Particle Accelerators

Livingston
and
Blewett

McGraw-Hill
Book Company

Particle Accelerators

INTERNATIONAL SERIES IN PURE AND APPLIED PHYSICS

LEONARD I. SCHIFF, CONSULTING EDITOR

Allis and Herlin Thermodynamics and Statistical Mechanics
Becker Introduction to Theoretical Mechanics
Clark Applied X-rays
Collin Field Theory of Guided Waves
Evans The Atomic Nucleus
Finkelnburg Atomic Physics
Ginzton Microwave Measurements
Green Nuclear Physics
Gurney Introduction to Statistical Mechanics
Hall Introduction to Electron Microscopy
Hardy and Perrin The Principles of Optics
Harnwell Electricity and Electromagnetism
Harnwell and Livingood Experimental Atomic Physics
Harnwell and Stephens Atomic Physics
Henley and Thirring Elementary Quantum Field Theory
Houston Principles of Mathematical Physics
Hund High-frequency Measurements
Kennard Kinetic Theory of Gases
Lane Superfluid Physics
Leighton Principles of Modern Physics
Lindsay Mechanical Radiation
Livingston and Blewett Particle Accelerators
Middleton An Introduction to Statistical Communication Theory
Morse Vibration and Sound
Morse and Feshbach Methods of Theoretical Physics
Muskat Physical Principles of Oil Production
Present Kinetic Theory of Gases
Read Dislocations in Crystals
Richtmyer, Gennard, and Lauritsen Introduction to Modern Physics
Schiff Quantum Mechanics
Seitz The Modern Theory of Solids
Slater Introduction to Chemical Physics
Slater Quantum Theory of Matter
Slater Quantum Theory of Atomic Structure, Vol. I
Slater Quantum Theory of Atomic Structure, Vol. II
Slater and Frank Electromagnetism
Slater and Frank Introduction to Theoretical Physics
Slater and Frank Mechanics
Smythe Static and Dynamic Electricity
Stratton Electromagnetic Theory
Thorndike Mesons: A Summary of Experimental Facts
Townes and Schawlow Microwave Spectroscopy
White Introduction to Atomic Spectra

The late F. K. Richtmyer was Consulting Editor of the series from its inception in 1929 to his death in 1939. Lee A. DuBridge was Consulting Editor from 1939 to 1946; and G. P. Harnwell from 1947 to 1954.

PARTICLE ACCELERATORS

M. Stanley Livingston, Ph.D.

PROFESSOR OF PHYSICS
MASSACHUSETTS INSTITUTE OF TECHNOLOGY
DIRECTOR, CAMBRIDGE ELECTRON ACCELERATOR
HARVARD UNIVERSITY

John P. Blewett, Ph.D.

SENIOR PHYSICIST
BROOKHAVEN NATIONAL LABORATORY

McGRAW-HILL BOOK COMPANY, INC. 1962
New York San Francisco Toronto London

PARTICLE ACCELERATORS

 Library of Congress Catalog Card Number 61-12960

THE MAPLE PRESS COMPANY, YORK, PA. 38140

Preface

The history of particle accelerators has not yet been compiled. Most of the literature on the subject is published in research journals or in laboratory reports, available only to a restricted group of readers. A few monographs have been published on selected subjects; a few journal issues have described individual machines; and several review volumes have included survey chapters on accelerators. But there are no books published in which the scientist, the engineer, or the student can find complete and general descriptions of the physical principles of all types of accelerators.

A comparative, critical analysis of the several accelerators can show the relative advantages and disadvantages for the different energy ranges. It will illustrate the way in which the different machines supplement each other as tools for the study of the broad range of phenomena in nuclear physics and high-energy particle physics. It can demonstrate one of the most significant features in accelerator development, the cross-fertilization between science and engineering which leads to the transfer of ideas and techniques between experts working on different parts of the problem or on different types of accelerators.

The need for such a critical study and compilation is clear. Many a student wants to know more about basic principles to guide his further studies; nuclear physicists must understand accelerators to evaluate experimental evidence; scientists or engineers in the field of atomic energy are curious about the machines which are the sources of nuclear data; and directors of laboratories need to appreciate the relative merits of the several machines as a basis for plans or decisions.

The layman gets his information about accelerators largely from newspapers or illustrated magazine articles. Newspapers have done much toward popularizing the field, but very little toward informing the public on basic principles. In the eyes of the press the "atom smasher" is a mysterious symbol of science. The layman has been led to think of atom

smashers as huge, complicated "Rube Goldberg" machines, built by prodigies with long beards for futile or slightly dangerous purposes. Yet many laymen are intrigued by their mechanisms and show much interest in qualitative descriptions. This is because most accelerators are simple in their basic principles, and a technically trained person finds that he can grasp these principles easily. Accelerators are no more complex than other machines which are commonly understood and accepted, such as the modern automobile or the synchronous motor; they are no more huge than many of the accepted devices of our civilization, such as the diesel locomotive or the multimotored aircraft. Their complexity depends on the detail with which they are studied. Basic principles of all accelerators are understandable in relatively simple concepts available to any technically trained person, and analogues can be found to extrapolate thinking to the more complicated principles.

A dozen authors would be required to describe expertly all the machines and techniques in the accelerator field. However, a compendium by many authors suffers from differences in content and style and cannot show the pattern of growth and development in the field. The authors of this volume recognize their limitations and have made every effort to supplement their personal experience by study of references and discussions with other experts. It is possible that some significant publications have been missed, unintentionally. This is an unfortunate consequence of the breadth of this rapidly developing field, lying as it does on the borderline between physics and engineering. A great deal of the material in this book is based on the authors' personal experiences in the accelerator field, covering the cyclotron, betatron, electron synchrotron, proton synchrotron, linear accelerator, and alternating-gradient synchrotrons. Much of the information has been acquired through private discussions, ranging over the whole field of accelerators. The authors wish to acknowledge their debt to the following for their generous and helpful criticisms and valuable advice: Mrs. M. Hildred Blewett, Prof. Sanborn Brown, Dr. F. T. Cole, Prof. E. L. Ginzton, Prof. D. W. Kerst, Dr. S. J. Lindenbaum, Prof. B. J. Malenka, Prof. J. C. Trump, Prof. Lloyd Smith, Prof. C. M. Van Atta, and Prof. Richard Wilson.

The organization of the material is primarily in terms of individual accelerators. Each type has been treated in a separate chapter essentially complete in itself. The emphasis is on the physical principles of operation, particle orbits and their controlling fields, and the design principles of the basic components. No attempt is made at complete coverage, but certain installations are chosen as typical and are described in some detail to demonstrate a particularly effective and well-coordinated system. Certain components such as ion sources, magnets, and shielding, which are common to many accelerators, are discussed in separate chapters. It has been the urge of the authors to show the

similarities in principle of the several machines, especially in the way they depend on the basic equations of motion of particles in electric and magnetic fields. To emphasize the similarities and to minimize repetition, the mathematical analysis of particle motion as applied to most accelerators is presented with a consistent nomenclature in separate chapters where the common features of acceleration, focusing, and stability are derived from the equations of motion.

The meticulous reader will note some inconsistencies in the use of symbols and units. The authors feel it is wiser in some instances to retain traditional and accepted symbols than to force a new symbolic terminology. Some of the fields discussed in the separate chapters have developed almost independently, and the same symbols have been used for different parameters in these fields. In some instances the symbols used in this volume have two or more definitions; these definitions are listed in the Table of Symbols. Similarly, several different systems of units have become customary in different fields. The authors prefer to use mks units wherever possible, primarily because of the major simplifications in the fields of electricity and electrical engineering which result. However, most scientists still use cgs units in many areas of scientific research and the data are frequently reported in these units; also, the mechanical engineering profession in the United States is wedded to the English system of units (inches, pounds, etc.). For consistency with the published data, the authors have chosen to use these alternate systems of units, with suitable conversion factors to the mks system where needed for clarity.

Accelerators are undergoing continuous development, and some of the material published here must necessarily be out of date. It is hoped that the basic principles presented and the general conclusions derived are now scientifically established, although it is expected that later work will extend the phenomena and improve on techniques and design.

M. Stanley Livingston
John P. Blewett

Contents

List of Symbols

(Page references are included to indicate the pages where nonstandard symbols are first defined)

c	velocity of light, m/sec
e	particle charge, coulombs
f	frequency, cycles/sec
h	harmonic order in synchrotrons (p. 302)
i	total current, amp
k	constant in water-flow formulas (p. 261)
m	particle mass, kg
m_0	particle rest mass, kg
p	particle momentum, kg-m/sec
p_0	momentum of equilibrium particle, kg-m/sec (p. 290)
p^*	$p_0/(m_0c)$ (p. 296)
r	radius in cylindrical coordinates (goes with θ and z)
s	position coordinate along an orbit, m
t	time, sec
u	scalar potential for magnetic field (p. 251)
v	velocity, m/sec
v_g	group velocity (p. 321)
A	vector potential (p. 252)
	atomic weight
B	magnetic flux density, webers/m^2 (p. 118)
	build-up factor (p. 521)
C	capacitance, farads
E	electric field, volts/m
F	force, newtons
G	gradient of a field (p. 112)

H	magnetic field, amp/m
I	current density, amp/m^2
J_n	Bessel function of order n
K	abbreviation used in phase-stability theory (p. 298)
	abbreviation used in synchrotron theory (p. 304)
L	inductance, henry
N	Avogadro's number
N_n	Neumann function of order n
P	pressure
Q	quantity of charge, coulombs
R	resistance, ohms
T	kinetic energy, joules or ev
	temperature
U	power, watts
V	potential difference, volts
W	total particle energy, joules or ev
W_0	rest energy, joules or ev
Z	atomic number
α	first Townsend coefficient (p. 75)
β	$= v/c$
γ	second Townsend coefficient (p. 77)
ϵ (or ϵ_0)	dielectric constant of free space, farads/m
η	$= (\mu_0/E_0)^{1/2} = 377$ ohms
	wavelength, m
μ (or μ_0)	permeability of free space, henrys/m
μ	microns: a parameter in AG theory; X-ray absorption coefficient
ρ	resistivity, ohms/m
	radius of curvature
σ	charge density
	collision cross section
ϕ	phase angle
ϕ_0	equilibrium phase (p. 297)
ω	2πf

1

Introduction

1-1. THE ROLE OF ACCELERATORS IN NUCLEAR SCIENCE

Particle accelerators have undergone a tremendously rapid development during the past 30 years. In few fields of science has progress been so spectacular. During this relatively short time, particle energies available for research have increased from a few hundred kilovolts to many billions of volts. Research in nuclear physics and on the properties of fundamental particles owes much of its progress to the continuously increasing energy achieved by a series of electronuclear machines, each larger and more effective than its predecessor. Also, much of the public awareness and support of the field of nuclear physics rests on popular interest in these gigantic atom smashers.

The purpose of this book is to present a description of the several particle accelerators. Fundamental principles will be discussed, and as much of the theoretical analysis of particle motion will be developed as is necessary to understand the operation of these principles in focusing and accelerating particle beams. The historical development will be outlined for each accelerator, and original contributions credited as fairly as possible. The over-all purpose is to show by comparison of their relative advantages and characteristics how the various accelerators supplement each other as tools for the study of nuclear physics and high-energy particle physics.

The record of accelerators in research is impressive. The complexity of nuclear processes has been demonstrated by hundreds of different reactions coming from artificial disintegration of nuclei by protons, deuterons, neutrons, alpha particles, gamma rays, and electrons, and by several

heavy ions. Induced radioactivities produced in targets bombarded by ion beams have been studied in detail to measure the lifetimes and analyze the decay schemes. New modes of disintegration and new complexities in the properties of nuclei have been discovered. Precise measurements of reaction thresholds and studies of the emergent radiations have led to an ever-increasing knowledge of atomic mass values and nuclear energy levels.

Radioactive elements have been used as tracers in many fields of scientific research: physics, chemistry, biology, medicine, metallurgy, and agriculture, to mention a few. A start has been made in the application of the radiations to medical therapy, notably for hyperthyroidism and leukemia. Neutrons from the cyclotron have been used in many fields of research, including cancer therapy. The properties of neutrons have been widely explored, and high-energy neutrons have themselves been utilized for disintegration. More recently the synchroaccelerators have succeeded in producing mesons, previously available only in cosmic rays, and studies of meson production and interactions are leading to important new knowledge about the fundamental nuclear force. New particles have been discovered, such as the neutral meson, the negative proton, and the antineutron, and it is clear that still more new knowledge is awaiting discovery. The record shows that particle accelerators have been most productive tools in exploring the nucleus of the atom.

Accelerators have found a permanent place in the science laboratories of the world. Every modern nuclear research laboratory must have some form of accelerator capable of disintegrating nuclei and producing induced activities; most of the larger laboratories have several machines to cover a wider range of phenomena. Direct-voltage accelerators, such as the electrostatic generator, are most useful in precise studies at low energy, such as the measurement of reaction thresholds or nuclear energy levels. The cyclotron is more powerful and produces particles of higher energy; it has been used as a high-intensity source of neutrons in the production of induced activities and for the study of high-energy disintegration processes. The betatron and electron linear accelerators produce high-energy electrons, and the resulting X rays are uniquely adapted to the study of photonuclear processes. Now the synchroaccelerators are rapidly taking over from cosmic rays the field of high-energy particle physics.

Each type of accelerator has made significant contributions. Because of their different capabilities, they supplement each other in covering the energy range needed for nuclear studies. Each accelerator fills a unique role, and all of them are needed. For example, the Nuclear Science Laboratory at the Massachusetts Institute of Technology has several electrostatic generators, a cyclotron, a linear accelerator, and a synchrotron, and all are being used effectively for research.

By 1940 much of the accumulated knowledge of nuclear physics had come from research using particle accelerators. However, radium-beryllium neutron sources were also in wide use and led in fact to the discovery of fission in 1939. Immediately following the first announcement, accelerators all over the world were applied to studies of this new phenomenon and rapidly exploited the field. Shortly thereafter a voluntary censorship was applied to reports of fission experiments in this country, and work was channeled into secret laboratories where accelerators were teamed with other scientific tools to produce the atomic pile and the atomic bomb. The speed with which accelerators were put to work is indicated by the transfer to Los Alamos of a working electrostatic generator from the University of Wisconsin and a cyclotron from Harvard University; both of these machines were in operation a few weeks after arrival at Los Alamos.

At the end of World War II, when physicists returned to their laboratories, the enhanced status of nuclear physics was immediately evident. The exciting and dangerous development of atomic energy, with its tremendous implications for national security, stimulated strong popular support for spending government funds on building still larger and higher-energy accelerators. With such impetus the new synchroaccelerators were rapidly developed.

Atomic reactors are finding many uses in research laboratories, but they have in no sense displaced accelerators for nuclear studies. The very high neutron intensities available from large reactors have made them the natural source of supply of induced radioactivities, which are distributed to the scientific world through the Isotope Distribution Division of the Atomic Energy Commission laboratory at Oak Ridge, Tennessee, and similar laboratories in other countries. This has relieved cyclotron laboratories of the tedious chore of production of long-lived isotopes. However, the accelerator is still essential for the radioactivity research laboratory. Positron emitters resulting from proton or alpha-particle bombardment of targets in an accelerator cannot be produced by neutrons. The very-short-lived neutron-induced activities cannot be shipped from the reactor to a distant laboratory and are best produced locally in an accelerator. Special research problems may require higher specific activities than are available from a reactor, but which can be obtained in the high concentration of neutrons in targets mounted directly behind the particle target in a cyclotron.

1-2. PROGRESS IN ACCELERATOR DEVELOPMENT

When Rutherford demonstrated in 1919 that the nitrogen nucleus could be disintegrated by the naturally occurring alpha particles from radium and thorium, a new era was opened in physics. For the first time

man was able to modify the structure of the atomic nucleus. The alpha particles used had energies of 5 to 8 million electron volts (Mev), far in excess of the energies available in the laboratory. During the 1920s X-ray techniques were developed so machines could be built for 100 to 200 kev. Development to still higher voltages was limited by corona discharge and insulation breakdown, and the multi-million-volt range seemed out of reach.

Physicists recognized the need for artificial sources of accelerated particles. In a speech before the Royal Society in 1927 Rutherford[1] expressed his hope that accelerators of sufficient energy to disintegrate nuclei could be built. Then in 1928 Gamow[2] and also Condon and Gurney[3] showed how wave mechanics could be used to describe the penetration of nuclear potential barriers by charged particles and made it seem probable that energies of 500 kev or less would be sufficient to observe the disintegration of light nuclei. This more modest goal seemed feasible. Experimentation started around 1929 in several laboratories to develop the necessary accelerating devices. Details of this race for higher voltages are given in the chapters to follow. Urged on by Rutherford, the first to succeed were Cockcroft and Walton[4] in the Cavendish laboratory at Cambridge. They reported the successful disintegration of lithium by protons of about 400 kev energy in 1932. The date of this first artificial transmutation can be taken as the starting point in accelerator history.

Four successive waves of development have swept the accelerator field, characterized by four different concepts in the acceleration of particles. The first stage was the application of direct-voltage techniques in which the particles were accelerated through a single large potential drop. The magnitude of the potential drop was increased to its practical limit by using electrode terminals of large radius of curvature and by improving insulation. Voltage breakdown of the accelerating tube was minimized by subdividing the potential along the length of the column.

The second concept was the application of resonance acceleration, in which the particles were constrained to pass and repass many times through a low potential drop in resonance with an oscillating electric field, until their final energy was many times greater than the maximum potential difference in the apparatus. The chief examples of resonance accelerators are the cyclotron and the early linear accelerators.

The third stage was the application of the principle of phase-stable acceleration to resonance accelerators, from which developed the family of synchroaccelerators. Here, with an exact knowledge of the forces producing stable orbits, it has been possible to keep particles in resonance for an indefinitely large number of accelerations to attain ultimate energies up to 10 billion electron volts (Bev).*

* The symbol "Gev" is used in England and in most European countries to represent 1000 Mev, rather than the symbol "Bev" used in the United States.

The fourth stage is in its preliminary phase of development. This is the new category of superenergy accelerators utilizing the alternating-gradient (AG) principle of magnetic focusing, which reduces the size and cost of magnets for circular machines so that a much higher energy range becomes economically feasible. In 1959 an AG proton synchrotron which produces 28-Bev protons was completed at the CERN laboratory in Geneva; a similar machine which produces protons of 33 Bev energy was completed in 1960 at Brookhaven National Laboratory.

Progress of accelerator development can be followed in more detail by noting the dates at which new machines entered the race, or at which they made new voltage records. The Cockcroft-Walton voltage multiplier was soon able to operate up to 750 kv. Later a 1.25-Mv installation was built by the Philips Company (Eindhoven) for the Cavendish laboratory, following the same design principles. This has proved to be about the practical limit for the voltage-multiplier type of accelerator when operated at atmospheric pressure.

Meanwhile, the magnetic resonance accelerator now known as the cyclotron was under development by Lawrence and Livingston at the University of California. Following a proposal by Lawrence, the principle of resonance acceleration was proved by Livingston in 1931 in a laboratory model experiment. The first practical cyclotron produced protons of 1.2 Mev in 1932. These were immediately put to use for nuclear studies. Deuterons of 5 Mev were obtained in a larger machine (the "27-inch") in 1934. Other laboratories joined in the development; 10 Mev was attained by 1936 and 20 Mev by 1940. However, the energy range of 20 to 25 Mev has proved to be a practical limit for the fixed-frequency cyclotron.

The betatron went through a similar development, starting with the first small model in 1940, with which Kerst produced 2.3-Mev electrons. A rapid development at the General Electric Research Laboratory produced 20 Mev by 1942 and 100 Mev by 1945. Kerst's 300-Mev betatron at the University of Illinois is the largest, and it will probably be the last of the big betatrons; before it was completed, the synchrotron came on the scene with a more efficient principle of acceleration.

Each new instrument has had a similar history; some of them have approached the practical ceilings even more rapidly. And just as one type of accelerator was approaching its upper limit, a new invention arrived to maintain the steady increase in energy. The cyclotron, betatron, synchrocyclotron, electron synchrotron, and proton synchrotron have each held the voltage record temporarily and have raised the energy scale still higher. Finally in 1952 the principle of AG focusing was published, allowing the latest extension of the energy scale.

This development of accelerators to higher and higher energy is illustrated graphically in Fig. 1-1. In this graph the energies achieved with

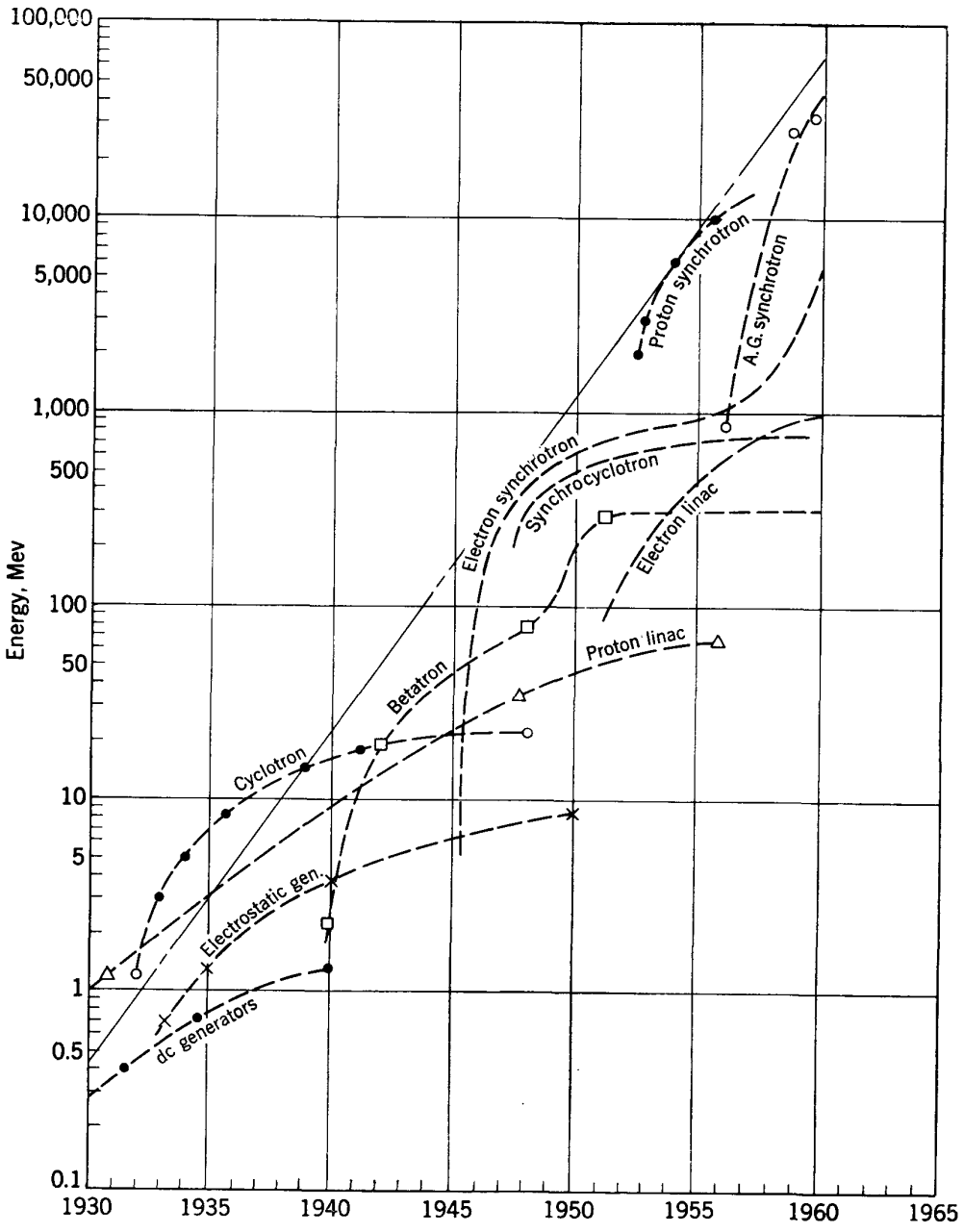

Fig. 1-1. Energies achieved by accelerators from 1930 to 1960. The linear envelope of the individual curves shows an average tenfold increase in energy every six years.

the several accelerators are plotted against the date of publication of the first announcement (which may lag many months behind the actual date of operation). When energy is plotted on a logarithmic scale, the envelope of the points is remarkably close to a straight line, indicating an increase in energy by a factor of 10 every six years. The progress of the individual machines in reaching their respective ceilings is indicated by the labeled

curves below the linear envelope. The exponential increase of energy indicated by this record is impressive. The plot also serves a useful purpose in orienting the various accelerators on the energy scale. An extrapolation beyond the highest points on the curve is intriguing. It is interesting to note that the principle of strong focusing (see Chap. 15) has offered a new opportunity of extending the energy range of accelerators and has come close to fulfilling the extrapolation.

1-3. COLLABORATION BETWEEN PHYSICS AND ENGINEERING

The development of accelerators has paralleled and sometimes paced progress in the electronics industry and in several branches of electrical and mechanical engineering. In few scientific developments has there been such effective and happy collaboration with the engineering profession as in the accelerator field. These machines were conceived by physicists who saw the need for high-energy particles in research, and the physical principles are based on fundamental scientific laws. However, the physicist who continued in the field ultimately metamorphosed into a practical engineer in order to produce a reliable, working machine. Of necessity he became accomplished in wide areas of electrical and mechanical engineering and utilized fully the advice and services of professionally trained engineers. On the other hand, many men trained in engineering have found in the accelerator field a challenge and opportunity to apply their training to new problems, frequently more exciting than the problems available in engineering practice. So the design staff of the modern accelerator laboratory is composed in almost equal numbers of experimental physicists and professionally trained engineers.

The first ion accelerators were simple applications of direct high voltage to evacuated discharge tubes. Nuclear physicists leaned on experience in the X-ray industry, and as the accelerator art progressed, it stimulated further development of higher-energy X-ray machines. Focusing requirements forced intensive studies and improvements in the field of ion and electron optics. Some of the developments have since been applied in the electronics industry. New techniques for the production of X rays, such as the resonance transformer, were stimulated by accelerator developments. The electrostatic generator has found almost equal application to positive-ion acceleration for nuclear physics and to electron acceleration for the production of X rays for medical therapy and radiography. The betatron has also found an important application as a source of very-high-energy X rays.

Magnetic accelerators, of which the cyclotron was the first, employed high-frequency electric fields for acceleration and drew heavily on experience in short-wave radio transmission at the start. It is significant that many of the early cyclotronists and their technician helpers were "ham"

radio operators. However, as numbers and experience grew, cyclotronists were able to make important contributions to the radio and radar fields. For example, the original roster of the Massachusetts Institute of Technology Radiation Laboratory, which developed microwave radar for the military services during World War II, consisted largely of nuclear physicists many of whom were cyclotronists. Cyclotron experience in magnetics and in high-frequency electronics was of real value in the early days of radar in such areas as the development of the magnetron.

We can follow this cross-linkage between accelerators and electronics still further. At the end of the war the accumulated experience in the electronics of high frequencies and pulsed circuits coming from the radar field fed back new techniques and concepts into accelerator design. The modern linear accelerator would have been impossible to conceive or build before the radar field reached its present high stage of development. The synchroaccelerators with their pulsed operation are also dependent on radar techniques. But it should be noted that the modern high-powered klystron tube with all its radar applications was originally developed in the Stanford accelerator laboratory. Modern accelerators are progressing further in adapting and utilizing the more sophisticated implications in the equations of motion and have already shown that they can offer new techniques and concepts to the engineering field. The principle of AG focusing appears to have a variety of applications, to traveling-wave vacuum tubes and to ion and electron optics.

Vacuum engineering is another technical field in which accelerator development contributed directly to engineering advances. The first all-metal vacuum systems were developed for accelerators such as the cyclotron, and techniques for making tight seals and high-speed pumps grew with the increasing size and energy of accelerators. The early metal pumps produced by commercial firms were based largely on this experience. As the field of vacuum engineering grew to meet the needs in vacuum distillation and isotope-separation problems, metal pumps were developed to still larger sizes. The well-known Westinghouse "30-in." fractionating oil-diffusion pump was developed for the isotope-separation plant at Oak Ridge. Even larger sizes with higher pumping speeds have since become available. These pumps have been applied directly to the recent synchroaccelerators and are a satisfactory answer to the vacuum-pump problems in these large metal-chamber machines. The most recent contribution to vacuum engineering from accelerator laboratories is the titanium-vapor pump, now in commercial production.

This healthy interchange of ideas and experience between accelerator scientists and practical engineers has been one of the most important factors leading to the rapid development in this field. Once the physical phenomena have been analyzed and understood, the remaining problems in accelerators are primarily those of engineering development. Ulti-

mately, as in any new application of basic principles, the engineer takes over to perfect techniques and produce a reliable product. Many of the machines conceived and designed by scientists are now ready for this detailed application of engineering, and some, such as the electrostatic generator, the cyclotron, the betatron, and the linear accelerator, are already being built by commercial engineering firms. In the construction of the new supervoltage accelerators the engineering profession is also making major contributions. The variety and scope of the engineering problems involved in the accelerator field will become evident in the chapters to follow.

1-4. THE MODERN RESEARCH LABORATORY

The modern research laboratory is far different from the "ivory tower" of the traditional individual scientist who pored over his books and retorts for years before announcing precedent-making discoveries. Neither does progress in scientific research depend solely on the inventions or flashes of genius of a few outstanding wizards, as conceived by many of the lay public. Rather, the modern laboratory is an organized cooperative team of specialists, each supreme in his own field but depending on others to supplement him in the attack on the complicated problem. Usually one or more senior scientists of wide experience and ability act as advisers and critics for the younger members and coordinate their efforts.

In no field are these characteristics more evident than in the modern accelerator laboratory. Here physicists with the insight to appreciate the new knowledge available from experiments with high-energy particles and the urge to create the necessary instruments are teamed with engineers who take pride and delight in invention of the unique devices, with theoretical scientists eagerly grasping the new experimental evidence to expand our knowledge of fundamentals, with young students just beginning to see the significance of their training and trying their wings on their first flights into the unknown, and with a group of loyal technical helpers each interested in doing his best for the project but only vaguely seeing the whole outline. Such a team constitutes the modern research laboratory, and each member plays a part. The morale and spirit of the team is of great importance, and much depends on the personality of the leaders to stimulate and maintain the proper spirit.

The thrill of discovery is the reward of exploration. The exploration of the unknown in science is just as rewarding as the discovery of a new river or mountain range, and nowhere in the field of science are the rewards more dramatic than in the accelerator field. The pleasure and excitement of the working crew when a new accelerator is first tuned in to set a new voltage record is something to be remembered for a lifetime.

The senior author (MSL) well remembers the sparkling eyes and dramatic gestures of his professor and supervisor, the late Ernest O. Lawrence, when the small cyclotron at the University of California produced 1-Mev protons for the first time in scientific history. An equal thrill comes to the experimentalist when, for example, a new ion source produces a beam current of ions greater than had been previously achieved. But even greater is the thrill of a significant scientific discovery or the observation of a new physical phenomenon. An equally dramatic moment at the University of California was the first observation of artificially induced radioactivity using 3-Mev deuterons. It is easy to understand why young scientists have been willing to labor for years to build and tune up a big accelerator in order to participate in these thrills of discovery when it is completed and brought into operation.

Wholehearted cooperation is essential for the members of a laboratory team if an instrument as complicated as the modern accelerator is to run smoothly. Each man has his special skill and is depended on to keep his component in good condition. The experienced operator, who knows just how to manipulate the controls to get the maximum beam intensity, comes to have a pride in his machine that admits no criticism. Pride in the machine and mutual respect for the other members of the group bring a team spirit frequently reminiscent of school days, and to a significant extent this team spirit improves the effectiveness and output of the laboratory.

A real insight into the spirit of such a laboratory is revealed by the spontaneous humor and intralaboratory jokes. A few samples have come into public view, notably the songs composed by Arthur Roberts. Some of these songs have been recorded for the phonograph, and the lyrics and scores of a few have been published.[5]

Large accelerators need large laboratories as well as large financial support. It is a paradox of science that the study of the smallest particles in nature requires the use of the largest and most expensive instruments. In the early days particle accelerators were built on a shoestring in academic laboratories, using or modifying old laboratory apparatus and depending on students for the labor of construction. There was a time when designers took pride in the low cost of their accelerators, but as the scientific results justified expansion to higher energies, the chief scientists or laboratory directors had to locate larger sources of funds. A new qualification became important in science—the ability to raise money. Some of the more colorful personalities in the nuclear field owe their reputations as much to their promotional and organizational abilities as to their scientific contributions.

In recent years financing has come increasingly from government sources, primarily the Office of Naval Research and the Atomic Energy Commission in the United States. Most of the large accelerators built in

this country since World War II have been financed by governmental grants-in-aid. Perhaps only in a government laboratory, or one supported by government funds, is it possible to undertake a development such as the cosmotron or the bevatron which costs many millions of dollars.

Costs increase with size of machines and with energy, as would be expected. Some machines are more efficient as power transformers than others, but power is not so important for research as the equivalent beam energy. The cost per unit of beam energy has actually decreased with the increasing energy of accelerators. On this basis, a dry cell costs about 50 cents per volt; the electrostatic generator produces ions of a few Mev energy at a cost of roughly 5 cents per volt. With the cyclotron, the cost at 15 Mev is below 1 cent a volt, and with the largest synchro-accelerators the cost approaches 0.1 cent per volt. It is well to recognize this steady improvement in cost efficiency when considering the magnitude of the investments in the larger accelerators.

1-5. REFERENCES AND BIBLIOGRAPHIES

Exchange of information between accelerator laboratories has done much to speed the rate of development. In addition to the formal publications of designs and results, many of the more detailed techniques have been written up in the form of reports circulated to other laboratories. This practice has been expanded considerably in recent years by the requirement of periodic progress reports to the sponsoring governmental agencies. The chief criticisms of this technique of reporting results are that the circulation of such reports is far too limited and that it tends to decrease the detail in regular publications. Only the larger laboratories in this country and a few foreign laboratories, for example, are supplied with copies of the progress reports handled by the Office of Naval Research or the Atomic Energy Commission.

Personal visits still remain the most effective means of acquiring information on recent developments. The practice is widespread among accelerator designers. Through such visits and occasional discussions at Physical Society meetings, news of developments travels rapidly across the country. Unfortunately this avenue of communication is limited to a relative few in the field, and others must depend on rumors or second-hand information. The accelerator field is still in many respects an art, and its practitioners are often unable to describe their techniques adequately in writing.

In the chapters to follow, references will be made to many publications and laboratory reports, listed at the end of each chapter. A serious attempt has been made to identify and credit the originator of each important new concept or technique. References are given, where

known to the authors, in justification of most of the arguable statements and conclusions. Specific references are made to papers summarizing the technical features or performance of individual accelerators which can be taken as typical of the species.

No attempt has been made to cover all publications in the accelerator field. This very valuable chore has been performed by others, resulting in a series of bibliographies which list and index essentially every significant publication. The first compilation was a Brookhaven National Laboratory report[6] published July 1, 1948. It was followed by University of California Radiation Laboratory reports in 1951,[7] 1952,[8] 1954,[9] and 1958.[10] In each case the new bibliography started from the date of the previous report and included only the new publications in the interim; so the entire series of bibliographies is needed to obtain a complete listing. The total number of publications listed is over 1500.

Others have listed the locations of high-energy installations in the United States and abroad, with dimensions, particle energies, and other parameters. The first listing was in the BNL report;[6] the most detailed listing is in the latest UCRL report,[10] which is reproduced in the "American Institute of Physics Handbook,"[11] 1957. The most recent compilation is an Oak Ridge laboratory report.[12] The total number of accelerators in this latest (but not up-to-date) listing is 525 throughout the world. Of these, about half are in the United States and half abroad; also about half are relatively low-voltage dc generators, and the others are resonance and synchronous accelerators.

We go now into a discussion of the early days of accelerator development to trace the evolution of the modern accelerator from the crude electric machines at the turn of the century to the present highly efficient sources of beams of accelerated particles. As we follow the story, we shall see how invention followed invention so rapidly at times that it was difficult to keep informed about the latest energy record. Each of the modern accelerators will be treated in a separate chapter in approximate order of development, which is also the approximate order of particle energy. The relationships between the several accelerators will become apparent, as will the way in which they supplement each other to cover the wide range of energies and phenomena in nuclear physics. The equations of motion of particles in electric and magnetic fields will be developed and applied to each machine. The principles of energy generation and particle acceleration will be described. Basic components will be identified and described in detail, and a few components will be discussed more thoroughly in separate chapters. So the story starts with the low-voltage generators of the early 1930s, the first of the series of particle accelerators.

REFERENCES

1. E. Rutherford, *Proc. Roy. Soc. (London)*, **117**:300 (1927).
2. G. Gamow, *Z. Physik*, **52**:510 (1928).
3. E. U. Condon and R. W. Gurney, *Phys. Rev.*, **33**:127 (1929).
4. J. D. Cockcroft and E. T. S. Walton, *Proc. Roy. Soc. (London)*, **A137**:229 (1932).
5. A. Roberts, *Phys. Today*, **1**:17 (1948).
6. E. Thomas, P. Mittelman, and H. H. Goldsmith, BNL-L-101 (July 1, 1948); AECU-31 (July 1, 1948).
7. B. E. Cushman, UCRL-1238 (March, 1951).
8. S. Shewchuck, UCRL-1951 (September, 1952).
9. F. E. Frost and J. M. Putnam, UCRL-2672 (Nov. 16, 1954).
10. G. A. Behman, UCRL-8050 (Jan. 1, 1958).
11. "American Institute of Physics Handbook," pp. 8–182, McGraw-Hill (1957).
12. F. T. Howard, ORNL Report-2644 (Nov. 17, 1958).

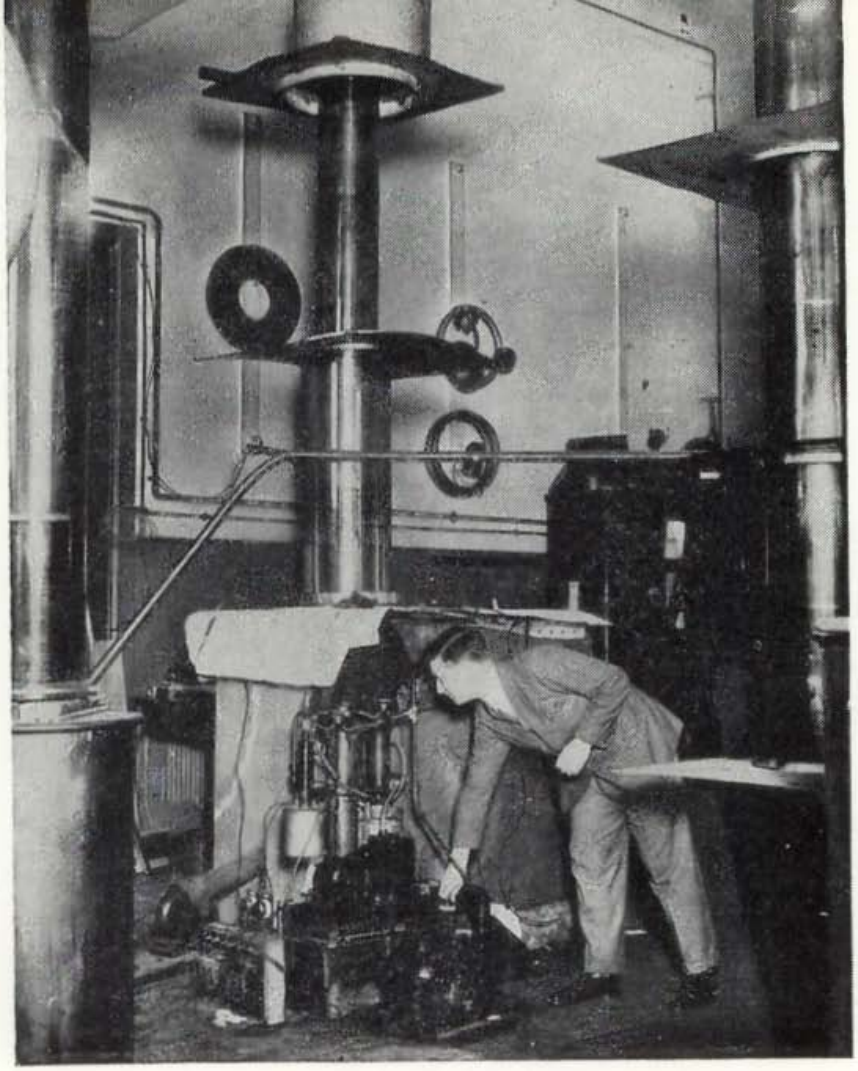

2

Low-voltage Generators

Particle accelerators of less than 1 million volts (Mv) have filled an important role in nuclear physics. In the early days they were the first in the field, and many significant discoveries were made at energies well below 1 Mev. Although higher-energy machines have now taken the spotlight, their more modest brothers are still turning out data of major importance. Some laboratories cannot afford the larger and more expensive machines, but scientists in such laboratories have nevertheless found the low-energy range a fruitful field for research. Many of the more interesting nuclear phenomena occur at relatively low excitation energy; to study them it is frequently better to use low bombarding energy so they are not concealed by competing reactions or by high background intensities.

Many different types of voltage generators have been applied to discharge tubes in this voltage range. Those that have been successful are the ones that produce steady direct voltage: the voltage multiplier, the transformer-rectifier, and the belt-charged electrostatic generator.

Others, such as the surge generator, the cascade transformer, and the Tesla coil, have been unsatisfactory largely because the voltage could not be controlled to sufficient accuracy. However, some of those which were unsatisfactory as positive-ion generators have been used successfully for high-voltage X rays where the requirements for voltage stability are not so severe. The different potential supplies will be described and their limitations discussed in turn; the parallel development of accelerating tubes will also be presented in this and the following chapters.

2-1. ELECTROSTATIC GENERATORS

Electrostatic generators may be considered in two general categories: the influence or induction machines and the separation-of-charge type. Influence generators of the Toepler-Holtz or Wimshurst types can be found in nearly every physical laboratory and are widely used in classroom demonstrations of static electricity. References dated 1870 to 1890 can be found in numerous texts. More recently, Simon[1] has developed the theory of operation of the induction generator; the theory of the Wimshurst machine is quite complicated, involving induction between eight sets of carriers on each of the counterrotating disks and using neutralizing brushes set at definite angles. "Leyden jar" capacitors are traditionally used to store the charge and smooth out potential fluctuations. A demonstration machine with 16- to 18-in. disks can develop 100 kv and can deliver currents of several milliamperes. Motor-driven units have been used occasionally as potential sources for X-ray tubes.

In the early days of accelerator development (1935), Dahl[2] (then at the Carnegie Institution of Washington) investigated the possibility of using a Holtz-type generator for nuclear studies. He built a double 24-in.-disk machine which developed up to 200 kv with a current capacity of 10 ma and concluded that it was practicable to use such a source in a higher-voltage installation. He suggested mounting several such machines on insulated platforms and connecting them in series for higher potentials. However, this potential source was not so steady as the belt-type generator and was abandoned. Still more recently (1951) Malpica[3] in Mexico City has described a rotating-disk friction generator for 300 kv intended for the acceleration of particles.

Before World War II the Wimshurst machines had been relegated to the category of museum pieces or, at best, classroom demonstrators. More recently, however, the techniques have been modernized and the device has been reduced to a practical dc power supply by a French company (SAMES of Grenoble). The SAMES generators are dielectric

---

At the head of the facing page is an illustration of the Cavendish laboratory generator for 700 kev. (Courtesy of Sir John Cockcroft.)

cylinders rotating in a hydrogen atmosphere. These compact, reliable machines are finding application in many European laboratories, wherever power supplies are required for dc currents up to a few milliamperes at voltages between 50 kv and 1 Mv.

Electrostatic generators which depend on separation of charge also have a long history in static electricity. In the early machines, positive and negative charges were separated by friction and then transported mechanically to charge a capacitor, which was often a metal sphere of large radius. Lord Kelvin is reputed to be the originator of the "charged water drop" generator; water drops electrified by friction on issuing from a nozzle fell into an insulated metal container which became charged to high potential. Others experimented on modifications of this method of conveying charge to an insulated terminal, including falling charged metal spheres. In about 1890, Righi improved the method by using a belt formed of alternate links of insulating and conducting material to carry charge to a hollow spherical terminal. Then for many years there was no activity in this field. A more recent revival was the development in the SAMES laboratory in France of an electrostatic generator which used air blasts of electrified dust to transfer the charge.

R. J. Van de Graaff[4] started the modern development of the belt-charged electrostatic generator in 1930. Charges sprayed from corona points onto a moving silk belt were transported to charge a 2-ft-diam aluminum sphere mounted on a glass rod. The immediate success of the belt-charged machine showed it to be superior to all other forms of static generators. It has become so important a tool in nuclear physics that it deserves detailed treatment and is therefore described and discussed fully in Chap. 3.

2-2. TESLA COIL

The Tesla coil utilizes electromagnetic induction to generate oscillatory pulses of high potential. In its usual form two resonant oscillatory circuits are coupled magnetically; the primary circuit has large capacitance and low inductance, while the secondary has a small distributed capacitance and large inductance owing to its being wound of many turns of fine wire. Figure 2-1 illustrates the traditional circuit for a spark-excited Tesla coil of the double-ended type. The capacitor in the primary circuit is charged to sufficiently high potential to cause breakdown of a spark gap in series with the primary windings, which produces an oscillatory discharge at the frequency determined by the inductance and capacitance in the circuit. The oscillatory current of high frequency in the primary coil induces bursts of high-potential oscillations in the coupled secondary, which are repeated at the sparking frequency. Voltage amplitude is a maximum when the two circuits are tuned to resonance.

This device was one of the first to be investigated in the search for a potential source for particle acceleration. A research team at the Department of Terrestrial Magnetism of the Carnegie Institution of Washington, consisting of Breit, Tuve, Hafstad, and Dahl, were among the first to attempt this application. They reported their results in a series of publications[5–9] in 1930 covering the Tesla coil, its voltage calibration, and the discharge tubes for accelerating particles. They used an oil-insulated secondary coil closely wound on a glass tube ending in spherical electrodes with a resonant frequency of 100 kc/sec, and reported peak potentials of 3 Mv at 1 atm oil pressure and 5 Mv when the oil was under high pressure. Their voltage calibrations, based on sphere-gap measurements, are now believed to be in serious error. The potentials attained were probably considerably lower than the values reported.

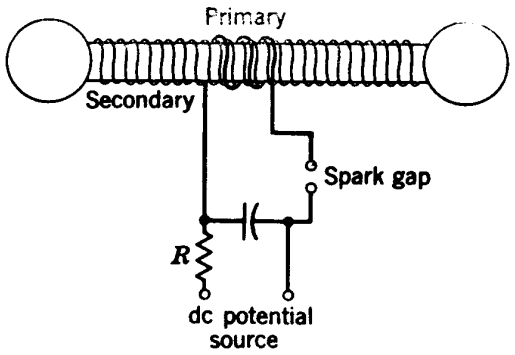

Fig. 2-1. Circuit diagram for a double-ended Tesla coil.

The most significant result of the early Carnegie experiments was not the voltage source but the development of the accelerating tubes. The first attempt, using long, evacuated glass tubes with an electrode at each end, showed a limiting voltage for breakdown at about 300 kv. The next step was to divide the potential between multiple electrodes, following the concept of the Coolidge "cascade" type of X-ray tube. This type of tube had been perfected for the acceleration of electrons in high-voltage X-ray installations, primarily at the General Electric Company. It used a column of tubular electrodes in line, with relatively short gaps between the rounded ends of the electrodes. Electrons were accelerated in a sequence or cascade of several potential drops uniformly spaced along the length of the tube. This distributed the potential drop along the accelerating tube and prevented high local field concentrations; also the tubular electrodes shielded the insulating walls and prevented charging of the walls by stray electrons from the beam. Figure 2-2*a* is a sketch of a two-stage Coolidge-type X-ray tube. In the Carnegie laboratory the early designs used many glass bulb sections sealed together in line with concentric cylindrical electrodes supported at the seals; tubes of 15 or more sections were developed. Figure 2-2*b* illustrates one of the early Carnegie tubes.

The accelerating tubes were immersed in an oil bath with the Tesla coil. Breakdown potentials of up to 1.9 Mv were reported, but were probably overestimated in view of later corrections to the spark-gap voltage calibrations. In any case, the oscillatory character of the potential obtained from the Tesla coil made it unsuitable for particle accelera-

tion. The Carnegie group abandoned it in about 1932 in favor of the belt-charged electrostatic generator developed by Van de Graaff. But they were able to utilize the accelerating tubes, which have proved to be forerunners of the modern tubes.

Modifications of the Tesla coil have taken several forms. In 1933 D. H. Sloan[10] at the University of California developed a continuous-wave radiofrequency type called the "resonance transformer" (Fig. 2-3). The secondary coil was made of heavy, internally cooled copper tubing of 10 to 15 turns, supported from one end in a vacuum chamber for voltage insulation, resonant at frequencies of about 6 megacycles/sec. The primary was a one-turn coil coupling with the secondary at the grounded

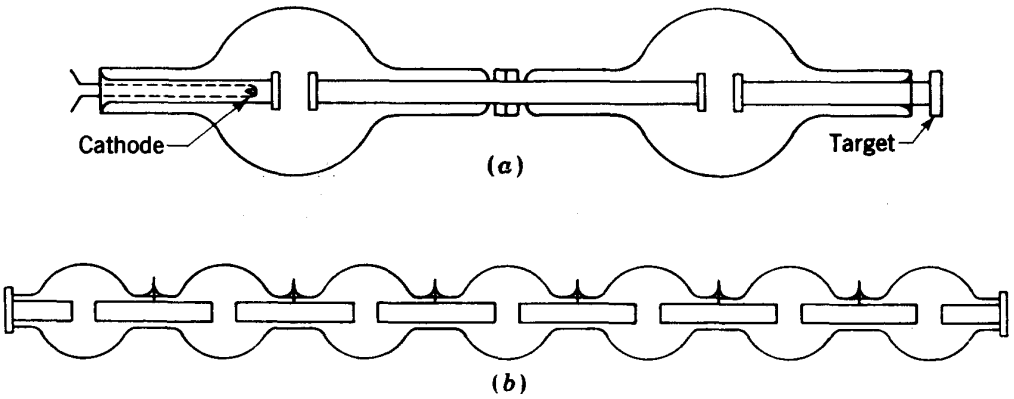

Fig. 2-2. (*a*) Coolidge cascade X-ray tube. (*b*) Carnegie Institute multisection accelerating tube.

end and driven by a vacuum-tube oscillator circuit at the resonant frequency.

The resonance transformer has been used successfully for production of X rays; a thermionic cathode in the side of the vacuum chamber provides electrons which are accelerated toward and strike a gold-surfaced target on the high-voltage end of the coil. An installation of this type was built in 1933 at the University of California Hospital in San Francisco by Livingston and Chaffee following Sloan's designs; it has given many years of service for X-ray therapy at voltages up to 1.25 Mv.

An experimental unit at the physics laboratories of the University of California, developed by Sloan and J. J. Livingood, had a hot cathode in place of the target on the end of the coil and a thin-foil window in the side of the vacuum chamber through which a beam of 1-Mev electrons emerged. Sloan had hoped to use the resonance transformer for producing positive ions of twice the nominal energy by providing two accelerations. In this arrangement ions would be injected from a source at ground potential on the chamber wall and those of proper phase would

be accelerated toward and enter a hollow cylindrical tube supported on the end of the resonant coil; ions which traversed the tube in one half-period of the oscillation would emerge when the tube had a reversed polarity and would be accelerated toward the opposite chamber wall, where they could be used for experiments. This principle of energy-doubling is a modification of the resonance principle used in the linear

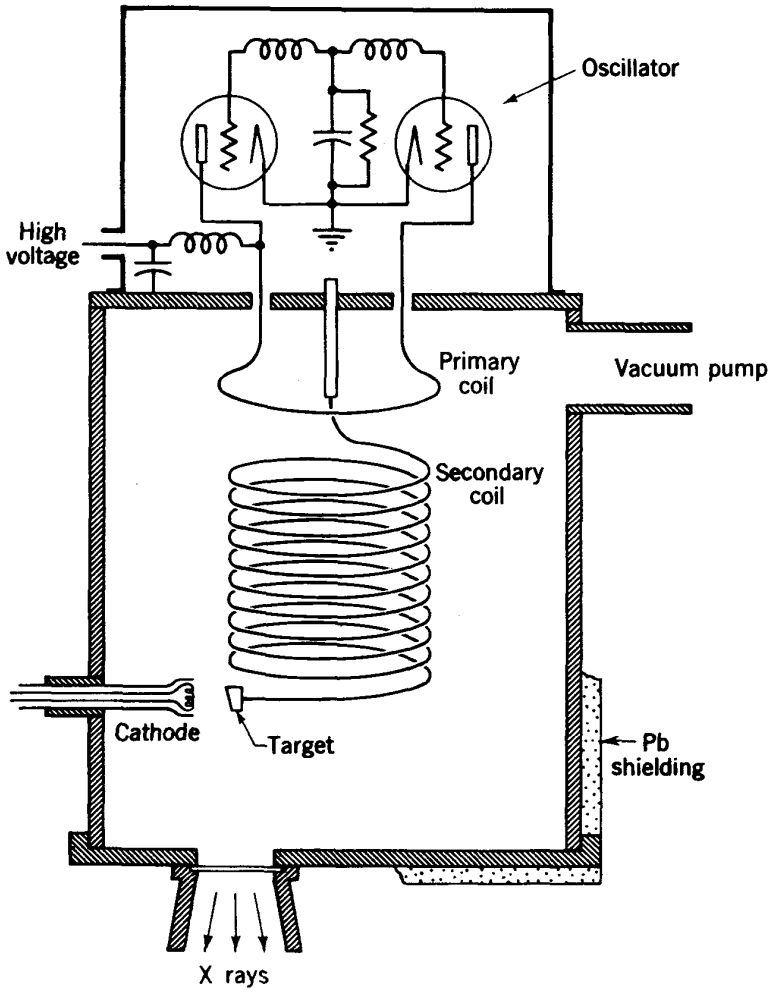

Fig. 2-3. Radiofrequency resonance transformer for 1-Mv X rays, University of California Hospital in San Francisco.[19]

accelerator. However, many technical difficulties were encountered, and this device was not sufficiently attractive to compete with the cyclotron or other positive-ion accelerators.

Another modification of the induction coil is the low-frequency resonance transformer developed before 1934 by Charlton, Westendorp, Dempster, and Hotaling[11] at the General Electric Company. Figure 2-4

is a schematic diagram of the apparatus. In this instrument the secondary coil was made of very many turns of fine wire, wound in compact coils. It had a laminated iron core and was resonant at 180 cps. The coil was mounted in a housing containing gas at high pressure for insulation. The primary coil was made to resonate at the same frequency by using a large

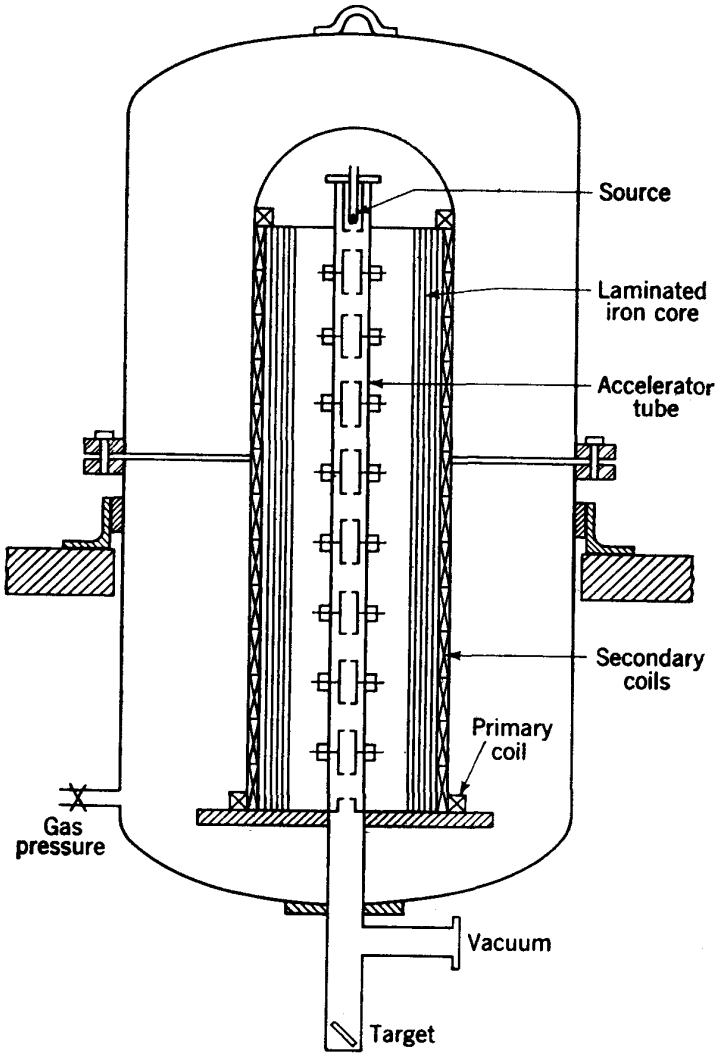

Fig. 2-4. 180-cycle resonance transformer for 1-Mv X rays, General Electric Company.[11]

capacitor and was supplied by a frequency-tripling circuit from a 60-cycle power supply. An evacuated accelerating tube installed along the axis of the coil was used to accelerate electrons. The cathode was heated by current from a low-voltage secondary winding at the high-potential end of the main coil, and the target was at the grounded end. This machine has been produced commercially as an X-ray generator operating at 1 Mv and 3 ma electron current.

2-3. SURGE GENERATOR

The "Marx" circuit has been widely used by electrical engineers to produce surges of high voltage for testing electric equipment. A stack of capacitors is charged in parallel from a dc potential supply and then

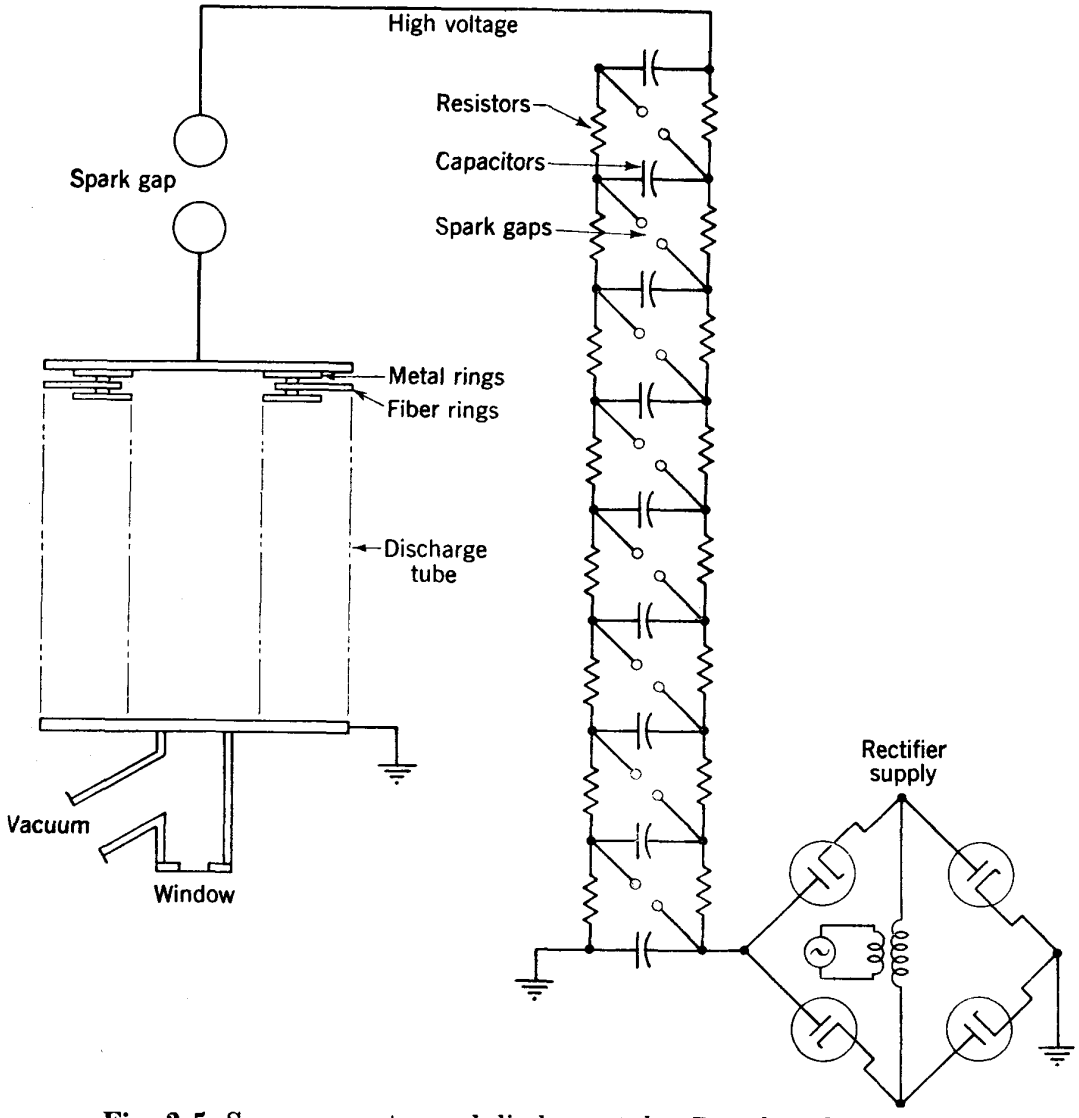

Fig. 2-5. Surge generator and discharge tube, Brasch and Lange.[13]

discharged through cross-connected spark gaps (Fig. 2-5). The potential difference developed momentarily across the stack of capacitors can be extremely high and can cause sparks many feet long in air—miniature lightning—but the duration of the voltage pulse is only of the order of a few microseconds, and it is oscillatory in character. The highest-energy surge generator was built at the General Electric plant at Pittsfield, Massachusetts, in about 1932; it was capable of producing voltage surges of over 6 Mv.[12]

Surge generators have been used primarily to test the flashover and

breakdown characteristics of insulators and electric equipment and have seldom been used for the acceleration of particles. However, in 1930 Brasch and Lange[13] in Germany developed a crude vacuum tube made of alternate rings of metal and fiber tightly compressed between end plates, to which they applied a 2.4-Mv voltage surge from a stack of capacitors. The peak surge current was of the order of 1000 amp; the discharge tube practically exploded on each surge and had to be cleaned and reassembled frequently. A metal-foil window at the grounded end of the tube allowed a beam of high-energy electrons and gas ions to emerge into the air. The emergent beam has been described as having an intensely brilliant blue color, brightest near the tube window but still visible at a distance of over a meter. Presumably this discharge was attended by some nuclear disintegration and also by considerable dangerous radiation; however, at that time the former was not suspected and the latter was not appreciated. Figure 2-5 is a schematic drawing of such a generator arranged to apply a surge to a discharge tube.

The surge generator has excited considerable enthusiasm as a demonstration of electric power. The tremendous sparks and the loud reports are very impressive. However, the short-pulse character of the surge and the irregular voltage obtained are not suitable for studies of accelerated particles, and the surge generator has not been significantly useful in nuclear research.

An interesting attempt to convert a surge generator into a steady source of dc potential difference was reported by W. C. Anderson[14] in 1936. He used a number of capacitors connected permanently in series and charged successively by motor-driven rotating brushes which were supplied with a dc voltage. The capacitors were arranged around a circular commutator, and the high series potential difference was developed between the final pair of unconnected capacitors. The model was qualitatively successful in magnifying 110 volts to over 5000 volts, but has not found further application.

At this point it may be of interest to mention an attempt to utilize the high potentials developed in the atmosphere during electrical storms. In 1932 Brasch and Lange[13] stretched an insulated cable across a valley between two peaks in the Alps; from this cable a conducting cable supporting a terminal was suspended. During thunderstorms high potentials would develop between this terminal and a grounded terminal on the valley floor; sparks several hundred feet long were obtained. Plans had been made to install a discharge tube for the acceleration of particles, but experiments were abandoned when Lange was killed.

2-4. CASCADE TRANSFORMER

The requirements of high-voltage power transmission in the western United States, where 220-kv lines at 50-cycle frequency were used for

long-distance transmission, led to the establishment of a high-voltage laboratory at the California Institute of Technology in the early 1920s, sponsored by the Southern California Edison Company. In this laboratory Sorensen[15] built the first cascade-transformer unit to reach 1 Mv from line to ground. A schematic diagram is shown in Fig. 2-6. Three 250-kv 50-cycle Westinghouse transformers were arranged in series. In addition to the usual low-voltage primary and high-voltage secondary windings, a third "exciter" winding at the high-potential end of the secondary was used to supply the next transformer. The transformers

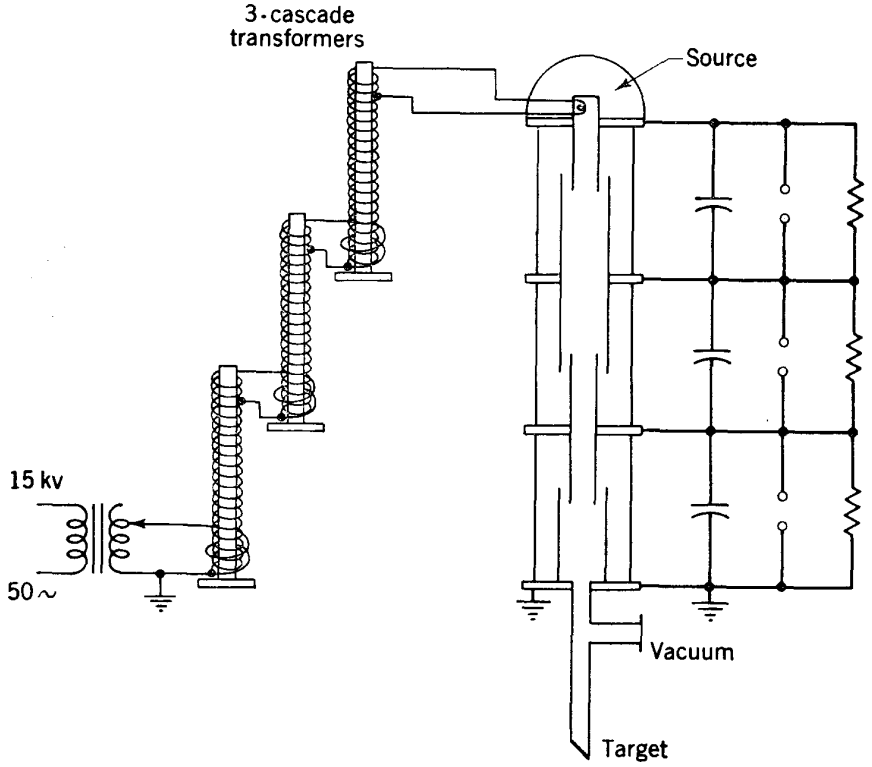

Fig. 2-6. Cascade transformer and discharge tube for 0.75 Mv, California Institute of Technology.[15]

were mounted on insulating platforms. The root-mean-square (rms) ac potential of the terminal of the last transformer was 750 kv, and peak voltage exceeded 1 Mv above ground. This installation was used for many years for the study of high-voltage breakdown of insulators, corona losses, and calibration of sphere-gap voltmeters.

After some years of service as a high-voltage test equipment for electrical engineering, the cascade transformer was taken over by C. C. Lauritsen about 1928 as a voltage source for the acceleration of particles. X-ray tubes were developed first,[16] operating at potentials up to 750 kv. Crane and Lauritsen[17] started with a simple type of X-ray tube built of a single porcelain bushing. In 1934 Crane, Lauritsen, and Soltan[18] installed a single-step positive-ion accelerating tube which would operate

at potentials up to 1 Mv and initiated a program of nuclear research, using H^+ and He^{++} ions to produce neutrons from Li and Be targets. Another tube, developed by Stephens and Lauritsen,[19] was characterized by having an extremely short path for the acceleration of ions. Positive-ion optics were not yet understood in those days, and the beams obtained had poor focal properties.

The "Caltech" nuclear research laboratory under Lauritsen has had a long period of productivity and has trained a notable succession of research students. Eventually the superior properties of the belt-charged electrostatic generator as a steady dc potential source were recognized, and the cascade transformer was replaced. However, the transformer served an important purpose at the start and made possible a great deal of valuable research.

2-5. TRANSFORMER-RECTIFIER

The X-ray unit, using a high-voltage transformer to produce alternating voltage for an X-ray tube which also acts as a rectifier, has been developed to a high stage of perfection by many engineering laboratories. Coolidge, at the General Electric Company, introduced the thermionic cathode and perfected the high-voltage sealed-off X-ray tube. Others have developed the necessary high-potential ac transformers. The classically simple circuit of a transformer, a sealed-off X-ray tube with a thermionic cathode, and a capacitor is shown in Fig. 2-7*a*. Years of intensive engineering effort have failed to improve significantly on the performance of this simple circuit.

For positive-ion acceleration it is necessary to insert a rectifier tube in the circuit (see Fig. 2-7*b*) to maintain direct voltage across the accelerating tube, since the gas evolved from the ion source becomes ionized and would otherwise support a large electron current during the negative half-cycle.

In a strict sense the X-ray tube was the first particle accelerator, although possibly the emergent cathode-ray beams obtained by Lenard in 1894 also fit the modern definition. In 1926 Coolidge[20] produced an emergent beam of electrons at 350 kev from a sealed-off tube with a thin metal-foil window. These electron beams were never used for nuclear investigations and will not be considered further here.

However, after the early successes by Cockcroft and Walton and others in producing nuclear disintegrations by positive ions of modest energy, the simple transformer-rectifier voltage supply came into use as a positive-ion accelerator. The low-voltage accelerator has several definite advantages. Neutrons coming from exoergic reactions, such as Li(p,n), have a precisely determined minimum energy (1.89 Mev), and the lower the bombarding energy, the better the uniformity of the neutrons. The yield of neutrons from the D(d,n) reaction is large, and the energy

depends on the angle of observation relative to the deuteron beam; a precisely controlled, low bombarding energy makes this reaction unique as a source of neutrons of known energy below 1 Mev. Several other reactions have resonances for bombarding energies below 200 kev.

Many descriptions of low-voltage accelerators have been published. As illustrations we shall cite three references. Zinn[21,22] started in 1936 with an extremely low-potential supply (60 kv) and then extended it to 200 kv as a source of neutrons from the D(d,n) reaction. Beam currents of over 1 ma of deuterons were obtained. In 1937 Slack and Ehrke[23]

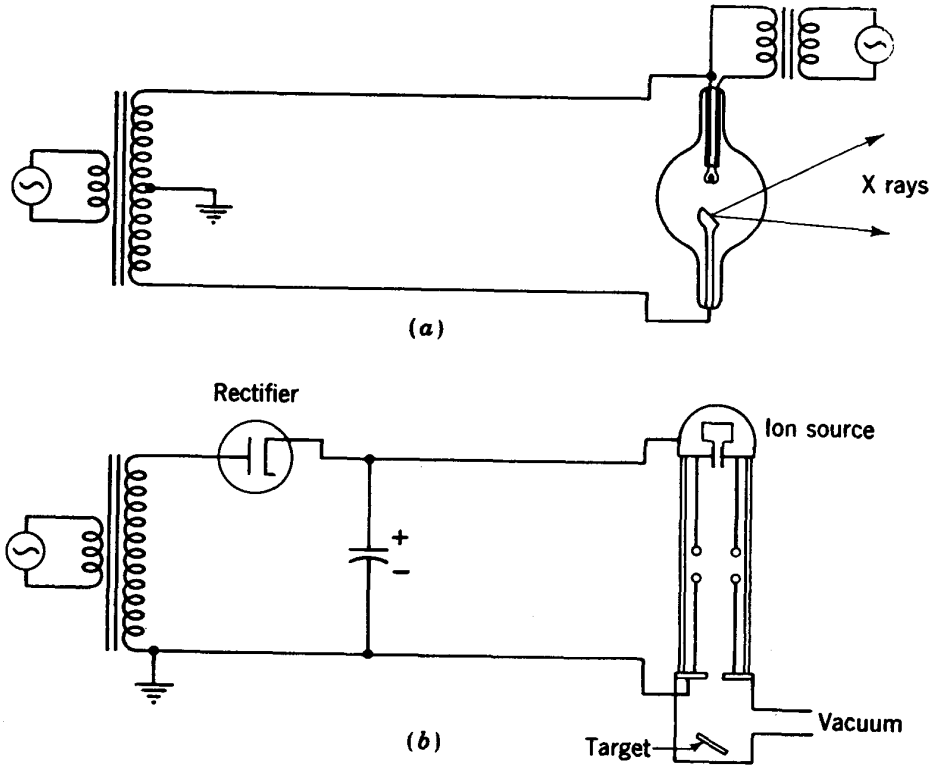

Fig. 2-7. Transformer-rectifier circuit producing high dc potential. (*a*) X-ray tube acts as a self-rectifier. (*b*) Rectifier required for positive-ion acceleration.

described a similar 200-kv unit used as a neutron generator. A more recently developed 200-kv accelerator (1950) is reported by Almqvist, Allen, Dewan, Pepper, and Sanders[24] and includes a voltage stabilizer.

For precise work the voltage must be stabilized by a regulating circuit such as that reported by Dewan,[25] which reduces fluctuations to 0.1 per cent. This corresponds to only 25 volts variation at the lowest energy used (25 kv).

The primary problem with this low-voltage accelerator has been to obtain sufficiently high intensities from an ion source. Many types have been tried, and several have been successful in producing beams of over 1 ma. These will be described more fully in Chap. 4, in the general discussion of ion sources. Large beam intensities are required to compen-

sate for the low yields owing to the small probability of potential barrier penetration at less than 200 kv. The lowest energy at which such an accelerator has produced observable intensities of nuclear disintegrations, observed as neutrons from the D(d,n) reaction, is about 30 kv.

2-6. VOLTAGE MULTIPLIER

The first successful disintegration of nuclei by electrically accelerated particles was achieved in 1932 by Cockcroft and Walton[26] using about 400-kev protons accelerated by a capacitor-rectifier circuit which multiplied the available potential by 4. Voltage-doubling or voltage-multiplying circuits had been developed as early as 1920[27,28] and were adapted by Cockcroft and Walton to meet their needs, but the accelerating apparatus utilizing this principle is usually called a Cockcroft-Walton machine.

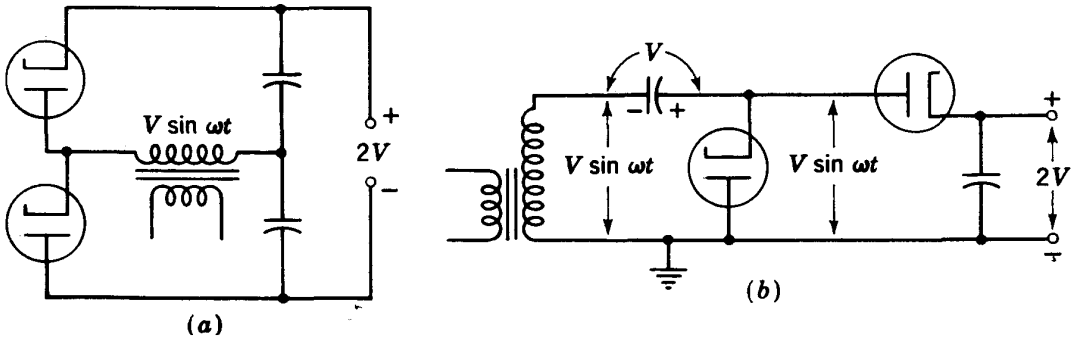

Fig. 2-8. Voltage-doubling circuits. (*a*) Symmetrical circuit. (*b*) Circuit which allows the negative terminal to be grounded.

The voltage multiplier is in principle a circuit for charging capacitors in parallel and discharging them in series. It differs from the surge generator in that it operates on alternating current, using rectifiers to charge capacitors during one half-cycle and other rectifiers to transfer the charge during the other half-cycle, so a steady direct voltage results.

The elementary voltage-doubling circuit is shown in Fig. 2-8. In the circuit shown in Fig. 2-8*a* the two capacitors are charged on successive half-cycles and a doubled voltage appears across the capacitors in series. Since neither end of the output is at the potential of one end of the transformer secondary, this circuit has some disadvantages in making ground connections. For this reason the circuit of Fig. 2-8*b* is usually preferred. Here the voltage applied to the output capacitor includes the transformer output ac voltage plus the dc charge of the first capacitor. This circuit is appropriate for addition of further stages of multiplication (Fig. 2-9*a*). By adding units to a total of N capacitors and N rectifiers one can obtain voltage multiplication by a factor of N. The circuit shown in Fig. 2-9*a* to give a fourfold voltage multiplication was the one used by Cockcroft and Walton.

The other half of the accelerator is the ion-accelerating tube, which Cockcroft and Walton had spent some years in perfecting. The two-stage tube used is illustrated in Fig. 2-9*b*. The papers describing their early results are classics in nuclear physics and give full details of the technical development, voltage calibrations, and experimental observations. The series of papers describing the first disintegrations[26] has earned enduring fame for the authors, who shared the Nobel Prize in physics for 1951. Their apparatus deserves recognition as the first successful particle accelerator for nuclear research.

Later Cockcroft and Walton installed a 1.25-Mv voltage multiplier of the same type in the Cavendish laboratory, engineered and constructed

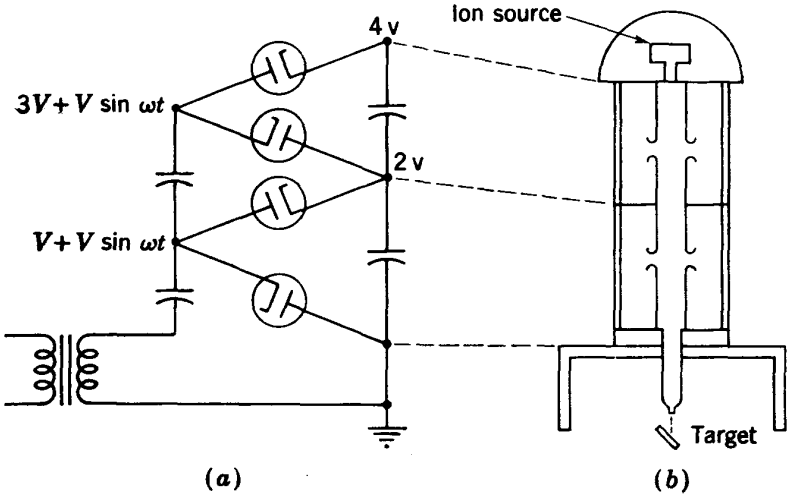

Fig. 2-9. (*a*) Cockcroft-Walton voltage-multiplying circuit.[26] (*b*) Accelerating tube for 0.7-Mev positive ions.[26]

by the Philips Company of Eindhoven, Holland. Similar potential supplies have been used in several English and European laboratories. A photograph of the 700-kev generator at the Cavendish laboratory is shown as the chapter headpiece, page 14. The arrangement of components has become standard in most installations. Capacitors are stacked in two vertical columns capped by a large rounded terminal. The rectifiers are located in a zig-zag pattern between the capacitor stacks. A stack of filter capacitors to reduce voltage ripple is frequently added as an extra vertical array, as can be seen in the photograph. The accelerating tube is also a vertical assembly with ion beam brought down through the floor to an experimental room beneath. Shielding for the X rays produced in the tube is necessary, and the floor is usually built up to provide this shielding.

The voltage multiplier has been so successful as a potential supply for energies of around 1 Mev that it has been widely copied and modified in other laboratories. One of the first laboratories in this country to build such a unit was the University of Illinois. In 1937 Haworth, King,

Zahn, and Heydenburg[29] described such an apparatus operating at 300 kv, chiefly characterized by the economy of construction. Capacitors of glass plates and metal foil were built in the laboratory; rectifiers were constructed of glass and metal cylinders and continuously pumped. The result of a continuous development of accelerating tubes was reported by Haworth, Manley, and Luebke.[30]

The circuit operates as described above, with an output-voltage multiplication factor N equal to the total number of capacitors (or the number of rectifier tubes) with no current drain. With finite current drain the voltage is reduced below this optimum, and ripple appears in the output. Bouwers and Kuntke[31] in Germany analyzed the circuit on the assumption of perfect rectifiers and capacitors. The theory has been extended and checked experimentally by Arnold,[32] Peck,[33] and Lorrain.[34] Lorrain gives the results in the following form, in which the output voltage V is given in terms of the peak input voltage V_i, frequency f, capacitance C of an individual capacitor, and load current I:

$$V = NV_i - \frac{I}{12fC}(N^3 + \tfrac{9}{4}N^2 + \tfrac{1}{2}N) \tag{2-1}$$

The ripple voltage is given by

$$\pm V = \frac{I}{16fC} N(N + 2) \tag{2-2}$$

It is clear that high frequency is an advantage, both to minimize ripple voltage and to reduce size of capacitors. The optimum number of stages can be obtained by differentiation of Eq. (2-2).

Arnold[32] used selenium rectifiers instead of vacuum tubes in the design of a 500-kv generator operating at 750 cps. In his paper he checked the performance of his circuit against the theory and found it in good agreement. Lorrain[34] reports on a 500-kv generator using 24 stages and operating at 32 kc/sec; he was able to utilize available low-cost radio and television equipment. The problem of insulation against corona breakdown was solved by housing the generator in a pressure vessel with 30 psi pressure of CO_2 and Freon gas.

This type of generator is now available commercially from several suppliers, using selenium rectifiers and providing output voltages up to more than 1 Mv.

REFERENCES

1. A. W. Simon, *Rev. Sci. Instr.*, **4**:67 (1933).
2. O. Dahl, *Rev. Sci. Instr.*, **7**:254 (1936).
3. J. M. Malpica, *Rev. Sci. Instr.*, **22**:364 (1951).
4. R. J. Van de Graaff, *Phys. Rev.*, **38**:1919A (1931).

5. G. Breit and M. A. Tuve, *Nature*, **121**:535 (1928).
6. G. Breit, M. A. Tuve, and O. Dahl, *Phys. Rev.*, **35**:51 (1930).
7. M. A. Tuve, G. Breit, and L. R. Hafstad, *Phys. Rev.*, **35**:66 (1930).
8. M. A. Tuve, L. R. Hafstad, and O. Dahl, *Phys. Rev.*, **35**:1406 (1930).
9. M. A. Tuve, L. R. Hafstad, and O. Dahl, *Phys. Rev.*, **36**:1261 (1930).
10. D. H. Sloan, *Phys. Rev.*, **47**:62 (1935).
11. E. E. Charlton, W. F. Westendorp, L. E. Dempster, and G. Hotaling, *J. Appl. Phys.*, **10**:374 (1934).
12. Bellaschi, *Trans. AIEE*, **51**:936 (1932).
13. A. Brasch and F. Lange, *Naturwiss.*, **18**:769 (1930); *Z. Physik*, **70**:10 (1931).
14. W. C. Anderson, *Rev. Sci. Instr.*, **7**:243 (1936).
15. R. W. Sorensen, *JAIEE*, **44**:373 (1925).
16. C. C. Lauritsen and R. D. Bennett, *Phys. Rev.*, **32**:850 (1928).
17. R. Crane and C. C. Lauritsen, *Rev. Sci. Instr.*, **4**:118 (1933).
18. H. R. Crane, C. C. Lauritsen, and A. Soltan, *Phys. Rev.*, **45**:507 (1934).
19. W. C. Stephens and C. C. Lauritsen, *Rev. Sci. Instr.*, **9**:51 (1938).
20. W. D. Coolidge, *J. Franklin Inst.*, **202**:693 (1926).
21. W. H. Zinn and S. Seely, *Phys. Rev.*, **50**:1101 (1936).
22. W. H. Zinn and S. Seely, *Phys. Rev.*, **52**:919 (1937).
23. C. N. Slack and L. F. Ehrke, *Rev. Sci. Instr.*, **8**:193 (1937).
24. E. Almqvist, K. W. Allen, J. T. Dewan, T. P. Pepper, and J. H. Sanders, *Phys. Rev.*, **79**:209 (1950).
25. J. T. Dewan, *Rev. Sci. Instr.*, **21**:771 (1950).
26. J. D. Cockcroft and E. T. S. Walton, *Proc. Roy. Soc. (London)*, **A136**:619 (1932); **A137**:229 (1932); **A144**:704 (1934).
27. Schenkel, *Elektrotech. Z.*, **40**:333 (1919).
28. H. Greinacher, *Z. Physik*, **4**:195 (1921).
29. L. J. Haworth, L. D. P. King, C. T. Zahn, and N. P. Heydenburg, *Rev. Sci. Instr.*, **8**:486 (1937).
30. L. J. Haworth, J. H. Manley, and E. A. Luebke, *Rev. Sci. Instr.*, **12**:591 (1941).
31. A. Bouwers and A. Kuntke, *Z. tech. Physik*, **18**:209 (1937).
32. W. R. Arnold, *Rev. Sci. Instr.*, **21**:796 (1950).
33. R. A. Peck, *Rev. Sci. Instr.*, **26**:441 (1955); R. A. Peck and H. P. Eubank, *Rev. Sci. Instr.*, **26**:444 (1955).
34. P. Lorrain, R. Beique, P. Gilmore, P. E. Girard, A. Breton, and P. Piché, *Can. J. Phys.*, **35**:299 (1957).

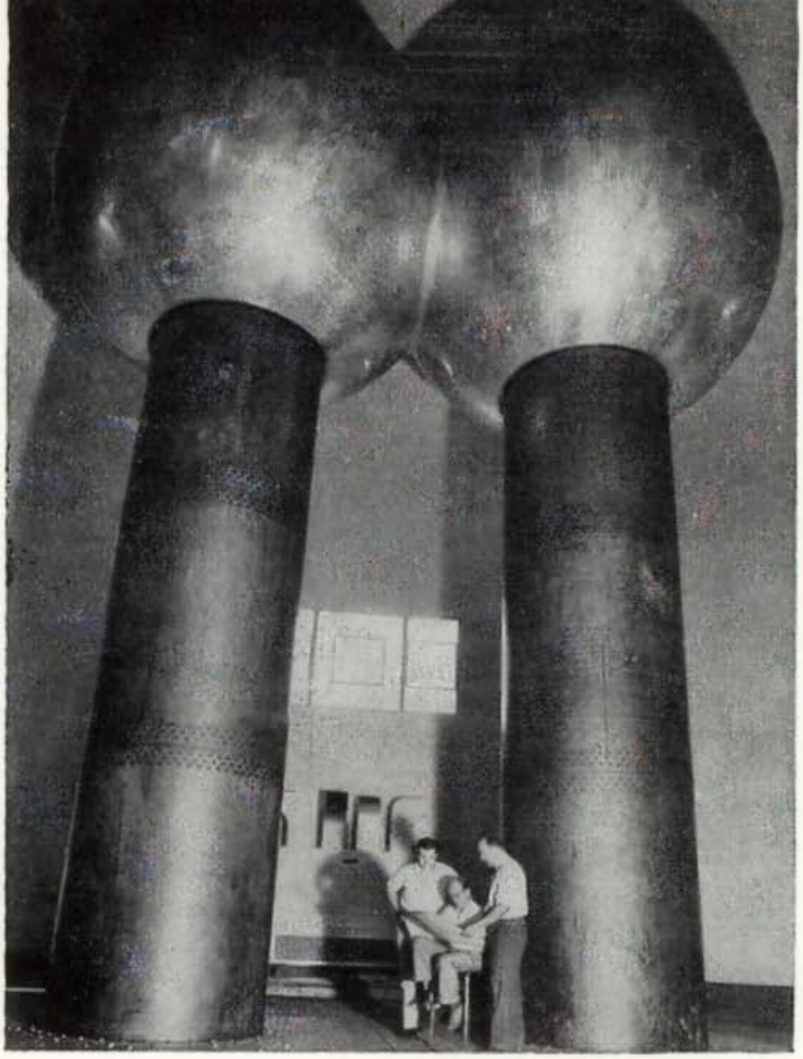

3

*The Electrostatic Generator**

The belt-charged electrostatic generator has been so successful as a voltage source for particle acceleration that it has displaced all other static machines and most of the other types of direct-voltage generators. The use of high-pressure gas insulation has freed the generator from atmospheric disturbances, and has resulted in a relatively compact design. In the energy range up to 4 or even 6 Mev to which it has been developed, it can deliver a steady, parallel beam of particles free from stray radia-

* The name "statitron" has also been applied to the belt-charged electrostatic generator. In an informal poll conducted some years ago by the editor of *The Review of Scientific Instruments* among most of the users of these machines in the United States, the name "statitron" received majority but not unanimous approval. It has not been generally accepted, however. Some people prefer to call the belt generator the "Van de Graaff," as it has been known to many in the past. However, in recent years the High Voltage Engineering Corporation has used the name "Van de Graaff" as a trademark for its products. In this chapter the writers have felt it more appropriate to retain the full title "electrostatic generator."

tion, which makes it ideal as a source for nuclear studies in this energy range.

The most important property of this accelerator is the unusually homogeneous beam energy. In modern electrostatic generators equipped with a beam analyzer, the energy spread of the beam and the stability with which it can be maintained are of the order of 1 to 2 kv, and experimental measurements can be made to this accuracy. The beam can be focused to small cross section at the target, and intensities have proved adequate for most purposes. Furthermore, the voltage can be varied at will, so nuclear processes can be studied as a function of bombarding energy. The electrostatic generator is supreme in the precise measurement of nuclear energy levels, and for the study of excitation functions. A large fraction of our quantitative data on nuclear properties has come from these machines. They have also been very successful as sources of X rays for medical and industrial uses. The most complete survey article was published in 1948 in an English journal by Van de Graaff, Trump, and Buechner.[1]

3-1. HISTORICAL DEVELOPMENT

The original suggestion of a belt-charged electrostatic generator seems to have come from Righi about 1890 as a modification of the "charged-water-drop" generator of Lord Kelvin. The significant principles were all known in the late nineteenth century, but the method was not developed as a source of potential for particle acceleration until the 1930s. As a Rhodes scholar in Oxford in 1927 and 1928, R. J. Van de Graaff became interested in the need for high-voltage machines to develop the field of nuclear physics, then in its infancy. He decided to experiment with the belt-charged electrostatic generator as a potential source, and on his return to Princeton University as a National Research Fellow in 1929, he built his first model.

Van de Graaff[2] described his first generator before the American Physical Society in 1931. It was simply conceived and built of inexpensive parts. Two 24-in.-diam spherical aluminum electrodes were mounted on 7-ft glass rods, each with a motor-driven silk belt to transport the charge. One sphere was given a positive charge; the other, a negative charge. An estimated 1.5 Mv potential difference was developed between terminals, limited only by corona from the terminals. The simple construction and the steady, direct voltage made the machine attractive as

---

At the head of the facing page is an illustration of the original air-insulated electrostatic generator at MIT designed by Van de Graaff and his collaborators,[5] now at the Boston Museum of Science. Shown in the photograph are C. M. Van Atta, D. L. Northrup, and L. C. Van Atta. (Courtesy of R. J. Van de Graaff.)

a voltage source for positive-ion acceleration. The possibility of extending the method to higher voltages was evident, and groups in several other laboratories became interested and joined in the development.

In 1932 Van de Graaff went to the Massachusetts Institute of Technology, where, with the support of President K. T. Compton, he started on design and development tests for a really large generator. A preliminary design study by Van de Graaff, Compton, and L. C. Van Atta[3] described the installation, which was later built in an airship hangar at the Round Hill estate of Col. E. H. R. Greene near South Dartmouth, Massachusetts. Two 15-ft-diam spherical metal terminals mounted on vertical hollow Textolite cylinders were charged, one positively and one negatively, by two 4-ft-wide belts within the cylinders. A discharge tube for accelerating ions was to be supported horizontally between the terminals, and the laboratory for observing nuclear experiments was to be within one of the 15-ft shells. The concept of the project was exciting and the scale tremendous for that time. It was essentially complete by 1936 and was described in detail by L. C. Van Atta, Northrup, C. M. Van Atta, and Van de Graaff.[4] It developed 2.4 Mv on the positive terminal and 2.7 Mv on the negative one, with a possible total of 5.1-Mv potential drop. However, the difficulties of mounting an evacuated discharge tube between terminals were extreme, and the machine never performed satisfactorily as a particle accelerator. Furthermore, voltage limitations caused by the high humidity and unclean conditions within the hangar near the ocean made it evident that this location was unsuitable.

The installation was moved to MIT in 1937 and installed in a tight metal-domed building in which dust and humidity could be controlled. In this reassembly the two columns and terminals were mounted adjacent to each other; one column was used for the belts of the electrostatic generator and the other for a vertical discharge tube, so experiments could be performed in a basement room below the floor. With this modified assembly, the machine was completed as an accelerator by 1940, accelerating electrons or positive ions to 2.75 Mev energy.[5] It was developed to be a reliable and steady source, and gave many years of valuable service as a research tool under the direction of Professors Van de Graaff and Buechner. However, this original MIT "Van de Graaff" has become obsolete as a scientific instrument and has been replaced by others of more modern design. The original dual-terminal generator is now located as a permanent exhibit in the Museum of Science in Boston.

The popular appeal of this gigantic generator has been tremendous. It was an awe-inspiring experience to stand beneath the huge spheres and feel the hair rise as potential increased, and then to see the long,

jagged strokes of man-made lightning as the terminal discharged to the roof or down the column. An even more exciting experience was to ascend by a ladder, stand within the hollow terminal by an open port as it was charged, and watch the sparks striking (or more exactly, originating) a few inches away on the port rim. Photographs of this Van de Graaff generator have been used as illustrations for many scientific articles. To many people it typifies the atom smasher of the nuclear physicist. Largely for its historical interest a photograph of the Massachusetts Institute of Technology 15-ft dual-terminal generator is shown in the chapter headpiece, page 30.

Soon after Van de Graaff had demonstrated the potentialities of the electrostatic generator in his first model, and while he was engaged in studies and designs for the large dual-terminal machine, a group headed by M. A. Tuve at the Carnegie Institution of Washington decided to abandon its previous attempts to build a Tesla-coil voltage source and to adopt instead the electrostatic generator. A project was started with the cooperation of Van de Graaff to study the technical possibility of applying an electrostatic generator to the high-voltage discharge tubes already developed in the Carnegie laboratory. Spherical shells of 1 and 2 m diam were mounted on Textolite columns in air, and tests were made establishing the prediction that terminal voltage is proportional to radius of curvature. The problems of corona formation, of destructive sparks down the insulating columns, and of the measurement of potential with spark gaps and generating voltmeters were studied with the aim of developing a reliable, steady source for nuclear experiments.

The Carnegie Institution group built first a 1-m-diam generator which supplied 600-kv ions by 1933. Then they developed a concentric-shell generator with a 1-m inner shell and a 2-m outer shell, mounted on a tripod arrangement of three Textolite columns. Two charging belts crossed the room horizontally, and a vertical discharge tube led through the floor, so that the beam of ions could be analyzed magnetically and experiments performed in a basement room. Potentials of up to 1.3 Mv could be maintained with the terminal positive (for accelerating positive ions to ground). These two machines have been fully described by Tuve, Hafstad, and Dahl.[6] They were put to immediate use in accelerating protons and deuterons for nuclear experiments. These were the first practical electrostatic accelerators, and an important series of research papers followed the completion of the 2-m generator in 1935, starting with measurements of excitation functions which showed sharp nuclear resonances.[7] A sketch of the 2-m generator is shown in Fig. 3-1.

One of the most important technical developments of the Carnegie Institution group was the study of voltage calibration for such air-insulated generators. It was found that sphere-gap calibrations could not be

extended to this voltage range with any confidence, but were a function of the meteorological and surface conditions of the gap electrodes. The generating voltmeter, which measures field intensity, was also found to be unreliable at potentials where corona discharge occurred. A high-energy proton beam could be brought through a thin vacuum window and the range measured, but the inherent errors in range straggling and the imperfectly known range-energy relations made this calibration also suspect. The first satisfactory calibration was obtained by deflecting

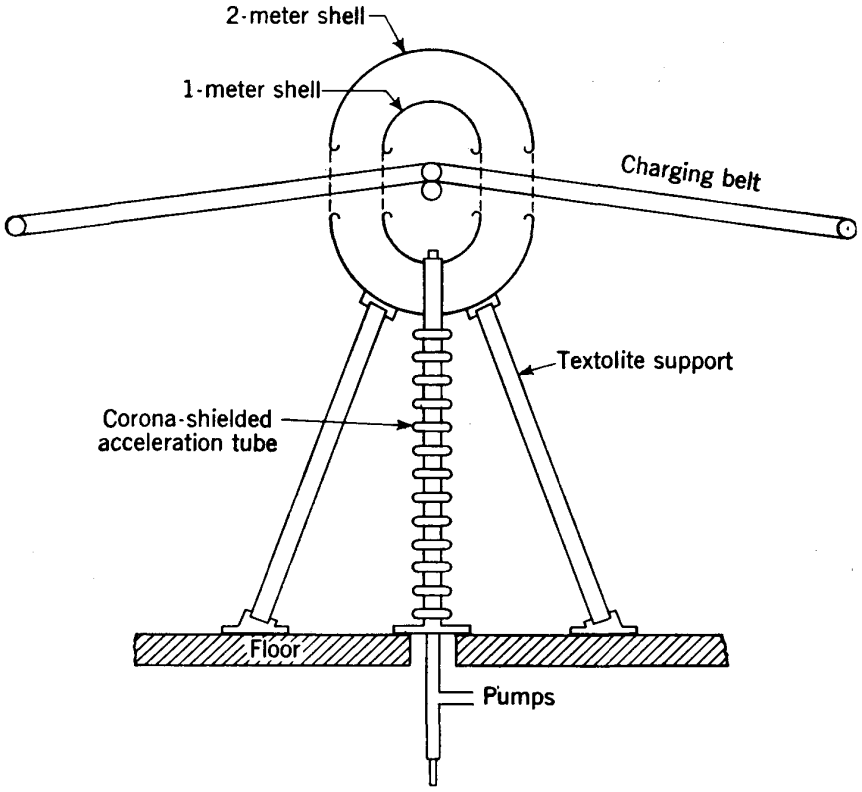

Fig. 3-1. Schematic diagram of 2-m electrostatic generator at Carnegie Institution,[6] showing the arrangement of supports, charging belts, and accelerator tube.

the emergent beam of protons by a magnetic field through a system of slits. This result was used to establish proton range-energy relations and to calibrate the generating voltmeter. The limit of accuracy was the measurement of magnetic field including the fringing effects.

The most accurate calibrations were based on the use of a column of precision resistors paralleling the discharge tube.[8] Accurate current measurements with this 10,000-megohm resistor column gave an absolute calibration which was of tremendous value to the scientific world at that time. Nuclear resonances, such as the $C(p,\gamma)$ resonances at 400 and 480 kv, the $Li(p,\gamma)$ at 440 kv, and the three $F(p,\gamma)$ levels at 328, 892, and

942 kv,[7,8] were observed and measured using extremely thin targets. These and other nuclear resonances have since been determined with such precision that they are used as substandards for calibrating instruments in other laboratories and in providing a cross-calibration of results from the different laboratories.

Meanwhile a parallel development started in other laboratories, based on the use of high gas pressure to insulate the terminal and increase the potential. Barton, Mueller, and L. C. Van Atta[9] at Princeton were the first to experiment with this modification. They used a cylindrical electrode supported by two Textolite cylinders along the axis of a horizontal pressure tank. Their first small machine developed 1-Mv potential at 7 atm air pressure, showing an almost linear increase in breakdown potential with increasing pressure. The chief advantages were the smaller size of the installation and the positive control of humidity within the pressure tank.

This principle was utilized by Herb, Parkinson, and Kerst[10] at the University of Wisconsin in the design of a series of pressure-insulated generators. The first model reached 0.75 Mv. The second, described in 1937 and again after further development and operational experience[11] in 1938, operated at 2.4 Mv and was equipped with an electronic voltage stabilizer to maintain the steady potentials needed for nuclear research. The third model, reported by Herb, Turner, Hudson, and Warren[12] in 1940, introduced the use of three concentric high-potential electrodes to distribute the potential drop and reached a potential of 4.0 Mv.

The Herb design, utilizing pressure insulation and having concentric terminal shields, has been adopted in most modern accelerators. The horizontal arrangement—with the terminal cantilevered on insulators from a grounded face plate, enclosed within a pressure housing which rolls on rails to open the chamber for servicing, and employing a horizontal discharge tube—has also found many converts. The practical limit seems to have been reached, however, at about the 4-Mev machine,[13] owing primarily to the difficulties of supporting the terminal and horizontal discharge tube as the size is increased.

During the early years other laboratories exploited the vertical mounting, with its apparent advantage in mechanical stability. In this arrangement, the insulation column sustains only compressional forces, and a large number of designs have been developed using insulation in the form of ceramic standoff insulators or short disk-shaped buttons separating metal-plate equipotential electrodes. Large pressurized generators were built at the Westinghouse Research Laboratory,[14,15] at the Carnegie Institution, and at the University of Minnesota.[16] These were designed to operate at relatively low (60 to 120 psi) gas pressure, in the hope that higher voltages could be most readily obtained by increasing the gap and the radius of curvature of the terminal. Recognition of the

adverse effect of large terminal area, of the importance of polished surfaces, and of the value of multiple-shell terminals came later. As a consequence, all have been restricted to less than their theoretical limits, operating at about 3 Mv.

Another line of development has been the small, inexpensive generator for low voltage. A good description has been published of such a small machine (rated at 1 Mv) at Johns Hopkins University.[17,18]

Meanwhile, at the Massachusetts Institute of Technology a new series of developments in which J. G. Trump was prominent was started in about 1938 in the Electrical Engineering Department. Trump and Van de Graaff[19] reported on the first of a series of generators for electrons intended for use as a source of X rays for medical and industrial purposes. Years of comprehensive study of the engineering problems of high dc potential made this group acknowledged leaders in the technical field. Their studies have included such problems as the flashover potentials for solid dielectrics in vacuum and in compressed gases, the influence of electrode material on breakdown potential, the relative dielectric strengths of various gases such as Freon, CCl_4, and SF_6, and ionization as a function of depth in tissuelike material for high-voltage X rays and electrons. The use of compressed gases as insulating media was investigated experimentally at an early date, and test equipment was set up to study the problems and determine the limitations. A large share of our technical knowledge of high-voltage engineering has come from this continuous and comprehensive program.

During the war the MIT High-Voltage Laboratory developed and built several X-ray generators of 2-Mv rating for the United States Navy and in the process studied and solved many technical problems. The results are reported by Buechner, Van de Graaff, Sperduto, McIntosh, and Burrill.[20]

The next step in the development of the electrostatic generator at MIT was a large, vertical, pressurized proton accelerator designed by Buechner, Trump, Van de Graaff, and others but not described in the published literature. This machine was financed by a grant from the Rockefeller Foundation and is duplicated at the Atomic Energy Research Establishment in Harwell, England. Results of the years of comprehensive study on electrostatic problems at MIT are incorporated in the design, and the wide experience of the staff has gone into its construction. It was completed in 1950. Beams of 10 to 20 μa of resolved protons at 4 Mev are obtained[21] with occasional operation at still higher energy. This beautifully built instrument is in full operation as a research tool.

The latest step in electrostatic-generator development at MIT is the "12-Mv" generator now operating at voltages up to 9 Mv. This will be described more fully at the end of this chapter. It is a fitting climax to the story of the development of these machines at the MIT laboratories.

In 1947 Trump, Van de Graaff, Denis Robinson, and others formed the High Voltage Engineering Corporation (HVEC) in Cambridge, Massachusetts, for commercial production of Van de Graaff generators. As the first commercial firm engaged solely in the business of designing and building accelerators, HVEC holds a unique position in the field. This company has produced several compact models of the pressure-insulated electron accelerator using sealed-off accelerating tubes and operating in the 1- to 2-Mv range. It has also developed a 5.5-Mv vertical-mount pressurized proton accelerator based on the design of the MIT research machine, a 4-Mv horizontal proton accelerator of the Herb type first built for the Brookhaven National Laboratory,[22] and a variety of other sizes and types.

The most recent HVEC development (1958) is a double-ended horizontal generator,[23] called a "tandem," in which negative hydrogen ions produced in a special source at ground potential are accelerated to the positively charged high-voltage terminal in the center of the machine. Here, they traverse a gas jet in which they are stripped of their electrons to become protons. Then they are repelled by the positive terminal and are accelerated back to ground potential to emerge with an energy corresponding to twice the potential of the high-voltage terminal. The first of these units, installed at the Chalk River Laboratory in Canada, gives 1-μa beams of H^+ or D^+ ions with energies up to 9 Mev.

Since there are several hundred electrostatic machines in laboratories around the world, it is impossible here to mention any but a few outstanding historical examples. Impressive electrostatic machines have been built and important contributions to the art have also been made in many other centers: Los Alamos National Laboratory, Brookhaven National Laboratory, University of California at Los Angeles, British Atomic Energy Research Establishment, Saclay Centre d'Études Nucléaires in France, Christian Michelsens Institut in Bergen, Norway, and many other places.

3-2. PRINCIPLES OF OPERATION

The electrostatic machine is simple in concept, but the techniques and designs needed to obtain engineering perfection are complicated with details and are bounded by fundamental limitations, such as the electrical breakdown of insulation. The principle of operation is readily understood by reference to Fig. 3-2, which is a schematic diagram of a vertically mounted belt generator. The structure consists of a rounded high-voltage terminal supported on an insulating column and a moving belt to carry charge to the terminal. Charge of one polarity is sprayed on the belt at the grounded end, is carried up into the terminal by a moving belt, and is removed by a collecting device within the terminal

where there are no high electric fields to disturb the collecting process. This steady current, $i = dQ/dt$, produces an electrostatic potential on the terminal. If C is the capacitance of the terminal to ground, the terminal will be raised to a potential V by a charge $Q = CV$, and the rate of increase of potential with time is given by

$$\frac{dV}{dt} = \frac{i}{C} \tag{3-1}$$

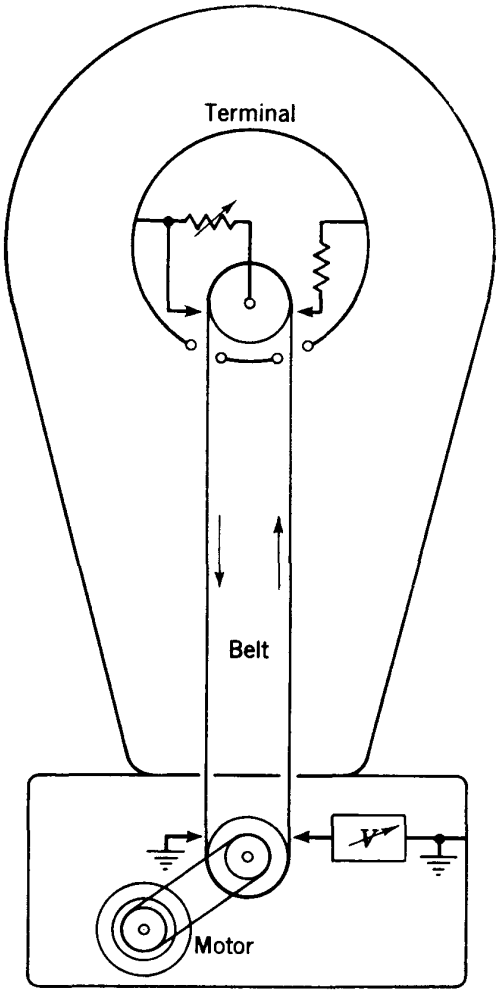

Fig. 3-2. Schematic diagram of generator enclosed in a grounded pressure tank. Circuits are shown for spraying charge on both the ascending and descending faces of the belt.

The capacitance of a spherical shell, if insulated and a long distance from ground, is given by

$$C = 4\pi\epsilon_0 r = 1.11 \times 10^{-10} r \quad \text{farads} \tag{3-2}$$

where r is the radius in meters and ϵ_0 is the dielectric permittivity of free space in mks units. If a terminal of radius r_1 is enclosed within a grounded concentric shell of radius r_2, the capacitance is given by

$$C = 1.11 \times 10^{-10} \frac{r_1 r_2}{r_2 - r_1} \quad \text{farads} \tag{3-2a}$$

For a typical large accelerator in which the inner terminal has a radius of 1 m and the outer pressure housing a radius of 2 m, the capacitance is about 220 $\mu\mu$f. Such an outer grounded shell is indicated in Fig. 3-2 to represent the wall of a pressure-containing vessel such as is used in most generators. This grounded shell is not necessary to the operation of the machine and is in fact missing in some of the earlier designs using air at atmospheric pressure.

Another common geometry is a cylindrical terminal with spherical end caps. The capacitance per unit length of coaxial cylinders having radii r_1 and r_2 is

$$\frac{C}{l} = \frac{2\pi\epsilon_0}{\ln (r_2/r_1)} = \frac{0.55 \times 10^{-10}}{(\ln r_2/r_1)} \quad \text{farads} \tag{3-2b}$$

For a 1-m-long cylindrical section with 1-m-radius hemispherical caps enclosed in a 2-m cylinder, the total capacitance is about 300 $\mu\mu$f. Capacitances for other shapes used in accelerator designs are of the same order. The dielectric constant of the gas between terminal and housing makes a small but usually negligible change in capacitance. Additional capacitance to ground is introduced by the metallic equipotential electrodes used in the supporting column and by the equipotential concentric shells used in most modern installations. Measured values of capacitance are, therefore, usually somewhat higher than those illustrated above.

Maximum charging currents used in modern generators are a few milliamperes. The time rate of increase of potential given by Eq. (3-1) is of the order of 10^6 volts/sec. At 2 ma a 500-$\mu\mu$f terminal would reach 4 Mv in 1.0 sec. After a spark breakdown or discharge, the generator requires a finite time of this order to regain its charge.

The belt runs between a motor-driven pulley at ground potential and a pulley in the terminal. Electric charge is sprayed on the belt at the grounded end from a fine wire or from a row of corona points (phonograph needles have been used) extended across the width of the belt and directed at the pulley or at a grounded plate behind the belt. A corona discharge maintained between these points and ground produces gaseous ionization in the air, and charge is deposited on the moving belt. If the terminal is to be charged positively, the points must have a positive potential relative to ground, so that positive ions will go toward the grounded pulley or plate and will be intercepted by the belt. If the terminal is to have a negative charge (for accelerating electrons), the corona points are made negative.

The charge is removed from the ascending belt within the terminal by a similar corona-point collector connected electrically to the terminal. If the pulley within the terminal is insulated, it will rise to a potential sufficiently above that of the terminal to maintain the necessary corona discharge. The charge appears on the outer surface of the terminal, so that (except for the effect due to the pulley potential) the inside of the terminal is field-free. Thus the charging process occurs within the grounded base, and the discharging of the belt takes place within the equipotential terminal; both operations are separately controllable and independent of terminal voltage.

The electric-power supply used to produce the corona discharge from the needle points is indicated schematically in Fig. 3-2. Potentials of 20 to 30 kv are sufficient, and a current capacity of several milliamperes is required. Almost any rectifier which meets these ratings is satisfactory. A half-wave, hard-vacuum-tube rectifier is common, using 60-cycle power. Filtering to reduce the ac ripple is useful in giving more uniform belt charge, but not essential. The magnitude of the corona spray current is usually controlled by varying the primary ac voltage.

This corona current determines the potential to which the terminal will rise, as will be described later.

It is also possible to spray charge of the opposite sign on the descending belt run within the terminal and to take it off at the grounded end. In this way the belt carries charge both ascending and descending, and the charging current is doubled. A charging circuit to achieve this result is also shown in Fig. 3-2. The resistor placed between the insulated upper pulley and the terminal can be adjusted to control the upper spray potential and arranged to make the charge densities equal on the upward and downward runs.

The power required to charge the terminal is calculable from charging current and terminal potential. For example, the necessary motor power (above that required for friction and windage) at 2 ma and 4 Mv is 8 kw. This assumes that belt speed is constant and that the 2-ma current returns to ground through some other path such as the discharge tube accelerating ions or electrons.

Current returns to ground from the high-voltage terminal in many ways. In a positive-ion accelerator the useful current is the beam of positive ions being accelerated down the accelerator tube. However, stray ions may strike the tube walls and may release secondary electrons, which are accelerated up the column to produce X rays on striking the ion source. Frequently a resistive load is built into the insulator column to serve as a potential divider. This may be of the order of 1000 to 10,000 megohms, uniformly distributed along the length of the accelerator tube and connected to appropriate electrodes along the column. The ultimate limit to terminal potential in the absence of an accelerator tube is corona discharge from the terminal. This is caused by the breakdown of insulation (either gas or solid) due to excessive fields at the surface of the terminal. In most installations adjustable corona-point units are installed opposite one point on the terminal surface to increase or decrease total load current and so to maintain a constant terminal potential. Occasionally a corona streamer in the gas will develop into a spark which discharges the terminal completely.

The required charging current is the sum of these several components, which behave differently with terminal voltage:

1. Positive-ion current is generally constant, determined by ion-source conditions rather than by total voltage.
2. Current in the resistive potential divider or leakage down the column is directly proportional to terminal potential.
3. Secondary electron current in the tube will be described in more detail in a later section, where it is shown to increase rapidly with voltage above an apparent threshold.
4. Corona current behaves similarly, being zero at low voltages and rising rapidly above a threshold value.

The charging-current versus terminal-voltage characteristic is illustrated qualitatively in Fig. 3-3, which shows the way in which the components listed above vary with potential. The equilibrium potential V_e to which the terminal will rise is determined by the maximum charging current available. Terminal voltage can be controlled by regulating the charging current or by varying the amount of corona load current with adjustable needle points. The extremely rapid change of corona current with voltage tends to stabilize voltage at the equilibrium value, as can be observed in the graph.

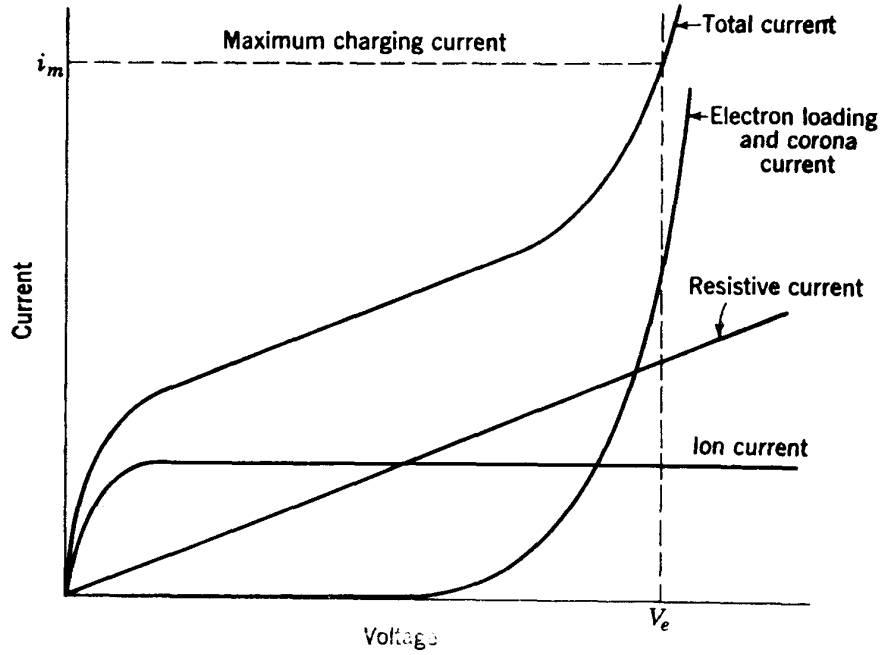

Fig. 3-3. Typical current-versus-voltage functions for the several components of the total charging current in an electrostatic generator. Terminal potential V_e is determined by the available charging current i_m.

After a spark has discharged the terminal and while the total load current is small, the excess charging current causes terminal voltage to rise rapidly. However, as terminal voltage approaches its equilibrium value again, the excess current becomes smaller and the rate of charging decreases. In principle the terminal voltage will approach the equilibrium value asymptotically, but in practice the corona-control system for voltage stabilization allows an overshoot. The time constant of this control system varies inversely with the magnitude of the corona-current variation used in the control.

The operation of the generator is simple to describe. First the belt motors are started; then the belt-spray charging unit is turned on and the rate adjusted to bring the terminal up to the working voltage, balancing the currents on the ascending and descending belt runs. Next the ion source is turned on and its potentials adjusted to bring the ion current up

to normal. This extra current load will decrease terminal voltage, which is trimmed back to the desired operating value by increasing the charging current. The corona-control circuit can now be locked in to maintain this voltage. Adjustments of ion-source or focusing-electrode voltages to improve beam focusing may require still further trimming of the control circuit.

It is well to avoid excess potential on the terminal in order to reduce the chance of destructive sparks. Such sparks will occur frequently on first tuning up a generator, and many days of operation with slowly increasing voltage are usually required to condition the generator to hold its rated voltage. A well-designed generator will eventually stabilize at that voltage set by the maximum allowed charging rate, i.e., when the total load current equals the charging current. Further increase in potential can only be obtained by decreasing the electron loading, which generally improves with time if the vacuum system is tight and the discharge tube clean. These problems will be described in more detail later.

3-3. ELECTRICAL BREAKDOWN IN COMPRESSED GASES

The breakdown potential of an insulated electrode in gas depends on several factors, which can be discussed separately:

1. Radius of curvature, area, and surface smoothness of the terminal
2. Electrode material and surface contaminations
3. Composition and pressure of the gas
4. Shape, material, and surface conditions of the insulating supports
5. Potential distribution along the insulator

Many of these factors are interrelated. The designer of an electrostatic generator must consider the limitations of each component and eliminate weak points.

Elementary theory of electrical breakdown predicts that breakdown potential should be directly proportional to the radius of curvature of the terminal. This is based on the assumption that ionization in the gas occurs and corona leakage develops at a fixed maximum potential gradient at the surface. The breakdown potential gradient in air at atmospheric pressure is of the order of 3×10^6 volts/m. This limit would be reached at a potential of 3 Mv for a spherical terminal of 1 m radius if corona did not distort the field. The early studies by Van de Graaff and by Tuve and his associates at the Carnegie laboratory showed that this relationship was approximately correct for 1- and 2-m spheres, although practical limitations on maintaining ideal surface conditions led to lower potential limits. Under stable conditions, however, the linear relationship between breakdown potential and radius was verified.

Paschen first formalized the relationship between breakdown potential V_m for plane-parallel electrodes, gas pressure, and interelectrode spacing as

$$V_m \text{ (in volts)} = k \text{ (pressure in atmospheres} \times \text{interelectrode spacing in cm)} \quad (3\text{-}3)$$

where k is a coefficient called the specific breakdown strength, which is a function of the composition of the gas and of the electrode materials. This coefficient was originally measured and found to be 30,000 for dry air at atmospheric pressure and with a 1-cm gap. It was this figure which led to the maximum field limit quoted for air of 3×10^6 volts/m. However, it was soon found that the coefficient was not a constant but varied with pressure, gap length, and electrode composition.

The type of discharge that results from breakdown depends on the shape of the electrodes, gap length, pressure, and the constants of the external circuit. The most common type of discharge is a spark. Between plane-parallel electrodes, the initial spark normally develops into an arc discharge with the current limited only by the external circuit resistance. Between small spheres spaced far apart, a corona or brush discharge may be visible near the surfaces, with the center of the gap appearing dark. With a large spherical terminal such as is used with the electrostatic generator, corona discharge usually occurs first at the surface, with the rest of the space dark. Then, occasionally, a corona streamer will develop into a spark to ground, discharging the terminal completely.

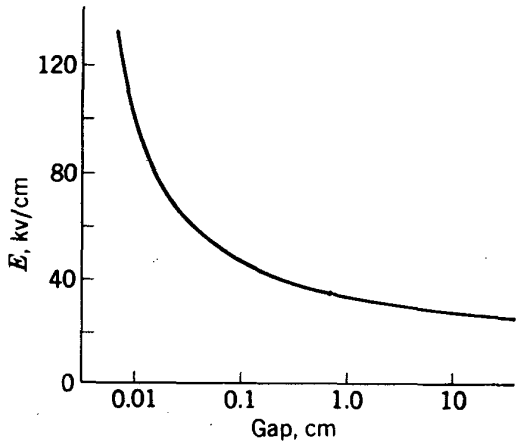

Fig. 3-4. Electric field for spark breakdown between plane-parallel electrodes in air at atmospheric pressure.

Experimental studies of spark breakdown show strong dependence on geometric arrangements, and the electric field intensity for breakdown is by no means constant. Figure 3-4 shows the electric field for spark breakdown between plane-parallel electrodes in air at atmospheric pressure as a function of gap length. Figure 3-5 shows the breakdown voltage between 25-cm-diam spherical terminals at atmospheric pressure as a function of spacing; grounding one of the terminals changes the results, an indication of the complicated influence of geometry on the fields. Sphere-gap measurements of voltage are subject to considerable error, owing to variations in corona discharge and in surface conditions. The presence of oxide films, oil, fingerprints, or even adsorbed gases will make marked changes in the sparking limit. Dust particles or surface

roughness may increase fields locally, and spheres must be carefully polished and cleaned. It has also been observed that a change of relative humidity from 0 to 100 per cent increases sparking potential in air by about 3.5 per cent.

In applying these considerations to a generator terminal, we can understand why such large-radius surfaces do not reach the predicted maximum

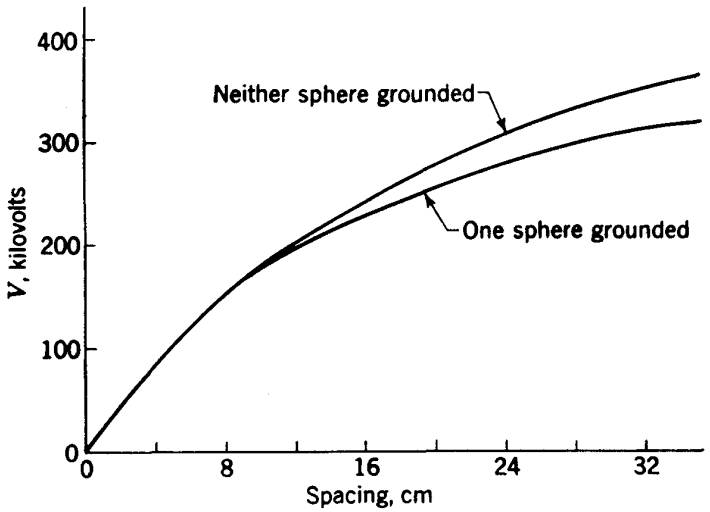

Fig. 3-5. Spark-breakdown voltage between metal spheres of 25 cm diam in air at atmospheric pressure, with and without one sphere grounded.

potentials. The charge on a spherical terminal of radius r required to produce the breakdown field of 3×10^6 volts/m at the surface is given by

$$Q = 4\pi\epsilon_0 E r^2 = 3.33 \times 10^{-4} r^2 \quad \text{coulombs} \tag{3-4}$$

The corresponding terminal potential would be

$$V = \frac{E}{r} = \frac{3 \times 10^6}{r} \quad \text{volts} \tag{3-5}$$

A 1-m-radius terminal at atmospheric pressure should have a charge of 333 microcoulombs and should rise to a potential of 3 Mv. The best value obtained consistently at the Carnegie laboratory was 1.3 Mv. The 15-ft-diam terminals of the Round Hill installation had a theoretical limit of 6.8 Mv each. The actual potential attained was 2.4 Mv on the positive and 2.7 Mv on the negative terminal.

Surface irregularities can reduce the potential limit by decreasing radius of curvature and increasing electric field locally. It was early observed that breakdown potential was reduced for terminals exposed to dust. One of the worst limitations at Van de Graaff's Round Hill installation was sparking due to droppings from birds roosting within the hangar. An insulating oil film will also reduce breakdown voltage by allowing large local fields to build up across the film. The contamination

problem is largely solved in modern generators by enclosing the terminal in a pressure housing and by filtering and purifying the gas. However, great care must be taken in construction to polish the terminal and, after exposure to air, to wipe and clean the surface.

It is an experimental fact that even with polished surfaces the field cannot be pushed much above 50 per cent of the theoretical limit. Total gap length to the outer grounded walls is not a significant factor. Breakdown occurs at about the same terminal potential for all gaps longer than a practical limit. The practical minimum gap is about 1 m for a 1-m-radius terminal and is roughly proportional for other sizes.

The surface field at the terminal can be reduced by using one or more concentric terminal shells. If the potential drop between each set of shells is to be equal and the electric field at the surface of each shell is to be the same, the radii of concentric spherical shells must be in the ratio

$$\frac{r_1}{r_2} = \frac{r_2}{r_3} = \frac{r_3}{r_4} = \cdots \tag{3-6}$$

With a terminal constructed of several such shells replacing a single terminal within a given size of outer housing, the total breakdown potential can be increased about 50 per cent. The inner shell can be reduced to a size sufficient to house the ion source and power supplies essential to accelerator operation. The chief disadvantage is loss of accessibility to the terminal apparatus, causing increased complexity of maintenance. The shells are mounted on equipotential rings suitably spaced along the column to obtain the desired potential distribution. This requires that the column be designed with steps of decreasing diameter to accommodate the several shields. Figure 3-6 illustrates an arrangement for mounting such shields.

Experience with the use of concentric shells has exposed certain limitations. With increased terminal area (required for many shells) it is found that the reliable operating-potential gradient is reduced. The most recent designs use one or, at the most, two shells inside the outer terminal.

The metal used for terminals also has an effect on breakdown potential. Aluminum is commonly used because it can be spun to the desired spherical shapes and has a low density. Stainless steel is known to have a higher breakdown limit but is more difficult to form. Measurements[24] of the breakdown-potential gradients for the two metals, in the form of flat disks formed with rounded edges and buffed to a mirror finish, showed stainless steel to be much superior, especially at high gas pressure. The maximum fields obtained in these tests, at 400 psi pressure of air, were 800 kv/in. for aluminum and 1200 kv/in. for stainless steel. These values are representative of the ultimate limit for short gaps and high pressures; they are not directly applicable to the long gaps and nonuni-

form fields of the generator terminal. Other comparisons of electrode materials were made in vacuum, to simulate the accelerating-tube electrodes. It was found that highly polished aluminum had breakdown-potential gradients equivalent to stainless steel under high vacuum.

The use of compressed gases around the terminal to increase the breakdown potential is based on Paschen's law [Eq. (3-3)], which predicts a

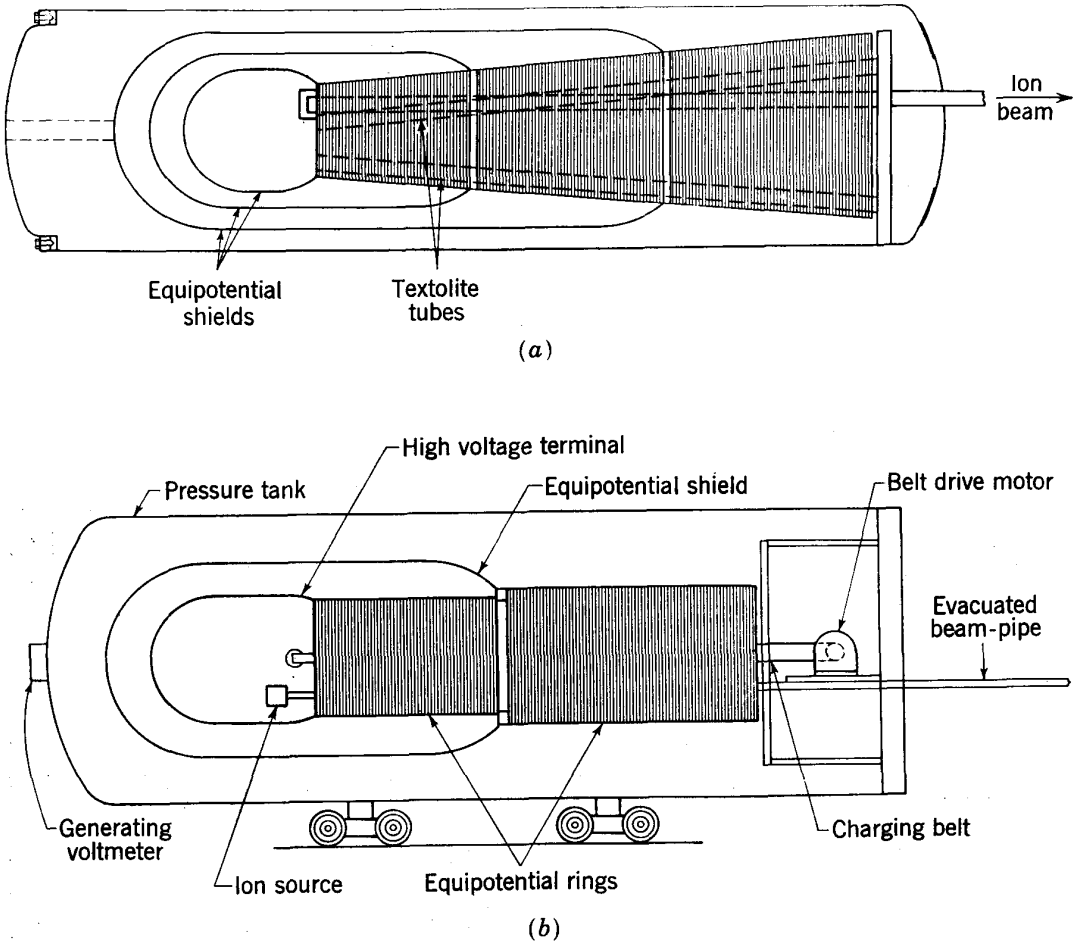

Fig. 3-6. (*a*) Diagram of early University of Wisconsin pressurized generator with concentric equipotential shields, supported at the grounded end by three Textolite tubes. (*b*) Horizontal Van de Graaff generator for 4-Mev protons.

linear increase of sparking potential with pressure. This is found to hold over a considerable range of pressure but to fail at high pressures. An early curve of breakdown potential as a function of air pressure, by Herb and Bernet,[25] shows a considerable deviation from linearity (see Fig. 3-7). Such deviations are found to depend on the geometry and material of the electrode, the gas composition, and the surface conditions. Under controlled laboratory conditions using plane electrodes and short gaps, Trump and his collaborators found that a useful increase can be extended up to 20 atm. With the nonuniform fields of large terminals in acceler-

ators, the sparking-potential curves always deviate from linearity above some value of pressure, which varies from one installation to another. No single curve can be cited to predict results, but sufficient data are now available for typical geometries to estimate the effect of pressure variation with reasonable accuracy. An example of the data available is the curve taken with a modern accelerator at MIT[20] (Fig. 3-7*b*).

Breakdown potential depends strongly on gas composition, particularly at high pressures. Air, nitrogen, and carbon dioxide were used in early pressure generators. Air has the advantage of availability but the disadvantage of supporting combustion; Textolite insulators and charging

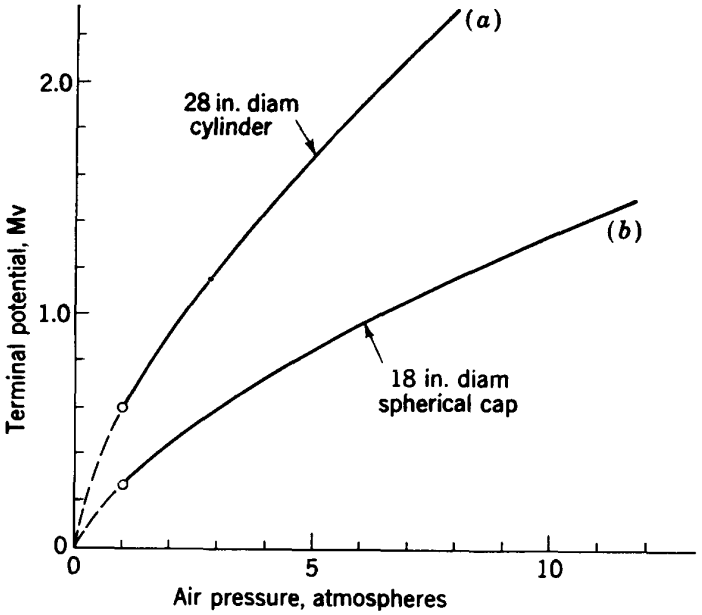

Fig. 3-7. Typical curves of terminal potential versus air pressure for electrostatic generators. (*a*) University of Wisconsin,[25] 28-in.-diam cylinder. (*b*) MIT,[19] 18-in. hemispherical cap.

belts were occasionally ignited by sparks in the compressed air. Herb et al.[12] discuss the problem of the fire hazard in compressed air in some detail and show that it can be minimized by suitable choice of nonflammable materials. Largely for this reason N_2 and CO_2 were tried in several generators, but in general gave lower spark-breakdown limits. Trump, Cloud, Mann, and Hanson[24] studied the relative sparkover limits for these gases and for mixtures of N_2 and CO_2, finding air to be superior in all cases.

It has been known since the work of Natterer (1889) that certain gaseous compounds containing chlorine, fluorine, or other "electronegative" gases gave a higher insulating strength than air. The dielectric strength of air is increased by the addition of any gas whose atoms or molecules have an electron affinity, i.e., can capture electrons and suppress discharges until the electron concentration becomes materially higher than

if the electronegative gas were not present. However, the advantages of these gases are somewhat offset by the formation of corrosive products when discharges do occur, or even when heavy corona discharge is permitted.

Several laboratories[26,27] have studied the increase in dielectric strength of air by the addition of a saturated vapor of CCl_4 (2 psi at room temperature) and have found that the increase is maintained at approximately

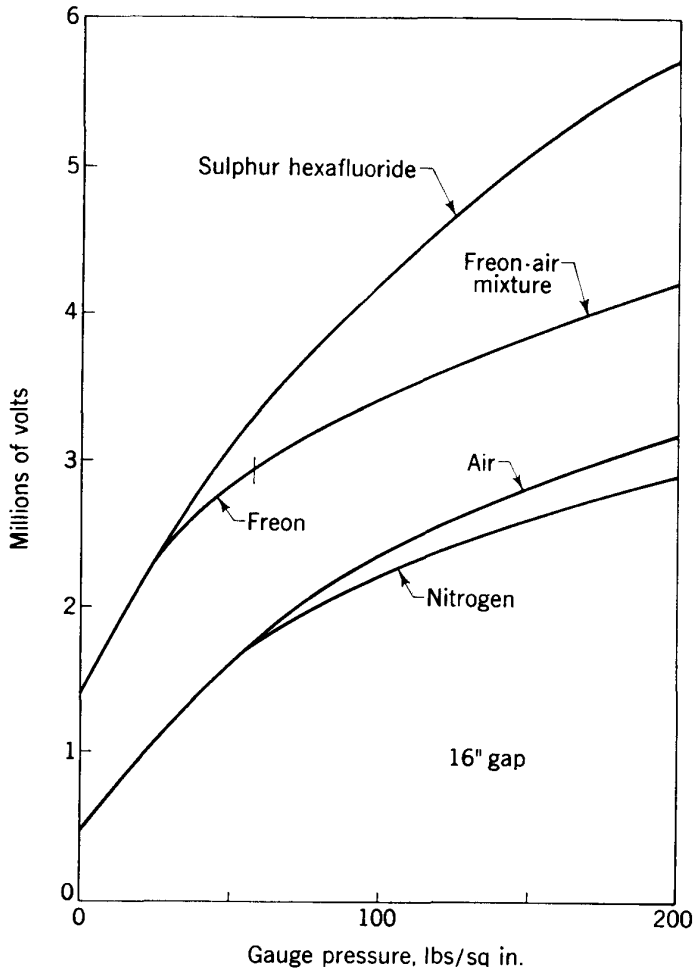

Fig. 3-8. Spark-breakdown voltage versus gas pressure for several gases in the MIT experimental generator.[20]

the same ratio at higher pressures. Others[28,29] investigated the characteristics of Freon (CCl_2F_2) and sulfur hexafluoride (SF_6) and found them to be particularly promising as insulating media. Freon, developed primarily as a refrigerant, was readily available and was studied by Trump, Safford, and Cloud[30] both in the pure state and when mixed with air at pressures above its vapor-pressure limit. Schumb[31] first developed techniques for producing SF_6 in a quantity sufficient to make tests at the Massachusetts Institute of Technology laboratory.[20]

A summary of the properties of these gases is given in the curves in Fig. 3-8, taken from MIT publications. The best gas tested was SF_6, up to a pressure of 200 psi, which almost doubled the maximum potential obtained with air at the same pressure. It has a vapor pressure of 330 psi at 25°C and can be run to even higher pressure by warming the generator housing. It can now be obtained commercially at reasonable prices and so affords a method of improving compactness and raising voltage limits of electrostatic generators. Freon, which has a vapor pressure at room temperature of only 85 psi, gives similar sparking potentials up to its vapor-pressure limit, but it is not quite so good as SF_6 at higher pressures, when air or another gas must be mixed with the Freon.

Despite the obvious advantages of the electronegative gases for high-voltage insulation, most laboratories have concluded that the corrosive products of dissociation make their use undesirable. The gases used in most installations are mixtures of nitrogen and carbon dioxide.

For all gases other than air, it is necessary to provide gas-storage reservoirs into which the gas can be pumped when the generator is to be opened for maintenance or repair. Such reservoirs are now common in new installations. The reservoir is usually made about equal in volume to the generator, and valves are arranged so that gas can be pumped either way. In a typical installation at Brookhaven, the pump-up or pump-down time is of the order of 30 min.

3-4. THE INSULATING COLUMN

Solid insulators are used to support the terminals in both vertical- and horizontal-type accelerators. The most common form of insulator is a hollow cylinder of fiber laminate. Textolite was used in the MIT 15-ft air-pressure generator, in the form of cylinders 6 ft in diameter, 22 ft in length, and $\frac{5}{8}$ in. in wall thickness. In the horizontal pressure generators designed by Herb and his associates, a truss structure of three or four smaller Textolite tubes, of 4 to 6 in. diam, is used to support the terminal.

The flashover voltage for Textolite columns depends more on the design of the connection at the terminal than on any other single factor. With a flush mounting (Fig. 3-9*a*) the concentration of field in the dielectric material of the column initiates corona discharge at the surface of the Textolite at lower potentials than those producing corona in the air. If the column is led through a hole in the terminal with internal edges well rounded (Fig. 3-9*b*), the situation is improved, but this is still the weak point. Without some form of shielding, sparks initiating at this point will flash down the surface of the column. The 6-ft-diam columns of the 15-ft MIT generator are scored with many such spark tracks. The

voltage limit is dependent not so much on length of column as on the initial breakdown at the connection to the terminal. With such an unprotected single insulating column, the limit is less than 3 Mv.

In all modern generators the supporting insulators are surrounded by closely spaced equipotential rings (Fig. 3-9*c*), so arranged that the electric field is approximately constant along the length of the column and the weak point at the terminal connection is shielded from high fields. Such rings surround the Textolite tube truss of the Herb-type horizontal generator and are equipped with corona-point gaps between rings to equalize the potential drops. The rings are also connected internally to corresponding accelerating-tube electrodes and to "field control" bars near the belt. A 10-ft column with such equipotential rings will insulate well

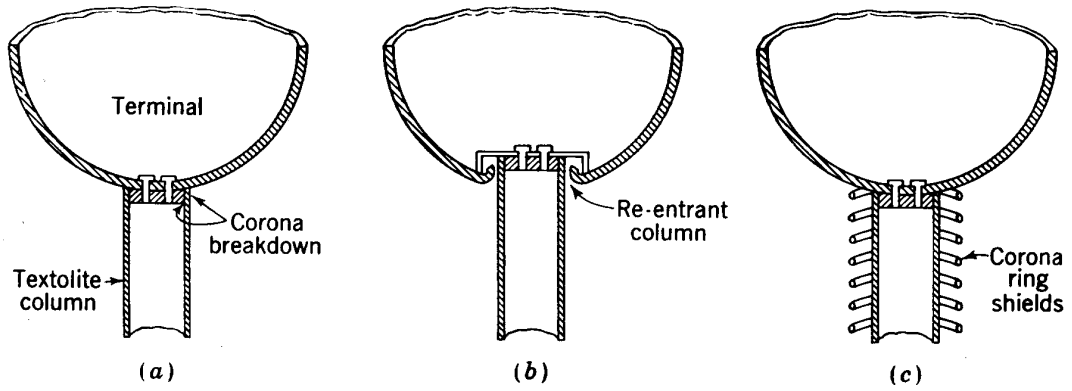

Fig. 3-9. Steps in the development of the connection between terminal and supporting column: (*a*) flush mounting results in corona breakdown of the insulating column; (*b*) reentrant column reduces but does not eliminate corona; (*c*) spaced ring shields along the column give a uniform potential gradient and eliminate corona.

over 4 Mv at 200 psi pressure of air, and such sparkovers as do occur go down the line of corona points without damage to the insulators inside.

The MIT vertical pressure generators use stacks of short glass or ceramic insulators, located between flat equipotential metal plates. Small bushing-type disk insulators are adequate to support a compressional load but are impractical for horizontal mounting. The use of modern adhesives has recently allowed this electrically superior construction to be applied to a horizontal mounting for short stacks capable of insulating over 2 Mv. The bushings can be corrugated to increase surface-path length. Flashover voltage for short solid insulators of this type in compressed nitrogen was studied by Trump and Andrias.[32] They used plain and corrugated cylinders of Lucite, Textolite, and Isolantite and found the limit to be set by surface flashover rather than by volume breakdown, and to be markedly improved by increased surface-path length, particularly for high gas pressures. The results of such studies have led to the design of compact generators with very short insulating columns, reaching a gradient of 1 Mv/ft without breakdown.

Despite the mechanical differences between vertical and horizontal mounting and the radically different type of column insulation, the overall outline of the terminal, column, shields, and pressure housing is surprisingly similar. This is illustrated by comparison of Fig. 3-10, which shows the MIT vertical 4-Mev "Rockefeller" generator, and Fig. 3-6*b*, the

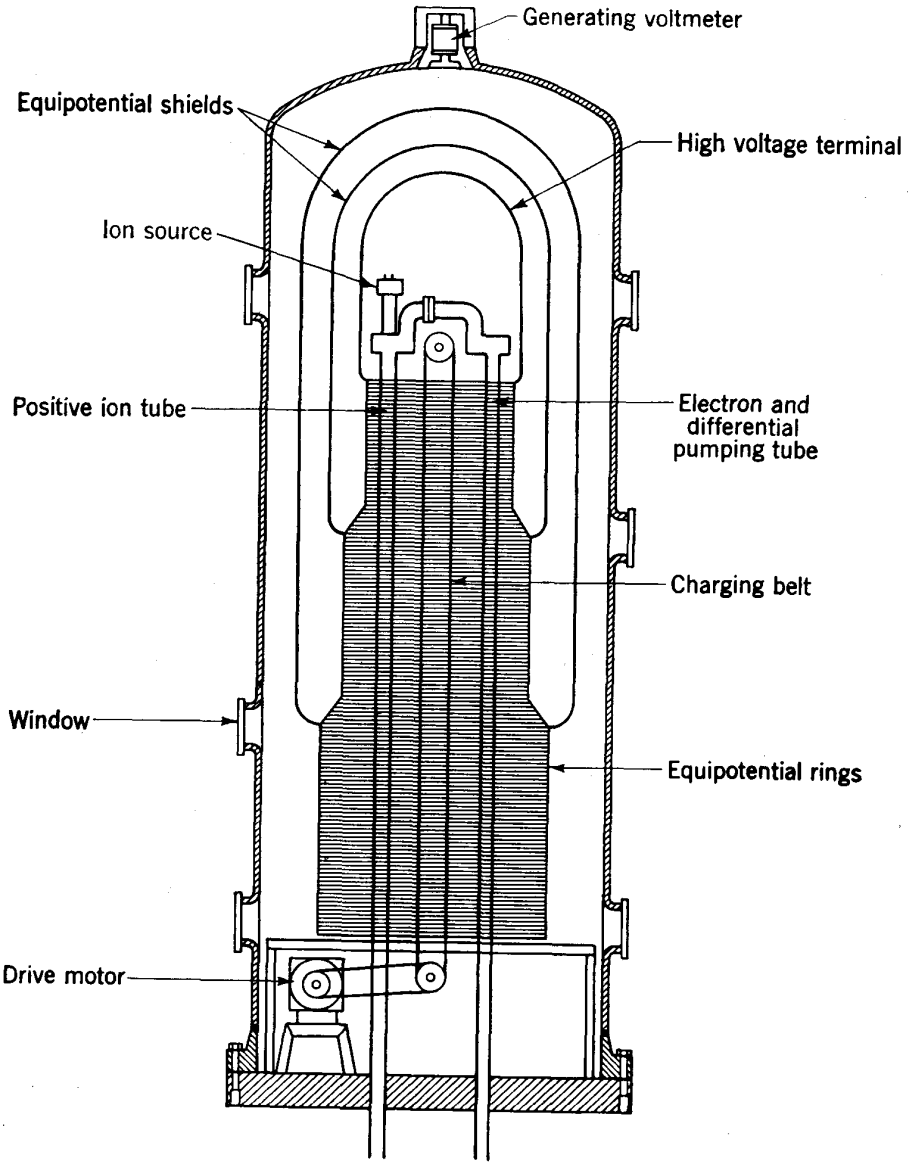

Fig. 3-10. Vertical electrostatic generator for 4 Mv at MIT.[1] Two accelerating tubes are shown, one for positive ions and the other for an electron beam with reversed terminal potential.

Herb-type horizontal 4.0-Mev generator built by the High Voltage Engineering Corporation for the Brookhaven National Laboratory. The similarity in outline is an indication of present agreement on fundamental design principles, since the two machines are culminations of experience in two separate laboratories.

3-5. CHARGE-CARRYING BELT

Flat, endless belts of insulating material have thus far proved to be the most effective charge conveyors for both air-insulated and compressed-gas electrostatic generators. Many kinds of materials have been used for belting, and opinions differ in the several laboratories as to the best material. The belt must have high mechanical strength, high surface and volume resistivity, and high dielectric strength, and it should be fire-resistant if air is to be used as the insulating medium. Another important requirement is that the belt should not absorb moisture when the housing is opened to the atmosphere for maintenance or repair, or else that the time required for dehumidifying the belt be short.

Two belts of electrical insulation paper 0.017 in. thick and 47 in. wide were originally used in the large Round Hill generator. The seams were made on a 45° bias and tapered to preserve a uniform belt thickness. Nevertheless, later experience showed that such belt joints produced a small but measurable pulsation in terminal voltage, and endless belts are now common.

The belts used and recommended at the MIT laboratory are made by the Fabreeka Products Company. They are endless woven cotton belts which are neoprene or rubber impregnated and vulcanized. The belts are oven-dried before being placed in the generator and are further dried during operation by recirculating the compressed gas in the tank through a dry-ice cooling coil until the dew point has reached $-35°C$ or lower. It is necessary to have this low air-moisture content (0.1 grain of water per cubic foot) to obtain the maximum voltage gradient on the belt. In using gases other than air, which are stored and reused, such a gas dehumidifier and circulator is also essential to remove the moisture absorbed on the various insulators when the tank is opened.

The belting used by Herb and his associates is a rubberized balloon fabric made by the Goodyear Rubber Company. These belts also must be thoroughly dried to prevent sparks along the belt which might rip the fabric.

Belts tend to stretch slightly during initial operation and must be readjusted to preserve proper tension. Pulleys are flat cylinders slightly crowned to make the belt ride true. A 2° taper over a short distance at each end of the pulley is usually sufficient. Pulley alignment is critical, and bearing supports must be capable of delicate adjustment.

Belt speeds are commonly between 3000 and 5000 ft/min, and windage losses are significant. An empirical formula for windage losses in air, relating the speed of the belt, its surface area, and the air pressure, was given in one publication[19] as

$$\text{Windage loss (hp)} = \text{pressure (atm)} \times \text{belt area (ft}^2\text{)} \times \frac{[\text{velocity (1000 ft/min)}]^3}{6000} \tag{3-7}$$

For a typical belt of 20 in. width, 20 ft total length, and a speed of 4000 ft/min at 200 psi pressure, the power required to overcome windage is about 5 hp.

In pressure-insulated generators, belts are driven by motors installed within the pressure housing below a false floor at ground potential and connected by short power-drive V belts to the lower pulley. The motor must be of the fireproof, glass-insulated type manufactured by several reputable firms.

Belt charge density is limited by gas breakdown, and the same limiting field applies as for terminal potential; in air at atmospheric pressure, this field E_m is about 3×10^6 volts/m. If the electric field due to belt charge is uniform and directed normal to the belt surface in both directions, the maximum charge density σ_m is given by

$$\sigma_m = 2\epsilon_0 E_m \simeq 5.3 \times 10^{-5} \text{ coulomb/m}^2 \tag{3-8}$$

In practice about 50 per cent of this maximum charge density is commonly attained. It is controlled by the rate of charging indicated by the corona spray current and the belt speed. If it is exceeded and the air becomes ionized at the belt surface, sparks can occur which might burn or rip the belt.

Higher gas pressure increases the permissible belt charge density by the same factor that terminal potential is increased. In fact, the higher charging rates possible in compressed gases constitute one of the primary advantages of the pressure generator. To obtain the necessary charging rate at atmospheric pressure, the belt area and speed must be large, but at high gas pressures a single belt of reasonable dimensions and speed is adequate to provide the charging current. The current delivered by a belt of width w (in meters) and speed v (meters per second) is given by

$$i = \sigma w v \qquad \text{amp} \tag{3-9}$$

To give an example: At 10 atm pressure where belt charge density can be 2×10^{-4} coulomb/m^2, a 50-cm-wide belt carrying charge both ways at a speed of 4000 ft/min will provide a charging current of 4.5 ma.

In the operation of the MIT vertical pressure generator, it was observed that a large fraction of the variation in terminal potential was due to static charge on the inside of the belt surface, caused by friction on the pulley. It was found, furthermore, that these variations could be reduced by spraying the main charge on the inside rather than the outside of the belt surface, which was the accepted procedure previously. This change improved the voltage regulation of the generator by about a factor of 3.

Another development at MIT is the use of a layer of slightly conducting rubber on the inside surface of the belt. Such a conducting layer can be charged by induction rather than by corona spray, thus eliminating the

ionization near the belt, which is believed to be the cause of much of the observed belt damage and of some of the voltage fluctuation. The method was first tested with conducting paints, which were found to wear off after a time; the conducting-rubber layer is a more permanent surface. The conductivity must be sufficient to obtain a suitable charge by induction, but not so large as to carry an appreciable current down the belt; the surface resistivity found suitable is about 10^7 ohm-m.

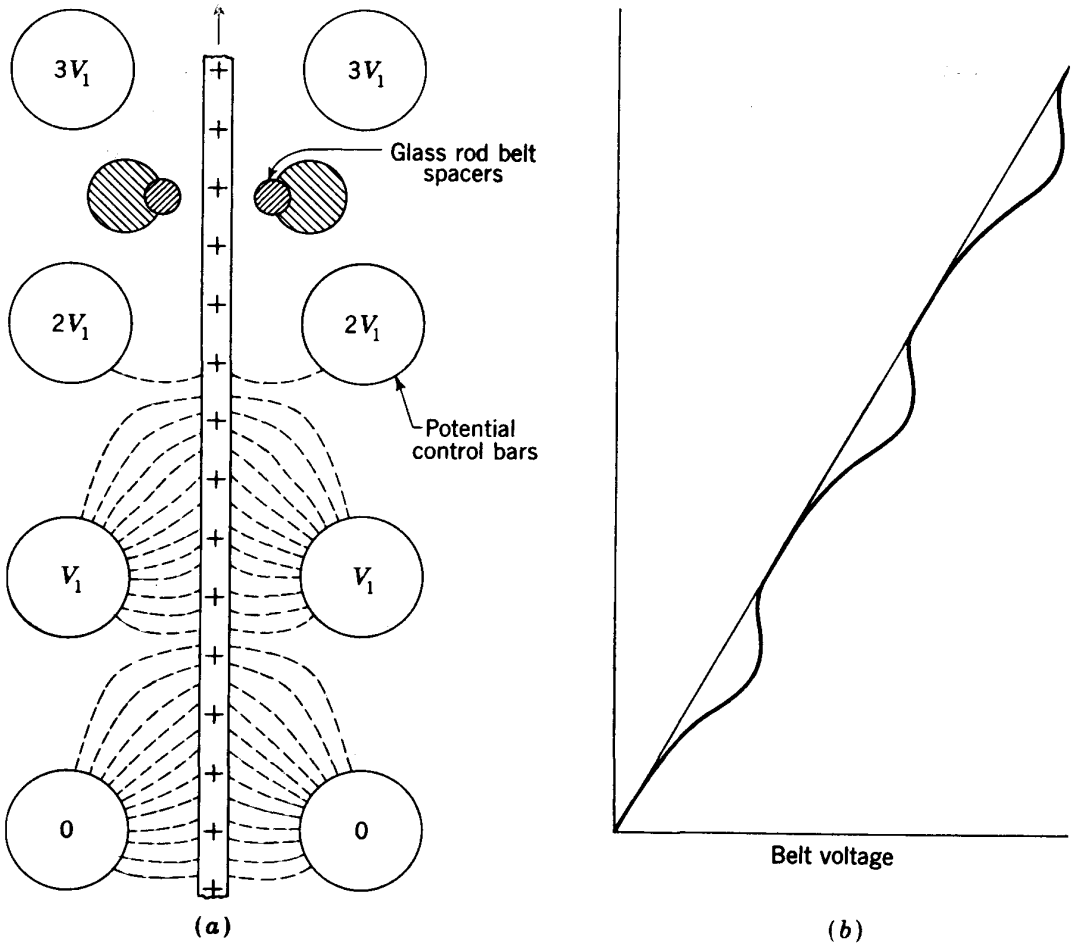

Fig. 3-11. (*a*) Computed electric-field pattern near belt and control bars with belt charged and moving.[1] A set of glass rods used as belt spacers is also shown. (*b*) Potential distribution along the belt due to the electric-field pattern shown in (*a*).

To maintain the necessary uniform transverse fields at the belt, a set of closely spaced field-control rods is located close to the belt. These rods are located in the planes of the equipotential rings and are electrically connected. A resistance voltage divider or suitable corona gaps maintain the uniform potential distribution along the column and the belt. Each belt run (up and down) rides between these parallel rods, so the electric field is closely confined to a region adjacent to the belt surface. With uniform belt charge and closely spaced equipotential planes, the gradient

along the belt is very nearly uniform, and the chance of breakdown is reduced. Figure 3-11 shows the fields around the belt and field-control rods as computed and plotted at the MIT laboratory.

The electrical force of attraction between the charged belt and the control bars is so large that the belt may rub against the bars and transfer charge irregularly if it is not precisely centered. The method developed by Trump and his group to prevent such contact is to use at intervals along the column small glass rod or bead spacers which have a narrower spacing than the bars and so keep the belt centered. These belt spacers or guides are supported on additional metal bars which parallel the belt surface (Fig. 3-11).

3-6. THE ACCELERATING TUBE

The evacuated tube for accelerating ions is one of the most critical components. After long development in many laboratories, it is still the ultimate limiting factor in total potential. The tube must be constructed of insulating material, commonly porcelain or glass cylinders several inches long and of large diameter, with vacuumtight seals to metal-plate electrodes between sections. These electrodes are connected to corresponding equipotential rings in the column to maintain a uniform distribution of potential along the tube. The metal electrodes have large-diameter holes or tubular electrodes aligned along the axis of the tube, through which the particle beam passes as it is accelerated. The electrodes produce an accelerating and focusing field for the charged particles and also are arranged to protect the walls of the tube from the beam to reduce the possibility of flashover and to shield the beam from the effects of static surface charges on the insulator wall.

Flashover limits are usually lower on the vacuum side of the insulator wall than on the gaseous insulator side, probably owing to local fields developed by surface charges. Studies at MIT[1] on the flashover of solid dielectrics in high vacuum have shown that hard glasses have a higher limit than electrical porcelains; Corning Vicor (96 per cent silica glass) and Corning 7070 (a high-resistivity borosilicate glass) were reported to have the best properties. It was found, for example, that six 1-cm sections of Vicor in a total gap length of 2½ in. can insulate 500 kv.

The vacuum seals at the joints are extremely critical, especially when operating with external gas pressures which may be as high as 300 psi. Gasket-bolted joints have largely been displaced by cementing techniques. Vinylseal (a plasticized polyvinyl acetate) has been found to have excellent properties for this purpose, being remarkably strong and vacuumtight and having a negligible vapor pressure after baking at 200°C in an oven.

The tube is run through a series of aligned holes in the equipotential

planes, which produce a uniform gradient along the tube. An important consideration in horizontally mounted tubes is the support of the heavy tube structure. It can be hung on slings at frequent intervals along the column, carefully adjusted to eliminate bending torques.

The early accelerating tubes were constructed of rather long sections of insulator, and "drift tube" tubular electrodes were mounted along the axis, so the charged particles experienced their acceleration in a series of discrete steps as they passed across the gaps between the drift tubes. This is illustrated in Fig. 2-2*b* showing the first Carnegie accelerator. These gaps represent a set of electric lenses for the particles, with most of the focusing occurring in the first few gaps at the source end of the tube where the charged particles move slowly.

Progress in design to higher voltage gradients along the tube has resulted in successively decreasing the spacing between electrodes and increasing the number of gaps. This development reached its ultimate

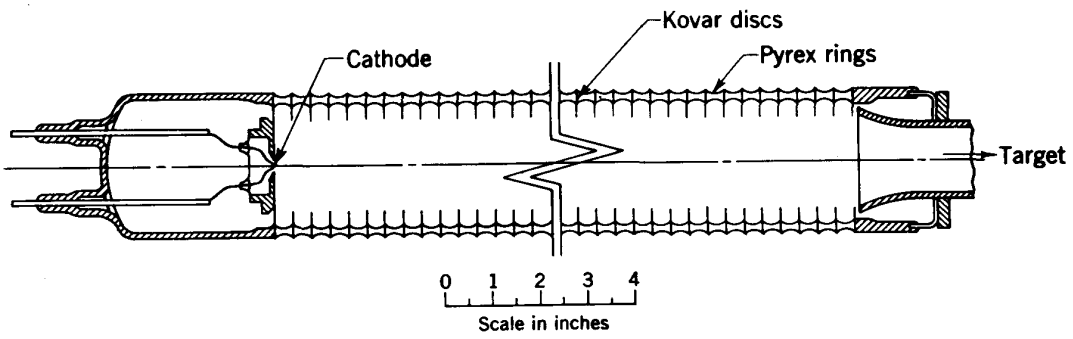

Fig. 3-12. Cross section of uniform-field accelerating tube for an electron beam.[1]

limit in the "uniform field" tube produced by the Machlett Laboratories for electron acceleration in the MIT X-ray generators built for the military services. This was a permanently sealed tube built of large numbers of Kovar disks and short Pyrex rings, with the thermionic cathode at one end. Figure 3-12 illustrates such an electron-accelerating tube. The present X-ray tubes used for medical and industrial applications are assembled from short glass or porcelain rings with intervening polished aluminum electrodes, sealed with Vinylseal and baked to form a mechanically strong tubular structure.

Modern designs for positive-ion tubes use much larger diameters, owing to the necessity of providing adequate pumping speeds to accommodate the gas flow from the source. Herb and others have developed 10-in.-diam tubes, which allow the vacuum pumps to be placed at the grounded end. Other laboratories use smaller tubes, with a pumping outlet near the source and a second insulating tube running the length of the column to provide a gas pump-out. This technique is known as "differential" pumping. In one case (Berkeley) the second tube was not used and the gas discharged from the differential pump outlet at the source was

pumped into a storage tank in the terminal, which had to be discharged occasionally. A typical positive-ion tube developed by the High Voltage Engineering Corporation for the Brookhaven electrostatic generator is shown in Fig. 3-13.

Vacuum pumps for the accelerator tubes must have pumping speeds compatible with the tube diameter or with the electrode aperture diameter, if that is the limitation. The required speed is relatively low as compared with pumps for cyclotrons or other large-volume vacuum chambers. The requirements for ultimate vacuum and low vapor pressure are more severe, however, primarily because of the problem of electron loading, to be discussed in the section to follow. A typical figure for ultimate vacuum demanded by most experimenters is 2×10^{-6} mm Hg.

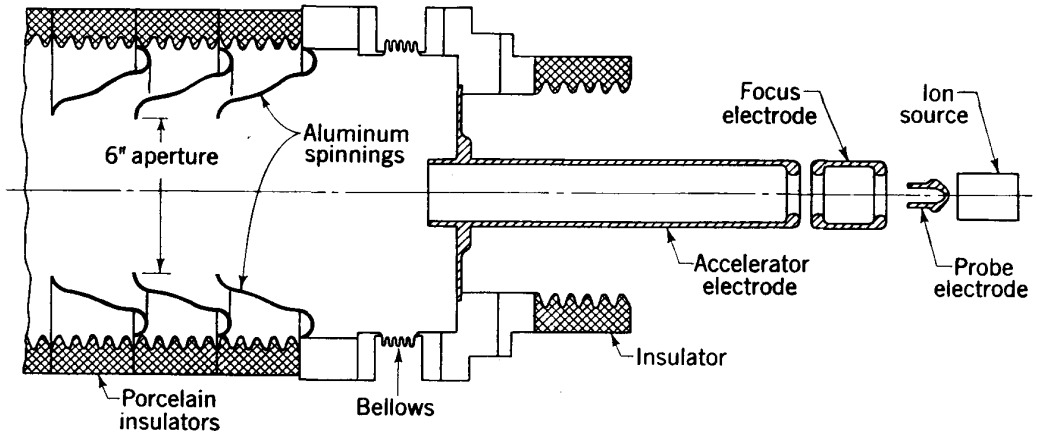

Fig. 3-13. Positive-ion source, focusing electrodes, and accelerating-tube structure for the Brookhaven 4-Mv generator.[22]

Vapor traps and baffles are essential, and these are almost universally refrigerated to low temperatures. The practice at the MIT laboratory has been to use only mercury-vapor pumps, with refrigerated baffles. The elimination of organic vapors originating from oil-vapor pumps seems to have reduced the electron-loading problem and to justify the practice. Other laboratories have used oil-vapor pumps successfully when suitable baffling has been provided, but an occasional burst of oil vapor into the tube has sometimes caused serious trouble from electron loading, and tubes must be cleaned more often.

3-7. ELECTRON LOADING

One of the most serious problems of the positive-ion electrostatic generator is the limitation on terminal potential due to electron loading.[33] The loading is caused by electrons, usually released by secondary emission processes from the electrodes or walls of the accelerating-tube structure,

which traverse the tube in the opposite direction and increase the tube current so as to limit terminal potential at constant charging rate. This beam of electrons is focused by the electric fields within the tube and strikes the ion source at the terminal end, producing X rays with an energy distribution extending up to the maximum tube potential. Such X rays are observed from the terminals in all positive-ion accelerators and, in fact, constitute one of the chief radiation hazards of the electrostatic generator. Shielding around the ion source within the terminal is difficult because of the weight of material required; shielding of the entire high-pressure shell or of the room in which the generator is housed is expensive. Nevertheless, most modern high-voltage generators have such shielding built into the walls of the room. Intensities equivalent to the gamma-ray output of several kilograms of radium have been observed occasionally in some generators.

This limitation of the accelerator tube has resulted in positive-ion energies well below the practical operating limit of the generator without the tube. Installations confidently designed for potentials of, say, 5 Mv have frequently been found to have a practical limit for positive ions of only 3 to 4 Mev. The practical voltage limit has been so difficult to estimate in advance that many generators have never reached their designed voltage when used with positive ions. The electrostatic generator has accordingly suffered from a rather bad reputation of seldom performing to specifications.

Electron loading is most conspicuous in tubes whose inner surfaces have become contaminated. One of the chief contaminants is the oil vapor or the discharge decomposition products of the vapor, when oil-diffusion pumps are used in the vacuum system without adequate baffling. The significance of oil vapor in the electron-loading problem has only been recognized in recent years. For many years experimenters had ascribed the phenomenon to other causes, such as improperly cleaned or polished electrode surfaces, gas pressure in the vacuum tube, or lack of adequate pumping speed. At the MIT laboratories early difficulties with oil-vapor pumps led to insistence on mercury-vapor pumps or on extremely cold baffles when oil was used. Nevertheless, they also have had difficulties and limitations due to electron loading, which can probably be ascribed to other contaminants such as vapor from gaskets or sealing compounds. There has been a running argument between two schools of thought for many years, in which one group argued for mercury-vapor pumps with the associated requirements of low gas flow and small-volume chambers, and the other group exploited large-diameter chambers, fast pumping speeds, and oil-vapor pumps. With the present understanding of the phenomenon the two lines of development have merged, and all agree on the importance of the minimum possible vapor pressures and surface contaminations.

The phenomenon was known in the early days of accelerator development. The first study of secondary-electron emission by positive ions, by Hill, Buechner, Clark, and Fisk[34] in 1939, was based on the urge to solve the loading problem. They measured electron yields from metallic surfaces placed in the beam of positive ions of several Mev energy, observing 4 electrons per positive ion for protons, 6 for hydrogen molecular ions, and 13 for helium ions, from molybdenum targets. The effect was nearly independent of the target metal and no method was discovered for reducing or controlling it.

The magnitude of the loading phenomenon in an operating generator will usually decrease slowly with continued operation. It can definitely be reduced by using faster pumps, better baffles, or refrigerated traps. It is a function of the gas pressure in the vacuum tube; the threshold for incidence of loading is raised by increasing gas pressure to about 10^{-5} mm Hg, and heavy gases like nitrogen or argon are more effective than hydrogen or helium in suppressing the effect. It is believed by some operators to be a function of tube diameter, in that large-diameter tubes seem to have a lower potential threshold than smaller tubes in the same generator; however, this may be associated with the relative pumping speeds. The effect is altered by surface conditions inside the tube; a tube which is subject to loading can be improved by careful cleaning.

In the past few years the problem of electron loading has been more widely recognized and studied. Experimental tests have been run at several laboratories to attempt an analysis of the mechanism of the phenomenon. Blewett[33] has suggested that it may be a consequence of the large local fields developed across thin layers of insulating contamination on electrode surfaces, such as pump oil or oxide layers, first studied by Malter[35] in 1936 at much lower energies. Malter observed large yields of secondary electrons from such surface layers when bombarded by electrons in the presence of high electric fields. He interpreted this as field emission due to extremely high local fields across an insulating surface layer.

Turner[36] showed that a large fraction of the secondary electrons came from the final slit at the grounded end of the tube in the Brookhaven proton accelerator and that they could be trapped by electric retarding fields between the last electrode and ground; reduction in electron loading current was observed as a decrease in X-ray intensity from the terminal. McKibben and Boyer[37] used magnetic fields at the base of the tube of the Los Alamos generator to deflect the secondary electrons, and from the results they concluded that negative-ion emission was also partially responsible for the effect.

New light was thrown on the effects of electron loading by Turner in some unpublished work performed during 1957. He made careful measurements of the locations of all currents which left the high-voltage

terminal of one of the Brookhaven electrostatic generators and established the fact that a large fraction of the loading current returned to ground through the high-pressure insulating gas. This current he attributed to ionization of the high-pressure gas by the X rays emanating from the region around the ion source. This secondary effect was found to be contributing a large fraction of the load current. By careful shielding of the ion-source structure with sheets of lead he was able to reduce the loading current by a significant factor and so to push the terminal potential to materially higher voltages than had been previously attained.

There is reason to hope that a combination of clean techniques, low vapor pressures, and fast pumping speeds can control contaminations, that electric or magnetic clearing fields can be designed and located to reduce the magnitude of the residual effect, and that X-ray ionization can be controlled by shielding. The recent successes in this direction suggest that with this problem under control the electrostatic generator can be extended to considerably higher energies than have been available in the past.

3-8. VOLTAGE MEASUREMENT AND CONTROL

The problem of voltage calibration is fundamental, since the primary usefulness of the electrostatic generator has been for studies of reaction energies and nuclear energy levels. Our present precise knowledge of nuclear energy constants rests to a large extent on the measurements made with these machines.

In the historical summary at the beginning of this chapter, the early calibrations in the Carnegie Institution laboratory were described. Techniques for measurement of particle energy have advanced steadily in the years of development. At present, in most laboratories using electrostatic generators, particle energy is known to within 1 or 2 kev in 4 Mev, and techniques for controlling the potential to this accuracy are available. Many laboratories and individuals were concerned in the development, and the techniques are generally known and used. The ones to be described here are representative of the latest methods leading to the highest accuracy.

The "generating voltmeter" has been for years the basic instrument for observing terminal potential with single-terminal machines.[12,38] Its operation depends on the static charge induced on an insulated metal plate or vane near the outer pressure housing surrounding the terminal. The magnitude of the induced charge is determined by the electric field established by the charged terminal at the location of the vane. In the usual form an insulated vane rotates at constant speed behind a grounded shield shaped so the vane is covered during half its travel and exposed to the electric field during the other half (see Fig. 3-14). The alternating

electrostatic voltage induced on the vane is amplified and rectified, and its magnitude is displayed on a dc meter at the control panel as a measure of terminal potential. The geometry of the system limits the precision of calibration from calculations of the capacitance and the electric field. The voltage scale is usually calibrated against other standards of potential. The most serious limitation is the distortion of electric fields due to corona discharge from the terminal, as discussed earlier. In most installations the generating voltmeter is used as a qualitative instrument for monitoring operations, such as in tuning up the generator or in observing spark discharges. With the advent of multiple-terminal shields its

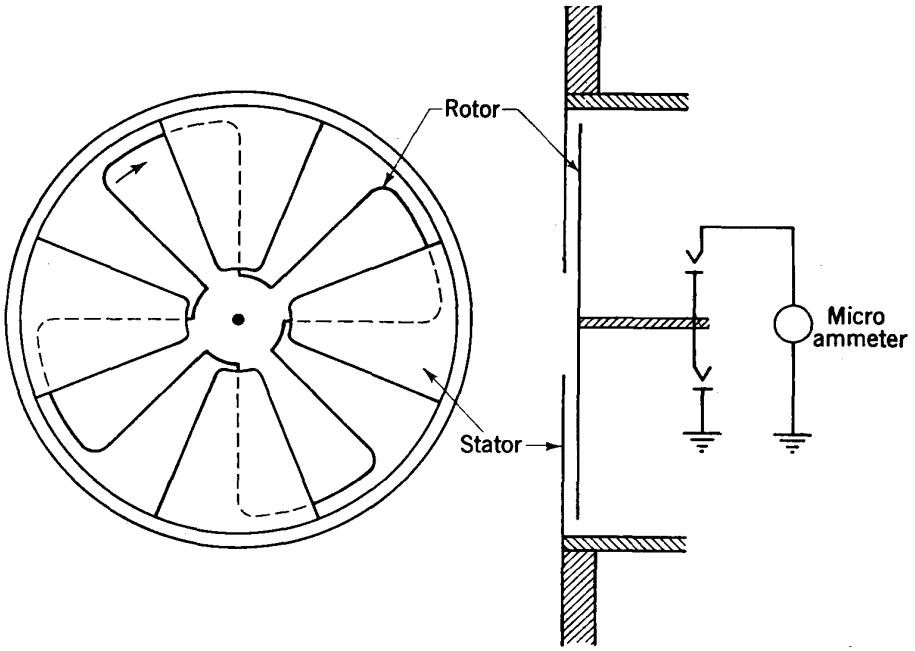

Fig. 3-14. Schematic diagram of generating voltmeter for measurement of terminal potential.[12]

usefulness is somewhat reduced, since it reads only the potential of the outer shield and its calibration depends on a constant ratio of potential drops between shields.

Another method of measuring terminal potential is to observe the current in a string of calibrated high resistors running from terminal to ground. To give a valid reading these resistors must be free from corona losses, not an easy matter unless they are carefully shielded. However, the resistor string can also be utilized to provide a uniform potential distribution of many small steps by connecting the resistors between successive equipotential rings. If this is done, corona loss can be made negligible, and the resistors serve a dual purpose. The total resistance is high, so the current drain down the stack is a small fraction of the charging current. A typical value is 10,000 megohms per million volts, or a current of 100 μa. A microammeter is inserted at the grounded end of the

resistor column. When used to calibrate terminal potential, the individual resistors must be measured to high precision. If other more accurate voltage calibrations are used, this current can still be displayed on the control panel as a visible check on terminal potential.

Most modern accelerator installations use magnetic or electric deflection of the particle beam to calibrate voltage. In some cases the instrument is itself calibrated by using natural alpha-particle groups whose energy is precisely known from measurements made at the Cavendish laboratory. An illustration is the MIT laboratory, where Buechner uses a calibrated 180° magnet to focus and measure the energy of protons scattered from the accelerated beam. The precision attained in absolute energy calibration is of the order of 0.1 per cent.

An important means of cross-calibrating the proton-energy scales in the several laboratories is provided by nuclear resonances. Certain reactions are found to have extremely sharp resonances at definite proton energies when thin targets are used, and the yields from such reactions show sharp peaks. Several resonances at energies useful for voltage calibration were measured at an early stage by the Carnegie Institution group,[7] using their precision resistance voltmeter. Others at higher energy values have been added as the energy scale increased. The most precise measurements in the 1- to 2-Mev range came from the Wisconsin group, reported by Herb, Snowden, and Sala.[39] The results of their proton-energy calibration are given in the form of exact values for the thresholds of three nuclear reactions, as follows:

$$\begin{aligned} \mathrm{Li}^{7}(p,n)\mathrm{Be}^{7} &- 1.882 \pm 0.1\% \text{ Mev} \\ \mathrm{A}^{27}(p,\gamma)\mathrm{Si}^{28} &- 0.9933 \pm 0.1\% \text{ Mev} \\ \mathrm{F}^{19}(p,\alpha\gamma)\mathrm{O}^{16} &- 0.8735 \pm 0.1\% \text{ Mev} \end{aligned} \tag{3-10}$$

The energy calibration used by Herb, Snowden, and Sala came from the use of a large electrostatic analyzer, in which the protons were deflected through 90° between curved plates by an electric field which could be determined from the dimensions, and from potentiometer measurements of the applied voltage. The analyzer was accurately constructed and end effects were calculated carefully. Protons were passed through very narrow slits by the focusing inherent in the 90° electrostatic deflection. Uncertainties are reported to be 0.1 per cent, or about 1 kv/Mv, including the error in the e/m value for the proton taken from latest measurements of the physical constants. This energy scale is independent of alpha-particle energies and represents an absolute and independent calibration.

At Rice Institute in Texas, Bonner has also used magnetic deflection, using alpha-particle calibration for energy measurement. However, he has developed a new absolute method for calibration of the magnetic field based on nuclear resonance with the proton magnetic moment.

This "proton moment" method of calibrating a magnetic field is described in more detail in Chap. 8 in the section on magnetic measurements. The value of the proton moment is known to extremely high precision, even better than alpha-particle energies. The chief source of error in the method comes from uncertainties in the geometry and in calculating the end effects in the analyzing magnet. The precision attained is equivalent to that in the two laboratories mentioned previously.

It is of interest to note that the three independent techniques of calibration outlined above are in excellent agreement, well within the experimental errors. Each laboratory has provided cross-checks by measuring the thresholds or resonance energies for several nuclear reactions, and these results agree. As an additional check, Herb and his group have measured the energy of the polonium alpha-particle group with their electrostatic analyzer and find agreement with the accepted value to within the experimental limits of error. So it is now possible to rely on energy calibrations in those laboratories to within 0.1 per cent. Other laboratories have in general relied on the energy scale given by the most accurately measured values of nuclear resonances, and calibrate their deflecting magnets and energy scales by using the resonances as substandards.

The techniques for voltage control are similar in the several laboratories. All depend on error signals from a slit system at the exit of the magnetic or electrostatic analyzer. In the magnetic analyzer, for example, the beam traverses narrow slits at the entrance and exit. If the magnetic field is constant, a variation of terminal potential will cause the beam to strike one side or the other of the exit slit. The slit edges can be insulated and currents to the edges measured and compared. A lack of balance indicates a variation of particle energy, and the sense of the difference gives the direction of deviation.

In most installations using protons for target bombardment, the mass-2 ions from the source (singly charged hydrogen molecular ions) are used for the voltage control. In a magnetic field these ions are deflected through an angle which is $1/\sqrt{2}$ that for the protons in the analyzer, and this beam is allowed to fall on the double-edged slit used for control. In this way the proton beam can be kept free from confining slits and allowed to pass through the analyzer to the target.

An amplified error current from the control slit is used to correct terminal potential. Several methods of applying this control are available. The error signal can be used to modulate the voltage of the belt-corona-spray power supply. This may be done either by controlling primary voltage of the high-voltage transformer or by varying grid potential of a vacuum tube placed in the grounded lead of the rectifier set. In the latter case the potential drop across the tube is in series with the spray points and the lower grounded pulley and hence can control the

corona voltage and current. This system is limited to a speed of response corresponding to the belt travel time. The load current is assumed to remain essentially constant.

Another control method depends on maintaining constant charging current and varying a component of the load current. Corona points are located at the wall of the pressure housing opposite the terminal, and the current in this steady corona discharge is varied by the error signal from the energy analyzer. The corona-control points are usually arranged in a package of 6 to 12 points, each sticking through a hole in a grid plate. This grid plate may be grounded and the control voltage applied to vary the negative potential on the points, or the control voltage may be applied to this grid plate to vary the electric field at the points. The corona package as a whole can be moved close to the terminal for low terminal potentials and back to the wall for maximum potentials. Corona currents from such a negative point are very sensitive to variation of point potential.

An alternate method of controlling load current is to modulate a beam of electrons going up to the terminal from the grounded end in a second accelerating tube, which may also be used for differential pumping at the ion source. A thermionic cathode and control grid similar to those in a standard triode are used to produce and control electron-beam current. A disadvantage of this system is the X rays produced at the terminal end of the electron-accelerating tube.

Any such control scheme depends on varying the potential of the terminal, which is of large capacitance and has a relatively long time constant. The variation in corona load current or electron loading current must be large to keep the time of response short. Current variations as great as 1 ma have been used, although the usual range is a few hundred microamperes. To give a numerical example: Consider a generator operating at 4 Mv, with a capacitance of 300 $\mu\mu$f, and a control-current variation of 100 μa. Equation (3-1) can be used to calculate the rate of change of potential. The time required to change terminal potential by 1 per cent (40 kv) is about 0.1 sec.

The control systems described above can usually be adjusted to maintain terminal potential constant to within 0.1 per cent over long periods. The limit of precision is frequently not the control circuit but the magnet current stabilization circuit in the magnetic analyzer.

Practical techniques for switching and adjusting ion-source controls within the high-voltage terminal range from the extremely simple to the highly ingenious. The classic method is to use strings as insulating belts extending from the base up within the shielded column to the terminal; these strings give direct mechanical coupling to the potentiometers and other controls within the terminal. At the other extreme, beams of light are projected up the column and activate photocells in the terminal.

Modulation of light intensity is used to regulate photocell current for control. In most installations the simplicity and direct mechanical control of the system of strings have proved to be most satisfactory.

3-9. THE 12-MV GENERATORS

The last word in electrostatic-generator development is in the form of two supergenerators both originally rated for 12 Mv. One, at MIT, represents the culmination of years of research and engineering on the problems of high-voltage insulation by Professors J. G. Trump, W. W. Buechner, and their associates. The other, at the Los Alamos Scientific Laboratory, has been designed and built by Dr. J. L. McKibben, a graduate of the Herb school of accelerator design at the University of Wisconsin. Both machines are in operation, but at considerably less than the expected maximum voltage. It is still uncertain whether they can be tuned up to their original rating as proton accelerators.

The two machines are similar in general outline, but differ in many features of structural design and in many details. Both are mounted vertically and pressure-insulated. The most obvious difference is in the structure of the pressure vessel and the buildings to house the instruments. The Los Alamos machine is an enlargement of the removable-housing design. The pressure vessel can be lifted bodily off the terminal column, so the building to house it is five stories high. The MIT pressure housing is permanently installed in the laboratory building, with a removable cap at the top through which the terminal column can be assembled. The general designs are illustrated in Figs. 3-15 and 3-16.

A complete description of the MIT generator has not been published, but many technical details are available in the form of laboratory reports of the MIT Laboratory of Nuclear Science and Engineering. The following description has been made available by courtesy of Professor Trump (see Fig. 3-15).

The pressure tank is 12 feet in diameter and 32 feet high. It is rated for 400 lb/in.^{2} pressure. The removable tank cover can be lifted by overhead crane and moved aside for the assembly of the column. A movable working platform fits inside the tank and around the column. The filling gas used is 80% N_2 and 20% CO_2. This can be pumped into storage cylinders outside the building when the tank is to be opened. The insulating column is 18 ft long, of which the upper 6 ft is 8-inch diameter, and supports a 38-inch diameter terminal, and the lower 12 ft is 60-inch diameter and supports a 68-inch equipotential shield. In operation at 12 Mv the voltage distribution will apply 4 Mv between the inner shells and 8 Mv across the outer gap. One belt 18 inches wide is driven by two 5 hp, 1800 rpm motors. Space is available for two accelerating tubes, one for positive ion acceleration and one for differential pumping. Mercury diffusion pumps are located below the baseplate. An analyzing magnet on a swivel base

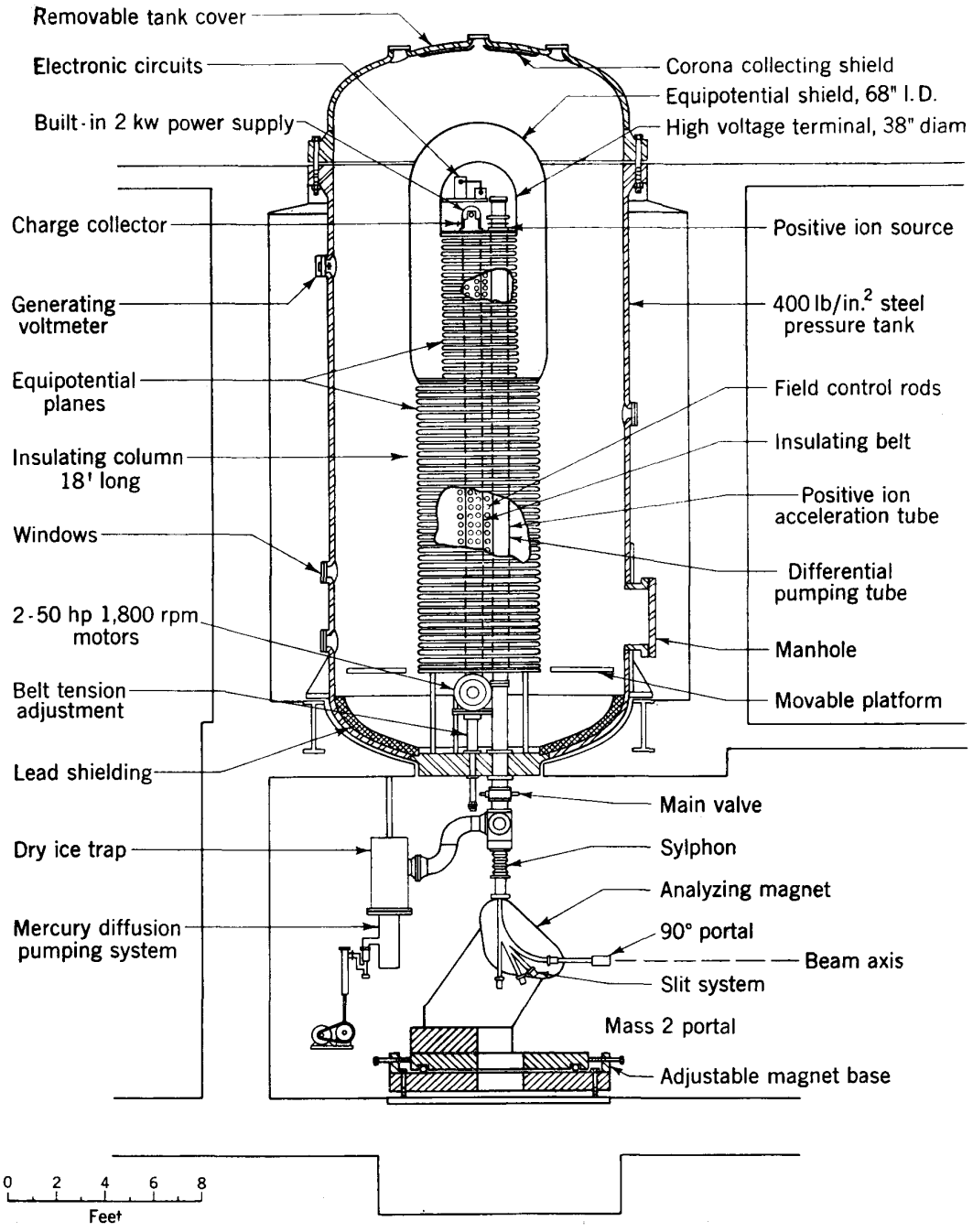

Fig. 3-15. 9-Mv electrostatic generator at MIT. (Courtesy of J. G. Trump.)

allows the beam to be swung to alternate experimental stations within the large well-shielded laboratory room.

Under the direction of Professor Buechner, this MIT generator is now operating as a research instrument, normally at 7 to 8 Mv, but with maximum proton energies of 9 Mev. It is the highest-energy single-stage electrostatic generator in operation.

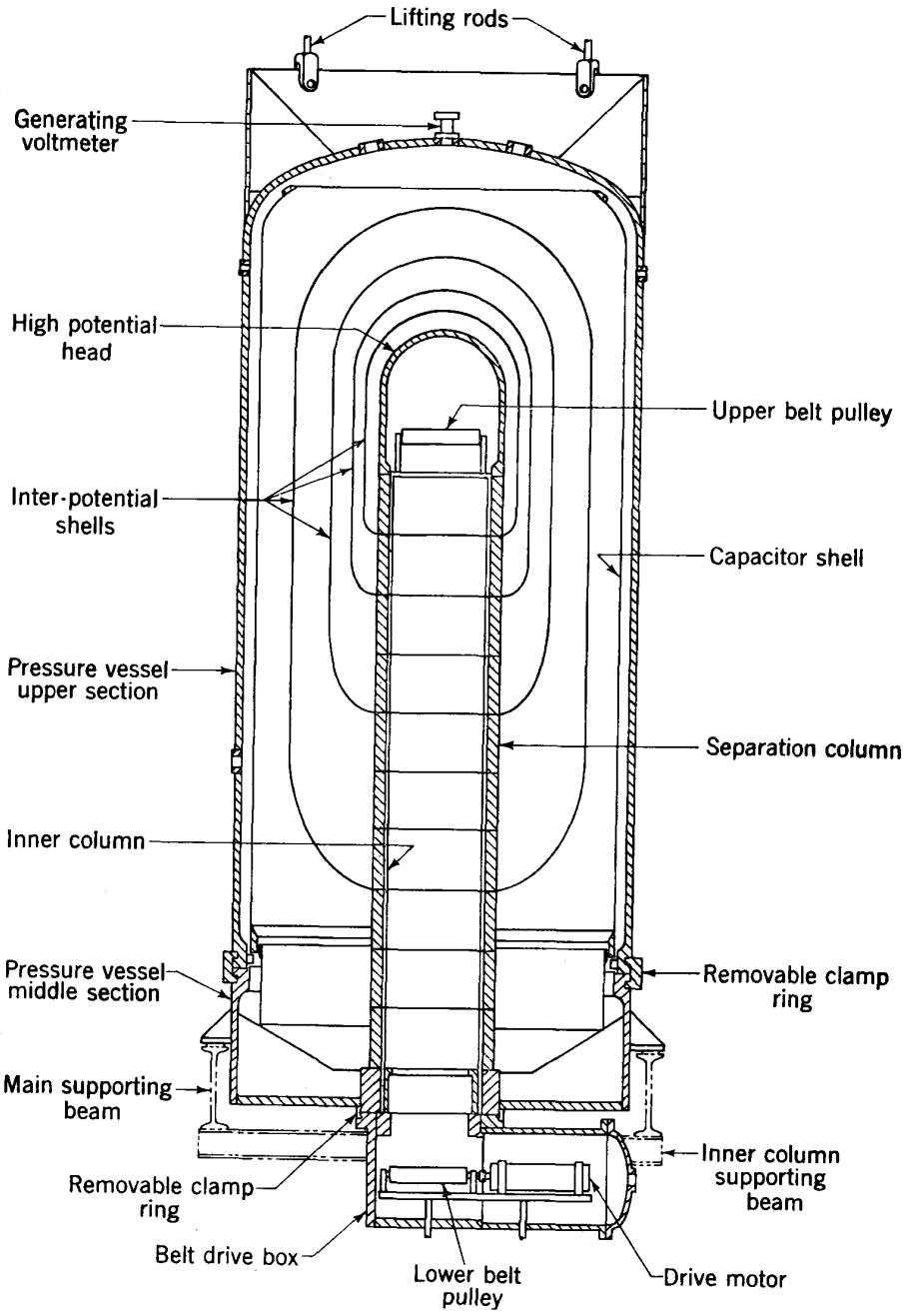

Fig. 3-16. 8-Mv electrostatic generator at Los Alamos. (Courtesy of J. L. McKibben.)

3-10. ELECTRON ACCELERATORS

Electrostatic electron accelerators have found a large field of usefulness as sources of high-voltage X rays. The 1- to 2-Mev X rays obtained have been used with good results in the field of medical therapy and in radiography of metal castings and forgings.

The electron accelerator differs from the positive-ion accelerator only in that the terminal is charged to negative potential and a thermionic

cathode replaces the ion source. However, the cathode does not evolve gas, as do positive-ion sources, so the vacuum pumping problem is much simpler and the accelerator tube can be of smaller diameter. Furthermore, voltage stabilization is not so important, since the X rays are distributed in a continuous energy spectrum having a maximum equal to the electron energy. Manual control of terminal potential through adjustment of charging current is usually sufficient. Because of the smaller tube and simpler construction, an electron accelerator can be more compact for the same voltage rating.

A number of X-ray generators developed by Trump[19,40] and later by the High Voltage Engineering Corporation have been installed in hospitals and sold to industrial firms. The most popular model is rated at 2 Mv and accelerates a beam of about 250 μa of electrons, producing an X-ray beam of quality and intensity equivalent to the gamma-ray output of 5000 g of radium. Accelerator tubes with permanent cathodes and water-cooled gold targets are of the uniform-field type developed by Trump and his associates. The entire instrument is only 3 ft in diameter and 6 ft in over-all length. It is mounted in gimbals, so it can be swung into any position to direct the X-ray beam.

The most detailed description of an X-ray generator is by Buechner, Van de Graaff, Sperduto, McIntosh, and Burrill.[20] This reports the results of a design contract with the United States Navy for a group of 2.0-Mv generators for radiographic purposes. The schematic diagram of this generator (Fig. 3-17) shows the assembly within the pressure tank.

The most successful medical application has been to cancer therapy. The high skin tolerance for 2-Mev radiation and the great depth of penetration in tissue make it particularly effective for the irradiation of deep tumors. Exposure from different angles can provide a cross fire of radiation on a deep-seated tumor many times as intense as the skin dose. Study of therapeutic problems has resulted in a full understanding of the dosage, the filtering techniques, and the physiological limits. The sharp beam due to the small focal spot on the target, the freedom from side scattering at these energies, and the uniform intensity over the radiation field make this type of X-ray therapy an ideal alternate to radium therapy.

A recent summary of the medical applications and the experimental techniques is given by Trump in Glasser's[41] "Medical Physics," vol. 2.

These same properties are advantageous in radiography. In particular, the small focal spot on the target gives a sharpness of definition much to be desired in studying flaws in metal castings or in any other of the uses of X-ray radiography. The low absorption coefficient in metals for this radiation provides deep penetration.

An alternative use of the electron accelerator is to obtain an emergent

electron beam through a thin metal vacuum window. This beam can be used to produce ionization directly in target materials. Since the beam is essentially monoenergetic, it can be deflected in magnetic fields or focused to an extremely small focal spot, of the order of 0.5 mm. The

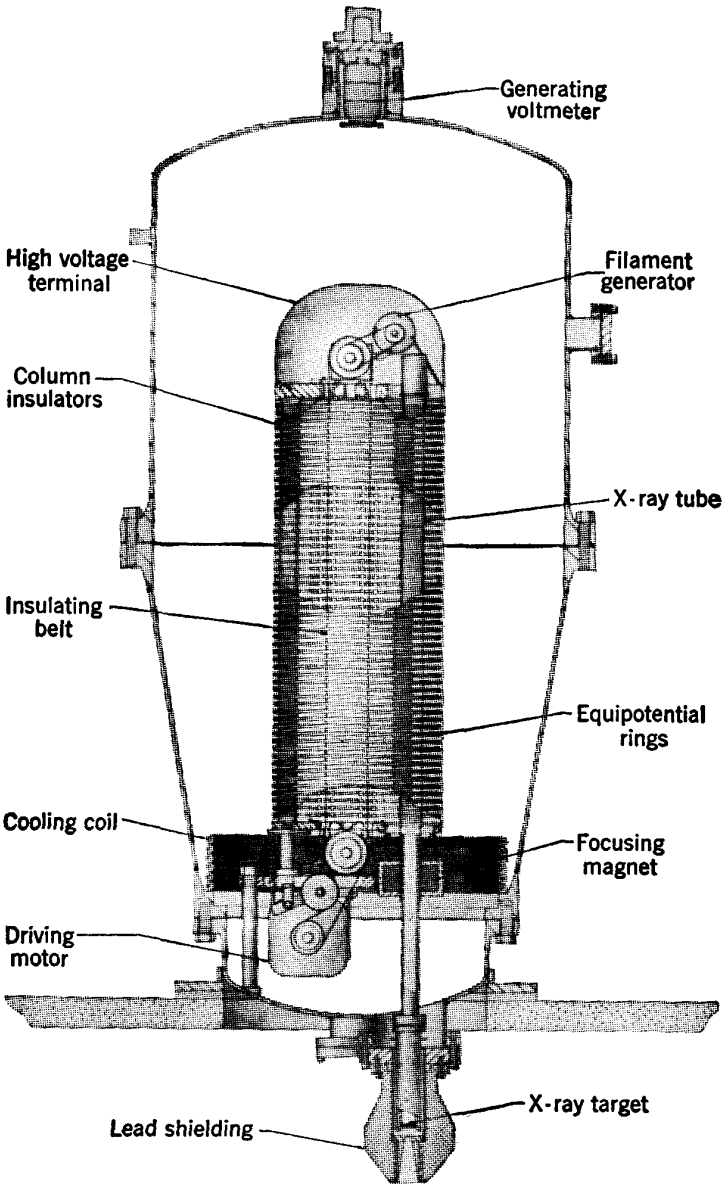

Fig. 3.17. 2-Mv electron accelerator for generation of X rays, developed at MIT.[20]

electron beam can be used for many purposes, such as sterilization of packaged goods or direct irradiation of shallow tumors, with a remarkable concentration of ionization at the end of the range of the beam. Such electron beams of controlled energy have also been used in the study of photonuclear disintegration processes.

3-11. TANDEM ELECTROSTATIC GENERATORS

The most recent development in the electrostatic-generator field is a technique for utilizing the terminal potential several times in sequence, to obtain output energies of two or more times that available in a single acceleration. The technique involves reversing the charge of the accelerated ions in successive accelerations. Such charge-exchange processes result in a significant reduction in beam intensity. However, for a wide range of experiments in nuclear research a few microamperes of accelerated ions are adequate, and the higher energy is greatly to be desired.

The concept of the tandem generator has been discussed for many years and has been specifically proposed by W. H. Bennett[42] and by L. W. Alvarez.[43] However, the first practical application was made by the High Voltage Engineering Corporation in a machine constructed for the

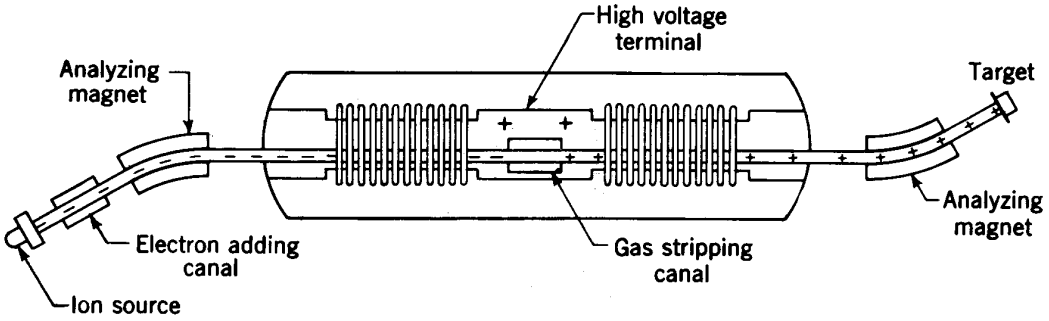

Fig. 3-18. Two-stage tandem electrostatic generator.[23]

Chalk River Laboratory of the Canadian Atomic Energy Agency and reported by Van de Graaff.[23] Figure 3-18 shows a schematic diagram of the "two-stage" tandem principle as used in this machine. The arrangement includes a horizontal pressure tank with the high-voltage terminal supported from both ends on insulating mounts; an evacuated accelerating tube extends for the full length. When a hydrogen-ion beam traverses a region containing hydrogen gas at low pressure, the emerging beam consists of a mixture of protons, neutral hydrogen atoms, and negative hydrogen ions, in relative amounts depending on ion velocity and gas pressure. Protons produced in a high-intensity radiofrequency ion source at one end of the accelerator traverse an "electron-adding" canal with hydrogen gas at sufficient pressure so that about 1 per cent of the protons emerge as negatively charged atomic hydrogen ions. These negative ions are accelerated up the accelerating tube to the positively charged terminal; there they traverse a "stripping" canal with hydrogen gas where most of them are stripped of their electronic charges and emerge as protons to be accelerated down the other accelerating tube to ground potential; the final energy is twice the terminal potential. In initial tests 1.5 μa of protons was obtained at 13.4 Mev energy, with a terminal potential of 6.7 Mv.

The technical features which make the tandem generator practical are themselves the consequence of long development in several laboratories. Ion sources capable of delivering several milliamperes of positive ions through a small canal with uniform velocities have become practical only in the late 1950s (see Chap. 4). Electrode alignment and beam focusing in the electrostatic generator have progressed over the years to produce extremely small-diameter, well-collimated beams. For example, the stripping canal in the terminal of the Chalk River generator is only 0.18 in. diam; the mechanical and technical perfection of the accelerating column which allows the beam to be passed through this small canal is itself the result of many years of development and is primarily responsible for the success of this machine.

The tandem principle can be extended to more than two stages of acceleration, but at the cost of inserting additional stages of charge exchange and further reduction in intensity. Van de Graaff has proposed a three-stage tandem which would use two double-ended horizontal electrostatic generators in line. Positive ions from an external source would first be neutralized in a gas-filled canal and would then coast through to the first negative terminal where they would traverse an electron-adding canal, accelerate down to ground potential and up to the positive terminal of the second generator, be stripped to positive ions in the second terminal, and be accelerated down to ground potential again with a total energy of three times the terminal voltage. Another technique is to use 180° bending magnets to return the beam externally to the ion-source end of the system and reuse the initial potential differences; with this scheme the energy could be raised to four times the terminal potential, but the target would be inside the first terminal.

REFERENCES

1. R. J. Van de Graaff, J. G. Trump, and W. W. Buechner, *Repts. Progr. in Phys.*, **11**:1 (1948).
2. R. J. Van de Graaff, *Phys. Rev.*, **38**:1919A (1931).
3. R. J. Van de Graaff, K. T. Compton, and L. C. Van Atta, *Phys. Rev.*, **43**:149 (1933).
4. L. C. Van Atta, D. L. Northrup, C. M. Van Atta, and R. J. Van de Graaff, *Phys. Rev.*, **49**:761 (1936).
5. L. C. Van Atta, D. L. Northrup, R. J. Van de Graaff, and C. M. Van Atta, *Rev. Sci. Instr.*, **12**:534 (1941).
6. M. A. Tuve, L. R. Hafstad, and O. Dahl, *Phys. Rev.*, **48**:315 (1935).
7. L. R. Hafstad and M. A. Tuve, *Phys. Rev.*, **47**:506 (1935); **48**:306 (1935).
8. L. R. Hafstad, N. P. Heydenburg, and M. A. Tuve, *Phys. Rev.*, **50**:504 (1936).
9. H. A. Barton, D. W. Mueller, and L. C. Van Atta, *Phys. Rev.*, **42**:901A (1932).
10. R. G. Herb, D. B. Parkinson, and D. W. Kerst, *Rev. Sci. Instr.*, **6**:261 (1935).
11. D. B. Parkinson, R. G. Herb, E. J. Bernet, and J. L. McKibben, *Phys. Rev.*, **53**:642 (1938).

12. R. G. Herb, C. M. Turner, C. M. Hudson, and R. E. Warren, *Phys. Rev.*, **58**:579 (1940).
13. I. Michael, E. D. Berners, F. P. Eppling, D. J. Knecht, L. C. Northcliffe, and R. G. Herb, *Rev. Sci. Instr.*, **30**:855 (1959).
14. W. H. Wells, *J. Appl. Phys.*, **9**:677 (1938).
15. W. H. Wells, R. O. Haxby, W. E. Stephens, and W. E. Shoupp, *Phys. Rev.*, **58**:162 (1940).
16. J. H. Williams, L. H. Rumbaugh, and J. T. Tate, *Rev. Sci. Instr.*, **13**:202 (1942).
17. B. Jennings, C. D. Swartz, and H. H. Rossi, *Rev. Sci. Instr.*, **15**:64 (1944).
18. D. R. Inglis, R. W. Krone, and S. S. Hanna, *Rev. Sci. Instr.*, **20**:834 (1949).
19. J. G. Trump and R. J. Van de Graaff, *Phys. Rev.*, **55**:1160 (1939).
20. W. W. Buechner, R. J. Van de Graaff, A. Sperduto, L. R. McIntosh, and E. A. Burrill, *Rev. Sci. Instr.*, **18**:754 (1947).
21. W. M. Preston and C. Goodman, *Phys. Rev.*, **82**:316A (1951).
22. E. L. Rogers and C. Turner, *Rev. Sci. Instr.*, **21**:805 (1955).
23. R. J. Van de Graaff, *Nuclear Instr. and Methods*, **8**:195 (1960).
24. J. G. Trump, R. W. Cloud, J. G. Mann, and E. P. Hanson, *Trans. AIEE* (November, 1950).
25. R. G. Herb and E. J. Bernet, *Phys. Rev.*, **52**:379 (1937).
26. F. Joliet, M. Feldenkrais, and A. Lazard, *Compt. rend. acad. sci. Paris*, **202**:291 (1936).
27. M. T. Rodine and R. G. Herb, *Phys. Rev.*, **51**:508 (1937).
28. E. E. Charlton and F. S. Cooper, *Gen. Elec. Rev.*, **40**:438 (1937).
29. H. C. Pollock and F. S. Cooper, *Phys. Rev.*, **56**:170 (1939).
30. J. G. Trump, F. J. Safford, and R. W. Cloud, *Trans. AIEE*, **60**:132 (1941).
31. W. C. Schumb, *Ind. Eng. Chem.*, **39**:42 (1947).
32. J. G. Trump and J. Andrias, *Trans. AIEE*, **60**:986 (July, 1941).
33. J. P. Blewett, *Phys. Rev.*, **81**:305A (1951).
34. A. G. Hill, W. W. Buechner, J. S. Clark, and J. B. Fisk, *Phys. Rev.*, **55**:463 (1939).
35. L. Malter, *Phys. Rev.*, **49**:478 (1936).
36. C. M. Turner, *Phys. Rev.*, **81**:305A (1951).
37. J. L. McKibben and K. Boyer, *Phys. Rev.*, **82**:315A (1951).
38. G. P. Harnwell and S. N. Van Voorhis, *Rev. Sci. Instr.*, **4**:540 (1933).
39. R. G. Herb, S. C. Snowden, and O. Sala, *Phys. Rev.*, **75**:246 (1949).
40. J. G. Trump and R. W. Cloud, *Am. J. Roentgenol. Radium Therapy*, **49**:531 (1943).
41. O. Glasser (ed.), "Medical Physics," vol. 2, Year Book Publishers (1950).
42. W. H. Bennett and P. F. Darby, *Phys. Rev.*, **49**:97, 422, 881 (1936).
43. L. W. Alvarez, *Rev. Sci. Instr.*, **22**:705 (1951).

At the head of the facing page is an assembly photograph of a duo-plasmatron ion source developed at the Oak Ridge National Laboratory. (Courtesy of Dr. C. D. Moak.)

4

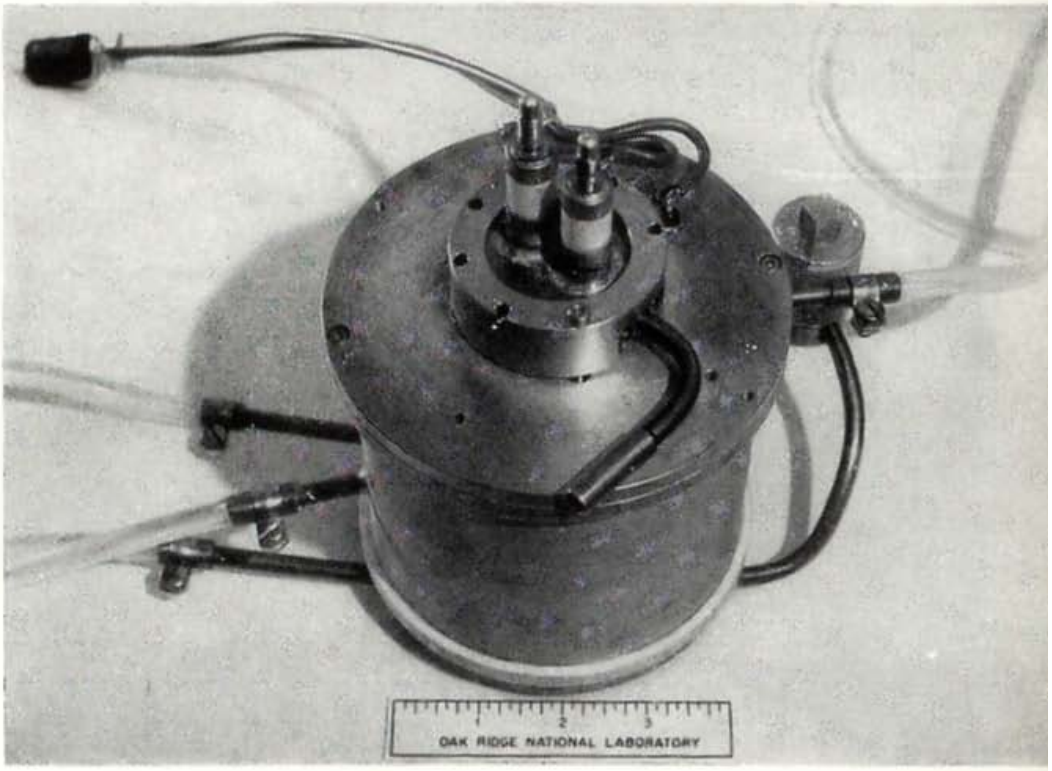

Ion Sources

Ion sources for low-voltage dc accelerators and for the electrostatic generator have similar requirements and characteristics. The basic requirement is a parallel beam of protons, deuterons, or other light positive ions, aimed along the axis of the accelerating electrodes. There are few space limitations except that ions should emerge from the source through a small, round hole on the axis, to maintain cylindrical symmetry. Plenty of space is generally available for the electrodes and discharge chamber. Cyclotron ion sources, on the other hand, have severe restrictions on dimensions and must operate in the intense magnetic field at the center of the cyclotron chamber. They are of a special type and will be described in Chap 6. The purpose of this chapter is to discuss the problems of positive-ion formation and the several ion sources used in producing a linear beam of ions.

All ion sources utilize the ionization produced in a gaseous discharge, but the mechanisms for producing this ionization and for concentrating the discharge into a small, parallel beam vary considerably. Several classes or types of source can be recognized, grouped according to the nature of the discharge phenomena or the different physical arrangements used to produce the ionization:

1. Cold-cathode canal-ray tube
2. Spark discharge

3. Hot-cathode arc
4. Low-voltage capillary arc
5. Discharge in an axial magnetic field
6. Radiofrequency electrodeless discharge
7. Electron oscillation (P.I.G.) discharge

These sources will be described and discussed individually. However, it is possible to identify several features of an ion source which are common to all types.

4-1. PROPERTIES OF A GASEOUS DISCHARGE

In all ion sources the ionization is produced by electron impact in a gaseous discharge. The general requirements are a source of electrons, a small region of relatively high gas pressure separated from the accelerating tube, an electric field to accelerate electrons and maintain the discharge, and some mechanism for concentrating the discharge and for

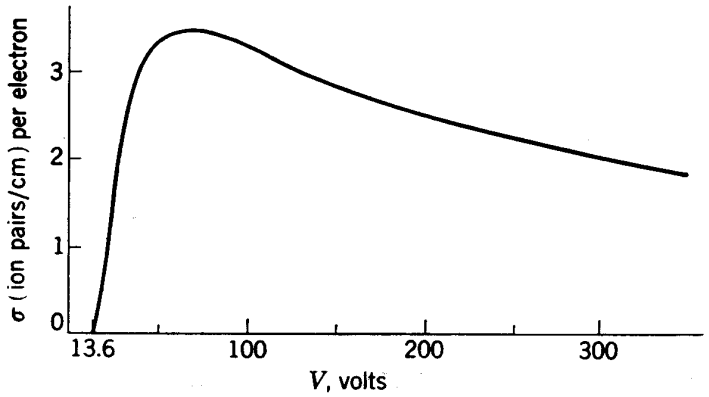

Fig. 4-1. Ionization efficiency for hydrogen at 1 mm Hg pressure and 0°C, as a function of electron energy in volts.

pulling positive ions out in a parallel beam. Usually the high-pressure discharge region is separated from the accelerating tube by a diaphragm with a small hole. This is frequently combined with differential pumping between the diaphragm and the acclerating tube to eliminate the gas. The adjustable parameters of an ion source are electron emission, gas pressure, voltage across the discharge, magnetic field, size of exit hole, geometry and surface properties of the electrodes, and the general shape and dimensions of the enclosing discharge chamber.

Ionization occurs in gases when the electron energy equals or exceeds the ionization potential of the gas. The ionization potential of the hydrogen molecule, forming H_2^+, is 15.6 volts; that for the formation of atomic ions H^+ from H atoms is 13.6 volts; the ionization potential of helium to form He^+ is 24.5 volts; and for He^{++} it is 54 volts. Ionization probability increases with electron energy, having a maximum for

hydrogen at about 75 volts. This function is shown in Fig. 4-1. Electrons make collisions in the gas; their average energy depends on the energy acquired in a mean free path between collisions and so varies inversely with pressure. The potential drop across the discharge is usually considerably greater than 75 volts in hydrogen and depends strongly on the pressure.

Many texts[1] are available which present the theory and observations on gaseous ionization. It is sufficient here to note only a few of the pertinent conclusions.

Townsend studied the non-self-maintaining or dark discharges observed at fields below the spark breakdown limit and developed the theory known by his name which explains this phenomenon. Suppose a number of electrons N per second traverse the gas at a distance x from the cathode. The number of new electrons dN released per second in a distance dx owing to ionization is proportional to N and to dx:

$$dN = \alpha N\, dx \tag{4-1}$$

The proportionality constant α is known as the "first Townsend coefficient." This leads, upon integration, to

$$N = N_0 e^{\alpha x} \tag{4-2}$$

where N_0 is the number emitted from the cathode ($x = 0$) per second. This can be expressed in terms of the current density in the gas I and the emitted current density I_0 as

$$\frac{I}{I_0} = e^{\alpha x} \tag{4-3}$$

The ratio I/I_0 is the gas multiplication factor.

In nonuniform fields, such as may exist in ion sources with nonplanar geometry, the electric field varies from point to point. Since α is a function of the field, a correct calculation requires summation over varying values of α, described by the relation

$$\frac{I}{I_0} = e^{\int_0^{\alpha} \alpha\, dx} \tag{4-4}$$

The value of the first Townsend coefficient will depend on pressure, which determines the number of collisions in a given length of path, and also on the energy of the electron at the time of collision. This energy depends on the mean free path (an inverse function of pressure) and on electric field intensity E. Thus α is proportional to pressure P and also

to some function of E/P. The customary expression is

$$\frac{\alpha}{P} = f\left(\frac{E}{P}\right) \tag{4-5}$$

The value of this function can in principle be computed from the ionization probability curve (Fig. 4-1). Usually, however, it is determined directly from experimental observations. Values of α/P for hydrogen

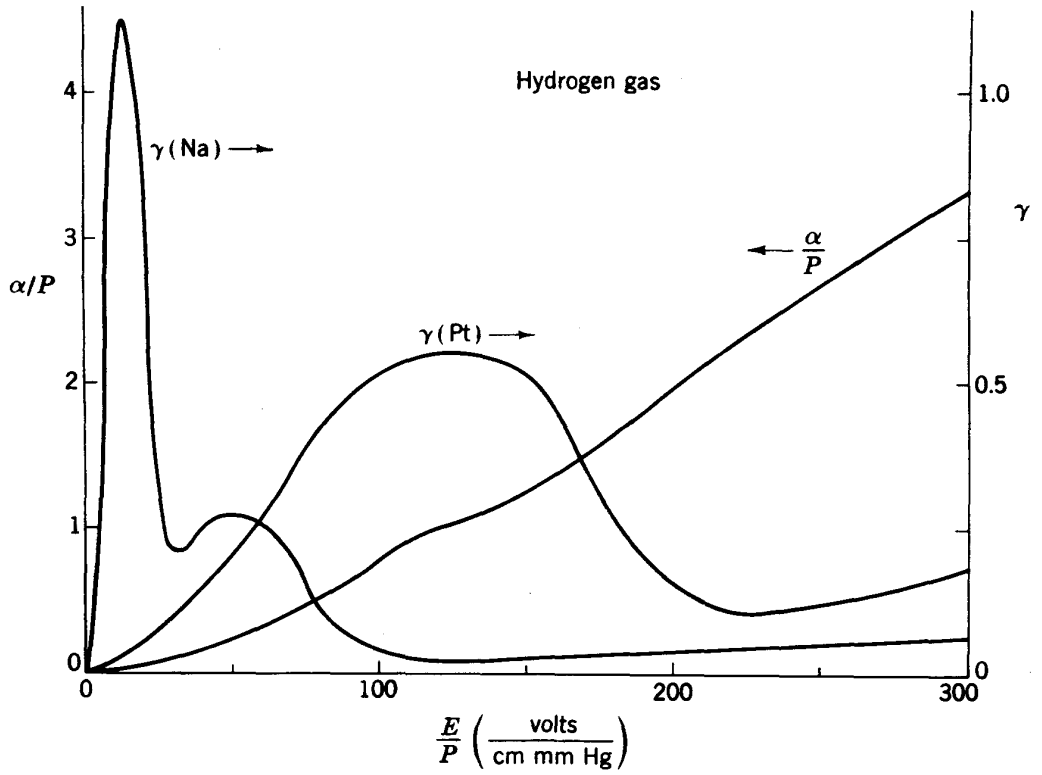

Fig. 4-2. Coefficients of ionization by electrons and positive ions in hydrogen gas, as a function of E/P [volts/(cm) (mm Hg)]. The electron coefficient α/P is in units of ion pairs/cm at 1 mm Hg and 0°C. The positive-ion coefficient γ is the number of secondary electrons produced at the cathode per positive ion in the discharge.

gas are shown in Fig. 4-2 as a function of E/P. More accurate and more extensive data can be obtained from the standard texts on gaseous discharge.

In his early theory Townsend assumed a "second Townsend coefficient," which was the ionization per centimeter per positive ion in the gas. From this assumption Townsend developed his theory of cumulative breakdown of the gas and expressed the result in terms of his two coefficients. Direct gaseous ionization is not now believed to be the dominant mechanism by which positive ions affect the discharge. Other phenomena are more important. Positive ions produce secondary electrons on striking the cathode surface, with a probability which is a function of

ion energy and also varies widely for different surfaces. Another important mechanism is production of photons in the gas by positive ions through excitation of molecules, formation of metastable molecular states, etc. These photons, on striking the cathode, also produce secondary electrons, with a probability primarily dependent on the nature of the surface. The sum of all these effects can be lumped into a coefficient γ, which is the number of secondary electrons entering the discharge per positive ion. Using this modern form of the second Townsend coefficient, we find that the current density in the discharge becomes

$$\frac{I}{I_0} = \frac{e^{\alpha d}}{1 - \gamma(e^{\alpha d} - 1)} \tag{4-6}$$

where d is the electrode spacing.

The expression above reduces to Eq. (4-3) for $\gamma = 0$. For finite values of γ it leads to a prediction of cumulative ionization or breakdown when the denominator goes to zero. This Townsend sparking criterion is for

$$\gamma(e^{\alpha d} - 1) = 1 \tag{4-7}$$

Experimentally measured values of the secondary-electron coefficient γ for positive ions are also available for most gases and many cathode materials, usually presented as a function of E/P. Illustrative curves for γ for two surfaces Na and Pt in H_2 gas are also plotted in Fig. 4-2.

Under the conditions applying at breakdown, it can be shown[1] that the quantity $e^{\alpha d}$ is very much greater than unity. So the criterion of Eq. (4-7) can be simplified to

$$\gamma e^{\alpha d} = 1 \tag{4-7a}$$

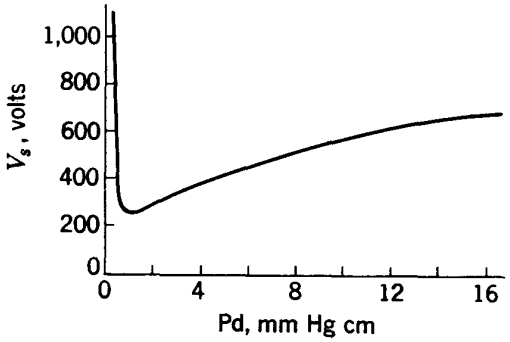

Fig. 4-3. Sparking-potential curve for nickel cathode in hydrogen gas.[2]

Using values of α/P and γ as functions of E/P (Fig. 4-2), it is possible to compute the electric fields required for breakdown under various conditions. For example, Hale[2] has computed the values of breakdown or sparking voltage for an Ni cathode in H_2 gas as a function of Pd (pressure times electrode spacing) and compares these computed values with the measured sparking voltages. The measured and computed values were in excellent agreement over a wide range of conditions. Figure 4-3 shows the curve of sparking potential obtained by Hale. It has a minimum value (about 230 volts) at about 1 mm Hg gas pressure for 1 cm spacing (or 0.1 mm Hg pressure for 10 cm). Dimensions of ion sources are in the range between 1 and 10 cm, so we can expect H_2 gas breakdown at minimum voltage to be obtained with pressures between 0.1 and 1.0 mm Hg.

Some ion sources operate at this gas breakdown limit, where the discharge is self-maintained and limited only by the constants in the external power-supply circuit. These are the plasma-type sources. The discharge becomes stabilized at that balance of electrons and positive ions in the gas which leads to the equilibrium condition expressed by Eq. (4-7).

Other ion sources are operated below the breakdown limit and depend on electron emission from a heated cathode to maintain the discharge. With a hot cathode the arc current can be controlled and the voltage drop adjusted to give average electron energies near the optimum shown in Fig. 4-1.

Gas pressure in the discharge must be relatively high in order to reduce the required potential to a practical value. Ionization density is directly proportional to pressure for the same discharge current, so high pressure is an advantage when ions are to be brought through small exit holes. In most ion sources the pressure is between 10^{-1} and 10^{-3} mm Hg. However, gas pressure in the accelerating tube outside the hole must be much smaller (10^{-5} mm Hg or less) to prevent electrical breakdown. Therefore, small holes are used in the walls of the chamber and also in the probe electrodes employed to pull ions out of the discharge; frequently differential pumping is applied to this region between exit hole and probe to remove the gas flowing out of the hole. Rather wide variations in the chosen conditions are noticeable in the several types of sources. Some have quite low pressures and very large holes. Others use concentrated discharges at high gas pressure and depend on differential pumping to remove the gas. Still others are designed for minimum gas flow with very small exit holes, to economize on the use of rare gases such as H^3_2 (tritium) or He^3 when these are used for source gases. No general conclusions can be derived, since each type has been considered best for some application.

Within an arc discharge a high density of ionization exists. Electrons (and some negative ions) move toward the anode. Because of their low mass the mobility of electrons is high, and they move rapidly through the gas. Positive ions go to the cathode, but because of their larger mass and lower mobility they take a longer time. An equilibrium is established with approximately equal numbers of positive ions and electrons, in which a slight excess of ions produces a positive space charge and a radial electric field. The potential of the central region, or plasma, becomes 5 to 10 volts positive relative to the walls, so positive ions are forced outward. In addition, a longitudinal potential gradient develops along the discharge column just sufficient to maintain cumulative ionization. Under equilibrium conditions the plasma is an almost uniform mixture of gas, drifting ions, and electrons, with very low internal potential gradient. In such a plasma most of the current is carried by electrons because of their much higher mobility.

Another feature of the discharge is the sheath which develops near the walls—a sharp, visible boundary of the region of ionization associated with the potential drop caused by the difference between the mobilities of electrons and ions. The outward field for positive ions exists largely across a narrow dark layer between the plasma sheath and the walls. Positive ions which originate in the plasma drift to the sheath and are directed outward, where they can emerge through an exit hole cut in the wall of the discharge chamber. Other positive ions are attracted toward the cathode and will emerge through a canal cut in the cathode.

In a molecular gas such as H_2 the formation of atomic ions (H_1^+) is believed to be a complex process involving the intermediate step of formation of atomic gas (H_1) followed by ionization of this atomic gas. Evidence for this is the observed threshold of ionization at the 13.6-volt ionization potential of atomic hydrogen gas. The molecules can be either dissociated directly or, more probably, ionized first to H_2^+, which then dissociates on collision with another molecule to form $H_1 + H_1^+$. Wall material is important in this process, since one of the limitations is the recombination of atomic gas to form molecules at the wall. Another effect is the recombination of atomic ions with electrons to form atomic gas, which tends to increase atomic-gas concentration. In the design of proton sources precautions are frequently taken to control the recombination processes by such techniques as the use of special coatings or by maintaining the walls at high temperature.

Positive ions which emerge from the side of the discharge column have low velocities, equivalent to the 5- to 10-volt potential difference between plasma and walls. They also have random directions because of thermal impacts with gas atoms. It is usually necessary to locate a probe electrode outside the exit hole in the wall of the discharge chamber, with a somewhat larger hole through which ions pass, and to maintain the probe electrode at a high potential relative to the walls. The electric field due to this probe potential will penetrate the exit hole and may distort the electric fields within the discharge. This accelerating field is the first and most important of the ion lenses used in focusing the beam of emergent ions. The physical shapes of exit hole and probe tip become very important in determining the focal properties. These problems are discussed in more detail in the following chapter, but our understanding of the focusing problem is far from complete. Much is left to the inspiration and ingenuity of the experimenter, and we observe wide differences in designs and techniques for bringing out an emergent beam.

Ions which strike the cathode have much higher energies. The cathode fall of potential between the plasma and the cathode may be a large fraction of the total arc voltage. In most arcs the ions emerging through a canal in the cathode have maximum energies of 100 to 200 volts, and they have a rather large variation in energy. On the other hand, these ions

are more sharply collimated in direction than those discussed above, coming through the side sheath of the plasma. The probe electrode described above may not be needed, but an accelerating field is required, and this first accelerating lens serves the same purpose of focusing the beam. Geometry again is all-important.

A general characteristic of all ion sources is that they behave best on bench tests and almost universally fail to reach test performance when applied to an accelerator. A variety of factors are responsible. In testing a source, the usual method is to measure the emergent ion current

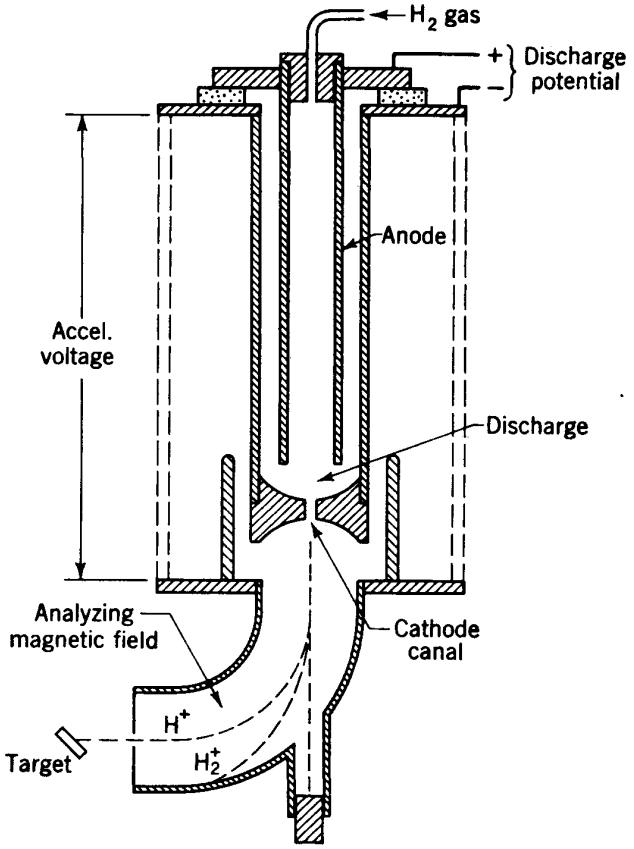

Fig. 4-4. Canal-ray ion source used by Oliphant and Rutherford.[3]

after it has been accelerated by a few kilovolts potential applied to a probe electrode. The beam observed may be strongly divergent, and only a fraction would be acceptable in an accelerator. Or gas flow may be excessive, owing to the use of large exit holes. When applied to an accelerator tube under high voltage, this gas flow might result in breakdown or in excessive electron loading currents. For accelerator use a source must have small exit holes or differential pumping arrangements to prevent loading with gas. Furthermore, the total ion beam from a source is a mixture of singly and multiply charged ions and molecular ions, while that desired for an accelerator is a single type of ion. As a consequence,

reports of new high-intensity sources have frequently raised hopes, but the sources have failed to demonstrate their superiority in service. Publications describing only bench tests are often misleading. The final test of a source is the level of stable operation in service, with the beam focused, accelerated, and analyzed. In the descriptions to follow it is well to remember that most publications cite beam intensities obtained in bench tests.

4-2. COLD-CATHODE CANAL-RAY TUBE

The ion source used by Cockcroft and Walton in their earliest experiments on artificial transmutation was a high-voltage cold-cathode canal-ray tube. A potential of about 20 kv was required to maintain suitable discharge currents. A typical design is described by Oliphant and Rutherford.[3] The cathode and anode were long coaxial cylinders with the anode inside and having a sufficiently close spacing to the cathode to prevent discharges between the walls. The discharge was restricted to the space around the end of the anode cylinder, just opposite a small hole in the cathode end plate through which ions emerged. The arrangements are shown in Fig. 4-4. The discharge was operated at 20 kv and between 10 and 100 ma current. The source was oil-cooled at the base, and the tip of the cathode could be run at red heat. Gas was admitted through the base into the interior of the anode. Gas pressure was not specified but, by comparison with other high-potential discharges, must have been of the order of 10^{-2} mm Hg. Magnetic deflection of the accelerated ions allowed measurements of separated ions. At first the emission was largely hydrogen molecular ions, but after some hours of operation the proton component increased to about 20 per cent. Beams of about 1 μa of protons were normally obtained.

The disadvantage of this source is the wide spread in energy of the emergent ions. A spread of 20 kv would not be acceptable in modern accelerators.

4-3. SPARK DISCHARGE SOURCE

Experimentalists in the field of mass spectroscopy have been faced with the problem of producing ions of essentially every element in order to complete mass-spectra and mass-defect tables. Intensities required were extremely low in comparison with present demands for accelerators, but sensitive detectors were available and exposures of several hours could be used if necessary to obtain adequate data for analysis. One of the techniques which was most successful for a wide range of atomic and molecular ions was the spark source, in which high-voltage sparks were

developed between electrodes of the chosen material. Typical of such spark sources are those described by Dempster.

Several of the high-energy accelerators, such as the linac and the proton synchrotron (see Chaps. 11 and 13), accelerate short pulses of particles to high energy so the source duty cycle may be as small as 1 part in 10,000. For example, the proton synchrotron requires a pulse of injected ions of about 100 μsec length at about 5-sec intervals. A continuously operating ion source is inefficient for such service, and considerable effort has gone into developing pulsed sources with high peak pulse currents but low average current.

One of the more intriguing pulsed sources is an "occluded gas" spark source reported by Ehlers, Gow, Ruby, and Wilcox[4] for use with the pulsed high-intensity linacs at the University of California Radiation Laboratory. The technique uses electrodes of titanium metal which have been heated and cooled in a hydrogen or deuterium atmosphere until the metal is saturated with interstitial hydrogen. Under optimum conditions about 400 cm^3 of hydrogen gas can be occluded per gram of titanium. The titanium is formed in washers stacked with mica spacers to form the electrode of a spark discharge chamber. An electrical "delay line" of capacitors and inductors develops a voltage pulse of 10 to 20 kv for a pulse length of up to 500 μsec, which is applied across the discharge chamber. Auxiliary electrodes and fields are arranged to pull out and focus a beam of atomic-gas ions produced in the spark. Ion currents as large as 300 ma are observed during the pulse; the intensity decays slowly with time as the gas occluded in the electrodes is exhausted. With this source the pulsing rate was limited to one per second to avoid overheating the Ti electrode. The disadvantages are relatively short life and inclusion in the beam of a large titanium ion component.

4-4. HOT-CATHODE ARC

A common feature of many modern ion sources is the use of a heated cathode to supply electrons by thermionic emission. Copious emission can be obtained from heavy tungsten or tantalum filaments or from oxide-coated cathodes. This source of electrons makes it possible to operate the arc at considerably lower potentials than required for the canal-ray discharge. A typical value is 200 volts. As a consequence, the energy of ions emitted from the source is much more uniform. It is also possible to maintain the necessary ionization density at somewhat lower pressures and so to reduce gas flow. A wide variety of designs has been used with different arrangements for the cathode, anode, and exit hole. In general the volume allowed for the discharge is reduced considerably below that used in the high-potential cold-cathode discharge tubes. Many ingenious devices have been invented to mount the elec-

trodes and cool them and to concentrate the discharge; a wide variety of cathode shapes has been employed.

The use of a hot cathode in a gaseous discharge as a method of increasing positive-ion density was proposed by Langmuir and Jones[5] in 1928. One of the first research teams to apply it to proton sources was Lamar and Luhr[6] at the Massachusetts Institute of Technology. In these early designs the cathode served the simple purpose of maintaining the discharge and was located inside a rather large anode cylinder. Ions were pulled out of the discharge through a canal in a probe electrode which could be biased with a negative potential. The physical arrangement of electrodes was not efficient in concentrating the discharge, and ion currents were low.

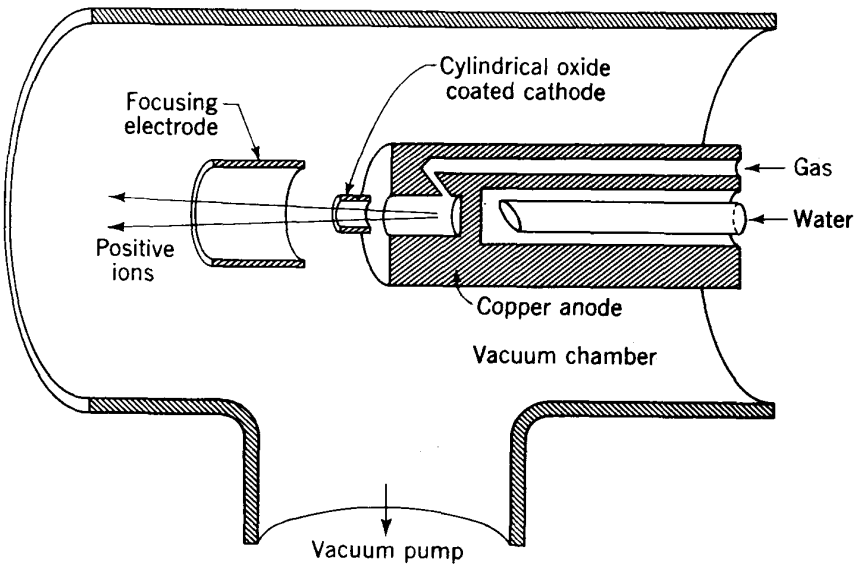

Fig. 4-5. Hot-cathode "focused beam" positive-ion source developed by Scott.[9] A hollow cylindrical cathode is used, through which the ions emerge.

The next step in the development of the hot-cathode source was the result of a more deliberate study of the properties of the discharge, as well as the physical arrangement of electrodes to favor positive-ion emission. Fowler and Gibson[7] used a circular-loop filament close to and surrounding the exit canal through which positive ions produced in the discharge could emerge. Beams of several milliamperes of positive ions were produced in bench tests, but with a large-diameter canal and with a small atomic-ion fraction.

A thorough empirical study of the hot-cathode arc was reported by Tuve, Dahl, and Hafstad[8] using a variety of arrangements for the electrodes and the probe. The best arrangements gave about 25 μa of resolved protons after acceleration. This report came after the Carnegie Institution group had found that they could obtain higher intensities from

a capillary arc, but the simpler hot-cathode source was satisfactory for several years of operation with the Carnegie electrostatic generator.

One of the most impressive bench tests of a hot-cathode hydrogen-ion source was reported by Scott.[9] The design was based on the conclusions reached in a theoretical analysis of ion sources by Smith and Scott;[10] the test apparatus is shown in Fig. 4-5. The most significant feature was a cylindrical cathode of large area to give high electron emission, aligned along the axis of the arc so that the positive ions emerged in a parallel beam through the cathode cylinder. The cathode was formed of nickel strip, oxide-coated for emission and heated by a low-voltage supply. The anode was water-cooled and located close behind the cathode, with a cup in the surface into which the gas was admitted and into which the electrons plunged from the cathode. With a cathode-anode potential difference of about 800 volts, positive-ion beams as large as 4 ma were obtained on bench tests, including nearly 50 per cent protons. The chief advantage of the source is in the high beam densities obtained because of the focusing action of the accelerating fields. However, the experiments reported did not use a canal to provide a pressure differential, and the gas flow from this source was too high to apply directly to an accelerating tube.

4-5. CAPILLARY ARC

The ionization density in the plasma of a low-voltage hot-cathode arc can be increased by concentrating the discharge in a constriction between cathode and anode. This constriction, or capillary, not only increases current density in the arc, but makes it possible to choose the wall surface to improve the atomic-ion concentration. In the constriction the high ion density forces the plasma sheath close to the walls. Positive ions are ejected radially through the sheath and can emerge through a small aperture in the wall of the capillary with only 5 to 10 volts variation in energy. Furthermore, if the wall material has a large coefficient of recombination, positive ions will rebound as neutral atoms, releasing thermal energy and heating the gas as well as increasing the atomic-gas component. Ionization in this atom-rich gas will yield a higher proportion of protons. A double advantage is gained: increased beam intensities and increased atomic-ion percentage.

The first report of such a capillary arc was by Tuve, Dahl, and Van Atta,[11] in which they credited Dr. F. L. Mohler of the National Bureau of Standards with the suggestion. They first used a quartz capillary, but then found that a metal capillary, the potential of which could be adjusted, gave equivalent results and had longer life. A later report by Tuve, Dahl, and Hafstad[12] gave a good diagram of the source (Fig. 4-6). The capillary was transverse to the direction of the emitted ion beam,

with anode and cathode in separate enlarged chambers on the two sides. A probe with a small-diameter hole was located outside the 1-mm canal in the side of the capillary. Potentials of up to 7 kv were applied to extract and focus the ions. Beams of over 1 ma of ions were obtained on bench tests, with over 30 per cent protons.

Experience in other laboratories brought recognition of the advantages of the capillary-arc source and extended the development. Lamar, Samson, and Compton[13] started on similar studies at the Massachusetts Institute of Technology. Lamar, Buechner, and Van de Graaff[14,15] described a series of sources. In some they revived the use of quartz or Pyrex capillaries to increase the atomic-ion output. The MIT sources were characterized by very short capillaries and small exit holes. Ions

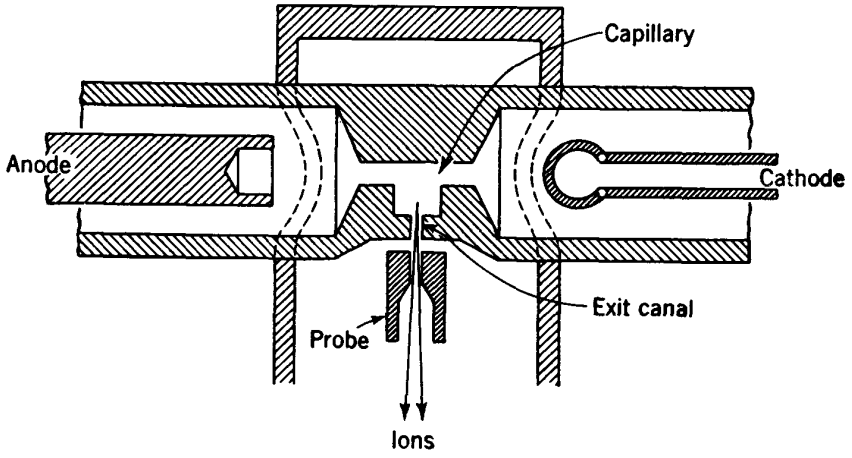

Fig. 4-6. Metal-walled capillary arc, by Tuve, Dahl, and Hafstad.[12]

diffused out of the hole at low velocity, and no high-voltage probe was used. Ion beams of several milliamperes were obtained with atomic-ion percentages up to 40. A differential pumping outlet was usually located just outside the exit hole. However, when applied to the electrostatic generators for which they were designed, the sources have in almost all instances so loaded the accelerating tube with gas that it would not hold voltage. Lower gas pressures and lower beam currents were found necessary in order to maintain voltage on the accelerator. As a consequence the available ion intensities have not proved to be practical, and in operation the sources were run below maximum yield.

Zinn[16] developed a capillary arc with an interesting axial geometry which still maintains the constriction but pulls ions out of the capillary along the axis (Fig. 4-7). This source is one of the most highly developed and has resulted in beam currents up to 500 μa when used with a low-voltage accelerator. Total ion currents up to 4.3 ma were reported, using a canal 1 mm in diameter and 6 mm long through a probe electrode maintained at 10 kv potential. Magnetic analysis showed that the beam

included 15 to 20 per cent protons. The potential drop used for the arc was about 100 volts, although higher potentials were required to start it; the maximum arc current was about 2 amp. Pressure in the arc was estimated at 3×10^{-2} mm Hg, and gas consumption was measured as 15 cm^3 of hydrogen or deuterium at atmospheric pressure per hour.

Allison[17] reported on a rugged capillary-arc source which has given good service for 8 years in a 400-kv accelerator. It operates on an arc current of 0.75 amp and consumes 25 cm^3 of gas per hour, producing a total beam current of 1.1 ma with a probe potential of 3500 volts. About 50 μa of resolved atomic ions are magnetically analyzed and focused on the target.

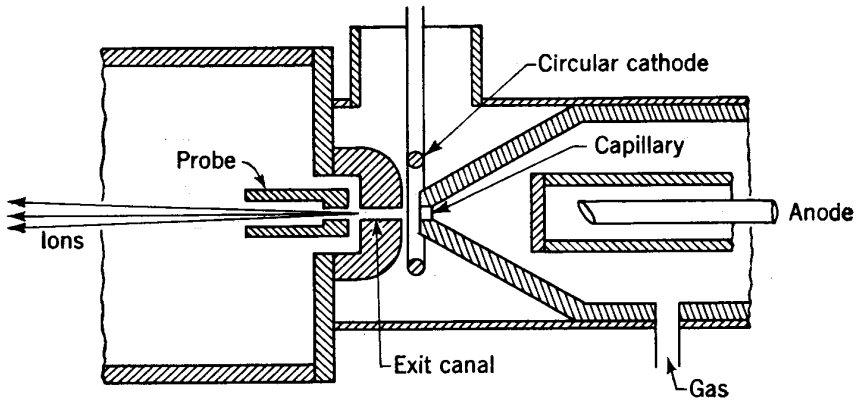

Fig. 4-7. Axially concentric capillary arc developed by Zinn.[16]

Timoshenko,[18] following the MIT development, built a high-intensity source using argon gas which produced 400 μa of singly charged argon ions through a 1-mm-diam exit hole.

4-6. MAGNETIC ION SOURCE

Axial magnetic fields can be used to concentrate the discharge in a hot-cathode arc in the region near the exit hole where a high density of ionization is needed. Several functions are served by the magnetic field. The electron beam is tightly collimated (see Sec. 5-5), so the discharge is limited to a cross-sectional area essentially equal to the area of the emitting surface of the cathode. The yield is also increased because the field keeps positive ions from diffusing to the walls of the chamber and being lost. The ratio of ion density to arc pressure is thus higher in the presence of the magnetic field. To reach maximum effectiveness the average radius of curvature of ion paths in the field should be about the size of the exit hole. The magnetic field required can be computed from typical ion velocities to be of the order of 1000 gauss. In practice, an optimum field of about this magnitude is observed.

The use of a magnetic field does not make the magnetic ion source a unique type. This technique of concentrating the discharge can be superimposed on other types such as the capillary arc or the rf source to increase ionization density in the discharge. It is also useful in concentrating the electron oscillation discharge to be described later.

One of the early ion sources which employed an axial magnetic field to concentrate the discharge in a hot-cathode arc was reported by Bailey, Drukey, and Oppenheimer.[19] Figure 4-8 shows the location of the field coil around the arc chamber, designed to produce a field of 1000 gauss within the chamber. The arc itself uses a tight spiral tungsten filament to maintain the discharge. The magnetic field collimates the emission from this cathode, so a beam of electrons is projected into the field-free region in which ionization occurs. Ions emerge from $\frac{1}{16}$-in.-diam exit hole on the axis and are accelerated and focused by the potential of 3 to 5 kv on a probe electrode. The report describes a beam of 500 μa of resolved atomic ions after acceleration to 200 kv.

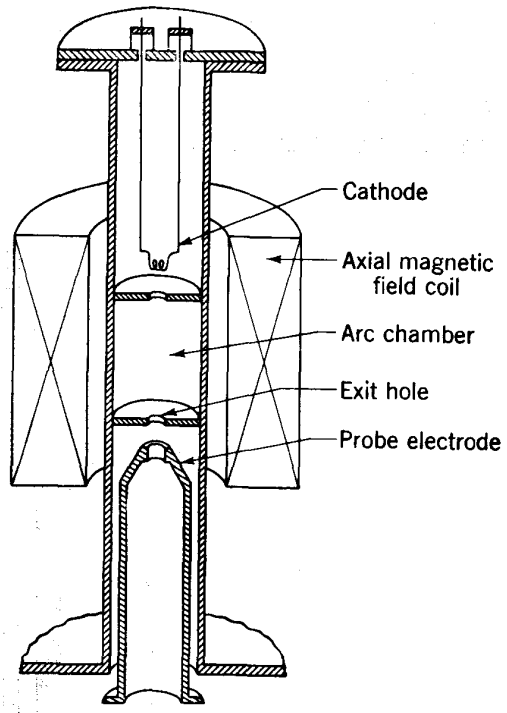

Fig. 4-8. Magnetic ion source using a hot-cathode arc, by Bailey, Drukey, and Oppenheimer.[19]

Setlow[20] described a source which is similar in principle but was not equipped with the necessary probe canal and differential pumping to use with a high-voltage accelerator. It was intended as the source for a single-stage resonant-cavity radiofrequency accelerator in which gas pressure and breakdown of insulation were not limiting factors. Because of these unusual opportunities, larger apertures could be used, resulting in extraordinarily high beam intensities. When pulsed with a duty cycle of 250 μsec 60 times a second, peak ion currents of 100 ma were obtained, with 30 to 40 per cent protons.

The most intense ion source of the low-voltage, hot-cathode, magnetic-field-concentrated type described in the published literature was reported by Lamb and Lofgren[21] of the University of California Radiation Laboratory (UCRL). It represents the culmination of many years of development of high-intensity sources for the large-aperture, high-current linear accelerators developed in the UCRL and in the Livermore laboratory of the Atomic Energy Commission. It was used as an injector for the

"A-48" proton linac at Livermore (see Chap. 10). It is literally a monster source in all respects—in size, power requirements, and cost, as well as in the phenomenal beam intensity obtained. The output beam current of ions was 750 ma (95 per cent atomic ions) at 85 to 100 kv energy; the beam was very broad and could be focused only to a 3-in.-diam spot with $\pm 5°$ angular spread. A very large and powerful solenoid magnet around the discharge region of the source supplied 7000 gauss at the location of the arc aperture, and a second solenoid provided magnetic focusing for

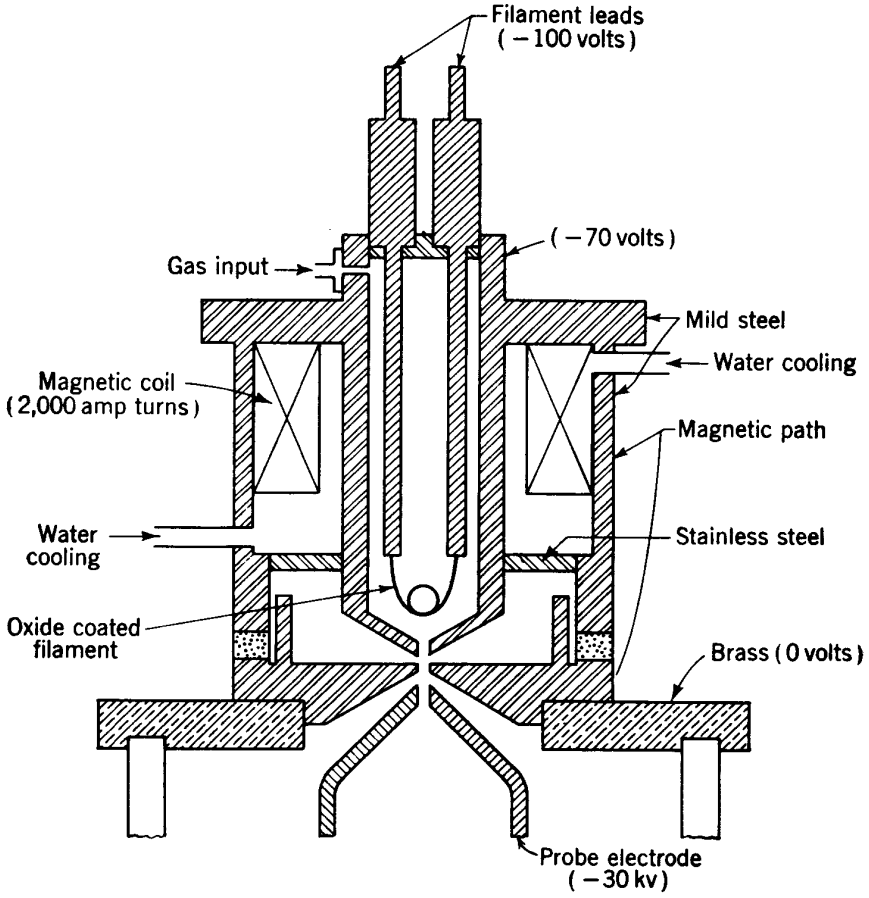

Fig. 4-9. Duo-plasmatron ion source.[23]

the emergent beam. The aperture was a ¾-in.-diam circle of twelve ⅛-in. holes, and two 20-in. mercury-diffusion pumps were used to evacuate the blast of gas emerging through the holes. This tremendous source should make practical the dream of accelerator designers for a really high-intensity accelerator.

A somewhat more elegant development of the hot-cathode magnetic ion source is due to von Ardenne.[22] This device, christened the "duo plasmatron" by its inventor, was evolved in the U.S.S.R. and in East Germany. The most important innovation in this source is concentration of the magnetic field at the exit hole by an ingenious combination of

electromagnet and electrodes in a structure where the plasma-forming electrodes are also the poles of a small electromagnet (Fig. 4-9). Thus the plasma is formed only in the region where it is useful. In his original publication von Ardenne claimed output currents as high as 500 ma through a 1-mm-diam hole. He claimed further that almost all the escaping gas is ionized and that almost all ions are protons. The current and exit-hole diameter mentioned indicate ion current densities of the order of 100 amp/cm^2. Later studies of this ion source substantiate this figure, although developments have been in the direction of 10- to 100-ma sources with smaller exit holes. Analysis of the ion beam indicates that at least two-thirds of the emitted ions are protons. The source has been studied extensively at Oak Ridge[23] and elsewhere in the United States. It is now available commercially from the High Voltage Engineering Corporation of Burlington, Massachusetts, and from the VEB Vakutronik Corporation of Dresden, East Germany.

4-7. RADIOFREQUENCY DISCHARGE

The electrodeless discharge which can be produced in gases by radiofrequency fields is a well-known phenomenon. An axial magnetic field is often used to enhance the ion yield. One advantage of the electrodeless discharge is that cathode life is not a limitation. Another is that the electrons circulate in orbits through the gas, multiplying the probability of collision and increasing the atomic-ion concentration. The ions are removed through a canal in a probe electrode inserted into the discharge chamber along the axis of the discharge and of the magnetic field; probe potentials of a few kilovolts are required. The chief technical problems have been to concentrate the discharge in a small volume and to feed the rf energy into the discharge. The application of this type of discharge to the production of positive ions has been investigated by several experimenters in England[24,25] and in Canada.[26] Frequencies of 100 to 200 megacycles were used, developed in resonant circuits with a coil of a few turns surrounding the discharge chamber. The rf power required was quite low, of the order of 100 watts. On bench tests the ion output looked encouraging, and the large atomic-ion percentage (about 50) was favorable.

A radiofrequency source of advanced type which combines most of the advantageous features has been described by Hall.[27] He used very high frequencies (450 megacycles) and a small barrel-shaped quartz discharge chamber about ½ in. in diameter and ¾ in. long placed at the open end of a resonant quarter-wave coaxial transmission line. An axial magnetic field of 1000 gauss was produced by a coil surrounding the discharge tube and was found to increase the ion yield greatly. The physical arrangement is shown in Fig. 4-10. A 1-mm hole in the end of the chamber

allowed the ions to emerge into the first accelerating gap, to which a differential pumping outlet was connected. The pressure in the quartz discharge chamber was roughly 0.1 mm Hg, and the gas flow was about 30 cm^3/hr at atmospheric pressure. This source was applied to a 120-kv accelerator, and the results reported are for focused and accelerated ions at the target. Hall reports obtaining 400-μa beams containing 60 per cent protons, with an oscillator power of 60 watts.

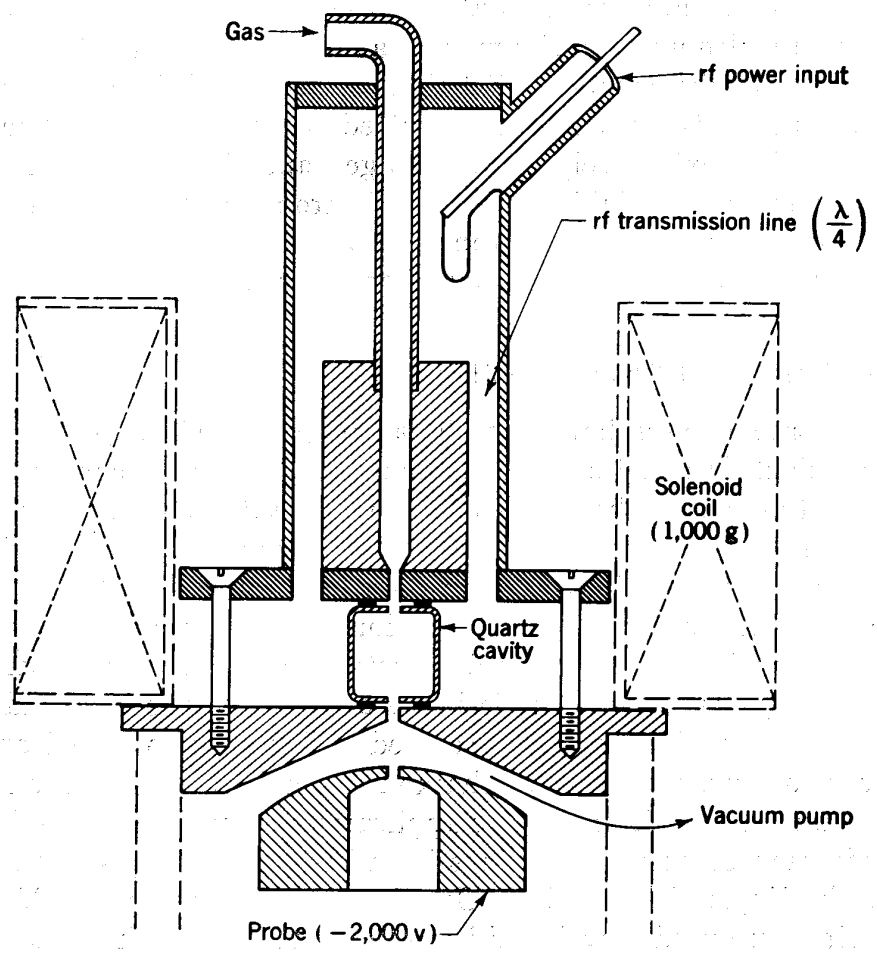

Fig. 4-10. Radiofrequency discharge ion source developed by Hall.[27] An electrodeless discharge within a quartz cavity is concentrated by an axial magnetic field.

The radiofrequency source is capable of much higher emission when operated under pulsed conditions. At the CERN laboratory in Geneva, Switzerland, a radiofrequency source yields currents of the order of 100 ma in pulses 10 μsec long.[28] This source requires about 7 kw of radiofrequency power at 139 megacycles.

4-8. ELECTRON OSCILLATION (P.I.G.) ION SOURCE

One of the most recently developed high-intensity ion sources utilizes electron oscillations to increase the density of ionization in the discharge.

This principle was first utilized in the Philips laboratories ionization gauge, and ion sources of this type are frequently known as P.I.G. sources. The principle was presented by Penning[29] in 1937 and was incorporated in the Philips gauge immediately. The first practical ion source of this type was reported by Finkelstein[30] in 1939, but it received relatively little attention for some years. With the developing need for high-intensity pulsed sources, the technique was revived by a group at the University of California as a pulsed source for an electrostatic generator feeding a proton linear accelerator. A detailed discussion is given by Backus[31] in the National Nuclear Energy Series, and a description of a revised source is given by Gow and Foster.[32]

The mechanism of the discharge can be described by reference to Fig. 4-11, which shows the Gow and Foster source. The discharge occurs between a cylindrical anode and two disk-shaped, secondary-emission cathodes at the ends of the anode cylinder. Hydrogen gas pressure of about 2×10^{-2} mm Hg, an axial magnetic field of about 1000 gauss, and a potential difference of a few hundred volts between anode and cathodes provide the necessary conditions for the discharge. An electron released from either cathode will be accelerated into the anode, its radial motion constrained by the magnetic field. As it coasts through the field-free region inside the anode, it loses some energy to the gas and produces some ion pairs, so it emerges from the anode with less energy than on entering and is retarded and reflected by the negative potential of the other cathode. The electron then reenters the anode and continues the axial oscillation until its energy is reduced below that required for ionization. Eventually it drifts to the anode to become part of the external-circuit current. The average energy required to form an ion pair in hydrogen is about 35 ev, so each primary electron can form 5 to 10 ion pairs. The secondary electrons formed by ionization also oscillate axially, but since their energy is low, they are less effective in ionization.

Positive ions formed in the discharge are also constrained by the magnetic field to motion in the axial direction. When the ions approach the cathode, they are accelerated toward it and strike with several hundred electron volts energy. With suitable cathode surfaces each positive ion releases several secondary electrons on impact. If more secondaries are produced than the number of ions formed per primary electron, the discharge will become cumulative and the current will increase until it is ultimately limited by the external circuit. The discharge will stabilize as a self-maintaining phenomenon at that balance of current and potential drop which results in equal numbers of ions per electron and electrons per ion. A plasma column forms through the center of the anode, terminating in a thin cathode sheath at the surface of each cathode. This sheath is estimated to be about 0.01 cm thick from considerations of the space-charge limitation of emission of secondary electrons from the

cathode surface. Most of the potential drop in the discharge occurs across this cathode sheath, and it is here that the oscillating electrons are turned back. The diameter of the plasma column is small, with a suitable constraining magnetic field; in the source illustrated in Fig. 4-11 it was observed to be about $\frac{3}{16}$ in. diam.

The primary advantage of this source over the hot-cathode type is in the large ratio of ion current to electron current in the discharge. With the hot-cathode type, this ratio depends on the ratio of velocities (the mobility) of ions to electrons and is of the order of $(m_e/m_p)^{1/2}$, which for

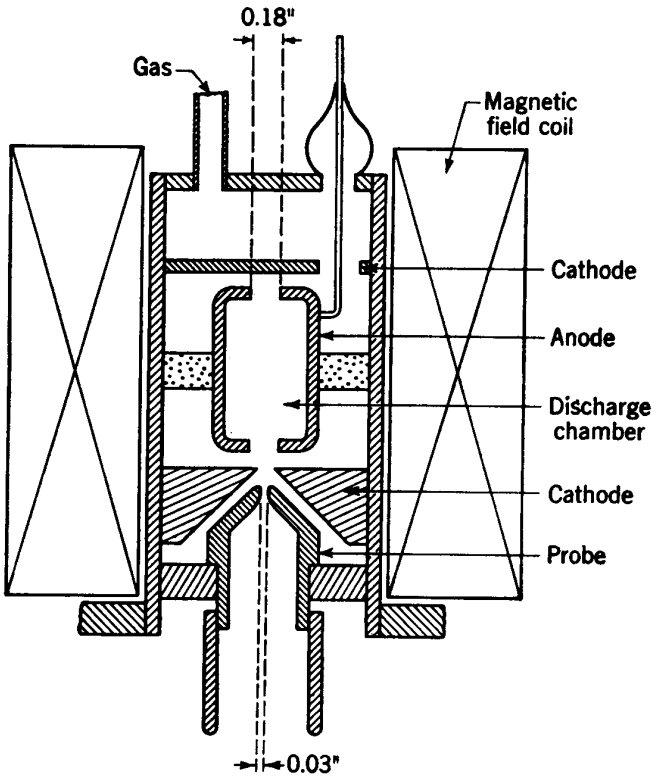

Fig. 4-11. Electron oscillation ion source by Gow and Foster,[32] based on the P.I.G. principle.

hydrogen is about 0.03. With the oscillation source the number of ions formed per electron from the cathode is increased by a factor of 5 to 10, and up to 0.3 of the current is carried by positive ions. This concentrated blast of positive ions striking the cathodes allows a relatively large number to emerge through a canal cut through one cathode. For example, if the arc current is 2 amp, about 400 ma of positive ions will strike a $\frac{3}{16}$-in.-diam spot on one cathode, and as much as 1.5 ma can emerge through a 0.030-in.-diam canal. This estimate is in good agreement with the observed emergent beam intensities. The ratio of atomic to molecular ions improves with current density, as would be expected from such a concentrated discharge, and the atomic component is

observed to be about 60 per cent of the total ion output in practical sources.

Cathodes must have large secondary-electron-emission coefficients under positive-ion bombardment. An oxide film on the cathode surface plays a key role. The mechanism of secondary emission is believed to involve a layer of positive charge built up on the surface of the oxide layer by the positive ions. This provides extremely high electric fields across the layer, pulls electrons from the base metal by field emission, and releases them into the discharge. The base metals which have been found most satisfactory on tests are aluminum and beryllium. Others, such as magnesium and duralumin, are subject to loss of the oxide film and erosion by sputtering of the metal. The oxide layer on aluminum or beryllium cathodes wears away after some period of operation and must be replaced. Oxidation can be accomplished by heating and decomposing silver oxide in a side tube with the discharge running. Such conditioning takes about ½ hr and must be repeated after about 100 hr of normal operation of the source.

The positive-ion beam emerging from the cathode canal is accelerated and focused by potentials on a probe electrode and by successive accelerating electrodes which act as ion lenses. The potential on the probe, of 5 to 15 kv, determines the beam current. This probe lens is divergent by itself, but the conical shaping is arranged to give a beam as nearly parallel as possible. Focusing is accomplished primarily by the lens between the probe and a following accelerating electrode. In continuous operation the source will produce over 100 μa of resolved protons, limited by heating of the source and by discharges in the accelerating tube.

The P.I.G. source has been very successful when applied to pulsed operation. With a pulse duty cycle of $\frac{1}{100}$ or smaller, the heating in the discharge can be readily controlled, and high current densities are used. Proton beams of 5 to 50 ma peak current during the pulse have been obtained after acceleration to several Mev in linear accelerators and electrostatic generators. A real advantage of this source over others offering equivalent beam intensities is the low gas flow through the small cathode canal, of the order of 25 cm^3/hr at standard conditions. This allows the source to be used without differential pumping at the probe canal.

A modification of this electron-oscillation source has been highly successful as a cyclotron ion source[33] (see Chap. 6). The secondary-emission cathodes avoid the cathode life limitations of hot-cathode sources, and the strong axial magnetic field in the cyclotron is helpful in collimating the discharge. In the cyclotron application, instead of ions being pulled out through an aperture in one of the cathodes, they emerge through a slit along the side of the discharge column, which can extend over much of the internal aperture of the cyclotron electrodes. As a result, very

high intensities can be obtained, roughly proportional to the aperture of the slit.

The advantages of the cyclotron modification of the P.I.G. source, with its long-slit geometry, are retained in a source described by Anderson and Ehlers,[34] which is intended for use with a linear accelerator. They use a transverse magnetic field to deflect and analyze the emergent beam from the slit, so as to obtain a momentum-analyzed beam of ions. On emerging from the deflecting magnet, the beam is broad in the direction of the slit and has angular divergence in the other coordinate, so it must be further focused to provide a beam of suitable geometry to be used in linear acceleration. Such a diffuse beam is suitable for a linac of large aperture, but not for small-aperture accelerating structures.

REFERENCES

1. J. M. Meek and J. D. Craggs, "Electrical Breakdown of Gases," Oxford (1953); L. B. Loeb, "Basic Properties of Gaseous Electronics," University of California Press (1955); J. D. Cobine, "Gaseous Conductors," McGraw-Hill (1941).
2. D. H. Hale, *Phys. Rev.*, **56**:1199 (1939).
3. M. L. E. Oliphant and E. Rutherford, *Proc. Roy. Soc. (London)*, **A141**:259 (1933).
4. K. W. Ehlers, J. D. Gow, L. Ruby, and J. M. Wilcox, *Rev. Sci. Instr.*, **29**:614 (1958).
5. I. Langmuir and H. A. Jones, *Phys. Rev.*, **31**:357 (1928).
6. E. S. Lamar and O. Luhr, *Phys. Rev.*, 44:948 (1933); **46**:87 (1934).
7. R. D. Fowler and G. E. Gibson, *Phys. Rev.*, **46**:1074 (1934).
8. M. A. Tuve, O. Dahl, and L. R. Hafstad, *Phys. Rev.*, **48**:315 (1985).
9. G. W. Scott, Jr., *Phys. Rev.*, **55**:954 (1939).
10. L. P. Smith and G. W. Scott, Jr., *Phys. Rev.*, **55**:946 (1939).
11. M. A. Tuve, O. Dahl, and C. M. Van Atta, *Phys. Rev.*, **46**:1027 (1934).
12. M. A. Tuve, O. Dahl, and L. R. Hafstad, *Phys. Rev.*, **48**:241 (1935).
13. E. S. Lamar, E. W. Samson, and K. T. Compton, *Phys. Rev.*, **48**:886 (1935).
14. E. S. Lamar, W. W. Buechner, and R. J. Van de Graaff, *J. Appl. Phys.*, **12**:132 (1941).
15. E. S. Lamar, W. W. Buechner, and R. J. Van de Graaff, *J. Appl. Phys.*, **12**:141 (1941).
16. W. H. Zinn, *Phys. Rev.*, **52**:655 (1937).
17. S. K. Allison, *Rev. Sci. Instr.*, **19**:291 (1948).
18. G. Timoshenko, *Rev. Sci. Instr.*, **9**:187 (1938).
19. C. Bailey, D. L. Drukey, and F. Oppenheimer, *Rev. Sci. Instr.*, **20**:189 (1949).
20. R. B. Setlow, *Rev. Sci. Instr.*, **20**:558 (1949).
21. W. A. S. Lamb and E. J. Lofgren, *Rev. Sci. Instr.*, **27**:907 (1956).
22. M. von Ardenne, "Tabellen der Elektronenphysik und Übermikroskopie," Deutscher Verlag der Wissenschaften (1956).
23. C. D. Moak, H. E. Banta, J. N. Thurston, J. W. Johnson, and R. F. King, *Rev. Sci. Instr.*, **30**:694 (1959).

24. P. C. Thoneman, *Nature*, **158**:61 (1946).
25. J. C. Rutherglen and J. F. I. Cole, *Nature*, **160**:545 (1947).
26. A. J. Bayly and A. G. Ward, *Can. J. Research*, **A26**:69 (1948).
27. R. N. Hall, *Rev. Sci. Instr.*, **19**:905 (1948).
28. E. Regenstreif, "Le Synchrotron à Protons du CERN," chap. 5, p. 22, CERN, Geneva (1959).
29. F. M. Penning, *Physica*, **4**:71 (1937).
30. A. T. Finkelstein, *Rev. Sci. Instr.*, **11**:94 (1940).
31. J. Backus, National Nuclear Energy Series, div. I, vol. 5, McGraw-Hill (1949).
32. J. D. Gow and J. S. Foster, Jr., *Rev. Sci. Instr.*, **24**:606 (1953).
33. C. B. Nulls, C. F. Barrett, and R. S. Livingston, Oak Ridge National Laboratory Report Y-542 (Nov. 8, 1949).
34. C. E. Anderson and K. W. Ehlers, *Rev. Sci. Instr.*, **27**:809 (1956).

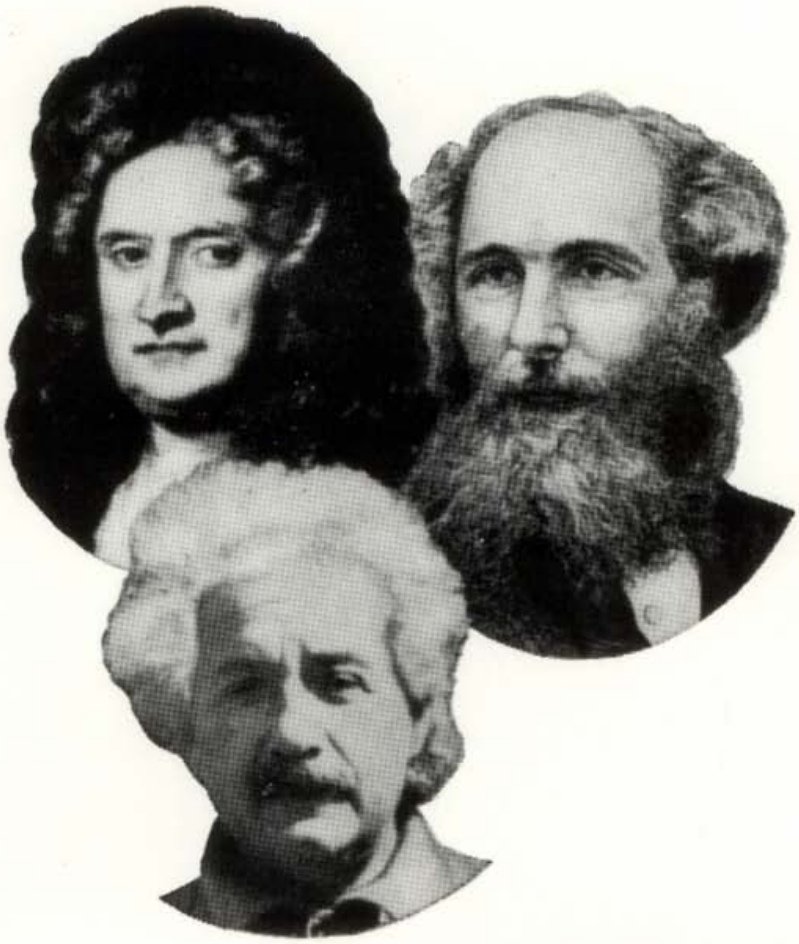

5

Particle Motion in Electric and Magnetic Fields

The accelerator designer depends heavily on two mathematical tools. The first is Maxwell's statement of the interrelation of the components of electric and magnetic fields, and the second is the formulation of Newton's second law of motion for charged particles in these fields. In this chapter these relations will be tabulated and presented in the coordinate systems most useful for application to accelerators. They will then be applied to two general classes of problems.

The first class of problems relates to the accelerating systems of direct-voltage accelerators described in the preceding chapters, including the problems of focusing particle beams which travel in straight lines. Focusing analysis is required in the design of systems for extraction of beams from ion sources. Furthermore, in many high-energy accelerators the attainable electric accelerating fields are not strong enough to reach high energies in short accelerating chambers, so focusing systems are necessary which will maintain beams of small cross section over long distances. Four focusing systems will be discussed: the electrostatic lens,

the axial-magnetic-field lens, the alternating-gradient lens, and the magnetic edge-focusing lens.

The second class of problems relates to the orbits of charged particles in static or slowly varying magnetic fields. A foundation will be laid for the discussion in chapters to follow on the circular magnetic accelerators such as the cyclotron, the betatron, and the synchrotron. Superficially these machines are radically different. But the basic arrangement of fields is the same in all three: a magnetic field restrains the motion to a roughly circular orbit, and tangential electric fields provide the acceleration.

5-1. MAXWELL'S EQUATIONS

For the derivation of Maxwell's equations from the results of experimental physics the reader is referred to any text on electromagnetic theory. Here we shall merely tabulate these equations in the forms most useful to the accelerator designer. In vectorial form they are as follows (in rationalized mks units):

$$\begin{aligned} \text{div } \mathbf{E} &= \frac{\rho}{\epsilon} \\ \text{div } \mathbf{B} &= 0 \\ \text{curl } \mathbf{E} &= -\frac{\partial \mathbf{B}}{\partial t} \\ \text{curl } \mathbf{B} &= \mu \mathbf{I} + \mu\epsilon \frac{\partial \mathbf{E}}{\partial t} \end{aligned} \tag{5-1}$$

where $\mathbf{E}$ = electric field strength, volts/m
$\mathbf{B}$ = magnetic flux density, webers/m^2
ρ = charge density, coulombs/m^3
$\mathbf{I}$ = current density, amp/m^2
μ = permeability of the medium, henrys/m
ϵ = dielectric constant of the medium, farads/m

In free space

$$\mu = \mu_0 = 4\pi \times 10^{-7}$$
$$\epsilon = \epsilon_0 = \frac{1}{36\pi} \times 10^{-9}$$

so that $\mu_0\epsilon_0 = 1/c^2$, where c is the velocity of light in free space.

In rectangular coordinates Maxwell's equations are as follows:

$$\frac{\partial E_x}{\partial x} + \frac{\partial E_y}{\partial y} + \frac{\partial E_z}{\partial z} = \frac{\rho}{\epsilon} \tag{5-2}$$

At the head of the facing page are pictures of the three men who laid the foundations for the study of particle dynamics: Isaac Newton, James Clerk Maxwell, and Albert Einstein.

$$\frac{\partial B_x}{\partial x} + \frac{\partial B_y}{\partial y} + \frac{\partial B_z}{\partial z} = 0 \tag{5-3}$$

$$\frac{\partial E_z}{\partial y} - \frac{\partial E_y}{\partial z} = -\frac{\partial B_x}{\partial t}$$

$$\frac{\partial E_x}{\partial z} - \frac{\partial E_z}{\partial x} = -\frac{\partial B_y}{\partial t} \tag{5-4}$$

$$\frac{\partial E_y}{\partial x} - \frac{\partial E_x}{\partial y} = -\frac{\partial B_z}{\partial t}$$

$$\frac{\partial B_z}{\partial y} - \frac{\partial B_y}{\partial z} = \mu I_x + \mu\epsilon \frac{\partial E_x}{\partial t}$$

$$\frac{\partial B_x}{\partial z} - \frac{\partial B_z}{\partial x} = \mu I_y + \mu\epsilon \frac{\partial E_y}{\partial t} \tag{5-5}$$

$$\frac{\partial B_y}{\partial x} - \frac{\partial B_x}{\partial y} = \mu I_z + \mu\epsilon \frac{\partial E_z}{\partial t}$$

In accelerator design the cylindrical coordinate system is probably the most useful. In cylindrical coordinates Maxwell's equations are

$$\frac{1}{r}\frac{\partial}{\partial r}(rE_r) + \frac{1}{r}\frac{\partial E_\theta}{\partial \theta} + \frac{\partial E_z}{\partial z} = \frac{\rho}{\epsilon} \tag{5-6}$$

$$\frac{1}{r}\frac{\partial}{\partial r}(rB_r) + \frac{1}{r}\frac{\partial B_\theta}{\partial \theta} + \frac{\partial B_z}{\partial z} = 0 \tag{5-7}$$

$$\frac{1}{r}\frac{\partial E_z}{\partial \theta} - \frac{\partial E_\theta}{\partial z} = -\frac{\partial B_r}{\partial t}$$

$$\frac{\partial E_r}{\partial z} - \frac{\partial E_z}{\partial r} = -\frac{\partial B_\theta}{\partial t} \tag{5-8}$$

$$\frac{1}{r}\frac{\partial}{\partial r}(rE_\theta) - \frac{1}{r}\frac{\partial E_r}{\partial \theta} = -\frac{\partial B_z}{\partial t}$$

$$\frac{1}{r}\frac{\partial B_z}{\partial \theta} - \frac{\partial B_\theta}{\partial z} = \mu I_r + \mu\epsilon \frac{\partial E_r}{\partial t}$$

$$\frac{\partial B_r}{\partial z} - \frac{\partial B_z}{\partial r} = \mu I_\theta + \mu\epsilon \frac{\partial E_\theta}{\partial t} \tag{5-9}$$

$$\frac{1}{r}\frac{\partial}{\partial r}(rB_\theta) - \frac{1}{r}\frac{\partial B_r}{\partial \theta} = \mu I_z + \mu\epsilon \frac{\partial E_z}{\partial t}$$

In a static electric field the field components can be derived from a potential function V by the vector relation $\mathbf{E} = -\text{grad } V$. In rectangular coordinates

$$E_x = -\frac{\partial V}{\partial x} \qquad E_y = -\frac{\partial V}{\partial y} \qquad E_z = -\frac{\partial V}{\partial z} \tag{5-10}$$

In cylindrical coordinates

$$E_r = -\frac{\partial V}{\partial r} \qquad E_\theta = -\frac{1}{r}\frac{\partial V}{\partial \theta} \qquad E_z = -\frac{\partial V}{\partial z} \tag{5-11}$$

In dynamic fields a more sophisticated representation in terms of scalar and vector potentials is necessary. Since no use will be made in this book of this representation, it will not be included here.

When the first Maxwell relation is written in terms of the potential function V it becomes

$$\text{div grad } V = \frac{-\rho}{\epsilon}$$

In this form it is known as Poisson's equation. If the charge density ρ is zero, the same equation is referred to as Laplace's equation.

5-2. EQUATIONS OF MOTION

Charged particles are accelerated in the direction of motion only by electric fields. Magnetic fields exert forces at right angles to the direction of particle motion and to the direction of the magnetic field. In vector notation the equation of motion of a particle of charge e and mass m in a combined electric and magnetic field is

$$\frac{d}{dt}(m\mathbf{v}) = e\mathbf{E} + e\mathbf{v} \times \mathbf{B} \tag{5-12}$$

In rectangular coordinates Eq. (5-12) becomes

$$\begin{aligned} \frac{d}{dt}(m\dot{x}) &= eE_x + e\dot{y}B_z - e\dot{z}B_y \\ \frac{d}{dt}(m\dot{y}) &= eE_y + e\dot{z}B_x - e\dot{x}B_z \\ \frac{d}{dt}(m\dot{z}) &= eE_z + e\dot{x}B_y - e\dot{y}B_x \end{aligned} \tag{5-13}$$

where the dots indicate differentiation with respect to time. In cylindrical coordinates Eq. (5-12) is

$$\begin{aligned} \frac{d}{dt}(m\dot{r}) - mr\dot{\theta}^2 &= eE_r + er\dot{\theta}B_z - e\dot{z}B_\theta \\ \frac{1}{r}\frac{d}{dt}(mr^2\dot{\theta}) &= eE_\theta + e\dot{z}B_r - e\dot{r}B_z \\ \frac{d}{dt}(m\dot{z}) &= eE_z + e\dot{r}B_\theta - er\dot{\theta}B_r \end{aligned} \tag{5-14}$$

All particle motions in accelerators follow from special cases of these equations. For nonrelativistic motion the mass m is a constant. For relativistic motion $m = m_0(1 - v^2/c^2)^{-\frac{1}{2}}$, where m_0 is the rest mass of the particle.

5-3. THE ELECTROSTATIC LENS

From early work on the formation of electron beams in X-ray tubes and other electronic devices it was well known that a sequence of accelerating electrodes with cylindrical symmetry had lens-like properties. This is a consequence of the radial components of the fields around and between the accelerating electrodes; these field components will act either to focus or to defocus deviant particles in the accelerated beam.

Early studies of ion-beam focusing by Tuve, Dahl, and Hafstad[1] were largely empirical and consisted of observations of the focal properties of a variety of electrode arrangements. The first accelerating gap between ion source and accelerating column was found to be the dominant lens. Studies were made with various sizes of cones, cylinders, and planes, and with one and two gaps. The properties of such electrostatic lenses were determined qualitatively as a function of electrode potentials and ion-beam energy. It was found that almost any arrangement of electrodes could give reasonably good focal properties if electrode potentials were properly adjusted. The results were used chiefly to design electrodes so that inconveniently high voltages were not required.

Buechner, Lamar, and Van de Graaff[2] investigated focusing by electrostatic lenses using photographic detection of the focused beam. They were able to show that beam divergence due to space-charge forces could be compensated by appropriate lens design. Eventually the group at the Massachusetts Institute of Technology was able to report focal spots as small as 1 mm in diameter at distances as great as 10 ft from the ion source. Important to this success were precise construction and alignment, large lens apertures, and carefully regulated electrode potentials.

In all this early work the results were largely empirical and applied only to the particular electrode configuration tested. It was difficult to separate the optical properties of the source and its electrodes from those of the accelerating tube.

The first attempts at theoretical analysis of electrostatic lenses came in the field of electron optics, stimulated by the requirements of electronic devices such as the cathode-ray tube and the electron microscope. Electron optics is now a mature field and its results are to be found in many textbooks, such as those written by Zworykin,[3] Pierce,[4] Cosslett,[5] and Terman.[6] We present here the basic treatment of electrostatic lenses with cylindrical symmetry around the beam axis.

We assume that, whatever is the particular electrode configuration, it yields a potential distribution along the z axis which we represent by

$$V(r = 0) = V_0(z) \tag{5-15}$$

Also we assume that this potential is referred to a zero at a point where the particle energy is zero so that V is a measure of particle energy. The

particle energy T in electron volts is given by $T = -V$. We now can satisfy Laplace's equation if we write for the potential in the region where r is not zero

$$V = V_0 - \frac{r^2}{4}\frac{d^2V_0}{dz^2} + \frac{r^4}{64}\frac{d^4V_0}{dz^4} - \cdots \tag{5-16}$$

From this potential function we can derive the axial and radial field components. For most lens systems it is necessary to retain only the leading terms in the expansions, so we shall use

$$\begin{aligned} E_z &= -\frac{dV_0}{dz} \\ E_r &= \frac{r}{2}\frac{d^2V_0}{dz^2} \end{aligned} \tag{5-17}$$

The radial equation of motion ($m\ddot{r} = eE_r$) can be written

$$m\ddot{z}\frac{dr}{dz} + m\dot{z}^2\frac{d^2r}{dz^2} = eE_r \tag{5-18}$$

But $$m\ddot{z} = eE_z = -e\frac{dV_0}{dz} \quad \text{and} \quad m\dot{z}^2 = -2eV$$

so Eq. (5-18) can be rewritten

$$Vr'' + \frac{V'r'}{2} + \frac{V''r}{4} = 0 \tag{5-19}$$

where the primes indicate differentiation with respect to z. This "paraxial ray equation" is well known in electron optics. It does not lend

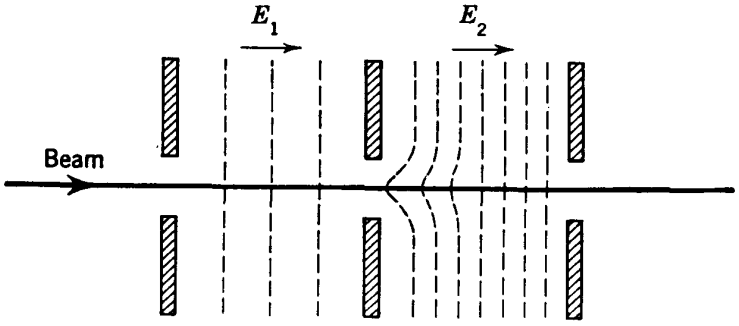

Fig. 5-1. Convergent aperture lens showing equipotentials for $E_2 > E_1$.

itself to precise solution, but it has been solved numerically for a variety of cases. The results can be found in great detail in Terman's Handbook.[6]

For weak lenses some of the properties of the electrostatic lens can be derived from approximate solutions of Eq. (5-19). Two types of lenses are of primary interest. The first type is the aperture lens shown in Fig. 5-1. In this lens the ray travels from a region of constant $E_z = E_1$ through an aperture into another region of constant $E_z = E_2$. Focusing

occurs in the region around the central aperture. The focusing region is short and the radial displacement of the particle does not change appreciably as it passes through this region. In this case it is appropriate to write Eq. (5-19) in the form

$$\frac{d}{dz} r'V + \frac{r^3}{4}\frac{d}{dz}\left(\frac{V'}{r^2}\right) = 0$$

In view of the approximate constancy of r, we can integrate this relation to give

$$\left(r'V + \frac{rV'}{4}\right)_{\text{final}} = \left(r'V + \frac{rV'}{4}\right)_{\text{initial}}$$

If, initially, the beam was traveling parallel to the axis so that the initial value of r' is zero and if we note that $(-r/r')_{\text{final}}$ is equal to the distance the beam will travel before it crosses the axis, we can rewrite the integrated equation in the form

$$\frac{1}{f} = -\left(\frac{r'}{r}\right)_{\text{final}} = \frac{V'_{\text{final}} - V'_{\text{initial}}}{4V} = \frac{E_2 - E_1}{4T} \qquad (5\text{-}20)$$

where V is the potential of the central diaphragm and f is the focal length of the system. We have thus shown that (for accelerating fields) if the second field is the stronger, the lens is converging; if the first field is stronger, the lens is diverging. If the fields are decelerating, the converse will be true.

A second type of electrostatic lens is that produced by the field between the ends of two coaxial cylinders. In Fig. 5-2 we show the case where the two cylinders have the same diameter. In the lower half of the figure, plots are included of V, V', and V'' along the axis of the system. Equally useful as lenses are other examples of this configuration in which the cylinders have different diameters. This lens class differs from the class described in the last paragraph in that the particle travels from a region of zero field, traverses the lens, and enters another region of zero field. Consequently, a different mathematical approach is appropriate. In this case we rewrite the paraxial ray equation (5-19) in the form

$$\frac{d}{dz} r'V^{1/4} + \frac{d}{dz} rV^{-3/4}V' + \tfrac{3}{16} rV'^2V^{-7/4} = 0$$

When this equation is integrated between entrance and exit points through the lens, the second term disappears since V' is zero initially and finally. In its integrated form the equation becomes

$$(r'V^{1/4})_{\text{final}} - (r'V^{1/4})_{\text{initial}} = -\frac{3}{16}\int_{\text{entrance}}^{\text{exit}} rV'^2V^{-7/4}\,dz$$

As in the previous case, the radial displacement r will not change appreciably during passage through the focusing region. Also, if the lens is weak, the difference in potential between the cylinders will be small compared with the absolute value of V. If the initial value of r' is zero (ray

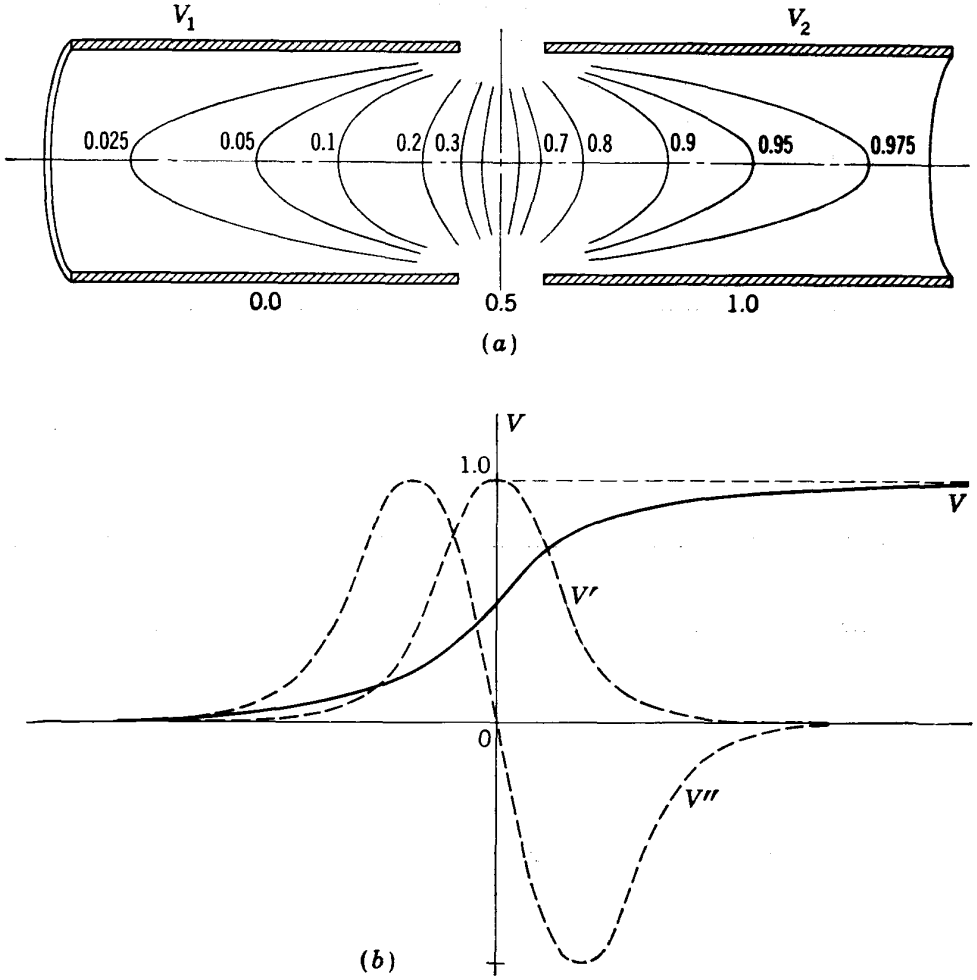

Fig. 5-2. (*a*) Two-cylinder lens showing equipotentials. (*b*) Variation of axial potential V and of its first (V') and second (V'') derivatives in the two-cylinder lens.

parallel to the axis), we can write the integrated equation in the approximate form

$$\frac{1}{f} = \frac{-r'_{\text{final}}}{r_{\text{initial}}} \cong + \frac{3}{16}\left(\text{avg value of } \frac{V'^2}{V^2}\right) \tag{5-21}$$

Since the right-hand side of this equation is always positive, lenses of this type are always converging lenses regardless of which cylinder has the higher potential.

This result could have been predicted on qualitative grounds. The character of the particle path through an accelerating and a decelerating

lens of this sort is shown in Fig. 5-3. In the accelerating lens the fields around the gap force the particle inward as it approaches the gap. At the gap it is accelerated, and it proceeds through slightly weaker radial fields pushing it outward. Its velocity is higher, so these weaker fields have even less effect and it is pushed outward less than it was originally deflected inward and leaves the lens with an inward component of radial velocity. In the decelerating lens the particle is pulled away from the axis as it approaches the gap. Leaving the gap with decreased velocity, it enters a focusing field stronger than it felt before, and it also leaves the lens with an inward velocity component.

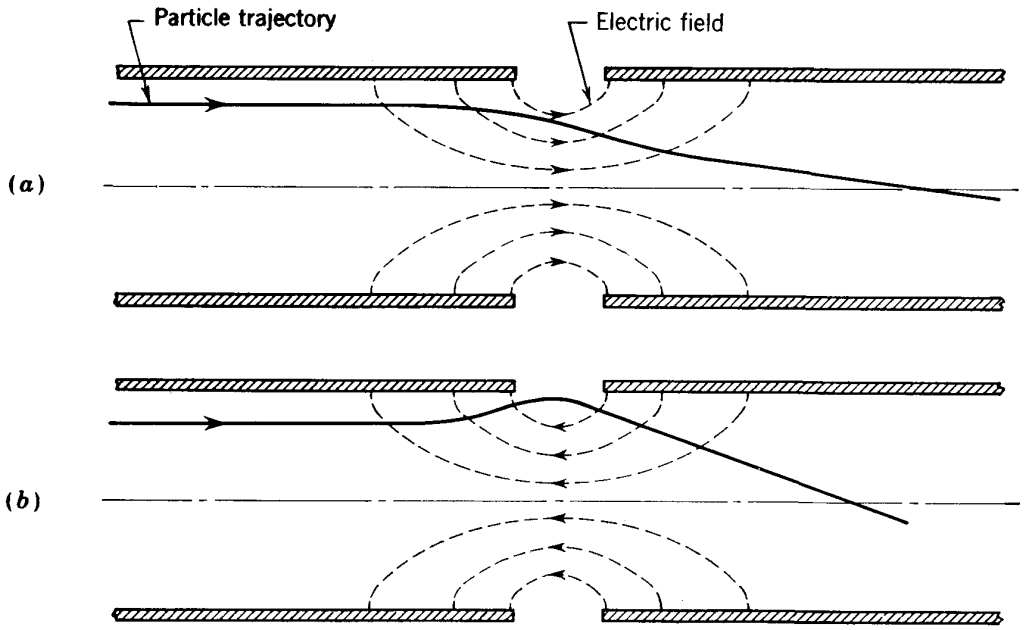

Fig. 5-3. Particle trajectories in (*a*) accelerating lens and (*b*) decelerating lens.

The focal lengths for accelerating and decelerating lenses of this type will differ slightly because of the somewhat different orbits traversed. In Fig. 5-4 focal lengths are plotted for lenses having cylinders of the same diameter for the two cases. The coordinates used are the ratio of focal length to cylinder diameter and the ratio of the cylinder voltages; with these units the plot is independent of units or dimensions. These graphs were obtained by numerical integration of the paraxial ray equation through fields computed for this particular geometry.

The theoretical approach presented above is somewhat naive; more sophisticated discussions will be found in the references cited. Detailed studies of electrostatic lenses show many analogies with optical lenses. A more precise treatment can be made to show the presence of principal planes and focal points similar in every way to the cardinal points of optical systems. Aberrations of the sorts observed in optical systems are also present. This is particularly true if the beam diameter is a large

fraction of the diameter of the focusing electrodes since, in this case, many of the assumptions made in the derivation of the paraxial ray equation are no longer valid.

The properties of a two-cylinder electrostatic lens are profoundly modified if a conducting grid is placed across the end of one of the cylinders. With a dense grid the field approaches that between a cylinder and a plane, effectively removing either the focusing or the defocusing half of the two-cylinder lens field. A grid across the second cylinder of an accelerating lens makes the lens strongly focusing; one across the end of

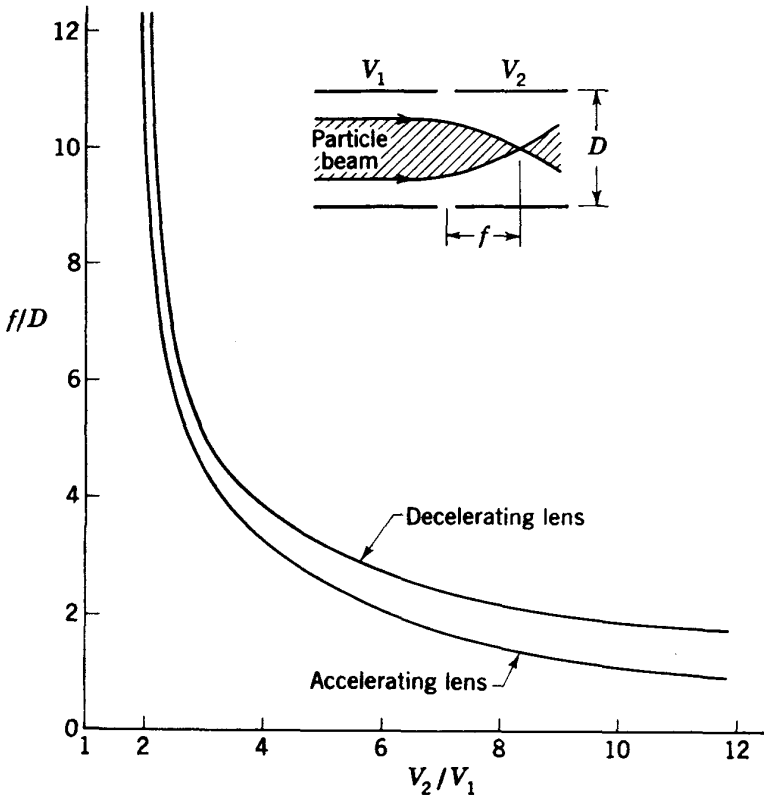

Fig. 5-4. Focal lengths for double-cylinder lenses.

the first cylinder makes it defocusing. The grid will obstruct a portion of the aperture and reduce beam transmission. Yet if the grid is made too transparent, field penetration through it will reduce its effectiveness. A practical compromise which does not reduce beam intensity unduly has made the grid lens useful for some linear-accelerator applications (see Chap. 10). Grids are used also in lens systems for focusing beams from accelerator ion sources.

Also of interest to the accelerator designer is the ion optical behavior of a uniform accelerating field with no radial components. In this system the particle trajectory is modified because the paraxial velocity is continually increasing although the radial velocity component is unaffected. Consequently a diverging beam tends to be slightly converged during

acceleration and a converging beam has its convergence slightly decreased. The general tendency during acceleration is to bring the beam closer to parallelism.

Many combinations of focusing fields have been used with the various direct-voltage accelerators. A typical system used in the Van de Graaff preaccelerator for the cosmotron (see Fig. 3-13) includes a probe electrode maintained at a potential of the order of -20 kv with respect to the ion source, a focus electrode maintained at about -10 kv, and an accelerate electrode at about -60 kv with respect to the ion source. The potential difference between source and probe is kept high to extract as large an ion current as possible. The diverging beam is decelerated in the focus electrode so that it can more easily be focused; then the beam (reduced in diameter and more nearly parallel) is carried through the accelerate electrode into the uniform field of the accelerating column. Electrode potentials are computed and adjusted to give the desired beam properties at the output of the accelerator. Usually this emergent beam will be approximately parallel and will be reduced in diameter from more than 1 cm at the probe electrode to 1 or 2 mm at full energy.

5-4. SPACE-CHARGE EFFECTS

If the density of charge is high in a beam to be focused by an electrostatic lens, it may be necessary to take the space-charge field into account in designing the lens. Since like charges repel each other, this is always a defocusing field; its effect can be included in the paraxial ray equation. We assume streamline flow in the beam so that, inside the radius defined by a particular particle path, the total current i is constant. To simplify the problem, we assume that the charge density is uniform as a function of radius, although it will vary as a function of z. With these assumptions the charge density is given in terms of the current by

$$\rho = \frac{i}{\pi r^2 v} \tag{5-22}$$

where v is the particle velocity and is given by $v = (-2eV/m)^{1/2}$. The potential pattern in the beam must now satisfy Poisson's equation rather than Laplace's equation. Poisson's equation states that

$$\frac{1}{r}\frac{\partial}{\partial r} rE_r + \frac{\partial E_z}{\partial z} = \frac{\rho}{\epsilon}$$

which indicates that E_r now has the value

$$E_r = \frac{rV''}{2} + \frac{i}{2\pi\epsilon r(-2eV/m)^{1/2}}$$

instead of the value $rV''/2$ given by Eq. (5-17). When the new radial field is inserted in the derivation of the paraxial ray equation, we obtain

$$Vr'' + \frac{V'r'}{2} + \frac{1}{4}\left[r\,V'' + \frac{i}{\pi\epsilon r(-2eV/m)^{1/2}}\right] = 0 \qquad (5\text{-}23)$$

The new term introduces severe limits because it indicates a defocusing radial field that goes to infinity as r tends to zero. Thus it would appear that a beam of appreciable density can never be brought to a focus. This is not strictly true, since our simplifying assumptions are not usually justified to this degree. However, it is good practice not to attempt to include beam crossovers in lens systems for intense beams. For weak lenses in which the beam is not strongly concentrated and in which r and V do not change drastically during passage through the focusing region, it is quite possible to include the space-charge term as a correction term in computing the lens optics.

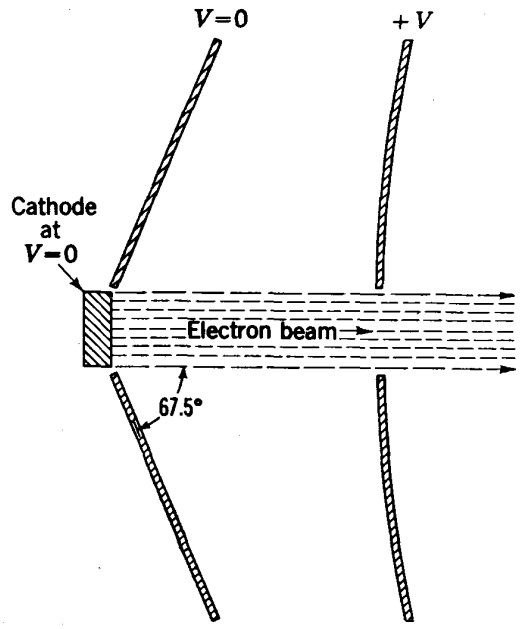

Fig. 5-5. Pierce electron gun with electrodes shaped to make $V \propto z^{4/3}$ along the edges of the electron beam.[4]

The special case of a lens system to keep a beam parallel in the presence of space charge follows from setting $r'' = r' = 0$ in Eq. (5-23). The equation is satisfied if, along the boundary of the beam, V is proportional to $i^{2/3}z^{4/3}$. Electrode structures which satisfy this criterion have been worked out by Pierce (see Fig. 5-5).[4] An electron gun designed in this

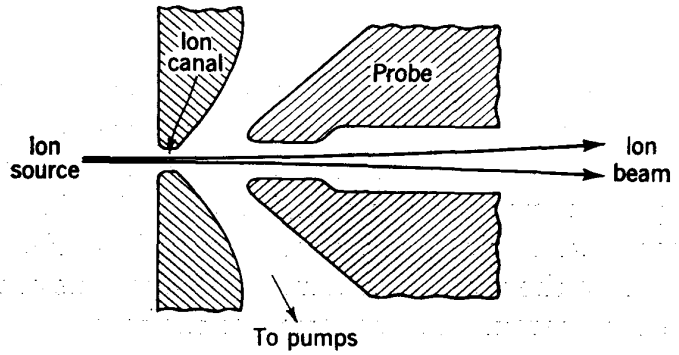

Fig. 5.6. Pierce lens for extracting ions from an ion source.

fashion is usually known as a "Pierce gun." Many variations of Pierce's electrode geometries have been evolved for maintaining desired convergence or divergence in dense charged-particle beams. The problem of

space-charge limitation is most frequently encountered in accelerators at the exit of the ion source where high currents of low-velocity ions are to be extracted through small apertures. Here the Pierce electrode shape is usually modified to a reentrant cone (Fig. 5-6). The tip of the probe or first accelerating electrode is then formed as shown as a reentrant coaxial cone with a somewhat larger aperture at its tip. If desired, the space between source and probe can then be connected to a vacuum pump to evacuate the gas coming from the source.

5-5. FOCUSING BY AXIAL MAGNETIC FIELDS

Although the mathematical method for treating the magnetic lens is analogous to that just used for the electrostatic lens, the mechanism of the magnetic lens is quite different. This lens usually takes the form shown in Fig. 5-7. A solenoid coaxial with the beam, and usually sheathed in iron to decrease stray magnetic fields, provides a magnetic field generally parallel to the axis but having radial components at its ends. We assume that the entering beam has only axial and radial components of velocity. As the beam crosses the radial-magnetic-field components at the entrance to the lens, the cross-product interaction between these field components and the particle velocity [Eq. (5-12)] introduces a corkscrew motion into the beam. Inside the solenoid both the angular and the radial velocity components of this corkscrew motion interact with the axial magnetic field to give further spiral motion around the axis. Finally the radial field at the exit introduces further cross-product interaction with the axial velocity. This sounds complicated, but the mathematical treatment yields a simple result. Just as in the electrostatic case, we set up expansions of the radial and axial field components in terms of a general axial field distribution $B_z(r = 0) = B_0(z)$. We introduce these fields into the radial and azimuthal equations of motion (5-14) and arrive at a new paraxial ray equation of the form

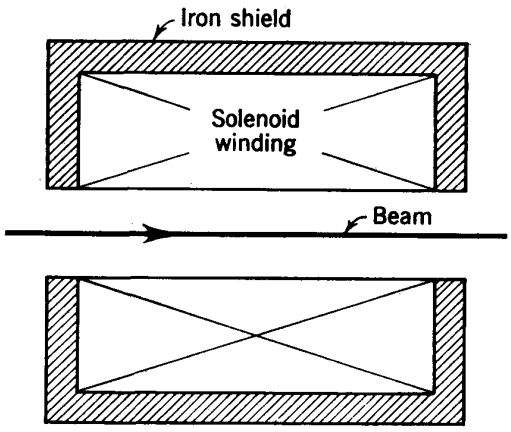

Fig. 5-7. Cross section of a cylindrical magnetic lens for focusing by an axial magnetic field.

$$r'' + \frac{eB_0^2 r}{8mT} = 0 \tag{5-24}$$

If the magnetic field is approximately uniform throughout the length of the lens, the solution to the ray equation is a sinusoidal oscillation in

radius and it will be possible to choose the lens length so that the system is either focusing or defocusing.

Because of the focusing mechanism, the beam will be rotated around its axis as it passes through the lens. If the beam was not originally symmetrical around the axis, the asymmetry will be rotated during the focusing process. With initially symmetrical beams this effect will be observable only through rotational velocity components left in the beam after it has been focused. The amount of the rotation can be derived from the relations used in the derivation of Eq. (5-24).

If very strong magnetic fields are used, the restoring forces indicated by Eq. (5-24) become very strong and the radial extent of the beam is small. Even in the presence of dense space charge a beam can be restrained from expanding by such an axial magnetic field. This is the mechanism (see Chap. 4) used in many ion sources to keep the ionizing electrons in the discharge from escaping.

Short magnetic solenoid lenses are also used where it is desirable to minimize the physical extent of the lens system. The field is confined to a short axial gap between the end plates of the iron sheath. The length of the uniform-field region is greatly reduced relative to the nonuniform end fields. The focal length of a short magnetic lens can be derived approximately if it is assumed that the magnetic flux density $B = B_0$, a constant, for a distance d in the middle of the lens and is zero elsewhere. The paraxial ray equation (5-24) can now be integrated and the focal length f of the lens can be derived. The result is

$$f = \frac{8mT}{eB_0^2 d} \tag{5-25}$$

where T is the kinetic energy of the particles in electron volts. If the exciting winding includes NI amp-turns, then, since $B_0 d = \mu_0 NI$,

$$f = \frac{8mTd}{e\mu_0^2 N^2 I^2} \tag{5-26}$$

For electrons $f \cong 30Td/(NI)^2$; for protons $f \cong 53{,}000Td/(NI)^2$. As an example we consider a magnetic lens to have a focal length of 1 m. Magnetic field will be maintained over a distance of 3 cm along the axis, and the particles to be focused will have an energy of 1 Mev. From the above relations, a lens for electrons will require about 900 amp-turns to maintain a flux density of about 4×10^{-2} weber/m^2 (400 gauss). For protons the lens will require 40,000 amp-turns and will have a flux density of about 1.6 webers/m^2 (16,000 gauss).

5-6. EDGE FOCUSING

Wherever particle beams enter or leave magnetic fields, the fringing fields and pole geometry will affect the beam optics. Under certain

conditions the magnet may act as a lens that can be converging in both planes.

First we consider the beam optics in the plane normal to the direction of the magnetic field. A parallel beam will be assumed to enter normally a region of field bounded by the lines A and B of Fig. 5-8. As the beam enters the field, its direction is unaltered. Had the other boundary been the line C parallel to A, the beam would also emerge as a parallel beam, though somewhat reduced in cross section. But, since the line B is inclined at an angle θ with respect to C (or A), the upper part of the beam has been deflected through a larger angle than has the lower part and the beam will emerge converging. By some rather simple geometric construction the reader will easily discover that the distance f_1 from the boundary B to the focal or crossover point of the beam is given by

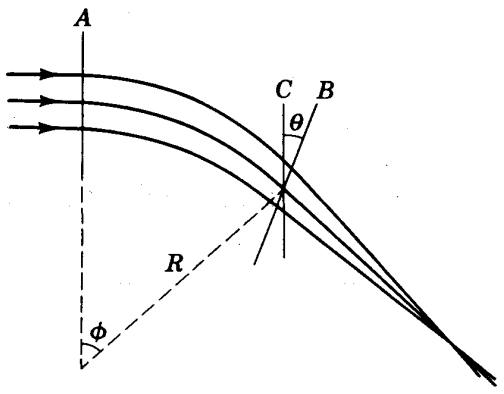

Fig. 5-8. Passage of initially parallel beam through an edge-focusing lens.

$$f_1 = \rho \frac{\cos(\phi - \theta)}{\sin \theta} \tag{5-27}$$

where ρ is the radius of the curvature of the beam in the magnetic field and ϕ is the angle through which the axial ray of the beam is bent in the magnetic field.

In the other plane the focal properties of the field are not so evident. In this plane the field well inside the magnet has no appreciable effect; here only the fringing field is important. We assume a coordinate system whose origin of coordinates is at the point where the axial ray crosses the boundary B. The y axis is parallel to B, the x axis is normal to B in the plane of the diagram, and the z axis is normal to the plane of the diagram. The fringing field will now have x and z components; from symmetry there will be no y component. Focusing effects will follow from interactions of the beam with the x component of the fringing field B_x. From Eqs. (5-13)

$$\frac{d}{dt}(m\dot{z}) = -e\dot{y}B_x \tag{5-28}$$

We now need some clue as to the form of B_x. From experience we know that the z component B_z will have in the xy plane the general character shown in Fig. 5-9. Above and below this plane it will decrease gradually and symmetrically around the median xy plane. We can represent this

behavior by the expression

$$B_z = f(x) - \frac{z^2}{2!} f''(x) + \frac{z^4}{4!} f''''(x) \cdots$$

To satisfy Maxwell's equations, B_x must now have the form

$$B_x = zf'(x) - \frac{z^3}{3!} f'''(x) + \cdots$$

To a first approximation, good enough for the present purpose, we can say, so long as z is small,

$$\begin{aligned} B_z &= f(x) \\ B_x &= zf'(x) \end{aligned} \qquad (5\text{-}29)$$

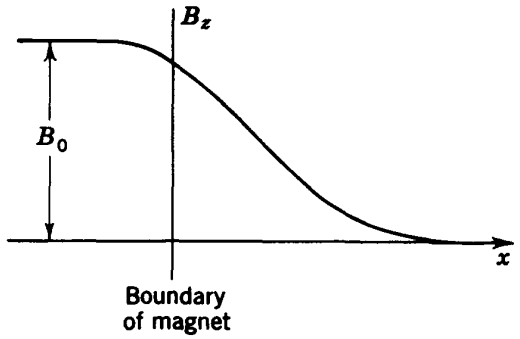

Fig. 5-9. Distribution of magnetic field around the edge of a magnet gap.

When this is substituted in Eq. (5-28), it becomes

$$\begin{aligned} \frac{d}{dt}(m\dot{z}) &= -e\dot{y}zf'(x) \\ &= -ez\left(\frac{\dot{y}}{\dot{x}}\right)\frac{d}{dt}[f(x)] \end{aligned} \qquad (5\text{-}30)$$

During passage through the fringing field, $\dot{x}$, $\dot{y}$, and z of the beam are sensibly unchanged. Moreover, if v is the velocity of the particles in the beam, $\dot{x} = v\cos(\phi - \theta)$ and $\dot{y} = v\sin(\phi - \theta)$. Hence Eq. (5-30) can be integrated to give

$$\begin{aligned} m\dot{z}_{\text{final}} - m\dot{z}_{\text{initial}} &= ez\tan(\phi - \theta)[f(x)_{\text{final}} - f(x)_{\text{initial}}] \\ &= ez\tan(\phi - \theta)(0 - B_0) \end{aligned}$$

where B_0 is the field strength well inside the magnet. The beam has thus been deflected by an angle

$$\begin{aligned} \frac{\dot{z}}{v} &= -\frac{eB_0}{mv} z\tan(\phi - \theta) \\ &= -\frac{z}{\rho}\tan(\phi - \theta) \end{aligned}$$

and the focal distance f_2 in the vertical plane is given by

$$f_2 = \frac{zv}{\dot{z}} = \rho\cot(\phi - \theta) \qquad (5\text{-}31)$$

A range of the angles ϕ and θ exists over which Eqs. (5-27) and (5-31) indicate focusing in both planes. By inclining the entrance plane of the magnet to the beam, similar focusing can be attained as the beam enters the magnet.

Focusing of this sort is used to restrain the excursions of the circulating beam in the zero-gradient synchrotron (ZGS) of the Argonne National Laboratory. Edge-focusing effects are included also in the fixed-field alternating-gradient (FFAG) designs presented in Sec. 15-10. In many other cases where beams pass through analyzing magnets this effect must be included in analysis of the beam optics.

5-7. FOCUSING BY ALTERNATING GRADIENTS

The most recently discovered technique for restraining the radial motions in beams of charged particles is that of alternating-gradient (AG) focusing. Since it gives much stronger restraining forces than most of the other available methods, it has often been described as "strong focusing." The basic principle as it applied to magnetic-gradient focusing in the synchrotron was first proposed by Christofilos in Athens, Greece, in 1950, in a manuscript which was not published. The principle was independently discovered in 1952 by Courant, Livingston, and Snyder[7] at Brookhaven National Laboratory and expanded to cover the application of magnetic gradients to the focusing of linear beams. Blewett,[8] also at Brookhaven, presented the basic formulation for focusing with electrostatic gradient fields. When Christofilos became aware of the Brookhaven publications and visited the laboratory to compare notes, his priority was immediately evident and was acknowledged by the Brookhaven group early in 1953.[9] He later joined the Brookhaven laboratory and has been active in the further development of accelerators using this principle. The theoretical formulations and techniques have been improved and generalized for the magnetic-field application[10] (see Chap. 15). It seems more appropriate in this chapter to start with the specialized application to the focusing of linear beams in electrostatic gradient fields.

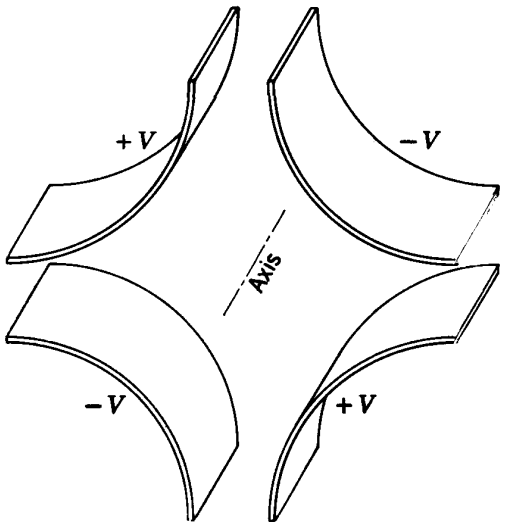

Fig. 5-10. Electrostatic quadrupole lens for use in AG focusing.

If a beam of charged particles whose axis is the z axis passes through a region where the transverse field E_x has the form $E_x = -Gx$, G being a constant, the beam will be focused in the xz plane. But, since div **E** must be zero, it follows that E_y must have the form $E_y = +Gy$ and the beam will be equally strongly defocused in the y plane. The discovery of AG

focusing revealed the fact that if the beam now passes through a second region of reversed gradients in which $E_x = +Gx$ and $E_y = -Gy$, the net effect of the combination will be focusing in both planes. As was pointed out by the Brookhaven group, the system has its analogy in optics, where it has long been known that a beam of light passing in succession through focusing and defocusing lenses of equal but opposite strength will be focused no matter which lens comes first.

The field pattern just described is derivable from a potential function having the form

$$V = \frac{G}{2}(x^2 - y^2) \tag{5-32}$$

The equipotentials are rectangular hyperbolas, so such a field pattern can be set up by a quadrupole system of electrodes having the shape shown in Fig. 5-10.

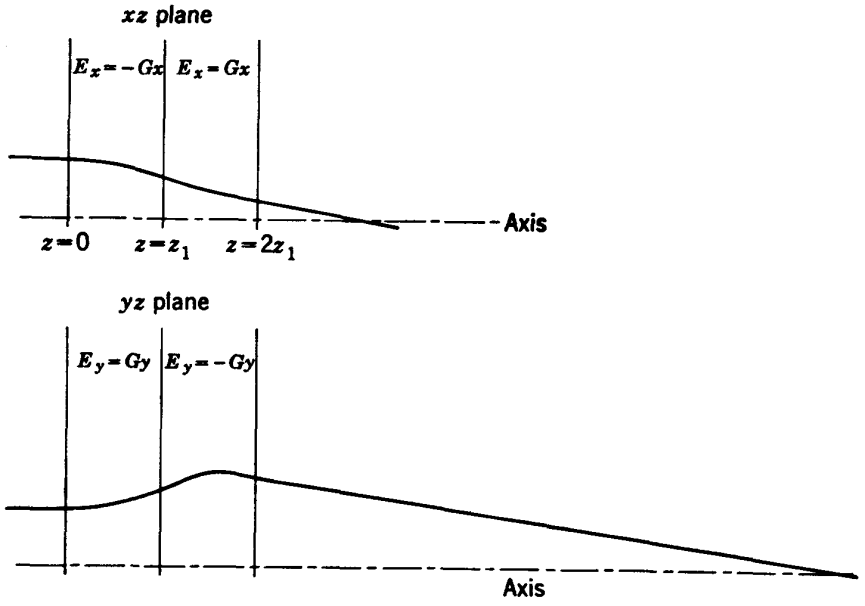

Fig. 5-11. Focusing in a two-element AG lens having $k = 0.5$ and $kz_1 = 45°$.

The precise behavior of the system can be derived by tracing a particle through the system geometry (see Fig. 5-11). In the xz plane the equation of motion in the first region is

$$m\ddot{x} = -eGx \tag{5-33}$$

whose solution is

$$\begin{aligned} x &= x_0 \cos\left(\frac{eGt^2}{m}\right)^{1/2} + \dot{x}_0\left(\frac{eG}{m}\right)^{-1/2} \sin\left(\frac{eGt^2}{m}\right)^{1/2} \\ &= x_0 \cos\left(\frac{eGz^2}{mv^2}\right)^{1/2} + \dot{x}_0\left(\frac{eG}{m}\right)^{-1/2} \sin\left(\frac{eGz^2}{mv^2}\right)^{1/2} \end{aligned} \tag{5-34}$$

where the zero subscripts indicate the initial conditions.

At $z = z_1$ the position and velocity of the particle are given by

$$\begin{aligned} x &= x_0 \cos kz_1 + \frac{\dot{x}_0}{kv} \sin kz_1 \\ \frac{\dot{x}}{v} &= -kx_0 \sin kz_1 + \frac{\dot{x}_0}{v} \cos kz_1 \end{aligned} \tag{5-35}$$

where $k = (eG/mv^2)^{1/2}$. Equations (5-35) can be written in the form of a matrix transformation:

$$\begin{vmatrix} x \\ \dot{x}/v \end{vmatrix} = \begin{vmatrix} \cos kz_1 & (1/k) \sin kz_1 \\ -k \sin kz_1 & \cos kz_1 \end{vmatrix} \begin{vmatrix} x_0 \\ \dot{x}_0/v \end{vmatrix} \tag{5-36}$$

If the sign of the gradient G is reversed, the transformation matrix becomes

$$\begin{vmatrix} \cosh kz_1 & (1/k) \sinh kz_1 \\ k \sinh kz_1 & \cosh kz_1 \end{vmatrix} \tag{5-37}$$

The displacement and velocity of the particle after passage through the two successive field regions can now be written

$$\begin{aligned} \begin{vmatrix} x \\ \dot{x}/v \end{vmatrix} &= \begin{vmatrix} \cosh kz_1 & (1/k) \sinh kz_1 \\ k \sinh kz_1 & \cosh kz_1 \end{vmatrix} \begin{vmatrix} \cos kz_1 & (1/k) \sin kz_1 \\ -k \sin kz_1 & \cos kz_1 \end{vmatrix} \begin{vmatrix} x_0 \\ \dot{x}_0/v \end{vmatrix} \\ &= \begin{vmatrix} x_0(\cosh kz_1 \cos kz_1 - \sinh kz_1 \sin kz_1) + \frac{\dot{x}_0}{kv} (\cosh kz_1 \sin kz_1 + \sinh kz_1 \cos kz_1) \\ kx_0 (\sinh kz_1 \cos kz_1 - \cosh kz_1 \sin kz_1) + \frac{\dot{x}_0}{v} (\cosh kz_1 \cos kz_1 + \sinh kz_1 \sin kz_1) \end{vmatrix} \end{aligned} \tag{5-38}$$

In the yz plane the particle position and velocity are obtained by applying the transformation matrices in the reverse order to obtain

$$\begin{aligned} &\begin{vmatrix} y \\ \dot{y}/v \end{vmatrix} \\ &= \begin{vmatrix} y_0(\cosh kz_1 \cos kz_1 + \sinh kz_1 \sin kz_1) + \frac{\dot{y}_0}{kv} (\cosh kz_1 \sin kz_1 + \sinh kz_1 \cos kz_1) \\ ky_0(\sinh kz_1 \cos kz_1 - \cosh kz_1 \sin kz_1) + \frac{\dot{y}_0}{v} (\cosh kz_1 \cos kz_1 - \sinh kz_1 \sin kz_1) \end{vmatrix} \end{aligned} \tag{5-39}$$

It is not immediately evident from these rather complex expressions that we have achieved focusing in both planes. This fact can be made clear if we make the simplifying assumption that kz_1 is small enough that we can use the approximate substitutions

$$\begin{aligned} \cosh kz_1 &= 1 + \frac{(kz_1)^2}{2} \\ \cos kz_1 &= 1 - \frac{(kz_1)^2}{2} \\ \sinh kz_1 &= kz_1 \left[1 + \frac{(kz_1)^2}{6} \right] \\ \sin kz_1 &= kz_1 \left[1 - \frac{(kz_1)^2}{6} \right] \end{aligned}$$

We consider a beam that is initially parallel so $\dot{x}_0 = \dot{y}_0 = 0$. Now, to the order of the approximation

$$\begin{aligned} x &= x_0(1 - k^2 z_1^2) \\ \frac{\dot{x}}{v} &= -\tfrac{2}{3} x_0 k^4 z_1^3 \\ y &= y_0(1 + k^2 z_1^2) \\ \frac{\dot{y}}{v} &= -\tfrac{2}{3} y_0 k^4 z_1^3 \end{aligned} \tag{5-40}$$

The two velocities are equal for the same initial displacements and both are directed toward the axis.

In Fig. 5-11 we have traced the orbits in the two planes for the particular case $k = 0.5$ and $kz_1 = 45°$. From the figure it can be seen that the greatest displacement occurs in the focusing sector in both planes; the

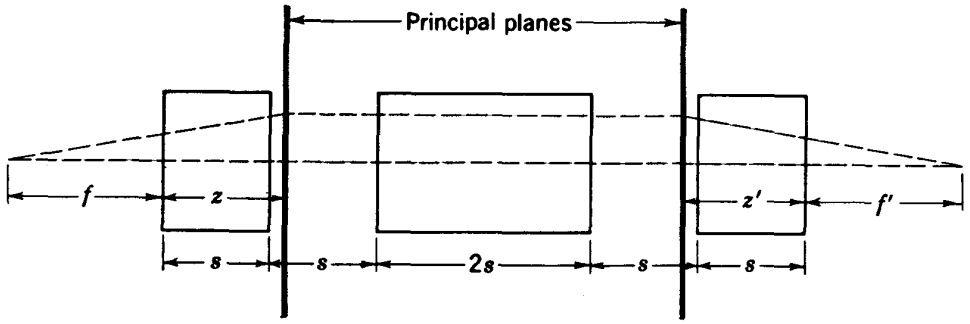

Fig. 5-12. Triplet AG lens. Principal planes and focal distances are indicated.

particle thus experiences the strongest force when it is in the sector where the force is directed toward the axis.

The same focusing effects can be obtained if a field-free space is included between the two sectors, as is necessary in the physical arrangement of electrodes or quadrupole magnets. Analysis of the system becomes a little more complicated but is still manageable, and the applied fields are somewhat reduced.

As can be seen from Fig. 5-11, the two-element AG lens is highly astigmatic; the focal points in the two planes are at very different locations. This means that a beam initially circular in cross section will pass through a focal line in the yz plane and somewhat later will pass through a focal line in the xz plane. When better optical properties are desired, it is preferable to use triplet lenses. A favorite triplet-lens arrangement is illustrated in Fig. 5-12; the three elements of the lens can be equal in length or, as in the case illustrated, the central element can be longer; here it is twice as long as the two other elements.

Alternating-gradient lenses can be analyzed by the methods of geometric optics in terms of focal lengths and principal planes. If focal distances f and f' are defined as distances of focal points from the extreme ends of the lens array and the distances of the principal planes from the

ends of the array are represented by z and z' (Fig. 5-12), it will be found that these parameters satisfy the relation

$$\frac{1}{f' + z'} + \frac{1}{f + z} = \frac{1}{F}$$

where F, z, and z' are constants for all values of f and f'. Thus the parameters F, z, and z' are constants for the lens system. Moreover, if the fields in the first and last lens element are equal, it will be found that $z = z'$.

Tabulations of F, z, and z' have been assembled at the Brookhaven National Laboratory for a variety of AG lenses with two and three elements and with various spacings between elements. Typical figures for the lens illustrated in Fig. 5-12 are collected in Table 5-1.

TABLE 5-1
PARAMETERS FOR THE TRIPLET LENS OF FIG. 5-12

$k_1^2 = eG_1/(mv^2)$ and refers to the first and third lens element
$k_2^2 = eG_2/(mv^2)$ and refers to the central lens element

Initially focusing plane					
$k_1 s$	$2k_2 s$ =	0.4	0.8	1.2	1.6
0.4	F/s =	6.258	17.56	−6.259	−1.753
	z/s =	4.584	4.486	4.344	4.181
0.8	F/s =	−1.904	−1.825	−1.704	−1.555
	z/s =	−5.143	−5.340	−5.672	−6.143
1.2	F/s =	−0.2250	−0.1908	−0.1487	−0.1092
	z/s =	−0.8047	−0.8157	−0.8328	−0.8548
1.6	F/s =	−0.0901	−0.0736	−0.0547	−0.0384
	z/s =	−0.1767	−0.1804	−0.1861	−0.1933
Initially defocusing plane					
$k_1 s$	$2k_2 s$ =	0.4	0.8	1.2	1.6
0.4	F/s =	−3.240	8.968	1.477	0.8207
	z/s =	2.269	2.291	2.332	2.402
0.8	F/s =	−0.2997	−0.5783	1.973	0.3561
	z/s =	1.374	1.380	1.390	1.407
1.2	F/s =	−0.0573	−0.0888	−0.3976	0.1476
	z/s =	0.8985	0.8999	0.9025	0.9069
1.6	F/s =	−0.0144	−0.0208	−0.0579	0.0629
	z/s =	0.6524	0.6528	0.6536	0.6548

If the expressions (5-38) and (5-39) are examined for higher values of kz_1 than those which are suitable for the approximation applied to yield the results of Eqs. (5-40), it will be discovered that the AG system discussed above is not always a focusing system. When kz_1 passes the value of π, the system suddenly becomes strongly defocusing. For still higher values of kz_1 the combination can again become focusing, but these higher-order systems have no advantage over the systems which keep kz_1 below π.

The AG method is a powerful means for maintaining beams over long distances. Quadrupole lenses can be arranged in an AG sequence involving many quadrupoles. When this is done, it can be shown by the methods of matrix analysis[10] that the condition for continuous focusing is that $\cosh kz_1 \cos kz_1$ must lie between -1 and $+1$. If the gradients in successive lens elements are different, the condition becomes more complicated but will also be found in the reference cited.

The method is equally powerful if magnetic quadrupoles are used. The theoretical treatment is essentially the same as that given above except that the electric-field gradient must be replaced by the product of particle velocity and magnetic-field gradient.

The most spectacular application of AG focusing is in the AG synchrotron (Chap. 15). The method is also applicable to the linear accelerator (Chap. 10). It would appear also to be promising for beam focusing in direct-voltage accelerators. A practical technique might result from the use of permanent-magnet quadrupoles along the accelerating column. Permanent-magnet quadrupoles of Ferroxdur or Indox (nonconducting permanent-magnet ceramics) have been produced at Brookhaven.[11] A theoretical study of AG focusing in accelerating tubes has been made at the University of California Radiation Laboratory. Since both studies have given encouraging results, it would appear that it is only a matter of time until the permanent-magnet-quadrupole technique becomes practical.

5-8. THE CONCEPT OF EMITTANCE AND LIOUVILLE'S THEOREM

Particle beams in general are not the idealized assemblies of parallel rays thus far represented. They do not come to perfect focal points, but because of imperfections in the methods of beam generation, they can be focused only into regions of finite size. When every attempt has been made to make a beam parallel, the particles will still have a finite angular distribution. Generally it will be found that, if the individual particles are plotted as points in a region where, say, the x component of velocity is plotted against the x coordinate, the particles will all lie in a region like that illustrated in Fig. 5-13, having, for most beams, a generally elliptical shape. A similar plot will be found in the other plane, although the shape

and orientation of the region will probably be different. If the beam is passed through lenses or is otherwise affected by fields, or if it is merely allowed to drift, the shape of the region enclosing the particles will change. But it will be found, in linear systems, that the area of the region is constant. This constant area is a characteristic of the beam and is known as the "emittance" of the beam. So long as the energy of the beam is not changed, the emittance will be constant.

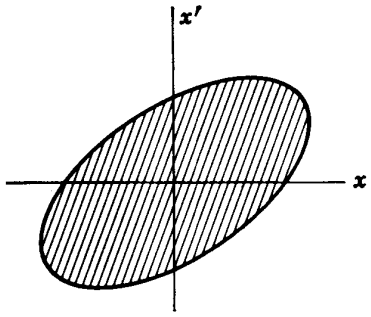

Fig. 5-13. Emittance plot in x-x' phase space.

A lens system whose defining apertures are such that it can barely accept a beam of a given emittance is said to have an "admittance" equal to the emittance of the beam that it can accept.

The constancy of the emittance of a beam is a consequence of Liouville's theorem, which says that the area in phase space occupied by an assembly of particles whose properties p_k and q_k are derivable from a Hamiltonian H by the relations

$$\frac{dp_k}{dt} = -\frac{\partial H}{\partial q_k} \qquad \text{and} \qquad \frac{dq_k}{dt} = +\frac{\partial H}{\partial p_k}$$

will remain constant throughout the motion. For the proof of this theorem the reader is referred to texts on the classical statistics. Here the application is evident since positions and momenta of particles are derivable from a Hamiltonian representing the total energy, kinetic and potential, of the system. Strictly speaking the phase space is a six-dimensional space for particle beams. But if the motions in the three planes are not coupled, two-dimensional plots like that in Fig. 5-13 are useful and represent areas that remain constant through systems of lenses and deflecting fields.

Other cases will emerge later in which other pairs of conjugate variables will yield constant areas in "phase space" plots. Energy and time are often found to be such variables.

5-9. ORBITS IN UNIFORM MAGNETIC FIELDS

In a uniform magnetic field the simplest form of motion of a charged particle which satisfies the equation of motion (5-12) is circular motion at constant velocity in a plane normal to the magnetic field. The equation of motion in cylindrical coordinates simplifies to

$$mr\dot{\theta} = erB \tag{5-41}$$

where $B = -B_z$ = a constant. Since $r\dot{\theta} = v$, the particle velocity, Eq. (5-41) represents the linear momentum of the particle, which is propor-

tional to the product Br. The motion can be visualized by reference to Fig. 5-14, in which the cylindrical coordinates of circular motion (r, θ, and z) represent the radius of the circular orbit, the angular location, and the distance from the central orbit plane of a particle between the poles of an electromagnet which produces an axial field B_z.

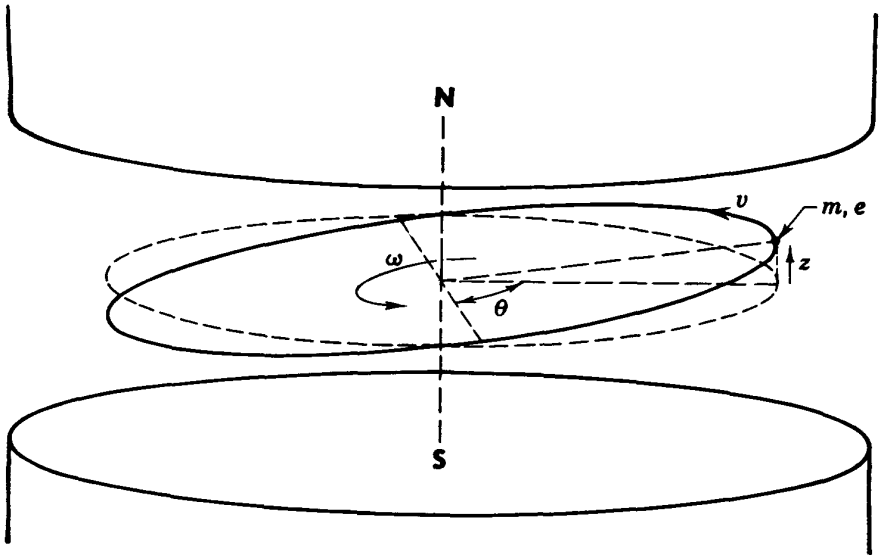

Fig. 5-14. Cylindrical coordinates for orbital motion in a magnetic field. A particle of mass m, charge e, and velocity v in a magnetic field B moves in a circle of radius r. The angular position θ and the axial displacement z are shown.

The frequency of revolution of the particle can be obtained from the momentum relation as

$$f = \frac{\dot{\theta}}{2\pi} = \frac{eB}{2\pi m} \tag{5-42}$$

This linear relation between frequency of particle revolution and magnetic field shows that frequency is constant in a uniform and steady magnetic field if the mass of the particle remains constant, i.e., for nonrelativistic velocities. This relation determines the applied frequency of the accelerating electric field in the cyclotron and is known as the cyclotron resonance relation.

For light positive ions having energies less than about 20 Mev, the nonrelativistic expression for kinetic energy can be used, from which we have

$$T = \tfrac{1}{2}mv^2 = \frac{e^2r^2B^2}{2m} \tag{5-43}$$

In this energy range the kinetic energy increases with the square of magnetic field and the square of the orbit radius. In the mks system of units, kinetic energy is measured in joules. We shall more often have occasion

to define kinetic energy as

$$\frac{T}{e} = \frac{\frac{1}{2}mv^2}{e} = \frac{er^2B^2}{2m} \tag{5-44}$$

In this form the kinetic energy is measured in electron volts or, if we wish to include the appropriate factor, in millions of electron volts. This definition assumes the charge to be that of a single electron. If multiply charged ions are involved (such as He^{++}), the numerical value of T/e in Mev units must be divided by the multiplicity of charge to obtain the kinetic energy.

The radii of orbits can be obtained from a rearrangement of the above relation:

$$r = \frac{10^3}{B}\left(2\frac{m}{e}\frac{T}{e}\right)^{\frac{1}{2}} \tag{5-45}$$

where B is in webers/m^2, e/m is in coulombs/kg, and T/e is in Mev units for a singly charged particle. Orbit radii obtained from this relation for H^+, D^+, H_2^+, and He^{++} ions in a magnetic field of 1 weber/m^2 are plotted in Fig. 5-15 to illustrate the dimensional requirements for accelerators in

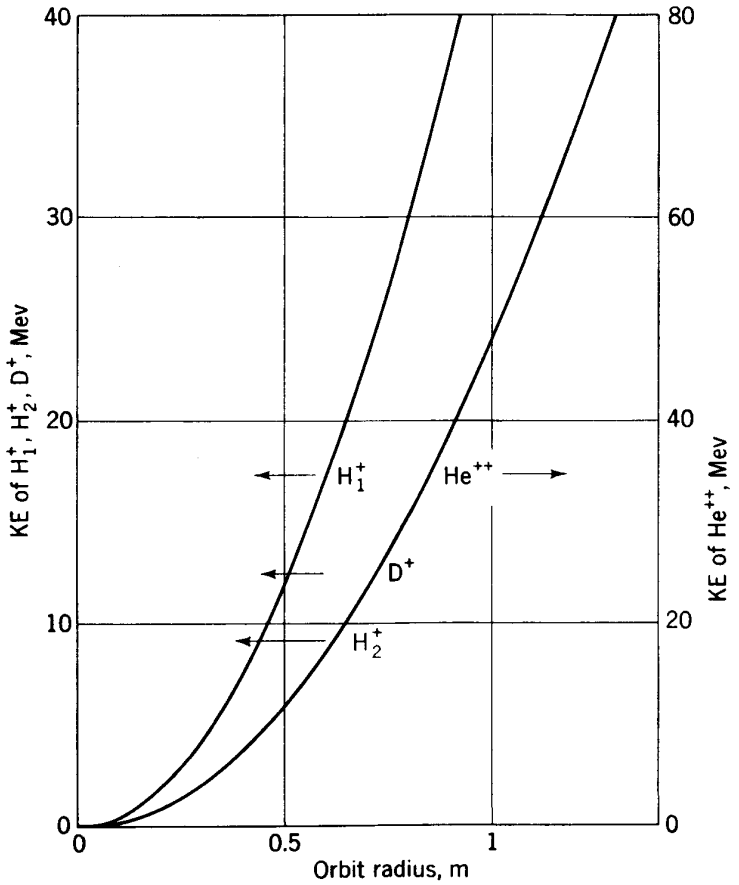

Fig. 5-15. Orbit radii (meters) for light ions in a magnetic field $B = 1.0$ weber/m^2 as a function of energy in Mev.

the nonrelativistic energy region. The influence of multiple charge is illustrated by the curve for He^{++}, which is essentially identical with that for H_1^+, although the charge-to-mass ratio e/m has a value approximately the same as that of the H_2^+ or D^+ ions.

5-10. RELATIVISTIC EQUATIONS OF MOTION

The motion of particles at high energies is also described by Eq. (5-41), but in this case the momentum must be expressed in its relativistic form. The relativistic expression for total energy W of a particle is

$$W = mc^2 = \frac{m_0c^2}{(1 - v^2/c^2)^{1/2}} = W_0 + T = m_0c^2 + T \tag{5-46}$$

whence

$$\frac{v}{c} = \left(1 - \frac{W_0^2}{W^2}\right)^{1/2} \tag{5-47}$$

The momentum p of a relativistic particle is given by

$$p = mv = \frac{m_0v}{(1 - v^2/c^2)^{1/2}} = \frac{1}{c}(W^2 - W_0^2)^{1/2} = \frac{1}{c}[T(T + 2W_0)]^{1/2} \tag{5-48}$$

where m_0 = rest mass of particle
c = velocity of light
W_0 ($= m_0c^2$) = rest energy of particle
T = kinetic energy of particle

Values of rest energy W_0 in Mev units are given in Table 5-2 for the particles used in accelerators.

TABLE 5-2

Particle	*Rest energy, Mev*
Electron	0.511
Hydrogen atomic ion (proton)	938
Heavy hydrogen atomic ion (deuteron)	1877
Hydrogen molecular ion	1876
Doubly ionized helium (alpha particle)	3733

From Eq. (5-41) the orbit radius is now (in meters)

$$r = \frac{mv}{eB} = \frac{[T(T + 2W_0)]^{1/2}}{ceB} \tag{5-49}$$

When T and W_0 are expressed in Mev units and B is in webers/m^2, this becomes

$$r = \frac{[T(T + 2W_0)]^{1/2}}{300B} \tag{5-50}$$

The relationship given in Eq. (5-50) between orbit radius, magnetic field, and kinetic energy is plotted in Fig. 5-16 for electrons, protons,

deuterons, and alpha particles. Three coordinates are used: B, r, and T; as an aid to using the plot, the product Br is also introduced. Logarithmic scales are used to encompass a wide range in the variables. Orbit radius extends from 1 cm to 100 m, magnetic field from 0.01 weber/m^2 (100 gauss) to 10 webers/m^2 (100,000 gauss), and kinetic energy from 1 to 10,000 Mev (10 Bev).

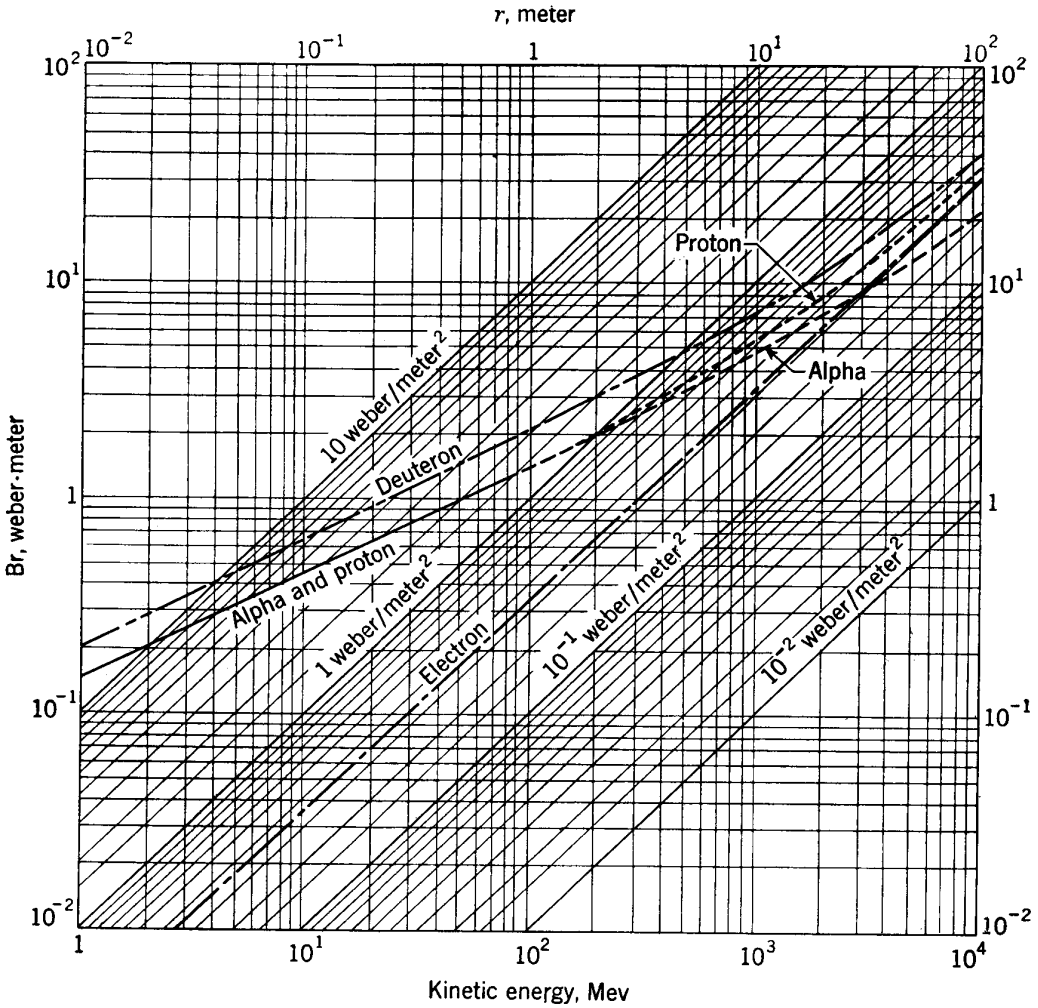

Fig. 5-16. Orbit radius as a function of energy and magnetic field. First find the Br value for the desired particle and particle energy; follow this Br value to the intersection with the chosen value of field B; read orbit radius on the upper scale.

In Table 5-3 a few typical values are listed to show the dimensional requirements of magnetic accelerators. Note the approach to a linear relation between radius and energy for relativistic energies where $T \gg W_0$. Note also the converging dimensions for electron and positive-ion accelerators at very high energies.

When rearranged to solve for kinetic energy, Eq. (5-49) becomes

$$T = (W_0^2 + c^2e^2B^2r^2)^{1/2} - W_0 \qquad (5\text{-}51)$$

T can be read from the plot of Fig. 5-16 by reversing the procedure in the legend. This equation illustrates one feature characteristic of very high energies: when T becomes very large compared with W_0, the relation simplifies to

$$T \simeq ceBr \qquad \text{(high energies)} \tag{5-52}$$

At high energies, energy and momentum become linearly proportional and as a result the particle energy becomes linearly proportional to the product Br. To give an easily remembered example, the relation is

TABLE 5-3
ORBIT RADIUS IN METERS
(At 1 weber/m²)

T, Mev	Electrons	Protons	Deuterons	He^{++} ions
1	0.00485	0.143	0.206	0.144
10	0.0347	0.454	0.643	0.454
100	0.330	1.47	2.05	1.45
1,000	3.30	5.60	7.22	4.85
10,000	33.0	36.0	38.7	21.8

evaluated for a magnetic field of 1.0 weber/m² (10 kilogauss), which is representative of fields obtained with iron-cored magnets:

$$T \text{ (in Mev)} \simeq 300r \text{ (in meters) at } B = 1.0 \text{ weber/m}^2 \tag{5-53}$$

For example, an electron moving in an orbit of 1 m radius in a 10-kilogauss field must have an energy of 300 Mev.

The relativistic expression for orbital frequency follows from Eqs. (5-46) and (5-49):

$$f = \frac{v}{2\pi r} = \frac{eB}{2\pi m} = \frac{eB}{2\pi m_0}\frac{W_0}{W} = \frac{eB}{2\pi m_0(1 + T/W_0)} = \frac{f_0}{1 + T/W_0} \tag{5-54}$$

Here f_0 is the nonrelativistic "cyclotron frequency." The frequency is constant only as long as $T \ll W_0$. This same relation will be used later to show the magnitude of frequency variation involved in the acceleration of positive ions to high energies in the synchrocyclotron; as particle energy increases, with B constant, the frequency of the electric field applied to the accelerating electrodes must decrease.

Orbital frequency can also be expressed in terms of orbit radius by using the relativistic relation for velocity:

$$f = \frac{v}{2\pi r} = \frac{c}{2\pi r}\left[1 - \left(\frac{W_0}{W_0 + T}\right)^2\right]^{1/2} \tag{5-55}$$

The numerical constant is readily evaluated; as long as T and W_0 are expressed in the same units and r is in meters, we have

$$f = \frac{47.8}{r}\left[1 - \left(\frac{W_0}{W_0 + T}\right)^2\right]^{1/2} \quad \text{megacycles/sec} \qquad (5\text{-}56)$$

As an example, consider a high-energy electron in an orbit of 1 m radius (the magnetic field must have the proper value). For energies above a

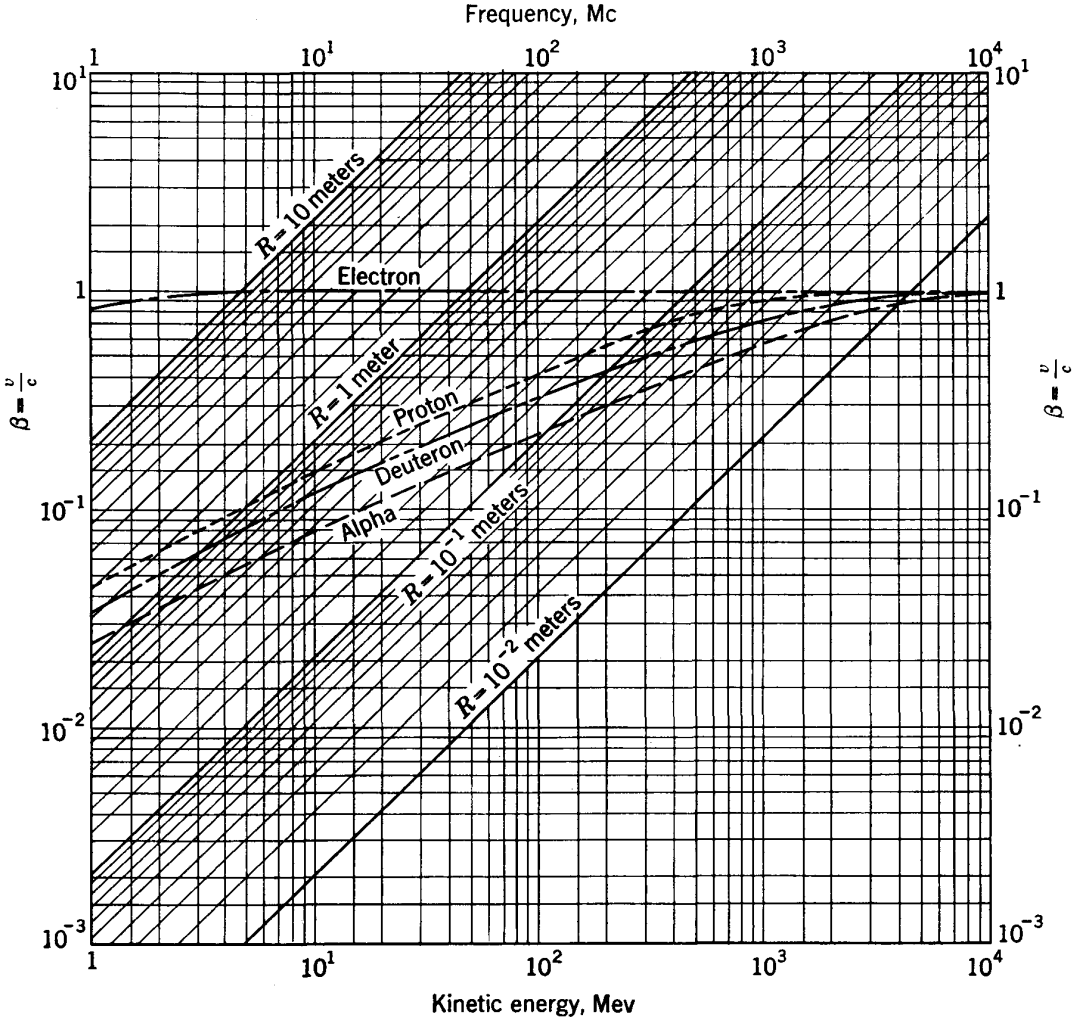

Fig. 5-17. Orbital frequency as a function of energy and orbit radius. First find the β value for the desired particle and particle energy; follow this value of β to the intersection with the chosen orbit radius; read orbital frequency on the upper scale.

few Mev, the second term involving the energies becomes negligible and the frequency approaches a constant value of 47.8 megacycles/sec.

The frequency relation of Eq. (5-55) is plotted in Fig. 5-17 over a wide range in energy and radius for electrons, protons, deuterons, and He^{++} ions. In this plot logarithmic coordinate scales are used, and the parameter $\beta = v/c$ is used as an intermediate step.

A few typical values of ion-revolution frequency are listed for the several particles in Table 5-4. The magnetic field is 1 weber/m^2, and the orbit radii are those given in Table 5-3. Note the converging values of frequency for all particles at very high energies. The revolution frequencies for different magnetic fields are inversely proportional to the flux density.

TABLE 5-4
ORBITAL FREQUENCY
(In megacycles/sec at 1 weber/m^2)

T, Mev	Electrons	Protons	Deuterons	He^{++} ions
1	9,120	15.2	7.60	7.61
10	1,380	15.2	7.60	7.61
100	145	13.8	7.34	7.40
1,000	14.5	7.46	5.00	6.05
10,000	1.45	1.32	1.22	2.11

The equations developed above give all the necessary information to determine the orbital motion of particles in a uniform magnetic field which is normal to the plane of their orbits. This special symmetry

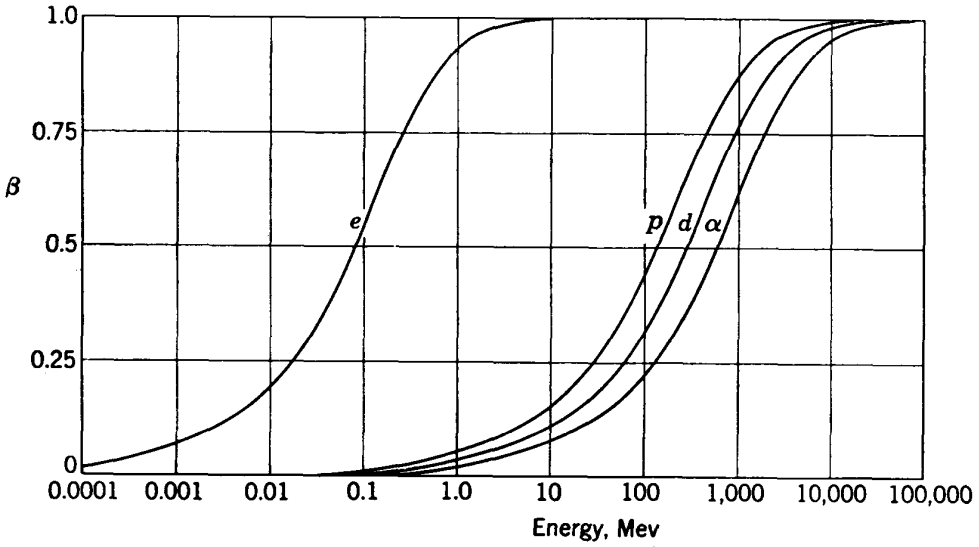

Fig. 5-18. Plot of $\beta = v/c$ for light particles as a function of energy.

has been chosen in all existing magnetic accelerators. Basic parameters can be determined by using Figs. 5-16 and 5-17. The transition from nonrelativistic to relativistic regions is evident. For electrons the relativistic region is reached at a few Mev ($v = 0.98c$ at 2 Mev); protons and other positive ions reach the equivalent region at energies of several Bev ($v = 0.98c$ at 4 Bev for protons). This result points out the essential difference between the acceleration of electrons and of positive ions, yet it shows that the problems become essentially identical at extremely high energies.

Another method of plotting the velocity of particles as a function of energy is shown in Fig. 5-18. Here the ratio $\beta = v/c$ obtained from Eq. (5-47) is plotted against energy T on a logarithmic scale for the several particles. This presentation shows the relativistic approach to constant velocity and serves to identify the energy range which requires the use of the relativistic equations for the different particles.

5-11. ORBITAL STABILITY

An additional requirement for accelerators is that they provide restoring forces for particles which deviate in direction from the orbit plane. This is a necessary requirement, as can readily be noted by considering the effect of a small, angular deviation from the plane for a particle which is traversing hundreds or thousands of revolutions. In an absolutely uniform magnetic field the orbit would be a helical spiral of small pitch,

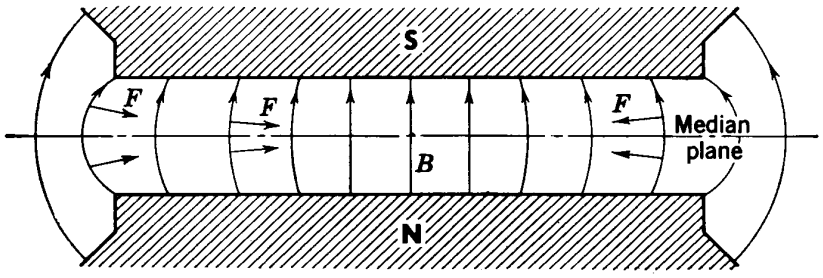

Fig. 5-19. Radially decreasing magnetic field in the cyclotron, showing the concave shape of the lines of flux and the direction of the magnetic forces acting on orbiting particles to restore deviant particles to the median plane.

and the axial displacement from the plane would increase linearly with the number of revolutions. In a magnetic field or vacuum chamber of finite extent most of the particles would be lost against the poles or the walls. It is essential that the magnetic field provide restoring forces to focus the particles about the central orbit plane.

Such restoring forces can exist in a *magnetic field which decreases in magnitude with increasing radius.* In this field the lines of magnetic flux are concave inward. Figure 5-19 is a diagram of the magnetic field between cyclotron pole faces and shows the direction of the forces on charged particles moving in orbits above or below the median plane. The direction of the force on the moving particle is normal to the local direction of the magnetic flux. It will have a downward component for particles above the median plane and an upward component for particles below the median plane. It is evident that field shaping of this sort will provide the desired restoring forces to prevent the particles from wandering off in the vertical or axial direction.

The considerations leading to appropriate field shaping to prevent particle loss in the radial direction are best seen through a study of the

general equations of motion (5-14). For our present purpose these equations simplify materially. There is no electric field involved and there is no azimuthal component of B. Also we shall assume that the radial and vertical excursions are so small that they do not affect the velocity in the θ direction; we can then write $r\dot{\theta} = v$ and assume that v does not change materially during the period under consideration.

We know that the field must decrease in the radial direction for vertical restoration of the particles to the orbit. To give this statement a mathematical form we shall write

$$B_z = B_0\left(\frac{r_0}{r}\right)^n \tag{5-57}$$

where n = positive constant
r_0 = radius of "equilibrium orbit"
B_0 = value of B_z at equilibrium orbit

Since we assume that r makes only small excursions from r_0, we can write Eq. (5-57) in the approximate form

$$B_z = B_0\left(1 - \frac{n\,\Delta r}{r_0}\right) \tag{5-58}$$

where $\Delta r = r - r_0$. The other magnetic-field component B_r follows from Maxwell's equations (5-1), which state that for this case curl $\mathbf{B} = 0$ and

$$\frac{\partial B_z}{\partial r} = \frac{\partial B_r}{\partial z} \tag{5-59}$$

From Eqs. (5-58) and (5-59)

$$B_r = -\frac{nB_0 z}{r_0} \tag{5-60}$$

We are interested only in the radial and axial components of the equations of motion (5-14). With the substitutions just outlined, they become

$$\frac{d}{dt}(m\,\Delta\dot{r}) - \frac{mv^2}{r_0}\left(1 - \frac{\Delta r}{r_0}\right) = evB_0\left(1 - \frac{n\,\Delta r}{r_0}\right) \tag{5-61}$$

and

$$\frac{d}{dt}(m\dot{z}) = \frac{evBn_0 z}{r_0} \tag{5-62}$$

But we define the equilibrium orbit as that orbit for which both $\Delta\dot{r}$ and Δr are always zero. For this case Eq. (5-61) simplifies to

$$\frac{mv^2}{r_0} = -evB_0 \tag{5-63}$$

This equation is identical with Eq. (5-41), which was presented in connection with pure circular motion; the circular orbit discussed then has now become the equilibrium orbit for the more general motion under study.

Equations (5-61) and (5-62) become still simpler when Eq. (5-63) is used as a substitution for all terms including B_0. We make the further substitution of the symbol ω for the angular velocity v/r_0 and obtain finally

$$\frac{d}{dt}(m\,\Delta\dot{r}) = -m\omega^2(1-n)\,\Delta r \tag{5-64}$$

and

$$\frac{d}{dt}(m\dot{z}) = -m\omega^2 nz \tag{5-65}$$

These two equations have the general form of equations of motion. On the right-hand side of each equation is the term that represents the force which restores the particle to the orbit or repels it from the orbit. So long as the sign of the term is negative for positive displacements and positive for negative displacements, the particle will continually be forced back to the equilibrium orbit whenever it becomes displaced from that orbit. Evidently this can be true only if n and $(1-n)$ are both positive, in other words, if n lies between 0 and unity.

From the qualitative discussion of the vertical motion presented earlier it seemed essential that n should be positive so that the field would decrease with increasing radius. The reason for radial restoring forces existing only when $(1-n)$ is positive is not so easily seen but may become clearer from the following argument: In the coordinate system of the particle the centrifugal force term mv^2/r must be balanced by the magnetic force evB_z. If these two terms are plotted as a function of radius (Fig. 5-20), it becomes evident that, so long as B_z does not fall off faster than $1/r$ [with $(1-n)$ remaining positive], there will be a radius at which the curves cross and the two forces are balanced. This will be the radius of the equilibrium orbit. Outside of this radius the inward magnetic force will be greater; inside of this radius the outward centrifugal force will be greater; thus there will always be a net force restoring the particle to the equlibrium orbit.

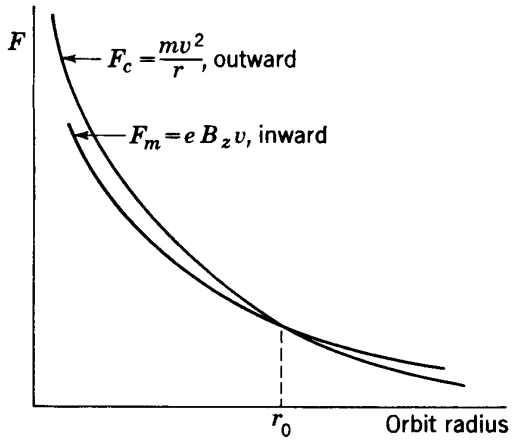

Fig. 5-20. Forces acting on a particle in a circular orbit in a radially decreasing magnetic field, showing a net force acting to restore a deviant particle to the equilibrium orbit r_0.

These restoring forces are sufficiently strong to restore a deviant particle fairly rapidly to its orbit. In the case of a 300-Mev electron traveling in an orbit of 1 m radius in a field whose n value is 0.5, the restoring force on a particle which strays 1 cm from the orbit is the same as that which would be exerted by an electric field of about 1.5 Mv/m.

5-12. THE FREE OSCILLATIONS

Equations (5-64) and (5-65) not only show that restoring forces can exist for a proper field shape, but also give the character of the motion under these forces. The general form of these equations is similar to that for simple harmonic motion, which can have the form

$$\frac{d}{dt}(\dot{x}) = -\omega_0^2 x \tag{5-66}$$

where x = displacement
$\dot{x}$ = velocity
ω_0 = angular frequency of oscillatory motion
[For example, in an oscillatory system of mass and spring, the angular frequency $\omega_0 = (K/m)^{1/2}$, where K is the spring constant and m the mass, and the motion is described by $x = x_m \cos \omega_0 t$.]

In order for Eqs. (5-64) and (5-65) to represent harmonic motion, the quantities m and ω must be essentially constant over the period of motion. We shall assume this to be the case in order to estimate the frequency of oscillations about the equilibrium orbit. Referring to Eq. (5-66) we find

$$f_r = \frac{\omega}{2\pi}(1 - n)^{1/2} \qquad \text{(for radial motion)} \tag{5-67}$$

$$f_z = \frac{\omega}{2\pi} n^{1/2} \qquad \text{(for axial motion)} \tag{5-68}$$

But $\omega/2\pi$ is the frequency of revolution f_0 of the particle in the equilibrium orbit. Evidently the oscillations about the orbit take place with a frequency only slightly lower than the particle frequency of revolution, since n must lie between 0 and 1. For example, if $n = 0.5$, both oscillations have a frequency of $0.707 f_0$ and would complete one period during 1.41 revolutions. This oscillation is sufficiently rapid to justify the assumption above that no important changes will take place in m or ω during an oscillation period.

These oscillations in radius and in vertical position are known as the "free oscillations" since they continue, once started, without the action of any but the guiding field. Since the free oscillations were first studied in connection with the betatron,[12] they are also known as "betatron oscillations" in spite of the fact that they are observed in many other accelerator species.

The free oscillations usually are initiated early in the accelerating cycle. They may be due to errors in the injection system or to the finite size of the injector, or they may be initiated by small-angle scattering by the residual gas in the vacuum chamber. Gas scattering rapidly decreases in importance as particle energy increases, and the free oscilla-

tions which remain as acceleration proceeds are merely a continuation of those generated at or shortly after injection.

It is now important to assure ourselves that the amplitude of these oscillations will not grow with time. Since both the mass of the particle and the restoring force (proportional to $m\omega^2$) increase during the acceleration, we should expect that the oscillation amplitude would decrease, and this is indeed the case. Since we are now considering a long time relative to one free oscillation period, it is no longer legitimate to make the assumptions which led to the simple harmonic solution of Eqs. (5-64) and (5-65). We must now make a more precise solution of these equations. The next higher approximation to the solution of the equations of motion takes the form

$$\Delta r = C_1(m\omega\sqrt{1-n})^{-\frac{1}{2}} \sin\left(\int \omega\sqrt{1-n}\,dt\right) \tag{5-69}$$

$$z = C_2(m\omega\sqrt{n})^{-\frac{1}{2}} \sin\left(\int \omega\sqrt{n}\,dt\right) \tag{5-70}$$

These solutions are valid to a high order of accuracy and are sufficient for application in almost all practical cases. They show that the oscillation amplitudes damp like $(m\omega)^{-\frac{1}{2}}$. From Eq. (5-41) this is equivalent to damping like $B_0^{-\frac{1}{2}}$. At low, nonrelativistic energies, kinetic energy is proportional to B_0^2, so in this range the free-oscillation amplitude is proportional to the inverse one-quarter power of the kinetic energy $T^{-\frac{1}{4}}$. At high relativistic energies the kinetic energy becomes proportional to B_0, and the rate of damping of the free oscillations increases to the point where the amplitude is proportional to the inverse one-half power of the kinetic energy $T^{-\frac{1}{2}}$.

The assumptions used in the derivation of the damping equations (5-69) and (5-70) are valid unless one of the quantities m, ω, $1 - n$, or n approaches zero. In actual accelerators m and ω are always finite. Only in the case of the cyclotron do we run into difficulty with n, which is approximately zero at the beginning of acceleration. Since this problem relates only to the cyclotron, we postpone its consideration to the next chapter.

5-13. CONSIDERATIONS AFFECTING ACCELERATOR DESIGN

In the design of a particle accelerator one of the most important decisions is the choice of aperture dimensions. The costs of the most expensive components usually depend strongly on the size of the aperture. Since the aperture must be large enough to contain the free oscillations of particles around their equilibrium orbit, the probable amplitudes must be estimated at an early stage of design.

In the cyclotron, where an approximately uniform magnetic field must be maintained over a large radial extent, it is not possible to use a large

value of n. The n value chosen is that which is just sufficient to provide the necessary axial focusing and usually varies from less than 0.01 near the center to slightly higher values as the outer periphery is approached.

In ring-shaped accelerators with iron-cored magnets, such as the betatron and the synchrotron, it is usually more economical to widen the region of useful magnetic field in the radial direction than it is to enlarge the gap between poles and provide space for axial oscillations. Consequently the n value chosen is as high as possible to provide strong restoring forces in the axial direction. The usual choice is an n value of about 0.7. In the few ring-shaped accelerators which have used air-cored fields without iron magnetic circuits, on the other hand, axial extension of the field is easier and cheaper than radial extension, so n values of the order of 0.3 are appropriate.

The damping of free-oscillation amplitudes is of major significance in accelerator design and operation. Amplitudes have been shown to decrease with increasing particle energy, varying with $T^{-\frac{1}{4}}$ at low energies and with $T^{-\frac{1}{2}}$ at relativistic energies. This means that the available aperture of useful field at the start of acceleration determines initial amplitudes and is the limiting factor on the intensity of the accepted beam. The damping causes the beam to decrease in cross section during acceleration, so the high-energy beam is much smaller. Beam dimensions have a direct bearing on the design of targets or of ejection systems for emergent beams. In an electron synchrotron, for example, an initial beam width of more than 10 cm will be reduced to a few millimeters at high energy.

If a mechanism for coupling exists between the radial and axial free oscillations and if the frequencies are in fundamental or harmonic resonance, oscillation energy can be transferred from one mode to the other. Small imperfections in the uniformity of the magnetic field are sufficient to provide significant coupling. The frequencies of the two modes are identical for $n = 0.5$, so this value of n is usually avoided in design. This is not a serious limitation if the available apertures in the two coordinate directions are similar in size, but it becomes important when the axial dimension is reduced significantly below the radial dimension. Harmonic resonances can occur for n values of 0.2 and 0.8, for which the ratios of frequencies are 1:2 or 2:1; these values also are avoided in design. In the standard cyclotron the number of revolutions required to cross the $n = 0.2$ resonance is small, so effective coupling is not observed and the particle beam can remain in orbit out to larger n values. In the synchrocyclotron, however, the rate of acceleration is much slower and the beam is observed to "blow up" axially at the radial location where $n = 0.2$. These points will be discussed in more detail in the following chapters on magnetic accelerators.

REFERENCES

1. M. A. Tuve, O. Dahl, and L. R. Hafstad, *Phys. Rev.*, **48**:241 (1935).
2. W. W. Buechner, E. S. Lamar, and R. J. Van de Graaff, *J. Appl. Phys.*, **12**:141 (1941).
3. V. K. Zworykin et al., "Electron Optics and the Electron Microscope," Wiley (1945).
4. J. R. Pierce, "Theory and Design of Electron Beams," Van Nostrand (1949).
5. V. E. Cosslett, "Introduction to Electron Optics," Oxford (1950).
6. F. Terman, "Radio Engineers' Handbook," McGraw-Hill (1943).
7. E. D. Courant, M. S. Livingston, and H. S. Snyder, *Phys. Rev.*, **88**:1190 (1952).
8. J. P. Blewett, *Phys. Rev.*, **88**:1197 (1952).
9. E. D. Courant, M. S. Livingston, H. S. Snyder, and J. P. Blewett, *Phys. Rev.*, **91**:202 (1953).
10. E. D. Courant and H. S. Snyder, *Ann. Phys.*, **3**:1 (1958).
11. J. P. Blewett, N. C. Christofilos, and A. M. Vash, *Phys. Rev.*, **99**:652 (1955).
12. D. W. Kerst and R. Serber, *Phys. Rev.*, **60**:53 (1941).

At the head of the facing page is an illustration of the 16-Mev cyclotron at the Massachusetts Institute of Technology.

6

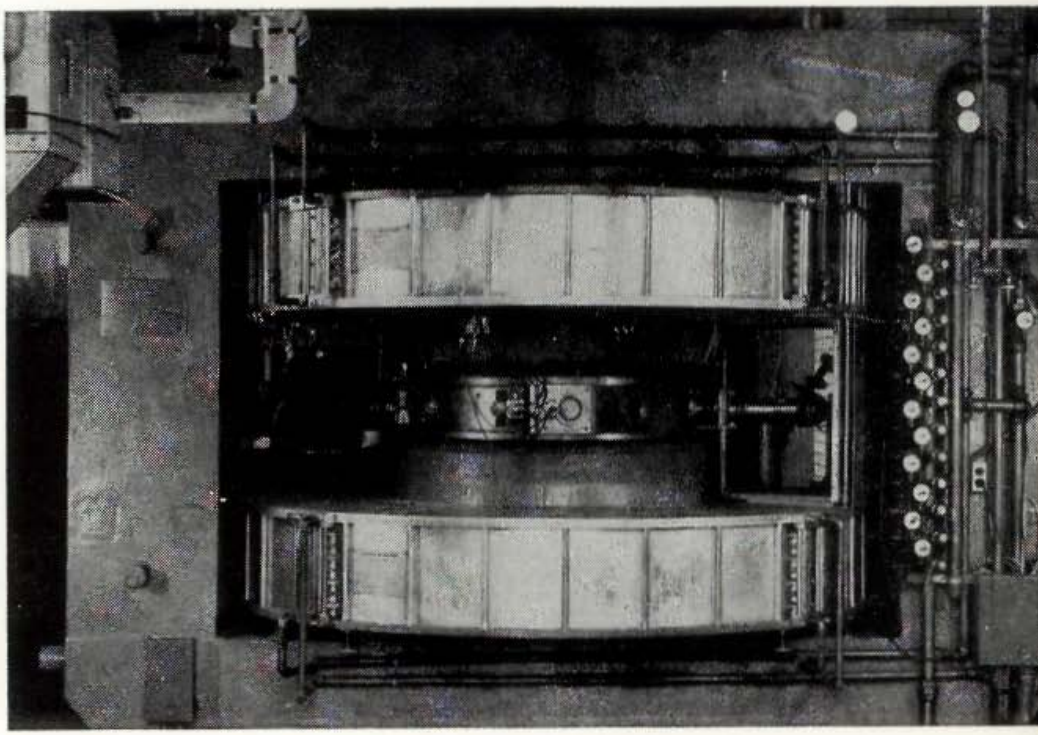

The Cyclotron Magnetic Resonance Accelerator

The cyclotron accelerates light positive ions to high energy without the use of high voltage, thereby avoiding the limitations of insulation breakdown. Ions move in widening semicircular paths in a uniform magnetic field, crossing back and forth between two electrodes in resonance with an oscillatory electric field. The ions are accelerated at each traversal of the electric field, attaining a final energy hundreds of times greater than that available from the impressed voltage on the electrodes. A simple analogy is the garden swing which can be urged to large amplitude by successive small pushes, each push timed with the natural period of the swing.

This is the principle of resonance acceleration, and the technical name for the machine is the "magnetic resonance accelerator." However, the more concise term "cyclotron," which developed as laboratory slang, has become the popular name for the instrument. The name is so well known, in fact, that it is often loosely applied to designate any type of particle accelerator, and is essentially synonymous with "atom smasher." The cyclotron was the first of the resonance accelerators. It supplied the principle and the basic concepts for the development of the modern high-energy accelerators. The simplicity of the concepts and their prompt success stimulated a rapid development which can scarcely be matched in any other field of science.

6-1. HISTORICAL DEVELOPMENT

The cyclotron principle was proposed in 1930 by the late Ernest O. Lawrence[1] of the University of California. It was suggested by the experiment of Wideröe[2] in 1928 in which ions of sodium and potassium were accelerated to twice the applied voltage in traversing two tubular electrodes in line between which an oscillatory electric field was applied—an elementary linear accelerator (see Chap. 10).

The conception* of the idea occurred in the library of the University of California in the summer of 1929, when Lawrence was browsing through the current journals and read Wideröe's paper in the *Archiv für Electrotechnik*. Lawrence speculated on possible variations of this resonance principle, including the use of a magnetic field to deflect the particles in circular paths so they would return to the first electrode and thus reuse the electrical field in the gap. He discovered that the equations of motion predicted a constant period of revolution, so the particles could be accelerated in resonance with an oscillatory electric field.

The principle of acceleration was announced in a short article in *Science* by Lawrence and Edlefsen[1] in 1930. Edlefsen was a graduate student who had just completed a thesis in another field; on Lawrence's request he attempted a brief preliminary experimental test of the principle. The experiment was not successful in demonstrating resonance, and no experimental results were reported. However, the basic soundness of the principle was evident and justified the public announcement in advance of experimental proof.

The senior author (MSL) was a graduate student at Berkeley at that time; this problem was suggested by Professor Lawrence as the subject for an experimental research investigation to demonstrate the validity of the resonance principle. A doctorate thesis by Livingston[3] dated April 14, 1931, reporting the results of the study, is on file in the University of California library. This was the first experimental verification of the principle of cyclotron resonance.

For this preliminary study only small-size laboratory equipment was available, including an electromagnet of 4 in. pole diameter. An illustration from this thesis (Fig. 6-1) shows the arrangement of components which is still a basic feature of all cyclotrons. A vacuum-tube oscillator provided 2000 volts radiofrequency potential to the electrode, with a frequency which could be varied by adjusting the number of turns in the resonant inductance. Hydrogen ions (H^+ and H_2^+) were produced by ionization of hydrogen gas in the chamber by electrons emitted from a tungsten-wire cathode near the center. Resonant ions which reached the edge of the chamber were observed in a shielded collector cup. Sharp peaks were observed in the collected current at the magnetic field of resonance for H_2^+ ions (and later for H^+ ions), as illustrated in Fig. 6-2, which

* As told to the senior author (MSL) by Professor Lawrence.

shows a typical resonance curve taken from the thesis. At the collector radius and for the highest field used, the expected energy of the H_2^+ ions was 80,000 ev, confirmed by electric-field deflection measurements. By varying frequency of the rf accelerating fields (reported as wavelength), resonance was observed over a broad range of frequencies and magnetic fields (Fig. 6-3), proving conclusively the validity of the resonance principle.

The next step in the development, the first practical cyclotron, used a magnet with pole faces 10 in. in diameter and produced protons of over

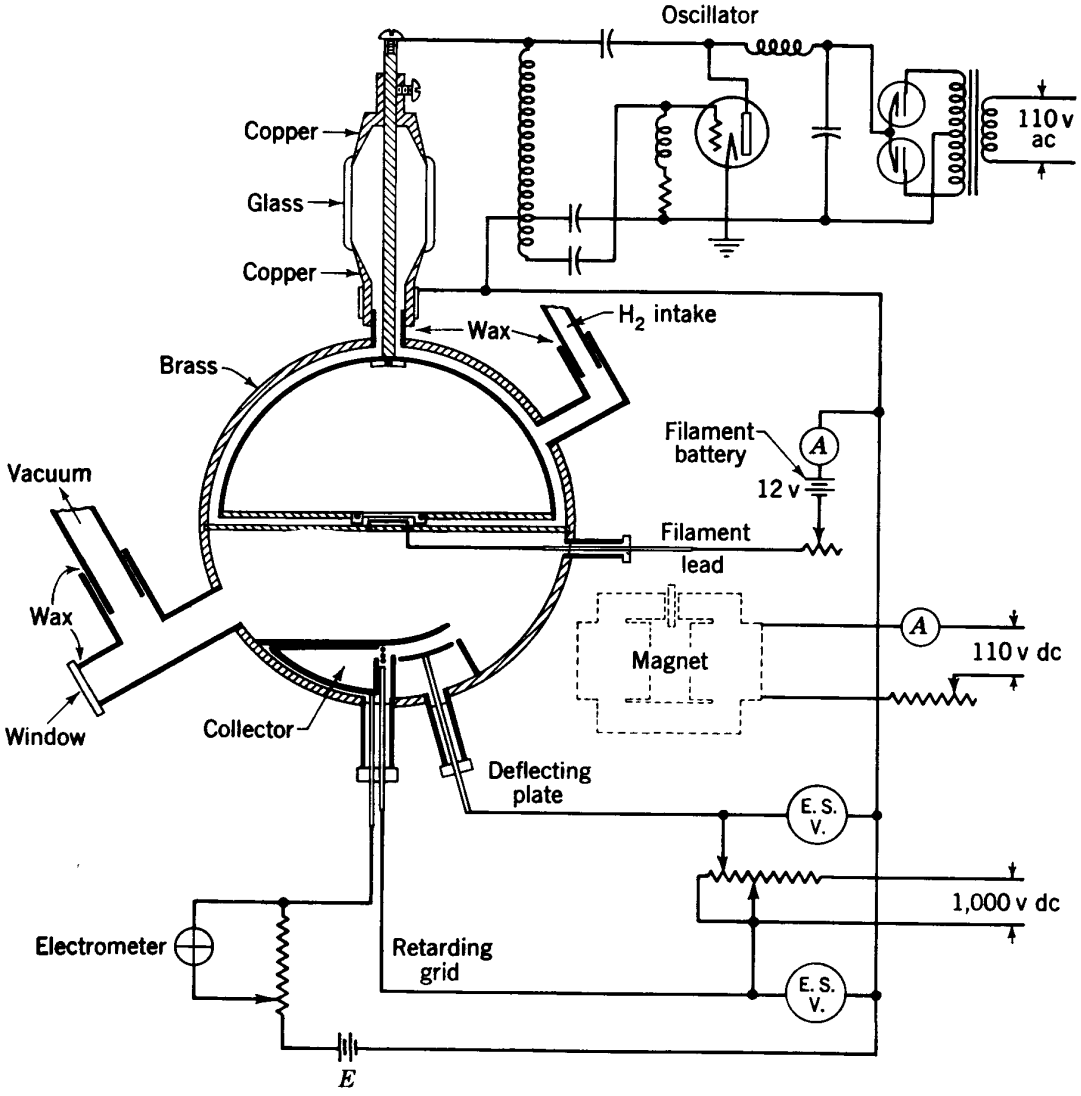

Fig. 6-1. Schematic diagram of original cyclotron chamber and associated circuits. (Livingston.[3])

1 Mev energy, the first time that controlled particles of this energy had been obtained in scientific history. The development is described in a paper by Lawrence and Livingston[4] in 1932.

A few months before this instrument was completed, Cockcroft and Walton[5] at the Cavendish laboratory had observed for the first time the

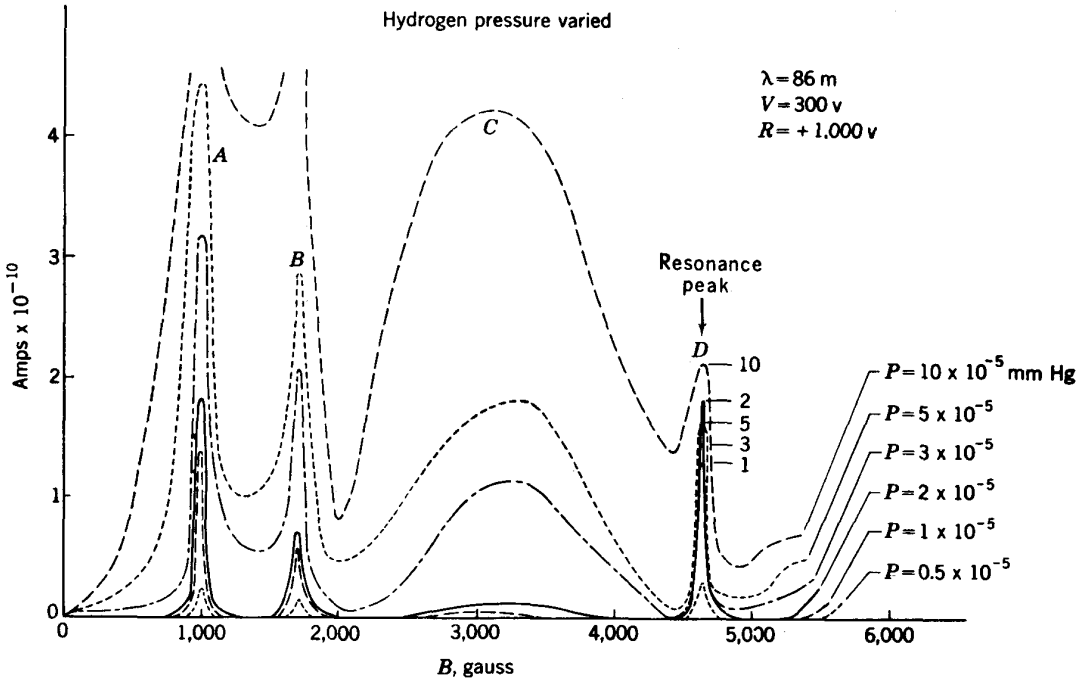

Fig. 6-2. Typical resonance curve of beam current versus magnetic field. (Livingston.[3])

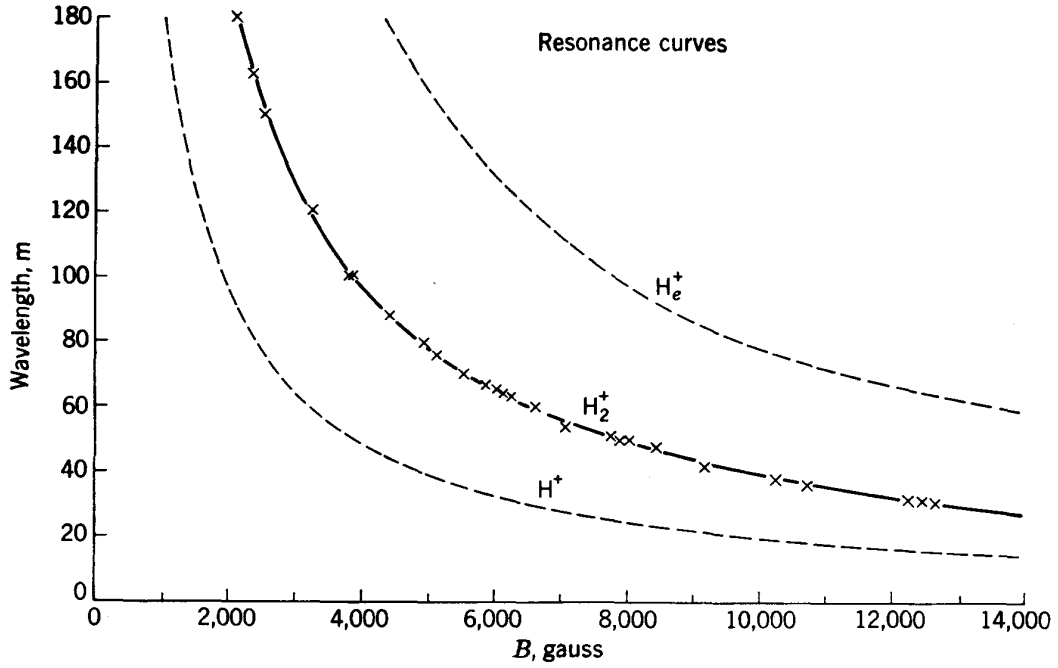

Fig. 6-3. Experimental verification of cyclotron resonance relation. (Livingston.[3])

disintegration of Li nuclei by artificially accelerated particles, using protons of 400 kev energy (see Chap. 2). The 1-Mev protons from the first cyclotron were promptly used to confirm and extend the British results. Disintegrations were observed in Li and in several new targets, as reported in 1932 by Lawrence, Livingston, and White.[6]

These early successes stimulated interest in many laboratories. In Berkeley, plans were made for higher energies, and Professor Lawrence obtained financial support from the Research Corporation, which led to the design and construction of a much larger cyclotron, the "27-inch." The iron core for this large electromagnet was taken from a dismantled Poulson-arc radio transmitter donated by the Federal Telegraph Company. By the time the cyclotron was completed in 1933, ions of the newly discovered and separated heavy-hydrogen isotope (deuterons) were available, obtained from heavy-water samples supplied by the late Prof. G. N. Lewis of the chemistry department of the university. The machine was rapidly tuned up (primarily by "shimming" of the magnetic field) to produce 3-Mev and then 5-Mev deuterons. A team of young, enthusiastic scientists explored the new fields of deuteron reactions, induced radioactivity, and neutron production; a dozen or more short papers were published describing the progress. The 5-Mev deuteron cyclotron was described by Lawrence and Livingston[7] in 1934. At this time Livingston left Berkeley to join the physics department at Cornell University and to build another research cyclotron. A later stage, after expansion of the pole faces to 37 in. diam and further development to 8 Mev energy, was reported by Lawrence and Cooksey[8] in 1936.

Potential medical applications of high-energy neutrons, available in adequate intensity for the first time, justified the design and construction of the 60-in. "Crocker" cyclotron and the development of an associated medical laboratory on the University of California campus. This machine was completed in 1939, first operating at 16 Mev and later producing 20-Mev deuterons or 40-Mev helium ions. It is the prototype of the modern standard cyclotron and was described by Lawrence, Alvarez, Brobeck, Cooksey, Corson, McMillan, Salisbury, and Thornton.[9]

In 1939 Professor Lawrence was awarded the Nobel Prize in physics in recognition of his achievements in the conception and development of the cyclotron. His untimely death in 1958 terminated an impressive career as Director of the University of California Radiation Laboratory and in many positions of scientific responsibility for the United States government.

Meanwhile cyclotrons were constructed in many other laboratories, at first largely designed by graduates of the Berkeley school. Soon these laboratories were able to make important contributions to the development. Among the laboratories contributing significantly to the progress of cyclotronics in the early years were those at the University of Michigan,

Cornell University,[10] Columbia University, Princeton University,[11] University of Rochester, Washington University at St. Louis, Bartol Research Laboratory,[12] University of Illinois,[13] University of Indiana, Purdue University, Carnegie Institution of Washington, Harvard University, and the Massachusetts Institute of Technology.[14] A monograph by W. B. Mann[15] (1940) describes the fundamental principles and tells some of the story of cyclotron development in the Berkeley laboratory.

As a result of widespread effort, closely coordinated by publications, correspondence, visits, and exchange of personnel, the modern cyclotron is the composite product of many laboratories and scores of individual contributions. A large number of the technical developments have not been published, but after alteration and improvement as they passed from one laboratory to another, they have become part of the general store of technical information. One of the more detailed publications, by Livingston[14] in 1944, describes some of these features, illustrated by the design and performance of the MIT cyclotron, which operates at 16 Mev for deuterons or 32 Mev for helium ions.

Several commercial firms have joined in the development of the fixed-frequency cyclotron. The Collins Radio Company designed and constructed two 60-in. machines, for the Brookhaven National Laboratory and the Argonne National Laboratory, under the direction of W. W. Salisbury. The General Electric Company has built a machine of the same size for the National Committee of Aeronautics Laboratory in Cleveland. The Philips Laboratory at Eindhoven and Brown-Boveri in Switzerland have built several cyclotrons for European laboratories.

Theoretical analysis of the principles of operation and of focusing was developed by Rose[16] at Cornell University and by Wilson[17,18] at the University of California in 1938. A much more comprehensive theoretical treatment by Cohen[19] of the Oak Ridge National Laboratory gives a sound basis for the design of the modern high-energy, high-intensity cyclotrons.

The cyclotron has become a symbol of nuclear physics, and its simple principles are taught in most high-school and college physics courses. Small working models have been built by students in several high schools, and a report of one such installation has been published.[20]

A new field of special scientific interest has been opened with the development of ion sources for multiple-charge heavy ions for acceleration in a cyclotron. The Oak Ridge National Laboratory[21] has been a leader in this field of ion-source development. Ions such as C_{12}^{++}, C_{12}^{3+}, N_{14}^{3+}, and N_{14}^{4+} have been produced in adequate intensities to be accelerated in the cyclotron[22] and have been used for many research studies. An ion such as C_{12}^{3+} has almost the same e/m value as He^{+} and can be accelerated at similar values of frequency and magnetic field.

However, because of its triple charge, the energy is three times that of an He^+ ion under these conditions. Ions with other e/m values can be tuned for resonant acceleration by adjusting the applied frequency of the cyclotron. Machines in other laboratories have been adapted to heavy-ion acceleration; an example is the 225-cm cyclotron at the Nobel Institute in Stockholm.[23] Interest in the field, notably at Oak Ridge, has resulted in designs for cyclotrons specifically planned for this purpose.

6-2. THE RESONANCE PRINCIPLE

In the cyclotron an electromagnet is used to provide a nearly uniform magnetic field between the flat faces of cylindrical poles of large radius. A vacuum chamber fits between the pole faces, and two hollow copper

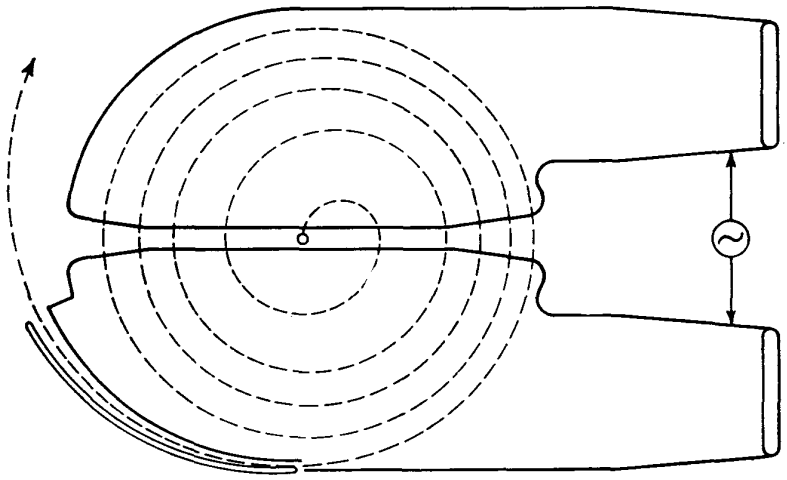

Fig. 6-4. Schematic diagram of cyclotron electrodes showing ion paths.

electrodes (Fig. 6-4) are mounted inside the vacuum chamber. These electrodes were originally semicircular in shape, as though a flat, hollow pillbox had been cut through a diameter. Because of their shape, the electrodes are frequently referred to in laboratory slang as D's or dees. A radiofrequency power supply provides an alternating electric field between the diametral faces of the two D's. Ions are accelerated in this region of crossed electric and magnetic fields.

Positive ions are produced near the center of the chamber between the D's by an ion source and are accelerated toward and into the electrode, which is negatively charged at the instant. In the electric-field-free region inside the D the ions are acted upon only by the uniform magnetic field and travel in circular orbits in a plane normal to the field. After traversing a semicircular path, each ion returns to the diametral gap between electrodes and comes again under the influence of the electric field. For the condition of resonance, the magnetic field is adjusted so the time required for an ion to complete a half-circle is equal to the time

for reversal of the oscillatory electric field. So, after completing the first half-circle the ion experiences another acceleration, acquires higher velocity, and traverses a path of larger radius within the other electrode. As long as this resonance is maintained, the ions are accelerated each time they cross the gap, traveling in ever-widening semicircles until they reach the periphery of the electrodes.

As was shown in Chap. 5, the force on an ion of mass m, charge e, and velocity v moving at right angles to a uniform magnetic field B has the magnitude evB and is exerted in a direction normal to the magnetic field and to the direction of motion of the ion. This force causes the ion to travel in a circular path of radius r whose value is obtained by balancing the centrifugal force and the magnetic force thus [cf. Eq. (5-41)]:

$$\frac{mv^2}{r} = evB \tag{6-1}$$

The frequency of revolution in the circular path is [cf. Eq. (5-42)]

$$f = \frac{v}{2\pi r} = \frac{eB}{2\pi m} \tag{6-2}$$

This frequency is constant in a uniform magnetic field so long as the mass m is constant.

For acceleration in the cyclotron the frequency of the alternating electric field applied to the electrodes is set equal to the ion revolution frequency. The linear relation between applied frequency and magnetic field is the fundamental equation of cyclotron resonance. When evaluated for the e/m values characteristic of light ions, it gives

Protons:	f (megacycles)	$= 1.52B$ (kilogauss)
Deuterons:	f	$= 0.76B$
He^{++}:	f	$= 0.76B$

These relations are plotted in Fig. 6-5 to illustrate the range of frequencies required to produce resonant acceleration in magnetic fields up to 20 kilogauss.

A voltage-time graph of the potential between the electrodes of a cyclotron is shown in Fig. 6-6. On each traversal of the gap between electrodes the particle will acquire an increment of kinetic energy $\Delta T = eV$ of magnitude determined by the phase of crossing the gap. Particles will be moving in opposite directions in successive passages, so the energy increments are cumulative. A resonant particle crossing at the phase of peak field (point 1) will continue to cross the gap at the same phase and will reach maximum energy in the minimum number of turns. Particles crossing at other phases, such as points 2 and 3, will acquire smaller increments but will remain in resonance for a larger number of turns to reach

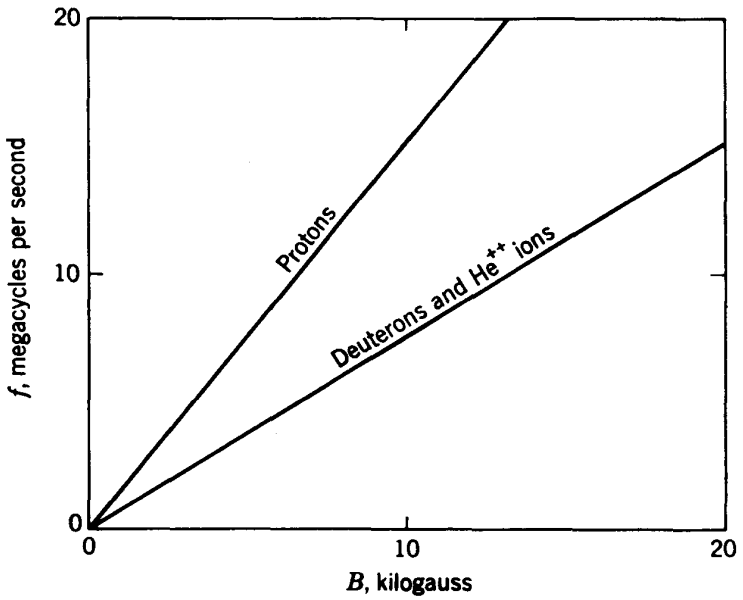

Fig. 6-5. Plot of cyclotron resonance relation for H^+, D^+, and He^{++}.

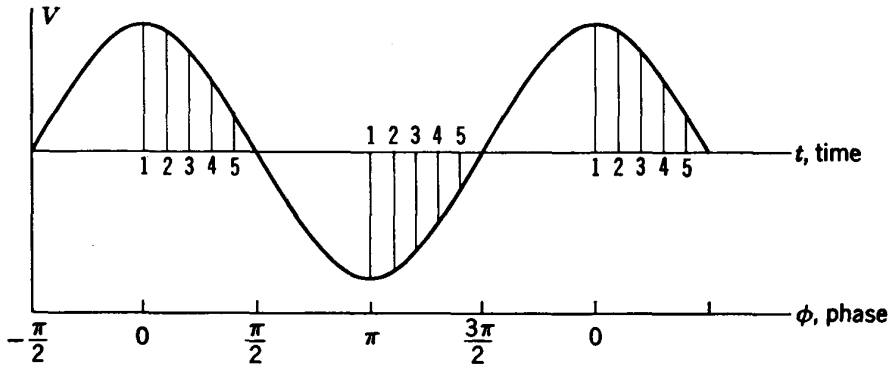

Fig. 6-6. Voltage-time graph of the alternating electric potential between D's of a cyclotron. Resonant ions which cross the gap at the phases 1, 2, 3, . . . are accelerated on each traversal.

maximum energy. If there are N accelerations and the average potential difference between D's each time the ions cross the gap is V, the final energy will be

$$T = NVe = \frac{1}{2} m v_m^2 \tag{6-3}$$

Kinetic energy can also be written in terms of magnetic field B and final orbit radius R by use of Eq. (6-1):

$$\frac{T}{e} = \frac{1}{2} \frac{e}{m} B^2 R^2 \tag{6-4}$$

Here the kinetic energy per unit charge is shown to be proportional to the square of the momentum in units of BR. It is evaluated for the light

ions in Mev units, with B in kilogauss and R in inches (units established by long usage in the cyclotron field), as

Protons:	T (Mev)	$= 3.12 \times 10^{-4} B^2 R^2$
Deuterons:	T	$= 1.56 \times 10^{-4} B^2 R^2$
He^{++}:	T	$= 3.12 \times 10^{-4} B^2 R^2$

Note that although He^{++} has essentially the same e/m value as the deuteron, its double charge gives it twice the kinetic energy of the deuteron.

In using these relations to determine the dimensions of a cyclotron magnet we must remember that the radius R applies to the extent of the uniform magnetic field; the physical radius of pole faces must be larger by about one-half the gap length. Since the saturation limit of iron prescribes a maximum magnetic field in iron-cored magnets of about 18 kilogauss (depending somewhat on quality of iron and on the specific design), the maximum energy is roughly determined by the square of the pole-face radius or diameter. With a chosen magnet size, the ion energy obtainable at radius R increases with the square of the magnetic field.

An informative expression for orbit radius can be obtained by eliminating T from Eqs. (6-3) and (6-4):

$$r = \frac{1}{B}\left(2\frac{m}{e}V\right)^{\frac{1}{2}} N^{\frac{1}{2}} \tag{6-5}$$

We note that the radii of successive paths increase with a sequence of square roots of integral numbers $N^{\frac{1}{2}}$, getting closer together as N becomes large. This relation was used to draw the schematic ion path of Fig. 6-4, in which N is an impractically small number, but which illustrates the expanding paths.

These basic relations can be illustrated by data representative of the MIT 42-in. cyclotron. At the maximum magnetic field used (17.7 kilogauss), the useful region of uniformity extends to a radius of 18.75 in. The resonant frequency for deuterons, from Eq. (6-2), is 13.5 megacycles/sec. The maximum kinetic energy, from Eq. (6-4), is 16.0 Mev. The peak radiofrequency voltage between D's when operating at full beam intensity is measured to be 140 kv (70-kv peak between each D and ground). Ions experience phase shifts as they are accelerated, as will be shown later, so a representative ion might make 100 revolutions or receive 200 accelerations of an average value of 80 kv before attaining the final energy of 16.0 Mev. Successive ion path radii, computed from Eq. (6-5) and assuming an initial 40-kv and subsequent 80-kv accelerations, would be 0.9, 1.5, 2.0, 2.3, . . . in. Actually the first few paths will be distorted spirals rather than semicircles, as shown later. The difference in radius between the ninety-ninth and one-hundredth revolutions, Δr, is found to be about 0.1 in.

After acceleration to the maximum practical energy and orbit radius R the ions enter a deflection channel defined by a septum of somewhat larger radius of curvature. An electric field is maintained across this channel by a negative dc potential on an insulated electrode paralleling the septum. The difference in radius Δr between the last two orbits is sufficient for a useful fraction of the beam to pass behind the septum, where it is deflected outward in an opening spiral path as an emergent beam.

6-3. MAGNETIC AND ELECTRIC FOCUSING

An understanding of the detailed motion of the particles in their orbits is important, in order to appreciate the reasons for the specialized techniques which have evolved. The basic resonance principle applies to an idealized particle moving in an orbit located on the median plane of the cyclotron chamber and crossing the accelerating gaps in perfect synchronism with the electric field. However, essentially all ions being accelerated deviate from these ideal conditions; they perform oscillations about the median plane and they migrate in phase of crossing the gap. Those which remain in resonance are enclosed within an envelope inside the D's which is limited both in the transverse spread about the median plane and in an azimuthal sector enclosing the accepted phase band. During each radiofrequency cycle such a loose bunch of ions starts from the source, and the center of the bunch follows the idealized expanding orbit described previously. In each subsequent cycle another bunch is emitted and follows in the same track. We shall see that the bunches are discrete only for the first few revolutions; eventually they overlap and merge into an almost continuous radial distribution of all possible energies, contained within the limiting envelope in the transverse dimension but bounded in phase to an azimuthal sector which is probably not greater than one-quarter of the chamber. Our purpose in this section is to describe the magnetic and electric forces acting on the individual ions and holding the ions within the enclosing envelope.

The feature which makes the method of multiple acceleration practical is the focusing resulting from the shape of the magnetic field. Ions making 100 or more revolutions in a cyclotron traverse a path hundreds of meters in total length. In a uniform magnetic field, in which field lines are strictly parallel, there would be no vertical deflections and no focusing. Ions traveling at a small angle to the median plane would follow a helical path and would strike against the top or bottom surfaces of the D's; the probability of an ion reaching the collector at the periphery would be vanishingly small.

Magnetic focusing results from a small decrease in magnetic field with increasing radius, so that lines of magnetic flux are concave inward.

This shape of field exists naturally near the periphery of cylindrical poles as a result of "fringing." In the central region an adequately decreasing field can be obtained by shaping the pole faces so that the gap widens slightly with increasing radius, or the effective gap length in the center can be shortened by inserting disk-shaped iron shims in gaps between the vacuum chamber and the magnet poles. At any point off the median plane in such a concave field the field has a radial as well as an axial component (see Fig. 6-7). Deviant particles traversing such a field experience restoring forces due to the radial field component tending to return them to the median plane. The direction of forces acting on orbiting particles is also illustrated in Fig. 6-7. The magnitude of the radial component of magnetic field, and thus of the restoring force, is proportional to the displacement from the equilibrium orbit.

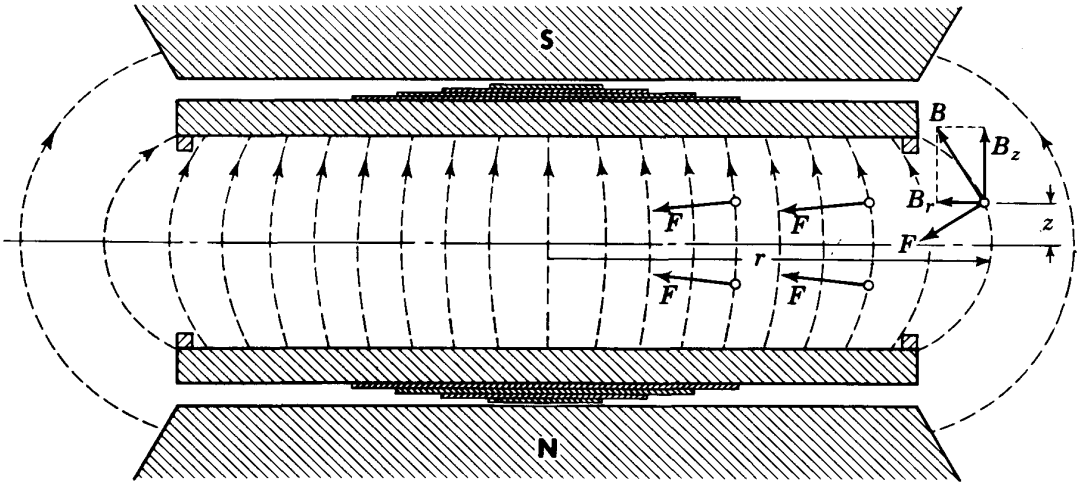

Fig. 6-7. Radially decreasing magnetic field between poles of a cyclotron magnet, showing shims for field correction.

Motion of any system under a restoring force which is proportional to the displacement is oscillatory in nature. In Chap. 5 the equations of motion were analyzed and general solutions were obtained of the resulting oscillatory motion. The results, as they apply to the type of field used in the cyclotron, can be summarized briefly. It was found useful to express the radial rate of decrease of field in terms of a radial exponent or index n defined by the relation [cf. Eq. (5-57)]

$$B = B_0 \left(\frac{r_0}{r}\right)^n \tag{6-6}$$

where B_0 is the field at some fixed radius r_0 and B is the field at a different radius r. The index n is obtained by differentiation to be $n = -\dfrac{r}{B}\dfrac{dB}{dr}$. In applying this concept to the cyclotron we determine the n value at any radius r from the field B and the local radial field gradient dB/dr at r.

Numerical n values will range from 0 at the center to values larger than 2 in the fringing field at the edge of the poles. In Chap. 5 it was shown that for particle oscillations about an equilibrium orbit to be stable for both axial and radial coordinates, the value of n must be in the range $0 < n < 1$.

The requirement of a radially decreasing field for axial focusing limits the range of validity of the basic resonance relation, in which a uniform field is required for resonance at constant applied frequency. The compromise which makes the cyclotron a practical accelerator is that the radial decrease in field be kept small so that resonance can be maintained over a sufficient number of accelerations for the ions to reach maximum energy. Experience is the best guide to the optimum magnitude of this radial decrease and the shape of the field. Those cyclotrons which have achieved high efficiency in acceleration of ions and a high-intensity beam show a consistent shape of magnetic field. This is an approximately linear decrease over most of the pole face out to the region where peripheral fringing sets in and where the decrease becomes more rapid. For medium-energy cyclotrons (15 to 20 Mev) the total decrease below the value of the central field out to the exit slit is about 2 per cent. The radial decrease can be larger (3 to 4 per cent) in small machines in which D voltage is relatively high and the number of revolutions small. It should be smaller ($\sim$1 per cent) for very large cyclotrons which approach the relativistic limit of ion energy (see Sec. 6-12) where maintenance of resonance over the maximum number of revolutions is a prime requisite.

A typical radial field distribution is that of the MIT cyclotron (Fig. 6-8). This field gave the highest beam intensities and was the culmination of an exhaustive empirical program of field shaping. This program used thin disk shims of various radii inserted in the two shimming gaps outside the pole faces as well as ring shims of several sizes mounted on the inner periphery of the pole faces. The values of the index n computed from this curve are also indicated in Fig. 6-8. The n value rises almost linearly from zero at the center to 0.02 at 15 in. (where fringing effects start), then increases rapidly to 0.40 at 18.75 in. (exit-slit location) and to 1.0 at 19.25 in.

Returning to the discussion of particle oscillations, we found in Chap. 5 that a particle displaced from the median plane in such a radially decreasing field experiences restoring forces which produce transverse oscillations about the median plane. The frequency of these axial oscillations is

$$f_z = n^{1/2} f_0 \tag{6-7}$$

where f_0 is the cyclotron resonance frequency given by Eq. (6-2). The initial amplitude z_0 of these oscillations will be determined by the internal aperture of the D's near the ion source. For the radial field distribution described above, the frequency of axial oscillations is small compared

with the orbital frequency over most of the pole face. At $r = 15$ in., where $n = 0.02$, for instance, $f_z = 0.14f_0$, so seven or more revolutions are required to complete a vertical oscillation cycle. Frequency increases to a maximum of about $0.6f_0$ at the maximum practical exit-slit location.

The amplitude of the vertical oscillations decreases with acceleration to higher energy and to larger orbit radii. This can be seen qualitatively as a consequence of the increase in strength of the restoring forces while the energy of transverse oscillations remains essentially constant. The

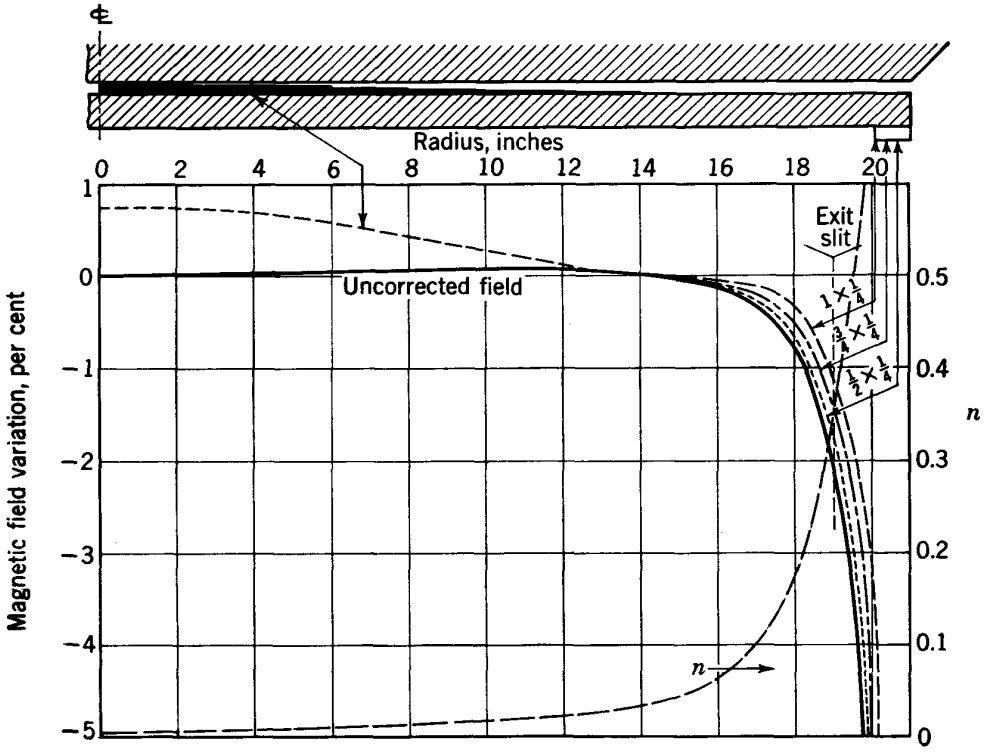

Fig. 6-8. Measured values of magnetic field as a function of pole-face radius for the MIT cyclotron.[14] The curves show the uncorrected field and the field obtained with disk shims and three sizes of ring shims at the edge of the poles.

damping relation of Eq. (5-70) shows that the amplitude is a function of the quantity $\omega n^{1/2}$, but it is not valid when the n value is extremely small, such as near the center of a cyclotron. For this special case in which the motion is nonrelativistic, we return to a study of the equation of this oscillatory motion [Eq. (5-65)], which can be written

$$\ddot{z} + \omega^2 n z = 0 \tag{6-8}$$

The optimum shape of magnetic field in a cyclotron was found to be one in which the n value rises approximately linearly with radius. The angular frequency is nearly constant, and in Eq. (6-5) it was shown that the orbit radius varies with the square root of the number of revolutions and hence with the square root of the time of acceleration. Conse-

quently, n is proportional to $t^{1/2}$, and Eq. (6-8) can be rewritten

$$\ddot{z} + (\text{const})\, t^{1/2} z = 0 \tag{6-9}$$

This constant is an arithmetic combination of machine parameters, which for the MIT cyclotron has the value 4.3×10^{16}. Equation (6-9) has an analytic solution involving fractional-order Bessel functions. It will not be quoted here since it is valid only in the case where n is proportional to r; in other cases it is necessary to integrate the equation of motion numerically. In the particular case of the MIT cyclotron the solution indicates a weak damping in the region in which n varies linearly with r, with a value $(z/z_0)_1 = 0.53$ at $r = 15$ in., where $n = 0.02$.

At larger radii the n value rises sharply, and Eq. (5-70) can be used to estimate the additional damping. Amplitudes vary approximately with $n^{-1/2}$, so the damping factor is given roughly by $\frac{z}{z_0} = \left(\frac{n_1}{n_2}\right)^{1/2}$. For the special case of the MIT cyclotron between $r = 15$ in. and $r = 18.75$ in. (exit slit) the n value rises from 0.02 to 0.4, and the additional damping factor $(z/z_0)_2 = 0.22$.

Combining the damping factors for these two regions of acceleration, we estimate the over-all damping from center to exit slit to be 0.12 for the MIT machine. The internal aperture of the D's in the central region is 1.6 in., so a possible initial amplitude is 0.8 in. and the final amplitude should be about 0.1 in. The observed height of the emergent beam (double amplitude) is about $\frac{1}{4}$ in., in reasonable agreement with this estimate.

A more detailed calculation of damping of axial-oscillation amplitudes would require numerical solution of the equations of motion and should also include the electrostatic focusing effects at the accelerating gaps, which will be discussed later in this chapter.

A practical consequence of this compaction in axial width of the envelope enclosing the ion oscillations is to make the problem of deflection of an emergent beam considerably simpler. Beam width is a basic parameter in the design of the exit-slit septum. On the other hand, the narrow beam width is a disadvantage when targets are used in the circulating beam, causing a serious problem in target cooling.

Radial oscillations also occur, about the ideal or concentric equilibrium orbit location, with a frequency given by

$$f_r = (1 - n)^{1/2} f_0 \tag{6-10}$$

Such oscillations can be induced at the start of acceleration by off-center location of the ion source, which produces a lack of concentricity of ion orbits with the magnetic field. At the start, where n is so small as to be negligible relative to unity, the frequency of these radial oscillations is

essentially equal to the ion orbital frequency. An orbit which is displaced relative to the center of the magnetic field will continue to expand in widening semicircles about the location of the displaced center. However, as the ions approach the radius of the exit slit, where the n value rises to about 0.40, the radial-oscillation frequency decreases to

$$f_r = 0.78 f_0$$

The decrease in f_r causes the orbits to precess, so the azimuth of maximum amplitude moves forward around the circumference, first by small steps and ultimately by large angular jumps in each turn. For the above example of $f_r = 0.78 f_0$ the angle of precession per turn is about 80°. The precessional motions of the individual particles are not coherent, so particles of all possible phases of precession exist within the resonant bunch. Particles of essentially the same energy will have a radial spread given by their residual double amplitude of radial oscillation and will also have an angular deviation from the equilibrium orbit. To illustrate with a practical case, a radial-oscillation amplitude of 0.50 in., at an orbit radius of 18.75 in. and an n value of 0.40, would result in an angular divergence of 0.019 radian.

Precession of orbit centers during acceleration can occur as a consequence of the unequal voltages between D's along the D faces. Since the D's are the terminating capacitances of quarter-wave resonant circuits and have a physical extension along their faces which is a significant fraction of the quarter wavelength, there will be a somewhat lower potential at the ends of the D faces nearest the lines relative to that at the extreme ends of the lines. This difference has been measured in some cyclotrons to be as great as 5 per cent. The resonant ions will receive an average smaller acceleration when crossing in one direction across D faces than in the other direction. This will cause the orbit centers to precess. The result is similar to that of a "bump" in the magnetic field at one azimuth. The effect of such a precession is to increase radial-oscillation amplitude. It can be partially compensated, under steady conditions, by displacing the ion source away from the geometric center. In some cyclotrons a displacement of the ion source of over 2 in. has been necessary to give maximum emergent beam intensities.

The radiofrequency electric field between D's also produces forces on deviant particles, depending on the shape of the electric field and on the phase of the rf cycle when particles cross the accelerating gap. The gap between D faces can be considered a cylindrical electric lens. In Fig. 6-9 a schematic cross section of the D gap is shown, indicating the lines of electric field and the direction of the forces on a particle crossing the gap. We note that there are convergent forces on entering the gap and divergent forces on leaving.

The first effect noted is a net displacement toward the median plane. This is equivalent to the "thick-lens" displacement of off-axis rays in an optical lens system. As for the optical case, it can be shown to be proportional to the displacement z from the median plane. It is also proportional to the ratio of energy acquired in a single crossing to particle energy. It will be most significant for the first few gap crossings when ions are at low energy.

The effect of the electric fields in a cyclotron was first analyzed and published independently by Rose[16] and Wilson[17,18] in 1938. Both authors considered the combined effect of the electric and magnetic fields, focusing at various stages of the acceleration, the phase shifts occurring during acceleration, and the significance in terms of the theoretical maximum

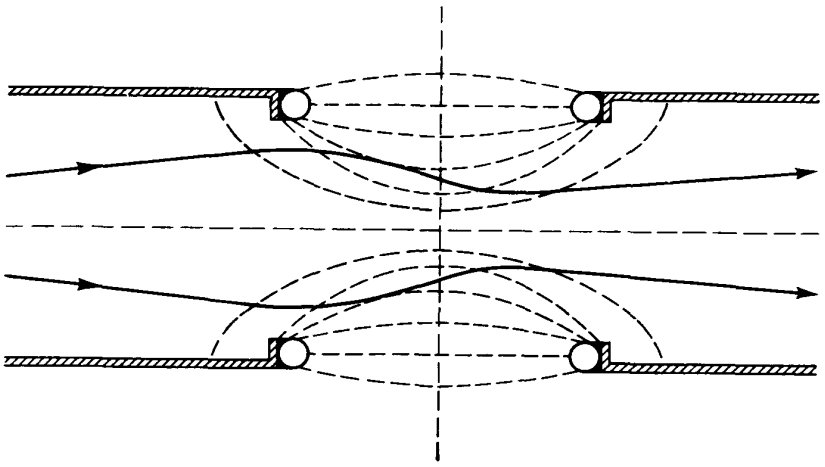

Fig. 6-9. Cross section of the electric-field pattern between the D's of a cyclotron. A typical ion path (exaggerated) illustrates the mechanism of electric focusing.

energy obtainable with a cyclotron. Their terminology and points of view were different, but the conclusions were essentially identical. Both described the vertical oscillations, and both showed that under certain conditions the electric field is defocusing. A recent and more complete analysis of the effects of the cyclotron fields by Cohen[19] has corrected a few errors and has also identified some additional defocusing terms in the equations of motion. We shall not attempt here to duplicate the detailed analysis, but shall describe the effects qualitatively.

Two mechanisms in electric focusing can be isolated and discussed. First, since the ion is being accelerated to higher velocity during its passage across the gap, the time spent in the convergent field on entering is longer than that in the divergent field. This "energy change" effect is most pronounced in early accelerations when ion energy is low and the change in velocity is most significant. Wilson has shown that it is most effective for a narrow gap between D's with wide D aperture.

Second, particles crossing the gap will experience an electric field which changes during the time of transit. In that portion of the rf cycle when

the rf field is decreasing in magnitude, the convergent force on entering the gap will be larger in magnitude than the divergent force on leaving, so the net result is convergence. During the other quadrant of the accelerating half-cycle, the effects will be reversed and the result will be divergence. The magnitude of this "field variation" effect also decreases with increasing particle energy and orbit radius, since the time spent in crossing the gap, and hence the magnitude of the potential change, becomes smaller.

The net result of these two major effects is an effective focusing only during early stages of acceleration and for particles within a rather limited phase band. The focal length of the equivalent electric lens is relatively short for low-energy ions of the proper phase, but becomes very long for high-energy particles. Each ion traverses the lens about 200 times. If we visualize the spiral path of the ions as unrolled into a straight line, the successive lenses of increasing focal length would be spaced at increasing intervals proportional to the square roots of a series of integers [see Eq. (6-5)]. The paths of ions through such a combination of converging lenses has been analyzed by Rose. He finds them to have long-period oscillations about the median plane, with an envelope which diverges slowly, with $T^{1/4}$. We note that with electric-field focusing only, the ion beam would diverge at large radii.

Electric focusing is strong enough to be significant only in the first few accelerations; it is maximum during the initial quarter-cycle as the ions are pulled out of the ion source and into the D. Such focusing can be observed visually under conditions of high gas pressure in the chamber when the beam of ions pulled from the source produces a faint blue glow. This glow is observed to converge as it leaves the column of ionization at the source and enters the D. Extensions on the D faces opposite the source, called "feelers" or "auspullers," have been used to improve beam intensity; they decrease the physical spacings and increase the electric field at the source. They also change the dimensions and focal properties of this first electric lens.

Quantitative experimental evidence on the effect of electric focusing or defocusing is lacking, since it is difficult to isolate this feature from the other factors which affect beam intensity. The long-period oscillations due to electric forces have not been observed, since they are submerged beneath the higher-frequency damped oscillations caused by the radially decreasing magnetic field. The few empirical studies which have been made with different shapes of feeler electrodes and ion sources have not been sufficient to show the full effect of geometry on ion-beam intensity.

The combined effects of electric and magnetic fields would predict an envelope which first increases in transverse thickness until it is limited by the internal D aperture, followed by a steadily decreasing amplitude with increasing ion energy and orbit radius due to the decreasing magnetic

field. A few experimental studies have been made of the size of this beam envelope. One technique has been to measure the width of the region of induced radioactivity on the leading edge of probes inserted to different radial locations. In one such test reported by Wilson the beam width was found to be limited by the internal aperture of the D's out to about one-third of the final radius and then to narrow in a nearly linear fashion out to the exit slit. The envelope calculated by Cohen[19] for the Oak Ridge cyclotron reaches its maximum at about one-half of the final radius. In some cyclotrons the D's have been shaped to conform roughly to such a beam envelope, having wide inner vertical aperture in the central region and tapering to a narrower width at the outer edge. In several cyclotrons holes have been melted in the D's in the inner region where beam amplitude is large. Good design practice uses closely spaced water-cooling tubes on the D's in the central region to absorb the heat produced by ions of excessive amplitude. A general conclusion is that all cyclotrons experience a considerable loss in intensity during the early stages of acceleration. In this situation a more detailed analysis of fields, forces, and particle orbits during the initial accelerations might yet yield useful and significant results.

6-4. PHASE RELATIONS DURING ACCELERATION

An ion crosses the gap between electrodes twice in each revolution, each time gaining energy from the electric field. Since the rf potential between electrodes varies harmonically with time, particles can be accelerated only during half of the cycle; during the other half they would be decelerated. Those crossing the gap when the field is maximum will require the smallest number of turns to reach maximum energy; those crossing at other phases gain energy at a slower rate and make more revolutions to attain maximum energy. We can express the time variation of electric field as

$$E = E_0 \cos \omega(t + t_0) \tag{6-11}$$

where the phase $t_0 = 0$ for maximum accelerating field. At the start of acceleration ($t = 0$) ions released from the source, which is midway between electrode faces, will gain maximum energy when the phase $\omega t_0 = 0$. The ion current pulled from the source by the rf field is greatest at the instant of maximum field, since it seems certain from experimental observations that the emission of ions is space-charge-limited.

We shall show that the ions which constitute the resonant beam start their acceleration near zero phase but experience phase shifts during acceleration. At all times, however, the ions of the resonant beam must remain within the accelerating half-cycle. The phase relationships at the start of acceleration can be understood by analyzing the initial ion

paths in the region of essentially uniform electric field between the electrode faces.

Consider a positive ion of charge-to-mass ratio e/m formed in a region in which there is an electric field E [given by Eq. (6-11)] along the x coordinate and a constant magnetic field B in the z direction. Motion will be confined to the xy plane, and the equations of motion in cartesian coordinates are

$$m\frac{d^2x}{dt^2} = eE + Be\frac{dy}{dt} \tag{6-12a}$$

$$m\frac{d^2y}{dt^2} = -Be\frac{dx}{dt} \tag{6-12b}$$

For cyclotron resonance the frequency of the applied electric field will be equal to the ion revolution frequency:

$$\omega = 2\pi f = \frac{Be}{m} \tag{6-13}$$

Using the accepted symbols for time derivatives the equations of motion become

$$\ddot{x} = \frac{eE_0}{m}\cos\omega(t + t_0) + \omega\dot{y} \tag{6-14a}$$

$$\ddot{y} = -\omega\dot{x} \tag{6-14b}$$

We consider the ion to start from rest ($\dot{x} = \dot{y} = 0$) at $t = 0$ from the origin. Solutions of the equations of motion above give the position of the ion at any subsequent time:

$$x = \frac{eE_0}{2m\omega^2}[\sin\omega t_0 \sin\omega t - t\sin\omega(t + t_0)] \tag{6-15a}$$

$$y = \frac{eE_0}{2m\omega^2}[\cos\omega t_0 \sin\omega t - t\cos\omega(t + t_0) - 2\sin\omega t_0(1 - \cos\omega t)] \tag{6-15b}$$

Initial ion paths have been computed from these equations for deuterons at a frequency $f = 13.5$ megacycles (for which $B = 17.7$ kilogauss) and an electric field $E_0 = 25{,}000$ volts/cm, for several phase conditions. The paths are plotted in Fig. 6-10. In this diagram the electric field is in the x direction (D faces parallel to the y axis).

Several interesting results become apparent from the paths plotted in Fig. 6-10. The central orbit is for zero initial phase, the optimum cyclotron resonance condition, in which ions leave the source when voltage between D's is a maximum. The opening spiral path is in exact resonance with the electric field, crossing the y axis at intervals of π, 2π, 3π, etc. One limiting phase condition ($\omega t_0 = -\pi/2$) is for D-voltage zero and increasing at the start; this particle travels in a wider orbit than the

resonant particle. The other limiting phase is not shown ($\omega t_0 = \pi/2$), but would be a mirror image of the $-\pi/2$ case. Intermediate orbits are shown, for phases of $\pm\pi/6$ and $\pm\pi/3$. As stated earlier, the bulk of the emission from the ion source will be concentrated in the interval when electric fields at the source are high, roughly between the phase curves

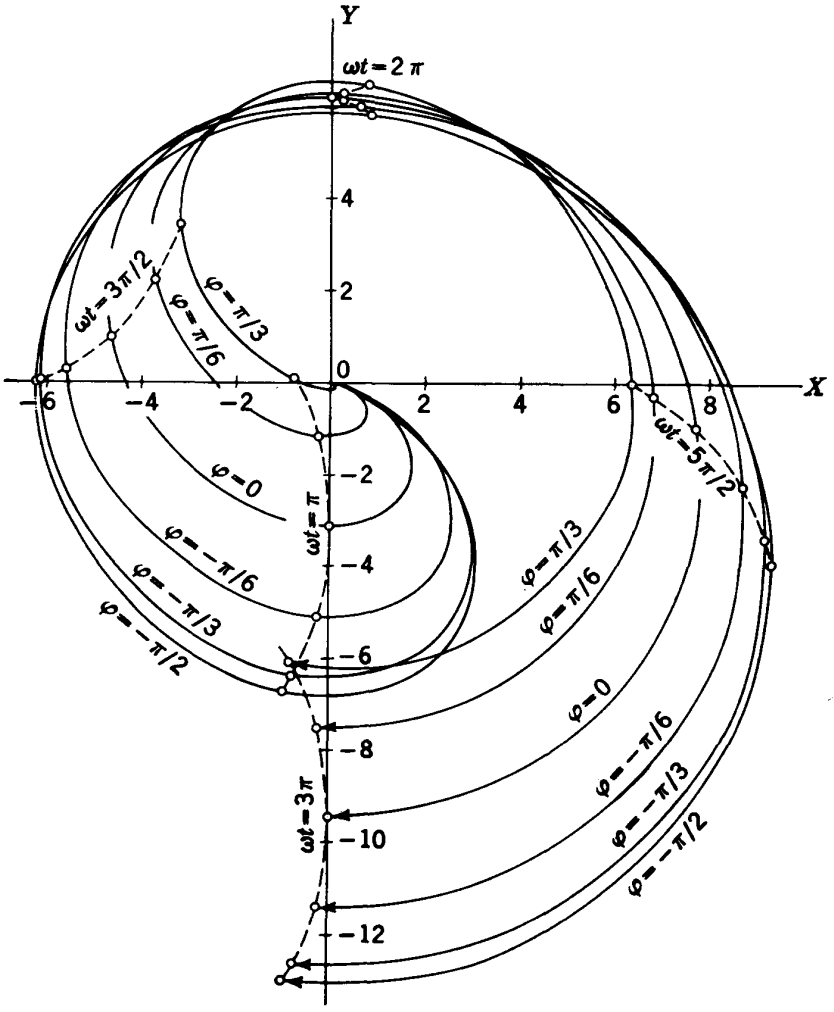

Fig. 6-10. Initial ion paths in a uniform sinusoidal electric field along the x axis and a magnetic field along the z axis. Orbits are shown for particles starting at the center at several phases of the electric field.

for $\omega t_0 = \pi/3$ and $-\pi/3$. This family of curves represents ions starting toward the right D.

The most interesting result is the phase focusing for off-phase ions. Small circled points on each curve in Fig. 6-10 show the positions of particles at $t = t_0$, when D voltage is a maximum. These points cluster closely around the y axis, even after only one half-cycle, and approach zero phase asymptotically in subsequent passages. This means that all ions from the source are bunched near zero phase, regardless of their initial phase.

It may also be noted here that cyclotron resonance exists even without having electric-field-free regions within the D's as was assumed in the simple theory. The paths are opening spirals, rather than semicircles, but the resonance condition is still satisfied.

Another significant feature of these initial orbits is the spatial concentration for ions of all possible phases. With the exception of a narrow band near $\omega t_0 = \pi/2$, all orbits swing clear of the ion-source location, allowing the use of a tubular jacket around the column of ionization if desired, or a support for a hooded source (see Sec. 6-6). Furthermore, the whole family of orbits come to an approximate focus near the second crossing of the y axis. This physical separation of successive orbits will be sharper the narrower is the phase band being accelerated. Experimental evidence for such separation of orbits near the ion source has been reported by several experimenters. The most obvious evidence is the observation of blackened circular bands on the interior surfaces of the D's after long operation. Presumably, these bands are due to dissociation and deposition of contaminant vapors in the chamber by those ions of the resonant beams which have large vertical oscillations and so approach or strike the inner D surfaces.

The above calculation and the plot of Fig. 6-10 were made on the simplifying assumption that the electric field was uniform. However, in practice the D faces are closely spaced and the electric fields do not penetrate far into the D's, so the larger orbits are shaped solely by the magnetic field. A better approximation is to assume that the electric field goes to zero at planes $x = \pm x_D$, which are typical of the D spacing in cyclotrons. Another set of orbits have been computed for this case, in which $x_D = 2$ cm, and in which the orbits become segments of circles outside x_D (Fig. 6-11). The phase focusing and spatial focusing are less complete than in the uniform-field plot, but are still observable. After a relatively few turns the orbits approach the pattern of connected semicircles assumed in the elementary cyclotron theory.

As the acceleration continues, a phase shift will result if the ion frequency differs from the applied frequency of the electric field. A decrease in ion frequency does occur as a result of the small radial decrease in magnetic field required for focusing, of about 2 per cent as described in the preceding section. At high ion energies the relativistic increase in mass will cause an additional drop in ion frequency, of about 2 per cent for 20-Mev protons or 1 per cent for 20-Mev deuterons (see Sec. 6-12). If the applied frequency were maintained at the initial ion frequency, this would cause the ions to lag behind the voltage maximum so the phase would shift into the decelerating part of the cycle and the beam would be lost.

The method used in practice to avoid loss of resonance is to use an applied frequency intermediate between the initial and final ion fre-

quencies. The ions will first lead the voltage maximum causing a phase shift toward, but not exceeding, the phase of zero voltage. Then, when ions reach a radius at which the magnetic field corresponds to an ion frequency equal to the applied frequency, the phase shift stops, and for further acceleration the shift reverses and approaches again the phase of

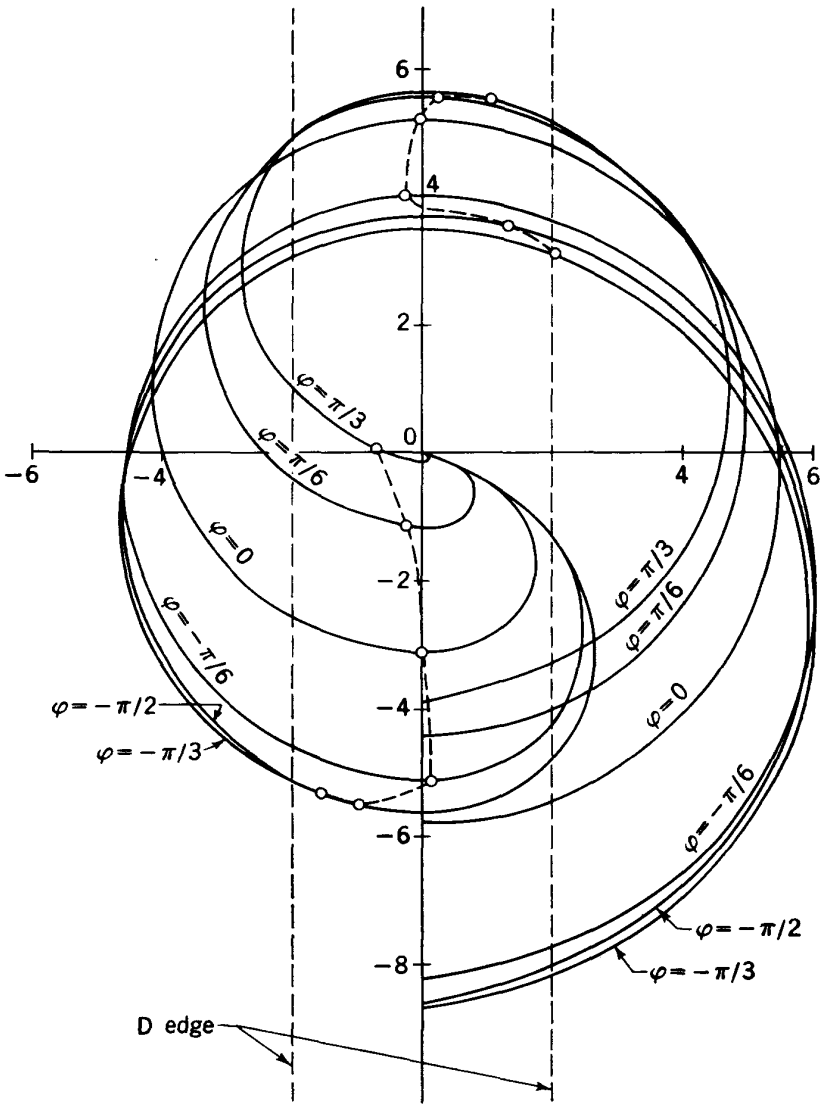

Fig. 6-11. Initial ion paths with the electric field confined between D edges.

maximum field. When the ions reach the radius of the exit slit and enter the deflector channel (see Sec. 6-7), they should again be close to zero phase. This is necessary so the difference in radius of successive paths, Δr, is large enough for them to pass behind the septum and enter the channel. So the practical maximum migration in phase will be from zero to $-\pi/2$ and back to zero, a total phase migration of π radians or one half-cycle.

The actual technique used to control resonance in a cyclotron is to vary the magnetic field, with the applied frequency held constant. The result is the same as discussed above. At the start of acceleration the central field is higher than that specified by the applied frequency, so the ions lead the voltage wave and the phase shifts toward $-\pi/2$; at large radii the field is lower and phase shifts in the opposite direction.

The shift in phase during acceleration is illustrated in Fig. 6-12, in which three half-cycles of the radiofrequency are shown. The initial electric acceleration will produce focusing for particles within the shaded quarter-cycle (while potential is decreasing in magnitude during passage of the particle across the gap), but intensities are a maximum and acceleration greatest for a band (labeled A) at near maximum voltage or near zero phase. An intermediate acceleration shows this group of ions

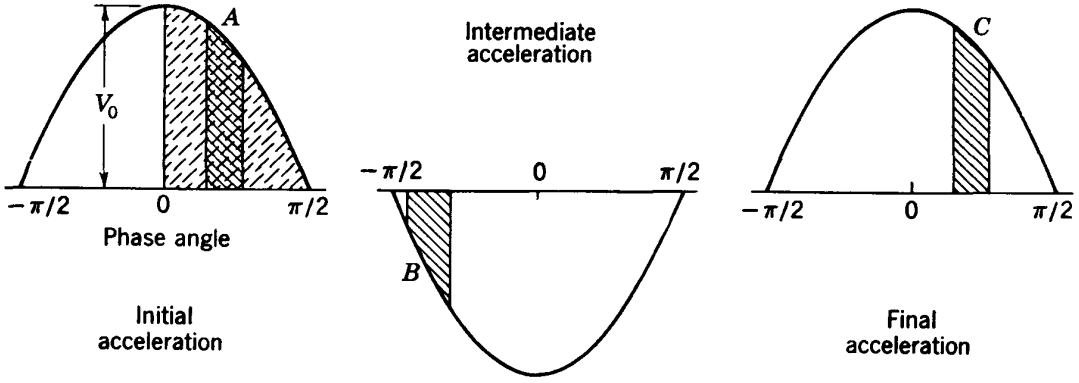

Fig. 6-12. Phase shift during acceleration of a preferred band of ions, labeled A at the start, B at an intermediate time, and C at the final acceleration.

(labeled B) at the extreme phase shift almost to $-\pi/2$. In the final acceleration the band (labeled C) is again near zero phase to provide sufficient change in radius per turn to emerge through the deflector channel.

Tuning of a cyclotron to obtain the highest energy and highest-intensity emergent beam depends on keeping the total phase shift within the limits described above. The location of the exit slit is extremely critical in this respect, since the magnetic field is falling steeply in this region and increasing the radius causes the phase shift to increase rapidly. Increasing the D voltage requires fewer turns for acceleration to maximum energy and will compensate for a larger phase shift. However, D voltage is usually limited by technical considerations of power and spark breakdown and cannot easily be pushed above a practical maximum operating value for a given cyclotron chamber and D assembly. D voltage can also be raised by decreasing the loading current to the D's, for example, by decreasing gas flow to the source, but the yield of ions is also reduced. In each cyclotron a practical compromise is reached between these several factors, which usually results in accepting a smaller exit radius

and lower beam energy than the maximum obtainable value in order to maintain the desired beam intensity.

When internal targets are used to intercept the resonant beam, the Δr limitation applying to an emergent beam is removed. The practical phase shift will be from zero to $-\pi/2$ and back to π radians, a considerable increase in total phase shift. As a consequence, the resonant beam intensities on such a target will be considerably higher than the emergent beam, and target location can be at a somewhat larger radius, resulting in higher ion energy.

6-5. VACUUM CHAMBER AND ELECTRODES

The chamber which fits between the poles of the electromagnet and contains the D's, the ion source, and the deflecting electrode is arranged to serve many purposes. It must be vacuum-tight, mechanically designed with adequate structural strength to resist distortion when under vacuum, constructed of nonmagnetic materials to prevent any disturbance of the symmetrical magnetic field, of high electrical conductivity to provide low resistance for the radiofrequency currents, and equipped with a large number of ports and apertures for inserting the many electrodes and controls. The design that has evolved is a framework of thick walls with many ports through the sides and with large circular apertures top and bottom filled by iron chamber lids which are extensions of the magnet poles. A photograph of the Massachusetts Institute of Technology chamber which is typical of present design is shown in Fig. 6-13. Its design features will be described below.

The structural frame of the chamber has been formed successfully in several laboratories from rolled brass hoops; others have used welded structures of thick plates of nonmagnetic stainless steel. Still others have used soldered or brazed assemblies of copper-alloy plates. A few have been successful in obtaining vacuum-tight bronze castings. Improved metallurgical techniques now make it possible to obtain large castings free from porosity. The MIT chamber is such a casting. All surfaces are machined, and many tapped screw holes are provided to bolt ports over the apertures and retain vacuum seals.

The soft-iron chamber lids rest on ledges machined in the chamber walls, with faces accurately parallel. The circular edge is sealed by a gasket joint under pressure of a packing ring held by a ring of bolts. Most cyclotrons use water-cooled copper sheet liners on the inner faces of the lids to provide a high-conductivity surface for rf currents. However, at MIT the inner surface of the lid is copper-plated to allow maximum clearance to the D's.

The D's are inserted through a large rectangular port in the rear of the chamber. Rectangular ports on the side faces are used to mount the

movable trimmer capacitor plates, the probe target, and the emergent beam port. A circular window allows inspection or insertion of probes along the diametral line between D's. The ion source is mounted opposite the window between D stems, with the cathode and anode leads paralleling the D faces.

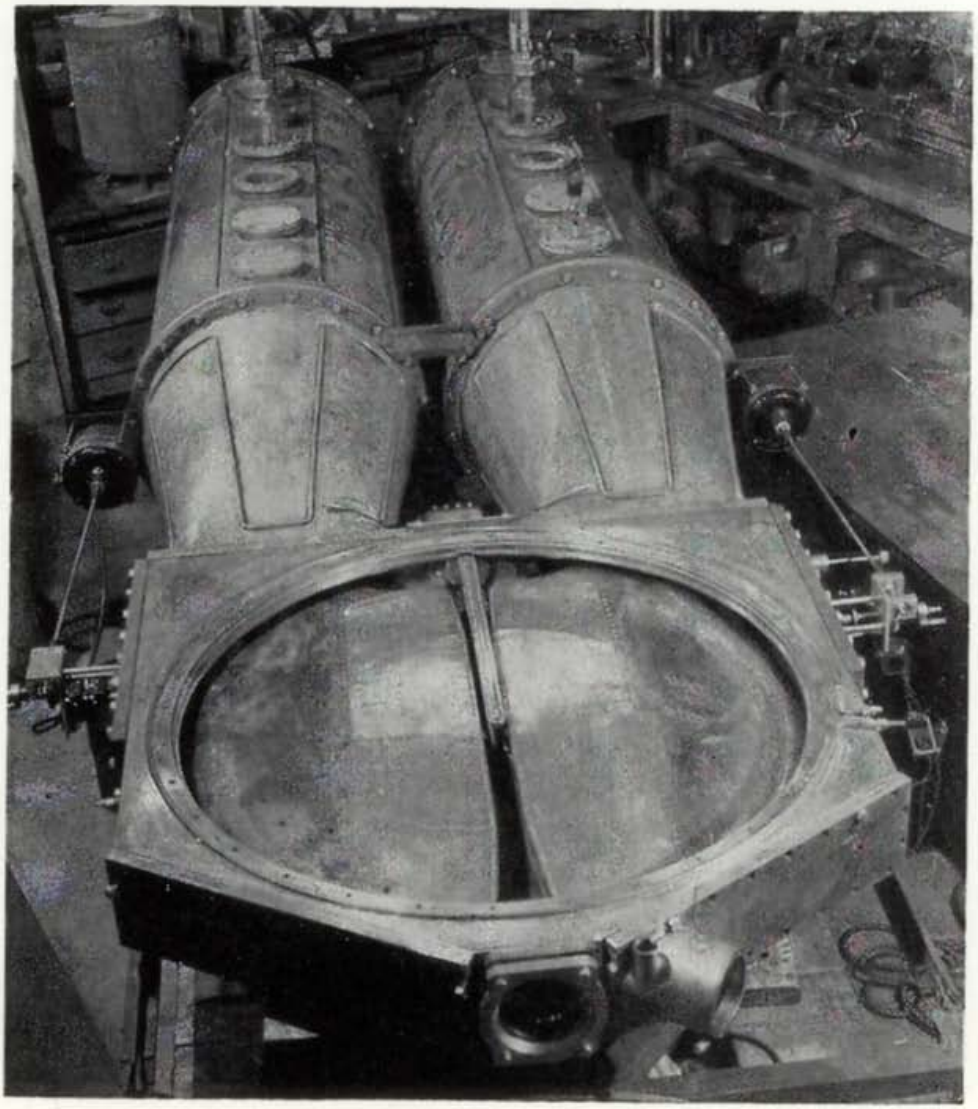

Fig. 6-13. Shop assembly photograph of the MIT cyclotron chamber.

The D's are supported on large-diameter (8-in.) stems within even larger (24-in.) cylinders which form a resonant circuit for the radio-frequency electric oscillations used for acceleration. The electrical properties of the rf system are described in a later section.

The coaxial D lines are connected to the chamber through tapered cones with oval cross section at the chamber wall. The inner stem which supports the D is formed from heavy copper tubing of 8 in. diam flattened into an oval shape where it enters the chamber, and the D structure is

built onto and supported by this flattened tubing. This oval shape of D lines at the throat improves mechanical rigidity, increases surface area, lowers rf resistance, and results in higher electrical efficiency. Many water-cooling tubes are soldered internally to the D's and D lines. In fact, it has been found necessary to have these tubes spaced as closely as 2 to 3 in. to prevent local heating and warping of the D's under power. Approximately 10 kw of heat is dissipated in each D and D line during operation. Other water-cooling circuits are distributed liberally around the coaxial lines, cones, and chamber walls, where experience shows the need.

The D's in the MIT cyclotron have a maximum outer width of $2\frac{1}{2}$ in. in the central region and are tapered over the outer half of their radius to a rounded edge having a 2-in. diam. The gap between chamber lids was chosen to be 5 in., leaving $1\frac{1}{4}$-in. clearance between D's and lids. This relatively short gap and small clearance are just adequate for maximum energy operation of this machine, resulting in a D-voltage limit of about 70 kv due to breakdown. Larger clearances are required for the higher D voltages needed in larger cyclotrons.

The deflector electrode and ejection septum are mounted within one D; the high-voltage electrode is supported coaxially along the center of the D stem on suitable insulators. The design of this deflector system is described in more detail in a later section of this chapter, as are the other components such as ion source and targets.

6-6. THE ION SOURCE

The source of ions used in most modern cyclotrons is a low-voltage, hot-cathode arc discharge. The discharge produces a dense column of ionization which is collimated by the strong magnetic field and crosses the center of the cyclotron chamber between D's. Positive ions formed in this region of ionization are pulled out and accelerated by the radio-frequency electric field of the D's.

The arc discharge itself is produced in a small metal-walled cavity located on the floor of the chamber against one pole face; it encloses a hot cathode which maintains a discharge current of 2 to 3 amp at relatively low potential, commonly 100 to 150 volts. In a typical ion source an intense beam of electrons of 1 to 2 amp emerges from the cavity through an exit hole in a truncated cone, aligned with its axis along the direction of the magnetic field. Gas is admitted to the discharge cavity from an external supply and flows out the exit hole with the electrons. This exit hole also permits a pressure differential to maintain an adequate gas pressure for the discharge within the cavity (estimated to be 10^{-2} mm Hg). The beam of electrons ionizes gas emerging from the exit hole, so ions are formed in place between the D's.

In the earliest cyclotrons an exposed cathode was used, located against one pole face near the center of the chamber. Ions were formed in the gas at low pressure which filled the entire chamber, and very low beam intensities were obtained (1-μa resonant beam). Such an exposed cathode can be seen in Fig. 6-1, which shows the first model-sized cyclotron.

The use of an arc source was first reported by Livingston, Holloway, and Baker[24] at Cornell University in 1939. It was an adaptation of the metal-capillary arc (Chap. 4). This first installation was in a small cyclotron with low-speed pumps. The discharge column was contained within a $\frac{1}{8}$-in. copper tube extended across the chamber, with a small

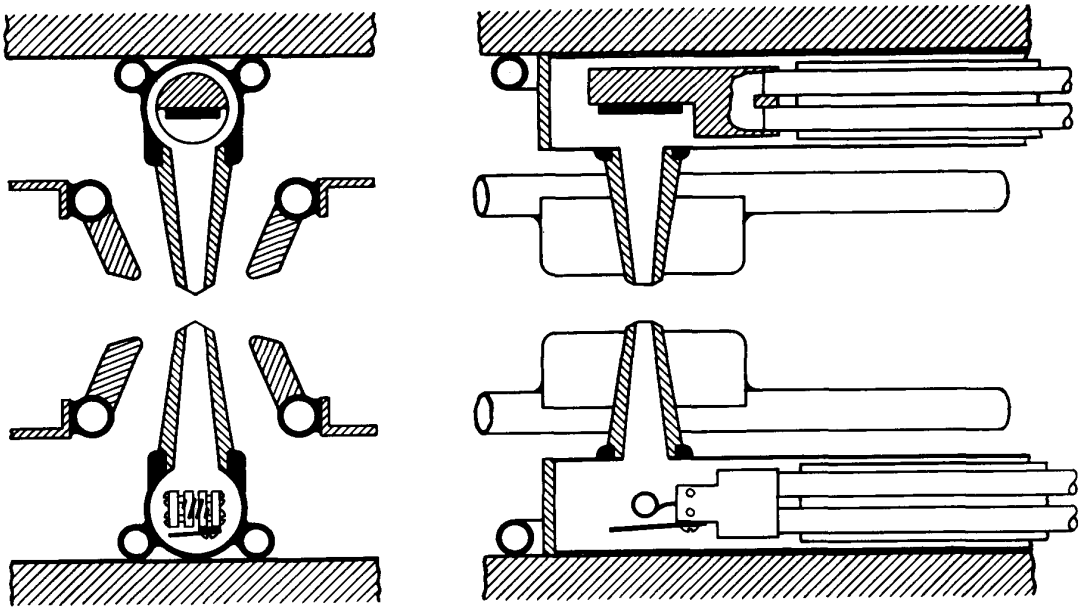

Fig. 6-14. An early MIT ion source using symmetrical cones and probes.

exit hole in the side opposite one D. The ion paths were large enough to clear the tube in their first accelerations.

With the development of high-speed pumps for larger cyclotrons the exit hole has enlarged so the capillary can be removed and the surface of the discharge column can be exposed to the electric fields of the D's. The shape of the arc-discharge cavity and of the cones for the exit hole has been the subject of competitive development in several laboratories, and many rather distinct types have proved successful. A review article on cyclotron ion sources[25] described the several designs and techniques developed by 1946.

Three stages of the development to higher-intensity sources are shown in Figs. 6-14 to 6-16. An early MIT source[14] used a symmetrical, double-cone structure in which the second cavity housed a test anode which was useful in aligning the cathode with the exit hole and in monitoring ion-source operation. Others used a single cone which terminated short of

the median plane and a water-cooled plate on the opposite side of the chamber to absorb heat from the electron beam. An improved version of the single-cone source is the "hooded arc"[26] (Fig. 6-15). The hood limits the length of the exposed column of ionization and avoids loading of the rf power supply for the D's with currents due to nonuseful ions coming from a more extended source. A more recent development, by

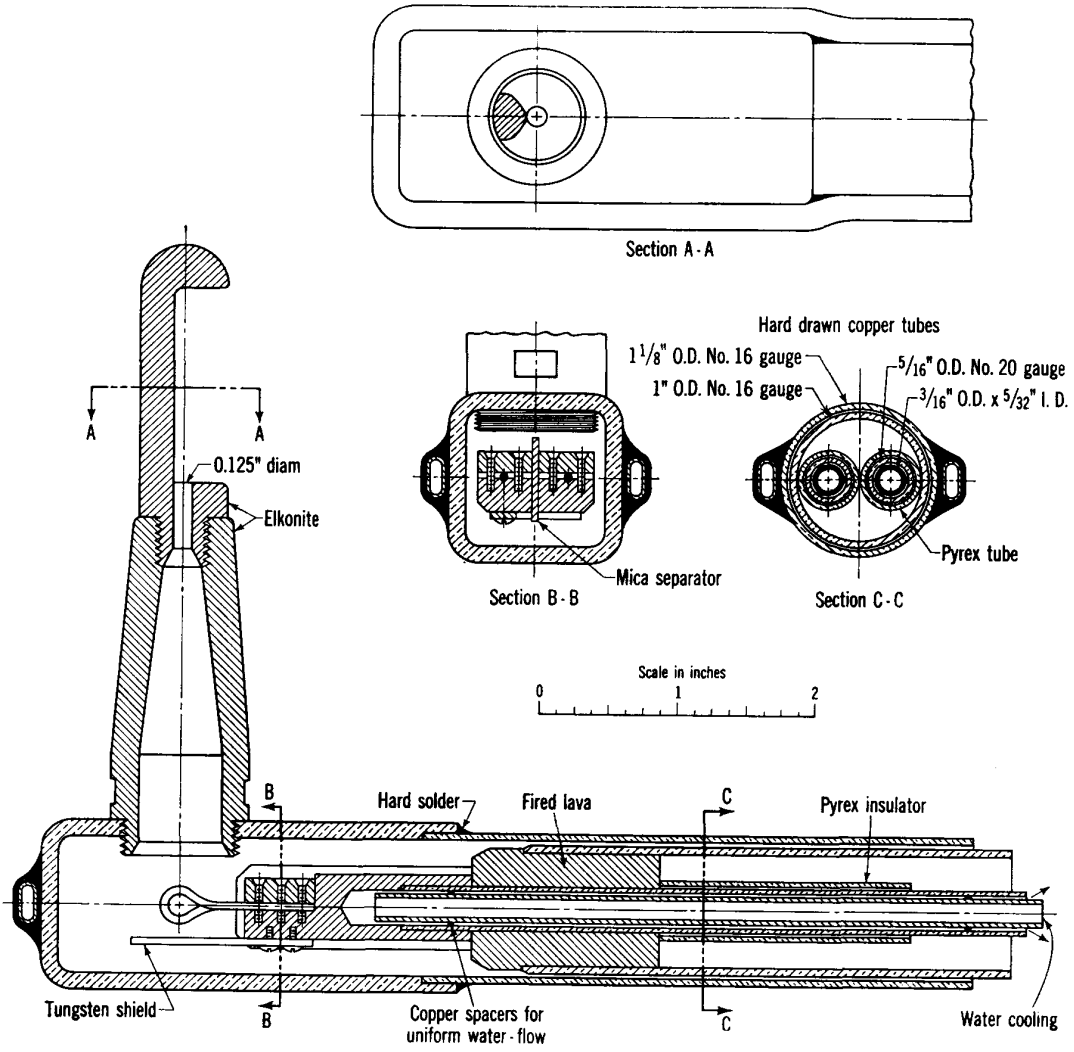

Fig. 6-15. Hooded-arc ion source. (Carnegie Institution.[26])

R. S. Livingston and R. J. Jones[27] of Oak Ridge, is designed for a cyclotron of wide D aperture and has an arc-discharge cavity extended across the D face with a long, narrow slit facing a slotted accelerating electrode mounted on one D.

Techniques have steadily improved with years of development. The cathode is now formed of heavy tungsten or tantalum rod, formed as a short-stemmed "V" or "U," clamped in terminating lugs and using large-diameter water-cooled leads. The largest cathode reported is the

0.170-in.-diam tantalum rod used in the Oak Ridge source; it requires 500 amp at 4 volts dc for heating. The heating power is either dc or high-frequency ac (~100 kc) to avoid damage from vibration in the magnetic field at low frequencies. Cathode life is a function of gas composition and is materially shortened by traces of oxygen. Lifetimes in service of 100 to 200 hr have been reported. The limit is due to erosion of a small area the size of the exit hole on the cathode surface, which represents the effective emitting surface.

Erosion of cone tips or arc-cavity slits is another limit to ion-source operation. Metals such as copper-tungsten alloy have been used, and water cooling of the arc body is common. Graphite is coming into wide use for cones, arc bodies, and also for D feelers or accelerating electrodes; it operates at high temperatures with a minimum of sputtering or evaporation. Many variations on cone-and-slit design have been used, and no one design has yet gained general acceptance.

The length of the exposed column of ionization seems to determine beam intensity. It is limited by the vertical aperture of the D's or the space between D feelers. If the column is too long, off-focus ions tend to load the D circuit and increase rf power requirements; if power is limited, D voltage is reduced. At various times this optimum length has been studied for a particular cyclotron. At MIT, with an internal D aperture of 1.6 in. the optimum length of ionization column was $\frac{5}{8}$ in. For 4-in.-wide D's in the Carnegie Institution 60-in. machine it was $1\frac{3}{8}$-in. The Oak Ridge cyclotrons have been designed for very high intensities, and the source described above has a slit $2\frac{1}{2}$ in. long. For each cyclotron there will be an optimum length depending on the D aperture, the shape of the ion source and accelerating structures, the available rf power, and the available pumping speed for evacuating gas from the source.

Typical operating characteristics of a hot-cathode arc of modest power and beam output would be: arc current, 3 amp; arc voltage drop, 100 volts; electron beam from exit hole, 2 amp; gas flow, 2 cm^3/min at atmospheric pressure. The resonant ion beam pulled from such a source by the rf fields of the D's might be about 0.5 ma. The beam intensity is limited by space charge in the column of ionization and can be improved by careful design of the electrode structures or by the use of feelers on the D edges to increase the electric field.

Another development of the Oak Ridge group is the "hollow-anode ion source,"[28] used for both light and multiply charged heavy ions (Fig. 6-16). It is a modification to cyclotron conditions of the electron oscillation source known as a P.I.G. (see Sec. 4-8). It was specifically developed for large cyclotrons with wide D faces and high rf power. In this source electrons are emitted from two secondary-emission cathodes at the ends of a hollow graphite anode with quartz sleeves. A long, narrow slit in the anode allows ions to emerge, where they are pulled into the D's by

the field on a slotted accelerator electrode. A potential of about 5 kv is required to strike the arc, dropping to about 600 volts in operation. Gas is introduced into the anode cavity from an external supply, and the narrow slit acts as a flow resistance. Resonant beam intensities of up to 3 ma of H^+ ions have been obtained from such a source.

Even higher-intensity sources are possible if adequate power is available for acceleration. There seems to be no practical limit to intensity if sufficient effort is spent on development of other components of the cyclotron to control heat and prevent damage.

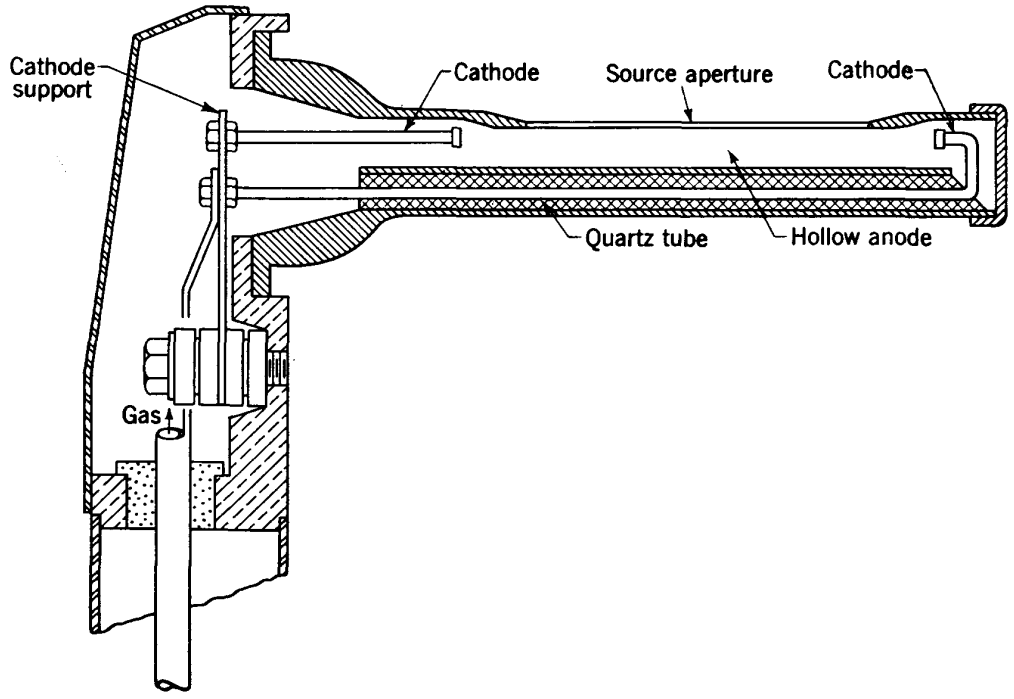

Fig. 6-16. Hollow-anode (P.I.G.) ion source, Oak Ridge National Laboratory.[28]

6-7. DEFLECTOR

The purpose of the deflecting electrode is to pull the resonant ion beam out of its circular path and direct it against an external target. At a chosen maximum radius R a thin septum is inserted having a larger radius of curvature $R + \Delta R$ which splits the resonant beam and allows a fraction of the ions to pass into a channel behind the septum. This is shown schematically in Fig. 6-17. An insulated electrode mounted behind and parallel to the septum is maintained at high negative dc potential, which provides an electric field to deflect the ions outward. The deflected beam traverses an opening spiral as the ions cross the weakening magnetic field at the pole edges and passes out of the chamber through a suitable port, beyond which external targets can be located.

Voltage needed for deflection depends on ion energy T, the width of channel to contain the ion beam d, and the deflected orbit radius $R + \Delta R$.

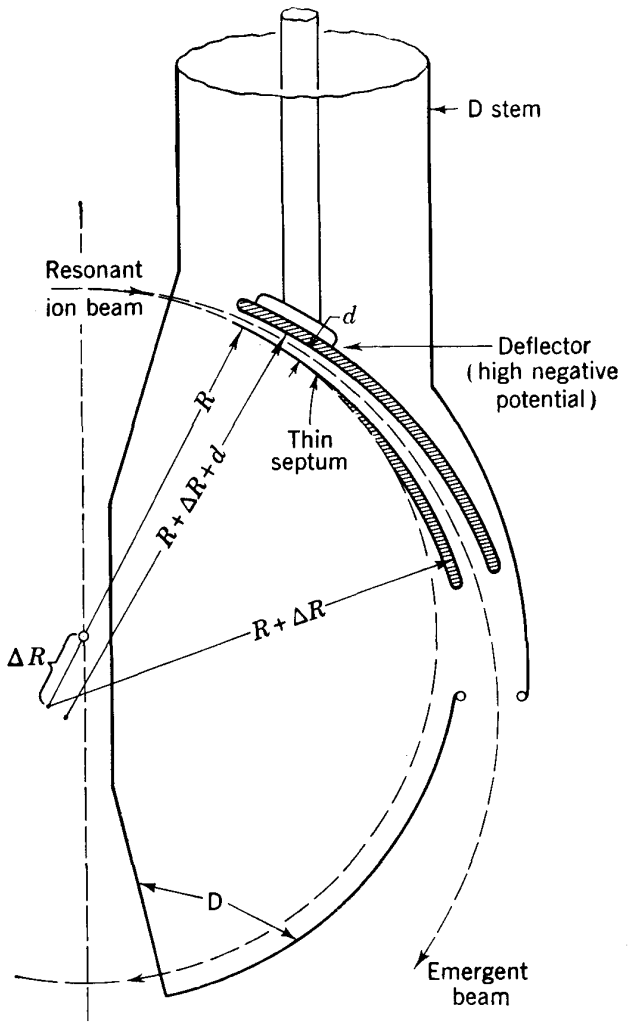

Fig. 6-17. Internal deflector electrode and septum for obtaining an emergent beam.

An estimate can be obtained by combining the relations for orbit radius with or without the deflecting potential V_d:

$$\left.\begin{aligned} \frac{mv^2}{R} &= Bev \\ \frac{mv^2}{R + \Delta R} &= Bev - \frac{V_d e}{d} \end{aligned}\right\} \qquad \frac{V_d}{d} = \frac{2T}{R}\frac{\Delta R}{R + \Delta R} \tag{6-16}$$

Evaluating for the 18.75-in. radius and 16-Mev deuterons of the MIT cyclotron, with an average deflector spacing $d = 0.3$ in., we find

For $\Delta R = 0.1R$: $V_d = 47{,}000$ volts
For $\Delta R = 0.2R$: $V_d = 87{,}000$ volts

A small value of ΔR means that the deflector channel diverges from the particle orbit slowly, so a long channel is required to pull the beam out through the fringing magnetic field. A large ΔR requires high potential on the deflector, which may exceed the breakdown limit. Under operating conditions an intense beam of ions traverses the channel and divergent ions bombard the electrodes; this produces ionization in the residual gas and limits the gap breakdown potential. The optimum choice depends on the individual characteristics and physical dimensions of the cyclotron. A typical figure, used in the MIT cyclotron, is a ΔR of $0.15R$.

The deflector gap is usually tapered to accommodate the diverging beam. Spacings as small as $\frac{1}{8}$ in. can be used at the entry slit, opening to $\frac{1}{2}$ in. or greater at the exit. The limit at the entry is set by the Δr between successive turns at this radius, which can be obtained from Eq. (6-5) in the form

$$\frac{\Delta r}{R} = \frac{1}{2}\frac{\Delta T}{T} = \frac{V_{rf}}{T} \tag{6-17}$$

since $\Delta T = 2V_{rf}$ (two accelerations). For $V_{rf} = 80$ kv, $T = 16$ Mev, and $R = 18.74$ in., we find $\Delta r = 0.1$ in.

The beam entering the exit slit has a finite energy spread and also an angular divergence associated with the residual radial oscillations of the resonant beam. In Sec. 6-4 the properties of these radial oscillations were discussed. It was shown that they lead to precessional motion of the individual particle orbits and an angular divergence of the particles entering the exit slit of up to 0.019 radian, for a radial-oscillation amplitude of 0.5 in. In a deflector channel of 20 in. length this would cause a beam spread of about 0.4 in. The deflector channel is tapered from $\frac{1}{8}$ to $\frac{1}{2}$ in. along its length so as to accept particles with this radial-oscillation amplitude. Amplitudes are apparently considerably larger than this for a considerable fraction of the resonant beam, so we expect that the channel dimensions will limit emergent beam intensity to a fraction of the available intensity in the resonant beam. Again, the designer and experimenter attempt to achieve a practical compromise based on channel dimensions and the voltage breakdown limit for deflecting potential. The reduction of radial amplitudes by careful shaping of the magnetic field becomes an important feature in achieving the best emergent beam intensities.

With such an initial angular divergence and radial width of the deflected beam, it will diverge even more rapidly as it passes through the rapidly decreasing magnetic fringing field. At the location of the emergent beam port it will have a wide radial spread. The observed radial width of the emergent beam in the MIT cyclotron is over 2 in., at a distance of about 60 in. measured along the spiral path. Emergent beam intensities

up to 25 per cent of the resonant beam intensity have been obtained under optimum conditions; for example, deuteron emergent beams of up to 150 μa have been obtained with a resonant beam of about 600 μa. However, such perfection in tuning and alignment is difficult to maintain, and practical operating intensities would in this case be limited to 80 or 100 μa.

The maximum orbit radius R, at which the deflector septum is located, is determined primarily by the radial decrease of magnetic field. Techniques for shaping of magnetic fields by shimming will be described in a

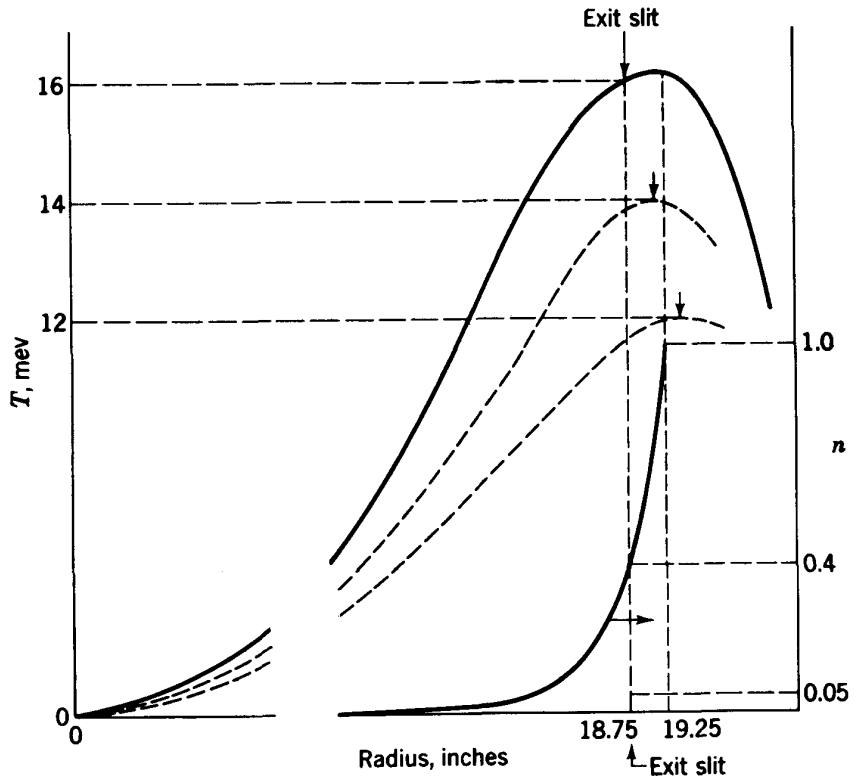

Fig. 6-18. Computed energy of deuterons as a function of orbit radius in the MIT cyclotron, showing location of exit slit. The n value computed from the magnetic field is also shown.

following section. A typical plot of magnetic field as a function of radius, obtained after suitable field shaping of the MIT cyclotron, was shown in Fig. 6-8. The maximum energy obtainable with a particular cyclotron is determined by the maximum value of the product B^2R^2, following Eq. (6-4). Using the measured values of field, the energy in the MIT cyclotron has been computed for each radius, and the result is plotted in Fig. 6-18.

The plot of energy as a function of radius falls below the theoretical curve for constant field, first slowly because of the small radial decrease required for focusing and then more rapidly because of fringing fields at

the pole edge. It reaches a maximum value at a point well inside the pole edge and then decreases for larger radii. This point represents the maximum energy obtainable with a given central field. The septum defining the exit slit for the deflector should be located as close to this maximum energy radius as is compatible with maintenance of resonance and of a high-intensity emergent beam. In the plot of Fig. 6-18 for the MIT cyclotron the radius of maximum energy is 19.25 in. and the experimentally determined location of the septum is at 18.75 in. On this same figure a curve is plotted of the computed values of the index $n = \frac{r_0}{B_0}\frac{dB}{dr}$, also shown in the field plot of Fig. 6-8. The n value is observed to rise steeply in the fringing field, reaching 0.40 at the location of the septum and 1.0 at the point of maximum energy.

Also shown as dashed curves on Fig. 6-18 are the computed values of energy versus radius for two lower values of magnetic field (with different shimming) used earlier in the process of tuning the cyclotron to higher energy. The maximum energy radius is not a definitely established position, but is actually larger at lower fields. This is associated with saturation of the corners of the pole edges at high flux densities. The locations of the deflector septum for these lower-field conditions were found to be at correspondingly larger radii, shown in the figure.

In order to adjust the location of the deflector septum to optimum in the MIT cyclotron, the deflector was designed to have an adjustable radial location. This was accomplished by pivoting the septum bar at the exit end of the channel; the water-cooling tubes which pass out of the D stem were used as levers to swing the entry end across a short arc so that R could be varied between 18 and 19 in.

Designing the correct, curved shape for the deflector septum and its paralleling deflector electrode is a straightforward but laborious process. The ion trajectory can be plotted step by step through the decreasing magnetic field and the decreasing electric field in the tapered channel, choosing appropriate values for deflecting potential, ion energy, and exit radius R. A set of such plots can be used to pick a set of diverging orbits which will emerge at the desired place on the chamber wall and for which the required deflecting potentials are acceptable. It will be found that the opening spiral can be fitted adequately by a septum which is a circular arc of radius $R + \Delta R$, where ΔR is about $0.1R$ or $0.2R$, as discussed above. Nevertheless, such calculations and designs can only be approximate, and it is desirable to have adjustable controls on deflector spacing and location which can be trimmed empirically for maximum beam intensity in operation.

A septum made of a thin solid-metal sheet will be bombarded by a considerable fraction of the resonant ion beam and will be damaged unless carefully designed and cooled. The energy in the resonant beam can be

greater than 10 kw for medium and large cyclotrons. Tungsten sheet was one of the earliest materials to be used successfully for a solid septum, but even tungsten is melted in a 10-kw beam. One technique used to prevent melting is to form the septum with a narrow slot on the median plane, of about the width of the resonant-ion beam. This narrow slot does not decrease the deflecting field seriously and allows most of the resonant beam to pass into the deflector channel without striking the channel walls. In the MIT cyclotron the septum is formed of two strips of tungsten, 0.020 in. thick and 12 in. long and with the edges spaced $\frac{1}{8}$ in. apart. Each strip is silver-soldered to a copper bar bent to the correct curvature, with copper tubing also soldered to the bar for cooling. Other designers use a long V slot in a tungsten-strip septum, so the heat is distributed over an extended surface area.

In the modern cyclotron with large-diameter D stems, the deflecting electrode is mounted on the end of a long supporting rod along the axis of one D stem, and the electrode itself is totally enclosed within the D. The electrode must be insulated for the 50 to 100 kv required, and the positioning adjustments work through insulators. It can be noted that no rf potential is transmitted to the deflector power supply with this mounting. The dc potential for the deflector is provided by a high-voltage rectifier unit equivalent to the power supply for an X-ray tube, and offers no unusual problems.

Some cyclotrons have been designed with deflector electrodes mounted through the chamber wall outside of the D, shaped to form the deflecting channel and extending around the outside of the D for 60 to 70° of arc. The rf field between D and deflector adds to the dc field in varying amount along the length of the channel, depending on the rf phase as a function of the angular position of the ions. This reduces somewhat the dc potentials required. In this position large rf potentials are induced on the electrode, and rf bypass capacitors are required to prevent the radio-frequency from damaging the deflector voltage supply; these are normally located just outside the chamber wall and enclosed within a metal shield to prevent rf power radiation into the laboratory. The control of discharges in the narrow channel between D and deflector has been a serious problem with this design. Nevertheless, some laboratories have been successful in obtaining very-high-intensity emergent beams.

6-8. RADIOFREQUENCY OSCILLATOR

The design of the radiofrequency power supply for the D's of a cyclotron should be a straightforward radio engineering problem. Many of the features of the rf power unit have in fact been taken bodily from experience in transmitter engineering for radio broadcast systems. However, the cyclotron system has an unusual property associated with the

variable ion loading and electrical discharges in the chamber which affects load impedance, so that the impedance is not constant as it is for a transmitting antenna. As a consequence, most transmitter experience and much of the advice from radio engineers have proved inapplicable. Physicists and their helpers in the cyclotron field have, of necessity, become specialists in high-frequency electronic engineering. In early cyclotrons the oscillator required a great deal of effort in the form of improvisation and rebuilding to keep pace with the growing need for higher D voltage. The accumulated experience has led to a variety of answers to the special problems of the cyclotron, several of which have proved satisfactory.

The problem is to produce a high-frequency potential difference of 100 to 200 kv in the frequency range between 10 and 20 megacycles/sec, between the opposing faces of the D's. Resonant circuits are required to transform from the potentials available with conventional high-frequency circuits using vacuum power tubes. These resonant circuits must be mechanically rigid to maintain a stable frequency and must have high electrical efficiency (high Q) to keep power requirements reasonable. The oscillator circuit must maintain suitable D voltage under all conditions of ion loading, recover automatically from extreme load conditions such as sparks or gas discharges, and protect the power tubes from damage.

The resonant circuit is electrically equivalent to a pair of quarter-wave coaxial transmission lines with the D's supported on the ends of the inner conductors. In large modern cyclotrons these coaxial lines are of large diameter and solidly constructed so the inner electrodes and D's are self-supporting and no solid insulators are required. D lines are made of copper and are water-cooled by tubes soldered to the inner surfaces, to obtain low resistances and high Q. The outer conductors provide shielding against radiative losses and can also be incorporated as part of the cyclotron chamber vacuum system, where they can serve as large-diameter pump leads. Inner and outer conductors are connected at the electrical node by a copper disk which is movable, so the electrical length of line can be varied to cover the desired range of frequency; clamps to make positive electrical contact are essential. Usually the inner electrode support is brought out through a vacuum seal beyond the node, with screw adjustments which are used to position the D's.

The coaxial lines and D's for the MIT cyclotron, which is typical of modern design, are illustrated in Fig. 6-19. In this machine the outer conductor is formed of 24-in.-diam copper pipe and the inner conductor of 8-in.-diam copper pipe. Even larger coaxial lines are used in higher-energy cyclotrons, up to 48 in. outer and 12 in. inner diameters in some cases. In the MIT design the inner conductor is flattened into an oval shape at the edge of the chamber, and the D is a smoothly shaped exten-

sion of the oval pipe. The tapering and the smooth, rounded shape of the D are intended to provide maximum mechanical strength and to minimize electric fields at the surfaces.

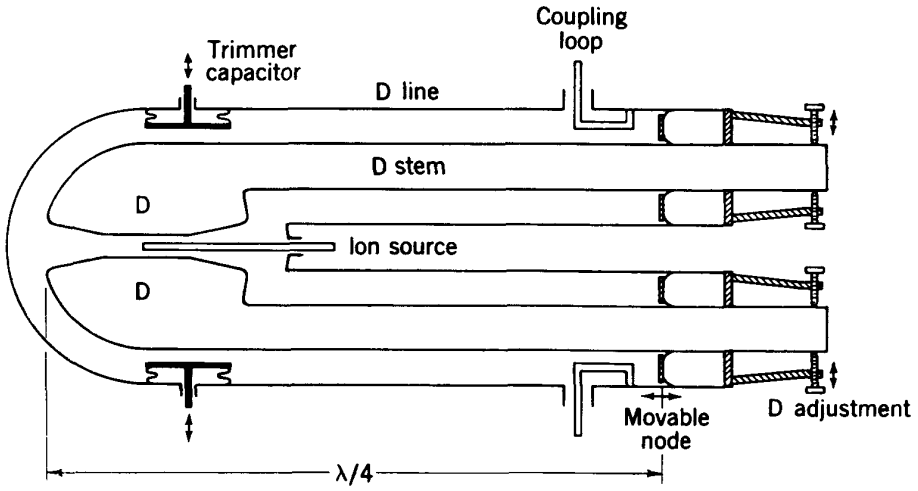

Fig. 6-19. Schematic diagram of the coaxial quarter-wave D-line circuit of the MIT cyclotron.

The equivalent circuit of the cyclotron is shown in Fig. 6-20, in which the distributed inductance, capacitance, and rf resistance of the lines and D's are represented by the lumped constants L_1, C_1, R_1, and L_2, C_2, R_2 for the two similar circuits, and C' is the D-to-D capacitance between the diametral faces which couples the two circuits. The resonant-ion load

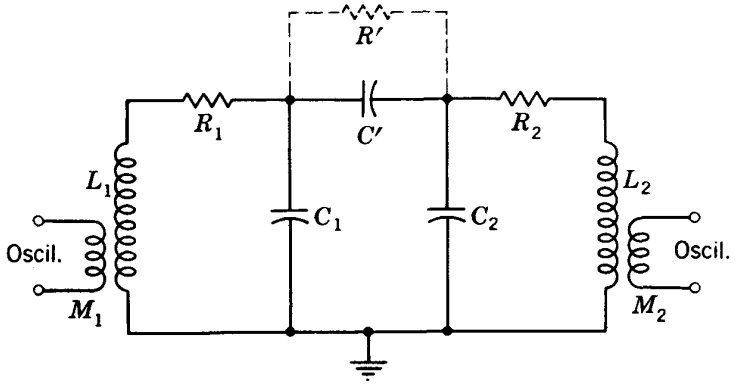

Fig. 6-20. Equivalent electric circuit for the D's and D lines of a cyclotron. The two quarter-wave resonant circuits L_1, R_1, C_1, and L_2, R_2, C_2 are coupled by the D-to-D capacitance C' and loaded by the ion beam load R'.

might be represented as an additional resistance R' paralleling C'. The two circuits are precisely tuned to resonance at the same frequency. If the two coupled circuits are mistuned, two shunt resonant frequencies will result, and the D voltages will be unequal.

Input power can be coupled most conveniently to the D circuits at the outer end of the coaxial line. This is near the voltage node, where cur-

rent is a maximum, and magnetic coupling is the obvious method. This is accomplished by a loop coupling the magnetic field inside the coaxial line, inserted through holes in the outer conductor through vacuum seals. The area of the loop determines the linkage and can be varied by raising or lowering the loop to match the impedance of the load. In principle a single loop driving one D line is sufficient, with the other D being coupled through the D-to-D capacitance. In practice a symmetrical system using two power tubes in push-pull and two coupling loops is the more common arrangement. In the equivalent circuit (Fig. 6-20) these loops are shown, with schematic connections to the oscillator circuit and with the mutual coupling inductances indicated as M_1 and M_2.

The circuit illustrated has several modes of oscillation. The normal push-pull mode, in which the two D's operate with phases opposed, provides maximum D-to-D voltage for ion acceleration. In a simplified case where the constants of the two circuits are identical ($L_1 = L_2$, $C_1 = C_2$, etc.) and coupling to the oscillator is neglected, the frequency of the push-pull mode is given by

$$f_{pp} = \frac{1}{2\pi[L(C + 2C')]^{1/2}} \tag{6-18}$$

Another fundamental mode of oscillation is the push-push or parallel resonance mode, in which the D's are in the same phase. Since in this mode there is no voltage between D's, the coupling capacitance C' is not effective, and the frequency is given by

$$f_{par} = \frac{1}{2\pi(LC)^{1/2}} \tag{6-19}$$

The resonant-ion load is zero when there is no voltage between D's, so the circuit has a higher Q and will tend to oscillate in this mode unless suppressed.

Other modes are possible when the coupled circuits in the oscillator are considered; these can be lumped together as parasitic oscillations. They are generally of higher frequency than the normal mode, and D voltages are much smaller or zero. These depend strongly on the physical dimensions of the external oscillator circuit and so are dependent on the particular design. They can be identified by an expert and suppressed by the addition of suitable grounding straps, bypass capacitors, etc. The only general rule is: The simpler the physical structure and the shorter the leads and connections, the less subject is the oscillator to parasitics.

A satisfactory alternative to two coaxial lines is a single shielded-pair arrangement, with similar large dimensions for the conductors. Although the mechanical construction is more complicated, it has certain advantages as an electric circuit. The D-to-D capacitance is increased by the paralleling line-to-line capacitance, separating mode frequencies and

making the circuit more stable in the desired push-pull mode of oscillation. The location of the node of zero radiofrequency potential is more readily available for tapping or adjustment, and the loop coupling the power oscillator to the resonant circuit can be designed more efficiently. This arrangement has been adopted in several of the larger cyclotrons, notably those built by the Collins Radio Company for the Brookhaven National Laboratory and for the Argonne National Laboratory. The most serious fault was found to be the mechanical problem of the movable node. Original designs did not provide adequate contact in the brushes to carry the high rf currents, and solid clamps had to be installed. The physical shaping of the node plate to carry the large rf currents has required detailed study. The node plate must also have large holes or apertures if pumps are located behind the node.

A technique frequently used to adjust or trim the relative resonant frequencies of the two D-line circuits is to use one or more trimmer capacitors which can be adjusted by remote control under full power operation. Such a variable capacitance can be provided by a movable plate on the side wall of the chamber facing one edge of the D. It must have excellent electrical contact to the walls for the radiofrequency currents and a range of motion sufficient to tune over about 1 per cent in frequency. The availability of such a tuning device makes it possible to adjust relative D voltage as desired for optimum operation.

The large amount of gas ionization produced between the D's when voltage is applied to the electrodes usually sets up a low-voltage, high-current discharge which is self-maintaining. This is the familiar "blue-glow" plasma discharge, maintained by secondary emission or electron "multipactoring"; this discharge causes gaseous ionization at high pressures. In the cyclotron the heat generated in the discharge liberates large quantities of gas from the metal surfaces and maintains the high pressure. This is particularly true at the start of operation after the chamber has been opened to air. Continuous operation under vacuum outgasses the surfaces, and the rate of gas evolution is eventually reduced. Fast pumps are required to evacuate this gas as it is produced and to keep the pressure as low as possible. Even the fastest pumps employed to date in any cyclotron are insufficient to keep the pressure below the threshold for blue-glow discharge during initial operation, but after some conditioning of the surfaces, fast pumps can maintain a low enough pressure to reduce the occurrence of such discharges significantly. This loading of the D circuit by discharge currents holds the D potentials down to a few hundred volts, too low to be effective in accelerating resonant ions. The radiofrequency D potential is also too low to provide adequate excitation for a self-excited oscillator. Unless the loading is removed, the chamber will continue to operate in the low-voltage, blue-glow discharge condition indefinitely.

When the circuit is operating at high D potentials, a different kind of discharge occurs frequently during conditioning. This is high-voltage sparking between a D and the grounded chamber lids, collimated by the magnetic field and sharply localized in position. It is apparently caused by secondary-electron emission from points, dust particles, or hot spots on the surfaces and is most frequent in regions where spacing is short or where curvature is sharpest, such as along D faces. In conditioning a fresh chamber these spark discharges occur like rain above and below the D's, until the whole surface is speckled with small discolored spots. This sparking will gradually decrease under high-voltage operation, but it sets the ultimate limit on D voltage for a cyclotron. The voltage limit can be raised by designing for greater clearance between D's and chamber lids and by providing round, smooth contours and clean, polished surfaces. It is common experience, however, that no amount of smoothing or polishing will eliminate the necessity of some high-voltage conditioning under vacuum. Clean laboratory techniques in preparing a chamber for reassembly after opening are essential; dust should be controlled and all grease removed (even fingerprints), and under no circumstances should steel wool or coarse abrasives be used in cleaning.

The oscillator circuit must be capable of driving the cyclotron through these varied conditions of sparking and discharge, without the necessity of tuning or of manual resetting of overload relays. Operation should be independent of minor frequency variations caused by ion loading or by vibrations or warping of the D's. The circuit must provide an electric field to sweep ions and electrons out of the chamber rapidly enough to prevent cumulative ionization and must be able to pull out of the blue-glow discharge condition automatically.

A variety of oscillator circuits have been developed, with varying success. Competing philosophies of circuit design have led to many friendly arguments between cyclotronists. Since each system has ultimately succeeded in its prime purpose of powering a cyclotron, it is difficult to assess the relative merits of the widely different systems. These circuits can be classified in two major divisions: (1) the master-oscillator, power-amplifier (MO-PA) circuits and (2) the self-excited oscillator circuits. In addition an intermediate form might be called the booster-oscillator circuit. The self-excited oscillator has the greatest number of variations and is used in the largest number of cyclotrons. The master oscillator has proved satisfactory for the high-power requirements of some large cyclotrons.

The MO-PA circuit follows most closely traditional radio engineering practice. Frequency is determined and excitation power is provided by a low-power self-excited master oscillator. This is used to drive the power-amplifier stage which supplies the D circuit. The MO-PA circuit has the advantage of maintaining D voltage during gas discharge conditions, if

properly coupled to the D circuit, and provides at all times the electric fields to sweep out ions. However, the circuits and coupling systems required to drive the variable-impedance load of the cyclotron efficiently prove to be complex and subject to parasitic modes of oscillation. The circuit will not follow changes in D-circuit frequency due to vibrations or warping under heat, so some method of controlling frequency from the D circuit is necessary. This can be provided by a feedback from the D circuit to the frequency-determining master oscillator, sometimes called a "rubber crystal." In some installations radio engineers have solved these special problems and have developed a satisfactory power supply.

The "booster oscillator" is basically a self-excited power supply similar to those described in the following paragraphs, but is also equipped with a low-power, master-oscillator exciter stage for the main oscillator which provides excitation when the self-excitation of the main oscillator is too small. So, during blue-glow discharges when the D circuit has low impedance, the booster provides sufficient excitation to develop enough voltage across the D's to sweep out the ions. Then, when the rf D potential is high enough to provide proper excitation, the main oscillator takes over as a self-excited system and the master oscillator is no longer needed. In one or two cyclotrons it has provided a method of controlling the blue-glow discharge condition.

The self-excited oscillator is basically a tuned-plate, tuned-grid system, so closely coupled to the D circuit that frequency is determined by and excitation is taken from the high-Q resonant D circuit. In its simplest form the tuned-plate circuit is the resonant D circuit of the cyclotron; grid excitation is derived from this same circuit. This oscillator will follow changes of frequency without retuning, has a minimum number of components, and has the advantage of circuit simplicity. However, special arrangements are required to obtain sufficient excitation to quench blue-glow discharges; this problem has been the subject of much development and has led to several variations in the design.

The power-oscillator tubes can be operated either with grounded cathode, grounded grid, or grounded anode, and examples of each type exist in cyclotron laboratories. The traditional circuit is with the cathode grounded, using grid excitation and insulating the high dc anode potential from the coupling loops in the D lines with capacitors. In this circuit the grid-plate capacitance of the power tube allows possible excitation of parasitic modes of oscillation.

The grounded-grid self-excited oscillator uses cathode excitation of the power tube from a loop coupling one D circuit and feeds power from the plate (using isolating capacitors) through another loop coupling the other D circuit. In this circuit the grounded grid serves as an electrostatic shield between tube cathode and anode, so the effect of interelectrode capacitance is negligible. With power fed to one D line and grid excita-

tion taken from the other D line, excitation occurs in the desired push-pull mode and other modes are suppressed.

A successful grounded-grid system, reported by Backus,[29] was developed for the Berkeley 60-in. cyclotron. Figure 6-21 is a schematic diagram of the circuit. Transmission lines are used to transmit power from the oscillator to the D-line coupling loop and from the other loop to the oscillator cathode. These lines must be properly terminated to avoid reflections and power loss, illustrated by the tuned stub lines shown in the figure. Power tubes can be used in parallel if required to increase power

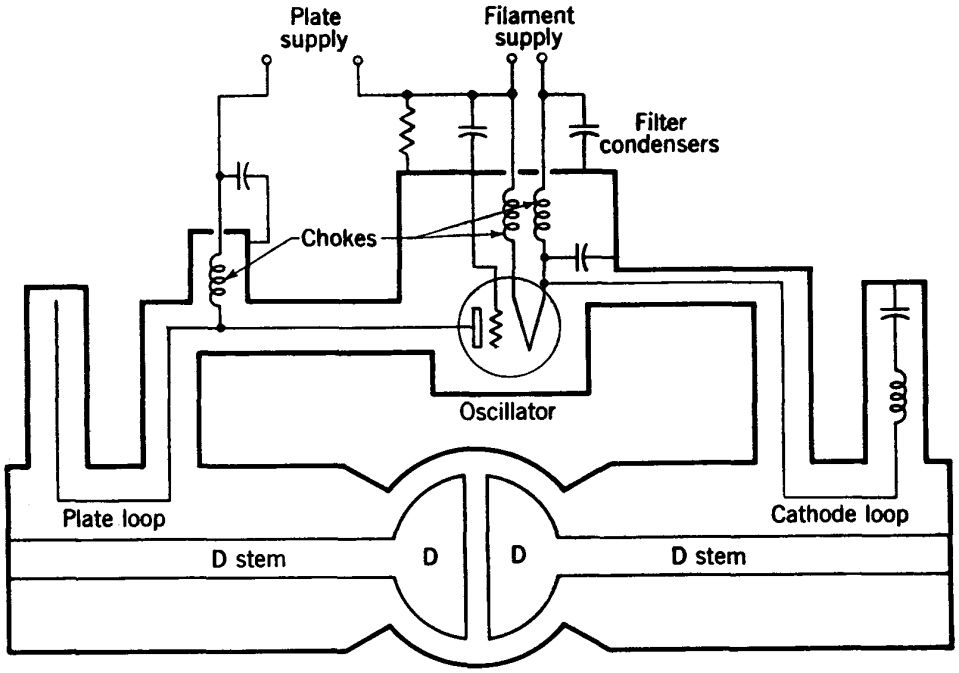

Fig. 6-21. Grounded-grid self-excited oscillator circuit for the University of California 60-in. cyclotron. (Backus.[29])

output. Cathode heating current is supplied through a choke-capacitor filter, in order to allow rf excitation of the cathode. The anode dc voltage supply must be insulated and filtered on both terminals, a slight additional complication. Blue-glow discharge reduces excitation severely and prevents high-voltage operation unless circuits are carefully tuned; in one installation (Brookhaven) a booster oscillator was installed to provide sufficient cathode excitation. In summary, it appears that in the hands of experts this grounded-grid system can be a reliable and efficient oscillator; but it is so large and complicated, so difficult to design and tune, and so subject to parasitics, that it has given considerable maintenance trouble to less experienced operators.

The grounded-anode type of self-excited oscillator has been used in several of the medium-size cyclotrons. It has some unique properties

which greatly reduce the physical complexity of the system. In this circuit the anodes of two power tubes are directly connected to loops coupling the two D circuits, and since they are at ground potential, no isolating capacitors are needed and the water to cool the tube anodes can be introduced through the tubing of which the coupling loops are made. The power tubes can be located directly above the D lines in a small, compact cabinet. The two tubes are operated in push-pull, with grid excitation provided by a pair of "crossed" capacitors of the variable vacuum-capacitor type, between opposite grid and plate terminals of the tubes. When these capacitors are adjusted to cancel the interelectrode capacitance of the power tubes, the cross-connection provides excitation only for the useful push-pull mode. Cathode heating power

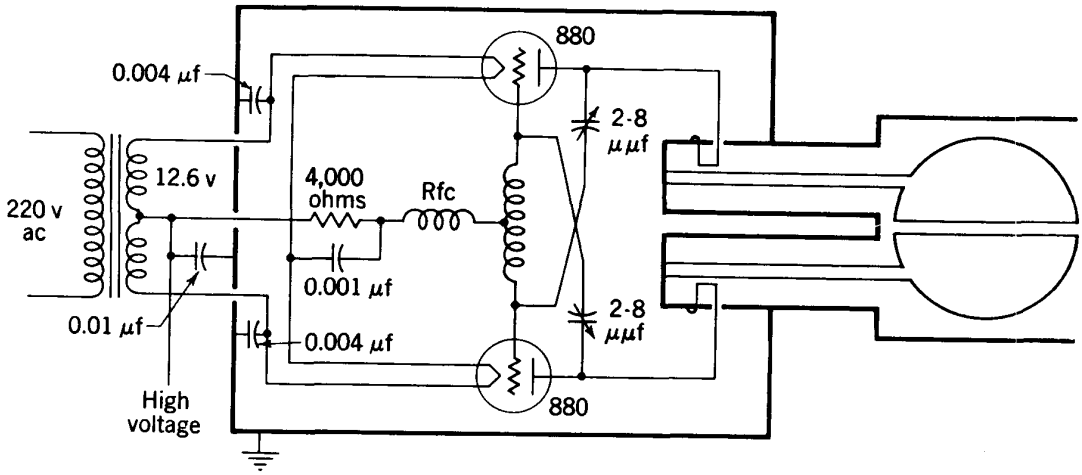

Fig. 6-22. Grounded-plate self-excited oscillator circuit of the University of Illinois 42-in. cyclotron. (Courtesy of G. F. Tape.)

comes from a low-voltage transformer insulated for the anode high voltage, which must be of negative polarity when used with grounded anode. The tuned-grid circuit is a low-Q inductive coil between grid terminals and is tuned to the resonant frequency. This symmetrical circuit suppresses the push-push mode of oscillation and, because of the compact arrangement, is essentially free from parasitics and easy to shield. However, if the excitation provided by the feedback capacitors to the grids is adjusted to optimum for high-power, high-impedance operation of the D circuits, it will be insufficient under the low-voltage blue-glow discharge condition. A reasonable excess grid excitation which provides sufficient power to suppress blue glows is allowable if tubes are not being run at full ratings. However, this limits the tube output power capability.

The grounded-anode circuit was developed at the University of Pittsburgh; a modification has been in service for many years at MIT. The most complete description (in an unpublished laboratory report) is for the oscillator of the University of Illinois 42-in. cyclotron, from which the circuit diagram of Fig. 6-22 is taken. The power tubes used were

"880s," made by several manufacturers, and rated for 50-kw rf power output. In service they are operated well below ratings; the total input power required for this size cyclotron is about 60 kw. The most significant advantage of this circuit is its simplicity and compactness along with the freedom from delicate tuning requirements or precise construction.

6-9. THE MAGNETIC FIELD

Cyclotron magnets are classically simple in their design features. Essentially all designers have arrived at the same basic structure of two cylindrical tapered poles, two rectangular yokes, and two rectangular uprights. Customarily the six pieces are machined forgings or castings of soft iron, although in a few cases (Berkeley 60-inch) the units are welded stacks of 2-in. mild steel rolled plate. Where castings have been used, corners are shaped to conform to magnetic flux lines and conserve weight of iron. With machined forgings it is usually cheaper to use rectangular blocks. In the largest magnets it has been necessary to assemble the basic units from narrower slabs, but for small- or medium-energy cyclotrons each of the six pieces is a single machined block. Precise machining of the surfaces in contact is necessary to make pole faces accurately parallel. The required machine tolerance is about 1/50,000 of the pole diameter and calls for the best machine practice. The structure of a few heavy blocks with machined faces in contact is quite rigid and requires very few bolts; alignment can be maintained by dowel pins or keys.

The design of magnets of this type is discussed in Chap. 8. However, the properties and requirements of each type of accelerator set certain limitations on design. We shall discuss here those features which are pertinent to the cyclotron.

A basic decision in the design of a magnet is whether pole tips should be cylindrical or tapered. The purpose of the taper is to keep flux density approximately constant along the length of the pole, to compensate for fringing flux entering the pole sides. For a designed flux density of 18 kilogauss in the gap of a 42-in. cyclotron, for example, the pole base would have to be about 52 in. in diameter to keep flux density in the base of the pole below the practical limit set by the permeability of the iron (about 20 kilogauss). Without such tapering the field in the gap is considerably lower, but the radial extent of the uniform field useful for acceleration is larger. In fact, particle energy is determined by the BR value at this maximum useful radius, which is largest for cylindrical poles. However, this advantage is offset by other considerations. With tapered poles the D's will be smaller and require less rf power for excitation. Other factors enter, such as the problem of deflecting an emergent beam through the fringing field. Within these several factors lies a wide region

for designer's choice, so we find cyclotrons with and without tapering and with all degrees of sophistication in magnet design.

The length of magnetic gap inside the chamber is also a designer's choice, depending on the evaluation of several other design problems. Internal dimensions of the D's are chosen on the basis of the anticipated amplitude of ion oscillations, the physical size of the ion source, and the importance of high intensities. The D's are often tapered to a narrower width at the periphery to conform to the ion beam envelope; this decreases capacitance to the chamber lids and reduces rf power requirements. The structural rigidity of the D's must also be considered in choosing their thickness. Once D dimensions are chosen, the clearance between D's and chamber surfaces can be considered. This clearance depends on the designed maximum energy and the corresponding maximum D voltage, and to a smaller extent on the smoothness of surfaces. Water-cooled copper plates are used as chamber liners by some designers, and these occupy space in the pole gap. This space was saved in the MIT chamber by copper-plating the surfaces of the iron pole faces; no serious heating due to rf currents was observed. Naturally, the longer the magnet gap the larger is the power required for excitation, varying approximately with the square of gap length. Furthermore, a wider gap reduces the maximum useful radius for acceleration due to fringing field penetration and so reduces maximum energy. Experience in evaluating these problems has led to the use of 5- to 6-in. gaps for 42-in. poles and 8- to 9-in. gaps for 60-in. poles for most cyclotrons in which maximum energy was the primary consideration. Wider gaps have been used when high intensity was considered more important.

Another engineering decision is the balance between magnet power and magnet cost. Excitation coils can be made with a large cross section of conductor, so the power for excitation is small. However, the larger physical dimensions and weights of both coil and iron yoke increase initial construction cost. A rough balance is frequently made by minimizing total cost of construction plus cost of power for 10 years.

The power source commonly used for excitation is a dc generator driven by an ac three-phase motor, usually with a smaller dc generator on the same shaft to supply the excitation current for the main generator. The magnet field must be accurately regulated to maintain a steady beam and be subject to delicate adjustment by the operator. A constant-current regulator is needed, capable of reducing fluctuations to better than 1/1000. A typical current-regulating circuit takes an input signal from the potential drop across a standard temperature-controlled resistor in series with the magnet coils and compares it against a standard potential obtained from a constant-potential battery. The difference voltage is amplified electronically and used to provide excitation for the exciter generator. A feedback control circuit maintains constant magnet cur-

rent automatically. Controls are also provided for adjusting the magnitude of the regulated current manually and are used in tuning for peak beam current. In some laboratories a further control circuit senses the beam current and automatically tunes the magnet current to maintain peak beam intensity. Techniques for magnet control vary widely, and several systems have been developed which will maintain a steady cyclotron beam for hours.

One of the more serious problems in tuning up a cyclotron is the shaping of the magnetic field to preserve resonance and maintain beam intensity. The shimming of a cyclotron has been a mysterious blockade to efficient operation in many laboratories and has required many weeks of cut-and-try experimenting in almost every machine built to date. In the early days, practitioners of the art of shimming devised many empirical techniques for bringing in a beam, but individual differences between cyclotrons usually made these formulas unsuccessful on other machines. However, with accumulated experience and with the modern techniques of field measurement, it is now possible to anticipate the proper magnetic-field shape for a cyclotron and to design the optimum shimming.

Although all cyclotron magnets are designed to give an ideally perfect uniform field, they all require special pole-face machining or shimming to develop the necessary radial decrease, and they all show imperfections and inhomogeneities which require correction. The magnetic inhomogeneities which must be measured and corrected can be identified separately as:

1. Radial decrease required for focusing
2. Radial decrease at the periphery due to fringing
3. Azimuthal variations of field, at all radii
4. Deviations of the magnetic median plane
5. Local variations due to machining errors, blowholes, etc.

The optimum radial decrease in field was described in Sec. 6-3 as one which decreased almost linearly from the center out to the region where peripheral fringing sets in, with a magnitude of decrease out to this point of about 2 per cent of the central field. Although this field shape can be achieved by machining of the surfaces of the pole faces, it is usually obtained by inserting a flat pyramidal stack of thin iron shims in shimming gaps outside the pole-face plates. Figure 6-8 shows the field shape in the MIT cyclotron obtained by the use of such stacks in the two shimming gaps, each consisting of four disks of 0.020-in. soft iron sheet of 6, 14, 18, and 22 in. diam. The instrument used to measure this radial decrease consisted of a small search coil and an integrating electronic fluxmeter (see Chap. 8). The coil was slid smoothly on a radial arm out from the center, in several azimuthal locations, to observe the radial

decrease. A series of measurements with different sets of shims led to the final choice.

Peripheral fringing causes the field to drop sharply at large radii, faster than is desirable for focusing. Rings of soft iron fastened to the extreme edge of the poles will limit this sharp drop and extend the region of slow decrease to larger radii. They are limited in physical size because they reduce clearance to the D stems where the stems go out of the chamber. At MIT the optimum ring section was $\frac{3}{4}$ by $\frac{1}{4}$ in.; the measured shape of field with and without this shim is shown in Fig. 6-8. Shims which are too large produce a minimum in the radial field plot which would cause defocusing. Also, a set of shims which are correct at high fields will be too strong and produce a defocusing minimum in the plot at lower fields, so the use of ring shims restricts the flexibility of varying the output energy of a cyclotron.

The modern technique for adjusting the radial decrease in magnetic field is to use corrective windings or shimming coils in place of the edge ring shims and the stacks of thin iron shims. These are flat-wound coils of many concentric turns with individual leads brought out radially from the inner turns. They can be located in the shimming gaps outside the pole-face cover plates or inside the vacuum chamber on the inner surface of the pole faces, where they must be covered with copper-plate liners for the rf circuit. Currents can be adjusted individually in the concentric turns to provide any desired radial decrease in field. For most of the central area of the pole face the excitation required is less than 1 per cent that of the main excitation coils of the magnet, so small currents can provide the desired radial decrease for focusing. Near the edge the currents must be considerably greater to offset the fringing fields. Although the technical problems are severe, especially those associated with the mechanical clamping structures, control of heating, and the many seals for bringing electric leads out of the vacuum chamber, the advantages of such an electric shimming system are obvious. One of the more important advantages is that the electrical corrections can be varied to provide optimum shimming at any magnetic field, allowing the cyclotron to be developed into a variable-energy machine.

Azimuthal variations of field can cause serious perturbations of the particle orbits, primarily through inducing radial oscillations. The figure of merit used to describe azimuthal uniformity is the maximum per cent variation around a circle of constant radius, and the most critical region is near the exit-slit location. Experience, again, is the only guide to the necessary uniformity. Most operators agree that a variation of less than 0.1 to 0.2 per cent is desirable in large cyclotrons.

Instruments for measuring azimuthal variation are described in Chap. 8. The same type of search coil with integrating electronic fluxmeter can be used as for the radial measurements, with the coil mounted on a

radial arm which is pivoted at the center and can be swung around a full circle. Before corrections, measurements of the MIT magnet showed variations as large as 2 per cent of the average field. These were due to inhomogeneities in the iron of the cast poles and to the asymmetric shape of the yokes. After careful correction by use of sector-shaped and wedge-shaped shims, the errors were reduced to less than 0.1 per cent for all radii out to the exit slit.

The magnetic median plane may deviate from the geometric median plane; the ion beam will follow the magnetic plane. A special search coil can be used to observe the median plane in the radially decreasing field, using two opposed identical coils equally spaced about the center and with the axis precisely aligned normal to the pole surfaces. At MIT the uncorrected field showed a median plane displaced ½ in. below the central plane on which targets were located. This was adequately corrected by reducing excitation in the upper magnet windings relative to the lower ones, after which the beam emerged on the geometric median plane.

Still other inhomogeneities can be observed in a thorough program of magnetic-field measurements. A local weak spot in the field (0.5 per cent low) was observed in the MIT magnet which was presumed to be due to a blowhole in the pole casting; it was corrected by a local spot shim.

The techniques described above make it possible to design a cyclotron field which will be satisfactory without relying on the cut-and-try empirical shimming of early days. The experience at MIT is typical. After several years of empirical shimming, with continual difficulties in maintaining high-intensity operation, a careful program of measurement and correction was carried out as indicated in the illustrations above. When this program was completed, the cyclotron was reassembled and on the first operation gave the highest beam intensities ever obtained, with no further empirical shimming.

6-10. VACUUM PUMPS AND SEALS

The large-volume vacuum chambers resulting from the coaxial D-line design and the high rate of gas evolution in discharges require high-speed pumps. A good rule of thumb is to provide a pumping speed of at least 1 liter/sec at 10^{-5} mm Hg per liter of volume. Oil-diffusion pumps of large diameter which have two or three pumping stages and automatic fractionation of the oil are best suited to this purpose. The pumps must be equipped with adequate baffles to prevent back streaming of the oil vapor, so there is minimum deposition of oil within the vacuum chamber. The mechanical pumps must have sufficient displacement to pump down the chamber volume from atmospheric to the backing-pressure limit of

the diffusion pumps in a relatively short time; 15 to 20 min is considered a good design figure. They must also maintain backing pressure under the high gas-evolution conditions of discharge, so the chamber will recover quickly from the bursts of gas pressure produced.

The techniques for evacuating large metal chambers have undergone steady improvement, speeded in recent years by the developments for the large synchroaccelerators. Most of these techniques originated in cyclotron laboratories and have been enlarged and extended for application to the larger machines. Concepts are radically different from those used for high-vacuum glass systems, in which surfaces are outgassed by heating under vacuum and vapors are condensed in refrigerated traps. Outgassing of the large metal surfaces in a cyclotron is impractical, and vapor evolution is small compared with gas flow, so refrigeration is less important with cyclotrons. Reliance is placed in such high pumping speeds that evolved gas and vapors are evacuated as rapidly as they are formed.

The MIT cyclotron vacuum-pumping system is typical and illustrates the techniques, although it does not contain all the features used in other installations. Two oil-diffusion pumps are used, bolted to 15-in. apertures on the bottom of the two D lines. Figure 6-23 is a diagram of the 12-in., three-stage, fractionating oil-diffusion pump. Various oils have been used successfully. A silicone-base oil has been most satisfactory and has given the longest service. The water-cooled baffle at the top of the pump is designed to intercept back-streaming oil vapor, yet to give maximum transmission for gas diffusing in the forward direction. It consists of a conical spiral of narrow, overlapping half-rings of thin copper with water-cooling tubing soldered along one edge of the rings. No refrigerant other than this water-cooled baffle is used.

The heating units at the base of the pump are formed of three 1-kw Calrod elements, cast into an aluminum block. Power can be adjusted separately on the three units to give maximum pumping speed. In operation the total power requirement for each pump is 1.8 kw.

In test runs with a calibrated air leak, the diffusion pumps developed a speed through the baffle of 1200 liters/sec each at 10^{-5} mm Hg. The total effective pumping speed for the two pumps of 2400 liters/sec is adequate for the 2000-liter volume. With no gas flow, chamber pressures of better than 1×10^{-6} mm Hg are obtained. With the deuterium gas flow from the ion source, the operating pressure is about 2×10^{-5} mm Hg, and pumping speed is materially increased by substitution of deuterium for air.

In the MIT installation no high-vacuum valves are used between D lines and pumps. Diffusion pumps are allowed to cool for a half-hour before admitting air. Valves were considered unnecessary in view of the infrequent need for opening the chamber to atmospheric pressure. Valves are commonly employed, however, in other installations.

Two mechanical pumps are connected to the low-pressure manifolds of the diffusion pumps, cross-connected so they can be operated in parallel for pump-down; a single pump can be used for normal operation. These pumps are two-stage units with a displacement of 7 liters/sec. The pair

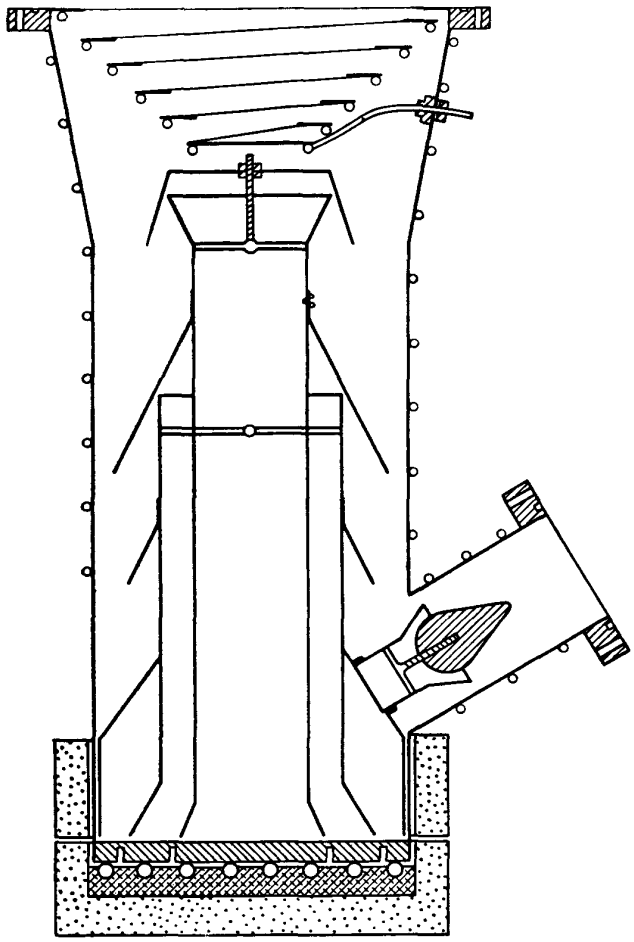

Fig. 6-23. Fractionating oil-diffusion pump of 12 in. diam developed for the MIT cyclotron. Two pumps are used.

will pump down the 2000-liter-volume chamber to the backing-pressure limit of the diffusion pumps in 20 min, about the time needed for the diffusion-pump heaters to rise to operating temperature.

The design and technique of vacuum seals have made steady progress through years of development. Simple, reliable seals are available for most of the special types of joints needed in an all-metal vacuum system. A basic design for a seal between parallel surfaces or flanges consists of a groove machined in one surface to hold a strip gasket in position, with suitable bolts between flanges to compress the gasket. The gasket may be a rectangular strip of rubber, taper-lapped at the joint and about 50 per cent thicker than the depth of the groove to allow for compression, or it may be an endless rubber ring of square cross section cut from a sheet, or it may be a continuous band of round cross section. This latter

form is available commercially in a variety of sizes and materials and is known as an O-Ring. A double-gasket seal is frequently used with a pump-out connection to the space between gaskets. This arrangement makes it possible to test the seal for vacuum-tightness quickly and with certainty or to provide a pump-out port in case of a leak. Small grooves and gaskets can be used for small apertures where bolt pressure is small. On the other hand, ¼-in. gaskets have proved adequate for even the largest seals, if surfaces are machined and bolt pressure is uniform.

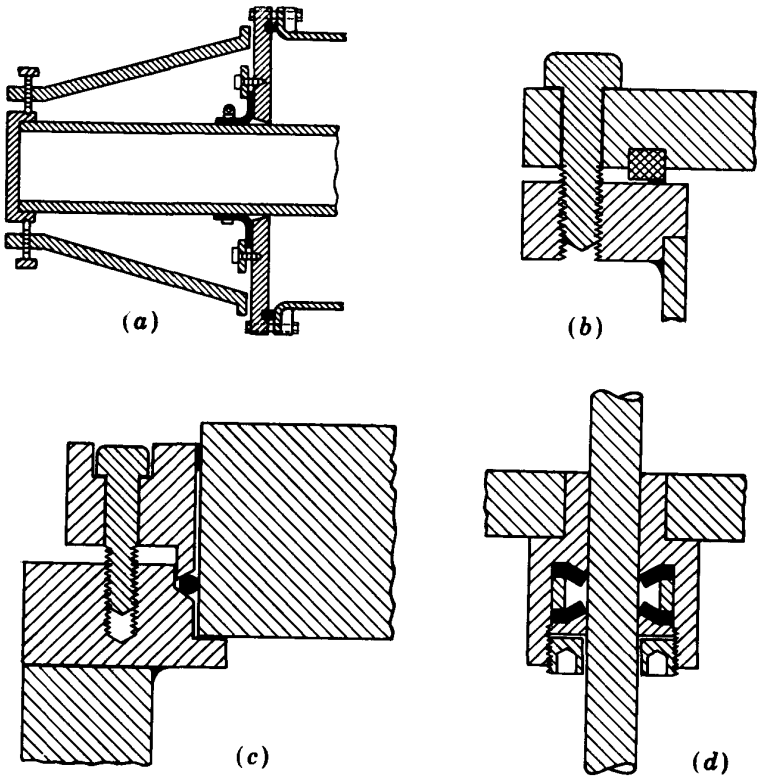

Fig. 6-24. Gasket vacuum seals for several purposes: (*a*) D-stem flexible joint and D-line ring-gasket seal; (*b*) detail of ring-gasket seal; (*c*) chamber lid seal using O-Ring and packing gland; (*d*) shaft seal allowing lateral and rotary motion.

Conductivity for rf currents through such a seal can be assured by half-covering the gasket with a thin copper-foil strip. Conversely, it can be adapted as an insulator with thick gaskets and fiber insulation around the bolts. For semipermanent seals soft fuse-wire or aluminum-wire gaskets have been successfully used.

Many movable joints are required for adjustments of the cyclotron D's, ion source, deflector, trimmer capacitors, etc. Figure 6-24 illustrates several of the seals developed for special purposes: a flexible diaphragm seal used for the adjusting motions of the large D stem (Fig. 6-24*a*); a square gasket in a groove for cover-plate seals (Fig. 6-24*b*); a typical pack-

ing-gland seal used for the chamber lids (Fig. 6-24*c*); and a seal which utilizes atmospheric pressure and the elasticity of rubber to make a movable vacuumtight joint which allows in-out and rotary motion of a shaft (Fig. 6-24*d*). Similar results can be obtained with O-Ring seals available commercially.

Several grades of rubber and of synthetics are available as gasket material. Low vapor pressure is the primary requirement; physical strength and resilience come next. Most natural or artificial rubbers have unacceptable vapor pressures and also deteriorate when used with lubricating greases. Neoprene is free of these faults and is widely used in cyclotrons. Myvaseal has even lower vapor pressures.

With the steady growth of a commercial vacuum industry, it is now possible to buy all the essential parts of the vacuum pumping system, including pumps, baffles, valves, and gauges. This eliminates much of the design and development effort which went into the vacuum systems of early cyclotrons.

6-11. TARGET ARRANGEMENTS

Targets for the cyclotron are of many types, depending on the needs of the particular experiment. For some purposes probe targets are used to intercept the resonant beam; these are mounted on stems with sliding vacuum seals at the chamber wall. In this location the targets are bombarded by the full intensity of the resonant beam, which may be from 0.5 to 1.0 ma at energies between 10 and 20 Mev, giving a beam power between 5 and 20 kw. Because of the small axial width of the beam in the fringing field and the small radial spread which is desirable when operating with an emergent beam, the cross section of the beam may be less than 1 cm^2. Experience has shown that it is almost impossible to cool targets with such high power densities. Any target would be destroyed by melting except those formed of metals of very high thermal conductivity and high melting point. A variety of techniques have been used to reduce power density by increasing surface area of the target.

An oscillating probe target developed at MIT was able to dissipate up to 10 kw of beam energy for certain target materials. The target was formed of flattened copper tubing, in which the water-flow channel was about 0.020 in. thick and 0.5 in. wide; water pressures of 40 psi resulted in flows of about 1 gpm. The face of the target was also tilted relative to the direction of the beam to increase surface area. This unit was arranged with a flexible vacuum seal at the chamber wall so that it could be oscillated transversely at 10 to 20 oscillations per second by external motor drive, moving the face of the target across the beam and extending the effective surface area to 1 in. length by ½ in. width. Thin plates of

beryllium and other metallic targets were silver-soldered to the face of this target for bombardment.

Still other techniques have been developed to utilize the resonant beam, such as deliberate detuning of the cyclotron to expand the transverse dimensions of the beam and decrease beam power density. However, in most high-intensity cyclotrons the beam intensity must be reduced below the available maximum because of this limitation on target cooling, and only the most refractory of target materials can be bombarded successfully. Nevertheless, probe targets are still used for special experiments in which the high current density is advantageous. When suitable target materials are available, the high beam density results in a high specific intensity of induced radioactivity and minimizes the inactive residue. With a Be target the concentration of fast neutrons beyond the target exceeds the neutron density in nuclear reactors by several orders of magnitude, so fast-neutron-induced activities can be produced efficiently in small target samples behind the Be target. The largest total yields of neutrons from a cyclotron are usually obtained with a water-cooled Be probe target in the resonant beam, through the Be(d,n) reaction; so probe targets are used whenever the cyclotron is used as a neutron source. The yield of neutrons from this reaction is about 1 neutron per 200 deuterons at 15 Mev energy.

Targets for the emergent beam of deflected particles are located in a target box at the chamber wall where the beam emerges. This box can be separated from the cyclotron vacuum by a thin-foil window to allow rapid interchange of targets and to allow bombardment in a gaseous atmosphere if desired. For many target materials such a gaseous atmosphere (usually He) is essential for surface cooling and to limit evaporation and sputtering. With high-intensity emergent beams the thin-foil window is a limit to beam intensity; double-foil windows have been developed with gas cooling (He gas) of the foil surfaces by a gas jet introduced between the two foils. Occasionally, thin targets are used in the target box to limit bombardment energy to a narrow range, so the beam channel extends beyond the target box to a well-shielded "catcher" target at a distance. For the production of induced radioactivities in target materials which cannot readily be obtained in thin plate or foil form, a more extended target can be used which is tilted to present a large surface area to the beam; powder targets have been used in the emergent beam with this technique. Thin targets of special materials can be supported in polyethylene films.[30]

The radiation hazard to personnel from induced radioactivity in targets is a serious problem. Quick-acting valves and gates are essential to keep handling time a minimum; protective gloves and shields and long-handled tongs are important. A fully automatic target-handling mechanism would reduce the danger, but few practical systems have been

devised and no system will eliminate all exposure for the maintenance staff. Cyclotron laboratories should adopt the best handling techniques from those developed for reactors.

Research studies of the primary processes of disintegration or scattering do not require high beam intensity but do require good energy resolution and low background radiation intensities. Many cyclotrons are now used primarily for the production of such low-intensity, well-focused emergent beams. These beams are brought out of the cyclotron vault through a narrow channel in the shielding wall into an external observation room in which the experimental apparatus is located, in some installations at distances of 20 to 40 ft from the cyclotron. A few such installations have been described in publications.[31,32] Usually a carefully designed set of focusing magnets is located near the cyclotron, and an analyzing magnet is used to select a narrow momentum band from the emergent beam. A typical result would be a 1-μa beam on a target of 1 cm^2 area at a distance of 20 ft, with an energy resolution of ± 0.5 per cent.

6-12. MAXIMUM ENERGY AND OPTIMUM SIZE

The relativistic increase in mass of the ions at high energies would need a magnetic field increasing radially outward to maintain resonance. This is forbidden by focusing requirements; in fact, a field which decreases with radius is essential. This conflict between the requirements for focusing and for ion resonance results in a theoretical and practical upper limit to the energy obtainable with a fixed-frequency cyclotron.

To evaluate this limit the resonance relation of Eq. (6-2) must be modified to the relativistic expression developed in Sec. 5-10, which expresses the mass in terms of particle rest energy W_0 and kinetic energy T using the relation $mc^2 = W_0 + T$:

$$f_i = \frac{c^2 eB}{2\pi(W_0 + T)} \tag{6-20}$$

Both decreasing magnetic field and increasing kinetic energy cause the resonant-ion frequency to decrease. The frequency of the electric field applied to the D's is fixed and has a magnitude intermediate between the initial and final values of ion frequency. As discussed in Sec. 6-4, this situation produces a phase shift, first toward a phase $\omega t_0 = -\pi/2$ and then back toward or beyond $\omega t_0 = 0$, with a total phase migration of about π radians. The applied rf voltage on the D's must be large enough that the number of accelerations is sufficiently small for the total phase migration to be within the above limit. Otherwise the ions move into a decelerating phase and go out of resonance.

Although this energy limit was recognized at an early date in cyclotron development, it was first analyzed in a publication by Bethe and Rose[33]

in 1937. This was followed by a more detailed paper by Rose[16] in 1938. The energy limit was found to depend on the phase shift discussed in Sec. 6-4 and on the peak radiofrequency voltage applied to the D's. Rose gives the relation for the limiting energy in the form

$$T_m = KV^{1/2}(\cos \omega t_0)^{1/2} \tag{6-21}$$

where V = peak voltage between D's
ωt_0 = initial phase
K = a constant involving the e/m of the ion and numerical conversion factors

The numerical estimates were based on the low D voltages obtained in small cyclotrons up to that time and on a theoretical shape of magnetic field for focusing. Assuming a D-to-D voltage of 50 kv, the predicted energy limits were 15 Mev for protons, 21 Mev for deuterons, and 42 Mev for He^{++} ions.

As might be expected, this theoretical threat to the future of the cyclotron was not taken seriously by experimentalists, who were convinced that technical improvements would raise the limits almost indefinitely. In fact, much larger cyclotrons have been built than were originally contemplated and much higher D voltages have been obtained. For large cyclotrons (60-in. or larger), continuous development of the rf power supplies to higher power and higher efficiency has resulted in D-to-D voltages well over 200 kv. When Rose's energy limit expression is reevaluated for this higher D voltage, it gives 30-Mev protons and 42-Mev deuterons.

A more complete analysis by Cohen[19] expresses the energy limit in terms of the minimum D voltage required to obtain a given proton energy. Figure 6-25 illustrates the D-voltage requirements to attain a given proton energy for various (linear) magnetic-field fall-off rates given in terms of the fractional decrease δ from center to edge of the field. The maximum energy limits indicated are in reasonable agreement with those cited above.

The limiting energy for a given cyclotron depends on the useful radius of magnetic field, the D spacing from the chamber lids, and the rf power available. A machine designed for high D voltage will require a long magnetic gap and high magnet power, as well as large rf power. So the cost of the magnet and rf components increases steeply, for a relatively small gain in ion energy as the limiting energy condition is approached. As a consequence, few of the existing cyclotrons approach the theoretical limits. The two largest fixed-frequency cyclotrons are the 86-in. machine at the Oak Ridge National Laboratory and the 88½-in. machine at the Nobel Institute in Stockholm. Both machines have produced protons of 22 Mev energy and deuterons of 24 Mev. Practical limitations on rf power and on the perfection of magnetic shimming have restricted the

energies to values considerably below the theoretical limits. Still larger and more powerful fixed-frequency cyclotrons could be built, but present installations appear to have come close to the practical economic limit for ion energy.

There is no longer any great pressure to push the standard cyclotron to its ultimate energy limit, since much higher energies can be attained with the frequency-modulated synchrocyclotron (see Chap. 11). This is obtained, however, at the cost of a considerable decrease in beam intensity due to the pulsed duty cycle of the synchrocyclotron. When the

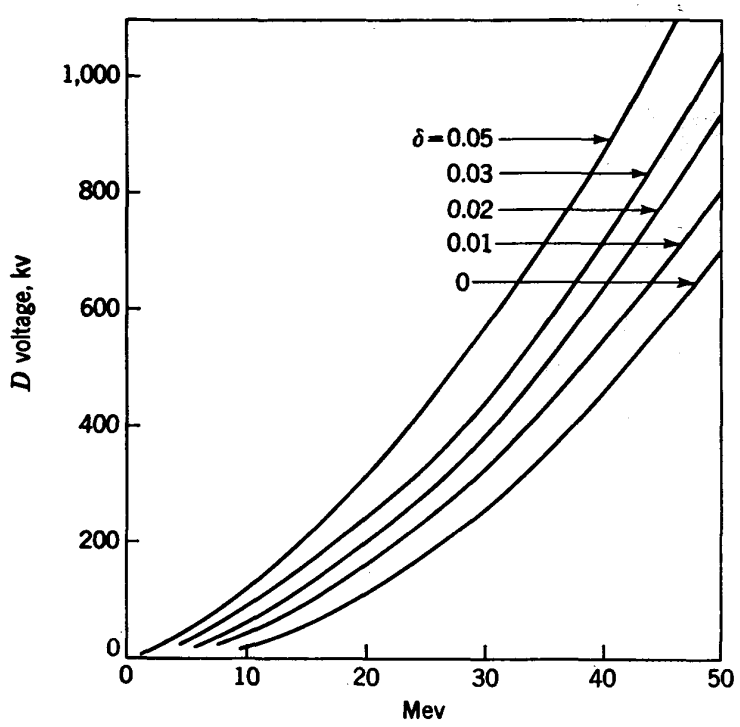

Fig. 6-25. Minimum D voltage required to obtain a given proton energy. Curves for various (linear) magnetic-field fall-off rates, δ. (Cohen.[19])

need arises for much higher beam intensities at energies above those available at present, the probable direction of development will be the strong-focusing cyclotron which is a variant of the alternating-gradient synchrotron described in Chap. 15. The principle of the strong-focusing cyclotron was proposed by Thomas[34] in 1938, long before the more general theoretical development of alternating-gradient focusing came along in 1952, but it was neglected in favor of the synchroaccelerators in the intervening years (cf. Sec. 15-11).

The optimum size for a cyclotron depends on the planned use and is not necessarily the largest size. Cyclotrons have had their greatest application in research laboratories, as sources of high-energy particles for studies of nuclear disintegration at energies surpassing nuclear potential barriers. They have served as high-intensity sources of neutrons and

for the production of a wide spectrum of induced radioactivities. A large fraction of research problems in these fields can be handled adequately with energies of less than 20 Mev.

Other accelerators supplement the cyclotron and help define its useful energy range. Electrostatic generators excel in the energy range below about 5 Mev to which they have been developed. The proton linear accelerator is the most direct competitor, producing protons of 60 Mev, and still higher-energy models are under construction. However, its short duty cycle results in considerably lower beam intensity than the cyclotron. For much higher energies, above 100 Mev, the synchro-accelerators take over. We can conclude that the cyclotron is the only instrument which accelerates light ions in the energy range from 5 to 25 Mev at high beam intensity. This energy range covers a wide variation in type of research program and in cost.

An estimate of the present cost of a 5-Mev cyclotron would be $20,000. The MIT 16-Mev cyclotron might be reproduced for about $120,000 exclusive of buildings or shielding. A modern 60-in. machine built by a commercial firm would cost at least $800,000, again exclusive of buildings. Magnet costs vary roughly with weight and so are proportional to (pole diameter)^3 or to $T^{3/2}$. However, total costs rise more steeply at larger sizes because of the additional requirements for high-power rf supplies and the surcharges on apparatus of a size approaching the limit of commercial availability. Most small cyclotrons were built 10 to 15 years ago and in academic laboratories where student help and surplus apparatus were available; they could be housed in existing buildings and operated by the existing staff. Large, modern installations require new laboratories, heavy shielding, and a staff of technical personnel for maintenance; most of the equipment must be purchased commercially and requires skilled labor for installation. So total costs rise far more rapidly than with $T^{3/2}$ in the high-energy range.

The productivity of a cyclotron, on the other hand, does not vary by such a large factor. Consider the production of neutrons or of a typical radioactivity. Yield increases exponentially at low energies where nuclear barrier penetration is the determining factor, then increases further only with target penetration as energy increases (roughly with $T^{3/2}$), and even falls below this rate of increase at high energies when target cooling is a limitation. Unit costs in the production of neutrons or radioactivity are considerably less for the medium-energy installations (15 Mev) than for larger machines (20 Mev and higher).

Other factors may be more important than cost comparisons. Research laboratories may experience a point of diminishing returns if the size and the complexity of the accelerator overburden the available staff. If the effort required for supervision, administration, and maintenance involves too large a fraction of the time of the research staff, productivity

decreases. The size of the installation should not be disproportionate to the resources of the laboratory.

All sizes of cyclotron have their special areas of usefulness. A small institution with a limited budget will find that a small and inexpensive cyclotron in the 5- to 10-Mev range will be useful in providing student training and experience in nuclear physics. One in the 15-Mev range will provide a source of continuing scientific usefulness for research at minimum cost. For laboratories which have sufficient resources to take a leading role in exploring new research fields, the highest energies and highest intensities become important.

REFERENCES

1. E. O. Lawrence and N. E. Edlefsen, *Science*, **72**:376 (1930).
2. R. Wideröe, *Arch. Elektrotech.*, **21**:387 (1928).
3. M. S. Livingston, "The Production of High-velocity Hydrogen Ions without the Use of High Voltages," Ph.D. thesis, University of California, Apr. 14, 1931.
4. E. O. Lawrence and M. S. Livingston, *Phys. Rev.*, **37**:1707 (1931); **38**:136 (1931); **40**:19 (1932).
5. J. D. Cockcroft and E. T. S. Walton, *Proc. Roy. Soc. (London)*, **136A**:619 (1932); **137A**:229 (1932).
6. E. O. Lawrence, M. S. Livingston, and M. G. White, *Phys. Rev.*, **42**:1950 (1932).
7. M. S. Livingston, *Phys. Rev.*, **42**:441 (1932); M. S. Livingston and E. O. Lawrence, *Phys. Rev.*, **43**:212 (1933); E. O. Lawrence and M. S. Livingston, *Phys. Rev.*, **45**:608 (1934).
8. E. O. Lawrence and D. Cooksey, *Phys. Rev.*, **50**:1131 (1936).
9. E. O. Lawrence, L. W. Alvarez, W. M. Brobeck, D. Cooksey, D. R. Corson, E. M. McMillan, W. W. Salisbury, and R. L. Thornton, *Phys. Rev.*, **56**:124 (1939).
10. M. S. Livingston, *Rev. Sci. Instr.*, **7**:55 (1936).
11. M. C. Henderson and M. G. White, *Rev. Sci. Instr.*, **9**:19 (1938).
12. A. Allen, M. B. Sampson, and R. G. Franklin, *J. Franklin Inst.*, **228**:543 (1939).
13. P. G. Kruger et al., *Rev. Sci. Instr.*, **15**:333 (1944).
14. M. S. Livingston, *J. Appl. Phys.*, **15**:2 (1944); **15**:128 (1944).
15. W. B. Mann, "The Cyclotron," rev. ed., Methuen's Monographs, Wiley (1953).
16. M. E. Rose, *Phys. Rev.*, **53**:392 (1938).
17. R. R. Wilson, *Phys. Rev.*, **53**:408 (1938).
18. R. R. Wilson, *Am. J. Phys.*, **11**:781 (1940).
19. B. L. Cohen, *Rev. Sci. Instr.*, **24**:589 (1953).
20. El Cerrito Cyclotron, *Phys. Today*, **1**:10 (1948).
21. R. J. Jones and A. Zucker, *Rev. Sci. Instr.*, **25**:562 (1954).
22. R. J. Jones, *Phys. Rev.*, **91**:223 (1953).
23. H. Atterling, *Arkiv Fysik*, **7**:503 (1954).

24. M. S. Livingston, M. G. Holloway, and C. P. Baker, *Rev. Sci. Instr.*, **10**:63 (1939).
25. M. S. Livingston, *Rev. Mod. Phys.*, **18**:293 (1946).
26. D. B. Cowie and C. J. Ksanda, *Rev. Sci. Instr.*, **16**:224 (1945).
27. R. S. Livingston and R. J. Jones, *Rev. Sci. Instr.*, **25**:552 (1954).
28. R. J. Jones and A. Zucker, *Rev. Sci. Instr.*, **25**:562 (1954).
29. J. Backus, *Rev. Sci. Instr.*, **22**:84 (1951).
30. N. S. Wall and J. W. Irvine, Jr., *Rev. Sci. Instr.*, **24**:1146 (1953).
31. B. R. Curtis, J. L. Fowler, and L. Rosen, *Rev. Sci. Instr.*, **20**:388 (1949).
32. K. Boyer, H. E. Gove, J. A. Harvey, M. Deutsch, and M. S. Livingston, *Rev. Sci. Instr.*, **22**:310 (1951).
33. H. A. Bethe and M. E. Rose, *Phys. Rev.*, **52**:1254 (1937).
34. L. H. Thomas, *Phys. Rev.*, **54**:580, 588 (1938).

At the head of the facing page is an illustration of the University of Illinois 300-Mev betatron.[8]

7

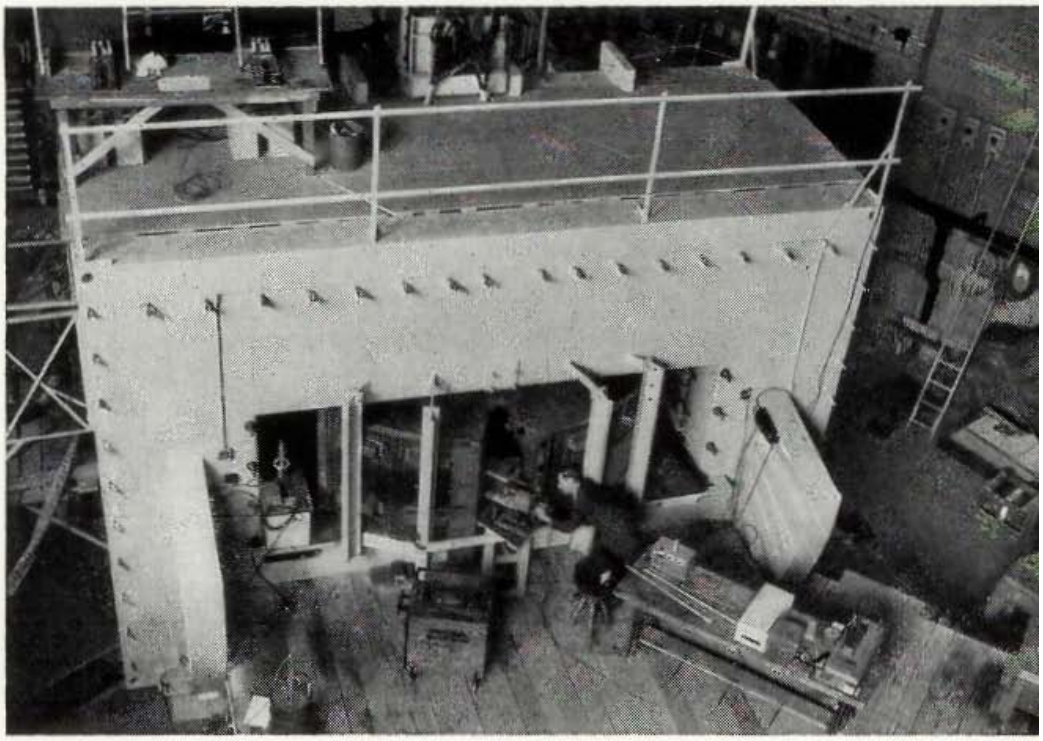

The Betatron—Magnetic Induction Accelerator

In the betatron, electrons are accelerated by the electric field induced by a changing magnetic flux linking the electron orbit. The magnetic field at the orbit provides the central force (which produces circular motion) and increases with increasing electron energy so the orbit is of essentially constant radius. A basic arrangement is a doughnut-shaped vacuum chamber in the gap between ring-shaped poles of an electromagnet, with a shorter gap and higher fields in the central region to provide the flux linkage required for induction. Figure 7-1 is a schematic cross section of such a magnet and vacuum chamber.

The concept of using a time-varying magnetic field to provide an electric field for the acceleration of electrons to high energy has been considered by physicists for many years. It has the advantage of avoiding the limitations of insulation breakdown characteristic of direct-voltage generators, and the magnetic guide field retains the electrons in circular orbits of small dimensions so the size of the accelerator can be small. The energy gained by an electron in one revolution is equivalent to the induced voltage in a one-turn coil, if it were located at the orbit. The magnitude of this induced voltage is given, as for the transformer, by the time rate of change of magnetic flux linking the orbit, $d\Phi/dt$. Since electron velocities are large, approaching the velocity of light at a few Mev, the electrons can make many revolutions in a short time and acquire high energy.

7-1. HISTORICAL DEVELOPMENT

Among the many investigators who have attempted to accelerate electrons by magnetic induction, none were successful until D. W. Kerst[1,2] of the University of Illinois produced 2.3-Mev electrons in 1940. His success depended on careful magnet design based on the detailed orbit stability calculations of Kerst and Serber.[3] This first model was amazingly successful, producing X rays with an intensity in the forward direction equivalent to the γ-ray intensity from 1 gm of radium. It was immediately evident that much higher energies could be produced in this way. Kerst next transferred his base of operations to the General Electric Company Research Laboratory, where with the collaboration of this

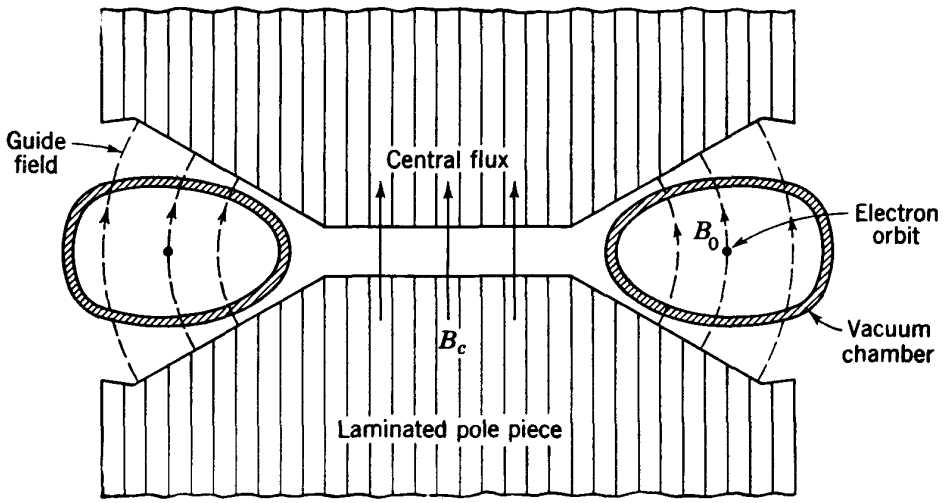

Fig. 7-1. Schematic diagram of a betatron magnet and vacuum chamber, showing the orbit field B_0 and the central core supplying the linkage flux B_c for acceleration.

experienced laboratory staff, a 20-Mev betatron was completed in 1942.[4] Westendorp and Charlton[5] of the General Electric Company continued the development with a 100-Mev machine in 1945. Commercial production was started at GE and also at Westinghouse and Allis-Chalmers companies, primarily in the 20-Mev energy range, to meet the rising demands from research laboratories, hospitals, and industrial plants. In Europe electrical manufacturing companies have also entered the field. The chief developments have come from the Philips Laboratory at Eindhoven, where Bierman[6] has built small betatrons both with and without iron yokes, and at Brown-Boveri in Switzerland, directed by Wideröe.

Meanwhile Kerst returned to the University of Illinois to build first an 80-Mev model[7] and ultimately a 300-Mev machine[8] which represents the largest and possibly the ultimate betatron.

It is of some interest, however, to look back at the early years before 1940 to see how the concepts gradually developed. Kerst[9] has made a

careful survey of published and unpublished work to find the origins of the induction accelerator.

The significance of the magnetic term curl $\mathbf{E} = -\frac{d\mathbf{B}}{dt}$ in the equations of the electromagnetic field had been recognized by many scientists, and the formulation $\oint E\,ds = -\frac{d\Phi}{dt}$ for the induced voltage per turn due to a changing flux Φ is taught in all elementary courses in electricity. That this electric field would accelerate free charges as well as the conduction electrons in a wire coil of a transformer was obvious. However, the first proposal to apply this principle to the acceleration of electrons seems to have come in 1922, in J. Slepian's U.S. Patent 1,645,304. Kerst has shown that this first proposal was impractical because of the lack of suitable focusing fields. In 1927 Breit and Tuve[10] studied the possibility of using the induction principle to develop a source for nuclear studies. In their apparatus a rapidly increasing magnetic field was produced by spark discharge of a large capacitor through a coil; electrons started at the outside would spiral inward in this field and would increase in energy. However, they failed to appreciate the need for a radially decreasing field to give focusing. If the focusing feature had been added, the apparatus might have worked as an X-ray source of low efficiency, but it was abandoned in favor of the more controllable electrostatic generator for the projected nuclear studies.

Wideröe[11] in 1928 came closer to a practical accelerator. He made a major advance in recognizing the requirements for acceleration at constant radius and developed the 2:1 rule (see Sec. 7-2). However, he did not at first recognize the necessity for magnetic-field shaping to produce axial and radial focusing, and his method of injection using an external cathode gun was cumbersome and unsuitable for the relatively slow rise in magnetic field. Walton[12] built an apparatus based on the electrodeless ring discharge principle, which can be considered a forerunner of the modern betatron without iron yoke. Although he was unsuccessful experimentally, Walton made an important contribution in solving the theoretical problem of radial focusing forces (see Chap. 5). Jassinsky[13] extended the calculations of orbit stability, considering a magnetron-like situation with an axial magnetic field and radial electrostatic field. M. Steenbeck developed an idea based on the Wideröe accelerator and in 1937 took out U.S. Patent 2,103,303 on an experimental apparatus; however, the patent does not indicate that it was based on an operating machine. This was followed by unpublished work on an operating model, and Steenbeck has since claimed[14] to have obtained high-energy X rays.

Several other workers are known to have made attempts to accelerate electrons by induction; apparently all of these were unsuccessful and unpublished. However, the concept was discussed and speculations

exchanged over a period of several years by many others. It seems clear that the complete stability theory of Kerst and Serber and the careful and thorough magnet design calculations of Kerst were a prerequisite to a practical accelerator. The major credit for the development of the betatron justifiably goes to D. W. Kerst.

7-2. THE ACCELERATION PRINCIPLE

The fundamental problem in the design of an induction accelerator is to maintain the necessary proportionality between magnetic field at the orbit, B, and electron momentum $p = mv$, so that orbit radius remains constant.

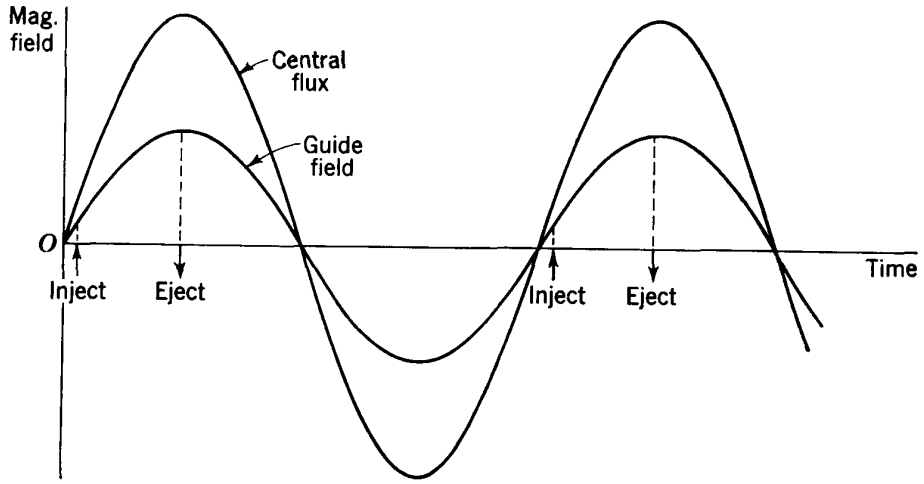

Fig. 7-2. Time cycle for acceleration of electrons in a betatron with sinusoidal magnet excitation; the guide field and central flux are in phase.

The magnetic field at the orbit must increase with time to maintain constant radius for electrons of increasing energy. This is usually accomplished by powering the magnet cyclically from an ac supply. Acceleration occurs during the quarter-cycle when the field is increasing from zero to its maximum. The time cycle for acceleration is illustrated in Fig. 7-2, on a sinusoidally varying magnetic-field plot. Electrons are injected at low energy when the guiding field at the orbit is small; they reach maximum energy at the peak of the field cycle. As the electrons approach maximum energy, they can be diverted against a target, producing X rays. The X rays occur in a sequence of short pulses at the frequency of the power supply. In order to avoid losses due to eddy currents, the iron is laminated as in a transformer.

The magnetic field required to produce circular motion depends on the energy of the electron. It is given in mks units by [see Eq. (5-49)]

$$B = \frac{mv}{er} = \frac{(T^2 + 2TW_0)^{1/2}}{cer} \tag{7-1}$$

where T = kinetic energy
W_0 = rest energy (m_0c^2)
r = orbit radius
e = charge
m = relativistic mass of electron

Evaluating this relation for a numerical example where $r = 0.5m$ and $T = 100$ Mev, we find

$$B = 0.67 \text{ weber/m}^2 \text{ or } 6700 \text{ gauss}$$

This shows that high-energy electrons can be retained in reasonably small orbits by readily available magnetic fields.

The time rate of increase of momentum is a measure of the electrical accelerating force acting on the electron and can be expressed in terms of the time rate of change of flux linking the orbit. In rationalized mks units this is given by

$$\frac{dp}{dt} = \frac{e}{2\pi r}\frac{\partial \Phi}{\partial t} \tag{7-2}$$

Integrating to find the momentum acquired owing to a finite flux change, we have

$$p = \frac{e(\Phi_2 - \Phi_1)}{2\pi r} \tag{7-3}$$

But from Eq. (7-1) we have for momentum $p = eBr$, where B is in the same direction as $(\Phi_2 - \Phi_1)$, so

$$\Phi_2 - \Phi_1 = 2(\pi r^2)B \tag{7-4}$$

Thus the flux change within the orbit must be *twice* the value obtaining if flux density were uniform and equal to the field at the orbit. This is the now-famous 2:1 rule. To satisfy the requirement there must be a strong central field linking the orbit and a weaker field at the orbit. Both fields must increase proportionately with time, the central field to provide the acceleration and the field at the orbit to retain the particle of increasing energy in an orbit of constant radius. The particular orbit for which this 2:1 ratio applies can be called the equilibrium orbit. We use the symbols r_0 for the radius and B_0 for the magnetic field at this orbit, so the equilibrium momentum p_0 is given by

$$p_0 = eB_0r_0 \tag{7-5}$$

An electron having momentum $p_0 + \delta p$ differing from that of the equilibrium electron will describe an orbit of radius $r_0 + \delta r$ given by

$$p_0 + \delta p = eB(r_0 + \delta r) \tag{7-6}$$

where B represents the field strength at the new radius. The new orbit will enclose a total flux whose rate of change is

$$\frac{\partial \Phi}{\partial t} = 2\pi {r_0}^2 \frac{\partial B_0}{\partial t} + \int_{r_0}^{r_0+\delta r} 2\pi r \frac{\partial B}{\partial t}\, dr$$

Since B will not change materially in the neighborhood of the equilibrium orbit, we can rewrite this relation as

$$\frac{\partial \Phi}{\partial t} = 2\pi r_0(r_0 + \delta r) \frac{\partial B_0}{\partial t} = 2\pi r r_0 \frac{\partial B_0}{\partial t}$$

Consequently, for this nonequilibrium particle, Eq. (7-2) gives

$$\frac{dp}{dt} = \frac{e}{2\pi r} \frac{\partial \Phi}{\partial t} = e r_0 \frac{\partial B_0}{\partial t} \tag{7-7}$$

But this is the same rate of change of momentum as obtains for the equilibrium particle. Consequently, this particle will gradually tend to have the same momentum as does the equilibrium particle, since its total momentum will eventually become so large that the initial momentum error will become negligible.

The fact that the rate of change of momentum is independent of radius leads to the conclusion that [from Eq. (7-6)]

$$d[B(r_0 + \delta r)] = r_0\, dB_0$$

whence, since B will not differ appreciably from B_0,

$$\frac{d(\delta r)}{\delta r} = -\frac{dB_0}{B_0} \left(= -\frac{dT}{2T} \text{ for nonrelativistic particles} \right) \tag{7-8}$$

We conclude that a particle released on an instantaneous orbit such that its momentum corresponds to its radial distance from the center according to Eq. (7-6) will spiral asymptotically toward the radius at which the 2:1 rule is satisfied. If the momentum and radius do not correspond to this relation, the particle will oscillate around the instantaneous orbit given by Eq. (7-6) in the fashion already discussed in Secs. 5-9 and 5-10. The path of this particle will gradually tend toward the equilibrium orbit as just shown, but it will now include an oscillation around the instantaneous orbit whose radius is tending asymptotically toward the equilibrium radius.

To summarize, we have shown that a particle injected at any point in the neighborhood of the equilibrium orbit will gradually tend toward an orbit satisfying the 2:1 rule. This concept, first developed by Kerst and Serber, is fundamental to the demonstration of the soundness of the betatron design.

The shift in orbit radius toward the equilibrium orbit described above led Kerst to the concept of an injection system which proved successful. He reasoned that electrons released from a cathode or injection gun outside of the equilibrium orbit would have subsequent orbits of smaller radius and some of the electrons could miss the back of the injector and be accelerated. With an electron gun displaced 1.5 cm from the equilibrium orbit injecting 200-volt electrons, he noted that Eq. (7-8) indicates a decrease in orbit radius of 1 mm per revolution provided only that the rate of increase of energy is about 25 volts per turn. The gun was to emit electrons continuously at the indicated energy. As the magnetic field increased, there would be a short period when the orbits would satisy the correct relations and a fraction of the injected electrons could be captured and accelerated.

The injection scheme was successful but, as is now known, not for the reasons given. As the injection energy was increased through the range where all electrons should have been lost on the back of the injector, the intensity of the accelerated beam continued to increase. The present interpretation of this discrepancy will be discussed in Sec. 7-8, Electron Injection.

7-3. ORBITAL STABILITY

An additional requirement for acceleration is that there be spatial focusing for particles which deviate in direction from the equilibrium orbit. During acceleration the electrons must make many revolutions and so have very long total paths. In the first Illinois betatron it was estimated that the electrons made about 200,000 revolutions and traveled a total distance of 100 km during a quarter-cycle of the 60-cycle applied magnetic field. In order that the electrons do not wander to the walls of the chamber during these many revolutions, it is essential that the magnetic field provide strong focusing forces restoring the particles to the median plane and the equilibrium orbit. (It is also necessary that the gas pressure be small so beam intensity will not be drastically reduced by gas scattering.) As has been shown in Chap. 5, such focusing forces can exist in a magnetic field which decreases with increasing radius. Here we present a qualitative review of the stability conditions; the detailed equations of motion were presented in Chap. 5.

In a radially decreasing field specified by the relation

$$B_z = B_0 \left(\frac{r_0}{r}\right)^n \tag{7-9}$$

a particle will experience restoring forces both toward the median plane and toward the equilibrium orbit provided only that n lies between zero and unity. The radial restoring force will be proportional to $(1 - n)$

and the vertical restoring force will be proportional to n. The frequencies of oscillation around the equilibrium orbit were given by Eqs. (5-67) and (5-68); both are slightly lower than the frequency of revolution of the electrons in their orbits. Specifically, the frequency of the radial oscillation is

$$f_r = (1 - n)^{1/2} f_0 \tag{7-10}$$

and the frequency of the vertical oscillation is

$$f_z = n^{1/2} f_0 \tag{7-11}$$

where f_0 is the frequency of revolution of the electrons and is given by

$$f_0 = \frac{eB_0}{2\pi m} \tag{7-12}$$

As was shown in Eqs. (5-69) and (5-70), the amplitude of these oscillations is damped as the electron energy increases. While the electrons are in the low, nonrelativistic range, the amplitude decreases in proportion to $T^{-1/4}$; in the high-energy, relativistic range the amplitude damps more rapidly in proportion to $T^{-1/2}$.

So long as no perturbations are introduced, the amplitude of these free or betatron oscillations will be determined by the injection conditions. The relative amplitudes of the radial and vertical oscillations will also be affected by the relative restoring forces; for n values close to unity the radial oscillations will tend to be large and the vertical oscillations will be more strongly restored. If n is close to zero, the vertical amplitudes will tend to be large and the radial oscillations will be more strongly focused. Since vertical space in an electromagnet is usually more costly than radial space, n values are usually nearer to unity than to zero; preferred values have been between 0.6 and 0.75.

Thus we see that the equations of motion of an electron in such a radially decreasing magnetic field lead to stable oscillations about the particle orbit. During the early stages of acceleration these oscillations will be centered on the instantaneous orbit, which itself will approach the equilibrium orbit asymptotically. Oscillation amplitudes are damped by the increasing magnetic field so the cross section of the circulating beam of electrons will decrease with increasing energy. Figure 7-3*b* illustrates a radial oscillation about the equilibrium orbit; Fig. 7-3*c* combines this oscillation with the asymptotic damping of the instantaneous orbit (Fig. 7-3*a*) to illustrate a more general case. Axial oscillations, not shown in the figure, give the true orbit a three-dimensional envelope shaped like a thin, flattened doughnut.

The location of the equilibrium orbit can be changed by changing the proportionality in the betatron relation during the progress of the cycle. It is possible to make the equilibrium orbit drift inward or outward to

strike a target on the wall of the chamber. For example, if the central flux change is made more rapid than indicated by Eq. (7-4) as the particle approaches maximum energy, the momentum will increase and the equilibrium orbit will expand. This motion is slow enough to be essentially adiabatic, and the spatial focusing is not disturbed. Electrons will

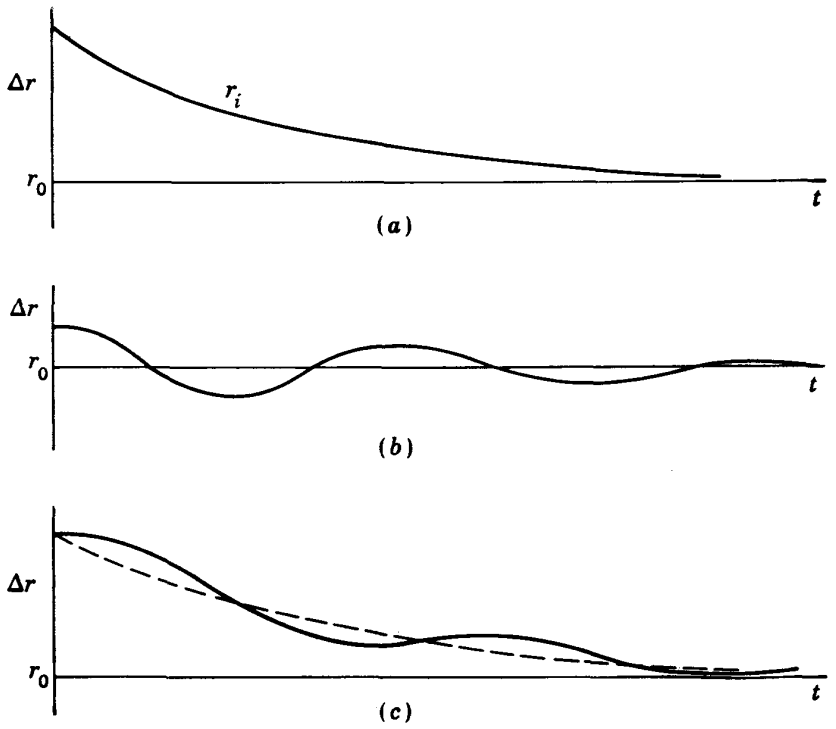

Fig. 7-3. Paths of electrons unrolled into a straight line and plotted as the displacement Δr from the equilibrium orbit r_0: (*a*) tangential injection on the instantaneous circle r_i; (*b*) damped oscillation around the equilibrium orbit; (*c*) damped oscillation around the instantaneous circle which contracts toward the equilibrium orbit.

peel off against the edge of a target, requiring hundreds of revolutions for all the electrons to reach this radius.

7-4. MAGNET DESIGN

The magnet of a betatron provides two components, the field at the orbit and the central flux required for acceleration. These components are linked through the requirement of the betatron relation: The central flux must change at a rate *twice* that obtaining if the central field were uniform and equal to the field at the orbit. Two basically different magnet structures have been employed. In the smaller betatrons a single magnetic circuit carries the return flux for both the guide field at the orbit and the central flux; the central flux density is increased by use of a shorter air gap to establish the betatron condition. For the larger machines, separate magnetic circuits are used and the central flux core is

biased to allow a larger flux change for induction; in this case the exciting coils for the separate circuits are powered in parallel to maintain the proportionality of field and flux.

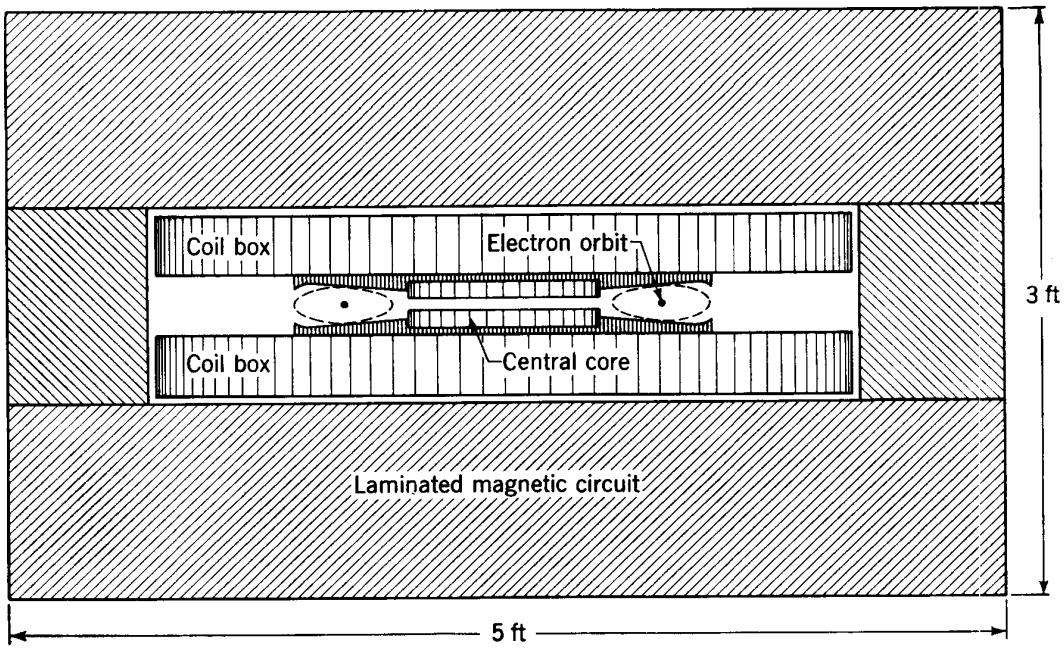

Fig. 7-4. Diagram of the magnetic circuit for the 20-Mev betatron designed by Kerst.[4]

A good example of the simple single-circuit type is the magnet for the 20-Mev betatron[4] (Fig. 7-4). This magnet has a 19-in.-diam pole face with an 11-in.-diam central core. It is constructed of stacks of 0.014-in. silicon steel transformer laminations. Laminations of different lengths are grouped into tapered radial sectors to form the cylindrical poles. The return for the magnetic circuit consists of packages of laminations assembled as an external yoke as in transformer design, but with the packages separated by spacers to provide ducts for air-blast cooling. The total weight of iron is about 3.5 tons. The assembly is clamped together by maple planks and long bolts. Laminations forming the pole face between the 5.5-in. and 9.5-in. radii are shaped to provide a radially decreasing field with a value of $n = 0.75$; measurements on a small dc model were used to obtain the correct shape. A plot of the field shape near the orbit location (at a radius of 7.5 in.) is shown in Fig. 7-5; here B

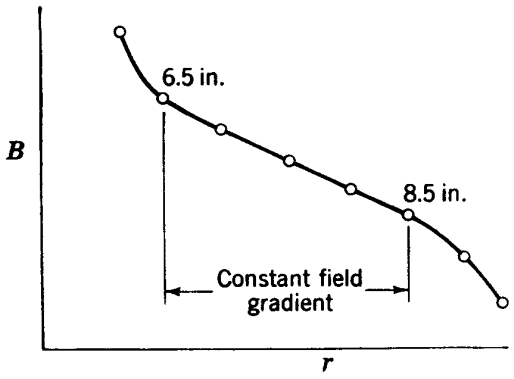

Fig. 7-5. Magnetic field versus radial position in the 20-Mev betatron, showing the region of constant magnetic gradient.[4]

is plotted against r and the straight-line portion between 6.5 and 8.5 in. indicates a constant value of n. This rate of variation of field with radius is approximately 10 per cent per inch; at 6.5 in. the required field is $1.11B_0$ and at 8.5 in. it is $0.91B_0$, which specifies dimensions for the tapered gap.

The shorter air gap in the central core is obtained by inserting two disks of laminated iron bonded into a rigid structure by a thermosetting resin. The thickness of the disks determines the residual gap length and the flux density through the core and thus establishes the orbit radius for which

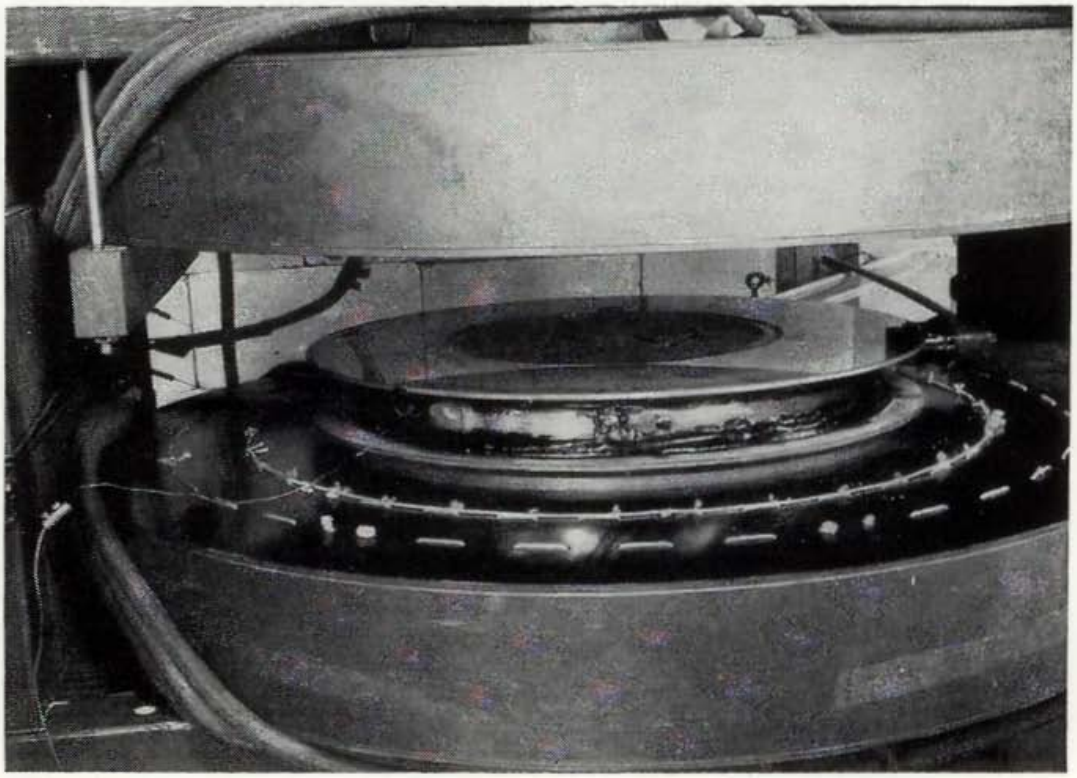

Fig. 7-6. The 20-Mev betatron with magnet coils and vacuum chamber in place. The top pole is removed.

the betatron condition holds. This was predetermined by model measurements to give an equilibrium orbit radius of 19 cm (7.5 in.). The vertical location of the two disks within the central gap can be varied to modify the shape of the field in the adjacent region enclosing the vacuum chamber and is adjusted to extend the region of uniform n to the smallest possible radius. Figure 7-4 illustrates the arrangement of poles and vacuum chamber of the 20-Mev machine; Fig. 7-6 is a photograph of the magnet and chamber assembly showing the excitation coils, with the upper pole removed.

Exciting windings for the 20-Mev magnet consist of 81 turns of stranded wire about each pole, firmly clamped and contained in Textolite coil boxes. At the chosen operating frequency of 180 cps, and with the

coils in series, an external capacitor bank of 5.5 μf is required for resonance. A resonant circuit is desirable in order to relieve the generator of the otherwise large reactive current. With the resonant capacitor in series, the current and voltage in the exciting winding are almost 90° apart in phase and the generator has to supply only the resistive and eddy-current losses. The circulating power required to excite the magnet for the 20-Mev betatron is 1750 kva; losses in the windings, the capacitors, and the iron total only 26 kw. One of the most expensive components of the betatron is the capacitor bank to handle the large circulating currents; power ratings for the capacitors must be adequate for 1750 kva in this case.

The 180-cps power is obtained from a 3-phase 60-cycle line by means of a frequency-tripling circuit (Fig. 7-7). Three separate transformers are run at very high flux density so that saturation effects, which develop third harmonics in voltage, become noticeable. Primaries

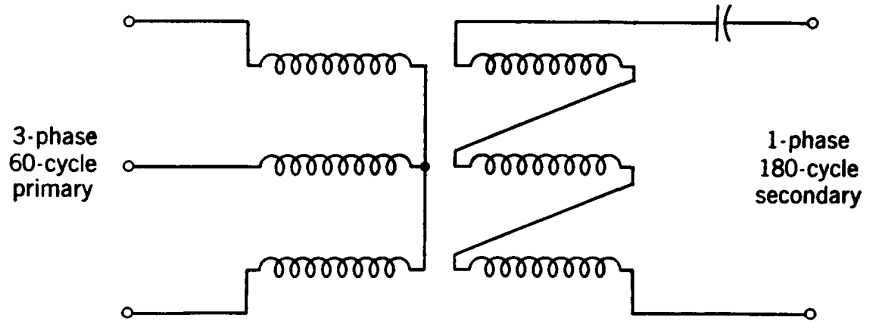

Fig. 7-7. Frequency-tripling circuit with resonant capacitor for 180 cps.

are connected in Y so the tripled-frequency voltage cancels out at the primary terminals, and the secondaries are connected in series so that the 60-cycle voltage cancels at the secondary terminals. This output is connected in series with a six-turn primary winding coupling the magnet coils and a smaller resonant capacitor bank capable of handling the 26-kw load.

The magnetic field at the orbit for 20-Mev electrons can be computed from Eq. (7-1) to be

$$B_0 = \frac{(T^2 + 2TW_0)^{1/2}}{cer_0} = 0.36 \text{ weber/m}^2 = 3600 \text{ gauss}$$

To maintain the betatron flux condition, the total change in flux within the orbit given by Eq. (7-4) would be

$$\Delta\Phi = 2\pi r_0^2 B_0 = 0.082 \text{ weber}$$

We shall consider the simple case where central flux and orbit field are proportional, and compute the magnitude of the central flux density, B_c. If we assume this central core field to be uniform inside the 5.5-in. radius

and to have an average value of $1.11B_0$ between 5.5 and 7.5 in. (the value at 6.5), and if we compute the areas of these two regions, we obtain as an estimate of the central field

$$B_c \sim 1.0 \text{ weber/m}^2 = 10{,}000 \text{ gauss}$$

This illustrates the high central flux density required for such a single-circuit magnet.

Precise calculations of the flux linking the orbit, from the peak ampere-turns in the winding and the dimensions of the magnetic circuit, can be used to compute electron energy and predict the equilibrium orbit radius. An experimental method available in model studies is to use a one-turn coil at the orbit location in series with an integrating capacitor and a high resistance. The voltage developed on the capacitor at the time of ejection can be measured with a vacuum-tube voltmeter; it is proportional to the flux change within the orbit and so gives the equivalent electron energy. Both methods were used for the 20-Mev betatron, and the results agreed within 1 per cent. This indicates that the location of the equilibrium orbit was known to good precision.

The magnets for the 300-Mev betatron[8] and the 80-Mev model[7] for this machine utilize separated magnetic circuits. A sketch of the assembly of the 80-Mev magnet is given in Fig. 7-8. The flux magnet is a continuous iron core with dual return legs similar to a transformer core. The excitation windings are distributed in four symmetrical coils about the top and bottom yokes. The field magnets consist of six C-shaped cores which fit between the yokes of the flux magnet so as to produce the orbit field in an annular region surrounding the core. Laminations for these six segments are bent and stacked to form a radial array and thus produce the most uniform field possible at the orbit. This bundling into six packages leaves six V-shaped notches of sufficient dimensions to allow the passage of an X-ray beam or to insert leads for the electron injector or for measuring instruments. The careful design of this field magnet resulted in an extremely uniform magnetic field at the orbit, described as being "two orders of magnitude smoother than the fields of earlier conventional betatrons." Copper shielding is provided between the two magnetic circuits to eliminate flux leakage which might distort the fields. Excitation windings are circular and located close to the magnet gap. They consist of two equal coils—one split between top and bottom, which provides the field excitation, and one backwound coil in the gap between pole tips, which confines the field to the region between pole faces and eliminates fringing flux.

The reason for this extreme care in magnet design and the strenuous efforts to obtain uniform fields is that injection must occur at very low fields. Known techniques of injection make it possible to produce electron beams of between 50 and 100 kv, but not much higher. At 60 kv,

for example, the field at the orbit at injection is 22 gauss for the 80-Mev model, but injection occurs at only 7 gauss for the 300-Mev betatron. It is obvious that small asymmetries in the field such as might result from physical irregularities or variations in remanent field would be much more serious for the large machine. Separation of the flux and field magnets was essential to obtain the field uniformity needed.

The magnetic-field shape chosen for the 80- and 300-Mev machines does not have a constant value of n, but varies from $n = 1$ at injection

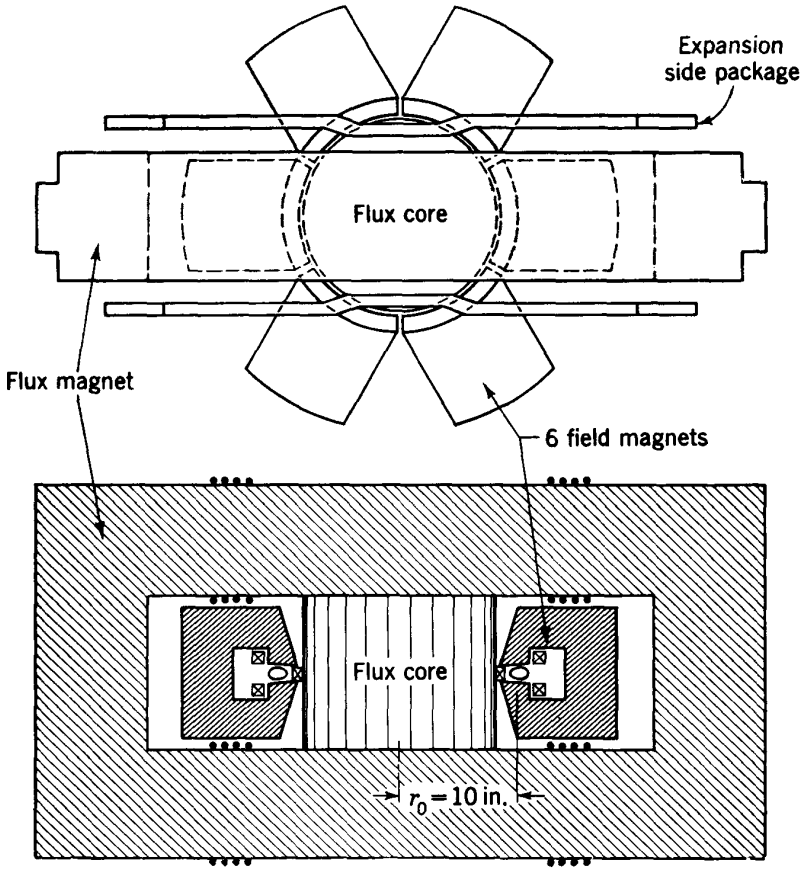

Fig. 7-8. Assembly sketch of magnetic circuits for the 80-Mev betatron, showing the separation of flux and field magnets.[7]

radius to $n = 0.2$ at the inner wall of the chamber. The value at the computed equilibrium orbit radius is $n = 0.5$; this orbit radius is 26.5 cm for the 80-Mev model and 122 cm for the 300-Mev betatron. In such a field with n a function of radius, the radial and axial oscillations are much more complicated functions than for constant n, and the shape of the orbits cannot be described simply. One advantage is that orbit position can be set for any desired n value by varying the betatron balance, and the optimum orbit location can then be determined experimentally. Also injection and ejection are both facilitated near $n = 1$ because of the spiral-shaped paths and wide spacing between turns. However, the most

important reason for choosing a small value of n over most of the orbit region is that it minimizes the shrinkage in orbit radius caused by radiation loss as the electrons reach high energy. This conclusion comes from a more detailed study of the equations of motion. The problem of energy loss by radiation is described in Sec. 7-7.

7-5. BIASED BETATRONS AND FLUX FORCING

Probably the most significant improvement in betatron design occurred with the introduction of the concept of field biasing, which forces the flux to change through a larger numerical value of $d\Phi/dt$. This concept makes use of the relation found in Eq. (7-4), that the flux *change* $(\Phi_2 - \Phi_1)$ is the quantity proportional to maximum orbit field B_0. In early betatrons both orbit field and central flux passed through zero $(\Phi_1 \simeq 0)$ at the same instant, and the resulting acceleration was limited by saturation of the core at the peak central flux Φ_2; furthermore, to satisfy the proportionality of Eq. (7-4), orbit field is limited to a much smaller value than can readily be obtained with iron magnetic circuits. For larger betatrons this single magnetic circuit is inefficient, and it is advantageous to excite the two field components separately so both central flux and orbit field can approach the limits set by saturation of the iron. An increase in orbit field by almost a factor of 2 can be achieved by having the flux in the central core reverse direction while orbit field rises from zero to maximum. This can be accomplished by suitably biasing either of the two magnetic circuits with a direct current in the winding.

This feature was appreciated by several workers in the field. Independent publications by Kerst[15] and Westendorp[16] first described the principle of biasing and flux forcing, but it appears that other workers in Italy[17] and Germany had arrived at the same conclusions by that time and were also designing betatrons to take advantage of flux forcing.

The power required to produce a given central flux can be greatly reduced by eliminating the air gap in the central core. This follows from the fact that the energy stored in the field in iron is small compared with that in even a short air gap. With no air gap the inductance of the exciting winding is increased and the size and power rating of the resonant capacitor bank is greatly reduced. The size and cost of the capacitor can be reduced to about one-third that for a conventional betatron of the same electron energy. This saving is significant in the design of high-energy betatrons.

One way to eliminate the air gap is to have two separate magnetic circuits powered with separate exciting windings. If these windings have the correct number of turns to satisfy the betatron relation of Eq. (7-4), and if they are powered in parallel from the same resonant capacitor bank, the fields in the two circuits will rise proportionately. This

arrangement for parallel powering of the two magnetic circuits is called "flux forcing." An elementary circuit showing the parallel connections for field and flux coils is illustrated in Fig. 7-9. A fine adjustment of the induced voltage and hence of orbit radius can be made by moving taps of a small autotransformer connected to one of the coils.

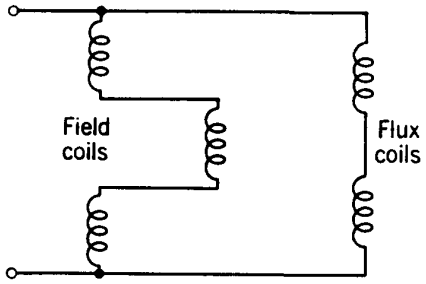

Fig. 7-9. Elementary flux-forcing circuit.

The advantages of flux forcing can be obtained in another way by isolating the two magnetic circuits of a single magnet core electrically and magnetically, even though they are not physically separated. This was in fact the first proposal and was applied to the first betatron single-circuit magnets to increase the energy output. This separation can be achieved by the use of another coil in the magnet windings. Kerst called it a "backwound" coil and located it in the magnet gap just inside the doughnut-shaped vacuum chamber; Westendorp proposed a split coil having two components located in grooves in the pole faces at the same location; he called these "groove" coils. The effect of this backwound

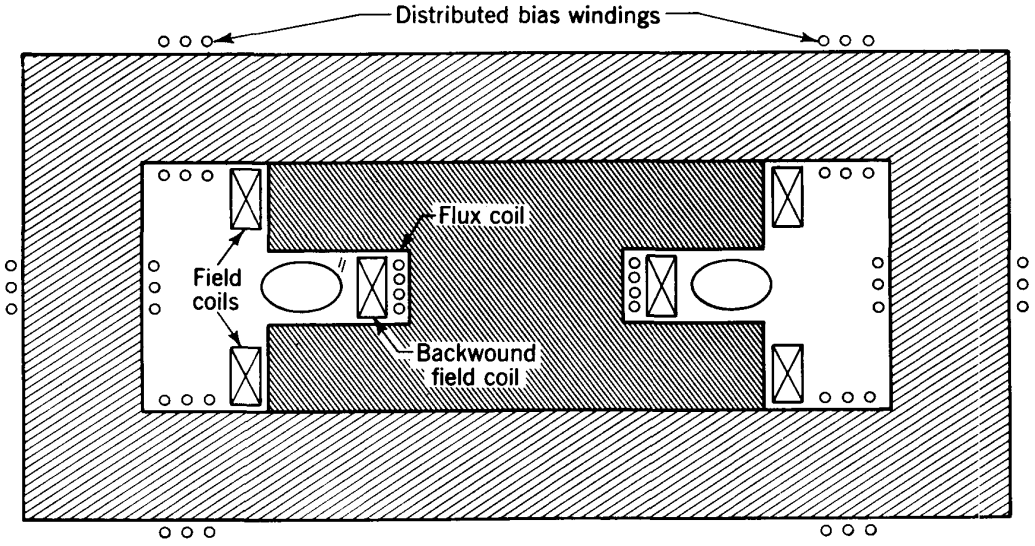

Fig. 7-10. Location of exciting and bias coils in a flux-biased betatron having a single magnetic circuit.[7]

coil is to cancel out the flux in the central core produced by the main windings, thereby confining the guide flux to the annular region near the orbit. The number of turns and the geometry of the coils can be adjusted so the central flux is completely canceled; if so, another separate flux winding is required to produce the central flux. Or the ampere-turns in the backwound coil can be smaller than for the main coil, leaving an

excess to provide the central flux for acceleration. The location of such a backwound coil is illustrated in Fig. 7-10.

A disturbing feature of the use of flux forcing in a closed flux core is introduced by the variable reluctance of the iron. The air gap in the orbit field has essentially constant reluctance, but as the flux-core iron approaches saturation its permeability drops and its reluctance increases. This effect causes a distortion of the proportionality of flux to field, and the radius of the equilibrium orbit shifts. Since increased core reluctance reduces central flux, the result is a slower acceleration than required for the betatron balance, and the orbit contracts. In a betatron economically designed to have a small region of stability around the orbit this effect can be serious and requires correction.

Small changes in radius of equilibrium orbit can be corrected by adding more flux in a separate magnetic circuit; such a compensating circuit is needed also to correct for radiation losses (see Sec. 7-7) and is used in the 300-Mev betatron.

Kerst has suggested another method of maintaining the flux-field proportionality. Two auxiliary coils can be used, one linking the central flux and one the orbit-field flux; the turns ratio can be adjusted so induced voltage is the same across the coils for the desired flux-field relation, and when the coils are connected in opposition, there will be no current in them. Then if this relation is disturbed by the iron-saturation effect, a current will circulate in this pair of coils and will set up fields to oppose the change. The residual error in the flux forcing system with such correcting coils will be determined by the resistive voltage drops in the auxiliary coils and can be held to any desired value. Such techniques make it possible to use flux densities in the core as large as 14 to 16 kilogauss.

Two methods are available for biasing a betatron to provide the advantage gained by flux forcing. These depend on whether the dc bias is applied to the orbit field or to the central flux.

In *field biasing*, the magnetic field at the orbit is arranged to have a steady component by a dc component in the windings. If this steady field is approximately half the maximum set by saturation of the poles and if the ac component has the same magnitude, the field will vary from zero to maximum during a half-cycle of the applied ac current. During this half-cycle the central flux will vary from its maximum negative to its maximum positive value, a total flux change approaching twice that available without biasing. Electrons can be accelerated to nearly twice the energy at the same orbit radius. Figure 7-11*a* illustrates the field and flux waveforms for such a field-biased betatron.

Injection of electrons occurs at low electron energy when the orbit field is just starting to rise from zero. However, the rate of change of field should be fairly large at injection to obtain a fast build-up of energy

and provide good focusing forces at the start, so in practice the bias is made somewhat smaller than the amplitude of the ac component. Ejection also occurs slightly before the peak of the cycle, before magnetic field has reached its maximum. The total variation of field and flux that

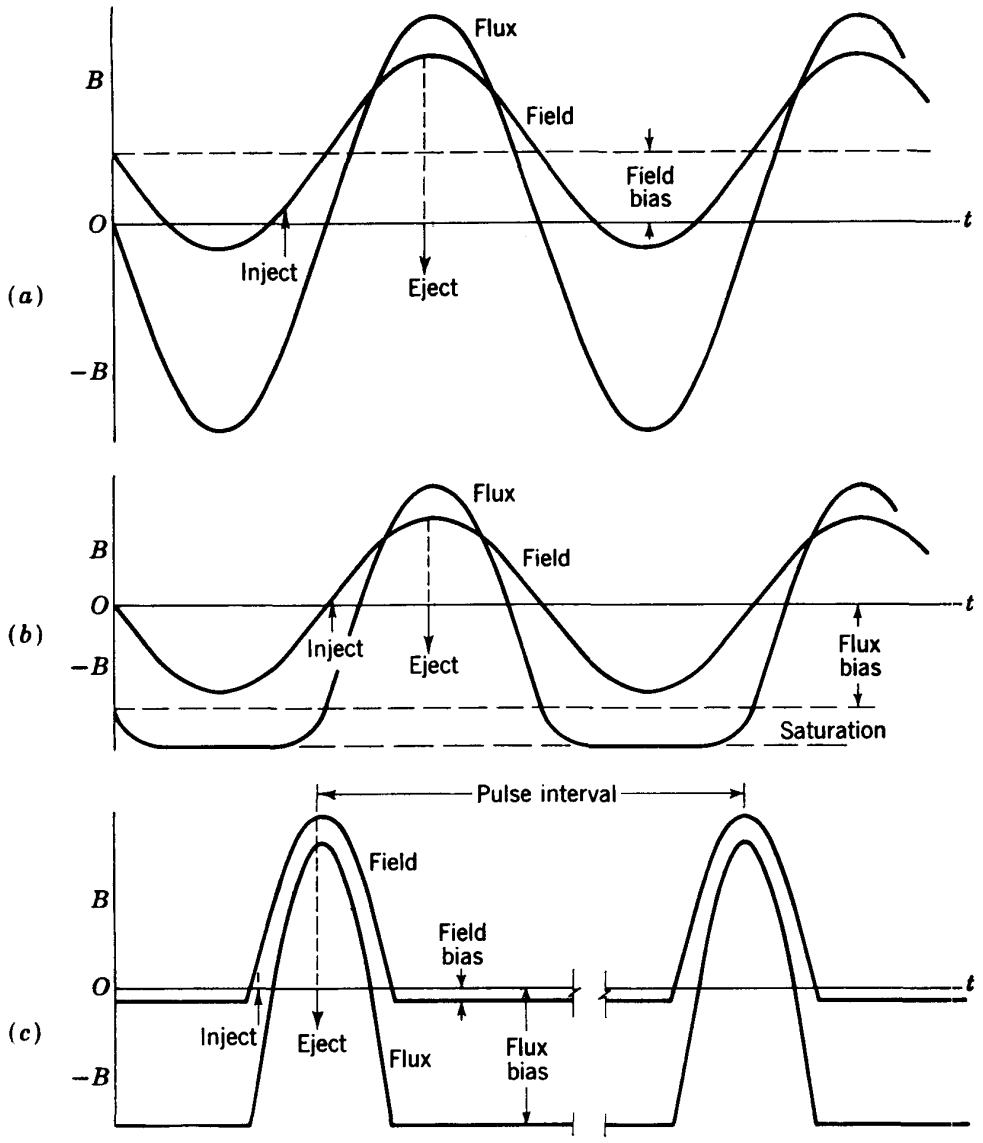

Fig. 7-11. Orbit field and central flux waveforms for (*a*) field biasing, (*b*) flux biasing—continuous operation, and (*c*) flux biasing—pulsed operation.

can be utilized, as chosen by designers, is about 86 per cent of the maximum possible.

Figure 7-12 is a simple schematic circuit for supplying dc bias current to the orbit field. The direct current is supplied in series to the groove coils and the main coils. The groove coils are used here merely to cancel the dc component in the central flux core; the main coils provide ac com-

ponents for both orbit field and core flux. An ac filter is placed in series with the dc generator in this circuit to limit the ac current in the windings of this machine.

Flux biasing utilizes a dc magnetic component in the central flux field, which nearly saturates the iron in the negative sense. The ac component superimposed on this bias carries the flux density through zero and to a positive maximum during the quarter-cycle when orbit field is going from zero to maximum. The orbit field can now be powered to approach its maximum practical value, and the doubled electron energy comes from the doubled change in central flux, from $-\Phi_c$ to $+\Phi_c$ during the quarter-cycle. The waveforms for continuous operation are shown in Fig. 7-11*b*; here the negative half of the ac flux cycle is shown lopped off by the saturation of the iron. It should be noted that flux biasing oversaturates

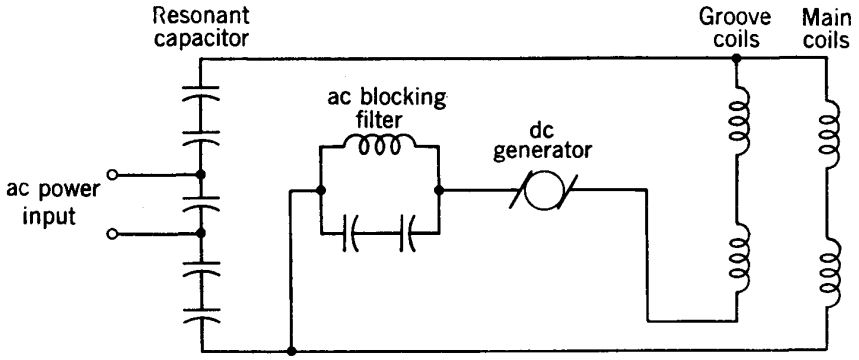

Fig. 7-12. Powering circuit for a field-biased betatron, showing the dc generator and a filter to reduce ac current in the groove coils.[16]

the central core during the negative half-cycle. In a large magnet this results in such large and undesirable magnetic losses due to hysteresis that it is impractical to operate continuously. However, pulsed operation is possible, and the duty cycle can be adjusted to reduce losses and heating to a satisfactory level and to hold input power to a practical value. Figure 7-11*c* illustrates the waveform for unidirectional pulsing which can be used with flux biasing.

Flux biasing was chosen for the 300-Mev betatron for several reasons. First, fewer bias ampere-turns are required to saturate the central core, which has no air gap, than to half-saturate the field magnet, which does. Second, the choke coil needed in the ac filter to limit the magnitude of current induced in the bias coil during the flux change is smaller by one-tenth than for field biasing. Third, flux biasing lends itself to unidirectional pulsing rather than continuous operation. For the large magnet used in the 300-Mev betatron, the power consumption would have been excessive for continuous operation. Unidirectional pulsing allows a design for lower power input, smaller coils, and reduced coil heating; magnet design is more compact, leakage flux is minimized, and capacitor

ratings and costs are reduced. The smaller duty cycle due to pulsing results, however, in lower average beam intensity.

The flux bias supply for the 300-Mev betatron is not described in detail in the publications. However, that for the 80-Mev model[7] can be cited to illustrate the design. Separated bias windings are distributed about the flux core to give maximum magnetic efficiency and minimum leakage flux. Power comes from a high-capacity 4.8-volt battery, supplying 97 amp to the windings. During the flux pulse large voltages and high currents would be induced in this winding, which would oppose the flux change and essentially short-circuit the voltage pulse. A simple but clever arrangement is used to prevent this short-circuiting. A choke coil which has its secondary winding installed in series with the bias supply has a primary winding connected to the betatron terminals. As the voltage pulse builds up on the terminals, a secondary voltage is produced

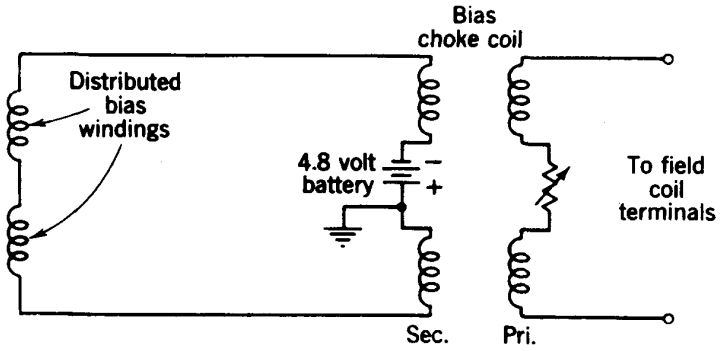

Fig. 7-13. Flux bias circuit for the 80-Mev betatron, with a choke coil to oppose the induced voltage.[7]

in the choke coil which just bucks out the induced voltage in the bias windings. The circuit for the dc-bias-coil connections, including the choke coil, is shown in Fig. 7-13. Note the center-tapped coils used for both magnet winding and choke coil; this allows mid-points to be grounded to give a balanced circuit and reduce capacitance effects.

7-6. PULSE POWERING

Continuous operation of a betatron magnet on an ac power supply is limited by heating of the iron due to hysteresis and eddy currents. As electron energy is increased, all considerations tend to increase this heating. The time of acceleration must be short to reduce losses due to gas scattering and radiation; this requires high-frequency operation, which increases the eddy-current heating. Magnetic-field intensity in the iron approaches saturation at the peak of the cycle and actually exceeds saturation in the negative cycle for flux biasing; this also increases heating. Furthermore, heating is proportional to volume and increases with

the third power of a linear dimension of the magnet, while surface area, through which it can be cooled, increases only with the second power.

Oil-immersion cooling of the laminations, which is common for power transformers, is impractical for the betatron. The efficiency of air-blast cooling is limited to a fraction of that obtainable with oil cooling, and air ducts are difficult to install in a betatron magnet without seriously crippling accessibility to the vacuum chamber.

In the design of the 300-Mev betatron it was found that heating of the iron limited the duty cycle during which the magnet could be powered to about one-twentieth of the total time. Pulsed operation was chosen, with a unidirectional pulse of $\frac{1}{120}$-sec duration (essentially a half sine wave at 60-cycle frequency) repeated at a maximum rate of 6 pulses/sec. In the 80-Mev model, which was operated at the same flux densities, the limitation imposed by the scaled-down current-carrying capacity of the windings reduced the duty cycle to 1 pulse every 3 sec. As a consequence, the 80-Mev machine was not so flexible and did not produce as high intensities as could have been attained had the windings been designed efficiently for that energy.

Pulsed operation does not reduce the size or cost of the capacitor bank, which is one of the most expensive components. The size of the capacitor bank is determined by the fact that it must be able to store all the energy required to power the magnet a quarter-cycle later. Once the magnet is designed and its maximum stored energy determined, the requirements of the capacitor bank are fixed. Frequency can be adjusted by changing the series-parallel connection of the capacitor bank. In higher-frequency operation the capacitor losses will be higher and their kva rating lower, so the costs may be increased somewhat.

The pulse power supply for the 80-Mev betatron is shown in Fig. 7-14*a*, producing the sequence of operations indicated in Fig. 7-14*b*. A three-phase full-wave rectifier using six thyratrons, which has a dc output of 1100 volts, provides a charging current of 30 amp to the 5000-μf capacitor bank. The charge-discharge cycle is controlled by a pair of solenoid-type contactors, arranged as a reversing switch. The main pulse is triggered by a mercury-pool ignitron. Voltage on the capacitor bank reverses during the discharge through the exciting coils, and the final voltage is about 25 per cent less than the initial voltage owing to dissipation in the coil windings and the ignitron. This loss is made up by recharging the capacitors from the rectifiers.

The flux-forcing circuit is also indicated in Fig. 7-14*a*. It involves a fairly intricate balance between induced voltages in the several coils and resistive voltage drops. Field windings are represented by coils A (back-wound) and coils B (main winding) in series; the flux windings are the distributed C coils. The location of these coils in the magnet is shown in Fig. 7-8. A variable series resistor R_T in the flux circuit is used to obtain

a first-order balance between the resistive voltage drops in the two windings; since this is alternating current, the resistance must be measured and balanced for the fundamental frequency of the exciting pulse. Higher harmonics in the flux windings, which are due to the effect on

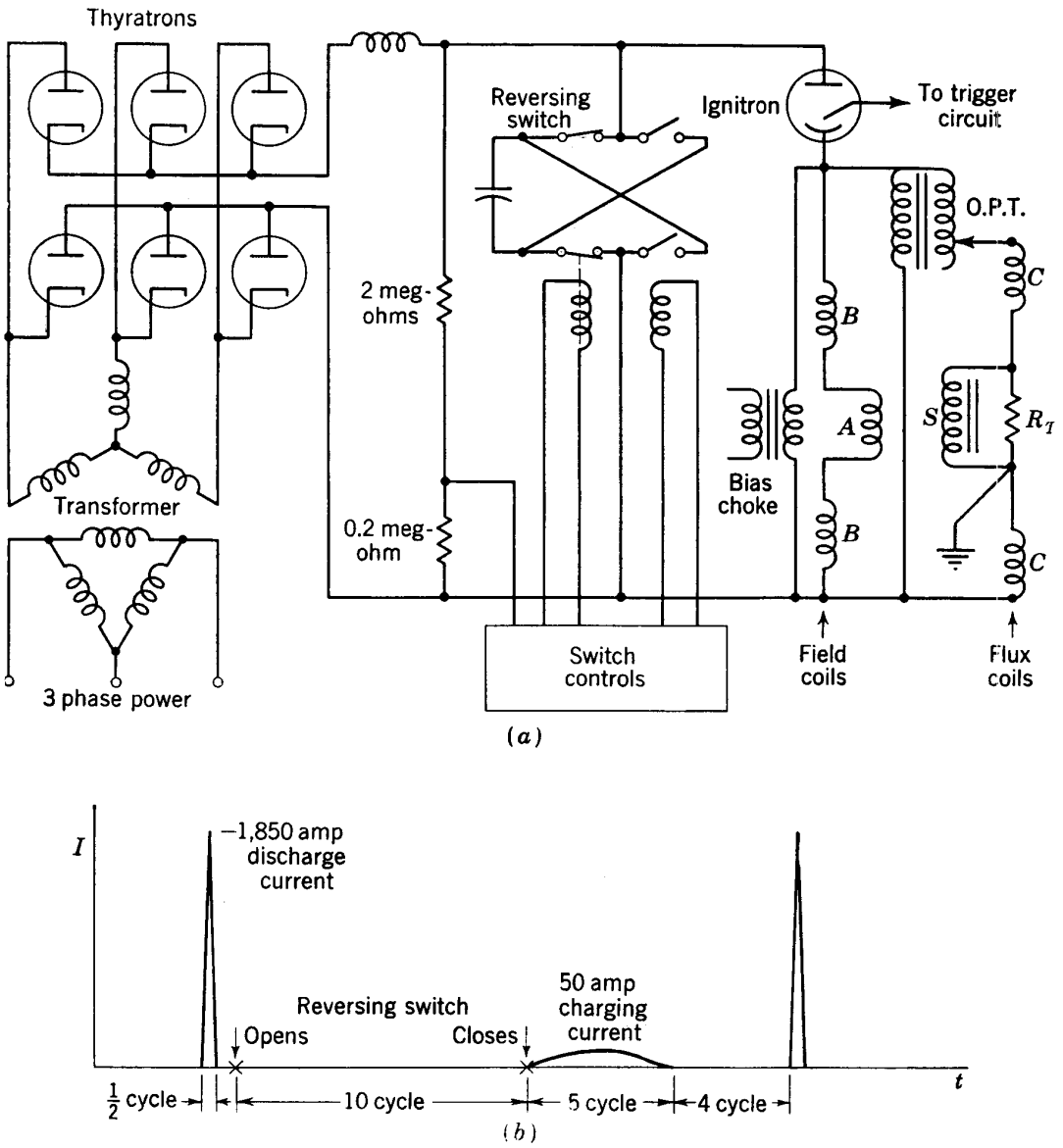

Fig. 7-14. (*a*) Pulse power supply for the 80-Mev betatron.[7] (*b*) Sequence of power-supply operations at 3 pulses/sec.

inductance of the varying reluctance of the iron flux core, are corrected by a saturating reactor (S) placed in parallel with R_T. An orbit positioning transformer (labeled O.P.T.) varies the potential applied to the flux windings by a small amount, to change the field-flux ratio and position the orbit as desired. The exciting coils are grounded at their mid-points to

provide symmetrical circuits and equalize the effects of capacitance in the windings.

The large and steep rise of current at the start of a pulse induces eddy-current transients in the iron which take a finite time to become established. This is the time required for the magnetic field to penetrate the iron and depends on the thickness and condition of saturation of the laminations. This flux penetration time is given by[7]

$$t = \frac{\pi \mu d^2}{3 \times 10^9 \rho}$$

for the rise time to 95 per cent of full value for the eddy currents; ρ is resistivity in ohm-cm, d is the thickness in centimeters, and μ is the differential permeability. For the heavily biased 0.014-in. silicon-steel laminations used in the 300-Mev magnet, this time is 7.5 μsec.

During the time required to establish the eddy currents the proportionality between field and flux will be changing, so the equilibrium orbit will not have constant radius. This time may be longer than the time for the field to rise to the injection value, which depends on injection voltage. The technique used to correct for this starting transient with the 300-Mev magnet was to apply a small negative field bias (about 28 gauss) to allow time for eddy currents to become established (see Fig. 7-11*c*).

The only published description of the 300-Mev betatron[8] is very brief. It can be summarized by the dimensions and constants given in Table 7-1. The best photographic illustrations are published in *Life* magazine.[18] The primary purpose in building the 300-Mev machine was to attain energies at which mesons could be produced. This result has been achieved, and present activity in the Illinois laboratory centers on scientific studies of meson properties and interactions.

TABLE 7-1
CONSTANTS OF THE 300-MEV BETATRON

Maximum electron energy	315 Mev
Orbit radius	122 cm
Maximum orbit field	9.2 kilogauss
Initial flux density	−14 kilogauss
Final flux density	16 kilogauss
Weight of flux magnet	275 tons
Weight of six field magnets	66 tons
Energy stored in capacitor bank (field magnet, 85 per cent; flux magnet, 15 per cent)	170,000 joules
Flux-core bias winding	2,600 amp-turns
Injection energy	80–135 kv
Peak injection current	1–3 amp
Pulse repetition rate	6 pulses/sec
X-ray output at 1 m, ⅛ in. Pb	14,000 r/min

7-7. RADIATION LOSS

A charged particle constrained to move in a circular orbit by a central accelerating force radiates energy because of this acceleration. The magnitude of this radiation loss can be computed from the classical theory of the electromagnetic field. Iwanenko and Pomeranchuk[19] first pointed out that this effect would disturb the betatron relation and would ultimately set an upper limit on the energy that could be attained by this machine. Blewett[20] analyzed the problem as applied to betatrons, and Schwinger[21] has presented a complete study of classical radiation by accelerated electrons. A valuable analysis of radiation by accelerated relativistic electrons is available also in chap. 7 of "Electrodynamics," by Page and Adams.

These various authors have shown that an electron having velocity v and acceleration a in a direction normal to the velocity vector will lose energy by radiation at a rate given by

$$U = \frac{2 \times 10^{-7} e^2 a^2}{3c(1 - v^2/c^2)^2} \quad \text{watts} \tag{7-13}$$

It is worthy of note that application of a Lorentz transformation to modify this relation to a reference frame in which the electron is instantaneously at rest changes the formula to

$$U = \frac{2 \times 10^{-7} e^2 a^2}{3c} \quad \text{watts} \tag{7-14}$$

which is the classical formula first derived by Larmor for radiation from a slowly moving electron.

For an electron constrained to travel in a circular path of radius r, a is v^2/r; since the radiation effects are appreciable only in the extremely relativistic range, we can replace a by c^2/r. The quantity $(1 - v^2/c^2)$ can be replaced by $\left[\frac{m_0 c^2}{e(W/e)}\right]^2$, where W/e represents the energy of the electron in electron volts. With these substitutions Eq. (7-13) becomes

$$U = \frac{2 \times 10^{-7} e^6 (W/e)^4}{3 m_0^4 c^5 r^2} \quad \text{watts} \tag{7-15}$$

After substitution in this formula for the fundamental constants we obtain

$$U = 6.76 \times 10^{-43} \frac{(W/e)^4}{r^2} \quad \text{watts} \tag{7-16}$$

or

$$U = 4.22 \times 10^{-24} \frac{(W/e)^4}{r^2} \quad \text{ev/sec} \tag{7-17}$$

But one revolution takes $2\pi r/c$ sec and therefore

$$U = 8.85 \times 10^{-32} \frac{(W/e)^4}{r} \quad \text{ev/revolution} \tag{7-18}$$

From this relation it is evident that appreciable energy loss will not be experienced until W is of the order of 100 Mev. Above this energy the loss will increase very rapidly until, for example, a 1-Bev electron in a betatron with a radius of 10 m would lose 8850 ev of energy per revolution, an amount that would be difficult to supply by betatron techniques.

A useful concept in the mathematical treatment of radiation effects is that of an effective retarding electric field E'. The radiation loss has the same slowing-down effect on the electron as would be experienced in a continually retarding field E', which can be obtained from Eq. (7-18) as

$$E' = 1.408 \times 10^{-32} \frac{(W/e)^4}{r^2} \quad \text{volts/m} \tag{7-19}$$

Two other features of the radiation are derived in the references cited; the derivations are beyond the scope of this book, but the results can be stated. The radiation is generally emitted in the forward direction, and the higher the particle energy the more sharply is the radiation collimated. The half-intensity contour is a rough cone whose internal half-angle is approximately equal to m_0c^2/W radians. For 100-Mev electrons this angle is about 0.3°. The second feature of interest is the spectral distribution of the radiation. It is spread over 10^7 or more harmonics of the fundamental revolution frequency with an energy distribution whose maximum is usually in the visible spectrum. As a consequence of these phenomena it is easy to see the radiation by looking along a tangent to the orbit (with a mirror) at the side where the electrons are approaching the observer. A bright spot of light is clearly visible; its intensity can be used as a measure of beam intensity. In Chap. 12, The Electron Synchrotron, observations will be discussed which give experimental checks of all of the predictions of the theory.

The total energy loss during acceleration can be obtained by integration of Eq. (7-17) over the acceleration cycle. For the 300-Mev betatron the total loss is about 13 per cent of the total energy. If no compensating means were included, the orbit would shrink about 20 per cent and the beam would be lost by collision with the inside wall of the vacuum chamber.

To correct for this loss the relation between orbit and flux change must be modified; central flux must rise at a faster rate than for strict proportionality. Or, alternatively, the orbit field can increase less rapidly, which can be accomplished by designing the magnet so that saturation

sets in and reluctance increases in the orbit-field circuit faster than for the central flux.

A betatron with flux forcing can be arranged to have more flux added at the peak of the flux cycle to compensate for this radiation loss, at least up to some practical limit. In the 300- and 80-Mev magnets a section of the central pulse-transformer core was reserved for the dual purpose of adding flux to correct for radiation loss and for expanding the orbit against a target at ejection time. This section has about 7 per cent of the cross section of the central core and is supplied by a magnetic return circuit which does not link the exciting coils for the central core (see Fig. 7-8). Separate windings on these "expansion side packages" are excited late in the cycle by a separate power supply, with a voltage rise time designed to give the correct rate of flux increase and orbit expansion.

It is necessary to shield the side packages of laminations from the main flux in the core to prevent partial saturation by leakage flux. This is done by copper shields wrapped around the core, with an insulated, overlapped split to prevent short-circuiting currents in the shield. Eddy currents developed in the copper sheet by the leakage flux set up reverse fields which cancel the leakage flux. This also results in a lower inductance of the side-package circuit, making it possible to pulse it with a sharply rising voltage pulse.

In the design of the 300-Mev betatron the radiation loss has been carefully considered and corrected for. Both methods are used: modifying the field-flux proportionality in the windings and forcing additional flux through the core. The fractional radiation loss is held to about 8 per cent by allowing electrons to remain in the machine for only 75° of the magnetic excitation cycle, which means that ejection occurs at 3.5 per cent below peak magnetic field. The corrections are sufficient to maintain essentially constant orbit radius up to the ejection pulse and to have an excess adequate to expand the orbit out to the target radius. This required very delicate balancing of many factors entering in the design.

The fourth-power increase of energy loss by radiation suggests that it will be impractical to attempt to push betatron designs to much higher energy. Most designers feel that the present 300-Mev machine represents the practical maximum energy for a uniform-n betatron. With the introduction of the synchrotron principle of electron acceleration it is possible to add energy electrically through use of an accelerating gap; the necessary volts per turn can be added more economically this way than through magnetic induction. So it seems probable that synchrotrons will provide a more satisfactory method of attaining higher energies. However, in practice, higher beam intensities have been attained with betatrons than with synchrotrons, and in the lower energy range, where magnet cost is not a limitation, the betatron has a distinct advantage.

7-8. ELECTRON INJECTION

Electrons are injected into the betatron tangentially at an instantaneous orbit located just inside the radial position where the magnetic field becomes defocusing. The injector gun consists of a heated cathode, a focusing electrode, and an outer shield. A typical structure is shown in Fig. 7-15, taken from the description of the 20-Mev betatron. A tight helical spiral of tungsten wire is used for the cathode, giving a line source some 0.5 to 1.0 cm long. The focusing electrode is a curved reflector behind the cathode, having a potential slightly negative relative to the cathode and shaped to produce a focused beam of electrons. The outer shield, constructed of molybdenum or tungsten sheet with a slot for the beam to emerge, is at ground potential. The cathode is operated at high negative potential, so the electrons have high injection energy. Potentials of 600 volts for the first 2.3-Mev accelerator, 20 kv for the 20-Mev machine, 60 kv for the 80-Mev model, and up to 135 kv for the 300-Mev machine have been reported, indicating a steady development to higher injection energy. Peak injection currents of several amperes can be obtained from such a source. The beam emerging from the injector gun is not sharply focused but diverges at an angle of 5 or 10°. A large fraction of the beam is lost to the walls within the first turn.

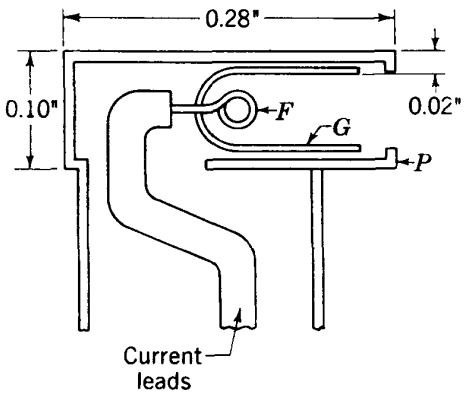

Fig. 7-15. Electron injector gun, showing filament F, focusing electrode G, and outer shield P, which is grounded. Peak beam current pulses of 1 to 3 amp are produced.

The success of this injection scheme depends on the chance that an electron will miss hitting the back of the injector on subsequent turns. Calculations of the rate of decrease of instantaneous orbit radius as it spirals into the equilibrium orbit show the change per turn to be extremely small. The contraction will follow Eq. (7-8):

$$\frac{d(\delta r)}{\delta r} = -\frac{dB_0}{B_0} = -\frac{1}{2}\frac{dT}{T}$$

where δr = displacement from the equilibrium orbit
B_0 = magnetic field
T = kinetic energy

A sample calculation of the magnitude of this contraction per turn will be informative.

Consider injection of 20-kev electrons into an orbit at 8.5 in. radius in the 20-Mev betatron, in which the equilibrium orbit is at 7.5 in. To

calculate the increase in energy per turn we must find the flux change or the energy change per turn at the start of the acceleration cycle. In a previous section we showed that the total flux change corresponding to 20-Mev electrons at peak orbit field was 0.082 weber. The total acceleration time is a quarter-cycle at 180 cps, or 0.0014 sec, and the slope of a sine wave at the start of the cycle is $\pi/2$ times the average slope. So the initial induced voltage per turn is

$$V_i = \frac{(\pi/2)\,\Delta\Phi}{\Delta t} = \frac{1.57 \times 0.082}{0.0014} = 92 \text{ volts/turn} \qquad (7\text{-}20)$$

At the injection energy of 20 kev this represents a change in energy of 1 part in 460; from Eq. (7-5) this is equivalent to a change in displacement (δr = 1 in.) of 1 part in 920, which is roughly 0.001 in. This is much smaller than the dimensions of the injector; if it were necessary to depend on this effect alone, essentially all electrons would strike the back of the injector and be lost.

Another feature which must be considered in injection is the radial and axial oscillation of the electrons about their instantaneous orbits. For the value of $n = 0.75$ chosen for the 20-Mev betatron magnet these oscillation frequencies are $f_r = 0.50f_0$ and $f_z = 0.864f_0$. Particle orbits will be complicated three-dimensional curves which cross the equilibrium orbit once each revolution and which cross the median plane once each 208° in azimuth. A plot of the path of a typical electron projected on the median plane (which shows only the radial variations) is shown in Fig. 7-16. The damping motion is exaggerated in the illustration to show successive circles, which are numbered in order. The plot shows that the electron will miss the injector in the first, third, fifth, etc., passages and will be closest to the injector on the second revolution. However, the axial oscillations will be out of phase after two turns (720° of azimuth) and will have approximately maximum amplitude at this point, so the electron has a good chance of missing the injector vertically. Such considerations suggest that on the average an electron will traverse 5 to 10 revolutions before again having large positive radial amplitude and small axial amplitude at the location of the injector. The orbit contraction will be five to ten times greater by this time, and it might be supposed that some of the electrons would miss the back of the injector and be captured in stable orbits. The injector unit in modern betatrons is made as narrow as possible in the axial dimension in order to increase the chance of missing the injector through the vertical oscillations.

The analysis of orbit contraction above predicts the largest radial displacement at low injection energy. Early designers assumed this to be valid; note the 600-volt maximum designed for the 2.3-Mev machine. Nevertheless it was found experimentally from the start that beam intensity increased with increasing injection energy, approximately with

$V^{3/2}$. It was a mystery to all concerned how electrons could miss the injector in early betatrons. Designers accepted the experimental fact and used the highest practical injection energy.

Kerst[22] has proposed a theory of self-contraction to explain the high injection efficiencies. It offers a specific mechanism and Kerst cites some evidence to support it, but other workers feel that self-contraction is not the most important factor.

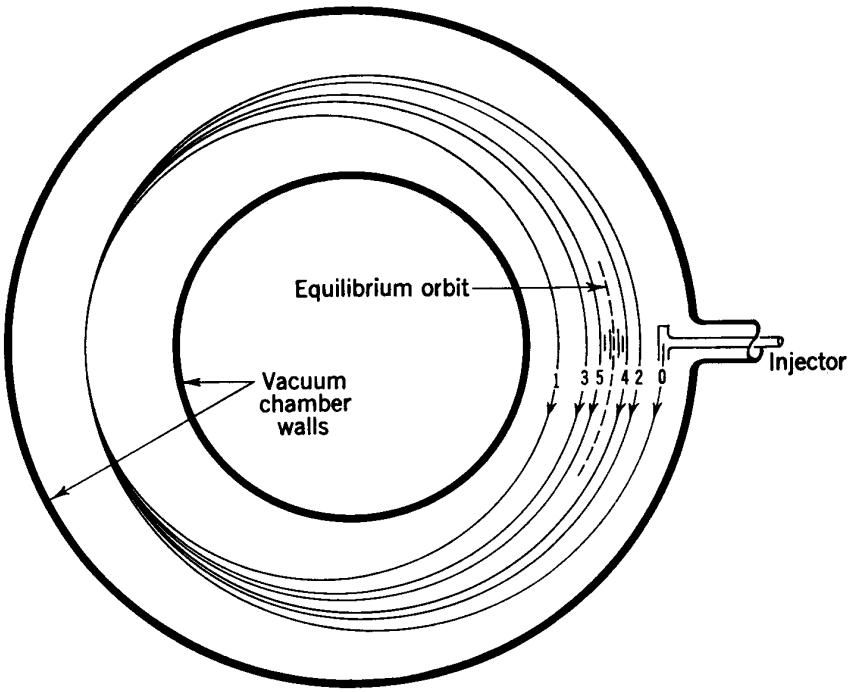

Fig. 7-16. Successive electron paths in a magnetic field for which $n = 0.75$ ($f_r = \frac{1}{2}f_0$). Damping is exaggerated to show contraction toward the equilibrium orbit following injection.

Self-contraction is due to energy withdrawn from the kinetic energy of the beam in setting up an electromagnetic field. It can be visualized most simply in terms of current in a wire loop at the location of the beam. Consider that a current is established in this loop in a time comparable with one revolution; it will produce a magnetic field within the loop which opposes the flux already threading the loop. Kerst has computed the inductance L of such a loop in the 20-Mev betatron to be about 4×10^{-6} henry, mainly because of the large central flux present. The voltage drop around this loop is given by $L(di/dt)$; if 1 amp were to be set up in one revolution, approximately 10^{-8} sec, the voltage would be

$$V = -L\frac{di}{dt} = -4 \times \frac{10^{-6}}{10^{-8}} = -400 \text{ volts} \qquad (7\text{-}21)$$

So the electron beam might be reduced in energy by 400 ev in one revolution owing to this effect alone. If several revolutions are required to

establish the circulating beam, the loss might be spread out over these several revolutions.

The existence of the beam of electrons at the orbit location also means that a concentration of space charge has been set up which produces an electrostatic field. The energy in the electrostatic field due to this charge can also be estimated. Kerst has computed that the energy required to set up this electrostatic field subtracts from the beam 150 ev energy per electron in each turn. Others believe that space-charge effects can be even more important and that a detailed and precise analysis would justify this opinion.

It is clear that the complete interpretation must include the effect of magnetic-field inhomogeneities, electrostatic repulsion within the beam, build-up of electrostatic charges on the walls, damping of oscillations due to these various factors, and possibly other unrecognized influences. For example, Heyman[23] has found that it is possible to increase injection efficiency and beam intensity by applying a negative bias to the metallic coating of the chamber relative to the injector shield.

One useful improvement in experimental technique has resulted from studies of orbit contraction. This is the orbit contractor reported by Adams.[24] Adams uses a wire loop on each pole face above and below the orbit location; these loops are connected to a pulsed power supply which produces a rising current pulse during injection. The direction of current in the loops is such as to retard the rate of rise of flux within the orbit. This causes electrons in orbits outside the equilibrium orbit to be suddenly drawn in toward this orbit. The action is similar to the action of the beam on itself in self-contraction and provides a practical method of controlling this phenomenon. The increasing current in these loops reduces magnetic field inside the orbit radius relative to that outside. This change of field shape represents a decrease in n value near the orbit. Radial-oscillation frequency will be increased, as will the damping of these oscillations, by this change in n value. The complete theory of the orbit contractor is obviously complicated. Experimentally it has resulted in a considerable increase in X-ray yield from all betatrons to which it has been applied, indicating an increase in the percentage of electrons trapped at injection.

Orbit contraction is a consequence of the increase of circulating current in the beam. Consequently electrons which are injected after the time when they can be trapped, but which can circulate for a few revolutions before striking the walls, will also retard the rate of rise of central flux and hence serve to contract orbits for the useful electrons injected earlier. It was noted at a very early stage that beam intensity could be increased by continuing injection for a short time past the acceptance interval, but that there was a drop in yield if injection was continued through the full cycle. This optimum length for the total injection pulse was reported[4]

to be about one-twelfth the full quarter-cycle for the small betatrons. Only a fraction of the injected electrons are actually accelerated; one author estimates[25] a final peak beam current of 0.2 amp, although the injection beam was of the order of 1 amp. It has been observed that a low-intensity beam from a very short pulse can be increased in intensity by a larger factor than that from a long pulse when the orbit contractor circuit is utilized. We can conclude that the postinjected beam is useful chiefly in supplying orbit contraction to the trapped beam. Modern betatrons such as the 80-Mev machine, which is equipped with orbit contractor coils, do not require as long an injection pulse; the optimum pulse for this machine was found to be 5 μsec.

Continuous injection results in lower intensities than pulsed injection. The decrease seems to be due to the disturbing magnetic and electrostatic fields set up by the delayed electrons. Late in the cycle, at high magnetic fields, the orbits of electrons injected at the constant injection energy will be small spirals. These asymmetric circulating currents can set up distorting magnetic fields near the injector. Also the electrostatic charge collected on the walls may become large enough to deflect and defocus the trapped beam. So pulsed injection is now standard procedure, with a variable pulse length which is adjusted experimentally to give maximum beam intensity.

A rising voltage pulse on the injector is found to give higher intensities than a flat-topped pulse. This is understandable from the simple concept of matching injection energy to magnetic field over a longer time interval. Other effects may be involved, such as the rising emission current from the injector, which aids in orbit contraction. The optimum pulse shape also is obtained by experimental manipulation.

Azimuthal inhomogeneities in the orbit field at injection time can have a serious effect on beam intensity. This problem was studied in detail by Adams, Kerst, and Scag[26] for four similar 22-Mev betatrons built for commercial sale; the azimuthal fields were measured using the peaking strip technique (see Sec. 7-9, Magnetic Measurements). Fluctuations as large as ± 5 gauss were observed at different azimuths, and all four magnets were different. Such bumps in the field can produce electron oscillations of sufficient magnitude to reduce intensity significantly. They are due to phase differences in the field at different portions of the magnetic circuit, caused by variations in lamination thickness, hysteresis and eddy-current losses, or by accidental short circuits between laminations. The out-of-phase components can be corrected by coils located beneath the orbit at the indicated locations, powered with out-of-phase currents to correct the phase angle. The use of such correcting coils increased yield in all betatrons to which they were applied by from 20 to 50 per cent. When the field variations were reduced to about 3 per cent of injection field (1 to 2 gauss at 45 gauss), no further improvement could be obtained.

This criterion for "smoothness" of the magnetic field applies to the geometric aperture of the 22-Mev machines; other betatrons with relatively smaller vacuum chambers would require proportionately smaller fluctuations in field.

It should be noted that the injector could be located alternatively inside the equilibrium orbit, if desired, rather than outside. The instantaneous orbit would spiral outward toward the equilibrium orbit in this case. Focusing forces for deviant electrons exist as before. The orbit contractor could be arranged as an orbit expander by reversing the direction of the current pulse. This injector location is particularly useful when an emergent beam is to be extracted from the betatron, in which case it would be advantageous to have the outer region of the chamber free from obstructions except for the extractor device. Similarly, the injector could be located above or below the orbit, in which case vertical injection oscillations would be the limiting factor.

The most complete theoretical analysis of the injection problem in the betatron was published by Schwartz[27] in a German journal. He has considered the problem of a divergent electron beam and has determined the envelope of particle paths in the first few revolutions after injection. With this more detailed analysis most of the phenomena observed at injection are explained. The time interval of acceptance into stable orbits is found to increase with injection voltage. The effect of field inhomogeneities is studied and the necessary uniformity computed. The angle of divergence at the source which can be accepted into the available aperture is found to be independent of injection voltage and to improve with improved field uniformity. During the acceptance time interval the allowed angle of divergence increases from zero to a maximum and falls back to zero. So injection efficiencies can now be fairly well computed if all constants are known.

7-9. MAGNETIC MEASUREMENTS

Probably the most significant contribution to electrical science and practice coming from the development of the betatron has been the improved knowledge of principles, methods, and techniques for magnetic measurements and magnet design, largely as a result of the design study of the 80-Mev model by Kerst and his associates. The emphasis placed by Kerst on perfection paid off in a striking way in the 300-Mev betatron, which operated at full designed energy almost from the start. It is a noteworthy example of the importance of careful design. An excellent description of these design studies and model measurements has been published.[8] We shall summarize here some of the more significant results.

The criterion for producing an azimuthally uniform magnetic field is that the reluctance be the same through any section of the magnetic

circuit. The bundles of C-shaped laminations used for the orbit-field circuit were designed to have essentially equal length of iron through each path. The radial tapering at the pole face was obtained by chopping laminations of different lengths and assembling the long and short ones symmetrically, with the short ones distributed so that the magnetic inhomogeneities introduced were "fine-grained." The assembly technique was aimed at preventing any magnetic flux from having to cross from one lamination to another.

The radial variation of field across the pole face was chosen to have the index n vary from 0.2 at the inside wall to 0.5 at the orbit radius and to 1.0 at the location of the injector. The contour to provide this field shape was determined by successive trials with a dc model of one-tenth scale of the 300-Mev machine, constructed with $\frac{1}{8}$-in. laminations. Measurements were taken with a search coil and ballistic galvanometer actuated by the reversal of field in the dc model.

Excitation windings must be installed in such locations that the lines of field H are everywhere parallel to the laminations in which the induction B is to be established. This was accomplished for the orbit-field circuit by using simple circular windings, axially symmetrical with the poles. It would not have been sufficient to distribute these windings over the six back-legs of the C's.

Distortions can exist in the field because of different thicknesses of iron or imperfections in the geometry of assembly. Other distortions are observable primarily near zero field or the low fields at injection. Leakage flux from the pulsed excitation of the core can be eliminated by suitable copper shielding. Residual magnetism can vary in different samples of iron because of variations in manufacturing or handling procedures. The magnitude of the remanent field observed in the model was about 3.5 gauss, and the variations were less than 0.1 gauss. Eddy-current fields can be inhomogeneous, depending on the presence of short circuits between laminations. This was sufficiently corrected by inserting paper insulation between laminations at $\frac{1}{4}$-in. intervals. Phase lags at the pole tips caused by the distribution of eddy-current electromotive forces about the circuit may also be important; they have the effect of increasing the value of n at injection time. Although correction was not necessary in this case, it was found that such phase lags can be corrected by distributed windings about the circuit sufficient to compensate for the distributed losses in the circuit.

Several instruments have been devised for measuring small field variations at or near zero field. The "peaking-strip"[26,28] method uses narrow strips of permalloy or Hypernik, which saturate at very low fields, wound with a small solenoidal coil of many turns. Use of the peaking strip for magnetic measurements is discussed in Sec. 8-8.

A "zero-field detector" has been developed[8] which is essentially a

cathode-ray gun which shoots a beam of 100-volt electrons through fine slits and against a collector. As the field passes zero, an electron pulse is collected. A bias coil can be used and pulses from two detectors can be observed in coincidence, to measure the field difference. Much shorter pulses can be obtained with this detector than with the peaking strips, and the method is free from possible errors due to variable magnetic properties of the strips. When this detector was used, no variation of orbit field with azimuth was observed as great as 0.1 gauss in the 80-Mev model.

A small milligaussmeter reported by Adams, Dressel, and Towsley[29] is capable of high precision and is a novel application of magnetic amplifier technique. The method consists in measuring the second-harmonic content of the exciting current for a ferromagnetic peaking strip which is normally excited to partial saturation. The second-harmonic component appears when the strip is biased by an external magnetic field, and the amount is directly proportional to this field. The magnitude of the sharp pulses induced in the peaking strip increases significantly with very small applied fields. The instrument has been used to measure magnetic fields from 1 milligauss to 100 gauss in flux density, using a probe of the order of $\frac{1}{4}$-in. dimensions.

Another careful study of the azimuthal variations of field in a betatron magnet is reported by Lasich, Muirhead, and Wright.[30] They claim to be able to separate the contributions to the azimuthal variations due to iron inhomogeneities, eddy currents between laminations, and eddy currents in the laminations themselves.

The rate of rise of magnetic field in the 80-Mev betatron is 4 gauss/μsec at injection, so it is necessary to be able to estimate the time of zero field within one-twentieth of a microsecond to observe field errors of 0.1 gauss. The tolerance limits of 0.1 gauss for both axial and azimuthal components of field at the orbit were set by the computed orbit displacements which they would produce. If half the field were 0.1 gauss too high and the other half 0.1 gauss too low at injection time, a radial orbit oscillation would be set up which would remove about 6 per cent of the usable radial space. If the radial field component were to vary similarly by 0.1 gauss, it would set up vertical oscillations of equivalent amplitude. A radial component at the orbit which is either inward or outward around the full azimuth can result from a phase shift caused by an asymmetry between top and bottom poles. Another way of describing this situation is to say that it results in a median plane which is not at the geometric center of the gap. The orbit will locate itself at the magnetic median plane automatically, and a radial component at the orbit averaging 0.1 gauss is capable of shifting the orbit location vertically by 1.5 in.

Instruments had to be devised to measure the radial component of field at the orbit. The best results were obtained by using the zero-field

detector placed against the top and bottom poles and computing the radial component from the difference in the time of zero at the two locations.

7-10. VACUUM CHAMBER AND GAS SCATTERING

The toroid-shaped vacuum chamber enclosing the annular space between poles has undergone steady development. A glass-walled chamber was used for the first 2.3-Mev betatron, blown to a shape which fitted snugly between magnet poles and with tubulations on the outer rim for the pumping port and the injector assembly. The inside was coated with chemical silvering to shield the beam from electrostatic fields and prevent charges from building up on the walls. A resistance of the order of 100 ohms between test probes put in the side arms was used. The coating must be thin to prevent the development of excessive eddy currents which would distort the magnetic field.

The first 20-Mev chamber was assembled from flat glass washers and short glass cylinders cut from large-diameter tubing, waxed together in a rectangular cross section. Holes drilled in the outer cylinder were used for attaching the injector structure and the vacuum pump. A silver coating was applied on a sandblasted interior finish. Later developments for the GE 20-Mev chambers were of blown glass with a transparent conducting coating of tin chloride which made it possible to observe the internal components and the acceleration radiation at all azimuths. The glass chamber for the 100-Mev betatron in Schenectady, one of the largest glass doughnuts ever built, is impressive in its mechanical features and its careful design.

Other developments of betatron chambers have used ceramic materials, molded in sectors having the desired cross section and sealed end to end in place. This development has largely been the work of Almy and his associates at the University of Illinois; it is described in detail in laboratory reports. A good description of the 80-Mev chamber is published.[7] The six glazed porcelain sections have inner walls coated with Hanovia liquid bright palladium No. 62 for shielding. They are joined together by wrapping Scotch electrical tape around the joints and painting the overlap with Glyptal. Mica spacers are inserted at three of the joints; the acceleration voltage appears principally at these insulated joints. Resistors are connected between sections, and one section is left insulated to use for observing an injected beam pulse, found to be useful in tuning up the machine.

The vacuum chamber for the 300-Mev betatron is also made of molded porcelain sections, each of 20° extent. Groups of three are joined together by soldering to the metal coatings. The six 60° sections are manipulated into place in the pole gap, and final seals are made by the

atmospheric compression of neoprene gaskets. This tube, built for an orbit radius of 122 cm, has an approximately elliptical cross section with minimum inside dimensions of 4⅞ and 9⅛ in.

Scattering of electrons due to residual gas in the vacuum chamber has not proved to be a serious problem. Ordinary good vacuum techniques are capable of maintaining gas pressures of the order of 2×10^{-6} mm Hg, with the usual requirements that the container be clean and nonporous and that all leaks be stopped. The glazed porcelain chambers developed by Almy and his associates have proved to be quite satisfactory. Fast pumps, large-diameter pumping leads, and refrigerated traps or baffles to remove vapors are required if the chamber is to be continuously pumped. Sealed-off porcelain chambers of this type have been produced commercially for the 22-Mev betatrons, using standard vacuum-tube manufacturing techniques. The electron injector guns are permanently sealed into such chambers.

Gas scattering is a maximum at the start when electron energy is low, but it becomes less significant at high energies as the mean free path between collisions lengthens. Collision cross sections are known or computable, and the effect of gas scattering on beam intensity has been estimated.[31] This includes the fact that some electrons which are scattered through very small angles are refocused by the magnetic field and are not lost. Results of such calculations show that a significant loss of beam intensity due to gas scattering will be noticeable at pressures of the order of 2×10^{-5} mm Hg. Experimental observations of low-energy X rays produced by scattered electrons hitting the walls of the tube in the early part of the cycle are in agreement with the calculations.

7-11. INTERNAL TARGETS AND EMERGENT BEAMS

As the electrons approach maximum energy, their orbits can be expanded so they spiral outward and strike a target at the periphery. This can be done by pulsing a set of orbit expansion coils located above and below the orbit. This sudden rise in the rate of increase of central flux upsets the betatron balance so that equilibrium orbit radius increases. In principle the same coils can be used as were described for orbit contraction during injection; the method of operation is identical but reversed in sense. If desired, separate ejection coils can be installed to simplify switching and controls.

If the orbit expanding circuit is not used to eject the high-energy electron beam while the accelerator is in operation, electrons will follow the magnetic-field decrease and will be decelerated down to low energies again. In this case X radiation observed coming from the walls occurs mainly after the energy has been reduced to a few Mev, when oscillations have again built up to large amplitudes.

The rate of orbit expansion depends on the rise time of the voltage pulse. This is limited by the inductance of the orbit expander coils. Kerst has proposed a method using two sets of coils which reduces inductance to a minimum and increases the rate of expansion. In this scheme a one-turn coil at the orbit radius is in series with an oppositely wound two-turn coil at a larger radius, so chosen that the reluctance of the magnetic circuit linking the two-turn coil is double that of the one-turn at the orbit. This means that the net induced voltage across the two coils is zero. As a consequence of the difference in ampere-turns, the central flux change is equivalent to that for a single-turn coil. Yet the magnetic flux through the external field return circuit is zero. This has the effect of introducing a radial field gradient across the orbit region, essentially increasing n and causing the electrons to spiral out more rapidly.

The oscillations will have been damped to small amplitude by the time the electrons reach maximum energy. The cross section of the beam is estimated to be of the order of 1 to 2 mm^2. This narrow beam will be swept across the target by orbit expansion in a short time, producing a burst of X rays; X-ray pulses as short as 0.6 μsec have been observed. This is the equivalent of some 200 revolutions and indicates an orbit expansion rate of about 0.0002 in. per revolution. Only an extremely thin surface of the target is struck by the electrons. The target is usually the molybdenum or tungsten surface of the injector shield, which is the first obstacle that the electrons encounter.

The X rays have a strongly forward distribution, required by momentum conservation in the interaction which is almost entirely due to electron-electron impacts. The angle between half-intensity points has been measured as 9° for 20-Mev and 3° for 100-Mev electrons. The X rays have the continuous spectrum characteristic of bremsstrahlung or deceleration radiation, with a maximum energy equal to the energy of the electrons. They penetrate the porcelain tube wall with ease, but for some applications it is desirable to have a tangential spout with a thin window to transmit the X-ray beam in order to reduce scattering by the wall. A bremsstrahlung spectrum for 330-Mev electrons from a synchrotron is shown in Fig. 12-11.

A review of nuclear experiments with high-voltage X rays by Bosley and Craggs[32] describes experimental techniques, some experimental results on such processes as photofission, nuclear photoeffect, (γ,p) reactions, and a measurement of the X-ray spectrum from betatrons.

A beam of electrons can be extracted from the betatron by using a magnetic shield or "peeler" located at the outer edge of the chamber. The first adaptation to the Illinois 20-Mev betatron was reported by Skaggs, Almy, Kerst, and Lanzl[33] in a brief note; it has been improved and developed in later applications to other betatrons. The shield is a small laminated iron bar with a channel tangent to and facing the beam. As

the equilibrium orbit is expanded by the injection pulse, the beam enters the shielded channel, where magnetic field is reduced, and moves outward. Usually the peeler is located at a radius outside the $n = 1$ point. When the orbit has expanded into the region where the field falls off faster than $1/r$ ($n > 1$), the radial focusing disappears and orbits spiral outward. Electrons can enter the channel by this spiraling action after being forced out to this radius by the orbit expander.

Those electrons which traverse the peeler channel itself emerge as a well-defined beam. Those which first experience the effect of the weakened field caused by the peeler before reaching the radius of the channel are deflected less, so the beam is fanned out radially. Figure 7-17 is a sketch of such a peeler with electron orbits indicated to show the production of such an emergent beam, which can be brought out of the vacuum chamber through a thin-foil window.

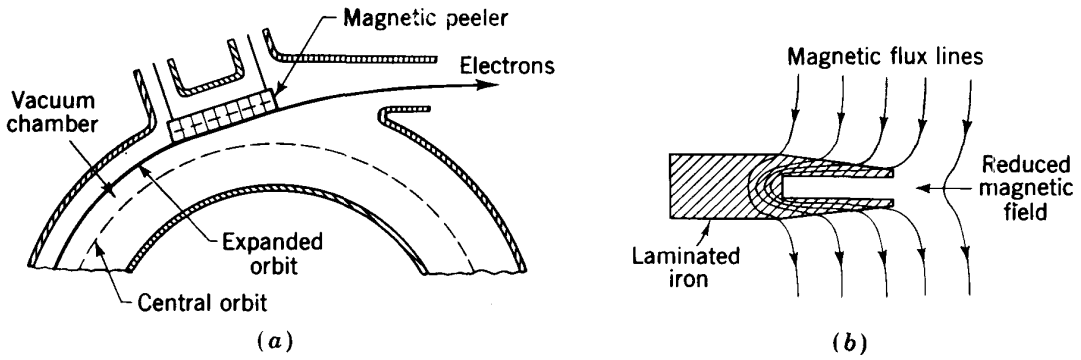

Fig. 7-17. (*a*) Location of magnetic peeler for removal of an electron beam. (*b*) Cross section of laminated iron peeler, with flux lines sketched to illustrate the magnetic shielding.

The emergent beam obtained at 20 Mev was observed to have a height of about 2 mm and a width of about 6 mm. In air outside the chamber it expands to a much larger cross section because of scattering; or it can be piped further in an evacuated spout if desired, in which case the beam remains fairly sharp. Time-average currents obtained have been of the order of 10^{-8} amp. They are emitted in pulses with a duration of less than 1 μsec, repeated 180 times per second, so the peak current during the pulse is of the order of 50 μa.

Another method of displacing the electron beam to make it available for ejection was proposed by Clark, Getting, and Thomas[34] of MIT as a mechanism for obtaining a short pulse on the target in a synchrotron. Wideröe[35] has adapted this to the betatron. The principle is that of generating radial oscillations of large amplitude by increasing magnetic field on one-half of the orbit and decreasing it on the other. If the n value is near 0.75, the frequency of radial oscillations is $0.5f_0$ and forced oscillations can be built up with maximum amplitudes at a fixed azimuth.

The method uses two coils, wound oppositely on symmetrical halves of the magnetic circuit for the orbit field, which are powered by pulsing from a resonant capacitor at ejection time. If the two coils are balanced, they have zero coupling with the main exciting coil and a correspondingly low inductance, so the resonant frequency of the pulse circuit can be high and the beam can be expanded entirely past the target in times of the order of 2 μsec. Calculations of oscillation amplitude build-up predict a displacement of 1.7 per cent of the radius in this time.

The ejection technique described above has been installed on the 300-Mev betatron and is used whenever pulses of microsecond duration are desired.

The resonant build-up of oscillations depends on a uniform value of n, of about 0.75. If electrons move out into a region where n approaches 1, the radial-oscillation frequency decreases toward zero and the orbits precess rapidly. This would result in the electrons "spilling out" around the full periphery. The amplitude build-up must proceed rapidly enough to take only a few turns if the unidirectional character of ejection is to be retained.

An alternative device for spilling electrons out in a fairly well-defined beam was proposed by Crittenden and Parkins;[36] it uses a distorted magnetic field over a short sector of the orbit. This technique could serve as an alternative method of getting the beam out to the location of a magnetic peeler. Kerst and Koch[37] have discussed the relative merits of the different methods of displacing the beam, and they conclude that the orbit expansion procedure is most satisfactory for betatrons.

Still another method of extracting an electron beam is based on scattering by a thin foil. If the foil is thin enough, the energy loss by ionization is small; an undeviated particle traverses an orbit of smaller radius but still within the focusing region of the field, so that it is reaccelerated and can traverse the foil a second and third time. Small-angle scattering induces oscillations, and these are damped to smaller amplitudes during reacceleration. In the process some electrons are scattered through rather large outward angles, sufficient to enter an electrostatic deflection channel as in the cyclotron, and are deflected as an emergent beam. Gund and Reich[38] have described experiments with such a scattering ejector using a 4.6-Mev betatron. They report extraction of up to 70 per cent of the circulating electrons in an emergent beam of narrow solid angle. However, this high efficiency could not be expected at higher energies. The scattering foil used was 0.015-in. aluminum for this beam energy, thin enough that 95 per cent of the electrons were scattered through an angle of less than 1.15°. The foil is made narrow vertically so that it does not interfere seriously with vertical particle oscillations as they are being reaccelerated. An electrostatic deflector follows the foil; it uses 30 kv across a 2-mm gap and deflects the beam out of the chamber

through a thin-foil window. Just outside the window the ionization was measured to be 3×10^5 r/min, an extremely high ionization density.

An instrument for measuring betatron magnetic fields during ejection has been described by Gregg.[39] It uses a cathode-ray-oscilloscope presentation of the field, on which the ejection pulse is observed. Such measurements are useful in designing peelers or electrostatic deflectors for an emergent beam.

7-12. MEDICAL AND INDUSTRIAL APPLICATIONS

Ever since X rays were first used for the treatment of cancer, there has been a demand for higher energy and deeper penetration. Early experiments in the 1- to 2-Mev energy range showed a much lower skin reaction than had been anticipated. This was found to be due to the fact that the X rays at the skin surface carried a smaller complement of secondary electrons than at a greater depth where X rays and secondaries were in equilibrium. This reduced skin dose and the deep penetration of high-energy X rays has made it possible to use a cross fire on a deep-seated tumor and to build up dosage at the tumor to successful levels without skin damage. With the first successful operation of the betatron, it was clear that higher energies could be obtained than from any previous X-ray sources, and development of the 20-Mev betatrons at the General Electric Company was greatly stimulated by the known application to medical problems.

The 20- to 22-Mev betatrons give a beam of X rays from an internal target with a yield of up to 100 r/min at 1 m in the forward direction, as measured by the accepted Victoreen thimble chamber. The beam is primarily forward, with an angle of 9° between half-maximum intensity points. Intensity in the backward direction is 0.1 per cent of the forward maximum, making shielding problems simple. Kerst and Skaggs[40] have published an excellent review of the use of betatrons for medical therapy. This paper describes the instrument and the properties of the radiations, as well as the biological and medical applications.

The opportunity of using a beam of electrons directly for therapy became possible at adequate energies with the emergent beams from the betatron. Skaggs, Almy, Kerst, and Lanzl[41] have discussed the problem of electron therapy and have described the application of betatron beams for this purpose.

The betatron has also proved itself a valuable tool in industrial radiography. The X-ray beam from a high-energy betatron can be used in showing the internal structure of steel sheets or mechanisms several inches thick. A particularly ingenious application of the betatron to radiography is due to Wideröe.[42] Working at the Brown-Boveri Company in Switzerland, he has developed a betatron in which beams are

accelerated in opposite directions on successive half-cycles of the magnetic field wave. Two injectors are necessary and two targets are located on opposite sides of the orbit but displaced slightly so the two X-ray beams converge toward each other. With this device it is possible to make stereo-radiographs; with a suitable viewer of the X-ray pictures the structure viewed stands out in an apparent three-dimensional display.

7-13. AIR-CORE BETATRON

Bierman[6 43] of the Philips Laboratory at Eindhoven, Holland, has perfected a small betatron (9 Mev) in which the iron in the yoke and return circuit is dispensed with. He claims the advantage of a much lighter machine (110 lb) and of simpler construction. The magnetic fields required are produced with properly dimensioned air coils. Much larger currents are required to obtain the same magnetic induction as with the use of iron, but the magnetic stored energy is not excessive for small sizes, and capacitors of reasonable cost can supply the high current for pulsed operation.

The field is produced by two coils, each having 25 turns of heavy high-tension cable, mounted in sturdy coil frames to resist the strong expansive forces between turns. The doughnut-shaped vacuum chamber fits between the coils and is of much larger relative cross section than chambers for iron-cored betatrons, allowing a larger amplitude for ion oscillations. The size and spacing of the coils produce a radially decreasing field with a value of $n = 0.5$ at the orbit. The central flux is brought up to that necessary for the betatron balance by the insertion of two laminated iron bars as a core, but with an air return circuit. The separation of the bars at the center can be adjusted to obtain the correct flux balance and to aid in shaping the field near the orbit. The bars are of such diameter that they saturate at the peak of the magnetic cycle, causing orbits to contract toward a target located at a smaller radius. Figure 7-18 shows the design of this air-core betatron.

The power supply is a high-potential rectifier charging a 6.5-μf capacitor to 50 kv. A spark-gap breakdown discharges the capacitor through the coils. The discharge is oscillatory with a frequency of about 2500 cps and is highly damped, so acceleration occurs in a decreasing sequence of pulses. The injection potential for the electron gun is obtained from a small coil linking the field of the large ones, in which maximum potential is induced at the start of acceleration when the magnetic field passes through zero. The peak pulse intensity from the machine is larger than from conventional betatrons. With a pulse repetition rate limited by heating of the coils and capacitors to one per second, the average output is low.

The designer's claims for simplicity and light weight are valid. This is

a much simpler and cheaper instrument than any iron-cored machine of the same electron energy. It would be ideal as a demonstration model for university lecture halls or for use in a research laboratory as a pulsed source for cloud chambers or other instruments utilizing high peak intensity. However, the pulsed operation results in a short duty cycle and

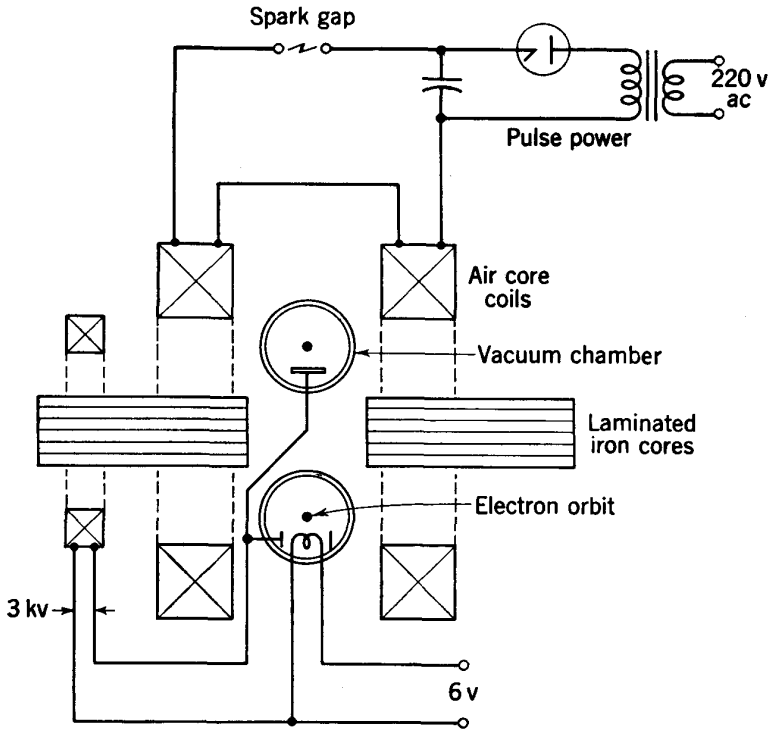

Fig. 7-18. Schematic diagram for an air-core betatron.[41]

low average intensities, so it is not so useful as a continuously operating betatron for medical therapy.

REFERENCES

1. D. W. Kerst, *Phys. Rev.*, **58**:841 (1940).
2. D. W. Kerst, *Phys. Rev.*, **60**:47 (1941).
3. D. W. Kerst and R. Serber, *Phys. Rev.*, **60**:53 (1941).
4. D. W. Kerst, *Rev. Sci. Instr.*, **13**:387 (1942).
5. W. F. Westendorp and E. E. Charlton, *J. Appl. Phys.*, **16**:581 (1945).
6. A. Bierman, *Nature*, **163**:649 (1949).
7. D. W. Kerst, G. D. Adams, H. W. Koch, and C. S. Robinson, *Rev. Sci. Instr.*, **21**:462 (1950).
8. D. W. Kerst, G. D. Adams, H. W. Koch, and C. S. Robinson, *Phys. Rev.*, **78**:297 (1950).
9. D. W. Kerst, *Nature*, **157**:90 (1946).
10. G. Breit and M. A. Tuve, *Carnegie Inst. Year Book*, **27**:209 (1927–1928).
11. R. Wideröe, *Arch. Electrotech.*, **21**:400 (1928).

12. E. T. S. Walton, *Proc. Cambridge Phil. Soc.*, **25**:569 (1929).
13. W. W. Jassinsky, *Arch. Electrotech.*, **30**:500 (1936).
14. M. Steenbeck, *Z. Physik* (February, 1943).
15. D. W. Kerst, *Phys. Rev.*, **68**:233 (1945).
16. W. F. Westendorp, *J. Appl. Phys.*, **16**:657 (1945).
17. E. Amaldi and B. Ferretti, *Rev. Sci. Instr.*, **17**:389 (1946).
18. *Life*, Mar. 20, 1950, pp. 129–132.
19. D. Iwanenko and I. Pomeranchuk, *Phys. Rev.*, **65**:343 (1944).
20. J. P. Blewett, *Phys. Rev.*, **69**:87 (1946).
21. J. Schwinger, *Phys. Rev.*, **75**:1912 (1949).
22. D. W. Kerst, *Phys. Rev.*, **74**:503 (1948).
23. F. F. Heyman, *Phys. Rev.*, **75**:1951 (1949).
24. G. D. Adams, *Rev. Sci. Instr.*, **19**:607 (1948).
25. L. Bess and A. O. Hanson, *Rev. Sci. Instr.*, **19**:108 (1948).
26. G. D. Adams, D. W. Kerst, and D. T. Scag, *Rev. Sci. Instr.*, **18**:799 (1947).
27. E. Schwartz, *Z. Naturforsch.*, **4a**:198 (1949).
28. A. F. Clark, *Phys. Rev.*, **70**:444 (1946).
29. G. D. Adams, R. W. Dressel, and F. E. Towsley, *Rev. Sci. Instr.*, **21**:69 (1950).
30. W. B. Lasich, E. G. Muirhead, and I. F. Wright, *J. Sci. Instr. Phys. Ind.*, **26**:91 (1949).
31. J. M. Greenberg and T. H. Berlin, *Phys. Rev.*, **74**:1243 (1948).
32. W. Bosley and J. D. Craggs, *Repts. Progr. in Phys.*, **12**:82 (1948–1949).
33. L. S. Skaggs, G. M. Almy, D. W. Kerst, and L. H. Lanzl, *Phys. Rev.*, **70**:95 (1946).
34. J. S. Clark, I. A. Getting, and J. E. Thomas, Jr., *Phys. Rev.*, **70**:562 (1946).
35. R. Wideröe, *Rev. Sci. Instr.*, **19**:401 (1948).
36. E. C. Crittenden and W. E. Parkins, *J. Appl. Phys.*, **17**:444 (1946).
37. E. W. Kerst and H. W. Koch, *Rev. Sci. Instr.*, **18**:681 (1947).
38. K. Gund and H. Reich, *Z. Phys.*, **126**:383 (1949).
39. E. C. Gregg, Jr., *Rev. Sci. Instr.*, **20**:841 (1949).
40. D. W. Kerst and L. S. Skaggs in O. Glasser (ed.), "Medical Physics," vol. 2, p. 11, Year Book Publishers (1950).
41. L. S. Skaggs, G. M. Almy, D. W. Kerst, and L. H. Lanzl, *Radiology*, **50**:167 (1948).
42. R. Wideröe, *Stahl u. Eisen*, **73**:706 (1953).
43. A. Bierman and H. A. Ĉele, *Philips Tech. Rev.*, **11**:65 (1949).

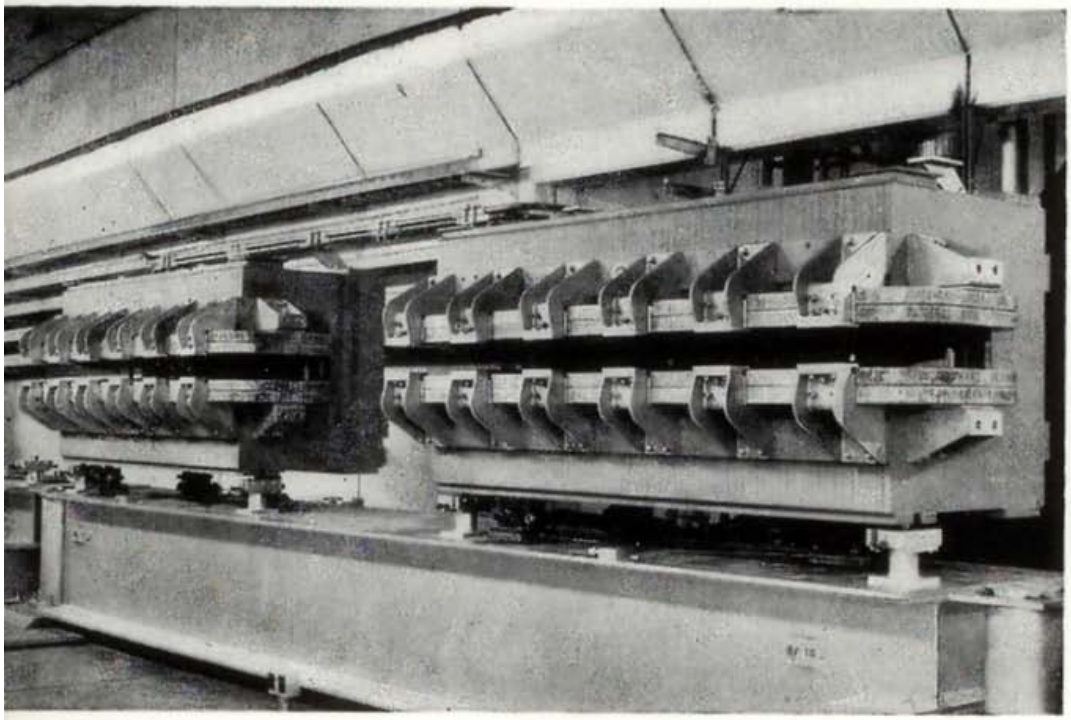

8

Magnet Design and Measurement

The design of iron-cored magnets calls upon the resources of the physicist, the electrical engineer, and the mechanical engineer. The fundamental principles of magnet design were established by the physicists of the nineteenth century. These principles then found application in the apparatus of electrical engineering—transformers, motors, generators, and other electrical machinery. With the development of the accelerator art, new requirements were set up which went beyond normal engineering practice; higher precision was needed in structures involving magnetic forces far beyond those usually experienced. New physical methods were evolved and new electrical and mechanical techniques were developed to meet these requirements. These procedures, in turn, have stimulated the engineering profession to make improvements in the industrial applications of electromagnets.

Theoretical knowledge of magnet design is precise in principle but has been considered inadequate in application to design problems. Until quite recently magnet designers have solved their problems by very approximate theoretical procedures and by cut-and-try magnet modeling. Although these methods are powerful and are still in vogue, a change in approach is now in process. The difficulties of the past have been introduced by the nonlinear characteristics of iron, whose permeability is a strong function of flux density; because of this, design of magnetic circuits is extremely complicated, and it has been easier to make the final steps using models which served, so to speak, as analogue computers. With

the advent of the modern electronic computer these problems are becoming soluble in reasonable times, and in 1961 the time appears not far off when a complete magnet design can be done rapidly without recourse to the laboratory.

At present, methods for formulation of the problems are at hand; procedures for solution of the problems using computers are in the process of evolution. Some of the methods have been tested by hand computation with completely satisfactory results. For example, the shape of the magnet for the Brookhaven AG synchrotron was deduced theoretically by methods to be discussed below. The final magnets were found to agree completely with the theoretical predictions.

In this chapter the physical principles of magnet design will be presented. Classical design techniques will be discussed, and new developments will be mentioned where they appear to be adequately established. Detailed design problems relating to individual accelerators will be reserved for discussion in the separate chapters on those machines.

The instruments and techniques employed in magnetic measurement will also be described. Different methods are used in studying the various properties of the magnetic field, and techniques differ according to whether the field is to be steady or time-varying; the two categories will receive separate treatment.

Although air-cored coils have found many applications in the accelerator field—Helmholtz coils, for example, are generally used in search-coil calibration—they will not be discussed here since methods necessary for their design and construction are fully covered in standard works on electricity and magnetism.

8-1. SPECIAL REQUIREMENTS FOR ACCELERATOR MAGNETS

Accelerator magnets depart from engineering experience primarily in the need for precise shaping of the fields in the air gap, which sets rigorous requirements on pole-face shape. This feature has been of less concern in engineering applications, where the detailed shape of the field is seldom important and gaps in the iron circuit are deliberately minimized. The accelerator scientist has had to design new types of precise instruments for measuring fields in order to determine the special shapes needed for the poles. In return the engineering field has supplied machine practice of the highest order to produce the necessary contours and has also provided magnetic materials of improved quality which have been of great value in accelerator magnets.

The desire for engineering perfection and electrical economy of the magnetic circuit is limited by other factors in the design of accelerator magnets. In general, the advantages of simple structures and precision

---

At the head of the facing page is an illustration of magnets for the Brookhaven AG synchrotron.

in manufacture, as well as the need for space around the poles to provide access to the vacuum chamber and other components, outweigh the importance of compact shapes or perfection in magnetic design. The exact field shape required to control particle orbits cannot always be determined in advance, so magnets are frequently equipped with removable pole faces or provided with arrangements for installation of shims or corrective windings during experimental manipulations. In other cases the uncertainties in planning research experiments justify considerable flexibility in the physical arrangements; magnets are needed which can be dismounted and reassembled by a laboratory crew. Most magnets represent compromises with such other requirements.

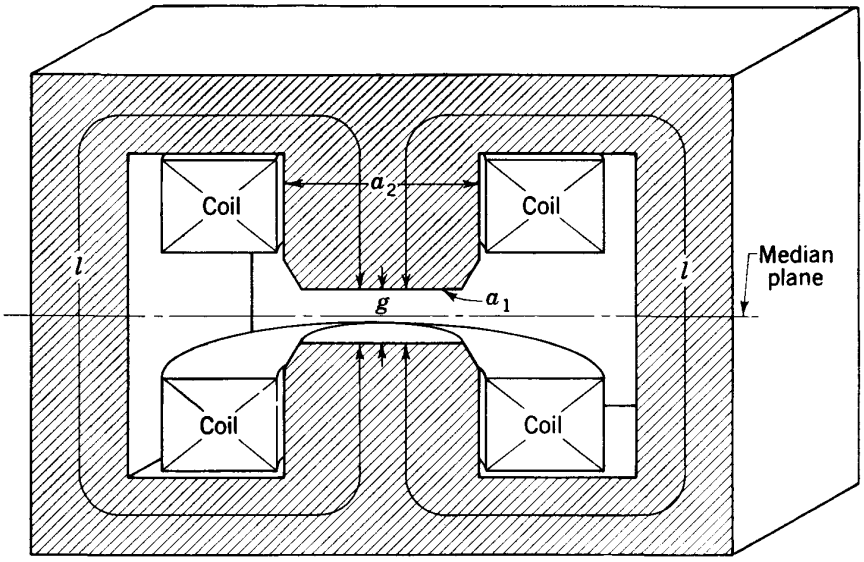

Fig. 8-1. Cross section of magnetic circuit for steady-field magnets used for cyclotrons.

Two basic magnet shapes cover most accelerator applications. First is the cylindrical-pole magnet used for cyclotrons to produce an approximately uniform field of high flux density across a cylindrical volume of large area. The field in a cyclotron magnet is constant in time. The magnetic circuit is assembled in large blocks, formed of solid iron forgings, castings, or plate. Pole faces are nearly flat and parallel, and gap spacing is small compared with the pole diameter. The excitation coils are formed in two units which are equally spaced about the magnetic median plane, to preserve symmetry about this plane. The coils are wound in layers with many turns of solid (or hollow) conductors and are arranged for oil or water cooling. Figure 8-1 is an illustration of a typical dc magnet for a cyclotron.

Ring-shaped magnets are used to accelerate particles in orbits of approximately constant radius, as in the betatron and the several types of synchrotron. A doughnut-shaped vacuum chamber fits in the gap between pole faces, which are not quite parallel but slightly tilted to pro-

duce a field which decreases with increasing radius for focusing. Since the particles must stay in orbits of nearly constant radius, the magnetic field must increase in magnitude during acceleration. The magnet is excited cyclically from low to high fields, either pulsed unidirectionally or powered by alternating current. The iron must be laminated, as in a transformer, to minimize eddy-current losses, and the material must have low magnetic hysteresis losses. The magnetic circuit is formed of blocks of iron laminations, which require clamping structures or resin-bonding procedures. Again, excitation coils are formed in two units, above and below the magnetic gap. They must have a small number of turns (of large cross section) to keep the applied voltage within reasonable limits

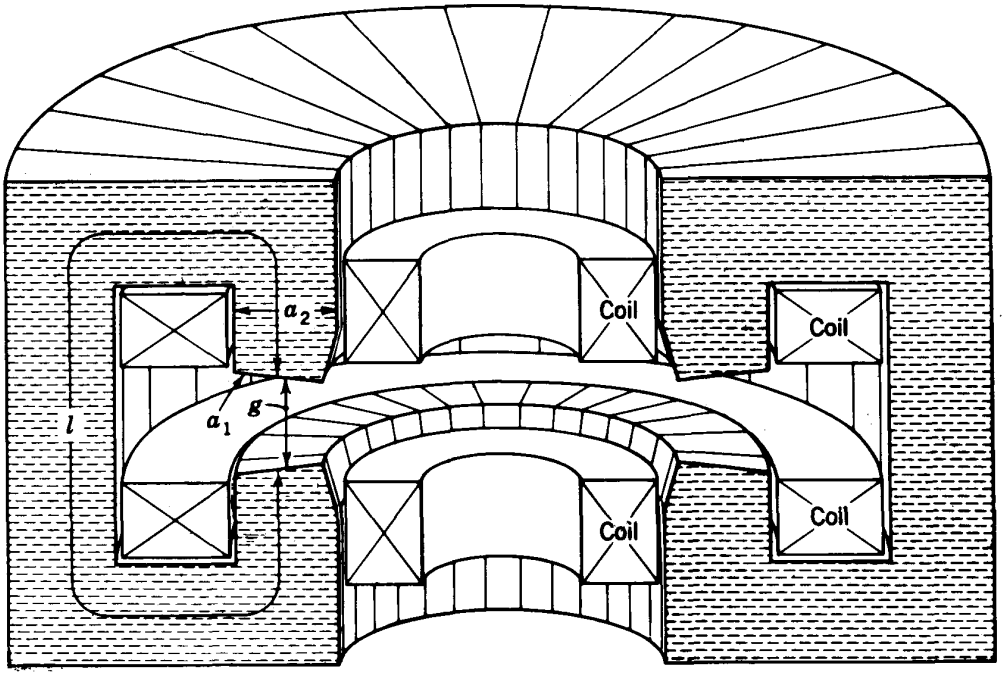

Fig. 8-2. Cross section of the C-type ring magnet with external return circuit used for some electron synchrotrons.

and are often formed of stranded cable to reduce eddy currents in the conductors. The cross section of such a ring magnet, which is typical of those used for electron synchrotrons, is illustrated in Fig. 8-2.

The magnet shown in Fig. 8-2 has the iron return circuit located outside the orbit. This is called a C magnet and has the advantage that one side of the magnet gap is readily available for installation and maintenance of the vacuum chamber. With larger orbits the return leg can be located inside the orbit, as in the Brookhaven cosmotron (a proton synchrotron), which simplifies the injection or ejection of particle beams. Still other ring magnets, such as the Berkeley bevatron, have return legs both inside and outside the orbit; these are known as H magnets. Such a magnet is usually formed in quadrants or octants with open field-free straight runs

between sectors to provide access for pumping ports, power systems, and beam ejection.

One significant difference between dc and ac magnets is in the quality of iron and the maximum flux densities possible. The soft iron used for dc magnets has a much higher permeability than the silicon steel with low hysteresis loss used for laminations in ac magnets. This, with the looser packing of a laminated structure, makes maximum fields lower in ac magnets. Few betatron or electron synchrotron magnets exceed 14 kilogauss flux density, but most modern cyclotron magnets are designed for over 18 kilogauss. Other differences have to do with the effect on the shape of the magnetic field of eddy currents in the iron under ac or pulsed operation; detailed measurements of the dynamic properties of the field are required, particularly at low flux densities.

Another category of magnets used in accelerator laboratories includes the auxiliaries employed for beam focusing and analysis. With the larger accelerators these auxiliaries are so large and heavy as to be equivalent to cyclotron magnets, and they deserve detailed study and design. They are normally excited with dc power for steady fields and are formed of blocks of soft iron as for cyclotron magnets. The most common pole-face shape is rectangular, to provide a linear extent of magnetic field. Frequently the pole faces are wedge-shaped or tilted to provide a gradient field for focusing. An example is a magnet to deflect and analyze particle beams of 1 Bev energy, which might have pole faces of 12 in. width and 4 ft length which are spaced to form a 6-in. gap. The magnetic circuit in such a unit would be formed of rectangular iron blocks machined from forgings, with a few bolts to hold the assembly. A common shape is the H-type frame with dual magnetic return legs for which a cross section would look much like that shown in Fig. 8-1. The excitation coils would be rectangular in cross section and rectangular in plan, arranged to fit closely around the poles. Usually the poles are fitted with pole-face plates which can be removed and replaced to obtain different gap lengths, modify the taper, or change the shape for focusing.

8-2. THE MAGNETIC CIRCUIT

All the magnet types described in the preceding section serve a single purpose, that of producing a high-flux-density field between nearly flat and parallel poles. The useful region is the approximately uniform field between the pole faces; the flux outside the poles is generally of no value and is called the leakage flux or fringing flux. For this type of magnetic circuit a primary consideration in design is to make the useful flux as large a fraction of the total as practical and to reduce the energy stored in the fringing flux. Since the iron return circuit must carry the total flux, it must be larger in cross section as the fringing increases.

The two magnetic circuits illustrated in Figs. 8-1 and 8-2 will serve to illustrate our analysis. Each circuit can be considered as an air gap of length g and area a_1 and an iron return path of length l and area a_2 (divided in two legs each of area $\frac{1}{2}a_2$ for the H-type circuit). For present purposes the flux density can be assumed constant throughout the circuit, obtained by suitable tapering and shaping of the iron return circuit. The excitation coils fit closely around the poles and are arranged in two identical units, so the magnet is symmetrical about the median plane through the air gap.

The first relation describing the properties of a closed magnetic circuit is the fourth Maxwell equation (5-1), in which the time variation has been set equal to zero. It can be expressed in the integral form as

$$\oint \left(\frac{\mathbf{B}}{\mu}\right) \cdot d\mathbf{l} = \iint I \, da \tag{8-1}$$

where the line integral is around a closed loop and the surface integral is bounded by the loop. The right-hand side of Eq. (8-1) thus represents the total number of ampere-turns linked by the loop of integration.

The second relation of importance in analyzing magnetic circuits follows from the second Maxwell equation (5-1). Since div $\mathbf{B} = 0$, Gauss' theorem yields the relation

$$\iint B_n \, da = 0 \tag{8-2}$$

where B_n is the component of B normal to the surface of integration. From this equation it follows that the total magnetic flux crossing any plane through the magnetic circuit is constant. For most purposes we shall be able to assume that the magnetic flux density across any plane throughout the circuit is reasonably uniform; hence the total flux $\Phi = Ba$ (where a is the area of cross section of the circuit) will be a constant.

Where the magnetic circuit consists of an iron path of length l and an air gap of length g (as in the circuits shown in Figs. 8-1 and 8-2), the simplified forms of Eqs. (8-1) and (8-2) lead to the relation

$$\Phi = Ba = \frac{Ni}{g/(\mu_0 a_1) + l/(\mu a_2)} \tag{8-3}$$

where Ni = number of ampere-turns in exciting windings
a_1 = area of magnet pole face
a_2 = cross-sectional area of iron magnetic return circuit

Equation (8-3) is extremely useful in making the first approximation to a magnet design since, for a prescribed field and air-gap geometry, it gives the number of ampere-turns necessary for magnet excitation and indicates the effect to be expected at high fields when iron permeability begins to decrease. This equation also suggests the traditional analogy between

magnetic and electric circuits. If an electric circuit includes two resistors having resistances $g/(\mu_0 a_1)$ and $l/(\mu a_2)$, if the emf in the circuit is Ni, and if the current in the circuit is Φ, then Ohm's law for the circuit has exactly the form of Eq. (8-3). For this reason, Ni is called the "magnetomotive force" of the circuit, and the quantities $g/(\mu_0 a_1)$ and $l/(\mu a_2)$ are called the "reluctances" of the air gap and the iron circuit, respectively. In these terms Eq. (8-3) is equivalent to

$$\text{Flux} = \frac{\text{magnetomotive force}}{\text{total reluctance}} \qquad (8\text{-}4)$$

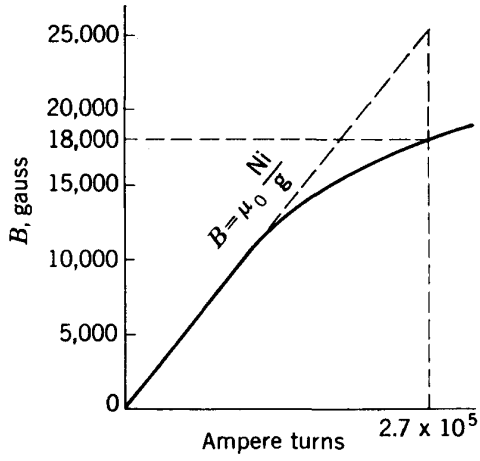

Fig. 8-3. Flux density in the gap versus excitation for the MIT cyclotron magnet.

For soft iron at flux densities up to about 10 kilogauss the permeability μ is more than 1000 times greater than that for air or vacuum μ_0, and the reluctance of the iron portion of the circuit can be neglected. If so, the flux density in the air gap is a linear function of current. Figure 8-3 is a plot of B versus i for a typical cyclotron magnet (MIT), showing the linear portion of the curve extending up to a field of about 10 kilogauss in the gap. In this region of excitation the flux density is given quite accurately by

$$B = \frac{\mu_0 Ni}{g} \qquad \text{webers/m}^2 \qquad (8\text{-}5)$$

where $\mu_0 = 4\pi \times 10^{-7}$
Ni = ampere-turns
g = air gap in meters

To produce a field B of 1 weber/m^2 (10 kilogauss) in a gap of 10 cm length, the number of ampere-turns required is 7.95×10^4; with a 1000-turn coil the current would be 79.5 amp.

The permeability of iron varies with flux density, rising rapidly to a maximum value at low fields and falling off at high fields. Figure 8-4*a* is a plot of magnetic flux density B against magnetic field H (in amperes per meter). In this plot we show curves for a typical silicon steel used in transformers and for a low-carbon steel of the type used in dc magnets. For explanations of the form of the characteristic hysteresis loop shown here the reader is referred to standard texts on electricity and magnetism. In Fig. 8-4*b* the permeability μ is plotted against flux density B for the same two steels. Although the silicon-steel permeability rises rapidly to much higher values than those for the soft iron, the latter displays higher permeability at the high fields used in cyclotron magnets.

At high flux densities the linear relation of Eq. (8-5) must be replaced by the more complete Eq. (8-3), because of the increasing reluctance of the iron. This is observable in Fig. 8-3, where the plot of observed field falls below the straight line extrapolated from low-field values. The point where this deviation starts and the magnitude of the deviation are

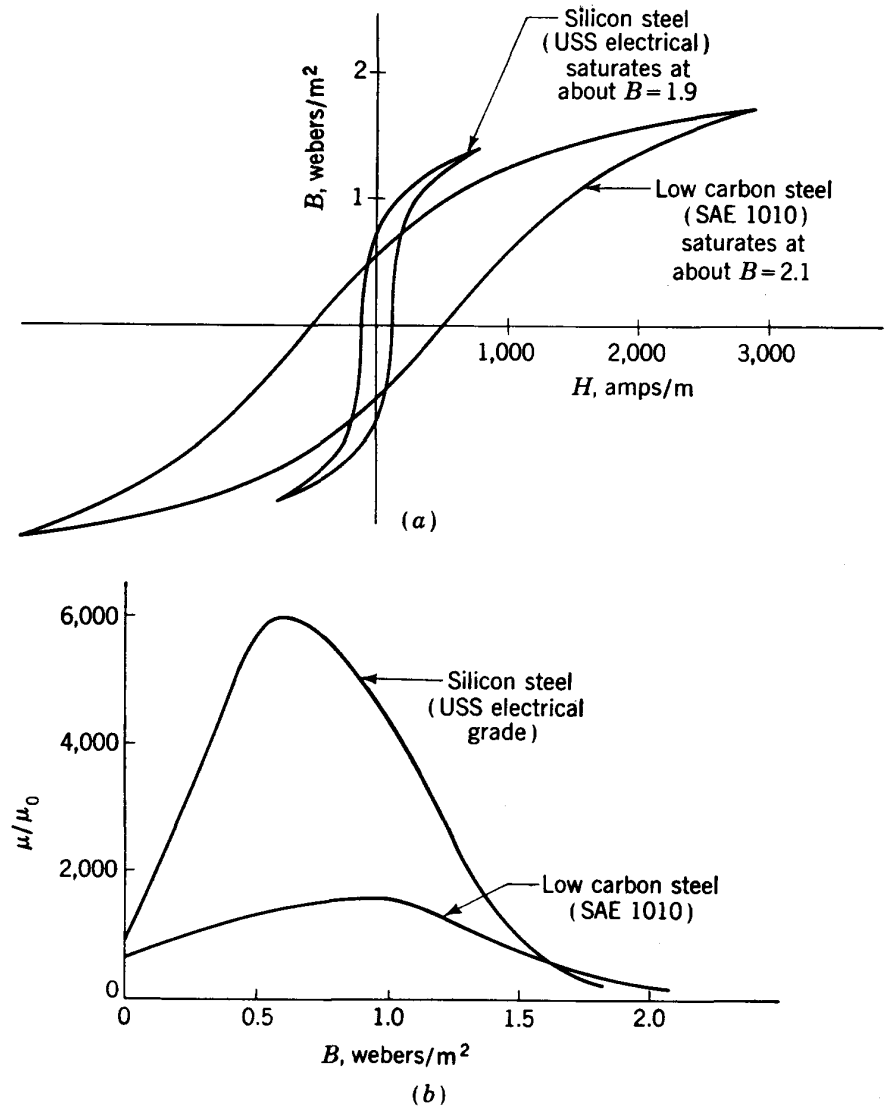

Fig. 8-4. Magnetic properties of soft low-carbon steel and silicon steel: (*a*) B versus H; (*b*) μ versus B.

affected by other features of the design. As iron permeability decreases, the pattern of fringing flux changes, with a larger fraction of flux being forced outside the geometrical boundaries of the poles. The degree of tapering of the poles depends on the chosen flux density and is characterized by the ratio of areas a_2/a_1. The shape of the tapering contour near the pole tip is the most important factor in determining the flux pattern in this fringing region; the sharp corner at the pole boundary is usually

the first portion of the iron to become saturated. The leakage flux pattern is also affected by the location of the exciting windings. In a qualitative sense the exciting coils tend to "compress" the leakage flux between them, so the total leakage flux is a minimum when the coils are closest to the air gap. In the iron circuit the "base" of the poles away from the air gap is the location of maximum total flux, and since it is limited in cross section by the coil dimensions, it is usually a region of high flux density and saturates before the rest of the iron circuit.

As a consequence of this complex situation at high flux densities, no simple relation is valid for computing excitation requirements. However, useful design estimates can be obtained from observations with circuits similar to the one being considered. A great deal of empirical information is available as the result of experience with a wide variety of magnetic-circuit shapes and for different magnetic materials. For example, consider a circuit similar to that shown in Fig. 8-1, for which an excitation curve like that in Fig. 8-3 is typical. Excitation requirements can be represented by the empirical relation

$$B = \frac{KNi\mu_0}{g} \tag{8-6}$$

where K is an "efficiency" factor which decreases with increasing excitation. At 18 kilogauss, for example, the observed value of B is 0.73 of that predicted by the straight-line extrapolation of the air-gap relation of Eq. (8-5), so $K = 0.73$. In a circuit under design which is reasonably similar to the shape and arrangement of the circuit just discussed, a judicious guess of the factor K will usually be sufficient to obtain adequate preliminary design estimates of the excitation requirements.

The dimension of pole-face diameter or width must be determined at an early stage of design, to provide the desired area of uniform field. Since fringing flux extends outside the pole boundaries, the flux just inside the boundaries is weakened and the region of uniform field is reduced. Experience shows that the edge of the usable region is inside the pole boundaries by about one-half the gap length. For example, with the MIT cyclotron magnet the region useful for acceleration (see Chap. 7), which is roughly defined as a point where the field is reduced to about 0.98 that of the central field, was observed with and without any special shaping of the pole face. Without shims the useful region was inside the pole edge by $0.6g$; with the chosen ring-shaped shims it was inside by $0.45g$. It should be noted that this boundary of useful field is closer to the pole boundary at low fields and is forced inward at higher fields, because of saturation of the outer corners of the pole tips.

Another general design problem is the degree of tapering of the poles and the optimum shape of tapering. The leakage flux enters or leaves the poles on the sides and at the tapered sections and adds to the total

flux in the return circuit. A simple explanation of the need for tapering the poles is that the return circuit should, at each transverse section, have sufficient area to carry the total flux (including the leakage flux) without exceeding the saturation limit of the iron at any point. The area ratio a_2/a_1 can be determined if the fringing-flux distribution is known, from which an estimate can be made of the total fringing flux. The graphical technique of flux plotting, described in a following section, provides a useful method of obtaining an approximate flux plot. However, the flux pattern depends on the degree of excitation as well as on the shape of the magnetic circuit and the location of the coils. So, for excitations approaching the limit of saturation in the iron or exceeding the flux density used in earlier experience, it is usually necessary to measure the field pattern directly with scaled models employing the same quality of iron.

The shape of the taper can be estimated theoretically for low flux densities where simplifying assumptions are allowable, such as the assumption that the iron surfaces are magnetic equipotentials or that the iron has infinite permeability. An analysis developed by Bethe was used to design the tapering for the Purdue University cyclotron magnet, reported by Howe and Walerstein.[1] The criterion applied in determining the shape of taper was to secure the highest value of BR (a measure of particle momentum) between flat poles, for a given central field. The results were given in terms of the radius of pole, $r = r(z)$, at a distance z from the median plane:

$$r^2(z) = r_0^2 \left[1 + \left(\frac{2}{\pi}\frac{g}{r}\right) \ln\left(\frac{2z}{g}\right)\right] \Big/ \left[1 - \left(\frac{2}{\pi}\frac{g}{r}\right) \ln\left(\frac{2z_0}{g}\right)\right] \tag{8-7}$$

Here r_0 is the pole-base radius at a distance z_0 from the median plane, and g is the gap width. The values of BR in the gap are also given:

$$BR = B_i r_0 \Big/ \left[1 + \left(\frac{2g}{\pi r}\right) \ln\left(\frac{2z_0}{g}\right)\right]^{1/2} \tag{8-8}$$

where B_i is the chosen maximum flux density in the iron pole (at its base). The tapering profile of the magnet pole resulting from this calculation is shown in Fig. 8-5, along with the relative shapes and spacings of the lines of flux in the fringing field.

Another criterion for shape of taper was used in the scaled-model studies at the Carnegie Institute of Technology.[2] This was essentially to obtain the highest value of uniform field in the gap for a given magnitude of excitation in ampere-turns. The result is shown in Fig. 8-6. We note that the shape of the taper is convex in the Purdue design and concave in the Carnegie design.

This difference illustrates one of the problems in magnet design, which is the determination of the essential criteria on which decisions are to be

based. There is no unique answer. Individual designers attach importance to different properties of the field, based on the evaluation of other aspects of the accelerator as a system. For example, the Carnegie design gives the sharpest fall-off of field in the fringing region, which simplifies beam deflection and in principle would provide a more concentrated

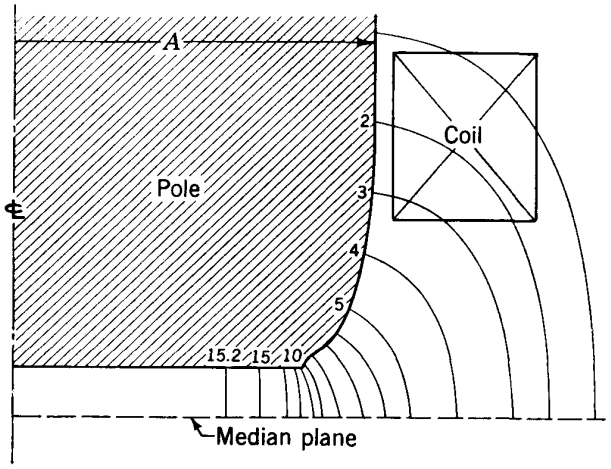

Fig. 8-5. Tapering profile of the Purdue University cyclotron magnet pole, showing the fringing-flux pattern.

emergent beam. The Purdue design, on the other hand, is less affected by saturation at the pole edges and allows shimming to obtain the maximum orbit radius and so the highest energy of internal resonant beam.

During past years the trend in design has been toward higher fields, using better-quality magnetic materials and more electric power. In this

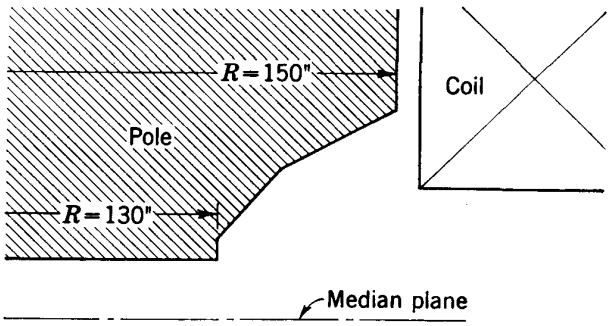

Fig. 8-6. Pole taper for the Carnegie Institute of Technology synchrocyclotron magnet[2] which resulted in the best excitation efficiency.

development the simple magnet-circuit shapes of the early accelerators have evolved into more compact structures which are more efficient at higher flux densities. Improved techniques have been found for coil cooling, allowing for more efficient coil designs. To illustrate this change in structural shape, Fig. 8-7 shows schematic representations of three

typical magnetic circuits, all of the H-type frame; for comparison the three magnets are scaled to the same pole-face diameter and gap length. One shape is representative of early low-energy cyclotron magnets using cylindrical poles for which the maximum field would be about 12 kilogauss. The second is typical of high-flux synchrocyclotrons, with tapered poles and large-diameter coils, which might operate at 18 kilogauss. The third is an example of a "poleless" circuit in which the excitation coils are fitted closely around the gap, and which can produce uniform fields

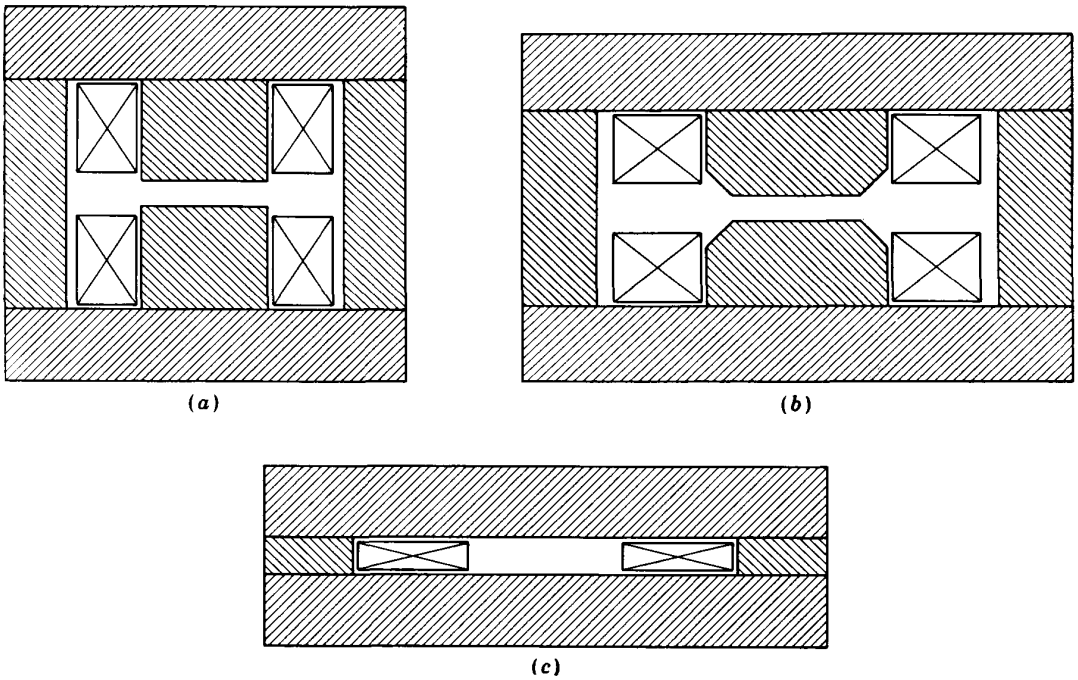

Fig. 8-7. Trend of steady-field magnet design: (*a*) early cyclotron magnet, B_m = 12,000 gauss; (*b*) synchrocyclotron magnet, B_m = 18,000 gauss; (c) poleless magnet, B_m = 22,000 gauss.

of between 20 and 22 kilogauss; this very compact circuit is being used in some modern synchrotrons and for high-flux analyzing magnets.

8-3. FIELD MAPPING AND FLUX PLOTTING

In the design and use of electromagnets it is frequently desirable to obtain a map of the magnetic field in part or all of the air gap, around corners of the pole or, perhaps, in and around the exciting coils. This map can be used to indicate the onset of local saturation, to show necessary changes in pole contour, or to evaluate forces on poles or conductors. The desired maps are almost always two-dimensional because symmetry in the structure makes the third dimension unnecessary.

The field properties used in field mapping follow from Maxwell's equations div $\mathbf{B} = 0$ and curl $\mathbf{B} = \mu\mathbf{I}$. If I is zero, these equations indicate

that B can be derived from a potential function u defined in two dimensions by

$$B_x = -\frac{\partial u}{\partial x} \qquad B_y = -\frac{\partial u}{\partial y} \tag{8-9}$$

Since div $\mathbf{B} = 0$, it follows that $\nabla^2 u = 0$. Whether or not I is zero, B can also be derived from another potential function A defined by

$$B_x = \frac{\partial A}{\partial y} \qquad B_y = -\frac{\partial A}{\partial x} \tag{8-10}$$

Since curl $\mathbf{B} = \mu\mathbf{I}$, it follows that $\nabla^2 A = \mu I$. This A is the z component of the vector potential which, in a three-dimensional problem, would also have x and y components.

Lines of constant A are defined as "lines of force," while lines of constant u are known as "equipotentials." In a field where I is zero, both equipotentials and lines of force can be drawn. The equation of a line of force is obtained by writing

$$dA = \frac{\partial A}{\partial x}\,dx + \frac{\partial A}{\partial y}\,dy = 0$$

whence

$$\frac{dy}{dx} = -\frac{\partial A}{\partial x} \Big/ \frac{\partial A}{\partial y} = \frac{B_y}{B_x} \tag{8-11}$$

Similarly the equation of an equipotential is

$$\frac{dy}{dx} = -\frac{B_x}{B_y} \tag{8-12}$$

Since

$$\left(\frac{dy}{dx}\right)_{A=\text{const}} \left(\frac{dy}{dx}\right)_{u=\text{const}} = -1 \tag{8-13}$$

it follows that the line of force through a given point is always normal to the equipotential through that point.

The "Electrolytic Tank" Method

The equations for lines of force and equipotentials in an electric field are exactly analogous to those in a current-free magnetic field. Accordingly, experimental methods used for mapping electric fields between conductors can be adapted to the magnetic-field problem. Iron surfaces in the magnetic field will be equipotentials for flux densities below the saturation limit and so can be modeled by metallic electrodes shaped like the poles. Electric potential differences between these electrodes and points in the electric field simulate the corresponding magnetic potential differences. Several methods have been used for exploiting this analogy.

The best-known electrical analogue is the electrolytic tank—usually a flat tank of glass or other insulating material filled with a shallow layer of a slightly conducting liquid such as a weak solution of copper sulfate. The magnetic poles and the iron return circuit are simulated by shaped metallic electrodes, and between them a dc or audiofrequency ac potential difference is maintained. A probe is used to determine the local potential, usually a short piece of Ni or Pt wire of small diameter. The probe potential is set by connecting it to a potentiometer whose fixed terminals are connected to the electrodes in the tank. The probe is then moved in the electrolyte until a detector (a galvanometer for dc signals, or earphones for ac signals) indicates a null. The position of the probe is read from a cross-section plot underlying the electrolyte and can be transcribed or transmitted by a pantograph to an external plot. Usually 10 or more equally spaced equipotentials are plotted; intermediate equipotentials are included in regions where the field is highly divergent.

The lines of force are now sketched in normal to the equipotentials. It is customary in drawing plots of lines of force to make the density of lines proportional to the field strength; thus the space between adjacent pairs of lines of force will include a constant quantity of flux. Since the separation of the equipotentials is also a measure of the field strength, this means that the ratio $\frac{\text{separation of adjacent lines of force}}{\text{separation of adjacent equipotentials}}$ must be kept constant for all the little rectangles enclosed by lines of force and equipotentials.

An example of contour maps obtainable by this technique is the map of flux density in the fringing field, which can be used to determine the flux entering the sides of a tapered pole (see Fig. 8-5). Another useful plot gives the flux density on the median plane as a function of radial position similar to that shown in Fig. 6-8 for the MIT cyclotron.

Other methods for utilizing the electrical analogy involve the use of "conducting paper," a paper sheet coated with a uniform layer of high-resistance material. Sheets of metal of high resistivity have also been used. In both cases the technique is the same as that already described; the conducting material merely replaces the sheet of electrolyte in the electrolytic tank.

The electrical analogy suffers from several faults. The surface of a magnet pole is a true equipotential only if the permeability of the iron is effectively infinite. At high flux densities, as local saturation occurs, the equipotential no longer coincides with the iron surface and the electrical analogy gives erroneous answers. Another difficulty lies in the breakdown of the analogy when current-bearing coils lie in the region of interest. Other electrical analogues have been developed for this case, but their application is limited and they are in the process of being super-

seded by the more sophisticated numerical techniques to be described later.

Conformal Mapping

Freehand flux plotting as a technique for magnet design has been highly developed by the engineering profession and is described fully in several engineering texts.[3,4] This has become an art and requires considerable practice for proficiency. It can give results correct to about 10 per cent,

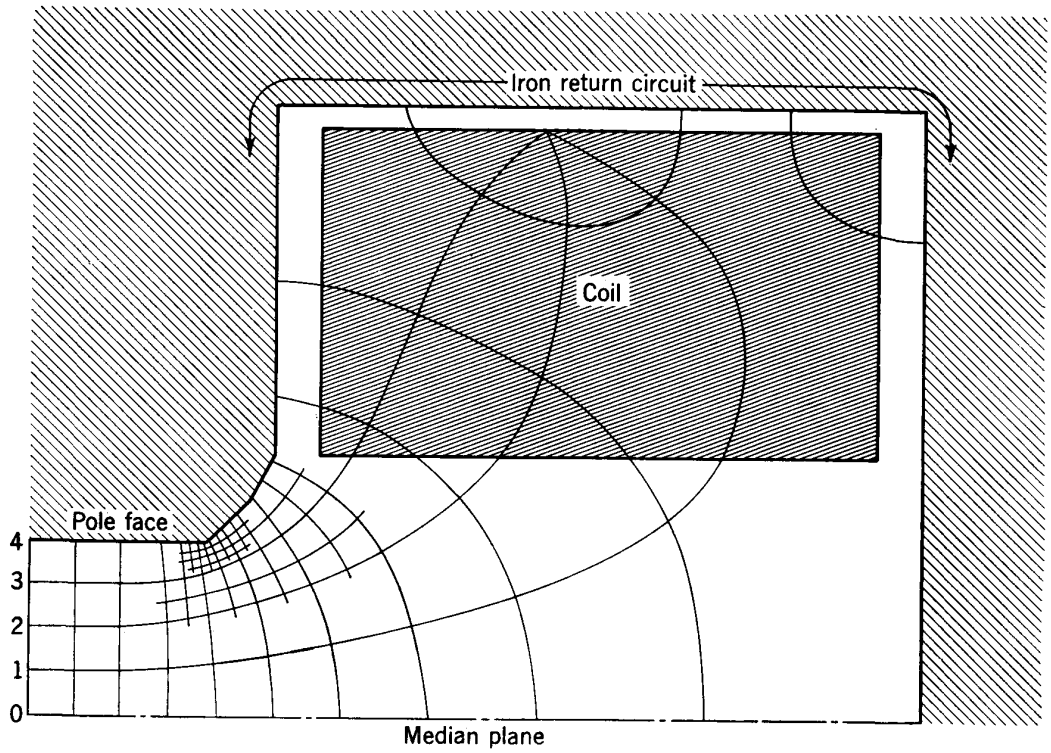

Fig. 8-8. A freehand flux plot for a cyclotron magnet with tapered poles. The lines of flux and the equipotentials intersect orthogonally and form curvilinear squares.

but in inexperienced hands it can also lead to gross errors. The amateur is advised to stick to the numerical methods described below.

The freehand flux plotter usually chooses to make the rectangles between adjacent equipotentials and lines of force into squares by appropriate choice of spacing between lines of force. He makes a freehand guess at the equipotential pattern, fits in a set of normal lines of force, and then, by liberal use of the eraser, corrects the first guess until a complete pattern of squares emerges. Figure 8-8 is an example of such a freehand plot of the field in the MIT cyclotron magnet. Values of flux density determined from the spacing of flux lines are in adequate agreement with measured values. Further refinements in the freehand tech-

nique are described by Dwight and Abt,[5] who used the method to design a continuously curving shape for the pole tip of a cyclotron magnet.

Numerical Methods for Flux Plotting

Several iterative numerical processes have been developed for establishing field patterns. In these methods one or other of the potential functions is obtained by numerical solution of the second-order equation which describes it. We shall consider first the methods used with the scalar potential u, which satisfies the relation $\nabla^2 u = 0$. First, a large-scale plot is drawn with the known potential boundaries, and a square net of points separated by a distance δ is laid out to fill the region between the boundaries. Figure 8-9 represents a small region of this net. If the potential at the various numbered points is u_1, u_2, etc., we can rewrite the equation for u at the point 0 in the form of a finite difference equation thus:

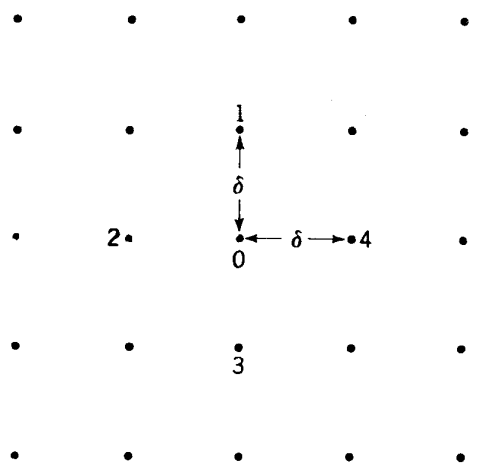

Fig. 8-9. Form of net used in relaxation flux plotting.

$$\nabla^2 u = \frac{\partial^2 u}{\partial x^2} + \frac{\partial^2 u}{\partial y^2} = \frac{u_1 + u_2 + u_3 + u_4 - 4u_0}{\delta^2} = 0 \qquad (8\text{-}14)$$

The most powerful method for obtaining a solution to this equation for all net points is the Southwell "relaxation" method[6] in which the errors in an assumed potential distribution are relaxed by consecutive revisions. The errors are expressed in the form of residuals, the residual at a given point being given by

$$\text{Residual at point } 0 = u_1 + u_2 + u_3 + u_4 - 4u_0 \qquad (8\text{-}15)$$

When, for the assumed distribution, the residuals have been determined for each net point, they are used to modify the potential at that point. The process converges rapidly, and a final solution is obtained when all of the residuals have been reduced below some previously accepted limit of error. Thus the solution can be carried to any desired accuracy.

The relaxation procedure in its simplest form involves reduction of the potential at the points of large residuals by one-quarter of the residual at that point. This reduces the residual at these points to zero and modifies the residuals at the neighboring points. By concentrating on the points of high residuals, the distribution is corrected step by step until it satisfies

the field equations. Procedures of block relaxation are described in the references cited for correcting large regions that have residuals of the same sign. Many other techniques are available for speeding up the correction process. But the primary virtue of the method is that it converges in a positive fashion even in the hands of a relatively unskilled operator.

Figure 8-10 shows a plot of a quadrant of the fringing field around a cyclotron pole, with the magnetic potential at the median plane assumed to be zero and to have the relative value 100 at the iron pole-face boundary. Values of potential indicated at each point in the square grid were

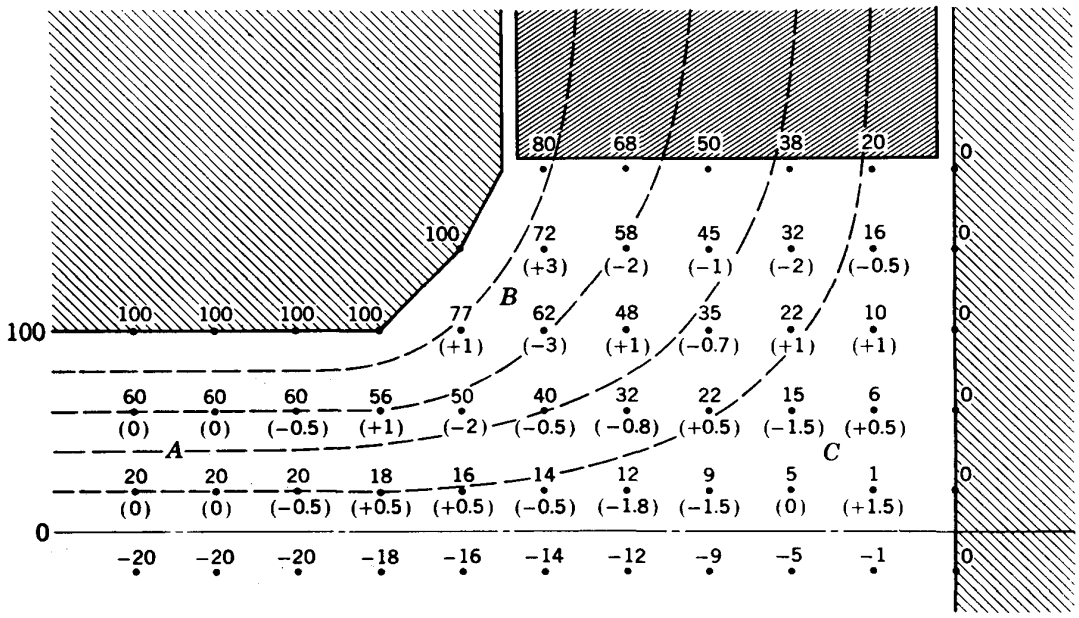

Fig. 8-10. Numerical flux plot showing the value of magnetic potential at each net point, with residual errors below in parentheses.

interpolated from the freehand potential plot which is sketched in dashed lines. The residuals for each point are shown in parentheses beneath the value of potential. It can be noted that the worst errors occur in the regions in which the divergence of field is the greatest, such as points B and C.

If the region of interest includes current-bearing conductors, the scalar potential can no longer be used. Solutions can be obtained for these cases by using the vector potential A, which must satisfy $\nabla^2 A = \mu I$. For this case the residuals take the form

$$\text{Residual at point } 0 = A_1 + A_2 + A_3 + A_4 - 4A_0 - \mu Ia \quad (8\text{-}16)$$

where a is the area of a net mesh.

The relaxation process is the same as that used for the scalar potential. When the vector potential is used, the situation at the iron boundaries is

more complicated than in the case of the scalar potential. In the latter case the potential at the boundaries was specified, and no residuals appear at net points on a boundary. With the vector potential the boundary condition of normal incidence of the lines of force on an iron surface results in a zero normal derivative of A. This is taken into account by inclusion in the net of "virtual net points" just inside the iron surface. The vector potential at these points is set equal to that at the point in the air gap, which is a mirror image in the iron surface of the virtual point.

For dealing with complicated and curved boundary surfaces a composite potential function has been evolved and used by M. H. Blewett of Brookhaven National Laboratory. Her work is unpublished, and the authors are indebted to her for the following description of her procedure:

When computing magnetic fields in a region with nonrectangular boundaries, a major disadvantage in using the vector potential in relaxation calculations arises from the necessary condition at the iron-air boundary that the normal derivative of the vector potential be zero. Thus, the virtual points used for this type of boundary condition are no longer on true net points, and a considerable amount of auxiliary computation must be carried out. Another difficulty arises when computing fields in C-shaped magnets where all boundaries but one have this normal-derivative type of boundary condition. In this case, the relaxation calculations become very tedious since all of the residuals, to use the Southwell terminology, must be "swept out" through quite a narrow region and dissipated in the infinite region beyond the area of interest to the computation.

To overcome these disadvantages, a modified potential function ψ may be derived as follows: If A is the usual vector potential, then let

$$-\frac{\partial \psi}{\partial y} = B_y = -\frac{\partial A}{\partial x} \tag{8-17}$$

and so

$$-\frac{\partial^2 \psi}{\partial x\, \partial y} = -\frac{\partial^2 A}{\partial x^2} = \mu I + \frac{\partial^2 A}{\partial y^2} \tag{8-18}$$

Integrating with respect to y gives

$$-\frac{\partial \psi}{\partial x} = \int_0^y \mu I\, dy + \frac{\partial A}{\partial y} + \text{integration constant} \tag{8-19}$$

But $\dfrac{\partial A}{\partial y} = B_x$ and the integration constant is zero if the problem has the usual symmetry about the x axis. Thus

$$-\frac{\partial \psi}{\partial x} = B_x + \int_0^y \mu I\, dy \tag{8-20}$$

We see that, in the non-current-bearing regions, ψ is like a scalar potential, and in the current-bearing regions it is related to the total current enclosed at a given point.

The Laplacian of ψ can then be found and is given by

$$\Delta^2\psi = -\frac{\partial}{\partial x}\int_0^y \mu I \, dy \tag{8-21}$$

It is noteworthy that the Laplacian of ψ is zero, not only in the current-free regions, but also throughout the coils except at each vertical boundary.

If a given problem makes it more convenient, it is, of course, also easy to find another potential-like function ψ' whose Laplacian will be given by

$$-\frac{\partial}{\partial y}\int_0^x \mu I \, dx$$

From the above, and particularly from Eq. (8-20), it can also be seen that the function ψ will have fixed values on an iron-air boundary. In regions enclosing a coil, it will vary with x as $\int_0^y \mu I \, dy$ varies. In regions between coils, it will have a value proportional to the total ampere-turns enclosed.

Figure 8-11 shows a plot of the lines of force in the Brookhaven alternating-gradient synchrotron (AGS) magnet (see Chap. 15) by the method

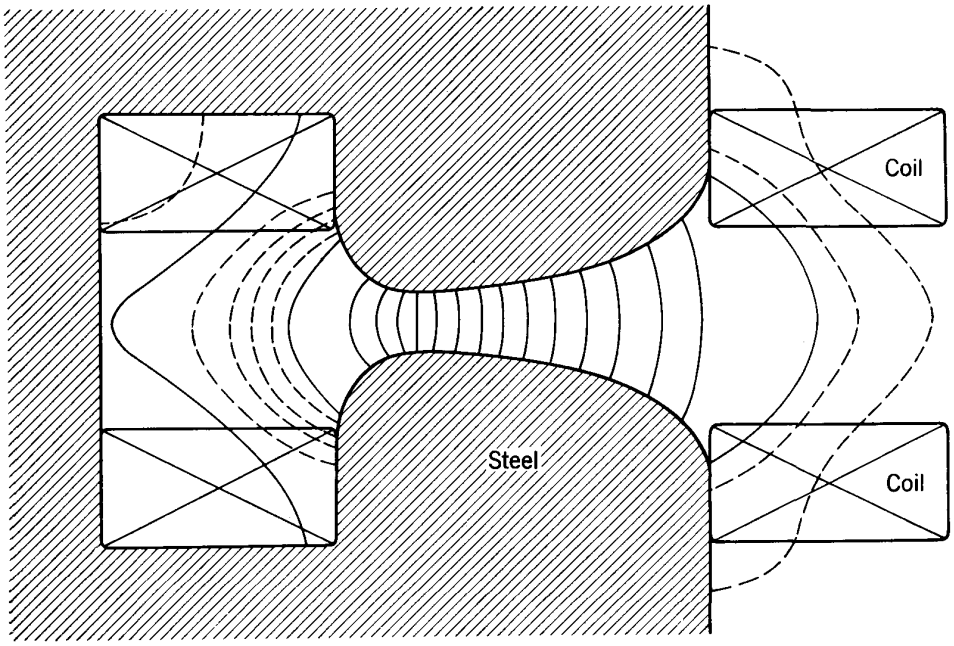

Fig. 8-11. Lines of force in the Brookhaven AGS magnet obtained by the relaxation method of M. H. Blewett. The spacing between the solid lines is a measure of the field strength. The dashed lines are interpolated in regions of weaker field; their separation indicates a field strength one-fifth as strong as would be indicated by an equal separation between solid lines.

just described. The potential function was determined to about 1 part in 100,000 at each net point, and by this means it was possible to define the pole shape, to give the desired field, to an accuracy of about 0.002 in.

Recent developments in the fields of numerical flux plotting have been in the direction of preparing programs for electronic computers that will permit rapid solutions by the methods just described.

The relaxation method can be used equally effectively to derive the field pattern in the iron of an electromagnet. With iron of uniform permeability the problem can easily be solved by hand. Although the solution is not valid as the iron saturates, it can be used to indicate the regions where saturation will first take place. When the variation of iron properties with flux density is taken into account, the problem becomes too complex for rapid hand solution but can still be handled by an electronic computer. Development of this method is now in its early stages but is progressing rapidly. The day appears not far distant when a magnet design can be completed without approximation by purely computational techniques.

8-4. USE OF MODELS IN MAGNET DESIGN

At present, most designers still find that experimental measurements with scaled models provide the most useful and exact information. Almost without exception, models have been used in determining final construction details and pole-face shape for the sequence of larger and larger magnets needed for accelerators.

Linear scale factors are used to provide the same magnetic flux pattern as in the full-scale unit, and models must be operated at the same flux density. The scale factor used depends on the kind of information desired from the model, on the accuracy demanded of the measurements, and on the dimensions of the measuring instruments available. Frequently the effort expended in developing small and precise measuring instruments is comparable to that required for the model itself. Small models are cheaper to build and modify, but measurements are more difficult and extreme precision is required in machining and instrumentation. For the Brookhaven cosmotron a scale of 1:4 was used to study the properties of a laminated magnet with 36-in.-wide poles to be excited with pulsed power; since eddy-current effects vary with the square of lamination thickness, the pulse length was also scaled to provide equivalent magnetic response. With the Cambridge electron accelerator the laminated magnet with AG pole faces of 6½ in. width had a sufficiently small iron circuit to allow the use of full-scale (but short-length) models. At the other extreme, the 130-in.-diam steady-field magnet for the Carnegie Institute of Technology synchrocyclotron was studied with a model of 2-in. pole face, a scale factor of 1:65. The scale factor used in any case is the designer's choice.

In model studies the fixed parameters are usually pole-face diameter (or cross section) and gap length. These quantities are essentially determined by the choice of particle energy, calculations of particle orbits, and the necessary aperture for the accelerating chamber between poles. The spacing between coils may also be limited by the physical space require-

ments for auxiliary apparatus such as the vacuum chamber or the D lines of a cyclotron. The general structural shape of the circuit is also usually conceived at an early stage of design.

Other physical parameters which may be studied in a model are the shape of pole taper, the length of pole and area of the pole base, the dimensions of the iron return circuit, and the size and location of the exciting coils. Electrical measurements are needed to predict full-scale power requirements, such as the ampere-turns in the coils and power losses in coils and core. The most significant results, however, come from precise measurements of the field in the gap and outside the gap, in order to determine pole-face shape and the leakage flux pattern. Removable pole-face disks or plates are normally built into the model; these can be remachined or replaced to study the effects of small changes in shape on the field distribution in the pole gap.

The most serious technical problem in small-scale models is that of coil cooling, since power requirements do not scale linearly. If the same magnetic flux density is to be maintained in the model as in the final magnet, the magnetomotive force, i.e., the total number of ampere-turns in the coil, will be proportional to the scale factor [cf. Eq. (8-3)]. For example, a quarter-scale model will require only one-quarter as many ampere-turns as does the full-scale magnet. But the cross-sectional area of the coil decreases like the square of the scale factor. Consequently, the current density in the coil will be inversely proportional to the scale factor. The power dissipation per unit volume in the coil is proportional to the square of the current density and hence to the inverse square of the scale factor. In a quarter-scale model the dissipation per unit volume of the coil is increased by a factor of 16!

Cooling of small-scale models of water-cooled coils is further complicated by the reduced water flow in the smaller cooling channels, since water flow rate is proportional to a high power of tube diameter. Consequently, it is often not possible to operate small models continuously; data must be taken during short pulses to avoid overheating. Special model coils using a small number of turns and very high water pressure have been used to obtain adequate cooling efficiency. Occasionally the model-coil cooling problems have been so severe as to require the use of larger-scale models than would otherwise have been required.

One of the most detailed reports of a model study is that of Foss, Fox, Sutton, and Creutz,[2] used in the design of the 130-in.-diam synchrocyclotron magnet at the Carnegie Institute of Technology. This study represents an extreme case in that the scale factor used was 1:65. Using a technique already tested in betatron magnet design, the group constructed only half of the model; the other half was mirrored in an effectively infinite half-space of iron plate located at the midplane of the air gap. This reduced gap length and ampere-turns to half those of a full

model and saved on machining of the pole shape. The permeability of the reflecting iron must be essentially infinite for field patterns and flux densities to be undisturbed; the authors estimate that a maximum error of less than 1 per cent was caused by the finite permeability for fields up to 20 kilogauss. In their model studies the Carnegie Tech group used a wide variety of shapes and sizes of iron for the poles and return circuits as well as many different shapes and sizes of copper exciting coils. The design was optimized for minimum excitation (ampere-turns) to obtain the designed peak flux density of 20 kilogauss in the gap. The final result (see Fig. 8-6) was a magnet with a flux efficiency of 86 per cent at 20 kilogauss, defined as the fraction of the total magnetic flux enclosed within the physical boundaries of the pole faces. It might be noted that the model was too small to show the detailed shape of the field between poles with sufficient accuracy. The necessary shimming to give the correct radial decrease needed for focusing was determined later with the full-scale magnet.

With pulsed or ac magnets, models have been an absolute necessity. In the development of the 300-Mev betatron Kerst used several stages of model studies. The first step was a solid-core small-scale model to ascertain the gross flux and field patterns in order to determine efficient shapes and sizes for the iron cores. He next built the 80-Mev machine, which was a scaled model of the projected 300-Mev betatron, with laminated cores and stranded cable coils, and used it with pulse powering to determine magnetic losses, field distributions, and the transient effects on the field distribution due to pulsed operation. Because it was a scaled model, the 80-Mev machine could not be cooled adequately and was operated at reduced pulsing rates.

A series of models of increasing scale factor was used in developing the magnets for the Brookhaven cosmotron, starting with $\frac{1}{12}$-scale solid-iron cores and culminating in a $\frac{1}{4}$-scale laminated-core model section of short length which was used for detailed pulsed-power measurements to determine the full-scale pole-face profile.

In many laboratories the development of accelerator magnets has justified the humorous quotation in one of the accelerator songs written by A. Roberts: "This machine is just a model for a bigger one, of course!"

8-5. COIL DESIGN

The excitation coils provide the magnetomotive force or the ampere-turns Ni used in the circuit equations of Sec. 8-2. In dc magnets the first parameter to be determined is the power to be dissipated in the resistance of the excitation windings. As will be shown below, power varies inversely with volume of conductor, so to a first approximation it can be chosen at will.

Consider a coil of N turns (usually arranged in two identical units) of total cross-sectional area a so that the area of one turn is a/N. Let the average length of a turn be l. If the conductors are formed of a material of resistivity ρ (evaluated for the average temperature expected in the windings), then the total resistance of the coil will be

$$R = \frac{Nl\rho}{a/N} = \frac{N^2\rho l}{a} \tag{8-22}$$

The maximum current i is specified by the chosen peak excitation Ni. At this current the power dissipated U is

$$U = i^2R = \frac{\rho(Ni)^2 l}{a} = \frac{\rho(Ni)^2 l^2}{\text{coil volume}} \tag{8-23}$$

from which the coil conductor volume can be obtained once power is chosen. To be sure, the average length of turn is not independent of conductor volume but is related through the dimensions of the coil units and the distribution of the insulation material. However, a well-designed coil will have a "packing ratio" greater than 0.5, meaning that the conductor area is more than half of the total cross section of the coil or that the space for insulation, cooling, and clamps occupies less than half of the total volume. The average length per turn l can be taken as that for a turn halfway between outer and inner dimensions of the coil.

The number of turns N, which then determines the conductor size, can be adjusted to match the current-voltage ratings of the power supply. Frequently the availability of machines of standard ratings will influence the choice of voltage V. Direct-current generators are commonly produced in standard voltage ratings of 115, 230, 500, etc., volts and for a sequence of power ratings determined by the size of the machine. With voltage V, power U, and ampere-turns chosen, the number of turns is given by

$$N = \frac{NiV}{U}$$

The number of turns must be even if two identical coil units are planned. Furthermore, the number is usually taken to be divisible by the number of coil layers chosen in design (i.e., with two coil units of four layers each, the number N must be a multiple of 8). Other conditions may enter, such as possible alternate series-parallel connections of the coil layers, which would modify the choice of number of layers. If coil design departs from the normal rectangular cross section, in which all layers have equal numbers of turns, still further modifications are involved. A simple rectangular cross section is usually found to be the most economical, since it simplifies the structures of the cooling system and mechanical supports as well as the process of coil winding. With the

above restriction on number of turns, limited to a multiple of some large number such as 8 or 16, the choice of voltage is also restricted to a set of values. The common decision is to choose a value of N for which the corresponding required voltage V is somewhat less than that available from the power supply, allowing a margin for surplus excitation.

The conductor shape which provides the desired cross section is heavily influenced by the technique chosen for cooling. Several alternative methods of providing the cooling will be described below.

Air cooling is standard for the windings of rotating dc machinery and is provided by the motion of the armature. With static magnets air-blast cooling is less attractive. Air ducts are bulky and interfere with other components of the accelerator; the efficiency of thermal transfer is low unless air speed is high, in which case the noise may be objectionable. Air cooling has been used in several cyclotrons and in the Berkeley bevatron and has the advantage of eliminating the problems of water cooling. However, more recent developments have made other techniques preferable, and air cooling is no longer in favor.

Oil-immersion cooling has been used for many cyclotrons, with multilayer coils enclosed in oil tanks and with forced circulation of the oil through a heat exchanger. Sturdy mechanical brackets are required to support the tanks and hold the coils in place against magnetic forces. The most serious problem is the fire hazard, since most oils used for this purpose are inflammable. At least two damaging fires have occurred in cyclotrons with oil-immersion cooling, and insurance underwriters' rates have reflected the hazard. For this reason oil-immersion cooling is no longer considered suitable for large magnets.

Water-cooling techniques have been developed largely for accelerator applications. One successful design employs alternate layers of conductor and water-cooled metal, with thermal conduction through thin intermediate layers of insulation. The metal cooling layer may be formed as a spiral-wound flat plate of rectangular hollow tubing through which cooling water circulates. This "dry-wound" water-cooled coil is compact and easy to mount and clamp. Its limitations are the relatively high conductor temperatures and the possibility of water leaks. Figure 8-12 is an illustration of cyclotron coils which employ this technique of cooling.

In each of the three methods described above, the conductor edge or face is exposed to the cooling medium. The conductors are usually formed as thin strips of bar copper, wound in a flat helical spiral with interleaved ribbons of insulation between turns; the edges of the strips are bare and in contact with the cooling medium. Typical dimensions are those for the MIT coil (see Fig. 8-12) in which the copper conductor has a rectangular cross section of $\frac{1}{8}$ by $\frac{3}{4}$ in. The most useful feature of such strip-wound layer coils is that the coils can be designed for a large number of turns and can use a high-voltage power supply.

Internal cooling through hollow conductors is possible only with conductors of relatively large cross section. In a small magnet this means a small number of turns and an undesirably low-voltage power supply. In large magnets the conductor cross section is large enough to use hollow conductors. Extruded copper (or aluminum) bars have been used which have a rectangular external shape and a water channel along the center. This design excels in cooling efficiency and allows the use of high current densities. Small-size copper tubing has occasionally been used for model coils; for these, high water pressures are needed. In large magnets the

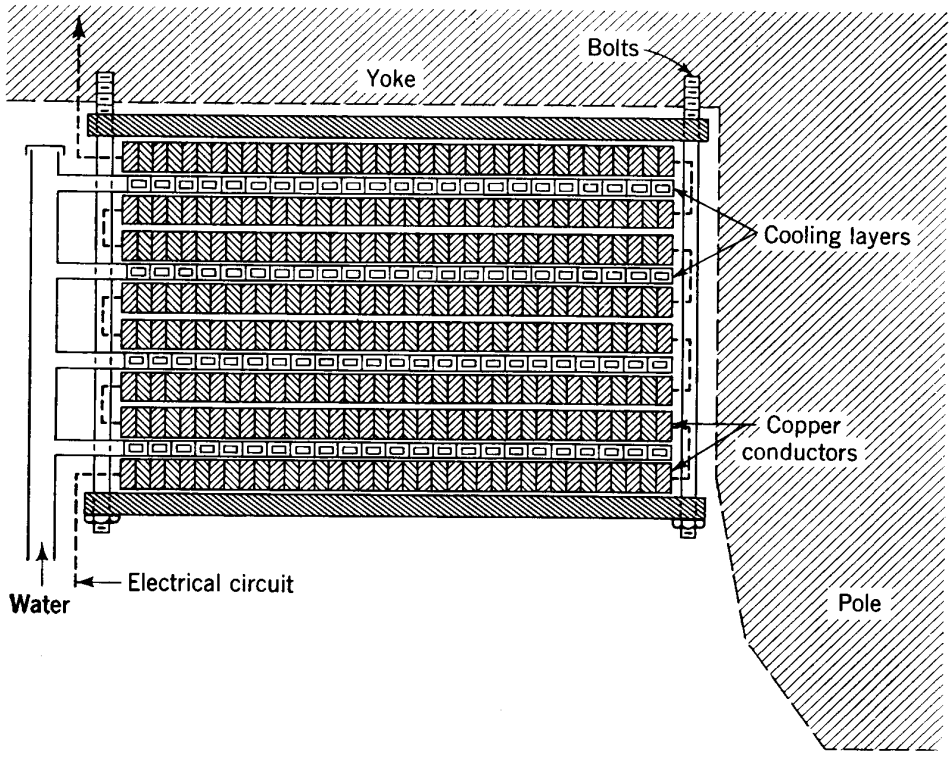

Fig. 8-12. Layer-wound coils with layers of water tubing inserted for cooling (similar to those in MIT cyclotron magnet).

chief disadvantage has been the large number of brazed or welded joints in the conductor and the consequent risk of water leaks. This is not a serious problem for dc cyclotron magnets in which magnetic forces are steady, but has been seriously objectionable in pulsed magnets as in the cosmotron, which has had several conductor-joint failures requiring major coil repairs.

The size of the cooling channel is the most critical dimension in the design of internally cooled coils, since the water pressure required to produce a given flow is a steep function of the size and shape of the channel. The water flow required to dissipate the heat generated in the coil can be determined from the known power losses and the allowed temperature rise in the water. In engineering units, the flow q (in gallons per minute)

required to dissipate an amount of power U (kilowatts) for a temperature rise ΔT (degrees Fahrenheit) is

$$q = \frac{6.82U}{\Delta T} \quad \text{gpm}$$

Water velocity and tube diameter determine whether the flow is streamlined or turbulent; in most cases it will be found that accelerator cooling systems are in the turbulent-flow range.

To compute the pressure drop required it is necessary first to derive the Reynolds number for the case in question. In terms of the flow q (in gallons per minute) and the tube diameter d (measured in inches) the Reynolds number is given for water at temperature T°F by

$$\text{Reynolds number} = \frac{3400q}{d} \frac{\text{viscosity of water at 75°F}}{\text{viscosity of water at } T\text{°F}}$$

The viscosity ratio necessary for substitution here can be derived from the following table:

Temperature T,°F.....	32	40	60	80	100	140	212
Viscosity at 75°F / Viscosity at T°F	0.52	0.59	0.82	1.07	1.35	1.95	3.13

The necessary pressure drop ΔP (measured in pounds per square inch) can now be obtained from the formula

$$\Delta P = \frac{kq^2l}{d^5} \quad \text{psi}$$

where q = flow, gpm
d = tube diameter, in.
l = tube length, ft
k = friction constant given as function of Reynolds number in Table 8-1

TABLE 8-1

Reynolds number	k	
100	0.0086	Streamline flow
300	0.0028	
1,000	0.00081	
2,000	0.00044	
3,000 (rate of flow increasing)	0.00032	
3,000 (rate of flow decreasing)	0.00059	Turbulent flow
5,000	0.00049	
10,000	0.00042	
30,000	0.00032	
100,000	0.00024	
1,000,000	0.00015	
10,000,000	0.00011	

The above formula and tables suffice to make approximate estimates of pressure drop for circular pipes without too many sharp bends. More refined calculations can be made with the assistance of methods to be found in such texts as "Heat Transmission," by McAdams,[7] or "Hydraulics," by Daugherty.[8]

The casting of preformed coils with epoxy or polyester resins to form solid mechanical structures is now a well-developed technique. Several competent commercial firms in the United States and Europe offer this type of coil as a standard product. The coils for several of the accelerators now under construction, and for many auxiliary magnets used in the research laboratory, incorporate this feature. Resins which are either thermosetting or room-temperature-setting are commercially available and have a wide range in their mechanical and electrical properties. When glass-fiber cloth or cotton mesh is used as a base and impregnated with such a resin, the tensile strength is in the range 1000 to 3000 psi. Individual conductors are tightly bound so as to prevent any motion under magnetic forces, and the coil is rigid enough to be self-supporting with the minimum number of clamps or brackets. This technique is a completely satisfactory answer to the problems of coil distortion and motion under magnetic forces and provides a coil having a long life expectancy against failures.

Special insulating techniques are required to obtain the necessary quality and uniformity in the insulation properties of resin-impregnated coils. The mechanical and electrical properties of resin-bonded material are so interrelated that it is in general not possible to choose resins for optimum mechanical strength and at the same time obtain reliable electrical insulation. The voltage breakdown strength of a resin-impregnated layer of glass cloth or cotton mesh is usually over 100 volts/mil thickness for thin layers (10 to 30 mils) when used for low potentials, such as for turn-to-turn insulation. However, it has usually been found necessary to utilize mica-sheet or mica-flake insulation to obtain the higher voltage-to-ground insulation.

A basic technique in making resin-bonded coils is to wrap individual conductors with a porous insulation tape made of glass cloth or cotton mesh after bending and forming these conductors into the desired shapes. The coil is enclosed within an airtight form from which the air is evacuated, and the fluid (hot) resin is flowed into the form to permeate the entire coil and fill the porous insulation with the resin dielectric. After setting, the coil unit is normally baked in an oven for a final cure and the entire coil is wrapped with an outer layer of special high-voltage insulation. The technique can be used with hollow conductors, in which case the water-channel connections are brought out of the casting with the conductor terminations. Figure 8-13*a* shows a cross section of the coil

for the Brookhaven AGS magnet (see Chap. 15), which is pulsed at 3-sec intervals, and for which a large hollow conductor is acceptable.

A special problem in coils for fast-pulsed or ac excitation is the requirement for low inductance, which means that the number of turns must be small and therefore of large cross section. Solid conductors lead to excessive eddy-current losses; stranded cables require complex clamping and insulating structures to resist magnetic forces and are difficult to cool. Although this problem exists in the electrical industry, it has

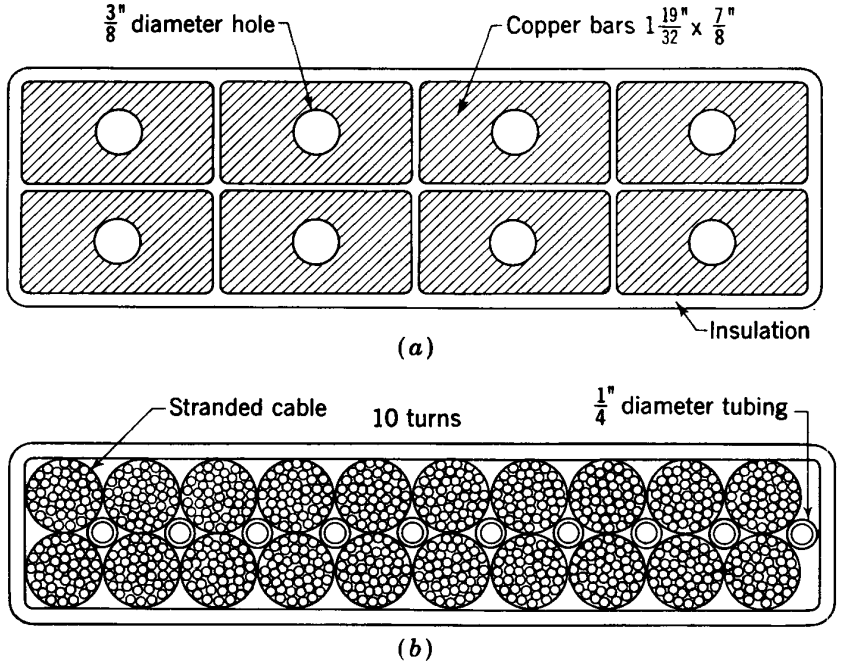

Fig. 8-13. (*a*) Resin-bonded hollow-conductor coil for the Brookhaven AGS magnet (see Sec. 15-8), designed for pulsing 20 times per minute. (*b*) Resin-bonded stranded-cable coil with internal water-cooling tubing for the Cambridge electron accelerator (see Sec. 15-9) designed for 60-cps pulsing.

become more acute in accelerator applications in which the coils are located near air gaps where fringing fields and magnetic forces are much greater. In the Cambridge electron accelerator, which operates at 60 cps, this problem is met by utilizing the resin-casting technique. Figure 8-13*b* shows a cross section of the stranded-cable coil used for the conductor, as well as the thin-walled tubing which is also embedded in the casting for removing the heat.

The forces on coils in electromagnets are often very large. For example, the coil in the magnet gap of the Brookhaven cosmotron experiences a peak magnetic pressure of about 1000 lb/in. of its length. These forces are generally in such a direction as to push the coil away from the region of high magnetic field. Their magnitude and direction can be

established from flux plots of the sort described in Sec. 8-3. Clamps must then be designed to prevent excessive motion under these forces, since coil motions will result in abrasion of insulation and in fatigue of the copper coil components.

8-6. METHODS OF MAGNETIC MEASUREMENT

Although magnetic fields are just as important to an understanding of natural phenomena as are electric fields, they have not reached the degree of practical importance that ensures the availability of commercial measuring equipment such as is readily available for the measurement of voltage and electric current. Until quite recent years the accelerator physicist has been faced with the necessity of building all his own magnetic measuring gear. For accurate measurement of magnetic fields it is still, in 1961, necessary to build almost all magnetic measuring equipment with the exception of a few types of approximate survey instruments which now are commercially available.

A number of magnetic-field-dependent phenomena are available for use in measurement of magnetic fields. Those whose applications will be discussed below are as follows:

1. A conductor-bearing current in a magnetic field will experience a force normal to the current and to the direction of the field.
2. A loop of wire which links a changing magnetic flux will exhibit an induced voltage.
3. Nuclear magnetic moments precess in a magnetic field at a measurable frequency whose value is a measure of the field.
4. Certain materials, notably bismuth, show a strong dependence of electrical resistance on magnetic field.
5. A potential difference appears across a current-bearing strip in a magnetic field (the Hall effect).
6. Some materials of high permeability (such as permalloy) saturate at very low magnetic fields.
7. A magnetized needle of ferromagnetic material will align itself with a magnetic field (as every sailor knows).

Varying degrees of accuracy are achievable using these phenomena. For convenience, linearity, and precision the induction of voltage in a conducting loop or search coil has always been the favorite effect, and a great variety of measuring equipment has been designed around it. Even higher precision is attainable using nuclear resonance, but the signal obtained is weak and easily lost in the presence of electrical noise. Saturation of permalloy strips can give accurate measurement of low fields in the 100-gauss range. The other effects are also capable of precision but usually only with very careful control of temperature, mechanical construction, or other pitfalls for the unwary.

We shall consider the various measuring techniques under three headings: dc measurements, measurements in pulsed fields, and measurements in high-gradient fields. The arrangement of material under these headings will be, to some extent, arbitrary and historical since, in principle, many of the methods are applicable in two or three of these categories. The dc-field section will include several methods for locating magnetic median planes.

A useful review of the techniques of magnetic measurement will be found in the paper of Symonds[9] of the Birmingham (England) proton synchrotron group.

8-7. MAGNETIC MEASUREMENTS IN DC FIELDS

Measurements Using the Force on Current-bearing Conductors

Magnetic field intensity is defined in terms of the force exerted on a wire carrying a current, following the vector cross-product relation of Eq. (5-12). The force is a maximum when the wire is normal to the field, and it is directed at right angles to the plane established by the wire and the field. The magnitude of this maximum force is given by

$$F_m = ilB \tag{8-24}$$

where l is the length of the wire. In the mks system of units the force is in newtons (1/9.8 of the weight of 1 kg) if current is in amperes, length in meters, and magnetic field intensity in webers/m^2. One method for observing the magnetic force is to measure the torque on a pivoted loop of wire. The torque on a loop of area A and N turns, carrying current i in a magnetic field B and located with the axis of the loop normal to the field, is

$$\tau = NiAB \sin \alpha \tag{8-25}$$

where α is the angle between the field and the normal to the loop.

Instruments have been developed for measuring uniform fields based on these fundamental definitions. One which is typical of the precision required for high-quality accelerator applications (about 1 part in 10,000) is that of Chang and Rosenblum.[10] They describe two techniques for measuring uniform fields, using large rectangular coils having precisely known dimensions, in which the magnetic torques are balanced by gravitational weight torques. The large size of the coils makes this method impractical for direct measurement of accelerator magnet fields. However, it finds a useful application in the measurement of calibrating fields such as Helmholtz coils.

Measurements Using EMFs Induced by Changing Flux

A more useful definition of magnetic field intensity comes from another basic relation, given in Eq. (5-1), for the electromotive force induced in a closed circuit by a change in the magnetic flux linking the circuit. For our present purpose we consider a coil of N turns of area a located in a magnetic field B. If the flux density linking the coil changes at the rate dB/dt, the instantaneous induced voltage V is

$$V = Na\frac{dB}{dt} \tag{8-26}$$

The induced current $i = V/R$, where R is the resistance of the coil and circuit. During any finite change ΔB in time Δt the accumulated charge Q is

$$Q = \int_t^{t+\Delta t} i\,dt = \frac{Na}{R}\Delta B \tag{8-27}$$

In a uniform field such a flux change can be produced by "snatching" the coil from a position at rest in the field to a position removed from the field; in this case the change ΔB is numerically equal to the field intensity B. The instrument to measure the charge (such as a ballistic galvanometer) must have a time constant long compared with the time Δt, so the accuracy of measurement will be independent of the rate of change. Magnetic field intensity is given by

$$B = \frac{Q(R_{\text{coil}} + R_{\text{gal}})}{Na} \tag{8-28}$$

Note that R includes the resistance of the coil and the galvanometer. Precision of measurement depends on the accuracy of knowledge of the dimensions and constants of the coil and on the galvanometer calibration. Or the coil can be calibrated for the coil constant Na in a standard magnetic field produced by a Helmholtz coil of precise dimensions.

The "snatch coil," or "search coil," is one of the earliest and most common of the instruments for measuring dc fields. Small coils of many turns can be used to study the details of a field pattern. In this case the coil is usually calibrated (with the galvanometer) by observing the charge induced using a known or standard magnetic field.

A modification called a "flip coil" uses a mechanical device such as a spring to flip the coil rapidly through 180°, while the coil remains in place. The 0° position must be accurately normal to the field, and the angle of flip exactly 180°. The reversal in direction of flux through the coil doubles the magnitude of the current pulse and the charge passing through the galvanometer, relative to the simple snatch coil described above. Flip coils capable of an accuracy better than 0.1 per cent have been built.

Another modification is the rotating coil equipped with brushes to transmit the ac output to an ac amplifier. Rotation speed must be constant and the brushes must be of high quality. The accuracy obtained with commercial instruments is about 0.5 per cent. Such an instrument can serve a useful purpose in obtaining relative values at weak fields, but is not suitable for absolute calibration.

With very small magnets (such as models) having a short-time-constant circuit in the power supply and excitation coils, the magnet excitation current can be reversed suddenly to obtain a doubled induced pulse in the measuring coil, leaving the search coil fixed. This is also the basic technique for measuring permeability of small iron samples, in which case the measuring coil is wrapped around the (ellipsoidal) specimen, which is placed inside a solenoidal excitation coil. Magnetization curves and values of permeability which are essential in magnet design can be obtained from such small-specimen measurements.

The Integrating Fluxmeter

The integrating coil fluxmeter used in most laboratories for measuring steady or dc fields is the modern application of the search coil and is the most generally useful instrument in the laboratory. Similar developments have occurred in several magnet design laboratories, with varying sensitivity and precision, but only a few have been described in detail. Usually there are three components to the fluxmeter: a coil, an integrating dc amplifier circuit, and a recording meter. Many coil shapes have been used, from tiny coils a few millimeters in diameter wound with extremely fine wire for detailed mapping of fields in small models, to large flat coils of a few turns of heavy wire to measure average fields. A typical "exploring" coil for a cyclotron magnet would have about 1000 turns of fine wire wound on a core ½ in. inside and 1 in. outside diameter and about ½ in. long; it might have a resistance of the order of 100 ohms.

Circuits for dc integrating amplifiers have been developed successfully in several laboratories. The primary problem is to maintain stability of the zero or base-line reading with time. A typical method is to use a dc-ac electronic converter or "chopper," which provides an ac signal which is readily amplified, and then to reconvert the amplified signal to direct current with a second phased converter. The integrating feature is provided by a feedback from the output to the input through a capacitor and a high resistance. Charge is stored in the capacitor proportional to the amplified input, and the potential across the capacitor is a measure of the integrated current. The circuit is essentially an RC integrator with an amplifier across the capacitor; the result is equivalent to increasing the magnitude of C without decreasing the output signal level, so that high integrating precision is achieved at high output level. Gains of

the order of 10^6 are needed to obtain sufficient sensitivity for the most precise measurements and to provide the high output level needed in the recording instrument.

A recording microammeter is usually used, such as those produced by Esterline-Angus or by Brown. With such a recording meter the data are plotted on a moving chart with the paper-drive mechanism geared to the physical location of the search coil in the magnetic field. Such a chart can be used to plot fields as a function of radial location, azimuthal position, or vertical height.

A good description of such a recording fluxmeter is given in the first University of Chicago Progress Report.[11] A later report (III) describes the use of the instrument for measurements and shows some of the chart records. This can be taken as typical of such instruments; many other laboratories have developed similar fluxmeters.

As usually used, the fluxmeter is a relative instrument only, depending for its calibration on another absolute instrument. One satisfactory method of calibration is to observe the deflection in an air-cored Helmholtz coil for which the magnetic field is accurately known from current and dimensions. The fluxmeter can be calibrated on the high-sensitivity scale, and electronic scale changers can be used for other ranges. In general each coil-amplifier-recorder hookup used must be separately calibrated. Usually the absolute value of magnetic flux density at high fields is not so important as the relative changes. So accurate plots of magnetic fields can often be made with relatively crude absolute calibrations.

In the cyclotron, one of the chief uses of the integrating fluxmeter has been the measurement of azimuthal variations of field at constant radius. Such variations can cause particle oscillations, as described in other chapters. For these measurements a coil is located at fixed radius on a radial arm pivoted to rotate about the center of the magnet. The arm is swept through a full circle, with the mechanical motion geared to the paper drive of the recorder. Connecting wires from the coil to the integrator must be twisted together and led out from the central pivot to prevent extraneous effects. If the field varies in magnitude around the circle, the variation will be plotted on the recorder as a wavy line. Total deflection should be zero after a full circle; this provides a check on the stability of the amplifier.

A series of such azimuthal plots for different radii will show the main features of the field distribution. Figure 8-14 shows a fluxmeter record from the Chicago synchrocyclotron measurements before magnetic corrections. The roughly sinusoidal variation is such as would result from pole faces which were not quite parallel, or from the pivot being off the center of the field. This fundamental harmonic error can be removed

by moving the pivot (the particles will rotate around this same magnetic center). For correcting higher-frequency variations, metal shims can be cut and tried until the error is reduced adequately; then the shims may be installed permanently.

Another important measurement in cyclotron and synchrocyclotron magnets is the radial decrease in field from center to the periphery. The recording fluxmeter described above can be used to make these measurements, with the chart driven in direct proportion to the radial location of the coil. A radial supporting beam of nonmagnetic material allows the coil to be located in azimuth and to be moved radially along the median plane of the field by strings or gears. The change in flux density produces a deflection on the chart when the coil is moved; if the field decreases linearly with radius and speed is constant, the plot will be a diagonal straight line across the chart. The magnitude of the flux change between radial locations is determined from the calibration of the fluxmeter and can be used to compute the field gradient. Since the instrument integrates the flux change, the final reading after moving the coil from center to edge and back to center should be identical with the original reading; this can be used to check the stability of the amplifier. A typical curve obtained in this way for the MIT cyclotron magnet is shown in Fig. 6-8, along with the computed value of n as a function of radius.

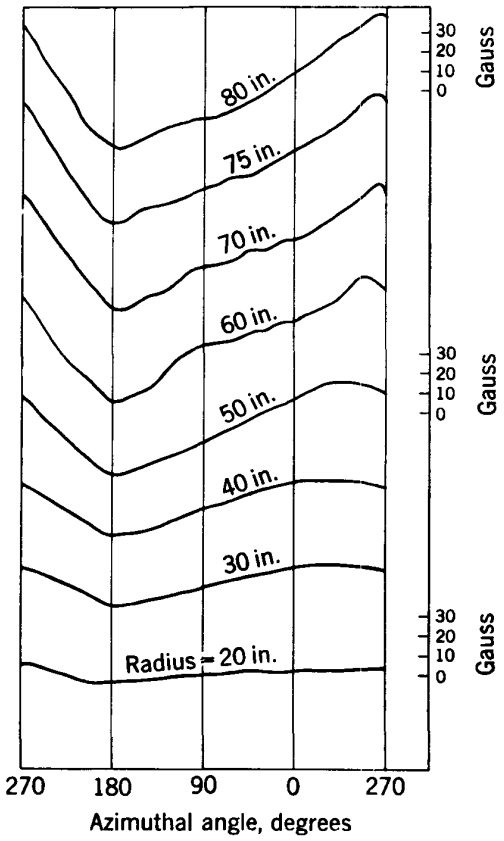

Fig. 8-14. Azimuthal variation of field for different radii, before correction, in the University of Chicago synchrocyclotron magnet.[11]

In such a radial plot the field changes very rapidly as the coil approaches the edge of the pole face. Scale-changing circuit elements can be used to shift to another range for plotting. However, it is frequently more convenient to measure the slope of the field, dB/dr, directly rather than the field itself. For this purpose the integrating capacitor in the amplifier circuit can be disconnected and the current observed directly. Then if the coil is moved at constant rate (using a screw feed to give uniform speed), the reading on the chart will be proportional to the slope of the field, and the gradient can be directly observed.

Measurements Using Nuclear Resonance

The proton magnetic moment will precess about an applied external magnetic field with a Larmor frequency which is directly proportional to field intensity. The methods of nuclear absorption or nuclear induction[12,13] can be used to observe this resonant frequency and so to measure magnetic field. This is an absolute method of calibration, dependent only on the magnitude of the proton magnetic moment, which is known to a precision of 0.03 per cent. Relative measurements can be made to even greater accuracy, limited only by the precision of measuring radio-frequencies or the homogeneity of the field.

The earliest suggestion for using this property for the measurement of magnetic fields was by Roberts,[14] although others working independently have reported similar devices. Packard[15] describes a magnetic-field regulator using the nuclear induction signal from a water sample in the field. Hopkins[16] reports a portable instrument using nuclear absorption of protons in a distilled-water sample which has a precision of better than 0.2 per cent at fields up to 19 kilogauss.

The fluxmeter developed by Hopkins uses an oscillating regenerative detector with an audioamplifier whose output is presented on an oscilloscope. The proton sample can be a thin-walled glass vial holding about 0.5 gm of distilled water, located in a small coil which is a part of the resonant circuit and can be moved about in the field. The coil is set with its axis at right angles to the field, and rf oscillations are set up in the coil at a frequency determined by a tuning capacitor. When this frequency corresponds with the Larmor precessional frequency of protons, transitions occur which result in an absorption of energy from the rf field. With the regenerative detector this energy drop appears as a sharp dip in an oscilloscope trace. The technique used to locate and identify the nuclear resonance is to apply a small 60-cycle component to "wobble" the magnetic field back and forth through its resonant value, using small auxiliary coils around the sample. The frequency for resonance can be measured and reduced to magnetic field through the relation

$$B = (234.82 \pm 0.13)f$$

where B is in gauss (10^{-4} weber/m^2) and f is in megacycles per second. The width of the resonance dip depends on the homogeneity of the field and also on the material used in the proton-moment sample holder. The radial decrease built into cyclotron magnets gives a resonance width of several gauss across the sample and is found to be the limit to precision.

The Bismuth Spiral

The resistance of bismuth wire increases in a magnetic field by as much as 50 per cent for fields of the order of 20 kilogauss. At low fields the

resistance-versus-field characteristic is nonlinear, but over the range from about 3 to 25 kilogauss the characteristic becomes roughly linear. This effect has been known for a long time, and bismuth resistors have often been used for magnetic-field measurements. Usually these resistors are in the form of cast spirals. The method suffers from the fact that the resistance of bismuth is also strongly temperature-dependent and is, moreover, sensitive to mechanical deformations. With adequate mechanical protection and temperature control the bismuth resistor can be very useful for survey measurements. A refined bismuth resistor probe was used by Dols, Skiff, and Watson[17] in magnetic measurements during the 1956 modification of the 184-in. synchrocyclotron at the University of California. The precautions necessary are discussed in detail in the paper describing these measurements.

The Hall Effect

The Hall effect (discovered by E. H. Hall in 1879) is the name given to the appearance of a potential difference across a strip of metal carrying a current in an external magnetic field. This is a relatively small but roughly linear effect which can be used fairly easily for measurement of magnetic fields to accuracies of the order of 1 per cent. It also suffers from sensitivity to temperature variations, but alloys can be found which are relatively temperature-insensitive over limited temperature ranges. A simple field-strength meter using the Hall effect was described by Pearson[18] in 1948, and since that time a great deal of unpublished work has been done in various laboratories, notably the CERN laboratory in Geneva, Switzerland. Commercial field-strength meters using the Hall effect and useful over the range of fields up to and above 20 kilogauss are now (1961) available. Plates of indium arsenide are available from the German firm of Siemens for use in such Hall-effect fluxmeters. With a current of 0.2 amp these plates give about 20 mv per thousand gauss.

Cyclotron Resonance

A simple method of determining the average magnetic field in a cyclotron magnet is to use the cyclotron resonance condition

$$f = \frac{1}{2\pi}\frac{e}{m}B$$

When the cyclotron is in operation, in resonance with an ion of known e/m value at a frequency f, the magnetic field can be determined with high precision, since e/m is known and the frequency of the resonant circuit can be measured to high accuracy. This is a useful method of

obtaining points on the magnetization curve of the magnet. But the field in a cyclotron is always slightly tapered, decreasing with increasing radius, so this resonance frequency represents an average value of the magnetic field from the center out to the exit radius. It cannot even be identified with a particular radial location, since phase migrations of ions are a consequence of this decreasing field and the details of such phase migrations are difficult to analyze. In attempting to evaluate the central field from this average value an error of the order of 0.5 per cent is possible.

Median-plane Location by the Tilt Needle

Several methods have been developed to locate the position of the magnetic median plane in cyclotron-like magnets. Some laboratories have used variations of the pivoted steel tilt needle with a mirror on the needle and a long light beam to indicate deflections. The needle aligns itself in the magnetic field quite accurately if bearing friction is small and the needle is exactly balanced. The needle mount can be raised and lowered in the field between poles to locate that level where the light beam indicates a vertical needle position. In the slightly convex field between cyclotron poles this position can be located within a few millimeters. The unit must be placed at many points over the pole surface to obtain a plot of median-plane location.

A common phenomenon in such magnets is to find the median plane dished into a shallow saucer shape caused by asymmetries in the magnet iron or of the reinforcing iron in the foundations. A similar shape will result if the coils are not located symmetrically or if there is a shorted turn. This property can be used to compensate and correct this type of deviation in median plane. At MIT such a "dished" median plane was corrected by connecting an external resistor in parallel with one of the coil layers, which reduced the current in this layer and in this case had the effect of flattening the median plane.

In using the magnetic needle for median-plane studies, an improved technique is to superimpose a small high-frequency transverse magnetic field on the needle (using a pair of small ac coils) to set it into vibration and cancel out bearing-friction effects. The frequency can be chosen to resonate with the mechanical oscillation frequency of the needle; this resonant frequency is itself a good measure of the axial component of magnetic field.

Median-plane Location Using Balanced Coils

Another technique for observing the median-plane location is the use of two small identical coils connected in series opposition and observed with

the integrating fluxmeter. The coils are located one above the other and arranged so the pair can be moved transversely across the median plane, keeping exact alignment. A net current pulse results if one coil moves through a stronger field than the other, which will occur in the convex field if the pair of coils is not balanced about the median plane. The magnitude and sense of the pulse can be observed for equal displacements with the center of the pair at different locations relative to the geometric central plane. The location of the magnetic median plane will be halfway between positions where the current pulses (of opposite sign) are equal in magnitude.

Median planes can also be located by very carefully designed search coils set on edge so that they measure only the radial component of the magnetic field. Such coils and their mechanical supports must be made and located with very high precision. The small residual errors in location can be eliminated by precise reversals of the coil around horizontal and vertical axes.

The Wire Orbit

One of the more ingenious devices for locating the median plane, and at the same time finding the magnetic center of the field between poles, involves the use of a current-carrying loop of wire. The technique is described in the third University of Chicago *Synchrocyclotron Progress Report.*[11]

A flexible wire carrying a current in a uniform magnetic field is acted upon by a force normal to the wire and to the field, so it will be stretched into a circular loop. The magnetic force per unit length of wire, which is given by the vector cross product $\mathbf{i} \times \mathbf{B}$, is balanced by the radial component of tension F in the wire:

$$Bi = \frac{F}{r} \qquad \text{or} \qquad Br = \frac{F}{i} \tag{8-29}$$

A charged particle in the magnetic field traverses a path of radius of curvature r if

$$\frac{mv^2}{r} = Bev \qquad \text{or} \qquad Br = \frac{mv}{e} \tag{8-30}$$

where mv is the momentum of the particle and e is its charge. If the weight of the wire is neglected, it will take up a position in the field in which

$$\frac{F}{i} = \frac{mv}{e} \tag{8-31}$$

So current and tension in a wire loop can be observed and used to obtain a measure of particle momentum at that radial position.

Actually the wire will have a finite weight. In the vertical field of a cyclotron magnet the loop will lie in the horizontal plane, and its weight will cause it to fall below the magnetic median plane in which the particle orbit is located. If the wire is supported at one point, where the leads adjoin, it will sag in the form of a catenary. Such a flat catenary can be approximated by a parabola, and the center of mass will be at one-third the height from the bottom to the top of the curve.

The method used to observe the median plane at Chicago was to support the current-carrying loop at one point, where flexible current leads were brought out, by a hydrometer float which allowed the loop to seek its own position of stability in the field. The outward forces stretch the loop into a circle, with the tension becoming greater as the current increases. The loop tends to move horizontally on the float until it

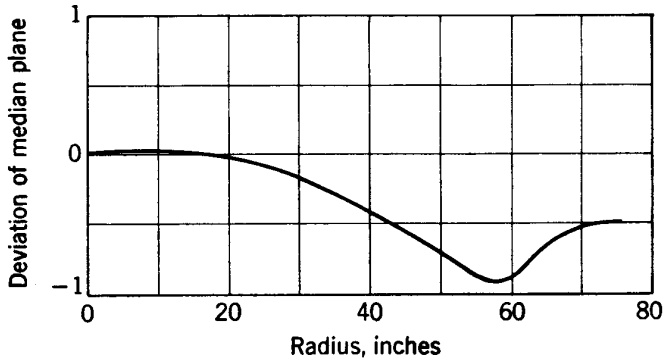

Fig. 8-15. Vertical location of magnetic median plane, before correction, in the University of Chicago synchrocyclotron magnet.[11]

encloses the maximum number of flux lines, so it picks the magnetic center of the field. The hydrometer stand can be varied in height, and the level of the float can be used to measure the combined weight of the loop plus any vertical unbalance in magnetic forces. If the magnetic forces are zero, the position of the float will not change with increase in current and tension. So the height of the stand is varied until loop position does not change with change in current. At this level the float supports just the weight of the wire loop. Heights at which this balance occurs can be measured for different loop radii. A correction must be applied for the catenary curve followed by the wire because of its distributed weight. The results of such a measurement for the Chicago synchrocyclotron magnet (Fig. 8-15) show a deviation of the median plane from the center of the geometrical gap by nearly 1 in. This deviation was corrected by suitably placed shims of iron.

The location of the center of the stretched wire loop is a measure of the displacement of the magnetic center. In the uncorrected Chicago magnet the mean center for large loops was 2 in. away from the geometrical center of the 130-in.-diam pole faces. To correct this deviation, iron

shims were added to the pole faces on the side away from the displacement. The magnitude of the correction needed (shim thickness) was estimated from the force required to displace the floating wire loop sideward. The final shim pattern obtained after experimental studies was spot-welded to the pole faces, resulting in an essentially constant center for orbits at all radii.

Another good discussion of the wire-orbit method is a report by Cranberg[19] at Los Alamos, available through the United States Atomic Energy Commission.

8-8. MEASUREMENTS IN TIME-VARYING FIELDS

The measurement of alternating or pulsed magnetic fields involves techniques entirely different from those used for steady fields. Snatch coils, balanced loops, and pivoted needles are all useless. The wire orbit is stable only under very restrictive conditions. On the other hand, a varying field has the inherent property of inducing emfs in stationary coils, so a useful measure of the rate of change of flux is readily available. Instruments which can integrate this rate of change from zero field up to some higher field point in the cycle will record the magnitude of this higher field. The most critical problem is the timing of the integrating instrument, so as to obtain an instantaneous measure of the field.

The kinds of measurements required for pulsed fields also differ from those needed for dc fields. One of the most important properties is the time rate of change. This is readily obtained from the output of a fixed coil if the coil has been suitably calibrated. Absolute values of field as a function of time measured from the start of the cycle are also important, to determine orbit radius, particle energy, and frequency of rotation. A more difficult problem is to observe the variation with time of the field distribution across the pole face, due to the varying permeability of the iron circuit or to the varying magnitude of eddy-current fields in the poles or conductors. So special techniques have been developed to study the dynamic properties of the fields in pulsed accelerators.

The Integrating Fluxmeter

The integrating fluxmeter, already discussed in connection with measurements of dc fields, is equally applicable to measurements of pulsed fields. The principle is the same, but the flux change through the search coil is achieved not by moving the coil to a different field, but by leaving the search coil fixed in the changing field. Since the measurement takes place fairly rapidly, problems of zero drift in amplifiers are not so serious and often can be neglected.

The integrating fluxmeter measures only the total change in flux

through the search coil; the "integration constant," which may correspond to an appreciable initial remanent field, does not register. Consequently a measurement of total field as a function of time must include a preliminary measurement of the initial field by dc techniques.

To determine the flux density at a particular instant a variety of techniques have been employed. The integrator output can be displayed on an oscilloscope with a sweep circuit giving a time base, and time markers from an electronic clock can be superimposed on the trace; the output can be observed visually and measured at any desired instant. Or the scope trace can be photographed on a moving-film camera, providing a permanent record for study and measurement. Or an electronic technique can apply the output potential to the grid of a trigger tube such as a thyratron; when the potential reaches a predetermined value, the tube fires, giving a time mark representing a given value of magnetic field which can be compared with time signals from an electronic clock. Experimenters will be able to invent other devices for displaying the signal as a function of time.

A detailed description of the application of the integrating fluxmeter to a pulsed field will be found in the paper of Green, Kassner, Moore, and Smith[20] describing magnetic measurements on the magnet of the Brookhaven cosmotron.

The Peaking Strip

An instrument which gives a precise measure of field at low field intensities is the magnetic peaking strip. The effect is based on the voltage pulse induced in a coil surrounding a sample of magnetic material when the direction of magnetization is reversed. The sample should have the highest possible permeability and the steepest or most "rectangular" B-versus-H hysteresis loop, in order that the induced voltage pulse should be a maximum. The sample should also have a large ratio of length to diameter, to minimize the "demagnetization coefficient" associated with the poles induced in the sample. The principle has been employed in magnetics laboratories for many years; a good published description of such an instrument is that by Kelly[21] as part of the program of measurement in the Brookhaven cosmotron laboratory.

A typical peaking strip would use a molybdenum-permalloy wire as a sample; the one used by Kelly was 0.002 in. diam and 2 in. length, sealed inside a small-bore quartz tube and carefully annealed. A small pickup coil of fine wire is wrapped around the center of the sample, and the unit is enclosed in a bias coil of solenoidal shape with which known bias fields can be imposed on the sample. Figure 8-16 is a schematic illustration of a peaking strip within a bias coil. The applied field on the sample can be made to traverse the hysteresis loop by applying a small-amplitude

60-cycle excitation to the bias coil, which induces voltage pulses in the pickup coil when the sample passes through zero excitation. Two pulses of opposite polarity are induced as the sample traverses the hysteresis loop. Figure 8-17 illustrates the hysteresis loop and the induced pulses of emf which are developed in the pickup coil.

For the measurement of steady magnetic fields a dc bias current is applied to the bias coil; this current produces a field on the sample equal

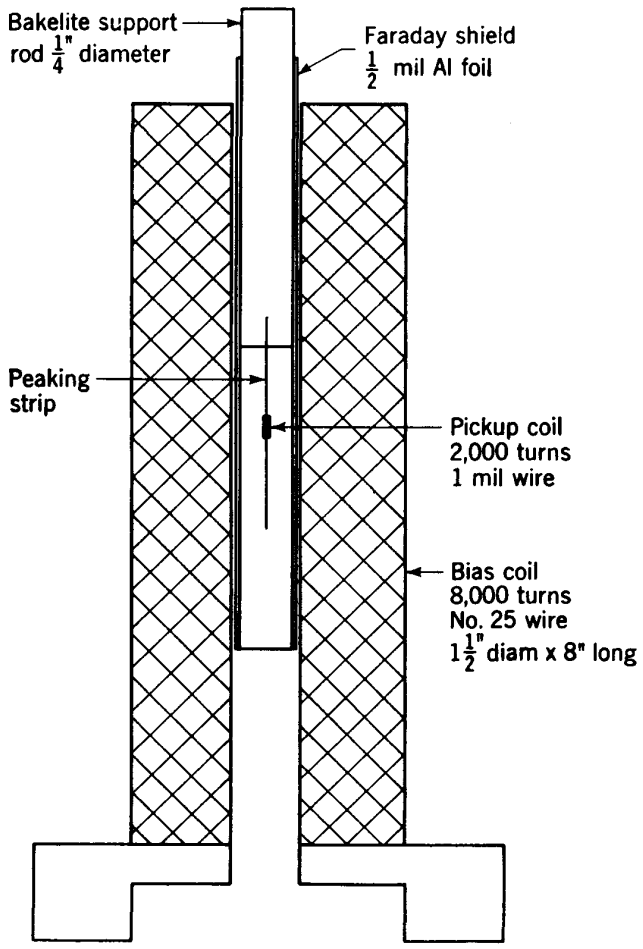

Fig. 8-16. Peaking strip and bias coil used with the cosmotron.[21]

and opposite to the one to be measured, so the net field will be zero. The small-amplitude 60-cycle excitation will result in a double-peak signal (Fig. 8-17) which can be presented on an oscilloscope with a phased 60-cycle sweep circuit to form a stabilized pattern. A balance is obtained when the two peaks of the output signal are equalized. The bias current which gives this result is a measure of the dc field.

Another useful application of the peaking strip is to the measurement of ac or pulsed fields. Since the field to be observed develops the necessary dB/dt, the 60-cycle oscillating component of field is not required, but the

dc-bias measuring field is retained. With a pulsed magnet, one output peak is observed when the rising field passes through the value imposed by the bias coil; the other output peak occurs on the falling side of the magnet cycle at the same flux density. The output peaks are quite narrow compared with the excitation pulse, so they provide time signals indicating the instant when the pulse traverses the value set by the bias coil. For comparative measurements, such as the radial flux distribution across a pole face, one peaking strip can be in a fixed location to give a time signal and another can be moved from point to point across the field. If the two pulses, displayed on the same oscilloscope, coincide in time, the fields in the two locations are equal; if they differ, the bias on one coil can be adjusted to bring them into coincidence, and the bias current difference is a measure of the difference in fields at the two locations.

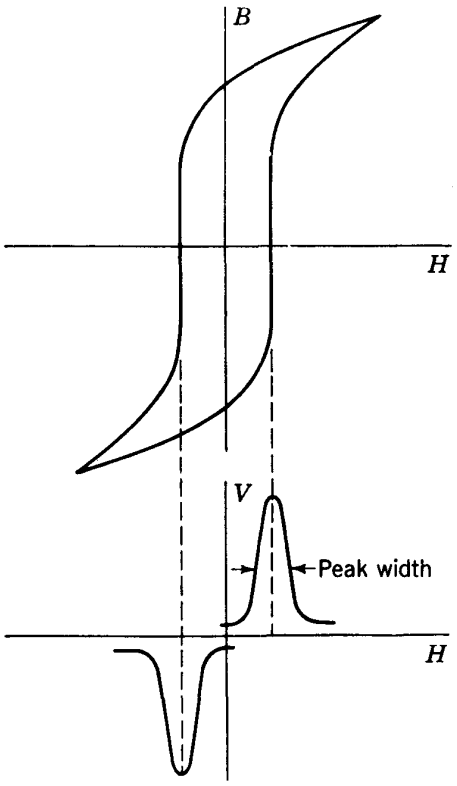

Fig. 8-17. Hysteresis loop for a peaking strip and induced voltage pulses in a pickup coil.

Pulses from such a peaking strip can be used to give a precise time signal for operation of other devices in a pulsed accelerator installation, such as the beam-injection circuits and other phased operations.

The sensitivity of the peaking strip depends on the width of the output peak, which is a function of the rate of change of field (dB/dt) and of the uniformity of the field over the length of the wire. The time width of the peak as observed on an oscilloscope can be translated into the width in gauss if the rate of change of field is known. In the Brookhaven studies[21] a rate of 10^6 gauss/sec gave an output peak with a half-power width of about 0.02 gauss; at a slower rate of 10^4 gauss/sec the observed width was 0.2 gauss.

The output peak is also broadened if the field is not uniform over the length of the wire sample. Again at Brookhaven it was found that a variation in field of 1 gauss/in. along the length of wire led to an undesirable increase in output peak width. This means that a long peaking strip is restricted in use to relatively uniform fields. A shorter strip can be used to measure fields with a finite gradient, but it suffers from a reduced effective permeability due to the demagnetization effects of the induced poles, which reduces the amplitude of the output peak and also widens the peak.

A serious limitation on the use of the instrument is the physical length of the bias coil; it can be used only in magnets with widely spaced poles. The useful range is limited to a few hundred gauss, set by the field which can be produced in the bias coil. Although larger coils could produce higher field, the larger size is a handicap. A strong bias-coil field can also distort the field distribution to be measured by changing the flux distribution in the iron pole faces, which will disturb the results.

Nuclear Resonance Fluxmeter

The fluxmeter described in the previous section, which utilizes the precessional frequency of the proton magnetic moment as a measure of magnetic field, can also be adapted to measurements in pulsed or alternating fields. The calibrating relation between magnetic field and the resonance frequency was given in Sec. 8-7. In the application to a varying field a predetermined microwave frequency is applied to the coil surrounding the sample; when the magnetic field passes through the value which is in resonance with this frequency, the oscillating power in the coil will drop. The output of the regenerative detector supplying the coil can be displayed on an oscilloscope with a calibrated time base; when the magnetic field traverses the nuclear resonance, the output will show a sharp dip which can be located to good precision with any one of the several techniques mentioned previously.

Nuclear resonance frequencies are in the 100-megacycle range at high magnetic fields (86 megacycles/sec at 20 kilogauss, for example) but are well within the range of modern techniques. The high frequency is an advantage in measurement of pulsed fields, increasing the sharpness of the resonance. The sharp pulse output can be used, like a peaking-strip pulse, to trigger other circuits in the accelerator; it has the advantage that it can be used near the maximum in the magnet excitation cycle for such purposes as triggering beam ejection systems or target-moving devices.

The chief difficulty in the use of this instrument is the electronic problem of electrical "noise" generated in the magnet pulsing circuits. The highest quality of electronic design practice is required in the construction, filtering, and shielding of the regenerative detector and the display circuits.

8-9. MEASUREMENTS IN HIGH-GRADIENT FIELDS

The ratio of magnetic gradient to field, $\frac{1}{B}\frac{dB}{dr}$, used in AG synchrotrons (Chap. 15) is a quantity which should be independent of the magnitude of field B if AG focusing is to be maintained throughout the accelerating

cycle in the pulsed magnet. A typical problem in AG-magnet pole-face design is to observe the gradient directly at different flux densities without depending on computations from field plots.

Gradient-to-field ratios used in AG accelerators are about 0.1/in., which means that the flux density varies by about 10 per cent across a 1-in. radial extent of pole face. So the magnitude of the field changes significantly across the width of even very small search coils. Fortunately, the most useful form of gradient field is one which has a constant gradient across the pole faces, so the errors introduced by using search coils of finite size compensate and measured values of gradient are not seriously perturbed. However, measurements in a region where gradient is changing rapidly may be in serious error if large coils are used. These errors can be removed to any desired order by special coil designs discussed by Garrett.[22] By the use of correct dimensions of search coils and by inclusion of auxiliary coils, higher-order terms in the field can be canceled out to any desired point so that the emf induced in the search coil is a true measure of the field at its center.

Measurements on AG magnets are further complicated by the fact that the nonuniform field is usually changing rapidly with time. The field pattern must be known at all times in order that the perturbing effects of eddy currents in the magnet poles and in vacuum-chamber structures can be evaluated.

A detailed discussion of the problems of measurement of fields of AG magnets will be found in the published thesis of B. De Raad,[23] which describes the methods used and considered by the CERN group.

In each magnet design program the first steps have been taken by a combination of computational methods and measurements on rough models. These establish the gross shape of the field and the magnitude of gradient between pole faces. Instruments and techniques described in Sec. 8-6 have been employed. Laminated models are then built and excited with pulsed or ac power to study the electrical properties such as inductance, magnetic and eddy-current losses, and power consumption.

The "Grad-coil"

Magnetic-field and gradient measurements at high flux densities, at or near the peak of the excitation cycle, can be obtained with fixed coils, using the integrating fluxmeter described in the last section. In order to integrate from zero to the maximum field being measured, time-trigger pulses are required. These can be obtained from peaking strips at low field or from a nuclear-resonance fluxmeter at high fields.

A typical gradient coil (grad-coil) used with the integrating fluxmeter consists of a pair of coils of identical size and shape spaced a short distance apart radially and located with the geometric center of the two coils at

the chosen position in the field. When properly calibrated and balanced, the gradient $\frac{1}{B}\frac{\Delta B}{\Delta r}$ is given by the ratio of the difference in output of the two coils to the sum of the outputs. With two coils of $\frac{1}{4}$ in. diam spaced $\frac{1}{2}$ in. between centers, the gradient can be measured to 0.5 per cent accuracy. Such coils are used to survey the field between poles and to study the radial distribution. Even smaller coils can be used to observe the details in the fringing field at the ends of the magnet sectors. Long coils which span the full length of a magnet sector can also be used to obtain average values of gradient including the fields outside the ends of the sector.

The "Vibrating Coil"

The vibrating coil is an instrument which has been developed[24] to measure field gradients directly. A small coil is made to vibrate at constant frequency and constant amplitude across the nonuniform field; the voltage output is proportional to the difference in field ΔB from one end to the other of the stroke. The output of the coil is a sinusoidal voltage of maximum amplitude given by

$$V_m = 2\pi f \, \Delta x \, Na \frac{\Delta B}{\Delta x} \tag{8-32}$$

where f = frequency of vibration
Δx = amplitude
Na = coil constant (number of turns times area)
$\frac{\Delta B}{\Delta x}$ = magnetic gradient

The instrument can best be calibrated in a known field with known gradient; computing the gradient from dimensions and vibration amplitudes is inexact. The instrument referred to above used a very small, light coil of several hundred turns mounted on a soda straw attached to the diaphragm of an audio speaker which was driven by an audio amplifier at frequencies up to 200 cps and for which the amplitude was about 0.02 in. It was used primarily for measuring gradients in dc models of strong-focusing magnets.

Remanent-field Measurements

Most synchrotron magnets are pulse-powered unidirectionally, with the field varying from zero (or close to zero) to maximum and back to zero cyclically. The magnitude of the remanent field is strongly affected by the detailed shape of the preceding cycle during which the field is decreasing to zero. The flux distribution and field gradient between pole

faces due to the remanent field is not necessarily the same as that for a powered field. At low flux densities (injection conditions) the remanent field adds to the powered field to produce the total field between poles, and the resulting gradient may differ from that at higher excitations. A technique of measurement is needed which measures total field, not just that fraction due to the applied excitation. Unfortunately, the output of induced current in coils measures only the component due to the rate of change dB/dt. This measurement problem is most severe at the low-field portion of the excitation cycle, so the instruments required must be able to detect small fields with adequate precision during early times in the cycle without being disturbed by the high fields during the remainder of the cycle.

One technique which has proved successful[25] utilizes the peaking strip discussed in Sec. 8-8. Two peaking strips are used, separated by a short distance and with axes parallel, so as to obtain two readings in the gradient field. Each peaking strip is enclosed in a bias coil and also has a pickup coil to generate signal peaks when the net field through the strip passes through zero. The two output signals are displayed on an oscilloscope. With equal bias fields applied to the two strips, the two signal peaks will be displaced in time in a gradient field. Then if the bias currents are adjusted to make the pulses coincide in time, the difference in field in the two locations can be measured directly by the currents in the bias coils. If the spacing is accurately known, the field gradient can be determined. The accuracy of the results, in terms of gradient in a field of 25 gauss, is about 0.5 per cent. Note that this technique is a measure of total field including the remanent field and will also include any distortions in field due to eddy currents.

Measurements of very high precision have been made on the magnets for the 30-Bev AG synchrotron at Brookhaven by comparing the outputs of search coils in two identical magnets. One magnet is used as a permanent reference. The output of a fixed search coil in its field is compared with the output of a search coil in the magnet undergoing test by balancing the outputs in a resistance bridge. By careful attention to the calibration and precision of the resistors used in the bridge, field measurements have been obtained which, over most of the range from 100 to 13,000 gauss, are precise to 2 or 3 parts in 10,000.

In making measurements of this order of precision the final limit to accuracy may be set, not by the magnetic measuring equipment, but by the mechanical devices used to locate the equipment. The search coil used in the Brookhaven measurements was a very carefully constructed 11-turn coil with a turn area of 1 cm by 3 m. Although the coil was made of 0.002-in. tungsten wire stretched around precisely constructed supports and was shielded from air currents by enclosure in a glass tube, and although the coil supports were constructed with the highest mechan-

ical precision attainable, still a large fraction of the final error in the measurements was due to inability to determine the exact location of the coil with respect to the magnet structure.

REFERENCES

1. J. D. Howe and I. Walerstein, *Rev. Sci. Instr.*, **9**:53 (1938).
2. M. Foss, J. G. Fox, R. B. Sutton, and E. C. Creutz, *Rev. Sci. Instr.*, **22**:469 (1951).
3. L. V. Bewley, "Two-dimensional Fields in Electrical Engineering," Macmillan (1948).
4. Ernst Weber, "Electromagnetic Fields," vol. I, "Mapping of Fields," Wiley (1940).
5. H. B. Dwight and C. F. Abt, *Rev. Sci. Instr.*, **7**:144 (1936).
6. R. V. Southwell, "Relaxation Methods in Theoretical Physics," Oxford (1946).
7. William H. McAdams, "Heat Transmission," 3d ed., McGraw-Hill (1954).
8. R. L. Daugherty, "Hydraulics," McGraw-Hill (1937).
9. J. Symonds, *Repts. Progr. in Phys.*, **18**:83 (1955).
10. W. Y. Chang and S. Rosenblum, *Rev. Sci. Instr.*, **16**:75 (1945).
11. H. L. Anderson and J. Marshall, University of Chicago, *Synchrocyclotron Progress Report*, I (July, 1947–July, 1948); II (July, 1948–July, 1949); III (July, 1949–July, 1950).
12. E. R. Andrew, "Nuclear Magnetic Resonance," Cambridge (1955).
13. P. Grivet, "La Resonance paramagnétique nucléaire," *Centre natl. recherche sci.*, Paris (1955).
14. A. Roberts, *Rev. Sci. Instr.*, **18**:845 (1947).
15. M. Packard, *Rev. Sci. Instr.*, **19**:435 (1948).
16. N. J. Hopkins, *Rev. Sci. Instr.*, **20**:401 (1949).
17. C. G. Dols, E. W. Skiff, and P. G. Watson, *Rev. Sci. Instr.*, **29**:349 (1958).
18. G. L. Pearson, *Rev. Sci. Instr.*, **19**:263 (1948).
19. L. Cranberg, "Magnetic Calibration by the Floating-wire Method," Los Alamos Report AECU-1670 (Nov. 23, 1951).
20. G. K. Green, R. R. Kassner, W. H. Moore, and L. W. Smith, *Rev. Sci. Instr.*, **24**:743 (1951).
21. J. M. Kelly, *Rev. Sci. Instr.*, **22**:256 (1951).
22. M. W. Garrett, *J. Appl. Phys.*, **22**:1091 (1951).
23. B. De Raad, "Dynamic and Static Measurements of Strongly Inhomogeneous Magnetic Fields," Uitgeverij Excelsior, 's-Gravenhage, Holland (1958).
24. J. F. Frazer, J. A. Hofmann, M. S. Livingston, and A. M. Vash, *Rev. Sci. Instr.*, **26**:475 (1955).
25. H. Nysater, *J. Nuclear Instr.*, **4**:44 (1959).

9

The Principle of Phase Stability

The discussion up to this point represents, in large measure, the status of the accelerator field in 1945. Although accelerator development continued during World War II, it was largely within closed laboratories, and very little was published. The prewar accelerators which have been described are all limited in maximum energy. Some, such as the electrostatic generators, are bounded by physical limitations such as the breakdown of insulation at high electric fields. In the cyclotron the relativistic increase in mass destroys the validity of the resonance principle at high energies. The betatron, although operating in the 100-Mev range, is limited by radiation loss. None of these machines can maintain acceleration to indefinitely high energies.

Postwar development of accelerators follows primarily from a new principle—the principle of phase stability. This principle was discovered independently and almost simultaneously in two countries; once again parallel developments in science led to an apparent coincidence. In 1944 Veksler[1] in the U.S.S.R. published a presentation of the new

principle. Early in 1945, before Veksler's paper reached the United States, the same principle was published by McMillan[2] of the University of California.

9-1. BASIC CONCEPTS

The new principle can be stated as follows: In a phase-stable accelerator, particles will be accelerated at a series of gaps by an alternating electric field. The gap separation and the frequency and strength of the field are adjusted so that a particle of a specified energy arriving at a particular gap at a specified equilibrium phase of the accelerating field will arrive at the next gap at the same phase. Now it can be shown that particles of the correct energy arriving at the gap at incorrect phases in the neighborhood of the equilibrium phase will experience an automatic correction toward the correct phase at succeeding gaps. In general, particles with slight phase or energy errors will continue to be accelerated with minor oscillations in energy and phase around the correct energy and the equilibrium phase. A mathematical demonstration of this principle will be given in the following sections.

This principle has found its most important applications in three accelerator types: the linear accelerator, the synchrotron, and the synchrocyclotron. Machines using this principle are known as synchronous or phase-stable accelerators as distinguished from the earlier resonance accelerators such as the cyclotron. The differences between the several types of synchronous accelerators come from different combinations of the geometric arrangements of magnetic and electric fields. They have the common feature that stable oscillations are set up in the phase at which the accelerating gap is crossed; particles remain in synchronism with the oscillating fields until they reach the physical limits of guiding and accelerating fields. In principle, acceleration can be continued to indefinitely high energies in synchronous accelerators. At present, upper limits for acceleration are set only by economic considerations.

In the linear accelerator, particles are accelerated in a linear path by a field of constant frequency. Separations between accelerating gaps increase as particle energy increases in such a fashion that the time taken by a particle to travel from any gap to the next gap is a constant, usually a full period of the accelerating field. The equilibrium phase in the linear accelerator is a phase on the rising side of the field wave across the gap. If a particle arrives too soon, it will receive too little additional energy at the gap; since now it travels too slowly, it will arrive at the next gap at a slightly later phase, which is closer to the correct equilibrium

---

At the head of the facing page are photographs of the discoverers of the principle of phase stability. On the left is E. M. McMillan; on the right is V. I. Veksler.

phase. If it arrives at the first gap too late, it will gain too much energy and will make the transit to the next gap faster than it should; again its phase at the second gap will be moved toward the correct phase. Thus the phase-correction mechanism becomes evident, at least for this particular case. If both phase of arrival and energy are incorrect, the situation becomes more complicated; we shall see later that phase stability is still effective.

The synchrotron was the machine whose invention by Veksler and by McMillan yielded the first understanding of phase stability. This is a machine in which particles are maintained in generally circular orbits by a magnetic field. As particle energy increases, the magnetic field is increased at such a rate that the radius of the particle orbit remains constant. Acceleration takes place at one or more gaps around the orbit. As the particle velocity increases, the frequency of the field must be increased to maintain a constant phase shift as the particle goes from gap to gap. Here the equilibrium phase is on the falling side of the field wave. Particles arriving too soon gain too much energy and travel on orbits of larger radius and hence larger circumference; they take longer to arrive at the next gap and so arrive nearer the equilibrium phase. Particles arriving too late gain too little energy, travel on a smaller orbit, and make too rapid a transit; they arrive, as before, nearer to the equilibrium phase.

The synchrocyclotron is a cyclotron in which the accelerating frequency is decreased as particles become relativistic. Stability of phase is maintained by essentially the same mechanism as exists in the synchrotron. This procedure was proposed by prewar cyclotronists, but its eventual success was not appreciated until the enunciation of the principle of phase stability.

The characteristics of these three machines may be summarized as follows:

Accelerator type	Frequency	Radius of particle orbit	Magnetic field
Linear accelerator	Constant	Infinite	Zero
Synchrotron	Increasing	Constant	Increasing
Synchrocyclotron	Decreasing	Increasing	Constant

In the sections which follow we shall enunciate the principle of phase stability for these various machines and examine the consequences for each case. First, however, we shall present a traveling-wave concept of the accelerating field; this concept will simplify the mathematical treatment and should clarify the description of the mechanisms which result in phase stability.

9-2. FIELD PATTERNS IN SYNCHRONOUS ACCELERATORS

The mechanism of acceleration in the synchrotron, the synchrocyclotron, and the linear accelerator can be described in rather simple, yet general terms. The particle to be accelerated crosses a gap across which is applied a radiofrequency field. If the particle is the equilibrium particle, it will traverse the gap at a prescribed phase of the accelerating field such that it gains a prescribed increment of energy. It now coasts through a region where it experiences no accelerating field and finally arrives at another gap (which may be the same gap as before), again at the prescribed accelerating phase. The sequence of acceleration and drift is repeated until the particle has gained the total energy for which the machine is designed.

For a mathematical representation of the accelerating field we shall consider the simplest case in which the gap is infinitesimal in length and in which the particle drifts from one gap to the next in one full period of the radiofrequency signal. If s represents distance along the particle path and s_n is the distance from the nth gap to the $(n + 1)$st gap, this means that

$$s_n = \frac{2\pi v}{\omega} \tag{9-1}$$

where v is the particle velocity and $\omega/2\pi$ is the radiofrequency.

The field configuration in the accelerator now consists of a high field for the infinitesimal distance across the gap and zero field over the distance to the next gap. This pattern can be represented by a Fourier series. If $V \sin(\omega t)$ is the gap voltage, the field along the particle orbit will be

$$E_s = \sum_n 2\frac{V}{s_n} \sin(\omega t) \cos\frac{n\omega s}{v} \tag{9-2}$$

which can be rewritten in the form

$$E_s = \sum_n \frac{V}{s_n}\left[\sin\left(\omega t + \frac{n\omega s}{v}\right) + \sin\left(\omega t - \frac{n\omega s}{v}\right)\right] \tag{9-3}$$

Equation (9-2) represents a standing-wave field pattern; Eq. (9-3) represents a traveling-wave pattern. Both representations are valid, but the traveling-wave picture is by far the most useful. In Eq. (9-3) only one term is significant. The wave represented by the term $\sin(\omega t - \omega s/v)$ is a wave which travels in the same direction as the particle and at the same velocity as the particle velocity. The particle may be considered

to be riding on this wave at an accelerating phase such that it continually gains energy from its electric field. All the other waves are traveling either at very different velocities or in the opposite direction to the particle motion. As a result these waves alternately accelerate and decelerate the particle, and their over-all effect after traversal of many gaps becomes completely negligible. The particle motion can, accordingly, be deduced from consideration of the effects of only the one significant traveling-wave component.

The traveling-wave concept has a further significance in accelerator design. Many other gap configurations and methods of gap excitation can be devised which, on analysis into traveling waves, yield a component with the same velocity and direction as those of the particle. These configurations are just as useful for acceleration of particles as the simple one described above. For example, the gaps can be separated by the distance traveled by a particle in one half-period of the radiofrequency. If the gap voltages alternate in polarity, the field pattern will include the same significant traveling-wave component. This system is the one used in the cyclotron and the synchrocyclotron.

Before we proceed to utilize this field component in analysis of particle motions, it is necessary to take into account the fact that the particle velocity is changing during acceleration. Also it may be necessary to vary the radiofrequency during acceleration so that the particle always arrives at the gap at the correct phase. The gap voltage may also vary along the complete particle orbit. We therefore represent the significant field component as follows:

$$E_s = E(s) \sin\left(\int \omega\, dt - \int \frac{\omega\, ds}{v} + \phi_0\right) \tag{9-4}$$

If the field E and the frequency are made to vary in the correct fashion, the first two terms in the argument of the sine will cancel and the particle will continually see an apparent accelerating field whose magnitude is $E \sin \phi_0$.

In the applications of these fields in the sections which follow, it will continually be necessary to remember that s and $\dot{s}$ are the position and velocity of the general particle, while v is the velocity of the accelerating wave.

9-3. THE PRINCIPLE OF PHASE STABILITY

We must now investigate the behavior of a particle which has fallen behind or has reached a phase ahead of the correct equilibrium phase on the traveling wave. First we consider the simplest case of the nonrelativistic linear accelerator in which the particle is traveling in a straight line with approximately the same velocity as the significant traveling-

wave field component. There will be two phases at which the particle can continue to gain energy at the correct rate. One of these phases will correspond to a point on the rising side of the wave; the other will correspond to a point on the falling side of the wave. A particle near the correct point on the rising side of the wave but delayed a little in phase will continually gain too little energy and so will slip farther and farther behind; another particle a little ahead of the correct point on the rising side will continually gain too much energy and also will move farther and farther away from the correct phase. Evidently particles on the rising side of the traveling wave are not stable in phase. On the falling side of the wave, however, the opposite is true. A particle lagging in phase will gain more energy and will tend toward the correct phase, and a particle leading in phase will gain less energy and will slip backward toward the correct phase. Stable oscillations will be set up around the correct phase; it will thus be possible to accelerate a group of particles which have the correct range of initial phases grouped around the stable phase on the falling side of the accelerating wave. The particle is behaving like a surf rider who continues to be accelerated so long as he rides ahead of the wave but is thrown back into the sea if he slips behind the wave crest.

Some confusion may arise in the reader's mind if he attempts to trace the particle orbit through the standing-wave pattern described by Eq. (9-2). In this case he will find that the stable phase in the linear accelerator is on the rising side of the standing wave observed when he maintains a fixed position in space and watches the particles go by. Since the traveling-wave concept is mathematically much more fruitful and conceptually clearer, we shall adopt the procedure of traveling with the equilibrium particle and observing only the significant traveling-wave component.

In the synchrotron and the synchrocyclotron the particle behavior is more complicated. A particle which has too much energy travels on a circle of too great radius and actually takes a longer time to return to the accelerating gap than does a particle of the correct energy. In other words, the faster the particle travels the farther it will lag behind the traveling wave. This "Alice through the Looking Glass" process reverses the arguments just outlined for the linear accelerator. In the circular machines the particle has phase stability around an accelerating phase on the rising side of the accelerating traveling wave.

The mathematical formulation of these qualitative ideas can proceed to some extent with such generality that it relates to all phase-stable machines. In our analysis we shall use time as the independent variable. Parameters describing the equilibrium particle will be distinguished by zero subscripts. The nonequilibrium particle will be assumed to have parameters which deviate from the equilibrium parameters by relatively small amounts. For example, the momentum p of a general nonequi-

librium particle will be written

$$p = p_0 + \Delta p$$

where Δp is assumed to be small compared with p_0. The particle which is not at the correct phase of the accelerating wave will have a position error Δs.

We shall write the equation of motion for the nonequilibrium particle for the most general case, in which the particle is bent on a circular arc of radius r by a magnetic field $-B_z$. The equation of motion will be the azimuthal component of the general equation of motion (5-14) in cylindrical coordinates:

$$\frac{1}{r}\frac{d}{dt}(rp) = \dot{p} + \frac{\dot{r}p}{r} = eE \sin\left(\int \omega\, dt - \int \frac{\omega\, ds}{v} + \phi_0\right) + eE' + e\dot{r}B_z \tag{9-5}$$

where the first term on the right is the traveling-wave component of the accelerating field and the second term eE' represents all other possible accelerating or decelerating fields such as those corresponding to betatron acceleration by a changing magnetic flux linking the orbit, or decelerating fields corresponding to energy loss due to electromagnetic radiation. But the momentum of a particle on an orbit of radius r in a field B_z is given by

$$p = erB_z \tag{9-6}$$

whence

$$\frac{\dot{r}p}{r} = e\dot{r}B_z \tag{9-7}$$

and Eq. (9-5) simplifies to

$$\dot{p} = eE \sin\left(\int \omega\, dt - \int \frac{\omega\, ds}{v} + \phi_0\right) + eE' \tag{9-8}$$

The radius r has disappeared from this equation except for its possible entry through E' or v. Since there is no E' term in the linear-accelerator case, Eq. (9-8) is a general equation describing the motion in all synchronous accelerators. It is valid for both relativistic and nonrelativistic motions.

We shall find it simplest to discuss the behavior of the nonequilibrium particle in terms of its phase. The particle phase ϕ is defined by

$$\phi = \phi_0 + \Delta\phi = \int \omega\, dt - \int \frac{\omega\, ds}{v} + \phi_0 \tag{9-9}$$

where $\Delta\phi$ is the phase error or deviation from the equilibrium phase ϕ_0. The precise evaluation of the phase error from this equation is rather

tedious; it is much easier to deduce its value from the sketch of the traveling wave shown in Fig. 9-1. A full wavelength of the traveling wave is v/c times the free-space wavelength corresponding to the radiofrequency field because the particle must cover one wavelength in one period of the accelerating field. Hence, in terms of the position error Δs of the nonequilibrium particle, the phase error is given by

$$\frac{\Delta\phi}{2\pi} = \frac{-\Delta s}{(v/c) \times \text{free-space wavelength}} = -\frac{\Delta s}{v/f}$$

where f is the frequency of the accelerating field. Hence

$$\phi = \phi_0 + \Delta\phi = \phi_0 - \frac{\omega\,\Delta s}{v} \tag{9-10}$$

In this notation Eq. (9-8) becomes

$$\dot{p} = eE \sin \phi + eE' = eE \sin (\phi_0 + \Delta\phi) + eE' \tag{9-11}$$

The general procedure for solution of the phase motion is now evident. Equations (9-10) and (9-11) must be combined and reduced to involve a

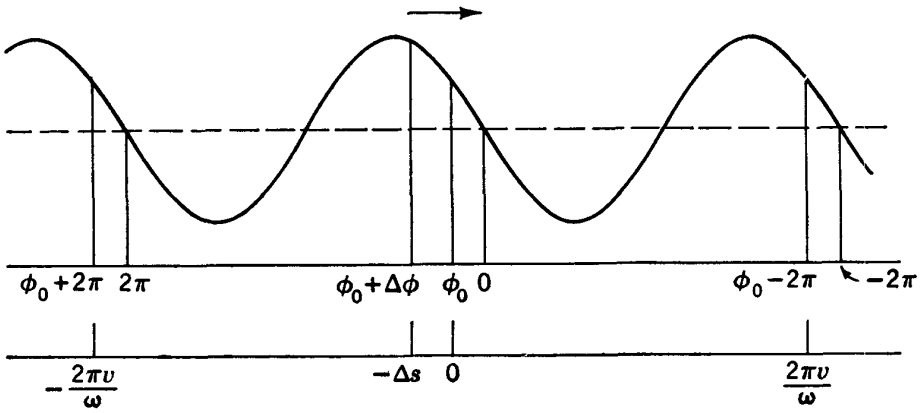

Fig. 9-1. Phase and distance scales for a wave traveling to the right. When $\Delta\phi = 2\pi$, $\Delta s = -2\pi v/\omega$; hence, in general, $\Delta\phi = -\omega\,\Delta s/v$.

single variable. The best procedures differ for the various accelerator types and will be treated separately in the sections that follow. Generally we shall derive a relation between the momentum error and the rate of change of the position error and so eliminate the momentum or position error between the two fundamental relations. This will leave us with a second-order differential equation for the phase error. If ϕ_0 has been chosen correctly, this equation will be found to describe a stable, usually damped, oscillation in phase around the equilibrium phase. It will be shown that, for a fairly wide range of initial phases, particles will continue to be accelerated without large deviations in energy from the design energy of the accelerator. Particles which fall outside of the

"acceptance phase range" will be lost early in the acceleration cycle. Particles which are accepted will undergo stable phase oscillations around the equilibrium phase during the acceleration cycle. This is a general statement of the principle of phase stability.

9-4. APPROXIMATE TREATMENT OF THE PHASE MOTION—THE PENDULUM ANALOGY

The general character of the phase oscillation can be shown by an approximate, nonrelativistic treatment in which the steady variations of frequency and equilibrium momentum are neglected in comparison with the more rapid periodic variations of the phase and momentum errors. We shall assume further that the electric field E is constant and that the term E' is negligible. Reminding the reader that v represents the wave velocity and p_0 represents the momentum of the equilibrium particle which is traveling at the wave velocity, we can now rewrite Eqs. (9-10) and (9-11) in the form

$$\frac{d\phi}{dt} = -\frac{\omega\,\Delta\dot{s}}{v} = -\frac{\omega\,\Delta p}{p_0} \tag{9-12}$$

and

$$\frac{d\,\Delta p}{dt} = eE(\sin\phi - \sin\phi_0) \tag{9-13}$$

We now differentiate Eq. (9-12) with respect to time, neglecting the relatively slow variation of ω and p_0. In the resulting expression we substitute from Eq. (9-13) to obtain

$$\frac{d^2\phi}{dt^2} + \frac{\omega eE}{p_0}(\sin\phi - \sin\phi_0) = 0 \tag{9-14}$$

This obviously represents an oscillation of ϕ about ϕ_0. For small deviations $\Delta\phi$ from the equilibrium phase ϕ_0 we can substitute $\Delta\phi\cos\phi_0$ for the quantity $(\sin\phi - \sin\phi_0)$ and Eq. (9-14) becomes the equation of simple harmonic motion provided that, as before, we neglect the slow variations of $\omega eE/p_0$. In this case we can write the solution of Eq. (9-14):

$$\Delta\phi = \Delta\phi_i \cos\left[\left(\frac{\omega eE}{p_0}\right)^{1/2} t\right] \tag{9-15}$$

where the subscript i indicates the initial value of the variable. The momentum error follows from Eq. (9-12); it is

$$\Delta p = \Delta\phi_i \left(\frac{p_0 eE}{\omega}\right)^{1/2} \sin\left[\left(\frac{\omega eE}{p_0}\right)^{1/2} t\right] \tag{9-16}$$

Generally it will be found that the values of E and ω in accelerators are such that the momentum error Δp is a small fraction of the equilibrium momentum p_0.

For oscillations of larger amplitude we must return to a study of Eq. (9-14). This is the equation of motion of a rather simple mechanical system. In one of its forms this system is a simple pendulum to which a constant torque is applied. A physical model of such a pendulum is illustrated in Fig. 9-2. It consists of a rigid pendulum mounted on a good bearing and having a cord carrying a weight wrapped around the hub. If the angle between the pendulum and the vertical is represented by ϕ, the angle at which it hangs at rest by ϕ_0, and if the length of the pendulum is chosen so that the ratio $\dfrac{\text{acceleration of gravity}}{\text{length of pendulum}}$ is equal to $\omega eE/p_0$, then the equation of motion of the pendulum will be identical with Eq. (9-14). Evidently the motion of this pendulum will be a stable oscillation around the rest position so long as displacements are small. If the displacements of the pendulum become so large, however, that it swings past the point where its mass is above the point of support, it will go into continuous rotation. The torque will continue to accelerate this motion, and the rotation will become continually more rapid so that never again can it stabilize itself. The particle-phase motion described by Eq. (9-14) is similar. If the phase oscillation carries the phase past certain safe limits, it will slip backward in phase with ever-increasing phase velocity. It will immediately be lost from the pattern of steady acceleration and will probably finish its career as a charged particle by drifting to one of the walls of the acceleration chamber.

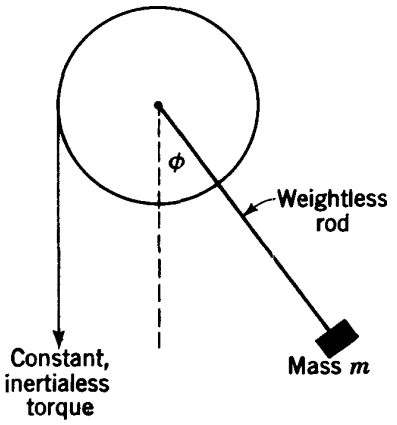

Fig. 9-2. Pendulum model for phase oscillations.

9-5. THE LIMITS OF PHASE STABILITY

A first integration of Eq. (9-14) is made possible by rewriting it in the form

$$\frac{d^2\phi}{dt^2} = \frac{1}{2}\frac{d}{d\phi}(\dot{\phi}^2) = \frac{\omega eE}{p_0}(\sin\phi - \sin\phi_0) \tag{9-17}$$

Integration of Eq. (9-17) yields

$$\dot{\phi}^2 = \frac{2\omega eE}{p_0}(\cos\phi + \phi\sin\phi_0 + \text{integration const}) \tag{9-18}$$

One of the limits of the stable phase oscillation is immediately evident. As ϕ increases through a range greater than ϕ_0, we see from Eq. (9-17)

that the second derivative of ϕ first increases, then decreases to pass through zero when ϕ reaches the value $(\pi - \phi_0)$. For larger values of ϕ the sign reverses and the phase oscillation is no longer stable. Consequently the limit of the oscillation in this direction is $(\pi - \phi_0)$ and the integration constant in Eq. (9-18) can be evaluated by setting $\dot{\phi}$ equal to zero for this value of ϕ. Equation (9-18) then becomes

$$\dot{\phi}^2 = \frac{2eE_0\omega}{p_0} [\cos \phi + \cos \phi_0 + (\phi + \phi_0 - \pi) \sin \phi_0] \qquad (9\text{-}19)$$

The other limit of the oscillation is given by the other value of ϕ for which the quantity in the square brackets in Eq. (9-19) vanishes. The phase-acceptance ranges for various values of the equilibrium phase and the accepted fraction of a continuous injected beam are given in Table 9-1.

TABLE 9-1

Equilibrium phase ϕ_0, deg	Limits of phase acceptance, deg	Accepted fraction of injected beam
0	−180 to 180	1.000
10	−99.6 to 170	0.749
20	−65.9 to 160	0.627
30	−38.7 to 150	0.524
40	−14.6 to 140	0.429
50	7.8 to 130	0.339
60	29.1 to 120	0.252
70	49.7 to 110	0.167
80	70.0 to 100	0.083
90	90.0 to 90	0.000

From this table it is clear that phase acceptance increases markedly as the equilibrium phase moves away from the peak of the accelerating wave. In other words, the higher the electric field relative to the minimum necessary field, the more particles will be accepted.

The discussion thus far has related only to the acceptance for particles with no momentum error. When particles have been accepted into phase-stable acceleration, momentum errors will develop, and the particles will move on "orbits" in a plot of momentum error against phase error. The shape of these orbits can be established from Eqs. (9-12) and (9-13). For large errors linear approximations are not adequate, and numerical integration is necessary. The result is shown in Fig. 9-3. Here a parameter proportional to energy error rather than momentum error has been plotted against phase error for various equilibrium phases. Energy error has been chosen because energy and phase prove to be Hamiltonian conjugates. From the arguments presented in Sec. 5-8, areas plotted in this manner will be preserved throughout the motion.

A group of particles plotted in this pattern will occupy a space whose area will not change with time, although the shape of the area may go through marked variations.

The Hamiltonian describing the phase motion has the form

$$H = eE \cos \phi - eE'\phi + \frac{\omega}{c}(W^2 - W_0^2)^{1/2} - \frac{\omega W}{v}$$

where W is the particle energy, W_0 is the rest energy of the particle, and the other symbols are as used earlier in these sections. It is not

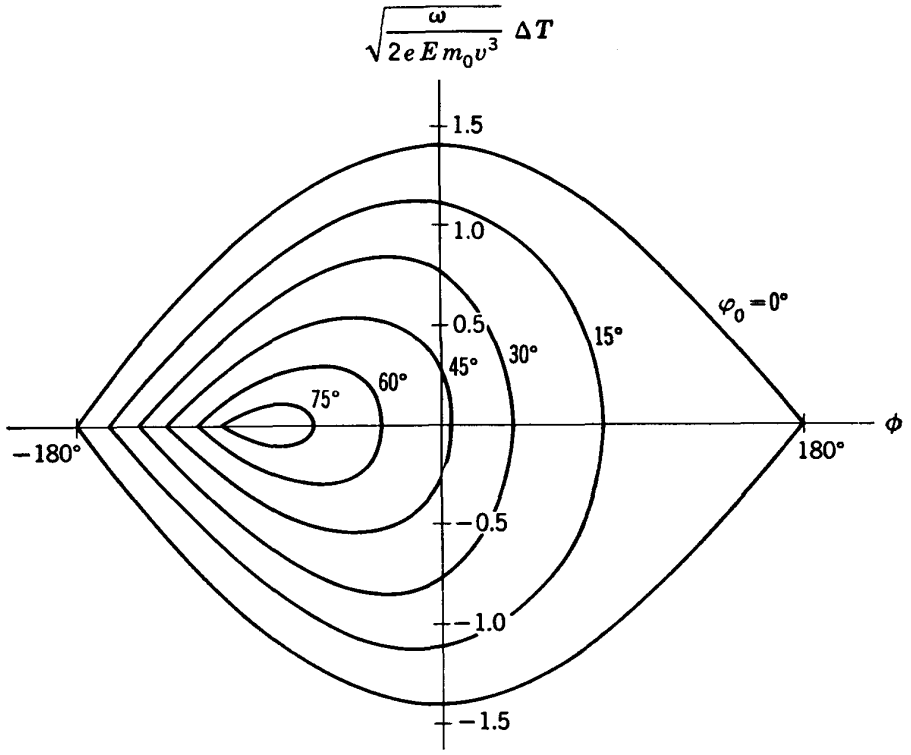

Fig. 9-3. Region of phase stability for various equilibrium phases ϕ_0.

difficult to show that Eqs. (9-10) and (9-11) can be derived from this function.

In spite of the approximate nature of the discussion in the two preceding sections, Table 9-1 is reasonably accurate for the initial phase of the acceleration cycle and gives a true picture of the amount of a continuous beam which will be captured in stable acceleration. As a precise description of the subsequent behavior of the particle phase and momentum error, the above discussion is entirely inadequate—its value is qualitative in showing the character of the oscillation. For a more detailed study we now consider the various accelerators in which phase stability is essential to operation. Fortunately the phase oscillations are damped in all

cases, and it will be possible to make an adequate study of the phase oscillations without consideration of oscillations of large amplitude.

9-6. PHASE STABILITY IN THE LINEAR ACCELERATOR

In the linear accelerator the frequency of the accelerating field remains constant and the wave velocity increases along the accelerator to match the increasing velocity of the equilibrium particle. There are no extra fields to produce a term of the form E' of Eq. (9-11). We shall restrict ourselves to small phase excursions around the equilibrium phase. Consequently we can write the fundamental equations (9-10) and (9-11) thus:

$$\Delta\phi = -\frac{\omega\,\Delta s}{v} \tag{9-20}$$

$$\Delta\dot{p} = eE\,\Delta\phi\cos\phi_0 \tag{9-21}$$

On differentiation with respect to time, Eq. (9-20) yields

$$\Delta\dot{s} = -\frac{1}{\omega}\frac{d}{dt}(v\,\Delta\phi) \tag{9-22}$$

To combine these equations into an expression in terms of $\Delta\phi$ we need to express Δp in terms of $\Delta\dot{s}$. For this purpose we use the relativistic expression for momentum discussed in Chap. 5:

$$p = \frac{m_0\dot{s}}{(1 - \dot{s}^2/c^2)^{1/2}} \qquad \text{and} \qquad p_0 = \frac{m_0 v}{(1 - v^2/c^2)^{1/2}} \tag{9-23}$$

where m_0 represents the rest mass of the particle, p_0 and v are the momentum and velocity of the equilibrium particle, and p and $\dot{s}$ are the momentum and velocity of the nonequilibrium particle. The expressions (9-23) can be inverted into the forms

$$m_0\dot{s} = \frac{p}{(1 + p^2/m_0^2c^2)^{1/2}} \qquad \text{and} \qquad m_0 v = \frac{p_0}{(1 + p_0^2/m_0^2c^2)^{1/2}} \tag{9-24}$$

whence it follows that

$$\frac{\Delta p}{p_0} = \frac{\Delta\dot{s}}{v}\left(1 + \frac{p_0^2}{m_0^2c^2}\right) \tag{9-25}$$

For abbreviation and simplification of the expressions which follow we now introduce the dimensionless variable p^* defined by

$$p^* = \frac{p_0}{m_0 c} \tag{9-26}$$

We note in passing that the ratio between p^* and unity is a measure of whether or not the treatment of the problem must be relativistic. So

long as p^* is small compared with unity, nonrelativistic treatments will be adequate. For electrons $p^* = 1$ if the electron energy is 212 kev. For protons $p^* = 1$ when the proton energy is 389 Mev.

We are now able to combine Eqs. (9-22), (9-24), and (9-25) to give a relation between Δp and $\Delta\phi$:

$$\Delta p = -\frac{m_0 c}{\omega}\left[p^*(1 + p^{*2})\frac{d\Delta\phi}{dt} + \dot{p}^*\,\Delta\phi\right] \tag{9-27}$$

The value of $\dot{p}^*$ we know directly from the equation of motion of the equilibrium particle:

$$\dot{p}_0 = m_0 c\dot{p}^* = eE\sin\phi_0 \tag{9-28}$$

Throughout this treatment we shall make the simplifying assumption that E is constant along the accelerator. Although solutions can be obtained for the more general case where E varies as some power of distance along the axis, these solutions are complicated and they do not correspond to the situation in any operating linear accelerator. If E is constant, Eq. (9-28) can be integrated to give

$$p^* = \frac{eEt\sin\phi_0}{m_0 c} \tag{9-29}$$

The phase equation can now be obtained by differentiation of Eq. (9-27) and substitution of the result in Eq. (9-21):

$$\frac{d}{dt}\left[p^*(1 + p^{*2})\frac{d\Delta\phi}{dt}\right] + \frac{eE\sin\phi_0}{m_0 c}\frac{d\Delta\phi}{dt} + \frac{\omega eE\cos\phi_0\,\Delta\phi}{m_0 c} = 0 \tag{9-30}$$

This is the general expression which describes the phase oscillations in the linear accelerator for both the relativistic and the nonrelativistic condition. In this form it is not easy to write an explicit analytical solution, although it is fairly evident that, if $\cos\phi_0$ is positive, the solution will have a generally periodic character with damping introduced by the second term.

The significance of the phase equation is much clearer if a change of variables is made. First we rewrite the equation in terms of the variable $p^*\,\Delta\phi$ instead of $\Delta\phi$ alone. We then introduce a new independent variable u defined by

$$u = \sinh^{-1} p^* = \sinh^{-1}\frac{eEt\sin\phi_0}{m_0 c} \tag{9-31}$$

The new variable is a monotonic function of p^* and so of t. For low values of p^*, u is approximately equal to p^* and so is proportional to t. For very large values of p^*, u increases more slowly and becomes approximately equal to $\ln(2p^*)$.

When the algebra attending these changes of variable has been carried through, we emerge with the new phase equation

$$\frac{d^2(p^* \Delta\phi)}{du^2} + \left(\frac{K}{p^*} - 1\right) p^* \Delta\phi = 0 \tag{9-32}$$

where the dimensionless constant K is given by

$$K = \frac{\omega m_0 c \cos \phi_0}{eE \sin^2 \phi_0} \tag{9-33}$$

The character of the phase oscillation in the linear accelerator is clear from Eq. (9-32). If K is positive, a stable oscillation will be maintained up to the point where p^* becomes equal to K. Although $p^* \Delta\phi$ will increase in amplitude, $\Delta\phi$ itself will be damped, as we shall show later. As p^* increases to such large values that K/p^* becomes negligible compared with unity and the variable u becomes equal to ln $(2p^*)$, then the phase equation (9-32) degenerates to

$$\frac{d}{dp^*}\left(p^{*3} \frac{d\Delta\phi}{dp^*}\right) = 0 \tag{9-34}$$

whose solution is

$$\Delta\phi = \text{a constant} + \frac{\text{another constant}}{p^{*2}} \tag{9-35}$$

Although the phase is no longer oscillating around a stable equilibrium value, it is now approaching a constant value; in other words, the particle continues to be "locked" to the accelerating wave.

A knowledge of the sign and value of the constant K is now essential to any further understanding of the phase oscillation. The phase oscillation is stable only if K is positive. From Eq. (9-33) this will be true only if cos ϕ_0 is positive; since sin ϕ_0 must also be positive for acceleration to take place, ϕ_0 must lie between 0 and 90°. For the traveling wave described by Eq. (9-4), this value lies on the falling side of the wave as we expected. [This fact may be verified by differentiating Eq. (9-4) with respect to distance s.]

The value of K for most operating electron linear accelerators is about 2. The phase oscillation, accordingly, ceases to be periodic when $p^* \simeq 2$ or when the kinetic energy of the electron is about 0.37 Mev. This energy occurs near the beginning of most electron machines; hence almost the whole electron accelerator is operating above the region where phase oscillations are observed. In most operating proton linear accelerators, on the other hand, K is of the order of 1000. But protons reach momenta given by $p^* = 1000$ only when the proton energy approaches 1000 Bev. Evidently all proton linear accelerators, operating or contemplated, will enjoy stable phase oscillations.

In the proton linear accelerator, up to the highest energies yet achieved, p^* is so small compared with unity that the variable u is effectively equal to p^* and a solution of the phase equation becomes possible. When u is replaced by p^* and the unity term is neglected in comparison with K/p^*, Eq. (9-32) becomes

$$\frac{d^2}{dp^{*2}}(p^* \Delta\phi) + K \Delta\phi = 0 \tag{9-36}$$

This is a modified form of Bessel's equation and has the solution

$$\Delta\phi = p^{*-\frac{1}{2}}\{C_1 J_1[2(Kp^*)^{\frac{1}{2}}] + C_2 N_1[2(Kp^*)^{\frac{1}{2}}]\} \tag{9-37}$$

where J_1 and N_1 are the Bessel and Neumann functions of the first order and C_1 and C_2 are constants determined by the initial conditions. When p^* reaches sufficiently high values, the asymptotic forms of the Bessel and Neumann functions can be used. For x large

$$J_1(x) \simeq \left(\frac{2}{\pi x}\right)^{\frac{1}{2}} \cos\left(x - \frac{3\pi}{4}\right)$$

$$N_1(x) \simeq \left(\frac{2}{\pi x}\right)^{\frac{1}{2}} \sin\left(x - \frac{3\pi}{4}\right)$$

and Eq. (9-37) can be rewritten in the form

$$\Delta\phi = \Delta\phi_i \left(\frac{p_i^*}{p^*}\right)^{\frac{3}{4}} \cos\left[2(Kp^*)^{\frac{1}{2}} - 2(Kp_i^*)^{\frac{1}{2}}\right] \tag{9-38}$$

where the subscript i indicates the initial value of the parameter in question. We see that the phase oscillation is damped and decreases in amplitude proportional to $p^{*-\frac{3}{4}}$.

Over the low-energy range of most proton linear accelerators the approximation involved in using the asymptotic form of the Bessel function is not a very good one; the qualitative conclusions are, however, valid over the whole energy range.

Associated with the phase oscillation of the nonequilibrium particle will be an oscillating momentum and energy error. This error can be evaluated from Eq. (9-22), which relates the velocity error to the phase error. If T_0 is the kinetic energy of the equilibrium particle and ΔT is the energy error of the nonequilibrium particle, the fractional energy error will be (for nonrelativistic particles)

$$\frac{\Delta T}{T_0} = \frac{2\,\Delta\dot{s}}{v} = -\frac{2}{\omega v}\frac{d(v\,\Delta\phi)}{dt} = -\frac{2\cot\phi_0}{Kp^*}\frac{d(p^*\,\Delta\phi)}{dp^*} \tag{9-39}$$

$\Delta\phi$ is given by Eq. (9-38). In taking the derivative we neglect the term derived from differentiation of the coefficient of the cosine term; this term will be found to make a negligible contribution compared with the term

derived from differentiation of the cosine itself. The result of this operation is

$$\frac{\Delta T}{T_0} = 2K^{-\frac{1}{2}} \cot \phi_0 p_i^{*\frac{3}{4}} p^{*-\frac{5}{4}} \Delta\phi_i \sin [2(Kp^*)^{\frac{1}{2}} - 2(Kp_i^*)^{\frac{1}{2}}] \quad (9\text{-}40)$$

This expression satisfies the usual initial condition of negligible energy error at the input end of the linear accelerator. The energy error builds up to a maximum in the first quarter of the phase oscillation and then oscillates with an amplitude which damps like $p^{*-\frac{5}{4}}$. Since, in the nonrelativistic range, the kinetic energy of the equilibrium particle is proportional to p^{*2}, the fractional energy error damps like $T_0^{-\frac{5}{8}}$.

In the intermediate energy range where relativistic effects become appreciable, it is necessary to solve Eq. (9-32) without approximation. This equation has not yet been given an analytic solution, but it can rather easily be solved numerically for any particular choice of parameters. It will be found that the damping of the phase oscillation becomes weaker as p^* approaches K but the oscillation never becomes unstable. As the oscillation finally becomes aperiodic, it is found that the fractional energy error approaches a constant value as does the phase error.

9-7. PHASE STABILITY IN THE LINEAR ACCELERATOR IF $v = c$

In the high-energy electron linear accelerator, the velocity of the electrons over most of the range of acceleration is very nearly equal to the velocity of light. It is therefore of interest to explore the possibility of setting the phase velocity v of the accelerating wave equal to the velocity of light throughout the whole machine; this will simplify the construction since the machine will now consist of a sequence of identical accelerating sections. This expedient proves to be quite satisfactory and is now used in all high-energy electron linear accelerators. A detailed analysis of this system is presented by Slater[3] and by Chodorow et al.[4]

The phase behavior for this case is rather simpler to diagnose than that in the nonrelativistic machines; in fact, the analysis can proceed without restricting the phase excursions to small amplitudes. If v is set equal to c, the two fundamental relations (9-9) and (9-11) become

$$\phi = \omega\left(t - \frac{s}{c}\right) + \phi_0 \quad (9\text{-}41)$$

and

$$\frac{dp}{dt} = eE \sin \phi \quad (9\text{-}42)$$

We differentiate Eq. (9-41) to obtain

$$\dot{\phi} = \omega\left(1 - \frac{\dot{s}}{c}\right) = \omega\left[1 - \frac{p}{(p^2 + m_0^2c^2)^{\frac{1}{2}}}\right] \quad (9\text{-}43)$$

Equations (9-42) and (9-43) are satisfied by the following relation between ϕ and p:

$$\cos \phi = \cos \phi_i + \frac{\omega}{eE}[p - (p^2 + m_0^2c^2)^{\frac{1}{2}} - p_i + (p_i^2 + m_0^2c^2)^{\frac{1}{2}}] \quad (9\text{-}44)$$

where the subscript i indicates initial values of the quantities concerned. As p becomes very large, ϕ approaches an asymptotic value ϕ_f given by

$$\cos \phi_f = \cos \phi_i + \frac{\omega}{eE}[(p_i^2 + m_0^2c^2)^{\frac{1}{2}} - p_i] \quad (9\text{-}45)$$

For any given injection momentum p_i this equation can be satisfied provided the accelerating field E is high enough that the cosine of the asymptotic phase is never greater than unity. In practice the value of E to satisfy this requirement is of the order of millions of volts per meter. When E is sufficiently high, we have a sort of phase stability because the phase continually approaches the asymptotic value given by Eq. (9-45). In other words, the electrons are bound to the accelerating wave and will continue to be accelerated indefinitely without falling out of step with the accelerating field.

9-8. PHASE STABILITY IN THE SYNCHROTRON

The synchrotron will be described in Chaps. 12 and 13. For the present discussion it will be sufficient to summarize its characteristics.

The equilibrium particle in the synchrotron has an orbit of constant radius r_0 given by

$$p_0 = B_0 e r_0 \quad (9\text{-}46)$$

where p_0 is the particle momentum and B_0 is the magnetic field at the orbit. Since r_0 is fixed, the field B_0 must increase with time as the particle momentum increases. Focusing forces are provided just as in the betatron by shaping the magnetic field so that

$$B = B_0 r^{-n} r_0^n \quad (9\text{-}47)$$

where n must lie between 0 and 1. Acceleration takes place at one or more gaps around the orbit and is accomplished by application of a radio-frequency field. As the particle is accelerated and its period of revolution decreases, the frequency of the accelerating signal must be increased. Consequently, in contrast to the linear-accelerator situation, the frequency of the accelerating signal is not constant but increases during the acceleration cycle.

Particles which arrive at the accelerating gaps at incorrect phases will vary in momentum from the equilibrium value and so will travel on orbits

with radii given by

$$p = Ber = B_0 e r^{1-n} r_0^n \tag{9-48}$$

The frequency of the accelerating signal is equal to the frequency of revolution $\omega/2\pi$ of the equilibrium particle or may be an integral multiple of that frequency. For generality we shall consider acceleration by the hth harmonic of the revolution frequency. The phase error now follows from Eq. (9-10):

$$\Delta\phi = \frac{-h\omega\,\Delta s}{v} \tag{9-49}$$

In the cylindrical coordinate system having the axis of the orbit as the axis of coordinates $\Delta s = r\,\Delta\theta$ and $v = r\omega$. Hence

$$\begin{aligned} \Delta\phi &= -h\,\Delta\theta \\ \text{and} \qquad \Delta\dot{\phi} &= -h\,\Delta\dot{\theta} \end{aligned} \tag{9-50}$$

$$\text{but} \qquad \Delta\dot{s} = \Delta(r\dot{\theta}) = \frac{v}{r_0}\,\Delta r + r_0\,\Delta\dot{\theta}$$

(We are assuming, as will subsequently be evident, that the radial velocity of the particle is negligible in comparison with its azimuthal velocity.) Therefore Eq. (9-50) can be written

$$\Delta\dot{\phi} = \frac{hv}{r_0}\left(\frac{\Delta r}{r_0} - \frac{\Delta\dot{s}}{v}\right) \tag{9-51}$$

The purpose of these manipulations is to express the phase error in terms of the momentum error so that the equation of motion (9-11) can be reduced to an equation describing only the phase error. Accordingly we transform the two terms on the right of Eq. (9-51) to terms proportional to the momentum error. From Eq. (9-48)

$$\frac{\Delta r}{r_0} = \frac{\Delta p}{p_0(1-n)} \tag{9-52}$$

The second term on the right-hand side of Eq. (9-51) has already been discussed in connection with the linear accelerator. From Eqs. (9-25) and (9-26)

$$\frac{\Delta\dot{s}}{v} = \frac{\Delta p}{p_0(1+p^{*2})}$$

The quantity v is expressible in terms of p^* by using Eqs. (9-24) and (9-26). With these substitutions Eq. (9-51) becomes

$$\Delta\dot{\phi} = \frac{h(n+p^{*2})\,\Delta p}{m_0 r_0(1-n)(1+p^{*2})^{3/2}} \tag{9-53}$$

We now return to the equation of motion (9-11). Before substituting from Eq. (9-53) in this relation, we must first make the appropriate substitution for the term E'. In the synchrotron the term E' represents two effects, first the accelerating or decelerating effect of the changing magnetic flux linked by the particle orbit and second, significant only in electron machines, the decelerating effect of the energy loss due to electromagnetic radiation by the accelerated electrons. For the present we consider only the first effect, the betatron effect of the flux within the orbit. Just as was done in discussing the betatron, we write this term

$$E' = \frac{1}{2\pi r} \int \frac{\partial B}{\partial t} 2\pi r \, dr$$

The accelerating field E in Eq. (9-11) is given by

$$E = \frac{V}{2\pi r}$$

where V is the sum of the peak voltages applied across all of the accelerating gaps. With these substitutions Eq. (9-11) can be written in the form

$$r\dot{p} = \frac{eV}{2\pi} \sin (\phi_0 + \Delta\phi) + e \int \frac{\partial B}{\partial t} r \, dr \tag{9-54}$$

In terms of momentum, radius, and phase errors this becomes

$$\dot{p}_0 \, \Delta r + r_0 \, \Delta\dot{p} = \frac{eV}{2\pi} \Delta\phi \cos \phi_0 + e \frac{\partial B_0}{\partial t} r_0 \, \Delta r \tag{9-55}$$

From Eq. (9-46) the first and last terms of this equation cancel each other, and we are left with

$$\Delta\dot{p} = \frac{eV}{2\pi r_0} \Delta\phi \cos \phi_0 \tag{9-56}$$

We have now only to combine Eqs. (9-53) and (9-56) to obtain a second-order differential equation in $\Delta\phi$. The result is

$$\frac{d}{dt}\left[\frac{(1 + p^{*2})^{3/2} \, \Delta\dot{\phi}}{n + p^{*2}}\right] = \frac{heV \cos \phi_0 \, \Delta\phi}{2\pi r_0^2 m_0 (1 - n)} \tag{9-57}$$

If $\dot{B}$ and the accelerating field remain constant, p^* will be proportional to time. Explicitly,

$$p^* = \frac{eVt \sin \phi_0}{2\pi r_0 m_0 c} \tag{9-58}$$

and p^* can be used as the independent variable in Eq. (9-57), which becomes

$$\frac{d}{dp^*}\left[\frac{(1+p^{*2})^{3/2}}{n+p^{*2}}\frac{d\Delta\phi}{ap^*}\right] = \frac{hK\,\Delta\phi}{1-n} \tag{9-59}$$

where

$$K = \frac{2\pi m_0 c^2 \cos\phi_0}{eV\sin^2\phi_0} \tag{9-60}$$

K is a dimensionless constant of the same character as the K that was used in analysis of the linear accelerator. In electron synchrotrons K is of the order of 1000; in proton synchrotrons K is of the order of 10^6.

Equation (9-59) describes the phase oscillations of the nonequilibrium particles. Since n must lie between 0 and 1 for radial and vertical focusing (as in the betatron), this equation can represent a stable oscillation only if $\cos\phi_0$ is negative. For acceleration to take place $\sin\phi_0$ must be positive. Accordingly the stable phase must lie between 90 and 180° on the standing wave and so must lie on the rising side of the traveling wave.

The frequency of the oscillation described by Eq. (9-59) is sufficiently high that the change of p^* during a complete phase oscillation is relatively small. For this reason an approximate solution of Eq. (9-59) will be sufficiently precise for our purposes. This solution takes the form

$$\Delta\phi = \Delta\phi_i\left(\frac{1+p^{*2}}{1+p_i^{*2}}\right)^{-3/8}\left(\frac{n+p^{*2}}{n+p_i^{*2}}\right)^{1/4} \cos\int\left[\frac{hK(n+p^{*2})}{(1-n)(1+p^{*2})^{3/2}}\right]^{1/2} dp^* \tag{9-61}$$

where the subscript i refers to the initial value of the parameter indicated. At nonrelativistic energies

$$\Delta\phi \propto \left(1-\frac{3n-2}{8n}p^{*2}\right)\cos\left[\left(\frac{hKn}{1-n}\right)^{1/2}p^*\right] \tag{9-62}$$

and we see that the phase oscillation is constant in frequency and is very weakly damped or undamped, depending on whether or not n is greater than $\frac{2}{3}$. In the extreme relativistic range where p^* is much greater than unity

$$\Delta\phi \propto p^{*-1/4}\cos\left(\frac{2hK}{1-n}p^*\right)^{1/2} \tag{9-63}$$

Equation (9-63) indicates that the frequency of the phase oscillation is decreasing as energy or momentum increases and that the oscillation damps like $p^{*-1/4}$.

Associated with the phase oscillation will be an oscillation in the momentum error; the amplitude of this oscillation is given by Eq. (9-53).

The momentum error will be reflected in a radial oscillation whose amplitude will be [cf. Eq. (9-52)]

$$\frac{\Delta r}{r_0} = \frac{\cot \phi_0}{hK} \frac{(1 + p^{*2})^{3/2}}{p^*(n + p^{*2})} \frac{d\Delta\phi}{dp^*} \tag{9-64}$$

In the nonrelativistic range it follows from Eq. (9-62) that, approximately,

$$\frac{\Delta r}{r_0} = \cot \phi_0 \, [hKn(1 - n)]^{-1/2} \frac{\Delta\phi_{\max}}{p^*} \tag{9-65}$$

where $\Delta\phi_{\max}$ represents the amplitude of the phase excursion. Since the damping or undamping of the phase oscillation is very weak, Eq. (9-65) indicates that the associated oscillation in radius falls off like $1/p^*$. When the particles reach extreme relativistic energies, Eqs. (9-64) and (9-63) give for the radial excursion the approximate result

$$\frac{\Delta r}{r_0} = \cot \phi_0 \, [2hK(1 - n)p^*]^{-1/2} \, \Delta\phi_{\max} \tag{9-66}$$

Since the phase oscillation is damping like $p^{*-1/4}$ in this range, the radial-oscillation amplitude will decrease like $p^{*-3/4}$.

It should be remembered in applying the above conclusions that $\dot{p}^*$, V, and ϕ_0 have been assumed to remain constant during the acceleration. If this assumption is not correct for a particular accelerator, it will be necessary to take this fact into account in solving Eq. (9-57). The more sophisticated treatments necessary in such cases will be found in the papers of Bohm and Foldy[5] or Twiss and Frank.[6]

A question may be raised as to the legitimacy of treating the betatron oscillations and the radial motions associated with the phase oscillations as though they were independent. In principle the general motion should be derived taking both effects into account. But it is always found that the phase oscillation is lower in frequency by a factor of 50 or more than the radial betatron oscillation. The mathematical consequence of this fact is that the oscillations are effectively decoupled and can be analyzed independently.

In electron synchrotrons the term E' of Eq. (9-11) must include a radiation-loss term. As was shown in Sec. 7-7 for the betatron, the radiation contribution to E' can be written

$$E' \text{ (due to radiation)} = -1.408 \times 10^{-32} \frac{W^4}{r^2} \quad \text{volts/m} \tag{9-67}$$

where W is expressed in electron volts. Radiation losses are important only in the extreme relativistic range where

$$W \text{ (in electron volts)} = \frac{pc}{e} \tag{9-68}$$

From Eq. (9-48)

$$r = r_0 \left(\frac{p}{p_0}\right)^{1/(1-n)}$$

Using these substitutions Eq. (9-67) can be rewritten in the form

$$rE' = -1.408 \times 10^{-32} \frac{1}{r_0} \left(\frac{p_0 c}{e}\right)^4 \left(\frac{p}{p_0}\right)^{(3-4n)/(1-n)} \tag{9-69}$$

Following the same reasoning that led from Eq. (9-54) to Eq. (9-57), we see that the radiation contribution to Eq. (9-56) is of the form $(e/r_0)\,\Delta(rE')$. From Eq. (9-69) and the extreme relativistic form of Eq. (9-53) this term is

$$\frac{e}{r_0}\Delta(rE') = -1.408 \times 10^{-32} \frac{(3-4n)e}{hcr_0} \frac{m_0 c^2 p^{*4}}{e} \Delta\phi \tag{9-70}$$

When this term is included in the derivation of the extreme relativistic form of Eq. (9-57) and the change is made to p^* as the independent variable, Eq. (9-59) becomes

$$\frac{d^2\Delta\phi}{dp^{*2}} + \frac{1}{p^*}\frac{d\Delta\phi}{dp^*}\left(1 + 6.03 \times 10^{-9} \frac{3-4n}{1-n} \frac{p^{*4}}{Vr_0 \sin\phi_0}\right) = \frac{hK}{(1-n)p^*}\Delta\phi \tag{9-71}$$

This is the complete relativistic equation for phase oscillations in the electron synchrotron. Since V will be of the order of 1000 volts and r_0 will be of the order of 1 m in most electron synchrotrons, it follows that the radiation term (the second term in the square brackets) will not become appreciable until p^* is of the order of 200 or until the electron energy is of the order of 100 Mev. The radiation term will be a damping or an undamping term, depending on whether or not n is less than $\frac{3}{4}$. As energy is increased above 100 Mev, the radiation effect will become more important very rapidly. Eventually, when the energy loss per turn becomes equal to or greater than the energy supplied by the accelerating system, the approximate method used in deriving Eq. (9-71) will no longer be valid. Obviously no further acceleration can take place unless V is increased.

9-9. PHASE STABILITY IN THE SYNCHROCYCLOTRON

The synchrocyclotron differs from the classical cyclotron primarily in the fact that the frequency of the electric field is varied during acceleration so that charged particles can be accelerated past the relativistic upper limit of the classical cyclotron (cf. Sec. 6-12). Just as in the

ordinary cyclotron, the path of the equilibrium particle is a spiral of ever-increasing radius r_0 given by

$$p_0 = B_0 e r_0 \tag{9-72}$$

where p_0 is the particle momentum and B_0 is the magnetic field at the orbit. Unlike the field in the synchrotron, B_0 does not vary with time, but it does decrease slightly with increasing radius to give focusing of the betatron type. Since this weak variation has very little effect on the phase oscillation, we shall neglect it in this section and shall assume that the magnetic field is constant in both time and space. This assumption will permit us to observe the general character of the phase oscillation; for a more precise treatment the reader is referred to the paper of Bohm and Foldy.[5]

Particles which arrive at the accelerating gap at incorrect phases will vary in momentum from the equilibrium value. They will then travel on orbits whose radii are given by

$$p = B_0 e r \tag{9-73}$$

The argument relating the phase error to the momentum error is identical with that presented in the preceding section on the synchrotron and gives the same result except that h is usually chosen to be unity in the synchrocyclotron and n has been assumed to be zero. Consequently, instead of Eq. (9-53), we obtain

$$\Delta\dot{\phi} = \frac{p^{*2}\,\Delta p}{m_0 r_0 (1 + p^{*2})^{3/2}} \tag{9-74}$$

where, as before,

$$p^* = \frac{p_0}{m_0 c}$$

Since r_0 is not constant in the synchrocyclotron, we express it in terms of p^* from Eq. (9-72) to obtain

$$\Delta\dot{\phi} = \frac{B_0 e}{m_0^2 c} \frac{p^*\,\Delta p}{(1 + p^{*2})^{3/2}} \tag{9-75}$$

The equation of motion (9-11) is simplified by the fact that there are no perturbing E' terms, since the magnetic field does not change with time and since radiation effects are negligible for the nuclear particles accelerated in synchrocyclotrons. The accelerating field in Eq. (9-11) is given by

$$E = \frac{V}{\pi r} \tag{9-76}$$

where V is the D-to-D voltage. Equation (9-11) then becomes

$$r\dot{p} = \frac{p\dot{p}}{B_0 e} = \frac{eV}{\pi} \sin \phi \tag{9-77}$$

whence

$$\frac{d}{dt}(p^* \Delta p) = \frac{e^2 V B_0}{\pi m_0 c} \Delta\phi \cos \phi_0 \tag{9-78}$$

As usual, Eqs. (9-75) and (9-78) in combination yield the phase-oscillation relation

$$\frac{d}{dt}[(1 + p^{*2})^{3/2} \Delta\phi] = \frac{(e/m_0)^3 V B_0^2}{\pi c^2} \Delta\phi \cos \phi_0 \tag{9-79}$$

Once again we have derived a phase-oscillation equation that describes a stable damped oscillation provided only that $\cos \phi_0$ is negative.

Approximate solutions of this equation valid only in the nonrelativistic or extreme relativistic ranges are of very little value here because a large part of the operating range of the synchrocyclotron is in the intermediate region where p^* is of the order of unity. Consequently detailed solutions must be obtained numerically for the particular set of machine parameters in question. For most cases of interest it will be found that the frequencies of phase oscillation are some tens of kilocycles per second. The energy spread after acceleration is derivable from Eq. (9-75) and the solution of Eq. (9-79) and will be found to be a fraction of 1 per cent—much narrower than the energy spreads encountered with conventional cyclotrons. These matters will receive further attention in Chap. 11.

9-10. PHASE STABILITY IN THE MICROTRON

The microtron is an electron accelerator originally proposed by Veksler[1] and discussed at length by Henderson,[7] Schmelzer,[8] Kaiser,[9] and others referred to in the references cited. It is designed for use with completely relativistic electrons and has a cyclotron-like structure. Since relativistic electrons have approximately constant velocity, the cyclotron principle cannot be used; instead the particles are made to arrive in the correct phase at the single accelerating gap by permitting them to slip one cycle in phase with each revolution in the magnetic field. The principle can best be understood by reference to the diagram of Fig. 9-4. A small radiofrequency accelerating cavity is located near

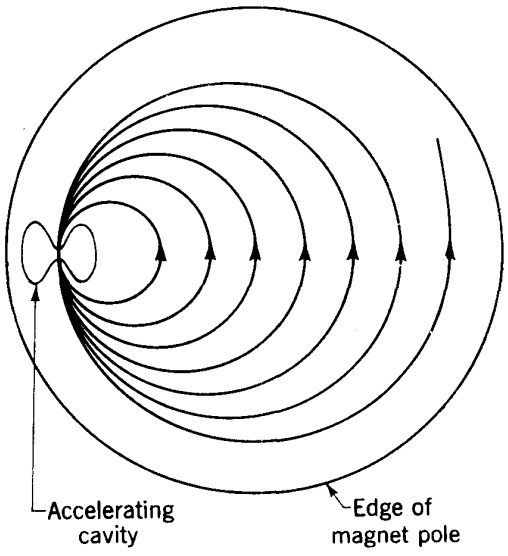

Fig. 9-4. Orbits in the microtron.

the edge of a cylindrical vacuum chamber. Particles traverse the resonator and are accelerated by the radiofrequency field. They then travel on a circular orbit in the magnetic field and return to the resonator in approximately an integral number of radiofrequency cycles so that they are again accelerated. The orbit is thus a sequence of circles of ever-increasing radius, all tangent at the resonator. This device is primarily useful for acceleration of electrons to a few tens of Mev. It has the advantage over the betatron that its accelerated beam is rather easily extracted for use outside the machine. If extracted beams are not required as, for example, in the case where the machine is used for generation of X rays, the microtron has no important advantage.

The particles in the microtron experience a variety of phase stability similar in general to that found in the synchrotron. Since the steps in energy at the accelerating unit are a large fraction of the total energy, it is no longer reasonable to describe the phase oscillation by a differential equation. The correct formulation of this problem is in a finite-difference equation whose solution must be numerical. For this treatment and its results the reader is referred to the paper of Henderson, Heymann, and Jennings.[7]

REFERENCES

1. V. Veksler, *Compt. rend. acad. sci. U.S.S.R.*, **43**:444 (1944); **44**:393 (1944); *J. Phys. (U.S.S.R.)*, **9**:153 (1945).
2. E. M. McMillan, *Phys. Rev.*, **68**:143 (1945).
3. J. C. Slater, *Rev. Mod. Phys.*, **20**:473 (1948).
4. M. Chodorow et al., *Rev. Sci. Instr.*, **26**:134 (1955).
5. D. Bohm and L. Foldy, *Phys. Rev.*, **70**:249 (1946); **72**:649 (1947).
6. R. Q. Twiss and N. H. Frank, *Rev. Sci. Instr.*, **20**:1 (1949).
7. C. Henderson, F. F. Heymann, and R. E. Jennings, *Proc. Phys. Soc. (London)*, **66B**:41 (1953).
8. C. Schmelzer, *Z. Naturforsch.*, **7a**:808 (1952).
9. H. F. Kaiser and W. T. Mayes, *Rev. Sci. Instr.*, **26**:565 (1955).

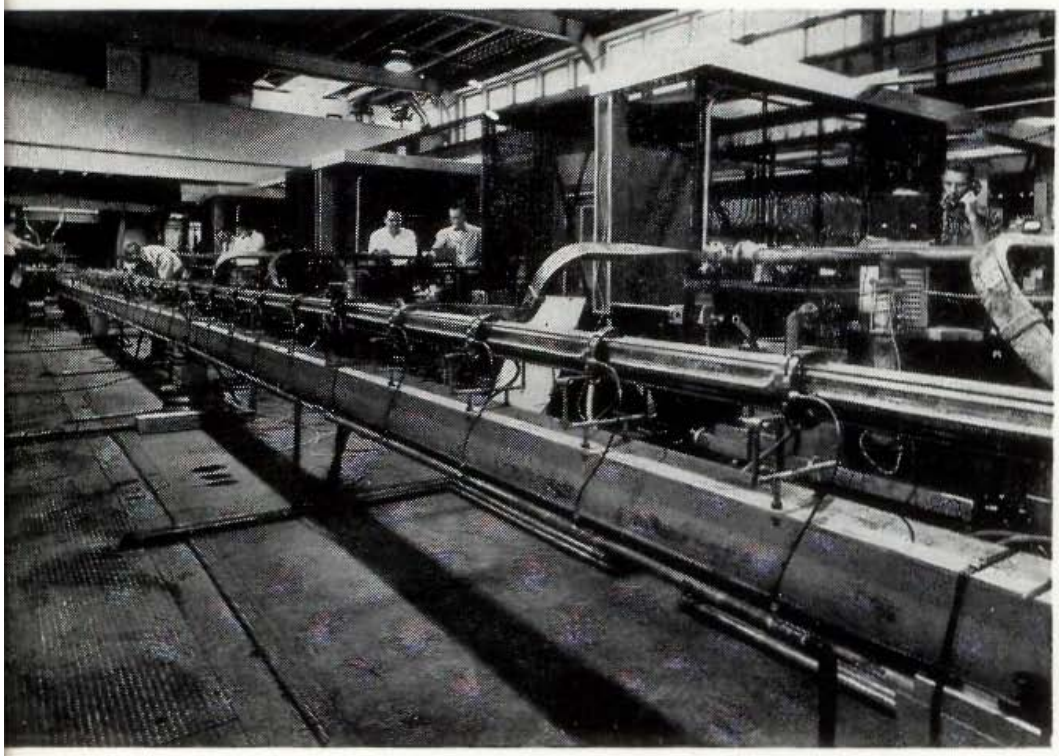

10

The Linear Accelerator

In the linear accelerator, as the name implies, particles are accelerated in a straight line by an oscillating electric field. Many different electrode structures have been devised and tested, but all have the common feature that their field pattern includes a traveling-wave component whose phase velocity is the same as that of the accelerated particles. Since the particle velocity is supposed to increase as the particle travels through the accelerator, the phase velocity of the accelerating wave must also increase with distance along the accelerating structure. At extreme relativistic energies when the particle velocity approaches very closely the velocity of light, it becomes possible to equate the phase velocity to the velocity of light, so the design of high-energy electron linear accelerators can be somewhat simpler than that of nonrelativistic accelerators used for heavier particles.

The chief advantage of the linear accelerator lies in the excellent collimation of the emergent beam, as compared with the spreading emergent beams from circular accelerators. The small size of the target spot and the high beam density improve and simplify experimental techniques for studies of small-angle scattering, angular distributions, and many other problems. Shielding is simplified because small beam channels can be used in the shields; background intensity due to scattered radiation is more easily controlled.

For energies of a few Mev the chief disadvantage of the linear acceler-

ator lies in the energy spread of the accelerated beam. This spread is of the order of 1 per cent or so. Direct-voltage machines such as the electrostatic generator yield much better energy uniformity. At higher energies linear accelerators are physically long. It is difficult to achieve energy gains of more than 3 to 5 Mev/ft of length, and the maintenance of the associated high electric fields requires enormous quantities of radiofrequency power derived from a multiplicity of power sources. For energies in the Bev range the limit appears to be economic.

Accelerator designers have hoped that, in addition to its technical advantages, the linear accelerator might eventually present an economic advantage for very high energies. This hope has been based on the approximately direct proportionality between cost and energy of the linear accelerator. Circular accelerators, on the other hand, require magnets whose cost increases roughly as the third power of the energy for relativistic particles. This difference in the cost equations suggests that linear accelerators should have an economic advantage for sufficiently high energies. However, the sequential developments of magnetic accelerators—from the cyclotron with its solid-core magnet, to the synchrotron with its much lighter ring magnet, to the AG synchrotron which still further reduces magnet dimensions and costs—have retained the economic advantage of the magnetic accelerators.

The linear accelerator has specific and sometimes definitive advantages over other machines when a compact, well-focused beam of accelerated particles is essential. It has found a useful application as an injector for high-energy machines such as proton synchrotrons (see Chap. 13). For this purpose the proton energy required lies between 10 and 50 Mev. Most of the development of proton linear accelerators has been in this range—by 1961 no proton linear accelerator had been built for energies higher than 70 Mev.

For acceleration of electrons into the Bev range the linear accelerator is a very strong contender. Circular electron accelerators are limited to energies of a few Bev by the rapid increase in energy loss by radiation of relativistic electrons traveling in curved paths. The electron linear accelerator has no such limitation and may become the most practical choice for accelerating electrons to energies above about 10 Bev.

Design problems for proton accelerators differ from those for electron accelerators. The slower velocities of protons in the range of interest dictate the use of radiofrequencies in the range between 100 and 200 megacycles. For ions heavier than protons still lower frequencies are used. However, the higher velocities of electrons and their approach to relativistic speeds at relatively low energies have made it possible to design simpler accelerating chambers for which the accelerating electric field has

At the head of the facing page is an illustration of the Stanford Mark III accelerator with the shielding removed.

frequencies in the microwave range, commonly around 3000 megacycles.

Among the fraternity of accelerator builders the rather cumbersome term "linear accelerator" is often abbreviated to "linac." This name has found its way into the literature and is now considered acceptable. It was originally applied to the proton linear accelerator, but the appeal of the abbreviation has caused it to be used for electrons also. Specialists occasionally argue for distinguishing titles, but thus far no suitable terms have become generally accepted. In the recently developing field of heavy-ion linear accelerators the identifying title "hilac" is used in several laboratories and appears to be gaining acceptance.

10-1. EARLY DESIGNS

The first proposal for a radiofrequency linear accelerator was made by Ising[1] in Sweden in 1925. He suggested the concept of resonance acceleration and proposed using a spark-gap oscillator and transmission lines to supply radiofrequency fields to accelerating electrodes. There is no record of any experimental test of the proposal. The first report of a working accelerator was that by Wideröe[2] in 1928, and his apparatus was the direct ancestor of all resonance accelerators. It consisted of three coaxial cylindrical electrodes; an alternating electric field was applied between the central electrode and the two electrodes on either side. The frequency of alternation was such that the electrode potentials were reversed during the time required for the injected ions (K^+ and Na^+ ions) to traverse the central electrode; the ions experienced two accelerations and attained a final energy twice that available from a single traversal of the field.

The report of Wideröe's experiment was noted by Lawrence at the University of California in Berkeley, and it provided the initial idea from which the concept of the cyclotron was developed (see Chap. 6). D. H. Sloan, then a student at Berkeley, extended the linear accelerator to include 10 or more accelerating electrodes. By 1931 Sloan and Lawrence[3] had accelerated mercury ions to 1.25 Mev, and by 1934 Sloan and Coates[4] reported 2.8 Mev. These fast mercury ions, incident on a target, were found to produce soft X rays characteristic of mercury and of the target element, but no nuclear effects were observed. Lithium ions were also used by Kinsey[5] at energies up to 1 Mev, at first with no evidence of nuclear disintegrations; later unpublished work by Kinsey showed that the well-known $Li(p,\alpha)$ alpha particles were produced from hydrogenous targets. Since these early accelerators could operate only at relatively low frequencies and so could accelerate only relatively heavy ions, their usefulness in nuclear research was insignificant.

A description of these early resonance accelerators will show the simplicity of the concepts. An array of coaxial cylindrical electrodes of increasing length (Fig. 10-1) was aligned along the axis of a long glass

vacuum chamber. The electrodes were connected alternately to two bus bars extending along the length of the chamber and supplied by the radio-frequency power source. The separation L between accelerating gaps is the distance traversed by the particles during one half-cycle of the applied electric field, whence

$$L = \frac{1}{2}\frac{v}{f} \tag{10-1}$$

where v is the particle velocity and f is the frequency. Each time a particle of charge e crosses a gap, it sees a field which gives it an energy increment $eV \sin \phi$, where V is the maximum gap voltage and ϕ is the phase at which the particle crosses the gap. The early machines were designed to accelerate only the particles which arrived at a phase close to 90°, so the energy gain at each gap was about eV.

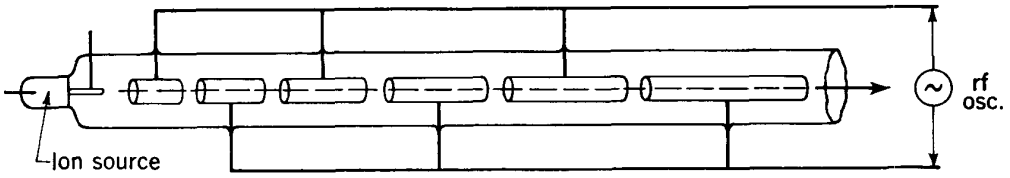

Fig. 10-1. Early linear accelerator for heavy ions with accelerating electrode lengths increasing with the square roots of a series of integers.

At low particle energies velocity increases with the square root of the energy, so successive gap separations were made to increase in a sequence proportional to the square roots of a series of integers. The gaps between the tubular electrodes were short and the positive ions spent most of their time in the field-free regions inside the electrodes or drift tubes. Relatively few electrodes were used (10 to 30), so the precision of spacing was not severe. Resonance was maintained by an experimental balance of the applied voltage V to the value required by the electrode spacing.

In a typical installation (Sloan and Lawrence[3]) 30 drift tubes were used. The first tube had an effective length of 1 cm, and the over-all length was 1.14 m. The radiofrequency power source operated at 10 megacycles (30 m wavelength), and a peak voltage of 42,000 volts was required for resonant acceleration of singly charged mercury ions, to give a final energy of 1.26 Mev. The beam of high-energy ions emerging from the accelerator was passed through slits and deflected by an electrostatic field through a small angle to direct it into a collector cup or against a target; this deflecting field served also to measure the energy of the emergent beam.

During this same period J. W. Beams[6,7] and his collaborators at the University of Virginia attempted the acceleration of electrons by traveling waves along a transmission line. The wave velocity of an artificial

transmission line was designed to match the electron velocity, and a sequence of potential surges was applied at one end of the line from a capacitor–spark-gap circuit. A linear array of short tubular electrodes with uniform separation was supported within a long, evacuated glass tube; the electrodes were electrically connected to the transmission line. Using 300,000-volt spark discharges, bursts of electrons were accelerated to 1.3 Mev. Although this early experiment was not successful in developing a reliable source of high-energy particles, it did presage the traveling-wave accelerator which became practical when suitable radiofrequency power sources became available.

10-2. MODERN LINEAR ACCELERATORS

The modern linear accelerators are founded on the work of two groups, one at Stanford University and one at the University of California. In the Stanford laboratory W. W. Hansen initiated a program in the 1930s for the development of high-frequency accelerators and power sources, with primary interest in the acceleration of electrons. One of the early concepts was a high-Q cavity resonator for single-stage acceleration of electrons. To excite this cavity, large quantities of radiofrequency power were required; accordingly a power-tube development program was initiated. Hansen collaborated with the Varian brothers in the invention and initial development of the klystron, which was destined to play an important role in the radar field. At the end of World War II a double-headed development was started on the iris-loaded waveguide as an accelerating structure for electrons and on the 3000-megacycle klystron to provide adequate power; in this program Hansen had the able assistance of E. L. Ginzton, M. Chodorow, and others. After Hansen's death in 1949 the program was continued and expanded by the Stanford group, utilizing radar techniques developed during the war. It has resulted in a sequence of electron linear accelerators of increasing length, power, and output energy, culminating in the present 1000-Mev linac which is described in Sec. 10-9.

Proton accelerator development started at the end of the war in the Radiation Laboratory of the University of California under the direction of L. Alvarez and with the important assistance of W. K. H. Panofsky. In this case also, radar developments made it possible to build practical accelerators with energies sufficient to be useful in nuclear physics.

The history of both of these fundamental design studies and a full description of the step-by-step developments are recorded in the Linear Accelerator Issue of *The Review of Scientific Instruments*[8] (February, 1955). A somewhat more concise discussion of modern linear accelerator design is available in the article by Lloyd Smith[9] in vol. 44 of the "Encyclopedia of Physics."

The two linear-accelerator types differ materially in appearance for a rather simple reason. As was shown in Sec. 9-2, the axial field component used in acceleration is a wave which travels with the particles and has the form

$$E_z = E_0 \sin\left(\omega t - \omega \int \frac{dz}{v} + \phi_0\right) \tag{10-2}$$

where z represents distance along the particle path and v is the particle velocity. Now in any real field pattern which satisfies Maxwell's equations E_0 must vary with radial distance from the axis of the particle beam. The exact solution will involve Bessel functions, but to a first approximation E_0 will have the form

$$E_0 = (\text{const})\left[1 + \left(\frac{\pi r}{\lambda}\right)^2 \left(\frac{c^2}{v^2} - 1\right)\right] \tag{10-3}$$

where r = distance from axis
λ = free-space wavelength of accelerating field
c = velocity of light

The correctness of this relation can be checked by substitution in Maxwell's equations [(5-6) to (5-9)]. The variation of accelerating field across the useful aperture should be small for several reasons. Variations will lead to increased phase oscillations and to an energy spread in the accelerated beam. Also, since the field increases with radius, higher applied fields are required at the aperture boundary to provide the desired axial field; this results in higher power input to the accelerator for a desired rate of energy gain. This phenomenon is often presented in terms of a "gap coefficient" between accelerating electrodes. A system having a large radial variation of field is said to have poor gap coefficients.

The maximum desirable operating frequency can be derived from the above argument. Suppose, for example, that the field variation is not to be greater than 10 per cent across the aperture. Then Eq. (10-3) states that the minimum permissible value of wavelength is given approximately by

$$\lambda_{\min} = 10 r_{\max} \left(\frac{c^2}{v^2} - 1\right)^{1/2} \tag{10-4}$$

where $r_{\max}$ is the half-aperture. This equation indicates that, for electrons whose velocity is close to the velocity of light throughout most of the accelerator, there is no real limitation on wavelength. For protons, however, for which the velocities at the low-energy end of the accelerator will be of the order of one-tenth of the velocity of light, the minimum permissible wavelength is severely restricted. If we consider 3 cm to be a reasonable dimension for the aperture, we see from Eq. (10-4) that the wavelength must be greater than 1.5 m and hence the highest permissible

frequency is 200 megacycles. This is the frequency actually chosen for most proton linear accelerators. For electron machines, on the other hand, it is possible to raise the operating frequency to 3000 to 10,000 megacycles before serious aperture limitations arise for other reasons. This permits the designer to use waveguide structures of a small and more convenient size. The result of this argument is that proton linear accelerators are housed in large tanks (of the order of 3 ft in diameter) resonant at 200 megacycles. Electron linear accelerators are sections of 3000-megacycle waveguides only a few inches in diameter.

TABLE 10-1
LINEAR-ACCELERATOR PARAMETERS

	Proton linear accelerator (Berkeley)	High-intensity proton linear accelerator (A-48, Livermore)	Heavy-ion linear accelerator (Berkeley, Yale)	Electron linear accelerator (Stanford)
Injection energy	4 Mev	85 kev	500 kev	80 kev
Final energy	32 Mev	3.7 Mev	10 Mev/nucleon	1 Bev
Length	40 ft	68 ft	105 ft	300 ft
Diameter	39 in.	About 12 ft	About 10 ft	3.25 in.
Frequency, megacycles/sec	202.5	48.6	70	2856
Axial field, Mv/m	3	0.5	1.9	9.6
Stable phase	64°	45–55°	Depends on e/m of particles	90°
Max beam current	60 μa	75 ma	1 ma	8 ma
Energy spread, %	0.5	8	1	3
Focusing	Grids	Solenoids	Grids + quadrupoles	None
Beam pulse length	400 μsec	Continuous	3 msec	1 μsec
Repetition rate	15/sec	Continuous	10/sec	60/sec
Peak power	2.1 megawatts	215 kw	3 megawatts	300 megawatts
Detailed description, see Sec.	10–12	10–15	10–14	10–9

For reasons to be discussed in Sec. 10-5, all high-energy linear accelerators require enormous amounts of radiofrequency power. The development of the necessary power sources has been the most difficult problem in the design of the modern linear accelerator, and an array of high-powered radiofrequency equipment is one of the more salient characteristics of a linear-accelerator installation.

Two other linear-accelerator types have been developed during the last decade. Although both are outgrowths of the proton linear accelerator they differ sufficiently to merit mention. The first is a linear accelerator for proton beams of high intensity. Here it has been necessary to increase aperture to accommodate the intense beams and, as we have seen, this has led to materially lower frequencies. These machines, accordingly, involve extremely large tanks and much lower frequencies. The second type is designed to accelerate heavier ions than protons.

Since heavy ions travel more slowly than protons of the same energy, we see from Eq. (10-4) that lower frequencies are required for heavy-ion linear accelerators than for proton machines operating over the same energy range. For this reason the resonant tanks used in heavy-ion machines are of the order of 10 ft in diameter.

The accelerating fields in linear accelerators vary from 1 to 3 Mv/m for proton machines to more than 20 Mv/m for electron machines. The 32-Mev proton linear accelerator built at the University of California (and later moved to the University of Southern California) is about 40 ft long. The 1-Bev electron linear accelerator at Stanford is 300 ft long.

In Table 10-1 we have collected some of the more important parameters of typical linear accelerators of the four types just discussed.

10-3. PARTICLE DYNAMICS IN THE LINEAR ACCELERATOR

The particles undergoing acceleration in the linear accelerator are subject to axial and radial forces. The axial field pattern and the particle motions in the axial direction have already been discussed in Chap. 9. In Secs. 9-6 and 9-7 we presented a general treatment of phase stability for all linear accelerators. The consequences of this treatment for particular accelerator types will be discussed further in the sections which follow.

The pattern of the fields which introduce radial forces is generally very complicated in an actual accelerating structure. Fortunately, this problem can be simplified by the same device as was used to simplify the problem of the axial motions. Any field pattern can be broken down by Fourier analysis into traveling-wave components traveling in the same direction as the particles and in the opposite direction. The one component which travels with the particles at the same velocity as that of the equilibrium particle will exert a continuous radial force on the particle stream. All other components will produce alternating deflections of small amplitude whose net effect will be negligible. Consequently we have to study only the field pattern which travels with the particles. The axial component of this pattern is the field [cf. Eqs. (9-4) and (10-2)]

$$E_z = E_0 \sin\left(\omega t - \omega \int \frac{dz}{v} + \phi_0\right) \tag{10-5}$$

already discussed in Sec. 9-2. The other field components associated with this one are derivable from Maxwell's equations. To a first approximation they are a radial electric-field component

$$E_r = \frac{\omega r E_0}{2v} \cos\left(\omega t - \omega \int \frac{dz}{v} + \phi_0\right) \tag{10-6}$$

and a circumferential magnetic-field component

$$B_\theta = \frac{rE_0}{2c^2} \cos\left(\omega t - \omega \int \frac{dz}{v} + \phi_0\right) \tag{10-7}$$

A more precise analysis of the field pattern would show that E_0 must depend on r; its exact form is a Bessel function of zero order, and the other field components also involve Bessel functions. The pattern is, in fact, the familiar TM_{01} field pattern found in cylindrical waveguides. For the present purpose, however, the approximate forms presented above are quite adequate.

Particle motion in the r direction follows from solution of the force equation

$$\begin{aligned} \frac{d}{dt}(m\dot{r}) &= eE_r - e\dot{s}B_\theta \\ &= \frac{er\omega E_0}{2v}\left(1 - \frac{\dot{s}v}{c^2}\right) \cos\left(\omega t - \omega \int \frac{dz}{v} + \phi_0\right) \end{aligned} \tag{10-8}$$

For simplicity we consider only the radial force on the equilibrium particle for which $\omega t = \omega \int dz/v$ and $\dot{s} = v$, so that

$$\frac{d}{dt}(m\dot{r}) = \frac{er\omega E_0}{2v}\left(1 - \frac{v^2}{c^2}\right) \cos \phi_0 \tag{10-9}$$

For low energies such that m does not vary appreciably from the rest mass and v is small compared with c, this equation indicates that the radial force is so strong that the particle will leave its orbit rapidly and will be lost in the radial direction. For higher energies the radial force decreases as v approaches c and finally becomes negligibly small. Some intriguing conclusions can be drawn from Eq. (10-9) if it is rewritten in the form

$$\frac{v}{(1 - v^2/c^2)^{1/2}} \frac{d}{dz}\left[\frac{m_0 v}{(1 - v^2/c^2)^{1/2}} \frac{dr}{dz}\right] = \frac{er\omega E_0}{2v}\left(1 - \frac{v^2}{c^2}\right)^{1/2} \cos \phi_0 \tag{10-10}$$

If v is approximately equal to c and if we make the substitution

$$dz' = \left(1 - \frac{v^2}{c^2}\right)^{1/2} dz \tag{10-11}$$

then our radial equation of motion reduces to the approximate form

$$\frac{d^2r}{dz'^2} = 0 \tag{10-12}$$

whose solution is

$$r = r_i + \left(\frac{dr}{dz'}\right)_i z' \tag{10-13}$$

where the subscript i indicates initial values of the parameters. The significance of this result emerges from a second glance at Eq. (10-11); dz' is the element of length in the frame of reference of the traveling particle. It has been shortened by the Lorentz contraction expressed by the equation defining it. (Proof of this statement will be found in standard references on the special theory of relativity.)

To acquire a feeling for the frame of reference of the traveling particle we assume that the accelerating field in the linear accelerator is independent of distance so that the kinetic energy $W - W_0$ of the particle is proportional to z. Let us say that

$$W - W_0 \left[= W_0 \left(1 - \frac{v^2}{c^2} \right)^{-\frac{1}{2}} - W_0 \right] = kz \tag{10-14}$$

Using Eqs. (10-11) and (10-14) an integration can be performed with respect to z and z' from which

$$z' = \frac{W_0 z}{W - W_0} \ln \frac{W}{W_0} \tag{10-15}$$

This seemingly simple relation has some startling connotations. The Stanford linear accelerator, designed for acceleration of electrons to 1000 Mev, is about 300 ft long. But in the frame of reference of the electrons, Eq. (10-15) indicates that the apparent length of the accelerator is only 35.3 cm. If the accelerator had been extended to twice its length to yield 2000-Mev electrons, its length in the electrons' frame of reference would have increased only to 38.5 cm. The consequence of these revelations is that the radial drift of relativistic particles is relatively very slow —so slow, in fact, that high-energy electron linear accelerators have little need of radial focusing mechanisms.

The results of these studies of radial motions will be seen in the discussions of specific designs for proton and electron linear accelerators.

10-4. THE TRANSVERSE-MAGNETIC FIELD PATTERN

In all conventional linear accelerators the field pattern is basically the transverse-magnetic field configuration well known to students of waveguides and resonant cavities. In every case tricks are used to modify the pattern so that the particles see an apparent traveling wave whose velocity is continually that of the equilibrium particle. These various devices do not alter the fact that the field pattern must have an axial electric field as one of its major components. Each linear-accelerator system can be understood as a combination of those modes known as transverse magnetic in which an axial electric field is always present. The field pattern follows directly from a solution of Maxwell's equations

in cylindrical coordinates. It has radial and axial electric-field components and an azimuthal magnetic-field component as follows:

$$E_r = \frac{\omega E_0}{vk_c} J_1(k_c r) \sin \frac{\omega z}{v} \sin \omega t \qquad \text{volts/m}$$

$$E_z = E_0 J_0(k_c r) \cos \frac{\omega z}{v} \sin \omega t \qquad \text{volts/m} \qquad (10\text{-}16)$$

$$H_\theta = \frac{\omega E_0}{ck_c \sqrt{\mu_0/\epsilon_0}} J_1(k_c r) \cos \frac{\omega z}{v} \cos \omega t \qquad \text{amp/m}$$

where r and z = usual cylindrical coordinates
E_0 = axial field amplitude on axis
v = phase velocity of wave
$\sqrt{\mu_0/\epsilon_0}$ = so-called impedance of free space = 377 ohms
$k_c^2 = \frac{\omega^2}{c^2} - \frac{\omega^2}{v^2}$
J_0 and J_1 = Bessel functions which have the following properties:

$$\text{For } x \text{ small:} \qquad J_0(x) \cong 1 - \frac{x^2}{4}$$

$$J_1(x) \cong \frac{x}{2} \qquad (10\text{-}17)$$

$$\text{For } x = 2.405: \qquad J_0(x) = 0$$

$$J_1(x) = 0.519$$

In a resonant cylindrical cavity of radius b the frequency must be such that, for $r = b$, $E_z = 0$. The field pattern of Eq. (10-16) becomes

$$E_r = 0.416 \frac{\omega b}{v} E_0 J_1\left(\frac{2.405r}{b}\right) \sin \frac{\omega z}{v} \sin \omega t \qquad \text{volts/m}$$

$$E_z = E_0 J_0\left(\frac{2.405r}{b}\right) \cos \frac{\omega z}{v} \sin \omega t \qquad \text{volts/m} \qquad (10\text{-}18)$$

$$H_\theta = 3.68 \times 10^{-12} \omega b E_0 J_1\left(\frac{2.405r}{b}\right) \cos \frac{\omega z}{v} \cos \omega t \qquad \text{amp/m}$$

In this case the ratio of the phase velocity v to the velocity of light is

$$\frac{v}{c} = \left[1 - \left(\frac{2.405c}{\omega b}\right)^2\right]^{-\frac{1}{2}} \qquad (10\text{-}19)$$

This transverse-magnetic field pattern is usually designated by the symbol TM_{01}. Several of its features are worthy of particular note. First, although the pattern has been expressed here as a standing-wave pattern, it can be expressed equally well in terms of traveling waves. Maxwell's equations are satisfied just as well if we change the

"$\sin \frac{\omega z}{v} \sin \omega t$" part of E_r to "$\cos \omega \left(t - \frac{z}{v} \right)$" and make the corresponding appropriate changes in E_z and H_θ.

We note also from Eq. (10-19) that the phase velocity must always be greater than the velocity of light. On the other hand, the group velocity v_g (the velocity at which information or power can be propagated) whose value for this mode is given by

$$vv_g = c^2$$

must always be less than the velocity of light. Since we wish to match the particle velocity in a linear accelerator with the phase velocity of the accelerating wave, it is obvious that we cannot use this wave without

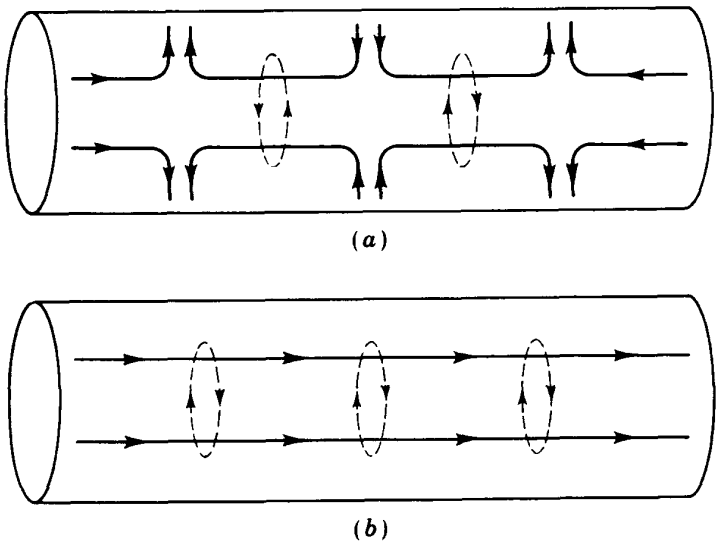

Fig. 10-2. Transverse-magnetic field patterns. Electric-flux lines are solid lines; magnetic-flux lines are broken. (*a*) The TM_{01} mode; (*b*) the TM_{010} mode.

modification because all particles have velocities less than the velocity of light.

A special case known as the TM_{010} mode arises when the phase velocity becomes infinite. In the resonant cavity this is achieved by setting $b = 2.405c/\omega$. In this case the radial field component and the group velocity disappear and the field pattern simplifies to

$$\begin{aligned} E_z &= E_0 J_0 \left(\frac{\omega r}{c} \right) \sin \omega t && \text{volts/m} \\ H_\theta &= 0.00265 E_0 J_1 \left(\frac{\omega r}{c} \right) \cos \omega t && \text{amp/m} \end{aligned} \tag{10-20}$$

As we shall see, this mode is used in all linear accelerators.

Figure 10-2 shows the field patterns in cavities supporting the TM_{01}

and the TM_{010} modes. Electric-field lines are shown as solid lines and magnetic-flux lines are shown as broken lines in this figure.

Further discussion of field patterns in waveguides can be found in standard electrical engineering texts.[10]

10-5. POWER REQUIREMENTS FOR LINEAR ACCELERATORS

In the previous section the transverse-magnetic field pattern used for acceleration in linear accelerators was shown to have an azimuthal magnetic-field component whose value is maximum at the wall of the cavity. Because of this magnetic field, paraxial currents flow in the cavity wall. From Eqs. (10-20) the amplitude of the total wall current is

$$I = 8.65 \times 10^{-3} bE_z \qquad \text{amp} \tag{10-21}$$

where b is the radius of the waveguide and E_z is the amplitude of the axial electric field on the axis of the cavity. The resistive losses in the walls due to these currents are the major power losses in the machine. Since linear accelerators are always lined with copper, we can evaluate these losses numerically. The resistance of the copper wall of a waveguide of radius b follows from the usual skin-effect formulas; it is

$$R = \frac{7.36 \times 10^{-4}}{b\sqrt{\lambda}} \qquad \text{ohms/m} \tag{10-22}$$

where λ is the free-space wavelength of the accelerating field. From the two relations above, the total loss in a machine of length l can now be estimated to be

$$P = \frac{2.8 \times 10^{-8} bE_z^2 l}{\sqrt{\lambda}} \tag{10-23}$$

But for the TM_{010} mode the radius of a waveguide is given by

$$b = \frac{2.405c}{\omega} = 0.383\lambda$$

Also, for singly charged particles, the maximum possible particle energy T emerging from the accelerator is given by $T = lE_z$. Consequently, we can rewrite Eq. (10-23) in the form

$$P = \frac{1.1 \times 10^{-8} T^2 \sqrt{\lambda}}{l} \tag{10-24}$$

This relation is not very accurate because in its derivation we have neglected the losses in all the auxiliary structures necessary to change the standard waveguide field pattern so that it will include the traveling-wave component essential for acceleration. It does, however, establish the

order of magnitude of power necessary. For example, suppose we wish to accelerate protons to 50 Mev in a machine 25 m long with a field whose free-space wavelength is 1.5 m. The power necessary, as given by Eq. (10-24), is 1.3 megawatts! To reach energies in the hundreds of Mev in a machine of reasonable length requires enormous quantities of power. It was this fact that held back the development of the linear accelerator until radar developments yielded sources of pulsed power in this range. The very high power requirements still make the linear accelerator a costly machine and have been a strong deterrent in its development even in the face of its several advantages as a research tool.

A more sophisticated derivation of Eq. (10-24) does not change its form but results in the expression

$$P = \frac{CT^2\sqrt{\lambda}}{l} \tag{10-25}$$

where C is a constant depending only on the geometric structure of the accelerating system. So long as the pattern is unchanged, it is possible to use this formula in scaling to different energies, wavelengths, and lengths. Its most interesting consequence is that power is inversely proportional to accelerator length; in designing a linear accelerator, power can be decreased by increasing length, and the designer can choose an optimum length for which the total cost of power plus cost of the accelerator is a minimum. But when the structure is changed, the constant C changes so much that the theorem is no longer very useful. For most proton linear accelerators C is about 2.5×10^{-8}, while for most electron linear accelerators it has values of the order of 10^{-7}.

10-6. THE CONCEPT OF SHUNT IMPEDANCE

A useful figure of merit for a linear-accelerator structure is one that provides an answer to the question: How much power is needed to provide a given accelerating field? Since, as we have seen in the preceding section, the power is proportional to the square of the accelerating field, a useful ratio should be that of the square of the maximum electric field on the axis to the power dissipated per meter of length. This ratio is called the shunt impedance and has the dimensions of ohms per meter. Usually it is expressed in megohms per meter thus:

$$Z = \frac{10^{-6}E_z^2}{P} \quad \text{megohms/m} \tag{10-26}$$

For almost all operating linear accelerators the shunt impedance Z lies between 25 and 50 megohms/m. This good agreement is, at least partly, a chance agreement. The possibility certainly exists that some

ingenious designer will invent a structure with a much higher shunt impedance. If this is achieved, the linear accelerator may become a much more popular device than it now is.

10-7. CAVITIES FOR ELECTRON LINEAR ACCELERATORS

The accelerating system for an electron linear accelerator consists of a sequence of small cavities (see Fig. 10-3). Each of these cavities operates in the TM_{010} mode, modified slightly by the fact that the end walls of the cavities are not solid but have openings into the adjacent cavities. These apertures have the dual function of permitting passage of the electron beam and of providing coupling from cavity to cavity so that many cavities can be excited from one power input. The size of the hole determines the degree of coupling and so determines the relative phase shift from one cavity to the next. When the dimensions have been

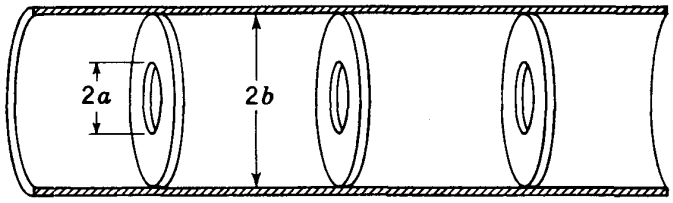

Fig. 10-3. Cutaway sketch of iris-loaded accelerating system for an electron linear accelerator.

tailored correctly, the phase changes from cavity to cavity along the accelerator to give an over-all phase velocity corresponding to the desired particle velocity. As was stated in Sec. 9-7, it is sufficient over most of the length of the accelerator to set this effective velocity equal to the velocity of light. This is true for electrons since, for energies above a few hundreds of kev, electron velocities are very close to the velocity of light.

The reason that this apparently complicated structure cannot be replaced by a simple waveguide is that the phase velocity in a simple waveguide cannot be reduced to the velocity of light. Consequently, the introduction of irises to subdivide the waveguide into separated cavities is often considered as slowing down the wave by iris loading. This picture is just as valid as the one presented in the preceding paragraph.

The arguments leading to the precise choices of the parameters of iris-loaded waveguides for electron linear accelerators have been presented by several groups. Outstanding among these studies are those of Slater,[11] of the Stanford group,[12] and of the British group at Harwell.[13] Five parameters must be determined: the wavelength of the accelerating

signal, the iris thickness, the iris spacing, the diameter $2a$ of the hole in the iris (cf. Fig. 10-3), and the diameter $2b$ of the guide proper. We shall discuss these choices in that order.

As has been shown in Sec. 10-5, the power required for a given final electron energy is proportional to (wavelength)$^{1/2}$. Consequently it would appear desirable to choose as short a wavelength as possible consistent with power sources and construction techniques available and yet not so small as to result in a very small waveguide with too restricted an aperture. These considerations have usually resulted in the choice of a wavelength of about 10 cm, which gives an over-all guide diameter of about 8 cm. It was a happy coincidence that power sources and other equipment at this frequency had been developed for S-band radar, and were available to scientists when they returned to their laboratories after World War II.

Iris thickness proves to have very little influence provided only that it is much less than the iris spacing. A thickness of about 0.5 cm provides adequate mechanical strength and can be contoured to prevent high field concentration and breakdown at sharp corners.

Iris separation has a fairly strong effect on shunt impedance. If too few irises are included, the desired traveling-wave amplitude for a given power input begins to decrease. When iris spacing is reduced too far, excessive power losses are introduced by currents flowing on the surfaces of the iris plates. The optimum shunt impedance occurs for 3.5 irises per wavelength, but for convenience in testing it is more usual to introduce 4 irises per wavelength, giving a shunt impedance lower than the optimum by only a few per cent.

The radii of the hole in the iris a and the guide radius b are not independent. For any choice of a there exists a value of b that will give an over-all phase velocity equal to the velocity of light. As a is increased, b also increases rather slowly. The precise relation is determined by a complex analysis, but for relatively small values of a, b is represented rather approximately by the relation

$$\frac{b}{\lambda} = 0.383\left[1 + 20\left(\frac{a}{\lambda}\right)^3\right] \tag{10-27}$$

It remains only to make a choice of a. For reasons to be discussed in the next section, most modern linear electron accelerators utilize traveling-wave field patterns. The flow of energy is strongly influenced by the size of the apertures; also, as we shall now demonstrate, there is an optimum rate of energy flow. The distribution of energy along the waveguide follows from two definitions and one self-evident relation as follows. The group velocity v_g is defined by the relation

$$v_g = \frac{\text{energy flow}}{\text{energy density}} \tag{10-28}$$

The self-evident relation is

$$\frac{d}{dz}(\text{rate of energy flow}) = \text{energy dissipated} \tag{10-29}$$

The Q factor of the waveguide system is defined by

$$Q = \frac{\omega(\text{energy stored})}{\text{rate of energy dissipation}} \tag{10-30}$$

From these three relations it follows that

$$\text{Rate of energy dissipation} \propto e^{-(\omega z/v_g Q)}$$

Since the energy dissipation is proportional to the square of the electric field, the electric field can be written

$$E_z = E_{z0}e^{-(\omega z/2v_g Q)} \tag{10-31}$$

It is usual to introduce energy at equally spaced points along the accelerator. The energy enters through a directional system such that energy flow is only in the direction of motion of the particle beam. The energy that remains at the next feed point is either reflected to become a useless backward wave or dissipated in an external load. If the distance between feed points is l, the total energy gain of a particle riding on the crest of the wave from one feed point to the next will be

$$e\int_0^l E_z\,dz = \frac{2ev_g Q E_{z0}}{\omega}(1 - e^{-(\omega l/2v_g Q)}) \tag{10-32}$$

The total power dissipation will be proportional to E_{z0}^2. Hence, if the amount of power available is constant, E_{z0} will be a constant. Q also will not change markedly with v_g; consequently the maximum acceleration will occur when the quantity $v_g(1 - e^{-(\omega l/2v_g Q)})$ has its maximum value. This occurs when v_g is chosen to give

$$\frac{\omega l}{2v_g Q} = 1.26 \tag{10-33}$$

(If electron beam loading is appreciable, this figure will decrease.) In other words, optimum operation is attained when the distance between feed points and the group velocity result in an attenuation of the wave between feed points to a little less than $1/e$ of its initial value.

It is now necessary to establish the relation between v_g and the iris aperture radius a. The rate of energy flow through the aperture is given by the integral of Poynting's vector over the aperture. For the TM waves here in question this integral is

$$\text{Energy flow} = \int_0^a E_r H_\theta 2\pi r\,dr \tag{10-34}$$

But from Eqs. (10-16) and (10-17), E_r and H_θ are proportional to r for r small. Hence, so long as a/b is a relatively small ratio, the energy flow given by Eq. (10-34) is approximately proportional to a^4. The constant of proportionality can be established either by a complicated analysis or by experiment. For a distribution of four irises per wavelength and for a/b in the neighborhood of 0.25, the value of v_g is given approximately by

$$\frac{v_g}{c} = 2.4\left(\frac{a}{b}\right)^4 \tag{10-35}$$

The choice of the aperture radius a is now clearly defined. When the distance l between feed points has been chosen and when the Q of the proposed structure has been measured or calculated, v_g is determined from Eq. (10-33). The two radii a and b are now defined by Eqs. (10-27) and (10-35).

Once these choices of parameters have been made, the dimensions must be maintained very precisely so that the phase velocity does not deviate from the chosen value. This is particularly important in electron linear accelerators, since these lack the self-compensating features of true phase stability. If the phase velocity is incorrect, the electrons will drift away from the acceleration phase and will not reach the design energy. If the phase velocity is wrong by as much as 1 per cent, the electrons will drift to a phase at which they lose energy instead of gaining energy before they have traveled more than 10 m. Consequently the accelerating system must be constructed very precisely. Mechanical tolerances in dimensions and locations are usually of the order of 0.0002 in., and temperatures must be precisely controlled in order that thermal expansions do not exceed these tolerances.

10-8. TRAVELING WAVES VERSUS STANDING WAVES

In the early days of the development of the modern electron linear accelerator it was not clear whether or not traveling-wave excitation of the cavity is preferable to standing-wave excitation. At first glance it would appear that traveling-wave excitation is preferable because the standing-wave mode is made up of a combination of a useful traveling wave going in the same direction as the electron beam and a useless traveling wave going in the opposite direction; thus half of the input power is wasted. But, as was shown in the previous section, traveling waves must be allowed to travel far enough that they are attenuated to about $1/e$ of their input amplitude. For this condition, the power required for the traveling-wave system is exactly the same as for the standing-wave system. The choice of system must thus be based on considerations other than power.

The choice of excitation is more strongly influenced by the type of power source available. After the World War II development of magnetrons for radar applications, several attempts were made to use magnetron oscillators to drive electron linear accelerators. No single magnetron was available with enough power to drive a machine of appreciable output energy; this left the accelerator designers with the two problems of keeping the magnetron frequency on the resonant frequency of the waveguide and synchronizing several magnetrons in phase. The first problem could be solved only by using a standing wave in the accelerator so that information from the backward component of the standing wave could be used in keeping the magnetron on frequency. The second problem was solved by the MIT accelerator group by light coupling between the various magnetrons and by a small amount of preexcitation. But by 1950 the Stanford group had developed klystron amplifiers to the point where they yielded several times as much power as could be derived from a magnetron. Many klystron amplifiers could be driven by a single power source, and by this means their relative phases were automatically maintained in the correct relation.

To the designer of the radiofrequency power supply for a linear accelerator, the accelerator cavity should look as much as possible like a pure resistive load. With a traveling-wave system this is rather easy since no reflected wave appears at the driving point to give reactive components of impedance. With the high-Q standing-wave system, on the other hand, difficulties of this sort are always experienced. If the system is matched at full load, bad mismatches of impedance are experienced during the build-up period.

A theoretical improvement in efficiency of the traveling-wave system is possible if the power left at the end of the section driven by one power source is not dissipated externally but is returned externally to the driving point and returned to the accelerator through systems of directional couplers. This technique has been worked out by Harvie and Mullett[14] of the Harwell group. It can give an appreciable increase in efficiency, but it adds complexity and changes the driven impedance to one characteristic of a standing-wave system. Consequently the technique has not become popular and is not used in modern electron linear accelerators.

10-9. THE STANFORD MARK III LINEAR ELECTRON ACCELERATOR

We begin a presentation of electron linear accelerators with the Stanford Mark III machine for several reasons. First, it has reached the highest energy yet achieved in any linear accelerator. Partly because of this fact and partly because it was built by an exceptionally gifted team, it is now accepted as the prototype for many other machines now under

construction. It will probably be some time before new developments change this situation. Finally, it has been completely described in the literature; the reader will be able to supplement the sketchy description possible here by reference to a number of publications; most outstanding is the Linear Accelerator Issue of *The Review of Scientific Instruments.*[8]

First we shall satisfy the reader's curiosity about the expression "Mark III" with a few historical comments. Ever since the mid-1930s the high-energy electron linear accelerator had been a dream of the late W. W. Hansen. Before World War II he was frustrated by the lack of radiofrequency generators with sufficient power output. The first device to fill this requirement was the magnetron, developed during the war for radar applications, and in 1947 Hansen and his associates built a 12-ft machine powered by a magnetron in which they accelerated electrons to 6 Mev. This was the Stanford Mark I.[15] Although this machine was reasonably successful, the magnetron left much to be desired as a power source and the Stanford group set about the development of the klystron for megawatt operation in the 3000-megacycle range. In the minds of most of their contemporaries the klystron was basically a milliwatt device useful only as a local oscillator or signal generator, and the Stanford project seemed fantastic. The klystron development proved, however, to be a brilliant success, and in 1950 the Stanford group brought into operation a new accelerator, the Stanford Mark II, also 12 ft long but yielding 35-Mev electrons. It was powered by a klystron amplifier which delivered between 10 and 20 megawatts at 2855 megacycles. The amplifier was powered by a 390-kv pulser delivering currents up to 250 amp. This machine was the prototype for the Mark III, designed for electron energies up to 1 Bev and consisting essentially of thirty 10-ft Mark II accelerators arranged in a line. After some years of operation at 700 Mev this machine was brought to its design energy in 1960. In the hands of W. K. H. Panofsky and R. Hofstadter it has proved itself a very powerful tool for explorations of nuclear structure. The Mark III machine is now a prototype for machines of still higher energies. For example, at the Orsay Laboratory in France a group is engaged in construction of a 2-Bev machine like the Mark III but roughly twice as long. The most ambitious proposal for the future comes from the Stanford group, which began in 1955 a design study for a machine 10,000 ft long aimed at eventual operation at 45 Bev.

A visitor to the W. W. Hansen Laboratories of Physics at Stanford will find the 300-ft machine buried under a tunnel of concrete shielding. If the concrete were removed, he would see a 300-ft tube supported above a row of 20-ft I beams. Along one side of the accelerator is packed the radiofrequency gear in a sequence of oil tanks and shielded high-voltage houses. The output end of the accelerator delivers the high-energy beam through a concrete shielding wall into an experimental hall full of analyz-

ing and deflecting magnets and experimental electronic equipment. Behind another shielding wall near the injection end of the accelerator is the main control panel, an impressive array of controls, safety devices, and trouble indicators.

The basic parameters of the Mark III machine are as follows:

Total length = 300 ft = 90 m
Length per section = 10 ft = 3.05 m
Frequency of rf power sources = 2856 megacycles
(wavelength = 10.5 cm)
Phase velocity $v = c$; velocity of light = 2.998×10^8 m/sec
Group velocity $v_g = 0.01c = 2.998 \times 10^6$ m/sec
Inside diameter of accelerating tube $2b = 8.247$ cm
Diameter of iris apertures $2a = 2.089$ cm
Thickness of irises = 0.584 cm
Iris spacing (center to center) = one quarter-wave = 2.625 cm
Q of cavity = 10,000
Time required to build up accelerating field = 1 μsec
Duration of acceleration = 1 μsec
Pulse repetition rate = 60 per second
Shunt impedance = 47.3 megohms/m

Figure 10-4 is a block diagram of the Mark III machine, and the chapter headpiece is a photograph of the accelerator with the shielding removed.

The machine was constructed in 2-ft sections, each assembled with extreme care and with techniques especially developed for the occasion to make possible the high precision essential to the success of the machine. The 2-ft sections were then clamped together to form the 10-ft acceleration units. Each 10-ft section is now effectively a continuous piece of iris-loaded waveguide, with one special section at the low-energy end. The end of this section is closed by a disk of the usual inside diameter but of much greater thickness than the other disks. To the high-frequency field this looks like a waveguide beyond cutoff and prevents the high-frequency energy from passing through the accelerator in the direction opposite to the electron beam. In the outer wall of this special section is an aperture opening into a waveguide which connects the radio-frequency power source to the accelerator. This aperture serves also as a pumping port for evacuation of the accelerator.

The 10-ft sections are arranged end to end on especially designed supports with which over-all alignment can be achieved. In the course of this assembly, numerous mechanical and rf tests are performed to ensure the precision of the machining and assembly.

The temperature of the machine must be controlled precisely. An over-all temperature change is not serious since it can be compensated by

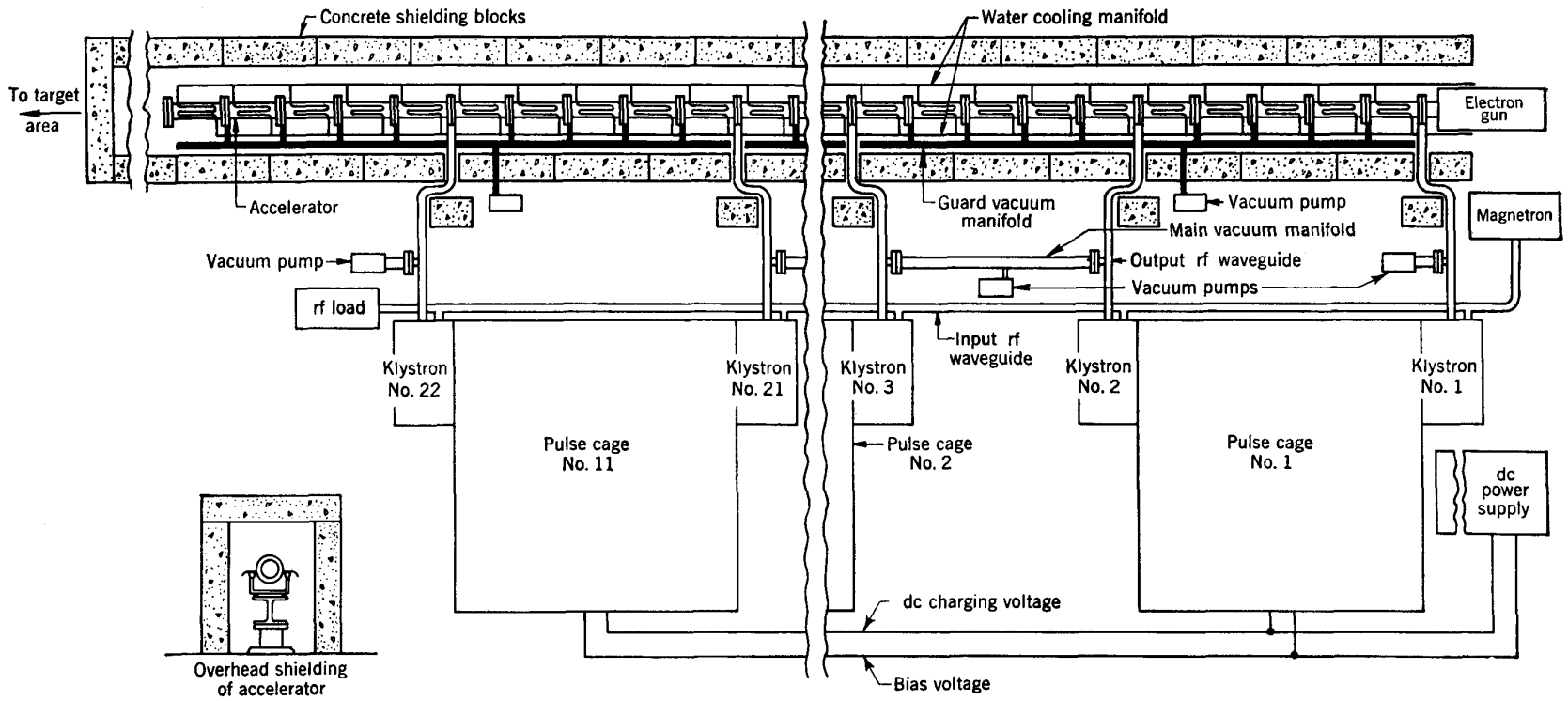

Fig. 10-4. Block diagram of Stanford Mark III accelerator.[8]

a change in operating frequency, but the relative temperatures of the sections of the machine must be maintained to better than 2°C. This is done by water cooling; copper cooling pipes are soldered along the outside walls of the 2-ft subsections.

After the accelerator itself the most spectacular Stanford achievement is the klystron development, in which the Stanford group has pioneered and which has laid the foundations for a now flourishing industry. This development involved extrapolation of klystron operation to power levels higher by a factor of 1000 than those previously achieved. Three-cavity klystrons of conventional design were reengineered to operate with 400-kv electron beams of 250 amp. Cathode problems, breakdown problems, problems of the behavior of relativistic electrons, and many other problems had to be solved. Solution of some of these problems still was not quite complete by 1961, but operation of klystrons at the 20-megawatt output level seems now to be quite predictable and reliable. Fortunately, in the relativistic electron accelerator, failure of one power source does not stop operation but merely decreases the final electron energy by about 5 per cent (for the Mark III).

A detailed description of the klystron amplifiers will not be included here since klystrons of this type are becoming shelf items with transmitting-tube manufacturers. Here we shall mention only one of the most troublesome problems encountered at Stanford. The klystrons on the Mark III machine were continuously pumped rather than sealed-off tubes, so that repairs could more easily be made on tubes which failed. The vacuum maintained in the accelerator was not good enough for the klystrons, however, since the oxide cathodes in the klystrons are very easily poisoned by traces of air. Consequently, the two vacuum systems were separated by an insulating ceramic window across the waveguide leading from the klystron to the accelerator. During the early days of operation many klystrons failed because of puncturing of this window by electrical discharges. It was thought that this was due to bombardment of the window by stray electrons from the klystrons, and a "dog-leg" bend was included in the waveguide so there was no direct path from klystron to window. This cured most of the difficulty, but residual difficulties still exist. Model tests indicate that these can be controlled by use of a double window with an evacuated space between.

The klystron development has now reached the point where 2000 hr is a conservative estimate of tube life. For some time a sealed-off-klystron development has been under way at Stanford, and it would appear that before long the continuously pumped klystron will be a thing of the past.

Injection into an electron linear accelerator can be a very simple process. In the Mark II machine the injector consisted of very little more than a hot tungsten spiral cathode biased to a negative potential of about 80 kv. Although 80-kev electrons have a velocity of only half the velocity of light, it still proved possible to inject into a section of wave-

guide in which the phase velocity was equal to the velocity of light. This does not seem so mysterious when it is realized that the high accelerating fields bring the electrons very rapidly to almost the velocity of light. But in the process many electrons which did not enter the first section at exactly the correct phase are lost. So in the Mark III a "bunching section" is included which pregroups the electrons around the correct phase. This can be done in either of two ways. The simplest method is that used in the klystron; the electrons pass through a gap at which they experience a relatively weak rf field, so some are accelerated and some are decelerated. They are then allowed to drift for a certain distance so the accelerated electrons catch up with the decelerated electrons of the previous bunch. With the correct drift distance the beam will be bunched around a particular phase. The bunching is, however, somewhat nonlinear and incomplete. For really tight bunching it is better to accelerate and bunch at the same time. The buncher used for this purpose is merely a section of accelerator in which the phase velocity is matched to the particle velocity. Still better bunching is achieved if the accelerating field increases along the buncher. In the Stanford buncher the field rises by a factor of 10 in its 0.8-m length. These variations of field strength and phase velocity are made automatic in the buncher (which is also an iris-loaded waveguide) by correct choices of the dimensions of the tapered pipe and the loading disks.

Two vacuum systems are required for evacuation of the klystrons and of the accelerator proper. Each klystron has its own pump which maintains a pressure in the klystron of 10^{-7} mm Hg with the cathode cold and about 10^{-6} mm Hg with the cathode hot. The vacuum requirements in the accelerator are not so stringent, and the pressure is reduced to about 2×10^{-6} before application of rf power; under full power the pressure rises to about 2×10^{-5} mm Hg. The accelerator is evacuated by 11 oil-diffusion pumps, each of which is connected to two 10-ft sections through a manifold. Although the ultimate pressure is not very critical, it is important for reasons to be discussed in Sec. 10-16 that oil from the pumps be prevented from migrating onto the surfaces of the accelerating cavity. For this reason each pump is equipped with a water baffle and a liquid-nitrogen cold trap. Addition of the cold traps was found to make a material improvement in the time required initially to bring the rf power to full operating levels.

In operation the Mark III accelerator yields an average current of about 1 μa in a beam about $\frac{1}{4}$ in. in diameter (this corresponds to an average power of almost 1 kw in the beam). Most of the output current is included in an energy spread of about 2 per cent. By magnetic analysis the energy homogeneity can be improved to be within any desired limits, with associated reduction of intensity.

After leaving the machine the accelerated beam passes into a beam-switching area where it can be displaced to right or left by deflecting

magnets or allowed to proceed undeflected. It then enters the experimental area through holes in a wall of heavy (iron oxide–loaded) concrete 5 ft thick. On the other side of the experimental area is a large earth mound which serves as a "backstop" to reduce the radiation level in the surrounding (university campus) area.

10-10. OTHER ELECTRON LINEAR ACCELERATORS

Dozens of electron linear accelerators in the energy range of a few tens of Mev are now scattered throughout the world, serving a variety of applications. Such machines are valuable implements in radiography and in medical applications and are commercially produced by several manufacturers. In design these machines follow the Stanford lead and it appears that, for some time, the Mark III accelerator will serve as a pattern for production. Four rather different electron linear accelerators are worthy of mention; three are of historical interest, and the other may indicate a future trend.

The first machine in the former category is the electron linear accelerator at MIT. It was constructed before the klystron development and was designed to be powered by magnetron oscillators. This machine is described in the 1952 paper of Demos, Kip, and Slater.[16] It also uses an iris-loaded waveguide structure, but to match the output requirements of the magnetron drivers it is a standing-wave machine. It is formed of 20 sections each about 1 ft long and each powered by a 2800-megacycle 500-kw magnetron. The final electron energy available is about 16 Mev. The difficult problem of keeping 20 magnetrons operating at the same frequency and at the correct relative phase was solved with less difficulty than had been generally expected. The problem of injection was simplified by use of a 2-Mev electrostatic injector so that injection energies were high enough to permit injection directly into a guide having its phase velocity equal to the velocity of light. Operation of this machine was quite successful and verified the predictions of its designers. Although it was constructed with the primary objective of advancing the linear-accelerator art, it has proved itself over a period of years to be a valuable research tool, and it was still in operation in 1961 some nine years after its completion.

During about the same period a traveling-wave linear accelerator for 4 Mev was designed at the British Atomic Energy Research Establishment at Harwell.[17] This machine was powered by a single 3000-megacycle 2-megawatt magnetron; energy was introduced at the injection end of the accelerator, and the energy which emerged at the high-energy end was dissipated in a waveguide load. Later Harwell studies showed that this energy could be returned to the input and added by a directional coupling system to the magnetron output.

The third approach in the historical category was radically different from those already described. At Yale an electron linear accelerator was built under the direction of H. L. Schultz[18] in which the operating frequency was reduced to the 600-megacycle range where triode power amplifiers were available in the 500-kw range. Instead of the iris-loaded waveguide, the Yale group chose to employ a series of uncoupled TM_{010} cavities. The holes through which the beam passed were made small enough that there was no appreciable coupling between cavities. Then each cavity was driven by its own power amplifier, relative phases of the cavities were adjusted for optimum performance, and finally the eight-cavity machine was brought into operation, delivering a current of the order of 0.2 μa average at 10 Mev. Although this approach has much to recommend it in the simplicity of the design and tune-up procedure, its relatively low efficiency compared with the 3000-megacycle machines makes it improbable that it will be duplicated.

Before passing on from these various machines, it should be emphasized that each has made its important contribution to the advancement of the accelerator art by adding to the store of experience of what can and what cannot be done. In the use of high rf fields and high power levels there have been and still are mysterious phenomena which plague the linear-accelerator designer. Some of these effects will be mentioned in Sec. 10-16.

The latest and most exciting modern development in the electron-linear-accelerator field is the result of many years of work at Harwell on dielectric loading of accelerator cavities. The most promising approach has been to load the accelerating waveguide with dielectric disks instead of metal irises. Disks of titanium oxide are used because they have high dielectric constants (of the order of 90 times that of free space) and low rf losses. To the rf field these present many of the same characteristics as do metal disks, but they do not show the resistive losses that are found with metal disks. Consequently the machine becomes much more efficient. In 1957 the Harwell group reported[19] on a 1.5-Mev dielectric-loaded machine which displayed a shunt impedance of 180 megohms/m. The possibilities of this system had been realized for some years, but model machines could not be made to hold the necessary high fields. Finally the trouble was cured by a thorough cleanup of the system and a change from oil pumps to mercury pumps. Apparently the troubles all were due to invisible oil films on the dielectric surfaces.

10-11. CAVITIES FOR PROTON AND HEAVY-ION LINEAR ACCELERATORS

The iris-loaded waveguide does not lend itself to the low phase velocities which must be used to accelerate protons or heavy ions. If such a system

is forced to low phase velocities and low frequencies, the efficiency becomes very low. Consequently a totally different approach has been made to this problem. The standard ion accelerator is a single standing-wave cavity operating in the TM_{010} mode. The electric-field lines are parallel to the axis of the cavity and terminate on the end walls of the cavity. In a 30-Mev ion linear accelerator the rf potential difference between the two ends of the cavity must be at least 30 Mev. But since an ion takes many periods of the rf field to travel from one end of the cavity to the other, some device must be introduced to shield it from the field while the field direction is such as to decelerate rather than to accelerate. This can be done rather simply by introducing a series of tubes along the axis through which the beam passes. The tube length is cut

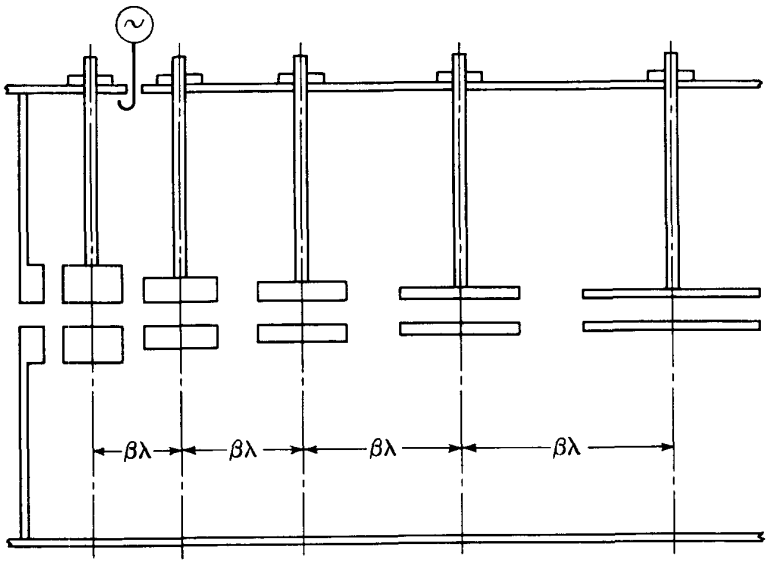

Fig. 10-5. Basic structure of positive-ion linear accelerator. As the drift-tube length increases, the diameter must decrease to maintain resonance.

so the ion takes exactly one full period to pass from the entrance of one tube to the entrance of the next. An ion which has the correct phase will see only accelerating fields; while the field is in the reverse direction, the ions are shielded by the tubes. These tubes are known as drift tubes since the ions experience no forces while they travel through them. Their length increases along the accelerator as the ion velocity increases. The over-all system presents the appearance shown schematically in Fig. 10-5. Fortunately the introduction of these drift tubes makes only local variations in the TM_{010} mode. The diameter of the cavity must be changed slightly from that of the empty TM_{010} guide, but the appropriate changes can be determined either by computation or by model studies. To the moving ion, however, all similarity to the TM_{010} mode has disappeared. The ion sees a complicated square-wave pattern whose important com-

ponent is the traveling-wave component having the same velocity as that of the ion at the equilibrium phase.

The use of drift tubes in a high-Q cavity as an accelerator structure was originated by a group at the Berkeley Radiation Laboratory under the direction of L. W. Alvarez and W. K. H. Panofsky. Shortly after World War II this group constructed a 32-Mev proton linear accelerator which serves as the prototype for all ion linear accelerators now under construction. Although many mechanical improvements have been made in the original structure, the basic principles have been preserved without appreciable modification. In the next section we present the design features of the Berkeley machine.

10-12. THE BERKELEY 32-MEV PROTON LINEAR ACCELERATOR

With the evolution of the cavity concepts just mentioned, the Berkeley group undertook, shortly after the end of World War II, to construct a 32-Mev proton linear accelerator. The details of construction and operation of this machine are presented in detail in the Linear Accelerator Issue of *The Review of Scientific Instruments*.[8]

Two additional factors entered the consideration of the Berkeley group. One was the discovery of phase stability with its obvious application to the linear machine. The other was the availability of a large amount of surplus radar equipment from the armed services. The radar tubes and power supplies were to be used to excite the accelerating cavity. In operation the performance of the radar equipment proved to be unsatisfactory, but by that time better rf sources were available.

The accelerating cavity was designed for operation at 200 megacycles and so was about 1 m in diameter. Average accelerating fields of about 2.5 Mv/m were believed to be achievable, so the machine length was made 40 ft or about 12 m. It was also felt desirable to separate the rf cavity from the vacuum tank so that distortions of the tank under evacuation would not detune the cavity. Therefore the rf cavity was built of copper sheets, using a light but rigid construction; the cavity was built by an aircraft company using standard aircraft production techniques. This cavity was then supported inside a large steel vacuum tank. Both the tank and the rf liner were split in a horizontal plane so both could be opened for installation of the drift tubes. The details of construction can be seen in Fig. 10-6. The drift tubes were hung from a supporting rail at the top of the liner by thin stems; these stems are normal to and make negligible perturbations in the rf field.

The drift tubes were basically cylinders with rounded ends and varied in diameter from 4.75 in. at the low-energy end to 2.75 in. at the high-energy end. Their precise shapes were determined by modeling. Since the radial planes through the center of the drift tube and midway between

drift tubes are planes of symmetry, the model cell could include only one-half drift tube; the planes of symmetry were replaced by copper sheets. In this unit cell the drift-tube shape was modified until the cell resonated at the correct over-all frequency. When the complete structure of all the unit cells was assembled, its over-all resonant frequency was the same as that of each cell. Both drift-tube diameter and relative gap spacing were modified to achieve this resonance. At the low-energy end the gap length was about 0.28 times the drift-tube length. This was gradually increased to about 0.33 at the 8.4-Mev point, and the ratio was held constant at 0.33 throughout the rest of the accelerator.

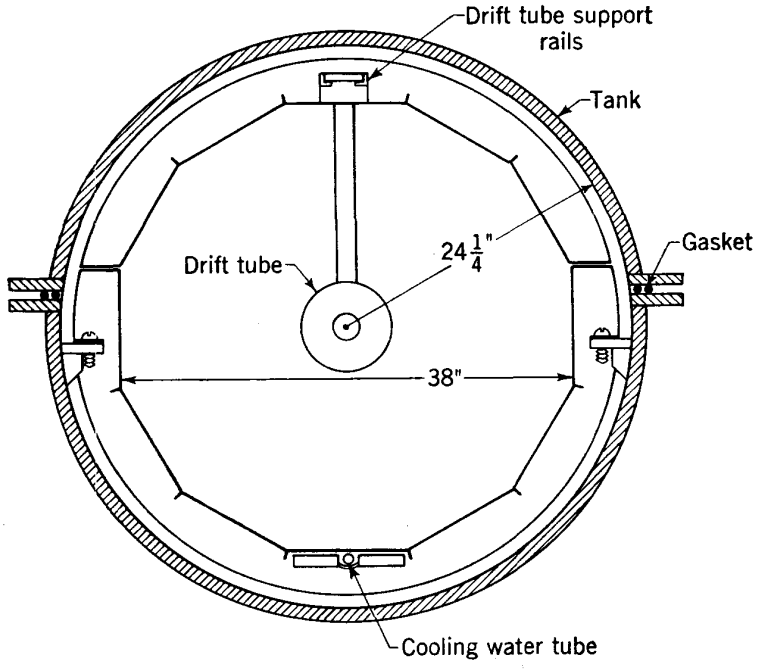

Fig. 10-6. Cross section through the Berkeley 32-Mev proton linear accelerator.[8]

One of the difficult problems facing the Berkeley group was rf defocusing of the beam. At velocities low compared with the velocity of light a phase-stable particle will be lost very rapidly by the radial components of the rf accelerating field (see Sec. 10-3). This is obviously the case because the phase-stable particle is riding at such a phase that the field is increasing as it crosses the accelerating gap. From the field pattern in the gap (Fig. 10-7*a*) we see that the inward force experienced by the particle as it leaves one drift tube will be more than counterbalanced by the outward force of the higher field present as it enters the next drift tube. It was realized by the Berkeley group that the radial field at the entrance to the drift tube could be largely removed if the upstream end was closed by a metal foil thin enough to permit passage of the proton beam without serious energy loss. The revised field situation can be visualized from

Fig. 10-7*b*. So beryllium foils 0.00003 in. thick were included in each drift tube. Unfortunately, after a few of the rf discharges inevitable in bringing the rf to full power, the foils evaporated and disappeared. They were then replaced by tungsten grids, which eventually were reduced to a few bent strips of tungsten strip located edge on to the beam. The grids solved the problem, although their optical properties were not so good as those of the foils and the rather poor focusing resulted in considerable beam loss. The structure of a typical drift tube in the Berkeley linac is shown in Fig. 10-8.

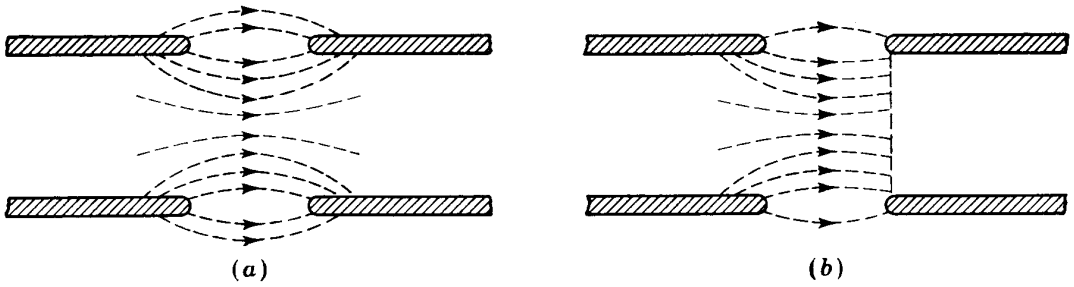

Fig. 10-7. Electric-field patterns between drift tubes: (*a*) normal defocusing-field pattern; (*b*) focusing-field pattern using grids or foils.

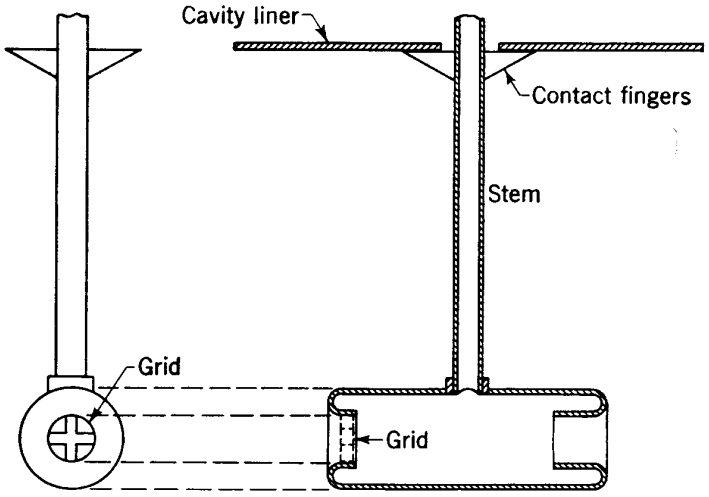

Fig. 10-8. Sketch of a typical drift tube in the Berkeley linear accelerator.

The rf power necessary to excite the tank to the desired level is about 2.1 megawatts. The Q of the tank is very high—about 70,000—consequently a period of about 200 μsec is required to bring the power up to the operating level. For good over-all efficiency a beam pulse length of 400 μsec was chosen to make the total pulse length 600 μsec, repeated 15 times per second. The power is supplied by nine self-excited power oscillators using Eimac 3W10,000A3 triodes and distributed at intervals along the tank. Coupling is such that the oscillator frequency is determined by the resonant frequency of the tank. This system will not rise

by itself to full power because of multipactoring (see Sec. 10-16), and it is necessary to start the rising field cycle by a single power amplifier used as a preexciter.

The injector for the 32-Mev machine is a 4-Mev electrostatic generator built by C. M. Turner. The high injection energy was chosen primarily because of the planned use of focusing foils which would cause serious beam scattering at lower energies. With the introduction of grids much lower injection energies are now possible, and in newer machines 500-kev injectors are common.

In operation the Berkeley machine yields an average beam current of about 0.4 μa about 3 mm in diameter. The energy spread in the beam is only about 0.3 per cent. This sharply focused and homogeneous beam is a very powerful research tool; it is more intense than any external cyclotron beam yet available.

In 1958 this historic machine was dismantled and moved to the University of Southern California, where it should continue its career as a valuable tool for research in nuclear physics.

10-13. OTHER PROTON LINEAR ACCELERATORS

Because the cost per Mev of proton linear accelerators is considerably higher than that for cyclotrons, the number constructed is smaller than for electron linear accelerators. Several noteworthy machines have been constructed, however, and others are in the process of construction.

At the University of Minnesota a group under the direction of J. H. Williams has built a 70-Mev machine[20] which is now in satisfactory operation and is shown in the artist's sketch of Fig. 10-9. This machine is subdivided into three tanks, each similar in construction to the Berkeley 32-Mev machine. Protons are injected at 500 kev into the first tank and are accelerated to 10 Mev in a distance of 18 ft. They leave the first tank to pass through a short section of pipe into the second tank, where their energy is increased to 40 Mev; in the final tank the energy is increased to 68 Mev; both the second and the final tanks are 40 ft in length. Deflecting stations are included at the exit of each tank so that 10-, 40-, and 68-Mev proton beams are available. The rf power for the three tanks is supplied by a power-amplifier system whose output consists of three tetrodes operating in parallel to power the three tanks. The tetrodes are of a spectacular size and of an unusual design with built-in resonant cavities. Tetrodes of this particular design are known as "resnatrons." They are not commercially available but were built specially by the Minnesota group.

At the British Atomic Energy Research Establishment at Harwell an ambitious proton-linear-accelerator project was initiated several years ago when plans were drawn up for a 600-Mev proton machine. Detailed

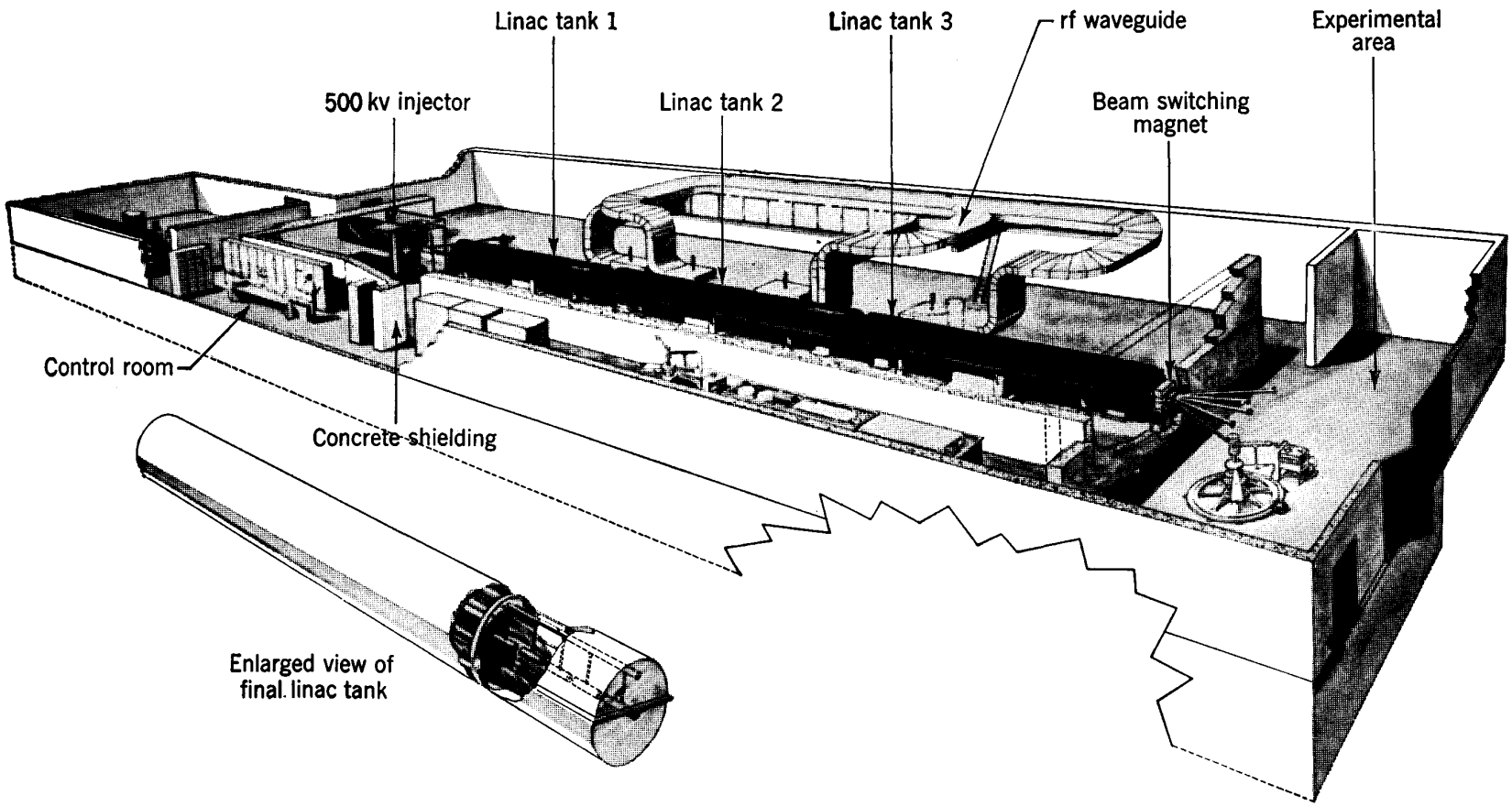

Fig. 10-9. 70-Mev proton linear accelerator at the University of Minnesota.[20]

design studies were made for the different types of accelerating cavities appropriate at the various energy ranges, and construction was started on the first 50-Mev part of the machine. Up to 50 Mev the design was for a three-tank machine similar to the Minnesota accelerator except that it was to be powered by laboratory-built triodes. In 1960 the 50-Mev machine was complete. Present plans call for extension to 70 Mev; work on still higher energies has been postponed.

Grid focusing in linear accelerators is now being superseded by AG focusing (see Chap. 5) using quadrupole magnets located in the drift tubes. Theoretical treatments of the old and new focusing methods will be found in the papers of Blewett[21] and of Smith and Gluckstern.[8]

Linear accelerators are used as injectors for large proton synchrotrons. For example, 10-Mev linacs are used as injectors for the 6-Bev Berkeley bevatron and for the Moscow 10-Bev "synchrophasotron." The 25-Bev AG proton synchrotrons at Brookhaven and CERN (Geneva, Switzerland)[22] use 50-Mev proton linacs as injectors. The CERN linac is similar to the Harwell machine. The Brookhaven linac is a single-tank machine and combines the rf liner and the vacuum tank by building the vacuum tank of copper-clad steel. Both of these linacs are powered by TH-470 triodes made by the French Thomson-Houston Company of Paris. Both machines use magnetic quadrupole focusing with quadrupoles embedded in the drift-tube structure. The CERN drift-tube configurations are similar to those used in the first Berkeley design. The Brookhaven drift-tube shapes were computed using a method due to N. C. Christofilos. Cross sections through a Brookhaven drift tube are shown in Fig. 10-10.

A discussion of linear-accelerator design would not be complete without a mention of another design for the accelerating system which has been much discussed but never tried. This system is well presented in the review by Johnsen;[23] it consists of a helical spiral enclosed in a conducting pipe. The technique has been used in traveling-wave tubes, which can be considered to be linear accelerators operated in reverse to deliver energy from a beam to a circuit. Consequently there seems no reason to doubt that it would work. It has not yet been developed, primarily because no one has devised a solution for the problem of focusing the beam in such a structure.

Extension of the proton linear accelerator to the billion-volt range has been proposed and discussed in many laboratories. It would not be difficult to build a conventional drift-tube accelerator in several sections to reach 200 Mev. At this energy the proton velocity has reached almost 60 per cent of the velocity of light, and it is quite possible to make a microwave cavity of the electron-linear-accelerator type for phase velocities in this range. Consequently the accelerator would change at this point to a microwave system. The phase velocity in the microwave

system would not equal the velocity of light but would of necessity be tapered along the accelerator to match the proton velocity. Since the cost per Mev of a drift-tube accelerator is much higher than that for a microwave system, the over-all cost of the machine per Mev will become lower as the ultimate energy increases. The 600-Mev Harwell proposal did not aim at an energy high enough to realize these economic advantages. In the U.S.S.R. a proposal has been studied for construction of a proton linear accelerator in the 1-Bev range. At Brookhaven a preliminary study has been made of a 10-Bev proton linear accelerator. The cost would be more than twice that of a proton synchrotron for the

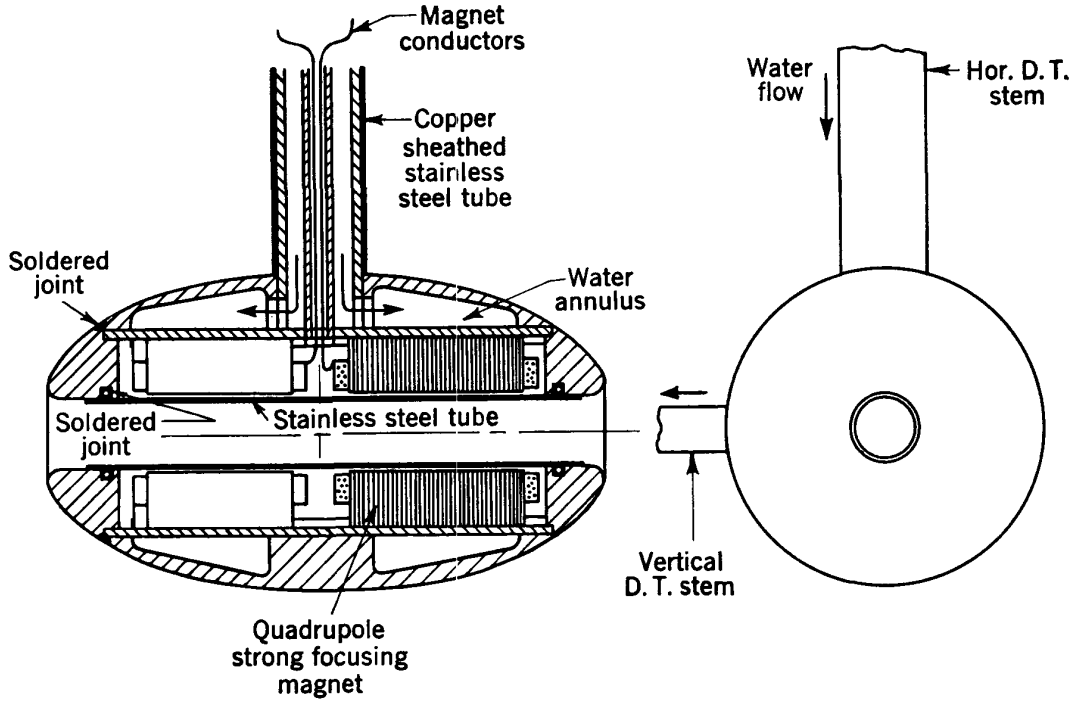

Fig. 10-10. Cross sections through a drift tube used in the Brookhaven 50-Mev proton linac, showing a focusing quadrupole.

same energy, but the beam intensity would be higher by a factor of 10^4 than that available from the proton synchrotron. Further study of the relative importance of cost, beam intensity, and beam characteristics will be necessary before such a project can be attempted.

10-14. HEAVY-ION LINEAR ACCELERATORS

Production of intense beams of ions heavier than protons is desirable for many experiments in nuclear physics and nuclear chemistry. For example, bombardment of uranium by carbon nuclei may give much information about formation of transuranic elements. Energies and intensities of heavy-ion beams produced in cyclotrons are too low for

these experiments. The linear accelerator seems ideal for this application, and a joint project was set up between Yale University and the Berkeley Radiation Laboratory for design of heavy-ion linear accelerators.[24] Groups directed by Beringer of Yale and Van Atta of the Radiation Laboratory completed a joint design, and in 1954 construction was started on two essentially identical machines in the two cooperating centers. Both machines are in operation and appear to justify the predictions of their designers.

Doubly charged He or C ions, triply charged N, O, or Ne ions, or several other possible ions of about the same charge-to-mass ratio are produced in special ion sources[25] and preaccelerated to 500 kev in a Cockcroft-Walton generator. The particles are then injected into a drift-tube accelerator 15 ft long and accelerated to energies of about 1 Mev per nucleon. The frequency of operation is 70 megacycles, and the tank diameter is about 10 ft. The tank is constructed of copper-clad steel.

The ion beam then passes through a "stripper," which is a gas jet in which the ions lose enough electrons so their charge-to-mass ratio is doubled. After stripping, electric accelerating fields will give twice the acceleration; the ion beam now enters the poststripper accelerator, which is 90 ft long and 9 ft in diameter. When the beam emerges from the poststripper, its energy has been raised to 10 Mev per nucleon. Focusing in the prestripper is accomplished by grids of the Berkeley type. In the poststripper AG focusing is achieved by inclusion of quadrupole magnets in the drift tubes. Radiofrequency power for both tanks is supplied at 70 megacycles by a power-amplifier system culminating in several RCA A2332 triodes.

10-15. LINEAR ACCELERATORS FOR HIGH CURRENTS

At the Livermore Laboratory of the University of California several linear accelerators have been built for acceleration of high currents of protons or deuterons. The authors are indebted to Prof. C. M. Van Atta for the following description of these developments.

At the Livermore site of the University of California Lawrence Radiation Laboratory several linear accelerators have been built for acceleration of proton and deuteron beam currents in the range of tenths of an ampere. This development was initially based upon use of the highest radio frequency for which high-powered, continuously operating oscillator tubes were then available, which was about 12 megacycles/second. The Mark I Accelerator, based upon this design limitation, consisted of a cylindrical cavity 60 feet in diameter and 60 feet in length and a high-powered injector capable of injecting beam currents of about ¾ ampere of protons (or deuterons) at 125 kev. Optimum performance of the Mark I Accelerator under continuous operation was an average beam current of about 50 milliamperes of protons at about 10 Mev. During pulse operation a

maximum peak beam current of 225 ma was attained and at a lower peak current and higher duty cycle (0.55) the maximum average beam output was 59 ma.

During construction and operation of the Mark I Accelerator improved oscillator tubes capable of continuous operation at frequencies as high as 50 megacycles/second at an output of 400 kilowatts became available. Using these new tubes and taking advantage of what had been learned from the Mark I Accelerator experience the A-48 Accelerator was designed and constructed. An improved injector system incorporating intense solenoidal magnetic focusing proved capable of injecting ¾ ampere of deuterons into a 3-inch diameter aperture at energies up to 130 kev with an angular divergence of about four degrees. With an injected beam of this quality it was feasible to design the rf accelerator with bore diameter of only 3 inches. The first stage of rf acceleration was accomplished by a two-stage, quarter-wave, resonant stem accelerator similar to a straightened out cyclotron operating at about 24 megacycles/second. Strong solenoidal focusing magnets were built into the drift tubes at the ends of the two quarter-wave stems and were also placed before, between and beyond the drift tubes to ensure that the intense beam would be kept under control. With rf pre-bunching of the injected beam the quarter-wave accelerator was capable of producing continuously 0.3 ampere of protons at 0.5 Mev, or of deuterons at 1.0 Mev. This section of the A-48 Accelerator was constructed and tested during the period April through December, 1954.

The remainder of the A-48 Accelerator consisted of two cylindrical cavities each twenty feet in length and resonant at about 48 megacycles/second. The two 20-ft cavities were completed and the A-48 Accelerator put into operation by December, 1955. The drift tubes of both cavities contained strong solenoidal focusing magnets. The output energy was 3.75 Mev for protons and 7.5 Mev for deuterons. Although the A-48 Accelerator was originally designed for a continuous output of 0.25 ampere of deuterons at 7.5 Mev, the actual currents attained during 1956 and 1957 were about 75 milliamperes of protons and 30 milliamperes of deuterons limited by the rf power input since the full design rf power was never installed. On the basis of experience with the A-48 Accelerator, those engaged in the project are confident that ion beam currents of ¼ ampere or more can be accelerated to any desired energy since the low-energy stages of acceleration are the most difficult. However, this development is not now being pursued. The A-48 Accelerator was shut down early in 1958 and has since been dismantled.

10-16. THE MULTIPACTOR EFFECT AND ELECTRON LOADING

Operators of accelerators which employ high electric fields have continually been plagued by the mysterious appearance of streams of electrons which load the power supply, induce emission of intense X radiation, and occasionally destroy parts of the machine. Such effects have already been mentioned in connection with the electrostatic generator and the cyclotron. When the fields alternate at high frequency, not only are the same effects present but also new effects appear. Most troublesome of these is the multipactor effect. This is an electron multiplication phe-

nomenon. If an rf electric field is set up between parallel metal surfaces and the field strength is such that an electron originating on one metal surface can take exactly one half-period of the radiofrequency to cross to the other surface, it can then knock out several secondary electrons which will return in exactly a half-period to the first surface. Secondaries from the first surface will now repeat the process with continual multiplication until the discharge becomes limited by space charge. In the linear accelerator multipactoring sets in at rather low levels between the closely spaced drift tubes at the low-energy end of the machine. If the machine is powered by self-excited oscillators, the build-up of the oscillator excitation will be stopped at this point. Consequently it is necessary to drive rapidly through the multipactor region with an externally excited power amplifier.

The important features of the multipactor effect can be established by the following derivation. We assume parallel plates in the yz plane, one at $x = 0$ and one at $x = x_0$. Between these plates exists an electric field $E_x = E \sin(\omega t + \phi)$. An electron leaving the $x = 0$ plane at time $t = 0$ with initial velocity $x = 0$ will have the equation of motion

$$m\ddot{x} = eE \sin(\omega t + \phi) \tag{10-36}$$

whence

$$\dot{x} = \frac{eE}{m\omega}[\cos\phi - \cos(\omega t + \phi)] \tag{10-37}$$

and

$$x = \frac{eE}{m\omega^2}[\omega t \cos\phi + \sin\phi - \sin(\omega t + \phi)] \tag{10-38}$$

If multipactoring is to occur, the time to travel from 0 to x_0 must be an integral number of half-periods, so $\omega t = (2n + 1)\pi$ and

$$x_0 = \frac{eE}{m\omega^2}[(2n + 1)\pi \cos\phi + 2 \sin\phi] \tag{10-39}$$

$$\dot{x} \text{ (at } x = x_0) = \frac{2eE}{m\omega}\cos\phi \tag{10-40}$$

In order for this mathematical picture to be physically realizable we must have $\ddot{x}$ positive at $x = 0$ and $\dot{x}$ positive at $x = x_0$. To satisfy these conditions [from Eqs. (10-36) and (10-40)] ϕ must lie between 0 and $\pi/2$. It can be shown by differentiation of Eq. (10-39) that the minimum possible value of E occurs when $\cot\phi = (2n + 1)\pi/2$. The maximum allowable value of E occurs when $\phi = \pi/2$. At $\phi = 0$, the value of E is intermediate between these limits. The values of the peak potential difference Ex_0 between the plates are

$$V_{\max} = \frac{m}{e}\frac{\omega^2 x_0^2}{2} \qquad \text{at } \phi = \frac{\pi}{2} \tag{10-41}$$

$$V_{\min} = \frac{m}{e}\omega^2 x_0^2[(2n + 1)^2\pi^2 + 4]^{-1/2} \qquad \text{at } \phi = \cot^{-1}\frac{(2n + 1)\pi}{2} \tag{10-42}$$

In Fig. 10-11 V/f^2 is plotted against x_0. From this figure, as from the above equations, the fact emerges that for a given electrode spacing there is a maximum field at which multipactoring can occur but there is no minimum field. Conversely, for a given field there is a maximum permissible electrode spacing for no multipactoring.

The case just discussed is the simplest possible situation in an rf cavity. In most regions of the cavity rf magnetic fields are present as well as rf electric fields. In many cases the magnetic fields make multipactor-

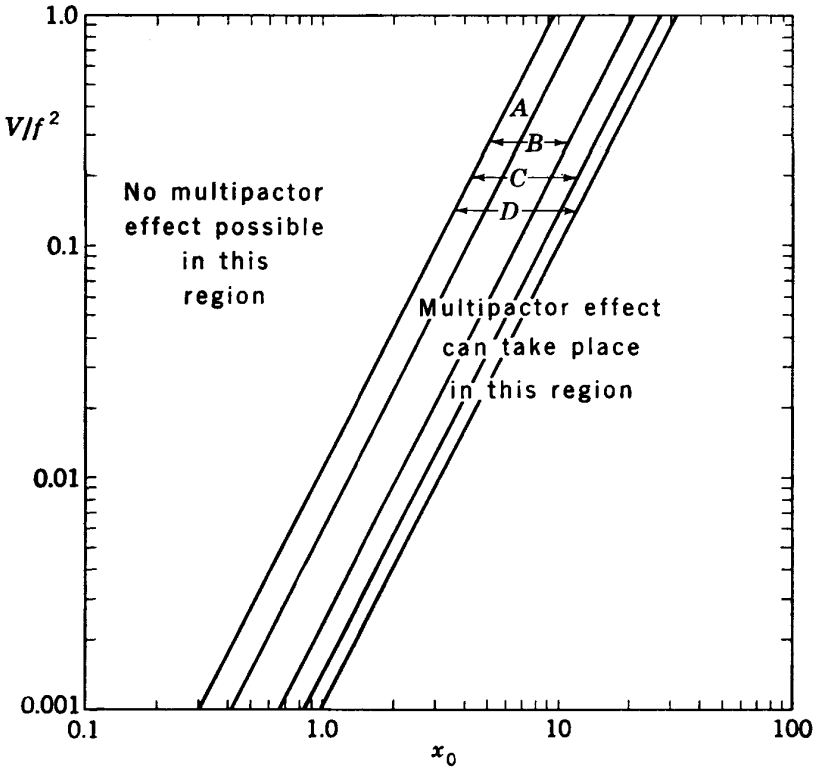

Fig. 10-11. The multipactor effect between parallel plates. In the region A the electrons require one half-period to cross from plate to plate; in region B the time required is three half-periods; in region C, five half-periods; and in region D, seven half-periods. Regions for still higher-order multipactoring are not shown but will extend indefinitely into the right-hand area of the graph. In this plot V is given in volts, f in megacycles, and x_0 in centimeters.

ing impossible. Sometimes, however, multipactoring occurs in and is dependent on the presence of rf magnetic fields. One such case is commonly found in proton linear accelerators. For many years the operators of these machines have been mystified by the appearance, after operation for some time, of discolored rings around the centers of the drift tubes. These rings appear in pairs separated by a few centimeters and symmetrically located on both sides of the vertical plane through the center of the drift tube. In the Brookhaven linac, where the drift-tube shapes are computed and all of the surrounding fields are known, it was possible

to compute electron orbits in this region. The rings were found to correspond to possible points of origin of multipactor electrons. Probably the continuous electron bombardment results in deposition and polymerization of the residual gas in the vacuum tank and so leads to visible discoloration. Fortunately, this effect is sharply dependent on voltage, so it takes place for very short periods and does not involve the dissipation of much rf power.

Other spurious electrons in linear accelerators originate from the thin insulating films which have been shown (Chap. 3) to be so troublesome in the electrostatic accelerator. These electron currents are easily distinguishable from multipactor discharges by the fact that they appear at a threshold voltage as the field is increased and then increase in intensity with a high power (usually about the sixth) of the electric field. If the metal surfaces in a proton linear accelerator are not kept scrupulously clean, these currents will rise to levels where the X-ray emission reaches dangerous levels and the electron currents begin to use up an appreciable fraction of the rf power. As an example of the difficulties experienced, it was found that the 32-Mev linac at Berkeley, which is pumped by oil-diffusion pumps, must be dismantled and cleaned every six months because the X-ray output of the loading electrons reaches intolerable levels. In the bevatron injector linac, which is pumped by mercury pumps, no such effect is observed.

10-17. TECHNIQUES FOR MEASUREMENT OF RF FIELDS

During the design and construction of the accelerating cavities for linear accelerators it is frequently necessary to make experimental studies of the rf field patterns set up throughout the cavity structure. It is difficult to use conventional probe techniques without distorting the field to the extent that the measurements are meaningless. Two special and unobjectionable methods are available. The first is fairly well known to microwave engineers. It involves the introduction of a small dielectric or metal bead into the region where the field strength is to be measured.[26] This bead produces a small perturbation in the resonant frequency of the cavity; this perturbation is proportional to the square of the field strength at the bead location. Since measurement of resonant frequency can be very precise, this is a powerful method and can give accurate results. If a spherical metal bead of volume δ is used, the fractional change in resonant frequency is given by

$$\frac{\Delta f}{f} = -\frac{3}{4}\frac{\delta}{W}(\epsilon_0 E^2 - \tfrac{1}{2}\mu_0 H^2) \tag{10-43}$$

where W is stored energy.

If a spherical dielectric bead of dielectric constant E is employed, the fractional frequency perturbation will be

$$\frac{\Delta f}{f} = -\frac{3}{4}\frac{\delta}{W}\frac{\epsilon - 1}{\epsilon + 2}\epsilon_0 E^2 \tag{10-44}$$

These two relations show that two measurements, one with a metal bead and one with a dielectric bead, can be combined to give both the electric field and the magnetic field at any given point. Only the absolute value of the field is determined; if field directions are desired, they can be deduced from measurements at several neighboring points.

The second method was developed by the linear-accelerator group at Berkeley; it is suitable for determination of electric-field strengths at higher levels. A small gas-filled spherical shell of glass or quartz is introduced into the field region and is observed by a photocell. If the size, gas filling, and pressure are adjusted correctly, the gas will break down and glow at a sharply defined field. These spheres are known to their inventors as "glo-balls."[27] Best results are obtained with Pyrex spheres about ½ in. in diameter filled with helium at a pressure of about 10 mm Hg. A ½-in. glo-ball prepared in this fashion breaks down at an electric field of about 120 volts/cm.

REFERENCES

1. G. Ising, *Ark. Math. Astron. Phys.*, **18**, Nr. 30, Heft 4, p. 45 (1925).
2. R. Wideröe, *Arch. Elektrotech.*, **21**:387 (1928).
3. D. H. Sloan and E. O. Lawrence, *Phys. Rev.*, **38**:2021 (1931).
4. D. H. Sloan and W. M. Coates, *Phys. Rev.*, **46**:539 (1934).
5. B. B. Kinsey, *Phys. Rev.*, **50**:386 (1936).
6. J. W. Beams and L. B. Snoddy, *Phys. Rev.*, **44**:784 (1933).
7. J. W. Beams and H. Trotter, Jr., *Phys. Rev.*, **45**:849 (1934).
8. Linear Accelerator Issue, *Rev. Sci. Instr.*, **26** (February, 1955).
9. Lloyd Smith, "Linear Accelerators," Encyclopedia of Physics, vol. XLIV, pp. 341–388, Springer (1959).
10. S. Ramo and J. R. Whinnery, "Fields and Waves in Modern Radio," Wiley (1944).
11. J. C. Slater, *Rev. Mod. Phys.*, **20**:473 (1948).
12. E. L. Ginzton, W. W. Hansen, and W. R. Kennedy, *Rev. Sci. Instr.*, **19**:89 (1948).
13. W. Walkinshaw, *Proc. Phys. Soc. (London)*, **61**:246 (1948); R. B. R.-Shersby-Harvie, *ibid.*, p. 255; L. B. Mullett and B. G. Loach, *ibid.*, p. 271.
14. R. B. R.-Shersby-Harvie and L. B. Mullett, *Proc. Phys. Soc. (London)*, **62**:270 (1949).
15. G. E. Becker and D. E. Caswell, *Rev. Sci. Instr.*, **22**:402 (1951).
16. P. T. Demos, A. F. Kip, and J. C. Slater, *J. Appl. Phys.*, **23**:53 (1952).
17. D. W. Fry, R. B. R.-Shersby-Harvie, L. B. Mullett, and W. Walkinshaw, *Nature*, **162**:859 (1948).

18. H. L. Schultz and W. G. Wadey, *Rev. Sci. Instr.*, **22**:383 (1951).
19. R. B. R.-Shersby-Harvie, L. B. Mullett, W. Walkinshaw, J. S. Bell, and B. G. Loach, *J. Inst. Elec. Engrs. (London)*, **104B**:273 (1957).
20. E. A. Day, R. P. Featherstone, L. H. Johnston, E. E. Lampi, E. B. Tucker, and J. H. Williams, *Rev. Sci. Instr.*, **29**:457 (1958).
21. J. P. Blewett, *Phys. Rev.*, **88**:1197 (1952).
22. Proceedings of CERN Symposium of 1956 (Geneva).
23. K. Johnsen, "On the Theory of the Linear Accelerator," A. S. John Griegs Boktrykker, Bergen, Norway (1954).
24. E. L. Hubbard, W. R. Baker, K. W. Ehlers, H. S. Gordon, R. M. Main, N. J. Norris, R. Peters, L. Smith, C. M. Van Atta, F. Voelker, C. E. Anderson, R. Beringer, R. L. Gluckstern, W. J. Knox, M. S. Malkin, A. R. Quinton, L. Schwarcz, and G. W. Wheeler, *Rev. Sci. Instr.*, **32**:621 (1961).
25. C. E. Anderson and K. W. Ehlers, *Rev. Sci. Instr.*, **27**:809 (1956).
26. S. W. Kitchen and A. D. Schelberg, *J. Appl. Phys.*, **26**:618 (1955).
27. J. F. Steinhaus, *Rev. Sci. Instr.*, **27**:575 (1956).

At the head of the facing page is an illustration of the University of California 184-in. synchrocyclotron, before the installation of shielding.

11

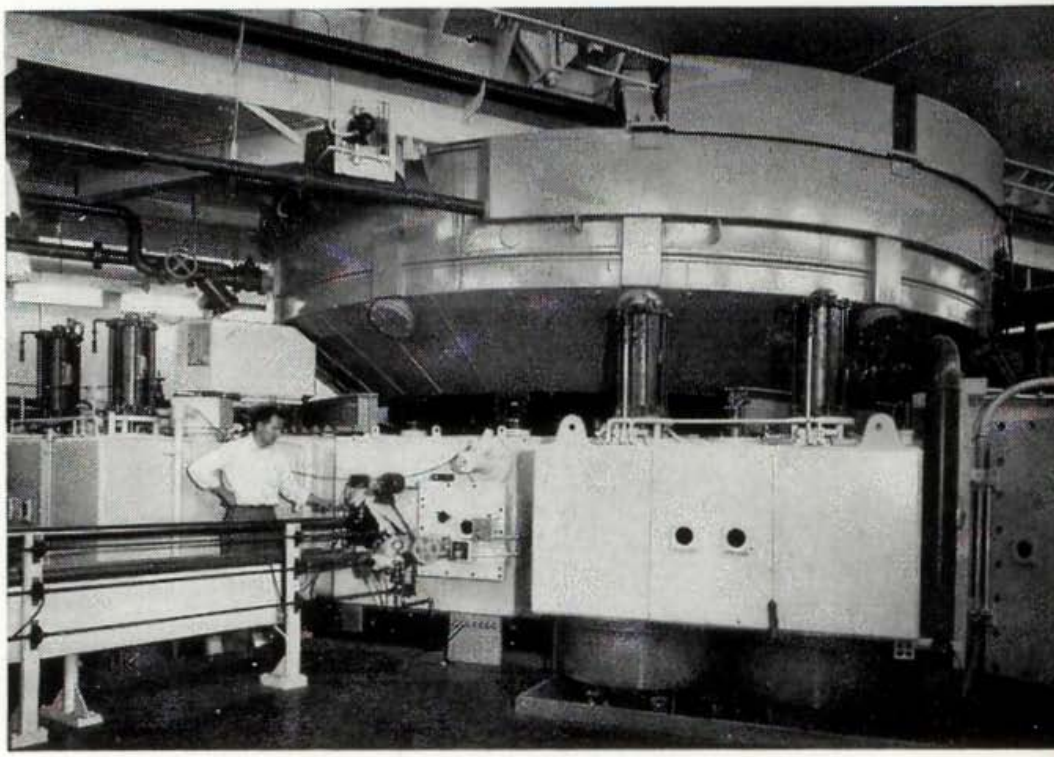

*The Synchrocyclotron**

The relativistic limitation on energy for fixed-frequency cyclotrons has restricted the useful size of magnets to about 60 in. pole-face diameter and the proton or deuteron energy to about 25 Mev. This limit is set by the relativistic increase in mass of the ions, which causes ion revolution frequency to decrease, so the ions fall out of resonance with the fixed-frequency applied electric field.

This maximum-energy limitation can be removed and the ions can be accelerated indefinitely if the applied frequency is varied to match exactly the ion revolution frequency. In Chap. 9 it was shown that particles in phase-stable orbits in a cyclotron-like accelerator will follow a slow change in applied frequency. The phase of crossing the accelerating gap oscillates about a mean value which allows just sufficient energy increase per turn to maintain resonance with the changing frequency.

When frequency is varied cyclically, a short bunch of ions will be accelerated to high energy in each frequency sweep, resulting in a sequence of such bursts occurring at the modulation frequency. The reduced effective duty cycle results in a much lower average ion output than in the conventional cyclotron (about 1 per cent), but it avoids the resonance limitation due to the fixed frequency and allows acceleration to much higher energies.

* Also known as the "frequency-modulated cyclotron."

11-1. EARLY DEVELOPMENT

The use of frequency modulation as a remedy for the relativistic limitations of the cyclotron was suggested as a consequence of the discovery of phase stability in 1945 by McMillan[1] of the University of California and independently by Veksler[2] of the U.S.S.R. The 184-in. magnet at the University of California had originally been conceived as a giant standard cyclotron by Prof. E. O. Lawrence and his coworkers. It was assembled and used for experimental purposes in the Manhattan District during World War II but was not completed as a cyclotron. At the end of the war, when McMillan proposed the use of frequency modulation, it became obvious that this method would result in higher energies, and plans were made to convert the machine into a synchrocyclotron.

The first test of the principle, at Berkeley, was made on the older 37-in. cyclotron magnet by an ingenious method of simulating the expected relativistic mass change with an exaggerated radial decrease in the magnetic field. Ion revolution frequency will decrease at very high energies because of the relativistic increase in mass; it can also be made to decrease with increasing energy in a small cyclotron if the magnetic field at large radii is reduced below the central field. The test was modeled on the anticipated operation of the 184-in. cyclotron. Deuterons of 200 Mev would experience an 11 per cent increase in mass during acceleration; the associated change in frequency, plus an additional 2 per cent for the radial decrease in field required for focusing, would require a total frequency change of 13 per cent during acceleration. To simulate this frequency change the field of the 37-in. magnet was equipped with radially tapered pole faces, requiring a 13 per cent modulation in frequency to maintain resonance with the low-energy (7-Mev) deuterons produced. With this arrangement the techniques of frequency modulation could be studied and the principle of phase-stable synchronous acceleration could be tested.

The results of the 37-in.-model test were reported by Richardson, MacKenzie, Lofgren, and Wright.[3] The test was completely successful. Very low D voltages were required, as compared with conventional cyclotron operation, and the deuterons remained in resonance for many thousands of revolutions. The frequency modulation was achieved with a rotating variable capacitor in the D circuit, using modulation frequencies up to 600 cps. The average deuteron current increased with modulation frequency as expected, to a maximum value of 0.2 μa. The results were in excellent agreement with those predicted from a theoretical analysis of phase-stable acceleration, and the success of the model experiment justified the modification of the 184-in. cyclotron to utilize this principle.

The 184-in. synchrocyclotron was brought into operation in November, 1946; it was immediately successful in producing good intensities of deuterons of 190 Mev and He^{++} ions of 380 Mev. The author list of the first report is a roster of the many members of the laboratory staff involved: Brobeck, Lawrence, MacKenzie, McMillan, Serber, Sewell, Simpson, and Thornton.[4] This impressive array of scientific and engineering talent makes it possible to understand how such a tremendous job could be completed in little more than a year. Yet another factor also entered. The fundamental soundness of the principle of phase stability and the simplicity of the basic techniques have impressed all observers. Equivalent success and speed in tuning up a synchrocyclotron have been achieved subsequently in other laboratories. In almost every installation to date, as soon as all components were completed and operable, resonant-ion beams have been obtained with a minimum of further experimentation. The synchrocyclotron has proved to be one of the simplest and most rewarding of all accelerators.

The immediate success of the Berkeley laboratory led others to build similar accelerators. The large size of this first machine stimulated others to plan for large sizes and high energies. Within a few years synchrocyclotrons were completed and in research operation in five university laboratories in the United States: at Rochester, Harvard, Columbia, Chicago, and Carnegie Tech. This rapid development was supported in large measure by government funds supplied by the Office of Naval Research and later by the Atomic Energy Commission, and it set a precedent in the United States for government support of university research laboratories.

Table 11-1 lists the larger machines in the United States and in other countries, with a few basic characteristics. They fall in two energy ranges. Those below 200 Mev energy are used for nuclear studies and single-particle scattering interactions. Those in the 400- to 700-Mev range have found their chief usefulness for the production of mesons and in the study of meson interactions.

Three machines in the 600- to 700-Mev range are the largest at present. At the University of California the rebuilt and repowered 184-in. cyclotron operates at 720-Mev protons; the U.S.S.R. Academy of Sciences has sponsored in the Joint Institute for Nuclear Research at Dubna a 6-m pole-face machine which operates at 680 Mev; and a 196-in. machine which produces 600-Mev protons was completed in 1958 at the CERN Laboratory, Geneva.

In addition to the large machines listed, small standard cyclotrons have been converted by a few laboratories (Princeton and University of California at Los Angeles) to the synchro principle to obtain higher energies than can be obtained with fixed-frequency operation.

TABLE 11-1
THE LARGER SYNCHROCYCLOTRONS

	Pole diam, in.	Magnet weight, tons	Magnetic field, kilogauss	Proton energy, Mev	Date first operated
United States:					
Univ. Calif.	184	4300	15.0	350	1946
			23.0	720	1957
Univ. Rochester	130	1000	17.0	240	1948
Harvard Univ.	95	700	20.0	150	1949
Columbia Univ.	164	2400	18.0	400	1950
Univ. Chicago	170	2200	18.6	450	1951
Carnegie Inst. Tech.	142	1500	20.7	450	1952
Foreign:					
Univ. Amsterdam	71	210	13.7	28(*d*)*	1949
AERE, Harwell	110	670	16.8	175	1949
McGill Univ.	82	260	16.4	100	1950
Werner Inst., Upsala	90	720	22.0	200	1953
Univ. Liverpool	156	1640	18.0	400	1954
Dubna, U.S.S.R.	236	7200	16.8	680	1954
CERN, Geneva	196	2500	20.5	600	1958

* (*d*) Deuteron energy.

11-2. PRINCIPLE OF OPERATION

In the synchrocyclotron light positive ions (protons, deuterons, He^{++}) are accelerated to energies significant relative to the rest energy of the particle. The ions traverse circular orbits in an approximately uniform and steady magnetic field, starting with small orbits at the center and increasing to larger radii as energy increases. In their circular motion they pass many times through the rf electric field of a large semicircular hollow electrode called a D. The frequency applied to the electrode is made identical with the ion revolution frequency, so that particles experience an acceleration on each traversal of the accelerating gap.

The steady magnetic field is produced by a solid-core electromagnet with dc excitation. For each value of particle energy in this field there is a particular equilibrium orbit radius and a specific frequency of revolution. Equations describing the orbital motion were developed in Chap. 5. Orbit radius is given by the relativistic relation (in mks units)

$$r = \frac{[T(T + 2W_0)]^{1/2}}{ceB} = \frac{[T(T + 2W_0)]^{1/2}}{300B} \quad \text{meters} \qquad (11\text{-}1)$$

The numerical constant above applies when kinetic energy T and rest energy W_0 are given in Mev units and magnetic flux density B is in units of webers/m^2 (1 weber/m^2 = 10,000 gauss). Ion revolution frequency is

given by

$$f = \frac{c^2eB}{2\pi(W_0 + T)} = 14{,}320\,\frac{B}{W_0 + T} \quad \text{megacycles/sec} \quad (11\text{-}2)$$

Units are the same as for Eq. (11-1).

The decrease in ion revolution frequency is caused primarily by the increasing kinetic energy of the ions but is also affected by the slight decrease in magnetic field with increasing radius required for orbit stability. The relations above are plotted in Figs. 11-1 and 11-2 to show

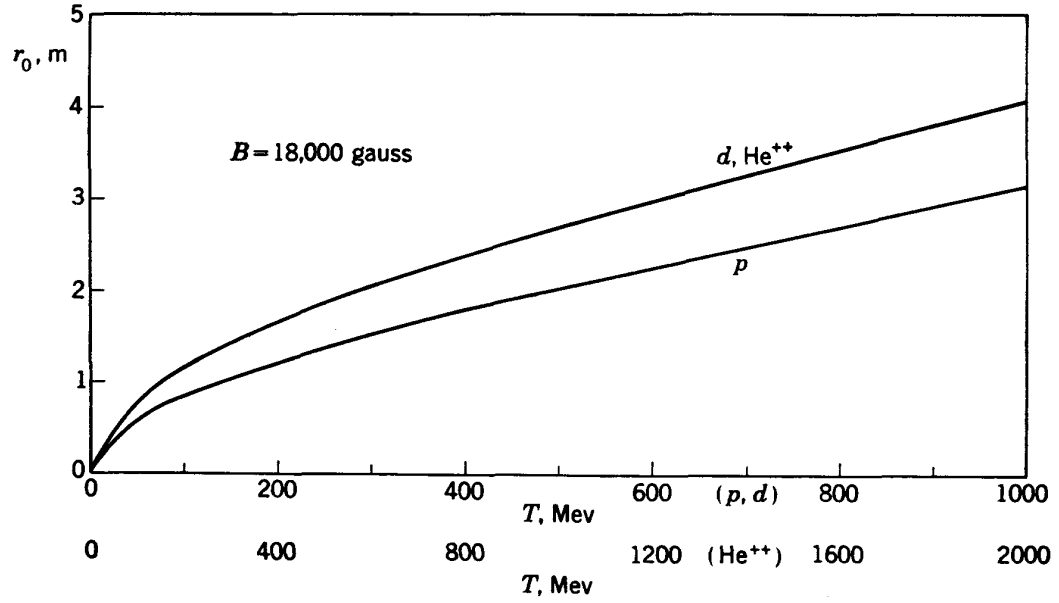

Fig. 11-1. Orbit radius versus energy for light positive ions in a magnetic field of 18 kilogauss.

the dimensional requirements and the orbital frequencies for the several light ions as a function of their kinetic energy, for a magnetic field of 18 kilogauss, which is typical of the fields used in synchrocyclotrons.

The D-shaped electrode is similar to the electrodes used in the standard cyclotron, but since the required acceleration voltage is low relative to that used in the standard cyclotron, a single D is used rather than the two D's customary in standard cyclotrons. Particles cross the acceleration gap, between the diametral face of the D and a dummy D at ground potential, twice in each revolution. The magnitude of the acceleration at each crossing depends on the instantaneous rf voltage, and so on the phase of crossing the gap relative to the rf wave. As the ions gain in energy on each traversal of the gap, they travel in circles of larger radii, ultimately reaching the maximum practical radius (see Fig. 11-3). The problem is to keep the ions in precise resonance with the applied rf field for a very large number of revolutions. Resonance is maintained auto-

matically in the synchrocyclotron through the principle of phase stability (see Sec. 9-9). A brief review of this principle as it applies to the synchrocyclotron will be useful at this point.

Consider a particle which crosses the gaps at zero phase ϕ_0 when the rf voltage is zero; its energy will not change, and it will continue to rotate in a circular orbit of constant radius. This orbit was defined as an equilibrium orbit. As long as the applied frequency is constant, a particle which deviates from equilibrium energy will oscillate around this value of energy and this location of the orbit. For example, consider a particle

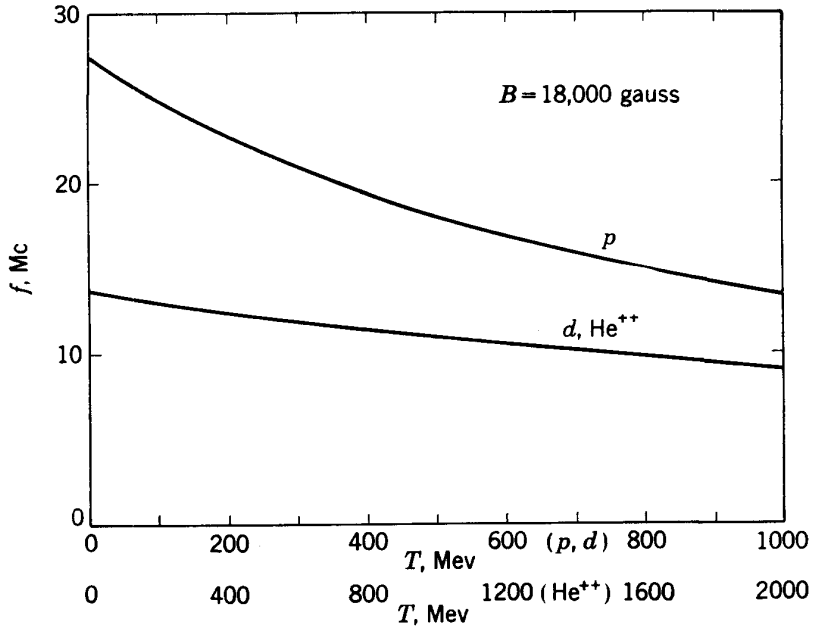

Fig. 11-2. Ion revolution frequency versus energy for light ions in a magnetic field of 18 kilogauss.

which is not in exact resonance but crosses the gap at a phase ϕ when the field is accelerating. Such a particle will acquire excess energy, will traverse an orbit of larger radius which requires a time longer than the rf period, and so will shift in phase toward the zero-phase position. This motion was shown to lead to an oscillation in phase about the equilibrium phase and to an associated oscillation in orbit radius about the position of the equilibrium orbit.

Consider next the effect on a particle in such an equilibrium orbit of a small decrease in the frequency applied to the electrodes. This change in frequency results in a phase shift, so the particle crosses the gap at a time when the voltage is accelerating. The particle will gain energy until it is in resonance with the new frequency; its equilibrium orbit radius will increase correspondingly. Furthermore, if the frequency is decreased slowly and continuously, the particles will follow this change, increasing

steadily in energy and orbit radius; phase oscillations will occur around that phase at which the particles acquire the average energy per turn which corresponds to the rate of change in frequency. This is the principle of the synchrocyclotron.

Because of the relatively slow decrease in accelerating frequency, the ions in the synchrocyclotron make many thousands of revolutions. For the accelerating fields ordinarily used, each phase oscillation takes several hundred revolutions. The ions, which are initially spread widely in azimuth, are slowly bunched as they are accelerated. As in the other

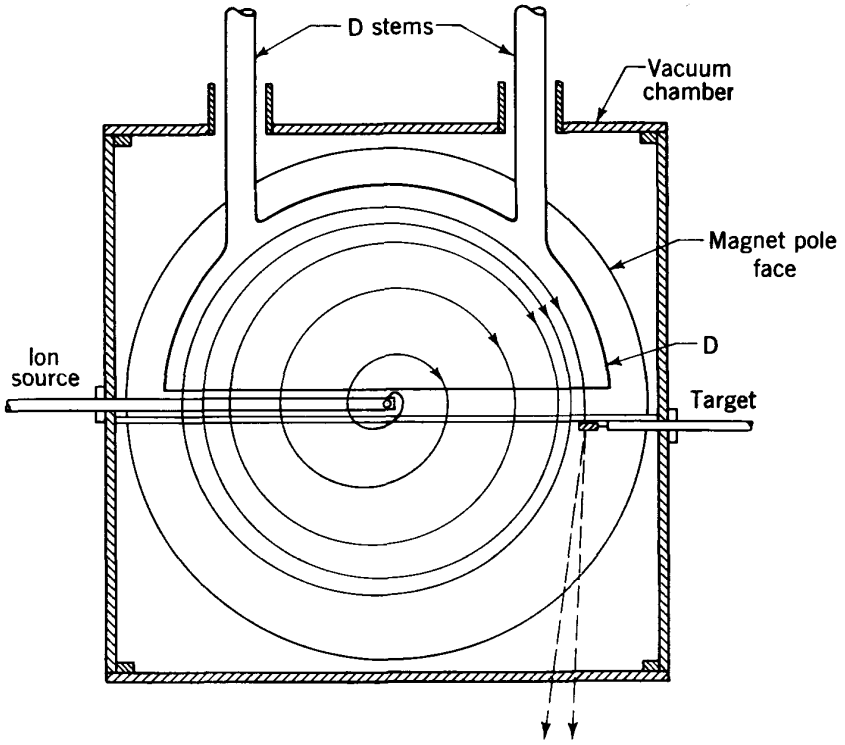

Fig. 11-3. Schematic diagram of the synchrocyclotron showing the arrangement of components within a vacuum chamber. Particle orbits shown are also schematic; in practice the particles traverse thousands of revolutions.

synchronous accelerators, a small radial oscillation around the expanding orbit is associated with the oscillation in phase.

Other motions, both in radius and in the vertical direction, are associated with initial errors in ion injection and with minor defects in the guiding magnetic field. These are oscillations of the same nature as those occurring in the betatron and have already been discussed in Secs. 5-9 and 5-10. The field index n required for adequate stability of these free oscillations is usually of the order of 0.05 in the synchrocyclotron. From Eqs. (5-67) and (5-68) it follows that the frequency of radial betatron oscillation is about 0.98 times the revolution frequency, while the frequency of vertical betatron oscillation is about 0.2 times the revolution

frequency. These rapid oscillations are superimposed on the much slower phase oscillations.

The existence of such stable orbits in which ions can be trapped was demonstrated at an early date by some unpublished observations with the 37-in. model at Berkeley. When the ion source was pulsed a single time and the capacitor was rotating continuously, an initial burst of high-energy ions was observed on a target at the periphery (using a cathode-ray tube with a sweep circuit to display the instantaneous current), followed by a sequence of bursts of decreasing intensity at the modulation frequency. The interpretation is that ions which were not trapped and accelerated in the first frequency sweep were captured on successive sweeps. In another test the capacitor was rotated slowly by hand, so that the frequency sweep required several seconds. A small burst of ions was still observed at the end of the sweep, indicating that the orbits are truly stable. Ions will stay in resonance indefinitely, limited only by losses from gas scattering.

For continuous operation the frequency is modulated cyclically by a variable capacitor in the resonant D circuit. The frequency change as a function of time for such a typical circuit is illustrated in Fig. 11-4. During each sweep a bunch of ions is accelerated, so in continuous operation a sequence of pulses of high-energy ions reaches the periphery at the modulation frequency. This pulsed character of the beam can be described in terms of the duty cycle (the ratio of the pulse length to the cyclic period of modulation), which is of the order of 1 per cent. A more meaningful description is stated in terms of the capture efficiency. Since ions are accelerated intermittently, there is only a limited time interval in which ions emitted from the source can be accepted into stable orbits. Capture efficiency is the ratio of the number of ions accepted to the total number available during one frequency-modulation cycle. The calculation of efficiency is one of the principal objects of theoretical studies, and the primary problem in design is that of maximizing the capture efficiency, or the effective duty cycle.

The ion source is quite similar to that used for the standard cyclotron. A more complete discussion is given in Sec. 11-11. Some intensity gain will usually result from pulsing the source at the modulation frequency, so that ions are emitted in bursts during the acceptance time intervals.

To summarize, we can describe the general motion of the ions in terms of the superposition of three components of motion:

1. Expansion of the equilibrium orbit at a steady rate determined by the rate of frequency modulation
2. Radial phase oscillations about the equilibrium orbit and azimuthal oscillations about the position of equilibrium phase, of all amplitudes up to a maximum value set by the stable phase limits

3. Free radial and axial oscillations about the instantaneous orbits, with frequencies determined by the radial gradient of the magnetic field and amplitudes set by initial conditions and physical limitations

The rotating ions are enclosed within a curved, sausage-shaped envelope; the center of this envelope rotates at the applied frequency about the magnetic center and traverses a slowly expanding spiral path. The angle in azimuth subtended by the envelope is determined by the extreme limits of phase oscillation. The radial width is made up of two components, since the radial free oscillation is superimposed on the radial synchronous orbits. The vertical or axial thickness of the envelope is given by the maximum amplitude of the axial free oscillations. Any single particle migrates around within the envelope, making a complete

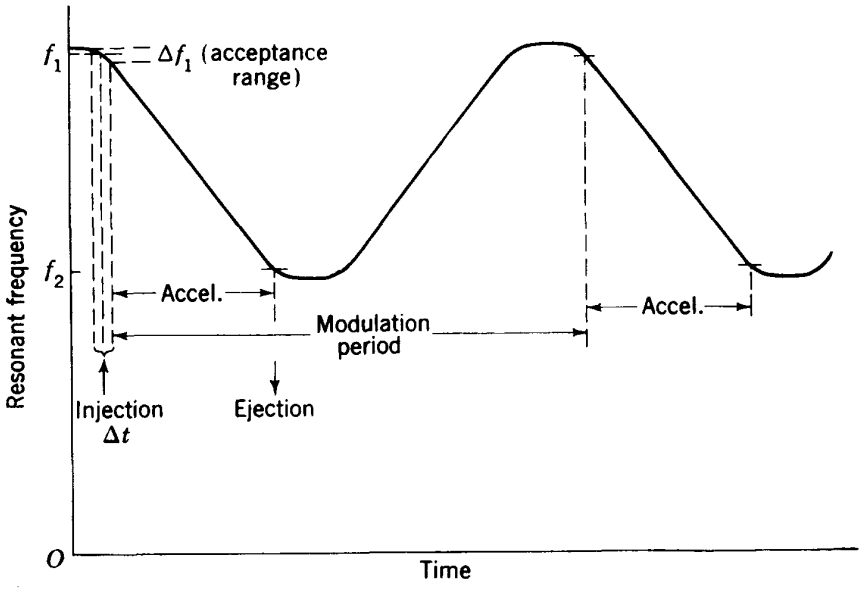

Fig. 11-4. Typical frequency-modulation cycle obtained with a variable capacitor in the D circuit.

circuit in its location within the envelope during a phase-oscillation cycle, which requires several hundred revolutions.

11-3. CAPTURE EFFICIENCY

A detailed theoretical analysis of phase-stable synchronous acceleration and of the phase oscillations was reported in two papers by Bohm and Foldy[5,6] of the University of California. The first is on the theory of synchronous oscillations in general, but with primary reference to the electron synchrotron; the second discusses capture efficiency for a synchrocyclotron and compares results with experimental observations from the Berkeley machine. A more detailed comparison of the operation of the 184-in. synchrocyclotron with theoretical predictions was

reported later by Henrich, Sewell, and Vale.[7] A brief derivation of the theory of synchronous oscillations has also been given in Chap. 9, with a unified terminology applying to all machines. However, in Chap. 9 the details of the cyclotron application were bypassed to emphasize the generality of the derivation. Some additional discussion of a qualitative nature is in order to describe the more pertinent details such as the factors affecting capture efficiency, the effects of orbit precession, and the loss of ions through coupling between the several types of oscillations at large n values.

Capture efficiency deals with conditions at the start of acceleration and during the first few phase oscillations. The process of acceleration starts at the ion source, when the cloud of ions formed during the ion-source pulse is drawn toward the D by the applied rf voltage. D voltage is relatively low, as compared with that of a fixed-frequency cyclotron, so the first accelerations and initial orbit radii are small. These first spiral orbits do not penetrate the interior, field-free region of the D, but are located in the D gap where the electric field is approximately uniform. Under these conditions it can be shown that the ions are rapidly bunched, or phase-focused, around the phase of maximum voltage, $\phi = \pi/2$. This phenomenon was described in Sec. 6-4 for the standard cyclotron and was illustrated by orbit plots showing the phase focusing and the concentration into radial bunches. Bohm and Foldy[6] have given the theory of this prebunching in some detail in an appendix. So, at the start of their motion the ions are closely bunched in phase around the phase of peak voltage.

During further acceleration the orbits grow larger and enter the D; the prebunching is distorted and spread into a wider phase band. Then, as the applied frequency decreases, the phase shifts to smaller values. Those ions within the stable phase limits are captured and set into phase oscillations. The fraction captured depends on the initial applied frequency and varies in magnitude as the frequency sweeps over an "allowed" range.

In Sec. 9-5 a general treatment of the limits of phase stability led to the conclusion that the range of initial ion phases that can be accepted in a synchronous accelerator depends on the value of the equilibrium phase; for low values of the equilibrium phase large fractions of the injected beam are accepted; for an equilibrium phase of about 30° about half of the beam is accepted; as the equilibrium phase approaches 90°, the accepted fraction becomes very small. Particles that arrive at phases different from the equilibrium phase, but within the acceptance range, will undergo oscillations in phase in the course of which their energy will change and they will move to paths of different radius. Thus we can draw an area in a plot of radius versus phase within which particles can be accepted and outside of which they will be rejected. Figure 11-5 is such a

plot derived for the Chicago synchrocyclotron.[8] In this plot the areas of stability are shown for several equilibrium phases. The direction of migration around the plot during the phase oscillation is indicated by arrows. The areas shown in this graph do not remain fixed in space but move out in radius as the particle energy increases and as the applied frequency decreases. Consequently, at least some of the particles will move clear of the injector before the oscillation returns them to their original azimuth and relative radial position. The problem of how many such particles will escape has been discussed by Bohm and Foldy.[6]

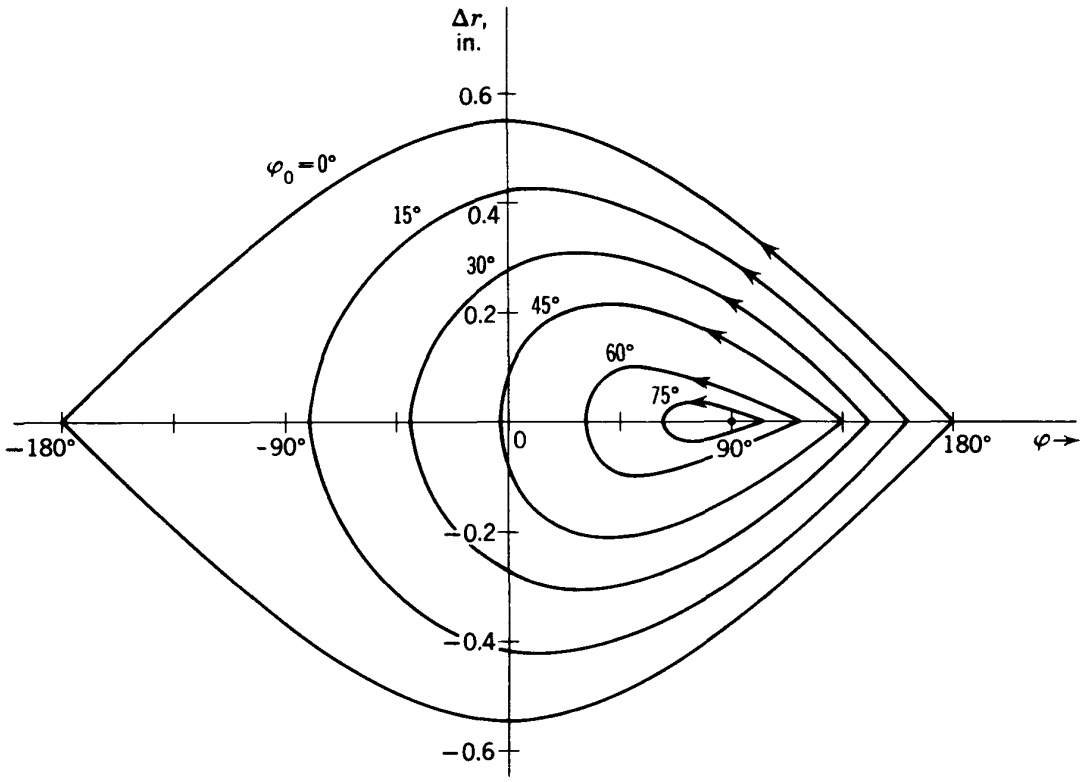

Fig. 11-5. Amplitude of radial phase oscillation Δr as a function of particle phase,[6] for several equilibrium phase angles ϕ_0 (cf. Fig. 9-3).

The results of Bohm and Foldy are presented in Fig. 11-6, taken from their paper. A particle circulating at the wrong radius will have a frequency of revolution that differs from the applied frequency, so the radial position error shown in Fig. 11-5 could just as well be presented as a frequency error. The ordinate in Fig. 11-6 is a function $f(\omega_0 - \omega)$ which is proportional to the difference between ion revolution frequency and applied frequency. The abscissa is the sine of the equilibrium phase angle. The double-branched curve labeled I gives the boundaries of the phase region in which ions would be captured into phase-stable orbits if there were no questions of interception by the injector. This curve could have been drawn from the data presented in Fig. 11-5. Curve II

is the boundary beyond which particles will be returned to the origin. The area to the right of curve II is the acceptance area. The vertical arrows indicate the magnitude of the allowable frequency error (or radial displacement).

From the data used in plotting these graphs it is possible to compute the capture efficiency as a function of the equilibrium phase angle. The results differ slightly, depending on whether the machine is tuned by changing the rate of frequency modulation or by changing the D voltage (either will have the effect of changing the equilibrium phase). In both

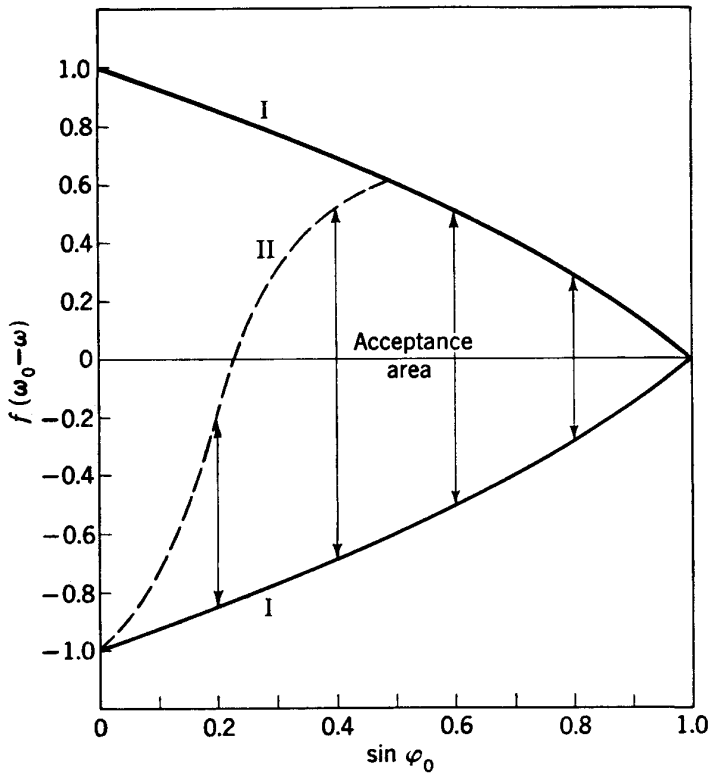

Fig. 11-6. Stable phase limits in terms of the difference between ion frequency and applied frequency, used to compute capture efficiency.[6]

cases, however, the efficiency as a function of equilibrium phase angle rises from zero at 0° to a peak between 20 and 30° and falls again to zero at 90°. Since the equilibrium phase angle should be between 20 and 30° for maximum capture efficiency, the peak applied voltage V should be between two and three times the equilibrium value of volts per turn $V \sin \phi_0$.

Experimental observations are in good agreement with the theoretical predictions. Bohm and Foldy show a plot (Fig. 11-7) of the way average beam current should vary with modulation frequency. When the experimental observations were matched in intensity to the theoretical curve at one point, they were found to be quite similar in general shape, except

for a tail on the experimental curve extending to higher modulation frequencies. This is explained as due to ions which fall out of synchronism but are picked up and accelerated in a subsequent modulation cycle. The absolute magnitude of the average beam current is also in reasonable agreement with the calculated intensities based on the known peak current from the ion source and the computed capture efficiency. More details on the agreement between operational results and computed capture efficiency are given by Henrich, Sewell, and Vale.[7] They show that

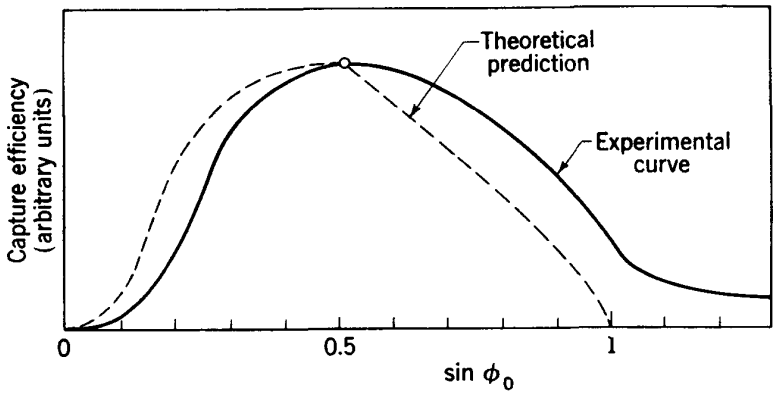

Fig. 11-7. Comparison of capture efficiency, calculated and observed, as a function of phase angle on the 37-in.-model synchrocyclotron,[6] obtained by varying the rate of frequency modulation.

the theoretical efficiency curve is valid over a wide range of D voltage and beam current.

11-4. ORBIT PRECESSION

Free radial oscillations are superimposed on the longer-period phase oscillations. The frequency is given by Eq. (5-67), and over most of the acceleration it is only slightly smaller than the resonant or orbital frequency. We would expect the azimuthal location of maximum outward amplitude of these free oscillations to precess around the chamber, with a precessional frequency given by

$$f_{pr} = [1 - (1 - n)^{1/2}]f_0 \tag{11-3}$$

For example, the precessional frequency at a radial location where $n = 0.04$ would be $0.02f_0$, and the period of precession would be fifty times the period of revolution. When such precession occurs, the ions would reach their maximum radial amplitude at the azimuth of a probe target at intervals of about 50 ion revolutions.

Evidence for such orbit precession is reported by Henrich, Sewell, and Vale[7] from the 184-in. machine. Oscilloscope pictures of the beam current striking a probe target show a series of pulses with an average time

separation of 10 μsec (see Fig. 11-8). When the probe was moved to different radii, the period was observed to vary, giving results in agreement with the precessional periods computed for the respective n values at the different locations. For this effect to be observed it is necessary for the ions to be sharply bunched in the phase of their radial oscillations and not continuously distributed in phase. We have indicated earlier how such bunching occurs during the first accelerations.

An envelope over the pulses illustrated on the oscillographic records in Fig. 11-8 shows a structure with two broad maxima separated by a longer time interval, of the order of 45 μsec. This separation agrees well with the computed period of phase oscillations and illustrates the "breathing" motion of the orbit. The fact that more than one phase-oscillation period is observable on the records means that the amplitude of free radial oscillations was larger than the radial increase during a phase period. In fact, this technique offers a method of estimating the ampli-

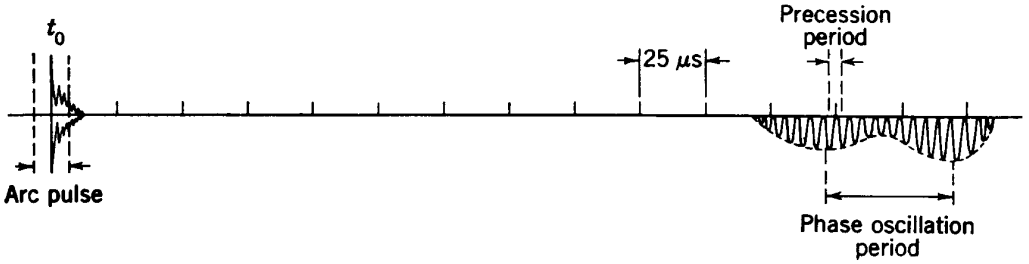

Fig. 11-8. Sketch of an oscilloscope pattern of beam intensity versus time with the 184-in. synchrocyclotron,[77] showing evidence for orbit precession and phase oscillations.

tude of the free oscillations, which in this case appears to be of the order of 3 in. and is roughly constant during acceleration.

Another experimental method of estimating the radial-oscillation amplitude of the beam is observation of the spread of the induced radioactivity on probe targets. Although the mean increase in beam energy per turn is very small (a few thousand electron volts) and the corresponding increase in orbit radius is almost undetectable, the combined effect of radial oscillations and precession of orbits spreads the beam over a finite radial width on the probe. The radioactivity observed in such tests at Berkeley was confined within 0.16 in. from the leading edge. Approximate calculations were made[7] of the spread expected for various radial-oscillation amplitudes at different radii, and the results suggest again that the free radial-oscillation amplitude was of the order of 3 in.

11-5. COUPLING BETWEEN OSCILLATIONS

A severe limitation on all synchronous accelerators is coupling between the several modes of oscillation. Under certain conditions excess energy

may be fed into one type, such as the axial free oscillations, so that particles are lost to the beam through striking the D. This phenomenon was first observed experimentally in the 184-in. machine as a complete loss of the beam at about the 81-in. radius ($n = 0.2$), even though it was originally expected that the beam would persist out to the limit of radial stability at $n = 1.0$. To study the effect, copper probes in the shape of a U—with the open side of the U toward the center—were placed in the beam; they were then removed and radioautographs were made which showed that most of the beam hit the top or bottom of the U-shaped probe at about the 81-in. radius. This blowing up of the beam was explained as due to a coupling between free radial and vertical oscillations at $n = 0.2$.

At $n = 0.2$ the frequency of the radial oscillation is a second harmonic of the axial frequency, as can be shown by applying Eqs. (5-67) and (5-68).

$$\frac{f_r}{f_z} = \frac{(1 - n)^{1/2} f_0}{n^{1/2} f_0} = \frac{(1 - 0.2)^{1/2}}{0.2^{1/2}} = \frac{2}{1} \tag{11-4}$$

The probability of transferring energy from the radial to the axial mode depends on the duration of the coupling interval. This interval can be computed from the time required for the particle to pass through the resonance value of $n = 0.2$. The amplitude and so the energy of the radial oscillations must be known, as well as the physical limits of axial oscillations set by the D aperture.

The theory of coupled oscillations is given in many studies, and it was applied to this problem by Henrich, Sewell, and Vale.[7] For an assumed radial amplitude of 1 in. in the 184-in. cyclotron, the time required to transfer sufficient energy into the other mode to exceed the vertical aperture limits was found to be about 10 revolutions, with even shorter times for larger initial amplitudes. These results show that most of the beam would be lost near the $n = 0.2$ radius because of striking the D. Some ions should have very small amplitude radial free oscillations, however, and so should not exceed the vertical aperture even though the entire oscillation energy is transferred to the axial mode. Yet it was observed that essentially all the beam was lost in the 184-in. machine before it reached the radius at which $n = 1.0$. This suggested the possibility of coupling between other types of oscillations or for other harmonics.

At $n = 0.25$, coupling could occur between the vertical free oscillation and the fundamental circular motion, if azimuthal inhomogeneities in the magnetic field exist to provide a mechanism for energy transfer. The frequency of vertical oscillation would be $0.5f_0$ for this value of n. It is known that a radial component of magnetic field can affect the vertical motion of the ions and provide coupling. A radial component B_r will exist at the particle orbit if the median plane varies in location around the orbit. Even if the median plane is flat, the radial component at a small

distance from the plane may vary with angle if the vertical component of field has azimuthal inhomogeneities. In the 184-in. machine the magnetic field was carefully measured as a function of angle and found to have inhomogeneities of the order of a few per cent. Henrich, Sewell, and Vale showed that this inhomogeneity was sufficient to account for the loss of essentially all ions at $n = 0.25$, even if they had survived the $n = 0.2$ resonance.

Detailed analysis of the coupling problem in the Chicago synchrocyclotron[8] showed that the $n = 0.2$ resonance is so tightly coupled as to predict almost total loss of the beam at this radius for this machine. On the other hand, the extreme care used in correcting the magnetic field for azimuthal variations led to a relatively weak coupling at $n = 0.25$. Operational experience has confirmed the predictions.

Other possible resonances can be analyzed similarly. Coupling can occur between vertical and radial oscillations, with $f_r = 3f_z$ at $n = 0.1$. Analysis of the coupling terms in the energy equation shows that for this second harmonic the coupling is insufficient to produce significant vertical amplitudes within the time interval available for resonance. The same is true for higher harmonics and for all other types of coupling which have been investigated.

At $n = 1.0$ the motion becomes radially unstable and particles enter orbits which are rapidly opening spirals. This feature might be used to advantage in ejecting an emergent beam in the simple manner used for the fixed-frequency cyclotron, if the ions could be brought out to this radius. However, the resonances at $n = 0.2$ and 0.25 effectively eliminate this possibility of obtaining a high-intensity emergent beam with the synchrocyclotron. Despite the strong coupling at the $n = 0.2$ and 0.25 resonances, some ions may survive to reach the $n = 1.0$ limit. This effect has been observed at the University of Rochester, where an oscillographic record of the secondary radiation from the chamber showed three peaks at times corresponding to the beam reaching successively the regions of $n = 0.2$, 0.25, and 1.0.

11-6. THE MAGNETIC FIELD

The largest and most costly component of the synchrocyclotron is the solid-core magnet of large pole-face area. The magnetic field must be steady and approximately uniform over the pole face, decreasing slightly with increasing radius to provide focusing forces. So poles are roughly parallel, with a suitable contour provided on the pole faces to give a radial drop of a few per cent from center to edge.

Magnet weight and cost of iron increase roughly with the cube of the pole diameter. In the low-energy nonrelativistic range, particle energy varies with the square of the orbit radius; so magnet weight for small

cyclotrons is given roughly by the $\frac{3}{2}$ power of the energy: Wt $\propto T^{3/2}$. But for high energies particle energy approaches a linear proportionality with orbit radius; so magnet weight increases more rapidly, approaching the relation Wt $\propto T^3$. This rapid increase in weight and cost is the chief limitation on the practical maximum energy for synchrocyclotrons. No insurmountable technical problems have been encountered up to the present largest sizes, capable of producing protons of 600 to 700 Mev. Designs for even larger machines seem practical. But the excessive cost of solid-core magnets for higher energies has transferred interest to the type of accelerator using constant orbit radius and a ring-shaped magnet (see Chap. 13), which is called a proton synchrotron.

The weight of iron is partially offset by the relatively simple design and structure of such a dc magnet. Cheap iron can be used in the form of thick plates or forgings, exciting coils are simple even though heavy, and power requirements are not excessive if a sufficient weight of conductor is used in the coils. The pole-gap length does not need to increase as fast as the pole-face diameter, since field shaping can be used to focus the resonant ions about the median plane; this results in relatively lower power requirements and smaller fringing-flux losses for large magnets and makes some reduction in weight of iron below the T^3 variation. Magnetic circuit dimensions tend toward broad, squat structures as size increases, and the magnetic efficiency is higher. These principles are discussed in more detail in Chap. 8 in the section on magnet design.

Maximum magnetic flux density is severely restricted by the permeability limits of iron, at around 18 to 20 kilogauss for soft iron forgings or rolled plates. Power requirements increase sharply above this limit, and most designers plan for fields in the gap of this magnitude. Once the maximum practical field has been established, the orbit radius can be determined for the type of ion and the ion energy desired. To illustrate the dimensions needed, Table 11-2 shows rough estimates of dimensions and magnet weight for several values of proton energy at an assumed magnetic field of 18 kilogauss at the maximum ion radius.

TABLE 11-2
ESTIMATED MAGNET WEIGHTS

Proton energy, Mev	Orbit radius at 18 kg (m)	Pole diam, ft (approx.)	Magnet weight, tons
100	0.83	6	200
300	1.50	11	1,200
600	2.26	16	4,000
1,000	3.16	22	11,000
2,000	5.18	36	40,000

The basic structure adopted by almost all designers of modern synchrocyclotron magnets is illustrated in Fig. 11-9. It is a straightforward extension of the classic H frame used for smaller cyclotrons to the larger dimensions required here. Machined low-carbon steel forgings are used for the major components, in unit sizes as large as are practical for production and assembly. The frame consists of six elements: two poles, two yokes, and two uprights. The yokes and uprights for the H frame are rectangular machined forgings arranged to carry the load of the structure and to have a magnetic flux path as short as is practical. The poles are cylinders, machined to a good finish and usually tapered to smaller diameter at the gap. The poles terminate in pole-face disks which form the

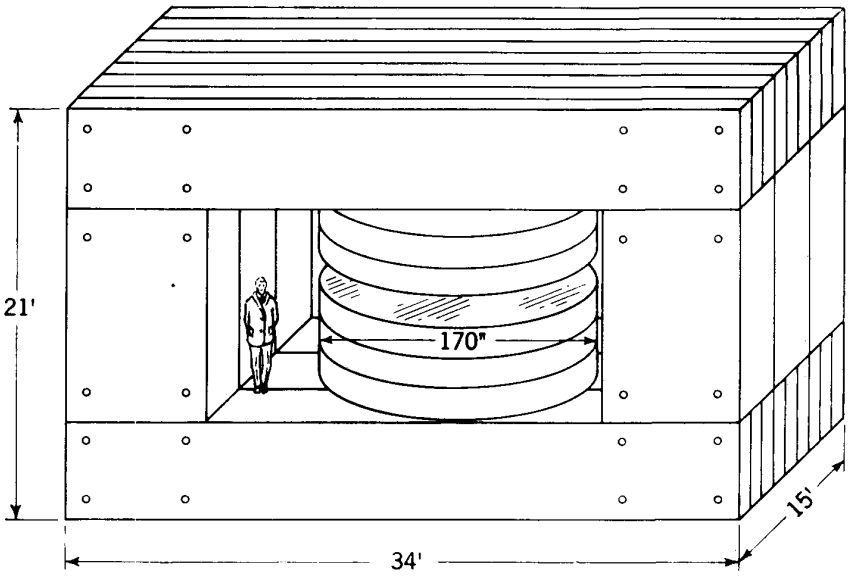

Fig. 11-9. Magnetic circuit for the University of Chicago synchrocyclotron,[8] showing the use of large rectangular forgings to form the structure.

lids of the vacuum chamber; these disks are contoured to give the radially decreasing field required for focusing.

In the smaller magnets at Harvard and at Rochester a single forging is used for each upright, and two parallel bars make up each yoke. The arrangement illustrated in Fig. 11-9 is for the 2200-ton magnet at the University of Chicago; here the maximum weight of each piece was chosen to be less than 100 tons, so the assembly could be handled with a 100-ton crane. For this large magnet three rectangular forgings are used in each upright and eight long slabs in each yoke.

Precision in machining is important to minimize air gaps at surfaces in contact, to give a mechanically stable structure, and to maintain accurately parallel pole faces. Specifications usually call for better than ± 0.010 in. precision in flatness and parallelism. After assembly the rectangular forgings are frequently welded together along the edges in

contact to prevent shifting under magnetic stresses and to make the structure mechanically more stable. In most machines the magnet poles also support the atmospheric load on the vacuum chamber, and the frame must be sufficiently rigid to prevent distortion under the combined load of atmospheric pressure and the magnetic force between poles. Very few bolts are needed in the assembly except those to support the upper pole. The pole assemblies are held together with long bolts through the yokes or occasionally are welded in place. In most cases, however, the pole-face disks are solid plates with blind-tapped holes in the face away from the gap, into which long bolts can be inserted to hold the disks in place.

Some few designers have used assemblies of thinner plates (bolted and welded together) such as in the original Berkeley 184-in. magnet, which uses 2-in. mild-steel rolled plate. However, with increased experience and new techniques in steel manufacturing plants it is now possible to obtain forgings at equivalently low prices. The structure assembled from large forgings described above has proved to be magnetically more efficient and structurally stronger, and the total cost including assembly is no greater than for an assembly of thinner plates.

Exciting coils for the magnet have also been developed into a nearly standardized design. Two stacks of flat layer-wound coils are used for the two windings, fitting snugly around the poles. Variations in design are chiefly in the method of cooling the conductors. Some designers use oil-bath cooling, with the coils stacked inside an oiltight tank and with the oil recirculated through a heat exchanger for cooling. Others prefer dry-wound coils, with the cooling fluid contained in separate layers in thermal contact with the conductors. One satisfactory arrangement is to interweave layers of conductor with layers of water-cooled plate or tubing and to depend on the thermal conduction through an intermediate thin layer of insulation to cool the conductors. Another method, popular in recent years with the development of new skills in the nonferrous-metals industry, is to use hollow conductors, with cooling water or oil flowing through the channel in the conductor and with electrical insulation provided for the cooling-fluid leads. The designers' choice of number of turns and of the current-voltage rating of the winding determines the conductor dimensions in each case.

Azimuthal asymmetry of the magnetic field can cause a shift in the center of the orbit and so might reduce the maximum ion energy obtainable at a fixed radius. Asymmetry can also induce radial oscillations, as described earlier. Although the presence of such oscillations would not cripple the operation of the accelerator seriously, it is advantageous to keep them to a minimum. Large radial oscillations, with the associated orbit precession, can add to the difficulty of extracting an emergent beam. An estimate of a reasonable radial amplitude is that it should be no larger

than the orbit increase during a phase-oscillation cycle. The maximum amplitude is of the order of 1 to 2 in. for most of the larger accelerators. When this is translated into the maximum allowable magnetic asymmetry, it is about 0.05 per cent, or 1 part in 2000. Pole faces must be flat and parallel to this same precision, a severe criterion in such a large machining operation.

In the Chicago report[8] of magnetic-field measurements azimuthal deviations were observed ten times greater than could be expected from the dimensional discrepancies in the gap between poles. The asymmetry was ascribed to variations in magnetic permeability of the iron in the poles. Empirical shimming was required to correct for these deviations, which was done by welding thin soft-iron plates to the pole tips where indicated. A figure showing these measurements was included in Chap. 8, with a discussion of the techniques used to correct the variations.

The radial tapering of the field needed for magnetic focusing is obtained by contouring the pole faces. This is normally determined by model tests on small-scale magnets using the same quality of iron and the same maximum flux density; in these tests the contour shape is determined by empirical machining of the model pole faces. Experience with smaller cyclotrons shows that a drop of 2 to 3 per cent from center to edge of the uniformly tapered region is adequate to establish a median plane and to provide vertical restoring forces. A larger decrease is acceptable in the synchrocyclotron from the point of view of phase stability, but it increases the range of frequency modulation required and decreases final energy. So the smallest magnetic decrease compatible with focusing is usually used to keep the frequency sweep to a minimum and seldom exceeds 5 or 6 per cent.

Electric focusing due to the accelerating voltage across the D gap is negligible for the synchrocyclotron, because of the relatively low D voltage used. It is essential to extend the region of magnetic focusing in to as small radii as possible, to preserve the beam during the first few hundred revolutions at low energy. To this end the radial decrease of field is sometimes maintained by severe contouring near the center, in the form of a sharp protuberance at the center on each pole face, which reduces the gap length.

Figure 11-10 is a plot of magnetic field versus radius for the Chicago 170-in. synchrocyclotron magnet, for several values of exciting current in the windings and several corresponding values of field. The pole faces are contoured to produce an approximately linear radial decrease from the maximum central field of 19 kilogauss at a rate of about 16 gauss/in., or a total drop over the linear region of about 6 per cent. The contour required to give this shape was obtained from model measurements at the same flux density. At lower flux densities this contour results in lower values of the slope dB/dr, and for central fields below 18 kilogauss

a minimum develops in the B-versus-r curve. If the accelerator were operated at fields below this limit, the ion beam would be lost through nonstable axial oscillations at the location of the $n = 0$ minimum. So the range of maximum central magnetic fields for which the slope is monotonic with this contouring is restricted to between 18 and 20 kilogauss.

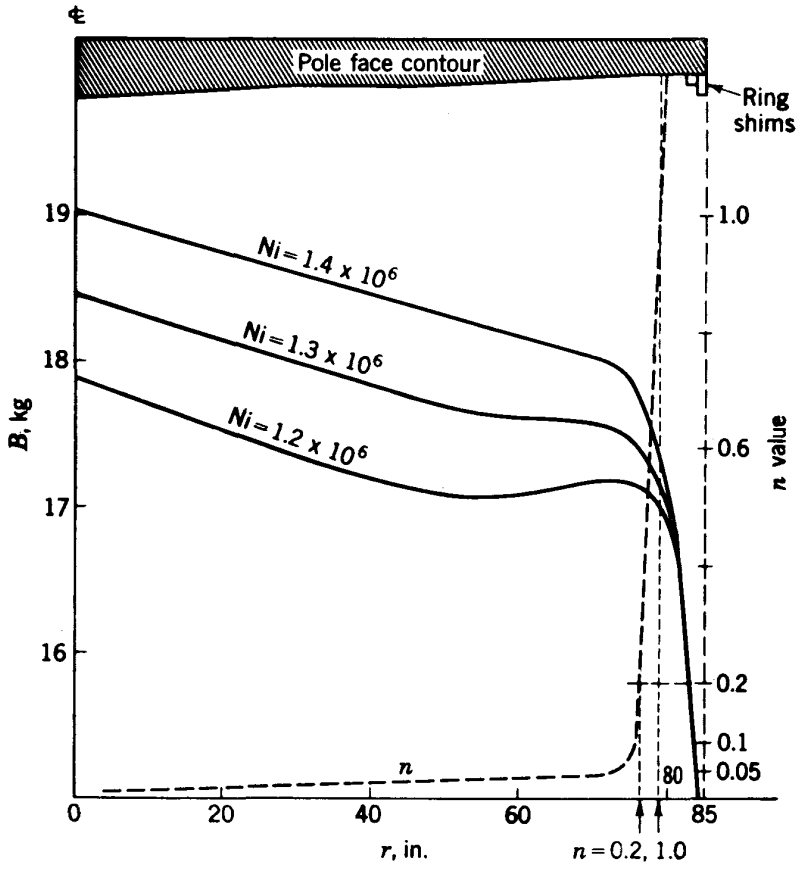

Fig. 11-10. Magnetic field versus orbit radius for the Chicago synchrocyclotron magnet.[8] The pole-face contour used to produce the radially decreasing field is shown, along with the variation of n value.

The numerical value of n in the region of acceleration varies smoothly from zero at the center to about 0.05 at large radii. Then, as the field falls off near the pole edge because of fringing effects, the value of n rises sharply. The extent of the region of small n value is also illustrated in Fig. 11-10, where the rise starts at about 75 in. radius. At $n = 0.2$ (76.5 in. in the Chicago magnet) the beam blows up because of resonance, as described previously. This point represents the maximum practical orbit radius and defines the maximum energy.

The magnetic field should also be symmetrical about a median plane, and this plane should be flat and at the geometrical center of the gap. During acceleration the beam will follow the median plane, so deviations

should be small compared with the vertical clearance inside the D to allow adequate clearance for vertical oscillations. In practice the median plane is frequently found to vary with radius; a variation of about 1 in. was observed with the Chicago magnet. This was not considered sufficient to require correction, but the relative currents in the two exciting coils were adjusted to shift the average vertical location of the median plane. An azimuthal variation of the median plane would be more serious, since it might set up vertical oscillations. Such a deviation would be observed in the azimuthal uniformity measurements described earlier and would require corrective shims.

11-7. VARIABLE-FREQUENCY OSCILLATOR

The radiofrequency system for powering the D in a synchrocyclotron depends for its frequency variation on the mechanical modulation of the resonant D circuit by a variable capacitor. A capacitor rather than a variable inductance is chosen largely for practical, mechanical reasons. The single-D system is simpler than the double-D used in the standard cyclotron, and it is adequate for the relatively low applied voltage. Electronic methods of frequency modulation were seriously considered in the early planning stages. However, the wide range of frequency modulation and the considerable change in energy stored in a large D and D-stem system make electronic modulation impractical. The mechanical system, on the other hand, acts as a reservoir to store and release electrical energy as required. The electrical efficiency or Q of a tuned mechanical system can be high, so power requirements are a minimum, while that of a broadly tuned electronic system must necessarily be low.

The rf oscillator and modulation system developed for the 37-in. model of the Berkeley synchrocyclotron was the first practical design and pointed the way for future developments. Schmidt[9] described the system in detail, discussing the several possible methods of coupling a variable capacitor to the D circuit. The system was intended to model and approximate the conditions required for the 184-in. machine. The arrangement adopted for the 37-in. model is shown in Fig. 11-11*a*. In this arrangement the capacitor is located at the far end of the D stem, forming a half-wavelength resonant line. The coupling loop to the oscillator is located along the stem near the rf node of the half-wavelength line.

The half-wave resonant circuit operates in the mode in which the D at one end and the floating plates of the capacitor at the other end have opposite phases or potentials. As the capacitance is varied, the resonant frequency of the circuit changes, and the location of the rf node shifts along the stem. For a frequency change of 10 to 20 per cent the physical shift in location of the node is not large, and a fixed coupling loop which

is optimum for some intermediate frequency can be used to feed power into the circuit from an external oscillator over the entire frequency range. The coupling must be tight, with large mutual inductance, so the oscillator frequency will be determined by the resonant frequency of the circuit. Other components of the oscillator must have high rf imped-

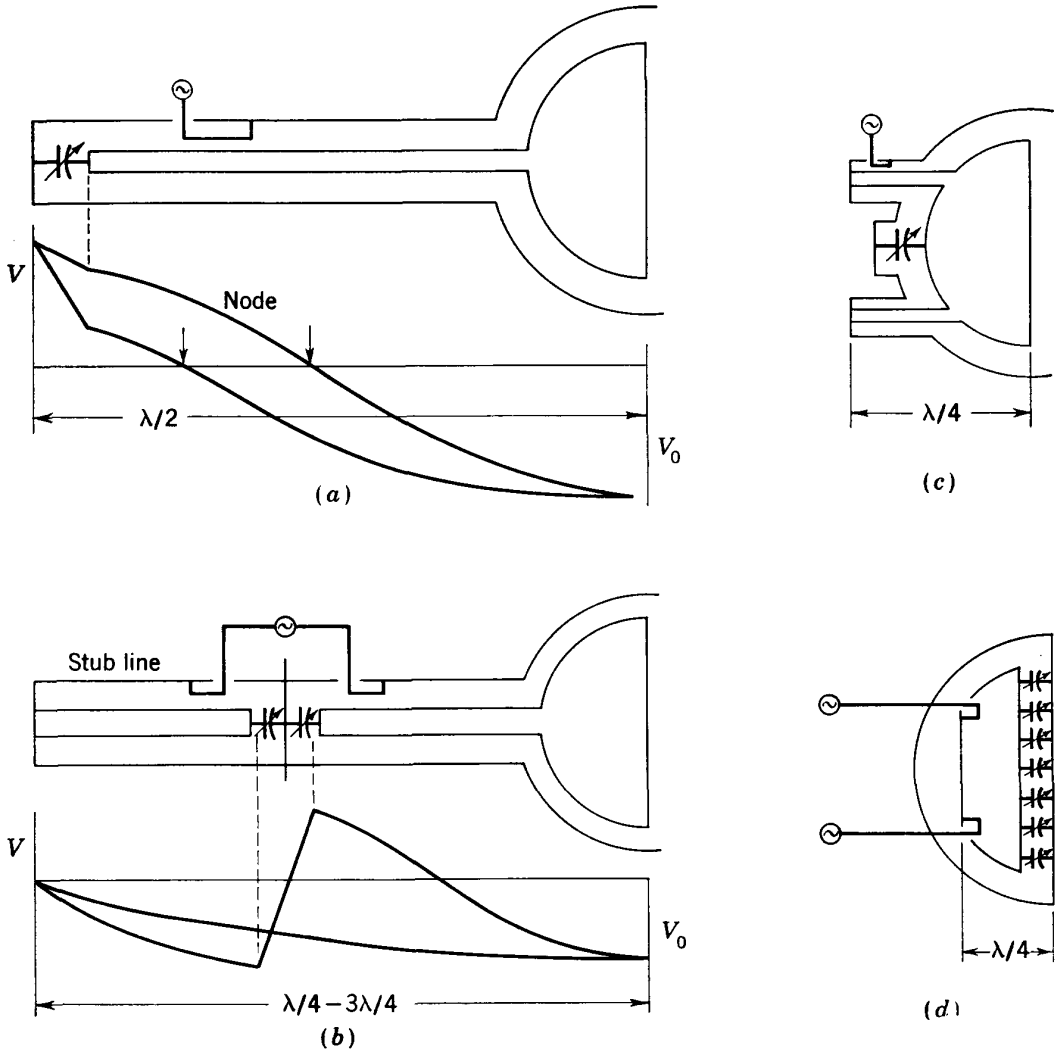

Fig. 11-11. Alternative frequency-modulation systems for the resonant D circuit in a synchrocyclotron: (*a*) λ/2 circuit; (*b*) ¾λ circuit; (*c*) λ/4 circuit for low energies; (*d*) λ/4 circuit for high energies.

ance or low Q, so they do not affect the frequency. The simplest circuit for this purpose is a grounded-grid self-excited system with cathode excitation supplied through a broadly resonant, fixed-frequency grid circuit. An alternative is a modified Hartley self-excited oscillator in which the excitation comes from a feedback connection from the plate circuit.

A more detailed description of the 37-in. oscillator system was pub-

lished by MacKenzie and Waithman,[10] after some experience with the earlier circuit. In this modification a wider range of frequency was provided. The grounded-grid oscillator is described and illustrated, and its coupling to the half-wave circuit is analyzed.

With this experience the 184-in. rf system was successful from the start. After two years of operation the results were reported by MacKenzie, Schmidt, Woodyard, and Wouters,[11] describing the acceleration of deuterons to 190 Mev and He^{++} ions to 380 Mev. They give the considerations involved in this initial choice as:

1. The rotary capacitor could operate outside the magnetic field.
2. Design and construction of the D and of the capacitor could proceed independently.
3. Many of the problems involved in the design of the capacitor had been worked out on the 37-in. model.
4. Vacuum systems for the cyclotron D and the capacitor could be independent.
5. The D could be insulated to provide a D bias to control discharges.
6. The oscillator could be coupled to the rf system in air near the nodal point of the transmission lines.
7. The system is readily adjustable to give the desired shape of the D-voltage-versus-frequency characteristics.

Many technical problems were studied and solved during the construction and testing phase. Suitable water cooling had to be installed on the D transmission lines, coupling loops, and the rotary capacitor. All steel surfaces exposed to rf fields were copper-plated to reduce rf resistance. The D was mounted on vacuumtight insulators mechanically arranged to support the extended structure. The capacitor was built with seven rotor disks having 24 teeth each, rotating between stator rings with matching blades and located in a large vacuum chamber with separate high-speed pumps. Scale-model tests were used to determine the capacitance and frequency range in advance of construction. The 100-kw grounded-grid oscillator was copied from the successful design used with the 37-in. magnet.

Operational experience showed a few weak points, which were corrected. Chief of these was the low-voltage glow discharge developed in the large spaces around the D because of electron oscillations in the electric and magnetic fields. The discharge tends to load the D circuit with nonuseful ion currents and so to reduce D voltage undesirably. The discharges were eliminated by adding grounded shields around the D to reduce the volume for electric discharge and by application of a negative bias to the D to sweep out the ions formed in the adjacent region. Another general problem was the elimination of spurious resonances or parasitics. These would show up at some intermediate frequency and cause a wiggle or kink in the frequency characteristic. Methods of identifying the source

of such parasitics and eliminating them by use of suitable grounding straps or other techniques call for a high level of experience and ingenuity in the designer, and they are individually characteristic of the particular oscillator circuit.

Later a revised rf system for the Berkeley 184-in. synchrocyclotron was substituted to enable the machine to be tuned for proton acceleration as well. This required a wider frequency range than for deuterons alone, and the entire system was rebuilt. The proton-deuteron system is described by MacKenzie[12] in considerable detail; Fig. 11-11*b* is a schematic illustration. The primary change was the addition of a stub line behind the capacitor, with a grounded node at the end of the stub line. This is equivalent to making the D circuit a three-quarter-wavelength resonant line, and the system is called a three-quarter-wave circuit. In tuning over the broad frequency range the circuit shifts gradually from a three-quarter-wave resonance at high frequencies to a quarter-wave resonance at low frequencies; the location of the two coupling loops was chosen to feed power over the entire range. The rotating capacitor was built with a sufficiently large change in capacitance to enable operation over the full frequency range required for both proton and deuteron resonance, from 23.2 to 9.5 megacycles. The mechanical details are well described in this article, as also is the electrical problem of suppressing parasitic modes of oscillation. The oscillator was built around two 9C21 tubes in parallel, in a grounded-grid circuit. The physical dimensions of the tubes and oscillator components restricted the tube location and required the use of transmission lines about three-eighths wavelength long to the coupling loop. With this arrangement the oscillator tubes could be located in the region of minimum magnetic field outside the magnet, where the reversed leakage flux cancels the useful flux; the tubes were also shielded magnetically. This new rf system was a complete success and has had a good record of steady operation.

At the University of Chicago[8] the arrangement chosen for the 170-in. machine is essentially the same as the one described above for the proton-deuteron system in the Berkeley 184-inch. It also uses a series capacitor and a quarter-wave stub to form a three-quarter-wavelength line. However, no attempt is made to cover the entire frequency range with a single capacitor, but a proton-deuteron switch system is used which shifts the range of frequency covered by the capacitor to operate with either kind of ion. The stub line is arranged with adjustable shorting bars so its electrical length can be adjusted from outside the vacuum; the lengths of the coupling lines are also adjusted to obtain optimum coupling for the two conditions; metal plates around the rotating capacitor are shifted to alter its series inductance. All these changes are arranged to be made quickly and without disturbing the vacuum when frequency is switched from proton to deuteron resonance. A rather simplified sketch of the rf

system is shown in Fig. 11-12. The oscillator power tube is housed in a metal shielded cabinet with transmission lines coupling to the cathode and the plate. The tube is an RCA 5770 triode with water-cooled anode. It is surrounded by a ½-in.-thick iron tube to shield it from the fringing magnetic field of the cyclotron magnet, estimated to be 300 gauss in this region.

Other laboratories have used different arrangements for the rotating capacitor and the rf resonant circuit. Smaller synchrocyclotrons such as the one at Harvard[13] (150-Mev protons) require a smaller range of frequency modulation, and the mechanical and electrical problems are considerably simplified. An elementary quarter-wave resonant circuit can be used, with the D mounted on short stubs supported at the rf node. At Harvard the frequency range is between 25 and 18 megacycles and is obtained with a relatively simple rotating capacitor mounted at the back of the D just outside the magnet poles. The eddy currents induced in the rotor by operation in the fringing magnetic field are not serious; the heating effect is not sufficient to require water cooling. The D is supported on two coaxial quarter-wave stub lines which are large and sturdy and have high electrical efficiency. A schematic diagram of the $\lambda/4$ circuit and oscillator is shown in Fig. 11-11*c*. In principle no insulators would be required in this type of support, since the shorted end of the $\lambda/4$ stub line is an electrical node. In practice, however, it is desirable to impress an electrical bias on the D to suppress discharges, so a ring of vacuumtight isolation capacitors is located around the node of each stub line so the D can be electrically insulated. The oscillator circuit uses a pair of 880 tubes in a grounded-plate circuit in which the power is fed directly from the plate to a coupling loop in one D stem through a transmission line, and excitation is taken from another transmission line leading to the cathode.

A similar arrangement of capacitor and D-support stems was chosen for the 240-Mev accelerator at the University of Rochester.[14] With large D size the capacitance is increased and the lengths of the quarter-wave stub supports are shorter. The variable capacitor must also tune over a wider frequency range.

The rf system for the Columbia University[15] 400-Mev synchrocyclotron at the Nevis Laboratory at Irvington, New York, is radically different from the other large machines. It is based on the use of a variable capacitor located along the leading edge of the D in the strong magnetic field between poles. The D is a quarter-wave cavity resonator, entirely enclosed within the main vacuum chamber. Figure 11-11*d* shows a schematic view of such a cavity-resonator D with the variable capacitor on the leading edge. The sketch illustrates the problem of using a $\lambda/4$ stub-line circuit for the D in such large-diameter magnets—the physical length of the oscillating circuit is shorter than the distance from center to

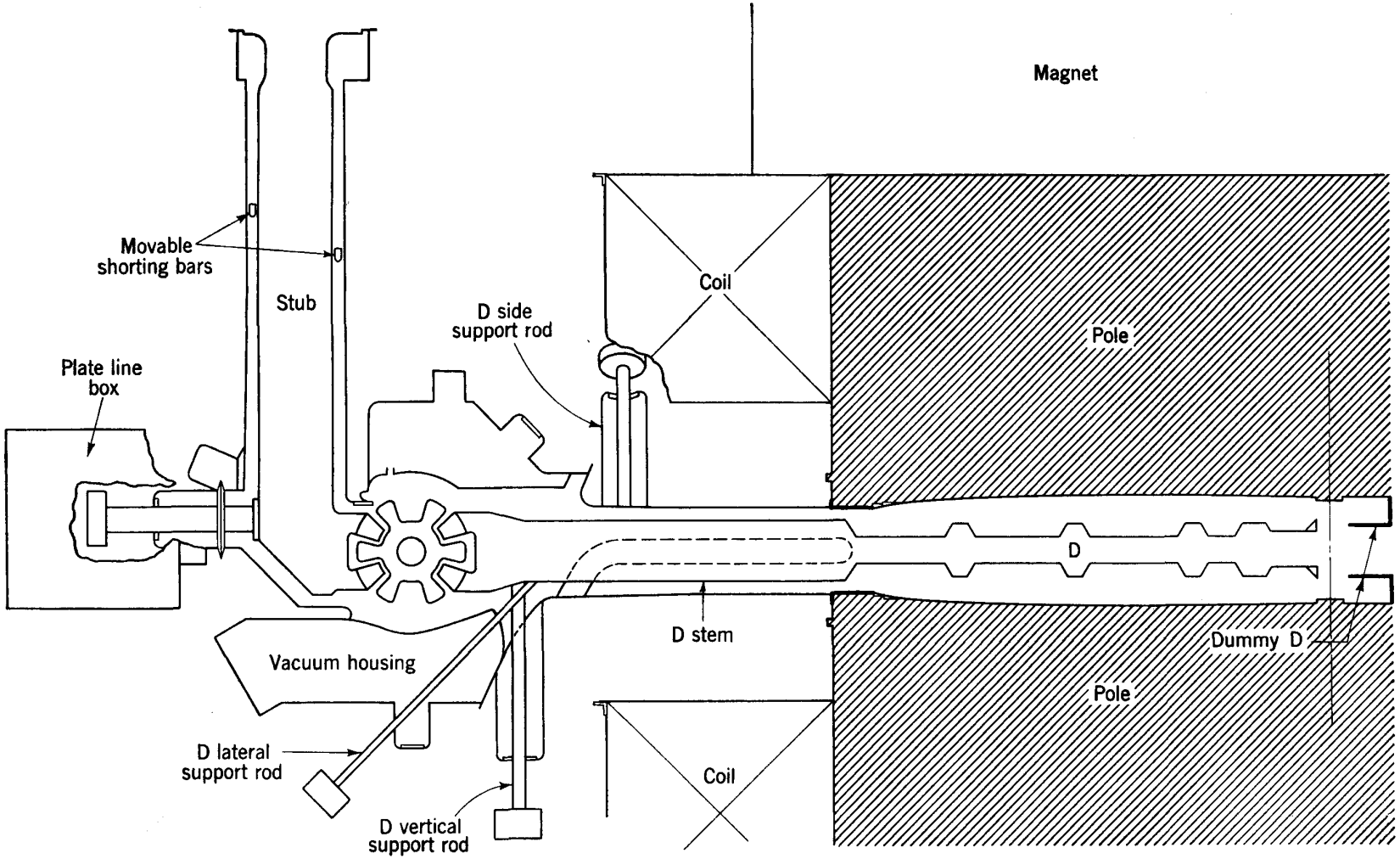

Fig. 11-12. Radiofrequency system for the University of Chicago synchrocyclotron.[8] The oscillator circuit is not shown.

edge of the cyclotron chamber. The capacitor is used to maximum effectiveness when located at the open end of the quarter-wave resonator, where voltage is a maximum, so its capacitance can be a minimum. This system has the advantage that it is essentially free from parasitic oscillations, and the energy is entirely in the fundamental mode. The only serious parasitic encountered was that associated with standing transverse waves from side to side of the flat, hollow cavity. It was eliminated by feeding the cavity symmetrically from two oscillator tubes in parallel with coupling loops located at opposite corners of the cavity. The oscillator circuit and coupling lines are of simple design.

The quarter-wavelength cavity resonator is the only existing type of circuit which could, in principle, be extended to indefinitely large pole-face diameters. However, the mechanical and technical problems of operating the rotating capacitor in the strong magnetic field are severe. Eddy currents generate heat in the rotating blades, and the rotor shaft must be water-cooled. Other problems were met in the maintenance of the insulating supports and bearings of the rotor to prevent frictional heating in vacuum. They have been solved by the development of nonlubricated Teflon bearings. A series of modifications were required before all the problems were solved. Nevertheless, the circuit has performed satisfactorily in operation, and the designers have confidence in the soundness of the principle.

11-8. VARIABLE CAPACITOR

The design of the variable capacitor depends on the range of frequency variation required, the type of circuit in which it is to be operated, and the physical location. As used in the half-wave and three-quarter-wave circuits, the capacitor is located at the outer end of the D stem and can have its own separate vacuum system. The primary problems with a rotating capacitor are the technical ones of structural strength in rotation and electrical insulation of the rotor. Electrical leads must be designed for low rf resistance. Maximum capacitance requires close spacing of the blades, and spark breakdown between blades is a limitation; smooth rounded corners, highly polished surfaces, and fast pumps which result in a good vacuum are essential. A cross section of the Chicago capacitor showing the shape of rotor and stator blades is illustrated in Fig. 11-12. A typical frequency-versus-time characteristic was shown in Fig. 11-4. An approximately linear frequency dependence on time is considered desirable over the operating frequency range, although the phase stability of particle motion holds for any decreasing function. The usual design uses rectangular blades; blade shaping to tailor the shape of the time variation is considered unnecessary.

Capacitors for quarter-wave circuits must operate in the fringing mag-

netic field at the back of the D. The same basic design of multiple parallel-plate capacitor is employed, with the plates rotating in the plane of the field. Thick metal plates have large eddy currents induced when rotated at high speeds in the magnetic field. The designs tend toward thin plates having high rf conductivity, and the shaft is usually water-cooled to remove the heat generated by the eddy currents. In a typical installation (Rochester) fixed stator blades are mounted on the back of the D, and the teeth of the rotor blades mesh accurately with 0.10 in. clearance (Fig. 11-13). The capacitor is in the main cyclotron vacuum chamber, and some sparking is observed when discharges occur in the chamber and raise the gas pressure.

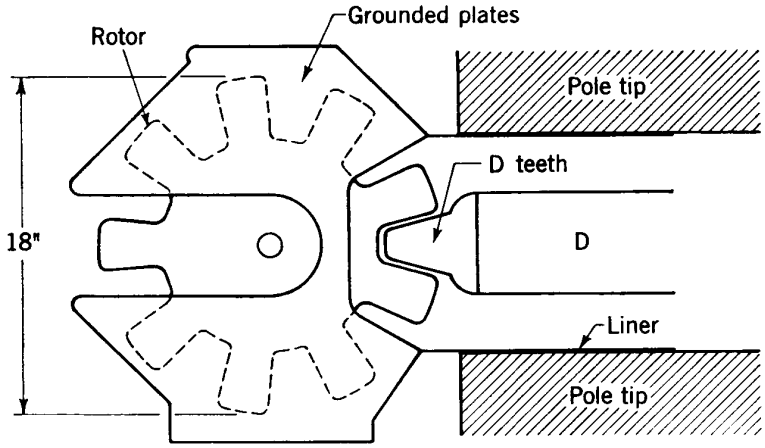

Fig. 11-13. Schematic cross sction of rotating capacitor for the University of Rochester synchrocyclotron.[14]

The rotating capacitor in the Columbia machine is of even more special design, since it must operate in the high central magnetic field and must also be physically small in diameter to fit in the regions between the outer D surfaces and the pole faces. A double capacitor is used for symmetry, one above and another below the D. Each consists of a long row of small-diameter blades having four teeth mounted on a shaft which goes across the vacuum chamber. Maintenance problems have led to the development of sectional units, each about 2 ft long, which can be readily replaced. The chief disadvantage of this system is the radiation exposure of personnel in maintenance operations, which is partially controlled by using graphite "beam catchers" on the lips of the D to reduce the intensity of induced radioactivity.

A new concept for the variable capacitor was developed at Berkeley in 1956 during the rebuilding of the 184-in. machine to produce 720-Mev protons. The principle of the vibrating reed or plate has been adopted; it allows a higher rate of frequency modulation than the rotating capacitor and results in a correspondingly higher average beam intensity. In the

Berkeley application a set of four stainless-steel plates are used, each about 4 ft long, 12 in. wide, and tapered in thickness from 2 in. at the fixed end to ½ in. at the vibrating end. These plates are tuned to identical mechanical vibration frequencies of 64/sec and driven by electromagnetic coils in a manner entirely similar to an electrically driven tuning fork. Vibration amplitudes of over 1 in. have been obtained. The vibrating plates provide a variable capacitance to the fixed and insulated D structure, modulating the frequency as desired. This system may well replace rotating capacitors in future synchrocyclotrons. It was also incorporated in the 600-Mev CERN synchrocyclotron.

11-9. ELECTRICAL DISCHARGES

Electrical discharges between the D and ground have caused considerable trouble in the development of synchrocyclotrons. The mechanism of the discharge is a combination of several processes. It closely resembles the cumulative type of blue-glow discharge common in standard cyclotrons, but in the large volumes surrounding the D in synchrocyclotrons it is incident at considerably lower D voltage. One phenomenon which is involved is secondary-electron emission at the surfaces of the D and the liner; another is the collimation of the discharge by the magnetic field, which localizes it around sharp points or surfaces of high electron emissivity and leads to spark breakdown. However, to obtain the ordinary type of dc plasma discharge with the available potentials, the gas pressure would have to be many times larger than the pressure normally used in the vacuum chamber. It is now recognized that electron oscillations in the radiofrequency electric fields are involved, and possibly also large positive-ion orbits, both of which would increase the probability of ionization.

Electron oscillation discharges are caused by oscillatory motion of electrons in the rf fields; the electrons make many traversals of the available space, and ionization in the residual gas is greatly increased. In the stray magnetic field between poles electron paths are restricted to tight helical spirals about the lines of magnetic flux, and the electric-field component effective in producing oscillations is that which parallels the flux lines. This means that the physical distance involved is usually the spacing between the D and the grounded pole faces. In the fringing region at the edge of the poles, however, these path lengths can be considerably greater.

Large amplitude oscillation of electrons with the radiofrequency field occurs over a narrow range of applied voltage and is a function of the frequency. We consider an electron of charge-to-mass ratio e/m in a field $E = V/d$, where d is the available gap length for electron motion and the electron is in an oscillating field of angular frequency ω. The

mathematical analysis is identical with that used in Sec. 10-16 in connection with the multipactoring effect. The conclusion is that there is a maximum voltage at which resonance can occur. From Eq. (10-41) this maximum voltage is given by

$$V_{\max} = \frac{\omega^2 d^2}{2e/m} \tag{11-5}$$

As an example, consider a synchrocyclotron operating at a frequency of 20 megacycles, and assume a typical gap 10 cm long. We find for the maximum resonant voltage: $V_{\max} = 450$ volts. This is sufficient to impart a maximum energy of 225 ev to the electrons, at which energy the probability of ionization is near optimum. As long as the peak voltage across the gap is below this limit, electrons will stay in the gap and oscillate in resonance with the field, causing a cumulative build-up of ionization which culminates in a blue-glow discharge. This heavy loading of the oscillator holds D voltage low, so the chamber continues in the discharge condition indefinitely. However, if the voltage can be made to exceed this resonant value, the amplitude will exceed the physical dimensions of the gap; electrons will impinge on the metal of the D or the chamber wall, and the cumulative ionization will be reduced. The discharge can be avoided if D voltage can be "jumped" through this resonance region rapidly, or if the free electrons in the region can be removed by some additional agency.

We note from Eq. (11-5) that the combination of high frequency and long gaps used in the synchrocyclotron raises the resonant voltage to a value at which ionization becomes efficient. If either the frequency or the gap spacing could be reduced, the voltage limit would be lowered and cumulative ionization would not be so probable. Yet frequency is fixed by the proton resonance relation, and the relatively wide spacings are necessary to keep capacitance low so as to have an efficient resonant D circuit at this frequency. So the problem of electron oscillations is inherent in the design parameters required for the larger proton synchrocyclotrons.

The electron multipactor effect, which has been a severe problem in proton linacs, was discussed in Sec. 10-16. It is probable that multipactoring is a factor in the synchrocyclotron discharge problem, although conditions are more complicated and it is difficult to identify multipactoring experimentally. In this effect the electron oscillations in resonance with the applied rf field would result in the production of secondary electrons at the electrodes on impact. Secondary emission would increase the electron density and so would aggravate the discharge.

Several mechanisms are available to control this type of discharge, once its nature is understood. The simplest and most practical technique

is to impose a dc bias field between the D and ground. This requires that the D be insulated. Such a field sweeps out electrons as they are formed, holding the electron density below that critical value required to initiate the cumulative blue-glow-type discharge. This technique was readily available in the Berkeley synchrocyclotron, since the design of the oscillator circuit required that the D be mounted on insulators. The application of a dc bias of several thousand volts was found to control the discharges. The opportunity to use dc biasing is one of the considerable advantages of the half-wave and three-quarter-wave resonant systems. It has been applied to all synchrocyclotrons of this design.

Circuits utilizing the quarter-wave resonant system do not have the advantage of an insulated D, since the simplest mechanical technique would be to support it on short stub lines attached to the chamber wall. At Harvard the designers inserted a ring of isolation capacitors in each stub line at the rf node in order to insulate the D and allow dc biasing to be used. At Rochester a set of small electrodes ("spot grids") was installed on the copper liners surrounding the D; these electrodes could be biased to provide a clearing field. Considerable development was required to find the proper number and location of such grids.

Another technique which might be useful in suppressing discharge would be to use a power amplifier rather than a self-excited oscillator to drive the D circuit, and to drive the circuit through the critical voltage region fast enough to avoid initiating the discharge. The electron-oscillation effect is a resonance phenomenon which is effective only over a certain range of applied voltage. If the voltage can be increased rapidly enough, the time during which it will be in the resonance range will be too short to allow a cumulative build-up of oscillations, and the discharge cannot start. This may be practical with the resonant circuits used in cyclotrons which have a relatively low Q. If driven by a power amplifier which is sharply pulsed, the sensitive voltage region could be traversed rapidly. Some designers believe that this technique might eliminate the need for D biasing.

11-10. VACUUM CHAMBER

The main vacuum chamber houses the accelerating electrode or D and provides an evacuated region between pole tips in which ions are accelerated. Designers of large synchrocyclotrons have found it desirable to support the atmospheric pressure load on the pole tips. The top and bottom surfaces of the chamber have large holes equipped with ring vacuum seals to accommodate the iron pole tips, which form the faces of the chamber. Large side ports are also required for inserting the D and for mounting pumps and probes. The chamber itself is little more than a structural framework, supporting the atmospheric load only on the

side surfaces. A typical and simple chamber is that for the Rochester[14] machine (see Fig. 11-14).

The most successful designs use nonmagnetic stainless-steel plate, welded to form the chamber shell and having machined pads around the port apertures to provide good gasket surfaces. The techniques of welding vacuumtight seals in nonmagnetic metals have been highly perfected during the past 10 years. It is now possible to obtain reliable welding jobs from many fabricating plants.

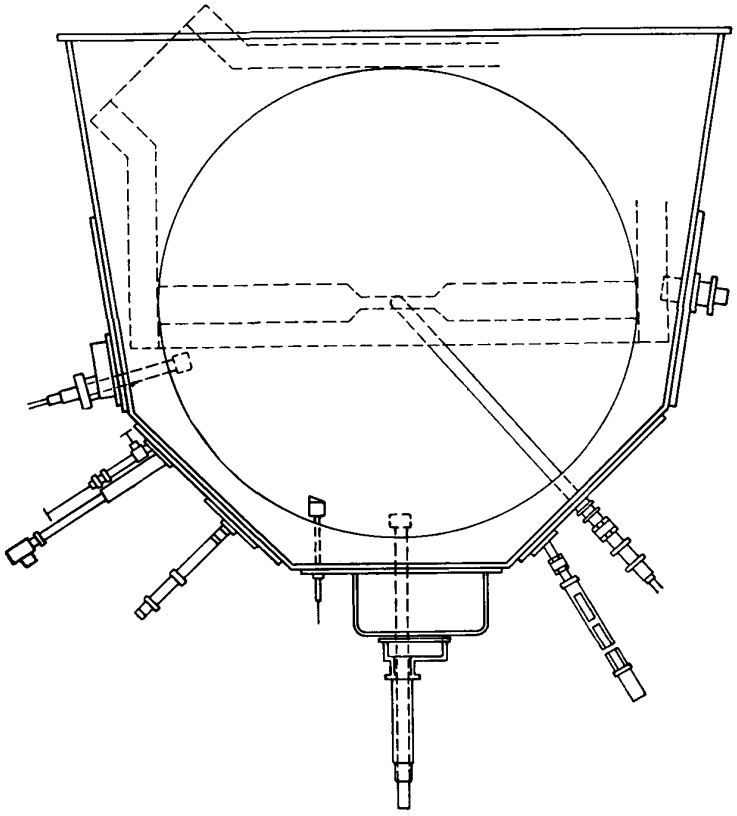

Fig. 11-14. Welded stainless-steel vacuum chamber of the Rochester synchrocyclotron,[14] showing ports for insertion of the D electrode, ion source, and various probe targets.

Vacuum-seal designs have been discussed in earlier chapters. The accumulated experience in vacuum engineering has led to a wide variety of excellent designs for all types of seals. In the synchrocyclotron chambers with their large volumes and many ports this experience has been put to good use. The number of satisfactory designs is so great that detailed description is impractical.

The inner surfaces of the chamber, including the pole tips, are usually lined with water-cooled copper sheet to provide a low-resistance return path for the rf currents in the D circuit. Good electrical contact must be maintained across any gasket joints, such as at port cover plates. A

variety of ingenious techniques have been developed to solve such technical problems, and these are adequately described in the several laboratory progress reports referenced earlier.

Vacuum techniques have also been described in some detail in earlier chapters. The pumps and the vacuum techniques needed for the synchrocyclotron differ only in scale from those successful in smaller vacuum chambers. Many competent designs showing great individuality are evidence of the high state of perfection to which the field of vacuum engineering has now progressed. The variety and scope of such designs and their many details cannot be reported here, but they are available in the form of blueprints and technical data in the several laboratories.

11-11. ION SOURCE

Many laboratories have engaged in independent development studies of the ion source, since it is a straightforward problem in gaseous discharge and electronics. In most cases the result has been a relatively minor modification of the hot-cathode arc common in standard cyclotrons (see Chap. 6). The chief problems encountered involve cathode life, erosion of the cone tip, cooling for high-current operation, and the mechanical manipulation of the source and cathode stems. A typical source is that developed at the University of California and copied in principle in several other laboratories. The source head is illustrated in Fig. 11-15. It uses a "hairpin" of large-diameter tungsten as a cathode and a graphite cone to condense the arc and limit gas evolution. In normal operation a potential of about 200 volts will produce a total discharge current of several amperes with a hydrogen gas flow of about 0.1 liter/hr. The useful ions are formed in the emergent stream of gas just outside the cone tip by the electron beam issuing from the discharge and collimated by the magnetic field. The ions are pulled from this region by the rf fields on the D; usually extensions or feelers are attached to the D near the center to increase the electric field near the source. The limiting factor is the chamber pressure due to the emergent gas, controlled by the size of the cone-tip aperture and the pumping speed. In each installation this balance is achieved by experiment, usually resulting in a chamber pressure of about 2×10^{-5} mm Hg. Beam intensities obtained with such a source are of the order of 200 μa peak during the acceptance pulse.

The mechanical features of ion sources also have much in common. In essentially all installations the source is installed through a side port on the end of a long tube, with an internal cathode stem. A vacuum lock is normally installed to enable replacement of the cathode without loss of chamber vacuum. Because of the length of the stem this involves a mechanism to retract the cathode many feet. Mechanical devices are also needed to locate the source tip both horizontally and vertically;

these usually include a flexible joint such as a metal bellows at the chamber wall and mechanical screws or adjustments

The source stem must be at ground potential, and special spring contacts have been developed to make contact with the adjacent copper liner in order to prevent rf potentials from building up along the length of the stem. Without this precaution an rf arc which may release gas and cause discharges can develop between stem and ground.

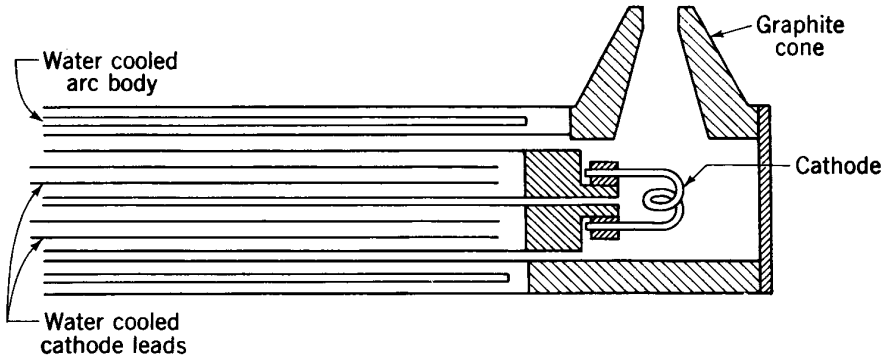

Fig. 11-15. Typical synchrocyclotron ion source.

11-12. BEAM INTENSITY AND PROBE TARGETS

Resonant-ion beam intensity is reduced below that obtained from fixed-frequency cyclotrons by the effective duty cycle or the capture efficiency, which is about 0.01, so the time-average intensities are about 1 per cent of those possible with the standard cyclotron. At Berkeley, where the development has proceeded for the longest time, resonant-ion beams up to 2.0 μa are obtained. Other laboratories report beams of between 0.1 and 1.0 μa.

The beam occurs in bursts at the modulation frequency, which for a typical installation is about 100 per second. Each burst extends over a time interval determined by the rate of expansion of orbits against a fixed target. This time interval represents 500 to 1000 ion revolutions, depending on conditions. If the amplitude of radial free oscillations is smaller than the radial phase amplitude, the time interval for the beam to clean up against the probe would be about a half-period of phase oscillations, or about 500 revolutions in a typical case. If the free oscillations have larger amplitude, the burst length may be extended to several phase oscillations. An example of the beam observed with the Berkeley machine was shown in Fig. 11-8, covering several phase periods and illustrating the effects of orbit precession. The total burst time observed, about 75 μsec, represents about 800 orbit revolutions.

Higher cycling repetition rates will increase average beam intensity and will also increase the efficiency of taking data with electronic detec-

tion equipment, which is frequently limited in the number of counts per pulse which can be recorded. The present trend toward using the vibrating-reed type of variable capacitor should result in higher intensities in future machines.

Many experiments with the synchrocyclotron can be conducted using targets mounted on probes inserted to various radial positions through a sliding seal in the chamber wall. The radial location of the probe is a measure of the ion-beam energy, and excitation functions or other experiments requiring variation of beam energy are readily performed by inserting the probe to different radii. Certain properties of the beam must be considered. For example, as ion-beam energy increases at large radii, the range of the ions in the target also increases, and ions may penetrate a thin target. If this happens, the ions of reduced energy will revolve in the magnetic field in smaller orbits; some will be reaccelerated and may again strike the probe. A given target may be a "thick" target when used at small radii and a "thin" target at the periphery. For some experiments a very thin target is desired, in order to study a narrow energy range. The ions will penetrate such a target many times. Scattering will occur, as well as absorption of energy, and many of the ions will be deflected by small angles. Such deflected ions will perform free oscillations and may strike the target in the next revolution over a wide surface area. This spreading of the beam can be observed by removing the target and scanning the surface for induced radioactivity. Any conclusions inferred from such observations regarding the size of the beam must take into account the possibility of penetration and scattering.

The radial oscillations of the beam, both synchronous and free, will affect the distribution of the beam over the leading edge of the target. The precession of orbits caused by the mismatch of radial-oscillation frequency with the circular motion has been described in an earlier section. Precession will cause the beam to strike the target at a finite distance back from the leading edge of the target. To observe it a thick target is required, in order to prevent penetration and scattering, which would also diffuse the beam. The spread in ion energy for particles striking the target is also affected by the magnitude of the radial phase oscillations; this effect has also been described in the earlier discussion of operational results with the Berkeley machine.

When deuterons strike a probe target, they can disintegrate into protons and neutrons. The neutrons emerge in the forward direction in a narrow cone; they have an energy distribution which is sharply peaked about a mean value of half the deuteron energy. The energy spread depends on momentum transfer in the interaction, including the effect of the distribution of internal momentum between the components of the deuteron. This beam of roughly monoenergetic neutrons is of considerable value for certain special experiments. Protons from the splitting of

the deuteron have a similar energy and angular distribution, but they are deflected by the magnetic field in circular orbits of roughly half that for the deuterons, so they return to about the center of the chamber after a half-revolution. Detection instruments such as photographic plates placed near the center of the chamber, located above or below the plane of the beam, have been used to observe such secondaries. The cyclotron magnetic field provides energy analysis of the protons.

When the synchrocyclotron is accelerating protons and they are allowed to strike a probe target, a beam of neutrons emerges in the forward direction with energies ranging up to the maximum proton energy.

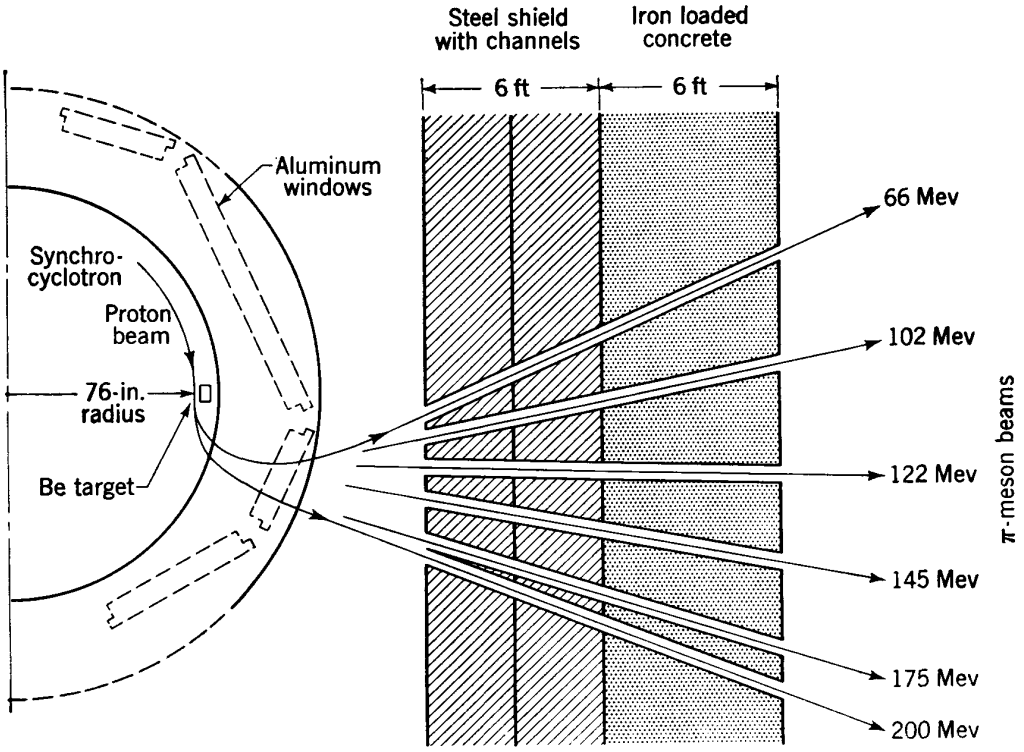

Fig. 11-16. Target and shielding arrangements for emergent meson beams in the Chicago synchrocyclotron.[8]

This is interpreted as an "exchange of charge" process between the protons and neutrons in the target nuclei. Maximum neutron energies are much higher than those from the deuteron split-up.

Mesons are produced above some threshold energy in targets by all particles. This threshold is about 150 Mev for protons, 190 Mev for deuterons, and 250 Mev for He^{++} ions. The "pi" mesons are produced directly in nuclear reactions and have the highest intensity; "mu" mesons are observed primarily as decay products of the pi's; neutral π mesons produce high-energy photons, a process investigated in detail for the first time in the Berkeley laboratory.

Mesons originating at a probe target can emerge from the cyclotron

and will be analyzed and partially focused by the cyclotron field. Beams of π mesons of a narrow energy spread can traverse channels in the shield and emerge to be used for experiments. At Chicago, for example, the intensity of mesons produced by 1 μa of 450-Mev protons on the probe target is about 4×10^{10} mesons/sec. In the most favorable energy channel about 10^3 π mesons/(cm^2)(sec) are available in an energy range of 122 $\pm$ 3 Mev. Figure 11-16 shows the arrangements in the Chicago installation to provide such analyzed beams of mesons for experiments.

11-13. EMERGENT BEAM

The deflection of resonant ions in the synchrocyclotron to produce an emergent beam is complicated by the fact that the change in orbit radius per turn is small. The method which was successful in the standard cyclotron cannot be applied directly for several reasons. A solid septum, even if accurately shaped and located, would intercept practically the entire beam. Furthermore, deflection must start inside the $n = 0.2$ point where the beam blows up into vertical oscillations, and it must extend at least as far as the $n = 1.0$ radius where radial stability ceases and the beam enters opening spiral orbits. So the deflector must pull the beam through a large radial distance. The electric field required to bring the beam out of the magnetic field within a reasonable length of arc is very high for the high-energy particles, and voltage insulation for the deflecting potential becomes a serious problem. Finally, because of their phase oscillations, the ions are not so tightly bunched in phase while crossing the accelerating gap as the resonant ions in the standard cyclotron. The energy gain in the last turn (and the equivalent change in orbit radius) varies widely over the range of phase oscillation, and it may be zero.

The rate of expansion per turn ΔR depends on the maximum accelerating voltage V, the phase of crossing the gap ϕ, particle energy and velocity, and the radial gradient of the magnetic field given by the index n. Bohm and Foldy[5] give this rate as

$$\frac{\Delta R}{R} \simeq \frac{1}{(1 - n)\beta^2} \frac{2eV \sin \phi}{W} \tag{11-6}$$

where W is total energy (including rest energy) and β is the relativistic parameter v/c. A simpler form of this relation was used in Sec. 6-7 to describe the rate of expansion for the nonrelativistic particles in the standard cyclotron; it led to ΔR's of the order of 3 mm, quite adequate to pass behind the thin septum used to form the inner face of the deflector channel. However, for the synchrocyclotron the calculated ΔR is less than 0.1 mm in practical cases; an example is given in the reference above.

Such a beam would be entirely lost against a septum if the orbits were concentric.

On the other hand, certain characteristics of particle motion in the synchrocyclotron can be utilized for ejection of a beam. The stability of free oscillations in the radially decreasing magnetic field makes it possible to excite wide-amplitude radial oscillations and throw the particles out locally beyond their equilibrium orbit location. At the maximum radius where $n = 0.2$ the frequency of such radial oscillations is about $0.9f_0$, so the location of maximum radial amplitude precesses about the cyclotron, moving about one-tenth of a cycle or 36° per turn. The combination of precession and large radial amplitude can spread the beam by a much greater amount than the ΔR calculated from the energy increase per turn. Phase oscillations produce a breathing motion of the equilibrium orbit and also affect the radial motion. A superposition of the maxima of radial phase oscillations and radial free oscillations gives the largest radial displacement. Vertical free oscillations can also be induced locally to deflect the resonant ions and may be utilized to pull a beam of emergent ions from the stable orbits.

The method used to eject an emergent beam in the Berkeley 184-in. machine was to set up large-amplitude radial oscillations with a pulsed electric deflector; the deflected ions then entered a magnetic shielding channel where the weakened field allowed them to fly out on an opening spiral path. A full description is given by Powell, Henrich, Kerns, Sewell, and Thornton.[16] A schematic view of the arrangement is shown in Fig. 11-17. The deflector system consists of four 1-in.-square bars spaced about the median plane, with the two inner bars pulsed negative and the two outer bars positive, extending around 120° in arc. Particles are deflected inward to set up radial oscillations, and the channel is curved to follow the trajectory. The next outward maximum of the radial oscillations comes at about one full turn from the location of the deflector, and the entry of the magnetic shield is at this point, placed about 2 in. radially outside the location of the deflector.

The pulsed voltage comes from a pulse transformer described by Kerns, Baker, Edwards, and Farly.[17] It produces a potential difference of ± 100 kv and has a pulse rise time of about 0.1 μsec. The electric deflector is pulsed by a timing system at the instant the expanding beam reaches the radius of the deflector entry. The vertical spacing between bars ($1\frac{3}{8}$ in.) allows about half the ions to reach orbits of this radius. The 0.1-μsec pulse rise is about equal to the period of one revolution of the ions, so a phasing circuit designed to time the pulse to the angular position of the ion bunch gave only a minor improvement. Measurements showed that about 10 per cent of the resonant beam which reached the deflector entry was deflected into sufficiently large oscillations to reach the entry to the magnetic shield.

The magnetic shield has undergone considerable development, starting with a structure of two concentric iron tubes, which were modified to a set of vertical bars designed to weaken the field on the median plane and finally to a tube of elliptic cross section. The presence of these shields affects the field inside the region where resonant ions circulate and must be corrected by still other shims in the form of bars which are carefully designed and located close to the pole faces. The magnetic channel is curved to follow the opening spiral path out through the fringing field of the magnet. About 10 per cent of the ions entering the magnetic

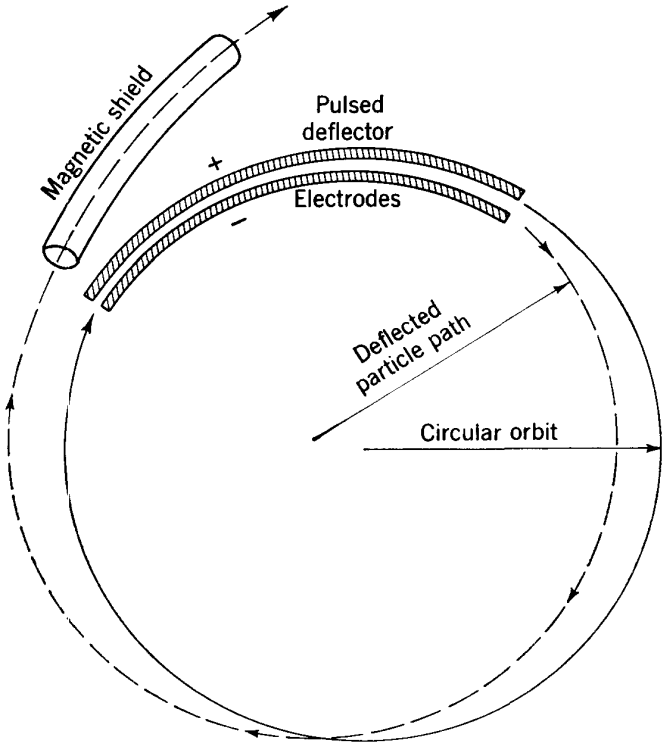

Fig. 11-17. Schematic arrangement of the pulsed electrostatic deflector and magnetic channel for the 184-in. synchrocyclotron at the University of California.

channel emerge in a reasonably well-collimated beam. The over-all efficiency of the Berkeley ejection system is about 1 per cent.

A more efficient system for ejecting an emergent beam is the "regenerative" deflector first proposed by Tuck and Teng[8] of the University of Chicago synchrocyclotron group and first successfully applied by A. V. Crewe at the University of Liverpool. In this system one of two magnetic anomalies is located in the vicinity of the $n = 0.20$ orbit radius to set up radial free oscillations of increasing magnitude. The primary advantage is that this "static" deflector operates on each particle in the resonant beam as it approaches the maximum radius.

The mechanism of the regenerative deflector can be explained most

readily by reference to the two-unit system proposed by Tuck and Teng. The first magnetic anomaly, called a peeler following the betatron usage, weakens the magnetic field over a short arc (about 8 in. long). The cross section of such a peeler is illustrated in the sketch of Fig. 7-17; magnetic flux is bypassed through the iron back-leg of the peeler, weakening the field between the jaws. In this weak field ions acquire an outward radial displacement relative to a circular orbit; this represents a radial free oscillation, which reaches its maximum outward amplitude after traveling about 90°. The second magnetic anomaly is a regenerator which strengthens the magnetic field locally, placed about 90° beyond the

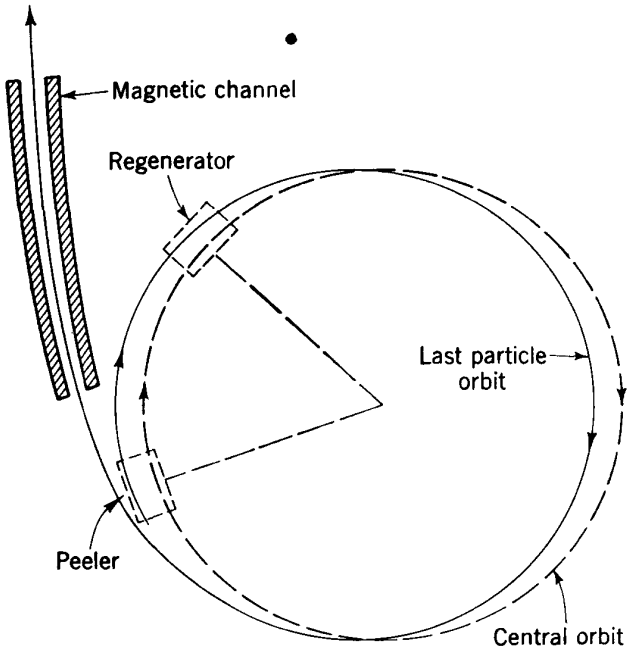

Fig. 11-18. Regenerative deflector system for ejecting an emergent beam, proposed by Tuck and Teng.[8]

peeler. It consists of iron bars above and below the central plane which concentrate magnetic flux and increase intensity at the center. The regenerator gives a second impulse, inward, which causes a further increase in radial amplitude. The increased amplitude causes the ion to swing first inward and then outward again, where it reaches the azimuthal location of the peeler with a net outward displacement. The increased penetration into still weaker fields produces larger amplitudes, so it penetrates more deeply into the regenerator field, etc. Since the process is regenerative, the displacement grows exponentially. Ultimately the amplitudes become sufficient for the change in radial location in a single turn ΔR to become large enough for the ion to pass behind the peeler and enter a magnetic shielding channel, which allows the beam to emerge from the field.

In the Liverpool application the peeler was used as described above, and the regenerator was located about 45° beyond. Analysis of the motion showed the importance of a linear (constant-n-value) decrease of field in the peeler and a linear increase in the regenerator, in order to have a constant coefficient in the exponential term describing the increase in amplitude. Magnetic measurements were made of the fields around the peeler, regenerator, and shield, and correcting shims were designed to preserve the uniformity of field on the central plane inside these magnetic anomalies. The ΔR obtained in the last turn, after exponential growth of amplitude, was about 3 in. About 20 per cent of the resonant beam entered the channel of the magnetic shield; with the initial shield about 5 per cent emerged as a collimated beam which formed a spot about 1 in. in diameter at a distance of 20 ft from the cyclotron.

A later revision of the Chicago deflector system, utilizing the experience and improved analysis of the Liverpool group, has resulted in an intensity of about 10 per cent in an emergent beam. In this revision the regenerator is used as before, but the peeler is eliminated. The property of the peeler of providing a radially decreasing magnetic field is not essential, since the fringing field of the magnet provides such a decrease around the entire orbit. New analyses showed the optimum location and strength of the regenerator unit relative to the opening of the magnetic channel. The back-leg of the peeler, formerly responsible for some intensity loss, is removed, so the final intensities are higher.

The most significant advantage of the magnetic deflector is that it acts on all particles of the beam sequentially as they expand progressively past some fixed radius and so spreads the deflection pulse over hundreds of cycles at the resonant frequency. Such a long ejection pulse is highly desirable for electronic detection instruments. The emergent beam can be focused to small diameter and passed through channels in a shield. Its monoenergetic character and its small size, which allows the use of small targets, make the emergent beam far more valuable for research than the resonant beam, which required the use of probe targets.

11-14. CONTROLS

An important part of the technical development of all accelerators is the design of circuits for supplying power to the several electrodes and other auxiliary equipment, along with the system of adjustments and controls. The most obvious component of the control system is the operator's console, on which are mounted all the switches, meters, and control devices. It is such a necessary feature in any accelerator installation that it is usually taken for granted; since it is considered to be primarily the product of electronic and electrical engineering, it is seldom featured in any physical design study. However, much experience has

gone into the design of control systems and the operator's console, and many technical improvements have been incorporated. This experience has followed the radio and electronics fields, and many of the improvements have been taken from these engineering developments. But the particular needs of accelerators have made each control system unique, and many special devices have been developed by the designers. This is particularly true in the synchroaccelerators, where the pulsed duty cycle requires special instrumentation to display and control the operation of the accelerator. For this reason an exception is made in this chapter by describing the control system in some detail, as representative of the special problems for synchronous accelerators.

The more recent development of control consoles has tended toward simplification, with the minimum of starting switches, meters, control knobs, pilot lights, etc., in order not to confuse the eye and hand of the operator. Small wires and low power levels at the console are the rule. Power-switching relays and adjustable controls used for more permanent settings are relegated to auxiliary relay racks which do not require continuous maintenance or attention. The usual layout of a synchrocyclotron control room includes a relatively compact console desk, with the necessary indicators closely grouped and available to an operator in a swivel chair, and rows of relay racks along the sides of the room in which the power controls are located.

The typical console is arranged in a three-sided arc like the mirrors on a dressing table. A flat table surface for keeping records, at the proper height for a seated operator, extends around the arc. Sloping panels within easy arm's reach have all necessary control buttons and switches. The important switches and controls are prominently located in the center, usually with a beam current indicator directly in front of the operator. Auxiliary switches are grouped on the sides according to function. Pilot lights and other indicators are displayed near the appropriate switches and controls, and banks of indicators for circuits such as cooling-water flow and pump heaters are located where the operator can keep them in view without strain.

The control room must be located behind suitable radiation shields, but should be as close as possible to the accelerator, so the operator or his assistants can move readily between the control console and the machine for maintenance and test operations. In some cases observation windows have been built into the shielding wall; an example is a water-filled tank equipped with glass windows. This is probably undesirable in modern high-intensity machines, but is a relic of the days when the operator's eye and ear were important instruments for observing spark breakdowns or other phenomena. A modern equivalent is a television camera, with a display at the console.

Cathode-ray tubes with time sweeps are prominently featured on the

consoles of all pulsed synchronous accelerators and are arranged to superpose successive pulses. Multiple-channel switches allow the operator to display any one of several variables on the scope. The time of sweep can be varied to expand the early stages for detailed study of injection phenomena or to observe the output beam at the end of the acceleration. Or, the frequency-modulation cycle in the resonant circuit can be displayed to observe any distortion of wave shape. A superimposed pulse from the ion-source pulser will show the frequency at the start of acceleration, and the effect of pulse-delay circuits can be studied. Another technique is to display the rf waveform and study the phase timing of the deflector pulse applied to the emergent beam.

Starting switches and adjustment controls for many circuits are needed on the console. The magnet current supply customarily is a dc generator connected permanently to the magnet coils and driven by an ac induction or synchronous motor. Excitation for the generator may come from a smaller dc generator which is itself excited by an electronically regulated field supply. Starting switches will operate power relays in the ac power lines. A reading of magnet current can be obtained from a shunt in series with the coils, and it is usually displayed on a panel meter. Fine variations in current are best observed through the magnitude of the electronically regulated exciter field current, often by use of a potentiometer which displays a small difference between the field current and a constant bias. The magnet current regulator should be capable of setting any value of magnet current and of maintaining constancy to within about 1 part in 1000 over the normal operating range. Controls for turning on and adjusting the regulator are also installed on the panels at the console.

Suitable overload relays, temperature indicators, pilot lights to indicate successive stages of the operation of starting, and other monitoring systems will also be grouped on the console. Vacuum systems require many control switches and indicators. Mechanical fore-vacuum pumps, rough-vacuum pressure gauges, cutoff valves, diffusion-pump heaters, water thermocouples, water-flow indicators, high-vacuum valves, valve-position indicators, and high-vacuum ionization gauges—these are the essential elements which require switches, interlock circuits, or pilot lights on the operator's console. Automatic interlocks of many types are helpful in such a complicated system. A high reading on a rough-vacuum pressure gauge or failure of the cooling-water flow can be used to close valves or turn off pump heaters. A common arrangement on the panel display is a compact group of associated display elements with the pilot lights, position indicators, and meters disposed in vertical columns above the appropriate starting switches.

A complete set of controls for the rf oscillator and a set for the motor driving the rotary capacitor are also needed. These must include all the

necessary indicating instruments for monitoring, such as grid-current, plate-current, grid-bias, and plate-voltage meters. Pulsed operation of the oscillator may be desirable, and it is used in some installations to reduce the average power requirements. If it is used, controls for these pulsing circuits are required. The variable speed drive of the rotary capacitor should be controllable from the console, as should the starting switches. Another item associated with the rf oscillator is the power supply to provide the dc field used for suppression of discharges in the chamber.

The ion source requires cathode heating power, arc voltage supply, and gas flow. Each of these requires controls at the console. The ion source is often sensitive to discharges and must be readjusted to maintain a steady output; this may require voltage and current regulator circuits as well. The mechanical adjustments for the location of the source should also be made by remote control from the console; directional drive controls and position indicators should be located at the operator's bench. Other mechanical adjustments, such as those which determine the location of the probe target, require similar controls. Servosystems are frequently used for such purposes.

For such complex systems a well-designed set of protective mechanisms and interlocks is essential. Water-supply circuits for cooling are generally equipped with flow indicators which are interlocked to turn off power circuits in event of water failure. High-voltage equipment is protected by screens or shields with hinged doors or removable panels for maintenance; electrical interlocks on such doors will turn off power supplies when the doors are opened. Operation sequences should also be interlocked; ion source, water-cooling circuits, cathode heaters, etc., should all be on and their interlocks open before rf power switches can operate. Doors or gates in the radiation shielding must also be interlocked to prevent personnel from entering a region of high radiation intensity accidentally.

The over-all problem of circuit design, controls, cabling, and protective equipment is highly involved in a large accelerator installation. The efficient operation of the machine requires that this problem be solved in such a manner that the controls actually handled by the operator are few and simple. The trend in design is toward increasing use of automation, so the operators can concentrate on operating problems which require human intelligence for their solution.

REFERENCES

1. E. M. McMillan, *Phys. Rev.*, **68**:143 (1945).
2. V. Veksler, *J. Phys. (U.S.S.R.)*, **9**:153 (1945).
3. J. R. Richardson, K. R. MacKenzie, E. J. Lofgren, and B. T. Wright, *Phys. Rev.*, **69**:669 (1946).

4. W. M. Brobeck, E. O. Lawrence, K. R. MacKenzie, E. M. McMillan, R. Serber, D. C. Sewell, K. M. Simpson, and R. L. Thornton, *Phys. Rev.*, **71**:449 (1947).
5. D. Bohm and L. L. Foldy, *Phys. Rev.*, **70**:249 (1946).
6. D. Bohm and L. L. Foldy, *Phys. Rev.*, **72**:649 (1947).
7. L. R. Henrich, D. C. Sewell, and J. Vale, *Rev. Sci. Instr.*, **20**:887 (1949).
8. "170 Inch Synchrocyclotron," Institute for Nuclear Studies, University of Chicago, I (July, 1948); II (July, 1949); III (July, 1950); IV (July, 1951).
9. F. H. Schmidt, *Rev. Sci. Instr.*, **17**:301 (1946).
10. K. R. MacKenzie and V. B. Waithman, *Rev. Sci. Instr.*, **18**:900 (1947).
11. K. R. MacKenzie, F. H. Schmidt, J. R. Woodyard, and L. F. Wouters, *Rev. Sci. Instr.*, **20**:126 (1948).
12. K. R. MacKenzie, *Rev. Sci. Instr.*, **22**:302 (1951).
13. "Harvard 95 Inch Cyclotron," Office of Naval Research Report NR-026-012 (July, 1950).
14. "130 inch Rochester Cyclotron," Office of Naval Research Report N6-ori-126, II (July, 1946–July, 1949).
15. E. T. Booth (ed.), Columbia Cyclotron Report (Mar. 30, 1950).
16. W. M. Powell, L. R. Henrich, Q. A. Kerns, D. C. Sewell, and R. L. Thornton, *Rev. Sci. Instr.*, **19**:506 (1948).
17. Q. A. Kerns, W. R. Baker, R. F. Edwards, and G. M. Farly, *Rev. Sci. Instr.*, **19**:899 (1948).

At the head of the facing page is an illustration of the 350-Mev electron synchrotron at the University of Glasgow. (Courtesy of P. I. Dee.)

12

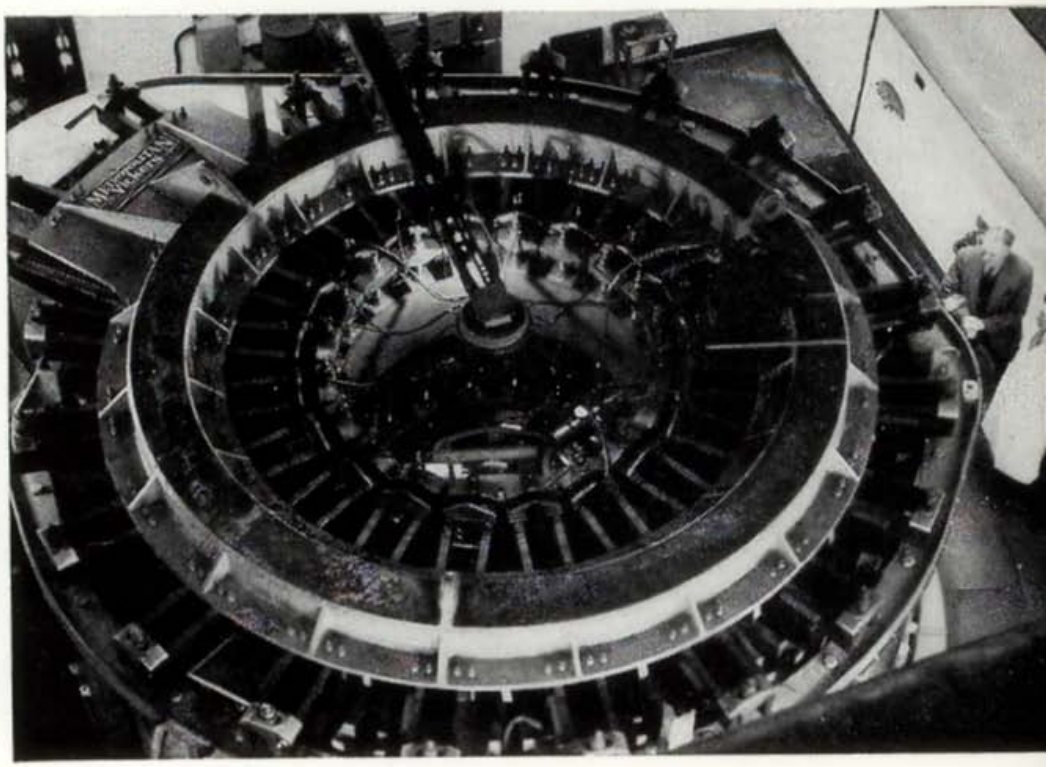

The Electron Synchrotron

In the synchrotron particles are accelerated to high energies in an orbit of roughly constant radius. Energy is supplied to the particles by a radiofrequency field provided at one or more points around the orbit. As particle energy increases, the magnetic guide field in the circular orbit also increases, at a rate which matches the increasing momentum of the particles. The magnet is operated cyclically from low to high magnetic fields as the particles are accelerated, resulting in a pulsed output of high-energy particles at the cycling frequency. Because of the varying magnetic field, the magnet cores are laminated as in a transformer.

Phase stability exists in the synchrotron (see Sec. 9-8) and provides a mechanism by which the particle energy is made to keep pace with the rising magnetic field. When electrons are accelerated, the phase-stable acceleration automatically follows any reasonable rate of rise of magnetic field and maintains constant orbit radius. This is due to the fact that electrons reach relativistic velocities at quite low energies ($v = 0.98c$ at 2 Mev), so the angular velocity at fixed orbit radius approaches a fixed value and the electrons can be accelerated by a constant-frequency radio-frequency supply which is basically simple in design and for which power requirements are modest.

At low energies the frequency of particle motion in a magnetic field depends strongly on energy, which means that the frequency of the

accelerating field must be varied to match the particle frequency. This is a major problem in the acceleration of protons, and it requires a wide range of frequency modulation during the acceleration cycle (see Sec. 13-7). With electrons the need for frequency modulation is minimal and can be removed by using an alternative system for acceleration up to a few Mev energy.

The synchrotron has to a large extent displaced the betatron as a source of high-energy electrons. The much lighter ring-magnet structure which provides the guide field in the synchrotron is simpler and less costly than the laminated-core magnet needed to supply induced voltage for acceleration in a betatron. In the synchrotron one or more compact cavity resonators provide radiofrequency electric fields for acceleration. Furthermore, the radiative losses by electrons at high energies are corrected automatically in the synchrotron by phase shifts which increase the accelerating fields; the complicated compensating devices necessary to achieve high energies in the betatron are not required. Even in the 20- to-50 Mev energy range, in which there are many medical and industrial applications, smaller synchrotrons are competing effectively with betatrons as sources of X rays.

12-1. STORY OF THE DEVELOPMENT

Unlike earlier accelerators, most of which required slow and tedious development starting with small sizes at low energies, the electron synchrotron was conceived in its full stature as a high-energy accelerator. The first installation (by McMillan at the University of California) was designed for 320 Mev, at which energy the radiations are capable of producing mesons. Within a few years a half-dozen machines of about this energy were started in the United States, with others abroad. Seldom has a new accelerator been exploited with such promptness. The reason is that the principle was announced in 1945, just at the end of World War II when scientists had returned to their universities and were eager to engage in the new field of high-energy physics.

The development started suddenly in 1945 with independent publications describing the principle of phase-stable acceleration by McMillan[1] at the University of California and by Veksler[2] in the U.S.S.R. In his first publication McMillan discussed the application of the principle to an electron accelerator and named it the synchrotron. Readers immediately recognized the soundness, simplicity, and completeness of this new proposal. No better method can be used to illustrate the features described above than to quote directly from McMillan's brief paper, which stands as a classic in accelerator history:

> One of the most successful methods for accelerating charged particles to very high energies involves the repeated application of an oscillating electric field, as in the cyclotron. If a very large number of individual accelerations is required,

there may be difficulty in keeping the particles in step with the electric field. In the case of the cyclotron this difficulty appears when the relativistic mass change causes an appreciable variation in the angular velocity of the particles.

The device proposed here makes use of a "phase stability" possessed by certain orbits in a cyclotron. Consider, for example, a particle whose energy is such that its angular velocity is just right to match the frequency of the electric field. This will be called the equilibrium energy. Suppose further that the particle crosses the accelerating gaps just as the electric field passes through zero, changing in such a sense that an earlier arrival of the particle would result in an acceleration. This orbit is obviously stationary. To show that it is stable, suppose that a displacement in phase is made such that the particle arrives at the gaps too early. It is then accelerated; the increase in energy causes a decrease in angular velocity, which makes the time of arrival tend to become later. A similar argument shows that a change of energy from the equilibrium value tends to correct itself. These displaced orbits will continue to oscillate, with both phase and energy varying about their equilibrium values.

In order to accelerate the particles it is now necessary to change the value of the equilibrium energy, which can be done by varying either the magnetic field or the frequency. While the equilibrium energy is changing, the phase of the motion will shift ahead just enough to provide the necessary accelerating force; the similarity of this behavior to that of a synchronous motor suggested the name of the device. . . .

The paper goes on to give the equations describing the phase and energy variations. These have been derived in Chap. 9 and are analyzed further in the sections to follow. The design parameters for a 300-Mev electron synchrotron were also presented; this is basically the same machine on which construction was started shortly afterward at the University of California. McMillan also recognized the limitations imposed by radiation from the orbiting electrons, and in a companion paper[3] he discussed the magnitude of this loss for 300-Mev electrons, concluding that it would not seriously affect the operation of the synchrotron. He was fortunate in finding immediate support for his proposal through the United States Atomic Energy Commission, which subsidized the Radiation Laboratory at the University of California.

The University of California machine came into full energy operation in January, 1949, with a maximum electron energy of 320 Mev. At a pulse rate of six per second, with a 0.02-in.-thick platinum target, the time-average X-ray output observed with a Victoreen thimble chamber inside $\frac{1}{8}$ in. of lead was 1000 r/min.

Meanwhile, before the large California synchrotron could be completed, Goward and Barnes[4] in England were able to demonstrate the validity of the principle with a much smaller machine (8 Mev) utilizing an old betatron magnet. A quarter-wave resonator in the form of a cage of wires was installed outside the vacuum chamber. Then the magnet excitation was increased so the flux core became saturated and the betatron phase was overrun. When the radiofrequency was turned on,

the electrons were accelerated in resonance with the applied rf electric field up to an energy twice the maximum betatron energy.

The next to succeed was a group at the General Electric Research Laboratory[5] with a 70-Mev synchrotron based on their previous experience in betatron design. A series of experiments with these early machines demonstrated the range of validity of the stability principle, worked out the necessary conditions for injecting electrons so they would be captured in synchronous orbits, and explored some of the properties of the high-energy beam of X rays. In the 70-Mev machine the forward-directed beam of visible light due to radiation by the radially accelerated electrons was observed for the first time.

The simplicity of the basic concept is reflected in the relatively few competing techniques which have been reported and in the comparatively small number of publications. A few theoretical papers have added detail to the original articles by McMillan and Veksler. Dennison and Berlin[6] analyzed the stability of the synchronous orbits and found that the amplitude of synchronous oscillations decreases with increasing particle energy. They also recognized the need for frequency modulation for electron energies below about 2 Mev, plus the fact that radiation losses at high energies would require increased accelerating potentials. Bohm and Foldy[7] at the University of California extended McMillan's calculations to describe the free oscillations in some detail; they also computed the radiation damping effects and exploited McMillan's proposal of using betatron operation at the start to avoid the difficulties of frequency modulation. Frank[8] and Blewett[9] examined in detail the process of transition from betatron to synchrotron action. All these studies are in basic agreement, varying only in the type of approximations used in the calculations and in the emphasis placed on the several aspects of the motion. Theoretical understanding of the synchrotron thus became quite adequate at an early stage.

The first wave of construction in this country was in the 300-to-350 Mev energy range. In addition to the machine at the University of California, synchrotrons of this energy were started at Cornell University,[10] Massachusetts Institute of Technology,[11] the University of Michigan,[12] and Purdue University. Most of these projects were supported by grants from the Office of Naval Research or the Atomic Energy Commission. During this early phase a 140-Mev machine was built at Oxford University, England. In general, these machines were put to immediate use for research studies, primarily in the production of mesons. An unusual design which developed the magnetic fields required without the use of iron magnets was started in the General Electric Company Research Laboratory by J. P. Blewett[13] and was carried on by J. L. Lawson[14] and his associates. Development in this energy range was climaxed by the completion in 1954 of a 350-Mev synchrotron at the

University of Glasgow; this machine was most carefully designed and engineered and incorporates all the best features of the earlier machines.

During this first phase of construction a series of papers was published giving more details on orbit theory, betatron injection, capture efficiency, magnetic properties, and other features. Others have been written following completion and testing of the machines, giving operational experience and results. These contributions will be referred to in the following sections, as they apply to specific problems or components.

More recently, the urge for still higher energies started another wave of construction in the 1000-Mev energy range. At the California Institute of Technology the magnet of the quarter-scale model of the bevatron (see Chap. 13), originally built at the University of California in Berkeley, was rebuilt and adapted for electron acceleration. In 1954 this Caltech machine came into operation at electron energies of 500 Mev; by 1958 power supplies were increased to allow operation up to 1.1 Bev. In 1959 a 1.2-Bev constant-gradient synchrotron was brought into operation at the Istituto Nazionale di Fisica Nucleare at Frascati near Rome.

Another group of large electron synchrotrons has incorporated the AG principle for the ring magnets. First of these was at Cornell University,[15] which had previously gained experience with a 300-Mev constant-gradient machine; by 1959 the larger Cornell synchrotron was in research use at 1.2 Bev energy. Three other electron synchrotrons using AG magnets reached essential completion in 1959, one at the Royal

TABLE 12-1
OPERATING ELECTRON SYNCHROTRONS

Location	Type	Orbit radius, m	Repetition rate, cps	Energy, Mev
United States:				
Univ. of Calif.*	H-type magnet	1.3	6	320
MIT	Constant-gradient	1.3	2	300
Univ. of Mich.*	Racetrack	1.2	...	300
Gen. Elec. Co., Schenectady	Air-cored	1.0	60	300
Purdue Univ	Constant-gradient	1.2	...	300
Cornell Univ	Alternating-gradient	5.0	30	1200
Calif. Inst. Tech	Quadrant	4.9	1	1100
Abroad:				
Univ. of Glasgow	Constant-gradient	1.4	...	350
Bonn Univ., Germany	Alternating-gradient	1.7	50	500
Royal Inst., Stockholm	Alternating-gradient	3.7	12	1200
Inst. Nucl. Phys. Frascati, Rome	Constant-gradient	3.6	20	1200
Univ. of Tokyo	Alternating-gradient	4.0	21	1300

* These machines were dismantled in 1959.

Institute of Technology in Stockholm with an energy of 1.0 Bev, one at the University of Bonn, Germany, at 0.5 Bev, and a 1.3-Bev machine at the University of Tokyo. The use of the strong-focusing property of AG magnets to reduce apertures in vacuum chambers and the physical size of the magnets are discussed in Chap. 15, along with other applications of the AG principle. However, for the purposes of this chapter we can restrict ourselves to the basic principles of the synchrotron as they are applied in the simpler magnets using the weak focusing of constant-gradient fields.

The larger electron synchrotrons which have been completed and are in operation for research are listed in Table 12-1.

12-2. PRINCIPLE OF OPERATION

The synchrotron accelerates electrons in an orbit of essentially constant radius by means of a radiofrequency electric field applied across a gap at one point in the orbit. The electrons are constrained to move in their circular path by a magnetic field which increases with time, from a low field which is just adequate to capture low-energy electrons at injection, to a maximum value permitted by the permeability of iron. A ring-shaped magnet provides the magnetic field over the doughnut-shaped vacuum chamber which encloses the electron orbits. The pole faces are accurately shaped to provide a field which decreases with increasing radius, with an n value of about 0.6, to supply focusing forces for the electrons; this feature is identical with the focusing principle in the betatron. During each rising pulse of the magnetic field a bunch of electrons is accelerated to high energy. Pulses are repeated at the repetition rate provided by the magnet power supply. Pulsed operation would result in eddy currents which would distort the carefully shaped magnetic field if the magnet core were of solid iron, so the core is laminated as in a betatron. The cyclic operation results in a sequence of pulses of high-energy electrons at the pulse repetition frequency.

Maximum energy of the electrons depends on orbit radius and on the maximum value of the magnetic field, following Eqs. (5-51) to (5-53):

$$T = ceBr_0 = 300Br_0 \qquad \text{Mev} \tag{12-1}$$

The constant on the right applies when B is in units of webers/m^2 and r_0 is in meters, to give energy in Mev units. For example, an orbit radius of 1 m and a field of 10 kilogauss (1 weber/m^2) will retain an electron energy of 300 Mev.

Synchronous acceleration normally starts when the electrons reach approximately the velocity of light, which in practice means an energy of 2 to 4 Mev. At this constant velocity the orbital frequency is given by

$$f = \frac{c}{2\pi r_0} = \frac{47.8 \times 10^6}{r_0} \qquad \text{cps} \tag{12-2}$$

where r_0 is in meters. The applied rf accelerating field must have a frequency equal to this electron orbital frequency, or to some harmonic of it. A 1-m-radius orbit, for example, requires an applied frequency of 47.8 megacycles (or 95.6 megacycles, etc.). If the injection velocity is materially less than the velocity of light, the equilibrium orbit for resonance at this frequency will be smaller. For example, at 2 Mev energy the velocity is $0.98r_0$, displaced 2 cm in the example above. Such a small displacement is acceptable if the radial aperture is adequate.

The applied rf voltage is developed in a resonant-cavity circuit built into the vacuum chamber and driven by a vacuum-tube oscillator-amplifier. The voltage amplitude is normally about twice the required acceleration in volts per turn, to provide an equilibrium phase angle near 30° (see Sec. 9-5).

The volts-per-turn requirement comes from the rate of rise of magnetic field and other constants of the motion including the radiation loss. By differentiating Eq. (5-52) with respect to time we obtain

$$V_e = 2\pi r_0^2 \frac{dB}{dt} \tag{12-3}$$

As an example, consider the field to rise from zero as a sine wave to a maximum value of 10 kilogauss, for an orbit radius of 1 m in a time of $\frac{1}{240}$ sec, which is one quarter-cycle at 60 cps. The initial rate of rise of field dB/dt (twice the average value for a sine wave) would be 480 webers/(m²)(sec). We obtain for the required initial acceleration

$$V_e = 3000 \text{ volts per turn}$$

Since the time per revolution $\tau = 1/f = 2.05 \times 10^{-8}$ sec and the total time of acceleration t is $\frac{1}{240}$ sec, the number of revolutions is given by $t/\tau = 2.0 \times 10^5$. The average value of acceleration per turn to attain a final energy of 300 Mev would be 1500 ev. With a sinusoidal magnetic-field cycle the required volts per turn would be twice this average value at the start and would decrease to zero at the end of the acceleration interval.

In order to obtain a more efficient use of the rf power supply, the magnetic-field pulse is usually arranged to rise in a more nearly linear manner. This is achieved by discharging a bank of capacitors through the inductance of the magnet coils. If the iron is pushed into saturation, the normal half-sine-wave pulse will be sharply peaked because of the decrease in inductance at high current. This type of pulse is illustrated in Fig. 12-1. With such a linear rise, for the same pulse length as used in the example above, the acceleration required at the start would be slightly over 1500 volts per turn and would remain constant until the iron approached saturation.

During acceleration the electrons are kept in step with the accelerating field by phase stability in the fashion already discussed in Chap. 9, par-

ticularly Sec. 9-8. The equilibrium electrons continue to return to the accelerating point at the correct phase; other electrons in the phase-stable range oscillate in phase around this equilibrium phase. The phase oscillations are accompanied by oscillations in energy and so in orbit radius. Hence the electrons are accelerated in a packet or bunch, as are the protons in the synchrocyclotron. The aspect of this bunch as it passes the accelerating gap is shown in Fig. 12-2. It is roughly banana-shaped; the electrons of correct phase near the center have maximum radial displacement, and the electrons of correct radius at the ends have maximum phase (or azimuthal) displacement.

The limits of phase stability were presented in Sec. 9-5. Figure 12-3 shows the region of radial displacement and phase error in which phase stability exists for an electron synchrotron for various values of the equi-

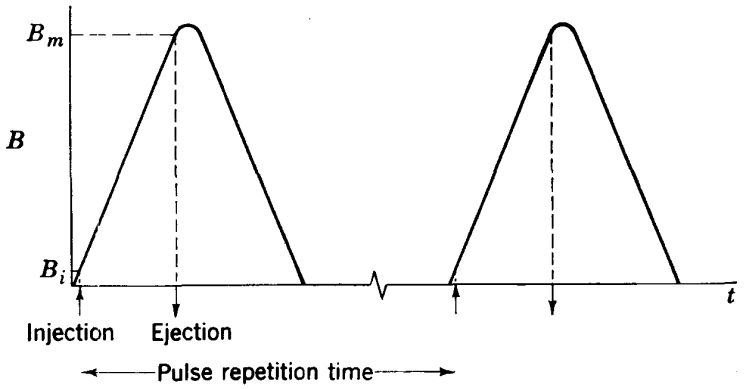

Fig. 12-1. Pulse-powering cycle of a synchrotron magnet. Electrons are injected at low energy at low magnetic field and are ejected when the field approaches a maximum value.

librium phase angle. This figure, redrawn from the work of Bohm and Foldy,[7] shows how much radial displacement is to be expected at various energies as a result of the phase oscillation. At high energies the function $f(W)$ simplifies to $[\pi(1 - n)W/eV]^{1/2}$. For example, in a synchrotron having an accelerating voltage of 1500 volts and an n value of 0.6, $f(W)$ at 300 Mev will be about 500. For an equilibrium phase angle of 30° the maximum radial excursion at this energy is given by the graph to be 0.16 per cent of the orbit radius. At 3 Mev the radial excursion is roughly ten times higher. For example, in a machine of 1 m radius the oscillations at 3 Mev cover a range of ± 1.6 cm.

The instantaneous frequency of the phase oscillation follows from Eq. (9-57). By a little manipulation of this equation it can be shown that, provided the electron energy is higher than 2 or 3 Mev, the ratio

$$\frac{\text{Frequency of phase oscillation}}{\text{Frequency of revolution}} = \left[\frac{heV \cos \phi_0}{2\pi(1 - n)W}\right]^{1/2} \tag{12-4}$$

where the parameters are as defined in Chap. 9.

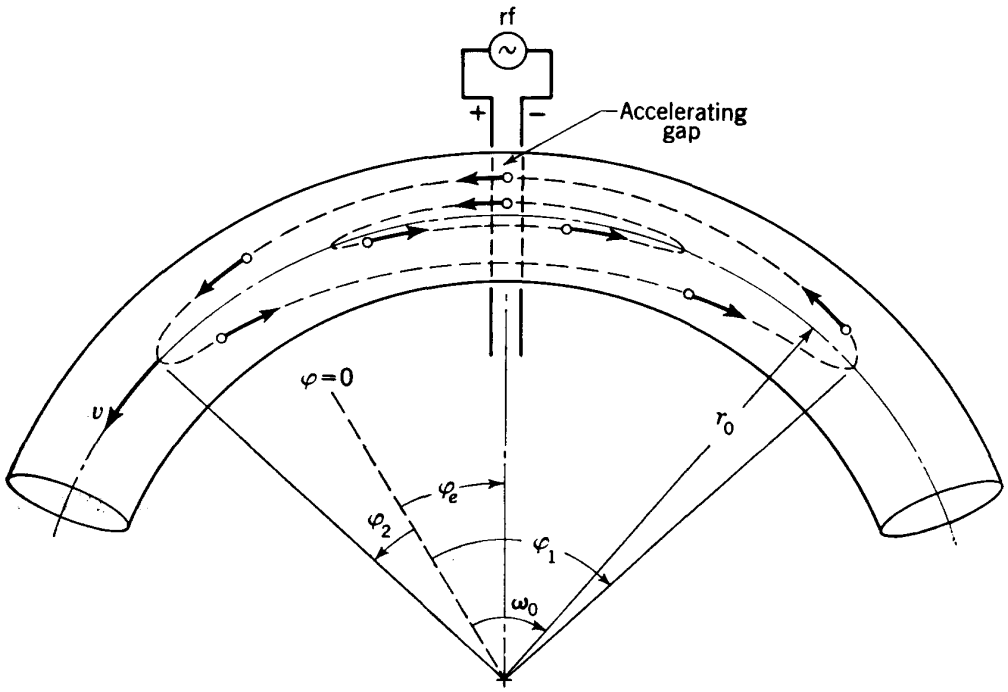

Fig. 12-2. Azimuthal phase oscillations around the equilibrium phase ϕ_0 between arbitrary limits. Electrons migrate in phase, as illustrated by the small arrows, resulting in oscillations in energy and orbit radius.

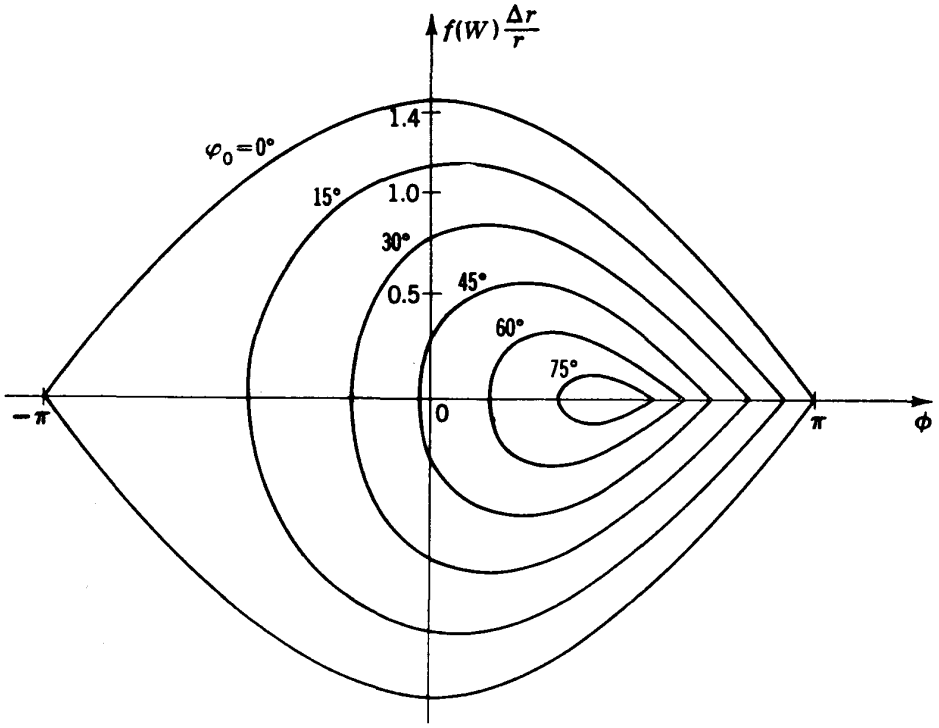

Fig. 12-3. Regions of phase stability in the electron synchrotron for various equilibrium phases. See text for discussion of the function $f(W)$.

For an electron synchrotron having an accelerating voltage of 1500 volts, a harmonic order h of 1, and an n value of 0.6, this formula indicates that at 3 Mev the phase-oscillation frequency is about 0.014 times the frequency of revolution. At 300 Mev this ratio has been decreased by another factor of 10 to 0.0014. This means that a single phase oscillation requires about 70 turns at 3 Mev or 700 turns at 300 Mev.

The usual method of bringing electrons up to the energy at which the synchronous drive can be started is to accelerate by induction, as in the betatron. The techniques in this "betatron start" will be described in Sec. 12-6, Injection. The flux linking the orbit is provided by high-permeability flux bars installed on the pole tips at the inner periphery of the magnet gap. This flux increases with time as in the betatron, providing a steady azimuthal accelerating field. Faraday's law of magnetic induction says that the induced voltage, in this case specified by the required volts per turn V_e given in Eq. (12-3), is supplied by the time rate of change of flux linking the orbit, $d\Phi/dt$. So the necessary rate of change of flux to provide betatron acceleration at constant radius is given by [cf. Eq. (7-4)]

$$\frac{d\Phi}{dt} = 2(\pi r_0^2)\frac{dB}{dt} \tag{12-5}$$

This equation is the betatron flux relation. It can be simply interpreted to read that the flux contained within the orbit must increase at a rate which is *twice* the value resulting from a uniform field of magnitude B_0 (the field at the orbit) if it were uniformly extended across the orbit, which is the betatron "2-to-1" rule.

The electrons supplied by the source are accelerated by this field and are distributed uniformly around the orbit. When they approach the constant-velocity condition, the rf accelerator unit is turned on at the chosen constant frequency. Further acceleration comes from this radio-frequency field, after the betatron flux condition is destroyed by saturation of the flux bars. The maximum limits of stable phase-oscillation amplitude mentioned above define the fraction of the uniformly distributed electrons in the orbit which will have the proper phase to be accepted into stable synchronous orbits. Others will gain or lose energy at too great a rate to remain within the aperture. When we consider an instantaneous transition from betatron to synchrotron drive, we find that about half of the betatron beam is accepted and bunched within the phase limits which allow synchronous acceleration. The transition from betatron to synchrotron drive is described in more detail in a later section, in which it is shown that under certain conditions nearly 100 per cent of the electrons can be captured in synchronous orbits.

During this initial betatron operation, free oscillations are set up about the equilibrium orbit in both radial and axial coordinates, because of

physical deviations of the instantaneous particle paths, exactly as in the betatron. The frequencies of these free oscillations, described in earlier chapters, are between 0.3 and $0.9f_0$, where f_0 is the orbital frequency, depending upon the n value of the magnetic field. These free oscillations are superimposed on the slower synchronous oscillations.

Since the free oscillations are of much higher frequency than the radial synchronous oscillation, they distort the instantaneous orbits, increase the radial extent, and also produce an axial width to the bunch. So the resonant bunch of electrons takes the form of a long thin sausage bent around the orbit. In a typical case at the start of synchronous acceleration (for the numerical example cited above) the bunch might extend around 180° in angle, have a radial width of about ± 5 cm (the sum of the two radial amplitudes), and have an axial thickness of about ± 2 cm.

As the magnetic field continues to increase with time, the amplitudes of both the synchronous and radial oscillations decrease (see Secs. 5-12 and 9-8). By the time electrons attain high energy, the transverse dimensions of the synchronous bunch are reduced by damping of both the phase oscillations and the free oscillations. The region occupied by the beam is now much smaller than at injection, so the area over which the magnetic field must be maintained at constant n value can become narrower. This is fortunate, since saturation of the iron sets in first at the pole edges, and fields are distorted in such a way that the central region of uniform n value narrows with increasing field.

An interesting and useful modification of the circular electron synchrotron was first suggested by H. R. Crane,[12] who proposed breaking the circular orbit into two semicircular sectors or four quadrants separated by field-free straight sections. The purpose of this change was to simplify the problems of introduction of rf cavities, injectors, and targets by inserting them into the open straight sections. The proposal was analyzed by Dennison and Berlin[16] and later by Blachman and Courant,[17] who showed that straight sections of moderate length would not destroy the stability of the particle orbits. Slightly more aperture is needed in such a machine, and the equations of particle motion are somewhat modified. The limits of stability are not so wide as in the circular machine, but the general character of both the betatron and the phase oscillations is essentially the same as that already discussed for the circular machines.

When the electrons approach their maximum energy, they can be made to strike a target on either the outer or the inner surface of the vacuum chamber. This can be accomplished in several ways. One method is to extend the magnet cycle past the point of saturation of the iron, where the condition of uniform n value is destroyed. The radial free oscillations become unstable if the n value exceeds 1, and the electrons will be spilled out of the orbit around the periphery. A reentrant target which

intercepts these particles before they can hit the walls will be a source of high-energy X rays which will emerge in a tangential direction.

Note that as long as the magnetic field retains a uniform n value less than 1, the focusing properties are retained. If the field is allowed to go over its peak and down the decreasing side of the pulse, the synchronous oscillations would follow this change to a negative value of dB/dt, the equilibrium phase would shift automatically into the decelerating region of the rf cycle, and the particles would be decelerated synchronously down to low energy. During this deceleration the oscillation amplitudes would increase, so the electrons would eventually strike the walls at approximately their injection energy; a burst of low-energy X rays would be the final result. This phenomenon has been observed.

Several other procedures are available to deflect electrons against targets, either inside or outside the orbit, when they have reached high energy. It is also possible to eject a reasonably concentrated beam of electrons, so experiments can be performed outside the chamber. These techniques will be discussed in Sec. 12-11.

12-3. APERTURE REQUIREMENTS

The intensity of the beam accepted into stable orbits is dependent on the dimensions of the aperture available for particle oscillations, as well as on any constructional errors or physical deviations from the ideal theoretical conditions. Oscillation amplitudes can be computed, and estimates can be made of the increase in amplitude expected from known deviations. The probability of obtaining the maximum possible intensity can be increased by using a large factor of safety in dimensions above those computed from oscillation amplitudes. On the other hand, as the size and weight of the magnet increase, costs go up approximately with the square of a magnet gap dimension. This sets an economic upper limit on aperture dimensions. The design choice for aperture is based on judgment of the proper balance between these limitations.

Other factors affect the choice of aperture dimensions. In the gap between poles of an iron-cored magnet the leakage flux from the pole edges weakens the field between poles for a distance which is approximately half the length of the magnet gap in from the edge. This means that the radial extent of the region in which the field will have a uniform n value is considerably narrower than the radial width of the poles. Furthermore, the number of ampere-turns required for excitation is directly proportional to gap length, and the power required to excite the magnet varies with the square of the gap length. As a consequence, most designers choose a short gap and a wide radial extent of pole. However, the practical problem of providing a thin-walled, mechanically sound vacuum chamber to fit between pole faces imposes a limit on such

radial extension. In an extreme case the vacuum-chamber wall thickness would occupy an undesirably large portion of the magnet gap. Here, a factor influencing the final choice is the success in obtaining a practical design for the vacuum chamber.

The limitations on magnet design discussed above determine the shape of the magnet gap. Since magnet economy favors a relatively short gap with wide radial extent, the n value is chosen to make the vertical (or axial) free oscillation amplitudes smaller than the radial amplitudes. This requires higher frequencies of oscillation in the vertical mode and is accomplished by choosing the n value larger than 0.5. Most designers have used n values in the range between 0.6 and 0.75. A consequence of the use of these rather large n values is that the magnet pole faces must be tapered and the vacuum chamber must fit in a wedge-shaped gap.

At the start of synchronous acceleration the aperture dimensions are determined in part by the initial phase conditions. There must be sufficient radial width to accommodate the radial phase oscillations. An example was used in the previous section of initial phase conditions which led to a radial synchronous amplitude of ± 1.6 cm at the assumed starting energy of 3 Mev. However, in design it might be desirable to allow more flexibility for choice of operating parameters. To extend the example above, if we chose to use a phase angle of 15°, requiring an applied voltage of nearly 6,000 volts, and assumed a starting energy of 2 Mev to reduce the duration of the betatron phase, the anticipated radial amplitude would be ± 2.7 cm. So a rather wide range of oscillation amplitudes occurs as a result of variations in choice of initial operating conditions. Or, put the other way around, a choice in aperture dimensions does not necessarily limit intensity but may restrict initial operating parameters. This conclusion holds only when the radial synchronous oscillations are the primary consideration, such as when particles are injected from an external source directly into the synchronous phase of acceleration.

When the betatron start is used to accelerate the electrons up to relativistic velocities before starting synchronous acceleration, the accepted intensities and so the aperture requirements are determined by the initial conditions for the betatron phase. The intensity-aperture problems of the betatron have been discussed at some length in Chap. 7. The primary problem is to prevent the injected electrons from striking the back of the electron gun on subsequent revolutions. Experience in betatron operation has shown that mechanisms exist which contract the orbits sufficiently to allow an adequate fraction of the injected beam to miss the gun and to be captured in stable betatron orbits. The trapping efficiency can be increased by the use of "contractor" coils located above and below the orbit, which are pulsed with large currents during the injection interval. It was shown in Chap. 7 that such current pulses distort the magnetic field and particle orbits contract rapidly.

During the betatron phase the energy increases from about 100 kev at the start to, say, 3 Mev. Magnetic field meanwhile increases from about 10 gauss at the start to 100 gauss. This increase in magnetic field causes a decrease in betatron amplitudes proportional to $B^{-\frac{1}{2}}$, to about 0.3 of the original values. We can assume that the original amplitudes were limited by the vacuum-chamber aperture (usually designed to enclose the useful magnetic-field region), so the betatron amplitudes are reduced to dimensions occupying about 0.3 of the chamber dimensions. With the start of synchronous acceleration the radial spread is increased by the magnitude of the radial synchronous amplitude. We must also allow surplus radial aperture to accommodate the reduced-radius equilibrium orbit at 3 Mev energy, estimated to be about 1.2 cm less than r_0 for a 300-Mev machine of 1 m radius.

To summarize, the radial aperture must be sufficient to accept a beam having the designed value of radial synchronous amplitude plus a radial betatron amplitude of approximately 0.3 of the half-width of the chamber, temporarily located at the radius of the initial central orbit. The vertical aperture should be balanced with the radial aperture to provide acceptance of the same angular spread of electrons from the source in the initial betatron condition; this balance comes from the chosen n value of the magnetic field.

In practice the early designs allowed quite large apertures, with a radial width of 10 to 15 per cent of the orbit radius. This is now believed to be unnecessarily conservative and costly. Later designs provide a radial width of about 5 per cent of r_0. However, as discussed above, the essential function of the aperture is to accept adequate intensity during the initial betatron phase from electron guns which cannot at present produce a sufficiently collimated beam to use the minimum aperture defined by the synchrotron requirements. As a consequence, choice of aperture is really determined by the designer's judgment as to the balance between beam intensity and initial cost of the machine.

12-4. MAGNET

In some early synchrotrons magnets were used which had H-type frames similar to those used for betatrons but without the large central laminated core, illustrated by the magnet for the 320-Mev synchrotron built by McMillan at the University of California. Accumulated experience in analyzing and applying field corrections has shown this H-type magnet to have several disadvantages besides the obvious one of making the beam inaccessible. The two external return yokes produce magnetic anomalies with measurable differences in the magnitude and the phase of the field in those portions of the orbit shadowed by the yokes. Such azimuthal inhomogeneities can introduce perturbing effects on the particle

oscillations and require correction, accomplished by installing special coils. The total weight of laminated iron required for the H-type frame exceeds that of the more compact designs described below, but construction is simpler. Costs of the two types are closely comparable.

Modern synchrotron magnets are formed of a ring of identical C-type units, each providing the field over a short section of the orbit. The purpose is to distribute the flux return path uniformly around the orbit, in order to reduce the magnitude of azimuthal inhomogeneities to a minimum. It is not necessary that the magnetic field be absolutely uniform in azimuth, but only that the periodicity of the irregularities be of a sufficiently high order that there are several units within each betatron oscillation wavelength. It is more important that the length and physical arrangement of return-path laminations be identical, so the eddy-current patterns are similar and the phase of the field the same in all units.

The basic arrangement of a ring magnet is shown in Fig. 12-4, representing the Massachusetts Institute of Technology synchrotron. This machine has 24 magnet units, each about 10 in. thick, assembled around an orbit of 40 in. nominal radius. The return legs of the C-type magnet frames are outside the orbit. Laminations are of 0.014-in. transformer steel and are assembled in blocks which are held together by external clamps. The pole tips are removable and especially shaped to give the desired radial field gradient; they are clamped in place with thin layers of insulation to prevent eddy-current short circuits.

The exciting coils are continuous circular windings threading all the sectors; these coils are installed after the iron units are in place. These are formed of stranded copper cable, similar to the cable used for winding transformers, and held in place by insulated brackets to restrict motion and abrasion. The requirement of low inductance, to allow pulsing with a large rate of rise of field, results in a coil having conductors of relatively large cross section and few turns. In the MIT machine the coil has 18 turns, and the peak current required to reach maximum excitation is 3800 amp.

The field index chosen in the MIT magnet was $n = 0.7$. The gap length between pole faces at the orbit is 2.9 in., and the width of the region of useful field is 3.5 in. (see Fig. 12-5). This is considered to be a relatively small aperture; most designers have chosen larger dimensions for the pole gap for orbits of this size.

A difficult technical problem in the design of such magnets is the mechanical clamping arrangement for holding the blocks of laminations, to avoid mechanical distortion under magnetic forces and to keep gap length constant. This is much more serious for laminated iron than for the solid block structures used in cyclotrons, since metal bolts cannot be used without insulating sleeves, and clamping brackets and bolts must be

insulated to prevent continuous metallic loops in which eddy currents could be established. In several installations the original brackets have not been completely satisfactory, but have allowed some slight vibration under magnetic forces which erodes the insulation and cuts laminations. One method of avoiding such faults has been to use preformed blocks of laminations bonded into solid structural units with thermosetting resin.

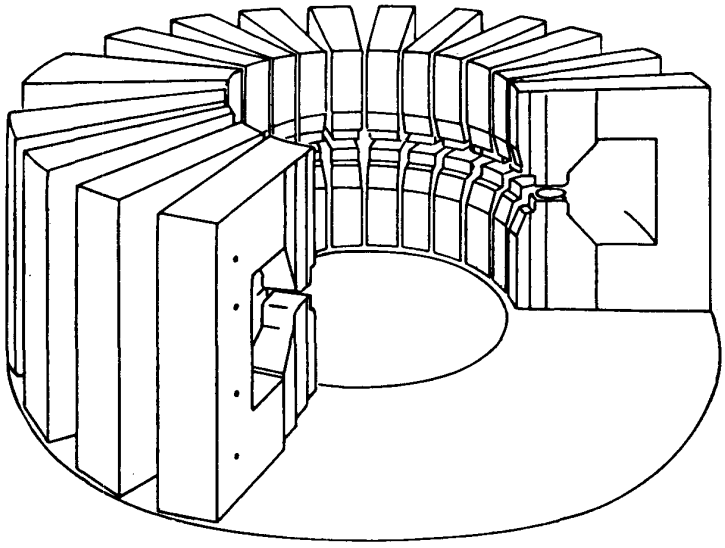

Fig. 12-4. C-type magnet of the MIT synchrotron.

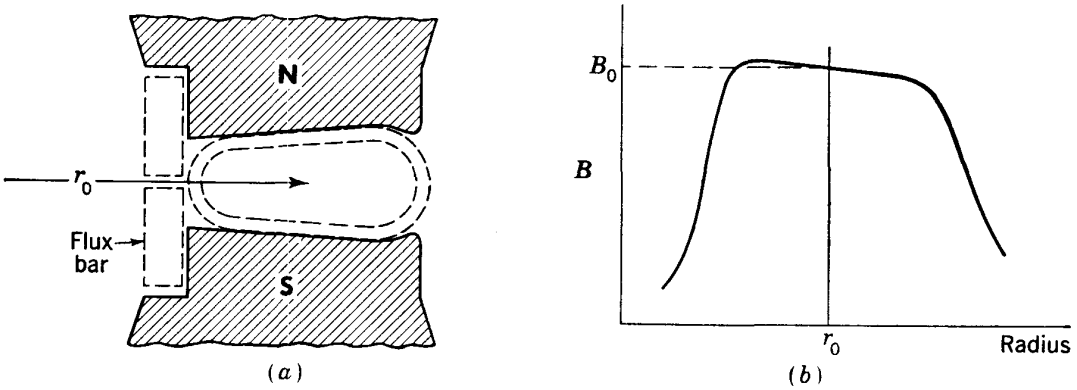

Fig. 12-5. (*a*) Sketch of pole face and vacuum chamber for the MIT synchrotron. (*b*) Plot of magnetic field across the pole face, showing a region of linear decrease with radius where $n = 0.75$.

The smaller machines use an external flux return path, since there is insufficient area within the orbit circle to accommodate the return legs. For larger machines, or for those with very small aperture and hence return circuits of small cross section, the flux return legs can be located inside the orbit. In this event the return flux threading the orbit is in the opposite direction to that required for betatron acceleration; specially

designed betatron flux bars carrying flux which parallels the orbit field are required to produce the betatron condition.

Another design problem is the contouring of the pole face to provide the radially decreasing field needed for focusing. A simple flat taper is usually sufficient to provide the desired n value of 0.6 or 0.7 over the central portion of the gap. However, the field is weakened at the edges because of fringing, similar to the effect at the periphery of cyclotron magnets (see Sec. 8-2). This can be partially compensated and the region of uniform-n field extended somewhat by adding shims or shaped protuberances on the pole faces near the edges. Such shaping is needed on both inner and outer pole edges.

The desired pole-face taper and the optimum shape of the edge shims are usually determined by model measurements. These measurements are made at the injection field, when oscillation amplitudes will be a maximum and the maximum aperture should be available. At higher field intensities the pole-edge shims saturate first, and the width of the useful region of magnetic field contracts. However, by this time oscillation amplitudes have been damped to smaller dimensions, so the narrowing of the uniform-n region is not a limiting factor. The maximum practical value of magnetic field is reached when the width of the useful field band becomes narrower than the space required by the beam. With the type of steel used for laminations, and for the density allowed in packing the laminations, this limit is about 12 kilogauss.

Eddy-current effects can be seriously disturbing, especially if they occur with an azimuthal variation. They cause the magnetic field in different portions of the gap to differ in time by small amounts. The magnetic field at any point can be considered as having a component in phase with the exciting current and another component 90° out of phase. At injection time, when the average field is very small, the out-of-phase component can become dominant. A radial variation of field such as is caused by eddy currents tends to change the n value. If there is an azimuthal variation in the eddy currents, the n value will also vary around the orbit.

Many laboratories have experienced difficulties due to eddy-current effects, and much time and effort have been required to find suitable corrections. Careful design is of first importance, particularly in making each lamination which carries guide flux have the same length and dimensions. Close packing of laminations at the orbit and elimination of gaps between laminations in which fringing fields can occur will reduce the risk of trouble. If variations still exist, they can be corrected by appropriately placed windings which carry small currents 90° out of phase with the magnet excitation current. Several laboratories have designed such correcting coils. Those used with the 300-Mev Cornell machine were arranged to correct for the first and second Fourier components of the

azimuthal field, with four controls to apply corrections proportional to sin θ, cos θ, sin 2θ, and cos 2θ.

Variations in the remanent magnetic field (the value at zero excitation) can occur for different portions of the iron in the magnet because of variations in the physical handling or the past magnetic history of the material. These differences can be quite significant at the low injection fields. Some experts advise a degaussing procedure for the blocks before assembly. Special care must be used in handling the blocks of laminations to prevent mechanical jars during assembly. Even when all possible precautions have been taken, the residual magnetism of structural steel in the foundations or in the building may induce an undesirable remanent field in the magnet after assembly. If the remanent field is nonuniform in azimuth, it can cause significant perturbations of the particle orbits. Such remanent fields can be corrected by dc currents in suitably located coils. Most designers try to keep the azimuthal variations below 1 part in 1000 at injection fields.

Another common magnetic fault is the displacement of the magnetic median plane from the geometric center plane of the gap. Since particle orbits follow the magnetic median plane, any displacement will shift the orbit plane. An azimuthal variation in the location of the median plane is even more disturbing, since it can feed energy into the vertical betatron oscillations. This type of fault is fairly common, since the sloping earth's field acts differently around the orbit. When such an anomaly is detected, it can be remedied by currents in correcting coils located appropriately.

12-5. MAGNET EXCITATION

Several methods are available for powering a synchrotron magnet. Alternating current can be obtained from the power lines or an ac generator to provide continuous full-wave excitation. However, the reactive current required for excitation is extremely large relative to the current needed to supply losses in the iron and copper. A simple arrangement for providing the large excitation current is to resonate the inductance of the magnet with a capacitor bank at the desired repetition frequency and to drive this resonant circuit and supply the losses from an ac generator at this frequency. This technique was used for the early synchrotrons and is still satisfactory for relatively small magnets. The limitation for the larger machines is the heat loss under continuous excitation, due to eddy currents in the iron and the resistance of the coil. Removal of the heat developed in the iron and copper because of these losses requires special cooling techniques, which are difficult to apply. The usual oil-immersion cooling used in transformers is impractical for the synchrotron magnet; air-blast cooling is noisy, bulky, and of much lower efficiency; no other

schemes of equivalent effectiveness have been developed. In the absence of practical designs for a high-capacity cooling system the only alternative has been to reduce heat losses by reduction of the duty cycle of operation. Most synchrotrons of the 300-Mev size or larger are pulse-powered, with a duty cycle chosen to keep the heat evolution within the capacity of the cooling system.

The requirement of pulse powering described above applies to the compact heavy magnets which use uniform n values and have relatively wide apertures and wide poles. The introduction of AG focusing (see Sec. 5-7 and Chap. 15) allows the use of much narrower apertures and smaller magnets. With such lightweight magnets it again becomes possible to use continuous full-wave excitation without exceeding the cooling capacity.

The power supply for a pulse-powering system uses capacitors to store energy for the magnet. The capacitance must be adequate to supply the full stored energy required for the magnet at maximum excitation. In operation, the capacitor is charged from a dc source and then discharged into the magnet. If one full cycle of oscillation is allowed per pulse, at the frequency determined by the inductance and capacitance in the series circuit, the capacitor will be returned to nearly its initial voltage. Between pulses the dc source supplies the system losses. It is also possible to operate on only one half-cycle per pulse. The average power consumption is only half that of full-cycle operation, but each pulse reverses the polarity of the capacitor voltage. In recharging the capacitor between pulses the capacitor polarity must be reversed by a mechanical or electronic switch. Grid-controlled rectifier tubes can be used to charge the capacitor or act as reversing switches.

In pulse operation it is customary to use ignitrons to control the capacitor discharge. A typical ignitron is the mercury-vapor GL-506, which will carry 2000 amp peak and withstand 20 kv peak inverse voltage. Such an ignitron can carry much higher currents than the rated value on low-duty-cycle pulsed operation, if properly protected by magnetic shielding from adjacent current-carrying bus bars (which might deflect the arc from the mercury pool to the wall of the tube with possibly damaging effects).

A typical pulse-powering system, for the MIT synchrotron, has a capacitor bank of 960 μf which resonates with the inductance of the magnet at a frequency of 45 cps. The total energy stored in the magnet or in the capacitors is 15,000 joules. The peak voltage applied to the capacitors is 15 kv, and the peak current 3,800 amp. The synchrotron operates at a pulse repetition frequency of two per second, limited by the power supply.

A simplified circuit diagram of the pulse-powering system for the MIT synchrotron is given in Fig. 12-6. The rectifier for charging the

capacitor bank is a full-wave, three-phase system using transformers and six rectifier tubes, delivering 15 kv. Four GL-506 ignitrons in parallel are used as switching tubes to connect the capacitor to the coil during the pulse and to disconnect at the end of the pulse.

Electrical problems in pulse-powered systems arise chiefly from transient voltage surges which occur during the switching and can lead to breakdown of tubes or other components. One serious transient occurs when the ignitrons first begin to conduct, applying voltage suddenly to the magnet terminals. This transient is associated with resonance of the stray capacitance of the magnet with the inductance of the leads from

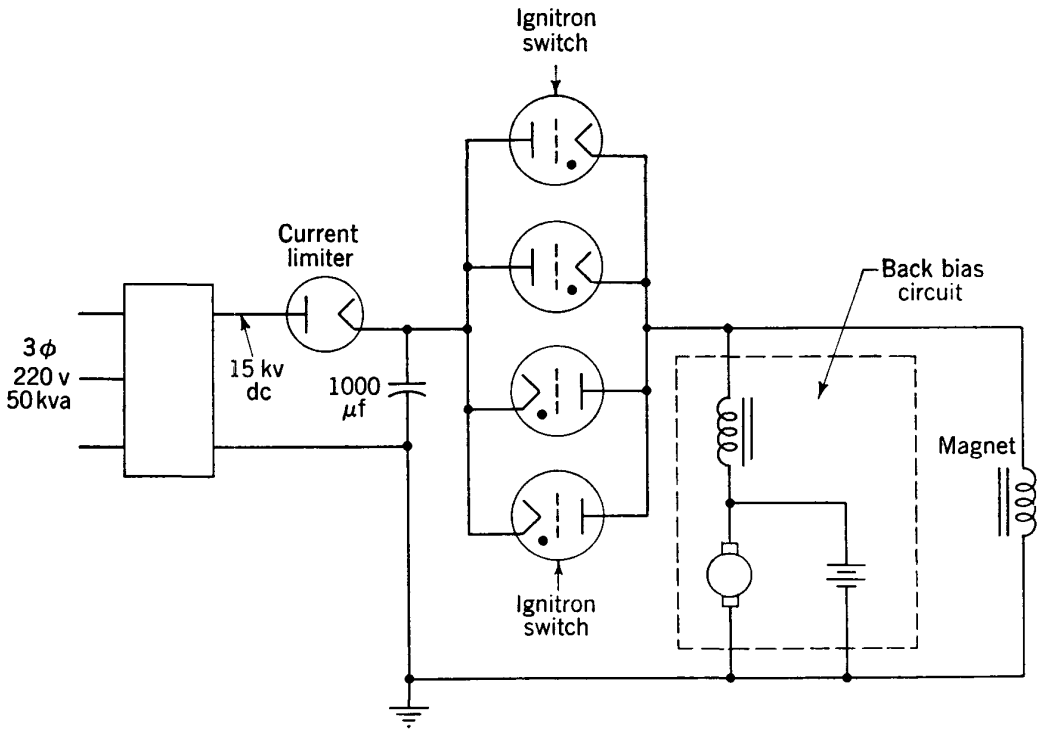

Fig. 12-6. Simplified circuit diagram for the pulse-powering system of the MIT synchrotron magnet.

the ignitrons and capacitor bank. It can be damped out by a series capacitor and resistor across the magnet terminals, in which the capacitor is several times the stray capacitance and the resistor is chosen to provide critical damping with the lead inductance. Another transient arises at the end of the conduction interval, when the inverse voltage builds up across the ignitrons. This transient is caused by resonance of the full inductance of the magnet with the stray capacitance of the leads. Again, it can be damped by a series resistance and capacitance, this time across the ignitrons.

The chief limitation of the system described above is its low repetition rate, which reduces the frequency of pulses for experimental work to an

undesirably low value. Operators are now convinced that a higher repetition rate is essential, even though it increases the power requirements and the cooling problems. Other installations have been powered for higher repetition rates, of up to 60 pulses/sec.

12-6. INJECTION

A betatron start is commonly used to accelerate electrons from their initial injection energy of less than 100 kev to 2 or 3 Mev energy at which they have a velocity of over $0.98c$ and so travel in an orbit of radius not significantly smaller than the geometric central orbit. This requires that the flux linking the orbit have a time rate of change proportional to the rate of change of the guide field flux at the orbit, following the betatron relation given by Eq. (12-5). The linkage flux is provided by flux bars on the inside of the orbit, attached to the poles of the guide field magnet. They are effective only during the early stage of acceleration while the guide field is still small, and for only a very short time interval, after which they become saturated and have no further effect. Since the guide field for 2- to 4-Mev electrons is low (<100 gauss in the example used in Sec. 9-12), while the flux density in the flux bars can approach saturation, the cross-sectional area of the flux bars needed to satisfy the betatron relation can be quite small. In order to obtain this high flux density in the bars, the air gap in the flux-bar circuit is made short relative to the gap between pole faces. So these flux bars are of negligible size compared with the heavy central core required in the betatron to provide acceleration to top energy.

One arrangement for installing flux bars on the magnet poles is illustrated in Fig. 12-7. This long flux bar is clamped in place with short spaces between the bar and the poles which can be adjusted to provide the correct total flux in the bars to satisfy the betatron condition, so the equilibrium orbit is at the center of the chamber. Another arrangement (see Fig. 12-5*a*) uses two short flux bars fastened against the inside edge of the pole with a short gap between the two bars on the central plane. This gap can likewise be adjusted, by loosening the clamping brackets and sliding the bars, to modify the reluctance of the circuit and vary the relative amount of flux in the bars.

Several authors have analyzed the betatron-flux condition and have shown how to compute the dimensions and properties of the flux bars. Goward[18] discussed the requirements from the point of view of providing adequate flux for betatron acceleration, but made simplifying assumptions regarding the transition from betatron to synchrotron operation. Wilkins[19] discussed the magnetic aspects of flux-bar design, including a more thorough analysis of the transition problem. He described the use of flux-biasing techniques to adjust the location of orbit radius in the

betatron phase and to provide a more efficient transition to the synchronous phase.

The rate of rise of flux density in the flux bars is much higher than in the iron of the magnet, so eddy currents are also greater. During the first few microseconds of the betatron phase such eddy currents have the effect of reducing the effective permeability of the bars. During this same interval the guide-field flux in the magnet depends almost solely on the pole-gap reluctance and is not much affected by eddy currents in the poles. So the betatron-flux condition is disturbed during the time

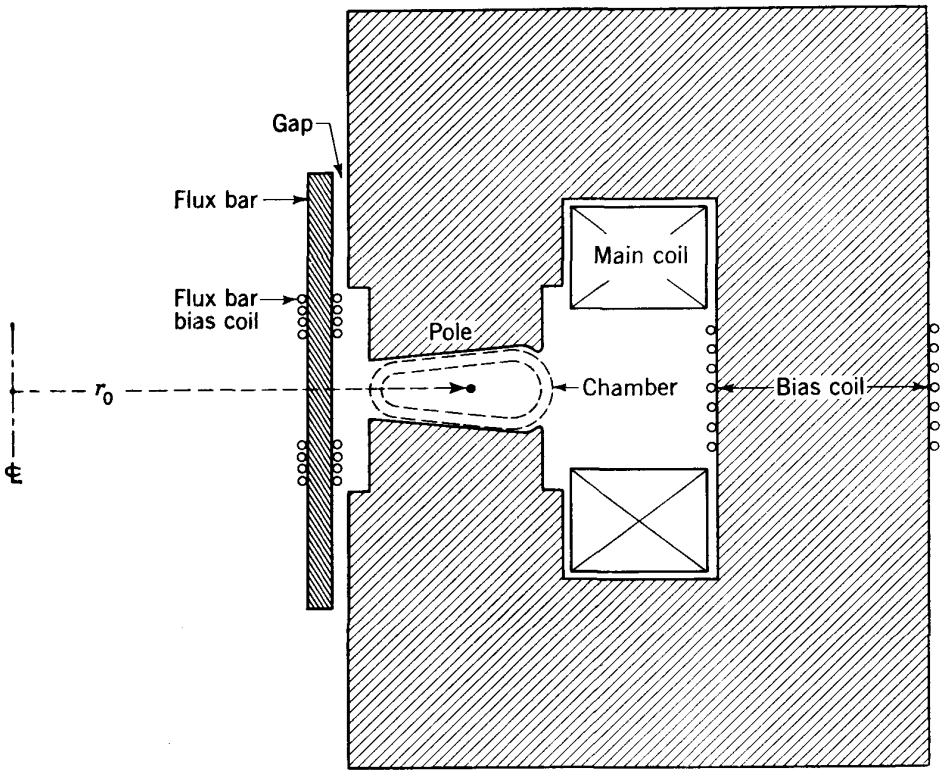

Fig. 12-7. One method of installing flux bars on the inside of the orbit of a synchrotron used for initial acceleration during the betatron start.

required for eddy-current equilibrium to be reached; this can delay the time when orbit stability becomes established beyond the normal time for injection. The difficulty can be avoided by applying a suitable negative bias to the main magnetic field, so there is adequate time for the eddy currents in the bars to reach equilibrium before the guide field reaches the injection value. A special winding of a few turns can be used for this purpose. Or direct current can be applied to the main magnet windings, using a suitable series inductor or choke in the dc leads to eliminate induced voltage surges in the dc source.

The high rate of rise of field in the flux bars requires that these bars be

formed of extremely thin laminations in order to reduce the eddy-current time lag. In some installations stacks of laminations are cemented together to form solid bars for ease in clamping and mechanical adjustment. Thin foils of high-permeability material such as permalloy can be used to reduce the dimensions of the flux bars. Another possibility is to use blocks of ferrite, which has a very high resistivity and so reduces eddy-current effects. The properties of ferrite as applied to the radio-frequency system of the cosmotron are discussed in some detail in Chap. 13. The disadvantage of ferrite is that it has a lower saturation limit than iron laminations and the dimensions must be correspondingly larger.

Another problem to be considered in designing flux bars is their effect on the guide field. If they are located too close to the main gap, they may shield the guide-field flux crossing the chamber and produce local areas of weak field. A further consideration is the mechanical mounting arrangement for the flux bars on the inside of the orbit. In this location they can obstruct access to the vacuum chamber. Simple mechanical mountings which can readily be removed for maintenance are quite important.

Several physical and electrical adjustments are available to control the betatron flux during the acceleration interval. Flux-bar cross section can be changed if needed; gap spacing in the flux-bar circuit can be adjusted; dc bias can be applied to either the main magnet or the flux bars to regulate the injection time phase and the rate of rise of flux in the bars. The significant times are at the start and at the transition to synchrotron drive. Experience with betatrons is directly applicable in obtaining maximum capture efficiency at the start. A problem unique to synchrotrons, however, is the transition to synchronous drive. This will be discussed in the section to follow.

The electron gun used for injection into the synchrotron is similar to those used in betatrons. The basic design is illustrated in Fig. 7-15. The function of the gun is to inject a very intense beam (several amperes) of electrons confined in a narrow cone and at high energy (50 to 100 kev). It is also essential that the gun have a narrow radial dimension, to improve the chance of electrons missing the back of the gun on subsequent revolutions. This requires small radial spacings and limits the voltage which can be applied to the gun. In order to focus the electrons into a narrow cone a third electrode, located between the cathode and the outer jacket which serves as an anode, is used as a control electrode. The outer jacket is normally grounded, so the cathode must be maintained at high negative potential. The focusing electrode is usually a rectangular plate with a rectangular slot, approximately the size of the cathode, located close to the cathode and having a potential applied which is positive by a few kilovolts relative to the cathode. A sequence of experimental modi-

fications has resulted in a standard gun design which produces a beam having an angular spread of 5 to 10° under operating conditions.

At the MIT laboratory Stone[20] has developed a special cathode formed of sintered molybdenum-thoria which is cut from a hollow cylinder of $\frac{5}{8}$ in. inner diameter. The sliver is about $\frac{3}{8}$ in. long and $\frac{1}{16}$ in. wide, mounted with the concave side of the cylinder facing the direction of emission. This shape seems to improve the focus to some extent over the usual tungsten spiral cathode and provides a copious current of several amperes. When installed in a conventional gun with a control electrode and an anode potential of 80 kv, it projects a beam with half the total emission concentrated within $\pm 2°$ of the axis.

The radial location of the electron gun is quite critical. It is usually mounted on an adjustable stem to allow this position to be determined experimentally. The normal position is with the leading edge of the gun located at the outer periphery of the uniform-n field where the n value is approximately unity.

Experience with betatrons shows that the intensity accepted into stable orbits increases with injection voltage, varying approximately with $V^{1.5}$. However, because of the narrow radial spacings required and technical limitations on insulation, the maximum practical voltage on such an electron source is found to be between 80 and 100 kv.

The rather wide angle of emission from the gun means that a large fraction of the beam is outside the limits of stability of the radially tapered field and is not accepted into stable orbits. This unfocused portion of the beam strikes the wall of the chamber within the first turn. One consequence is that static charges can be accumulated on the inner wall of the chamber, which would distort the electric fields and reduce intensity of the captured beam. So the inner surface of the chamber is coated with a grounded conducting layer to prevent the accumulation of charge. This layer must be sufficiently thin to prevent the development of eddy currents which would distort the magnetic field. A resistivity of about 100 ohms per square has been found satisfactory.

Accepted beam intensity is determined by the fraction of the injected beam contained within the narrow cone which is focused and set into stable oscillations about the equilibrium orbit in the radially decreasing magnetic field. It is further limited by the fraction which misses the back of the injector gun on subsequent revolutions, until such time as the damping of amplitudes due to the increasing field removes the beam from this obstruction.

Several mechanisms are involved in the injection process, which have been analyzed in Sec. 7-8 in their application to the betatron. Kerst[21] first pointed out the effect of self-contraction due to the injected electron beam. The electron-beam current is in a direction to oppose the increasing magnetic flux in the flux core (or the flux bars in the synchrotron). It reduces the induced voltage below that required to satisfy the betatron

relation so the electrons acquire too small an amount of energy per turn and their orbits contract, allowing them to miss the gun. The unfocused beam intensity which strikes the walls in the first turn thus serves a useful purpose in providing a large self-contraction effect. Further advantage of this mechanism is taken by pulsing large currents in contractor coils during the injection interval; such coils are located on the pole faces above and below the beam-orbit location in the chamber.

A second mechanism proposed by Kerst is the space-charge self-repulsion of the beam. Space charge in the beam gives forces opposite in direction to the normal guide-field restoring forces. This reduction in the effective restoring forces tends to decrease both the radial and vertical free-oscillation frequencies. At injection, when space-charge density is greatest, the band of oscillation amplitudes is determined by aperture dimensions. Then, as space charge is removed by losses to the walls and to the back of the electron gun, the free-oscillation frequencies increase and their amplitudes decrease. This is equivalent to a forced damping of the betatron oscillations, and the reduction in amplitude allows a considerable fraction of the beam to miss the injector gun.

Other methods have been proposed to improve acceptance. Davis and Langmuir[22] suggested a mechanism for producing a resonant distortion of the equilibrium orbit away from the injector by means of coils which are pulsed during the period of injection, to distort the azimuthal uniformity of the magnetic field. Resonance with the radial oscillations is possible when $n = 0.75$, and this value has been adopted by the group at the General Electric Company Research Laboratory[24] to increase intensity in their air-cored synchrotron.

For very large accelerators, where the voltage gained per revolution is a significant fraction of the injection voltage, the rate of contraction of the instantaneous orbits toward the equilibrium (betatron) orbit is also large. If the deviation of the instantaneous orbit is Δr, the contraction per turn δ is given by $\frac{\delta}{\Delta r} = \frac{\Delta E}{2E}$, where ΔE is the energy gain per turn. This may provide sufficient damping in a few turns to give a large increase in acceptance. Whenever possible, then, the magnitude of ΔE should be made large by using techniques which maximize the rate of rise of flux in the flux bars.

Although many of these techniques are empirical, a sufficient body of experience is now available, in both betatron and synchrotron operations, to provide useful suggestions. Adequate intensities have been obtained in most synchrotron laboratories.

12-7. RADIOFREQUENCY ACCELERATION

The accelerating system in a synchrotron is usually a quarter-wave resonant cavity, resonant at the electron orbital frequency determined by

orbit radius as given in Eq. (12-2), and driven by a radiofrequency oscillator-amplifier. It is located between magnet poles and forms an arc extending part way around the orbit. If cavity wavelength were the same as in vacuum, it would extend around one quadrant of the circumference. However, it can be made physically shorter by loading it with material of high dielectric constant which has adequately low losses at the applied frequency. A practical method of forming the resonator is to make it a section of the vacuum chamber, with the same aperture and dimensions. The electrodes are plated surfaces on the inside and outside of the sector, joined electrically at the node end and with an insulated gap at the open end of the quarter-wave cavity across which the rf voltage is developed. Particles which traverse this gap are accelerated by different amounts depending on the phase of the rf field at the instant.

Ceramics are available having dielectric constants of up to 80, which can be slip-cast into the structural shape needed for the vacuum chamber. Glass and fused silica have also been used. In most cases a sector of the material chosen for the vacuum chamber itself is adapted to be the resonant cavity. The voltages required are modest, and the electric fields in the body of the material are not excessive. So heating due to the rf fields has not been a serious problem for materials with reasonably low rf loss factors. One of the best materials from this point of view is fused silica,[5] which can be blown or cast in the proper shapes, has excellent mechanical properties so walls can be kept thin, and has a dielectric constant of 4. Wavelength is reduced by the square root of the dielectric constant, so the length of a quarter-wave resonator is half a quadrant or 45° in arc.

A good description of a fused-silica resonator used in the Berkeley synchrotron has been published.[25] An important technique in its construction is the application of the conducting coating to inner and outer surfaces. The surfaces were first etched with hydrofluoric acid to remove the glaze and were thoroughly cleaned. Then Liquid Bright platinum was painted on and fired in a furnace, in two or three successive coats. This surface was then sufficiently conducting to allow a copper electroplated surface of about 0.003 in. thickness to be applied.

The plated surfaces of the cavity are scribed longitudinally with closely spaced parallel cuts to insulate against eddy currents, which otherwise would be developed in the conducting surfaces and which might distort the magnetic field in this sector. When these cuts are approximately parallel to the direction of the rf currents, they have a negligible effect on the resonant efficiency or rf resistance of the cavity. The highest electric fields are developed across the short insulating gap at the open end of the quarter-wave line. It has been found useful in some laboratories to terminate the coating in small rounded electrodes which

cover the sharp edges of the gap. Use of such electrodes increased the breakdown voltage by as much as a factor of 3 at MIT.

The rf amplifier or oscillator is coupled to the resonant cavity by capacitative coupling near the rf node of the quarter-wave line. A sketch of the 50-megacycle resonator developed for the 330-Mev synchrotron at the Massachusetts Institute of Technology[20] is shown in Fig. 12-8.

The radiofrequency oscillator used to excite the cavity can be located at some distance from the magnet, with power transmitted through coaxial cable matched to the impedance of the cavity. The MIT oscillator operates at 46.5 megacycles and uses a WL530 triode as a power tube in a class-C self-excited oscillator circuit. With an input power of 7 kw, a peak voltage of 3.5 kv is developed across the gap at the open end of the resonator. Several other tubes have been equally satisfactory, such as the Eimac 3X2500A3 or the 7C24. In general, the radiofrequency

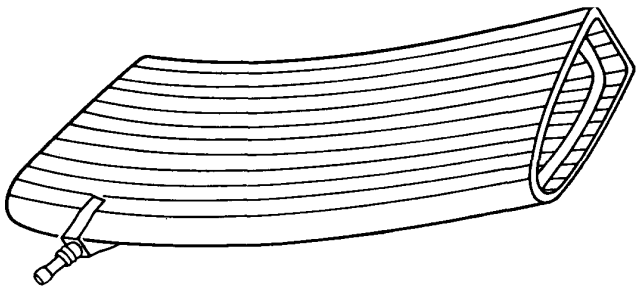

Fig. 12-8. Quarter-wave resonant cavity used for the rf accelerator in the MIT synchrotron. The cavity forms one sector of the vacuum chamber.

problems of the synchrotron have been minor and have been easily solved.

In such a radiofrequency system the quarter-wave resonator, the transmission line from the oscillator tube, and the tube with its associated circuit components form a single resonant circuit. The length of the transmission line must be adjusted to give the proper phase; one standard procedure is to make this line electrically one half-wavelength long. A schematic diagram of the Berkeley oscillator circuit[25] (Fig. 12-9) illustrates the physical arrangements and also shows the several supplementary circuits for suppressing parasitic oscillations, for supplying the triggering pulse to start the oscillator, and for "tickling" the circuit with an auxiliary oscillator which helps to initiate oscillations and reduce the "jitter" or uncertainty in the starting time. The oscillator is pulsed for about 8 msec, which is sufficient to overlap the acceleration interval. The pulse is initiated at an adjustable instant in time determined by the magnet excitation cycle, representing the end of the betatron acceleration period. It is terminated as soon as acceleration is completed. In the Berkeley machine this pulse length represents a duty cycle of one-twentieth at the repetition rate of 6 pulses/sec.

The resonant efficiency or Q of the resonant-cavity circuit is of the

order of 500, largely determined by the losses in the dielectric core of the cavity and in the iron pole faces of the magnet. In a high-Q system the radiofrequency voltage build-up time will be of the order of Q cycles. So when the rf oscillator is turned on, it takes a time of about 10 μsec to reach full voltage. During this build-up time the energy acquired from betatron acceleration is decreasing. An analysis of the phase relations during this transition by Kaiser[26] shows that the initial phase at which the electron crosses the accelerating gap is not so critical in determining whether the particle will be accepted in a stable synchronous orbit as would be inferred from the simple theory of phase acceptance described

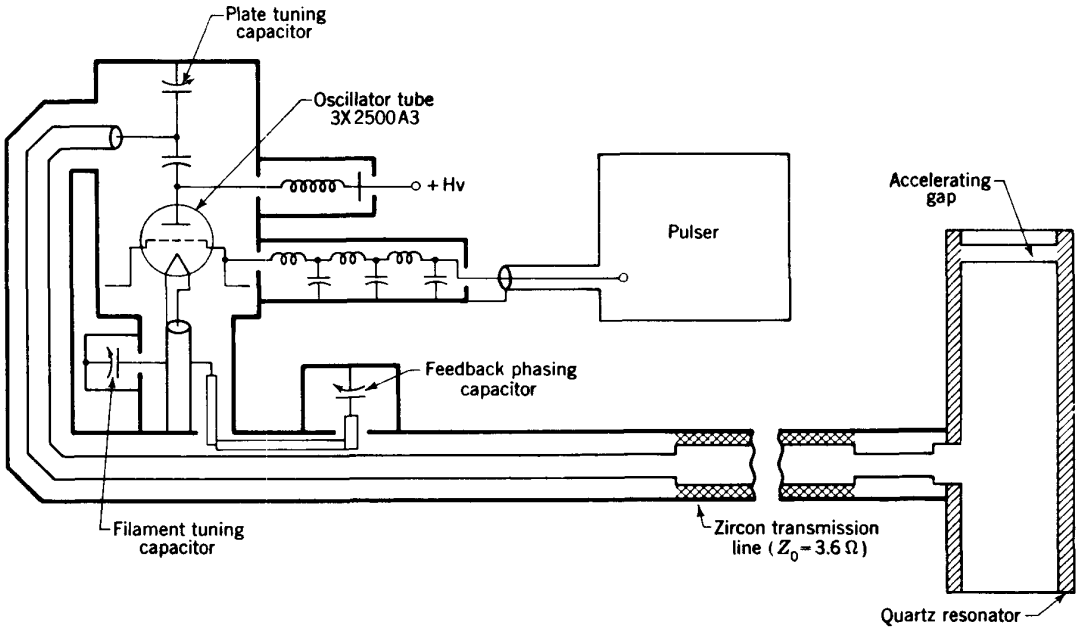

Fig. 12-9. Schematic circuit diagram of the rf oscillator for the Berkeley synchrotron.[25]

earlier. Rather, the critical parameter is the phase velocity, that is, the difference between the angular frequency of the particle and the angular frequency of the oscillator. Since the angular frequency of the particle at this time depends primarily on the orbit radius, in a machine of small aperture the spread in phase velocities can be kept small.

From the analysis described above, Kaiser verified previous predictions[9] that essentially all the uniformly distributed electrons in the orbit would be accepted into stable synchronous orbits, with the long build-up time expected from a high-Q resonator. This is in contrast to the simple theory of acceptance given by Bohm and Foldy,[7] Goward,[18] and others in which it was assumed that the transition between betatron and synchrotron drive was instantaneous. Kaiser and Tuck[27] tested this theory of electron capture in their 14-Mev synchrotron by turning off the rf accelerating voltage for a period long enough to allow the electrons to become

uniformly distributed in phase. Then, when the rf oscillator was again turned on, all the electrons were recaptured except those whose phase velocities were too great, as predicted.

DePackh and Birnbaum[28] have also studied the capture process, considering all possible initial phases and phase velocities at the transition between betatron and synchrotron phases. They find that a moderately slow increase of the rf voltage from zero to its final value will minimize oscillation amplitudes, and that an asymptotic approach to the final value is an advantage. With synchrotron chambers of relatively small aperture it is now generally agreed that the capture efficiency can approach 100 per cent by using such long rf build-up times.

During the early stages of operation of the University of California synchrotron a half-wave drift tube or C electrode was used as a resonator. By analogy with the D in a cyclotron in which the resonant particles experience two accelerations per turn, on entering and on leaving the D, a C-shaped electrode in the synchrotron extending around half the orbit will also provide two accelerations. It can be considered to be a half-wave resonant circuit. This type of electrode was originally built and installed in the Berkeley machine, formed as a hollow laminated tube supported in a concentric position inside the vacuum chamber by several short stub lines through the walls. The length was somewhat shorter than 180° in arc, and somewhat higher potentials were applied to compensate. The chief problem was the mechanical difficulty of supporting such a long hollow structure weakened by the longitudinal laminations. With the development of the quarter-wave cavity resonator, which involves fewer technical problems, the original C electrode was replaced. But in principle any electrode system which provides a phased radiofrequency voltage of proper magnitude and frequency would be satisfactory.

12-8. VACUUM CHAMBER

The vacuum chambers used in the electron synchrotron are doughnut-shaped rings of ceramic, glass, or quartz. For the smaller machines (up to 70 Mev) they can be cast in single units. A photograph of such a single-unit cast ceramic chamber has been used by the General Electric Company in its advertisements (Fig. 12-10*a*).

In the large machines the chamber is made up of segments cemented or clamped together with sealing gaskets. A description of the University of California chamber has been published,[25] including a photograph of one sector (Fig. 12-10*b*). It consists of eight 45° sectors of fused silica, assembled in the form of a toroid with an elliptical cross section of $3\frac{1}{2}$ by $6\frac{1}{4}$ in. and a wall thickness of $\frac{5}{16}$ in. The sectors are joined and vacuum-sealed by covering the eight joints with wide rubber

bands and using Lubriseal grease to ensure a good seal. Sector ends were separated and insulated by thin Teflon gaskets. A conducting coating on the inside was obtained by painting with Du Pont No. 4817 air-drying silver; this coating was grounded through a network of eight 1000-ohm resistors to avoid the accumulation of static charge. Such a resistor network is needed to allow the betatron accelerating voltage to develop

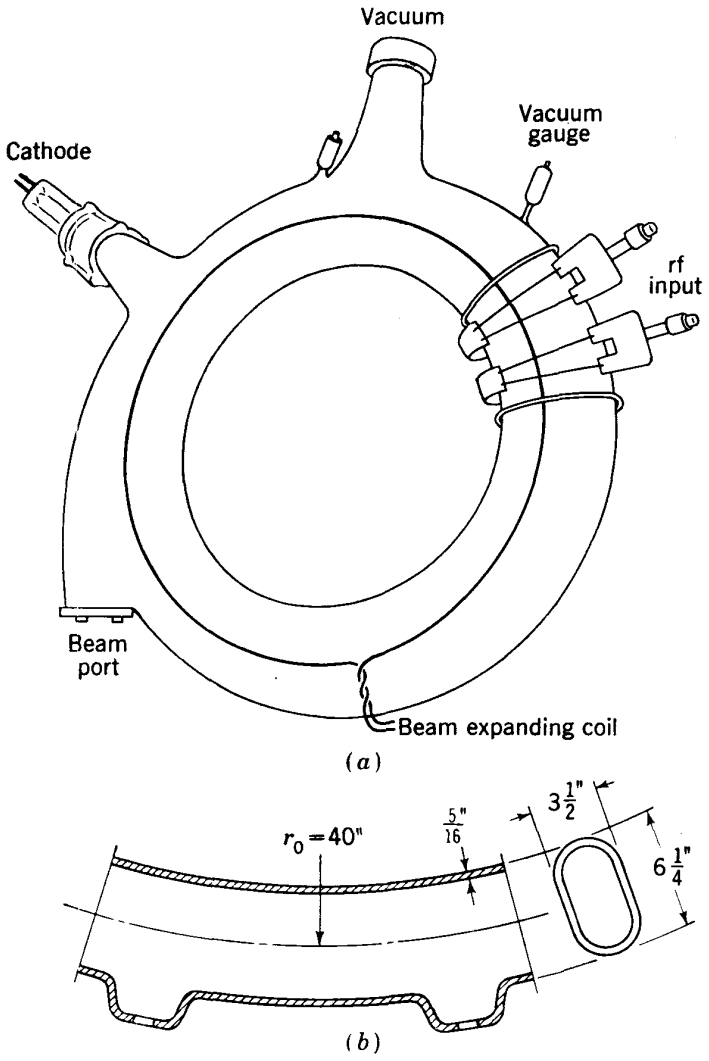

Fig. 12-10. (*a*) Cast ceramic vacuum chamber for the GE 70-Mev synchrotron.[5] (*b*) Sector of fused-silica vacuum chamber for the Berkeley 320-Mev synchrotron.[20]

between sectors. One of the sectors was specially plated and scribed to form the quarter-wave resonator for radiofrequency acceleration.

An operating pressure of better than 10^{-5} mm Hg is required to prevent loss of beam through gas scattering. Vacuum-pumping speeds are not large for this small chamber, and straightforward vacuum techniques are satisfactory. The pump used in a typical 300-Mev installation is a

6-in. oil-diffusion pump with an efficient refrigerated baffle cooled to −40°C.

12-9. FREQUENCY-MODULATED START

In a few installations the designers have chosen to avoid some of the difficulties and possible loss of intensity in the betatron start by injecting a prefocused beam of electrons from a low-voltage dc generator directly into the synchronous acceleration phase of operation. In one synchrotron a Cockcroft-Walton machine of 400 kv is used; in another the source is an electrostatic generator producing 1-Mev electrons. The well-collimated beam is directed toward the orbit at a shallow angle and is "inflected" into the orbit by an auxiliary dc electric field maintained between two curved plates. The inflector is located at the outer edge of the aperture, near the position where $n = 1$. If the energy is less than the 2 to 4 Mev at which electrons attain relativistic velocities, their orbital frequency at the desired orbit radius r_0 is lower than the constant frequency which they attain at higher energies. In order to provide synchronous acceleration at constant radius during this early phase, the frequency of the rf cavity must be modulated to match the orbital frequency.

Crane[12,29] at the University of Michigan was the original proponent of this technique. In his synchrotron the magnet is separated into four quadrant sectors spaced by straight field-free sections, one of which is used for installation of a large resonant cavity which can be frequency-modulated; another is used for the inflecting system for the beam from the external source. This has been called a "racetrack" orbit.

Several methods are available for producing the necessary frequency modulation. The accelerating-cavity unit can be broadly resonant, having a low Q, and can be driven at the desired frequency by a power amplifier which is controlled to follow the chosen cycle. The power requirement for such a system is undesirably large. Another method would be to have a mechanically modulated resonant cavity of high Q, for which power needs would be small. However, a mechanically tuned system which uses a variable capacitor or inductor has an inherent lack of flexibility in modifying the frequency cycle, and the precision of timing at the start of the cycle is poor. A more efficient technique, adequate for a rather small range of frequencies, is to use electronic modulation of a high-Q resonant-cavity resonator.

Crane used a resonant cavity in which part of the capacitance of the circuit was a symmetrically arranged circle of barium titanate capacitors. This material has the property of having its dielectric constant vary with the magnitude of the impressed electric field. The capacitors were arranged so that a dc bias field could be applied across the barium

titanate, and this dc field varied through a time cycle to control the capacitance and change the resonant frequency of the circuit.

Although the frequency-modulated start does avoid some of the difficulties associated with betatron operation, it introduces other difficulties. Injection of a narrow well-focused beam reduces the amount of space charge and eliminates the large loss of beam to the walls in the first turn, which is characteristic of injection from an electron gun. However, it is not clear that this is an advantage, since high beam intensities and space-charge effects seem to be useful in contracting orbits in betatron operation. The narrow inflected beam must also miss the back of the inflector plates on subsequent revolutions. The mismatch of free-oscillation frequencies with the orbital frequency at $0 < n < 1$ allows the electrons to make several turns before they again approach maximum outward radial amplitude at the azimuth of the inflector. During this time the increasing magnetic field will contract the equilibrium orbit radius and damp the oscillations. With careful adjustment, these effects are sufficient to allow a large fraction of the beam to miss the inflector and to be captured in stable orbits. Since injection continues for a time interval representing many turns, the beam is uniformly distributed in azimuth. Only about half these electrons have a phase relative to the rf phase which will allow them to be captured in stable synchronous orbits, as discussed in earlier sections.

As a consequence of the several limitations, beam intensity from the frequency-modulated synchrotron is lower than that normally obtained with a betatron start. Furthermore, the difficulties in the electrical problems of frequency modulation are significant. As a result, the method has not been widely used.

At Cornell University[15] the magnet for the 1.2-Bev synchrotron is of the AG type, with the return leg of the C on the inside of the orbit and with a very compact arrangement of iron and coils. There is not sufficient space on the inside of the orbit for flux bars, so betatron preacceleration is not used. Rather, a 1-Mev electrostatic generator was used to supply a focused beam of electrons, which were injected into the synchronous phase of acceleration. The frequency modulation required for a start at 1 Mev is only 6 per cent, and it was supplied by a separate radio-frequency cavity tunable over this range. The tunable power source was operated for only a short time at the start of each pulse; then the main rf constant-frequency cavity was turned on and provided acceleration to top energy. In 1961 the electrostatic generator was replaced by a 10-Mev linear accelerator, removing the need for frequency modulation. Beam intensities were greatly increased, reaching a level where radiation damage to the glass chamber became a serious hazard.

It seems probable that future development of higher-energy synchrotrons will tend toward the use of strong-focusing magnets and small

apertures and that injection energy will be increased to 3 Mev or higher, at which frequency modulation is unnecessary.

12-10. RADIATION LOSS

Since the electrons in the synchrotron experience a continuous central acceleration, they must radiate energy, in accordance with the classical theory. This effect has been discussed in Chap. 7 relative to the betatron and in Sec. 9-8, where the theoretical equations were presented. The total energy lost because of radiation increases with the fourth power of the electron energy, for fixed orbit radius, following Eq. (7-18). This electromagnetic radiation extends from very long wavelengths through the optical spectrum and into the ultraviolet and soft X-ray region. The peak for 300-Mev electrons in an orbit of 1 m radius occurs at about 70 A, or in the ultraviolet. In the visible region this radiation becomes noticeable, as a reddish light, at about 60 Mev. The peak is in the center of the visible spectrum for an energy of about 200 Mev and is observed as a brilliant white light.

The direction of propagation is normal to the acceleration vector, which is radial, and so the light is emitted in the forward or tangential direction in a narrow cone. With a transparent chamber wall it can be observed by eye when looking directly at the oncoming electrons. However, this radiation is highly dangerous to the eyes and should be observed only with mirrors. During a synchronous pulse it appears as a short flash when the electrons attain sufficient energy; frequently this spot appears as a line with a radial spread due to orbit contraction as the beam moves across the chamber.

The energy loss per turn due to radiation, for electrons in a 1-m orbit, is about 150 ev at 200 Mev and 800 ev at 300 Mev. If plotted on a time axis the loss is a sharply increasing spike occurring near the end of the acceleration interval. For this radius of curvature the energy loss is small compared with the applied rf accelerating voltage. When the particles lose energy, they tend to shift to a smaller orbit radius; this causes a change in phase of crossing the accelerating gap; the phase shift increases the amount of acceleration; so the particles remain in synchronism and at the synchronous orbit radius. This feature of the synchrotron, of providing automatic compensation for radiation loss, is one of the most attractive characteristics of the machine.

It would seem that this rapid increase of radiation loss with energy would set a practical limit to the size and energy which could be obtained with an electron synchrotron. Such a limit will depend on the volts per turn supplied by the radiofrequency accelerating system. For the type of machine described in this chapter, using a single accelerating cavity and limited by the breakdown of dielectric in the cavity, the practical limit to

energy would appear to be about 2 Bev. However, modern designs are utilizing field-free straight sections in the particle orbit, in which highly resonant cavities with vacuum insulation can be mounted. It is also possible to use two or more cavities, driven in phase. So the volts per turn can be increased by a large factor if desired, and the energy limit can be pushed much higher. In Sec. 15-9 is described a design for an AG synchrotron which uses 16 cavities each producing 500 kv; with this emphasis on the radiofrequency system, it is possible to design for 6 Bev, and higher. The limit in this case seems to be an economic one, when the cost of the rf component becomes excessive relative to other components of the machine.

12-11. TARGETS AND BEAMS

The simplest method of utilizing the synchrotron beam is to deflect it against a target at the edge of the chamber at the end of the acceleration interval, to produce a beam of high-energy X rays. The X rays are caused by deceleration of the electrons in the target and have the typical bremsstrahlung spectrum with a maximum energy equal to that of the electron beam, but with the intensity distributed over lower-energy quanta. The spectrum computed for 330-Mev electrons[30] is illustrated in Fig. 12-11. When a solid target is used, or if the X-ray beam must penetrate the chamber wall to emerge, the low-energy portion of the spectrum is absorbed and a peak is observed which shifts to higher energy with increased absorber.

The angular spread of the X-ray beam is small, with a half-angle in the forward direction which includes all but $1/e$ of the intensity given by

$$\theta_{1/2} = k\left(\frac{W_0}{W}\right)\ln\frac{W}{W_0} \tag{12-6}$$

where $k = 0.65 \pm 0.15$ over a wide range of electron energy, photon energy, and target material. The detailed variation of k is given in a paper by Stearns.[30] When evaluated for an electron energy of 330 Mev, the half-angle defined above is found to be less than 0.4°. Experimental measurements confirm these calculations and show that the X-ray beam emerges in a very narrow forward cone.

When the electrons approach maximum energy, they can be made to strike a target at either the inner or outer edge of the chamber. One simple method is to turn off the rf voltage while magnetic field is still rising. The beam spirals in to smaller radii, owing to both the increase in field and the energy loss by radiation, and will strike a target located on the inner wall. It might be noted here that the final maximum energy is lower for this smaller final orbit radius than if the beam were expanded outward against a target on the outer periphery.

Another method, which brings the beam outward, is to excite the magnet past saturation so the shape of the field exceeds the stable limit of $n = 1$ and radial oscillations become unstable. As radial amplitudes increase, the electrons usually strike first on the back surface of the injector gun, which serves as a target.

The duration of the beam pulse on the target can be varied over a wide range. Some experiments require a very short pulse, and others a long one. The normal rate of contraction per turn when rf voltage is turned

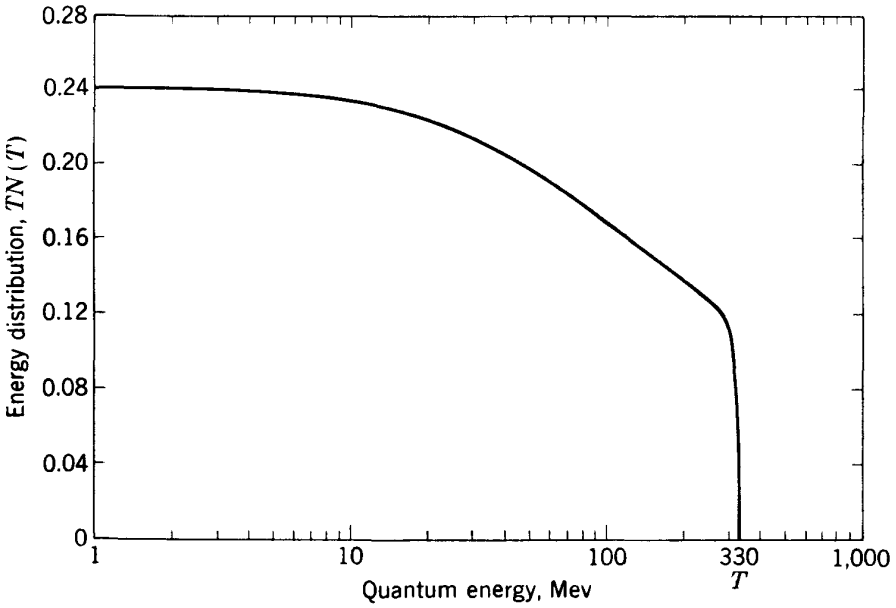

Fig. 12-11. Calculated bremsstrahlung spectrum from electrons of 330 Mev incident normally on a Pt target 0.02 in. thick.[30]

off rapidly is quite small. This rate of contraction has been variously estimated in different machines to be less than 0.001 in. per turn by the time it strikes the target. So only the extreme inner tip of the target is struck by the electrons. A time which is equivalent to many turns is required for all the electrons to be cleaned up against the target. Under normal conditions the resultant X-ray pulse lasts about 10 μsec.

Pulses of shorter duration can be obtained by setting up radial beam oscillations. The synchrotron group at the Massachusetts Institute of Technology[31] first proposed the use of a "figure 8" coil, wound in opposite directions about the two halves of the magnet, which has the effect of increasing field in one half and decreasing it in the other. A switch shorting this coil is timed to follow closely the turn-off of the rf voltage, before the beam has contracted into the target. If the n value is maintained at 0.75, the frequency of radial oscillations is

$$f_r = (1 - n)^{1/2} f_0 = 0.50 f_0$$

and the electrons traverse two revolutions in one radial-oscillation cycle. Weakening the magnetic field on one half of the orbit and strengthening it on the other induces a rapid increase in amplitude.

Ejection by induced oscillations can be accomplished with a variety of systems for inducing the oscillations. It is not necessary that the distortion of the field be symmetrical, but smaller exciting coils can be used. Davis[23] proposed the use of a transient pulse in a coil around a small arc. This is illustrated in Fig. 12-12, which portrays schematically the particle paths during the last few revolutions, showing how the beam can be made to strike a target. At Berkeley, a coil around one-eighth of the pole face

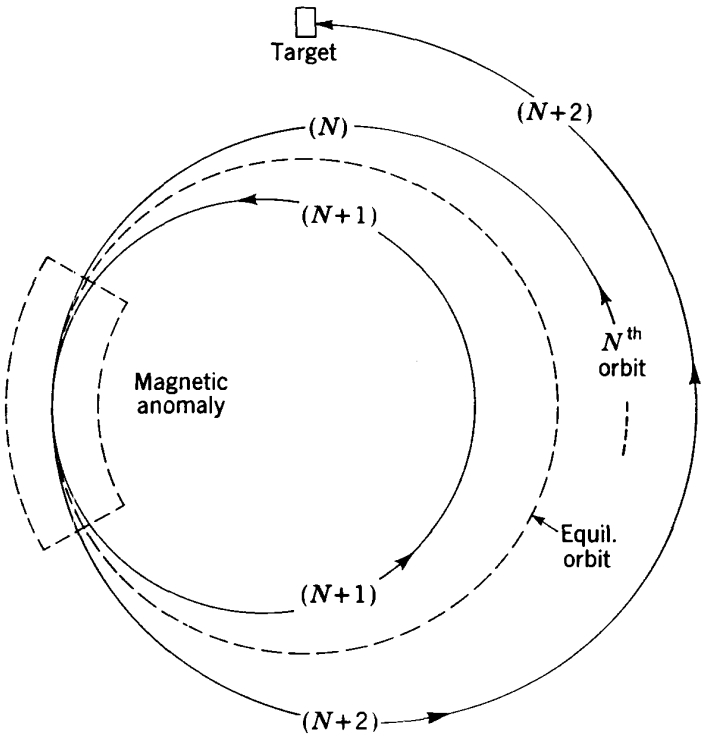

Fig. 12-12. Radial oscillations about the equilibrium orbit induced by a magnetic anomaly at one point in the orbit, useful in expanding the beam against a target.

gave a considerably increased output from the target. At Iowa State College[32] coils supported by the vacuum chamber are pulsed to change the n value over different portions of the orbit. Several of these methods have been successful in obtaining output X-ray pulses as short as 0.1 to 0.2 μsec, representing less than 10 revolutions of the electrons.

Long pulses can be obtained by decreasing rf voltage gradually. Electrons having the largest phase oscillations are first lost from synchronous stability and strike the target; others are kept in resonance until the rf voltage drops below the equilibrium value. This method has been used to stretch the target pulse length to over 2500 μsec. Such a long pulse is

frequently desirable when electronic coincidence instruments are used for measurement, in order to increase the time extent of the beam and the duration of observation.

It is also possible to eject a beam of electrons from a synchrotron, although not much use had been made of such an emergent beam up to 1961. The techniques described above for producing radial oscillations can bring a beam out to the edge of the magnetic field. The injector gun should be on the inside of the orbit, if an external emergent beam is to be obtained. The emergent beam is concentrated in a fairly narrow cone and can be brought through a tangential evacuated tube to a thin window. It is also possible to use the magnetic peeler (see Chap. 7), used for the betatron, to deflect the electron beam further and to obtain a more collimated beam.

12-12. X-RAY BEAM INTENSITY

The X rays produced by the synchrotron have much higher energy than those normally used for medical or industrial purposes, for which measuring instruments have been highly developed. At a peak energy of several hundred Mev the processes of energy loss are quite different, so different instruments are required. At these energies electron showers are produced, similar to those observed in cosmic rays. Shower production is the cumulative effect of electron-pair formation and bremsstrahlung radiation by the electrons. The phenomenon of pair formation is well understood theoretically, and the cross section can be computed with some precision. The problem of intensity measurement involves knowledge of the bremsstrahlung spectrum and the integration of the pair-production process over this wavelength spectrum.

The pair-production and bremsstrahlung calculations and calibration of the X-ray beam intensity have been done at Berkeley by Blocker, Kenny, and Panofsky.[33] Thin ionization chambers are used, behind absorbers or converters of different atomic number Z, in which the electron density N_e is known. The ionization due to Compton-effect electrons is a function only of N_e and can be subtracted to find the pair-production effect. By measuring the ionization behind converters of widely different Z and comparing with the theoretical cross section for pair production, the intensity in terms of number of quanta per unit area per unit time (the flux) can be determined. Detailed equations are given, as well as tables of averaged pair-production cross sections for bremsstrahlung of different energies and for absorbers of different Z.

A cruder method of measuring intensity, also described by the Berkeley group,[33] is to use the mean energy loss of an electron per unit path in an absorber of known Z, as a function of absorber thickness. Thin ioniza-

tion chambers are located at varying positions in the absorber, and the total intensity decrease is observed. Reasonably good data exist on the mean energy loss as a function of maximum energy for shower electrons. So the observed ionization absorption coefficient can be used to obtain a value for beam intensity. However, this method does not distinguish between X-ray and electron intensity in the beam.

Occasionally it has been desirable to express intensity in terms of the roentgen (r) familiar in radiation-therapy measurements. This unit is defined in terms of the ionization in air produced by a beam of photons in equilibrium with its secondary electrons. At normal X-ray energies equilibrium cannot be established in an air-filled chamber, so the practice has been to resort to "air-wall" ionization chambers. It is even more difficult to obtain equilibrium at 300 Mev, so the number of electrons associated with the X-ray beam is quite uncertain. It is for this reason that the pair-production intensity calibration is used, which is independent of the electron "contamination" of the X-ray beam. However, in order to have a practical standard of comparison, McMillan, Blocker, and Kenny[34] have proposed a standardized roentgen measurement for synchrotrons, using a Victoreen thimble chamber inside a lead cylinder of $\frac{1}{8}$ in. wall thickness, located transverse to the beam at a considerable distance. Table 12-2 gives the calibrations for the Berkeley synchrotron at two energies, expressed in units of ergs/(cm^2)(r), Mev/(cm^2)(r), and in "effective quanta," defined as the energy flux divided by the maximum energy, which is proposed as a more meaningful unit for high-energy radiation (see Sec. 14-4).

TABLE 12-2
VICTOREEN THIMBLE-CHAMBER CALIBRATION FOR BERKELEY SYNCHROTRON
(In $\frac{1}{8}$ in. Pb)

X-ray energy, Mev	Ergs/(cm^2)(r)	Mev/(cm^2)(r)	Effective quanta/(cm^2)(r)
320	5.3×10^3	3.3×10^9	1.04×10^7
160	3.5×10^3	2.2×10^9	1.38×10^7

The average output of the Berkeley synchrotron[34] with the above definitions for intensity is 1,000 r/min at 1 m. This is at full energy and with a pulse rate of six per second. This can be compared with the output of the Illinois 320-Mev betatron, which is 14,000 r/min at 1 m. The higher intensities from the betatron are a result of the higher repetition rate, larger aperture, and higher input beam intensity, obtained at considerably higher cost. There is reason to believe that synchrotrons can be designed and developed to give equivalent intensities if such higher intensities are found to be worth the increased cost.

12-13. IRONLESS SYNCHROTRONS

The magnetic fields required to deflect and focus electrons can be produced by air-cored coils, without the use of iron. Several proposals for such a machine have been published, such as that by Kaiser and Tuck.[35] The individual primarily responsible for the development of such machines is J. L. Lawson of the General Electric Company Research Laboratory.[24] Lawson's synchrotron, designed for 300-Mev electrons, has undergone a long period of development and is now in operation for research. It is difficult to assess the relative merits of this kind of machine. It does have some advantages, such as the absence of eddy-current distortions in the magnetic field and freedom from the flux-density limits set by the permeability of iron. However, it also has several disadvantages, of which the primary one is the distortion of field caused by the extremely large forces on the current-carrying conductors which produce the magnetic field. Since one of the opportunities of an air-cored magnet is the possibility of using very high magnetic fields, in order to reduce orbit dimensions, the currents in these conductors are very large. Furthermore, energy dissipation is a problem, since for practical reasons it is desirable to have the conductors located within the vacuum envelope. Practical limitations seem to restrict the size to about 500 Mev, and it is possible that the most economical range is around 100 Mev.

REFERENCES

1. E. M. McMillan, *Phys. Rev.*, **68**:143 (1945).
2. V. Veksler, *J. Phys. (U.S.S.R)*, **9**:153 (1945).
3. E. M. McMillan, *Phys. Rev.*, **68**:144 (1945).
4. F. K. Goward and D. E. Barnes, *Nature*, **158**:413 (1946).
5. F. R. Elder, A. M. Gurewitsch, R. V. Langmuir, and H. C. Pollock, *J. Appl. Phys.*, **18**:810 (1947).
6. D. M. Dennison and T. Berlin, *Phys. Rev.*, **70**:58 (1946).
7. D. Bohm and L. Foldy, *Phys. Rev.*, **70**:249 (1946).
8. N. H. Frank, *Phys. Rev.*, **70**:177 (1946).
9. J. P. Blewett, *Phys. Rev.*, **70**:798 (1946).
10. Cornell University Laboratory of Nuclear Studies, *Synchrotron Progress Report* (Nov. 1, 1949).
11. I. A. Getting, J. S. Clark, J. E. Thomas, Jr., and I. G. Swope, *Phys. Rev.*, **79**:208A (1950); *Engineer*, Apr. 6, 1951, p. 440.
12. H. R. Crane, *Phys. Rev.*, **69**:542 (1946).
13. J. P. Blewett, *J. Appl. Phys.*, **18**:976 (1947).
14. W. B. Jones, H. R. Kratz, J. L. Lawson, D. H. Miller, R. D. Miller, G. L. Ragan, J. Rouvina, and H. G. Voorhies, *Rev. Sci. Instr.*, **26**:809 (1955).
15. "The Cornell Bev Synchrotron," Cornell University, Floyd Newman Laboratory of Nuclear Studies (December, 1956).

16. D. M. Dennison and T. Berlin, *Phys. Rev.*, **69**:542 (1946).
17. N. M. Blachman and E. D. Courant, *Rev. Sci. Instr.*, **20**:596 (1949).
18. F. K. Goward, *Proc. Phys. Soc. (London)*, **62A**:617 (1949).
19. J. J. Wilkins, *Phil. Mag.*, **41**:34 (1950).
20. J. E. Thomas, Synchrotrons, *Ann. Rev. Nuclear Sci.* (1952).
21. D. W. Kerst, *Phys. Rev.*, **74**:503 (1948).
22. L. Davis and R. V. Langmuir, *Phys. Rev.*, **75**:1457 (1949).
23. L. Davis, *Rev. Sci. Instr.*, **21**:971 (1950).
24. W. B. Jones, H. R. Kratz, J. L. Lawson, G. L. Ragan, and H. G. Voorhies, *Phys. Rev.*, **78**:60 (1950).
25. M. H. Dazey, J. V. Franck, A. C. Helmholz, C. S. Nunan, and J. M. Peterson, *Rev. Sci. Instr.*, **21**:436 (1950).
26. T. R. Kaiser, *Proc. Phys. Soc. (London)*, **63A**:52 (1950).
27. T. R. Kaiser and J. L. Tuck, *Proc. Phys. Soc. (London)*, **63A**:67 (1950).
28. D. C. DePackh and M. Birnbaum, *Rev. Sci. Instr.*, **21**:451 (1950).
29. H. R. Crane, *Phys. Rev.*, **70**:800 (1946).
30. M. Stearns, *Phys. Rev.*, **76**:836 (1949).
31. J. S. Clark, I. A. Getting, and J. E. Thomas, Jr., *Phys. Rev.*, **70**:562 (1946).
32. C. L. Hammer and A. J. Bureau, *Rev. Sci. Instr.*, **26**:594 (1955).
33. W. Blocker, R. W. Kenny, and W. K. H. Panofsky, *Phys. Rev.*, **79**:419 (1950).
34. E. M. McMillan, W. Blocker, and R. W. Kenny, *Phys. Rev.*, **81**:455 (1951).
35. T. R. Kaiser and J. L. Tuck, *Nature*, **162**:616 (1948).

At the head of the facing page is a photograph of the cosmotron at the Brookhaven National Laboratory, before shielding was installed.

13

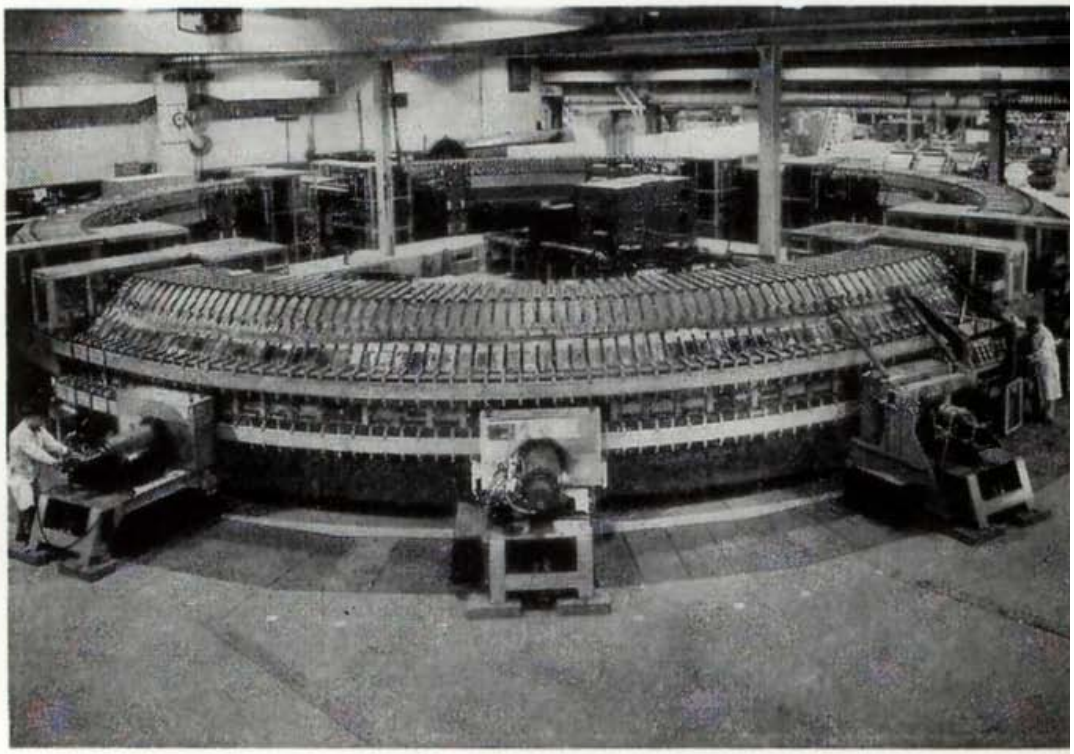

The Proton Synchrotron

The proton synchrotron is the culmination of the phase-stable accelerators and yields the highest energies yet achieved. By 1961 four proton synchrotrons were operating in the energy range between 3 and 10 Bev, and three more were under construction. It represents the ultimate development of the accelerator art, involving such complicated techniques that all the skills of mechanical and electrical engineering are taxed to provide the wide variety of complex components and to assure that they function as a unit. Advanced techniques of theoretical computation are required in design, and the electronic computer has become an essential tool.

The AG modification is the most recent development, which has resulted in the production of energies of over 30 Bev. In this form the proton synchrotron has no foreseeable limitation in energy except the practical considerations of size and cost. Although the AG proton synchrotron utilizes the same principle of acceleration, the unusually large step upward in energy and the unique physical characteristics of the AG synchrotron justify a separate category; it is described in some detail in Chap. 15.

In this chapter we limit the discussion to the original concept of the proton synchrotron utilizing the low, constant magnetic gradients which are just sufficient to produce orbit stability. As the first multi-Bev accelerators, they opened up the new research field of particle physics.

Costs of accelerators in the Bev energy range are outside the limits of university budgets. Essentially all proton synchrotrons have been built with funds supplied by the governments of the countries concerned. Nevertheless, the cost efficiency in terms of the beam energy achieved per dollar of construction cost is better than for earlier types of accelerators. Costs are 2 million dollars per Bev, or 0.2 cent per volt.

For the first time there are available in the laboratory particle energies larger than the rest mass of nucleons (0.938 Bev) or of the heaviest of the "strange" particles which have been observed in cosmic-ray studies. Cosmic-ray processes can be studied under controlled conditions with directed and focused beams having intensities millions of times higher than are available in nature. The processes of meson formation and the properties of the several types of mesons can be studied at energies extending well into the cosmic-ray region. Basic forces between nucleons and mesons are directly measurable. The scientific results obtained with the new multi-Bev accelerators have been impressive. Essentially all types of strange and unstable particles observed in cosmic-ray studies have been produced in the laboratory, and many new ones have been observed and identified. At the Brookhaven laboratory the cosmotron was used to produce and study the neutral Λ^0 particle, which is heavier than a nucleon and which decays into a nucleon and a meson. The bevatron at the University of California produced antiprotons and antineutrons for the first time, created directly from energy. The Nobel Prize in physics for 1959 was awarded to Drs. Emilio Segrè and Owen Chamberlain for the discovery of the antiproton. The search for more knowledge and new phenomena goes on. Scientists are having an exciting time in the early years of research with these great accelerators.

13-1. THE MULTI-BEV ACCELERATOR

Magnetic accelerators for electrons, such as the betatron and the constant-gradient synchrotron, have been shown to have practical energy limits because of the rapid onset of radiation losses by the orbiting electrons. As we have seen, this energy loss varies with $(W/W_0)^3$, a very steeply rising function, and the practical limit is reached when the radiation loss per turn approaches the maximum practical voltage per turn. However, protons have a much larger rest mass, and the equivalent limit for protons will not be reached until much higher energies are attempted, of the order of 10,000 Bev.

The synchrocyclotron, which has been so successful as a proton accelerator in the 100- to 700-Mev range, requires a solid-core magnet. At relativistic energies magnet weights and costs increase roughly with the cube of a magnet dimension such as pole-face diameter; power cost also increases with the volume of the magnetic field between poles, or with at least the square of a pole dimension. If the synchrocyclotron were to be

enlarged to produce protons of several Bev energy, the magnet would become exorbitant in weight and cost. The obvious method of reducing magnet cost is to use a ring magnet covering only a narrow annular band. Such a fixed orbit radius requires the synchrotron principle of acceleration, using a pulsed magnetic field. With a ring magnet the cost is very much smaller for the same particle energy, although it still increases with the cube of the radius if aperture dimensions are assumed to increase proportionally.

The only alternative principle of acceleration known is that of linear acceleration. The present stage of development is described in Chap. 10. Although plans are progressing for higher energies, practical experience with proton linacs is still (1961) in the range below 70 Mev; many problems must be solved to extend the proton linac into the multi-Bev range. Much higher energies have been obtained with electron linacs. The nominal advantage of a linear accelerator is that construction and power costs should be approximately proportional to energy. However, under present conditions the circular magnetic accelerators appear to be more economical and more practical for the multi-Bev energy range.

Qualitative reasoning such as the above suggests that, to attain energies of several Bev, it is preferable to use a ring magnet to reduce magnet cost and to operate on the principle of synchronous acceleration at constant radius. This extension of the principle was appreciated by machine designers in several laboratories. Several groups independently calculated the basic requirements and developed designs for proton synchrotrons.

The principle of operation is basically the same as for the electron synchrotron. A fixed orbit radius is chosen, and a ring-shaped magnet produces a magnetic field normal to the doughnut-shaped vacuum chamber enclosing the orbit. The magnetic field increases with time as the protons gain energy, to maintain constant orbit radius. Ions are injected into the orbit at low energy when the magnetic field is small, and energy is supplied by an accelerating electric field applied across a gap at one or more points in the orbit. But unlike electrons which approach the velocity of light at relatively low energies ($v = 0.98c$ at 2 Mev) and so have an essentially constant frequency of revolution during acceleration to higher energies, protons do not reach the equivalent limit until they have acquired about 4 Bev energy; so the velocity and the frequency of revolution increase during the entire acceleration interval. The applied electric field must synchronize with the changing orbital frequency of the particle, requiring frequency modulation over a wide range during acceleration, determined by the ion frequencies of revolution at injection and at maximum energy. This feature introduces new and complicated technical problems in the design of the accelerating electrodes and of the high-frequency oscillator.

The same type of phase focusing exists to bunch the particles about an

equilibrium phase of the accelerating field as for the electron synchrotron, and if the applied frequency is correct, the protons maintain a constant average orbit radius. But an error in frequency could cause the particles to gain energy at a rate not compatible with the increasing magnetic field and to spiral inward or outward, where they would be lost against the walls of the chamber. The required schedule of frequency modulation does not follow any simple law, but depends on the rate of increase of magnetic field, which is itself a function of the constants of the power supply and the properties of the magnet iron. So new problems of frequency control are encountered, which are unique to the proton synchrotron.

On the other hand, the design of proton synchrotrons is based upon a considerable body of experience acquired in the development of synchrocyclotrons and electron synchrotrons. Some of the techniques are directly applicable and can be expanded to accommodate the larger physical dimensions. An adequate theoretical analysis of the motions of particles is available to guide designers, checked by experience in earlier synchronous accelerators. Designers can anticipate many problems and compute quite precisely the magnitude of fields, the necessary uniformity, the effect of inhomogeneities, etc. Because of the larger investment much effort has been applied to model tests and engineering development. Commercial engineering firms, with their wide experience and large facilities, have been attracted by the challenge and by the opportunity to develop new and specialized equipment; they have supplied their best engineers for advice and assistance in the design of the major components. So the physical problems of design and construction have not been so formidable as might have been expected from the size of the machines.

13-2. HISTORICAL DEVELOPMENT

The first proposal of a proton accelerator using a ring magnet, in which both magnetic field and frequency of the accelerating electric field are varied, was made in 1943 by Prof. M. L. Oliphant of the University of Birmingham, England, to the British Directorate of Atomic Energy. Because of wartime security restrictions the proposal was not published at that time. It is reported in a detailed design study by Oliphant, Gooden, and Hide,[1] published in 1947 and accompanied by a theoretical analysis of orbit stability by Gooden, Jensen, and Symonds.[2] It will be noted that Oliphant's original proposal antedates the discovery of phase stability by two years. At the time of the first proposal there was no assurance that the principle was sound or technically practical. Perhaps, had it not been for the distractions of wartime work in Great Britain, analysis of this proposal might have revealed the principle of phase stability two years earlier.

An accelerator for protons following these designs was built at the University of Birmingham, and it has been in operation at 1.0 Bev since 1953. Professor Oliphant's return to his native Australia and the untimely death of Dr. Gooden, the chief scientist on the project, slowed progress toward completion of this machine, which was the first proton synchrotron to be started. This early start resulted in freezing the basic magnet design and starting construction before other components had been analyzed and designed in detail, and also before certain improved design concepts were developed in the United States. As a result the Birmingham machine lacks some of the advantageous features of the later machines and operates at rather low intensity. Despite the early difficulties and the small number of staff engaged, it has been brought into satisfactory operation for research.

Meanwhile the principle of phase stability in synchronous accelerators was announced independently in 1945 by McMillan[3] at the University of California and by Veksler[4] in the U.S.S.R. Both papers describe two techniques for synchronous acceleration, which have been described in earlier chapters. The use of frequency modulation of the applied accelerating electric field led to the development of the synchrocyclotron. The concept of constant frequency and constant orbit radius with an increasing magnetic field has been applied to the electron synchrotron. Both papers also include implicitly the possibility of acceleration of protons in a synchrotron by also varying the frequency of the accelerating field, but neither paper was primarily concerned with this more complicated application of the principle. By this combination of techniques the limitations of the two simpler machines are side-stepped and a new range of energies has been made available.

Design studies for proton synchrotrons in the United States started early in 1947 in two laboratories supported by the United States Atomic Energy Commission. Dr. W. M. Brobeck,[5] of the University of California Radiation Laboratory, made a preliminary report of a possible design for 10-Bev protons in 1948, which was primarily a study of the practicability of a pulsed power supply for the large ring magnet required. The name bevatron was given to this *b*illion-*e*lectron-*v*olt accelerator.

At the same time, preliminary designs for a similar accelerator were started at the Brookhaven National Laboratory under the direction of the senior author, on leave from the Massachusetts Institute of Technology, as chairman of the Accelerator Project. The stimulus for this development came from Prof. I. I. Rabi of Columbia University. The early Brookhaven plans were reported in papers by Livingston[6] and others before the American Physical Society in 1948. As the design approached completion, a description was published by M. S. Livingston, J. P. Blewett, G. K. Green, and L. J. Haworth[7] in January, 1950. This machine was soon given the laboratory name of cosmotron.

Both the Berkeley Radiation Laboratory and Brookhaven were

encouraged in these design studies by the AEC officials responsible for research and development of instruments. When preliminary designs and cost estimates became available in 1948, a decision was made by representatives of the two laboratories and of the AEC for the construction of two machines, a 2.5- to 3.0-Bev cosmotron at Brookhaven and a 5- to 6-Bev bevatron at the University of California. In both laboratories teams of scientists and engineers were assembled to complete designs and proceed with construction. Many of the members of these teams have contributed importantly to the designs, and the results are the product of the joint efforts of a large number of individuals.

The Brookhaven cosmotron was the first proton synchrotron to be completed (in May, 1952), and it was rapidly tuned up to 2.3 Bev, the maximum energy possible with the available power supply. A period of engineering consolidation and "bug-picking" brought it back into operation at the date of the dedication ceremonies on December 15, 1952. A year of research at this energy allowed the completion of the power supply. Operation at the maximum design energy of 3.0 Bev with a beam intensity of 2×10^{10} protons/pulse repeated at 5-sec intervals was announced in early 1954.

During the period of design and construction some of the progress was recorded in publications. R. Q. Twiss and N. H. Frank[8] of MIT made a theoretical study of orbital stability in the proton synchrotron, taking design parameters compatible with those being considered at Brookhaven. Some of the components have been described in a sequence of abstracts of papers presented to the American Physical Society[9] by members of the team. N. M. Blachman and E. D. Courant[10] analyzed the gas-scattering problem; A. I. Pressman and J. P. Blewett[11] described the electrically tuned variable-frequency oscillator. An over-all description of the accelerator by Livingston, Blewett, Green, and Haworth[7] has been mentioned earlier. Finally, after completion of the machine the entire staff collaborated in presenting a complete description of all components of the operating machine, which occupies a full issue of *The Review of Scientific Instruments*, edited by M. H. Blewett.[12]

At the University of California the designers of the bevatron chose to build first a working quarter-scale model to determine requirements for the full-scale machine. With this model they demonstrated the resonance principle and showed that the structure formed of four magnet quadrants and four straight sections did not disturb the stability of the orbits. Particle oscillation amplitudes were measured in the model, but the results were inconclusive (found later to be due to magnetic inhomogeneities and alignment errors). As a consequence the design proceeded with alternative pole-tip arrangements: a large-aperture design which would allow a maximum energy of 3.5 Bev, and a smaller aperture capable of reaching 6.4 Bev. This question was resolved by the report

of the initial performance of the Brookhaven machine, which showed that the smaller aperture was adequate. Accordingly, plans were quickly modified to use the small-aperture, high-energy arrangement. Initial operation at about 5 Bev at low intensity was reported in early 1954. Further development resulted in reaching full-power operation at 5.7 Bev in October, 1954, with a beam intensity of about 1×10^{10} protons/pulse repeated 11 times per minute. Maximum energy operation at 6.4 Bev is possible at a slower cycling rate. Since that date the research staff of the Berkeley laboratory has been engaged in a broad research program utilizing this high-energy beam.

Publications by the Berkeley group have been largely through laboratory memorandums and AEC progress reports, which have had a limited, although unclassified, distribution. Papers before the American Physical Society[13] have described the quarter-scale model and some of the components and include in the author list the major contributors to the design of the machine. Lofgren[14] published a brief description of the design parameters and the performance of the model in 1950. The most recent and inclusive survey is an internal laboratory report in 1957 by Brobeck.[15]

During the late 1950s several other proton synchrotrons were built, patterned to a large extent on the cosmotron or the bevatron. The largest is the 10-Bev synchrophasotron of the U.S.S.R. Joint Institute for Nuclear Research at Dubna (near Moscow), which was completed and reached its design energy in 1957. Difficulties with the magnet correcting systems and with the injector held beam intensity to low values in early operations; these difficulties appear to be solved, and the machine is now (1961) in active use for research. This machine is, for the most part, a scaled-up version of the bevatron. It is described in numerous papers in the Russian technical literature which can be traced through the papers of Veksler and others in the U.S.S.R. *Journal of Nuclear Energy*[16] and in the CERN (Geneva) symposium proceedings of 1956.[17]

Three machines are based on cosmotron design and experience. A 3-Bev proton synchrotron nicknamed "Saturne" was completed in 1958 at the Saclay laboratory of the French Commissariat a l'Énergie Atomique.[18] At Princeton University (collaborating with the University of Pennsylvania) a small-aperture rapid-cycling machine for 3 Bev energy and high beam intensity is nearing completion (1961), under the direction of M. G. White, G. K. O'Neill, and F. C. Shoemaker. At the Rutherford Laboratory at the British Atomic Energy Research Establishment at Harwell, a machine modeled on the cosmotron but scaled up to an energy of 7 Bev is under construction, directed by T. G. Pickavance.

At the Argonne Laboratory of the AEC near Chicago a proton synchrotron for 12.5 Bev energy of a somewhat different type is under construction. It is a "zero-gradient synchrotron" (ZGS) which uses a magnet of the bevatron type but with a uniform field in the magnet

proper; focusing is obtained by shaping the end faces of the eight magnet sectors to give the same effect as though a field gradient of $n = 0.6$ had been included (cf. Sec. 5-6). The magnet structure is of the poleless type with minimum-size aperture and will operate at fields up to 21.5 kilogauss. Because of the compact design the magnet weight is considerably smaller than for the bevatron-type magnet. The project was initiated by a group under J. J. Livingood and is now under the direction of A. V. Crewe. It is scheduled for completion in 1962.

The most unusual machine under construction is at the Australia National University under the leadership of M. L. Oliphant. This is to use an air-cored magnetic field in four quadrants, with fields of up to 80 kilogauss produced in a shaped coil structure which does not have an iron core. The coils are to be excited by a massive homopolar generator which can store a great amount of rotational energy but will operate at a very slow repetition rate of about one pulse every 10 minutes. Many challenging engineering problems are involved, in such features as the brushes to handle the extremely large currents and the structures for supporting the large magnetic forces on the coils. The injector will be an 8-Mev cyclotron placed inside the circular coils.

In Table 13-1 are collected some of the parameters of the nine proton synchrotrons operating or under construction in 1961, which use conventional constant-gradient magnetic focusing.

Some general reviews other than those already mentioned describe the design and applications of proton synchrotrons. Blewett[19] has written a survey article for the 1956 *Reports on Progress in Physics*, and Green and Courant[20] have authored a review article in the 1959 *Handbuch der Physik*. The CERN (Geneva) Symposium on High Energy Accelerators[17] in 1956 included many papers devoted to the technical design of proton synchrotrons, along with other accelerator types, which were published in the proceedings of the symposium. Another conference on high-energy accelerators and instrumentation was sponsored by the CERN laboratory in Geneva in September, 1959, and included brief papers on the construction status and special features of several machines; these papers are published in the conference report.[21] The latest conference in this series on accelerators was held at Brookhaven in 1961; its proceedings are scheduled for publication early in 1962.

In the following sections the problems of development of the special components of a proton synchrotron will be illustrated by a rather detailed presentation of the Brookhaven cosmotron. This emphasis recognizes the much closer association of the writers with the design and development of the cosmotron than with other proton synchrotrons. It is not intended to slight the design virtues of other machines, and the authors ask indulgence for this somewhat unbalanced presentation. In partial justification it can be argued that the cosmotron was the first proton

TABLE 13-1
PARAMETERS OF CONVENTIONAL PROTON SYNCHROTRONS

	In operation, 1961					Under construction			
Location	Birmingham, U.K.	Brookhaven, U.S.A.	Saclay, France	Berkeley, U.S.A.	Dubna, U.S.S.R.	Princeton, U.S.A.	Harwell, U.K.	Argonne, U.S.A.	Canberra, Australia
Accelerator nickname	.....	Cosmotron	Saturne	Bevatron	Synchro-phaso-tron	P.P.A.*	Nimrod	ZGS	
Maximum energy, Bev	1.0	3.0	2.5	6.4	10	3.0	7.0	12.5	10.6
Mean orbit radius, m	4.5	10.7	11	18.2	30.5	12.2	23.6	27.4	6.4
Number of magnet sectors	1	4	4	4	4	16	8	8	4
Peak magnetic field, kg	12.6	13.8	15	16	13	13.8	14	21.5	80
Magnet weight, tons	810	1,650	1,080	10,000	35,000	350	7,000	4,000	0
Aperture:									
Width, cm	50	91	60	122	150	18	91	81	22
Height, cm	21	22	10	30	40	7	24	15	22
Pulse rate, pulses/min	6	12	19	10	5	1,140	28	15	0.1
Injector	t.r.†	e.a.‡	e.a.‡	Linac	Linac	e.a.‡	Linac	Linac	Cyclotron
Injection energy, Mev	0.46	3.7	3.6	9.8	9	3.0	15	50	8
Number of accelerating stations	1	1	1	1	2	4	1	2	1
Harmonic order	1	1	2	1	1	8	4	8	1
Date of completion	1953	1952	1958	1954	1957	1962	1962	1962	1962–1963

* Princeton-Pennsylvania Accelerator.
† transformer-rectifier set.
‡ electrostatic accelerator.

synchrotron to be completed, has had a reasonably successful record of operations, and is thoroughly documented in the literature.

The discussion in this chapter is also confined to the conventional machine using constant-gradient magnetic fields. Although such magnets are large and costly compared with the more recently developed AG magnets, they have served their basic purpose well and illustrate all the essential properties of the proton synchrotron.

13-3. BASIC PARAMETERS

The largest and most costly component of a proton synchrotron is its magnet; to a considerable degree the choice of magnet parameters determines the characteristics of the other components. Consequently, the first step in design is a decision on magnet dimensions and properties. The designer's choice is based on minimizing the cost and complexity for a given value of BR, which is a measure of particle energy. Magnets for proton synchrotrons cover a wide range in their design features, which will be discussed further in a following section. This range includes a spread in orbit fields from 14 to over 21 kilogauss and wide variations in the structural shape of the magnetic circuit.

In the cosmotron, which was among the first to be started, the design involved the use of parallel bundles of iron laminations arranged in a radial array around a circle, leaving wedge-shaped spaces between bundles at the orbit. The magnetic circuit has a C-shaped cross section, so the vacuum chamber between poles is accessible around the entire outer periphery. With this arrangement the maximum magnetic field at the orbit, up to the point where saturation effects become significant, is about 14 kilogauss. At the other extreme, the magnet for the Argonne machine uses a very compact design of poles and coils, with iron return circuits both inside and outside the orbit. Maximum fields of over 21 kilogauss can be used; this results in a minimum orbit radius for the chosen energy. But the structure severely restricts accessibility to the vacuum chamber and may prove to have objectionable limitations in research operations.

The choice of magnet structure and maximum field determines the orbit radius for a chosen particle energy. The relativistic relation between particle kinetic energy T, magnetic field B, and orbit radius R is given [see Eq. (5-49)] by

$$T(T + 2W_0) = c^2e^2B^2R^2 \tag{13-1}$$

When T and W_0 are expressed in Bev units and B is in webers/m^2 (units of 10,000 gauss), the radius is given by

$$R = \frac{3.33[T(T + 2W_0)]^{1/2}}{B} \quad \text{meters} \tag{13-1a}$$

In the cosmotron, with a chosen proton energy of 3.0 Bev and with a maximum field of 14 kilogauss, the required orbit radius is 9.10 m. The mean orbit radius taken as the basic dimensional parameter was 30.0 ft (9.15 m).

The choice of orbit aperture depends primarily on the estimated amplitudes of the several types of particle oscillations at and shortly following injection. This problem will be discussed in more detail in Sec. 13-6, Injection. The choice also depends on the space allocated for the top and bottom walls of the vacuum chamber, and so on the structural design of the chamber. The most uncertain element in this decision is the geometric "factor of safety" in excess of the calculated aperture requirements to allow for the effect of magnetic inhomogeneities, scattering of particles in the beam by residual gas in the chamber, and alignment errors. Early designers tended to choose a large safety factor, which resulted in unnecessarily large aperture dimensions and increased the cost of the magnet and power supply. With experience it is now possible to compute the effects of such errors with some confidence and to reduce the safety factor to a more reasonable value. The decision on aperture balances the importance of maximum possible beam intensity against the costs for initial construction and for power during operations.

In the cosmotron the decision on aperture dimensions had to be made early, before designs were complete for the vacuum chamber and also before any model experiments could be carried out. Oscillation amplitudes were computed theoretically and estimates were made of the effect of inhomogeneities, gas scattering, and alignment errors. The gross aperture chosen was a 36-in. pole-face width and a 9-in. gap, planned to accommodate a vacuum chamber with a net internal clearance of 30 by 6 in. As will be shown in the discussion to follow, this allows a geometric factor of safety of about 1.5 times the calculated maximum oscillation amplitudes in both the radial and vertical dimensions. Operating experience shows that a large fraction of the ion beam initially captured in resonant orbits is retained within this aperture.

As indicated earlier, the bevatron designers were more conservative in their early planning and chose basic magnet dimensions which would allow alternative use of either a large-aperture chamber for low particle energy or a smaller-aperture chamber for higher energies. Their final decision was for an internal aperture of 10 by 40 in., resulting in proton energies up to 6.4 Bev.

As the design studies developed at Brookhaven and at Berkeley, it became evident that there were several reasons for providing sectors in the ion orbit free from magnetic field. An electron-synchrotron magnet with straight sections between two semicircular halves of a ring magnet, called a racetrack, had been proposed by Crane[22] for the University of Michigan synchrotron and had been shown theoretically by Dennison

and Berlin[23] not to cause defocusing or to set up excessive ion oscillations. A design was chosen, at Brookhaven and also at Berkeley, in which the circular magnet was spaced into four quadrants joined by four straight sections free of magnetic field. Later, Blachman and Courant[10] published the Brookhaven calculations justifying the quadrant design and showing that the four symmetrical straight sections do not disturb orbit stability; they do modify the calculations on oscillation amplitude and frequency slightly and require a slightly larger aperture within the quadrants. Finer-grained angular asymmetries in the field, such as those caused by spaced bundles of magnet laminations, were found to have an almost insignificant effect on ion oscillations; amplitudes can be computed by using the average field around the quadrant.

A field-free region is essential to accommodate the type of induction accelerator used for ion acceleration in the cosmotron or the drift tube used in the bevatron. Another field-free region is assigned to injection of the beam of protons from the preaccelerator. Still others can be used effectively for targets or for the ejection mechanisms needed to produce an emergent beam of high-energy protons. In the bevatron the four straight sections are used for vacuum-pump manifolds as well. The absence of such straight sections in the Birmingham machine has made it necessary to mount the inflector, radiofrequency accelerator, and targets between the magnet poles.

The magnetic field must decrease with increasing radius across the pole face to provide the necessary focusing for particles in the orbit. The significance of this decrease in field (specified by the n value) in providing stability for particle orbits is discussed in Chap. 5. It is shown there that in a gap having a vertical dimension small relative to the radial extent the n value should be between 0.5 and 1.0, for a circular orbit. In the quadrant-type magnet with straight sections these limits become 0.5 to 0.8.[10] In both the cosmotron and bevatron the n value for the magnetic field at injection was chosen as 0.6, obtained by sloping the pole faces so the gap on the outside of the orbit is longer than on the inside. In both cases also, the final detailed shape of the pole faces was obtained by analysis of the magnetic circuit and checked by model measurements.

Power for magnet excitation is another basic parameter. It is closely associated with the choice of pulse repetition rate and so with the time-average beam intensity. In pulse powering, the stored energy in the magnetic field must be removed at the end of each cycle. In the large magnets required for multi-Bev synchrotrons the stored energy between poles is in the range of 10^7 to 10^8 joules. If it were to be supplied at a repetition rate of one per second and dissipated in each cycle, it would require 10 to 100 megawatts of power. Some method of storing and of reusing the energy in the magnetic field is essential. Cyclic operation is

indicated, with a system which transfers the stored energy of the magnetic field to some other storage element in the circuit and returns it to the magnet in the following cycle.

Brobeck[5] first discussed the alternative possibilities of energy storage, using the preliminary conceptual design for a 10-Bev bevatron as illustration. Capacitors, while ideal for small installations using higher repetition rates, would be far too costly for such a large magnet with the long time constant inherent in the basic design. At an early stage of the cosmotron planning an estimate of the cost for the necessary capacitors was about 3 million dollars. Storage batteries can store adequate power, but they involve formidable control and switching problems as well as serious maintenance and charging problems. It was estimated at Berkeley that maintenance and charging of a battery storage system would require three shifts of 6 to 10 electricians each.

The choice of an energy storage system, at Berkeley and at Brookhaven, was a flywheel. A large flywheel can readily store ten or twenty times the magnetic stored energy in rotational kinetic energy, and 5 to 10 per cent of this energy can be delivered to the magnet during the excitation cycle by means of a generator and suitable high-current rectifiers. Furthermore, grid-controlled rectifiers can be used which act as inverters to drive the generator as a motor during the return half of the powering cycle and transfer the stored energy back to the flywheel. Losses due to heating in the magnet windings and friction in the rotating machines can be made up by a low-power motor which drives the flywheel back to full speed between pulses. The average power dissipated will be just that due to losses during the pulses and can be specified to supply any desired pulse repetition rate.

The electrical properties of the magnet windings, such as the inductance, resistance, and number of turns to provide the desired excitation, are chosen for optimum performance of the pulse powering system. Further details of the cosmotron magnet and power supply will be given in following sections.

Magnetic field increases with time during the pulse; the rate of this increase is determined by the characteristics of the power supply and the magnet windings. The time to reach maximum field, and so the time rate of increase in field, is influenced by several factors. A short rise time increases the peak value of kilovolt-amperes required to excite the magnet and so increases the cost of the power supply. However, it reduces the average power demand (at a fixed repetition rate) by reducing the heat in the windings. A short rise time also means a large dB/dt and so requires higher rf potentials from the radiofrequency accelerating system to provide the necessary volts per turn. A short accelerating time also decreases the interval at the start of acceleration during which particles can be lost from the beam because of gas scattering. Practical

considerations also enter, such as the properties and ratings of commercial electric equipment and the cost of this equipment.

The magnetic-field rise time at the cosmotron was chosen to be 1 sec, although an allowable range would have been between 0.5 and 2.0 sec. The interval for returning the stored energy to the flywheel, while the pulse is decreasing, is associated with the rise time and is also about 1 sec. An independent parameter is the pulse repetition rate, which determines average power requirements. This was taken to be 12 per minute for the cosmotron. So the magnet cycle is 1 sec rise, 1 sec fall, and 3 sec for the drive motor to bring the flywheel back to speed.

At the bevatron the rise time was also taken to be 1 sec and the repetition rate at full power was set at 10 per minute.

Another basic parameter is the injection energy. Protons are preaccelerated to injection energy in a separate accelerator usually located outside the ring of synchrotron magnets and are directed through a vacuum pipe to the injection straight section. In this location they pass through an inflecting field between shaped electrodes, which bends the particle beam into the direction of the synchrotron orbit at the chosen injection orbit radius.

Many considerations point to the desirability of high injection energy. The most significant of these is that the magnetic field at the orbit is most uniform and least subject to errors due to remanent fields and eddy currents for high injection fields. Another is that the initial orbital frequency of the particles increases with field, so a high field reduces the range over which the applied accelerating radiofrequency must be modulated. Still another is that gas scattering is minimized at high injection energy.

However, practical limits existed on the energies which could be obtained from the existing types of low-energy accelerators which were adaptable to this purpose. The types considered were the Cockcroft-Walton voltage multiplier, the electrostatic generator, the proton linear accelerator, and the cyclotron. Each type had its own limitations on energy, beam collimation, or reliability.

The physical dimensions and the general arrangements for the cosmotron are illustrated in Fig. 13-1. This shows the four magnet quadrants of 30 ft orbit radius spaced by straight sections of 10 ft length. It also shows the electrostatic generator used as a preaccelerator, which feeds pulses of protons to the inflecting plate system in one straight section; another straight section is used for the radiofrequency accelerator, a third for control electrodes and internal targets, and the fourth for the devices used to produce an emergent beam. The chapter headpiece, page 437, is a photograph of the assembled cosmotron before the surrounding shielding was added.

With the basic dimensions known, other parameters can be established,

such as the ion revolution frequencies at injection and at high energy which determine the range of frequencies required in the radiofrequency system. Equation (5-54) gives the frequency of revolution in a circular orbit as

$$f_c = \frac{c^2eB}{2\pi(W_0 + T)} \tag{13-2}$$

In the orbit with four quadrants of radius R and straight sections of length L the orbital frequency is decreased by the path-length ratio

$$\frac{f_0}{f_c} = \frac{2\pi R}{2\pi R + 4L} = 0.824 \text{ (cosmotron)} \tag{13-3}$$

The frequency of revolution f_0 for the cosmotron is plotted as a function of the magnetic field in Fig. 13-2 and shows a range of frequencies from

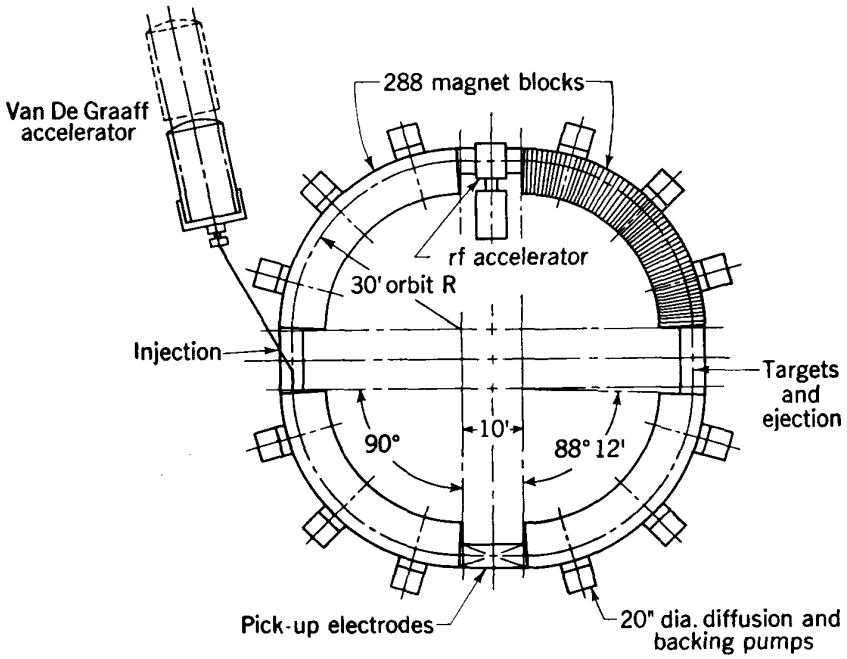

Fig. 13-1. Sketch of the cosmotron assembly showing the four quadrants and four straight sections.

0.40 megacycle/sec at 4-Mev injection where $B = 311$ gauss (or 0.35 megacycle at 3 Mev and 271 gauss) to 4.2 megacycles at the maximum energy of 3 Bev.

Ions must be accelerated on each turn by an average energy increment determined by the instantaneous rate of change of field, dB/dt, in order to maintain constant radius. The average value of dB/dt is given by the maximum field and the rise time, but is modified by the varying inductance of the magnet windings as magnetic permeability changes during the cycle, and also by the falling voltage characteristic of the generator

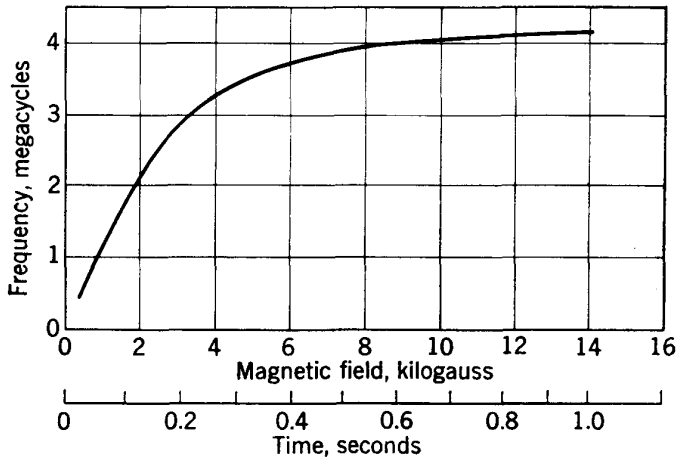

Fig. 13-2. Ion revolution frequency during the acceleration cycle for the cosmotron.

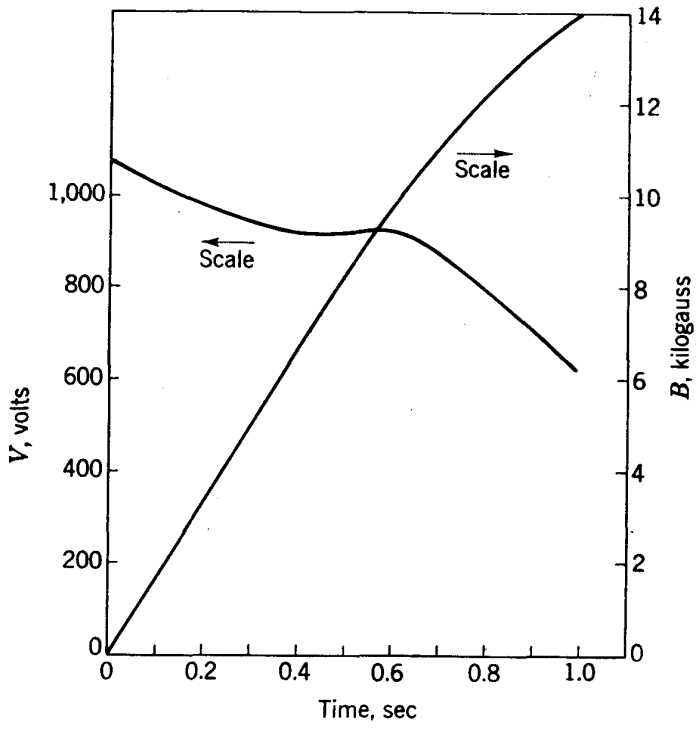

Fig. 13-3. Variation of magnetic field B and the volts per turn V required for acceleration during the cosmotron acceleration cycle.

as magnet current increases. These variations can be computed from the physical properties of the system or can be observed from scale-model studies using a time scale in proper ratio.

The measured value of B as a function of time during the 1-sec rise time of the cosmotron magnet is shown in Fig. 13-3. The values of dB/dt determined from this function start at over 16 kg/sec and drop to about 10 kg/sec near maximum field.

The rate of increase of particle energy with time is directly related to the rate of magnetic-field increase. By differentiation of Eq. (13-1) we find

$$\frac{dT}{dt} = \frac{c^2e^2R^2B}{T + W_0}\frac{dB}{dt} \tag{13-4}$$

A more useful quantity is the energy increase per turn. This can be obtained by dividing the above relation by the orbital frequency f_0 given in Eqs. (13-2) and (13-3):

$$\frac{\Delta T}{\text{Turn}} = \frac{2\pi eR^2}{0.824}\frac{dB}{dt} \tag{13-5}$$

The constant in the denominator of Eq. (13-5) is the value for the orbit radius and straight section length of the cosmotron. When evaluated for an average value of dB/dt of 14 kilogauss/sec, this relation gives ΔT/turn (average) = 880 ev/turn.

The volts-per-turn function for the cosmotron is also shown in Fig. 13-3, in units of electron volts. The maximum value occurs at injection and is about 1000 ev, decreasing to about 600 ev at maximum energy. The applied radiofrequency voltage across the accelerating gap must be higher, by about a factor of 2, to maintain phase stability in synchronous oscillations. This determines the voltage requirements for the rf accelerator. The frequency variation of the accelerator during the cycle is illustrated in Fig. 13-2.

The analysis above covers the basic interrelated parameters which must be determined at an early stage of design. From these, the other constants and design requirements can be obtained. We go now into a more detailed discussion of the characteristics of the several major components.

13-4. COSMOTRON MAGNET

The magnet design chosen for the cosmotron after a careful study of alternative structures involves several unusual features. It is basically a C section with minimum-size window for the windings. Choice of the C shape was influenced by the desire to provide ready access for pumping and for beam ejection on the outside of the magnet gap along the entire periphery. Pump leads can be located as frequently as desired along the length of the vacuum chamber, a valuable feature when vacuum requirements are severe and chamber cross section is small. Access to the chamber for inspection and maintenance is also simplified. When the slot opening of the C is on the outer face of the ring, high-energy particles can emerge tangentially from the accelerator around the entire circumference, with only thin windows in the chamber wall for absorption and

scattering of the radiations. To be sure, every effort is made to eject a concentrated beam in a narrow angle; however, the external C opening is good insurance that the high-energy particles can be utilized to the maximum for experiments.

The poleless C-shaped magnetic circuit has minimal dimensions and weight and requires only two accurately machined surfaces (the pole faces). The octagonal shape is a compromise between a square and the ideal circular shape; it is achieved by cutting off the corners of square plates in manufacture. The magnet cross section is shown in Fig. 13-4.

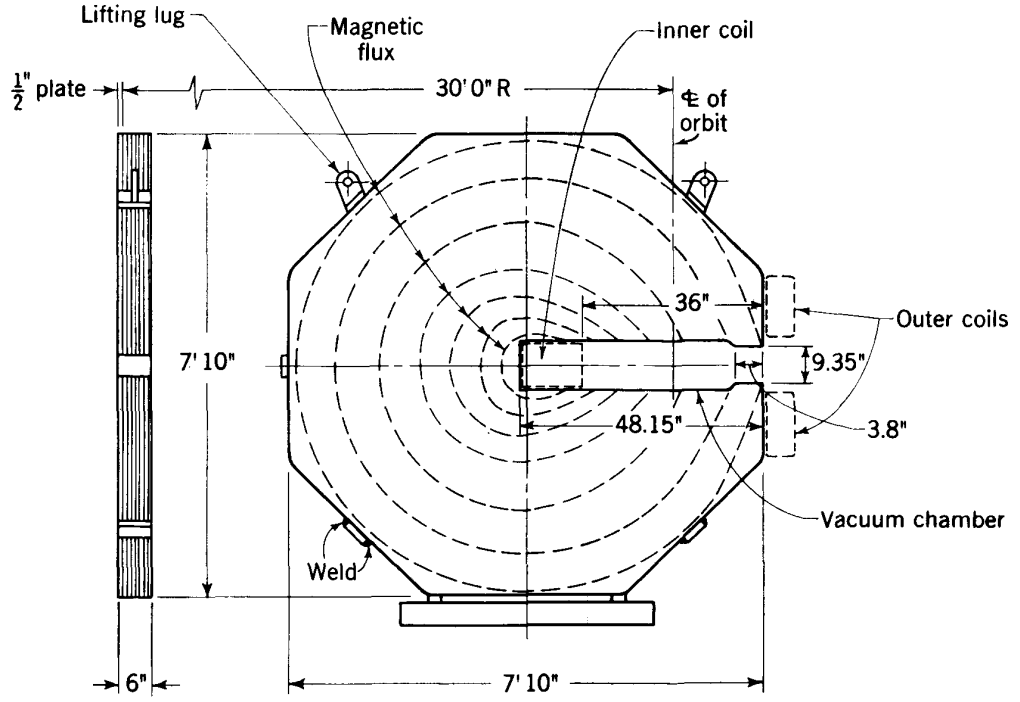

Fig. 13-4. Iron magnetic circuit for the cosmotron, showing assembly in bundles of 12 half-inch plates.

Since magnetic field increases at a rate up to 16 kilogauss/sec during the acceleration, eddy currents will be induced in the iron and it must be laminated. A detailed analysis of the eddy currents, checked by model measurements, justified the choice of ½-in. plate, which has the advantage of being readily available in large sheets and at a low base price. The material chosen was equivalent to SAE 1010 mild steel, having a low carbon content and magnetic properties closely approaching those for soft iron. The octagonal plates were sheared from 8-ft-wide strips and were supplied and fabricated by the Bethlehem Steel Company.

In order to simplify the problems of machining and handling the thousands of ½-in. steel plates, a procedure was devised for assembling the plates into blocks of 12, with interleaved insulation. The 12 plates in each bundle are welded together by tie bars at the outer edges. These

tie bars are outside the magnetic circuit and do not link any appreciable flux, so they do not produce significant eddy currents. The pole-face contours were machined in the block as a unit after assembly and welding; care was taken to remove all metal chips and burrs. Lifting lugs on the welded tie bars allow the blocks to be handled; the weight of each block of 12 laminations is about 5.7 tons.

Short circuits between laminations might produce serious eddy-current distortions if they occurred near the magnet gap. To test for such shorts, the insulation between laminations consisted of a sandwich of two layers of 0.007-in. insulation paper separated by a 0.001-in. aluminum-foil sheet. After processing and machining the blocks, these aluminum sheets were used to test for short circuits.

A total of 288 bundles, each about 6 in. thick, are arranged in four quadrants to form the complete magnetic circuit. Each quadrant occupies an angle of 88.4°, which was the angle found necessary from magnetic-field measurements to produce 90° deflection of particles, because of the fringing field which extends into the straight sections. The bundles were assembled on base plates and carefully leveled by accurate surveying techniques during assembly to keep the median plane of the gap flat. The inner edges of the bundles are in contact, and the center line of each bundle was located accurately on a surveyed radial line. After alignment the bundles were welded together at the tie bars to form the entire quadrant structure into a rigid unit. Settling of the foundation under the load of 2000 tons of steel was anticipated and provided for by elevation adjustments beneath the base plates. The precision attained in assembly was within 0.005 in. in the horizontal level and 0.015 in. radially, with additional precautions to maintain vertical alignment.

The pole-face contour was shaped to produce the widest possible region with a radially decreasing field of the correct slope to provide focusing. The n value chosen was 0.6, and the acceptable range is 0.5 to 0.8. Maximum aperture is most necessary during and immediately following injection, when ion oscillations have their largest amplitudes. So the pole was shaped to give the widest possible extent of the $n = 0.6$ slope at the injection flux density of about 300 gauss.

Measurements with a short section of a quarter-scale model were used to study the properties of the magnet and to obtain the pole-face shape. The model was in true physical scale, using $\frac{1}{8}$-in. laminations of equivalent iron plate, and consisted of seven blocks of laminations, formed around an arc of the scaled-down radius. Effects due to the quadrant ends were observed to extend in no further than two lamination blocks, so the three blocks at the center of the model were available for typical magnetic measurements. The exciting coils were also modeled to scale and were pulsed at the planned duty cycle. Certain physical problems were encountered, such as the spreading or fanning of the laminations

due to the repulsive forces between parallel laminations. These indicated similar problems in the full-scale magnet and were solved by installing bolts and clamps of nonmagnetic stainless steel to restrict the spreading.

Many types of measurements were taken with the models. In fact, the program of magnetic measurements continued in more and more detail for a period of over 2 years. These measurements included:

1. Average field at the orbit radius as a function of time during the pulse and of the current in the windings
2. Time rate of change of magnetic field, dB/dt, as a function of time
3. Radial decrease in field at injection time and at several higher fields extending up to the maximum, for a series of pole-face shapes
4. Eddy-current effects at short times, extended past injection until they became negligible
5. Remanent magnetic fields in the gap, as a function of previous excitation history
6. Effect of corrective pole-face windings, to extend the desired n value to high fields and over as large a gap area as possible
7. Fringing fields in the quadrant end region, at various fields
8. Fringing fields at large radii on the median plane off the front of the magnet gap, to compute trajectories for emergent particles
9. Location of the magnetic median plane

Average flux densities at a particular radius were obtained with a rectangular coil located on the median plane, narrow enough to give the desired resolution in radial measurements and of a length sufficient to extend from the center of one block to the center of the next and so to overlap the wedge-shaped space between. This coil was located at different radii to observe the radial decrease from which the n value could be computed. As an alternative, two such coils located at different radii were used to obtain a value for dB/dr directly, and the pair could be moved radially to survey the field.

The time rate of change came directly from the induced electromotive force (emf) in a coil. The emf was displayed on a cathode-ray tube with a time sweep, and photographs of the pulse were taken. Calibrations were obtained from several standards. A large precisely built Helmholtz coil was used to obtain known magnetic fields up to 1000 gauss in air, and the test coils were calibrated in this field. Calibrated voltage amplifiers were used for the measurement of emfs.

Eddy-current effects appeared in the dynamic measurements during the first 30 μsec of the pulse. Qualitatively the effect of eddy currents in the pole faces is to reduce the magnetic field at the midportion of the gap as compared with the field near the exciting windings. As a result, the rate of field decrease with radius, or the n value, is increased. If the time rate of increase of field were constant, this increase in n could be com-

pensated by a slightly different shape of pole contour. But the initial sharp change of dB/dt at the start of the pulse induces a transient which takes a finite time to die out and extends up to injection times. The magnitude of this increase in n value over steady-state conditions, Δn, was measured by observing the difference in induced voltage in two coils spaced a short distance apart radially and located at various positions across the gap. Photographic recordings of the integrated difference voltage displayed on a cathode-ray tube were analyzed to obtain a measure of Δn as a function of time. The results are shown by the dashed curve of Fig. 13-5. The effect was large at very short times, but had dropped to a value of $\Delta n = 0.3$ at the time corresponding to injection at 3 Mev, when the magnetic field is 271 gauss.

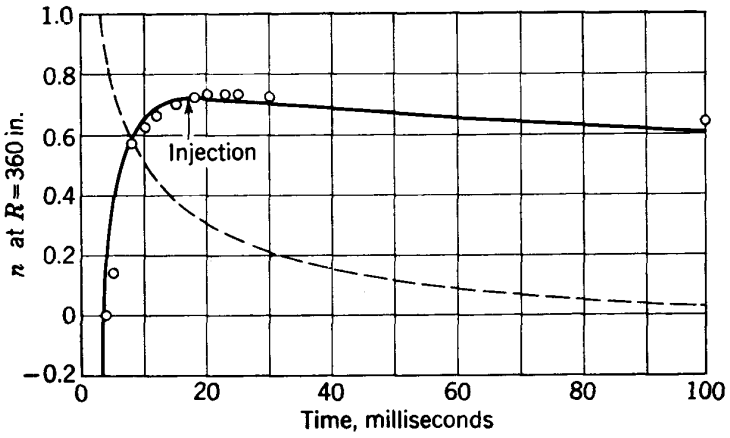

Fig. 13-5. Variation of the n value of magnetic field in the cosmotron at short times. The dashed curve is the calculated effect of eddy currents alone.

The remanent field in the iron resulting from unidirectional operation is significant and adds to the dynamic field at low flux densities. It is determined by the past history of excitation and can be removed by applying a reversed field after the main pulse, if needed. It was found to have an average value of about 25 gauss at the central orbit radius after a typical cycle of operation to maximum field and reduction to zero current. It was also observed to increase almost linearly by about 25 per cent from the inner to the outer radius of the aperture; this is due to the larger integrated coercive force in the long flux paths around the outer portions of the magnetic circuit. The radial increase due to the remanent field produced a negative Δn at injection time, which almost completely compensated for the positive Δn due to eddy currents. This was a fortunate coincidence associated with the shape of the magnetic circuit. The maximum resultant Δn, measured as the sum of both effects at injection time and over the useful width of the pole face, was of the order of ± 0.1. It was considered to be sufficiently small to make

further corrections for eddy currents unnecessary. The variation of n after correction for remanent field effects is shown by the solid curve of Fig. 13-5.

The machined taper needed to attain a value of $n = 0.6$ at injection time, after including the effects of eddy currents and of the remanent field, was derived from model experiments (see Fig. 13-6). The taper starts at the inner radius of the aperture (outside the magnet slot windings) at a gap length of 9.00 in. and is a straight taper cut on each face to a position about 4 in. inside the front face of the magnet where the gap length is 9.35 in. A 4-in.-wide lip of iron is retained at the periphery with the basic 9.00-in. gap to extend the region of uniform field to the maximum possible radius. The resulting magnetic field at injection time during a normal pulse decreases about 3 per cent from the inner to the outer extent of the useful field. Figure 13-7 is a plot of the n value as a

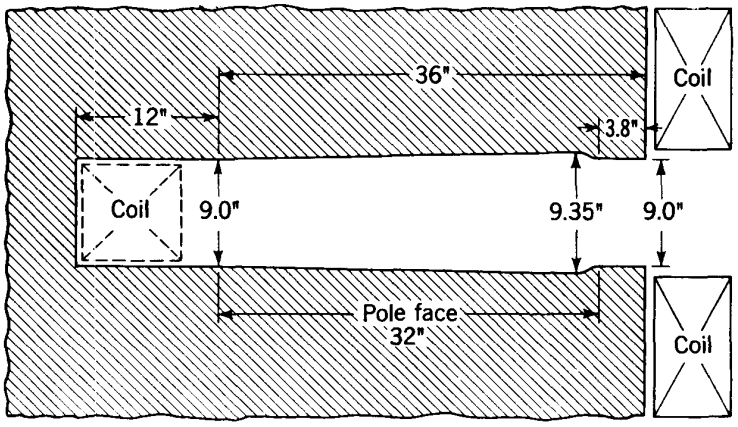

Fig. 13-6. Pole-face shape to produce an n value of 0.6 at injection fields in the cosmotron.

function of radius. The useful field region at injection is found to extend from a radius of 344 to 372 in., defined as the region in which n lies between the limits 0.5 and 0.8. No significant difference in the shape of this field was observed up to fields of about 6000 gauss.

At high fields the permeability of the magnet iron decreases and an appreciable fraction of the magnetomotive force appears in the iron. Because of the C shape of the magnetic circuit and the large difference in iron-path length for flux crossing at the two ends of the gap, the effect of decreasing permeability is to cause an increase in n value at high fields. This effect becomes significant at about 9000 gauss; it increases the value of n above the 0.8 limit over the entire pole face by the time the field reaches 12,000 gauss.

Such a large change in n value cannot be permitted, and must be compensated by auxiliary windings. Such windings need only be powered during the later part of the acceleration interval and need only change

the slope or shape of the field. An excessive n value means that the field at large radii is too small relative to that at small radii. A method of correction is to add magnetic flux at large radii, tapering off to zero at the center of the aperture and subtracting flux at smaller radii. This can be achieved most simply with a layer of windings distributed uniformly across the pole face, with suitably located return windings.

Before being assembled, each of the 288 blocks was checked in a detailed testing program, to determine its properties and the best order of assembly in the final magnet. A full-scale three-block sector was set up in which the block under test was placed between two fixed guard blocks. The unit was magnetized to full field using a 1-sec cycle to duplicate the operating condition. Measurements were made of the maximum field in the

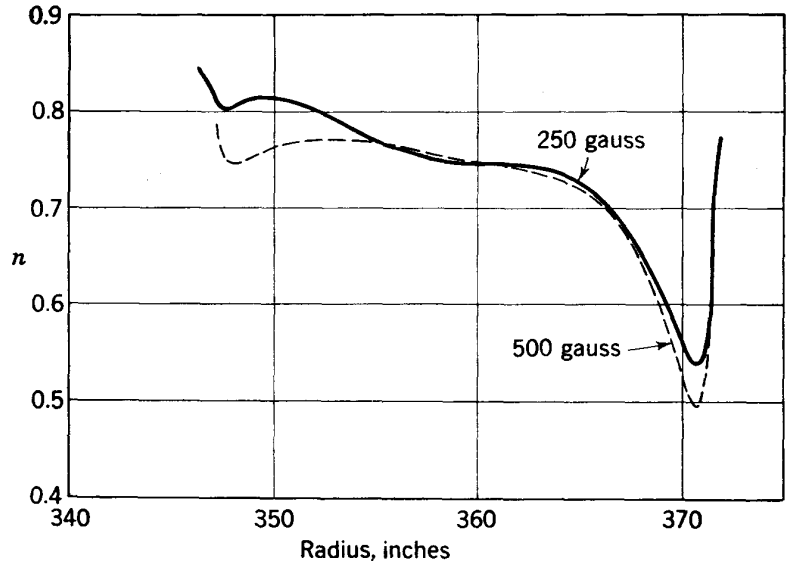

Fig. 13-7. Radial variation of n value across the pole face of the cosmotron, at injection fields.

gap, the initial dB/dt to check for shorts between laminations, the n value at injection fields, the location of the magnetic median plane, and the remanent field after a pulse. The variations observed in the dynamic field were negligible. Appreciable differences were observed in remanent field, however. A statistical analysis of the results led to a preferred order of assembly which gave a fine-grained azimuthal variation in remanent field and compensated for the blocks having extreme properties. The uniformity of average field attained in this way was much better than would have resulted from random stacking and gave the maximum possible useful area of magnetic field at injection.

The excitation windings for the magnet were designed to be compact and located as close as possible to the magnet gap. In principle a single circular winding located in the slot of the C magnet would provide excita-

tion. However, such a coil of large diameter would produce magnetic fields in the air both inside and outside the circular magnet. External fields well beyond the iron would be of the order of hundreds of gauss when the field in the gap was 14 kilogauss and would represent a large amount of stored energy. In early calculations and model studies with a single-slot coil the external stored energy was observed to be about 40 per cent of the stored energy in the gap itself. Return windings, split symmetrically above and below the slot on the outer face of the magnet, confine the magnetic fields more closely to the gap. Further studies with such return windings showed the external stored energy to be reduced to 13 per cent of the energy in the gap.

The slot windings were made as compact as possible to minimize the size of the coil window in the C structure and thereby to reduce magnet weight, stored energy, and power requirements. They consisted of 48 turns arranged in four layers. Each conductor was an extruded rectangular copper bar with a $\frac{3}{8}$-in.-diam hole down the center for water cooling. The bars were double-wrapped with insulation, formed to the proper circular shape, and clamped into the slot between fiber shields to prevent contact with the iron and to provide insulation.

The return windings do not have so severe a space limitation; they were designed with a 50 per cent larger cross section to reduce resistance. These are also rectangular, with a $\frac{3}{8}$-in. water-cooling channel. They are arranged in two bundles of 24 turns each, one above and one below the gap, clamped to the magnet face with many stainless-steel brackets.

Connectors joining the inner and outer windings at the quadrant ends are made of the same stock as the outer return windings, also water-cooled. Silver brazing was used to form the corner joints in the connectors, and the connectors were gasket-bolted firmly to the ends of the magnet windings. Thermal expansion was anticipated for the copper windings relative to the iron quadrant structure, and it was allowed for in the design of spring clamps to support the connectors. In the completed unit (Fig. 13-8) the windings form a continuous coil of 48 turns around each quadrant pole face, with two terminals brought out at one quadrant end.

Water-cooling leads for the 96 separate conductors in each quadrant are brought out in parallel to water manifolds located at the quadrant ends. Insulation of the $\frac{3}{8}$-in. cooling-water lines is provided by 5-ft lengths of plastic hose in each line. Water flow through the 384 parallel cooling tubes is about 500 gpm at 20 psi pressure. The water is purified to control conductivity and is recirculated through a heat exchanger.

After the assembly was completed, tests were made gradually increasing the length of pulse up to the full 1 sec and the peak current up to its maximum of 7000 amp. Small physical displacements of the connector bars at quadrant ends were observed due to the magnetic forces; the

maximum displacement observed was 0.060 in. Additional steel brackets ("spreader bars") were installed between quadrant ends to brace the connector-bar assembly, and the displacement was reduced to 0.020 in. under maximum power. A systematic routine of tightening all clamp bolts and the insertion of block spacers between magnet blocks resulted in a more rigid structure in which physical motions of the iron laminations and coil conductors were reduced to even smaller values. The compact assembly resulted in very little audible creaking when the magnet was pulsed. Some was observed at the start when the magnet was first excited, but was almost completely eliminated by the tightening program.

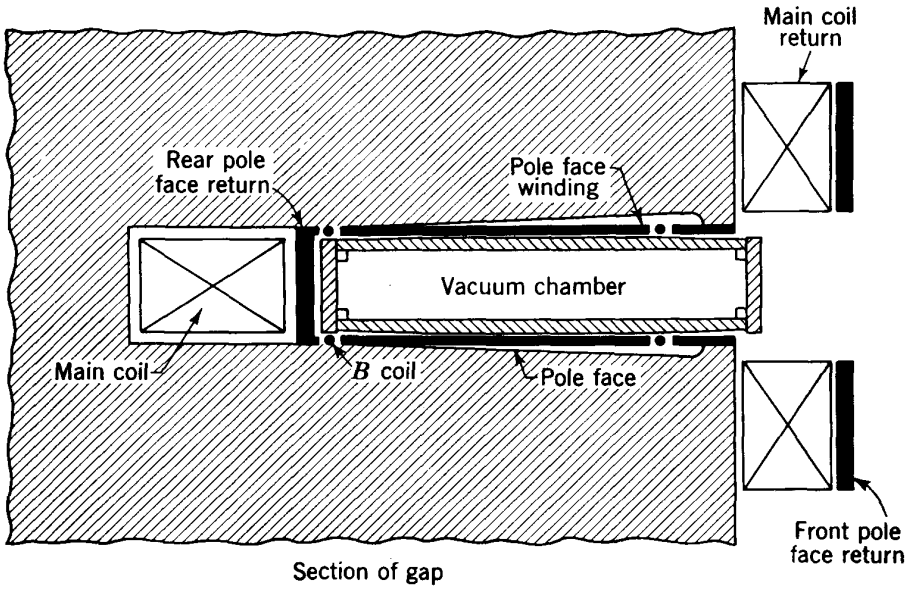

Fig. 13-8. Assembly sketch of water-cooled conductors forming the excitation coil of the cosmotron magnet. Correction windings on the pole face and return circuits are also shown.

After 2 years of operation (in November, 1954), a fault developed which led to an insulation breakdown between conductor bars near one of the quadrant end connections. The cause of the failure appears to have been a small water leak from a defective bar. Moisture seepage from this leak saturated the insulation and caused a destructive short circuit between adjacent conductors. This bar and adjacent bars were replaced and satisfactory operation was resumed.

In November of 1957 a more serious failure occurred when one of the coil conductors broke near the sharp bend at the end of the quadrant. Inspection of similar bars on other quadrants revealed the fact that the bars were suffering from metal fatigue due to their small motions in the fringing fields around the quadrant ends. Although these motions were very small, the magnet had, by this time, been pulsed more than 7 million

times. It was evident that a local repair would no longer be adequate, and the whole magnet coil was removed and redesigned. In the new coil the conductors extend past the quadrant end and are joined to the front coil by connectors which are spaced vertically 3 ft away from the gap. These connecting bars experience negligible forces due to stray fields, and no further fatigue failures are expected. This repair involved a shutdown of more than a year; fortunately this provided an opportunity for long-overdue modifications in other components and in the experimental laboratory.

The faults and limitations of the early designs for the cosmotron magnet and coils have been described in some detail to illustrate a typical development problem in the accelerator field. As a result of this experience new concepts and techniques have been developed and widely applied in subsequent designs. The physical motions of laminations and coils in the magnetic fields can now be essentially eliminated by bonding techniques using modern adhesives and resins. The laminated cores of pulsed magnets are now bonded into solid mechanical blocks with suitable adhesives. The most successful type is an air-drying, thermosetting artificial rubber; laminations are coated with a thin layer of liquid adhesive, air-dried, stacked, and clamped into bundles and baked in an oven with a carefully controlled temperature cycle. The resulting bundles of laminations can then be assembled, aligned, and clamped in place on suitable structural bases to form the magnet. Similarly, the conductors for magnet windings are bonded into solid units. The preferred technique is to wrap the individual conductors with porous cotton or glass-fiber cloth, wind or assemble the conductors into coil units in a vacuumtight housing or mold, and vacuum-impregnate the entire coil with an epoxy resin which has good electrical insulation properties. This technique for making solid resin-bonded coils is now standard throughout the electrical industry. Most accelerator laboratories are taking advantage of these new developments in the design of magnets and coils for new accelerators or auxiliary apparatus.

The pole-face windings used to correct the field at high flux densities consist of a single layer of 20 turns of $\frac{1}{4}$- by $\frac{1}{4}$-in. copper conductor spaced across each pole face. Each conductor is an arc of constant radius extending along the length of a quadrant. The 20 conductors are spaced at $\frac{1}{2}$-in. intervals and grouped near the center of the pole face, since it is necessary to correct the fields only over a radial-aperture width of about 10 in. at high magnetic fields when radial beam oscillation amplitudes have been damped to small dimensions. The correction windings were embedded in a $\frac{3}{8}$-in. layer of polyester with glass-cloth reinforcement, cast from a liquid thermosetting resin. The resin has good insulation properties and forms a strong and rigid unit for mounting on the pole faces. The return circuits for the pole-face windings are located partly

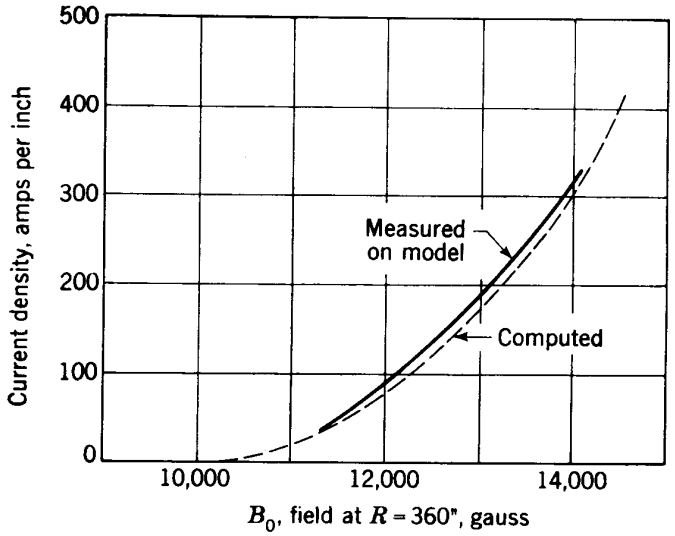

Fig. 13-9. Correction current pulse applied to pole-face windings used on the cosmotron to maintain uniform n values to high magnetic fields.

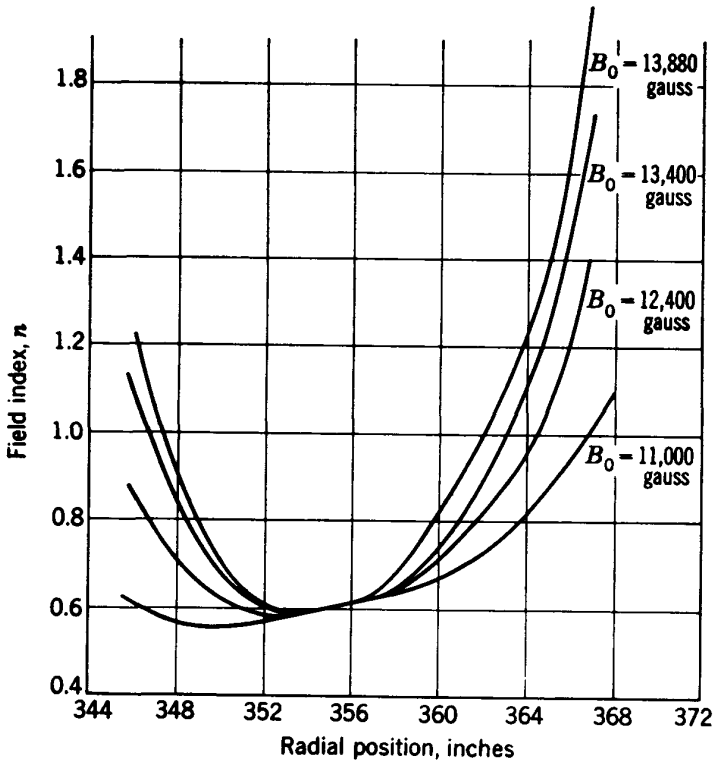

Fig. 13-10. Radial variation of n value at high magnetic fields using pole-face windings in the cosmotron.

outside and partly inside the main magnet gap. With a proper division of these turns there can be almost zero coupling between the pole-face windings and the main field pattern, so it is possible to power the correcting windings with an independent power supply. The pole-face return windings are also formed in a rigid arc and bonded with glass-cloth-reinforced resin.

The physical arrangements of the pole-face windings and return circuits are also shown in Fig. 13-8. The current-time pulse used to power

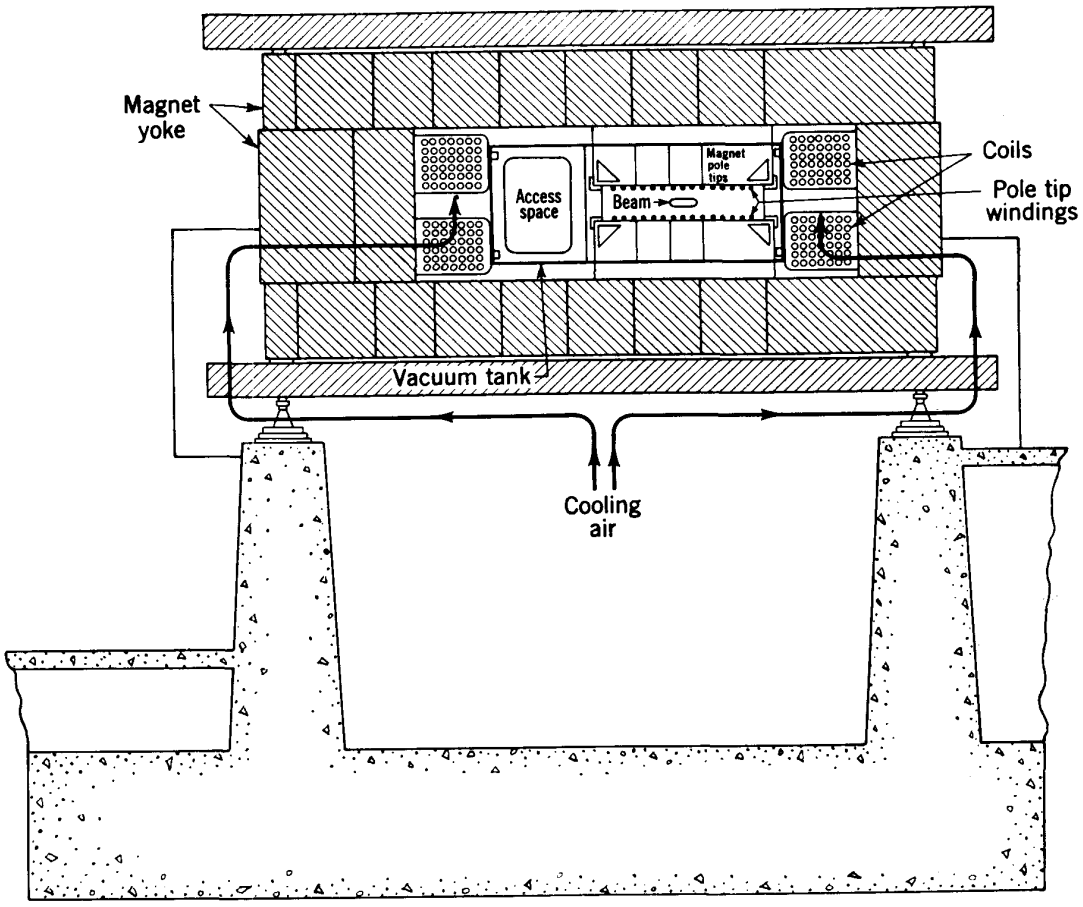

Fig. 13-11. Cross section of bevatron magnet at the University of California Radiation Laboratory.

the windings is illustrated in Fig. 13-9, and a plot showing the radial variation of n value after correction by currents in the pole-face windings is shown in Fig. 13-10. This plot shows that the region of useful n value contracts at high magnetic fields; fortunately the damping in amplitude of particle oscillations during acceleration reduces the width of the beam so the contracted region of focusing field is quite adequate.

The magnet for the Berkeley bevatron has iron return circuits both inside and outside the orbit (Fig. 13-11). This symmetrical structure is more efficient magnetically, in that saturation effects do not destroy the

useful field region until the field reaches about 16 kilogauss. This advantage is offset to some extent by the relative inaccessibility of the vacuum chamber; magnet yokes must be removed to install or to make significant modifications to the chamber. As mentioned earlier, the bevatron magnet was designed to allow the use of a large pole gap and wide aperture, because of concern over the possible effect of orbit inaccuracies and gas scattering in developing large-amplitude oscillations. Following the success at the cosmotron with a smaller relative aperture, the poles and vacuum chamber were redesigned for a 12-in. gap with pole faces of 5 ft width, a much smaller vacuum chamber than originally conceived. This arrangement is shown in Fig. 13-11, which also shows the access tunnel through which a man can crawl to service the chamber, if necessary.

A new principle of pole-face design has been developed by H. Bruck and his associates[24] for the 3-Bev accelerator at Saclay. The pole tips are bonded units of thin laminations of two or more different pole-face shapes, stacked in a sequence to give a fine-grained alternation in profile. These "crenelated" pole tips display the magnetic-field pattern at low fields established by the profile of the protruding laminations; at high fields when the protruding edges saturate, the field pattern is determined by the shape of the underlying base laminations. This technique allows the magnet to be operated much closer to saturation limits without requiring pulse-powered correcting coils. The Saclay machine has removable pole pieces to allow the use of such crenelated poles when desired. The same principle has been adopted to determine pole-face shape for the Princeton-Pennsylvania proton synchrotron.

13-5. PULSE POWER SUPPLY

The systems for providing pulse power to the magnet, at the cosmotron and also the bevatron, use large flywheels for energy storage. They consist of a motor, a flywheel, and a 12-phase ac generator on the same shaft, with the generator supplying a rectifier-inverter circuit connected to the magnet coils. The motor drives the flywheel up to speed; the flywheel supplies energy to the ac generator; the rectifier converts the multiphase ac output of the generator to direct current to supply the magnet. As energy is removed from the flywheel, it drops in speed. Then at the peak of the cycle the grids of the rectifier-inverters (Hg vapor ignitrons) are controlled to switch to inverter action; the inverter drives the generator as a motor, fed by the stored energy in the magnetic field; the stored energy (less heat losses) is returned to the flywheel, increasing its speed. During the remainder of the pulsing cycle the motor brings the flywheel back to the original speed.

The design of this power supply was worked out in collaboration with the makers, the Westinghouse Electric and Manufacturing Company.

The ratings of the power supply had to be coordinated with the properties of the magnet and its exciting coil. Peak current was chosen to supply the necessary ampere-turns for full excitation of the magnet, and voltage was designed to bring the magnet up to full excitation in the chosen 1-sec rise time.

In the cosmotron, scaled-model measurements showed that the excitation required to produce 14 kilogauss in the gap was

$$Ni = 3.36 \times 10^5 \text{ amp-turns}$$

The total flux in the magnetic circuit including stray field was

$$\phi = 88 \text{ webers}$$

and the initial rate of change to reach peak field in 1 sec was

$$\frac{d\phi}{dt} = 58 \text{ webers/sec}$$

The total stored energy in the magnetic field at peak excitation was found to be $W = 1.2 \times 10^7$ joules, and the peak power transfer was

$$\frac{dW}{dt} = 26{,}000 \text{ kva}$$

Generator output V is related to the number of turns N and the resistance R of the coil as

$$V = N\frac{d\Phi}{dt} + Ri \tag{13-6}$$

For practical engineering reasons the manufacturers recommended a peak voltage of 5 to 6 kv for the generator and rectifier system. The cosmotron designers desired a coil with an even number of turns which could be compacted into two identical rectangular bundles fitting inside the 9-in.-high window in the magnet; this required a number of turns divisible by 2, 4, 6, or other simple integers in order to assemble the bundles from rectangular copper conductors. The external dimensions of the space allocated to the coil were known, and good estimates were available of the total copper cross section A which could be packed into this space with suitable insulation.

The resistance of a coil can be expressed as a function of the number of turns N, the average conductor length per turn L, and the copper cross section A:

$$R = \frac{\rho L}{A} N^2 \tag{13-7}$$

where ρ is the resistivity of the conductor at operating temperature. For the cosmotron dimensions this becomes $R = 4.95 \times 10^{-5} N^2$ ohms. The

quantity Ri for use in Eq. (13-6) can now be obtained as

$$Ri = 4.95 \times 10^{-5} N(Ni) = 17.0N$$

The relation between voltage and number of turns can now be expressed as $V = 58N + 17.0N = 75N$. The choice of the cosmotron designers was for a coil of 48 turns, for which the applied potential at 14 kilogauss excitation is 3700 volts. Peak current is then found to be

$$i = \frac{Ni}{N} = 7000 \text{ amp}$$

This is the voltage and current required at full excitation, after the flywheel and generator have been reduced to minimum speed. At full speed at the start of the cycle, and with no load, the generator characteristics provide a potential of 5400 volts.

The inductance of the magnet changes during the cycle with the varying permeability of the iron core. Model measurements showed the inductance to have an initial value of 0.47 henry, rising to a maximum of 0.80 henry at about 1000 gauss and dropping to a final value of 0.25 henry as the iron saturates. When combined with the falling voltage characteristic of the power supply, this leads to a nonlinear increase in current (or magnetic field) with time. The measured curve of B versus t was given in Fig. 13-3.

The cosmotron power supply in service is an impressive installation. The motor is rated at 1750 hp and is of the standard wound-rotor induction type operating at 950 rpm. It is directly connected to the large flywheel, which is 9 ft in diameter and weighs 42 tons, and to the 12-phase, 60-cycle generator. This alternator has a nominal continuous-service rating of 20,000 kva, specially designed to withstand rectifier service; it will deliver 6000 volts at no load and a peak of 7000 amp at 4200 volts under full load. The power supply has taps for 50, 75, 87, and 100 per cent voltage output, with the 87 per cent tap corresponding to standard operation at 14 kilogauss field in the magnet. The rectifier inverter bank uses 24 ignitrons in a 12-phase circuit, with grids and igniters controlled to rectify the alternator output during the 1-sec acceleration interval, and then to switch to inverter action. The flywheel is reduced in speed by about 6 per cent at the peak of the cycle, representing a 12 per cent decrease in the rotational stored energy. The heat loss per cycle in the magnet windings represents an average power drain of about 800 kw; windage and thermal losses in the machines and losses in the ignitron rectifier add to make the total average power demand under full load about 1100 kw. A control system for the motor limits the line-surge demands to 2000 kva peak; it can be adjusted to make the power demand nearly constant over the 5-sec cycle.

Protection against failures in the power circuit is provided by a short-circuiting switch across the magnet terminals and by spark gaps between power leads to the magnet at each quadrant. Any voltage surge which raises voltage by 50 per cent above the designed maximum will cause the gaps to discharge, shorting the circuit. Simultaneously the ignitron excitation is removed. Under such a short circuit the magnet windings have adequate thermal capacity and cooling to discharge the peak stored energy.

The complete time cycle for the applied voltage and current is shown in Fig. 13-12. The dc voltage on the coil terminals starts at 5400 volts and decreases to 3700 volts during the 1-sec powering interval; it is

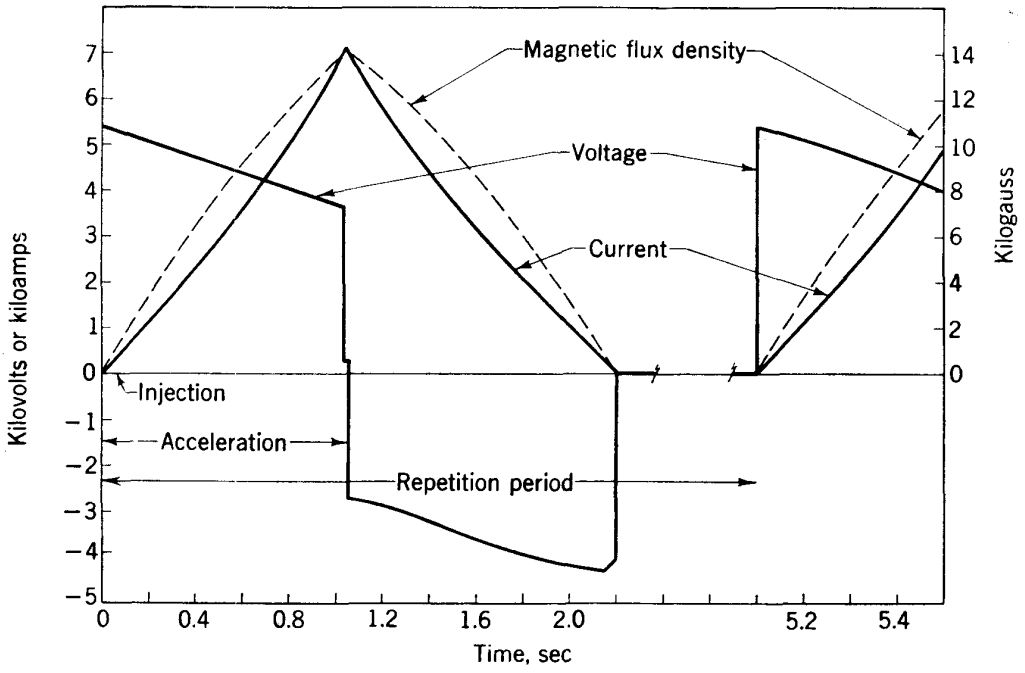

Fig. 13-12. Time cycle for applied voltage and current from the cosmotron magnet power supply. The magnetic flux density is also shown.

reversed by the ignitrons to −2800 volts and then increases in magnitude to about −4300 volts, by which time the current in the windings is reduced to zero; then the voltage is brought sharply to zero. The current cycle is also indicated, rising to 7000 amp at 1 sec and falling to zero in another 1.15 sec. The cycle is repeated at 5-sec intervals. Magnetic field varies with time in a slightly different manner than exciting current, because of the varying permeability. The remanent field of about 25 gauss is too small to be observable on the plot.

It is also possible to shorten the rise time and the time cycle if desired. For example, voltage can be reversed after 0.5 sec, at which time the current and magnetic field are approximately half their maximum values. With such reduced power demand the repetition rate can be increased.

This procedure can be used to eject protons at less than their maximum energy, in order to study nuclear processes at lower bombarding energies.

Another technique of completing the cycle after the magnet has been brought to full excitation is to short-circuit the magnet coils, removing ignitron excitation simultaneously. This technique is called "crashing" in laboratory parlance. When the coils are shorted in this way, all the energy stored in the magnetic field is dissipated in heat in the windings; the current circulating in the magnet decreases slowly, with a time constant given by the inductance and resistance of the windings. Or the coils can be shorted at any chosen time after the normal reversal of voltage has started to decrease the current. Such variations in the shape of the cycle are observed to affect the remanent fields strongly, and so may possibly have a useful function.

An auxiliary power supply is provided for the pole-face windings. This supply consists of four 40-kva dc generators on the same shaft, each supplying one quadrant. The excitation for each generator is separately controllable to adjust the time schedule of the corrective currents to optimum in each quadrant. The unit is capable of supplying a 0.3-sec pulse with a maximum current of 800 amp, sufficient to correct the field up to 14 kilogauss. When the main winding voltage reverses, induced voltages in the pole-face windings would produce large currents in the pole-face windings. This is controlled by reversing the voltage applied to the pole-face windings simultaneously with that of the main winding, and allowing current to fall to zero before opening the circuit.

The power supply for the Berkeley bevatron magnet is quite similar to that for the cosmotron, but has about twice the output capacity. This was obtained by using two generators and by paralleling twice as many ignitrons in the rectifier circuit. One major fault occurred during the early testing, because of failure of ignitrons in the pulsing circuit, which caused damage to one of the generators. The rate of ignitron "flashbacks" is higher at Berkeley than at Brookhaven, possibly because of operation closer to the power limits of the tubes.

13-6. INJECTION

The general requirements for the injection of particles into the orbit have been described in an earlier section. Protons are produced in an auxiliary accelerator, of an energy sufficient to give a high capture efficiency in the synchrotron orbit. A high-intensity, pulsed beam of particles is needed, with small energy spread, and delivered in a well-collimated beam of small cross section. The ion source for this preaccelerator is pulsed at the start of each magnet cycle, for a short time interval during which the magnetic field is in the range to accept the particles in stable orbits.

The preaccelerator chosen for the cosmotron was a Van de Graaff electrostatic generator rated for 4 Mev, built by the High Voltage Engineering Corporation. At the bevatron a 0.5-Mev Cockcroft-Walton source supplies a 10-Mev proton linac which was designed and developed at the Berkeley laboratory. Both machines give well-focused beams suitable for injection, and both have been copied in other installations.

The obvious method of directing the beam into the orbit is to deflect it between a pair of curved "inflector" electrodes which provide an electrostatic field and which are located in the field-free region at a straight section. These electrodes direct the beam into the synchrotron in a direction paralleling the equilibrium orbit and located at the outer edge of the useful aperture of the synchrotron. A basic requirement of the inflector system is that the injected particles should not strike the back of the inflector electrodes, or the chamber walls, in subsequent revolutions. The contraction in orbit radius due to the increasing magnetic field can be computed from Eq. (13-1a). For cosmotron parameters this is found to be 0.17 in. per turn at 4 Mev energy. In itself this orbit contraction would be insufficient to clear a practical injection electrode assembly, if the successive orbits were concentric.

The principle of injection utilizes the mismatch in frequency between the orbital motion of the particles and their betatron oscillations about the equilibrium orbit. Because of this mismatch the particles traverse many turns before their oscillations bring them again into the location of the inflecting electrodes. During this time the rising magnetic field causes the equilibrium orbits to contract sufficiently that the particle orbits can miss the electrodes completely.

The amplitude of the betatron oscillations depends on the spacing between the injected beam and the instantaneous location of the equilibrium orbit for a particle of injection energy. The acceptance interval starts when the equilibrium orbit is just inside the injection radius, when the oscillations are of small amplitude. As the equilibrium orbit contracts, the amplitudes increase to a maximum value which just fills the useful aperture when the equilibrium orbit reaches the center of the chamber. In the cosmotron this time interval is about 200 μsec, during which the ions make about 70 revolutions.

The parameters associated with injection into the cosmotron, at two injection energies, are listed in the following table:

Injection energy	3.0 Mev	4.0 Mev
Magnetic field at central orbit	271 gauss	311 gauss
Ion revolution frequency	0.35 megacycle	0.40 megacycle
Volts per turn for acceleration	1040 volts	1040 volts
Orbit contraction per turn	0.18 in.	0.17 in.
Time after $B = 0$	0.014 sec	0.017 sec

A charged particle directed into the synchrotron field on a path parallel to its equilibrium orbit but at a larger radius will oscillate in the radial plane about the equilibrium orbit. The frequency f_r of this radial oscillation is given by[10]

$$f_r = \left(1 + \frac{L}{\pi R}\right)(1 - n)^{1/2} f_0 \tag{13-8}$$

where f_0 is the orbital frequency in the quadrant and straight-section orbit given by Eqs. (13-2) and (13-3). When evaluated for cosmotron dimensions and n value, this gives $f_r = 0.70 f_0$. A full cycle of radial oscillation would require $360°/0.7 = 510°$ of azimuth, which is 150° beyond the angular location of the injector. Subsequent maximum outward amplitudes would be displaced from the injector position by 300°, 90°, 240°, etc. So the average particle will make 5 to 10 revolutions before the maximum outward amplitude again occurs at the location of the injector. During this time (15 to 30 μsec) the equilibrium orbit will contract by 1 to 2 in., sufficient for a large fraction of the beam to miss the inflector plates.

Angular divergence of the injected beam will cause a spread in the amplitudes of radial oscillations and will also result in a spread in the initial phase of the oscillations. An angular deviation on injection is equivalent to a radial oscillation of different amplitude with the phase shifted. The effect of angular divergence is to increase the chance of striking the back of the inflector electrodes for some particles and to decrease it for others. The average probability can be computed from the physical dimensions and the properties of the oscillations. It is not significantly changed by an angular spread of $\pm 0.5 \times 10^{-3}$ radian, which is typical of the beams coming from either a well-focused electrostatic generator or a proton linac.

Angular divergence also introduces vertical oscillations about the median plane, with a frequency

$$f_z = \left(1 + \frac{L}{\pi R}\right) n^{1/2} f_0 \tag{13-9}$$

For the cosmotron parameters this frequency is $f_z = 0.86 f_0$. These vertical oscillations are also mismatched to the orbital frequency; if amplitudes are sufficiently large and the beam is narrow, particles can pass above or below the inflector plates, even though the radial location of the particle orbit might be unfavorable. Such oscillations can be used to advantage by injecting the beam at a level above (or below) the median plane, to increase vertical amplitudes and improve the chance of missing the inflector plates. The number of free revolutions for the average ion can be increased in this way, improving the probability of capture in stable orbits.

The injection scheme described above is most efficient if ions are not being accelerated during injection. The radiofrequency accelerator can be turned on when the equilibrium orbit approaches the center of the chamber and can be brought up to full voltage within a few cycles if desired. By this time the entire chamber will be filled with oscillating particles, having a wide spread in amplitude and in phase.

In the cosmotron an unexpected perturbation of the remanent magnetic field simplified the injection problem and led to another technique for maximizing injection efficiency. It was found that the remanent median surface was not a plane in the region of the injection orbit, but was tilted upward. This distortion provides a mechanism for coupling between the vertical and horizontal betatron oscillations. In the cosmotron it was found that energy was removed from the radial oscillations at just the critical times to decrease the number of ions striking the inflector when the beam returned to its neighborhood. The magnitude of the remanent field perturbation was not exactly correct to obtain the optimum effect, so a few turns of the pole-face windings in this region of the orbit were powered and adjusted to give the desired degree of coupling. As a result, injection into the cosmotron results in almost no loss on the back of the inflector plate structure.

The 4-Mev Van de Graaff generator is a horizontal pressure-insulated electrostatic generator specifically designed and developed for operation at high pulse intensity (see Chap. 3). It produces a beam of about $\frac{3}{16}$ in. diam with an angular spread of $\pm 0.5 \times 10^{-3}$ radian. The ion source is the P.I.G. type developed at Berkeley (see Sec. 4-8) and produces pulses of up to 50 ma of hydrogen ions for about 100 μsec. Focusing of the high-intensity pulse is a problem differing considerably from the focusing of steady beams. The large positive space charge developed near the source aperture requires focusing fields different from those suitable for low-intensity operation. Voltage-stability problems also enter. Pulse-to-pulse voltages must be reproduced to a precision of about 0.2 per cent to stabilize injection conditions. This is done by operating with a low-intensity steady beam between pulses and using the analyzed "mass-2" beam of molecular hydrogen ions to control the voltage (see Sec. 3-8).

The potential of the generator terminal drops during the pulse because the ion current in the accelerating tube exceeds the charging current delivered by the belt, which is limited to about 300 μa. During a 100-μsec pulse of, say, 10 ma the 300-$\mu\mu$f capacitance of the terminal is lowered in potential by about 3000 volts, a 0.1 per cent drop. Furthermore, electron loading in the accelerating tube increases with operating voltage; at 4 Mev it can increase terminal current and cause a further drop in terminal potential. This decrease in injection energy during the pulse is opposite in sense to the rising magnetic field in the cosmotron orbit.

It results in shortening the effective injection interval and so in reducing the intensity of the injected pulse. In 1958 a pulsed capacitative liner was installed in the Van de Graaff generator to compensate for this effect. This liner is pulse-charged by a separate supply to maintain a steady terminal potential or can produce a rising voltage during the pulse, if desired.

The electrostatic inflector plates are located in a vacuum housing in a straight section. The beam from the Van de Graaff generator enters at a 30° angle to the equilibrium orbit and is deflected by this angle between electrodes which have a radius of curvature of 10 ft and an arc length of 5.2 ft. The two plates are spaced about 0.5 in. apart, and a dc potential difference of 20 to 30 kv is required to deflect the 3- to 4-Mev protons.

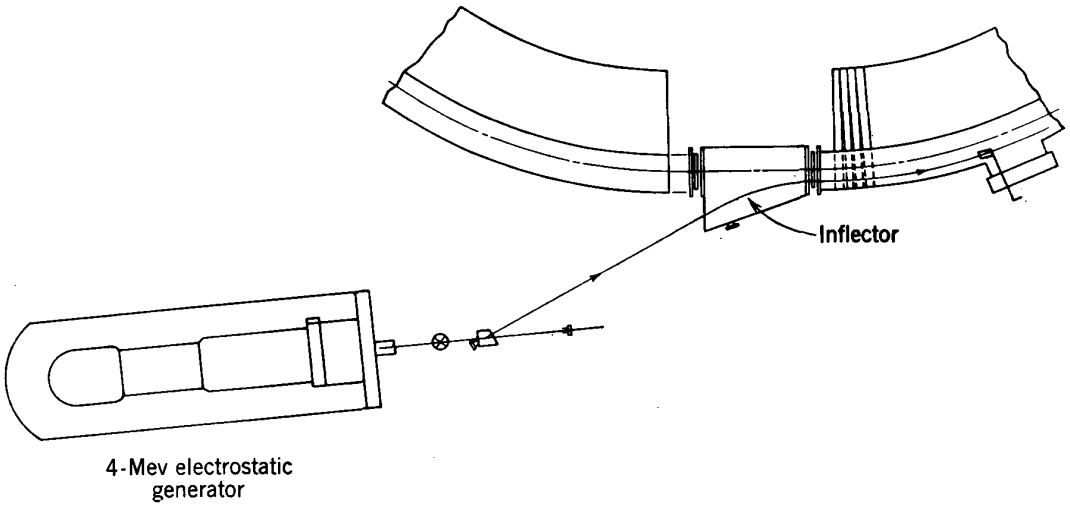

Fig. 13-13. Electrostatic inflector system for the cosmotron, using 4-Mev protons from an electrostatic generator.

The beam emerging from the inflector can be made accurately parallel to the equilibrium orbit by slight adjustments in the deflecting potential. The radial position of the exit end of the curved inflector channel can be varied by moving the inflector plate assembly on slides along the line of the entering proton beam from the Van de Graaff. This motion and other adjustments for elevation and alignment are controlled by mechanical devices with motors located outside the vacuum housing. Figure 13-13 shows a schematic view of the inflector system.

The energy spread of the 4-Mev proton beam from the electrostatic generator is of the order of ± 10 kv. This spread is equivalent to a band of equilibrium orbits in the magnet about 1.5 in. wide, centered on the mean orbit. The time required for an orbit to contract by this radial distance is about 25 μsec. For each value of energy the acceptance time interval is that required for the equilibrium orbit to contract from just inside the injector radius to the center of the chamber. This time is

about 200 μsec in the cosmotron, representing about 70 revolutions of the particles. The effect of the energy spread is to round off the beginning and end of the acceptance time interval over times of the order of 25 μsec.

The oscillations produced by angular divergence and beam width, along with the overlap resulting from the energy spread, reduce the effective acceptance interval. The capture probability will be a maximum at the center of this interval, decreasing to zero at the practical limits. With a long pulse overlapping this entire acceptance interval, the average capture probability is estimated to be about 10 per cent. A short pulse lasting for only a few revolutions and timed for the optimum location of the equilibrium orbit would have a higher probability of capture but lower total intensity. The need to start the rf acceleration slightly before equilibrium orbits pass the center of the chamber also reduces the length of the acceptance interval. The experimental optimum obtained by varying the pulse length and timing was found to be about 100 μsec, equivalent to about 30 turns. A current pulse of 1 ma would deliver 6×10^{11} particles into the orbit in this time.

When the rf field is applied to the accelerating gap, the particles will be set into synchronous phase oscillations, centered around that phase for which the energy gain per turn is correct to match the rise rate of the magnetic field. Since the particles will be uniformly distributed around the orbit after injection, only a small portion will have the azimuthal location which matches the synchronous phase. Most of the particles will be set into synchronous energy oscillations which will cause wide oscillations in the radial location of their equilibrium orbits. The equilibrium phase angle of 30° chosen for the cosmotron results in a range of acceptance into synchronous orbits of about 180° in azimuth, so only half the circulating particles could be captured. However, it has been shown that the particles injected in the orbit already have a wide spread in the initial amplitude and phase of their betatron oscillations, such that they essentially fill the available aperture. So the fraction captured in stable synchronous orbits within the useful aperture will be smaller than half. On the other hand, the frequency of synchronous oscillations is relatively low, such that the average particle takes about 1000 revolutions to complete a phase cycle. During this time some damping occurs, so some particles are salvaged. An over-all estimate is that about 20 per cent of the injected protons should be captured in synchronous orbits. If the number of protons injected is 6×10^{11} per pulse, as estimated above for a 1-ma source pulse, the number captured in synchronous orbits would be about 10^{11} protons/pulse. Beam intensities observed in operations are in good agreement with this estimate, but do not increase linearly with higher injection current. The reason for this is not yet understood.

As magnetic field rises and particle energy increases, the amplitudes of

the oscillations decrease. In Chap. 5 it was shown that the betatron amplitudes vary with $B^{-\frac{1}{2}}$. Amplitudes will have decreased to half by the time the field has increased to four times the injection value. Amplitudes may be increased temporarily by angular deviations due to gas scattering in the chamber, but will be continuously damped; gas-scattering losses should be negligible for energies above about 100 Mev. Synchronous amplitudes are also damped by the rising magnetic field, but at a slower rate, varying with $B^{-\frac{1}{4}}$ for these low energies. With further increase in field and in beam energy the intensity should remain, in principle, essentially constant.

To summarize, beam injection starts by filling the orbit with particles having a wide spread in oscillation amplitudes. Those particles which do not fall within the acceptance limits are lost against the chamber walls within the first betatron period, or within one to two turns. Then when the radiofrequency is applied, about 20 per cent are captured in stable synchronous orbits and the rest are lost to the walls during the first half of the first synchronous cycle or within about 500 turns. Further small losses can be anticipated during the next few synchronous cycles, and by gas scattering, up to an energy of about 100 Mev. Cathode-ray-tube displays of beam intensity in the orbit obtained from the pickup electrodes show that the intensity does, in fact, have the characteristics described above.

13-7. RADIOFREQUENCY ACCELERATOR

Performance requirements for the particle acceleration system were described in the earlier section on basic parameters. The particles must be supplied an energy increment on each turn determined by the rate of rise of magnetic field. The customary technique in synchronous acceleration is to apply a radiofrequency potential across a short insulated section in the metal vacuum chamber, located in a straight section. The applied frequency is either the fundamental orbital frequency of the particles or some preferred harmonic; in most proton synchrotrons the fundamental orbital frequency is used. This frequency increases during the 1-sec accelerating cycle, with increasing particle energy. In the cosmotron it extends from about 0.40 megacycle for injection at 4 Mev to 4.20 megacycles at maximum energy, following the schedule shown in Fig. 13-2.

In synchronous acceleration the voltage applied to the accelerating gap must exceed the average requirement of volts per turn to provide for a wide range in phase and energy oscillations. The choice of equilibrium phase angle, at which particles acquire the necessary volts per turn, determines the peak applied rf voltage. This choice in phase angle is a balance between the radial-aperture requirements and beam intensity.

In the cosmotron, it was taken as about 30°, for which the peak applied voltage is twice the volts per turn. This leads to energy oscillations during the synchronous cycle which have associated radial amplitudes of about ±8 in. at 4 Mev injection energy. In Chap. 9 it was shown that a synchronous phase angle of 30° led to a range of acceptance into synchronous orbits of about 180° in phase, which means that about half the particles distributed uniformly around the orbit could be accepted, if the radial aperture were sufficient to accept the radial oscillations. The applied voltage requirements change during the accelerating cycle, following the rate of rise of magnetic field. The volts per turn needed in the cosmotron were shown in Fig. 13-3. So the peak applied voltage must start at about 2000 volts (at 0.40 megacycle) and drop to about 1400 volts (at 4.20 megacycles) at high energy.

These accelerating potentials are modest, as compared with those used in cyclotrons or other resonance accelerators in which the time for acceleration is shorter and the number of accelerations is much smaller. This is one of the primary advantages of the synchronous acceleration principle. However, the wide range of frequency variation required and the need for the frequency to follow a predetermined schedule are unique to the proton synchrotron and pose some of the most difficult problems.

If the accelerating system is to be resonant, it must be tuned over the entire frequency sweep. A resonant-cavity circuit such as is used for the electron synchrotron would require excessive power to produce the necessary potentials when off resonance. A mechanically tuned system, similar to the circuit of a synchrocyclotron which uses a rotating variable capacitor, would have to cover a frequency range of about 12 to 1, a difficult design problem. Furthermore, the variable-capacitor plates would have to be precisely shaped to fit the predetermined time schedule. If such a system were broad-banded, however, the correct frequency schedule could be impressed on it by an external oscillator, although the efficiency of such a system is low. Broad-banding involves the use of a sufficiently high impedance system that it can operate untuned over the entire frequency range. An electronically tuned oscillator can then be used to impress the correct frequency schedule on the accelerating system. The primary problem is the design of the high-impedance circuit. This is the approach used for the cosmotron, and the method has been to use ferromagnetic loading materials to give the desired high impedance.

The accelerating system for the cosmotron is essentially a radiofrequency transformer. A ferromagnetic core surrounds the particle orbit at one of the straight sections. The core material is chosen to have a useful magnetic permeability at frequencies up to the maximum 4.20 megacycles. Power is fed to a primary winding from a radiofrequency power supply electrically tuned over the frequency range. The particle orbits can be visualized as one-turn secondaries linking the transformer

core. Each time a particle traverses the core it experiences an electromotive force equivalent to that which would obtain in a one-turn secondary winding of the transformer.

Another description of the accelerating system is that it is an induction accelerator depending on the time rate of change of flux linking the particle orbit, as in the betatron. During most of its path the proton is within a grounded metal vacuum chamber; the only time it can experience the electromotive force induced by the changing flux is while it is traversing the insulating gap at the location of the flux core. The rate of change of flux, $d\phi/dt$, within the magnetic core linking the orbit while the particle is crossing the gap determines the emf and so the energy acquired by the particle. In this sense the ferromagnetic core linking the orbit is equivalent to the flux core in a betatron.

A third way of describing the operation of the accelerating system is to say that it is a cavity resonator heavily loaded with material of high magnetic permeability and high dielectric constant. The cavity resonator is the copper shield around the core, and the potential is developed across the insulated gap in the vacuum chamber. If it were air-filled, this cavity would be resonant at an extremely high frequency because of its small dimensions. If loaded with low-loss high-dielectric material, as for the quarter-wave resonators used in the electron synchrotron, the resonant frequency would be lower but the impedance would also be low at resonance. When loaded with ferromagnetic material, the resonant frequency lies in the band of impressed frequencies; but the cavity is so broadly resonant and has such high impedance that it can be driven efficiently at frequencies far off its resonance.

The basic problem is the choice of ferromagnetic loading material. Iron cores, even if laminated, are subject to eddy-current effects which restrict their use to frequencies of less than 100 kc. Powdered iron and permalloy foil cores can be made to extend the frequency range to about 1 megacycle. But for higher frequencies even finely laminated metallic cores are impractical because of high costs and inefficient power transformation.

The core material chosen is a ferromagnetic ferrite, which is a semiconductor with conductivity about 10^{-7} times that for metals, so that eddy-current limitations are extended to much higher frequencies, and with an effective magnetic permeability of 500 to 1000 in the frequency range desired. This type of ferromagnetic material has been developed in several industrial laboratories within the past few years for use in pulse transformers, high-frequency chokes, and magnetic deflection yokes for television tubes. It is available under several trade names such as Ferroxcube and Ferramic. The electrical and magnetic properties of such ferrites have been studied in some detail in the various commercial laboratories. A study by Blewett, Plotkin, and Blewett[12] of the Brook-

haven staff discusses the properties of ferrites with particular regard to their application to the cosmotron. Since its publication innumerable studies of various ferrites have been printed in the engineering and scientific literature. The cosmotron application was, however, one of the first in the United States and was influential in bringing these interesting materials to public attention.

The material of the core is a synthetic manganese-zinc-ferrite, formed by the replacement of two of the FeO groups in Fe_3O_4 by the other metallic oxides. The oxides of iron and of the other metals are finely powdered in a ball mill, mixed in the correct proportions with an organic binder, and extruded or pressed to the desired shape, making due allowance for 15 to 20 per cent shrinkage which takes place on firing. The material at this stage has the appearance of molding clay, is reddish in color, and is not yet ferromagnetic. The shapes are then fired in a controlled oxygen atmosphere at temperatures below the melting point, so recrystallization occurs. The final product is a hard, black ceramic similar to porcelain. Electrically it is a semiconductor, and magnetically it is now ferromagnetic. It can be ground like glass or porcelain to obtain precise dimensions.

Different properties can be achieved by varying the proportions and the firing cycle. A typical ferrite has a saturation flux density of 2000 to 3000 gauss, a Curie point at about 400°K, a permeability of about 1000 at low frequencies (decreasing to about 500 at 5 megacycles), and a very high dielectric constant. In general, ferrites which have high permeability have a lower frequency cutoff, and those with good high-frequency properties have lower permeability. The losses in the material can be described by the Q of a coil wound on a toroid-shaped sample. For the material used in the cosmotron the Q varies from over 10 at 0.35 megacycle to 1.6 at 4.2 megacycles.

The 2800 lb of ferrite needed for the core was obtained from two sources, because of uncertainties in the production schedules and properties. The North American Philips Company supplied Ferroxcube III in the form of rectangular blocks 2 cm thick, surface-ground to a smooth finish. These blocks were assembled and cemented together in the shape of a "picture frame" with a total air gap of less than 0.001 in. The General Ceramics and Steatite Corporation supplied a similar material, Ferramic, in the form of extruded rods about 1 cm in diameter. These rods were supported in frames, the ends bevel-ground, and also cemented to form picture-frame units. Figure 13-14 shows the assembly of the two types of ferrite material. Although the amount of ferrite ordered from each supplier was sufficient by itself, both lots were included in the final assembly to increase the efficiency of the accelerator.

The primary winding, of $\frac{1}{4}$-in. copper rod, is distributed about the core for electrical efficiency, but is equivalent to a one-turn coil. The entire

core, except for the insulating gap in the straight-section vacuum chamber, is enclosed by a copper shield. Because of the high dielectric constants, such a large assembly might develop standing waves in the transverse dimensions unless care is taken to detune such modes by shielding or by physical spacing. The picture-frame core sections are separated by air spaces which serve the dual purpose of permitting forced-air cooling and of suppressing undesired modes of oscillation.

The amplifier which supplies the frequency-modulated excitation to the ferrite accelerator unit is a broad-banded system with an output power level of about 100 kw. The high-level amplifier itself has four stages of push-pull amplifiers, with two Machlett 5681 triodes rated at

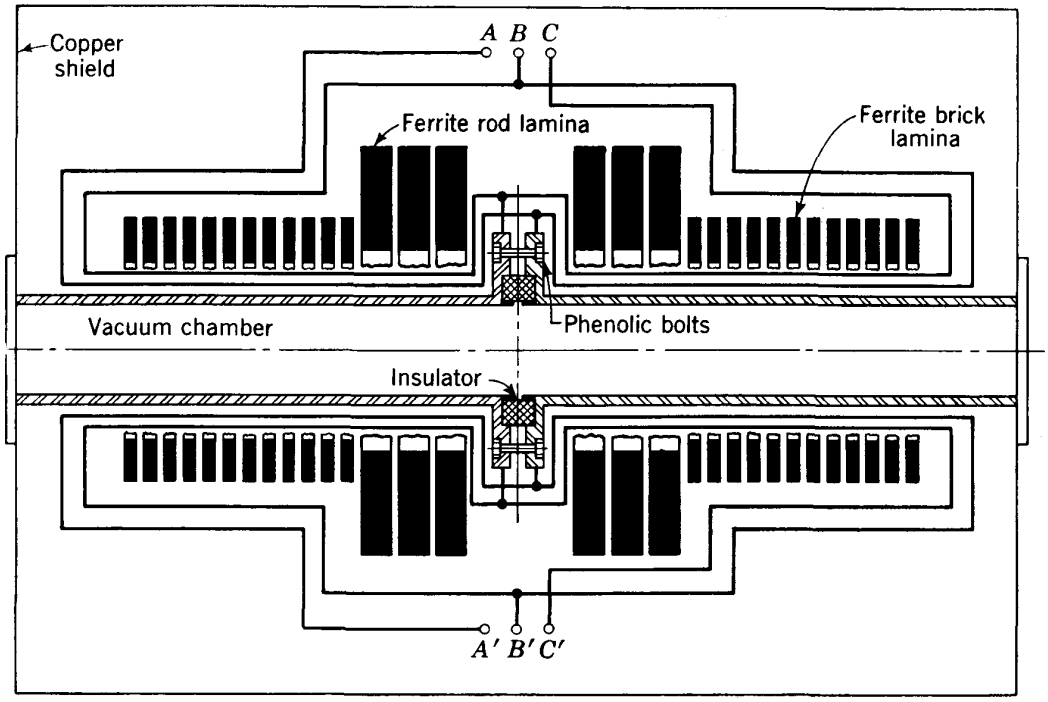

Fig. 13-14. Ferrite-core accelerating unit for the cosmotron.

75 kw plate dissipation each, in the final stage. It takes its excitation from the output of an intermediate amplifier which delivers a signal of about 15 volts through 70-ohm transmission-line cable from the central circuit room to the location of the accelerator unit. The intermediate amplifier is driven by a low-level (2-volt) signal developed by the frequency control system and master oscillator to be described in the following section. Full details are given in the report by the cosmotron staff.[12]

Continuous measurement of the gap voltage is used to observe waveform and amplitude during the cycle. For this purpose diodes are connected across the gap, or from one side of the gap to ground. One is used as a peak-reading voltmeter, another with a voltage divider is used for amplitude control, and a third with a short-time-constant circuit is used

to provide oscilloscope presentation of the gap voltage to check the waveform.

The accelerating unit in the bevatron at the University of California is a drift tube—a section of hollow rectangular conductor surrounding the beam aperture—located in one of the straight sections. If such a drift tube were extended around half of a synchronous wavelength (half of the circumference when the harmonic order $h = 1$, as in the bevatron), the full rf potential would be effective on both entry and exit, as in a cyclotron D. Space limitations in the bevatron prevent this configuration, so the drift tube is limited to a shorter length which can be contained in the straight-section vacuum chamber. Consequently the drift-tube voltage must be higher (by about a factor of 5) than the energy gain required per revolution. As the particles enter the drift tube, they are accelerated; as they leave the other end, they are decelerated. Because of the phase shift during the passage through the drift tube, the deceleration is less than the acceleration, and a net energy gain results.

The drift tube forms a resonant circuit with a ferrite-loaded inductor, and the circuit is driven by a power amplifier at the frequency of revolution of the protons. The inductor is tuned by varying a bias current in a primary winding which partially saturates the ferrite core, and the bias current is controlled to produce a variable-frequency cycle exactly matching the increasing frequency of particle motion.

13-8. FREQUENCY CONTROL IN THE COSMOTRON

The frequency of the accelerating electric field must be held to within about 0.2 per cent of the scheduled value during the cycle in order to limit the radial excursions of the equilibrium orbit and to prevent loss of particles to the walls of the chamber. The cycle must be triggered by a signal derived from the magnetic field and must start at the frequency which is compatible with the field at injection. The precision required is highest at the start of the cycle when oscillation amplitudes are greatest.

The allowed frequency error can be estimated from the magnitude of the allowable radial excursion. Equation (13-2) gives the simple form for orbital frequency. When this is modified for the effect of straight sections [Eq. (13-3)] and for the variation of magnetic field with radius, we have

$$f = \frac{c^2 e B_0}{2\pi(W_0 + T)} \frac{2\pi R_0}{2\pi R_0 + 4L} \left(\frac{R_0}{r}\right)^n \tag{13-10}$$

By differentiation and substitution, we find the frequency error associated with a given allowed radial deviation:

$$\frac{df}{f} = -\left[n + \frac{T(T + 2W_0)}{(W_0 + T)^2}\right] \frac{dr}{R_0} \tag{13-11}$$

Evaluation for a change in radius of 1 in., in the cosmotron, at injection, shows a frequency shift of 0.17 per cent; at maximum energy the shift is 0.60 per cent. In a similar manner the frequency error can be analyzed in terms of the deviation from ideal injection timing. It is found that a frequency error of 0.1 per cent corresponds to an error in timing of 16 μsec.

The variable-frequency signal is generated by an electronically tuned oscillator in which the tuning is accomplished by saturation of a small ferrite core in the inductance of the tank circuit.[12] The varying inductance changes the resonant frequency of this low-level oscillator, depending on the magnitude of the dc current in a winding used to saturate the core. The saturable inductance is a toroid of small radial thickness (to minimize eddy-current effects at high frequencies) ground from blocks of Ferroxcube and enclosed in a doughnut-shaped metallic jacket. The jacket serves as an oil container to maintain constant temperature and is made in two sections separated by a gasket to prevent circulating currents. The two windings, one for the dc saturating current and one for the radiofrequency signal, are wound to have minimum coupling. The rf winding is threaded through a rectangular hole cut in the side of the toroid, with a figure-8 winding which cancels out the dc flux. The dc winding is wound around the enclosing doughnut-shaped jacket, threaded through the toroid to produce the saturating flux in the core. Calibration studies have shown that the permeability varies from about 1000 to less than 10 as the magnetizing field is raised from zero to 20 amp-turns/cm in the dc windings. So the toroid inductance can be varied over a factor of 100.

The dc current in the saturating winding is controlled by a signal from a pickup in the magnetic field to produce the correct frequency-field function (see Fig. 13-2). A diode network with 28 parallel circuits of different biases is used to produce a signal having the proper output-current-versus-field function. This output current is used to saturate the core. By tuning the bias voltages and amplitudes of these parallel diode circuits, a cycle can be produced which is within 0.1 per cent of the calculated frequency cycle over the full 1-sec interval. Furthermore, the controls can be used to trim the shape of the cycle at will.

The "precut" frequency cycle established by the diode network described above is found to be extremely stable. Negative feedback in the amplifier is used to produce an amplitude control which is within 4 per cent over the cycle. This type of frequency control for the cosmotron accelerator unit depends only on the observed magnetic field during each cycle and so is independent of field variations from cycle to cycle.

The method used to start the frequency cycle on the correct frequency and at the correct time to match injection conditions is to obtain a short-pulse trigger signal from a peaking strip in the magnetic field (see Sec.

8-8). The time can be varied by varying the peaking-strip bias, which is calibrated in terms of the magnetic field. The frequency cycle is started at a magnetic field and at a frequency well below the usual injection energy, so the cycle is initiated and any transients have decayed before the protons are injected. This makes the frequency cycle independent of the precise value of injection energy or injection timing.

An alternative frequency monitoring system has also been developed, which takes its information from the radial position of the proton orbit. After the ions have been bunched and oscillations have damped out, which requires about 50 msec, the radial location of the mean orbit can be observed and used as a measure of the frequency error. A pair of hollow pickup electrodes, mounted radially inside and outside the chamber at one of the straight sections, have voltage pulses induced on them by the electrostatic charge of the bunched beam as it passes through the electrodes. The relative magnitudes of the pulses on the two electrodes will be different, depending on the radial location of the orbit. An error signal which can be used to correct the frequency cycle can be derived from this difference. At first glance it would appear simplest to apply the radial pickup electrode signal directly to the diode network system controlling the frequency cycle. A more sophisticated analysis reveals the fact that such a double-element system is subject to instability and loss of particles.

It is now agreed that it is preferable to combine the radial information with a system that does not use a programmed oscillator but derives the initial rf signal from the beam itself. If the beam is initially bunched by a frequency program shortly after injection, the master oscillator can be turned off and replaced by the induced signal from an electrode through which the bunched beam passes. Stability is obtained by controlling the phase of the accelerating signal by a phase shifter which, in turn, is controlled by the signal from the radial pickup electrodes. This system was tested on the cosmotron in 1953 by G. K. Green and E. C. Raka; its operation was quite stable and satisfactory. A short description is available in the *Handbuch* article of Green and Courant.[20]

Coherent phase oscillations in the cosmotron excited by noise in the frequency-control system were responsible for loss of some 50 per cent of the beam during acceleration until a phase-oscillation damping system, invented by E. J. Rogers,[25] was incorporated. In this system, phase differences between the rf accelerating field and the signal induced in the beam pickup electrodes are detected and fed back to the frequency control of the master oscillator in the required sense to oppose sudden phase shifts. This system improved the rf stability to the point where no detectable beam loss takes place after the initial capture process is complete.

The beam pickup electrodes just mentioned are mounted in one of the

straight sections. Electrodes are located inside and outside the orbit and yield induced signals which give a measure of the radial position of the beam and which thus enable the operator to apply necessary corrections manually to the frequency-determining network to keep the beam centered. Other electrodes above and below the orbit give an indication of vertical beam position during the accelerating cycle. The pickup electrode shapes are shown in Fig. 13-15.

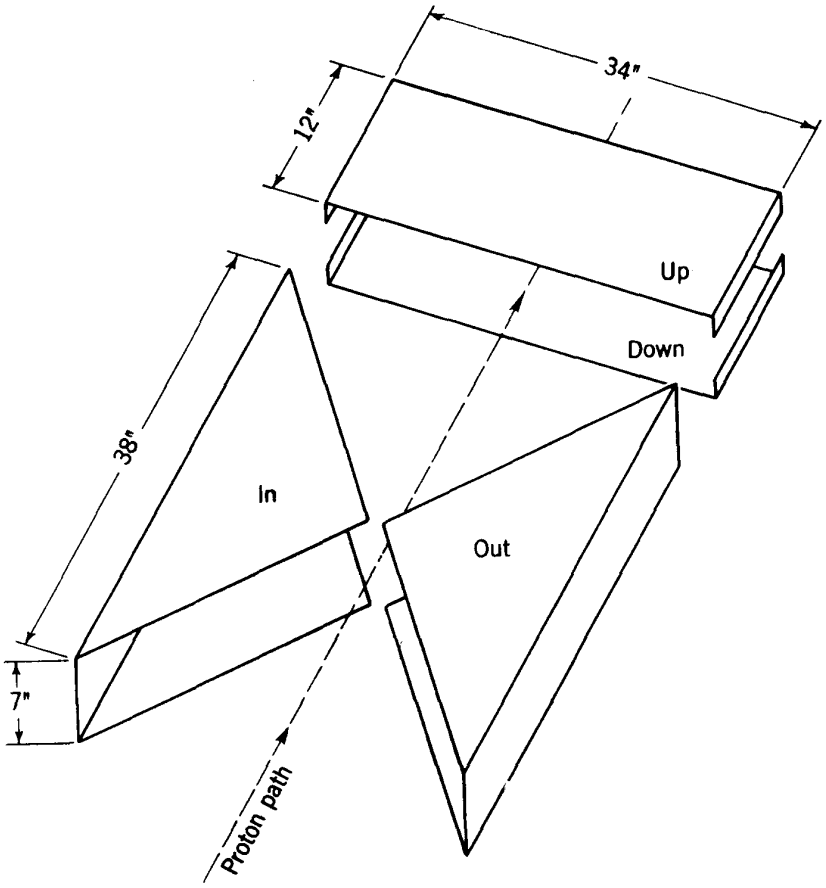

Fig. 13-15. Arrangement of pickup electrodes in the cosmotron.

13-9. COSMOTRON VACUUM CHAMBER

The vacuum chamber to contain the ion orbits during acceleration is subject to very stringent physical requirements. It must be entirely nonmagnetic so as not to disturb the carefully designed magnetic fields. It must also be constructed in such a way that eddy currents induced in metallic components of the chamber do not disturb the field; this limitation applies primarily to the field at injection. Not only must it be vacuumtight in the ordinary sense of having no air leaks, but all joints should be readily accessible for leak testing and gaskets should be made of materials having low vapor pressure. The physical dimensions are

also severely restricted to maintain the largest possible internal aperture for ion oscillations. So top and bottom walls, at least, must be physically thin and mechanically strong.

A natural division of the vacuum chamber is into four quadrants fitting between magnet pole faces, with four connecting straight sections. The internal aperture required in the cosmotron pole gap is about 6 by 30 in., so small that flow resistance limits the pumping speed. Pump stations must be distributed around the periphery to provide the necessary pumping speed to attain the desired ultimate pressure within the chamber. These considerations led to the choice of 12 pumping stations for the cosmotron chamber, 3 in each quadrant. Pump-out apertures of 6 by 40 in. are located in the outer wall of the chamber, connecting to the pump manifolds. Incidentally, the straight sections are free of pumps and available for other apparatus.

The quadrant vacuum chambers are constructed of bars and laminations of nonmagnetic stainless steel; rubber sheets form the vacuum wall. The steel structure supplies mechanical strength to support the atmospheric pressure load, and a rubber diaphragm bridges the narrow gaps between the steel lamination bars. The structure is assembled on two 1- by 8-in. bars on edge, preformed in 90° arcs of 342 and 378 in. radius, spaced with rectangular frames at the quadrant ends (where magnetic field is small). Bridged across the 36-in. chamber width are several hundred taper-shaped steel bars which form the top and bottom surfaces of the quadrant box structure. The 2-in. width of the bars limits eddy currents in the surface. Calculations of the eddy currents induced in the chosen high-resistivity stainless steel justify this choice of lamination thickness; model tests and operational experience bear out the calculations. The bars are attached by insulated pins at each end, and the conductivity of the rubber sheet is adequate to maintain dc ground potential to prevent accumulation of static charge.

The $\frac{1}{8}$-in. sheet material covering the top and bottom surfaces is Myvaseal rubber, produced by the Distillation Products Company. It is an artificial rubber having a vapor pressure of less than 1×10^{-7} mm Hg, considerably better in this respect than rubbers or plastics previously used in vacuum seals. Clamp bars are located around the periphery of the quadrant surfaces, and they press the sheet against the steel walls with an intermediate gasket.

Figure 13-16 is a schematic cross section of the quadrant chamber. Under atmospheric pressure the tapered bars deflect about $\frac{1}{4}$ in. The structure is mechanically designed so that no unit exceeds 50 per cent of the yield stress of the steel, but also arranged to approach this 50 per cent limit at every critical point in order to keep the thickness of metal to a minimum. The net internal clearance between bars under vacuum is about 6 in.

The gaskets used for sealing this box structure have a "dumbbell" cross section forming a double seal with a pump-out channel between seals to use for vacuum tests. The material used is also Myvaseal, extruded into the dumbbell shape. The triple joints at the box corners are sealed with molded sections of the same gasket. Many pump-out leads are provided to test the region between gaskets; all of these leads are made available at the quadrant ends or along the front wall of the chamber.

The same gasket design and technique is used to seal the ends and face-plate apertures of the straight-section vacuum boxes. In addition, flap valves located in the straight-section boxes can be closed to isolate each quadrant for independent vacuum testing or measurements.

Scattering by the residual gas in the vacuum chamber will result in some loss of ions from the beam. A series of theoretical studies of this problem was initiated by Blachman and Courant[10] as applied to the

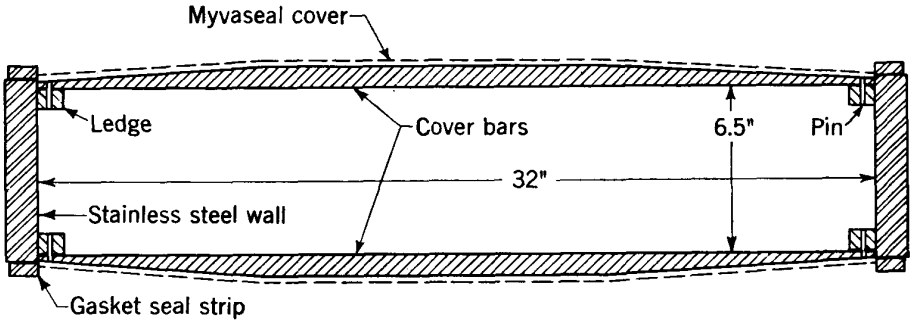

Fig. 13-16. Cross section of quadrant vacuum chamber for the cosmotron.

cosmotron conditions. Most of the scattering occurs within the first thousand revolutions, when ion energy is small and oscillation amplitudes are large. In each single-scattering process the proton is deviated from its orbit by a small angle. For most particles this angle is small enough to be within the aperture of the vacuum chamber. A small fraction have single-scattering angles sufficient to cause the particles to strike the chamber walls. Multiple scattering is also considered, and results in further loss of particles. Damping of the oscillation amplitudes in the increasing magnetic field, and the decreasing probability of scattering with increasing energy, eventually reduce scattering amplitudes so that no significant loss occurs after the protons reach an energy of about 100 Mev. The magnitude of scattering losses decreases with increased injection energy, and this is one of the chief reasons for using the maximum practical energy at injection.

The most significant factors in the calculation are the gas pressure and composition of this residual gas, proton energy and the rate of acceleration per turn, and the n value and physical dimensions which define the

effective aperture of the chamber. The results of the calculation are expressed in terms of the pressure for 10 per cent loss or for 50 per cent loss of protons. For cosmotron injection conditions these results are[12]

$$P \text{ (10 per cent loss)} = 0.8 \times 10^{-5} \text{ mm Hg}$$
$$P \text{ (50 per cent loss)} = 1.4 \times 10^{-5} \text{ mm Hg}$$

The vacuum pumping system consists of 12 identical high-vacuum pump stations, distributed around the chamber with three on each quadrant, located in the trench that surrounds the magnet ring. Each station

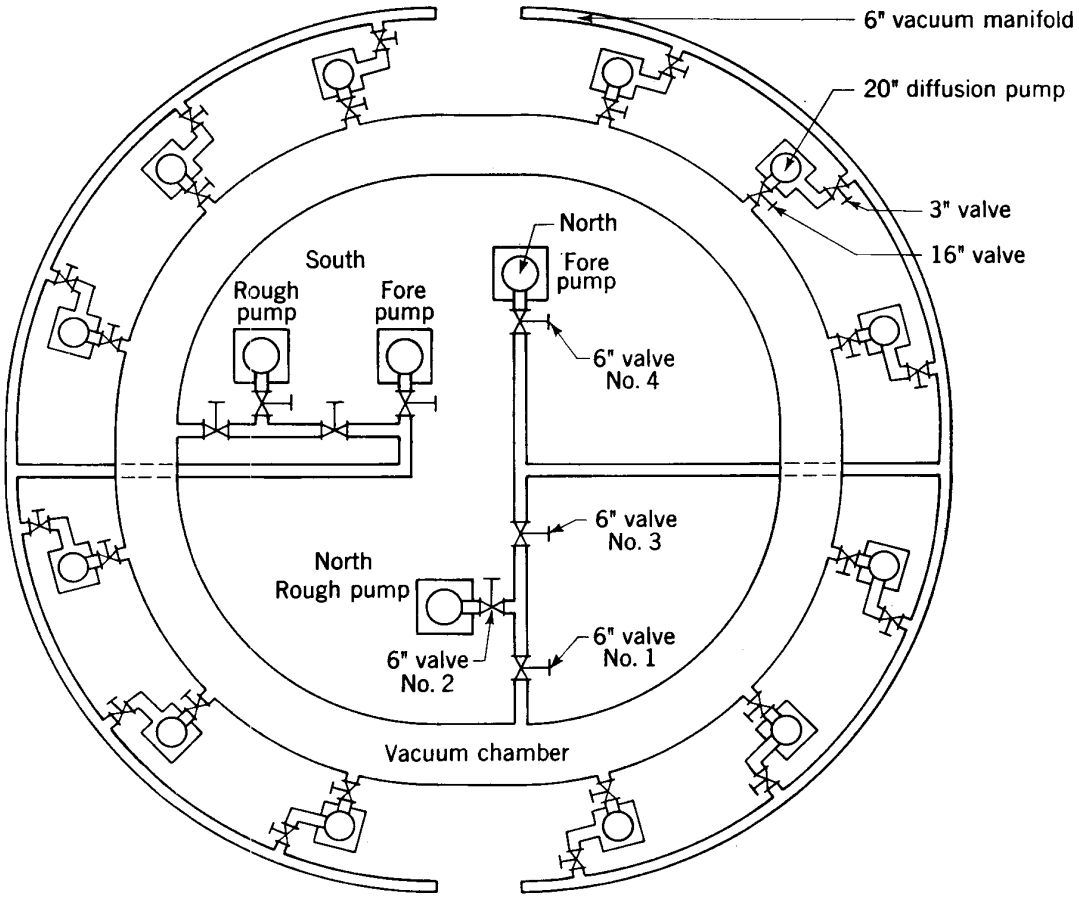

Fig. 13-17. Schematic diagram of the vacuum pumping system for the cosmotron.

is located at a manifold or plenum chamber attached to the quadrant vacuum chamber, and each manifold is equipped with a high-vacuum close-off valve, so pump units can be removed or interchanged without losing vacuum in the main chamber. A pump unit consists of a Westinghouse 20-in. oil-diffusion pump, an 8-in. booster diffusion pump, a cooled baffle and refrigeration compressor, and all associated electric equipment including pump heaters and vacuum gauges. A 6-in.-diam fore-vacuum manifold in the trench connects to four mechanical pumps located in the center of the magnet ring. Figure 13-17 is a schematic drawing of the

pumping system. A circular bank of pilot lights on the control panel, which looks much like the figure, shows which valves are open or closed so the operator can monitor pumping operations.

The 20-in. diffusion pumps are rated at 7000 liters/sec speed at 1×10^{-5} mm Hg air pressure and are equipped with three-stage fractionating jets. The oils used have been Lytton-C or Myvane-20, petroleum-base oils which have similar properties. A specially designed baffle for the large oil-diffusion pump prevents oil vapor from diffusing back into the manifold and chamber; it can be cooled by the mechanical refrigerator to $-40°C$. Minimum pressures observed in the cosmotron vacuum chamber are 0.6×10^{-5} mm Hg without refrigeration and 0.4×10^{-5} mm when the baffles were cooled, after several months of continuous pumping. As a consequence, very little loss of beam intensity due to gas scattering is observed.

Vacuum leak testing and sealing is a major problem in all accelerators. Techniques for reducing the time lost on leak hunting are essential in such a large and complicated system as the cosmotron. As a start, all joints and seals were designed to be mechanically sound and trustworthy. Furthermore, all major assembly joints and port closures have a double gasket seal, using the dumbbell-shaped extruded gasket described above. The space between gasket seals is tapped to allow circulation of helium in this space or connection to a rough-vacuum pump. The helium-flow leak-detector technique, using a mass spectrograph, covers essentially every inch of gasket closure in the chamber. Leaks are readily detected, even those so small that when sealed, no improvement in chamber pressure is noticeable. For larger leaks, if the maintenance problem of opening and resealing is too time-consuming, a rough-vacuum pump on the helium channel will suffice until repairs can be made. Alarm-type vacuum gauges are located at each pump station and can be set to call the attention of the operator to any failure in the pumping system. In the event of electrical power failure, air-operated valves will close, supplied from compressed-air storage bottles. If faults develop in one of the pumping units, valves can be closed and a spare unit inserted without loss of vacuum. The vacuum controls system is made fully automatic by a complete system of interlocks which provide suitable time delays for the sequential scheduling required when pumps are turned on.

13-10. INTERNAL TARGETS USED IN THE COSMOTRON

The basic design of a C magnet with the vacuum chamber available around the entire periphery provides a favorable situation for performing experiments within the chamber, using internal targets. This advantage was recognized from the start and was one of the primary reasons for the choice of magnet structure. Another advantage of the cosmotron over

electron synchrotrons is the long acceleration interval after injection, although this feature also reduces average beam intensity. With the 1-sec interval it is possible to insert electrodes, magnetic fields, or probe targets needed for observations, without having them in place to distort the fields or interrupt the beam at injection. By 0.1 sec the ions reach an energy of 300 Mev and the radial oscillations are damped to small amplitude around the central orbit. In the time remaining, targets and other devices can be inserted.

When the protons reach maximum energy, they are bunched tightly about the equilibrium orbit. Final beam dimensions are observed to be ¼ in. high by 2 in. wide, and the beam can be located wherever desired across the radial width of the uniform-field region by adjustments of the frequency cycle. The bundle of ions includes a synchronous phase spread occupying about 90° in azimuth.

The orbit can be expanded or contracted by a small variation in applied frequency. The maximum rate of expansion or contraction depends on the magnitude of the accelerating volts per turn. With an average value of 600 volts per turn required for resonance, and a peak rf potential of, say, 1400 volts, the maximum possible increase in energy per turn would be 800 ev. The practical value would be much smaller, because of the necessity of maintaining synchronous stability. Assuming expansion at the rate of 500 volts per turn, the increase in radius would be 0.0005 in. per turn. Thus, it would require 2000 revolutions or 0.5 msec to expand the orbit by 1 in., or about 3 msec to move the orbit 6 in. to intercept a target inserted to that location. Furthermore, it would require 4000 revolutions to sweep the 2-in. width of the beam across the target. Protons would strike the target in a sequence of some 4000 pulses at 4.2 megacycles frequency: each pulse would be about one-fourth of the cyclic period or 0.05 μsec duration.

Orbit contraction can be accomplished somewhat faster, by as much as 1000 volts per turn, or 0.001 in. per turn, by using frequency modulation. An alternative is to turn off the rf oscillator and allow the beam to contract while the magnetic field still increases. Although radial stability disappears for regions outside the $n = 0.8$ limit, vertical stability remains. So ions which have contracted inside the limit of uniform-n magnetic field are still well-focused vertically and spiral inward on the median plane. A target which is permanently mounted just inside the inner wall of the chamber will intercept the entire contracting beam. In practice, such a permanent target can be located on the back (inner) surface of one of the straight-section vacuum chambers.

A wire target has been used successfully without expanding or contracting the beam. The wire is mounted on a shaft above beam level which can be quickly rotated to turn the wire down into the center of the chamber. Only a small fraction of the particles in the diffuse beam will

strike the wire in any one revolution. Those that do strike the wire will have a rather small probability of making a nuclear collision; most of them will be reduced in energy or scattered through very small angles. Except for a very small fraction scattered through angles large enough to be thrown out of the chamber, the particles will be reaccelerated through many turns before again striking the wire. In this way the ions strike the wire many times, on the average, multiplying the effective thickness of target. Eventually, the small wire will clean up the entire beam, spread over tens of thousands of revolutions. The efficiency of the wire target is estimated as about 10 per cent.

Ram-in targets have been developed which can be thrust into position well inside either the inner or outer wall of the chamber in a very short time, using pneumatic cylinders. Such targets are normally located in one of the straight-section vacuum chambers.

Experiments using electronic particle detection are best served with very long output times, representing many thousands of revolutions. The slow-clean-up type of targets described above is useful, frequently aided by very slow rates of orbit contraction. The longest output pulse obtained is about 50 msec, representing 200,000 revolutions.

When still longer beam pulses are desired, it will be necessary to "flat-top" the magnetic field, that is, to maintain the field at its peak value for an appreciable period such as 0.1 sec while the beam is brought slowly to a target. Although flat-topping the field does not appear too difficult, additional problems are introduced by the necessity for simultaneous flat topping of the pole-face-winding current. In 1961 these problems had not yet been solved, but were receiving intensive study.

For other experiments very short beam pulses are desired, such as those utilizing time-of-flight techniques to observe very short lifetime processes. The shortest pulse possible by the method of contracting the beam against a target is about 0.1 msec.

13-11. EJECTION OF AN EMERGENT BEAM

The full potentiality of the proton synchrotron can be realized only when the high-energy protons can be ejected from the magnetic field as an emergent beam. This goal was included in the earliest plans and was one of the important reasons for the arrangement of magnet quadrants and field-free straight sections. It was anticipated that the straight sections would be useful for the apparatus required to produce an external beam of protons.

Several methods were available, based on analogous beam-removal systems in other magnetic accelerators. Among those considered was the magnetic peeler, used so effectively in the synchrocyclotron. Resonant build-up of radial free oscillations is another possibility which has

been equally useful, and it was considered seriously for the cosmotron. The method chosen, which has been successfully applied to the cosmotron[26] and has also been proposed for the bevatron,[27] goes back to first principles and straightforward techniques.

The basic technique proposed by Piccioni et al.[26] utilizes the energy reduction in a target to displace the proton beam so that it can traverse an auxiliary magnetic field placed just inside the usual beam aperture in a straight section. This auxiliary magnetic field then deflects the beam outward so strongly that it emerges about one quadrant later. In the original proposal, a second magnet outside the usual beam aperture was to be used to provide a further outward deflection and to focus the divergent beam. Later it was shown that a stronger deflection at the

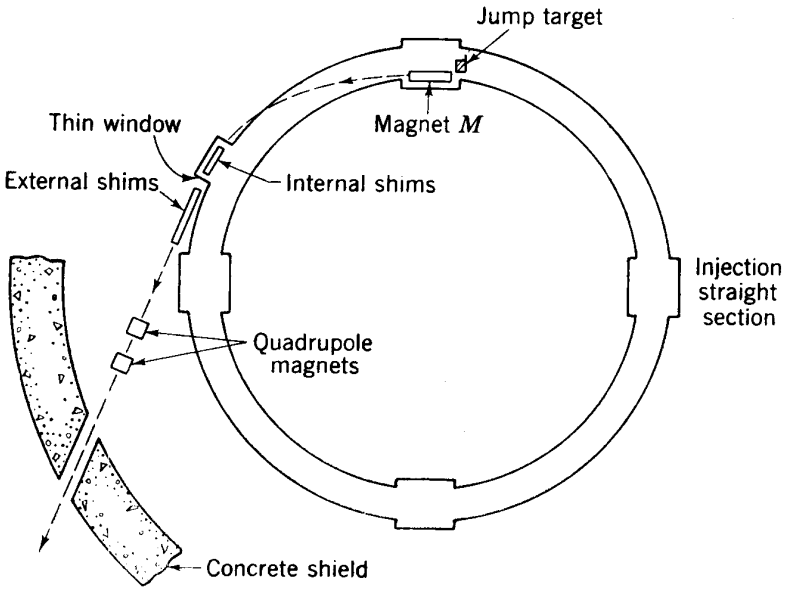

Fig. 13-18. Schematic diagram of the beam extraction system of the cosmotron. See text for description.

first magnet, together with selected field-distorting shims at the exit point, was adequate for extraction.

The "jump target" used for the original reduction in beam energy is a double structure. A beryllium "lip" 0.048 in. thick extends ¼ in. outward toward the beam from the main target, which is a beryllium block about ¾ in. thick in the azimuthal direction. By turning off the rf accelerating signal, the rising magnetic field causes the beam to contract in radius until those particles with maximum betatron oscillations strike the lip. The first effect of the lip is to reduce the amplitude of betatron oscillation, since the reduction in energy by ionization loss in the beryllium shifts the radius of the individual equilibrium orbit inward. When the betatron oscillation is effectively damped out, further energy loss causes the equilibrium orbit to contract and to pass through the thick

body of the main target. This results in a much larger energy loss and, unfortunately, in some energy spread (the Landau effect).[28] The average energy loss in the ¾-in. Be target causes a decrease in equilibrium orbit radius of several inches, the precise amount depending on the n value. To make this jump as large as possible, the field shape is modified by changing pole-face winding current to give an n value as close as possible to 0.8, at which radial instability occurs. Under these conditions the beam is displaced inward about 4.5 in. one revolution later and enters the gap of the auxiliary magnet, which is located in the same straight section as the jump target.

The arrangement of components is shown in Fig. 13-18, which also indicates the beam path after leaving the deflecting magnet. The beam emerges at a point about 75° downstream from the magnet through one of the pumping manifolds. Since the normal stray field of the cosmotron magnet would induce strong nonlinear defocusing of the beam, the stray field at the point of emergence is corrected by a set of steel shims carefully tailored to avoid disturbance of the field in the main magnet gap. The beam emerges through a thin aluminum window and is finally focused by a pair of quadrupole magnets. At a distance of 35 ft from the quadrupoles most of the beam is included in a circle 2 in. in diameter. The contour of half-intensity in the beam pattern is a circle approximately 1 in. in diameter. As much as 50 per cent of the circulating beam has been extracted in this fashion.

13-12. BEAM ANALYSIS AND USE

Use of the high-energy particle beams for research in nuclear physics or in the study of particle interactions is the ultimate purpose of any accelerator. Experiments should be planned as far in advance as possible, and the design of the machine should be adapted to provide the greatest utility and flexibility in research operations. Although this volume has dealt mainly with the technical and engineering problems of accelerators as electromagnetic machines, it should be clear that the ultimate goal is the efficient use of the particle beams. The proton synchrotron provides an opportunity to illustrate the ways in which the planned experimental use influences the basic design of the machine, and also how it develops the need for major modifications.

The cosmotron was designed at a time when the production and study of the properties of mesons was considered the most immediate problem. However, plans included the study of all known types of radiation, and a thorough analysis was made of all possible particle trajectories emerging from internal targets. Trajectories were computed for mesons of a wide range in energy, scattered protons, neutrons, γ rays, etc., for various target locations. These studies strongly influenced the basic design.

They influenced the choice of proton energy and indicated the advantage of a C-shaped magnet which would allow particles to emerge around the entire periphery. The structure of quadrants and straight sections was arranged to provide the best opportunity for inserting targets and other beam-handling devices. Thin windows of aluminum foil were located by beam plots and installed in suitable locations around the chamber. Vacuum-pump manifolds were modified to provide other ports through which particles could emerge.

The radiation shield originally planned to contain the anticipated secondary intensities was a circular tier of concrete blocks 8 ft thick, located 10 ft outside the magnet and surrounding the two quadrants where beams of secondary radiations were to emerge. A 6-in.-thick layer of dense concrete and Pb bricks was provided at the beam height, through which channels could be placed for the emergent beams. A set of channels was provided for mesons of different energies coming from known target locations, analyzed by the fringing field of the cosmotron; meson channels labeled "300 Mev," "500 Mev," "1.0 Bev," etc., were available for experiments outside the shield. Fast neutrons and γ rays emerged tangentially through other channels.

Experience in operations showed that the planning was inadequate in several respects. Beam intensity was increased steadily over the early years, requiring additional shielding. The space between the magnet and shield was inadequate for the large analyzing and focusing equipment later found necessary. Furthermore, the space beyond the shield proved to be much too small for the large equipment and long beam runs needed as the field of research broadened. This space soon became overcrowded. The most serious inadequacy was the limited space originally provided in the direction of the emergent proton beams.

During 1958 and 1959 major additions were made to the buildings housing both the cosmotron and the bevatron. At Brookhaven the radiation shielding was entirely rebuilt so as to enclose the machine completely, including overhead shielding. The improved shielding is considered adequate for intensities up to 10^{12} protons/pulse, which is 1000 times larger than the intensities anticipated prior to operation. Additional experimental space was provided, with power and cooling facilities for large experimental apparatus. The arrangements allow the use of three external beams. As a result, emphasis has been shifted from experiments using internal targets to those with the external beams.

The auxiliary instruments needed for an experimental research program at these high energies have exceeded all expectations in number, size, and cost. The need for momentum analysis of the radiations has led to the development of scores of magnets of varying types. Crossed-field velocity analyzers are needed to separate different particles in the emergent beams. Cloud chambers and liquid-hydrogen bubble cham-

bers, with their associated magnets, are large, complicated, and expensive. The development of AG magnetic lenses for focusing emergent beams offers a valuable improvement in beam density, but also requires longer beam runs. Power to supply these many magnets presents a major problem. Total power requirements exceed the power used for the cosmotron itself, and space to house the many generators has been added to the buildings. In addition, there are the steadily accumulating racks of electronic circuits for detecting and observing the radiations, lead-brick huts where photographic emulsions are exposed, and galleries of microscopes for scanning.

A general conclusion is that future planning for accelerators of this high-energy range must provide far more space, power, and facilities than had been anticipated for the cosmotron or bevatron.

REFERENCES

1. M. L. Oliphant, J. S. Gooden, and G. S. Hide, *Proc. Phys. Soc. (London)*, **59**:666 (1947).
2. J. S. Gooden, H. H. Jensen, and J. L. Symonds, *Proc. Phys. Soc. (London)*, **59**:677 (1947).
3. E. M. McMillan, *Phys. Rev.*, **68**:143 (1945).
4. V. Veksler, *J. Phys. (U.S.S.R.)*, **9**:153 (1945).
5. W. M. Brobeck, *Rev. Sci. Instr.*, **19**:545 (1948).
6. M. S. Livingston, *Phys. Rev.*, **73**:1258 (1948).
7. M. S. Livingston, J. P. Blewett, G. K. Green, and L. J. Haworth, *Rev. Sci. Instr.*, **21**:7 (1950).
8. R. Q. Twiss and N. H. Frank, *Rev. Sci. Instr.*, **20**:1 (1949).
9. J. P. Blewett; G. K. Green; W. H. Moore and J. P. Blewett; M. G. White; M. Plotkin and J. P. Blewett; J. P. Blewett; M. H. Blewett; *Phys. Rev.*, **75**:1288 (1949).
10. N. M. Blachman and E. D. Courant, *Phys. Rev.*, **74**:140 (1948); *Rev. Sci. Instr.*, **20**:596 (1959).
11. A. I. Pressman and J. P. Blewett, *Proc. IRE*, **39**:74 (1951).
12. Cosmotron Staff, *Rev. Sci. Instr.*, **24**:723–870 (1953).
13. D. C. Sewell, W. M. Brobeck, E. O. Lawrence, and E. J. Lofgren; Q. A. Kerns, W. R. Baker, G. M. Farly, and J. Riedel; E. J. Lofgren, W. M. Brobeck, E. O. Lawrence, and D. C. Sewell; L. Smith, A. A. Garren, and L. R. Henrich; *Phys. Rev.*, **78**:85 (1950).
14. E. J. Lofgren, *Science*, **111**:295 (1950).
15. W. M. Brobeck, UCRL-3912 (September, 1957).
16. V. I. Veksler et al., *J. Nuclear Energy*, **4**:333 (1957).
17. Proceedings of CERN Symposium on High Energy Accelerators of 1956 (Geneva).
18. Le Synchrotron à protons Saturne du Centre d'Études Nucléaires de Saclay, *L'Onde électrique*, **39** (1959).
19. J. P. Blewett, *Repts. Progr. in Phys.*, **19**:37 (1956).

20. G. K. Green and E. D. Courant, *Handbuch der Physik,* **44,** 1959.
21. Proceedings of CERN International Conference on High Energy Accelerators and Instrumentation of 1959 (Geneva).
22. H. R. Crane, *Phys. Rev.*, **69**:542 (1946).
23. D. M. Dennison and T. H. Berlin, *Phys. Rev.*, **70**:58 (1946).
24. G. Bronca, H. Bruck, J. Hamelin, G. Neyret, and J. Parain, *L'Onde électrique,* **39**:463 (1959).
25. E. J. Rogers, *Rev. Sci. Instr.*, **29**:215 (1958).
26. O. Piccioni, D. Clark, R. Cool, G. Friedlander, and D. Kassner, *Rev. Sci. Instr.*, **26**:232 (1955).
27. B. Wright, *Rev. Sci. Instr.*, **25**:429 (1954).
28. L. D. Landau, *J. Phys.* (*U.S.S.R.*), **8**:201 (1944).

At the head of the facing page is a photograph of the shielding around the Brookhaven cosmotron. Compare with Chap. 13 headpiece.

14

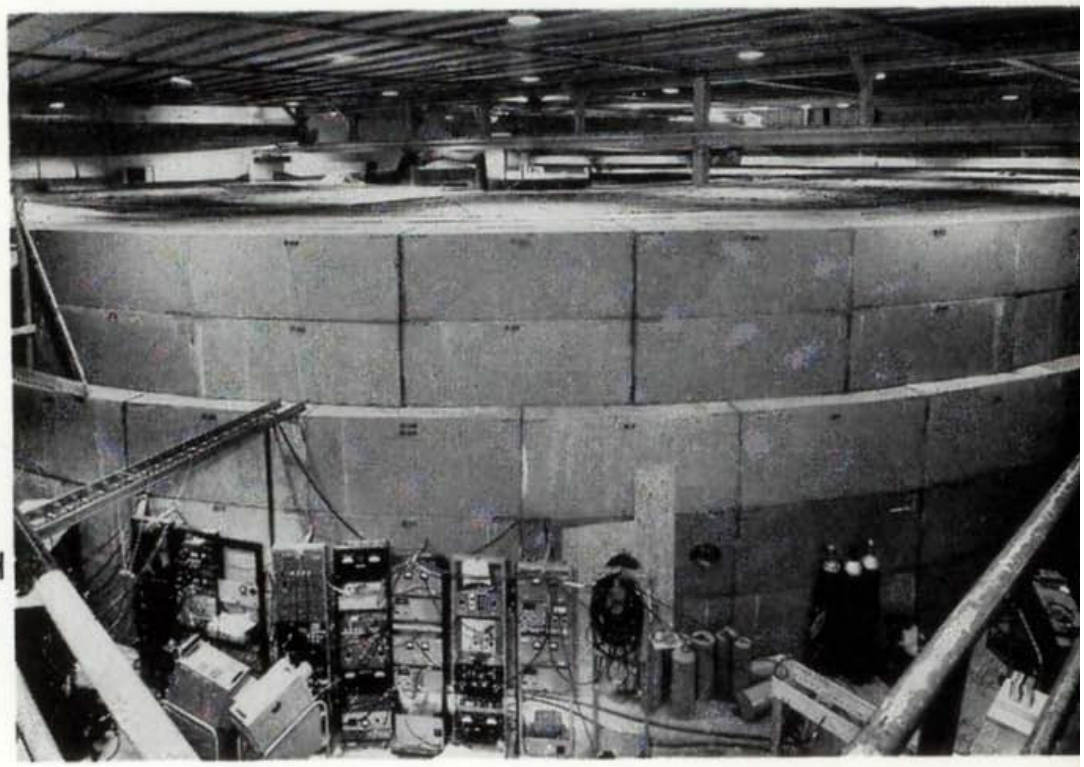

Shielding for Accelerators

The radiation shield is an important component of the modern accelerator. It is intimately connected with the design of the buildings to house the machine and the arrangement of experimental laboratories to use and study the radiations. A well-planned and effective shield can make the accelerator a useful and flexible instrument for research. But a poorly designed system can handicap experiments and limit the quality and scope of the research results.

Early accelerators were built without much regard for shielding. Intensities are usually low in the initial operation of a new type of machine or one exploring a new energy range, and ultimate intensities can seldom be anticipated. In some cases the properties of the new, higher-energy radiations were not calculable in advance, and could be determined only by laboratory measurements. But the most compelling reason for the imperfect shielding was that research experiments follow a step-by-step development, as in all new fields, and the arrangement of shielding had to be continuously adapted to the needs of the experiments. However, once the properties of the radiations have been determined and intensities measured, shielding can be installed to meet the needs and to accommodate the experiments. Beam intensity usually increases with continuous development; if so, further shielding must be added. In consequence of such experiences, the shielding system of a pioneering accelerator is usually clumsy and inefficient. A time comes when it is necessary to redesign and rebuild the original shield for more effective

protection. This has occurred in nearly all the early model accelerators, of all types.

With the steady development of accelerators to higher energy and higher intensity, the size and cost of machines and buildings have increased. The shielding system for a new accelerator should be planned in advance and incorporated in the building designs. Full information is needed on the properties of the radiations and on attenuation factors of shielding materials. The shield should anticipate the maximum possible energy and the ultimate beam intensity if possible. Yet the system must also allow sufficient flexibility to provide for future modifications of research experiments. In the larger accelerators, shields are massive and costly; an efficient design becomes an economic necessity.

Shielding serves two basic functions. Personnel must be protected from excessive radiation exposure, and background intensities must be minimized for experimental studies. The requirements for apparatus shielding usually exceed those for personnel protection.

In early accelerators with beams of low intensity, the scientists frequently overlooked the radiation hazard. Several have been burned by particle beams or scattered radiation, and some cyclotron operators have developed eye cataracts following overexposure to fast neutrons during tune-up. Appreciation of the hazards has grown with experience. Scientists and accelerator operators are now generally aware of the dangers, and proper precautions are taken to avoid overexposure. Government regulations limit dose rates and exposures. Laboratories are arranged to limit access to regions of high radiation intensity. "Health physicists" are employed in most large installations, with the responsibility of monitoring intensities and personnel exposures.

Shielding to minimize background radiation intensities for research experiments is a growing problem in all laboratories, with the use of more sensitive instruments and the demand for ever higher precision in measurements. Each type of instrument involves a different problem. Much can be done with electronic detectors by using multiple units in coincidence and anticoincidence circuits. However, in a typical research experiment an extensive arrangement of shielding is also required. For example, a narrow channel through a thick shielding wall is frequently used to obtain a collimated beam of the chosen radiation, lead or concrete enclosures may be needed around the detectors to reduce scattered radiation background, and the transmitted beam may be directed into radiation "traps" beyond the experimental apparatus to reduce back scattering. In such a system the shielding may be the largest and heaviest component of the experimental setup.

The radiations which are significant in the shielding of accelerators are those which have small interaction cross sections with the common materials used in shields, and so are of a penetrating character. They are also limited to those which are produced in considerable intensity. Other

radiations of shorter range or of low intensity, which may be of considerable interest to nuclear scientists, are not important in this application. In each shielding situation one radiation component will usually have the maximum penetration and will determine shield composition and thickness. Frequently this dominant component is a secondary radiation produced in the material of the shield. For other components this shield thickness will usually be more than adequate. The problem is to identify the dominant component and to determine its intensity.

Another typical problem in shielding analyses is the development within the absorbers of mixtures of radiations due to secondary and tertiary processes. Two types of "showers" can be identified, those which consist primarily of electromagnetic radiations and those which consist mostly of nuclear particles. High-energy electrons produce X rays which produce secondary electrons, etc., leading to the characteristic "soft shower" observed in cosmic rays; nucleonic components are also produced, such as neutrons from photonuclear processes, but the dominant components of the shower are electromagnetic radiations. Nucleonic showers are initiated by high-energy protons or neutrons, which produce mesons and other nuclear particles and which then cause nuclear interactions with the release of still other nucleons and mesons; nuclear gamma rays also come from excited nuclei and add to the shower, but the significant radiations are nucleonic.

In this chapter the most significant of these radiations and radiation interactions will be described. The physical processes of attenuation applying to the several radiations will be presented, and appropriate interaction cross sections will be cited, in order to obtain suitable attenuation coefficients for the common materials used for shielding. It will not be possible to present a complete theoretical analysis of the complex problems involved. Rather, we shall attempt to simplify each situation and to present approximate conclusions from which qualitative estimates of the shielding requirements can be obtained. For a more thorough treatment the reader is advised to study the basic references cited.

The over-all purpose is to treat the shield as a component of the experimental system, in order to provide the maximum flexibility and usefulness for research, but with due regard to personnel protection. We start with a discussion of the biological hazards and present the accepted standards for personnel protection.

14-1. PERMISSIBLE RADIATION DOSE

Ionizing radiation causes biological damage, although the detailed mechanism is unknown. The problem of specifying the biological effects was first encountered with X rays and γ rays and led to the choice of the roentgen as the unit of radiation dosage. The ionization effects produced in tissue were found to be closely similar to those in air, for which

electric instruments could be used for measurement. One roentgen is the quantity of X radiation (or γ radiation) which will release one electrostatic unit (esu) of electric charge per cubic centimeter by ionization, in an air-filled ionization chamber at standard temperature and pressure (0°C and 760 mm Hg pressure or 0.001293 gm/cm^3), in which secondary electrons are in equilibrium with the wall material.[1] (Note that 1 coulomb = 3×10^9 esu of charge.) Large parallel-plate ionization chambers were used with collimated beams of radiation to obtain basic calibrations. Then small "air-walled" ionization chambers were developed, with wall surfaces of plastic material which approximated air in average atomic number and in secondary-electron emission characteristics. One of the best known of the early instruments was the Victoreen thimble ionization chamber.

Radiation density decreases inversely with the square of the distance from an X-ray target and is expressed in r/cm^2. The intensity or the flux of the radiation is the amount traversing a unit area in unit time and is given in r/(cm^2)(sec) or r/(cm^2)(min). The output of a typical deep-therapy X-ray tube is about 500 r/(cm^2)(min) at 1 m distance from the target.

Absorbed Dose

Ionization in air, or in tissue, is caused primarily by the secondary electrons produced by the radiation. The average energy lost by a fast electron in liberating 1 ion pair in air is commonly taken to be 32.5 ev/ion pair (although more recent determinations[2] give the value 34.0 ev/ion pair). This energy loss per ion pair is almost independent of the energy of the ionizing electron and so holds for a wide range of X-ray and γ-ray quantum energies. Since 1 esu of charge is equivalent to 2.08×10^9 singly charged ions, it follows that 1 r corresponds to 5.24×10^{13} ev/gm air or 83.8 ergs/gm air (87.7 ergs/gm if the energy loss is 34.0 ev/ion pair).

The absorbed dose of any ionizing radiation is the energy imparted to matter by ionization and other absorptive processes. In air the absorbed dose per roentgen is the above 87.7 ergs/gm. The energy absorbed in tissue, such as within the human body, has been the subject of many calculations and also of experimental studies in "tissue-equivalent" ionization chambers. Results differ, depending on the type and energy of the radiations and the composition of the tissue, with values ranging between 90 and 150 ergs/(gm)(r). In "standard" soft human tissue (73 per cent oxygen, 12 per cent carbon, 10 per cent hydrogen, and 4 per cent nitrogen by weight) the absorbed dose is 97 ergs/gm tissue (for 34.0 ev/ion pair). Considering this variability, the Seventh International Congress of Radiology (Copenhagen, 1953) defined an international unit of absorbed dose called the "rad"[3] as one hundred ergs per gram tissue. One millirad (mrad) is equal to one-tenth erg per gram

tissue. By definition, this unit of absorbed dose can be applied to any type of tissue and to any type or energy of radiation which leads to the production of ionization.

Biological Response

Physical factors are responsible for some of the variations in biological response, although biological variability also has an important role. One of the most important of the physical factors is the density of ionization along the track of an ionizing particle. It is believed that the biological effect is a function of the number of ion pairs formed on the average within a single tissue cell. For example, a cell may recover from and survive a single ionization, while it might be seriously damaged by the cumulative effects of several simultaneous ionizations.

The specific ionization in air in ion pairs per centimeter varies inversely with particle velocity, being small at high velocities and increasing by a large factor as the particle slows down. This results in concentration of the ionization at the end of the particle range. The specific ionization is essentially the same for singly charged particles of the same velocity and is proportional to the square of the charge for multiply charged particles. In Table 14-1 are listed the values of specific ionization in air for electrons, protons, and alpha particles of 5 Mev energy, along with the maximum values of specific ionization for each particle near the end of the range. The same ratios apply for ionization in tissue, usually expressed in ion pairs per micron, or sometimes in ion pairs/(gm)(cm^2) of tissue.

TABLE 14-1
SPECIFIC IONIZATION IN AIR
(Ion pairs/cm)

	Energy, Mev	Specific ionization	Energy	Maximum specific ionization
Electrons	5	70	100 ev	1.0×10^4
Protons	5	2.5×10^3	25 kev	1.0×10^4
α particles	5	2.9×10^4	100 kev	4.0×10^4

The ionizing radiations produced by accelerators are of many types. X rays or γ rays release secondary electrons through three primary processes: photoelectric absorption, which is dominant for very low energies; Compton scattering, for intermediate energies; and positron-electron pair formation at high energies (the threshold energy for pair formation is 1.02 Mev). High-energy protons are produced directly in some accelerators and may also be formed in nuclear interactions. Alpha particles occur primarily as products of radioactive decay, but may also be accelerated directly or released in nuclear disintegrations. Fast

neutrons which are produced in nuclear interactions are not in themselves ionizing because of their zero charge, but they can project high-energy protons or other charged atomic nuclei from matter by direct recoil; these will produce ionization. Both fast neutrons and slow neutrons can cause nuclear interactions with the release of fast charged particles or gamma rays. All these primary or secondary radiations which cause ionization are significant in varying degree in producing biological effects.

Another physical mechanism which appears to have a direct biological effect is the removal of a proton or other atomic nucleus from a chemical molecule in the cell by direct recoil from a high-energy heavy particle such as a fast neutron. It is known that fast neutrons have an enhanced biological effectiveness compared with slow or thermal neutrons, which have insufficient energy to produce recoils. Part of this increased effectiveness is no doubt due to ionization by the recoil protons. It is also probable that the removal of an atomic nucleus from the molecule adds to the biological effect.

Biological and physiological studies of the effects of radiation show that the biological response varies markedly with the type of tissue or organ being irradiated. The damage in normal soft tissue is characterized by the killing of cells, which must be eliminated through blood circulation; the magnitude of the response depends on the blood supply to the tissue and on the rate of reproduction of tissue cells. In bones the damage is primarily associated with those tissues in the marrow which produce blood cells and is strongly influenced by chemical factors such as the selective concentration of radium or of radioactive strontium in the bones; a typical response is a reduction in the rate of production of blood cells. Radiation can cause mutations of the lens-producing cells in the crystalline lens of the eye, which may result in opaque cataracts; fast neutrons are specifically injurious in this respect. Harmful genetic mutations can also be produced in the gonad cells by radiation; however, most of the evidence of genetic damage has come from studies of fruit-fly or small-animal populations, and the application to the human population is inferred by calculations. In almost every case the magnitude of the biological response is also affected by subsidiary factors such as temperature, the chemical condition of the tissue or organ, and the absorbed dose rate.

This variability in biological response has led to the concept of the "relative biological effectiveness" (RBE) as a means of comparing the effectiveness of absorbed doses of radiation delivered in different ways and producing different biological responses. The RBE is taken as unity for the effects produced by X rays and γ rays, following the experience and practice in X-ray therapy and in the use of Co^{60} γ-ray sources. The definition of RBE is the ratio between the dose in rads from an X-ray or Co^{60} γ-ray source to produce a biological change and the dose in rads of the radiation under comparison to produce the same biological change.[4] So by definition the RBE for X rays or γ rays is 1.00.

For most biological phenomena the factor which determines the RBE is the specific ionization of the individual charged particles. As indicated in Table 14-1, this varies from about 70 ion pairs/cm in air for fast electrons to 4×10^4 ion pairs/cm for slow α particles. In water or in tissue with density of approximately 1.0 this spread would be between 6 ion pairs/μ for fast electrons and 3500 ion pairs/μ for slow α particles. If the phenomenon concerned is one which requires only a few ion pairs per micron to produce the biological response, the alpha particle would have an RBE < 1, as compared with an RBE of 1.0 for electrons. On the other hand, if the phenomenon requires a linear density of the order of 10^3 ion pairs/μ to produce a particular response, the alpha particle would have an RBE > 1 relative to electrons. Wide variations in the experimental values for RBE are reported, but for most biological changes of interest the values of RBE are larger than 1.0 for protons, alpha particles, and other heavy charged particles. The accepted values of RBE[5,6] as a function of specific ionization, in ion pairs per micron of water, are given in Table 14-2.

TABLE 14-2
RBE AS A FUNCTION OF SPECIFIC IONIZATION

Specific ionization, ion pairs/μ water	RBE	Radiations
0–100	1.0	X rays, γ rays, electrons
100–200	2.0	
200–650	5.0	
650–1500	10.0	Fast neutrons, protons, α particles
1500–5000	20.0	Heavy recoil nuclei

The usefulness of RBE is limited by the relative inaccuracy of biological measurements of response, associated with the problem of obtaining statistical accuracy from observations with a wide variability of individual response. It is further complicated by variations in experimental factors such as the rate and duration of radiation exposure, the physical and chemical condition of the biological samples, and the type and degree of biological damage. Those phenomena for which reasonably good measurements have been obtained are either for lethal doses or for gross pathological damage such as the production of cancer, leukemia, sterility, or cataracts. It is assumed that the same RBE values apply to the much smaller dose rates which are at the level of the permissible dose for laboratory workers.

The biological unit of radiation dosage is the "roentgen equivalent man" (rem). It is the dose of radiation which has the same estimated biological effect as 1 rad of X rays or γ rays. One rem is defined[4] as RBE times one rad. One millirem (mrem) is equal to RBE times one millirad. The rem has the same inherent limitations as the RBE;

assumed or estimated values are frequently used. Its use should be restricted to the field of radiation protection involving biological response. The unique feature is that it represents the same degree of biological response for all radiations and, with suitably adjusted RBEs, to all biological phenomena.

The radiations from accelerators are mixed types and occur in different proportions, depending upon the accelerated particle, the energy, and the target material. With such mixed radiation it is seldom possible to use a single instrument to measure the energy absorption dose in rads, and even more difficult to establish a significant value of RBE. The correct procedure would be to use separate instruments to measure the rad dose of each of the radiations selectively and to measure and assign a suitable RBE for each component of the radiation. Then the rem dose would be the sum of the individual products:

$$\text{Dose (rem)} = \Sigma[\text{RBE} \times \text{dose (rads)}]$$

However, such a detailed analysis of the radiation is seldom possible. The common procedure is to determine the rem dosage only for the biologically most dangerous component of the radiation (usually fast neutrons) for which an estimated RBE is available, using an instrument which will measure the intensity of this single component either in rads or in flux of particles/(cm^2)(sec). If the rem-dosage sum for the other components can be estimated to be small compared with that of the most dangerous component, the numerical value for this one component is used. In general this falls within the accepted limits of error in the definition of the rem dosage or in the definition of the maximum permissible dose.

Maximum Permissible Dose

The maximum permissible radiation dose for laboratory workers has undergone several revisions downward since the concept was initiated in about 1931, at which time the maximum permissible exposure (MPE) was set at 0.2 r/day. At first it was applied only to X-ray and γ-ray dosage, and the chief concern was the protection of radiologists and technicians. In 1934 the International Committee on X-ray Protection[1] adopted the value of 0.2 r/day as the "tolerance dose" without specifying the technique of measurement. Following the practice in X-ray technology in several countries, it was generally interpreted as the "skin dose," which includes back-scattered radiation from the surface of the body. A skin-dose rate of 0.2 r/day is roughly comparable to a rate of 0.1 r/day measured in air without back-scattered radiation. This rate of 0.1 r/day or 0.6 r/week measured in air was the generally accepted tolerance dose from 1934 to about 1946.

During the 1940s a great deal of detailed information became available

on the properties of different radiations and on biological response to radiation. It was recognized that standards for exposure of sensitive tissues or organs might differ from those for whole-body exposure. For example, clinical studies of radium poisoning showed the biological significance of α-particle radiation from radium deposited in the bones. The development of chain-reacting piles and the rapid growth of the atomic-energy industry increased the number of persons exposed to radiations and made it necessary to determine the specific effects of neutrons. Fast neutrons were identified as the damaging radiation in cyclotron-induced eye-lens cataracts. The significance of the time factor was recognized in radiation exposure, and studies were made of the biological response of different organs as a function of the time duration of exposure.

In 1949 the National Committee on Radiation Protection recommended a reduction in the permissible dose rate for whole-body exposure to 0.3 rem/week. This was adopted in 1950 by the International Commission on Radiological Protection and repeated with little change in 1954. These recommendations are summarized in the *National Bureau of Standards Handbook No.* 59, September 24, 1954,[5] and also in the report of the International Commission[6] in 1955. Since the permissible limit is expressed in rem, the same value applies to neutrons and other radiations as for X rays or γ rays. Certain exceptions and interpretations are noted. The limit is set by the exposure of the more sensitive organs, which in general are sufficiently below the skin surface to represent the internal body dose. A dosimeter at the skin surface could read 0.5 to 0.6 rem/week without exceeding the internal dose limit.

The flux of fast neutrons to give a dose of 0.3 rem for a 40-hr week depends on neutron energy and on the experimentally determined conversion factor between neutron flux and biological dose. Table 14-3

TABLE 14-3
NEUTRON FLUX AND BIOLOGICAL DOSE[7]

Energy, Mev	rem/(neutron)(cm^2)	Flux, neutrons/(cm^2)(sec) for 0.3 rem in 40 hr
Thermal	0.104×10^{-8}	2000
0.0001	0.134	1550
0.005	0.122	1700
0.02	0.25	830
0.1	0.83	250
0.5	2.30	90
1.0	3.80	55
2.5	3.41	60
5.0	3.80	55
7.5	4.16	50
10	4.16	50

gives these conversion factors in rem/(neutron)(cm^2) for a range of neutron energy; it also gives the flux in neutrons/(cm^2)(sec) to give 0.3 rem in 40 hr.[7] In the range of interest for fast neutrons from accelerators, the limiting flux is between 50 and 60 neutrons/(cm^2)(sec).

By 1956 a more intensive study of radiation hazards was prompted by a growing awareness of the significance of radioactive fall-out from atomic- and hydrogen-bomb tests. A committee on radiation hazards was established by the United States National Academy of Sciences, which published a report[8] in 1956. A parallel study was prepared by a committee of the British Medical Council. In 1955 the General Assembly of the United Nations authorized a Scientific Committee on the Effects of Atomic Radiation, which made a final report[9] in 1958. Also during these years the United States Atomic Energy Commission collected and analyzed a large amount of information on radiation fall-out intensities and supported many medical and biological studies of the effects of radiation.

The principal result of these studies has been to identify the results of radiation and to estimate their effect on the genetic heritage of the race. While the risk of radiation-induced genetic mutations has been considered negligible for the relatively small number of radiation workers, the effects cannot be neglected where large populations are exposed. Another hazard identified and studied is the incidence of leukemia and bone cancer due to ingestion of radioactive Sr^{90} from fall-out; strontium is taken up from the soil by plants which are eaten by animals and humans and is selectively concentrated in bone. For very long-term effects the accumulation of radioactive C^{14} in the biosphere also adds to the natural radioactivity and cosmic-ray background in producing both somatic and genetic effects.

As a consequence of this increased awareness of the hazards to large populations, the National Committee on Radiation Protection has recommended[10] certain modifications in the maximum permissible doses. A basic recommendation is that the total accumulated dose for radiation workers shall not exceed $5(N - 18)$ rem, where N is the age in years. This implies a maximum yearly permissible dose of 5 rem during the working life of the individual. So although no change is made in the basic maximum permissible dose rate of 0.3 rem/week for occasional exposures, it is in fact reduced, for occupational workers, to 0.1 rem/week. This is required if the total accumulated dose is not to exceed the limit of 5 rem/yr.

For the general population the maximum permissible dose is based on limiting the dose to the gonads so as not to exceed 14×10^6 rem per million population over the first 30 years of life and one-third of that amount in each decade thereafter. Of this average value of 14 rem per 30 yr for the individual, about 4 rem per 30 yr is expected from natural

background radiation. This leaves 10 rem per 30 yr for all other sources, including X-ray treatment, fall-out, or any other man-made source. The practical equivalent is a rate for large populations which is one-tenth that for occupational workers, or 0.01 rem/week.[7]

In accelerator operations it is customary to use these latest recommendations of the maximum permissible dose as the basis for calculations of shielding requirements. A dual standard of acceptable radiation intensities in and around accelerator installations is to be expected in the future. Two classes of persons are involved: laboratory workers and others within the controlled area, where measurements and records of the individual accumulated dose can be maintained, and the general public residing or working in areas external to the controlled laboratory area. The permissible weekly doses (pwd) for these categories are:

1 pwd (radiation workers)
= 100 mrem/wk, or 20 fast neutrons/(cm^2)(sec)
1 pwd (general public) = 10 mrem/wk, or 2 fast neutrons/(cm^2)(sec)

It might be noted that the natural background radiation at sea level and in the usual environment in inhabited areas is about 2.5 mrem/week, or about 25 per cent of the pwd for the general public. The natural cosmic-ray background increases with altitude above sea level, and the level of natural radioactivity is higher in certain environments. The permissible dose rates given above are considered to be conservative, and it seems unlikely that they will be reduced further in the future.

The most difficult problem in accelerator operations will be to determine the total rem dosage from the several types of radiation. Accepted practice at present is to monitor total radiation intensity continuously with an ionization chamber calibrated in millirads and to apply a local RBE factor estimated from the high-energy neutron content of the particular installation. This factor may be near 1.0 for low- and medium-energy accelerators, about 3 for the mixture of radiations from a cyclotron, and up to 10 for local areas near targets where the high-energy neutron component is dominant. It is essential to provide for continuous and permanent records of accumulated exposure for the individual workers; film badges or pocket ionization chambers are commonly required in all major laboratories. It is also desirable to have a continuous and permanent record of intensities at one or more key points within a laboratory, using ionization-chamber monitors and a recording system. An intensity contour plot of the laboratory should be made to reveal the areas of highest radiation intensity under the more commonly used arrangements for targets and beam handling; the permanent radiation monitors can be located in these highest-intensity areas. Such a permanent record should also be kept for monitors located outside the controlled areas, in regions where the exposure to the general public is likely to be a maximum.

14-2. RANGE-ENERGY RELATIONS FOR CHARGED PARTICLES

Primary protons, deuterons, etc., are frequently brought outside of the accelerator vacuum chamber through thin-foil windows as emergent beams. In the energy range of cyclotrons and other low-energy and medium-energy positive-ion accelerators, beams of such monoenergetic ions have a discrete range in absorbers.

The range-energy relations for protons, deuterons, and He^{++} ions in several materials have been computed by Bethe[11] from basic ionization-loss theory, corrected empirically to fit the experimental results of range

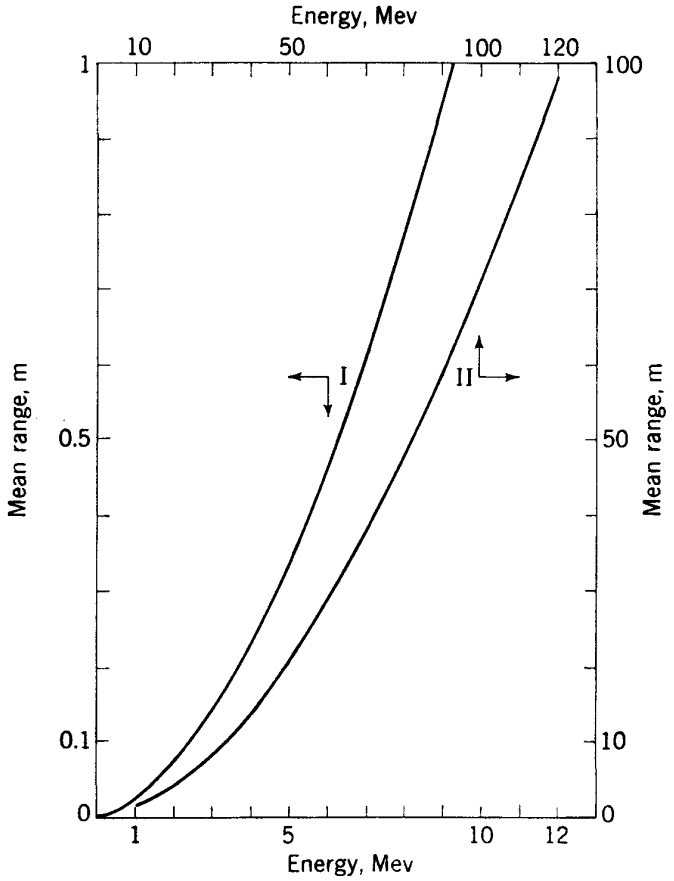

Fig. 14-1. Mean range of protons in air.[12]

measurements. The most complete compilation is in the form of graphs of mean range as a function of particle energy, in a Brookhaven report[12] by Bethe. A selected sample of these range-energy curves for protons in air and in several common foil materials, extending to over 100 Mev, is reproduced in Figs. 14-1 and 14-2. The statistical nature of the energy-loss processes results in range straggling, which extends the extreme (extrapolated) range beyond the mean range. The straggling corrections are also analyzed and presented as correction curves in the Brookhaven report; they are not reproduced here, since such precision is seldom neces-

sary for shielding calculations. In brief summary it can be shown that straggling extends the extrapolated range beyond the mean range by about 20 per cent in most materials at low energies (<20 Mev), and this extension decreases to about 10 per cent at 200 Mev.

The range of deuteron (D^+) or He^{++} ion (α-particle) beams can be related to proton (H^+) ranges through the approximate relations

$$R_D(T) = 2R_H(\tfrac{1}{2}T) \tag{14-1}$$

$$R_\alpha(4T) = R_H(T) + 0.2 \text{ cm} \tag{14-2}$$

where the symbol $R(T)$ means the range of a particle of energy T. If

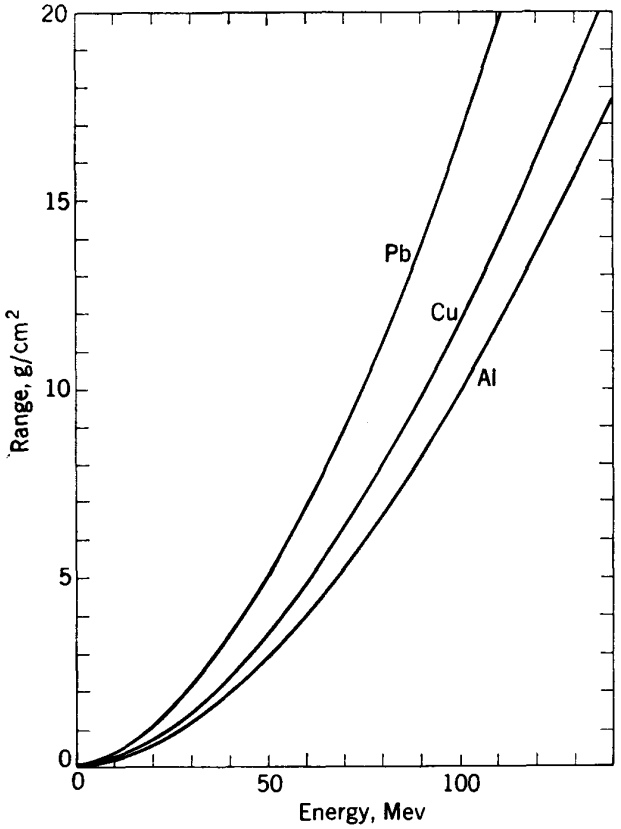

Fig. 14-2. Mean range of protons in metals.[12]

more precise values are needed, the detailed ionization-loss calculations of Bethe are available.

Beams from cyclotrons and other low-energy accelerators will be absorbed in the metal walls of the vacuum chamber. For example, 20-Mev protons have a range of 0.8 mm in Cu or 2.1 mm in Al. When brought outside the chamber through a thin-foil vacuum window, a beam of 20-Mev protons has a range of 4.0 m in air. A potentially dangerous by-product will be the radioactivities induced in the oxygen and nitrogen in the air; if such a beam is to be used in air, a suitable ventilation system must be provided. In this low-energy region

laboratory practice requires careful planning to avoid exposure of personnel to either the primary beam or scattered particles from the beam. Several scientists have suffered burns of the hands or arms from such scattered beam radiation. In general, however, this is a problem in laboratory arrangements rather than shielding.

Bethe's range-energy calculations and curves extend up to 1000 Mev for protons, but for energies above about 200 Mev other processes than ionization loss are involved, and range curves are no longer accurate. In general, processes such as nuclear interactions and meson production reduce the proton energy by large steps, so the mean proton range for higher energies is reduced below the ionization-loss curves. However, the secondary radiations produced in these interactions must themselves be analyzed for their penetration and ionization, and they may extend the observed ionization well beyond the extreme range of the primary protons. At energies above 400 or 500 Mev these other processes have such large yields that they become dominant features of the absorptive process. The ionization produced by the proton becomes less important than its nuclear interactions, and it behaves much like a fast neutron at these energies. The properties of such nucleonic particles are discussed further in Sec. 14-10, Nucleonic Showers.

14-3. ELECTRON ABSORPTION

Range of Electrons

Primary electrons have a reasonably well-defined range only for energies of less than a few Mev. At these low energies, energy loss is by ionization and excitation of the atomic electrons in the atoms of the absorber. The ratio of the number of electrons to atomic weight, Z/A, is approximately 2 for all materials except hydrogen. So range can be expressed in gm/cm^2 for all materials (except hydrogen) without serious error.

Each electron experiences many scattering collisions and follows a tortuous path before being brought to rest, so there are wide variations in the range of individual electrons, resulting in considerable straggling. The only significant observational quantity is the "maximum range," obtained by extrapolating the number-thickness curve on a linear plot at the extreme end of the range. For monoenergetic electrons of energy T between 0.7 and 3 Mev the observed maximum range in aluminum can be conveniently expressed by the "Feather rule":

$$R = 0.542T - 0.133 \text{ gm/cm}^2 \qquad (14\text{-}3)$$

The range rule holds approximately for other materials (except hydrogen). A useful rule of thumb is that the range in gm/cm^2 is half the energy in Mev.

For electron energies up to several Mev the range is short enough that the electrons will be absorbed by the metal walls of accelerator vacuum chambers. Thin-foil vacuum windows are frequently used to allow beams to emerge from the chamber. Such emergent beams have been used for localized irradiation for medical purposes, such as in the treatment of skin cancer, and for sterilization of packaged drugs or canned foods.

Energy loss by ionization depends on particle velocity. Electrons approach the velocity of light for energies above about 2 Mev, so the rate of ionization loss becomes essentially constant with further increase in energy. It is also nearly independent of the absorbing material. This limiting value of the rate of ionization loss is about 2 Mev/(gm)(cm^2) in light absorbers, becoming smaller with denser materials to reach a value of about 1.4 Mev/(gm)(cm^2) for Pb. It results in the formation of about 6.0 ion pairs/μ in material of unit density such as water or tissue. In cloud chambers or electron-sensitive photographic emulsions used for scientific observations, this minimum ionization rate results in the "thin tracks" which are characteristic of singly charged particles of "relativistic" velocities.

Radiation Loss

For electron energies above a few Mev the more important energy-loss process is the emission of radiation. This radiation is a continuous spectrum of X rays called bremsstrahlung (i.e., braking radiation) which is emitted in decelerating or deflecting impacts between the primary electrons and atoms in the target or absorber. The X rays which are produced are themselves absorbed through electromagnetic interactions such as photoelectric absorption, Compton scattering, or the production of positron-electron pairs. The attenuation of X rays due to these processes is discussed in Sec. 14-4. However, the secondary electrons which are emitted by the X rays cause further ionization and excitation of atoms, starting from the point within the absorber where they are produced, and may penetrate far beyond the range of the primary electrons. The difficulty in separating the effects of the primary and secondary electrons is the reason that range is not an appropriate measure of electron absorption above a few Mev energy.

The quantum-mechanical theory of the radiation emission process was originally developed by Bethe and Heitler;[13] simple approximations have been developed by Rossi and Greisen[14] and by Schiff.[15] Cross-section formulas and related data will be found in the article by Koch and Motz.[16] This theory predicts the spectral distribution of X rays as a function of incident electron energy and of the properties of the material in the target. A more complete description of the properties of the radiation will be given in the section to follow on X rays, where the energy

distribution will be illustrated. The theory describes, and experiments confirm, a distribution in which the largest number of X rays are emitted at low photon energy, with the number-versus-energy spectrum decreasing with increasing photon energy to an upper limit which is equal to the energy of the incident electron. From the probability of emission given by the theory, the total energy loss by the electron due to radiation can be obtained.

The fractional rate of energy loss through radiation is nearly independent of electron energy. It depends on the magnitude of the electric field within the atom, since it is this field that causes the phenomenon. This atomic electric field is associated with the atomic number Z of the atoms of the absorber. In a thickness x of absorber the fractional energy loss due to radiation may be represented by

$$\frac{W}{W_0} = F(W)e^{-x/x_0} \tag{14-4}$$

where W_0 is the initial and W the final value of the average particle energy, $F(W)$ is a slowly varying function of energy which involves the atomic number and other constants, and x_0 is a characteristic radiation length which is independent of energy.

The radiation length x_0 becomes a useful concept in the interpretation of energy-loss phenomena. Except for the modifying effect of the function $F(W)$, the radiation length can be visualized as the distance in which the electron energy is reduced to $1/e$ of its initial value. The concept has more validity when applied to a small fraction f of the radiation length; in a thickness fx_0 the particle will lose a fraction f of its energy, on the average, through radiation. The value of x_0 can be derived theoretically from the characteristics of the atoms in the absorbing material. When A is the atomic weight and Z the atomic number, the radiation length is given by[13]

$$\frac{1}{x_0} = 4.14 \times 10^{-3} \frac{Z^2}{A} (15.6 - \ln Z) \qquad \text{cm}^{-1} \tag{14-5}$$

In this relation the radiation length is given in centimeters. In practice this quantity is more conveniently measured in units of gm/cm^2 in which the calculated values form a smooth curve as a function of Z.

Since the radiation length is independent of electron energy and the function $F(W)$ is not strongly energy-dependent, it is convenient to present the variation of energy loss with electron energy as shown in Fig. 14-3. In this figure the fractional rate of energy loss per radiation length, $-\frac{x_0}{W}\frac{dW}{dx}$, is plotted as a function of energy for a dense (Pb) and a light absorber (air). This quantity increases asymptotically with energy to the maximum rate of 1.0 at very high energies.

In contrast, the competing process of energy loss by ionization is most important at very low energies, decreasing with increasing energy to minimum limiting values at 2 Mev/(gm)(cm^2) for air and 1.4 Mev/(gm)(cm^2) for Pb as the electrons approach relativistic velocities. Hence the fractional energy loss due to ionization per radiation length, $\left(\frac{x_0}{W}\frac{dW}{dx}\right)_{\text{ion}}$, decreases to a negligible fraction of the total for very high energies. For comparison, this quantity is also plotted in Fig. 14-3 for Pb and air absorbers.

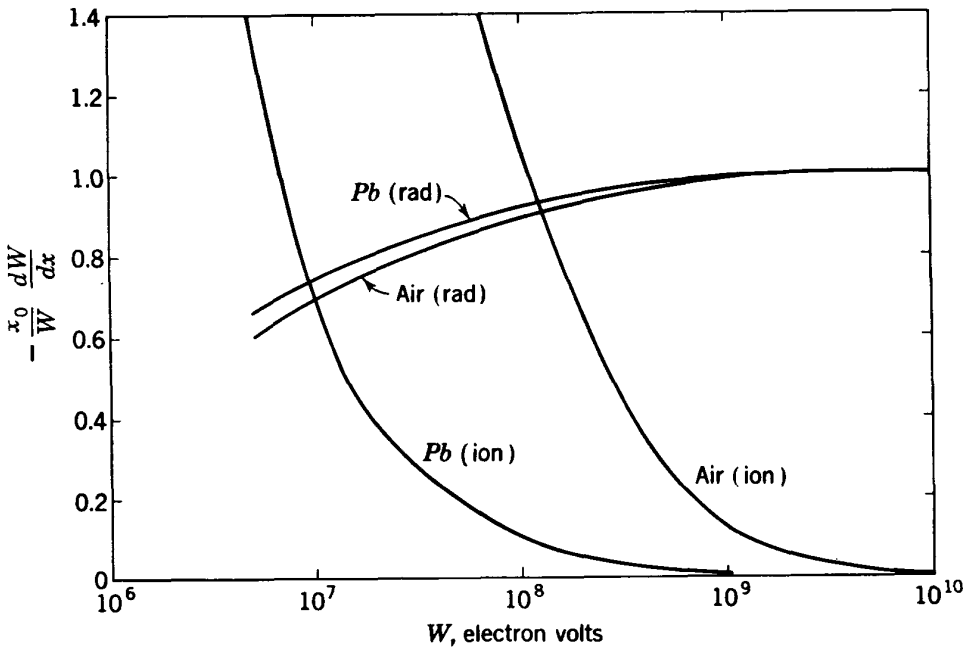

Fig. 14-3. Fractional energy loss by radiation and by ionization.[20]

Ionization loss and radiation loss are equal in magnitude at a critical energy W_c, which is given by the approximate relation[13]

$$W_c \cong \frac{800}{Z} \quad \text{Mev} \tag{14-6}$$

Theoretical computations of the magnitude of radiation loss are given in the *National Bureau of Standards Handbook No.* 55[17] and by Price, Horton, and Spinney,[18] Rossi,[20] and others. Results differ slightly, depending on the assumptions made in performing the computations, but are in general agreement as to the magnitude of radiation lengths and of critical energies. Table 14-4 gives numerical values of radiation length in gm/cm^2 and in centimeters for some of the common elements used in absorbers, taken from the above references, and also the critical energies

TABLE 14-4
RADIATION LENGTHS AND CRITICAL ENERGIES[20]

Substance	Z	Density, gm/cm³	Radiation lengths		Critical energy W_c, Mev
			gm/cm²	cm	
Hydrogen (liquid)	1	0.07	58	830	(400)[18]
Carbon	6	1.50	44.6	30.0	102
Nitrogen	7	.....	39.4	.....	88.7
Oxygen	8	.....	35.3	.....	77.7
Aluminum	13	2.70	24.5	9.1	48.8
Iron	26	7.85	14.1	1.80	24.3
Copper	29	8.94	13.1	1.47	21.8
Tin	50	7.28	8.9	1.22	12.5
Lead	82	11.34	6.5	0.57	7.8
Air	(7.37)	0.0012	37.7	31,000	84.2
Water	(7.23)	1.00	37.1	37.1	83.8
Concrete	(13.2)	2.35	24	10.2	47

in Mev. Figure 14-4 is a plot of these calculated values of radiation length and critical energy as a function of atomic number Z.

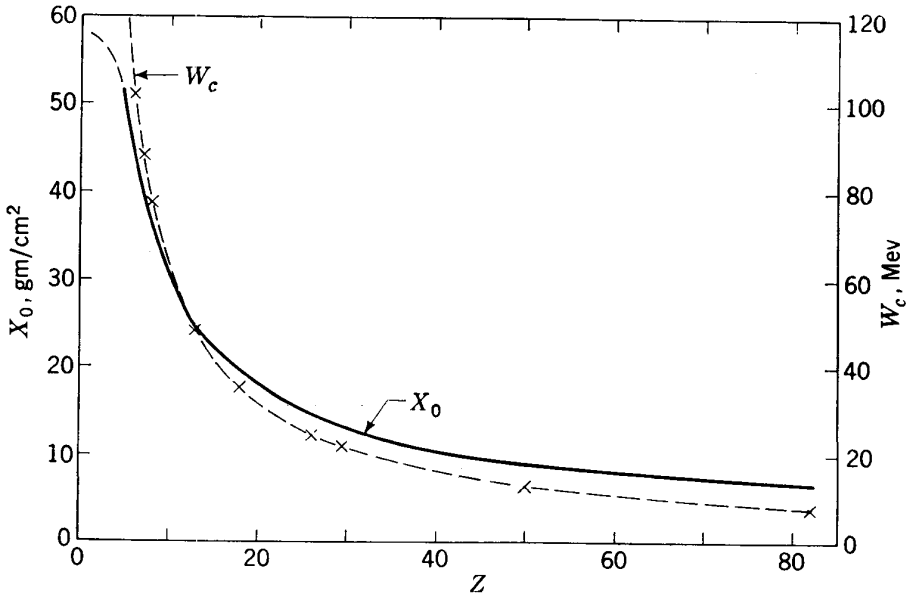

Fig. 14-4. Radiation lengths and critical energies as functions of atomic number.

For a mixture of elements, the radiation length can be obtained by summing the several individual values using the fraction of each element by weight f_i,

$$\left(\frac{1}{x_0}\right)_{\text{mixt}} = \sum \frac{f_i}{x_i} \tag{14-7}$$

Summary

We find that electrons are degraded in energy both by ionization and by radiation. At relatively low energies and in light absorbers ionization loss predominates. The residual energy W after traversing a thickness x of absorber of density ρ is given by

$$W = W_0 - \rho x \begin{bmatrix} 1.4 \text{ (high Z)} \\ 2.0 \text{ (low Z)} \end{bmatrix} \quad \text{Mev} \tag{14-8}$$

where ρx is in units of gm/cm^2 and the factor in brackets is the loss in Mev/(gm)(cm^2).

At very high energies where ionization loss is negligible, the attenuation by radiation loss follows the simple exponential law

$$\frac{W}{W_0} = F(W)_{\text{rad}}\, e^{-(\rho x)/x_0} \tag{14-9}$$

where ρx is the thickness of the target or absorber in gm/cm^2 and x_0 is the radiation length for this material in the same units. The factor $F(W)_{\text{rad}}$ is the fractional energy loss by radiation plotted in Fig. 14-3 and is a slowly varying function of electron energy with a magnitude between 0.6 and 1.0.

The production of X rays in the absorber follows the complementary relation

$$I = I_m(1 - e^{-(\rho x)/x_0}) \tag{14-10}$$

where I_m represents the intensity for complete conversion to X rays. So we see that X-ray intensity is a maximum in the initial layers of the absorber and falls off exponentially with thickness. Meanwhile the X rays are being absorbed and scattered by other electromagnetic interactions which release secondary electrons and positrons. These secondary charged particles lose energy through radiation, as well as by ionization, starting from the point within the absorber where they originate. The X rays also produce neutrons through the process of photoproduction, with a cross section depending on X-ray energy and the material of the absorber.

The concept of radiation length applies only to the loss of electron energy through radiation. Its primary utility is in computing the intensity of the secondary X radiation, preliminary to determining the X-ray shielding requirements. Nevertheless, it is occasionally useful as a unit of absorber thickness in describing the production of other secondary radiations such as photoneutrons and will be used in Sec. 14-9.

Some examples will illustrate the energy attenuation of the primary electrons, without consideration of the additional problems of absorption of secondary radiations. First, consider the attenuation in Al of a beam of 20-Mev electrons, as from an electron linear accelerator. The thick-

ness needed to reduce energy to zero by ionization alone is found from Eq. (14-8) to be 10 gm/cm^2 or 3.7 cm of Al. This represents 0.4 radiation length, in which the energy would also be attenuated by radiation to $0.41W_0$, following Eq. (14-9). Since both loss processes occur, the actual thickness needed to absorb the primary electrons is somewhat less than 10 gm/cm^2. However, computation of the exact thickness is of no significance, since it is insufficient in any event to provide adequate absorption for the secondary X rays produced in the Al absorber.

As another example, consider a beam of 200-Mev electrons and a Pb absorber. Ionization loss alone would require a thickness of 143 gm/cm^2 or 12.6 cm Pb. This represents 22 radiation lengths, in which the incident energy W_0 would be reduced by radiation to about $1.7 \times 10^{-10}W_0$, which is smaller than most shielding requirements for the incident electrons. The significant problem is again the attenuation of the secondary X rays and photoneutrons, which will be discussed in following sections.

14-4. X-RAY ATTENUATION

X rays are the principal secondary radiation from electron accelerators, emitted from all targets bombarded by the beam. They also occur as bremsstrahlung produced in absorbers by high-energy electronic components of the secondary radiation. Superimposed on the continuous energy spectrum of bremsstrahlung from targets or absorbers are the K, L, etc., line spectra, which are monoenergetic X rays associated with filling the inner electron energy levels in the target atoms. The energies of these line spectra are so low as to be unimportant in most shielding problems.

X-ray absorption is a complex problem which can only be discussed properly in terms of the several energy-loss processes, which vary in relative importance as a function of photon energy, and with due regard to the changing shape of the energy distribution as the relative intensities of the secondary and tertiary products change with increasing absorber thickness. Furthermore, the probabilities of the secondary interactions and the form of the energy distribution are also strongly dependent on the material of the absorber.

Our purpose in this section is to describe the properties of X-ray absorption for low-energy and medium-energy X rays, up to about 300 Mev, for which the interactions with matter are predominantly electromagnetic in character. To simplify the discussion, we shall consider the following topics:

1. Attenuation of monoenergetic X rays with narrow-beam geometry
2. Attenuation in thick absorbers and with broad-beam geometry
3. Bremsstrahlung energy distribution from thin targets

4. Attenuation of continuous spectra in thick absorbers
5. Photoneutron production

The probability of any atomic or nuclear interaction is given in terms of the cross section σ, measured in square centimeters. This is the idealized, equivalent "area" of the system, comprising the incident particle or radiation and the struck atom or nucleus. The probability is assumed to be 100 per cent if the projected path of the incident ray or particle falls within this area relative to the center of the atom, and zero if it is outside this area. From this we see that σ is measured by an interaction distance r_0, such that $\sigma = \pi r_0^2$. For example, if all photons coming within a distance r_0 of 10^{-8} cm of the centers of target atoms were to cause a particular interaction, while those at greater distances would not interact, the cross section would be 3.14×10^{-16} cm^2.

Experimental determinations of cross section are obtained from the observed intensity of an interaction involving a known number of incident particles and a known number of target atoms. If a beam of incident particles of N_1/sec strikes a thin target of N_2 atoms/cm^2 and produces an interaction with a number of secondary radiations N_3/sec, the cross section is given by

$$\sigma = \frac{N_3}{N_1 N_2} \qquad \text{cm}^2$$

To be more specific, consider a beam current i in amperes ($N_1 = i/e$ electrons or protons/sec) striking a target of atomic weight A, density ρ (gm/cm^2), and thickness l (cm). The number of target atoms/cm^2, N_2, is $\frac{N_0 \rho l}{A}$ atoms/cm^2, where N_0 is Avogadro's number. If the rate of emission of secondary radiations is N_3/sec, the cross section is given by

$$\sigma = \frac{N_3 A e}{N_0 \rho l i} \qquad \text{cm}^2 \tag{14-11}$$

The angular distribution of the secondary radiations is usually nonisotropic, with the emission frequently concentrated in the forward angles. In this event, the cross section per unit solid angle, specified for a particular angle, is more meaningful than the total cross section for 4π steradians. The total cross section σ_t is then 4π times the average value of the cross section per steradian.

Attenuation of Monoenergetic X Rays

The attenuation in energy of monoenergetic X rays can be computed from the theory of electromagnetic interactions. An extensive literature exists on the theoretical analyses and computations, covering a wide range in energy and for all types of absorbing materials. The results have been confirmed by many experimental measurements.

1. At very low energies "photoelectric absorption" is the dominant process; secondary electrons are emitted from the atoms in the absorber, and the full energy of the photon is absorbed. The cross section for photoelectric absorption decreases sharply with increasing energy, and it is of negligible importance for energies above 0.5 Mev. The secondary-electron energies are reduced below the incoming photon energy by amounts determined by the binding energies of the electrons in the atoms. Secondaries lose energy, by ionization of other atoms in the absorber, within a short distance because of their predominantly low energies. The angular distribution is essentially isotropic.

2. The Compton effect is an elastic collision between a photon and an atomic electron in which energy and momentum are conserved. Compton scattering refers to the secondary photons, which are reduced in energy and are scattered at a finite angle relative to the incident direction. For high-energy X rays or γ rays the scattering is largely forward, so the photon beam continues with the direction and penetrating power only slightly changed. The secondary electrons are emitted at wider angles, up to but not exceeding 90°, and with their energy dependent on the angle of scattering; for high photon energies the angles of emission of the secondary electrons are close to 90°. Again, these secondary electrons lose energy primarily through ionization in the absorber, although those of highest energy also emit tertiary X rays which are projected in the direction of the scattered electrons. The effect on a narrow beam is to degrade the energy spectrum of the forward radiation and to scatter a significant fraction of energy out of the beam as secondary electrons. The interaction cross section decreases with increasing X-ray energy, but at a much slower rate than the photoelectric interaction. This is the dominant process for most materials in the energy range above 0.5 Mev up to 10 or 20 Mev, and it is significant at even higher energies for low-Z materials.

3. Positron-electron pair formation becomes energetically possible above a threshold photon energy of 1.02 Mev ($2m_0c^2$), and the cross section rises with increasing energy. At high energies, the pairs are primarily projected forward, making small angles with the incident beam direction. For low-energy pairs the major energy loss is through ionization collisions in the absorber, at the customary rate of 2 Mev/(gm)(cm^2). After the positron slows down to thermal velocities, it is usually absorbed in an annihilation process with an atomic electron, releasing the total mass energy in the form of two quanta of 0.51 Mev energy, and with an isotropic angular distribution. The higher-energy secondary positrons and electrons also lose energy through radiation of bremsstrahlung, which is projected forward.

The fact that photoelectric absorption and Compton scattering decrease in probability with increasing energy, while pair formation increases in

cross section, leads to a minimum in the curve of absorption coefficient versus energy for monoenergetic X rays, with the location of the minimum a function of atomic number of the absorber. This minimum absorption coefficient μ_{min} occurs at about 3.5 Mev for Pb, 10 Mev for Cu, and 20 Mev for Al, for example. This minimum is at the energy where the cross section for pair production is approximately equal to the cross section for Compton scattering. X radiation of these energies is most penetrating in these particular absorbers. Note that these energies are considerably lower than the critical energies in these materials at which radiation loss by electrons becomes equal to ionization loss.

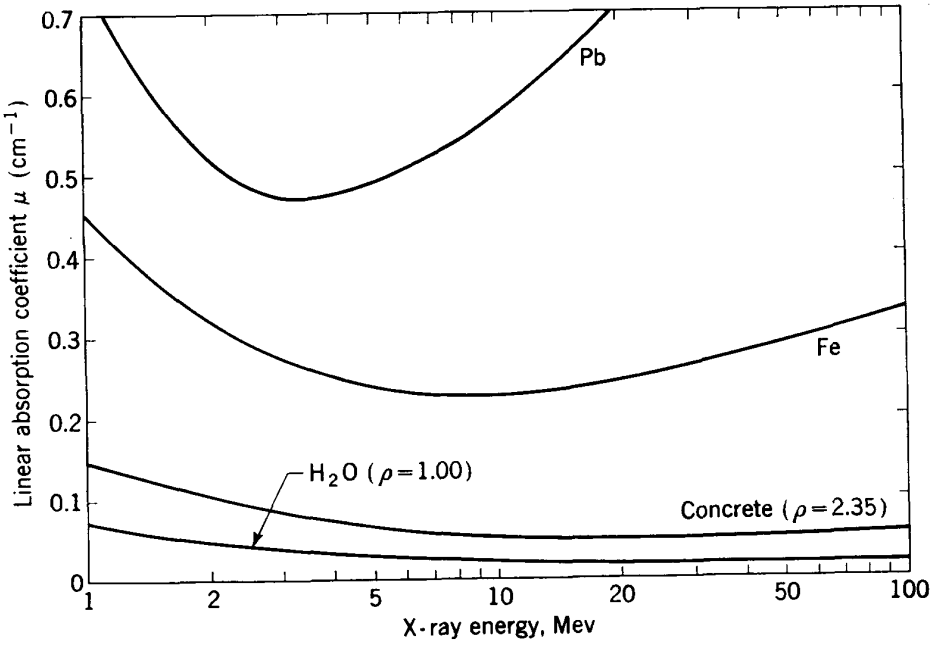

Fig. 14-5. Linear absorption coefficients for monoenergetic X rays.[17]

The ideal arrangement for computing or for measuring X-ray attenuation is with a narrow collimated beam of monoenergetic X rays traversing thin slabs of absorber composed of a single element. For this case the well-known law of exponential absorption holds:

$$\frac{I}{I_0} = e^{-\mu x} \tag{14-12}$$

where I_0 is the initial and I the final intensity after traversing a thickness x of absorber having a "linear absorption coefficient" μ. Experiments show that under ideal conditions the attenuation is exponential, as indicated by the relation above, and that the magnitudes of the observed absorption coefficients are in agreement with those computed from the interaction cross sections. Linear absorption coefficients for monoenergetic X rays in several materials are plotted as a function of energy in Fig. 14-5, taken from the *National Bureau of Standards Handbook No.*

55,[17] and each curve illustrates the minimum absorption coefficient described above.

The reciprocal of the linear absorption coefficient, $1/\mu$, is the thickness of absorber which reduces intensity to $1/e$, or to a value of $0.366I_0$; this distance is sometimes called the "e-folding length." A more widely used unit is the "half-value thickness," which, as its name implies, is the thickness of absorber which reduces intensity to $0.5I_0$; the half-value thickness is given by $L_{1/2} = (\ln_e 2)/\mu = 0.693/\mu$. Still another commonly used unit is the "10-folding length," which reduces intensity to $0.1I_0$; it is given by $L_{1/10} = (\ln_e 10)/\mu = 2.306/\mu$. When used for shielding calculations, the attenuation for absorber thickness x is given alternatively by

$$\frac{I}{I_0} = 10^{-x/L_{1/10}} \qquad \frac{I}{I_0} = 2^{-x/L_{1/2}} \tag{14-13}$$

The mass absorption coefficient $\mu_m = \mu/\rho$ has units of cm^2/g (ρ is the density in gm/cm^3), and the attenuation equation is

$$\frac{I}{I_0} = e^{-\mu_m(\rho x)} \tag{14-14}$$

where ρx is the mass per unit area of the shield, in units of gm/cm^2. When materials such as concrete are used for shielding, the mass absorption coefficient can be computed from the known fractional densities of the several elements comprising the materials and their respective absorption coefficients. The variation of μ_m with atomic number is smooth, and values can be interpolated from a few known elements. Table 14-5 gives a limited number of values of mass absorption coefficient

TABLE 14-5
MASS ABSORPTION COEFFICIENTS, μ_m, FOR MONOENERGETIC X RAYS AND γ RAYS
(In cm^2/gm)

Material	Z	Energy, Mev						
		0.01	0.05	0.10	0.50	1.0	5.0	10.0
Hydrogen	1	0.385	0.335	0.294	0.173	0.126	0.0502	0.0321
Carbon	6	2.13	0.178	0.149	0.087	0.0635	0.0270	0.0194
Oxygen	8	5.69	0.196	0.151	0.0871	0.0636	0.0276	0.0206
Aluminum	13	26.3	0.325	0.161	0.0840	0.0613	0.0282	0.0229
Silicon	14	34.1	0.389	0.172	0.0869	0.0635	0.0296	0.0243
Iron	26	178	1.83	0.344	0.0828	0.0595	0.0313	0.0295
Lead	82	80.1	5.19	5.29	0.145	0.0684	0.0426	0.0489
	Density:							
Air	0.00129	4.88	0.194	0.151	0.0869	0.0635	0.0274	0.0202
Water	1.00	5.09	0.212	0.167	0.0967	0.0706	0.0301	0.0219
Normal concrete	2.35	.....	.....	0.15	0.087	0.063	0.029	0.023

μ_m for several elements and common materials in the energy range below 10 Mev.

Attenuation in Thick Absorbers and with Broad Beams

A monoenergetic beam of X rays undergoes Compton scattering in the absorber which degrades photon energy; the energy distribution broadens and the average photon energy is reduced with increasing absorber thickness. In general, however, the higher-energy photons persist most nearly in the incident direction, while those of reduced energy tend to be scattered out of a collimated beam. The result is a relatively slow change in the penetration of the forward beam if measured with narrow-beam geometry. Under ideal conditions the absorption coefficient is constant out to very large absorber thickness.

Secondary electrons from Compton-scattering processes are emitted mostly at angles approaching 90°, and their energy content is spread laterally away from the collimated beam. Some lower-energy scattered photons are also deflected out of the direct beam, and tertiary processes extend the transverse spread still further. The result is a steady build-up in the initial layers of absorber of the ionizing particles which accompany the X-ray beam, along with a lateral broadening of the cross-sectional area of the envelope of these ionizing particles. A large ionization chamber placed behind absorbers will read a considerably higher intensity than a small one limited to the dimensions of the collimated beam. Such broad-beam measurements detect this build-up in ionization intensity which is not observed in narrow-beam geometry. A semilog plot of intensity as a function of absorber thickness shows wide deviations from the constant slope observed with narrow beams, especially for the initial layers, so that no unique absorption coefficient can be assigned. With increasing absorber thickness the mixture of primary, secondary, and tertiary radiations approaches an equilibrium, and the slope of the semilog plot approaches a constant absorption coefficient which is a true measure of the ultimate attenuation. However, the magnitude of this broad-beam thick-absorber coefficient is in all cases considerably smaller than that for a narrow collimated beam.

Practically all shielding applications involve the total energy transmitted through absorbing walls and so require analysis in terms of broad beams. The unique absorption coefficients for narrow-beam monoenergetic X rays illustrated in Fig. 14-5 and Table 14-5 do not apply. Furthermore, there is no simple and conclusive analysis to determine the magnitude of intensity build-up or the magnitude of the broad-beam attenuation coefficient for all situations. Rather, it is necessary to analyze each separate shielding problem in terms of the geometry of the absorbing shields, the amount of incident beam collimation, and the composition of the absorbers.

As an example of the difference in attenuation between narrow-beam and broad-beam geometry, Fig. 14-6 is a semilog plot of attenuation in steel of the essentially monoenergetic 1.2-Mev gamma rays from Co^{60} when observed through plane steel slab absorbers under broad-beam geometry; this plot is given in a paper by Halmshaw and Knapp reported by Price, Horton, and Spinney.[18] Also plotted on this figure is the attenuation curve for narrow-beam conditions using the monoenergetic absorption coefficient for this energy. It can be noted that the observed intensity is as much as five times greater for some absorber thicknesses than that predicted by the narrow-beam absorption curve, because of an initial build-up of ionization intensity. It may also be noted that the

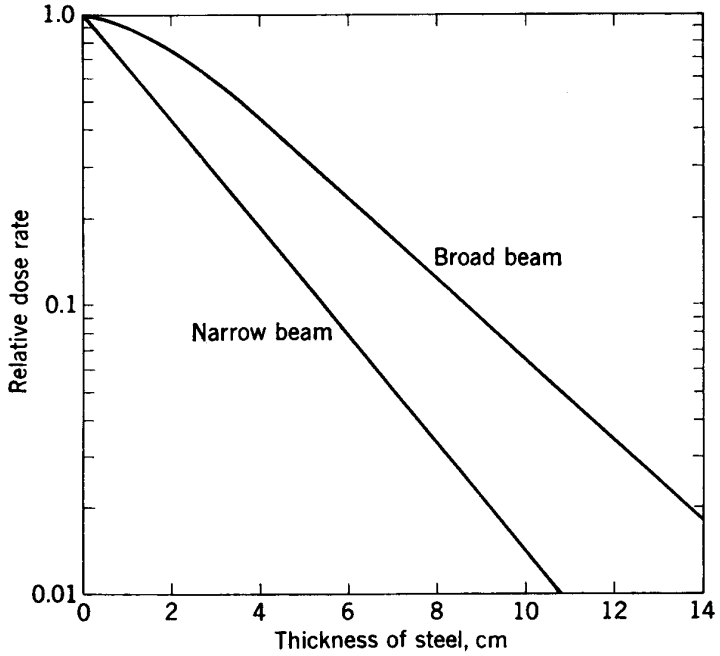

Fig. 14-6. Broad-beam and narrow-beam attenuation plots for 1.2-Mev γ rays.[18]

equilibrium value of broad-beam absorption coefficient is smaller than the narrow-beam coefficient, by about 25 per cent in this case. This apparent "hardening" of the radiation can be understood as a consequence of the production of secondary electrons and degraded photons deep in the absorber.

It is sometimes convenient to describe the difference between the results of measurements in narrow-beam and broad-beam cases by means of build-up factors. This problem is discussed by Price, Horton, and Spinney,[18] who present the results of build-up-factor calculations in a series of graphs and empirical relations. We shall not reproduce a detailed analysis of the problem, but shall present only some general results and conclusions:

1. The intensity increase in the initial layers of absorber can be described by a numerical build-up factor B in the attenuation equation

$$\frac{I}{I_0} = B \frac{1}{4\pi r^2} e^{-\mu_0 x} \tag{14-15}$$

where μ_0 is the monoenergetic X-ray linear absorption coefficient and the factor $1/(4\pi r^2)$ is the inverse-square reduction in intensity with distance r from the source.

2. The build-up factor B as defined above increases with absorber thickness, so the result is an apparent reduction in the value of μ_0.

3. The magnitude of the build-up factor is largest for low-energy radiation in low-Z shielding materials; however, this is of significance only in the shielding of very-low-energy accelerators.

4. Build-up factors depend on the geometry of the source and shield. They are largest for point isotropic sources with spherical shields (e.g., Co^{60} bomb) and smaller for plane absorbers with monodirectional sources characteristic of most accelerator shielding problems.

5. The build-up factor is of the order of 10 after 15 mean free paths (mfps) for higher-energy (10-Mev) X rays in dense absorbers. This means that additional absorber is required beyond that computed from the monoenergetic absorption coefficient, sufficient to increase the attenuation by about another factor of 10.

Bremsstrahlung Spectra from Thin Targets

The energy distribution of X rays from targets bombarded by high-energy electrons can be computed from the quantum-mechanical theory of Bethe and Heitler.[13] An expression derived by Schiff[15] gives the probability for emission of a photon of energy k in the range $d(k/W)$, where W is the incident electron energy. This expression has been used to compute the number of photons emitted in the forward direction, as a function of photon energy, for a sequence of incident electron energies between 5 and 100 Mev, given in the *National Bureau of Standards Handbook No.* 55.[17] In illustration, the spectral distribution for 16-Mev electrons is shown in Fig. 14-7, taken from the Handbook. The distribution is presented in two ways. One curve shows the relative number of photons per unit photon energy interval, which is given by the quantity $W^2\Gamma/k$, where W is total electron energy, Γ is a quantity proportional to the spectrum intensity in the forward direction, and k is photon energy. The other curve shows the X-ray intensity, which is number of photons times photon energy.

Experimental measurements of the X-ray energy distribution for a few discrete electron energies have been made with the Bureau of Standards 50-Mev betatron, and they are found to be in good agreement with the

theoretical distributions. There seems no reason to doubt that the theoretical representation is adequate for the purpose of this discussion.

The angular distribution of the radiation is a function of electron energy, photon energy, and the atomic number of the target. Stearns[19]

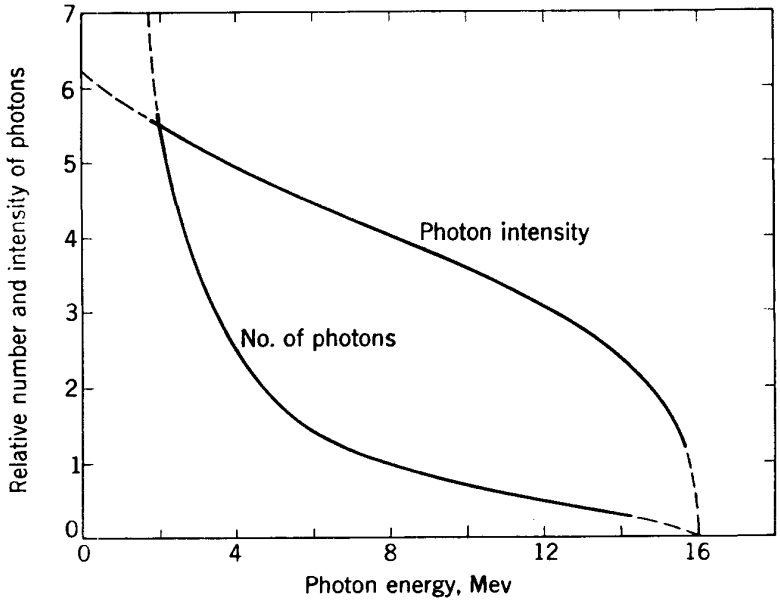

Fig. 14-7. X-ray photon spectrum and intensity spectrum for thin-target X rays from a 16-Mev betatron.[17]

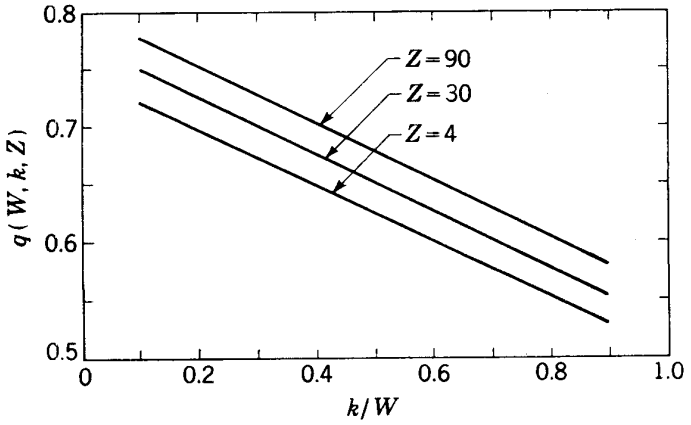

Fig. 14-8. Angular distribution function $q(W,k,Z)$ for bremsstrahlung spectra.[19]

has developed an expression for the root-mean-square (rms) angle of emission of photons, $\langle\theta^2\rangle^{1/2}$, which can be expressed as

$$\langle\theta^2\rangle^{1/2} = q(W,k,Z)\,\frac{m_0c^2}{W}\ln\frac{W}{m_0c^2} \tag{14-16}$$

where W is the total energy of the electron, $m_0c^2 = 0.51$ Mev is the electron rest energy, and $q(W,k,Z)$ is a function of electron energy, photon energy, and atomic number which is a slowly varying function of the ratio k/W and is of the order of magnitude of unity. Values of $q(W,k,Z)$ are plotted in Fig. 14-8 for several values of atomic number and for a wide range in the energy ratio k/W.[19] The radiation is strongly collimated in the forward direction, most sharply at the highest energies. For example, with 100 Mev electron energy and for a Pb absorber, the lower-energy photons have an rms angle of 2.1×10^{-2} radian (1.2°), and the higher-energy photons have a smaller angle of 1.5×10^{-2} radian; at 1000 Mev these angles are about 3.0×10^{-3} and 2.2×10^{-3} radian.

This sharp forward collimation of bremsstrahlung radiation is one of its most significant characteristics. The radiation from high-energy betatron and synchrotron targets is projected out of the orbit tangentially in such a self-collimated beam. Heavy shielding by dense materials is required in the forward direction, broad enough to encompass the diverging shower of secondary photons and electrons from the main beam; in other directions the shielding can be thinner, or of less dense materials.

Attenuation of Continuous Spectra in Thick Absorbers

In thick absorbers the energy spectrum of the X rays emitted from the primary target is degraded further, to a spectrum of still lower average energy. It differs from a monoenergetic beam in the sense that a continuous spectrum exists initially, so a distribution which is in equilibrium with its secondaries is reached at somewhat smaller absorber thickness. Nevertheless, scattering processes continue to broaden the beam, and the absorption coefficient observed with a broad beam is again lower than that for a collimated narrow beam. Since the magnitude of the attenuation depends in each case on the geometry and composition of the shields, on the collimation of the beam from the target, and on the thickness of the absorber, it is not possible to specify unique absorption coefficients for continuous spectra in thick absorbers.

Experimental measurements of the attenuation in concrete of the primary X-ray beam from the 50-Mev betatron at the National Bureau of Standards are reported in the *National Bureau of Standards Handbook No.* 55.[17] The results are shown in Fig. 14-9, as a semilog plot of the ionization intensity behind plane concrete barriers as a function of concrete thickness, and for electron beam energies of 6, 10, 20, 30, and 38 Mev. The density of the (normal) concrete was 147 lb/ft^3 ($\rho = 2.35$ gm/cm^3). On this semilog plot the attenuation curves show a small intensity build-up in the initial layers of absorber, similar to but of smaller magnitude than that for monoenergetic beams, but the curves become straight for thick absorbers, indicating a constant terminal absorption coefficient appropriate to the equilibrium mixture of radiations in each case. These

terminal absorption coefficients range from 0.172/in. for 6 Mev electron energy to 0.130/in. at 38 Mev. In fact, the terminal slope is essentially the same for all energies above 20 Mev; other observations and calculations in the same laboratory show that the same value is valid up to 100 Mev.

We conclude from these measurements that for this geometry and material a single, common value of terminal absorption coefficient holds for all continuous bremsstrahlung spectra coming from electrons of all energies from 20 to 100 Mev. In concrete this terminal value of the linear absorption coefficient is

$$\mu = 0.130/\text{in.}$$
$$= 0.0513/\text{cm} \qquad \text{(concrete)}$$

The equivalent mass absorption coefficient is

$$\mu_m = \mu/\rho$$
$$= 0.0218\ \text{cm}^2/\text{gm} \qquad \text{(concrete)}$$

Comparison with the monoenergetic absorption coefficients of Fig. 14-5 shows this value to be only slightly larger than that at the minimum of the absorption coefficient versus energy curve for this mixture of materials.

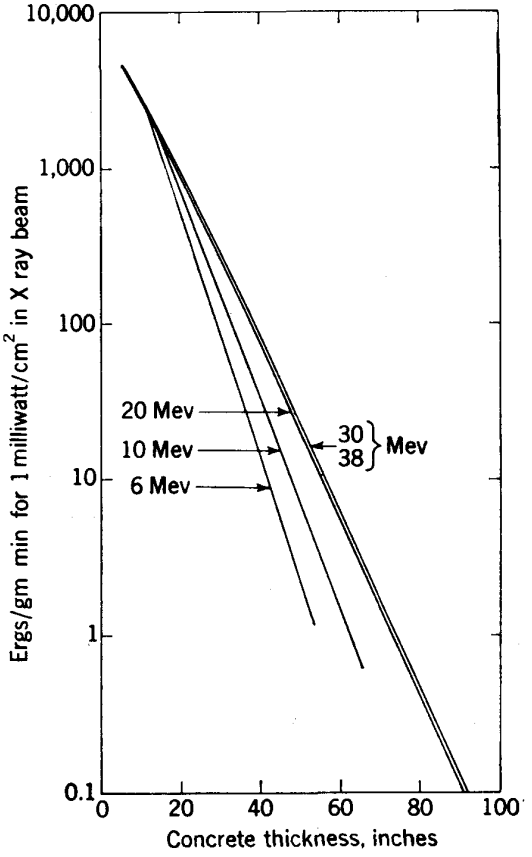

Fig. 14-9. Attenuation of X rays in concrete.[17]

A valid general conclusion is that the minimum absorption coefficient for monoenergetic radiation is a lower limit on, and a close approximation to, the effective terminal value of absorption coefficient for bremsstrahlung. This conclusion can be used to determine terminal absorption coefficients for other shielding materials. Figure 14-10 is a plot of these minimum mass absorption coefficients μ_{min} as a function of Z; for each element the value of the absorption coefficient plotted is for that energy at which monoenergetic X radiation is most penetrating.

Attenuation calculations which assume a single value of minimum absorption coefficient obviously will not give accurate results for thin absorbers, since these assumptions do not adequately describe the build-up in the initial layers; it is necessary to employ a more detailed analysis to estimate the build-up factor, as described earlier for mono-

energetic radiations. However, for thick absorbers the small error caused by neglecting the initial build-up in intensity is compensated by use of the minimum absorption coefficient. It is well to remember, however, that this terminal value is only an average or effective absorption coefficient which summarizes the complex effects of the broad energy distribution and of the mixture of radiations in the photon-electron shower.

As an example we shall compute the required thickness in each of several materials for shielding the X-ray beam from a 50-Mev betatron. We take the emergent X-ray beam intensity to be 500 r/min at 3 ft from the target (r_0). This is equivalent to about 5 milliwatts/cm^2 and is a

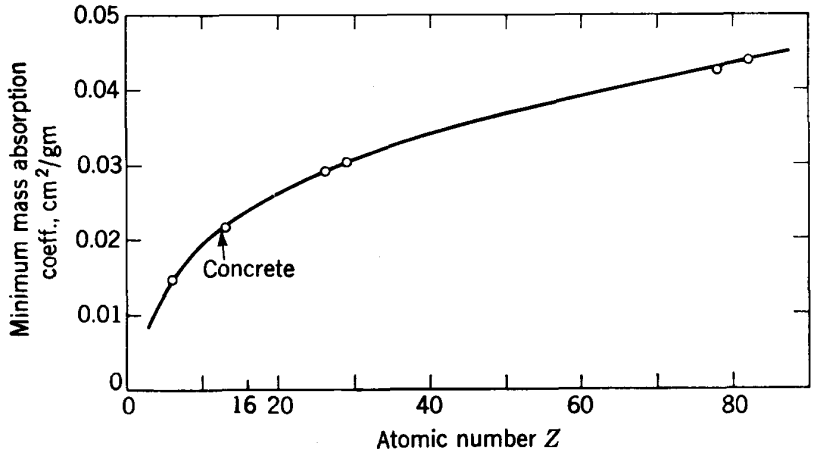

Fig. 14-10. Minimum values of mass absorption coefficients for monoenergetic X rays.

representative value of X-ray intensity from such a betatron as that reported in the *National Bureau of Standards Handbook No.* 55.[17] The intensity behind shielding walls at a distance of 30 ft (r) is to be reduced to the pwd rate of 100 mrad/week (see Sec. 14-1). We take a work week of 40 hr or 2.4×10^3 min. So the desired total attenuation is

$$\frac{I}{I_0} = \frac{0.100}{500} \times \frac{1}{2.4 \times 10^3} = 8.3 \times 10^{-9}$$

If we use the minimum mass absorption coefficient described above and include the inverse-square distance factor, the attenuation relation is

$$\frac{I}{I_0} = \left(\frac{r}{r_0}\right)^2 e^{-\mu_{\min}(\rho x)} \tag{14-17}$$

Values of the appropriate minimum mass absorption coefficients for concrete, iron, and lead are taken from Fig. 14-10. We obtain the following results:

Shielding material	Minimum mass absorption coefficient, cm^2/gm	Shield thickness		
		gm/cm^2	cm	in.
Concrete	0.0218	536	228	90
Iron	0.0290	403	52.5	21
Lead	0.0414	282	25.0	10

This concrete thickness is slightly greater than the comparable figure recommended for shielding in *National Bureau of Standards Handbook No.* 55, because of the use here of a lower value of the permissible dose. There are no equivalent experimental measurements to check the predicted thickness for iron or lead shielding.

Photoneutron Production

A word of caution is necessary with regard to drawing conclusions about X-ray shielding requirements solely from the X-ray attenuation calculations. This has to do with the production of neutrons in the absorber by the higher-energy X rays. In the foregoing analysis no attempt was made to include the special problems of neutron production or neutron shielding.

Photoneutrons from the (γ,n) process are produced in essentially all elements, with observed threshold energies varying from 2.2 Mev (deuterium) to nearly 20 Mev. Many of these processes lead to the production of radioactive isotopes, with which measurements have been made of the cross sections for production and the threshold energies. Table 14-6 lists the threshold energies of elements between $Z = 6$ and $Z = 79$, taken from the *National Bureau of Standards Handbook No.* 55.[17] Threshold energy falls irregularly with increasing Z, from 18.7 Mev for carbon to 7.7 Mev for tantalum. For the very heavy elements the threshold is at about 7.0 Mev, which is the average neutron binding energy in such elements.

Most of the measurements of photoneutron thresholds have been made with betatrons and electron linear accelerators of 20 to 50 Mev energy. At these energies the photoproduction yields are small, not exceeding a value of 10^7 neutrons/mole of radiated material for 1 r of radiation exposure (measured behind $\frac{1}{8}$ in. Pb) except for a few of the heaviest elements. From measurements at 50 Mev, Baldwin and Elder[21] report that the yield per mole roentgen is given by the empirical relation

$$\text{No. neutrons/(mole)(r)} = 1860Z^2 \qquad (14\text{-}18)$$

The total yield does not change significantly with energy from 20 to 50 Mev in Pb. This shows that the process is a resonance interaction, in

which only X rays within a rather narrow energy range are effective. The neutron yield is determined by the number of quanta within this energy band in the bremsstrahlung X-ray spectrum.

Photoneutrons are produced in the absorber, primarily in the initial layers where the major X-ray attenuation occurs. They have a roughly isotropic angular distribution (in the heavy elements), spreading out from their source within the absorber. The attenuation and absorption of these neutrons depend strongly on the material of the absorber. Low-Z, and especially hydrogenous, materials are most effective in moderating

TABLE 14-6
PHOTONEUTRON THRESHOLD ENERGIES

Element	*Threshold energy, Mev*
Carbon, C^{12}	18.7
Nitrogen, N^{14}	10.7
Oxygen, O^{16}	15.6
Magnesium, Mg^{24}	16.2
Aluminum, Al^{27}	14.4
Silicon, Si^{28}	16.8
Phosphorus, P^{31}	12.3
Sulfur, S^{32}	14.8
Potassium, K^{39}	13.2
Calcium, Ca^{40}	15.9
Iron, Fe^{54}	13.8
Copper, Cu^{63}	10.9
Copper, Cu^{65}	10.2
Zinc, Zn^{70}	9.2
Bromine, Br^{79}	10.7
Bromine, Br^{81}	10.2
Selenium, Se^{82}	9.8
Zirconium, Zr^{90}	11.9
Silver, Ag^{107}	9.5
Antimony, Sb^{121}	9.25
Praseodymium, Pr^{141}	9.4
Tantalum, Ta^{181}	7.7
Gold, Au^{197}	8.0

the neutrons to low energy, so they can be captured in nuclear interactions. However, the common slow-neutron capture process (n,γ), which has the largest cross section in most materials, releases gamma rays which are highly penetrating in such low-Z materials.

A general conclusion is that shielding for X rays of over 10 Mev must include some provision for attenuation of the photoneutrons. Although Pb and Fe are both highly efficient for X-ray attenuation and form compact shields, they are not suitable as neutron absorbers for neutrons of less than 1 Mev energy. For this reason concrete is preferred (it has a large fraction of hydrogen and low-Z materials), even though it makes a more bulky shield. Other alternatives are to use multiple layers of

different materials, such as Pb-concrete-Pb and Pb-paraffin-concrete. The optimum design depends on the energy of the X-ray spectrum. The neutron yield must be estimated in each case, and sufficient neutron absorber must be provided. Further details of neutron attenuation are discussed in Sec. 14-6.

14-5. GAMMA-RAY ABSORPTION

Gamma rays and X rays are actually identical in so far as their observed characteristics are concerned. The two names both describe electromagnetic radiation of relatively high energy. X-ray beams consist of photons generated by slowing down of electrons; they are, in effect, bremsstrahlung. Gamma rays, on the other hand, originate in nuclear interactions. Sometimes photons described as gamma rays may have lower energies than other photons described as X rays; sometimes the inverse is the case. The two terms are used only to discriminate between the mechanisms by which the photons originate. Consequently, absorption of gamma rays will follow from the same processes already discussed in the preceding section in connection with X rays.

Gamma rays are produced by excitation of nuclear energy levels, either in a target or in residual nuclei, in essentially all nuclear interactions. The line spectra observed are characteristic of the nuclei involved, and the relative intensity of the lines varies with the type and degree of excitation. Since many different targets may be used in an accelerator, shielding estimates can be based on a composite spectrum which is an envelope of the line spectra covering a large number of possible targets, incident particles, and interactions.

A composite spectrum representative of the energy distribution of γ rays from cyclotron targets is pictured in Fig. 14-11. It has been developed from the following considerations:

1. Most targets for nuclear research have low atomic number, for which the average excitation level spacing is about 0.5 Mev.
2. A few excitation states up to 10 Mev energy exist in a few light nuclei.
3. Average spacing of energy levels in heavy targets is less than 0.1 Mev.
4. γ rays occur primarily in cascade steps between energy levels, with small probability for high-energy quantum emission.

A similar situation exists in the decay of the fission products from U fission, for which the composite γ-ray energy distribution has been measured. For comparison the γ-ray spectrum for fission is also shown in Fig. 14-11. The assumed composite spectrum for accelerator reactions has a somewhat larger fraction of high-energy photons, associated with the wider energy-level spacings in light nuclei.

The composite γ-ray spectrum described above has a shape roughly similar to the X-ray bremsstrahlung distribution for an electron energy of about 10 Mev. As described in the preceding section on X rays, the attenuation of such a continuous distribution cannot be determined from monoenergetic absorption coefficients. The same conclusions are valid as those for X rays, which showed that a "terminal" absorption coefficient exists which can be approximated by the minimum absorption coefficient for monoenergetic photons in the material. However, because of the relatively low energy of the γ-ray spectrum, the terminal coefficient

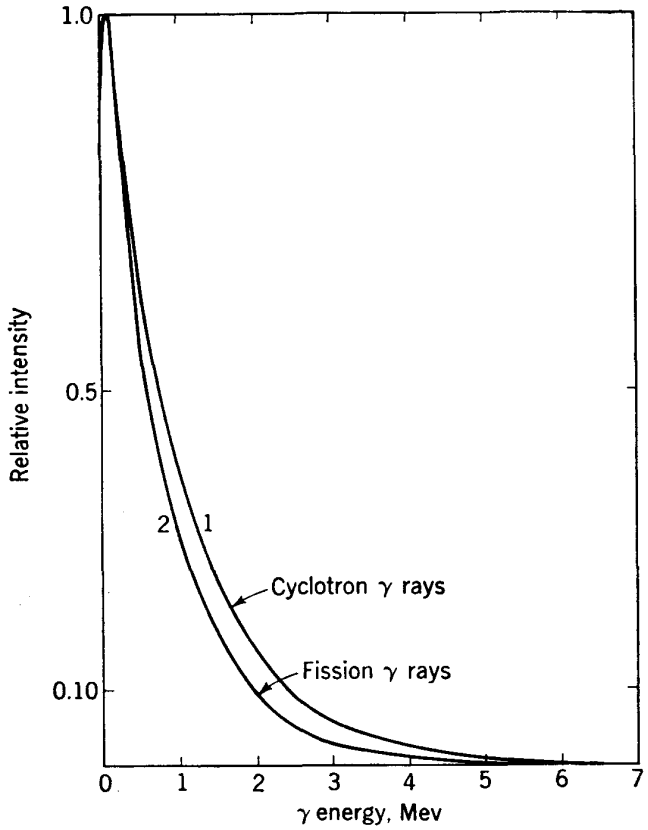

Fig. 14-11. γ-ray spectra, assumed for cyclotron (1) and observed for fission (2).[18]

will be somewhat larger than the minimum value recommended for high-energy X-ray spectra. A good approximation can be obtained from the terminal coefficient for 10-Mev bremsstrahlung (see Fig. 14-9), which is 0.155/in. concrete. The equivalent linear absorption coefficient in Pb would be about 0.55/cm, and the corresponding mass absorption coefficient is $\mu_m = 0.048$ cm^2/gm. This is somewhat larger than the minimum coefficient for Pb (0.042 cm^2/gm), which occurs at 3.5 Mev photon energy.

Photoneutron production by nuclear γ rays will be negligible, since only a small fraction have energies above the photoproduction thresholds for most materials. So, Pb absorbers of relatively small thickness are usu-

ally adequate for attenuating γ rays from an accelerator target. However, the shielding required for other radiation components, such as neutrons, will for most accelerators be considerably thicker than that required for γ rays alone. As a consequence, it is seldom necessary to analyze the γ-ray problem separately.

A more serious problem is the shielding for γ rays released in secondary reactions. Neutron capture, through the (n,γ) process, in the shielding material used for neutron attenuation releases γ rays deep in the shield. If the shield consists of low-Z materials, which are most effective for neutron attenuation, the γ-ray intensity emerging from the shield may be significant. One technique for controlling secondary γ-ray intensity is to add high-Z material to the shield. Another is to add a small amount of boron to the shielding mixture; boron has a large cross section for nonradiative capture of slow neutrons. These problems will be discussed in the section to follow.

14-6. NEUTRON SHIELDING

Neutrons are among the most penetrating of the secondary radiations from positive-ion accelerators and are potentially the greatest biological hazard. They are produced in the beam targets and also in the materials forming the defining channel for the emergent beams. They originate as fast neutrons released in nuclear disintegration reactions. Both the intensity of neutrons and their distribution in energy are determined by the particular nuclear interaction. Since a wide variety of target materials may be used in a laboratory research program and different charged particles may be accelerated, the shielding requirements for an accelerator should be based on the intensities anticipated for the highest-yield processes.

The attenuation and absorption of neutrons is a complex process involving many different kinds of interactions with atoms in the absorber, each of which has its own characteristic variability with neutron energy. The most probable interactions are elastic and inelastic collisions of the fast neutrons with nuclei in the absorber; these scattering processes involve large angular deflections and reduce neutron energy in large steps. Neutrons also produce disintegrations in which part or all of their energy is transferred to product particles or to excitation of the residual nucleus, which emits its excitation energy in the form of γ rays. After losing most of their energy through nuclear collision, the neutrons (if they survive) eventually come into thermal equilibrium with their surroundings by transferring the remaining energy by molecular excitation to the molecules of the absorber material, thereby raising the temperature of the absorber. Thermal neutrons diffuse through the absorber, making many elastic collisions before being absorbed. Their ultimate fate is to be

absorbed by capture in an atomic nucleus, and the most frequent reaction is that of radiative capture, in which the binding energy of the neutron in the nucleus is released in the form of γ radiation.

The problem of moderation of neutron energy lends itself to theoretical analysis, since elastic scattering involves the conservation of energy and momentum. Statistical features of the passage of neutrons through matter are described by the "transport theory." Analyses involving the time required to slow down neutrons are developed in the "age theory." Statistical studies of the number of impacts, and the times involved, lead to concepts such as the "slowing-down length" or the "relaxation length," which is the thickness of material in which neutron energy is reduced to $1/e$ of its initial value. When neutrons attain thermal equilibrium, their further motion is analyzed by the "diffusion theory." Many theoretical articles and books have been written on these subjects. It is now possible to compute the properties of some of the simpler reactor shield systems directly from the theoretical relations. We give here only a brief survey of the more important interactions and the most pertinent data on the properties of reactor neutrons. For a more complete understanding the reader is referred to the several books on the subject, such as "Radiation Shielding" by Price, Horton, and Spinney[18] of the Harwell Atomic Energy Research Establishment, "Attenuation of Gamma Rays and Neutrons in Reactor Shields," edited by Goldstein[7] for the United States Atomic Energy Commission, as well as the individual references which will be cited.

The purpose of the present discussion is to provide information sufficient for a qualitative understanding of the problems of neutron shielding in accelerators and for rough estimates of accelerator shielding requirements. Far less information is available than in the reactor field; basic constants of accelerator neutrons are not available for the precise treatment possible with reactor neutrons. Because of this lack of data, we are forced to accept and adapt many of the conclusions and much of the data coming from reactor studies. It should be noted, however, that accelerator neutrons can be quite different in their energy distributions and in their shielding requirements.

The cross section of a neutron interaction with an atomic nucleus is commonly given in units of 10^{-24} cm^2 or "barns."* As defined previously, the atomic cross section σ is the equivalent area of the neutron-nucleus interaction. When the cross section is calculated from reaction yields (see Sec. 14-4), the resulting value in square centimeters or barns can be visualized as the area of a circle centered on the nucleus, within

* The name of this unit appears to have developed early in the atomic-energy program in the United States, based on the observation of an unexpectedly large cross section for a particular slow-neutron process which was described as being "as big as a barn."

which the center of the neutron must pass if the probability of the interaction is taken as 100 per cent inside this area and zero outside.

The geometric cross section of an interaction is calculable from the physical dimensions of the particles. If we take as the radius of a proton or neutron the accepted value when these particles are bound in nuclei, $r_0 = 1.3 \times 10^{-13}$ cm, the interaction radius of a proton-neutron interaction would be $2r_0$. The geometric cross section would then be $\sigma_{geom} = \pi(2r_0)^2 = 0.21 \times 10^{-24}$ cm^2 = 0.21 barn.

Cross sections obtained from observed yields are in some cases smaller and in other cases much larger than the geometric cross sections. A smaller cross section means either that the neutron can penetrate the nucleus without interacting or that a more probable competing process is involved. A larger cross section can be interpreted as due to a neutron wavelength or effective size which is larger than that for a bound neutron, following the concepts of the wave-mechanical theory of nuclear interactions. The neutron wavelength is given by $\lambda = h/mv$, where h is the Planck constant of action and mv is the neutron momentum. For slow or thermal neutrons, the wavelength is hundreds of times larger than nuclear dimensions.

Sources of Accelerator Neutrons

The largest interaction cross sections for neutron production are for deuteron reactions on light elements, such as D(d,n), Li(d,n), and Be(d,n). At low deuteron energy the cross section increases with energy in a roughly exponential manner, following the potential-barrier penetration function for the incident deuteron. For energies above the potential barrier the cross section rises to a peak value and then falls off slowly with still higher energy, roughly proportional to $1/v$, where v is deuteron velocity. Individual reactions may show resonance peaks at particular energies, determined by the detailed energy-level structure of the nuclei involved. However, when averaged over the individual energy levels, the cross section has the general shape described above.

Total neutron yield from a thick target increases with energy, because of the increased depth of penetration with increasing particle range. Charged-particle range increases roughly with $T^{3/2}$, so the total yield at energies much higher than the potential barrier also increases approximately with $T^{3/2}$.

Target cooling limitations may restrict the maximum yield of neutrons from accelerators. Although the highest atomic cross sections are for deuterium (in the form of heavy ice) or lithium targets, the beam power which can be absorbed and cooled without damage to these targets is small. Larger beam currents can be used with metallic beryllium targets, with which more efficient cooling techniques have been developed. The highest neutron intensities are obtained with cyclotrons, for which the

beam power is greater than for other accelerators; the problems of cyclotron target cooling are described in Chap. 6. For cyclotrons in the 5- to 20-Mev energy range, the highest neutron intensities are observed with deuterons on water-cooled Be targets, using the internal resonant beam.

The thick-target yield for 15-Mev deuterons on a Be target has been measured (University of California 60-in. cyclotron) to be 1 neutron per 200 deuterons, or 3×10^{13} neutrons/sec for a 1-ma beam. Because of the small beam dimensions at the target, which with an internal resonant beam can seldom be made larger than a few square centimeters, there is a practical limit on the beam power which can be dissipated in the target with the present known techniques of cooling; this limit is about 5 kw for cyclotron internal targets. At 15 Mev this means that the beam current is restricted to about 0.33 ma, and the neutron yield is about 1×10^{13} neutrons/sec. Higher resonant-beam currents can be produced in a cyclotron, and they are used when the object is to produce a high-intensity emergent beam. However, the useful emergent beams are seldom larger than 20 to 30 per cent of the resonant beams, and emergent beams greater than 0.33 ma are a rarity. We conclude that a neutron yield of about 1×10^{13} neutrons/sec is a practical maximum for cyclotrons of this energy range.

Neutron output is smaller, in general, for other accelerators and for other incident particles. With incident protons the highest-yield process is the (p,n) reaction, in which the cross sections are less than 0.2 of those for the parallel deuteron reactions. Lower energy also reduces yield. A 1-ma beam of protons from a 4-Mev electrostatic generator will produce only about 10^{11} neutrons/sec. Neutron output is still smaller from electron accelerators, in which the neutrons are produced by the secondary X rays through the photoproduction or (γ,n) process, and mostly in the shielding materials used to define channels for the X-ray beam. A 50-Mev betatron, for example, will produce about 10^7 neutrons/mole of high-Z absorbing material, per roentgen of radiation.[17] With typical operating intensities the X-ray beam will be about 500 r/min at 3 ft from the betatron target; the total neutron yield would then be about 10^8 neutrons/mole of absorber.

Neutron energy distributions are line spectra, associated with the energy levels of the nuclei involved, and are roughly similar to the γ-ray energy distributions. Single levels can dominate the distribution in light elements where energy levels may be widely spaced; in a few examples the neutrons are essentially monoenergetic. In heavier targets where energy levels are more closely spaced, the intensity is distributed over a larger number of lines, which have a wide spread in energy. In all cases the imperfect energy resolution of measuring instruments makes the observed curves take on the appearance of continuous energy distributions.

A typical neutron energy distribution is that for 16-Mev protons on a Be target in a cyclotron, observed by Gugelot and White[22] (see Fig. 14-12). Neutron energy was observed by measuring the lengths of proton recoil tracks in photographic emulsions, with suitable calculations to determine the initial neutron energies; the statistical accuracy leaves much to be desired. This distribution has a peak at about 2 Mev and a tail extending up to 9 Mev energy. Note that the distribution may have a different shape for other neutron-production interactions or for incident particles of different energy.

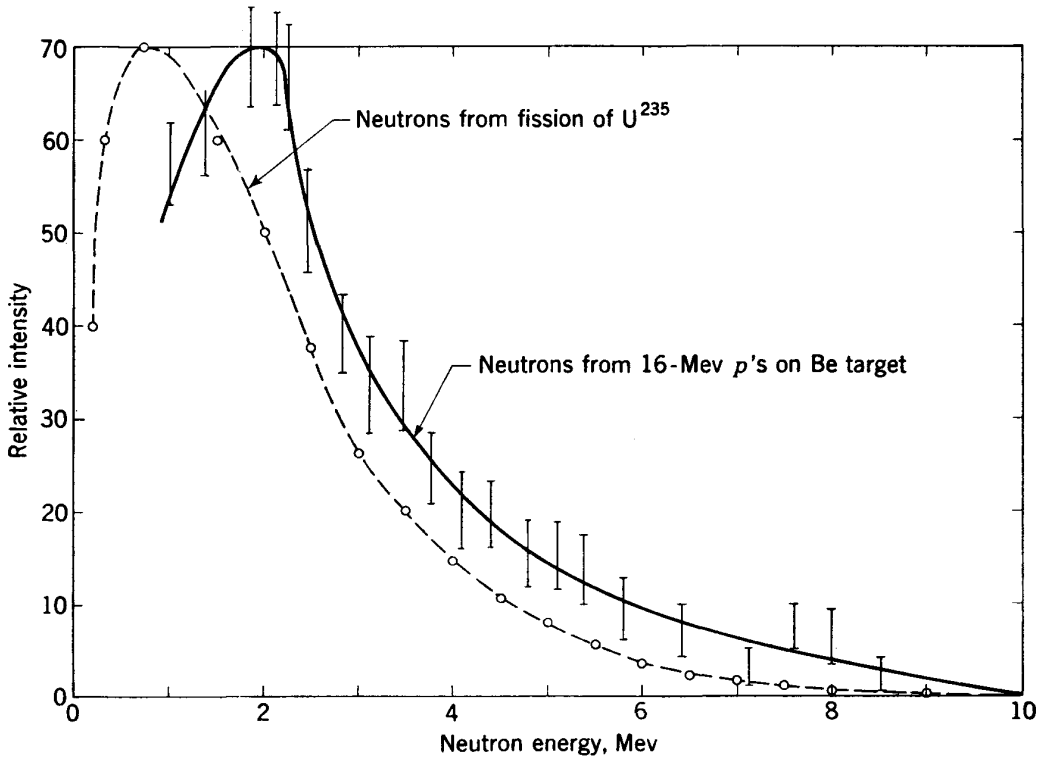

Fig. 14-12. Neutron energy distributions from 16-Mev protons on Be target[22] and from U fission.[18]

The spectrum of neutrons from the fission reaction of U^{235} is similar to the cyclotron spectrum in its basic shape. To illustrate, the U-fission spectrum[18] is also plotted in Fig. 14-12. The cyclotron spectrum observed by Gugelot and White is displaced to higher energy by about 1 Mev throughout, relative to the fission spectrum; this is a feature which may be characteristic only of this particular reaction. However, since the shapes of the neutron spectra are so similar, it is possible to utilize the extensive experimental studies and theoretical calculations of neutron attenuation in the field of nuclear reactors; these results can be applied, with slight modifications for the higher average energy, to the problems of shielding for accelerator neutrons.

The angular distribution of neutrons from a target is determined by

the energy-momentum properties of the individual interaction. At low and medium bombarding energies the distribution is essentially isotropic, with a slight peaking in the forward direction. The forward peak is more prominent at higher energies. However, scattering and absorption in the physical structures of the accelerator and in the target mounting usually dominate the angular distribution as observed. For example, the magnet poles of a cyclotron absorb and reflect neutrons from an internal target, and most of the flux emerges in the plane of the accelerator chamber.

Degradation in energy by scattering in the walls of the shielding enclosure of an accelerator will also severely modify the initial energy distribution. An equilibrium mixture of radiations is developed within the enclosure which includes fast neutrons, slow neutrons, γ rays, and other components. The "source intensity" of such a mixture of radiations is difficult to define or to measure. For shielding calculations the fast-neutron component usually can be taken as the dominant one, and the quantity needed for calculations is the flux of fast neutrons/(cm^2)(sec) at the shielding wall.

As an example, consider the neutron flux at the wall of a cyclotron enclosure at 10 ft from the target, with 10^{13} neutrons/sec emitted from the target. Without consideration of scattering, and assuming an isotropic distribution, the flux at the wall would be 0.85×10^7 neutrons/(cm^2)(sec). Back scattering from the walls, or forward peaking of the angular distribution, might increase the flux to about 2×10^7 neutrons/(cm^2)(sec). The attenuation factor required to reduce this flux to the level of the permissible dose rate, which is 20 neutrons/(cm^2)(sec), would be 10^{-6}. We conclude that the attenuation factors required for fast-neutron shielding in the horizontal direction of such an accelerator source of neutrons are of the order of magnitude of 10^{-6}.

Interactions between Fast Neutrons and Nuclei

Elastic Scattering. Fast neutrons lose most of their energy through elastic scattering impacts with atoms in the shield. The energy loss is greatest in hydrogen and least for the heaviest elements. Nonrelativistic particle mechanics can be used to compute the average energy loss ΔT per collision, for neutrons of energy T_0, in material of atomic weight A (atomic units). In hydrogen the average energy loss per collision is

$$(\Delta T)_{av} \simeq T_0/e = 0.37T_0 \qquad \text{for } A = 1, \text{ hydrogen} \qquad (14\text{-}19)$$

In heavier elements ($A > 2$) the average energy loss is given by the relation

$$\left(\ln \frac{T_0}{T_0 - \Delta T}\right)_{avg} = 1 + \frac{(A-1)^2}{2A} \ln \frac{A-1}{A+1} \simeq \frac{2}{A + \frac{2}{3}} \qquad (14\text{-}20)$$

For example, the average energy loss per collision is about 4 per cent of the incident neutron energy in Fe and 1 per cent in Pb.

The scattering cross section in hydrogen increases as neutron energy is reduced (see Fig. 14-13). It is smaller than geometric for energies above about 20 Mev and becomes larger than geometric at lower energies. Because of the large fractional energy loss per collision and the increasing cross section at low energies, elastic scattering in hydrogen is of unique significance in neutron attenuation. This process is almost the only one by which neutrons of less than 0.5 Mev energy can be degraded rapidly to very low energies. As a consequence, hydrogenous materials are almost universally used for slowing down neutrons.

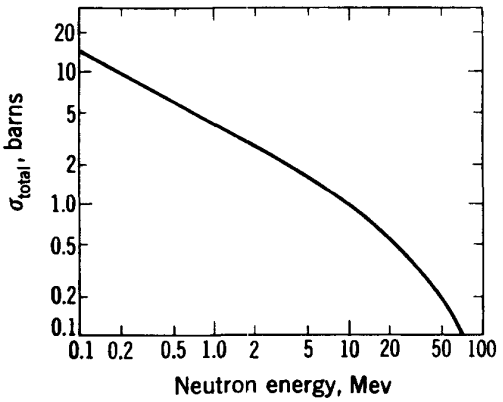

Fig. 14-13. Scattering cross section for low-energy neutrons in hydrogen.[18]

At sufficiently high energies, where the associated wavelength of the neutron becomes comparable with the radius of the nucleus, another process called "diffraction scattering" contributes to the elastic scattering. As with optical scattering by an opaque disk, the consequence of this phenomenon is that most of the neutrons are scattered into a forward cone of half-angle $\sim\lambda/R$, where $\lambda = h/2\pi mv$ is the "de Broglie" wavelength of the neutron. This phenomenon affects primarily the angular distribution of recoils in the scattering process.

Inelastic Scattering. Inelastic scattering increases the energy loss in heavy materials. Not only is neutron energy reduced by momentum transfer, but a further amount of energy is removed through excitation of the target nuclei. The magnitude of the cross sections in different nuclei depends on neutron energy and on the nuclear excitation levels available. In the common materials used in shields there are very few energy levels below 0.5 Mev, so inelastic scattering is significant only for the more energetic neutrons. In general the excited nucleus gives off its energy in the form of nuclear γ rays. Table 14-7 gives a selected sample of measured inelastic scattering cross sections for a few elements bombarded by monoenergetic neutrons in which the maximum value of the residual neutron energy was also observed.[18] The atomic cross sections indicated by these results are in the range of 0.1 to 3 barns, which add significantly to the elastic cross sections. Figure 14-14 is a more detailed study of the inelastic scattering from Fe as a function of neutron energy, showing a threshold at 0.85 Mev which is associated with the lowest effective energy level and a fluctuating increase in cross section as higher states of excitation become available. A more detailed compilation of

TABLE 14-7
INELASTIC SCATTERING CROSS SECTIONS FOR FAST NEUTRONS[18]
(Selected sample)

Element	Initial neutron energy, Mev	Final neutron energy, Mev	Cross section, barns
Carbon	4.1	3.2	0.08
	14	11	0.52
Oxygen	14	8.8	0.52
Magnesium	2.5	2.5	0.75
Aluminum	4.1	3.2	0.7
	14	~11	1.06
Iron	1.2	0.35	0.6
	4.1	3.2	1.5
	14	~11	1.5
Copper	14	~11	0.4
Cadmium	4.1	3.2	2.1
	14	12	2.2
Lead	2.5	1	0.55
	4.1	3.2	1.9
	14	12	3.3

inelastic scattering cross sections is given in a book by Price, Horton, and Spinney.[18]

A practical consequence of this inelastic scattering phenomenon is that for iron and for several other medium or heavy nuclei the rate of energy loss is increased and neutrons are rapidly reduced to energies of less than

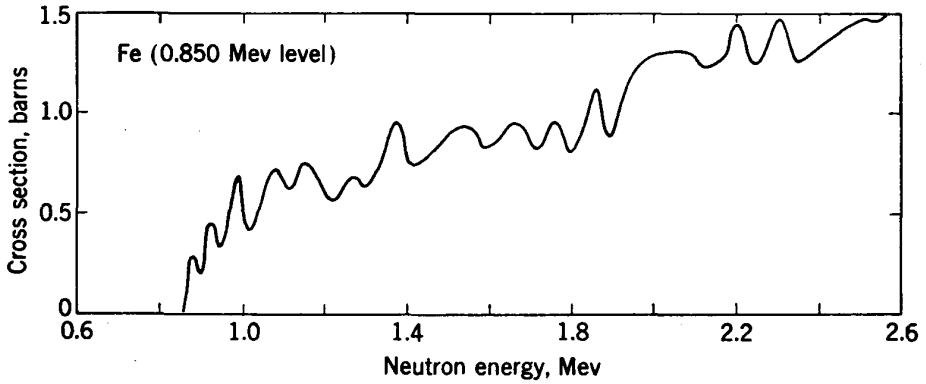

Fig. 14-14. Inelastic scattering cross section in Fe as a function of neutron energy.[18]

1 Mev. Neutrons emerging from such shielding materials have an energy spectrum with a prominent peak in the 0.5- to 1.0-Mev region. A corollary result is that iron is essentially transparent to neutrons of less than 0.85 Mev.

Nuclear Disintegration. Nuclear disintegrations which release charged particles have a smaller but finite cross section for fast neutrons

and serve to absorb a small percentage of the fast-neutron flux. In most elements the (n,p) and (n,α) reactions become energetically possible above a particular threshold energy; the probability increases with energy in excess of this threshold in a manner which is specified by the penetrability function of the charged-particle product in emerging through the coulomb potential barrier. A typical reaction is that for $O^{16}(n,p)N^{16}$, which results in a radioactive product nucleus with a half-life of 7.35 sec, for which the excitation function is illustrated in Fig. 14-15. It has a threshold at 10 Mev, and the cross section reaches its maximum value at 14 Mev. The maximum cross sections of these fast-neutron disintegrations are about 0.1 or 0.2 barn; they are significant over only a limited range in neutron energy, so they are of relatively small importance in shielding applications.

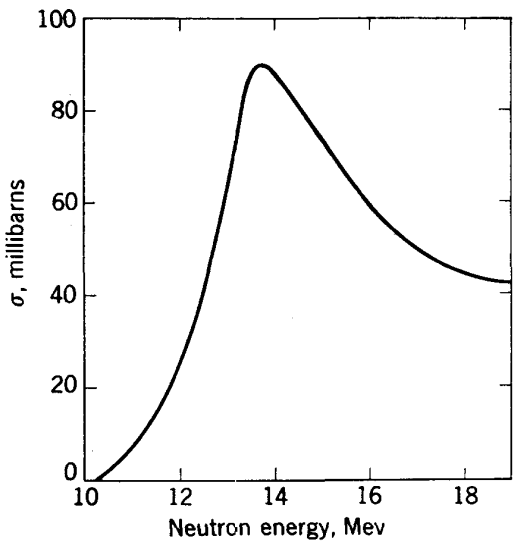

Fig. 14-15. Excitation curve for fast neutrons on oxygen, showing threshold.[18]

Some of the reactions which lead to radioactive products are useful as detectors of fast neutrons, however, where they serve to measure the intensity of neutrons in a characteristic energy band. Table 14-8 gives a list of the more common reactions used for fast-neutron detection, with the product half-life, threshold energy, and the energy at which the penetrability factor reaches 0.5.

TABLE 14-8
THRESHOLD REACTIONS FOR FAST-NEUTRON DETECTION

Reaction	Half-life	Threshold energy, Mev	Energy for 0.5 penetrability, Mev
$Al^{27}(n,p)Mg^{27}$	10.0 min	1.96	4.5
$Al^{27}(n,\alpha)Na^{24}$	14.9 hr	2.44	9.1
$Si^{28}(n,p)Al^{28}$	2.3 min	2.7	5.4
$P^{31}(n,p)S^{31}$	2.7 hr	0.97	3.8
$P^{31}(n,\alpha)Al^{28}$	2.3 min	0.91	8.3
$S^{32}(n,p)P^{32}$	14.3 min	0.96	5.6
$Fe^{56}(n,p)Mn^{56}$	2.6 hr	3.0	7.6

The $(n,2n)$ reaction becomes energetically possible at neutron energies in excess of the binding energy of the most loosely bound neutron in the target nucleus. At these high levels of excitation the $(n,2n)$ process competes with other possible modes of decay of the compound nucleus,

such as the (n,p) and (n,γ) processes. The low probability of an inelastic scattering collision's producing such high excitation means that the cross section for the $(n,2n)$ interaction is small, in general not exceeding 0.1 barn. Frequently the product nucleus is itself radioactive, which provides a simple technique for observation of the reaction. The threshold energies of fast neutrons required to produce the $(n,2n)$ reactions can be computed from the neutron binding energies. Table 14-9 lists the neutron binding energies for some of the common elements.

TABLE 14-9
NEUTRON BINDING ENERGIES FOR COMMON ELEMENTS

Isotope	Binding energy, Mev	Isotope	Binding energy, Mev
B^{10}	8.55	Ca^{40}	15.8
B^{11}	11.5	Mn^{55}	10.1
C^{12}	19.0	Fe^{56}	11.15
N^{14}	10.7	Cu^{63}	10.65
O^{16}	15.8	Cu^{65}	9.97
Na^{23}	12.05	Zn^{67}	7.0
Mg^{24}	16.4	Cd^{113}	6.48
Mg^{25}	7.33	Pb^{206}	8.25
Mg^{26}	11.15	Pb^{207}	6.91
Al^{27}	14.0	Pb^{208}	7.38
Si^{28}	16.9	U^{238}	5.88
Si^{29}	8.5		

Removal Cross Sections. In reactor theory the calculations of fast-neutron attenuation are simplified by utilizing the concept of a macroscopic "removal cross section"[7] which combines the atomic cross section of an interaction, in barns, and the physical properties of the absorbing material. The removal cross section Σ_r is given by

$$\sum_r = \frac{\text{Avogadro's number} \times \text{density}}{\text{atomic weight}} \times \text{atomic cross section}$$

or

$$\sum_r = \frac{0.602 \times \rho}{A} \times \sigma \text{ (in barns)} \qquad \text{cm}^{-1} \qquad (14\text{-}21)$$

We can use the removal cross section to summarize the properties of the materials used as fast-neutron attenuators. In comparing the relative cross sections of the different materials in the shields, the quantity Σ_r/ρ can be used; it depends only on atomic nuclear properties and is a smooth function of atomic weight.

The removal cross section gives the total of all processes tending to remove fast neutrons from the stream of neutron flux, for a slab of material embedded in a hydrogenous medium (such as water) which further attenuates and absorbs the reduced-energy neutrons coming from the

slab. It is averaged over the spectrum of neutron energies coming from U fission characteristic of reactors. It is of interest to note that the neutrons responsible for the residual intensity after attenuation by large thicknesses of hydrogenous material have cross sections characteristic of monoenergetic neutrons in the 6- to 10-Mev energy range. The numerical values obtained for fission neutrons do not apply to the different energy distributions coming from accelerator targets. Nevertheless, the general trends and the relative magnitudes of absorption coefficients obtained with fission neutrons are of considerable value, because of the scarcity of data from accelerator neutrons.

TABLE 14-10
SLAB REMOVAL CROSS SECTIONS FOR COMMON ELEMENTS[7]

Element	Atomic mass	Removal cross section Σ_r, barns
Hydrogen	1	1.00 ± 0.05
Deuterium	2	0.88 ± 0.10
Lithium	7	1.01 ± 0.04
Beryllium	9	1.07 ± 0.06
Boron	11	0.97 ± 0.10
Carbon	12	0.81 ± 0.05
Oxygen	16	0.99 ± 0.10
Fluorine	19	1.29 ± 0.06
Aluminum	27	1.31 ± 0.05
Chlorine	35	1.2 ± 0.8
Iron	56	1.98 ± 0.08
Nickel	59	1.89 ± 0.10
Copper	64	2.04 ± 0.11
Tungsten	184	2.51 ± 0.55
Lead	207	3.53 ± 0.30
Bismuth	210	3.49 ± 0.35
Uranium	238	3.6 ± 0.4

A listing of slab removal cross sections for some of the common elements for fission neutrons is given in Table 14-10, taken from the study by Goldstein.[7] The results show an essentially smooth variation with atomic weight, with cross sections varying from about 1.0 barn for the lightest elements to 3.5 barns for the heaviest ones.

Slow and Thermal Neutron Interactions

Elastic scattering is almost the only slowing-down process available for neutrons of less than 0.5 Mev energy. The largest cross section is for hydrogen, where it was shown in Fig. 14-13 to rise with decreasing neutron energy, reaching a value of about 20 barns for neutrons of a few kev energy. Other elements also moderate neutron energy by elastic scattering, but in general they require more impacts, a longer time, and a greater

density of material. A consequence is that the thickness of shield required to reach thermal equilibrium is shorter in hydrogenous materials than in others.

One special case is the use of graphite as a "thermal column" in reactor shielding, in which the shield thickness to reach thermal equilibrium is large but the absorption of thermal neutrons is a minimum, so the flux of emitted thermal neutrons is greater from a graphite shield than from a hydrogenous shield.

When neutrons have been slowed to a few electron volts energy, another type of inelastic scattering occurs in which energy is transferred to molecular vibrations and so is ultimately evolved as heat. Molecular energy states are mostly of lower energy than 1 ev, and the density of molecular energy levels is greatest at even lower energies. So the interaction cross sections for inelastic scattering involving molecular excitation

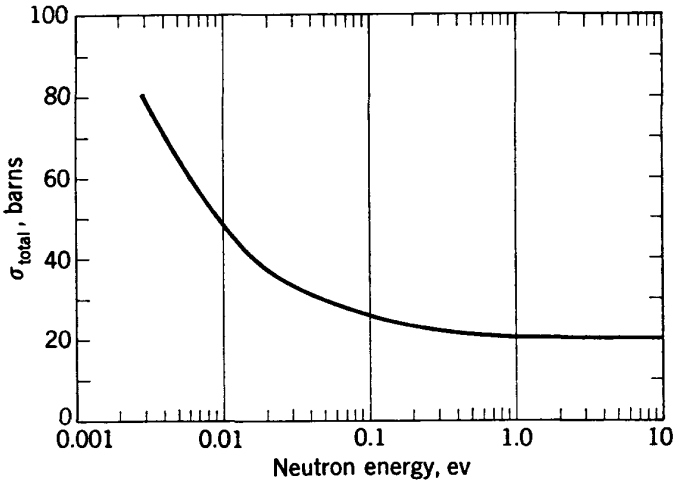

Fig. 14-16. Scattering cross section for thermal neutrons in hydrogen.[18]

rise with decreasing neutron energy for most materials. As an example, the cross section in hydrogen is shown in Fig. 14-16 for energies down to thermal equilibrium at room temperature,[18] which is about $\frac{1}{40}$ ev; the cross section in hydrogen rises to nearly 100 barns for thermal neutrons. These thermal neutrons diffuse within the material and migrate an average distance of several centimeters (depending on the material) before being absorbed.

The most probable absorptive process for thermal neutrons in most materials is the (n,γ) "radiative capture" process, in which the neutron is absorbed in a nucleus with emission of the neutron binding energy in the form of γ radiation. The capture cross section is tremendously large if neutron energy is equal to a resonance level in the nucleus formed. The magnitude of the cross section at other energies depends on how far neutron energy is from a resonance level and on the "width" of the levels.

For neutron energies which are far removed from a resonance, the cross section varies inversely with neutron velocity and is of the magnitude of a few barns for slow or thermal neutrons. At resonance, however, the radiative capture cross section can be 10^3 or 10^4 barns, for low-lying resonance levels.

A reaction of particular interest is the radiative capture in cadmium, due to a resonance level at 0.18 ev, for which the cross section at the peak is 8×10^3 barns. The level width overlaps the thermal Maxwellian distribution, and the cross section is still large ($>1 \times 10^3$ barns) for all energies below 0.3 ev. As a consequence, cadmium absorbs slow and thermal neutrons with great avidity and is commonly used in thin sheets of about 1 mm thickness as a slow-neutron capture shield. The γ rays from neutron capture in Cd are highly penetrating, having a peak emission at 3 Mev with some quantum energies up to 9 Mev. Additional shielding must be provided for these γ rays, if the slow-neutron flux is sufficiently intense.

Another absorptive process for thermal neutrons which is of significance in shielding is the $B^{10}(n,\alpha)Li^7$ reaction, in which the energy released ($Q = 2.8$ Mev) appears as the recoil energies of the product particles. These heavily ionizing charged particles have very short range and are locally absorbed. So boron is used in shielding applications to absorb slow and thermal neutrons without the production of capture γ rays. This is not a resonance-level capture process. The cross section follows the "$1/v$ law," being inversely proportional to neutron velocity. At a velocity of 2200 m/sec, which is the mean velocity of room-temperature thermal neutrons, the cross section for the B^{10} isotope is 4.0×10^3 barns. For the mixture of B^{10} and B^{11} isotopes existing in the natural element the average atomic cross section is 7.6×10^2 barns.

Other thermal-neutron absorbers of high cross section are He^3, Li^6, In, and a few rare earths. None of them are competitive, in a practical way, with Cd and B as thermal-neutron absorbers.

Measurements of Neutron Attenuation in Shields

The neutron intensity from high-yield medium-energy accelerators such as the cyclotron has been shown to require attenuation factors of about 10^{-6} for the fast-neutron component. The neutron energy spectrum is of somewhat higher average energy than for U-fission neutrons, but the general shape of the energy distribution is similar. Attenuation measurements and calculations for reactor neutron shielding give the most complete information. However, the attenuation factors needed for reactors are in the range of 10^{-8} to 10^{-10}, and the program of measurement and analysis had led to complex shielding systems which involve composite layer structures and mixtures of materials. Reactor shields are also designed to be specific for the neutron energy spectrum from

fission and to provide a proper balance of attenuation for the neutron and γ-ray components of pile radiation.

In general, simpler and more flexible structural arrangements are desired for accelerator shields, to allow for modifications in research experiments. Considerably less experimental effort has been applied to the study of shielding problems, and only a few basic types of shields have been tested with accelerator neutrons. The materials which have been used are of three general categories: hydrogenous substances, concrete mixtures, and iron plate. In the following pages each of these materials will be discussed and the experimental evidence presented, both from reactor shielding studies and from the more limited observations on accelerator neutrons.

Water. As the need for shielding developed, tanks of water were used for neutron shielding in early cyclotrons, largely because the laboratories had not been designed for more adequate arrangements. Water is very effective in moderating neutron energy and in reducing fast-neutron intensity. However, water has an undesirably low absorption for γ rays, which are emitted from targets and also produced within the water shield by capture of thermal neutrons, so the emergent γ-ray intensity has been excessive in most installations. Except for a few special applications in which B is added in solution, such as for viewing ports in shielding walls, water is no longer used.

Attenuation of the fast neutrons from a U-fission source in water has been measured in the AEC Shielding Facility Laboratory,[23] using the plane-collimated geometry applicable to practical shields. Fast neutrons were detected by observing the recoil protons in a fast-neutron counter. The semilog plot of intensity versus thickness shows an initial build-up which changes into an essentially linear decrease from 20 to 150 cm.[18] This equilibrium absorption coefficient has a value of 0.092/cm or 0.234/in. of water. Calculations from basic attenuation theory suggest that this value is equivalent to that expected for monoenergetic neutrons of about 8 Mev.[7] The total attenuation of 200 cm of water for fast neutrons is about 1×10^{-8}, more than is needed for most accelerator applications.

At still greater thicknesses and larger attenuations, other phenomena enter which further reduce the neutron absorption coefficient; these are associated with the production of photoneutrons within the water shield by the γ rays. This special problem of the production of photoneutrons was discussed in Sec. 14-4 and is analyzed for still higher photon energies in Sec. 14-9.

Gamma-ray attenuation in water cannot be described by a single absorption coefficient. The soft components of the incident γ rays from the fission reaction are absorbed in the initial layers, giving an initial large absorption coefficient. Thermal-neutron production and absorp-

tion and the resultant build-up of capture γ rays in the initial layers, combined with the absorption "hardening" of the incident flux, result in an absorption coefficient which decreases steadily with thickness of water. Total attenuation after 200 cm of water is only 7.5×10^{-4}, as compared with 1×10^{-8} for fast neutrons. A thickness of over 300 cm is required to give a γ-ray attenuation factor of 10^{-6}, at which thickness the absorption coefficient is about 0.071/in. of water. This comparison illustrates the basic limitations of a water shield for such mixed radiations.

Bor-paraffin. A somewhat more compact hydrogenous shield is a mixture of paraffin and boron. Paraffin has an even higher hydrogen content than water and so is more effective for fast-neutron attenuation. By the addition of about 2 per cent of boron by weight (usually in the form of borax), the nonradiative capture process in boron absorbs most of the thermal neutrons, so the capture γ-ray intensity can be reduced to an acceptable level. However, the absorption coefficient of the mixture for the incident γ rays is still much too small to provide adequate attenuation for this component. A layer of Pb blocks can be used inside the bor-paraffin shield to absorb such incident γ rays. In a typical application a melted mixture of bor-paraffin is cast into wooden or metal forms which are shaped to fit closely around the accelerator or the experimental apparatus, with an internal layer of Pb blocks. The chief limitation of such a composite shield is leakage of radiation through cracks and unshielded apertures. This technique has been used in a few cases to provide attenuation factors of 10^{-3} to 10^{-4} for fast neutrons.

Concrete. Concrete is the most frequently used of all shielding materials, usually incorporated in the walls and roof of the accelerator housing. Ordinary concrete, of density about 2.35 gm/cm^3 or 147 lb/ft^3, is by far the cheapest of all shielding materials. It has high water content for slowing down neutrons, about 33 per cent by weight of Si in the sand and gravel, and small amounts of heavier elements such as Fe and Ca which help absorb γ rays.

The attenuation of the fast-neutron component of U-fission neutrons in concrete[18] is illustrated in Fig. 14-17. This curve is based on a few experimental measurements with theoretical calculations to extend the curve to large attenuation factors. The initial absorption coefficient in the first 2 to 3 ft of concrete is about 0.24/in., decreasing to a value of about 0.18/in. for thicknesses in excess of 5 ft. The corresponding values of the 10-folding length, the thickness which reduces intensity to $0.1I_0$, are 9.7 and 12.8 in. of concrete. Because of the variable coefficient, it is necessary to compute the attenuation separately for each range of shield thickness. For example, a thickness of 3 ft will provide an attenuation factor of about 1.8×10^{-4}; a 6-ft thickness will give about 1.2×10^{-7}.

The U-fission γ-ray attenuation in concrete also has an absorption

coefficient which varies with thickness. The initial linear absorption coefficient is about 0.21/in., decreasing after 5 or 6 ft to a terminal value of 0.16/in. The terminal value is smaller than for the fast-neutron component, probably because of the production of new γ rays within the

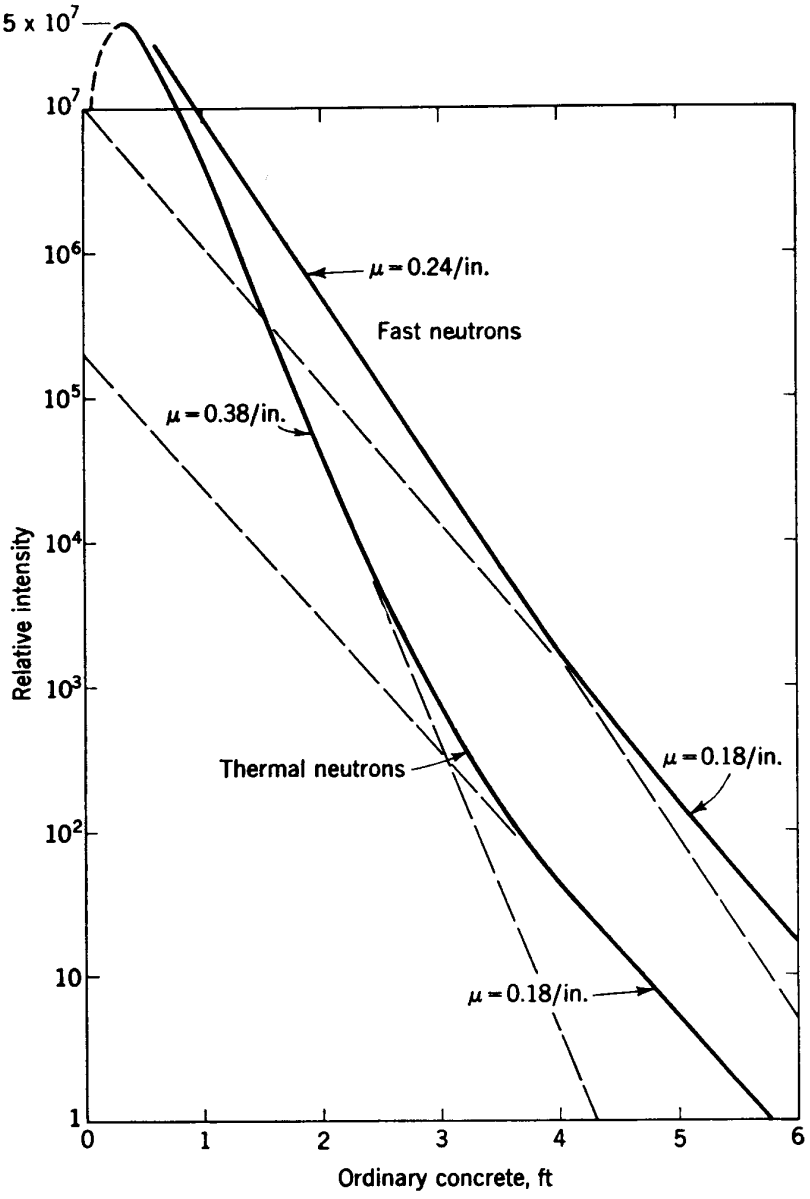

Fig. 14-17. Attenuation in concrete of fast neutrons and thermal neutrons from U fission.[18]

shield in neutron-capture processes. The initial attenuation coefficient for γ rays is considerably smaller than for fast neutrons. For example, 3 ft of concrete will provide an attenuation factor for γ rays of only 6.0×10^{-4}, and 6 ft will give 4.0×10^{-6}. Both of these factors are smaller than the neutron attenuation factors in concrete.

Lower-energy neutrons have a different type of attenuation. Figure 14-17 also shows a curve for the thermal-neutron intensities in a concrete shield, for neutrons coming from a U-fission reactor.[18] These thermal-neutron intensities were observed through the radioactivities induced in foil samples inserted in the shield. The initial build-up in intensity is greater than 50 per cent and occurs in the first 2 to 3 in. of concrete. This is followed by an initial attenuation with an absorption coefficient of about 0.38/in., changing steadily with increasing thickness to a value of about 0.18/in. after 5 ft of concrete. This final value is essentially the same as for the fast-neutron component and can be considered to be the terminal coefficient for an equilibrium mixture of fast and slow neutrons. At even greater thicknesses, which apply for higher-energy accelerators, the production of photoneutrons by the γ rays reduces the observed slow-neutron attenuation rate still further; this will be discussed in a following section.

The steep build-up of thermal-neutron intensity just inside the surface of the shield and the rapid attenuation of the thermal-neutron component mean that the ratio of thermal to fast neutrons is a function of the thickness of the shield; it is a maximum at the peak of the thermal-neutron intensity curve. For relatively thick shields, in which the intensity of the fast-neutron component has been reduced below the tolerance level, the surviving intensity of thermal neutrons is always well below tolerance. A general conclusion is that the fast neutrons are the dominant radiation and that shields should be designed for fast-neutron attenuation.

Accelerator neutrons have been used for attenuation measurements in only a few laboratories. Gugelot and White[22] studied the neutron and γ-ray attenuation in different concrete mixtures, using the radiations from the $Be^9(p,n)B^9$ reaction with 16-Mev protons from the Princeton cyclotron. They measured thermal and resonance slow neutrons through the activities induced in Ag foil detectors, but did not observe fast-neutron intensity directly. Furthermore, their measurements extended to only 15 in. of concrete, which is insufficient to observe the terminal values of absorption coefficients for large attenuations. The results showed the usual build-up of thermal-neutron intensity in the initial layers and an approximately linear attenuation after 20 cm with a half-value thickness of 10.7 cm for the thermal neutrons in normal concrete, equivalent to a linear absorption coefficient of 0.065/cm or 0.17/in. of concrete. This value is somewhat smaller at these thicknesses than that observed with fission neutrons and may be associated with the higher average energy of the neutron spectrum from this reaction. The comparative neutron spectra were illustrated in Fig. 14-12.

The major effort in the study by Gugelot and White was in comparative measurements of the neutron and γ-ray attenuations in several types of loaded concrete, involving substitution for the sand and gravel in the

ordinary concrete mixture of magnetite, limonite, scrap iron, and a composite of limonite and iron. A selected sample of their results is given in Table 14-11. The most effective mixture for neutrons and γ rays was shown to be concrete with 26.3 per cent limonite by weight, 59.4 per cent iron punchings, 4.7 per cent water, and 9.6 per cent cement; the mixture had a density of 4.41 gm/cm^3. The half-value thickness for thermal neutrons in this material was 5.4 cm, giving an absorption coefficient of 0.326/in. The coefficient for γ rays in this mixture was found to be 0.22/in., averaged over an attenuation factor range of 10^{-6}.

TABLE 14-11
NEUTRON AND γ-RAY ATTENUATION IN CONCRETE MIXTURES[22]

Absorber	Density, gm/cm^3	Neutron half-intensity thickness, cm	γ-ray half-intensity thickness, cm (at 20 cm)
H_2O	1.00	5.4	14.8
Concrete	2.35	10.7	13.3
Concrete + magnetite	3.78	8.5	9.0
Concrete + limonite	2.63	4.8	9.0
Concrete + limonite + iron	4.41	5.4	7.9

It is noteworthy that although the best neutron absorption (smallest half-intensity thickness) was observed with limonite concrete of density 2.63, which has the highest concentration of water, the strongest γ-ray attenuation came from the denser concrete including a large amount of scrap iron. We also note that in all cases the half-intensity thickness for γ rays exceeds that for neutrons.

Delano and Goodman[24] used neutrons from the MIT cyclotron coming from the $Be^9(d,n)B^{10}$ reaction with 15-Mev deuterons. The neutron spectrum was not measured, but is believed to have a somewhat lower average neutron energy than that used by Gugelot and White, from comparison of the results. Fast-neutron detectors were employed, by observing the induced radioactivities in samples of Al and Fe foil interspersed in the shield, as well as thermal- and resonance-neutron detectors. The fast-neutron-induced activities were the 10-min period from $Al^{27}(n,p)Mg^{27}$, the 14.9-hr period from $Al^{27}(n,\alpha)Na^{24}$, and the 2.6-hr period from $Fe^{56}(n,p)Mn^{56}$. These reactions are among those listed in Table 14-8, where they are shown to have thresholds at 1.96, 2.44, and 3.0 Mev, respectively; the energies calculated for 0.5 penetrability of the potential barriers are 4.5, 9.1, and 7.6 Mev. Despite this apparent difference in energy sensitivity, the three fast-neutron detectors showed similar attenuation curves, with an attenuation factor of 8.3/ft of concrete, equivalent to a linear absorption coefficient of 0.177/in. of concrete.

This value is essentially the same as that for the fast-neutron component of fission neutrons for equivalent concrete thicknesses.

Delano and Goodman also measured the attenuation for thermal neutrons to be a factor of 10/ft, which means an absorption coefficient of 0.19/in. of concrete. This can be compared with the Gugelot and White result of 0.17/in. and the terminal absorption coefficient for fission neutrons of 0.18/in. The attenuation of γ rays in concrete was also measured, giving 0.15/in. over the linear portion of the absorption curve, to be compared with 0.16/in. obtained for the fission γ rays.

Although the evidence is incomplete, it seems probable from the experimental studies that cyclotron neutrons are somewhat more penetrating in concrete than fission neutrons. This result must be associated with the higher energies of cyclotron neutrons. Since it can be expected that neutron energy spectra from accelerators in the several energy ranges will differ significantly, it follows that no single attenuation plot will be valid for all applications. Rather, each problem requires individual analysis to determine the specific shielding requirements. The absorption coefficients and attenuation factors described for fission and cyclotron neutrons are useful primarily in determining the order of magnitude of the shielding needed.

Another conclusion is that γ-ray attenuation is small relative to neutron attenuation in ordinary concrete. This imbalance is important in reactor shielding applications, where large attenuation factors are required. Ordinary concrete is seldom used in reactor shielding, where it is important to have similar attenuation factors for neutrons and γ rays. Accelerators require smaller attenuation factors, and space is usually not so critical, so an excessive thickness of ordinary concrete can be used to provide the necessary γ-ray attenuation.

Loading of concrete with iron ore or iron scrap increases the γ-ray attenuation and decreases the total thickness of shielding required for neutrons. Cost is materially increased, and the practical compromise is based on economic factors. Limonite or ilmenite ores can be substituted for the sand and gravel in concrete to obtain densities up to 250 lb/ft^3, and with a cost increase by about a factor of 4. These ores make strong concrete aggregates and are nonmagnetic. Magnetite has the disadvantage that the ore is magnetic and that dust from erosion of shielding blocks becomes a hazard to the magnets used in accelerator laboratories. The further addition of scrap iron (rivet punchings are common) can increase density to a maximum of about 450 lb/ft^3, but cost increases sharply. Engineering estimates[18] suggest that doubling the density by adding iron increases the cost by about ten times. For accelerator applications a shield of ordinary concrete of sufficient thickness to attenuate the γ-ray component is considerably cheaper than a thinner shield of loaded concrete which would provide a better balance of absorption coefficients.

Iron. Iron plate or forgings have been used in a few high-energy accelerators to provide a compact and dense shield when large attenuation factors are required and space limitations exist. At the University of Chicago synchrocyclotron laboratory concrete is used for most of the wall and overhead shielding, but iron is employed to form the channels for emergent beams in the wall facing the research laboratory.

As a neutron shielding material, iron has a fundamental limitation due to its small elastic cross section and the absence of energy levels for inelastic scattering at energies below 0.85 Mev, as discussed in the previous section. Compared with hydrogenous materials iron is very inefficient in slowing down neutrons, and the rate of build-up of thermal neutrons is slow. This is illustrated by the observation that the peak of thermal-neutron intensity in an iron shield is 40 cm behind the face of the shield,[6] while the peak is at about 5 cm from the face for a water shield and 10 cm for an ordinary concrete shield. However, from this point on, the fast-neutron attenuation in iron is reasonably high, having a linear absorption coefficient of 0.6/in. at 20 in., which decreases to 0.3/in. at 60 in. A 60-in. iron shield will provide a total neutron attenuation of about 10^{-8}.

Gamma rays are attenuated quite effectively in iron. The initial attenuation rate following the usual wide-beam-geometry build-up in intensity is nearly 1.0/in., and the terminal mass absorption coefficient after 3 to 4 ft is 0.030 cm^2/gm or a linear coefficient of 0.24/in. of iron. A 60-in. iron shield will provide a γ-ray attenuation factor of over 10^{-8}.

Effect of Channels and Ducts through Shields

For most accelerators there is a need to bring emergent beams of particles or radiation through a shielding wall, in order to perform experiments under low-background-intensity conditions beyond the wall. A typical problem is that of bringing a beam of charged particles through the shielding wall within an evacuated pipe. The limitation on the use of such beam channels is the current of neutrons or γ radiation which they also transmit, which increases the background intensity beyond the wall.

The transmission of a straight cylindrical duct of radius r and length z (shielding-wall thickness) can be computed under simplifying assumptions. If the source intensity of fast neutrons or γ rays, I_0, inside the shield is isotropic and these particles are assumed to suffer no reflections from the inner wall of the duct, the emergent intensity is given by the geometric limitations to be

$$I = I_0 \left\{ 1 - \left[1 + \left(\frac{r}{z} \right)^2 \right]^{-\frac{1}{2}} \right\} \tag{14-22}$$

This curve is plotted in Fig. 14-18 for a range of z/r from 2 to 100.

Slow or thermal neutrons have a somewhat modified penetration

through channels. Reflection by scattering from the interior wall of the duct plus leakage into the duct from the initial portions of the shielding wall increases the transmission above the geometric value for small duct ratios (up to $z/r = 20$), while it is smaller for greater lengths. Experimental measurements using fission neutrons from a reactor give the transmission curve for thermal neutrons in a cylindrical duct (see Fig. 14-18).

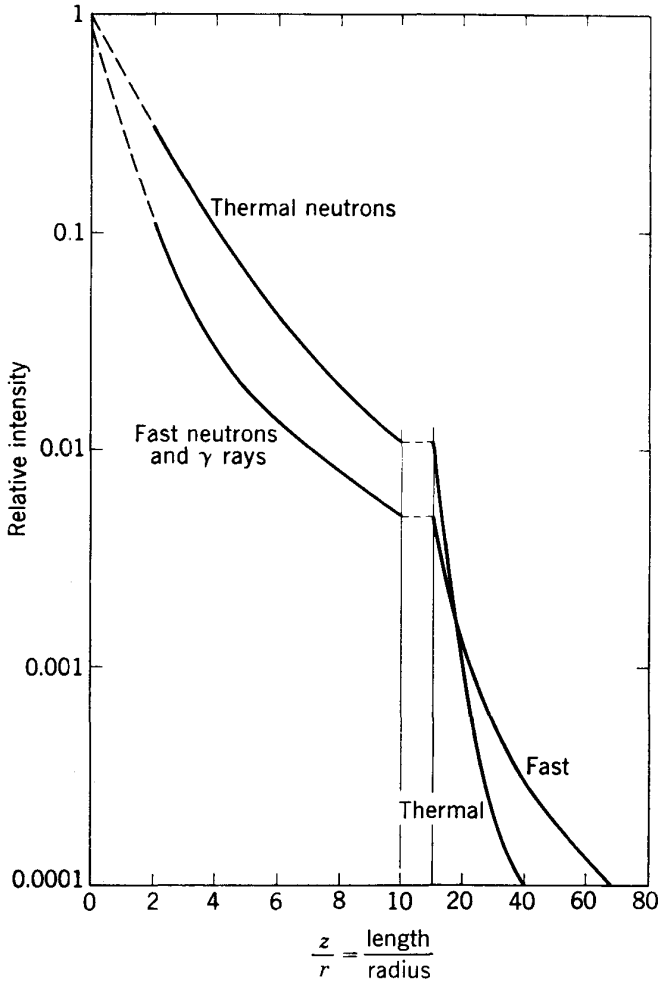

Fig. 14-18. Transmission of fast and thermal neutrons in straight cylindrical ducts of radius r and length z.

If it is possible to use an offset or bent duct, the transmission of fast neutrons and γ rays can be reduced to much smaller values. Because of internal reflection, offsets or bends are not so effective for thermal neutrons.

The intensities transmitted through channels or ducts may nullify the large attenuation factors for which a shield has been designed. For example, a 6-in.-diam channel through a 60-in. wall ($z/r = 20$) will transmit about 1×10^{-3} of the incident neutron flux over the area of the channel. If several such channels are used, the flux emerging from the

channels may exceed that transmitted through the body of the shield. In other words, if large channels must be used, large attenuation factors may be superfluous. In most situations, however, the limitation is on the size and number of channels which can be used with safety.

In several accelerator laboratories in which channels through the primary shields are used to bring out emergent beams, the intensity of radiation in the experimental area outside the shield has been excessive because of the total of the radiation leaking through channels or cracks in the shield plus the radiation produced by the emergent beam. In these cases the experimental area has also been provided with shielding, and the experiments have been operated by remote control.

14-7. INDUCED RADIOACTIVITY

One of the major hazards in accelerator operations is radiation exposure of personnel to induced radioactivity, both in the handling of targets and in repair operations on the machine. Remote-handling techniques and fast-acting systems are required for target changing, chemical processing of targets, and other routine operations. The intensities are in general smaller than those from reactor operations, but otherwise the problems are similar. The range of energies in the composite γ-ray and β-ray spectra from accelerators is similar to the fission-product spectrum, including in fact many of the same isotopes. Absorption coefficients in Pb and other shields are essentially the same as those for fission-product activities. Recommendations for handling techniques and shielding requirements can be taken directly from the experience and specifications available in the many studies and reports coming from reactor technology and radio chemistry. Useful summaries of the best practices are given in the "Handbook on Radiation Hygiene" edited by Blatz,[25] "Nuclear Engineering Handbook" edited by Etherington,[26] and other reference works.

The activities produced in accelerators cover a wide range in intensity and in half-life, coming from many radioactive isotopes. The many different materials used in and around an accelerator which can be bombarded by the positive ions, neutrons, and γ rays lead to a spread in half-lives nearly as great as in the fission-product spectrum from a nuclear reactor, and the composite decay curve is similar. A general observation on this composite decay is that the rate of decay measured at a time t after the machine is turned off shows a half-life of approximately t. The same is true for fission products where the apparent half-life is about $1.2t$.

The intensity of radioactivity within the shielding enclosure of an accelerator is closely proportional to the neutron intensity, which is an equilibrium mixture of fast, slow, and thermal neutrons. Most of the activities are products of the (n,γ) or neutron-capture reaction, which is

most probable for thermal neutrons, with smaller intensities coming from the (n,p), (n,α), and $(n,2n)$ fast-neutron disintegrations and a few high-energy γ-ray reactions.

Highest intensities come from accelerators such as the standard cyclotrons which have high neutron yields. At the MIT cyclotron the intensity following shutdown under normal operating conditions is sufficient to give one daily permissible dose in about 10 min, which is barely sufficient for target-handling or tune-up adjustments. Repairs and other maintenance tasks are postponed whenever possible until after an overnight or weekend shutdown, when the safe time for a daily dose is extended to several hours. Individual personnel exposure is monitored, and the working time within the enclosure is limited to prevent overexposure. Fast-acting mechanical systems are necessary for opening ports and changing targets. Long-handled tongs are used for removing the active target rapidly to a Pb-shielded carrying case. In a few laboratories remote-handling facilities have been developed for target changing or other routine operations. Nevertheless, in most well-shielded accelerator laboratories personnel exposure to radioactive γ rays and β rays is the dominant radiation dosage.

Something can be done in design to minimize the intensity of the induced activities, by careful choice of the materials used for chambers, ports, and probes. For example, the half-life of the activity induced in carbon by proton, deuteron, or neutron bombardment is short relative to that in copper. The D's of a cyclotron which are subject to bombardment by off-focus ions can be provided with graphite edges and linings; the intensity decays rapidly following shutdown, so radiation exposure during repairs can be minimized. Materials used for target holders, beam channels, and other parts subject to beam bombardment can also be chosen to reduce the activity level.

When a target is being bombarded for the purpose of producing specific radioactivities in the target, the bombardment can be usefully continued for a period of two or three half-lives; beyond this the increased yield is small. For short-lived activities the bombardment is short, and for longer-lived isotopes it can be maintained for much longer times. The highest intensity produced in a single cyclotron target, to the knowledge of the authors, is about 7 curies of Na^{24} ($T = 14.9$ hr) from a sodium target bombarded for 24 hr by deuterons in the MIT cyclotron. This occurred in about 1945, before even greater intensities of induced radioactivities could be obtained from nuclear reactors, which have now taken over the production of such high-intensity samples. For most research experiments the intensity produced in a sample seldom exceeds 100 millicuries and is more frequently in the range of a fraction of a millicurie.

Many induced activities cannot be produced by the neutrons in a

reactor, but can be formed only with charged-particle beams. This is true of essentially all positron emitters. So this large area of research is still reserved for accelerators.

Radiochemical processing of activities in targets is usually performed within shielded chemical hoods or "caves," with remote-handling facilities such as long-handled tongs or elementary master-slave manipulators, observed through thick windows in the shield or by mirrors. Most accelerator laboratories which produce activities in significant intensity have been equipped with such elementary "hot labs." Other technical devices may be useful, such as "ball-and-socket" tong manipulators, "glove boxes" for manual handling of β-active materials with thick gloves, and viewing periscopes. These devices have been developed to

TABLE 14-12
PB SHIELD THICKNESSES FOR Co^{60} AND Cs^{137} SOURCES OF INDUCED RADIOACTIVITY TO GIVE TOLERANCE DOSE, AT SURFACE OF 7.5 MREM/HR
(Spherical shields)

Pb thickness, in.	Activity, curies	
	Co^{60}	Cs^{137}
1	1.4×10^{-5}	1.3×10^{-4}
2	1.9×10^{-4}	7.5×10^{-3}
3	1.7×10^{-3}	2.5×10^{-1}
4	1.3×10^{-2}	6.4
5	9.0×10^{-2}	1.6×10^{2}
6	6.0×10^{-1}	3.7×10^{3}
8	2.3×10^{1}	
10	8.0×10^{2}	

an advanced state in the field of nuclear chemistry, and accelerator operators would do well to adapt this experience to their needs.

The basic shielding material for γ rays is lead, in the form of bricks, sheets, or carrying cases. Table 14-12 lists the source strengths of two common radioactive isotopes, Co^{60} and Cs^{137}, which can be shielded by given thicknesses of Pb to reduce the emergent intensity to the tolerance dose of 7.5 mrem/hr at the surface of the shield.[26] Note that about 3 in. of Pb is required to shield 1 millicurie of Co^{60}. Accelerator operators should be aware of the basic shielding requirements in the handling of targets and should monitor all such operations with suitable instruments.

In the energy range of cyclotrons and other low-energy or medium-energy accelerators used for production of radioactivity, an estimate of expected intensity can be obtained from the beam power, or the product of beam energy and time-average beam current. As a rough rule of

thumb, the slow-neutron intensity and so the level of induced radioactivity are proportional to beam power. In a standard cyclotron operating at 15 Mev and $\frac{1}{3}$ ma of deuterons, the beam power is 5 kw; intensities from operation at this range of beam power are potentially dangerous and require careful monitoring.

Induced radioactivity is a much smaller problem for the high-energy synchronous accelerators, because of the pulsed character of the beams and the low time-average beam current. The beam power from the Brookhaven 3-Bev cosmotron is about 10 watts, so the intensities of induced activities are proportionately lower. Furthermore, the more penetrating character of both the primary and secondary radiations from such high-energy machines means that much of the neutron attenuation occurs deep in the shields, so only a small fraction is available to produce radioactivity in the surface layers.

14-8. ELECTRONIC SHOWERS

High-energy electrons lose most of their energy in producing a cascade shower of X rays, secondary electrons, and positrons. This "soft shower," as it is called in cosmic-ray terminology, starts with a high-energy electron which loses energy by radiation. The X rays have a continuous energy distribution (see Sec. 14-4) with the maximum energy given by the energy of the incident electron, but with most of the intensity in lower-energy quanta. X rays are absorbed primarily through electromagnetic interactions which produce secondary electrons, lower-energy photons, and electron-positron pairs. This second generation of charged particles again loses energy primarily by radiation, with ionization loss becoming more important as energy decreases. The cascade process continues, with an increasing number of photons and charged particles, until the secondaries are sufficiently reduced in energy to be absorbed through ionization. The shower also grows in transverse width because of the predominantly transverse directions of the Compton secondary electrons, until the decreasing energy of the secondaries limits further transverse growth. For very-high-energy incident electrons (>1 Bev) the shower develops a columnar shape, with a central core of the higher-energy radiations and a surrounding sheath of lower-energy secondaries.

High-energy X rays also produce photoneutrons through photodisintegration processes. Although the neutrons carry only a small fraction of the total energy of the shower, they prove to be the dominant component after large attenuation through thick absorbers, because of their considerably greater penetration. The attenuation of the neutron component of such a shower will be described in more detail in Sec. 14-9. In this section we discuss separately the properties of the soft electronic shower components.

The basic properties of the cascade shower are well described by cosmic-ray shower theory.[14,20] The cross sections and angular distributions of the several electromagnetic interactions are known, including the variations with energy. Statistical calculations predict the growth and spread of secondaries and the attenuation resulting from absorptive processes. From such studies have come predictions of the number of secondaries in the shower, per incident electron, at different incident energies and as a function of absorber material and thickness. From the resulting transverse distributions the total ionizing intensity can be computed as a function of depth in the absorber. The validity of the results has been confirmed by experimental cosmic-ray observations.

Theory predicts an exponential build-up of ionizing radiations in the initial layers of absorber. The magnitude of this build-up depends on the incident energy in the shower. The energy of secondaries in low-energy showers rapidly falls below the energy at which radiation is the dominant process, and these secondaries are absorbed through ionization. For much higher incident energies the radiation-electron cascade continues for many more generations, and the exponential build-up continues to greater thicknesses. Eventually the mixture of radiations reaches an energy distribution in which the most penetrating component is the X rays of minimum absorption coefficient. This results in a terminal absorption coefficient of the shower having this minimum X-ray absorption coefficient. The "transition" curve of intensity versus absorber thickness shows an initial exponential build-up and a terminal exponential decay, with the magnitude and location of the peak-intensity point varying with incident energy and with absorber material.

As an aid to simplifying and correlating the results of calculations or measurements, absorber thickness is usually specified in units of radiation length x_0 (see Sec. 14-3). As used in shower theory, it is essentially the mean thickness, in gm/cm^2, in which one generation of the cascade process occurs, i.e., an electron radiates a photon and the photon is absorbed, giving another electron (or pair). Energies are also usually stated in units of the critical energy W_c at which radiation loss and ionization loss are equal and which has different values in the different materials. Values of x_0 and W_c for the common elements were listed in Table 14-4 and plotted in Fig. 14-4.

The results of cosmic-ray calculations and measurements are not directly applicable to accelerator shielding problems, since cosmic-ray data involve a spread in energy. Although it is possible to calculate attenuation curves for monoenergetic electrons from shower theory, it is more useful to observe the effects of accelerator electrons directly.

The best experimental evidence on the attenuation of an electronic shower comes from the Stanford linear accelerator.[27] Kantz and Hofstadter[28] studied the attenuation of the electronic shower component

from incident 185-Mev electrons, in the process of determining efficiencies and dimensions for scintillation and Cerenkov counters to be used for high-energy particles. They observed the ionization intensity with a small scintillation counter placed at various depths and transverse locations in a stack of slabs of absorber which was aligned in the direction of the electron beam. Absorbers of carbon (graphite), aluminum, copper, tin, and lead were used. These authors show that the output of the

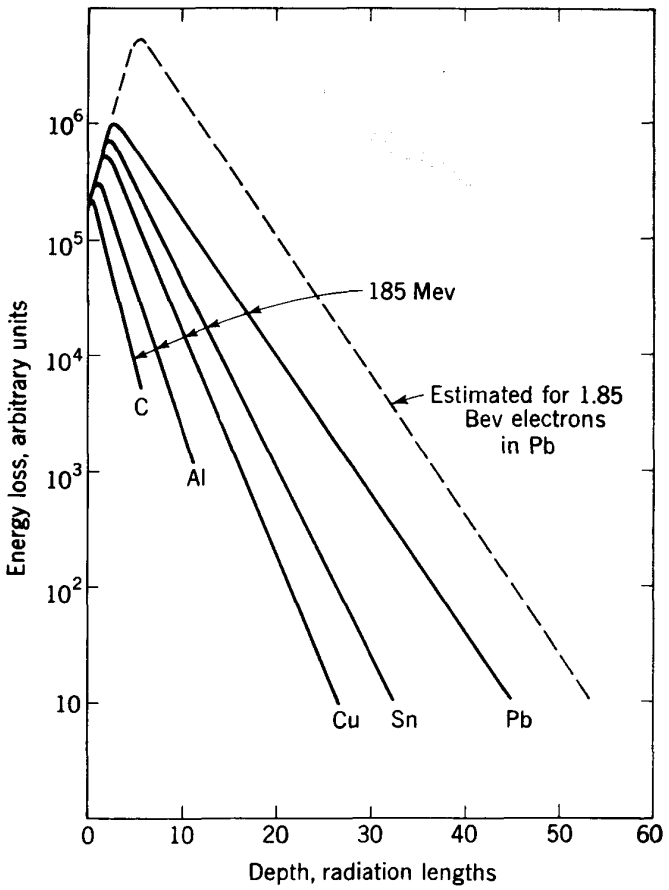

Fig. 14-19. Attenuation of electronic shower from 185-Mev electrons[28] and estimated attenuation of 1.85-Bev shower in Pb.

scintillation counter is proportional to the energy loss in this element of the stack. Intensities were observed over a wide transverse spread at each depth and summed graphically to obtain the total energy loss at this depth. Similar measurements were made over a series of depths in the absorber. Their results are shown in the semilog plot of Fig. 14-19 as the solid curves labeled with symbols for the absorbing materials.

The area under each curve (Fig. 14-19) is proportional to the total energy of the shower and so to the incident electron energy. Different fractions of the incident energy are transformed into the ionizing radia-

tions which actuate the scintillation counter in the different materials. In each curve the initial build-up shows an approximately linear increase on the semilog plot, in agreement with the predictions of shower theory. The magnitude of the build-up and the absorber thickness for peak intensity increase with atomic number of the absorber, again in agreement with theory. Beyond the peak intensity point each curve quickly reaches an essentially linear decrease, with a slope indicating the terminal absorption coefficient for each material. These terminal coefficients are in each case very close to the values of the minimum X-ray coefficients in the several materials, which were presented in Fig. 14-10 in the earlier section on X-ray absorption.

The close agreement of the experimental observations (Fig. 14-19) with shower theory makes it possible to predict the shape of similar energy-loss curves for higher incident electron energies. In any given material a higher-energy electron would have a transition curve with the same slope in the build-up portion and the same terminal absorption coefficient. The build-up would be extended to higher intensity and greater absorber thickness, but the slopes of both portions of the curve would be identical with those for 185 Mev. For example, an incident electron of 10-times-higher energy (1.85 Bev) would have an energy loss curve shifted vertically by a factor of 10, or one decade on the semilog plot. In illustration, a dashed curve is shown in Fig. 14-19 for 1.85-Bev electrons in a Pb absorber. The same incident intensity of 1.85-Bev electrons would require additional absorber to give an attenuation factor of 10^{-1}, in order to have the same emergent intensity. If the Pb absorber required for 185-Mev electrons were 45 radiation lengths thick (26.6 cm), the 1.85-Bev electrons would require 53 radiation lengths, an increase of 18 per cent in Pb thickness for 10-times-higher energy.

The above analysis and conclusion have oversimplified the problem considerably. A more complete study would require detailed analysis of the several competing electromagnetic interactions, including the angular distributions, and the simple results above would be slightly modified. However, it does present a reasonable approximation to the attenuation of the electronic components of the electronic shower. As stated earlier, the photoneutrons produced in the shower can become dominant components for large attenuations and must be considered for a more complete understanding of the shielding requirements.

The transverse spread of the electronic shower was also studied by Kantz and Hofstadter. They plot isoenergetic profiles as a function of depth and transverse spread within the absorbers, from which it is possible to determine the dimensions of a cylindrical volume within which any chosen percentage of the total shower energy would be contained. Their results show that a cylindrical volume with a diameter of about one-fourth the length would contain the shower in light-density material

such as C or Al, while a cylinder with a diameter of about one-half the length is needed in denser materials such as Cu or Pb.

The columnar shape of the electronic shower means that it can be absorbed locally in dense shields placed in the direction of the primary beam. Shielding requirements in transverse directions (for example, roof shielding) are small in comparison with those in the forward direction, as far as the electronic shower is concerned. However, it should be noted that the photoneutrons produced in the shower can have a much wider angular spread and will be the dominant components in determining the transverse shielding requirements.

14-9. PHOTONEUTRONS

The high-energy X-ray component of the electronic shower produces neutrons through the photonuclear disintegration reaction (γ,n) in essentially all elements. This process (see Sec. 14-4) was shown to have a characteristic threshold energy for each element (see Table 14-6). The cross section rises with increasing energy above threshold to a broad maximum known as the "giant resonance," at an energy of 15 to 20 Mev in most elements. This resonance represents a region of unusually high density of excitation states in the target nucleus. In the photodisintegration process the neutrons are emitted with energies in the range of 8 to 12 Mev, leaving the product nucleus in its ground state or a low-energy excited state.

X rays with energies above the giant resonance also release neutrons through the photodisintegration reaction, but with smaller cross sections; however, the neutrons emitted have proportionately higher energies and are more penetrating. In the discussion of high-energy neutron attenuation in the section to follow we shall show that the penetration of neutrons increases sharply in the 100- to 300-Mev energy range. Consequently, these high-energy neutrons become the dominant component for high-energy electron accelerators, despite the fact that photodisintegration cross sections are two orders of magnitude smaller than the electromagnetic interactions which lead to the electronic shower described in the preceding section.

We distinguish between two classes of photoneutrons in this analysis, of different energy ranges: (1) neutrons of less than 60 to 80 Mev energy which are produced at or near the giant resonance, and for which the attenuation in absorbers does not differ significantly from cyclotron or fission neutrons; (2) neutrons of more than 80 Mev energy produced by the direct photoeffect in essentially all nuclei at high energies, and for which the attenuation is much smaller than for the giant-resonance neutrons.

Giant-resonance Neutrons

The phenomenon of resonance in a nuclear interaction means that the production cross section is peaked at a particular value of photon energy k_0. Let $\sigma_r(k)$ be the atomic cross section for producing a photoneutron by a single photon of energy k in the region of resonance. The total atomic cross section, integrated over energy from threshold to well above the resonance, is determined only by the gross atomic properties of the target or absorber, such as atomic weight A, atomic number Z, and neutron number N. The magnitude of this integrated cross section has been shown[29,30] to be

$$\sigma_r(k)\,dk = 0.08\,\frac{NZ}{A} \qquad \text{Mev-barns} \tag{14-23}$$

The constant 0.08 applies for medium or heavy elements; a smaller constant of about 0.02 holds for light elements such as carbon. The yield of photoneutrons per incident photon is given by the product of atomic cross section and the number of atoms per square centimeter in the absorber along the track of the photon, which represents a mean free path for this interaction. This distance is given by the "track-length integral."

In cosmic-ray-shower theory the track length is essentially the thickness of absorber in which one generation of the electronic cascade occurs, i.e., in which a photon produces a secondary electron (or pair) and the electron generates another photon. In photoneutron production the track length is the average distance between neutron production interactions along the path of the photon. The integrated track length, integrated over the energy distribution of the photons radiated from an incident electron of energy W_0, and for a photon energy k, has been shown[20] to be given by

$$\pi(W_0,k) = 0.6\,\frac{W_0}{k^2} \tag{14-24}$$

Note that the integrated track length has units of (energy)$^{-1}$; the constant applies when W_0 and k are expressed in Mev. In photoneutron production the photon energy k can be taken as the value k_0 at the peak of the giant resonance.

The yield of photoneutrons per incident electron of energy W_0 can now be evaluated[20] from

$$Y(n)_r = \frac{N_0 x_0}{A} \times 10^{-24} \int \sigma_r(k)\pi(W_0,k)\,dk \qquad \text{neutrons/electron} \tag{14-25}$$

where N_0 is Avogadro's number and x_0 is radiation length in gm/cm^2.

In illustration we evaluate for an incident electron energy W_0 of 1 Bev. The yield will be directly proportional to electron energy. Table 14-13 lists values for A, Z, N, x_0, and k_0, for three typical absorbers: concrete, iron, and lead. Estimated values of the atomic constants are used for concrete. The radiation-length values come from Table 14-4. The resonance energy k_0 for the giant resonances decreases somewhat with increasing atomic number, and the values used are averages of the appropriate ranges of atomic number.

TABLE 14-13
PHOTONEUTRON YIELDS FROM 1-BEV ELECTRONS

	Concrete	Iron	Lead
A, atomic weight	(27)	56	207
Z, atomic number	(13.2)	26	82
N, neutron number	(14)	30	125
x_0, radiation length	24	14.1	6.5 gm/cm^2
k_0, resonance energy	22	18	14 Mev
Giant-resonance neutrons (W_0 = 1.0 Bev):			
$\frac{N_0 x_0}{A} \times 10^{-24}$	0.54	0.15	0.02
$\int \sigma_r(k)\, dk$, resonance cross section	0.27	1.0	4.0 Mev-barns
$\pi(W_0,k_0)$, track length	1.2	1.9	3.1 Mev^{-1}
$Y(n)_r$, yield at 1.0 Bev	0.18	0.27	0.23 neutron/electron
Photodisintegration neutrons (W_0 = 1.0 Bev):			
N_D, deuteron number	6	11	25
$\int \sigma_p(k)\, dk$, cross section	0.12	0.22	0.50 Mev-barn
$\pi(W_0,k)$, track length	9.0	9.0	9.0 Mev^{-1}
$Y(n)_p$, yield at 1.0 Bev	0.58	0.30	0.09 neutron/electron

Under the heading "Giant-resonance Neutrons" in Table 14-13, the yields are computed for the three absorbers. The yields are surprisingly similar for the different materials. Within the limits of precision applicable to these calculations, and to shielding problems in general, a single value can be used for all materials:

$$Y(n)_r = 0.25 W_0 \quad \text{neutrons/electron } (W_0 \text{ in 1-Bev units}) \quad (14\text{-}26)$$

The only significant error will be an overestimate of the yield at low energies and in light elements.

The angular distribution of these relatively low-energy photoneutrons is essentially isotropic. They spread in all directions from a line source along the core of the columnar photon-electron shower within the absorber. Other components, such as the high-energy photodisintegration neutrons, are more penetrating and determine the shielding require-

ments in the forward direction. The resonance photoneutrons are significant mostly in determining the transverse shielding requirements. For this purpose the attenuation coefficients for cyclotron neutrons can be used without serious error (see Sec. 14-6).

Photoneutrons of More than 80 Mev

The high-energy neutrons arise from the direct photoeffect. The most successful theory is that of the "effective deuteron" model, first developed by Levinger.[31] In this model, the photon is absorbed by proton-neutron pairs within the nucleus, for which the cross section is taken to be that for the photodisintegration of the deuteron, $\sigma_p(D)$. The cross section for any element is determined by the effective number of proton-neutron pairs in the nucleus, called the deuteron number N_D. In light elements the observed cross sections lead to a value of N_D close to the theoretical value, of about $1.5NZ/A$. In heavy elements the observed cross sections are smaller than the theoretical value, because of nuclear absorption of the outgoing neutrons (and protons) and the subsequent emission of lower-energy neutrons. Since these lower-energy neutrons have smaller mean free paths and are more readily absorbed, they do not contribute so effectively to the total photoneutron flux. Measured values by Odian[32] of the cross sections in lithium and oxygen lead to deuteron numbers $N_D(\text{Li}) = 3.0$ and $N_D(\text{O}) = 4.5$. Estimates have been made by Wilson[30] of the effective number of deuterons in iron and lead: $N_D(\text{Fe}) = 11$, and $N_D(\text{Pb}) = 25$. These values have been used to sketch the curve of N_D versus Z shown in Fig. 14-20, and appropriate values are also included in Table 14-13.

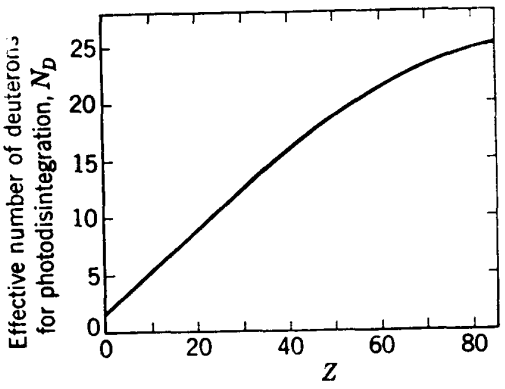

Fig. 14-20. Effective deuteron number photoneutron production as a function of Z.

At high energies the dominant contribution to the cross section is through the emission and subsequent absorption of mesons. Those mesons which are not internally absorbed will produce nuclear reactions in other nuclei with the release of other neutrons. So the total cross section for neutron production includes the alternate production of mesons. We shall calculate the intensity of emitted mesons in Sec. 14-11. It will be shown that their intensities are in general small and that they are not significant in shielding calculations relative to the fast neutrons discussed here.

The cross section for photodisintegration of the deuteron has been measured up to 900 Mev energy at the California Institute of Tech-

nology.[33] It is found to be essentially constant up to about 300 Mev, with a value of $\sigma_p(D) = 7 \times 10^{-5}$ barn, and to fall off with increasing energy to a value which is negligible for shielding calculations above 1 Bev. At 900 Mev it is decreasing at a rate faster than with $1/k^2$. Wilson[30] has shown that for the energy range between 300 Mev and 1 Bev the cross section can be approximated by

$$\sigma_p(D) = \frac{6}{k^2} \quad \text{barns} \tag{14-27}$$

where k is in Mev units. The total cross section when integrated over the energy range from above the resonance (taken as 80 Mev) to the upper limit of electron energy W_0 is

$$\int \sigma_p(D)\, dk = 7 \times 10^{-5} \int_{80}^{300} dk + 6 \int_{300}^{W_0} \frac{dk}{k^2} \quad \text{Mev-barns} \tag{14-28}$$

This results in a value of 0.02 Mev-barn at 1 Bev, and fits the Cal Tech data up to 900 Mev.

For other elements the cross section is given by the product of deuteron number and the deuteron cross section; values for the several materials are listed in Table 14-13. To determine the yield in neutrons per electron for thick absorbers, we again apply the principles of shower theory, using Eq. (14-25). The track-length integral is dominated by the value at the low-energy limit, taken rather arbitrarily as 80 Mev. For 1-Bev incident electrons the integrated track length has the value of 9.0 Mev^{-1}, and it varies directly with electron energy. Yields in the several materials are listed in Table 14-13 under the heading "Photodisintegration Neutrons." With these assumptions, the yield is found to decrease with increasing atomic number, having a value for medium-weight elements which is roughly equal in magnitude to the yield of low-energy resonance neutrons.

These high-energy neutrons are more penetrating than the resonance neutrons, as will be described in a following section. They become the dominant component for shielding calculations involving large attenuations in thick absorbers. The angular distribution is peaked in the forward direction, although not so sharply as the photon-electron shower. The high-energy neutrons which are the most penetrating are contained within a forward cone having a half-angle of about 30°. This requires the thickest and densest shielding in the forward quadrant.

In illustration, consider the neutron intensity which can be anticipated from a 1-Bev electron accelerator with a time-average beam intensity of 0.1 μa, or 6.25×10^{11} electrons/sec. This is characteristic of the intensities from electron linear accelerators or from high-repetition-rate electron

synchrotrons. Assume that the electron beam strikes a thick shield of ordinary concrete, at a distance from the accelerator of about 30 ft, collimated so the beam is narrow compared with the transverse width of the shower developed within the absorber. The transverse spread of the high-energy components of the electronic shower, and so of the photoneutrons, is about 1 m^2, so the emergent intensity is distributed over this area. This emergent intensity is to be reduced by shielding to below the tolerance level of 20 fast neutrons/(cm^2)(sec), or to a total of 2×10^5 neutrons/sec over the shower cross section. The total yield of high-energy photoneutrons within the absorber is about 0.6 neutron per incident electron, or 4×10^{11} neutrons/sec. The attenuation factor required of the shield in the forward direction is 5.0×10^{-5}, for the neutron component. The attenuation for such fast neutrons is discussed in a following section, where it is found to require about 21 ft of ordinary concrete to give this attenuation.

14-10. NUCLEONIC SHOWERS

Nuclear Star Production

Very-high-energy nucleons (protons or neutrons) produce another type of shower, composed primarily of nucleonic products of high-energy interactions. A typical interaction of a multi-Bev proton, for example, on striking a medium or heavy nucleus, is the production of a nuclear star in which a number of heavy-particle fragments such as protons, neutrons, and pi mesons (pions) share the energy and momentum of the incident nucleon. Residual nuclei may also be left in a state of high excitation energy, in which case further protons and neutrons are "evaporated" as low-energy nucleons. The charged-particle products can be observed in photographic emulsions or in cloud-chamber photographs; they show some "black" prongs due to relatively low-energy protons, "gray" prongs from higher-velocity protons or mesons, and some "minimum ionization" or "thin" tracks characteristic of very-high-energy pions or mu mesons. Neutrons and neutral pions leave no visible tracks, but their numbers can be estimated from statistical considerations; they are approximately equal to the number of charged products. The number of prongs in the star increases with incident nucleon energy and is also related to the atomic number of the struck nucleus.

Experimental evidence of star-type interactions comes from cosmic-ray studies as well as from observations with 3-Bev protons from the Brookhaven cosmotron and 6-Bev protons from the Berkeley bevatron. With 6-Bev protons Moyer reports[29] the "average star" produced in concrete to have the following composition and share of the incident energy:

		Bev
3 cascade or recoil protons 2 cascade or recoil neutrons	kinetic energy	3.0
4 evaporation protons 5 evaporation neutrons	kinetic energy	0.2
2 charged pions 1 neutral pion	kinetic plus rest energy	2.6
14 nucleons	total binding energy	0.2
Incident energy		6.0

The product particles are attenuated in the absorber through a variety of nuclear interactions. The higher-energy particles produce tertiary stars releasing still other nucleons and pions. Both protons and neutrons undergo elastic and inelastic scattering and also exchange-of-charge interactions. The charged components also lose energy through ionization. The result is a build-up in the number of particles and a decrease in the average energy. Some of the charged pions decay into mu mesons, which can lose energy only by ionization and which ultimately decay into electrons. Neutral pi mesons decay into pairs of γ rays of about 68 Mev each; these γ rays produce electron pairs and Compton electrons as they degrade in energy. Moyer[29] has estimated the intensity of these degraded components for each 6-Bev incident nucleon surviving and emerging from a thick shield of concrete to be:

Protons (from cascade and evaporation)	4
Charged pions	3
Muons	0.3
Neutrons (cascade, evaporation, and secondaries)	7
Slow neutrons	70
Electrons (from pion decay and nuclear γ rays)	10 (?)
Gamma rays (ionizing dose)	3×10^{-4} mr

This result is compatible with the evidence for build-up in cosmic rays.

The analysis above applies to the situation where the incident protons enter the shielding. If the primary beam impinges on a local target and does not strike the major shielding wall, the general radiation outside may not be as rich in high-energy protons or pions as indicated above.

A high-energy nucleonic shower will be strongly collimated in the forward direction. The highest-energy secondaries which carry most of the energy of the product particles will be projected forward, because of momentum conservation. Lower-energy evaporation particles will have a wider spread and may approach an isotropic distribution in angle. O'Neill[29] used a Monte Carlo calculation of the star-producing component of a nucleonic shower to predict the distribution of stars inside the face of an iron shield. He found that for incident energies over 1 Bev the rms angle from the beam direction of the stars was within $\pm 14°$ up to as much as 36 in. depth in the absorber. Particles projected at wider angles are generally of lower energy and are more rapidly attenuated in

the shield. In the Monte Carlo calculation described above, O'Neill found that the half-value thickness of iron was about 6.3 in. in the direction of the shower and only 4.5 in. in the transverse direction. The result was a roughly columnar shape of envelope enclosing the star-type interactions in the shower.

High-energy Neutron Attenuation

The attenuation of neutrons of up to 8 or 10 Mev energy was discussed in Sec. 14-6, where the absorption coefficient was found to approach a terminal value for thick absorbers. This terminal absorption coefficient is about 0.18/in. of concrete, for shields of more than 4 or 5 ft thickness. Equivalent coefficients for other materials can be obtained by comparisons with the data on removal cross sections for fission neutrons. Similar values are indicated for the attenuation of photoneutrons released by X rays or γ rays, although the rate of absorption of the primary photons is considerably smaller.

For neutron energies up to 50 or 60 Mev the same type of energy-loss interactions occur as for lower energies, and the absorption coefficient is believed not to decrease significantly. Above these energies the type of nucleonic cascade or shower described in the preceding paragraphs becomes energetically possible. Neutrons produce stars which release other neutrons, deep in the shield and directed primarily forward, although of lower energy. As long as the neutron energy exceeds that necessary for star formation, the neutrons tend to reproduce themselves. This multiplication of neutrons deep in the shield extends the effective range of the neutrons before they are absorbed and results in a significant decrease in the observed absorption coefficient, for sufficiently high-energy neutrons.

Experimental evidence on the attenuation of neutrons of 100 Mev energy or higher is quite incomplete. And cosmic-ray theory gives very little information on the nucleonic cascade process. Almost the only direct evidence comes from measurements of half-value thickness of concrete at two neutron energies, 100 and 300 Mev, taken by Moyer[29] and his associates at the University of California 184-in. synchrocyclotron. Concrete slabs were used in broad-beam geometry applicable to shielding walls, and the absorption of the fast-neutron component was observed directly. The half-value thicknesses obtained were 10 in. of concrete at 100 Mev and 18 in. of concrete at 300 Mev.

Panofsky[29] has summarized the available evidence in the form of a curve of half-value thickness in concrete as a function of neutron energy (see Fig. 14-21). The experimental points are supported by calculated values for other neutron energies, for the same broad-beam (poor geometry) condition. The most significant feature is the rapid increase in half-value thickness for energies between 100 and 300 Mev. This is due

to the development of the nucleonic cascade, as described above. Above about 300 Mev the production of pions becomes energetically possible; this provides an additional process through which fast neutrons can lose energy, so the half-value thickness again becomes essentially constant.

The most important elementary interaction in the energy range between 100 and 300 Mev is nucleon-nucleon scattering for which the cross section per nucleon varies with energy but depends only in a minor way on atomic number of the absorber. To a first approximation the absorption coefficient is directly proportional to the density of the material, and the half-value thicknesses are inversely proportional to density.

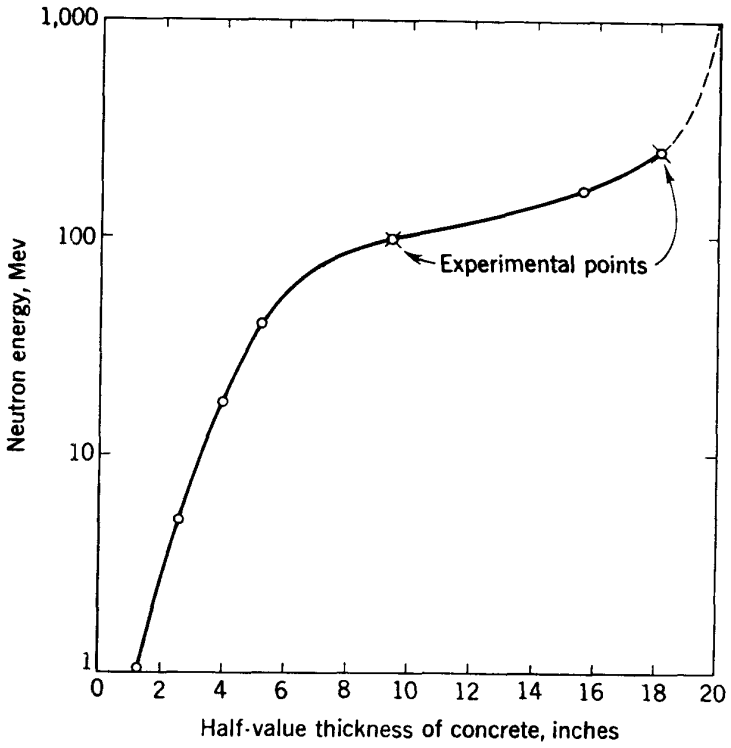

Fig. 14-21. Neutron attenuation half-value thickness as a function of neutron energy.[29]

Moyer's measurements on concrete can be used to predict the half-value thickness for other materials, in this same neutron energy region. Table 14-14, prepared by Wilson,[30] gives half-value thicknesses for several of the common materials used in shields and shows this close inverse proportionality.

An attenuation curve of total neutron intensity as a function of shield thickness can be developed from such half-value thicknesses and estimates of the number and energy distribution of neutrons within the shield. Such a curve was presented by Panofsky[29] for the attenuation in concrete of the neutron component of flux in the direction of the beam expected from a high-energy electron linac. This computed attenuation plot is

TABLE 14-14
HALF-VALUE THICKNESSES FOR HIGH-ENERGY NEUTRONS

	Earth	Concrete	Fe-loaded concrete	Iron	Lead
Density	1.5	2.35	4.0	7.8	11.3 gm/cm³
$L_{1/2}$ at 100 Mev	15	10*	7.5	4.5	4.5 in.
$L_{1/2}$ at 300 Mev	25	18*	13	8	8 in.

* Measured values.

shown in Fig. 14-22. Panofsky used three ranges of neutron energy in forming the composite curve. For $T < 80$ Mev he uses a half-value thickness of 4.8 in. equivalent to a constant absorption coefficient of

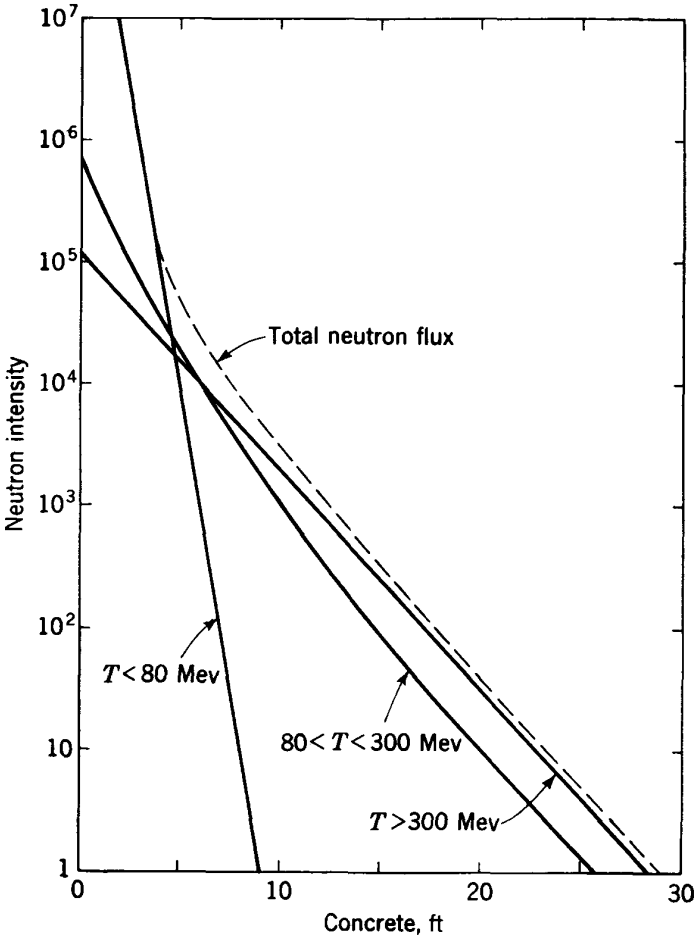

Fig. 14-22. Attenuation in concrete of high-energy neutrons.[29]

about 0.18/in. of concrete. For $80 < T < 300$ Mev he develops an attenuation curve with a coefficient varying with thickness, ranging from 0.07/in. to 0.035/in. of concrete. And for $T > 300$ Mev he uses a half-value thickness of 20 in. or a coefficient of 0.035/in. This curve can be

considered an extension of Fig. 14-17 to higher energies and greater thicknesses. For thicknesses greater than about 7 ft of concrete the highest-energy neutron component becomes dominant. It can be noted that this high-energy neutron absorption coefficient, of 0.035/in. of concrete, is lower by far than that for any other radiation component discussed in this chapter. Fast neutrons, in the energy range above a few hundred Mev, are the most penetrating of all radiations.

Attenuation of 3-Bev Protons

Measurements by Beebe, Cumming, Moore, and Swartz at Brookhaven, reported by Lindenbaum,[29] give the attenuation of the nucleonic shower initiated by a narrow external beam of 3.0-Bev protons in iron-loaded concrete of density 4.3 gm/cm^3. They measured both the number of penetrating particles and the ionization density at 12-in. intervals between blocks of concrete out to a total thickness of 13.5 ft. The beam was found to spread transversely to a half-intensity width of about 2 ft halfway through the stack. Build-up effects were still noticeable up to 4 ft. For larger thicknesses both the density of penetrating particles and the ionization intensity at the beam center followed a simple exponential attenuation with approximately the same half-value thickness of 8.5 in. Assuming that absorption coefficients are proportional to density, this corresponds to a half-value thickness in ordinary concrete of 15.6 in.

Ionization energy loss of the primary protons is about 200 Mev/ft in the loaded concrete, so proton energy is reduced to a few hundred Mev in penetrating the 13.5-ft shield. The average energy part way through the shield where measurements were taken would be less than 1 or 2 Bev, and nuclear interactions would produce a wide spread among the individual particles. Thus, the observed absorption coefficient cannot be assigned to any specific proton energy. Rather, this half-value thickness represents an average value applying to the mixture of radiations in a nucleonic shower initiated by 3-Bev protons. The Brookhaven workers state that geometric and other factors make their value a lower limit, and that their results are compatible with a half-value thickness for the more penetrating components of the shower of as much as 10 in., equivalent to 18.3 in. of ordinary concrete.

These results are in reasonable agreement with the half-value thicknesses observed at Berkeley with fast neutrons and show that the attenuation of a nucleonic shower is nearly independent of the type of particle which originates the shower.

Shielding for Nucleonic Showers

The dominant component of the nucleonic shower is high-energy neutrons, with energies of 300 Mev or higher. For such neutrons the thick-absorber half-value thickness is found to be about 20 in. of ordinary

concrete or the equivalent linear density of other materials. In concrete this terminal linear absorption coefficient is 0.035/in. and for other materials the mass absorption coefficient is $\mu_m = 0.0058/(\text{gm})(\text{cm}^2)$.

The intensity of these high-energy neutrons builds up in the absorber, primarily through nuclear star processes, reaching a maximum in the initial layers. High-energy charged particles are also released in the star processes, along with a much larger number of lower-energy particles and radiations. All these components degrade in energy at various rates through other interactions, including star production for those of sufficient energy. The neutrons of >300 Mev have the lowest interaction cross section. The number of these penetrating neutrons, per incident proton or neutron, reaches a maximum of 5 to 10 when the incident energy is 6 Bev. A reasonable estimate of the number at the peak of the shower build-up is one to two such fast neutrons per Bev incident energy. We conclude that an upper limit to the number is given by

$$N_n = 2W_0 N_{\text{incid}} \quad (W_0 \text{ in Bev})$$

At high incident energies the shower develops a columnar shape with a relatively restricted transverse cross section within the absorber, of the order of 1 m^2 or 10 ft^2 for the high-energy neutrons. Shielding in the forward direction must, in general, be sufficient to reduce the high-energy neutron intensity to below the tolerance level of 20 neutrons/(cm^2)(sec), which means a total of about 2×10^5 neutrons/sec for the cross section of the penetrating core of the shower.

As an example, we use the foregoing analysis to compute the shielding required in the forward direction for a beam of 10^{10} neutrons/sec of 5 Bev energy. The number of incident high-energy neutrons at the shower maximum is

$$N_n = 2 \times 5 \times 10^{10} = 1.0 \times 10^{11} \text{ neutrons/sec}$$

To reduce this to the tolerance value of 2×10^5 neutrons/sec beyond the shield requires an attenuation factor of 2×10^{-6} for the high-energy neutron component alone. Using the terminal absorption mean free path of 20 in. of ordinary concrete, this requires a thickness of 22 ft of ordinary concrete or 13 ft of iron-loaded concrete of density 4.0 gm/cm^3. To this must be added the thickness required for the shower to develop to maximum intensity, which is about 2 ft in ordinary concrete. We conclude a shielding requirement in the forward direction of 24 ft of ordinary concrete or 14 ft of iron-loaded concrete.

Obviously, much more detailed calculations are desirable in any specific shielding situation. The transverse spread can be calculated with statistical techniques using the specific energies and absorber materials, and the source intensity of high-energy neutrons should also include estimates for those of less than 300 Mev energy. Nevertheless, the crude estimate

above is in surprisingly close agreement with more detailed calculations of the shielding needed for the assumed intensity.

This technique of computing shielding requirements only for the dominant or most penetrating component of the radiation must be used with caution. It is suitable in this case only because the attenuation for all other components is much larger, sufficient to make the emergent intensities of these other components negligible. In this case, also, the source location of fast neutrons at the shower maximum is reasonably well defined; in other situations the source of radiation might not be so easily localized.

14-11. MESON PRODUCTION AND ATTENUATION

Meson Production by Photons

The simplest mechanism by which π mesons (pions) are produced is photoproduction, through the interactions

$$\begin{aligned} \gamma + P &\rightarrow N + \pi^+ \\ \gamma + N &\rightarrow P + \pi^- \\ \gamma + P &\rightarrow P + \pi^0 \end{aligned} \tag{14-29}$$

It is customary to write these relations using the symbols P and N for the protons and neutrons and identifying the charged or neutral pions with superscripts. Each of these processes has a threshold γ-ray energy for which the reaction becomes energetically possible, which can be computed from the pion masses and the kinematics of the collision. At this threshold the kinetic energy of the pion in the center-of-mass system of coordinates must be zero, from which it follows that the threshold photon energy is given by

$$W_t = m_\pi \left(1 + \frac{m_\pi}{2M}\right) \tag{14-30}$$

where m_π is the pion mass and M is the nucleonic mass. Present experimental evidence indicates rest masses and equivalent energies for charged and neutral mesons of

$$\begin{aligned} m_{\pi^\pm} &= (276.1 \pm 2.3)m_e = 141 \text{ Mev} \\ m_{\pi^0} &= (264.6 \pm 3.2)m_e = 135 \text{ Mev} \\ m_{\mu^\pm} &= (209.6 \pm 2.4)m_e = 107 \text{ Mev} \end{aligned}$$

In the laboratory system of coordinates the pion energy at threshold is a function of the angle of emission with respect to the incident photon direction. The kinematic equations are given in detail in "Meson Physics," by Marshak,[34] and in other reference texts. For our purposes

the threshold γ-ray energies for photoproduction can be taken as not significantly greater than the pion mass values.

Photoproduction of pions by γ rays is analogous to photoproduction of neutrons (see Sec. 14-9), except that production thresholds and resonance energies are higher. The most intense single group of pions comes from the $(\frac{3}{2},\frac{3}{2})$ resonance level identified in the "weak coupling" theory of photomeson production, for which the energy is about 300 Mev. At the peak of this resonance the cross section is known[34] to be about 2×10^{-4} barn. A total or integrated cross section can be obtained as in Eq. (14-23), integrating over the energy spectrum of γ rays coming from the incident electrons, from threshold to above the resonance energy. A track-length integral can be evaluated from Eq. (14-24), using a value of $k_0 = 300$ Mev for the resonance energy. The yield of resonance pions can then be determined from Eq. (14-25). When this yield is evaluated for an incident electron energy $W_0 = 1.0$ Bev, using appropriate constants for the different shielding materials (Table 14-13), we find

$$Y(\pi)_r = 1 \times 10^{-3} \text{ pion/electron} \quad \text{(earth or concrete)}$$
$$Y(\pi)_r = 2 \times 10^{-3} \text{ pion/electron} \quad \text{(iron)}$$
$$Y(\pi)_r = 4 \times 10^{-3} \text{ pion/electron} \quad \text{(lead)}$$

Comparison with the photoneutron yields given in Table 14-13 shows that the resonance photomeson intensities are about 1 per cent of the resonance photoneutron intensities. Most of the photomesons have energies of less than 100 Mev.

Pions are also produced by γ rays having energies above the resonance energy, through the direct photodisintegration process, again analogous to the production of high-energy photoneutrons. Measurements at the California Institute of Technology of the photodisintegration cross section in hydrogen with energies up to 1.2 Bev show it to be essentially constant for energies above 500 Mev, with a value of 6×10^{-5} barn. This can be taken as the cross section per nucleon in computing yields from other materials.

Yields can be obtained in a manner parallel to that used for photodisintegration neutrons, although the use of the track-length integral may lead to some error at these high energies. When the yield is evaluated for an incident electron energy of 1 Bev, we find

$$Y(\pi)_p = 1 \times 10^{-3} \text{ pion/electron} \quad \text{(earth or concrete)}$$
$$Y(\pi)_p = 5 \times 10^{-4} \text{ pion/electron} \quad \text{(iron)}$$
$$Y(\pi)_p = 2 \times 10^{-4} \text{ pion/electron} \quad \text{(lead)}$$

The intensities are only about 1 per cent of the high-energy photoneutrons shown in Table 14-13, and the cross section for pion production is in fact included in the photoneutron cross section.

Meson Production by Nucleons

Meson production interactions by nucleons become significant for energies above 200 to 300 Mev. Single pions are produced through a number of elementary processes such as

$$\begin{array}{ll} P + P \rightarrow N + P + \pi^+ & N + P \rightarrow N + N + \pi^+ \\ P + P \rightarrow P + P + \pi^0 & N + P \rightarrow P + P + \pi^- \\ & N + P \rightarrow N + P + \pi^0 \end{array} \tag{14-31}$$

The threshold kinetic energy of the incident nucleon is given by

$$\frac{T_t}{c^2} = \frac{(m_\pi + 2M)^2 - (2M)^2}{2M} \tag{14-32}$$

When evaluated for a single nucleon target (hydrogen), the threshold energy is 291 Mev for producing charged pions and 281 Mev for neutral pions. In complex nuclei the internal potential energy of individual nucleons in the nucleus—the Fermi energy—lowers the threshold. It can be as low as 180 Mev in heavy elements. From considerations of charge conservation and statistical weight the number of positive pions should be about twice the number of negative pions.

Experimental measurements, analyzed by Marshak,[34] show that the cross section for single positive pion production by protons of 340 Mev on protons is about 2×10^{-4} barn/steradian.

At higher bombarding energies, and in complex nuclei, the nucleonic shower phenomena (see Sec. 14-10) become energetically possible. Pions are emitted as components of the star processes, and several can be released in a single interaction. The evidence cited in Sec. 14-10 shows that the number of high-energy pions released in a 6-Bev shower is about half the number of high-energy cascade nucleons, and that they carry something less than half of the total energy.

Meson Attenuation

Charged mesons lose energy by ionization, with the rate of loss increasing as the velocity decreases. When they have been slowed down by ionization or collisions, the negative pions are captured by nuclei, releasing their mass energy in the form of γ rays or disintegrating the nucleus with the emission of neutrons. In about one-third of the negative pion interactions a neutron of about 7.0 Mev energy is released. On the other hand, slow positive pions cannot enter nuclei, and they usually decay into muons and neutrinos, with a characteristic half-life of 2.54×10^{-8} sec. The positive muon itself decays into a positron and neutrino with a half-life of 2.15×10^{-6} sec, and the positron loses energy by ionization, radiation, and annihilation. The neutral pions (π^0) have essentially no interaction with nuclei and decay promptly (10^{-15} sec) into two γ rays of

68 Mev each. These γ rays add to the soft component of the shower and are attenuated by pair production and other electromagnetic interactions.

High-energy charged pions have the same sort of nuclear interactions as protons of equivalent energies, and the cross section is essentially the same. For shielding considerations, the most significant of the interaction products are the high-energy neutrons. As was shown in a preceding section, protons in the Bev energy range develop nucleonic showers for which the attenuation is determined by the fast-neutron component. It is known that pions of these energies also produce star-type processes which are indistinguishable from those produced by nucleons. For example, the number of high-energy neutrons produced in such star processes is estimated by Moyer[29] to be 1 from 500-Mev pions, 2 from 1-Bev pions, and 3 from 3-Bev pions. These neutrons will be directed into a small forward angle, as is true for other high-energy neutrons in the shower.

We can conclude that charged pions are essentially equivalent to protons of the same energy in maintaining the nucleonic shower. Like protons, the rate of ionization associated with their charge means that they are attenuated more rapidly than the fast neutrons in the shower. So we return to the results of Sec. 14-10 and the attenuation plot of Fig. 14-22 as the basic data for estimating the shielding requirements for the nucleonic shower.

Properties of μ Mesons (Muons)

The muons formed by decay in flight of high-energy π mesons represent a special problem in shielding. Under certain conditions it is possible for the muons to penetrate shields which are otherwise adequate for attenuation of the nucleonic components. The reason is that muons have a negligibly small cross section for nuclear interactions, so ionization is the only process by which they can lose energy. The rate of energy loss, for singly charged particles of relativistic velocities, varies from 2 Mev/(gm)(cm^2) in light absorbers to 1.4 Mev/(gm)(cm^2) in Pb. This results in a penetration of about 7.0 ft/Bev energy in concrete, 2.5 ft/Bev in iron, or 2.1 ft/Bev in Pb. Depth of penetration is directly proportional to energy. In most installations the installed shielding for attenuating the nucleonic shower is sufficiently thick to absorb the total energy of the muons. However, for low-intensity multi-Bev accelerators the shielding required to reduce the emergent shower intensity to below tolerance may not be sufficient to absorb the entire energy of the muons.

The lifetime for decay of slow positive pions into muons is 2.54×10^{-8} sec. The negative pion decays only in the absence of matter, but the half-life is presumed to be the same. If the pion beam is allowed to traverse considerable distances in air or vacuum before entering a dense absorber, a significant fraction will decay in flight into muons. The mean

free path for decay is determined by the mean life, the velocity of the pions ($v \simeq c$), and the relativistic time-dilatation factor. In the multi-Bev energy range for which the muon component is a potential hazard, the time dilatation $W/m_\pi c^2$ is significant (W is pion energy and $m_\pi c^2$ is pion rest energy) and increases the decay mean life by this factor.

The mean free path for decay of pions is given by

$$L_m = c\left(\frac{W}{m_\pi c^2}\right)\tau \tag{14-33}$$

where τ is the mean life at low energies. As an example, for 5-Bev pions the time-dilatation factor is 35, and the mean free path for decay is 390 m. If the first dense shielding is at a distance of, say, 25 m or 80 ft, about 6.5 per cent of the negative pions will decay into muons. If the shielding is less than 35 ft of concrete or 12.5 ft of steel, this fraction of the incident muon flux will penetrate the shield. Even though the intensity is low in terms of biological hazard, it might impose an objectionably large background of ionizing radiation on detection instruments such as liquid-hydrogen bubble chambers or electronic scintillation counters.

The most obvious technique for removing the muon background is to place a shield of high-density material near the target where the pions are formed. This shield can have a conical or cylindrical shape with relatively small transverse dimensions, because of the forward collimation of the high-energy pions, and must be of sufficient length to attenuate the pion beam through nucleonic interactions. An iron shield for a beam of 10^{10} pions/sec of 5 Bev energy would be about 10 mean free paths or 7.5 ft long.

14-12. SKYSHINE

Upward-directed radiation which is scattered back toward the surface of the earth by collisions with air nuclei is known as "skyshine." Relatively low-energy fast neutrons (1 to 10 Mev) prove to be the significant radiation component for most accelerators. This is due to the fact that the cross section for elastic or inelastic scattering is large for neutrons in this energy range, while the absorption cross section is much smaller, so such neutrons can diffuse over considerable distances. The RBE of Mev neutrons is also larger than for γ rays or electronic components, so the biological effect of skyshine is determined predominantly by the low-energy neutron content.

The mean free path for scattering interactions with the O and N nuclei in air has been variously estimated; Lindenbaum[29] used 450 ft for 1- to 5-Mev neutrons, Williams[29] chose 270 m (685 ft) for 5 to 10 Mev, and Panofsky[29] used a mean free path of 1000 ft for his calculations. On the

average, each upward-directed neutron will have a scattering impact at this distance, so the source for skyshine is a diffuse hemispherical dome in the air above the accelerator with a mean radius of one mean free path. However, for purposes of calculation the source is usually presumed to be a point in air directly above the accelerator at an altitude of one mean free path.

Most accelerators are surrounded in the horizontal direction with thick barrier shields to attenuate the direct radiation to suitable intensity levels in adjacent laboratories. Skyshine radiation scattered over the barriers adds to the attenuated direct radiation intensity behind the shields. Relative intensity is determined by the distance and the geometric arrangement of the barriers. Close behind a barrier, where the solid angle of sky available for skyshine is reduced, the direct intensity may be dominant; at larger distances the skyshine frequently exceeds the transmitted intensity. We shall show that at large distances the rate of decrease of intensity due to skyshine varies roughly with the inverse first power of distance from the source, while direct radiation intensity falls off as the inverse square. So for locations well beyond the immediately adjacent laboratories or beyond project boundaries the residual intensities due to skyshine are usually dominant.

Accelerators of small physical size, such as cyclotrons, are usually housed in buildings with overhead roof shielding sufficient to reduce skyshine intensity outside the buildings to acceptable values. Larger, higher-energy machines such as the proton synchrotron are also normally placed in shielded tunnels to control the upward-directed intensity. However, the very-high-energy machines require extremely large laboratories within which experiments are performed on emergent beams. The cost of providing roof shielding for such large experimental areas sets a practical economic limit on the attenuation for upward radiation. In some cases it is more economical to shield the roofs of nearby occupied laboratory areas or to depend on huts for local shielding around the individual targets in the exposed experimental areas.

In a nonabsorbing medium of infinite extent the outward flux density at a distance r from a point source of N_0 neutrons/sec is

$$\phi(r) = \frac{N_0}{4\pi r^2} \qquad \text{neutrons/(cm}^2\text{)(sec)} \tag{14-34}$$

The attenuation of the outward-directed flux due to scattering interactions with a scattering mean free path λ is $e^{-r/\lambda}$. So the scattered flux intensity at a distance r is given by

$$\phi_s(r) = \frac{N_0}{4\pi r^2}(1 - e^{-r/\lambda}) \tag{14-35}$$

Panofsky first pointed out that the first term in the expansion of Eq.

(14-35) is an inverse first-power term of the form $1/4\pi r\lambda$, and that this first term becomes dominant at distances where $r > \lambda$.

A complicating factor is introduced by the effect of the ground surface on the intensity and energy distribution of the scattered neutrons. The heavier elements in earth or other solid materials have a larger absorption cross section for neutrons than oxygen or nitrogen, so the ground becomes a "sink" for neutrons, in the form of a horizontal plane bounding the hemispherical dome of skyshine. Since we are interested primarily in intensities close to the ground surface, the effect of this ground absorption is marked. However, earth is not a perfect absorber, and the "albedo" or back-scattering coefficient is estimated to be between 0.5 and 0.8 for neutrons of this energy. So the earth acts as an inelastic reflector for about half of the neutrons striking it. These reflected neutrons will then be rescattered by the air to add to the total skyshine intensity.

The general steady-state diffusion problem for neutrons under these conditions has not been solved. Partial or approximate solutions have been presented by Lindenbaum;[29] these were evaluated with constants and cross sections appropriate to incident neutrons of 1 to 5 Mev energy. The average total cross section for elastic and inelastic scattering in O and N was taken to be 1.5×10^{-24} cm^2 per nucleus, which is equivalent to a mean free path of about 450 ft in air. For convenience in plotting, the results are presented as the variation of the quantity $4\pi r^2\phi(r)$ as a function of radial distance r from the source in units of mean free paths. These results are shown in Fig. 14-23 for two conditions, with values of Lindenbaum's constant $C = \dfrac{\text{elastic cross section}}{\text{total cross section}}$ of 0.90 and 0.50. The value in air without any absorbing material such as the half-plane of earth is about 0.97; that adjacent to the ground plane is taken to be 0.50. The two curves in the plot represent extremes, with the upper curve more appropriate to large distances and intensities at considerable heights above the ground plane, while the lower curve is closer to that expected near the ground surface.

Lindenbaum notes that the general solution to the diffusion equation can be presented in the form of two terms, the first varying inversely with r^2, which is dominant near the source, and the second, which is the diffusion term, varying inversely with r. In drawing the curves he evaluates the two terms numerically. He also notes the differences between the low-energy and high-energy neutron components and suggests that the diffusion term could itself be expressed as two terms with different constants for low and high energies. His final result represents his own choice of approximations and simplifications, but is in reasonable agreement with the conclusions of Panofsky and of Williams, using different approximations.

Williams[29] uses a considerably simpler argument to estimate skyshine intensities, based on Eq. (14-35) and assuming that only the initially scattered radiation from the upward-directed flux is effective. From this assumption Wilson[30] has computed the skyshine flux as a function of

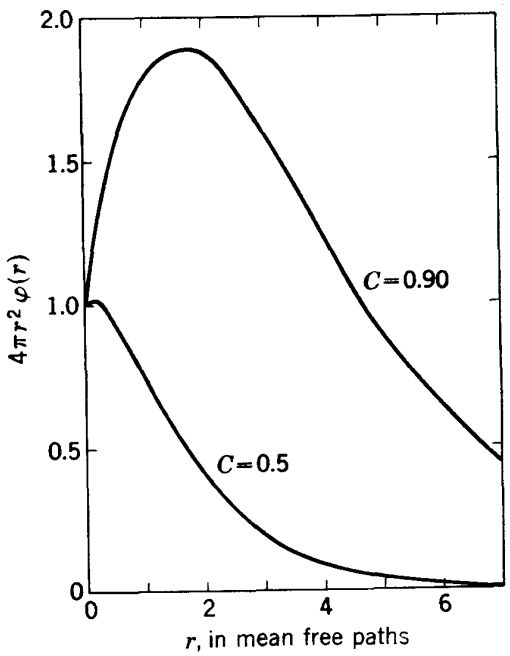

Fig. 14-23. Calculated total skyshine intensities[29] for two assumed values of the ratio $C = \dfrac{\text{elastic cross section}}{\text{total cross section}}$.

radial distance from a source of 1 neutron/sec. The results are based on an assumed mean free path of 1000 ft and are presented in Table 14-15.

TABLE 14-15
SKYSHINE INTENSITY FOR A SOURCE OF 1 NEUTRON/SEC

Distance, ft	*Flux, neutrons/(cm²)(sec)*
100	3.3×10^{-10}
200	1.7×10^{-10}
300	1.0×10^{-10}
400	0.7×10^{-10}
500	0.5×10^{-10}
1000	0.2×10^{-10}

Some practical examples show the magnitude of skyshine intensity. With the 3-Bev Brookhaven cosmotron and with barrier shields only (no overhead shielding) the intensity behind the barrier at 50 ft from the machine due to skyshine was observed to be 20 neutrons/(cm²)(sec) for a proton source intensity of 2×10^9 protons/sec and an estimated neutron source intensity of 10^{10} neutrons/sec. Overhead shielding was

installed to provide an attenuation factor of 10^{-3} in order to allow operation at higher intensities, requiring a layer of concrete beams 2.5 ft thick.

At the University of California 184-in. cyclotron a roof shield of one-fourth the thickness of the barrier shielding was required to reduce skyshine flux to a value comparable with the direct component in the beam direction. This ratio is characteristic only of the particular energy and intensity of the 184-in. cyclotron. If intensity were to be increased, say by a factor of e, the thickness of shield would have to be increased by one radiation length, both in the beam direction and in the overhead shielding for skyshine.

A general conclusion is that some overhead shielding is required to reduce skyshine intensities for essentially all accelerators for which neutron source intensity exceeds about 10^9 neutrons/sec.

REFERENCES

1. International Committee on X-ray Protection Report (1934).
2. W. P. Jesse and J. Sadaukis, *Phys. Rev.*, **97**:1668 (1955).
3. International Recommendations on Radiological Units, *Radiology*, **62**:106 (1954).
4. "Report of International Commission on Radiological Units and Measurements," *Natl. Bur. Standards (U.S.) Handbook No.* **62** (1957).
5. "Permissible Dose from External Sources of Ionizing Radiation," *Natl. Bur. Standards (U.S.) Handbook No.* **59** (1954).
6. *Brit. J. Radiol.*, Suppl. No. 6 (1955).
7. H. Goldstein (ed.), "Attenuation of Gamma-rays and Neutrons in Reactor Shields," U.S. Atomic Energy Commission (May 1, 1957).
8. Biological Effects of Atomic Radiation, National Academy of Sciences and National Research Council Report (1956).
9. United Nations Scientific Committee on the Effects of Atomic Radiation, U.N. General Assembly Official Records, XIII Session, Suppl. No. 17, A/3838 (1958).
10. National Committee on Radiation Protection and Measurements, *Radiology*, **68**:260 (1957).
11. M. S. Livingston and H. A. Bethe, *Rev. Mod. Phys.*, **9**:245 (1937).
12. H. A. Bethe, BNL-T-7 (June 1, 1949).
13. H. A. Bethe and W. Heitler, *Proc. Roy. Soc. (London)*, **A-146**:83 (1934).
14. B. Rossi and K. Greisen, *Rev. Mod. Phys.*, **13**:240 (1941).
15. L. I. Schiff, *Phys. Rev.*, **83**:252 (1951).
16. H. W. Koch and J. W. Motz, *Rev. Mod. Phys.*, **31**: 920 (1959).
17. *Natl. Bur. Standards (U.S.) Handbook No.* **55** (Feb. 26, 1954).
18. B. T. Price, C. C. Horton, and K. T. Spinney, "Radiation Shielding," Pergamon Press (1957).
19. M. Stearns, *Phys. Rev.*, **76**:836 (1949).
20. B. Rossi, "High Energy Particles," Prentice-Hall (1952).
21. G. C. Baldwin and F. R. Elder, *Phys. Rev.*, **78**:76 (1950).

22. P. C. Gugelot and M. G. White, *J. Appl. Phys.*, **21**:369 (1950).
23. "Reactor Handbook," U.S. Atomic Energy Commission, No. AEC-D-3465 (1955).
24. V. Delano and C. Goodman, *J. Appl. Phys.*, **21**:1040 (1950).
25. Hanson Blatz (ed.), "Handbook on Radiation Hygiene," McGraw-Hill (1959).
26. Harold Etherington (ed.), "Nuclear Engineering Handbook," McGraw-Hill (1958).
27. M. Chodorow, E. L. Ginzton, W. W. Hansen, R. L. Kylh, R. B. Neal, and W. K. H. Panofsky, *Rev. Sci. Instr.*, **26**:134–204 (1955).
28. A. Kantz and R. Hofstadter, *Nucleonics*, **12**:36 (1954).
29. "Conference on Shielding of High-energy Accelerators," New York (Apr. 11–13, 1957); U.S. Atomic Energy Commission No. TID-7545 (Dec. 6, 1957).
30. Richard Wilson, "A Revision of Shielding Calculations," Cambridge Electron Accelerator Report CEA-73 (May 12, 1959).
31. J. S. Levinger, *Nucleonics*, **6**:64 (May, 1950).
32. A. C. Odian et al., *Phys. Rev.*, **102**:837 (1956).
33. A. V. Tollestrup et al., *Phys. Rev.*, **101**:360 (1956) and **121**:630 (1961).
34. R. E. Marshak, "Meson Physics," McGraw-Hill (1952).

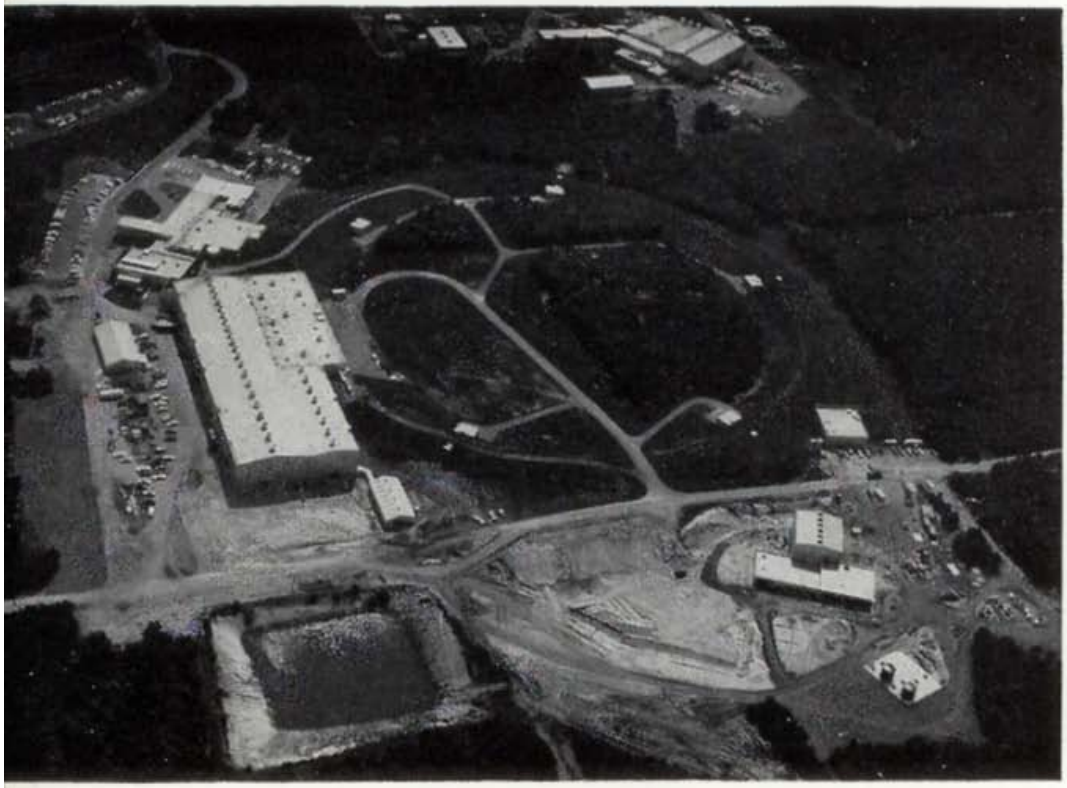

15

Alternating-gradient Accelerators

A new principle of magnetic focusing for accelerators, called alternating-gradient (AG) or "strong" focusing, which was started in 1952, has led to a series of machines capable of much higher energies than was economically practical with earlier techniques. The most dramatic applications are the several superenergy proton synchrotrons recently completed or under construction. At the CERN laboratory in Geneva the first of these large accelerators was brought into operation at 28 Bev in late 1959. At Brookhaven National Laboratory a machine of similar dimensions was completed in 1960, with a proton energy of 33 Bev. Two developments were under way in 1961 in the U.S.S.R.—a 7-Bev machine which was nearing completion and a 60- to 70-Bev machine on which construction was starting.

The principle of AG focusing has found applications to other accelerators. The method was first used and tested at Cornell University on a 1-Bev electron synchrotron. An electron synchrotron for 6 Bev using strong-focusing magnets is scheduled for completion in 1962 in Cambridge, Massachusetts, jointly sponsored by Massachusetts Institute of Technology and Harvard University. A similar electron synchrotron is under construction at the DESY laboratory associated with the University of Hamburg in West Germany. Another 6-Bev electron accelerator is under construction at Erevan in Soviet Armenia.

A modification of the principle called "sector focusing" has been adapted to the fixed-field cyclotron; it demonstrates that the proposal by Thomas[1] for such magnetic focusing (in 1938) can be viewed as a special case of AG focusing. A series of fixed-frequency cyclotrons using this principle has been built and others are under construction, primarily for the acceleration of multiply charged heavy ions. The feasibility of extending this principle of sector focusing to proton energies up to 850 Mev has been studied, primarily at the Oak Ridge National Laboratory and in England, and offers an opportunity to attain very-high-intensity beams up to this energy range.

Gradient fields developed by magnetic (or electric) quadrupoles have found applications in proton linear accelerators and in laboratory apparatus for utilization of particle beams in linear systems. The strong-focusing quadrupole magnetic lens is now an established component in all high-energy physics laboratories and in many other laboratory applications. Still other uses have been found for quadrupole focusing, as in traveling-wave electron tubes for amplification at microwave frequencies.

An extension of the concept by the use of AG focusing in fixed-field systems has led to the design of new types called fixed-field alternating-gradient accelerators (FFAG), primarily by the Midwestern Universities Research Association (MURA) now located in Madison, Wisconsin. This group of designers has built and tested a series of models involving several different ideas, some of which have the promise of much higher beam intensities than possible with the pulsed synchrotrons discussed above.

The AG concept has added a new dimension to accelerator design, with benefits to a wide range of accelerator types and techniques. A major contribution has been an improved theoretical understanding of orbit stability. The wide application to many different problems justifies the view that AG focusing has become one of the significant forward steps in accelerator development.

15-1. ORIGINS OF THE CONCEPT

The principle of AG focusing originated at Brookhaven National Laboratory in the summer of 1952, at a time when the cosmotron was nearing completion. A report of the early concepts was published by Courant, Livingston, and Snyder[2] late in 1952; it described the possible application to a high-energy proton synchrotron and also discussed the use of magnetic quadrupole lenses in focusing linear beams of particles. In a companion paper Blewett[3] showed that alternating electric-field gradients had the same focusing properties as alternating magnetic gradients and discussed the application to linear accelerators.

At the head of the facing page is an aerial view of Brookhaven 33-Bev AG synchrotron.

A brief description will now be presented of the factors which led to the conception of this focusing principle. The anticipated completion in 1952 of the cosmotron, which was the first multi-Bev accelerator, had attracted to Brookhaven many scientists who were engaged in developing experimental apparatus for research studies. It also attracted a delegation of European scientists representing the newly established CERN laboratory in Geneva, to assess the cosmotron as a model for a 10-Bev machine. In preparation for this visit, the senior author (MSL), on summer leave from MIT, initiated a study of the problems involved in a design for higher energy than 3 Bev. It was known that magnetic saturation effects limited the useful aperture of the C-shaped magnets of the cosmotron at high fields, although this limitation was not considered to be prohibitive in view of the other significant advantages of the C shape. A possible technique which would retain the C shape and also expand the useful aperture would be to alternate the back-leg locations from inside to outside the orbit. This would result, at high fields, in a corresponding alternation in magnetic gradients from positive to negative in the successive magnets as a result of saturation. The first concern was whether this alternation in gradients would destroy orbital stability.

E. D. Courant made a preliminary study of orbital stability under these conditions. A first guess involved pole faces sloped to produce alternating gradients with successive sectors having n values of about $+0.2$ and -1.0, which would give an average value of -0.6 as used in the cosmotron. Surprisingly, this preliminary study showed that orbit stability was improved rather than damaged by the alternation in gradient. A second calculation by Courant with n values of about 10 showed even stronger focusing and still smaller particle oscillation amplitudes. At this time H. S. Snyder joined in the speculative designing and helped to develop the general principle of dynamic stability involved in this use of alternating gradients. Larger and larger gradients were assumed in further stability calculations, each time based on sketch designs of magnets and estimates of the other parameters of a possible accelerator. Stability limits were identified, leading to suitable configurations of "positive" and "negative" magnet sectors and field-free straight sections between sectors around the orbit. Mechanical configurations were conceived which would produce the desired large magnetic gradients, and the requirements for magnet excitation power were estimated. Some of these early speculations led to such large gradients and such small vacuum chambers that construction was obviously impractical. However, it became more and more obvious that the basic concept was sound, and that the use of alternating gradients would allow major reductions in the transverse dimensions and the power requirements for magnets. Such a reduction in cost of synchrotron magnets for a given orbit radius would make it possible to design machines with much larger orbits and for much higher energies.

By the time the European delegation arrived at Brookhaven the concept had been developed sufficiently to be presented to them as a significant improvement over the cosmotron design. They were impressed by the new concept, and on their return they stimulated studies of AG orbit stability in British and European laboratories. For example, in England, Adams, Hine, and Lawson[4] identified and studied the problem of orbital resonances which might threaten orbit stability. This problem of orbital resonances will be discussed in following sections. When first presented by the British investigators, this seemed to raise a serious challenge to the practical use of alternating gradients. Further work showed that the objectionable resonances could be avoided by care in design and by use of suitable control systems to maintain constant gradients during the magnet excitation cycle. Confidence in the soundness of the new principle grew in all laboratories participating in the studies.

Several other laboratories contributed design studies of AG machines. The senior author (MSL) supervised a "Design Study for a 15-Bev Accelerator" at MIT, with the able assistance of R. Q. Twiss and J. A. Hofmann, and with consulting support from about 20 members of the MIT and Harvard Physics Departments. The result, published as a Report[5] of the MIT Laboratory of Nuclear Science in June, 1953, was the first relatively complete analysis of a practical design for an AG accelerator. The junior author (JPB) served for 6 months as a consultant to the new CERN laboratory, then returned to Brookhaven to join in the construction of the 33-Bev AGS. The Brookhaven and CERN groups moved ahead steadily in the theoretical analyses and engineering developments that culminated in the success of the large AG proton synchrotrons at both laboratories.

As so frequently happens in scientific research and development, this concept was developed independently elsewhere. N. C. Christofilos, an electrical engineer of American birth, educated and working in Athens, had been studying accelerators as a hobby for some years; he developed several new and unusual ideas on accelerator design in the form of private reports and patent applications. His unpublished report, "Focusing Systems for Ions and Electrons and Application in Magnetic Resonance Particle Accelerators," dated 1950, presented the concept of AG focusing and the conceptual design of an accelerator using this principle. He also applied for United States and European patents on the idea. A copy of his report was privately transmitted to the University of California Radiation Laboratory, but was not given serious consideration. After the Brookhaven publication in 1952, Christofilos came to the United States and demonstrated his priority, which was recognized in a brief note published by Courant, Livingston, Snyder, and Blewett[6] in 1953. Christofilos joined the staff of the Brookhaven Laboratory for a time, where he continued his speculative designing of accelerators and other

devices and also made contributions to the laboratory program leading toward the large AG machine. He became particularly interested in the linac injector for the synchrotron and made a number of valuable contributions to its design.

15-2. THE PRINCIPLE OF AG FOCUSING

Alternating-gradient focusing involves the use of much higher transverse gradients than those previously used in betatrons and synchrotrons. As was shown in Chap. 5, stability can be achieved by including gradients whose n values $\left(n = -\frac{R}{B}\frac{dB}{dr}\right)$ lie between zero and unity. In this case the free or betatron oscillation frequency is somewhat less than the frequency of revolution. This is now known as "weak focusing," in contrast to AG or "strong focusing."

In the AG system the particle passes alternately through strong focusing and defocusing lenses and is deflected alternately inward and outward. On the average it finds itself displaced farther from its orbit in focusing lenses than in defocusing lenses because in each focusing lens the particle has just been thrown outward by the preceding defocusing lens. But the focusing force or the defocusing force, as the case may be, is proportional to the field and hence to the displacement (in a field with a gradient). Consequently, the fact that the particle is generally further displaced in focusing sections indicates that the net force on the particle will be a focusing force.

Within rather wide limits the above conclusion is true. The net restoring force on the particle, though not nearly so strong as the individual focusing or defocusing force, is still much stronger than could be attained in weak-focusing systems.

This fact is reflected in the frequency of the free or betatron oscillations in an AG synchrotron. The strong restoring forces result in several betatron oscillations per revolution instead of less than one per revolution as in the weak-focusing case. In the accepted notation, ν (or Q, in European laboratories), the number of betatron oscillations per revolution, has been increased from the weak-focusing range of 0.2 to 0.6 up to the range between 5 and 100.

The most important consequence of the stronger restoring force is a decrease in oscillation amplitude and hence in necessary aperture. The amplitudes are decreased in approximately the same ratio that the free oscillation frequencies are increased. Strong focusing readily gives reductions of factors of 10 in aperture over weak focusing; this means factors of 100 or more in magnet cross sections and in tonnage of magnet steel.

Another consequence of the strong restoring forces is a reduction in the

radial spread of equilibrium orbits associated with momentum variations such as are introduced during synchronous oscillations. This "momentum compaction factor" is in the range of 0.05 to 0.02 for the several AG machines in being, compared with unity for a magnet with uniform field or values greater than unity for weak-focusing magnets. As a result, the transverse dimensions of the magnetic region between pole faces can be made much smaller than for weak-focusing machines, with a consequent decrease in the physical size of the magnets, the stored energy in the field, and the power required for excitation. The size of the vacuum chamber to fit between the smaller poles is materially reduced, to the extent that the conductance of the chamber for gas pumping is small and vacuum-pump ports must be closely spaced around the orbit.

As a result of this reduction in physical size of the magnets, the cost of the magnet component and the magnet power supply are reduced relative to costs of other components. It becomes practical to cycle such a magnet at higher frequency, increasing the number of beam pulses per second and so the time-average intensity of the beam. Other components become relatively more costly when cycling rate is increased, especially the radiofrequency system for accelerating particles. One parameter which cannot be reduced with increasing maximum energy is the orbit radius, which is associated with the limitation on the magnetic permeability of iron. The over-all orbit radius is larger, in fact, than for weak-focusing machines of the same energy, because of the necessity for many field-free spaces between AG magnet sectors. Thus the cost of buildings to house the machine becomes a dominating cost component for AG accelerators.

When the sequence of AG lenses is extended around an orbit to close on itself, other stability limitations enter which are associated with orbital resonances. If the frequency of the free oscillations is an exact integral harmonic of the orbital frequency, the pattern of orbit trajectories repeats identically in each turn. Any misalignment or magnetic anomaly which produces a small deviation in the trajectory at one point in the orbit is repeated at the same phase of the oscillatory motion in successive turns, which results in a rapid build-up of amplitude; the particle is quickly lost against the chamber walls. To avoid such a beam "blow-up," it is necessary to detune the free-oscillation frequencies from resonance with the orbital frequency. If they are nonresonant, the phase of the free oscillations changes in each turn at the location of the anomaly, so the effect is averaged out and excessive amplitude build-up does not occur.

The major resonance to be avoided is that for which the free oscillation is an integral harmonic of the orbital frequency. The restriction applies to both transverse coordinates, in the radial and axial directions. The integral resonances can be plotted on a "stability diagram" developed

in AG theoretical analysis (see Sec. 15-5), in which the two coordinates represent the free-oscillation phase shifts per turn in the radial and vertical directions. On this diagram the loci of points for which ν_r and ν_z have integral values show up as "integral stop bands" bounding diamond-shaped areas. A typical stability diagram (for the Cambridge electron accelerator) is shown in Fig. 15-9.

15-3. ANALOGUES OF AG FOCUSING

The physical principles of AG focusing can be illustrated by reference to analogies in other fields of science or engineering. In the mechanical field the rapid alternation of forces in opposite directions can produce a type of dynamic stability which has many similarities. A simple example is the inverted pendulum, which under static forces alone would fall to one side with any small displacement from the vertical. However, the pendulum becomes stable in the inverted position if the base is oscillated rapidly up and down through a short stroke.

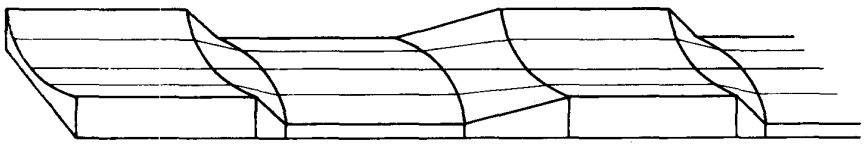

Fig. 15-1. The alternating trough.

Another mechanical system demonstrating dynamic stability, which is also useful as a model for AG focusing, is the "alternating trough" shown in Fig. 15-1. A ball will roll along a concave-upward trough, and if displaced from the axis will describe a harmonic trajectory about the center line. However, a ball will roll off the side of an inverted trough which is convex upward. Now if an alternating trough is formed of successive equal-length sections of concave and convex trough, with center lines forming a straight line and smoothly molded transition sections between, a ball will perform stable oscillations as it rolls along the trough, within a limited range of velocities. This stability range can be demonstrated by rolling the ball from different heights down an inclined plane to give it various initial velocities and directions. The shape of a displaced trajectory is a complicated curve which repeats periodically, with the shape depending on the initial phase of the motion relative to the phase of the trough periodicity. Within the stable range of velocities, rather wide deviations in physical displacement or angle of injection will result in trajectories which are confined to the trough. This system is useful as an analogue to AG focusing, since the trajectories of the rolling ball are quite similar in shape to the orbits of a particle in an AG ring-magnet accelerator, if the orbits were unrolled along a straight

line. A mechanical model serves to illustrate the wide variation in shape of orbits having different phases relative to the trough.

The most direct analogue to this type of magnetic focusing is in the field of lens optics. First, consider two thin lenses, one convex and one concave, with focal lengths f_1 and f_2 (negative), separated by a distance s. The optical relation for determining the over-all focal length F is

$$\frac{1}{F} = \frac{1}{f_1} + \frac{1}{f_2} - \frac{s}{f_1 f_2}$$

If for simplicity we take $f_1 = -f_2$, we find $F = |f|^2/s$, which is positive (convergent) for any finite separation distance and independent of the order of the lenses. If thick optical lenses are used in the example above, the focal lengths must be measured from the usual principal planes. Since the principal planes will have different locations for the converging and diverging lens surfaces, the location of the focal point depends on which lens comes first in the sequence.

Now let us extend the analogy by considering thick cylindrical lenses, for which each face has a double cylindrical curvature, such that a given lens would be converging in one transverse plane and diverging in the plane at right angles, with the two focal lengths f_1 and f_2 (negative) as before. A pair of such thick lenses with orientations rotated by 90° and separated by a distance s between principal planes would be converging in both transverse planes, with the same focal length. However, the image will be astigmatic, because of the different locations of principal planes in the two transverse coordinates. To obtain a point focus, one of the focal lengths would have to be modified.

A magnetic-gradient lens pair has the same focal properties for charged particles as the thick optical lenses described above have for light. The magnetic sectors have a physical extent, and the transverse gradients in the two perpendicular directions are equal in magnitude but opposite in their focusing properties on the particle beam. Figure 5-11 is a schematic illustration of particle paths through two such regions of alternating magnetic gradient, showing a net convergence in both transverse coordinates. The image is astigmatic, as with the optical lenses, but the two focal planes can be brought into coincidence by varying the excitation of one magnet sector. A complete analysis of this quadrupole magnetic lens was given in Sec. 5-6. Such a lens can be constructed using four symmetrical poles of alternating polarity, with pole faces shaped to a rectangular hyperbola. A simple two-element lens system (doublet) has the astigmatic aberration described above. A three-element system (triplet) using focusing-defocusing-focusing sectors in sequence can decrease the astigmatic and other aberrations. Other properties of quadrupole magnetic and electric lenses were discussed in Chap. 5.

To continue the optical analogy still further: A sequence of thin positive

and negative lenses of alternately positive and negative focal length can be arranged in a linear array to be continuously converging. (A modification of this principle is used in periscopes.) The sequence will be converging if spacings between lenses are arranged such that an off-axis ray never crosses the optic axis, which restricts spacings to the range $-2F < s < 2F$. Since the angular deviation is proportional to the distance from the axis in such a system, the ray trajectories will be spread most widely in the centers of the converging lenses, with minimum spread in the diverging lenses. This is an example of the general principle in lens optics that the converging lenses are the aperture stops. Magnetic-gradient lenses have the same property, in that the largest deviations in trajectory occur within the magnet sector which is converging (in that coordinate).

15-4. AG FOCUSING IN LINEAR SYSTEMS

The basic arithmetical methods used in analysis of AG focusing systems were presented in Sec. 5-6 with particular reference to lens systems consisting of a few quadrupole elements. In accelerators employing AG focusing the particles pass through many thousands of AG elements and

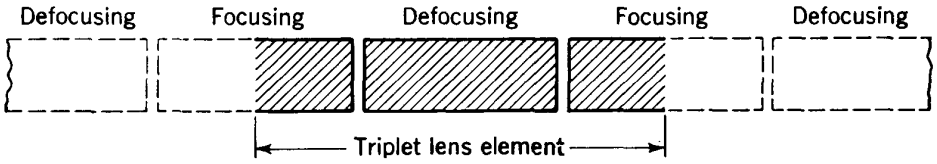

Fig. 15-2. Basic triplet lens element of an AG focusing system.

the methods of matrix analysis yield results so complicated that it is no longer easy to understand the results. In this section we shall present the basic methods of analysis together with some approximate representations that make the particle behavior more evident.

Although the single quadrupole is the basic element of the system, it becomes more profitable in thinking of AG systems to break the system down into a sequence of triplet lenses consisting (see Fig. 15-2) of the downstream half of one quadrupole, the whole next quadrupole, and the upstream half of the next one. Initially we shall assume that all quadrupoles are of length z_0 and have equal field gradients alternating in polarity from one quadrupole to the next. Since magnetic focusing is used in most accelerators, the analysis will be for quadrupole magnets rather than the electrostatic quadrupoles discussed in Chap. 5. In this case the parameter k used in Eqs. (5-35) will represent the quantity $(eB'/mv)^{1/2}$, where e, m, and v are the charge, mass, and velocity of the particles and B' is the gradient of the magnetic field. By the methods described in Sec. 5-6 we find that the exit position and transverse velocity

x and $\dot{x}$ of the particle are given in terms of the entrance position and velocity x_0 and $\dot{x}_0$ by the matrix transformation

$$\begin{vmatrix} x \\ \dot{x}/v \end{vmatrix} = \begin{vmatrix} \cos kz_0 & (1/k)\sin kz_0 \\ -k\sin kz_0 & \cos kz_0 \end{vmatrix} \begin{vmatrix} x_0 \\ \dot{x}_0/v \end{vmatrix} \tag{15-1}$$

for motions in the focusing plane, or

$$\begin{vmatrix} y \\ \dot{y}/v \end{vmatrix} = \begin{vmatrix} \cosh kz_0 & (1/k)\sinh kz_0 \\ k\sinh kz_0 & \cosh kz_0 \end{vmatrix} \begin{vmatrix} x_0 \\ \dot{x}_0/v \end{vmatrix} \tag{15-2}$$

for motions in the defocusing plane.

To trace a particle through our basic triplet, we must derive a transformation matrix by multiplication of the three matrices representing the three elements of the lens. The final position and velocity of the particle will be given, for the plane in which the first element is focusing, by the transformation matrix

$$\begin{vmatrix} \cos\frac{kz_0}{2} & \frac{1}{k}\sin\frac{kz_0}{2} \\ -k\sin\frac{kz_0}{2} & \cos\frac{kz_0}{2} \end{vmatrix} \begin{vmatrix} \cosh kz_0 & \frac{1}{k}\sinh kz_0 \\ k\sinh kz_0 & \cosh kz_0 \end{vmatrix} \begin{vmatrix} \cos\frac{kz_0}{2} & \frac{1}{k}\sin\frac{kz_0}{2} \\ -k\sin\frac{kz_0}{2} & \cos\frac{kz_0}{2} \end{vmatrix} \tag{15-3}$$

The result of this multiplication is the matrix

$$\begin{vmatrix} \cosh kz_0 \cos kz_0 & (1/k)(\sinh kz_0 + \cosh kz_0 \sin kz_0) \\ k(\sinh kz_0 - \cosh kz_0 \sin kz_0) & \cosh kz_0 \cos kz_0 \end{vmatrix} \tag{15-4}$$

This matrix looks remarkably like the element matrices of Eqs. (15-1) and (15-2). So long as the product $\cosh kz_0 \cos kz_0$ falls between -1 and $+1$, the matrix can be rewritten in the form

$$\begin{vmatrix} \cos\mu & (1/K)\sin\mu \\ -K\sin\mu & \cos\mu \end{vmatrix} \tag{15-5}$$

where

$$\cos\mu = \cosh kz_0 \cos kz_0 \tag{15-6}$$

and

$$K^2 = \frac{-k^2(\sinh kz_0 - \cosh kz_0 \sin kz_0)}{\sinh kz_0 + \cosh kz_0 \sin kz_0} = \frac{k^2(1 - \cosh^2 kz_0 \cos^2 kz_0)}{(\sinh kz_0 + \cosh kz_0 \sin kz_0)^2} \tag{15-7}$$

Evidently, for $\cosh kz_0 \cos kz_0$ between -1 and $+1$, both μ and K are real and the representation of Eq. (15-5) is legitimate. But this matrix has precisely the form of the focusing matrix equation (15-1), and hence it indicates that, for the condition stated, the triplet is a focusing lens. We can now add an indefinite sequence of identical triplets and be assured that this sequence will continue to restore a beam to the axis provided only that

$$-1 < \cosh kz_0 \cos kz_0 < +1 \tag{15-8}$$

This is known as the "criterion of stability" for an indefinite sequence of AG quadrupoles of equal length and strength. The condition given by Eq. (15-8) indicates that kz_0 must lie between 0 and 1.86 radians. Other stable regions exist for higher values of kz_0 for which low values of the cosine combined with the increasing values of the cosh still are able to satisfy the condition of Eq. (15-8); these regions are narrow and require high gradients; hence they are never used in practice.

Had we chosen as our basic element the triplet whose first element is defocusing, we should have obtained a slightly different matrix in place of Eq. (15-4), but the stability criterion would still be Eq. (15-8).

If the alternating elements in an AG system do not have the same lengths and field gradients, the analysis is a little more complicated but follows the procedures just outlined. If the quadrupoles have alternating lengths z_1 and z_2 and alternating k values of k_1 and k_2, the stability criteria prove to be, as before,

$$-1 < \cos \mu_1 < +1$$
$$-1 < \cos \mu_2 < +1$$

where

$$\cos \mu_1 = \cos k_1 z_1 \cosh k_2 z_2 + \frac{1}{2}\left(\frac{k_2}{k_1} - \frac{k_1}{k_2}\right) \sin k_1 z_1 \sinh k_2 z_2 \quad (15\text{-}9)$$

in the plane where the lenses numbered 1 are focusing and

$$\cos \mu_2 = \cosh k_1 z_1 \cos k_2 z_2 + \frac{1}{2}\left(\frac{k_1}{k_2} - \frac{k_2}{k_1}\right) \sinh k_1 z_1 \sin k_2 z_2 \quad (15\text{-}10)$$

in the other plane.

In Fig. 15-3 the region of stability is shown plotted in $k_1^2 z_1^2$ versus $k_2^2 z_2^2$ space for three different conditions: $z_1 = z_2$, $z_1 = 1.5 z_2$, and $z_1 = 2z_2$. Since k^2 is proportional to the field gradient B', the two coordinates of the plot are proportional to $B_1' z_1^2$ and $B_2' z_2^2$. The shape of the stable region in this plot has led to its nickname of the "necktie diagram." It is clear from these plots that the region is decreased when the quadrupole lengths are not equal; the necktie begins to look a little wind-blown.

The particle orbit through the sequence of quadrupoles has a character that is not at all clear from the arithmetic just presented. The triplet lens whose behavior is described by the matrix equation (15-4) is not nearly so strong a lens as one of the individual focusing quadrupoles; consequently, the effect of a sequence of such triplets will be to produce an oscillation around the axis whose wavelength is much longer than the length of an individual quadrupole. But superposed on this motion will be a smaller motion away from the axis in defocusing quadrupoles and toward the axis in focusing quadrupoles. The path will, in short, be an oscillation of several quadrupole lengths in wavelength with a "wiggly motion" superposed. Moreover, the maximum of the oscillation must

lie in a focusing quadrupole, since this is the only region where the curvature of the orbit is concave looking from the axis. There will not, in general, be a fixed relation between the phases of the slow oscillation and the wiggly motion; on different waves of the slow oscillation the wiggles

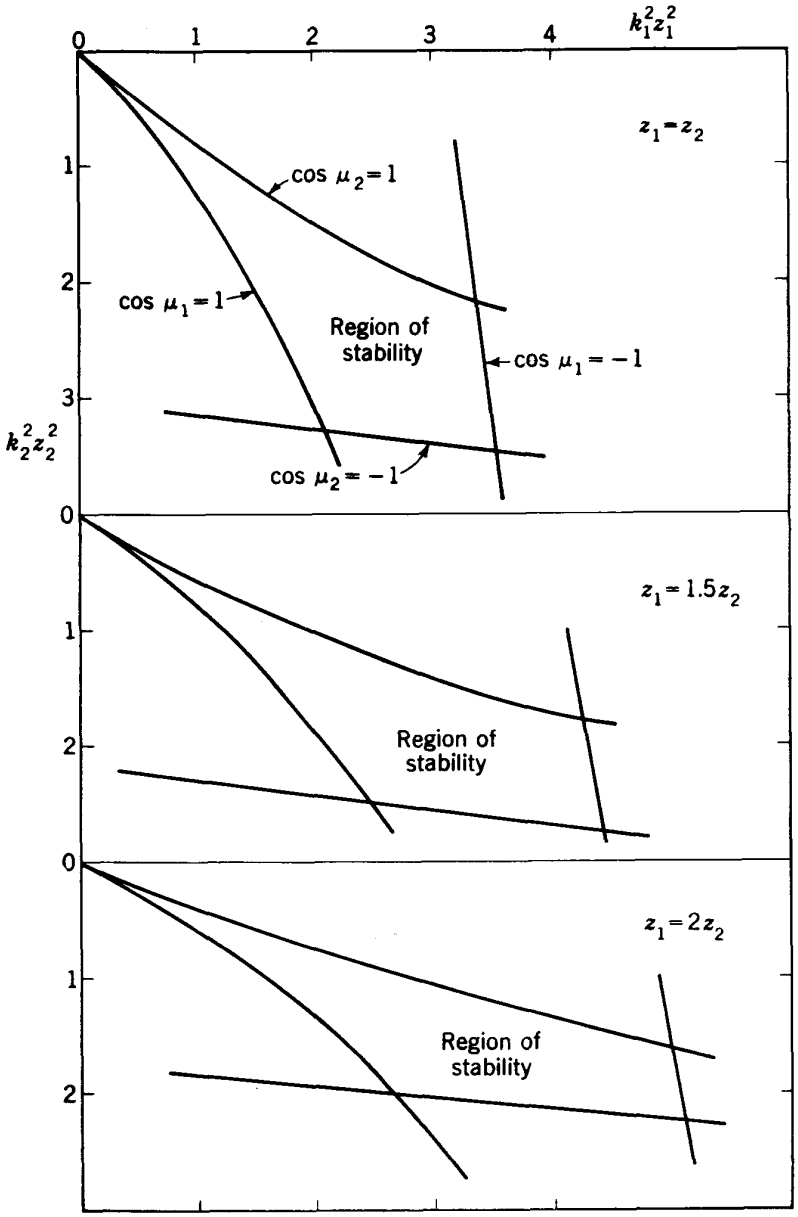

Fig. 15-3. Stability diagrams for AG systems.

will be different. But the envelope of all waves with different starting phases will always have maxima in focusing sectors. Hence focusing sectors will require somewhat larger apertures than will defocusing sectors. Sometimes advantage of this fact can be taken in design.

The only method for a precise orbit calculation appears to be an iterative application of transformation matrices; this operation can be done

easily with an electronic computer. Examples of such orbit calculations are presented in Fig. 15-4. The two orbits shown in that figure are for initial unit displacement in a sequence of quadrupoles of equal lengths

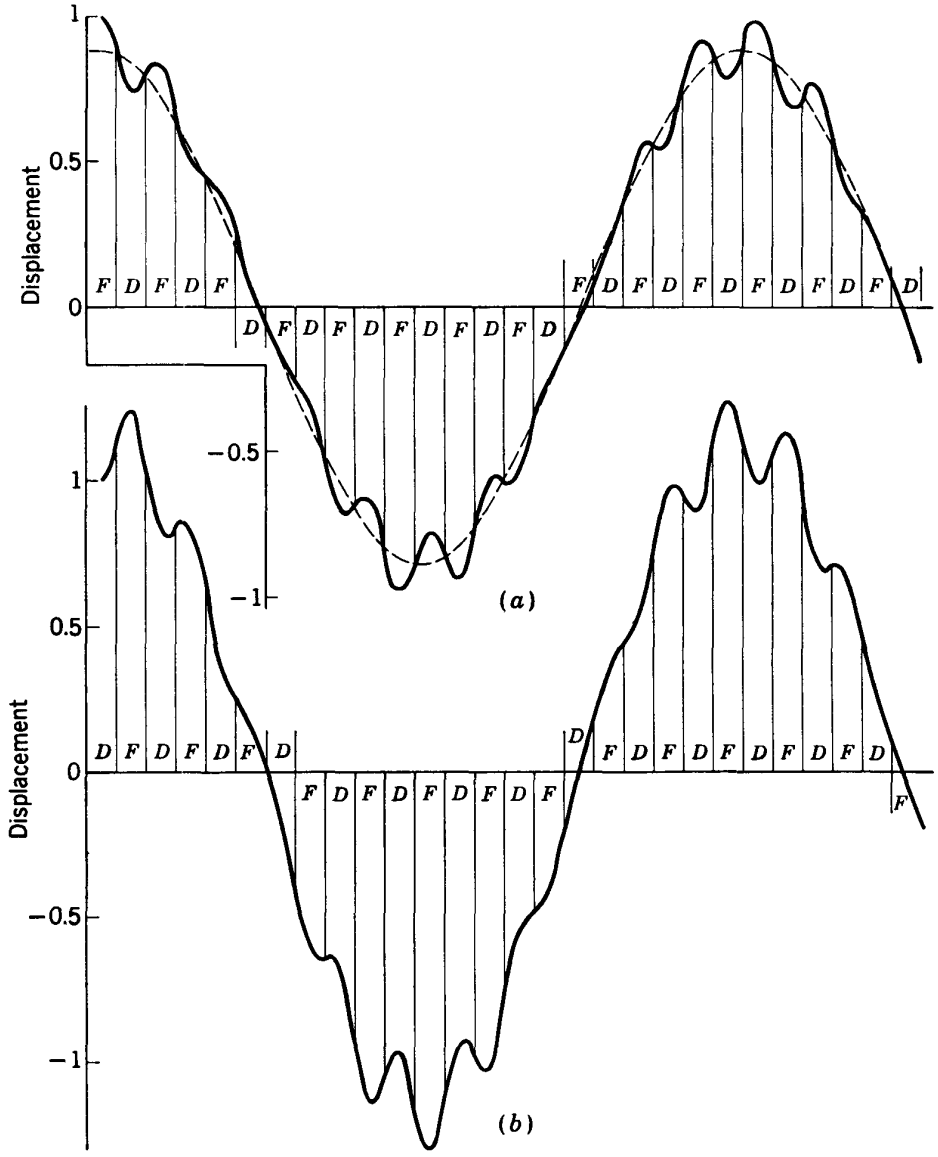

Fig. 15-4. Orbits through a 28-element linear AG focusing system having $k = 0.2$ and $z_0 = 5$. Particles are injected with unit displacement and parallel to the axis in the center of a lens element. (*a*) Orbit in the initially focusing plane; (*b*) orbit in the initially defocusing plane.

having $k = 0.2$ and $z_0 = 5$. One orbit begins in the center of a focusing quadrupole, the other in the center of a defocusing quadrupole.

In most accelerators using AG focusing the wavelength of the major oscillation covers several quadrupoles. For this case an approximate analytic solution describing the complete motion is possible and gives the important characteristics of the motion with sufficient accuracy for most

purposes. The general equation of motion through the quadrupole sequence can be written (cf. Sec. 5-7)

$$\frac{d^2x}{dz^2} + fk^2x = 0 \tag{15-11}$$

where f is a function that has the value $+1$ in focusing quadrupoles and -1 in defocusing quadrupoles. This equation is a form of Hill's equation; the reader who wishes more detailed analysis of this equation is referred to Whittaker and Watson's "Modern Analysis" or to Courant and Snyder.[7] For the present purposes, guided by our observations of orbit behavior thus far, we shall guess that an approximate solution might have the form

$$x = \cos\frac{\mu z}{2z_0}\left[1 + \delta \sin\frac{\pi z}{z_0}\right] \tag{15-12}$$

where the first term represents the long-wavelength oscillation and the term in the bracket represents the wiggly motion that is superposed. The value of μ will be given by Eq. (15-6), and the value of δ will be obtained by substitution in the equation of motion. When this substitution is made, we obtain

$$\cos\frac{\mu z}{2z_0}\left[\left(fk^2 - \frac{\mu^2}{4z_0^2}\right)\left(1 + \delta\sin\frac{\pi z}{z_0}\right) - \frac{\pi^2\delta^2}{z_0^2}\sin\frac{\pi z}{z_0}\right] - \frac{\mu\pi\delta}{z_0^2}\sin\frac{\mu z}{2z_0}\cos\frac{\pi z}{z_0} = 0 \tag{15-13}$$

We can obtain an approximate value of δ from this equation by averaging over the full period of the oscillation, i.e., over the length of two quadrupoles. We shall assume that, over this distance, the long-wavelength oscillation remains approximately constant so that the sine and cosine of $\mu z/2z_0$ can be considered to be constant. The average values of the function f and the sine and cosine of $\pi z/z_0$ will be zero. The quantity $f \sin(\pi z/z_0)$ will, however, have an average value of $2/\pi$. In view of these considerations Eq. (15-13) simplifies to

$$\frac{2\delta k^2}{\pi} - \frac{\mu^2}{4z_0^2} = 0$$

whence

$$\delta = \frac{\pi\mu^2}{8k^2z_0^2} \tag{15-14}$$

This rather rough and ready solution can be tested on the orbits plotted in Fig. 15-4. For these orbits, μ [from Eq. (15-6)] has the value 0.585. Hence, from Eq. (15-14), $\delta = 0.134$. The dashed curve in Fig. 15-4 is the cos $(\mu z/2z_0)$ part of our approximate solution (15-12). The deviations of the orbit from the dashed curve do indeed follow quite closely a sinusoidal oscillation of amplitude proportional to that of the long-wave oscillation. From the curve, δ is about 0.13 as predicted.

It should be reemphasized that this approximate solution is not valid unless the major oscillation covers eight or more quadrupole lenses. Generally, accelerators do not use shorter wavelengths than this because the lens strengths become inconveniently strong and call for higher gradients than are easily produced.

The exact solution of Eq. (15-11) is usually expressed in the form

$$x = A\beta^{1/2} \cos\left(\int \frac{dz}{\beta}\right) \tag{15-15}$$

where A is a constant. β satisfies the differential equation

$$\beta\beta'' - \frac{\beta'^2}{2} + 2fk^2\beta^2 - 2 = 0 \tag{15-16}$$

β is a periodic function, repeating over a distance $2z_0$. Its form is shown over one period in Fig. 15-5, for the two cases $kz_0 = \pi/2$ and $kz_0 = \pi/4$.

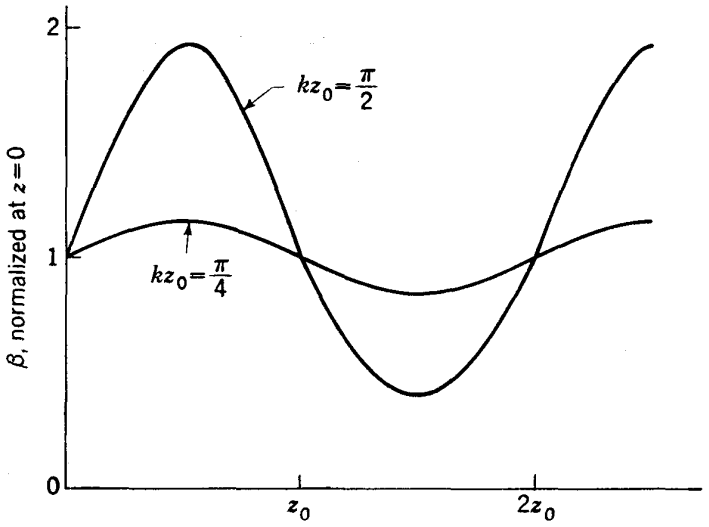

Fig. 15-5. Form of the factor β used in Eq. (15-15).

The factor $\beta^{1/2}$ in Eq. (15-15) corresponds to the factor $[1 + \delta \sin (\pi z/z_0)]$ that was introduced in the approximate solution of Eq. (15-12).

An important example of AG focusing in linear systems is the modern proton linear accelerator. Here, as was shown in Sec. 10-3, the particles are subject continually to a defocusing force of strength

$$\frac{er\omega E}{2v} z\left(1 - \frac{v^2}{c^2}\right) \cos \phi$$

This force is exactly the same as the proton would experience in a defocusing magnetic-field gradient of strength

$$B'_{\text{eff}} = \frac{\omega E}{2v^2} z\left(1 - \frac{v^2}{c^2}\right) \cos \phi \tag{15-17}$$

To find what applied B' required for stability, it is necessary to add the effective defocusing B'_{eff} to an applied alternating B' to see whether the combination lies within the stability diagram. We note that the defocusing problem is most severe for low values of v. Hence, for an example, we consider the low-energy end of a proton linac into which protons are injected at 500 kev (or $v = 10^7$ m/sec approx.). We assume that the linac is designed to operate at 200 megacycles/sec and that its average accelerating field E_z is 2 Mv/m. This gives an effective defocusing gradient

$$\begin{aligned} B'_{\text{eff}} &= 12.6 \cos \phi \text{ webers/m}^3 \\ &= 3200 \cos \phi \text{ gauss/inch} \end{aligned}$$

$\cos \phi$ in working linacs is usually of the order of 0.5; hence the effective defocusing gradient is of the order of 1600 gauss/in. From the stability diagram, the gradients that must be provided to overcome this defocusing are of the order of 10,000 gauss/in.

15-5. AG FOCUSING IN CLOSED ORBITS

If AG focusing is to be used in a circular machine, extra bending fields must be added to hold the particles in the circular orbit. Conceptually the simplest method for accomplishing this would be to alternate quadrupole lenses and bending magnets. This method has been given much

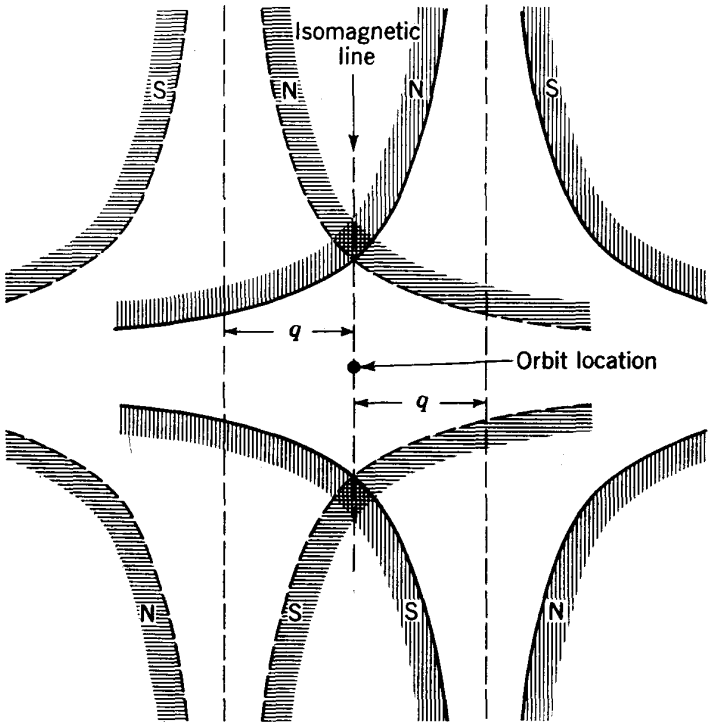

Fig. 15-6. Method of displacing successive quadrupoles to give a bending field in addition to the focusing fields.

thought but has lost out in competition with the more economical method in which quadrupole and bending fields are combined in the same unit. This is done quite simply by displacing the successive quadrupoles by a distance q in opposite directions (see Fig. 15-6) such that the particle feels a bending as well as a focusing field. Since at least half of the quadrupole is not used, it can be left out of the design. In principle it could be replaced by a sheet of iron (or "neutral pole") along the vertical plane of symmetry (see Fig. 15-7). But this refinement also has been eliminated by careful shaping of the magnetic poles to give a quadrupole plus bending field without further additions. The final shape of AG magnets used in synchrotrons is illustrated by Fig. 15-8, which is a cross section through the magnet used in the Brookhaven 33-Bev proton synchrotron.

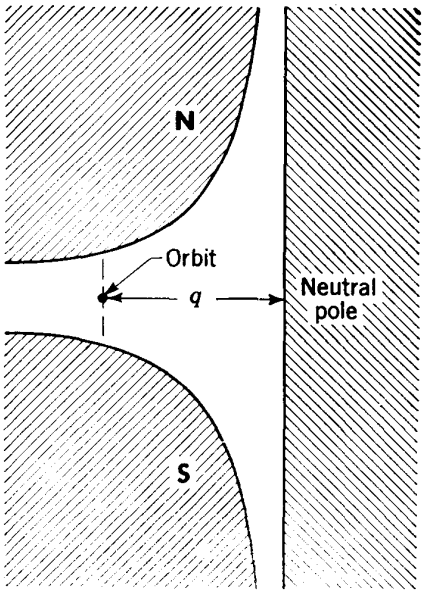

Fig. 15-7. Replacement of half a quadrupole structure by a neutral pole.

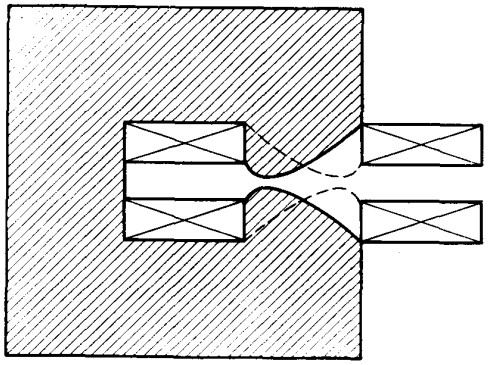

Fig. 15-8. Cross section through the magnet in the Brookhaven 33-Bev AG proton synchrotron.

In AG-focused machines having closed orbits the phenomena are essentially the same as those observed in linear AG systems, with two exceptions—one relatively unimportant and one of crucial importance.

The relatively unimportant consideration follows from the entry of the effects of centripetal force. This effect will become evident from a rederivation of the equations of motion [cf. Eqs. (5-14)]. The radial equation of motion has the form

$$m\ddot{r} - \frac{m\dot{s}^2}{r} = Be\dot{s}$$

where s represents distance along the orbit. This is easily converted to

$$\frac{d^2r}{ds^2} - \frac{1}{r} = \frac{Be}{p} \tag{15-18}$$

where p is the momentum of the particle. If we now make the substitutions

$$r = r_0 + x$$
$$B = B_0\left(1 - \frac{nx}{r_0}\right)$$
$$p = p_0 + \Delta p$$

where x/r_0 and $\Delta p/p_0$ are assumed to be small compared with unity, then Eq. (15-18) becomes

$$\frac{d^2x}{ds^2} + (1 - n)\frac{x}{r_0^2} = \frac{1}{r_0}\frac{\Delta p}{p_0} \tag{15-19}$$

For the present we consider only particles for which $\Delta p = 0$, and the equation of motion becomes

$$\frac{d^2x}{ds^2} - (1 - n)\frac{x}{r_0^2} = 0 \tag{15-20}$$

But
$$\frac{1 - n}{r_0^2} = \frac{n - 1}{-n}\frac{n}{r_0^2} = \frac{n - 1}{-n}\frac{eB'}{m\dot{s}} = \frac{n - 1}{-n}k^2$$

where k is the parameter defined in the preceding section. Consequently the equation of motion becomes

$$\frac{d^2x}{ds^2} + \frac{n - 1}{n}k^2x = 0 \tag{15-21}$$

In the next magnet sector n and B' will be reversed in sign, and the equation of motion will be

$$\frac{d^2x}{ds^2} - \frac{n + 1}{n}k^2x = 0 \tag{15-22}$$

These two equations can be combined in the form

$$\frac{d^2x}{ds^2} + \left(f - \frac{1}{n}\right)k^2x = 0 \tag{15-23}$$

where f is the quantity used in Eq. (15-11); it has the value $+1$ in focusing sectors and -1 in defocusing sectors; Eq. (15-23) is identical with Eq. (15-11) except that f has been replaced by $(f - 1/n)$. But in AG machines n is usually of the order of 100 or more, and hence the term $1/n$ is usually negligible. Therefore it will be found that orbits in circular AG machines will have essentially the same characteristics as orbits in linear machines in so far as radial deviations from the orbit are concerned.

In the vertical plane the equation of motion is identical with that derived in the linear case.

The second point of difference is much more serious. It is now very important that the orbit does not include an integral number of betatron oscillations per revolution. If the number ν of betatron oscillations per revolution is too close to an integer, the smallest orbit perturbation will build up a disastrous oscillation amplitude which, in a few revolutions,

will result in complete loss of the beam. This fact was first pointed out by Adams, Hine, and Lawson[4] shortly after the first publication of Courant, Livingston, and Snyder. For a time this observation was rather depressing to the early workers on AG focusing, since some premature optimism about pencil-sized vacuum chambers proved to be invalidated by a high density of resonances. But more sober consideration indicated that, by proper design, the resonance regions, or "stop bands" as they are now called, could quite safely be avoided.

As a result of these resonances the white-necktie diagram of the linear AG system takes on a plaid appearance. The location of the resonances can rather easily be determined from the fact that μ, whose cosine is the quantity presented in Eqs. (15-9) and (15-10), is the phase shift in the betatron oscillation per quadrupole pair. If the closed orbit includes N quadrupole pairs or $2N$ AG quadrupoles, the total phase shift around the orbit will be $N\mu$. If $N\mu$ is an integral multiple of 2π, a resonance will occur. Since μ can reach values as high as π ($\cos \mu = -1$) in the stable region, a system of N quadrupole pairs will have $N/2$ possible resonances in each plane. The location of these resonances for a machine having $N = 24$ is shown in Fig. 15-9. Except for minor corrections because of the inclusion of field-free straight sections between magnet units, this figure applies to the Cambridge AG electron accelerator discussed in Sec. 15-9.

Since the integral resonances cannot be crossed, the stable operating region for a closed AG machine is limited to one of the diamond-shaped regions between resonance lines. Higher-order resonances also are possible—for example, one in which an integral number of betatron oscillations is included in two or more revolutions. The first of these, the "half-integral" resonance, can cause some beam loss but does not appear to be disastrous. Higher-order resonances can be excited in badly distorted fields but do not appear to be very dangerous.

In the case of the half-integral values of ν_r and ν_z, the width of the stop band is small. "Sum" resonances occur where $\nu_r + \nu_z$ is integral; these cross the stability diamond at its mid-point. They also are narrow and need not disturb the beam significantly. The radial-axial resonance, for which $\nu_r = \nu_z$, is of some concern in that certain magnetic anomalies called "twists" can cause a transfer of oscillation energy between these modes; in this case the oscillation frequencies are shifted apart and may move uncomfortably close to an integral resonance.

In the design of constant-gradient AG magnets, the "working point" is chosen to be within the stability diamond at a location where any motion of the point during the acceleration cycle will not cross the more serious resonances. Integral resonances must be avoided; half-integral and sum resonances can be crossed only if the working point moves across the resonance rapidly; twist resonances can be eliminated from concern

by weak compensating fields. The exact location of the working point depends on the way in which magnetic properties vary during the cycle. If the magnets are to be pushed to high fields where saturation effects tend to reduce gradients and lower ν_r and ν_z, the initial location of the working point should be in the high-ν region of the stability diamond. Furthermore, low injection fields involve magnetic remanence effects

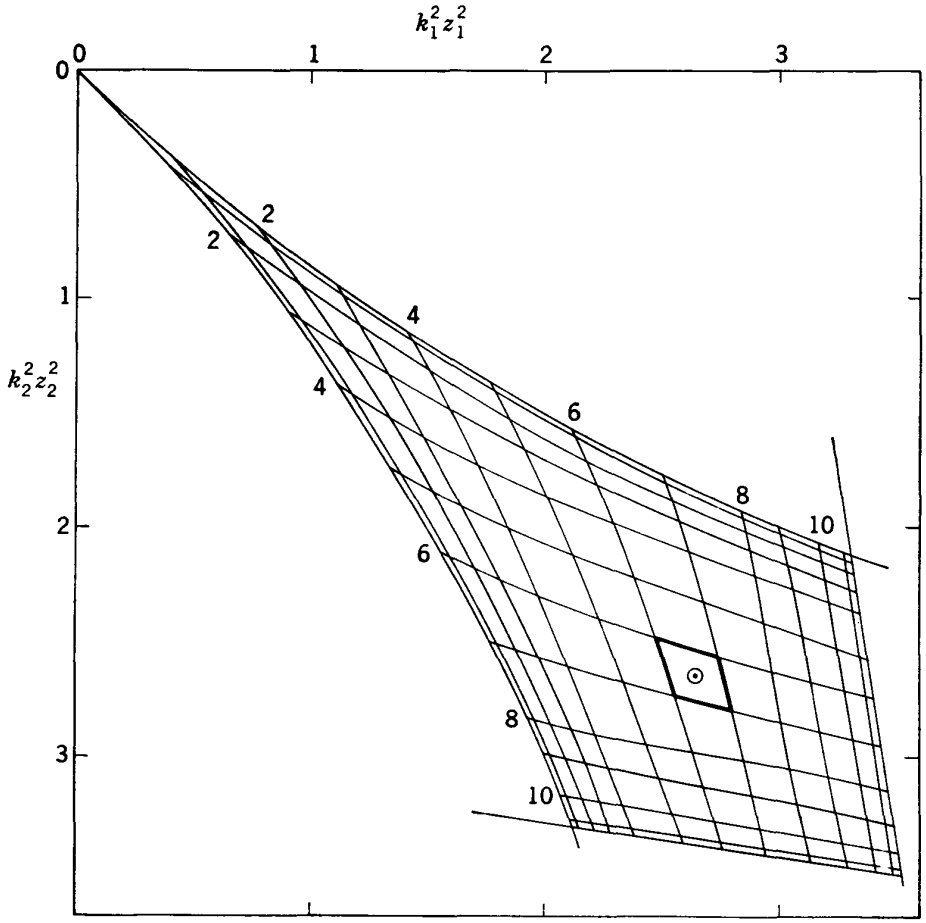

Fig. 15-9. Stability diagram for an AG synchrotron having 24 focusing and 24 defocusing sectors. Integral resonances only are indicated. A possible operating point at $\nu_r = \nu_z = 6.4$ is indicated in the diamond bounded by the sixth- and seventh-order resonances. With minor corrections because of the inclusion of field-free straight sections, this diagram applies to the CEA electron machine described in Sec. 15-9.

which tend to lower ν values; to minimize gradient corrections at and just following injection, the location should be in the high-ν region. Such design and planning considerations lead to a choice of ν either just below the center of the diamond (e.g., $\nu = 6.40$ at Cambridge) or just below the upper tip of the diamond (e.g., $\nu = 8.75$ at Brookhaven). Field correcting windings must be provided to compensate for any major change in location of the working point during the acceleration cycle.

Both linear and closed AG systems are extremely sensitive to misalignments of focusing quadrupoles because AG focusing, though relatively strong, is the net effect of focusing and defocusing forces which, separately, are several times as strong as their combined effect. For instance, it can be shown rather easily from the analysis already presented that the net focusing force in a system having the typical value of 1 for $k_0 z_0$ is lower by a factor of 12 than either of the focusing or defocusing forces that combine to give the AG focusing. This means that if one quadrupole is misaligned by a distance δ, its effects on the beam will be of the order of 12δ. Alternating-gradient focusing systems now in use generally must be aligned to between 0.1 and 0.01 of the tolerable deviation of the particle beam from its orbit. The precise figure depends on the choice of length and strength of the quadrupole focusing units.

15-6. MOMENTUM COMPACTION IN AG SYNCHROTRONS

In the preceding sections it was shown that restoring forces in circular machines with AG focusing are strong enough to reduce betatron oscillation amplitudes to values much lower than those found in machines with conventional or weak focusing. It may not be obvious, however, that particles having momenta that deviate from the equilibrium momentum will not make wide excursions from the equilibrium orbit. If this were so, the phase oscillations in an AG synchrotron would result in large radial motions, and the advantage of small betatron oscillation amplitudes would be lost. Fortunately, this is not the case—large momentum errors result in relatively small radial excursions.

The result just stated is not obvious and is not easily made obvious by qualitative arguments. It seems simplest to trace the orbit for a particle with a momentum error and establish its deviation mathematically. The equation of motion for a particle with a momentum error was established in the last section. It is

$$\frac{d^2x}{ds^2} + (1 - n)\frac{x}{r_0^2} = \frac{1}{r_0}\frac{\Delta p}{p_0} \tag{15-19}$$

where n alternates in sign when s increases by a distance s_0. If we set up an origin of coordinates in the center of each quadrupole element and write down the solutions of this equation, we shall obtain a trigonometric function in the radially focusing sectors and a hyperbolic function in the radially defocusing sectors. When these are matched at the boundaries in position and slope we obtain the solutions (assuming that $n \gg 1$) in the radially focusing sectors,

$$x = \frac{1}{k^2 r_0}\frac{\Delta p}{p_0}\left\{1 + \frac{2\cos ks}{\sin (ks_0/2)[\coth (ks_0/2) - \cot (ks_0/2)]}\right\} \tag{15-24}$$

and in the radially defocusing sectors,

$$x = \frac{1}{k^2 r_0}\frac{\Delta p}{p_0}\left\{-1 + \frac{2\cosh ks}{\sinh (ks_0/2)[\coth (ks_0/2) - \cot (ks_0/2)]}\right\} \tag{15-25}$$

The form of this orbit is illustrated in Fig. 15-10. The average value of x over a distance $2s_0$ is obtained by integrating. We obtain for $\bar{x}$, the average value of x,

$$\frac{\bar{x}}{r_0} = \frac{4}{k^3 r_0^2 s_0}\frac{\Delta p}{p_0}\left[\frac{1}{\coth (ks_0/2) - \cot (ks_0/2)}\right] \tag{15-26}$$

But $\coth x - \cot x = 2x/3 + 4x^5/945 +$ higher-order terms. For x less

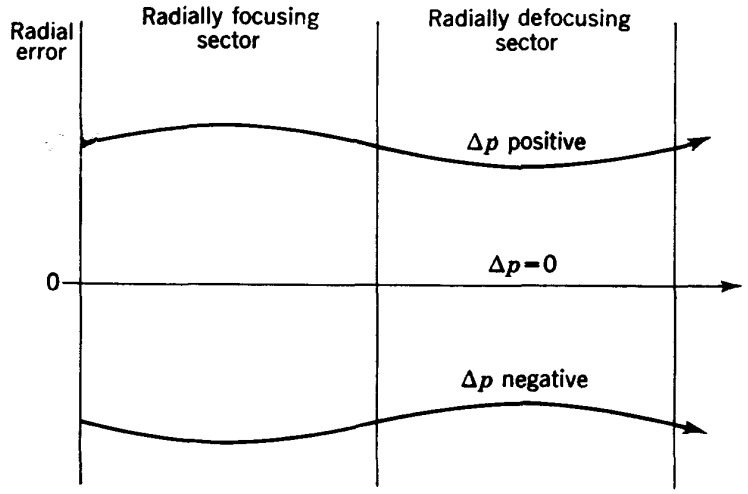

Fig. 15-10. Orbits of particles having positive, zero, and negative momentum errors in an AG synchrotron.

than about 1.1, we are correct to 1 per cent if we set

$$\coth x - \cot x = \frac{2x}{3}$$

So for all likely values of ks_0 the average value of x can be written

$$\frac{\bar{x}}{r_0} = \frac{12}{k^4 r_0^2 s_0^2}\frac{\Delta p}{p_0} \tag{15-27}$$

We now recall that μ, the phase shift in the betatron oscillation per $2s_0$, is given by

$$\cos \mu = \cos ks_0 \cosh ks_0$$

whence, if ks_0 is less than 1.1, we can write with an error of less than 2 per cent

$$\mu^2 = \frac{k^4 s_0^4}{3} \tag{15-28}$$

In terms of μ we can write for $\bar{x}$

$$\frac{\bar{x}}{r_0} = \left(\frac{2s_0}{\mu r_0}\right)^2 \frac{\Delta p}{p_0} \tag{15-29}$$

But N, the total number of pairs of quadrupoles around the ring, is $\pi r_0/s_0$, and ν, the total number of betatron oscillations in one revolution, is $N\mu/2\pi$. Hence

$$\frac{\bar{x}}{r_0} = \frac{1}{\nu^2} \frac{\Delta p}{p_0} \tag{15-30}$$

This will prove to be a very important result, since it shows that relatively large momentum errors in AG machines will not result in large displacements of the beam. For example, in the Brookhaven AG synchrotron, where $\nu = 8.75$ and $r_0 = 128.5$ m, the radial error for a 1 per cent momentum error is only about 1.6 cm. In a weak-focusing machine with an n value of 0.7 and a radius of 128.5 m, the radial excursion for a 1 per cent momentum error would be 4.1 m!

15-7. PHASE STABILITY IN AG SYNCHROTRONS

Derivation of the phase excursions in the AG synchrotron follows the same pattern as that deduced for the conventional synchrotron in Sec. 9-8. The one exception is that Eq. (9-52), which described the excursion in radius for a given momentum error, must now be replaced by the momentum compaction relation equation (15-30) derived in the preceding section. With this change the phase oscillation equation (9-57) becomes

$$\frac{d}{dt}\left[\frac{(1 + p^{*2})^{3/2}\,\Delta\phi}{1 + p^{*2} - \nu^2}\right] = \frac{heV \cos \phi_0\,\Delta\phi}{2\pi r_0^2 m_0 \nu^2} \tag{15-31}$$

where $\Delta\phi$ = phase error
eV = energy gain per revolution
ϕ_0 = equilibrium phase
$p^* = mv/m_0c$, whence $1 + p^{*2} = (1 - v^2/c^2)^{-1} = (W/W_0)^2$
ν = number of betatron wavelengths per turn
W = total energy of particle, ev
$W_0 = m_0c^2/e$ = rest energy of particle, ev

When $1 + p^{*2}$ is replaced by $(W/W_0)^2$, Eq. (15-31) becomes

$$\frac{d}{dt}\left[\frac{W\,\Delta\phi}{1/\nu^2 - (W_0/W)^2}\right] = \frac{hc^2V \cos \phi_0\,\Delta\phi}{2\pi r_0^2} \tag{15-32}$$

This equation has consequences somewhat more complicated than previous phase-stability equations since the quantity $1/\nu^2$ is usually much less

than unity in AG synchrotrons. For energies W less than νW_0 the phase oscillation will be stable only if $\cos \phi_0$ is positive as in the linear accelerator. For W greater than νW_0 the phase oscillation is stable only if $\cos \phi_0$ is negative as in the conventional synchrotron. The energy νW_0 is evidently a transition energy (and will be written W_{tr}) at which the equilibrium phase shifts discontinuously from one side of the accelerating wave to the other.

The reason for this behavior is that at low energies, momentum compaction effects prevent the orbit from wandering in radius enough to permit action of the conventional synchrotron mechanism. What remains of the synchrotron mechanism is overpowered by the linear-accelerator mechanism—particles which have too much energy return more quickly to their starting point, and vice versa. Above the transition energy, however, the particles have approached so closely to the constant velocity of light that the linear-accelerator mechanism is no longer strong enough to overpower the residual synchrotron mechanism and the machine suddenly begins to operate like a conventional synchrotron.

The phase transition phenomena predicted for AG synchrotrons troubled early designers who, at that time, were not confident of their ability to make the necessary sudden shift in phase of the accelerating signal. An ingenious, though cumbersome, design that avoided the phase transition was evolved by Vladimirskij and Tarasov,[8] and work was initiated in the U.S.S.R. on a model of this design. Further theoretical analysis of orbit behavior at phase transition was made at CERN[9] and at Brookhaven[7] with encouraging results, to be outlined below. Finally an electrostatically focused AG electron synchrotron (the "electron analogue") was built at Brookhaven, and it was shown that the phase transition could be passed with relative ease.

In the neighborhood of phase transition the phase-oscillation relation equation (15-32) must be rewritten. Since v is approximately equal to c in this region, the momentum equation (9-58) can be written

$$p_0 = \frac{eW}{c} = \frac{eVt \sin \phi_0}{2\pi r_0}$$

whence

$$W - W_{tr} = \frac{cV\,\Delta t \sin \phi_0}{2\pi r_0}$$

where Δt represents the difference in time between the achievements of energies W and W_{tr}. When these simplifications are inserted in Eq. (15-32), it becomes

$$\frac{d}{dt}\left(\frac{\Delta\phi}{\Delta t}\right) + K\,\Delta\phi = 0 \tag{15-33}$$

where

$$K = \frac{W_0^2 hc^3 V^2 \cos \phi_0 \sin \phi_0}{2\pi^2 r_0^3}$$

Equation (15-33) has a solution in Bessel functions of order $\frac{2}{3}$ which approaches finite limits as Δt approaches zero. For the details of this treatment the reader is referred to the work of K. Johnsen[9] and of Courant and Snyder.[7] It is, however, evident that Eq. (15-33) bears some resemblance to the equation of motion of a pendulum whose mass is increased without limit; at $\Delta t = 0$ the mass has become infinite and the motion is stopped momentarily. This analogy is qualitatively correct; at phase transition the amplitude of phase oscillation is momentarily reduced to a small value. At the same time the momentum errors are momentarily increased, since they are proportional to the rate of change of the phase error [cf. Eq. (9-53)]. Fortunately, in actual AG machines we find that the increase in momentum error and in radial position error does not reach, at transition, the values which have already been passed shortly after injection. For these reasons it has proved possible to pass the phase transition by the mere insertion of a discontinuous phase jump at the correct time. In the Brookhaven and CERN AG proton synchrotrons the timing of the phase jump must be correct to about 1 msec, an easily attainable precision.

15-8. AG PROTON SYNCHROTRONS

At the end of 1961 two large AG proton synchrotrons were in operation —the 28-Bev machine at CERN and the 33-Bev accelerator at Brookhaven. A third 7-Bev model in Moscow was scheduled for operation in 1962; it was to provide design information for a 50- to 70-Bev machine whose construction was beginning in the U.S.S.R. The AG proton synchrotron held undisputed sway over all other accelerator types. The Brookhaven and CERN machines achieved energies higher by a factor of 3 than any other accelerator types. The only possible competitor was the Stanford electron linac, still in the design stage. At the time of writing it appears that no particle energies higher than 33 Bev will be achieved before 1965.

Some of the history of the Brookhaven and CERN projects has already been told in the first section of this chapter. The collaboration between the two groups which began in 1952 with the discovery of AG focusing was maintained throughout the construction period, and, as a result, the two machines have striking similarities. An early debate was held in both groups about the wisdom of proceeding to construction around an untested idea. The theoretical groups in both centers were concerned about the validity of their analyses of the beam behavior at phase transition, and the interpretations of the effects of magnet misalignments were complex and subject to some question. In both centers proposals were made for construction of a low-energy AG-focused electron synchrotron as a check on the theory before the final commitment of some 30 million

dollars. Finally it was decided that the electron machine should be built at Brookhaven; for CERN this was a happy solution, since the CERN group could now proceed with design without drastic commitment before results emerged from the Brookhaven electron machine.

The AG electron accelerator was in no sense a model. It was designed for electrostatic AG focusing and for a final energy of 10 Mev. It was merely to serve as a computer to solve the problems of phase transition and misalignment, and so it came to be known as the "electron analogue." At the end of 1955 this machine was brought into operation; in every respect the electron beam supported the theoretical predictions.[10] Phase transition was passed with no detectable loss of beam, and beam resonances proved to be exactly as predicted. Both CERN and Brookhaven proceeded into construction with feelings of deep relief (except for certain members who had sufficient faith in theory that they believed the model to be unnecessary). The CERN proton synchrotron (generally known as the CERN PS) was completed and brought to energy in November, 1959; the Brookhaven AG machine (known as the Brookhaven AGS) reached its design energy in July of 1960. After a tune-up period of about 3 months both machines went into operation for high-energy experiments. Initial operation was at one shift per week. Within about 2 years it is expected that both machines will operate day and night, 7 days a week. Beam intensities of 3×10^{11} protons/pulse had been achieved both at CERN and at Brookhaven with no evidence of limitation by space charge.

The CERN project was initiated under the direction of O. Dahl of Norway and F. Goward of the United Kingdom. Later, Dahl returned to Norway; soon afterward, because of Goward's sudden death, direction of the PS passed to J. B. Adams of the United Kingdom and C. Schmelzer of Germany. The Brookhaven AGS was built under the direction of L. J. Haworth, G. K. Green, and the junior author (JPB).

The differences between the CERN PS and the Brookhaven AGS are almost entirely in mechanical design. No important differences exist in basic concepts. The writers, whose acquaintance with the Brookhaven machine is much more intimate, will therefore consider it sufficient to describe the AGS with only occasional reference to points of difference between Brookhaven and CERN.

The AGS includes 240 magnet sectors in an FFDD sequence (F is a focusing and D a defocusing sector), which means that the number N of quadrupole pairs (Sec. 15-5) is 60. The circumference of the ring is about 800 m, and the distances occupied by one lens element (in this case, two magnets) is 6.7 m. The ratio of magnetic-field gradient B' to magnetic field B is about 4.2 per cent per centimeter or 4.2 per meter. Hence k^2 ($= eB'/mv$ as before $= B'/Br_0$) is 0.033. The phase shift μ of the betatron oscillation per quadrupole pair [$\mu = k^2 s_0^2/\sqrt{3}$ from Eq. (15-28)] is 0.85. Hence the total number ν of betatron oscillations per

revolution should, on this approximate analysis, be 8.1. This is somewhat oversimplified, however, because the magnets in the AGS occupy only about two-thirds of the circumference of the ring and are separated by field-free straight sections of various lengths. When a detailed analysis is made of the orbits through magnets and straight sections, it is found that the correct value of ν for the AGS is 8.75.

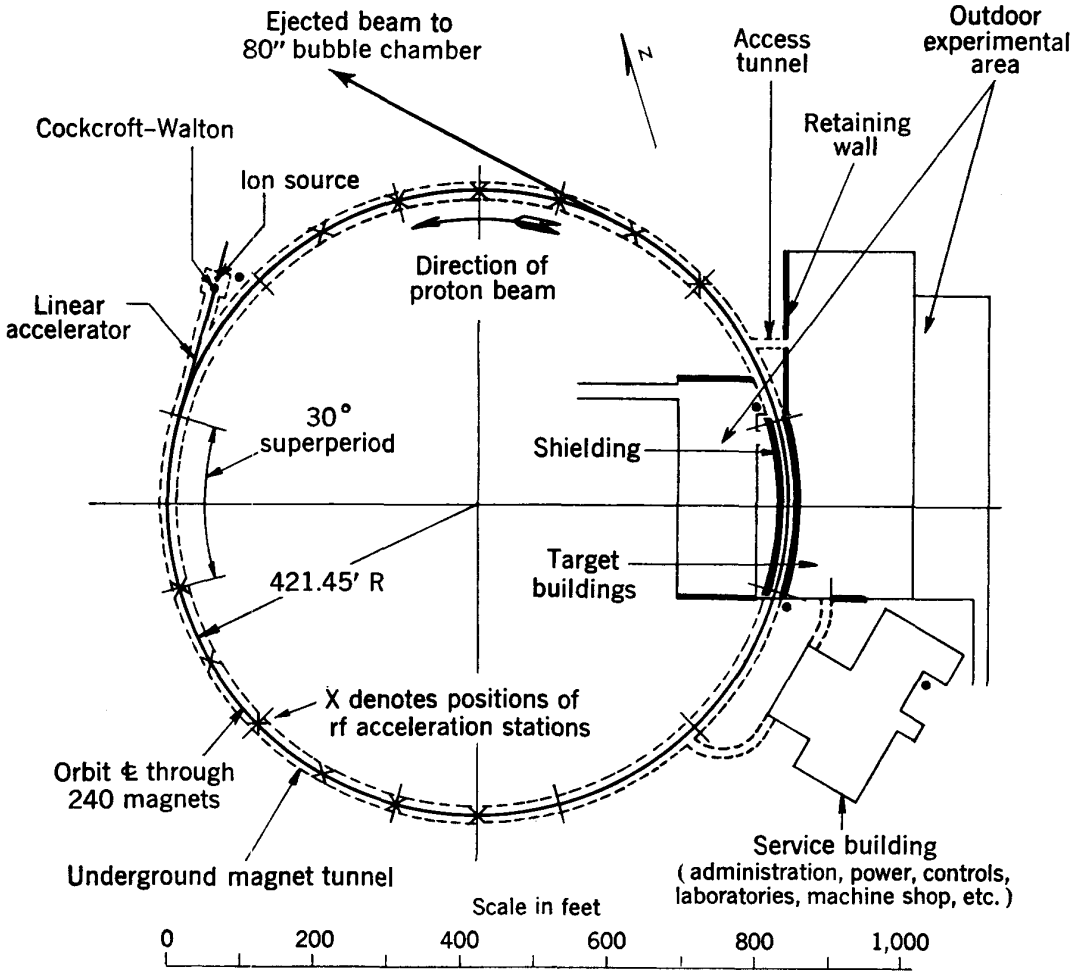

Fig. 15-11. The Brookhaven AGS.

The AGS magnets are arranged in 12 "superperiods" or identical groups of 20 magnets each. Between superperiods and in the middle of each superperiod is a 10-ft straight section that can be used either for one of the 12 accelerating stations, for injection, for targets, or for other beam ejection means. The magnets are C-shaped, and the first 10 magnets in each superperiod have their return legs outside the orbit; the next 10 return legs lie inside the orbit. This configuration allows ejected or scattered beams to clear magnet structures alternately inside and outside the orbit so experiments can be set up both inside and outside the ring.

Between the magnets within the half-superperiods 12 of the straight sections are 2 ft in length and 6 are 5 ft in length.

The general configuration of the AGS is shown in Fig. 15-11. Injection is roughly opposite the target area. The experimental area around the target region of the ring was expanded shortly after the machine became operative to a total of about 80,000 ft², or about 2 acres. This enormous area is needed because beam-handling and analyzing equipment for 30-Bev particles is inevitably massive and extensive. At this energy a magnet maintaining a 20-kilogauss field over a distance of 10 ft bends a particle beam by less than 3°. Counter telescopes are long and complex, bubble chambers have grown to lengths of 6 ft and more, and adjacent beams from the machine aimed at different experiments must be shielded from each other by enormous masses of concrete. Merely to protect the experimental area from the circulating beam in the synchrotron the target building requires a tunnel made of concrete blocks weighing a total of 14,000 tons.

The major components of the machine are as follows.

The Magnet

The AGS magnet configuration was shown in cross section in Fig. 15-8. Each magnet is about 36 by 39 in. in cross section and is about 8 ft long. Total weight of the 240 magnets is about 4000 tons. The pole contour was determined to give a constant field gradient over as wide a region as possible; it was computed by relaxation methods (see Sec. 8-3) and was verified by exhaustive model measurements. The magnet pole is 12 in. thick and gives a satisfactory field pattern over a radial region 7 in. in extent. This pattern is good up to about 11 kilogauss, where it begins to deteriorate, and it becomes unusable at about 13 kilogauss. If, to the cyclotron expert, this seems rather a low field, it must be emphasized that field gradients are high and that fields of 13 kilogauss at the orbit correspond to fields of over 20 kilogauss at the minimum gap.

The field in the AGS magnet reaches its peak in about 1 sec and is restored to zero in about the same period. At 30 Bev the cycle can be repeated every 2.4 sec. At 20 Bev the shorter cycle can be repeated every 1.6 sec, and at 10 Bev the repetition period can be reduced still further to 0.8 sec.

To keep eddy-current effects to a minimum, the magnet is constructed of 0.030-in. laminations. A study of the magnetic properties of steel by the Brookhaven magnet group revealed the fact that steel's most unreliable magnetic property is its coercive force and hence its remanent field. At injection field, about 120 gauss, remanent effects are very important. Accordingly, further studies were made of effects on remanence of chemical composition, heat treatment, etc., of steel. The conclusion of

the study was that no clear-cut predictions are possible at the present stage of the steelmaking art. The only solution appeared to be a thorough shuffling of magnet laminations from the complete series of production runs. Although this involved the use of a large area of a steel plant over a long period, the steel industry was very helpful, and all requirements of the magnet group were met. As a result the magnets as finally assembled were remarkably uniform in properties. All magnets were carefully measured; at intermediate fields they were found to be identical to better than 2 parts in 10,000. At injection fields they were identical to about 4 parts in 10,000, a quite acceptable figure.

The laminations were stamped by a carbide die whose precision was better than 0.001 in. They were stacked and welded into an open box structure under high pressure.

The magnet coils are in four units per magnet (see Fig. 8-13). Each unit was carefully insulated with mica and glass cloth and was cast in polyester resin; the individual units each include eight turns and are of such a thickness that they can be inserted through the gap of the assembled magnet core and moved into final position. A series-parallel connection of the coils gives the complete magnet a peak rating of 7000 amp at about 5000 volts.

In the AGS, errors in magnet location result in errors in orbit location about twenty times greater. It was agreed that orbit displacements up to 1 cm could be tolerated; thus tolerances on magnet location of about 0.5 mm or 0.020 in. were fixed. These tolerances proved, on more detailed analysis, to be valid over a limited range, specifically over a betatron wavelength. The greater the distance around the ring, the more relaxed became the tolerances. This fuzzy definition was clarified when it became evident that only misalignments which produced field errors including a harmonic close to the ν value of 8.75 were of paramount importance, and other harmonics were of lesser importance depending on their displacement from ν. Strict attention was paid to anything that could produce a seventh, eighth, ninth, or tenth harmonic in the field pattern. Correcting coils were included and connected for application of these harmonics. To date it has not been necessary to use these corrections.

A machine of ½ mile circumference to be aligned to 0.5 mm local precision raises unusual problems of soil mechanics. It is not customary to build structures to such precision, and few precedents exist for this undertaking. Both at CERN and at Brookhaven the earth and its underpinnings were studied very carefully. At CERN a test-tunnel section was built and observed over a long period. At Brookhaven load tests on the local soil were run by piling and unpiling some 2000 tons of concrete. The problems in the two sites proved to be completely different. At CERN a thin layer of shale covered a soft bedrock (the Molasse) that was subject to earthquake tremors and to seasonal dis-

placements with the snow load on adjacent mountains. At Brookhaven the laboratory is built on sand that extends in a relatively homogeneous fashion to a depth of 1500 ft down to bedrock. At CERN, accordingly, it was necessary to support the magnet on a monolithic concrete ring supported on springs, while at Brookhaven the magnet rests on concrete caps covering steel piles driven 50 ft into the sand. (It seems that it is not always unwise to build on the shifting sand.) Both foundations have proved stable and satisfactory.

Eddy-current effects at injection fields did not appear to be troublesome so far as the magnet was concerned. Serious field distortions appeared, however, in auxiliaries, particularly in the Inconel vacuum chamber where thickness tolerances could not be met with sufficient precision to guarantee azimuthal uniformity of eddy-current depression of the field. It was therefore decided at Brookhaven to decrease the initial rate of rise of the magnetic field by a factor of 4 by inclusion in series of a saturating inductor whose saturation characteristic was such as to hold $\dot{B}/B$ at or below its value at injection. This proved to be a 200-ton device whose performance was precisely as predicted. At CERN no series inductor has been included.

For adjustment of the initial ν values and for field corrections at high fields both Brookhaven and CERN have included a number of multipole magnets. In the AGS, 24 quadrupole magnets can be adjusted to keep the ν values constant as the magnet saturates; 36 sextupoles can be used to correct nonlinearities in the field pattern or, in other words, to keep ν constant with radius. At CERN a number of octupoles can be used to correct second-order field disturbances. These are not included in the AGS. Very careful and detailed orbit studies will be necessary to prove whether or not octupoles are useful.

The power supply for the AGS magnet system is similar to that used at the Brookhaven cosmotron (see Sec. 13-5). It includes a 35,000-kva 12-phase alternator driven by a 5000-hp motor and carrying on the same shaft a 40-ton flywheel for energy storage and equalization of load on the power line. The output of the alternator is rectified in a bank of 24 ignitrons and then supplied directly to the magnet through an extra magnet unit which supplies field to various timing devices necessary for timing injection, rf turn-on, etc. These are, for the most part, peaking strips or wires of high-permeability material which are located in biasing coils and which bear windings (see Sec. 8-8). As the field plus bias passes through zero, these strips go rather suddenly from negative to positive saturation. A peaked signal is induced in the windings and can be used for timing. The time of appearance of the peak can be adjusted by variation of the current in the bias winding.

The various multipoles also are powered by rotating machines, in this case dc generators with programmed field control.

Injection

Both at CERN and at Brookhaven, protons are injected into the synchrotron ring at 50 Mev. At Brookhaven, ions produced in a cold-cathode ion source are preaccelerated to 750 kev in a Cockcroft-Walton set built by Philips and consisting of a cascade-transformer voltage-multiplier stack and a filter stack supported on a 0.008-μf capacitor and supplied through a 5-megohm resistor from the cascade transformer.

The Brookhaven linear accelerator[11] is electrically a single tank of copper-clad steel. Mechanically it consists of 11 pipes of copper-clad steel about 3 ft in diameter and 10 ft long, flanged at their ends and bolted together. The shapes of the 124 drift tubes were computed,[12] and they were machined out of solid copper. At the low-energy end they are pancake-shaped; as their length increases along the tank, they become first almost spherical and then football-shaped. In each drift tube is a pulsed quadrupole magnet for compensation of the defocusing effects of the accelerating field. Radiofrequency power required is about 3 megawatts at 200 megacycles—this is supplied at the center of the tank by two TH-470 (French Thomson-Houston) triodes whose outputs are combined in a waveguide hybrid junction.

From the linac output the proton beam travels (see Fig. 15-12) about 140 ft through focusing and steering arrays, viewing screens, defining slits, and an analyzing magnet which is used to deflect the beam for measurement of energy and energy spread. The path approaching the injection point is parallel to the synchrotron orbit but displaced 3 in. outward. Approaching the inflector, the beam is bent by the stray fields of three magnet sectors and enters the inflector with an inward direction of 1.5°. The inflector consists of two plates on either side of the orbit, charged to + and −80 kv. This field straightens the proton orbit and directs the protons into the desired equilibrium orbit in the synchrotron. When the synchrotron vacuum chamber is filled, the field is turned off in a fraction of a microsecond; if it is left on, the beam is lost on its second traversal through the inflector.

The injection field in the AGS is 120 gauss; in the CERN PS injection is at about 150 gauss. In both cases the injection field is several times the remanent field. Higher injection energy would move injection into still higher and more uniform fields, but construction of injectors of energies higher than 50 Mev introduces serious problems of both cost and design of the electrostatic inflector. Independent studies at Brookhaven and CERN both resulted in the choice of 50 Mev as the optimum energy for injection.

The 50-Mev linac injector for the AGS has its output beam included in an area about 1 cm in diameter and with an angular spread of about 2 milliradians. This beam is easily matched to the synchrotron's require-

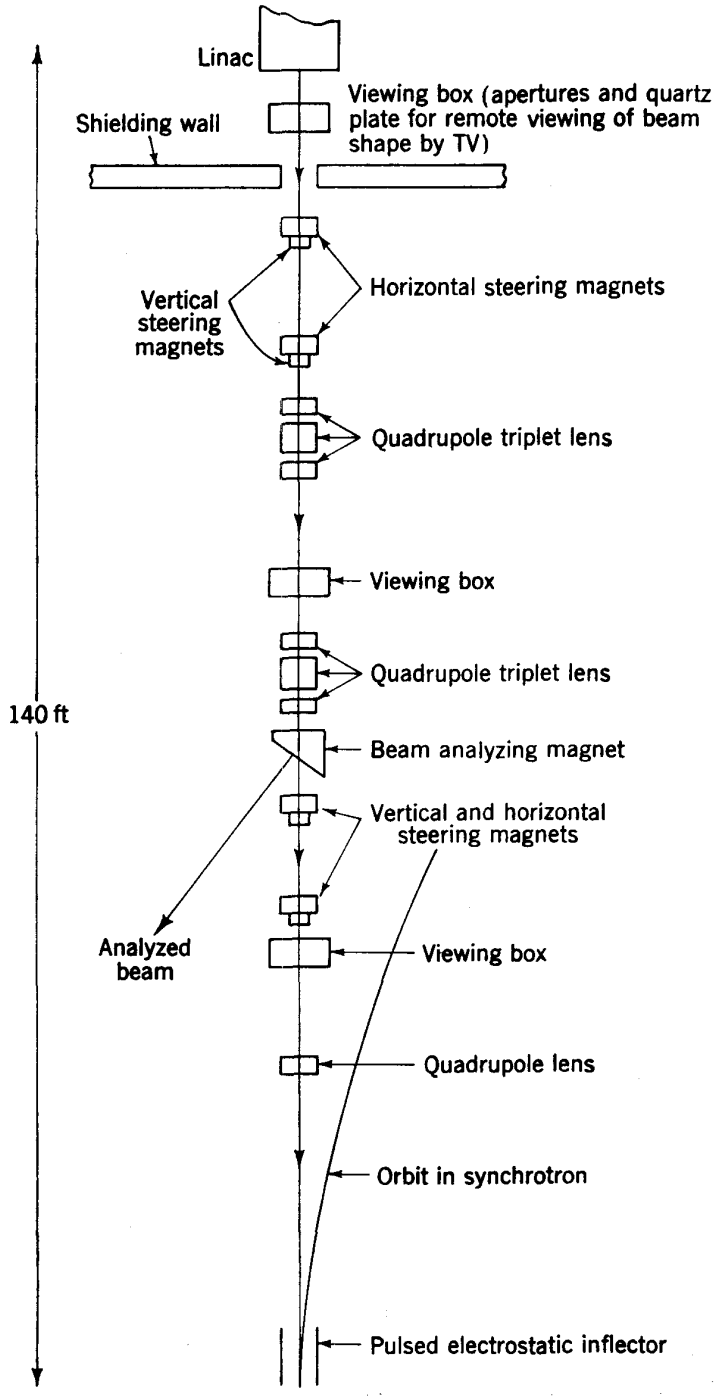

Fig. 15-12. Injection system of the Brookhaven AGS.

ments; no appreciable fraction of the beam is lost between linac output and synchrotron input.

RF Accelerating System

At 50 Mev the injected protons have about one-third of the velocity of light, while at 30 Bev the velocity has reached about 0.9995 of the velocity

of light. The frequency of the accelerating system must therefore vary over a factor of about 3. This variation takes place very rapidly during the first fraction of the cycle. Transition energy in the AGS is about 7 Bev and is reached in less than ¼ sec; by this time better than 99 per cent of the frequency range has been covered.

The frequency of revolution increases from its injection value of 125 kc to 375 kc at full energy. If this frequency were used in the accelerating system, however, the radial excursions due to the phase oscillation would be large, and the various accelerating stations around the ring would have small phase shifts with respect to each other to be maintained over the whole frequency range. To avoid these difficulties, the rf system uses the twelfth harmonic of the fundamental frequency and operates from 1.5 to 4.5 megacycles. Stations located in twelve of the twenty-four 10-ft straight sections are supplied from a central driver by cables of equal lengths; the stations run either in phase or 180° out of phase with each other, depending on their location.

Energy gain per turn is about 100 kev, or 8 kev per accelerating station. The accelerating units are double ferrite-loaded cavities kept in tune by saturation of the ferrite. The saturating current of about 1000 amp maximum passes through the wall of the accelerating cavity and is controlled by a bank of 100 paralleled power transistors.

The accelerating frequency in an AG synchrotron must be controlled with much higher precision than that in a classical synchrotron, particularly around transition. This problem is met in the AGS by deriving the accelerating signal directly from the proton beam. The beam is bunched in the first few revolutions after injection by a programmed oscillator, and the primary signal is then derived from a cylindrical electrode through which the beam passes. This signal is amplified and brought to the accelerating stations. It still is possible for slow phase drifts to cause the beam to drift inward or outward; this is corrected by derivation of a signal from a pair of pickup electrodes inside and outside the beam orbit and application of the signal to a controlled phase shifter in the chain to the accelerating units. The pickup-electrode signal is proportional to beam displacement and is fed back with such a polarity as to reduce this displacement. This system, used both at Brookhaven and at CERN, appears to hold the beam throughout acceleration with no detectable loss after the first few milliseconds. At transition, a sudden phase shift of about 120° transfers the operating phase from one side of the accelerating wave to the other. This phase shift must be made in a fraction of a millisecond at a time correct to better than 1 msec, tolerances that are rather easily met.

It was thought originally that losses at transition would be decreased by decreasing the amplitude of the accelerating signal as the phase is shifted, and the possibility of modulating in this fashion was incorporated

in the AGS rf system. Since, without changing amplitude, there is no apparent beam loss at transition, this modulation is not used.

Vacuum System

The vacuum chamber in the AGS is approximately elliptical in cross section, with the major axis horizontal and 7 in. in extent; vertically the maximum dimension is a little over 3 in. It is fabricated of Inconel, a stainless metal of high resistivity (over 100 μohm-cm) and 0.078 in. thick. In almost all magnet gaps the chamber has the configuration just described, but in some places special sections are fabricated of greater width to permit injection or beam ejection. In the straight sections are located bellows, vacuum pumps, valves, pickup-electrode stations, target boxes, beam-ejection mechanisms, and other miscellany.

The AGS is pumped entirely by Evapor-ion pumps, which operate by a combination of the gettering action of evaporated titanium and the pumping action of a glow discharge. These pumps were chosen since they do not require refrigerated baffles or cold traps. For the linear accelerator they seemed particularly appropriate since they would introduce no organic contamination into the high rf field regions. After about 18 months of operation this still appears to have been a wise choice, since the intense X rays emitted by linacs with oil pumps have not yet appeared.

Targets

In both the AGS and the PS, thin targets are used through which the beam makes multiple traversals. Scattering by atomic electrons is small enough that a proton that has not made a nuclear collision will continue to circulate, contained by the strong momentum compaction of the AG machines. Circulation continues until the proton makes a nuclear collision; thus very high target efficiencies are achieved.

An undesirable feature of the accelerated beam from the experimental point of view is its bunching by the rf accelerating signal which, at full energy, results in the containment of all protons in bunches occupying less than 10 per cent of the azimuth. This results in intermittent jamming and inactivity of counters used in detection of collision products. To avoid this problem the beam is debunched by turning off the rf accelerating field and allowing the beam to drift, under the influence of the still-rising magnetic field, to a target located an inch or so inside the equilibrium orbit. This requires a period of several milliseconds, during which the beam becomes rather thoroughly debunched.

The output of both machines includes large numbers of μ mesons (muons) which are weakly interacting particles. Consequently they appear in large numbers even after interposition of more than 15 ft of heavy (iron-loaded) concrete. These particles seem to present the worst

shielding problem and may be quite troublesome in experiments that require low background.

Operation

Both at Brookhaven and at CERN the hopes of the synchrotron designers have been exceeded by the performance of the AG machines. Reasonable care in meeting design tolerances has been rewarded by a steady beam that appears to deviate from the center of the vacuum chamber by not more than a centimeter. Variation of parameters of the magnetic field and its gradient results in observations of beam behavior in perfect agreement with theoretical predictions. Integral resonances are indeed impassable, but half-integral and other resonances can be crossed with impunity.

From the performance of the two large AG synchrotrons now operating it is safe to predict that the present method can be extrapolated upward in energy by at least a factor of 10 without serious technical difficulty. Cost appears to be the only visible limitation on extension of the AG art to hundreds or thousands of Bev.

15-9. AG ELECTRON SYNCHROTRONS

The principle of acceleration in the electron synchrotron is basically simpler than for the proton synchrotron, since electrons approach the limiting velocity of light at relatively low energies, and their orbital frequency becomes constant. This allows the use of high-Q resonant cavities for acceleration, without the need for frequency modulation and requiring much lower power. Some amount of preacceleration is required to reach constant orbital frequency. This was accomplished in the constant-gradient synchrotrons (see Chap. 12) either by use of an external preaccelerator and an inflection system to direct the linear beam into the orbit or by initial betatron acceleration in the synchrotron field.

In AG electron synchrotrons it is easy to avoid the technical difficulties associated with the phase transition; a transition energy exists, but usually it is below the injection energy. As was shown in Sec. 15-7, phase transition takes place at an energy of νW_0. For most AG machines now in operation or construction ν is of the order of 10. For electrons W_0 is about 0.5 Mev; the transition energy will thus be of the order of 5 Mev, which lies below the energy of the linac injectors planned for the AG electron machines in construction.

Alternating-gradient magnets allow considerable reduction in dimensions of the magnet and the gap between poles; at the same time they reduce the momentum compaction factor to make acceptable a much larger fractional spread in momentum than in the constant-gradient machines. The basic principle of acceleration is unchanged, and the

advantages of constant-frequency acceleration remain. The real significance of AG focusing is that much higher energies become economically practical and technically feasible. (However, the higher energies introduce new and serious design problems involving the energy loss by the orbiting electrons due to radiation.) Furthermore, the smaller size of magnets and the reduction in magnetic stored energy allow the AG magnets to be pulsed at a higher repetition rate than has been customary with constant-gradient magnets. The faster cycling rate results in significantly higher time-average beam intensities, as well as higher energies. The AG electron synchrotron is capable of producing beam intensities approaching those from linear accelerators, with similar cycling rates and with a considerably larger duty cycle for the high-energy beam; the long duty cycle has many advantages for research using electronic detection apparatus.

A fundamental limitation on any magnetic accelerator for electrons is the radiation loss due to radial acceleration in the magnetic field. The loss per turn (see Sec. 7-7) is

$$V = 8.85 \times 10^4 \frac{W^4}{r_0} \qquad \text{ev/turn} \tag{15-34}$$

where W is total electron energy in Bev units and r_0 is radius of curvature in meters of the orbit in the magnetic field.

Since radiation loss varies inversely with radius, problems can be minimized by using large orbit radius and a correspondingly low magnetic field. However, the fourth-power increase with energy limits the maximum energy for which practical designs can be conceived to about 50 Bev. Even at lower energies the economic advantage of the circular machine relative to the linac decreases. The large orbits (and low fields) result in increasing the size of buildings to house the ring-shaped accelerator, and the buildings become the most costly components.

The first large AG electron synchrotron aimed at approaching this practical maximum energy limit is the Cambridge electron accelerator (CEA), sponsored by MIT and Harvard University with a design energy of 6 Bev;[13] it is scheduled for completion in 1962. Two similar machines are now (1961) under construction, with the same design energy and based to a large extent on the CEA designs; one is at the Deutsches Elektronen Synchrotron (DESY) laboratory at Hamburg, Germany,[13] and the other at the Institute of Physics laboratory of the Armenian Academy of Sciences at Erevan, Armenia, U.S.S.R.[13] Since the Cambridge machine is further advanced and includes most of the features planned in the other laboratories, it will be described in some detail.

Several electron synchrotrons of lower energy utilize AG focusing. At Cornell University an electron synchrotron originally planned as a constant-gradient machine was modified to use AG pole faces, more as an

experiment in design than because of any fundamental requirement; it was brought into operation in 1954 and has been developed to deliver 1.1-Bev electrons. The Cornell machine was the first practical AG accelerator, and its success reinforced confidence in other laboratories in the design of still-higher-energy machines. Later, a 500-Mev AG synchrotron was built at the Physikalisches Institute der Universität, Bonn, and was completed in 1959. Two other AG electron synchrotrons are approaching completion (1961), each for about 1.2 Bev energy; one is at the University of Lund and the other at the University of Tokyo.

The Cambridge electron accelerator is sponsored by MIT and Harvard University, under the direction of the senior author (MSL); it is supported by the United States Atomic Energy Commission. Detailed design started in 1956. It was conceived as a research installation for the university scientists of the area for the study of high-energy particle physics. Electrons were chosen because of their obvious value as a supplement to protons in the field of high-energy interactions. The design energy of 6 Bev is five times greater than has been reached in existing electron accelerators and is sufficient for production of all known fundamental particles (except xi pairs). At this energy it will be possible to extend electron scattering experiments into a new energy range. The energy approaches the technically practical limit possible with circular machines, within the size of the available site of Harvard University.

The limitation on maximum energy due to radiation loss, based on Eq. (15-34), requires a relatively large orbit radius and lower magnetic fields than those normally used in proton synchrotrons. The choice of an orbit radius of approximately 118 ft leads to a peak magnetic field of about 7600 gauss for 6 Bev energy. This peak flux density is well below the value where magnetic saturation effects occur, and it removes the need for magnetic correcting devices at high energy; it also results in relatively small magnetic stored energy and low power requirements. Another valuable consequence is the opportunity to use a high repetition rate (60 cps), which minimizes the growth of radiation-induced oscillations and also results in a high time-average beam intensity. The several major components will be discussed in turn.

Magnet

The design of the system of AG magnets is based upon the requirement of strong momentum compaction, the need for a simple structure which can be assembled with precision to give the best obtainable uniformity between magnets, and the desire to minimize power requirements and cost of construction. The periodicity of the magnet structure ($N = 24$ AG units) and the number of betatron oscillations per turn ($\nu = 6.40$) were chosen to obtain a small momentum compaction factor (0.03). The periodic structure is a simple alternation of 24 F (focusing) and 24

D (defocusing) magnets spaced by field-free regions O; one AG period can be represented by the symbols FODO. The 48 magnets are identical except for the alternation in shape of pole faces, and they have equal field strengths at the "isomagnetic line" at the center of the magnetic-field region. The C-shaped back-legs of the magnetic circuit are all on the inside of the orbit, so beams of radiation can emerge tangentially from the vacuum chamber at any point around the orbit.

The pole-face shape is basically hyperbolic, to give uniform gradients in both radial and vertical coordinates. The distance from the isomagnetic line to the vertical axis of this hyperbola determines pole-face shape and is a measure of the focusing strength of the magnet; it is called the "characteristic length" and has the value $q = 11.38$ in. (see Fig. 15-6). The value of q determines the magnetic gradient through the relation

$$q = \frac{B_0}{dB/dr}$$

and it is associated with the n value of AG theory by $n = r_0/q$, where r_0 is the radius of curvature of the equilibrium orbit at the isomagnetic line. One of the primary advantages of the FODO structure is that the value of q can be varied (over a small range determined by the useful width of field) by moving one class of magnets radially inward and the other class radially outward. This independent adjustment of the effective gradient allows the ν value to be varied around the design value of 6.40 for high fields.

The pole-face profile varies slightly from the ideal hyperbolic shape to provide a small variation in gradient across the pole face. This variation is designed to keep betatron oscillation frequency independent of the radial location of the equilibrium orbit, coming from the "breathing" motion of the equilibrium orbit associated with the synchronous oscillations in particle momentum. If it were not applied, the betatron frequency would change (about 2 per cent per inch) with radial location, which could result in coupling between the betatron and synchronous oscillations and the introduction of satellite stop bands due to field or gradient errors; crossing such stop bands could lead to loss of beam intensity. This variation from hyperbolic shape produces a sextupole field distortion; it takes the place of the sextupole lenses used in proton AG synchrotrons to provide similar corrections at high fields. So quadrupole or sextupole magnetic lenses are not needed in the Cambridge accelerator for magnetic corrections at high fields.

The length of magnet gap is minimized to reduce excitation requirements; it is chosen as 2 in. at the isomagnetic line. Pole width is 6½ in., with the isomagnetic line 3 in. from the open face of the gap; this provides about 5 in. of useful width of essentially constant-gradient field. To minimize edge effects and extend the region of useful field, the "nose" at

the closed-gap side is rounded, and a flat step is provided at the open-gap side. This choice of vertical and radial aperture was based on computed oscillation amplitudes just following injection, assuming certain limitations on the properties of the injected beam from the linac preaccelerator. The aperture will accept an energy spread of 2.5 per cent, an angular divergence of 1.5×10^{-3} radian, and a beam diameter of 0.5 in.; it also includes a factor of safety to allow for growth of amplitudes due to alignment errors or magnetic inhomogeneities, and space for the walls of the vacuum chamber. The pole-face shape and vacuum-chamber dimensions are illustrated in the sketch of Fig. 15-13.

Magnet cores are formed of 0.014-in. sheets of high-silicon transformer steel, to minimize losses at 60 cps excitation, and are die-cut to the chosen

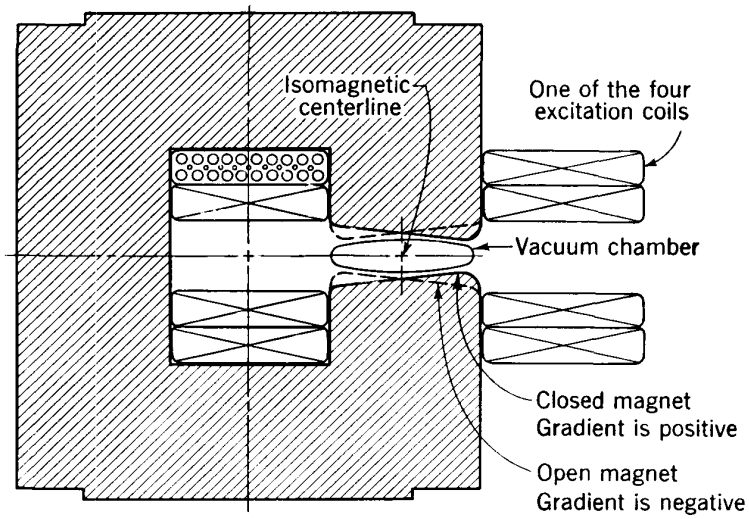

Fig. 15-13. Magnet configuration and vacuum chamber for the CEA AG electron synchrotron.

pole-face shape with 0.0005-in. precision. Sheets are sorted and preselected in sequence to randomize any nonuniformity of material or manufacture. They are bonded into blocks about 11 in. long with a rubber-base phenolic resin, utilizing an assembly and bonding jig which maintains 0.001-in. precision. The individual magnet is assembled on a heavy box girder about 12 ft long, using 12 core blocks in two straight assemblies of 6 blocks each, mounted on machined rails which make an angle of 3.75° (360°/96) to conform more closely to the circular orbit. The rails are machined flat and located with a precision of 0.002 in., and they provide the basic alignment for each magnet. Each set of six core blocks is clamped between nonmagnetic stainless-steel end plates by insulated stainless-steel tie rods. These end plates also carry a $\frac{3}{4}$-in. layer of laminations oriented normal to the ends of the magnet poles, to minimize eddy currents in the laminations due to fringing fields in the

magnet ends. These "end packets" of transverse laminations reduce heating of the end laminations to the extent that lamination cooling is not required for full-power operation. A wedge-shaped space at the center of the magnet between the two straight assemblies, about 4 in. long, is used to admit coil leads, cooling water tubes, etc.

Each magnet is energized by a 40-turn winding, in the form of four flat coils which enclose the 12 core blocks and end packets and are thin enough to be inserted between the magnet pole tips (1½ in.). The conductor is a double layer of stranded cable, with individual strands insulated to prevent circulating eddy currents, embedded in a resin binder (see Fig. 8-13). The heat is removed by water circulating in copper tubing meshed between the conductors and also embedded in the resin

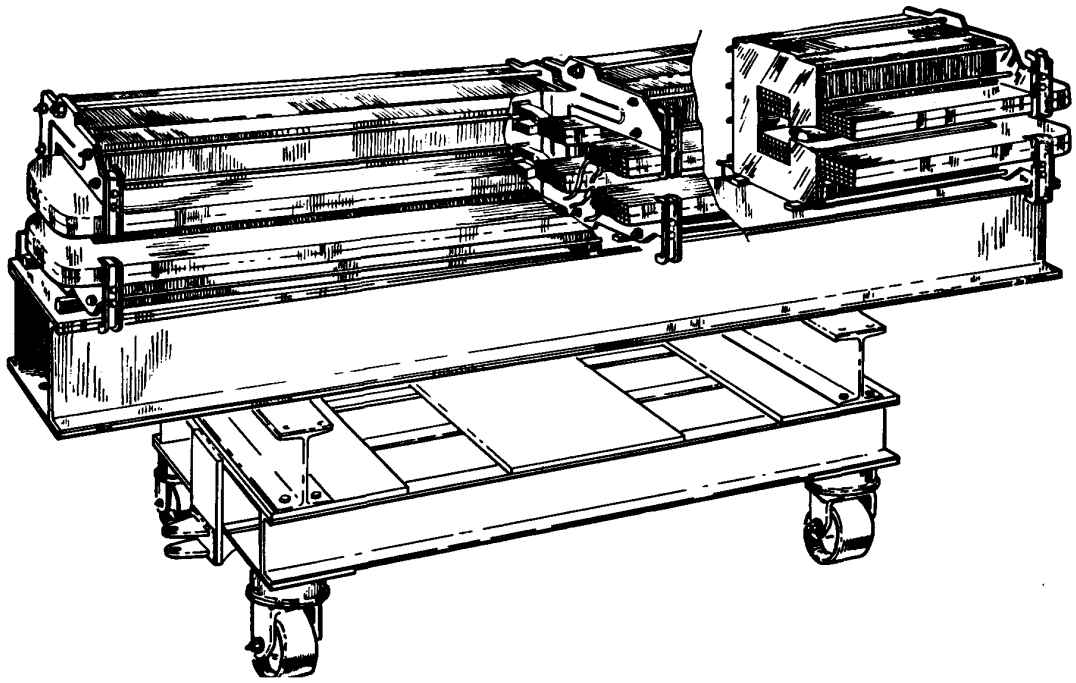

Fig. 15-14. Magnet assembly used in the CEA synchrotron.

binder of the coil. The structure and assembly of the magnet unit is illustrated in the sketch of Fig. 15-14.

Magnets are mounted on adjustable supports resting on piers which are physically separated from the floor of the circular tunnel and mounted on piles driven deep into the subsoil. These supports consist of jacks and hydraulically invoked ball bearings for transverse motion, capable of reproducible settings within 0.001 in. An optical surveying procedure is used to locate magnets with a positional accuracy of ± 0.01 in. (rms) in the radial and azimuthal coordinates and ± 0.005 in. in the vertical. This procedure uses a ring of 16 survey monuments outside the circle of magnets, along with accurately machined jigs to hold measuring instru-

ments mounted on the machined magnet rails and the die-cut surfaces of the magnet cores. The surveying techniques are adequate to obtain satisfactory alignment for initial operations.

Magnet Power

The magnet excitation cycle is a full-biased sinusoidal waveform obtained by superposition of a 60-cycle component of current with peak amplitude $\frac{1}{2}I_m$ and a dc component with amplitude $\frac{1}{2}I_m$, following the relation

$$I(t) = \tfrac{1}{2}I_m(1 - \cos 2\pi ft) \tag{15-35}$$

Full-biased excitation is desirable to make the time rate of change of field at injection $(dB/dt)_i$ small, which reduces eddy-current distortion of the field at this critical time. It also minimizes power requirements by reducing magnetic losses to those in a half-cycle.

The power-supply system for the magnet of the CEA has several unique features. It is entirely electronic and uses no motor-generator equipment. The dc bias current is provided by a three-phase full-wave rectifier circuit using commercial ignitrons. This supplies all 48 magnets in series, with an output of 420 amp at 840 volts.

The ac circuit is essentially a self-excited class-C oscillator, operating at a resonant frequency of 60 cps and having a Q of over 100. This circuit involves energy storage inductors (air-gap) and capacitors, connected to separate magnets (in pairs) in such a way that there are 24 resonant subunits of the circuit. The electric circuit is shown in Fig. 15-15. The air-gap inductor has minimum excitation when the magnets are fully excited and stores the entire magnetic energy when the magnets are at zero excitation; the capacitors are arranged in banks to transfer energy from magnet to inductor and back and to provide 60-cycle resonance. To ensure that current in the magnet does not go negative, silicon rectifiers are inserted in series. These rectifiers provide zero current and zero rate of change of current at the start of each excitation cycle, to maintain uniformity from cycle to cycle at injection time. The ac component slightly exceeds the dc component of current, so a "back voltage" is developed across the rectifiers which is used in a feedback circuit to maintain the correct ratio of ac/dc currents from the two power supplies. This feature allows the use of commercial-grade regulation in the power supplies.

For reasons of economy the energy storage inductor is built as a toroidal ring of 12 cores and 12 air gaps, with 24 identical coils mounted on the cores to supply the 24 magnet power units. The ac component of current in the resonant circuit is provided by a pulser circuit supplying primary windings on the choke. This pulser consists of a multiphase rectifier, a storage capacitor, and a pulse-forming network utilizing igni-

trons as switching elements. It develops short pulses of power synchronized with the resonant frequency and timed by a trigger signal to occur during the decreasing-current portion of the magnet excitation cycle. The ac power losses involved in the magnets, inductors, and capacitors

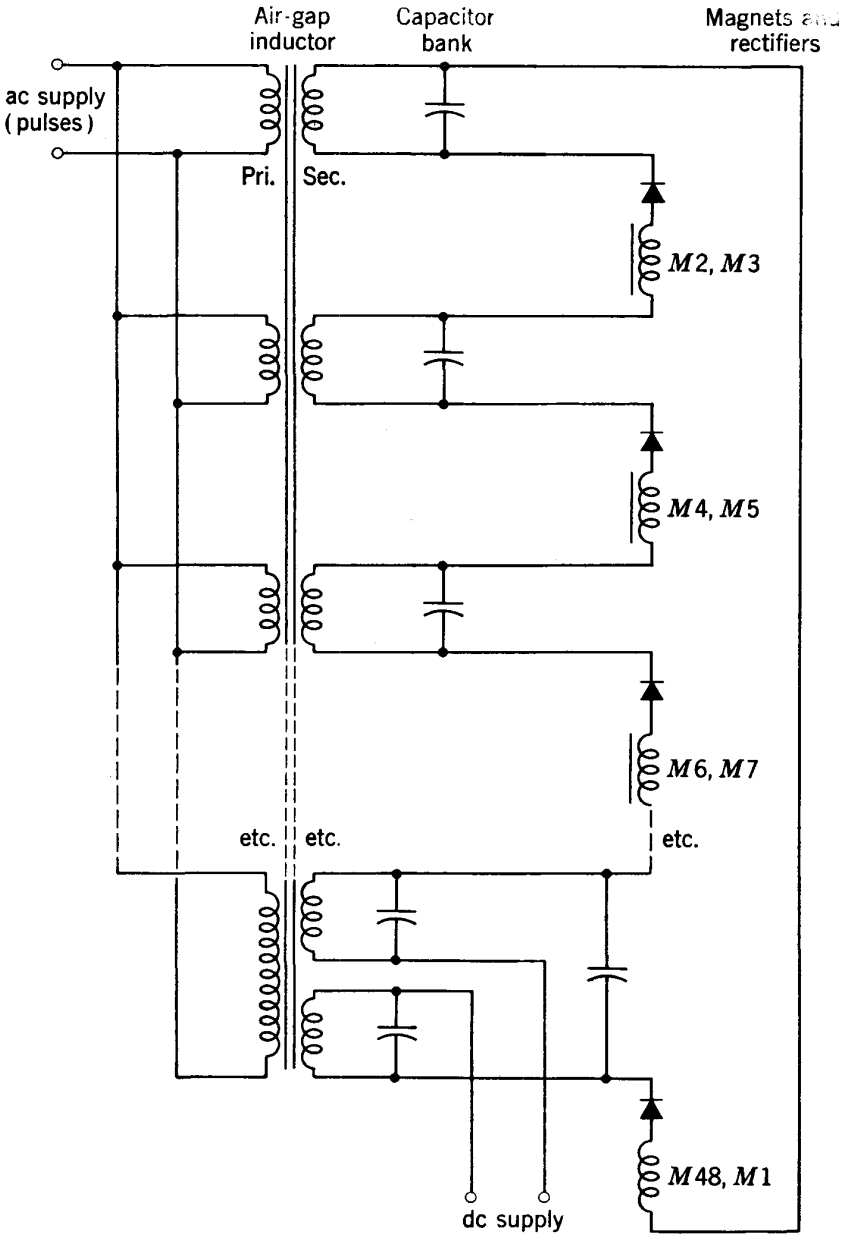

Fig. 15-15. Magnet power-supply circuit for the CEA synchrotron.

in the resonant circuit are about 700 kw. The total power losses are about 1100 kw.

The most important property of this power circuit is the uniformity of current in the 24 subunits of the power supply. The series connection requires that current be identical in each unit, to within the limit set by

leakage through insulation or variation in stray capacitance. Any variation in inductance or capacitance of the separate circuits results in a variation in the voltage across the unit, not in the current.

Injector

Electrons are preaccelerated to an energy of 25 Mev in a linear accelerator, directed tangentially toward the orbit from the outside, and are then inflected into the synchrotron orbit by a pulsed magnetic field located in one field-free space between magnets. The linac was constructed by Applied Radiation Corporation; it consists of two 10-ft sections of iris-loaded waveguide operating at a frequency of 2855 megacycles. It produces an output pulse of up to 200 ma of electrons at 25 Mev energy, in a pulse of about 0.7 μsec duration (sufficient to fill one turn in the orbit), within the energy spread and angular deviation required for injection.

The inflecting magnetic field, in the vertical direction, is located in one straight section and is developed by a shaped coil of conductors through which a pulse of current is sent from an auxiliary power supply. This power circuit is arranged to switch off the current (and inflecting field) in a time of about 0.1 μsec, which leaves most of the injected beam to circulate around the orbit. This modulation of the circulating beam by the switch-off interval of the inflector is a useful property for sensing current and location with pickup coils in the synchrotron orbit.

Radiation Loss

Radiation loss reaches a peak value of 4.5 Mev per turn at 6 Bev energy, following the relation given in Eq. (15-34). The radiation is emitted as discrete quanta distributed over a bremsstrahlung spectrum with a characteristic energy of 18 kv. The quantized emission causes momentum recoil of the electrons, which disturbs their orbits and excites certain modes of oscillation. On the other hand, the average loss of energy by radiation also provides damping for most of the modes of oscillation. This subject has been analyzed by Robinson[14] with special reference to the Cambridge accelerator conditions.

The emission of a quantum of radiation reduces the energy of the electron; this suddenly shifts the equilibrium orbit inward and initiates a radial betatron oscillation about the new equilibrium orbit. The rate of energy loss is greatest where radius of curvature is smallest, or at the location of the maximum outward amplitude in an existing betatron oscillation. This slight concentration also tends to increase the amplitude of the radial betatron oscillations. In addition, the change in energy disturbs the particle from synchronism and sets up synchronous phase oscillations about the equilibrium orbit. The effects due to individual quanta add with random phase to increase the amplitude of both phase and radial oscillations with time.

For radial betatron oscillations the net result is antidamping, or an exponential increase of amplitude with time, which could drive the electrons against the walls if it persisted. The choice of 60-cps excitation for the magnet reduces the time interval for radiation such that amplitudes will not exceed an estimated rms value of about 0.3 in. by the time they reach 6 Bev; this amplitude is acceptable within the aperture of the synchrotron. The synchronous oscillations are excited by radiation loss but also damped, so they approach an equilibrium distribution in which only a small fraction will exceed the allowable energy deviation determined by the peak radiofrequency accelerating potential. Vertical betatron oscillations are damped to small amplitudes and are not excited by radiation loss.

Radiofrequency

The radiofrequency accelerating system consists of a set of 16 high-Q resonant cavities, located in field-free gaps between magnets. They are tightly coupled by a circular ring of waveguide, fed through a radial waveguide from a power oscillator in the center of the ring, and operate as a single resonant circuit at a frequency of 475.8 megacycles. Each cavity consists of two half-wavelength resonators operating out of phase, with half-wavelength spacing between accelerating gaps; the double cavities are uniformly spaced around the ring with waveguide links which are electrically tuned to an odd half-integral number of wavelengths. Electrically, one may compare this system with a linear accelerator having 32 accelerating gaps spaced by one half-wavelength and operating in the resonant π mode.

The frequency is chosen to be a high integral harmonic (360th) of the orbital frequency (1.32 megacycles), primarily to reduce the amplitude of synchronous oscillations at injection, but also to give physical dimensions for the cavities which fit in the limited space between magnets and which have a high electrical efficiency. The frequency is also chosen to be the exact one-sixth subharmonic of the linac frequency; thus the linac can be synchronized with the rf system if desired. The physical structure is illustrated in Fig. 15-16. The two half-wave resonators are each partially loaded with reentrant drift tubes to reduce electron transit time and to provide a useful electric-field region slightly larger than the beam aperture. The two resonators are coupled by an inductive slot in the center wall, and each resonator has an inductive aperture on the side (top) surface for coupling to the waveguide with an alumina ceramic vacuum window closing the aperture. The separate components are overcoupled, which splits the mode separations sufficiently to allow each element to be tuned individually to resonance and ensures that the entire system operates in the chosen π mode. The measured Q of a prototype cavity unit is 25,000, and the shunt impedance is 7.0 megohms.

At the start of acceleration where $(dB/dt)_i$ is small, the peak rf voltage needed across each accelerating gap is about 20 kv, or about 0.6 Mv per turn. At the end of the cycle where radiation loss must be compensated, the requirement is about 200 kv per gap, or about 6 Mv per turn. The accelerated electrons, at an estimated maximum intensity of 10^{11} electrons per cycle, correspond to a circulating current of 20 ma. Peak power requirements for the system of 16 cavities and waveguide, including beam loading, are about 300 kw. Average power can be estimated from the expected schedule of rf voltage during the cycle to be about 60 kw. This

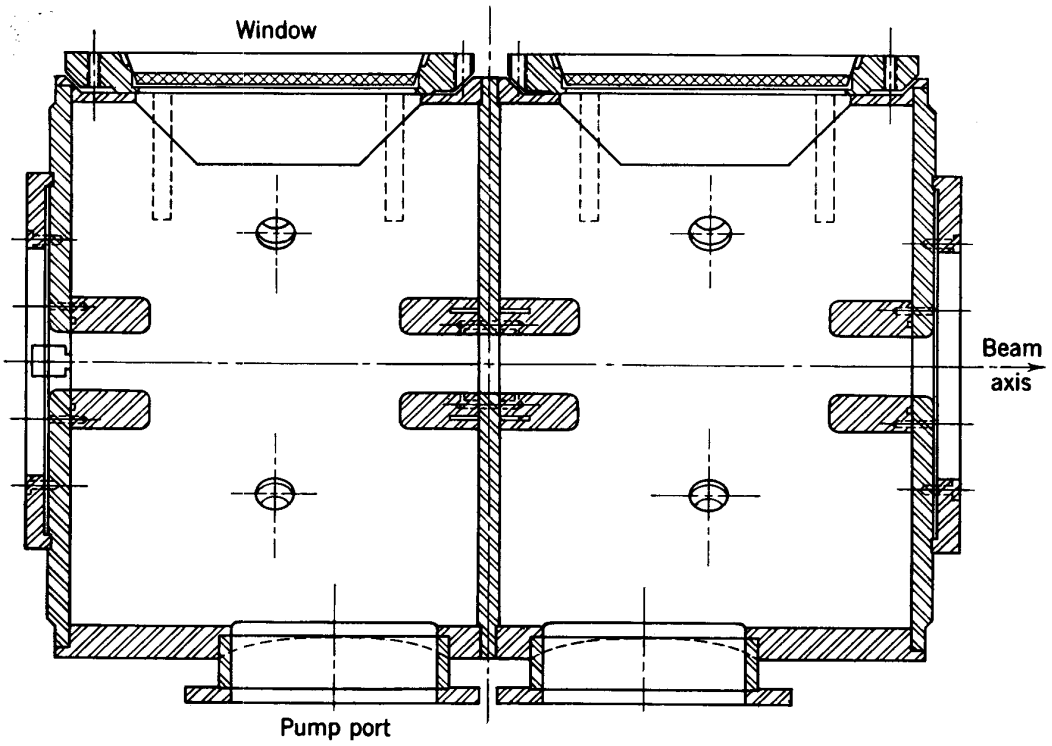

Fig. 15-16. Radiofrequency accelerating cavity for the CEA synchrotron.

power is supplied from an RCA superpower triode of the class A15040, which is the output tube in a power supply designed and constructed by RCA.

The effect of the circulating beam current on the rf system is most important when the rate of acceleration is small, just following injection. The circulating pulsed beam induces out-of-phase voltages on the cavities and will "pull" the phase of the resonant cavities away from the optimum synchronous phase angle. To compensate for this effect, the applied radiofrequency can be slightly mistuned from the resonant frequency, and the amplitude can be rapidly increased. It appears that beam loading will set an upper limit on the injected intensity of about 10^{11} electrons per pulse with the present radiofrequency system.

Vacuum System

The vacuum chamber fitting between magnet pole faces is formed of oval cross-section, stainless-steel tubing, deeply slotted transverse to the orbit to minimize eddy-current distortion of the field and covered with a layer of bias-wrapped glass cloth impregnated with an epoxy resin and baked to provide the vacuum surface. The narrow slots are spaced at ½-in. intervals, cut alternately from opposite sides, such that the stainless-steel chamber forms a continuous metallic circuit which can be electrically heated for vacuum bake-out. The metal wall will absorb the low-energy synchrotron radiation without structural damage; a glass or ceramic chamber would probably disintegrate under bombardment of this radiation, which has a power density estimated at 10 watts/cm^2 at the chamber wall. The chamber cross section is flat enough to allow the chamber to be assembled from the outside of the magnet ring through the pole-tip gap.

Straight sections between magnets are occupied by 16 radiofrequency cavities, 16 pickup coil housings, 1 inflector housing, and 15 other chambers for targets and beam-handling devices. Each of these 48 cavities has a vacuum-pump port and is evacuated by a high-voltage titanium-discharge pump (Drivac) manufactured by Consolidated Electrodynamics Corporation. Pump power supplies for the discharge pump are located in the central power building. Fore-vacuum pumps (Cenco #25 Hyvac) connected through liquid-air traps are used for initial evacuation; they are turned off—and sealed off by closing valves—when the titanium pumps come into operation.

The pumping speed of a Drivac is over 300 liters/sec. When tested on a radiofrequency cavity with full power, the observed pressure is less than 0.5×10^{-6} mm Hg. The average pressure in the vacuum chambers is expected to be below 1×10^{-6} mm, at which the gas-scattering losses should be negligible.

Targets and Beams

Targets can be mounted in six or eight straight-section cavities between magnets; from those targets gamma-ray and charged-particle beams will emerge in a tangential direction. Targets can be located at the edge of the beam aperture, where they will not intercept significant intensities at injection, and the high-energy beam will be contracted or expanded to strike the targets. One scheme for striking the targets is to distort the equilibrium orbit locally by pulsing auxiliary magnets located in other straight sections ahead of and behind the target location. Other schemes involve excitation of radial betatron oscillations. Gamma rays from such targets at the edge of the orbit are sharply collimated and can traverse small-diameter channels in a thick shield to emerge into a large

experimental hall. Charged particles can be analyzed for momentum in deflecting magnets and also directed through channels in the shield. Figure 15-17 shows the arrangement of target areas and shielding to provide emergent beams of radiation.

An emergent electron beam will be essential for some experiments. Such a beam can be extracted by use of a pulsed "current strip" at the edge of the aperture and parallel to the beam orbit. The pulsed magnetic

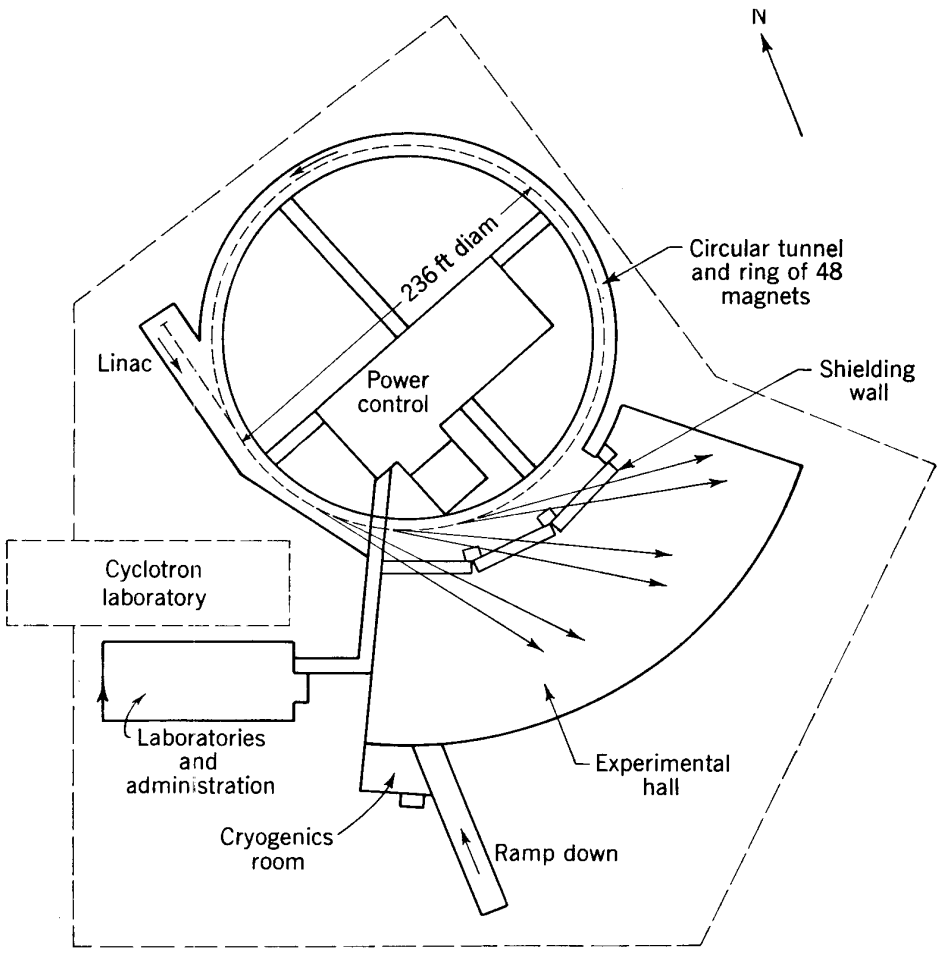

Fig. 15-17. Plan of the CEA synchrotron showing shielding and target areas.

field produced by this current strip will develop radial betatron oscillations, sufficient for a large fraction of the beam to "jump" the thin strip and be deflected out of the orbit.

Electronic control of the several orbit distorting devices will allow the beam to be directed alternately against different targets or out the emergent beam channel. When a full complement of beam-handling apparatus is developed, several experiments can be served simultaneously.

The maximum intensity anticipated with the Cambridge machine is about 10^{11} electrons/pulse, which at 60 cps is a time-average beam inten-

sity of about 1 μa or a beam power of 6 kw at 6 Bev. Control of the rate of orbit distortion should allow the beam to be ejected or directed against a target over a time interval of up to 1 msec; this represents a time duty cycle of the emergent beam of about 6 per cent of the total time, a feature which is highly desirable for experiments using electronic detection apparatus.

15-10. THE FIXED-FIELD ALTERNATING-GRADIENT PRINCIPLE

Shortly after the Brookhaven discovery of AG focusing in 1952 L. J. Haworth, director of the Brookhaven laboratory, realized that the strong momentum compaction in AG machines would make it possible to design an AG synchrotron with a magnet system whose field did not vary with time. He considered the case of a sequence of magnet sectors whose fields increase with radius but in which the polarity of the field alternates from one sector to the next. The particle beam is bent alternately inward and outward but will evidently travel on a closed orbit if the sectors which bend the beam outward are shorter or have weaker fields than the sectors which bend the beam inward. Although all fields increase outward, the gradients alternate because the field polarities are alternating. This idea was investigated by H. Snyder, who showed that the idea was sound but that the circumference of such a machine would be several times that of a more conventional AG synchrotron with a field that increases with time. The idea was not pursued further at that time and was not published. A year later the same idea was suggested by T. Ohkawa in Japan and by A. A. Kolomenskij, V. A. Petukhov, and M. S. Rabinovich in the U.S.S.R. (who called the machine a "ring phasotron"). Again the proposals did not receive general circulation. Finally in 1954 K. R. Symon, working in a group assembled to consider a high-energy accelerator for the American Middle West, reinvented the idea and was struck by a number of its advantages that previously had not been appreciated. The Midwest group plunged into an intensive study of FFAG (fixed-field alternating-gradient) accelerators and soon invented a number of interesting variants culminating in the so-called Mark V or "spiral-ridge" model, which was proposed by D. W. Kerst and which will be described later in this section.

True priority in this particular field of AG machines must be given to L. H. Thomas,[1] whose invention of an AG cyclotron in 1938 was so far ahead of its time that it attracted almost no attention. The consequences of FFAG advances on the cyclotron have been so important that they will be reserved for discussion in the next section.

Enormous numbers of internal reports on FFAG methods have been written in various laboratories, but probably the best references in this field are the Proceedings of the two CERN conferences in 1956[15] and

1959,[16] where the most important conclusions are presented by the various leading workers in the field.

In September of 1954 fourteen of the major universities and colleges in the Midwest formed the Midwestern Universities Research Association (MURA), whose primary function was to be the recommendation of a high-energy accelerator design to serve the physicists of the Midwest. The area covered centered roughly on Chicago, and MURA was incorporated in the state of Illinois. An enthusiastic and talented group was assembled, supported initially by finances contributed by the universities and later by Federal government agencies, and the FFAG principle was studied intensively. Initially the members worked in their own institutions, but by 1957 the group had been assembled in a rebuilt garage in Madison, Wisconsin; here models were assembled and operated, a digital computer was set into continuous operation, a large site was acquired and developed on the outskirts of Madison, and a series of conferences was held.

The enthusiasm and initiative of the MURA group constitute a phenomenon unique in accelerator history. Although its major proposals had not been accepted by 1961, it has made major contributions to accelerator theory and technique. The spiral-ridge cyclotron, a MURA sideline, has been widely studied, and several such cyclotrons are in construction or operating. Also the MURA group has been a major catalyst in the initiation of the Argonne 12.5-Bev ZGS project,[17] which is aimed at providing the Midwest with a high-energy machine at the earliest possible date.

The betatron field has also been profoundly affected by FFAG advances. The FFAG betatron, in which the guide field remains fixed in time, is capable of much higher intensity than the conventional betatron, and FFAG betatrons may well be serious competitors in the 10- to 100-Mev X-ray field where intensities of electron linear accelerators previously were unsurpassed.

Major advantages claimed for FFAG machines are as follows:

1. Since the magnetic field does not vary through remanent and saturation ranges, it can be set up and shimmed to any desired accuracy, as can the field in a cyclotron.
2. Eddy-current distortions of field are absent, and the magnet need not be laminated.
3. A metallic vacuum chamber can be used without field distortion.
4. Switchgear for pulsing high inductive voltage drops and intermittent forces on magnet coils are avoided.
5. The frequency modulation in the rf accelerating field is less critical.
6. High intensity can be attained by frequent repetition of the rf cycle.
7. Accelerated beams can be "stacked" in a circulating beam whose intensity can be built up to such high levels that it becomes possible to

think of collisions between particle beams circulating in opposite directions. Stacking at intermediate energies can permit acceleration at high repetition rate without the use of high rf voltages, because particles can be carried away from the injector at a rapid rate, stacked, and then carried the rest of the way at a lower rate. A third advantage of stacking lies in the increased flexibility in duty factor that becomes possible when the beam is stacked at maximum energy.

The MURA studies have shown that these advantages are offset by some serious difficulties, chief among which are those associated with the design of the large and complicated magnet structure that is necessary.

Of the several MURA schemes for utilizing the FFAG principle, two have emerged as most interesting—the so-called Mark I or radial-sector machine and the Mark V or spiral-sector accelerator. These will be presented in somewhat more detail.

The Radial-sector FFAG Accelerator

This is the machine independently proposed by Haworth, Ohkawa, Kolomenskij et al., and by Symon. Its general configuration is illus-

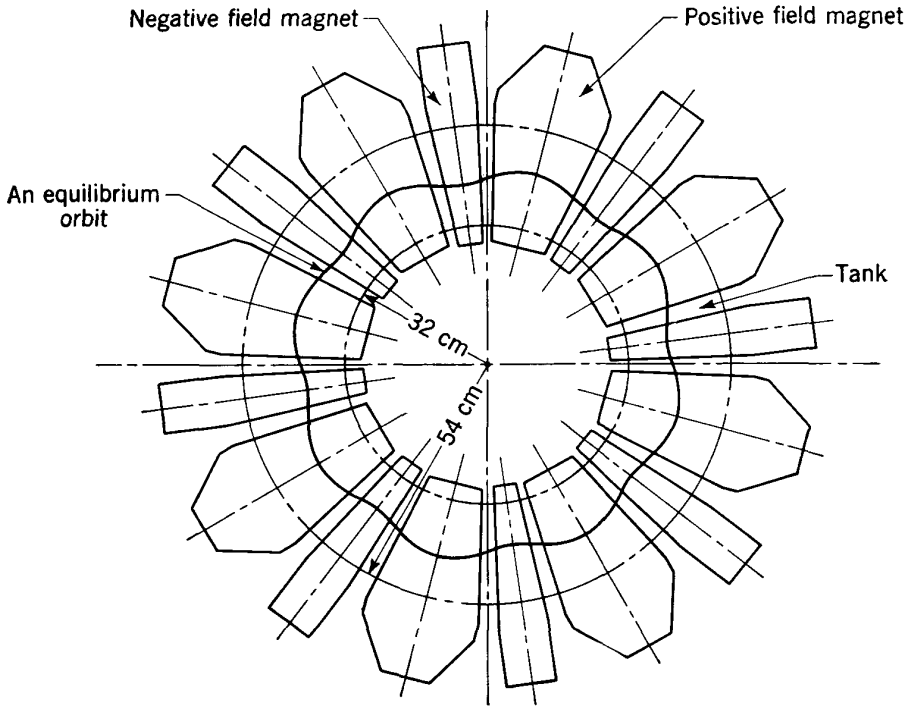

Fig. 15-18. Radial-sector FFAG accelerator. This configuration was used in the first MURA electron model.

trated in Fig. 15-18. On the median plane the magnetic field has only a z component, which can be written

$$B_z = B_0 \left(\frac{r}{r_0}\right)^k f(\theta) \tag{15-36}$$

where B_0 is the field at some arbitrary radius r_0 and at a point where $f(\theta)$ has the value unity, and $f(\theta)$, the azimuthal dependence of field, can be written as a Fourier series thus:

$$f(\theta) = \sum_n (g_n \cos nN\theta + f_n \sin nN\theta) \tag{15-37}$$

Here N represents the total number of identical sectors, each including a focusing and a defocusing magnet unit. Two more quantities must now be defined: the "flutter factor" F, which is a measure of the spatially varying part of the field, is defined by

$$F^2 = \sum_{n=1}^{\infty} (g_n^2 + f_n^2) \tag{15-38}$$

and G, a quantity important in deriving the free or betatron oscillation frequencies, is defined by

$$G^2 = \sum_{n=1}^{\infty} \frac{g_n^2 + f_n^2}{2n^2N^2} \tag{15-39}$$

Typical values of F and G for field patterns useful in radial-sector machines are given in the caption of Fig. 15-19. For field patterns in

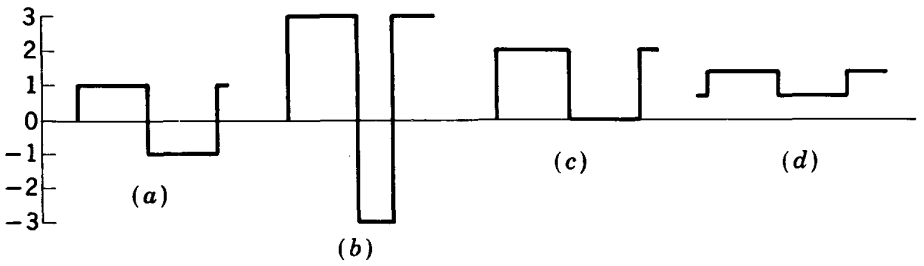

Fig. 15-19. Azimuthal field distributions possible in FFAG accelerators. (*a*) Sectors of equal length. Here $g_0 = 0$, $F = 1.4x$, $G = 0.9x/N$. (*b*) Positive curvature sector twice as long as negative curvature sector. Here $g_0 = 1$, $F = 4.0$, $G = 2.4/N$. (*c*) Sectors alternating with field-free regions of equal length. Here $g_0 = 1$, $F = 1.4$, $G = 0.9/N$. (*d*) Sectors alternating with regions of half-field strength. Here $g_0 = 1$, $F = 0.27$, $G = 0.15/N$.

which the magnet sectors are of unequal lengths and hence have g_0 not equal to zero, it is customary to normalize by choosing B_0 such that $g_0 = 1$. In these cases F will be of the order of 4 and G will be of the order of $3/N$.

Analysis of FFAG orbits is so complex that smooth approximations generally fail to give accurate results. Approximate methods are used only as a guide in preliminary design. From this point on it is necessary to make numerical computations of such complexity that a digital com-

puter is essential. It is significant that one of the first acquisitions of the MURA group was an IBM 704 computer.

Orbit characteristics are derived in two stages. First, the wavy equilibrium orbit through the alternating fields must be derived. Then it is possible to compute the free or betatron oscillations around this orbit. For the details of this analysis the reader is referred to the paper of Symon et al.[18]

From the smooth approximation the free-oscillation frequencies or, more precisely, the number of oscillation waves per revolution are given by

$$\begin{aligned} \nu_r^2 &\cong 1 + k + k^2G^2 \\ \nu_z^2 &\cong -k + k^2G^2 + \frac{F^2}{2} \end{aligned} \tag{15-40}$$

The magnet for a radial-sector FFAG machine must be designed to provide sufficient radial aperture for the whole energy range from injection to full energy and sufficient vertical aperture to accommodate the

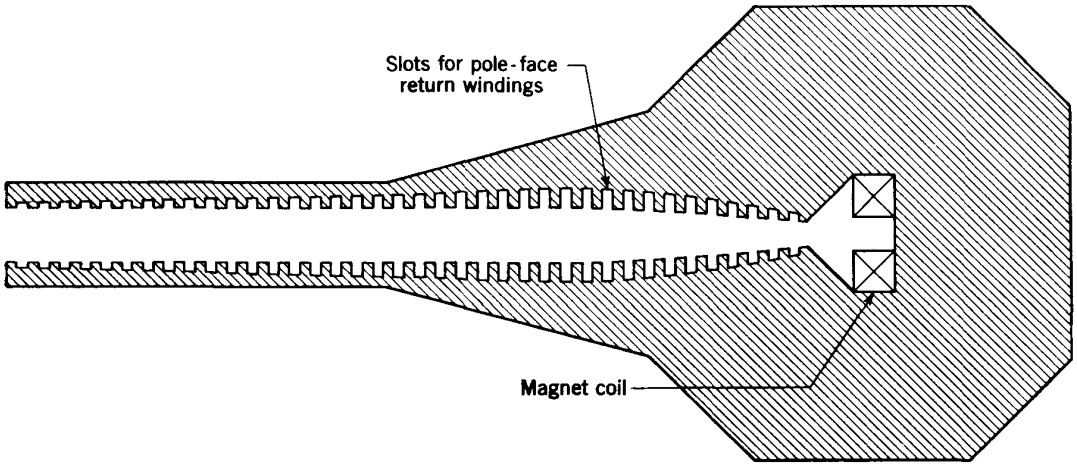

Fig. 15-20. Cross section through magnet for radial-sector FFAG accelerator.

large vertical oscillations at injection and the somewhat damped vertical oscillations at full energy. In cross section this magnet has the configuration illustrated by Fig. 15-20.

The circumference of a radial-sector FFAG synchrotron will be of the order of six times that of a conventional AG synchrotron without straight sections. When this factor is included in design, the mass of the magnet for an FFAG synchrotron becomes much larger than that of a conventional AG synchrotron.

Resonances in FFAG machines are just as important as those in conventional synchrotrons and are generally avoided by designing for "scaling" orbits—the field pattern is such that the betatron frequencies are the same at all radii. Recently the MURA group has shown that

some economies are possible in nonscaling machines, but in this case analysis becomes even more complicated.

A small radial-sector FFAG electron synchrotron was built by the MURA group at the University of Michigan and later moved to the MURA laboratory in Madison, Wisconsin. This model, designed for electron acceleration to 400 kev, was brought into operation in 1956.[19] Its general configuration was that of Fig. 15-18. Table 15-1 summarizes its major parameters. The performance of the MURA model was entirely satisfactory; it came into operation immediately, with very little initial adjustment, and was used for numerous studies of resonances and effects of misalignments of magnet sectors. In all cases the results were in agreement with the theoretical predictions.

TABLE 15-1
PARAMETERS FOR RADIAL-SECTOR FFAG SYNCHROTRONS

	MURA 400-kev electron model	Possible 10-Bev proton synchrotron
Number of magnet pairs N	8	64
k	3.36	192.5
Ratio of length of orbit in positive-curvature magnets to length of orbit in negative-curvature magnets	2.5 approx.	1.6 approx.
Injection energy	25 kev	5 Mev
Injection radius	34 cm	95 m
Final radius	50 cm	97.3 m
Aperture at injection	4 cm	30 cm
Aperture at full energy	2.4 cm	6 cm
ν_r	2.8	21.7
ν_z	2.1	3.9

Table 15-1 also includes a list of parameters for a possible 10-Bev radial-sector FFAG proton synchrotron. Several salient features emerge from this table and from the magnet design of Fig. 15-20. First, the magnet is enormous; its radial aperture is 2.3 m, and its total weight will be of the order of 15,000 tons or more. Its structure is complicated and presents severe mechanical problems. Since tolerances are tight as in the conventional AG synchrotron, the magnet pole faces must be restrained to a positional precision of the order of 0.2 mm, a severe problem in the extensive and weak magnet structure illustrated. On the other hand, a rapid repetition rate for acceleration to top energy makes possible in this machine a beam intensity of the order of 10^{14} protons/sec. This intensity is higher by a factor of 100 than that of any other proton accelerator in this energy range. The associated rf problems are not severe; they will be discussed later in this section.

The Spiral-sector FFAG Accelerator

This ingenious device is, perhaps, MURA's major contribution to the accelerator art. As described by Kerst (its inventor) and shown in Fig. 15-21, the device provides AG focusing either by spiral magnet sectors or by inclusion on the pole faces of spiral ridges to give regions of increased field over a spiraling configuration. To the novice the action of this configuration will be relatively incomprehensible except in terms of the mathematical results. The MURA group considers the spiral-ridge structure to be a case of alternating edge-focusing effects (see Sec. 5-6). The focusing mechanism will receive more detailed consideration in the next section, where it again appears in the sector-focused cyclotron. Primarily because the field need not reverse, this design results in an FFAG configuration much more economical than the radial-sector system.

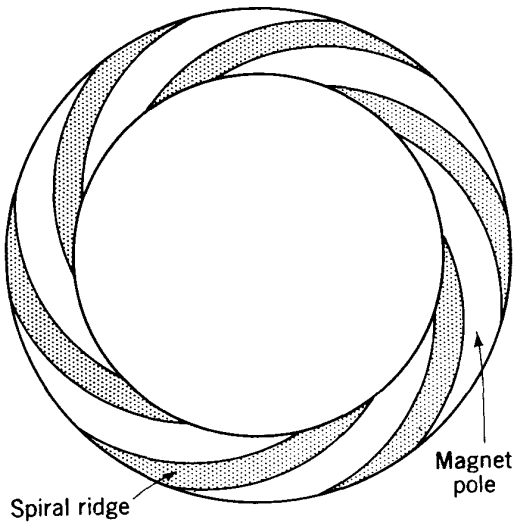

Fig. 15-21. Magnet configuration for a spiral-sector FFAG accelerator.

In this case, on the median plane the magnetic field has only the z component

$$B_z = B_0 \left(\frac{r}{r_0}\right)^k \sum_n (g_n \cos n\phi + f_n \sin n\phi) \tag{15-41}$$

where

$$\phi = K \ln \frac{r}{r_0} - N\theta$$

Aside from the term $K \ln (r/r_0)$, the field pattern is the same as that in the radial-sector machine. This is the term that gives the field its spiraling characteristic; the logarithmic form is such as to ensure scaling or constancy of betatron frequency with radius. K is related to the angle γ at which field spirals cut radial lines by

$$K = N \tan \gamma \tag{15-42}$$

Again the flutter factor F and the parameter G are defined as in Eqs. (15-38) and (15-39). In this case, however, the field does not reverse, and F and G have lower values than in the radial-sector case. Here F usually lies between 0.2 and 1.5 and G lies between $0.2/N$ and $1/N$.

Free-oscillation frequencies in the spiral-sector FFAG synchrotron are given by the smooth approximation

$$\nu_r^2 \cong 1 + k + k^2G^2 \tag{15-43a}$$

as in the radial-sector machine, and

$$\nu_z^2 \cong -k + k^2G^2 + F^2\left(\frac{K^2}{N^2} + \frac{1}{2}\right) \qquad (15\text{-}43b)$$

Since the field need not reverse in this design, the circumference factor can be reduced as low as 2. Orbit compaction is not so strong as in the radial-sector machine, however, and a larger radial aperture is required. The magnet weight for a spiral-sector machine can be about half that for a radial-sector machine. But this is still about ten times greater than the weight of a corresponding conventional AG synchrotron.

A spiral-sector FFAG electron synchrotron for about 120 kev final energy was built by the MURA group as a model on which to study orbits. This model was constructed at the University of Illinois and assembled at the MURA laboratory in Madison. Like the radial-sector model, it worked immediately and gave results in good agreement with the predictions.[20] The parameters of this model are collected in Table 15-2. Also included in this table are parameters for a possible spiral-sector 10-Bev proton accelerator.

TABLE 15-2
PARAMETERS FOR SPIRAL-SECTOR FFAG SYNCHROTRONS

	MURA 120-kev electron model	Possible 10-Bev proton synchrotron
Number of spiral sectors N	6	30
Angle of spiral with radius vector $[\tan^{-1}(K/N)]$	46°	84.3°
k	0.70	53
K	6.25	300
Injection energy	35 kev	50 Mev
Injection radius	31 cm	46 m
Final radius	52 cm	50 m
Final vertical aperture	3.8 cm	15 cm
ν_r	1.40	8.4
ν_z	1.12	7.2

It will be noted that the high-energy machine has a much larger spiral angle; the spiral is approaching much more closely to a circle. Whereas in the MURA model it was easy to make each spiral sector a separately excited magnet, for the high-energy machine it is much simpler to make the spiral sectors mere ridges on the pole face of one large magnet.

Colliding Beams and the Two-way ("Synchroclash") FFAG Accelerator

When the possibilty of beam stacking in FFAG machines was realized and analysis led to the conclusion that circulating beams of 10 to 100 amp

were quite possible, the MURA group began to think actively of the possibility of experiments involving colliding beams. At relativistic energies the kinetic energy available for nuclear reactions is disappointingly small when the target particle is at rest in the laboratory system. For proton-proton collisions the kinetic energy available is given by the expression

$$W_0\left[\left(2+\frac{2W}{W_0}\right)^{1/2}-2\right] \tag{15-44}$$

where W is the total proton energy and W_0 is its rest energy of 938 Mev. The following table indicates the result:

Energy of accelerated proton, Bev	*Kinetic energy available, Bev*
6.2	2
25	5.2
100	12
540	30

With these figures in mind the MURA group reasoned that it could make two 15-Bev FFAG accelerators and study reactions in the center-of-mass system where all the energy is available; this double machine would be equivalent, in terms of nuclear reactions possible, to a single machine of 540 Bev! With the possible circulating currents there should be about 10^7 collisions per meter of beam path; this would mean about 100 resulting particles per square centimeter per second at a distance of 1 m. Although the problems of direct observation of collisions would be formidable, this seemed sufficiently promising to merit further study. A detailed design study of the double clashing-beam accelerator using the spiral-sector design was completed in 1956. In the same year, however, T. Ohkawa[21] realized that the radial-sector FFAG design would work even if the length of the orbit in the positive-curvature magnets were made the same as the orbit length in the negative-curvature magnets. In this case identical radial sectors would alternate in polarity, and it should no longer matter in which sense the beam circulates. Consequently, beams could be made to circulate simultaneously in both directions, and beam collisions could be observed at a number of orbit intersections around the machine. Ohkawa showed also that spiral sectors can be used in a two-way machine.

Beam dynamics in the two-way radial-sector machine differ somewhat in characteristics from those found in radial-sector machines, where positive-curvature magnet sectors are longer than negative-curvature sectors. From the smooth approximation the betatron-oscillation frequencies are given by

$$\begin{aligned}\nu_r^2 &\cong 2k\\ \nu_z^2 &\cong \frac{F^2}{kG^2}\end{aligned} \tag{15-45}$$

The fact that g_0 for the two-way machine is zero and hence F and G cannot be normalized as before is rendered unimportant since only the ratio F/G appears in these equations.

The two-way radial-sector machine was now studied by the MURA group, and a possible 15-Bev design was completed. Simultaneously a 40-Mev two-way electron model was initiated;[22] it was completed early in 1960 and tested successfully. Parameters of the model and of the proposed 15-Bev proton accelerator are collected in Table 15-3.

TABLE 15-3
PARAMETERS FOR TWO-WAY FFAG SYNCHROTRONS

	MURA 40-Mev electron model	Possible 15-Bev proton synchrotron
Number of magnet pairs N	16	66
k	9.3	212
Injection energy	100 kev	50 Mev
Injection radius	124 cm	175 m
Final radius	198 cm	180 m
Vertical aperture at injection	7 cm	35 cm
Final vertical aperture	5 cm	15 cm
Circumference factor	8.0	5.8
ν_r	6.36	24.75
ν_z	5.34	4.30
Weight of magnet steel	32 tons	62,500 tons
Weight of copper in magnet coil	7 tons	3,000 tons

Detailed study of the two-way 15-Bev design led to some sobering conclusions. High-energy physicists were dubious about the possibilities of studying nuclear reactions in the inaccessible colliding-beam region. Unless the pressure in the vacuum chamber was kept to the order of 10^{-9} mm Hg, the colliding-beam reaction products would be obscured by a tremendous background because of collisions with residual gas nuclei. Finally, the cost of the machine proved to be astronomical. For these reasons, in 1960 it appeared improbable that colliding beams would receive very immediate consideration. In any case it appeared that colliding beams, if ever studied, would be produced by one accelerator and two storage rings, using the method discussed in the last section of this chapter.

RF Acceleration in FFAG Synchrotrons

The fact that stable orbits for all energies between injection and final exist continually in FFAG accelerators leads to several rather surprising conclusions with respect to methods of acceleration. It is, of course, quite possible to accelerate with a frequency modulated from initial to

final revolution frequency or a harmonic thereof just as in a conventional synchrotron. A transition energy exists in FFAG machines just as in other AG machines. Its value W_t is given by

$$W_t^2 = (k + 1)W_0^2 \tag{15-46}$$

This transition energy can be passed by making the appropriate shift in rf phase, as has been done with the CERN PS and the Brookhaven AGS.

The first point of difference with conventional practice lies in the fact that, while a frequency that is a harmonic of the revolution frequency carries the beam to high energy, it may also pick up injected particles on a different subharmonic and accelerate them to some intermediate energy. While the primary region of phase stability (cf. Fig. 9-3) is sweeping up in energy and carrying its content of particles with it, other regions of stability with different harmonic relations to the revolution frequency also are sweeping up in energy. As an example, suppose that protons are injected at one-eighth of the velocity of light (about 7.5 Mev) and are accelerated into the 10-Bev region, or virtually to the velocity of light. Suppose, further, that the accelerating frequency is the second harmonic of the revolution frequency. As the frequency increases to 1.5 times its initial value, it matches the third harmonic of the injection frequency; particles picked up on this harmonic will be accelerated to two-thirds of the final design velocity or to about $\frac{1}{3}$ Bev. When the frequency reaches twice its initial value, fourth-harmonic acceleration becomes possible with a final velocity of half the design velocity, here corresponding to about 200 Mev, etc. When the second harmonic has deposited its protons at the final radius and the rf is turned off, the groups accelerated on other harmonics will be left circulating at their respective radii until picked up by another rf signal or until eventually they are lost by scattering by the residual gas.

In the vocabulary of the MURA group (now generally accepted) the regions of stability are known as "buckets" taking part in a "bucket lift" carrying the particles to higher energies. Even more buckets can be added by simultaneous application of other frequency-modulated signals. The MURA group has shown, moreover, that successive buckets can be brought to full energy and dumped at the final radius to give a beam circulating at full energy and continually increasing in intensity until limited by the requirements of Liouville's theorem. This limit does not appear to set in until circulating currents of the order of 10 to 100 amp have been established.

One of the most disconcerting concepts of the FFAG acceleration picture follows from the conclusion from Liouville's theorem (cf. Sec. 5-8) that the phase space, of which the buckets are a part, is incompressible. Hence while the buckets are rising in energy carrying their particles with

them, particles that do not lie in the buckets must be forced down in energy. Conversely, if the buckets are pushed downward, the remainder of the phase space is pushed upward. In other words, if the frequency is modulated downward, particles not in phase-stable regions will be accelerated. From the MURA experiments this indeed appears to be the case.

Another intriguing idea in a fixed-field machine is that of "stochastic acceleration." This is one of the few concepts in this field not due to MURA; it was originally proposed in the U.S.S.R. by Burshtein, Veksler, and Kolomenskij[23] and tested on a small cyclotron by Keller, Dick, and Fidecaro[24] of CERN. These authors claim that, since all orbits exist simultaneously in an FFAG accelerator, it is necessary only to modulate the accelerating frequency at random, and sooner or later some particles will be accelerated. Other particles will be returned to the injector, but it seems reasonable to expect that this will be only about half of the injected particles. Indeed the frequency of the accelerating signal need not be distinguishable; the accelerating signal can be random noise. The CERN experimental results bear out these conclusions.

It is possible that these novelties will prove to be important. In 1961 this does not appear probable.

Some technical difficulties arise in connection with rf acceleration in FFAG accelerators, partly because of the difficulties of introducing field-free sectors and partly because of the large radial aperture. In the radial-sector machine, field-free sections are rather easily introduced, but in spiral-sector machines, introduction of radial straight sections requires redesign of the magnet structure, although it appears to be quite practicable. The large radial aperture makes for difficulty in construction of an accelerating system which can be modulated over a wide frequency range and which, simultaneously, is economical of power. The latter fact becomes important if rapid frequency modulation is required to produce high average beam intensity. The difficulty is associated with the large gap capacity that goes with large aperture and with the long path for magnetic flux linking the whole aperture. Saturating dielectric or ferromagnetic materials suitable for wide-range tuning under these conditions will perforce introduce large losses that will rise very rapidly as the rate of acceleration is increased. It is to be hoped that this problem, like so many others, will be solved by the inventive ingenuity of the MURA group.

15-11. SECTOR-FOCUSED CYCLOTRONS

The first proposal for a sector-focused cyclotron was made by Thomas[1] in 1938. This came at a time when early cyclotron designers were concerned with the maximum energy limitation at about 25 Mev imposed by the relativistic increase in mass of the accelerated particles. To maintain

resonance with the fixed-frequency accelerating electric field provided by the D's, as particle mass increases, the magnetic field should increase at large orbit radii. However, this requirement conflicts with the radially decreasing field needed to maintain axial stability of particle orbits. Thomas proposed the use of alternately high and low regions of magnetic field around the orbit, such as could be obtained with radial sectors of iron fastened to the pole faces to give alternately short and long gap lengths. The average field around an orbit could then increase at large radii to maintain resonance. Thomas showed that an orbiting particle in this azimuthally varying magnetic field would experience axial restoring forces which would provide the desired orbit stability.

This proposal of an azimuthally varying field (AVF) was recognized as being theoretically sound, but the computations were complex as compared with the simple relations then in use by cyclotron designers. The theory of particle orbits in magnetic fields was in its infancy, and Thomas's scheme was so far in advance of the general understanding by practitioners of the art that its virtues were not immediately accepted and put into practice. Furthermore, the cyclotron was in an early stage of development, and many practical problems of engineering development took precedence. As a result, the idea lay fallow for many years.

When the principle of synchronous acceleration was announced in 1946 and the use of frequency modulation and pulsed operation was proposed to overcome the relativistic limitation, it led to the speedy development of the synchrocyclotron and the construction of a sequence of machines of higher and higher energy. The only apparent restriction on energy was that of size and cost. Accelerator designers concentrated their efforts on such synchronous machines, and the low beam intensities which came as a consequence of pulsed operation were at that time considered acceptable.

It was not until 1949, when orbit theory was greatly advanced, that the AVF concept was revived under the stimulus of potential applications to national defense which required high beam intensities. Studies were started in 1949 at the University of California under security restrictions and became known to other laboratories only after declassification in 1955. The present sector-focused cyclotrons at the Livermore laboratory are a direct outgrowth of these studies. During this period two electron models were built at the University of California Radiation Laboratory to test the focusing principle, reported much later (1956) by Kelly, Pyle, Thornton, Richardson, and Wright.[25] Work also started in the early 1950s at the Oak Ridge National Laboratory, under the direction of R. S. Livingston and following the theoretical analyses of T. Welton.

Meanwhile, the discovery of the AG focusing principle led to the FFAG ideas discussed in the preceding section. The MURA group showed the advantages of spiral ridges on cyclotron pole faces over the radial sectors proposed by Thomas.

By the time these two lines of development merged, it became evident that Thomas's proposal of sector focusing was a special case of the general theory of AG focusing as applied to constant magnetic fields. The final result has been the development of a whole family of cyclotrons—"isochronous," or sector-focused, or AVF—some using radial and some spiral alternations in field. The common characteristic of all such machines is the use of fixed frequency for acceleration, which results in the large duty cycle and the high beam intensities characteristic of the standard cyclotron. The time-average beam current is about 100 times higher than for synchrocyclotrons, which accelerate pulsed beams by the use of frequency modulation.

The emphasis in the development of sector-focused machines has been on high beam intensity and on obtaining variable output energy. This latter feature can be obtained by using sector-shaped coils to control the magnitude of the azimuthal variation and circular coils of different radii on the pole faces to control the radial increase of average field. These coils maintain the field pattern as the main field is varied. Such coils can be powered to provide the necessary focusing fields for any chosen output energy, when combined with radiofrequency circuits which can be tuned over a suitable range in frequency. This technique solves a problem which has long been a handicap to research scientists using standard cyclotrons. The variable frequency and field property can also be used to provide the correct focusing fields for the acceleration of a variety of ions, such as H^1, D^1, H_2, D_2, He^3, or He^4.

The first practical cyclotron embodying these principles was the 42-in. standard cyclotron at Los Alamos, which was rebuilt by Boyer in 1954, using radial sectors and coils and with a variable-frequency oscillator. It has been highly successful in providing variable output energy and has been used for the acceleration of several types of ions.

A conference on sector-focused cyclotrons was held at Sea Island, Georgia, on February 2–4, 1959, at which most of the United States experts in this field were present. The published report[26] of the papers presented gives a full description of the status of the field at that date. A tabulation in an appendix to this report lists 15 sector-focused cyclotrons in various stages of design and construction; only two machines were in operation at that date, at Los Alamos and Delft, Holland, producing 16- and 12-Mev deuterons, respectively. By 1961, several machines in the 50- to 75-Mev proton energy range were approaching completion, at the University of California at Los Angeles, Oak Ridge National Laboratory, and the University of Colorado. Studies are in process for still higher energies at several laboratories; the largest is for 850 Mev, at Oak Ridge.

An AVF magnet has three or more (N) high-field regions (hills) and a corresponding number of lower-field regions (valleys) symmetrically located in azimuth. The average field around any orbit increases with

radius at the calculated rate to match the increase in particle momentum and to maintain constant orbital frequency. This oscillation in flux density on the median plane distorts the particle orbit from a circle into a curved polygon, illustrated in an exaggerated form in Fig. 15-22. Orbit-stability calculations are based on the fields encountered around such a

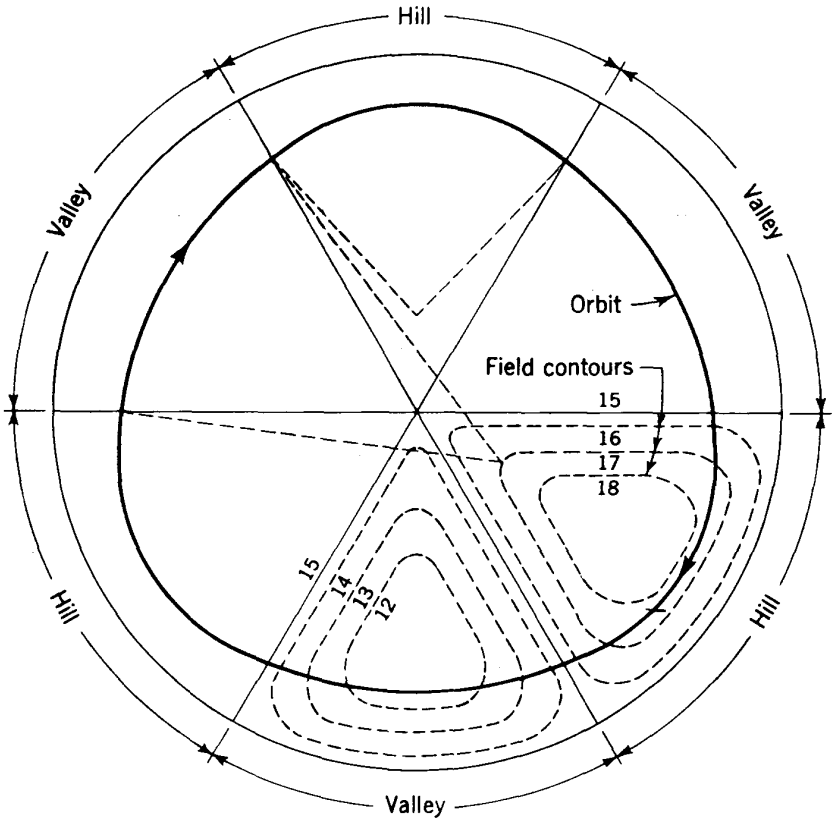

Fig. 15-22. Curved polygon orbit in a three-sector AVF cyclotron

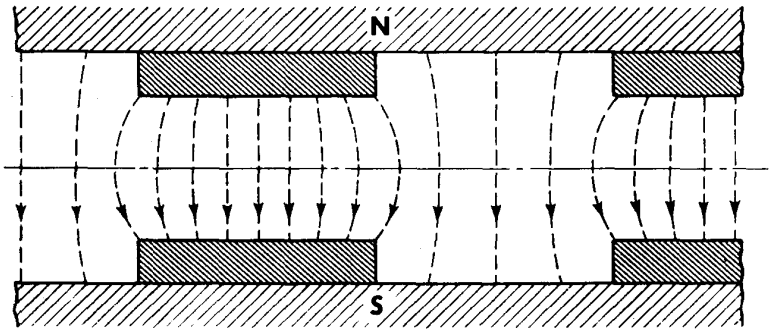

Fig. 15-23. "Unrolled" pole-face contour and flux pattern in an AVF cyclotron.

noncircular orbit and include a radial component of momentum mv_r. The field pattern off the median plane is also distorted from the parallel shape obtained in a uniform-field magnet. If the pole-face contour and flux-line pattern around an orbit were to be "unrolled" into a plane, it would appear similar to that illustrated in Fig. 15-23. The curvature of flux

lines produces azimuthal components of field B_θ at locations off the median plane.

The "Thomas" force F_z, which provides vertical stability in this field, is due to the interaction of the radial component of momentum mv_r with the azimuthal component of field B_θ. The direction of this force alternates as the particle moves around the orbit, from convergence to divergence about the median plane. This rapid alternation of focusing and defocusing forces provides the same type of stability which is characteristic of the forces in AG focusing, resulting in a net convergence. The mathematical analysis of the motion follows in a manner parallel to that discussed in Sec. 15-10. In general, this net focusing about the median plane must be large enough to more than compensate for the axially defocusing effect of the radially increasing average field.

Two additional axial restoring forces arise from the field pattern produced by a spiral-shaped azimuthal variation. The spiral shape can be defined by the angle γ between the direction of the spiral ridge and the radius vector; in a spiral this angle will increase with increasing radius. Because of this angle there will be a radial component of field B_r at points off the median plane, which will be directed alternately inward and outward as the particle crosses the boundaries of the hills and valleys. The azimuthal momentum of the particle mv_θ interacts with this radial field B_r to produce an alternating force in the axial direction, similar to and in addition to the Thomas force.

A second and different axial force due to the spiral pattern comes from an imbalance in the magnitudes of the axial forces at the boundaries of hills and valleys; these are not exactly equal, but the convergent forces are slightly larger. This can be understood by considering the noncircular shape of the orbit which results in the orbit's making a small angle δ (the Thomas angle) with a true concentric circle at these boundaries. The geometry can be visualized by reference to the sketch in Fig. 15-22. The Thomas angle is outward when the particle crosses the boundary between valley and hill and inward when it crosses the boundary between hill and valley. The particle spends a longer time going through the axially focusing region in the latter case than it does in traversing the defocusing region. Since the convergent force acts over a longer time interval, the result is a net convergence.

Each of the forces discussed above enters as a separate term in the equations of motion. The sum of the Thomas force and the two forces due to the spiral shape opposes the defocusing action of the radially increasing magnetic field. The problem in design is to balance the opposing terms, each of which is quite large, to obtain a net focusing action which is relatively small but sufficient to maintain axial stability.

If the field in a conventional cyclotron were to increase with radius at such a rate as to keep the frequency of revolution of the circulating par-

ticles constant, its radial dependence would follow from the fundamental relations

$$\frac{v}{c} = \frac{Be}{m} = \frac{Be}{m_0}\left(1 - \frac{v^2}{c^2}\right)^{1/2} = \text{const}$$

whence

$$B = B_0\left[1 - \left(\frac{B_0 er}{m_0 c}\right)^2\right]^{-1/2} \tag{15-47}$$

where B_0 is the field at zero radius.

If we define a field index k, as in the preceding section, to represent

$$\frac{r}{B}\frac{dB}{dr}$$

we obtain from Eq. (15-46)

$$k = \left[\left(\frac{m_0 c}{B_0 er}\right)^2 - 1\right]^{-1} = \left(\frac{c^2}{v^2} - 1\right)^{-1} \tag{15-48}$$

Evidently k cannot be kept constant with radius as in the spiral-sector FFAG machines, but will change from a very small value near the center of the machine through 0.2 at a radius where protons of 100 Mev would

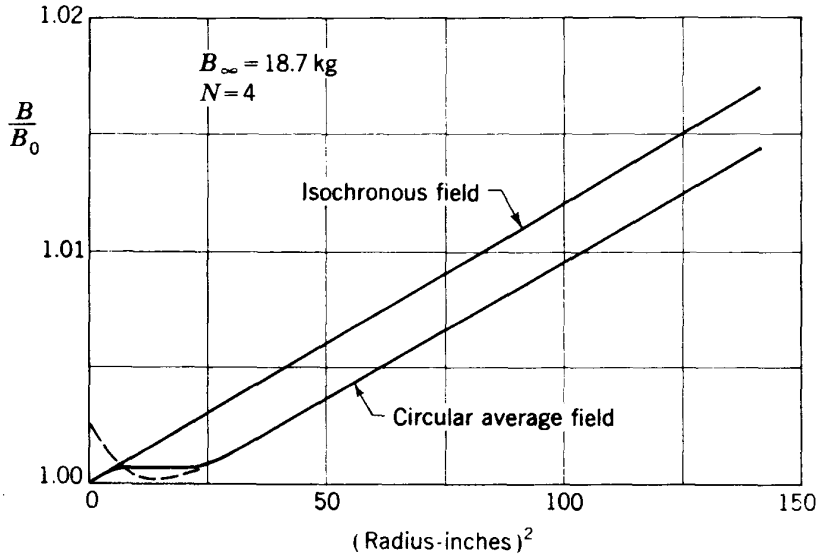

Fig. 15-24. Plots of magnetic field B and average field $\bar{B}$ for the 50-Mev AVF cyclotron at the University of California at Los Angeles.

circulate to very high values as v approaches c. This will result in a variation with radius of the frequency of radial oscillation—the machine cannot be a scaling accelerator in the language of MURA.

Inclusion of spiral ridges will compensate for the vertical defocusing in a field of the type described by Eq. (15-47), but the azimuthally averaged field must have the same general character as given by Eq. (15-47).

The radial and vertical oscillation frequencies will be given approxi-

mately by Eqs. (15-43), with the flutter factor F and the parameter G defined as before by Eqs. (15-38) and (15-39).

Ratios of maximum field under a ridge to minimum field between ridges have been chosen in various designs with values ranging from 1.3 to 3, giving flutter factors F ranging from about 0.2 to about 1. Near the center of the magnet, where the ridges come together, the field becomes essentially constant, and this region requires special treatment to provide adequate axial focusing. One technique is to shorten gap length to provide a slightly higher field at the center, so the average field decreases with radius from the center out to the point where the AVF fields become significant.

To arrive at an isochronous design, it is necessary to trace orbits through the AVF field pattern and derive an azimuthal average $\bar{B}$ which should satisfy Eq. (15-47). Deviations from this relation indicate the trimming that must be done on the spiral ridges. Figure 15-24 shows the radial field plots for $\bar{B}$ and B for the 50-Mev machine at the University of California at Los Angeles.[26]

Because of the relatively small values of k used in AVF cyclotrons the terms involving G in Eqs. (15-43), giving the betatron oscillation frequencies, are negligible, and these equations can be written

$$\begin{aligned} \nu_r^2 &\cong 1 + k \\ \nu_z^2 &\cong -k + F^2\left(\frac{K^2}{N^2} + \frac{1}{2}\right) \\ &\cong -k + F^2\left(\tan^2\gamma + \frac{1}{2}\right) \end{aligned} \tag{15-49}$$

where γ is the angle defined by Eq. (15-42). It is the angle at which field spirals cut radial lines.

The radial betatron frequency in a conventional cyclotron is always less than unity. Here, however, since k is positive and increases with radius, the radial frequency for an isochronous machine is always greater than unity. If it reaches the value of 1.5, a half-integral resonance can occur. For protons [from Eq. (15-48)] this occurs at about 450 Mev. It appears that this resonance can be passed, but the integral resonance that appears for $\nu_r = 2$ is regarded as an impassable barrier. This sets an upper limit of about 900 Mev on isochronous AVF cyclotrons. Above this energy it will be necessary to return to the frequency-variation methods used in the synchrocyclotron.

The vertical betatron oscillation tends to become unstable as k increases, unless the angle γ is increased. Vertical stability is improved also by increasing the flutter factor F.

The variables which can be adjusted in design to obtain a small positive value (about 0.02) for ν_z^2 are the number of sectors, the angle of the spiral, and the angular width of the hill. Although N, the number of

sectors, does not appear explicitly in the first of Eqs. (15-49), it does have an effect on the radial oscillation through the stability criterion which requires that ν_r be less than $N/2$. For radial stability it is best to have a large number of sectors and a small spiral angle; however, for axial stability a smaller number of sectors and a large spiral angle are desired, in order to obtain the largest possible flutter factor. The choice is the smallest number of sectors compatible with radial stability and the largest sector angle for which the hill angle can be adjusted to give axial stability. The higher the design energy, the more stringent these criteria become. For energies up to about 25 Mev, three sectors with zero spiral angle (radial sectors) are sufficient. For the energy range between 40 and 80 Mev the usual choice is four sectors and a maximum spiral angle at the periphery of about 45°. At still higher energies design parameters become more critical, and much more detailed analysis is required to avoid radial resonances. Design studies for the highest energies now being considered (850 Mev) involve massive programs for orbit computations and are beyond the scope of this book.

15-12. ACCELERATORS OF THE FUTURE

Scientists in the field of high-energy particle physics continue to press for accelerators of still higher energy. The scientific justification of this demand for ultra-high-energy machines goes far beyond the scope of this volume, but the evidence is impressive. Each new generation of accelerators in a new, higher energy range has brought new insights into the nature of the fundamental particles. Mesons, hyperons, and other short-lived strange particles have been discovered and their properties studied. New transitions between these excited states of matter have been observed, and new principles have been proposed such as the "conservation of strangeness." Studies of the scattering of high-energy particles have shown that the charge and mass distributions in the fundamental particles are so complex as to require new concepts in the theories of nuclear forces. Speculations are starting on the validity of some of the most basic physical laws such as those of quantum electrodynamics, and experiments have been conceived which would test the range of validity. Accelerators which started as tools for nuclear physics have progressed to be the essential instruments for this new field of particle physics, which goes as far beyond nuclear physics as nuclear physics went beyond atomic physics.

Still other scientists have conceived of new areas of research which might be opened by use of accelerators producing much higher intensities than are possible with existing machines. With an increase of several orders of magnitude in intensity and targets which could survive under the bombardment, the secondary radiations could themselves become

important tools for a wide range of new experiments. Pi-meson, K-meson, or even antiproton beams, which have the intensity and beam quality of present primary beams, might prove necessary to resolve the unforeseen problems of the future. Neutrino reactions are also of tremendous theoretical interest, but the flux required for detailed study is greatly in excess of the output from existing accelerators.

In the past, higher energies have resulted partly from a sequence of new concepts for acceleration and partly from technical developments which significantly improved the simplicity or economy of the machines. We could ask whether there are new concepts which would represent a major step in basic principles or whether there are new technical ideas which could be used to extend the energy range using present principles. The answer is that several such concepts have been proposed, and of both types.

Two new principles for acceleration were presented by U.S.S.R. scientists at the CERN conference on high-energy accelerators in 1956.[27] Budker proposed a "plasma betatron" which would utilize the self-focusing properties of an extremely large electron beam in the circular orbit of a betatron-type accelerator. It is known from studies of high-density plasmas that such an intense electron beam would collapse to small transverse dimensions and develop a toroidal magnetic field of such strength that extremely high-energy electrons could be retained in relatively small orbits. However, it is also known from studies with the plasma devices used in thermonuclear experiments that such a beam develops instabilities. Experimental work by Linhard at CERN was reported in the 1959 CERN conference[28] and was generally inconclusive. Although there are still some enthusiasts, there are few who believe this principle can be exploited in a high-energy accelerator, at least within the foreseeable future.

Veksler[27] discussed some theoretical calculations on an even more speculative concept—that of "coherent impact acceleration." This would utilize "collisions" between relativistic electrons in plasma bunches and single ions, in which, if the forces acting on the ion could be made coherent over the entire plasma bunch, the ion could be accelerated to extremely high energies. In the 1959 CERN conference[28] Veksler reported no significant progress, and there is little expectation that this concept will prove practical until there have been major advances in plasma physics and in the theoretical understanding of cooperative phenomena.

Several technical improvements have been proposed which, if they become practical, could lead to important changes in the characteristics of accelerators. The "plasma guns," which are just showing promise in thermonuclear experiments, could potentially be developed into ion sources of very high intensity. The use of cryogenic cooling for the exci-

tation windings of magnets, if developed to be economically practical, could revolutionize the field of magnet design; it might lead to air-cored coils producing extremely large magnetic fields and having correspondingly smaller dimensions. Cryogenic cooling of the radiofrequency systems used for acceleration, such as the waveguides in linacs, could also conceivably lead to greatly improved electrical efficiency in the transformation of rf power and provide faster rates of acceleration.

The synchroclash FFAG machine described in Sec. 15-10 is based on the concept of collisions between two counterrevolving beams; beam intensity must be several orders of magnitude greater than from present accelerators, but if it could be attained, the result would be a major increase in the effective energy of the interaction. For example, as shown in Sec. 15-10, protons of 100 Bev energy would be required, if directed against a fixed hydrogen target, to provide the same excitation energy available in collisions between two counterrevolving protons each of 6.0 Bev energy.

The "storage ring" utilizes the same principle. If the beam from an accelerator is diverted sequentially into two intersecting magnetic orbits, the circulating currents can be built up over reasonable times to hundreds of amperes, such that each beam becomes a target for the other and the sum of the kinetic energies is available for excitation. An electron storage-ring system has been designed and installed by G. K. O'Neill[28] for the Stanford 1-Bev linac to test the principle. Storage rings have also been proposed for proton accelerators, to provide excitation energy in the proton-proton interaction equivalent to very much higher output energies. If applied to the present 33-Bev Brookhaven AGS machine, they would provide 66 Bev of excitation energy in the center of mass, equivalent to that from a 2500-Bev proton beam against a fixed target. O'Neill estimates that a set of storage rings for a proton accelerator would cost approximately the same as the accelerator itself and would have similar dimensions. Somewhat higher estimates have been made at CERN.

The advantage of storage rings in providing high excitation energy means that they will probably be installed in some proton machines. However, the limitation to a single nucleon interaction and the unfavorable geometry for experiments on the secondary radiations make them less satisfactory as laboratory tools than existing high-energy machines. The storage ring should probably be considered as a useful but costly target arrangement rather than as a substitute for an ultrahigh-energy accelerator.

The most practical proposals for superintensity or ultra-high-energy accelerators are based on extensions of existing principles. Proposals for both types utilize AG magnetic fields to guide and focus the particles. This is not too surprising, since the development of the AG principle is still in its early stages; further elaboration and exploitation of the principle can be expected.

Accelerators for superhigh intensities must, almost by definition, be of the continuous-operation rather than the pulsed type, utilizing steady magnetic fields. We can also limit our speculations to those which produce sufficiently high energy to be in the range of interest of high-energy particle physics. Within these restrictions the most favored type is the isochronous cyclotron, discussed in Sec. 15-11. As mentioned, the fixed-field fixed-frequency cyclotron has the capability of being developed up to an energy of about 850 Mev, at which the integral resonance represents a practical limit. Intensities available from existing cyclotron ion sources will supply up to 20 ma of circulating beam, and much higher intensities could be obtained if suitable rf power sources for acceleration were available. Even if limited to 20 ma, the beam power at 850 Mev would be 17 megawatts! Engineering limitations on radiofrequency power and cooling are the most significant blockade to progress toward ultrahigh intensities, for this range of energies. Another major problem will result from the tremendous intensities of induced radioactivities produced in such a machine; remote-control devices would be required for most maintenance and repair operations, as in nuclear reactors.

With the outstanding success of the 30-Bev AG synchrotrons at CERN and Brookhaven, these high-energy pulsed machines have become strong competitors with the lower-energy continuous machines as high-intensity sources of secondary radiations. Such high energies lead to multiple production of mesons and increased output of hyperons, such that the most interesting secondary radiations have a more favorable ratio of intensity to background. The future may well show that the most intense beams of many secondary radiations will come from pulsed machines of the highest possible energies, rather than from lower-energy machines specifically designed for high-intensity primary beams.

The most practical present proposals of superenergy accelerators utilize the principle of the AG proton synchrotron. A study group at California Institute of Technology in the summer and fall of 1960, under the leadership of Prof. Matthew Sands, made a preliminary study and issued a report[29] on a proton AG synchrotron for 300 Bev. This speculative design study proposes a cascade synchrotron using two circular orbits—one of large aperture and small energy (10 Bev) for initial acceleration of a beam from an injection linac (50 Mev) and a second ring of small aperture and large radius (1300 m) for acceleration to 300 Bev. The beam would be extracted from the booster ring at 10 Bev in a single turn and injected into the larger orbit; studies of this transfer problem suggest that it is practical, using known techniques, and potentially highly efficient. Damping during acceleration in the booster accelerator will reduce the beam dimensions such that the aperture in the main ring accelerator can be made very small (2 cm by 5 cm), so the magnet is small and power requirements modest compared with the scaling factor. The AG magnet

would consist of 1200 sectors of alternating gradients, using an equivalent n value of 8600 and producing 43.25 betatron wavelengths around the orbit. In the judgment of several expert critics, the problems of orbit alignment and magnetic uniformity are within the scope of known techniques, and other parameters of the main accelerator and booster accelerator are not far outside the practical limits of present technology. In the preliminary cost estimates it is interesting to note that the buildings, tunnels, and facilities represent about half the total cost, which is of the order of 125 million dollars. In 1961, another design study for machines of 100 to 300 Bev was in progress at the Lawrence Radiation Laboratory of the University of California. Still higher energies were under study at the Brookhaven National Laboratory and in the U.S.S.R.

Enthusiasts for other accelerator types have also speculated about ultimate limits and the practicality of much higher energies. The proposed Stanford electron linear accelerator, which would be 2 miles long and initially powered to reach 15 Bev, could be extended by addition of many more rf power supplies to about 45 Bev, which would approach the technical limitations on maximum energy gain per unit length. The cost of the initial installation is estimated as about 100 million dollars; the higher-energy modification might increase this cost by half.

Proton linacs are potential competitors for high intensities, but the costs involved in extending energies into the multi-Bev range seem excessive. However, new technical concepts for increased efficiency of rf power transformation may change this situation. Such developments will be spurred by the need for proton linacs as injectors into large magnetic accelerators. Some designers conceive that a multi-Bev proton linac could be substituted for the booster synchrotron of the California Institute of Technology proposal, with significant improvement in the rate of cycling and the average beam intensity.

The electron synchrotron is limited by radiation loss caused by radial acceleration in the magnetic field used for containment. However, this limit can be raised by use of very large orbits and very low magnetic fields. In an orbit the size of the main ring for 300-Bev protons of the California Institute of Technology study, electrons could be accelerated to 40 or 50 Bev before reaching this radiation loss limit, in a fast-pulsed magnet having very low peak magnetic fields (about 2000 gauss). The radio-frequency power required to compensate for radiation loss would approach that needed for a linear accelerator and would be the most serious technical problem.

This speculative survey of possibilities indicates that there are no insurmountable technical limitations on the development of accelerators into the energy range of several hundred or even 1000 Bev. However, the size and cost will be at least an order of magnitude larger than for existing machines. Furthermore, each of these gigantic machines will require a

major laboratory installation. The complexity and cost of the apparatus and instruments required for meaningful experiments with modern high-energy accelerators have increased in recent years even more rapidly than for the accelerators themselves. The cost of a large liquid-hydrogen bubble chamber and its associated facilities is in the range of 5 million dollars; analyzing magnets for momentum analysis of the secondary radiations are as large as cyclotron magnets; Cerenkov counters and scintillation counters are as large as washtubs; data reduction and analysis systems require full-scale computers. The cost of the buildings, tunnels, and foundations to house and shield a large accelerator and its associated laboratories has become a dominant factor in the total cost, in some cases exceeding that for the machine and its power supplies. Electric-power requirements have risen much faster than accelerator energy and are already taxing the available supply in some areas. These trends will be continued in the ultra-high-energy machines of the future. It is conceivable that the cost of the accelerators will be a small part of the total cost of such a laboratory installation.

The question to be resolved is not so much whether higher-energy or higher-intensity accelerators can be conceived and constructed, but whether the field of high-energy particle physics justifies the investment of major funds in the extensive laboratories which will be required. One of the most significant factors is the need for a greatly expanded roster of scientists and engineers to staff the laboratories and conduct the experiments. For example, the staff at Brookhaven for construction of the 33-Bev AGS was about 175; this is barely adequate for minimum operations and will have to be increased considerably for most efficient use. The demand for manpower to construct and operate new laboratories for superenergy machines may prove to be a basic limitation to the rate of development.

Such gigantic enterprises may well tax the resources of individual countries, but might have meaning if conceived as international laboratories. The experiment in joint operation of a high-energy laboratory by the CERN group at Geneva, supported by 13 European countries, is an excellent illustration of the usefulness of such international cooperation.

It might be useful to summarize some of the more obvious factors involved in planning for an ultra-high-energy accelerator installation. Location of the site should be chosen for reasons better than those of political compromise. It should be accessible to visiting scientists and so should be reasonably close to a major airport; it should have very large electric-power facilities close at hand; it should have pure water supplies for cooling; it should be within reach of heavy transportation facilities, and if possible close to a major industrial center. The laboratory will require a large staff, and plans must include proper housing, recreational

facilities, and opportunities for intellectual stimulation. An important feature is close association with one or more major universities.

In choosing the type of accelerator and designing the system of components, several desirable features can be identified from past experience. It should be capable of providing for a wide variety of experimental uses, with multiple locations for targets and beams. Very long beam runs are essential for experiments with high-energy particles; experimental areas should be planned to allow expansion of space and facilities. A long duty cycle has many advantages over short pulses, for electronic detection experiments and for maximum intensity. Yet, short beam pulses have their own special utility and should be provided by beam control systems. Reliability of operation is essential and should be designed into the system through maximum use of duplicate replaceable parts and components and by conservative design. Simplicity, symmetry, and replaceability are good watchwords in design.

The history of accelerators is far from complete. This glimpse of the future suggests that the opportunities for further development to still higher energies are as hopeful as at any time in the past. As this book goes to press, the giant 30-Bev AG proton synchrotrons at CERN and Brookhaven are just coming into research operation, at an energy five times higher than that of earlier proton accelerators. The Cambridge accelerator will shortly be completed, with electron energies also five times greater than those of existing machines. Certainly, much will be learned in the next few years, from these and other high-energy machines and from advanced experiments in other laboratories. Yet, in the minds of many responsible scientists the need for still higher energies is already evident. A basic justification is that the time scale for design and construction of ultra-high-energy machines is so long that design and planning must even anticipate the need, to provide a fast start when the evidence becomes clear. As Robert Browning wrote many generations ago, "Ah, but a man's reach should exceed his grasp, or what's a heaven for?"

REFERENCES

1. L. H. Thomas, *Phys. Rev.*, **54**:580 (1938).
2. E. D. Courant, M. S. Livingston, and H. S. Snyder, *Phys. Rev.*, **88**:1190 (1952).
3. J. P. Blewett, *Phys. Rev.*, **88**:1197 (1952).
4. J. B. Adams, M. G. N. Hine, and J. D. Lawson, *Nature*, **171**:926 (1953).
5. "Design Study for a 15-Bev Accelerator," *MIT Research Lab. for Nuclear Sci. Tech. Rept. No.* **60** (June 30, 1953).
6. E. D. Courant, M. S. Livingston, H. S. Snyder, and J. P. Blewett, *Phys. Rev.*, **91**:202 (1953).
7. E. D. Courant and H. S. Snyder, *Ann. Phys.*, **3**:1 (1958).

8. V. V. Vladimirskij and E. K. Tarasov, *Z. Tekh. Fiz.* (*USSR*), **26**:704 (1956).
9. "Lectures on the Theory and Design of an Alternating-gradient Proton Synchrotron" (CERN-PS Group, Geneva, 1953).
10. G. K. Green and E. D. Courant, *Handbuch der Physik*, **44**:320 (1959).
11. J. P. Blewett, Proceedings of CERN Symposium of 1956 (Geneva), p. 159.
12. N. C. Christofilos, Proceedings of CERN Symposium of 1956 (Geneva), p. 176.
13. Proceedings of International Conference on High Energy Accelerators and Instrumentation of 1959, Session 3A (Geneva).
14. K. W. Robinson, *Phys. Rev.*, **111**:373 (1958).
15. Proceedings of CERN Symposium of 1956 (Geneva), pp. 32, 36, and 44.
16. Proceedings of International Conference on High Energy Accelerators and Instrumentation of 1959, Session 2A (Geneva).
17. Proceedings of International Conference on High Energy Accelerators and Instrumentation of 1959 (Geneva), p. 359.
18. K. R. Symon, D. W. Kerst, L. W. Jones, L. J. Laslett, and K. M. Terwilliger, *Phys. Rev.*, **103**:1837 (1956).
19. F. T. Cole, R. O. Haxby, L. W. Jones, C. H. Pruett, and K. M. Terwilliger, *Rev. Sci. Instr.*, **28**:403 (1957).
20. D. W. Kerst, E. A. Day, H. J. Hausman, R. O. Haxby, L. J. Laslett, F. E. Mills, T. Ohkawa, F. L. Peterson, E. W. Rowe, A. M. Sessler, J. N. Snyder, and W. A. Wallenmeyer, *Rev. Sci. Instr.*, **31**:1076 (1960).
21. T. Ohkawa, *Rev. Sci. Instr.*, **29**:108 (1958).
22. Proceedings of International Conference on High Energy Accelerators and Instrumentation of 1959 (Geneva), p. 71.
23. E. L. Burshtein, V. I. Veksler, and A. A. Kolomenskij, USSR Acad. Sci., 1955, p. 3.
24. R. Keller, L. Dick, and M. Fidecaro, *Compt. rend. acad. sci.* (*Paris*), **284**:3154 (1959).
25. E. L. Kelly, P. V. Pyle, R. L. Thornton, J. R. Richardson, and B. T. Wright, *Rev. Sci. Instr.*, **27**:493 (1956).
26. *Proc. Natl. Acad. Sci.* (*U.S.*) *Publ.* 656 (Feb. 2–4, 1959).
27. Proceedings of CERN Symposium of 1956 (Geneva), pp. 68 and 80.
28. Proceedings of International Conference on High Energy Accelerators and Instrumentation of 1959 (Geneva), pp. 139 and 160.
29. M. Sands, "A Proton Synchrotron for 300 Gev," Report No. 10, Synchrotron Laboratory, California Institute of Technology (June 30, 1960).

Name Index

Subject Index

Particle Accelerators

Livingston and Blewett

McGraw-Hill Book Company